AD-A200 903 PROCEEDINGS OF THE INTERNATIONAL WIRE AND CABLE SYMPOSIUM (IWCS 37TH) HEL..(U) ARMY COMMUNICATIONS-ELECTRONICS COMMAND FORT MONMOUTH NJ 1/9

UNCLASSIFIED 17 NOV 88 F/G 9/1 NL

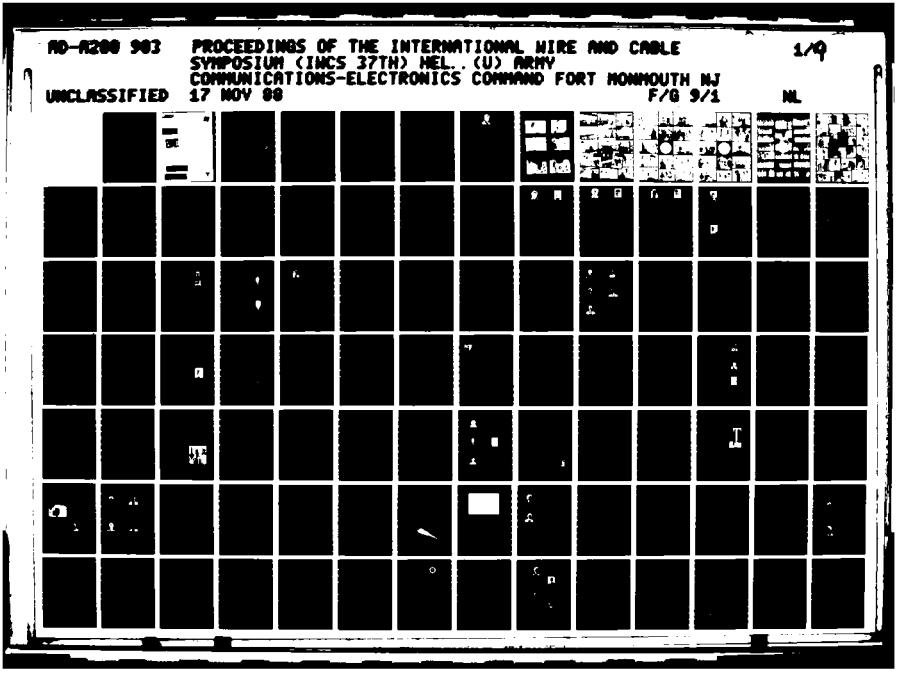

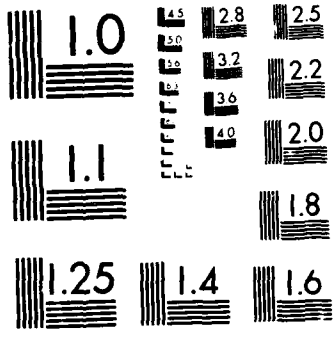

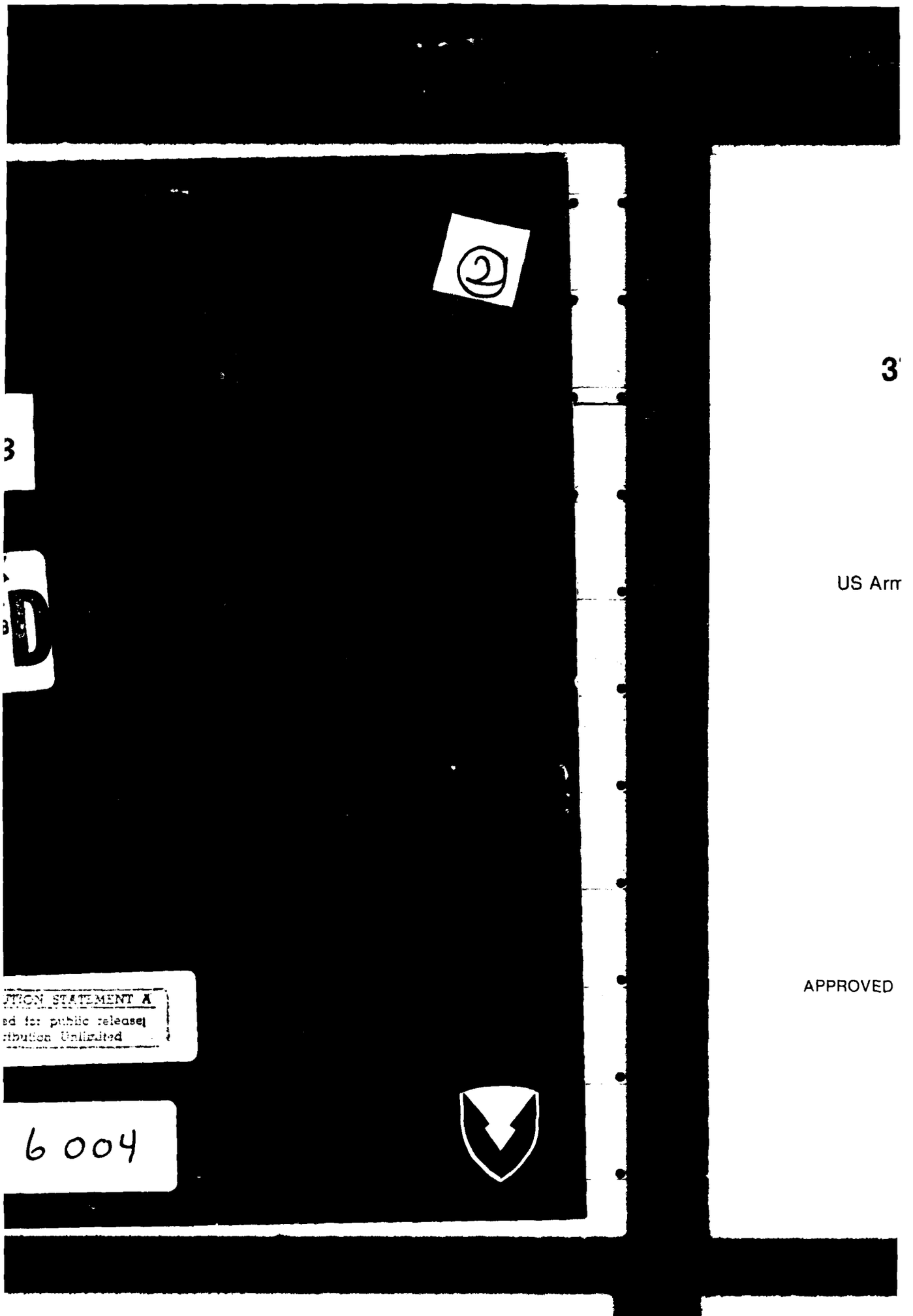

berg & Schubert GmbH

Quantum Chemical Corp., USI Division
Cincinnati, OH

(2)

PROCEEDINGS OF 37TH INTERNATIONAL WIRE AND CABLE SYMPOSIUM

Sponsored by
US Army Communications-Electronics Command
(CECOM)
Fort Monmouth, New Jersey

BALLY'S RENO HOTEL
RENO, NEVADA
NOVEMBER 15, 16 and 17, 1988

37TH INTERNATIONAL WIRE AND CABLE SYMPOSIUM

SYMPOSIUM COMMITTEE

Elmer F. Godwin, *Director*
GEF Associates
3A Buttonwood Drive
Shrewsbury, NJ 07701
(201) 741-8864

Susan Burgher, *Assistant*
US Army CECOM
ATTN: AMSEL-RD-C³-PB
Fort Monmouth, NJ 07703-5000
(201) 544-2770

Dr. Peter R. Bark
Siecor Corporation
489 Siecor Park
Hickory, NC 28603

Dr. Reiner J. Gerdes
Contel Laboratories
270 Scientific Drive—Suite 10
Technology Park/Atlanta
Norcross, GA 30092

Mr. Edward A. Gurney
GTE Service Corporation
3050 Harrodsburg Road
Lexington, KY 40503

Mr. L. G. "Les" Hewitt
Pacific Bell
2600 Camino Ramon
Room 4W401
San Ramon, CA 94583

Dr. Raymond E. Jaeger
SpecTran
50 Hall Road
Sturbridge, MA 01566

Mr. Tom Jones
Wyrough & Loser, Inc.
P.O. Box 5047
Trenton, NJ 08638

Mr. Vieney Mascarenhas
Canada Wire & Cable Ltd.
22 Commercial Road
Toronto, Ontario
Canada M4G 1Z4

Mr. Hans A. Mayer
Olex Cables, Division of
Pacific Dunlop Limited
207 Sunshine Road
Tottenham, 3012
Melbourne, Australia

Mr. James J. Pickering
Union Carbide Corp.
Weston Canal Center
CN 450
Somerset, NJ 08873

Dr. C. Ronald Simpkins
E. I. DuPont de Nemours & Co., Inc.
Polymer Products Dept.
P-182212
Wilmington, DE 19898

Mr. Robert Streich
AT&T Network Systems
505 North 51st Avenue
P.O. Box 13369
Phoenix, AZ 85043

Dr. Keiji Tachikawa
NTT
200 Park Avenue
New York, NY 10017

Mr. George Webster
AT&T Bell Laboratories
2000 Northeast Expressway
Norcross, GA 30071

SYMPOSIUM ADVISORY GROUP

Leo Chattler
DCM Industries, Inc.
13666 East 14th Street
San Leandro, CA 94578

Michael A. DeLucia
David Taylor Research Center
Energy R&D Office, Code 2759
Annapolis, MD 21402-5067

Marta Farago
Northern Telecom Canada Ltd.
P.O. Box 6122, Station A
Montreal, Quebec
Canada H3C 3J4

Irving Kolodny
Consultant
80-56 230th Street
Bellerose Manor, NY 11427

Frank Short
Consultant
1821 Howard Street
Saint Charles, IL 60174

MISSION

The International Wire and Cable Symposium provides a forum for the exchange of technical information amongst suppliers, manufacturers, and users on technological advancements in materials, processes, and products used for voice, data and video signal transmission systems.

TECHNICAL SESSIONS

Tuesday, 15 November 1988

9:30 a.m.	SESSION I	Tutorial—Technology, Regulation and the Consumer
1:30 p.m.	SESSION II	Materials
1:30 p.m.	SESSION III	Fiber Optic Cable Design for Special Applications I
1:30 p.m.	SESSION IV	Fiber Optic Aerial Cable

Wednesday, 16 November 1988

8:30 a.m.	SESSION V	Cable Networks I
8:30 a.m.	SESSION VI	Optical Cable Manufacturing, Installation & Testing
8:30 a.m.	SESSION VII	Reliability, Transmission Properties and Testing of Optical Fibers
2:00 p.m.	SESSION VIII	Cable Networks II
2:00 p.m.	SESSION IX	Fiber Optic Cable Design for Special Applications II
2:00 p.m.	SESSION X	Copper Cable Design/Testing
3:30 p.m.	SESSION XI	Poster Papers
5:30 p.m.		Special Session for International Attendees

Thursday, 17 November 1988

8:30 a.m.	SESSION XII	Physical and Electrical Stability of PIC Cable Insulation Systems
8:30 a.m.	SESSION XIII	Fire Hazard and Risk Assessment I
8:30 a.m.	SESSION XIV	Fiber Optic Splicing
8:30 a.m.	SESSION XV	Fiber Optic Military Applications
1:30 p.m.	SESSION XVI	Fire Hazard and Risk Assessment II
1:30 p.m.	SESSION XVII	Fiber Optic and Copper Connector
1:30 p.m.	SESSION XVIII	Bending Losses of Optical Fibers/Fiber Coatings

PAPERS

The papers in this volume were printed directly from unedited reproducible copies prepared by the authors. Responsibility for contents rests upon the authors and not the symposium committee or its members. After the syposium, all the publication rights of each paper are reserved by their authors, and requests for republication of a paper should be addressed to the appropriate author. Abstracting is permitted, and it would be appreciated if the symposium is credited when abstracts or papers are republished. Requests for individual copies of papers should be addressed to the authors.

PROCEEDINGS
INTERNATIONAL WIRE AND CABLE SYMPOSIUM

Bound—Available at Fort Monmouth

30th International Wire & Cable Symposium Proceedings—1981— $8.00
31st International Wire & Cable Symposium Proceedings—1982— $8.00
32nd International Wire & Cable Symposium Proceedings—1983— $8.00
33rd International Wire & Cable Symposium Proceedings—1984—$10.00
34th International Wire & Cable Symposium Proceedings—1985—$15.00
35th International Wire & Cable Symposium Proceedings—1986—$15.00
36th International Wire & Cable Symposium Proceedings—1987—$20.00
37th International Wire & Cable Symposium Proceedings—1988—$25.00

*Extra copies: 1-3 $25.00; next 4-10 $20.00; next 11 & above $15.00 each

Make check or bank draft payable in US dollars to the INTERNATIONAL WIRE & CABLE SYMPOSIUM and forward request to:

International Wire & Cable Symposium
P.O. Box 7597
Shrewsbury, NJ 07702

Telephone inquiries may be directed to Susan Burgher at (201) 544-2770.

NOTE: Overseas air mail will be an additional $25.00 per copy for Europe and $30.00 per copy for Asia.

Photocopies are available for complete sets of papers for 1964 thru 1987. Information on prices and shipping charges should be requested from the:

US Department of Commerce
National Technical Information Service
Springfield, Virginia 22151
USA

Include Title, Year and "AD" Number

13th Annual Wire & Cable Symposium (1964)	—AD 787164
15th Annual Wire & Cable Symposium (1966)	—AD A006601
16th International Wire & Cable Symposium (1967)	—AD 787165
17th International Wire & Cable Symposium (1968)	—AD 787166
18th International Wire & Cable Symposium (1969)	—AD 787167
19th International Wire & Cable Symposium Proceedings 1970	—AD 714985
20th International Wire & Cable Symposium Proceedings 1971	—AD 733399
21st International Wire & Cable Symposium Proceedings 1972	—AD 752908
22nd International Wire & Cable Symposium Proceedings 1973	—AD 772914
23rd International Wire & Cable Symposium Proceedings 1974	—AD A003251
24th International Wire & Cable Symposium Proceedings 1975	—AD A017787
25th International Wire & Cable Symposium Proceedings 1976	—AD A032801
26th International Wire & Cable Symposium Proceedings 1977	—AD A047609
27th International Wire & Cable Symposium Proceedings 1978	—AD A062322
28th International Wire & Cable Symposium Proceedings 1979	—AD A081428
29th International Wire & Cable Symposium Proceedings 1980	—AD A096308
30th International Wire & Cable Symposium Proceedings 1981	—AD A110859
31st International Wire & Cable Symposium Proceedings 1982	—AD A125662
32nd International Wire & Cable Symposium Proceedings 1983	—AD A136749
33rd International Wire & Cable Symposium Proceedings 1984	—AD A152119
34th International Wire & Cable Symposium Proceedings 1985	—AD A164384
35th International Wire & Cable Symposium Proceedings 1986	—AD A180828
36th International Wire & Cable Symposium Proceedings 1987	—AD A189610
Kwic Index of Technical Papers, International Wire & Cable Symposium (1952-1975)	—AD A027558

MESSAGE FROM DIRECTOR

The sponsor, U.S. Army Communication-Electronics Command (CECOM), Fort Monmouth, New Jersey and the Symposium Committee, welcomes each contributor and attendee to the 37th International Wire and Cable Symposium (IWCS). The symposium committee is dedicated to improving and broadening the technology and use of wire and cable for both military and industrial applications. Emphasis is always placed on making the symposium a learning environment where knowledge is freely exchanged and in many instances generated.

This year's technical program is extremely exciting, beginning with a tutorial session on "Technology, Regulation and the Consumer." The program includes seventeen additional sessions on various developments and uses of wire/cable components, including three special sessions on specific cable applications and testing. A poster session which was received with great enthusiasm last year should be a winner again this year. It is the committee's desire each year, to offer a program that represents a balance of the technical interest desired by all attendees and contributors. The technical program will, at all times, be a reflection of the current interest of the symposium participants, which is dictated by the response to the "Call-For-Papers." In addition to the technical presentations, many companies are planning special product demonstrations and hospitality functions.

Committee members Ed Gurney of GTE Service Corporation; Vieney Mascarenhas, Canada Wire and Cable; Raymond Jaeger, SpecTran and Tom Jones, Wyrough and Loser, are retiring from the committee. Each member was extremely dedicated and contributed significantly to the success of the symposium. On behalf of the sponsor and the committee, I extend to each, a very special thanks for their sincere dedication, cooperation and support of the symposium's activities.

The committee and sponsor offers their appreciation to all members of the wire and cable industry and solicit their continued support to ensure the future success of the symposium. Any comments and suggestions for improving the symposium are welcomed.

The 1989 symposium (38th) will be in Atlanta, Georgia at the Hyatt Regency Hotel and in 1990, the symposium will return to the Bally's Reno Hotel, in Reno, Nevada.

Elmer F. Godwin
Director, IWCS

Highlights of the 36th International Wire and Cable Symposium November 17, 18, and 19, 1987 Marriott Crystal Gateway Hotel Arlington, Virginia

Greetings by Mr. Eugene Famolari Jr., Director, Center For Command. Control and Communications C3 Systems, U.S. Army, CECOM, Fort Monmouth, New Jersey.

Luncheon Speaker—Dr. C. Kumar N. Patel, AT&T Laboratories, *Murray Hill, New Jersey.*

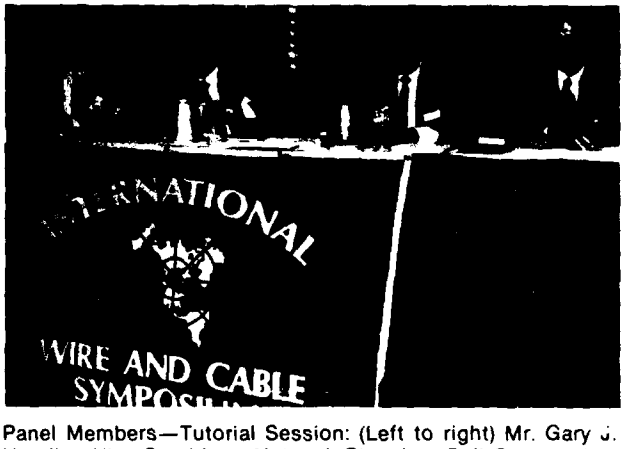

Panel Members—Tutorial Session: (Left to right) Mr. Gary J. Handler, Vice President, Network Planning, Bell Communications Research, Livingston, New Jersey: Mr. William J. Noll, Vice President, Network Technology, Bell Northern Research, Ottawa, Canada; Mr. Clark Barlow, Vice President, Operations Support, GTE Service Corp., Stanford, Connecticut; and Mr. Michael L. Bandler, Vice President, Network Engineering and Planning, Pacific Bell, San Ramon, California.

Committee Member Dr. Peter Bark (right), Siecor Corporation, presenting the Award for Outstanding Technical Paper to Dr. Simon D. Dadakarides, Stanford University, California.

Best Presentations—Two Winners

Committee Member Dr. Peter Bark (right), *Siecor Corporation* presenting the Award to Dave Fischer, Superior Cable Corporation.

Committee Member Dr. Peter Bark (right), Siecor Corporation presenting the Award to John C. Chamberlain, Siecor Corporation.


REGISTRATION GENERAL
INTERNATIONAL
WIRE AND CABLE
SYMPOSIUM
REGISTRATION









HIGHLIGHTS
OF THE
36TH
INTERNATIONAL
WIRE & CABLE
SYMPOSIUM


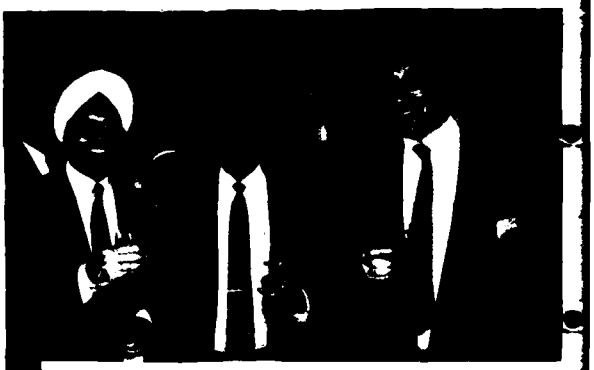








IWCS

CRYSTAL GATEWAY MARRIOTT HOTEL

ARLINGTON, VIRGINIA

Nov 17 18 and 19th 1987

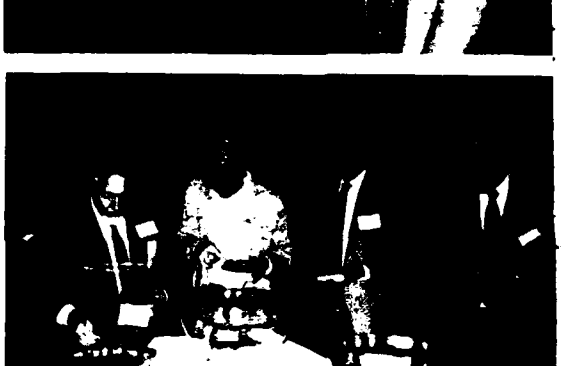






IWCS
TECHNICAL SESSIONS
SPEAKERS


IWCS
SESSION
IN PROGRESS
QUIET
PLEASE !

AWARDS

	Outstanding Technical Paper	*Best Presentation*
1968	H. Lubars and J. A. Olszewski, General Cable Corp.—"Analysis of Structural Return Loss in CATV Coaxial Cable"	N. Dean, B.I.C.C.—"The Development of Fully Filled Cables for Distribution Network"
1969	J. P. McCann, R. Sabia and B. Wargotz, Bell Laboratories—"Characterization of Filler and Insulation in Waterproof Cable"	J. D. Kirk, Alberta Government Telephones—"Progress and Pitfalls of Rural Buried Cable"
1970	D. E. Setzer and A. S. Windeler, Bell Laboratories—"A Low Capacitance Cable for the T2 Digital Transmission Line"	Dr. O. Leuchs, Kable and Metalwerke—"A New Self-Extinguishing Hydrogen Chloride Binding PVC Jacketing Compound for Cables"
1971	R. Lyenger, R. McClean and T. McManus, Bell Northern Research—"An Advanced Multi-Unit Coaxial Cable for Toll PCM Systems"	S. Nordblad, Telefonaktiebolaget L. M. Ericsson—"Multi-Paired Cable of Nonlayer Design for Low Capacitance Unbalance Telecommunications Network N. Kojima, Nippon Telegraph and Telephone—"New Type Paired Cable for High Speed PCM Transmission"
1972	J. B. Howard, Bell Laboratories—"Stabilization Problems with Low Density Polyethylene Insulations"	S. Kaufman, Bell Laboratories—"Reclamation of Water-Logged Buried PIC Telephone Cable"
1973	Dr. H. Margin, Kabelmetal—"High Power Radio Frequency Coaxial Cables, Their Design and Rating"	R. J. Oakley, Northern Electric Co., Ltd.—"A Study Into Paired Cable Crosstalk"
1974	D. Doty, AMP Inc.—"Mass Wire Insulation Displacing Termination of Flat Cable"	G. H. Webster, Bell Laboratories—"Material Savings by Design in Exchange and Trunk Telephone Cable"
1975	T. S. Choo, Dow Chemical U.S.A.—"Corrosion Studies on Shielding Materials for Underground Telephone Cables"	J. E. Wimsey, United States Air Force—"The Bare Base Electrical Systems"
1976	N. J. Cogelia, Bell Telephone Laboratories and G. K. Lavoie and J. F. Glahn, US Department of Interior—"Rodent Biting Pressure and Chemical Action and Their Effects on Wire and Cable Sheath"	Michael DeLucia, Naval Ship Research and Development—"Highly Fire-Retardant Navy Shipboard Cable"
1977	Thomas K. McManus, Northern Telecom Canada Ltd. and R. Beveridge, Saskatchewan Telecommunications, Canada—"A New Generation of Filled Core Cable"	William L. Schmacher, AMP Inc.—"Design Considerations for Single Fiber Connector"
1978	Fumio Suzuki, Shizuyoshi Sato, Akinori Mori and Yoichi Suzuki; Sumitomo Electric Industries, Ltd., Japan—"Microcoaxial Cables Insulated with Highly Expanded Polyethylene By Chemical Blowing Method"	Richard C. Mondello, Bell Labs.—"Design and Manufacture of an Experimental Lightguide Cable For Undersea Transmission Systems"
1979	S. Masaki, Y. Yamazaki and T. Ideguchi, Nippon Telegraph and Telephone Public Corporation, Japan—"New Aluminum Sheath Cable Used for Electromagnetic Shielding"	I. Wadehra, IBM Corporation—"Performance of Polyvinyl Chloride Communication Cables in Modified Steiner Tunnel Test"
1980	P. Kish and Y. BeBorgne, Northern Telecom Canada Limited, Montreal, Canada—"General Crosstalk Model For Paired Communication Cables"	J. J. Refi, Bell Laboratories—"Mean Power Sum Far-End Crosstalk of PIC Cables as a Function of Average Twist Helix Angle"
1981	C. J. Arroyo, N. J. Cogelia, Bell Laboratories, and B. J. Darsey, Western Electric—"Thermal Behavior of Experimental Plenum Cable Sheaths Determined in a Radiant Heat Chamber"	G. S. Anderson, Belden Corporation—"Installation of Fiber Optic Cable on 457 Meter Tower"
1982	R. H. Whiteley, Raychem Ltd.—"A Comprehensive Small Scale Smoke Test"	A. Yoshizawa, The Furukawa Electric Co., Ltd.—"Structure and Characteristics of Cables for Robots"
1983	V. A. Fentress, Raychem Corp. and D. V. Nelson, Stanford University—"Fracture Mechanics Evaluation of the Static Fatigue Life of Optical Fibers in Bending"	J. R. Bury, Standard Telecommunication Laboratories, Ltd., Hailow, England—"Development of Flame Retardant, Low Aggressivity Cables"
1984	M. Fujise and Y. Iwamoto, KDD Research & Development Laboratories, 1-23 Nakameguro, 2-Chome, Meguro-Ku, Tokyo, Japan—"Self-Core-Alignment Arc-Fusion Splicer Based on a Simple Local Monitoring Method"	William E. Dennis, Dow Corning Corporation, Midland, Michigan—"Hydrogen Evolving Tendencies of Cable Fillers and Optical Fiber Coatings"
1985	James A. Krabec and John W. Kincaid, Jr., Belden Technical Research Center—"Advances in the Optimization of Multi-Layer Shield Design"	Stephen Hornung, British Telecom Research Laboratories—"Manufacture and Performance of Fibre Units for Installation by The Viscous Drag of Air"
1986	Simon D. Dadakarides and Bruce B. Lusignam, Stanford University—"Magnetically Loaded Cables"	Dave Fischer, Superior Cable Corp.—"Progress Towards the Development of Lightning Test for Telecommunication Cables" John C. Chamberlain, Siecor Corp.—"Zero Halogen Fire Retardant Fiber Optic Shipboard Cable"

1987

Outstanding Technical Paper	*Outstanding Poster Paper*	*Best Presentation*
Stephen B. Pierce—Contel Laboratories—"Digital Transmission on Customer Premises Wiring"	William Wood—Bell Communication Research "Performance Analysis of Optic Fiber Cleavers"	Richard Rossi—General Cable Company "Cable Sheathing Design and Performance Criteria"

CONTRIBUTORS

ACOME
Paris & Mortain, France
AEG Kabel Aktiengesellschaft
Monchengladbache, West Germany
A.F.A. Industries
Garfield, NJ
Alambres Y Cables Venezolanos C.A. "ALCAVE"
Caracas, Venezuela
Alberta Government Telephones
Edmonton, Alberta, Canada
Alcatel NA, Inc.
Claremont, NC
Alcatel NA, Inc.
Roanoke, VA
Allied Corp.
Morristown, NJ
Allied Signal Inc.
Morristown, NJ
Alpha Wire Corp.
Elizabeth, NJ
Amoco Chemical Company
Naperville, IL
AMP Incorporated
Harrisburg, PA
Arvey Corporation
Cedar Grove, NJ
AT&T Network Systems
Phoenix, AZ
AT&T Technologies, Inc.
Phoenix, AZ
Austral Standard Cables Pty Limited
Clayton, Victoria, Australia
BASF Chemicals Corp.
Parsippany, NJ
BASF Corporation—Chemicals Division
Parsippany, NJ
Belden Technical Research Center
Geneva, IL
Bell Canada
Montreal, Quebec
Bell Canada
Toronto, Ontario, Canada
Bell Communications Research
Morristown, NJ
Bell-Northern Research Ltd.
Ottawa, Ontario, Canada
Berk-Tek Inc.
Reading, PA
BICC Cables Limited
Helsby, Warrington, Cheshire, England
BP Performance Polymers Inc.
Hackettstown, NJ
Breen Color Concentrates
Lambertville, NJ
Building Industry Consulting Service International (BICSI)
University of South Florida, Tampa, FL
Burgess Pigment Company
Sandersville, GA
Camden Wire Company, Inc.
Camden, NY
Canada Wire & Cable
Winnipeg, Manitoba, Canada
Carlew Inc.
LaSalle, Quebec, Canada
Chase & Sons, Inc.
Randolph, MA
Ciba-Geigy Corp.
Hawthorne, NY
C-I-L Inc.
Brampton, Ontario, Canada
Commercial Polymers P/L
Victoria, Australia
Copperthorne Industries 86 LTD
Vancouver, BC, Canada
Corning Glass Works
Corning, NY
Crellin Inc.
Chatham, NY
DCM International Corp.
San Leandro, CA
DeSoto Inc.
Des Plaines, IL
DuPont Canada Inc.
Mississauga, Ontario, Canada
Dussek Campbell Ltd.
Crayford, Kent. England
Dussek Campbell Limited
Ontario, Canada
Dussek Campbell Pty. Ltd.
Regents Park, Australia
EMS-Chemie AG
Switzerland
Engineered Yarns, Inc.
Coventry, RI
Ericsson Cables
Hudiksvall, Sweden
Essex Group Inc.
Decatur, IL
Fugikura Ltd.
Tokyo, Japan
Gary Chemical Corp.
Leominster, MA
Gavitt Wire and Cable Co.
Brookfield, MA
GE Plastics
Pittsfield, MA
Gem Gravure Company
West Hanover, MA
General Cable Company
Woodbridge, NJ
General Electric Plastics
Pittsfield, MA
B.F. Goodrich Company
Independence, OH
W.L. Gore & Assoc., Inc.
Newark, DE
Great Lakes Chemical Corp.
West Lafayette, IN
GTE Service Corp.
Lexington, KY
Himont, USA Inc.
Wilmington, DE
Hong Kong Telephone
Hong Kong
Hudson International Conductors
Ossining, NY
Judd Wire Inc.
Turners Falls, MA
Kabelmetal Electro GmbH
Hannover, West Germany
Kabelmetal Electro North America Inc.
Larchmont, NY

Kroschu-Kabelwerke Kromberg & Schubert GmbH
Wuppertal, West Germany
KT Industries Ltd.
Winnipeg, Manitoba, Canada
Lamart Corporation
Clifton, NJ
Lantor BV
Veenendaal, The Netherlands
LNP Engineering Plastics
Malvern, PA
Lonza Inc.
Fair Lawn, NJ
Mohawk Wire & Cable Corp.
Leominster, MA
The Montgomery Company
Windsor Locks, CT
NEK Cable, Inc.
Ronkonkoma, NY
NEPTCO Inc.
Pawtucket, RI
Nesor Alloy Corp.
W. Caldwell, NJ
Neste Chemicals Inc.
New Brunswick, NJ
The New Brunswick Telephone Company, Ltd.
Saint John, New Brunswick, Canada
Nippon Telegraph and Telephone Corp.
Ibaraki-ken, Japan
Nokia-Maillefer, Inc.
South Hadley, MA
Northern Telecom Canada
Lachine, Quebec, Canada
Northern Telecom Canada Ltd.
Saskatoon, Saskatchewan, Canada
NTT *America*, Inc.
New York, NY
Olex Cables, Div. of Pacific Dunlop Ltd.
Melbourne, Australia
Omega Wire Inc.
Camden, NY
Pacific Bell
San Ramon, CA
Pantasote Inc.
Passaic, NJ
Pennwalt Corporation
Philadelphia, PA
Penreco
Butler, PA
Philips Telecom Equipment Corp.
Brookfield, CT
Phillips Cables Limited
Vancouver, BC, Canada
Phillips Kommunikations Industrie
Cologne, West Germany
PPG Industries Inc.
Pittsburgh, PA

Quantum Chemical Corp., USI Division
Cincinnati, OH
RXS Schrumpftechnik-Garnituren GmbH
West Germany
Shuenn Feng Industrial Co.
Taipei, Taiwan, Rep. of China
Siecor Corporation
Hickory, NC
Siemens AG
West Germany
SILEC
Paris, France
The Stewart Group Ltd.
Markham, Ontario, Canada
Sumitomo Electric Fiber Optics Corp.
Research Triangle Park, NC
Sumitomo Electric Industries, Ltd.
Yokohama, Japan
Swedish Telecom
Farsta, Sweden
The Swiss Insulating Works
Switzerland
Syarikat Telekom Malaysia Berhad
Kuala Lumpur, Malaysia
Taconic Plastics, Ltd.
Petersburg, NY
Teledyne, Thermatics
Elm City, NC
Texas Instruments Inc.
Attleboro, MA
3M—Telecom Products Div.
Austin, TX
Telecom Australia
Melbourne, Australia
Times Microwave Systems, Inc.
Wallingford, CT
Trea Industries
N. Kingstown, RI
UBE Industries (America)
New York, NY
Union Carbide Corp.
Danbury, CT
Vista Chemical Co.
Houston, TX
Weber & Scher Mfg. Co., Inc.
Newark, NJ
Wilson-Fiberfil International
Nashanic Station, NJ
Wirex, Inc.
Wallingford, CT
Witco Corporation
New York, NY
Wyrough and Loser, Inc.
Trenton, NJ

TABLE OF CONTENTS

WEDNESDAY MORNING—8:30 AM-12:00 PM

Capital Room

SESSION V: CABLE NETWORKS I

Chairperson: Mr. Les Hewitt, Pacific Bell

Bijou Complex

SESSION VI: OPTICAL CABLE MANUFACTURING, INSTALLATION & TESTING

Chairperson: Mr. Hans A. Mayer, Olex Cables, Division of Pacific Dunlop Ltd.

Adelphia Room

SESSION VII: RELIABILITY, TRANSMISSION PROPERTIES AND TESTING OF OPTICAL FIBERS

Chairperson: Dr. Peter R. Bark, Siecor Corporation

AWARDS LUNCHEON

12:00 Noon-2:00 PM

Ziegfield Theatre

Guest Speaker: Mr. David G. Thomas, Executive Director, AT&T Bell Laboratories Transmission Systems Division, Holmdel, NJ

WEDNESDAY AFTERNOON—2:00 PM-5:00 PM

Capital Room

SESSION VIII: CABLE NETWORKS II

Chairperson: Leo Chattler, DCM Industries Inc.

Adelphi Room

SESSION IX: FIBER OPTIC CABLE DESIGN FOR SPECIAL APPLICATIONS II

Chairperson: Mr. George Webster, AT&T Network Systems, CA

Bijou Room

SESSION X: COPPER CABLE DESIGN/TESTING

Chairperson: Ms. Martha Farago, Northern Telecom Canada, Ltd.

WEDNESDAY AFTERNOON—3:30 PM-5:30 PM
Grand Ballroom

SESSION XI: POSTER PAPERS

Chairperson: Mr. Vieney Mascarenhas, Canada Wire & Cable Ltd.

THURSDAY MORNING—8:30 AM-12:00 Noon

Adelphi Room

SESSION XII: PHYSICAL AND ELECTRICAL STABILITY OF PIC CABLE INSULATION SYSTEMS

Chairperson: Mr. Vieney Mascarenhas, Canada Wire & Cable Ltd.

Moderator: Dr. James Tyler, Essex Group Inc.

Capital Room

SESSION XIII: FIRE HAZARD AND RISK ASSESSMENT I

Chairperson: Dr. C. Ronald Simpkin, E.I. DuPont de Nemours & Co.

Moderator: Dr. Frederic B. Clarke, Benjamin Clarke Associates, Inc.

Bijou Room

SESSION XIV: FIBER OPTIC SPLICING

Chairperson: Mr. Edward A. Gurney, GTE Service Corp.

Grand Ballroom

SESSION XV: FIBER OPTIC MILITARY APPLICATIONS

Chairperson: Mr. Michael A. DeLucia, David Taylor Research Center

Moderator: Mr. Vasilios E. Kalomiris, US Army Communications-Electronics Command

THURSDAY AFTERNOON—1:30 PM-4:30 PM

Capital Rooms

SESSION XVI: FIRE HAZARD AND RISK ASSESSMENT II

Chairperson: Dr. C. Ronald Simpkins, E.I. DuPont de Nemours & Co.

Adelphi Room

SESSION XVII: FIBER OPTIC AND COPPER CONNECTOR

Chairperson: Mr. Irv Kolodny, Consultant

Bijou Rooms

SESSION XVIII: BENDING LOSSES OF OPTICAL FIBERS/FIBER COATINGS

Chairperson: Dr. Raymond E. Jaeger, Spectran Corp.

TUTORIAL PANEL

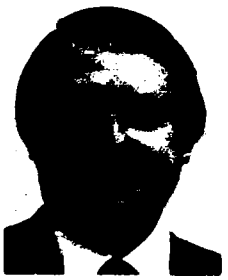

James J. Pickering (Chairman)
Union Carbide Corporation
Somerset, New Jersey

Mr. Pickering joined the Research and Development Department of Union Carbide in Bound Brook, N.J. in 1962. Following his R&D experience, Mr. Pickering was assigned to sales in the Chicago area in 1972 where he called on major wire and cable accounts in the midwest as an account representative.

In 1982 he was promoted to the position of Product Sales Manager for the Industrial Cable Market Area where he returned to Union Carbide in Bound Brook, N.J. He is presently Manager of Wire and Cable Product Applications interfacing with various end-users and specifying agencies.

Mr. Pickering is a member of the Society of Plastics Engineers, the Institute of Electronics and Electrical Engineers, The National Fire Protection Association, ASTM, New York Rubber Group, and the Wire Association.

Terry D. Appenzeller
Ameritech Services Corporation
Chicago, Illinois

Mr. Appenzeller joined Ameritech Services in August 1985 as Senior Director - Equal Access and Interexchange Carriers Account Management. He moved his wife and three daughters (Age 16, 13, 11) from the Washington, D.C. area to Barington Hills, Illinois in October 1985. Terry joined Ameritech following two years with Satellite Business Systems (SBS), and fifteen years with Pacific Bell.

At SBS, Terrry was the Director of Carrier Relations, with responsibility for their policy and planning interface with all Bell Operating Companies, Independents, AT&T, and other carriers. He was also responsible for SBS access charge expenditures and revenue expansion plans.

Prior to SBS, Terry was a Division Manager responsible for Carrier Relations at Pacific Bell. He was the primary policy and planning interface for IC's prior to divestiture. He held various management positions prior to this assignment - Network Special Services, Marketing, Business Offices, Installation & Maintenance, and Corporate Finance.

Terry is a national leader in the IC Industry from both an interexchange and exchange carrier perspective. He has played an active role in tall national carrier forums.

Terry graduated in 1969 from the University of Redlands in Southern California. He and his family have spent all of their lives in California, with the exception of the last five years.

Terry is currently holding the position of Senior Director - ONA Implementations and is repsonsible for representing Ameritech in Information Industry Liaison Committee (IILC) forums and before federal and state agencies and industry groups. Also, he is the primary open network architecture liaison with the Ameritech Bell Companies.

Brian R. Moir
Partner - Fisher, Wayland, Cooper & Leader
Washington, D.C.

Mr. Moir received his Juris Doctorate from the University of Denver College of Law where he received the International Legal Studies Award and was a member of the Denver Journal of International Law and Policy.

Prior to telecommunications law practice, Mr. Moir served for six years as Senior Legal Counsel to the Committee on Energy and Commerce of the U. S. House of Representatives where he was responsible for the telecommunications, foreign commerce, and trade jurisdiction of the Committee and was the Committee parliamentarian. Previously, he served as a staff attorney at the Federal Communications Commission, and as Assistant Corporate Counsel for Tele-Communications, Inc., the nation's largest owner of cable television systems and a miscellaneous microwave common carrier, in Dever, Colorado.

During Mr. Moir's more than fifteen years in the private and governmental sectors, he has gained experience in telecommunications and information law, and related government relations and trade matters. He has served as a member of numerous U.S. delegations on international telecommunications issues, has appeared as an expert witness before various Committees of the U.S. Congress, has written numerous articles on telecommunications issues, and has lectured extensively.

Frederic S. Topor
AT&T
Morristown, New Jersey

Mr. Topor was named vice president, manufacturing-Network Systems Media Division in May 1987. He is responsible for the manufacturing activities at the Atlanta, Omaha and Phoenix Works and AT&T Nassau Metals Corporation. His office is located at 475 South Street, Morristown, New Jersey.

Mr. Topor's diverse AT&T career began with Western Electric Co. in 1959, when he joined the Merrimack Valley Works as an engineer.

He served in a variety of managerial capacities in engineering and manufacturing at Merrimack Valley and North Carolina Works, Western Electric Headquarters in New York City, and in Newark, New Jersey.

In 1970, Mr. Topor was selected to participate in the Management Training Program in Princeton, New Jersey, and upon completion served as an engineering manager in Orlando, Florida.

Other positions Mr. Topor held in western Electric include installation manager and manager-installation planning and development in the Central Region, director of division staff for Bell Sales Division-East, director of operations in the Eastern region and regional vice president for the Northeastern Region.

Mr. Topor earned a bachelor's degree in Electrical Engineering from the University of Massachusetts in 1959, and a master's degree in electrical Engineering from Northeastern University in 1965. He is a past director of Renaissance Newark, Inc. and a former vice chairman of the Greater Newark Chamber of Commerce.

Mr. Topor and his wife make their home in Morristown, New Jersey. They have three children.

Barry Grossman
U.S. Department of Justice
Washington, D.C.

Professional Experience:

1. Chief of the Communications and Finance Section, Antitrust Division, United States Department of Justice (1984-Present)

2. Chief of the Appellate Section, Antitrust Division, United States Department of Justice (1975-1984)

3. Chief of the Evaluation Section, Antitrust Division, United States Department of Justice (1971-1975), Assistant Chief (1969-1971), Attorney (1967-1969)

4. Private Practice: Associate, Wilmer, Cutler & Pickering, Washington, D.C. (1964-1967)

Educational Background:

1. A.B. 1960, Georgetown University, Distinctions: Graduated first in class.

2. J.D. 1963, Harvard Law School Distinctions: Editor, Harvard Law Review 1961-1963; Recipient of Frank Knox Fellowship for Post-graduate Study in England.

3. Advanced Institute for Legal Studies and London School of Economics, University of London, 1963-1964 as Frank Knox Fellow from Harvard University.

Personal Information:

Age: 49
Married with two children

Leland W. Schmidt
GTE Service Corporation
a Subsidiary of GTE Corporation
Stamford, Connecticut

Mr. Schmidt was appointed Vice President - Industry Affairs of GTE Service Corporation, a subsidiary of GTE, in March 1987. For the four previous years, Mr. Schmidt served as the Assistant Vice President - Business Planning. Prior to that appointment he was Assistant Vice President - Revenues and Tariffs for seven years.

Mr. Schmidt joined GTE in its Wisconsin Operation in 1959 as a commercial representative prior to joining GTE Service Corporation.

Mr. Schmidt is a frequent guest lecturer and has made numerous presentations on the subjects of policy issues, strategic planning, and pricing related to telecommunications.

AWARDS LUNCHEON

Dr. Reiner J. Gerdes (Chairman-IWCS)
Contel Corporation
Norcross, Georgia

Dr. Gerdes is the Director of Contel Laboratories, an organization within the Telephone Operations Sector of Contel Corporation.

During the past two decades, he has been involved in the development and investigation of a wide range of materials and products used in the telecommunications industry. He is the author or coauthor of more than 150 technical papers and reports. He received his college education in the U.S., France, and Germany where he received a Ph.D. in physical chemistry.

Dr. Gerdes is the current Chairman, Board of Trustees, of the International Wire and Cable Symposium.

David G. Thomas (Guest Speaker)
AT&T Bell Laboratories
Holmdel, New Jersey

Mr. Thomas is Executive Director of AT&T - Bell Laboratories Transmission Systems Division. He is in charge of development for a variety of telecommunications transmission projects, including satellite, submarine cable, coaxial cable, and optical fiber transmission systems. He is also responsible for the development of high-speed digital transmission equipment and other communications apparatus.

Mr. Thomas joined Bell Laboratories in 1954, where he first conducted research into the solid-state chemistry of semiconducting materials. He later directed his research toward the optical properites of semiconductors, including their luminescence. After becoming Head of the Semiconductor Electronics Research Department in 1962, he conducted studies leading to the development of gallium phosphide light-emitting diodes, which are now used extensively as indicator lights on maintenance equipment, control panels, and some new multiline telephones and business telephone consoles.

In 1968, Mr. Thomas was appointed Director of the Electron Device Process and Battery Laboratory, with responsibilities that included the exploratory development of processes used to fabricate integrated circuits, and the development and engineering of batteries for Bell System use. A year later, he was appointed Executive Director of the Electronic Devices, Process and Materials Division responsible for the development of electronic devices, including their materials and fabrication. He assumed his present position in 1976.

Mr. Thomas received his Bachelor of Arts, Master of Arts, and D. Phil. degrees in Chemistry from Oxford Univeridty in 1949, 1950 and 1952, respectively. He is a Fellow of the Americal Physical Society and the IEEE, and a member of the American Association for the Advancement of Science.

He holds eight patents for materials and device developments, and has published numerous articles on the optical properties of semiconductors. IN 1969, he was corecipient of the Oliver E. Buckley Solid State Physics Prize of the American Physical Society for his theoretical and experimental work related to the interaction of light with solids.

GELS AND THEIR SEALING APPLICATIONS IN THE OUTSIDE PLANT

K. Dawes C. Debbaut A. P. P. Sutherland

Raychem Corp.
Fuquay-Varina, N.C.

Raychem Ltd.
Swindon, U.K.

ABSTRACT

Gels are relatively soft, pliable materials that readily conform to a range of substances. Under compression they generate a good seal, and do not loose the seal under temperature excursions.

The dynamic material analysis (D.M.A.) combined with other physical measurements produces a "characterization" window which defines gel properties required for functionality. Gel and non-gel materials are compared. Several applications are discussed which emphasize the good sealing characteristics of gels, compared to non-gel materials.

INTRODUCTION

Historically, many type of materials have been used to seal interfaces in the telephone networks. Crosslinked elastomers, hot melt adhesives, mastics and tapes comprise the majority of sealing systems in use today. In this paper we wish to discuss a new sealing system which offers advantages over many of the current sealing materials.

The materials to be discussed fall under the general classification of GELS. Gels are very soft pliable materials that easily conform to complex substrates. Several applications of gels for the sealing in the outside plant will be discussed.

THE GEL STATE[1]

Crosslinked polymers are insoluble in all solvents unless the solvent deactivates the crosslink, for example, in the case of a physical crosslink. Crosslinked polymers can be swollen and exist in the swollen state. The degree of swelling will depend on the following parameters:

A. Crosslink Density
B. Polymer Structure
C. Nature of the Solvent

In fact, the de gree of swelling of a crosslinked polymers by a given solvent has been used over many years as a measure of the crosslink density (Flory O Rehner Equation).[2]

Highly swollen crosslinked polymers (or macromolecules) are called GELS. The type of crosslink to form a gel may be either chemical or physical in nature. The gel state has properties very different to a solution or non-crosslinked system in that the gel state the polymer chains have restricted movement.

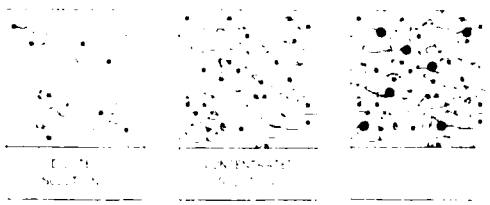

FLEXGEL[3], used for the filling of telephone cabies, is an example of a gel. It was formulated for some very specific properties related to the filling of telephone cables. It has, for example, a relatively low elongation at break and is mechanically weak. These properties are important characteristics since it allows easy removal at a splice opening.

Gels can be produced with a range of properties dependent on the specific application. They are very soft materials which when formulated correctly can be designed into devices that give a good seal but also allows reenterability and reusability.

EXPERIMENTAL

Gel Synthesis

Gels were prepared by either dissolving a monomer or polymer in the appropriate solvent and then curing the mixture.

Cone Penetration

Cone penetration was measured according to a modified version of ASTM D217 using a full-scale cone. The penetration was determined at 23c by releasing a standard full-scale cone assembly from the penetrometer and allowing the cone to drop freely into the gel for 5 seconds, the penetration depth is expressed as tenths of a millimeter.

Tensile Testing

Tensile testing of the gels used a modified version of ASTM D412. Samples for tensile testing were cut from sheets of gel of uniform thickness between 1 and 5 mm using a Type BS 2728/ISO 37 or a type 3 ASTM D412 dumbbell cutter. Tensile and ultimate elongation were measured at 23c.

Dynamic Mechanical Analysis[4]

Samples of the gels (and other materials) were cut from sheets having a uniform thickness between 1 and 5mm using a 25mm circular razor cutter. The samples were cleaned with lint-free wipes before testing to remove surface deposits.

The dynamic mechanical properties of the gels were measured using a RDS-7700 instrument. The oscillatory parallel plate mode (Figure 1) was used at 25c and 80c over an angular

Figure 1
Dynamic Analysis Parallel Plate Mode

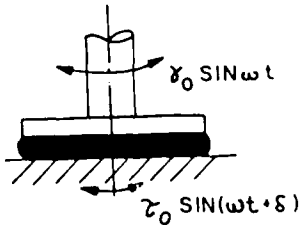

frequency range of 0.1 to 100 rad s^{-1}. The dynamic strain was generally maintained at 0.05 except for measurements at low rates and high temperatures where larger deformations were used to improve instrument signal resolution. The strain amplitude was kept within the region where the dynamic stress in linear with dynamic strain.

Stress Relaxation

Stress relaxation experiments were performed on samples prepared the same as for D.M.A. work. The analysis was performed on the RDS-7700 instrument using the transient parallel plate mode, allowing the input of a preselected step strain level up to 100%. The decay of the resultant torque modulus and normal stress were measured as a function of time at constant temperature.

RESULTS

The results for the dynamic mechanical analysis are shown in Table 1 for a range of gel materials with different polymer structures together with data for a silicone elastomer, a silicone grease and a mastic.

Figures 2 and 3 show the typical data for a gel and a non-gel material. For the non-gel material, the dynamic storage modulus (G') and the dynamic loss modulus (G'') show a crossover point, within the frequency range of 0.1 to 100 rad s^{-1}.

Figure 2
Gel DMA Spectrum

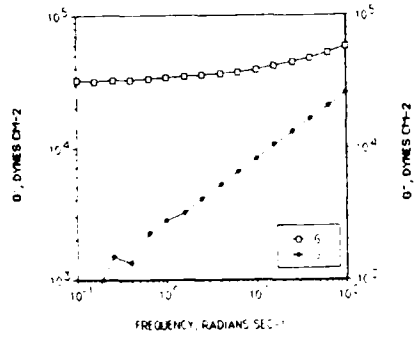

Figure 3
Non-Gel DMA Spectrum

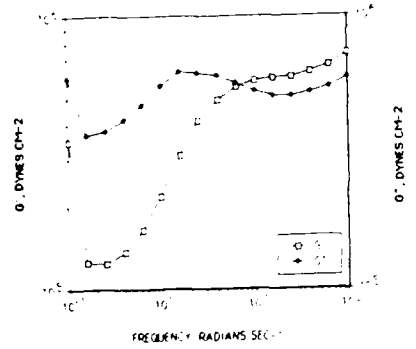

TABLE 1
DYNAMIC MECHANICAL ANALYSIS RESULTS MEASURED AT 1 Hz

Material	G (23c/80c) 10E2 dynes/cm²	Tan (23c/80c)	Eta* (23c/80c K poise
Gel A	376/372	0.18/0.05	6.1/5.9
Gel B	32/31	0.70/0.63	0.6/0.6
Gel C	32/34	0.15/0.04	0.5/0.5
Si Elastomer	10570/5394	0.06/0.11	167/86
Si Grease	233/24	1.47/1.65	6.6.2.4
Mastic	14540/3202	0.85/1.54	303/93

Tan δ = G (loss modulus)/ G (storage modulus)

For non-gel materials the value of the loss tangent, Tan δ shows an increase together with a substantial decrease in the complex dynamic viscosity, Eta* and G' with the increasing temperature. For the gel materials the temperature increase gives relatively stable readings for Eta* and G', and a slight decrease in Tan δ.

Table 2 gives data for the stress relaxation experiments carried out at 23c for 1 hr. The stress relaxation ratio, SRR, is defined as a ratio of the stress, or modulus, G(T), at time t divided by the peak stress achieved when the strain in applied at t=0, i.e., [G(T) at t]/G(T) max.].

TABLE 2
Stress Relaxation Data

Material	SRR (t= 3600 s)	Relaxation Time (s)
Gel A	0.835	>3600
Gel B	0.593	>3600
Gel C	0.740	>3600
Grease	0.235	49
Mastic	0.093	6

Figures 4 and 5 show the typical relaxation curves for a non gel and gel material. The non gel material shows rapid continuous relaxation indicative of polymer chain flow for a non crosslinked material.

Table 3 gives the values for the cone penetration and tensile properties for the range of materials. In the case of the silicone grease the tensile properties could not be measured and an elongation of 0% is assumed.

Figure 4
Gel Relaxation Spectrum

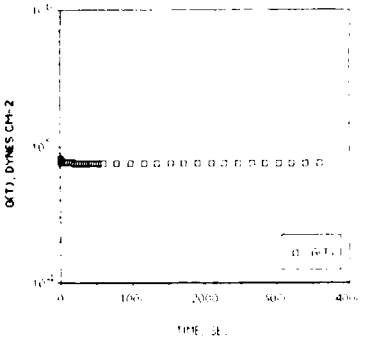

Figure 5
Non-Gel Relaxation Spectrum

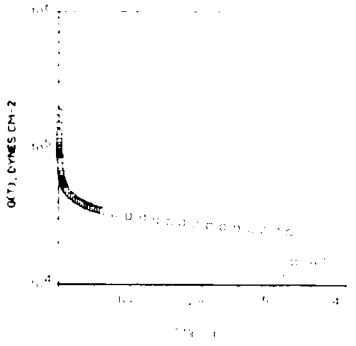

TABLE 3

Cone Penetration and Tensile Properties at 23c

Material	C.P. (0.1 mm)	T.S. (KPa)	UE (%)
Gel A	191	20	430
Gel B	307	7	315
Gel C	274	9.5	415
S. Sealant	14	1477	80
Si Grease	280	-	0
Mastic	65	47	35

DISCUSSION

The results of the dynamic mechanical analysis experiments clearly show differences between gels and non-gel materials. Although the gel materials are very soft and pliable, at elevated temperatures they maintain characteristics similar to ambient. In sharp contrast, the non gel materials show a decrease in properties at elevated temperature.

Figure 2 and 3 showing typical D.M.A. curves for gel and non gel materials clearly demonstrate substantial differences. For the gel material there is not a cross-over point for G' and G'', indicating the presence at all frequencies of a viscoelastic network system. The non gel materials show a cross-over of G' and G'' over the frequency range indicating a loss of the viscoelastic network which will lead to polymer flow. This cross-over is typical for a non-crosslinked material. Figure 6 shows the D.M.A. curves for the polymeric components of gel B but without curing.

Figure 6
Non-Cured DMA Spectrum

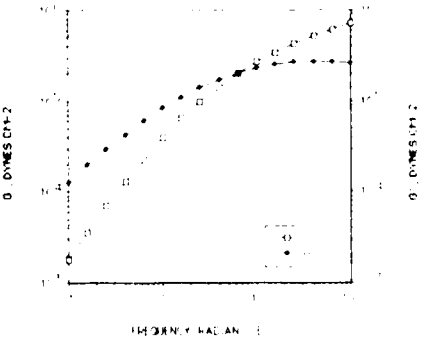

The Tan δ data together with the stress relaxation data also indicate some characteristics of gel materials. These are a reflection of the elastic response of the materials, and are specifically more related to tack and compliance of the gel to a substrate. A high Tan δ will give a very tacky material but will have a weaker elastic network which in turn will result in a high degree of stress relaxation. Greases and mastic show poor stress relaxation data and high Tan δ values relative to the gel materials, and they would not maintain a good seal under deformational stress.

In addition to the D.M.A. data, hardness

(cone penetration) and tensile properties further characterize gel materials.

The hardness as measured by cone penetration correlates well with the dynamic storage modulus, G', for the gel materials and both can be used as criteria to characterize a gel. The tensile properties show the materials to be relatively weak when compared to a conventional elastomer but to maintain a large amount of elasticity.

TABLE 4

Mechanical Criteria for Gel Characterization

Dynami Frequency Sweep @ 23c	G < 1 x 10E6 dynes/cm2 @ 1Hz Eta' < 2 x 10E5 poise @ 1Hz Tan < 1.00 @ 1Hz
Dynamic Frequency Sweep @ 80c	G > 1 x 10E2 dynes/cm2 @ 1Hz Eta' > 1 x 10E2 poise @ 1Hz Tan < 1.00 @ 1Hz
Dynamic Frequency Sweep	G < G at frequencies below 15Hz at 23 and 80c
Stress Relaxation	T > 900s
Cone Penetration	30 - 400 0.1mm
Tensile Testing	T.S. < 2 MPa U.E. > 100%

Table 4 gives a compilation of the preferred ranges of the previously discussed properties which define a functional gel from a mechanical point of view. These combined criteria clearly distinquish a macromolecular gel from greases, soft gums, mastics and elastomers.

All the properties discussed reflect the elastic behavior of these soft materials and are important in defining functional gel materials for a particular application.

APPLICATION OF GELS TO THE OUTSIDE PLANT

By their nature gels lend themselves to numerous applications in the outside plant. The general properties are as follows:

- They are precured in a specific container.
- They are very soft elastomers.
- They are easily deformable under a compressive force.
- Compression on a gel gives a good seal.[5]
- They are good void fillers and will deform to the elastic limit.
- They have elastic memory and removal of the compressive force will cause the gel to retract.
- Temperature excursions can be readily accommodated with a gel.
- When in contact with a metallic substrate and under compression they give excellent corrosion protection.

For a gel to perform well in the outside plant it must have good electrical properties, i.e. a good insulator, and also have good stability. Gels are formulated to the specific application requirements. In the following applications different gels are used since each application requires a different set of requirements.

Terminal Protection

Trouble reports in pedestals and aerial terminals are often due to moisture and corrosion. A cap has been designed which contains a gel. The gel is precured and the cap is simply placed on the terminal lug. The cap is also designed (Figure 7) to have a mechanical fit on the lug so that it will be retained and at the same time

Figure 7
Terminal Cap Cross Section

apply a compressive force to the gel. The properties of the gel are crucial to the performance, if it is too elastic the cap will lift off with time, too soft and the gel will not provide sufficient compressive force to maintain a seal. Table 5 gives the typical properties of a gel for this requirement.

TABLE 5

Properties of terminal protection Gel

Tensile strength (MPa)	1 x 10E-2
Ultimate elongation (%)	1100
Cone Penetration (0.1mm)	265
Water Uptake (7 day/ 100c, %)	0.056
Hydrolytic Stability (7 day/100c)	No Reversion
Heat Aging (21 day/100c)	3% weight loss
Volume Resistivity (ohm cm)	3.5 x 10E12

Re-entry and re-use are also important, the adhesive strength of the gel to the cap is larger than the adhesive strength to the substrate and the cohesive strength of the gel. On removal of the cap, the gel is retracted into the cap, leaving a clean terminal lug. The cap may then be replaced with no loss of functionality. Functional testing of the product shows excellent performance, some of the results on a WECO 9A1 terminal are shown in Table 6.

TABLE 6

Terminal Cap Functional Testing on WECO 9A1

Immersion in 5% NaCl solution (30 day/20c)	I.R. > 10E6 ohm
Re-entry of above (26% of samples)	I.R. > 10E6 ohm
Salt Fog (30 day, 35c, 95% RH)	No corrosion
Bell Cycling (21 cycles, -40 to +60c)	100% retention
Immersion in 5% NaCl solution	I.R. > 10E6 ohm

The data illustrates the excellent seal and corrosion protection offered by the gel. A good example of how well the gel seals is shown by installing a cap on a terminal lug underwater - the electrical integrity of the system is readily achieved on application of the gel filled cap. (Figure 8)

Figure 8
Water Displacement by Gel Compression

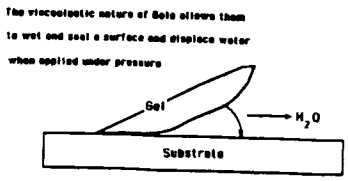

Figure 8
Water Displacement by Gel Compression

Further evidence[6] of the corrosion protection can be shown by measurement of the contact resistance at a terminal lug. After six weeks of salt fog testing on a closed terminal box with unprotected lugs resulted in an average increase of 14 milliohms, whereas the gel protected lugs showed no change.

In contrast to the above, a similar cap filled with a typical grease used in the outside plant would show failures within 2 days after Bell cycling. Temperature excursions cause greases to flow and generate potential leak paths.

Terminal Block

The terminal protection cap was designed for use on existing terminal lugs. As an extension of the concept of gel applications a new terminal has been designed which incorporates gel directly.

Figure 9 shows a simple diagram of the concept. During the manufacture of the terminal block gel is cured in the areas where metallic substrates are present. Wires ranging from 18.5 to 24 gauge can be readily accommodated without any modification, the gel allows easy entry for the wires and gives an excellent seal. The rotary action of the termination necessitates the need for a gel with very good mechanical properties, since the mechanical requirements are more severe than for the terminal cap protection gel.

Figure 9
Cross-section of Terminal Block

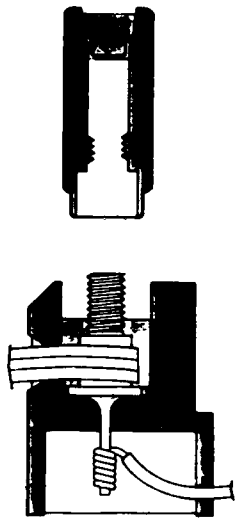

Figure 10 gives a schematic for the type of functional testing which is being applied to this terminal.

Figure 10
Terminal Block Performance Testing Program*

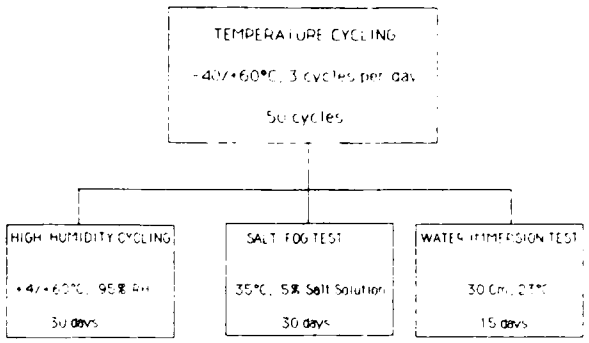

* 48 Vdc applied across tip and ring
50% samples re-entered 5 times

Aerial Closure End Pieces

The final application illustrates the use of a gel to generate a good closure to cable interface in an aerial application.

The gel for this application is somewhat harder than the other applications but the principles of design are similar. The closure end pieces comprise of two hinged half shells filled with gel to a specific pattern. The gel end pieces easily conform to the cable and help keep water out. The nature of the gel material makes the closure very easy to re-enter.

TABLE 7

Typical Gel Properties for End Pieces Application

Tensile Strength (MPa)	1.0
Ultimate Elongation (%)	1200
Cone Penetration (0.1mm)	80
Volume Resistivity (ohm cm)	>10E11

CONCLUSION

Dynamic mechanical analysis combined with hardness and tensile properties show clear differences between gel and non-gel materials. The mechanical characteristics of a gel are important to the functional sealing performance of a gel, as shown by the applications to outside plant products.

ACKNOWLEDGEMENTS

The authors would like to thank Mrs. Jerry Lachapelle for the preparation of this manuscript.

REFERENCES

1. Bruno Vollmert; "Polymer Chemistry", p. 543, Springer-Verlag (1973)

2. P. J. Flory; "Principles of Polymer Chemistry", Cornell Univ. Press, Ithaca, N.Y. (1953)

3. D. M. Mitchell and R. Sabia; "Development, Characterization, and Performance of an Improved Cable Filling Compound", Proceedings of the 29th International Wire and Cable Symposium, p.15 (1980)

4. J. D. Ferry; "Viscoelastic Properties of Polymers", John Wiley, New York, 2nd Ed. (1969)

L. E. Nelson; "Mechanical Properties of Polymers and Composites, Marcel Dekker, New York (1974)

5. C. Debbaut, "Apparatus and Method for Protection of Electrical Contacts", U.S. Patent # 4600261

6. J. Jervis, Personal Communication.

Keith Dawes received a first class honours B.Sc. degree in Chemistry from University of Newcastle-upon-Tyne in 1966 and obtained his Ph.D. from the University of Manchester in 1969. After post-doctoral fellowships at Columbia University and Oxford University, he worked at the Malaysian Rubber Producers Research Association. He joined Raychem Corporation in 1979 working in Corporate R & D at Swindon, England. He is now Development Manager for Raychem Telecommunications Division in North Carolina.

Chris Debbaut received his degree in Polymer Engineering from the Institute of Textile and Polymers in Gent, Belgium. He joined Raychem in 1973 and specialized in polymer compounds and adhesives for the European Telecom Division. Since 1978, he has been involved in product development for the US Telecom Division after spending two years in Corporate R & D, Menlo Park, California. He created the concept of applying polymeric gels for environmental sealing purpose and has several patents in this area.

Alistair Sutherland graduated from the University of Birmingham in 1979 with a B. Sc. degree in Chemistry. He subsequently gained a M.Sc. in Thermodynamics in 1980 and a Ph.D. in Polymer Physics in 1982 before joining Raychem, U.K. He worked as a specialist in the rheological and viscoelastic behavior of materials within Raychem;s European Corporate R & D Centre in Swindon before becoming Project Leader for Gel Materials. He was elected as a Chartered Chemist by the Royal Society of Chemistry in 1984.

OPTIMAL DESIGN OF JELLY COMPOUND FOR OPTICAL CABLE

T. Hattori, N. Akasaka, M. Fukuma, S. Masuda, S. Suzuki

Sumitomo Electric Industries, Ltd.

Abstract

The effects of each components on the characteristics of filling compound for optical fiber cables were investigated. It was found that the cone penetration and the oil separation of filling compound could be controlled by changing the mean molecular weight of base oil and the contents of silica. Further it made clear that the value of cone penetration at low temperature should be more than 200.
It was also found that it was desirable for base oil to have large mean molecular weight in view of long term reliability.

1.Introduction

It is necessary for the optical fiber cables to keep off water because the strength of glass fiber degradates by the water penetration. The transmission loss also increases due to hydrogen which is generated by a chemical reaction of water and components of the cable.[1] In order to prevent water penetration, there are two types of cables. One is the gas-filling type cable, and the other one is the cable with filling compound. Because of easy maintenance for transmission line, the cable with filling compound is widely used in the world.[2]
There are several essential requirements for the filling compounds to maintain stable characteristics of the optical fiber cables, and also easily to manufacture the cables. The main requirements of the filling compounds for optical fiber cables are as follows:

(1) Good water blocking property
(2) Exellent in thermal stability
(3) Appropriate viscosity for easy application
(4) Low temperature dependence of viscosity, especially at low temperature
(5) No drips from the cable
(6) Good compatibility with the components of optical fiber cables, especially with the coating materials of optical fiber

The relationship between required chemical and physical properties of filling compound and the characteristics of manufactured cable has not been established. The effects of each component of filling compounds on the characteristics of filling compounds also have not been clear. We produced the several kinds of filling compounds which have different compositions to investigate the characteristics of filling compound and manufactured cable. In this paper, the effects of each components on the characteristics of filling compounds and the properties of cable are discussed.

2.Characteristics of filling compound

Filling compound generally consists of base oil, silica, antioxidant, and the other ingredients. We investigated the effect of each components on the characteristics of filling compound.

2-1 Cone penetration

The relationship between cone penetration and components of filling compound, such as the mean molecular weight of base oil and the contents of silica, was examined. Several kinds of filling compounds were produced by a synthetic oil which showed good performance in thermal stability test. The composition of produced filling compounds are shown in Table.1. These compounds consists of 90 to 97% of base oils which have different mean molecular weight of 1440, 2330, and 3770, and 3 to 10% of silica.
The measurements of cone penetration of the filling compounds were conducted at 20°C and -40°C based on ASTM-D937 . As the contents of silica increased, the cone penetration of filling compound for each base oil became small as shown

Table.1 Composition of Filling Compounds

SAMPLE No.	1	2	3	4	5	6	7	8	9	10	11	12
M.M.W.*	1440	1440	1440	1440	2330	2330	2330	2330	3770	3770	3770	3770
CONTENTS OF SILICA	4.0	5.8	7.2	10.0	3.8	5.1	6.8	9.2	3.1	4.1	5.5	7.2

* M.M.W. : Mean Molecular Weight

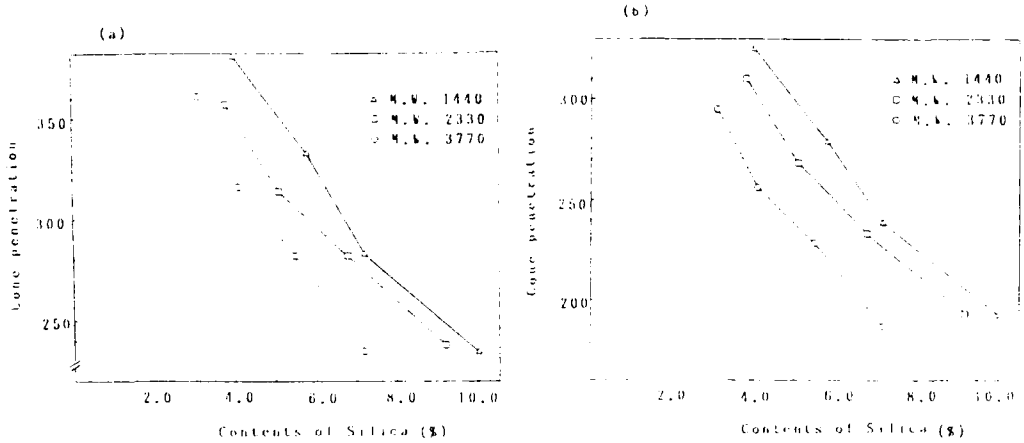

Fig.1 Relationship between Contents of Silica and Cone Penetration
(a) 25℃ (b) -40℃

in Fig.1. The cone penetration became small when the mean molecular weight of base oil became large. The same tendency was also observed at low temperature. It is found that the cone penetration of filling compound can be controlled at any temperature by changing the mean molecular weight of base oil and the contents of silica.

2-2 Oil separation

In order to improve the drip property of filling compound which is the one of the most important property for jelly-filled cable, the oil separation should be minimized. The measurements of oil separation after aging for 24 hours at 100°C for the filling compounds listed in Table 1 were conducted in accordance with JIS-K2220. Fig.2 indicates that the increase of silica contents has good effect to reduce oil separation of filling compound. AS contents of silica increased, oil separation reduced. However it was impossible to reduce the oil separation less than 3%. When the contents of silica was same level, higher molecular weight made lower oil separation. In order to reduce the oil separation to 0%, other ingredient is necessary to be mixed. Fig.3 shows oil separation of filling compounds added two types of resins. In both cases, oil separation could be reduced completely when 6% of resins were added.

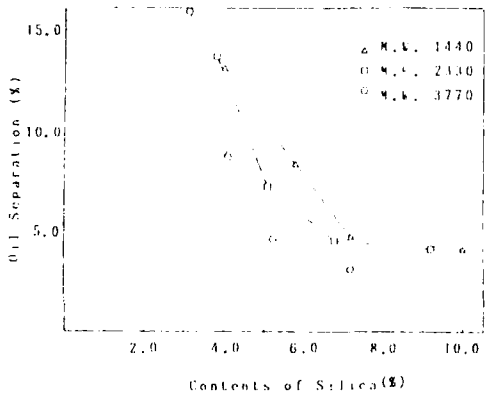

Fig.2 Relationship between Contents of Silica and Oil Separation

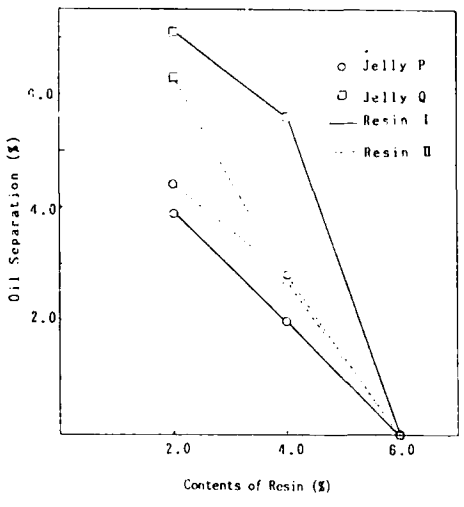

Fig.3 Effect of the Ingredients

3.Optimal cone penetration at low temperature

It is said that the attenuation of jelly-filled cable increases at low temperature, because of hardening of filling compound. In order to make clear the allowable hardness of filling compound, especially at low temperature, jelly-filled cables with the different filling compounds were manufactured. The cross-sectional structure of produced cables is shown in Fig.4. Eight rectangular slots were provided helically on the

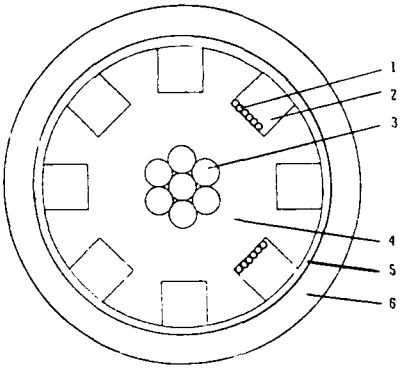

Fig.4 Structure of Jelly-Filling Cable

1. Optical fiber
2. Jelly compounnd
3. Galvanized steel wire strand
4. Grooved spacer
5. Wrapping
6. LAP sheath

spacer which were made of polyethylene. Stranded galvanized steel wire was used as the strength member in the center of the spacer. Six single mode fibers coated with UV curable resins up to 250 μm in diameter. The diameter of grooved spacer and LAP sheath were 12.2 mm and 16.3 mm respectively. Three types of filling compounds in Table 2 which have different temperature dependence of cone penetration value were used to investigate the relationship between attenuation increase at low temperature and the value of cone penetration. The attenuation of two cables filled with compound A and compound B increased similarly at low temperature. These loss increases at low temperature may be caused by shrinkage and hardening of filling compound. No loss increase was observed for the cable with compound C which had enough softness even in low temperature. The relationship between cone penetration value and loss increase at each temperature is shown in Fig.6. In order to prevent loss increase at low temperature, the value of cone penetration should be more than 200 at low temperature.

Table.2 Cone Penetration of Filling Compounds

	Compound A	Compound B	Compound C
20℃	118	220	296
0℃	61	163	286
-20℃	47	120	260
40℃	22	60	241

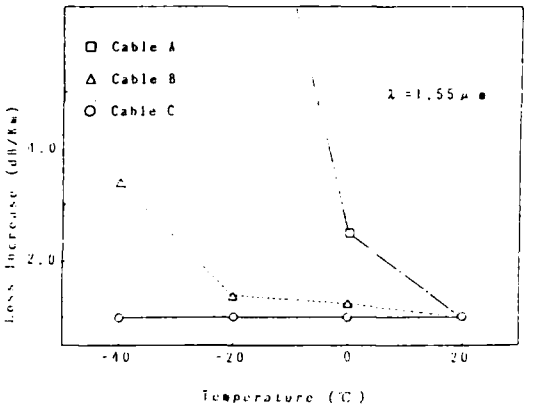

Fig.5 Temperature Dependence of Attenuation for Jelly-Filled Cables

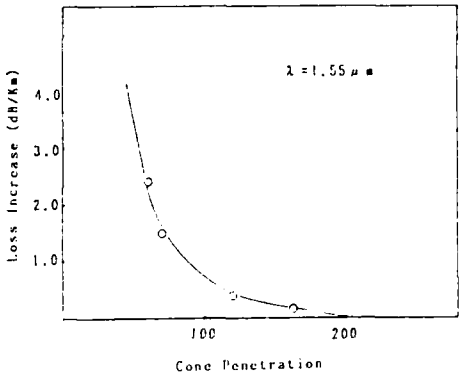

Fig.6 Relationship between Cone Penetration and Loss Increase

4.Compatibility with coating materials of optical fiber

Since the coating materials of optical fiber are most sensitive to filling compound among the components of cable, the compatibility with the coating materials of optical fiber was examined. For the examination of the compatibility with the coating materials, UV curable resin which was generally used as a primary buffer was selected. The sheet samples of UV curable resin were immersed at 60°C into the three kinds of base oil of filling compound. These base oils had different mean molecular weights such as 470, 1010, and 3770. The weight changes of the test specimens of UV curable resins before and after immersion were measured. Before the immersion, uncrosslinked portion of UV curable resin was extracted with methyl-ethyl-ketone in order to compensate outgoing of uncured extractable. The weight change of each test specimen was found to be saturated within 7 days as shown in Fig.7. The weight increase in the small mean molecular weight oil was clearly larger than that in the

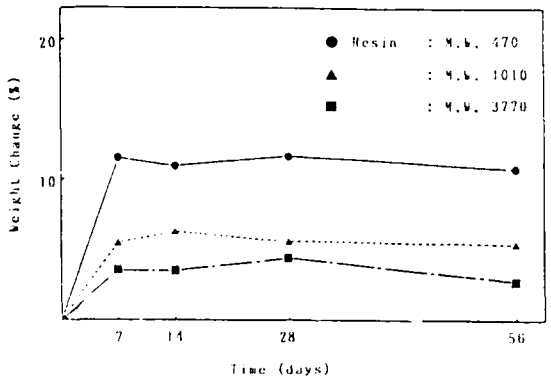

Fig.7 Weight Change of UV Curable Resin immersed in Base Oil at 60℃

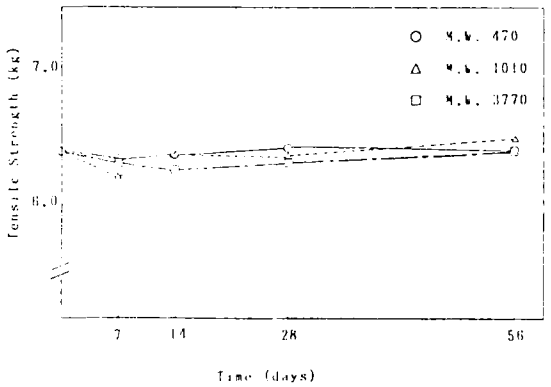

Fig.8 Strength of optical Fiber immersed in Base Oil at 60℃

large mean molecular weight oil. It was concluded that the small molecular weight oil could penetrate into UV curable resin more easily than the large mean molecular weight oil. In view of long term reliability, the mean molecular weight of base oil should be large, because the adhesion of the interface between glass and resin becomes lower due to penetration of base oil.
The stability of tensile strength of optical fiber immersed into the base oil of filling compound was also examined. The optical fiber coated with the above resin was immersed into the three types of base oil at 60°C. No degradation of the tensile strength of optical fiber immersed in each base oil has not been observed as shown in Fig.8.

5.Conclusion

The relationship between the components and the characteristics of filling compound was examined. In consequence, it was found that the cone penetration at any temperature and the oil separation could be controlled by changing the mean molecular weight of base oil and the contents of silica. Further it made clear that the value of cone penetration at low temperature should be more than 200. And it was also found that the weight change of UV curable resin immersed into filling compound could be lowered as the mean molecular weight of base oil increases.

References

(1) Y.Mitsunaga, T.Kuwabara, T.Abe, and Y.Ishida "Molecular Hydrogen Behavior for Loss Increase of Silica Fiber in Cable Filled with Water", Electron Lett. 20 pp 76 - 78 (1984)
(2) Y.Kameo, H Horima, S.Tanaka, and Y.Koyamada, "Jelly-Filled Optical Fiber Cable", IWCS 30 pp 236 - 243 (1981)
(3) US Patent 4,701,016

Tomoyuki Hattori

Sumitomo Electric Industries, Ltd.

1, Taya-cho, Sakae-ku, Yokohama, Japan

Tomoyuki Hattori received a M.S. degree in chemistry from Kyoto University in 1987. He joined Sumitomo Electrics Industries, Ltd. in 1987, and has been engaged in research and development of optical fiber and cables. He is a member of Transmission Media R & D Department in Yokohama Research Laboratories.

Shigeo Masuda

Sumitomo Electric Industries, Ltd.

1, Taya-cho, Sakae-ku, Yokohama, Japan

Shigeo Masuda graduated from the faculty of Engineering of Kyusyu University in 1966. He joined Sumitomo Electric Industries, Ltd. in 1966, and has been engaged in coating technology. He received a D.E. degree from Kyusyu University in 1979. He is member of the society of polymerscience, Japan, and a member of the society of Rheology, Japan.

Nobuhiro Akasaka

Sumitomo Electric Industries, Ltd.

1, Taya-cho, Sakae-ku, Yokohama, Japan

Nobuhiro Akasaka received a M.S. degree in Chemical Engineering from Tokyo University in 1983. He joined Sumitomo Electric Industries, Ltd. in 1983, and has been engaged in research and development of optical fiber and cables. Mr. Akasaka is a member of Transmission Media R & D Department, Yokohama Research Laboratories.

Shuzo Suzuki

Sumitomo Electric Industries, Ltd.

1, Taya-cho, Sakae-ku, Yokohama, Japan

Shuzo Suzuki received a M.S. in 1972 from Tokyo University. He joined Sumitomo Electric Industries, Ltd. in 1972, and has been engaged in research and development of optical fiber, cable and jointing technologies. He is a member of the Institute of Electronics and Communication Engineers of Japan.

Masumi Fukuma

Sumitomo Electric Industries, Ltd.

1, Taya-cho, Sakae-ku, Yokohama, Japan

Masumi Fukuma received a M.S. degree in Electrical and Electronic Engineering from Toyahashi University of Technology in 1985. He joined Sumitomo Electric Industries, Ltd. in 1985, and has been engaged in research and development of optical fiber and cables. Mr. Fukuma is a member of Communication R & D Department in Yokohama Research Laboratories.

AMORPHOUS POLYAMIDES AND BLENDS THEREOF SUITABLE MATERIALS FOR HIGH-PERFORMANCE LOOSE JACKETING

Dr. H.H. Dalla Torre

EMS-CHEMIE AG, 7013 Domat/Ems, Switzerland

Abstract

Very rigid, dimension and heat stable copolyamides and copolyamide-blends are suitable materials for the dual loose tube application.

For different application requirement, variation in the properties can be achieved by changing the chemical composition of the copolyamides, especially the amount of the lactam. Special properties like crack resistance and flexibility of the materials can be improved by blending them with similar semicrystalline polyamides.

In forming special blends of these copolyamides with polymers which show poor water adsorption, it is possible to create materials for the mono loose tube application.

1. Introduction

Among the various materials, which are needed for the construction of fiber optic cables, the buffer materials are of extreme importance to ensure long time of the optical fiber.
They can affect the optical, mechanical and connectional performance of the cable and must, therefore, be carefully selected.

The tight jacketing is usually applied on single fiber cables and needs rather flexible materials. The loose tube construction represents a more rigid system, which allows the use of one or a number of optic fibers embedded in a single tube.

The loose jacketing system is a sophisticated construction technology, which provides maximum protection against compressive and tension forces as well as chemical and environmental influences, provided the cable design and the selected materials are of appropriate quality.

2. Loose tube material quality:

The materials, which can be used successfully in loose tube construction must be able to fulfil all of the following very demanding requirements:

* good processability
* good melt behaviour
* high melt strength
* high shear modulus
* high stiffness
* high tensile strength
* high compressive strength
* good flexural strength
* sufficient tenacity
* good heat resistance
* good stress cracking resistance against all buffer filling materials and solvents used in splicing operations, such as alcohols or acetones
* low water uptake
* good dimensional stability
* sufficient abrasion resistance (hardness)
  and
* a competitive price

3. Available polymers

Considering the various polymers which would apparently be appropriate to a loose tube application, one would discover that most of them do not meet the specifications as outlined above.

- Polyolefines (polypropylene, polyethylene, copolyolefines, polyvinylchlorides, etc.) are not stiff enough and show poor dimensional stability and high coefficient of thermal expansion.
- Polyesters (PET and PBT) show generally good properties especially low water uptake, but fail because of weak compressive strength and stability against thermal hydrolysis.
- Polystyrene, ABS (Acryl-butadiene-styrene, PMMA (polymethylmetacrylates), SAN (polystyrene-acrylnitril) and others suffer due to poor stress cracking resistance.
- Polycarbonates show low water absorption and good mechanical properties, but are weak in stress cracking and chemical resistance.
- Polyamide 6, 6.6, 4.6, 6.10 are not very suitable because of dramatic changes in mechanical properties under water saturated conditions.
- Polyamide 12 and similar long chain polyamides are weak in stiffness and dimensional stability because of their tendency to post crystallize.
- Fluoropolymers, polysulfones, polyethersulfones, polyetheretherketones (PEEK), polyetherimides and liquid crystall polymer (LCP) generally has excellent mechanical and physical properties, but are not easy to process, have an unfavourably high density and are very expensive.

4. Quality of copolyamides

In comparison to the above polymers, amorphous copolyamides and blends thereof presently represent the ideal thermoplastic materials for the loose tube construction. These polyamides display advantages compared to the semi crystalline polymers, but also over other amorphous polymers currently available, which consists chiefly in the following areas:

* High stability of mechanical properties within a broad temperature range

* Extensive independence of the mechanical properties from moisture content

* Easy adaptability of properties to the requirements of different applications.

The properties of amorphous copolyamides can easily be varied in a wide range by changing the ratio of composition and nature of raw materials, which form the copolyamide resin.
A frequent combination consist of three to five compounds, of which at least two represent the diamine/dicarboxylic acid pairs and a third or fifth a monomeric lactam.

The first pictures (pictures $1^1/1^2$) shows some characteristic physical and mechanical properties of two representative types of copolyamides, the first a hexamethylene-isophthalic acid copolyamide called in this paper Copolyamide 3, and a laurolactam-isophthalic acid copolyamide called herein Copolyamide 5.

The shear modulus curves of the two copolyamides demonstrate their stability at elevated temperatures (picture 2^1 and 2^2).

Picture 1^1

Property	Test Method	Unit	CoPa 3
Specific gravity	DIN 53479	g/cm^3	1.18
Melt flow index (270°/325N)	DIN 53735	g/10'	20
Refractive index	DIN 53491		1.580
Glass transition temperature	DSC	°C	140
Heat distortion temperature			
0.46 N/mm^2 (B)	DIN 53461	°C	136
1.82 N/mm^2 (A)	ISO 75	°C	130
Coefficient of linear therm. expansion	DIN 52328		
-40° to 70°C		$10^{-5}xK^{-1}$	5.0
+70° to 100°C		$10^{-5}xK^{-1}$	7.0
Water absorption (esturated in water)	DIN 53495	%	3.6
Tensile strength a. break	DIN 53455	N/mm^2	88
Elongation at break	DIN 53455	%	20 - 40
Tensile modulus dry/cond.	DIN 53457	N/mm^2	3400/3400
Flexural modulus dry/cond.	DIN 53452	N/mm^2	3200/3200
Compressive strength	DIN 53454	N/mm^2	120
Impact strength	DIN 53453	KJ/m^2	nb
Notched impact strength (Charpy)	DIN 53453	KJ/m^2	2
	ASTM D 256	J/m	40
Shrinkage of a loose tube (0 1.2/2.0) after aging 24 hours at 100 °C		o/oo	2.0-2.8

Picture 1[2]

Property	Test Method	Unit	CoPa 5
Specific gravity	DIN 53479	g/cm^3	1.05
Melt flow index (270°/125N)	DIN 53735	g/10'	26
Refractive index	DIN 53491		1.530
Glass transition temperature	DSC	°C	155
Heat distortion temperature			
0.46 N/mm² (B)	DIN 53461	°C	145
1.82 N/mm² (A)	ISO 75	°C	135
Coefficient of linear therm. expansion	DIN 52328		
-40° to 70°C		$10^{-5}K^{-1}$	6.8
+70° to +30°C		$10^{-5}K^{-1}$	7.8
Water absorption (saturated in water)	DIN 53495	%	3.3
Tensile strength a. break	DIN 53455	N/mm²	60
Elongation at break	DIN 53455	%	50 - 120
Tensile modulus dry/cond.	DIN 53457	N/mm²	2300/2300
Flexural modulus dry/cond.	DIN 53452	N/mm²	2200/2200
Compressive strength	DIN 53454	N/mm²	105
Impact strength	DIN 53453	KJ/m²	nb
Notched impact strength (Charpy)	DIN 53453	KJ/m²	4 - 5
	ASTM D 256	J/m	60 - 70
Shrinkage of a loose tube (Ø 1.2/2.0) after aging 24 hours at 100 °C		o/oo	0.8-1.2

Picture 2[1]

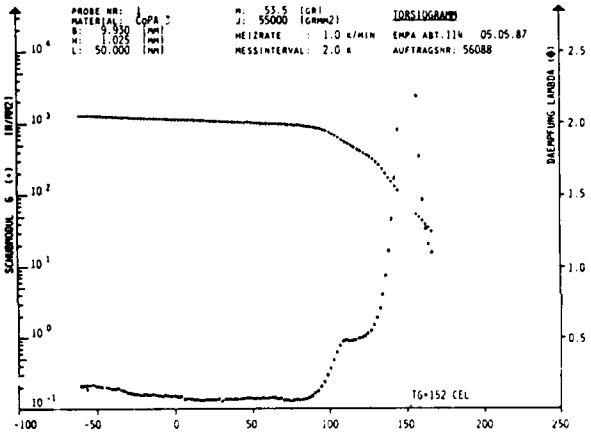

Picture 2[2]

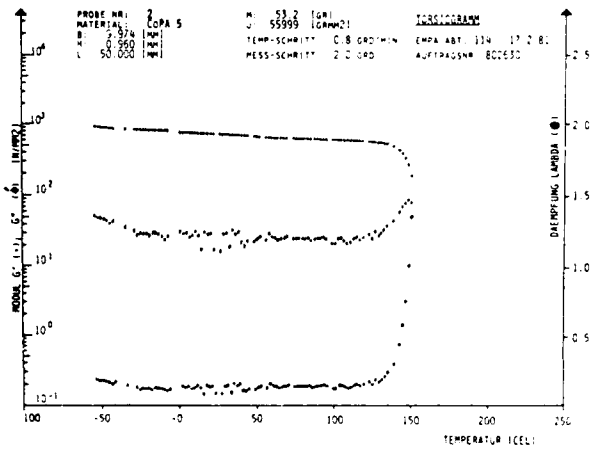

These properties do not change substantially when measured in water conditioned stage, which means these two copolyamides are able to retain their rigidity and dimensional stability in spite of water absorption. This compares favourably with the partially crystalline polyamides, the properties of which are strongly dependent on moisture content.
Specific properties like glass transition temperature, heat distortion temperature, tensile strength, flexibility, chemical resistance and others can be increased or decreased by varying the ratio of lactam to the diacid/diamine contents.
The more the lactam content is reduced, the more the heat deflection temperature and the stiffness increase. On the other hand it is possible to improve the flexibility and impact strength by increasing the lactam content.

The next pictures (pictures 3-11) show the dependence of the glass transition temperature, melt viscosity, water absorption, flexural modulus, tensile and impact strength on the amount of caprolactam or laurolactam used as co-component in the polycondensation of Copolyamide 3 and Copolyamide 5.

A similar variation in properties can be created by using (instead of rigid molecules like isophthalic acid or cycloaliphatic diamines) more flexible ones, such as long-chain diacides or diamines (azelaic acid, sebacic acid, dodecandioic acid) or, on the diamine side 5-methylnonandiamine or dodecamethylenediamine.

Dependence of glass transition temperature 1) on the amount of caprolactam in Copolyamide 3

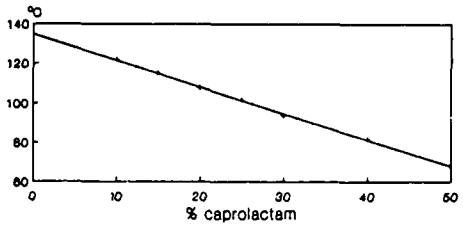

1) measured by DTA

picture 3

EMS

Dependence of tensile strength at break 1) on the amount of caprolactam in Copolyamide 3

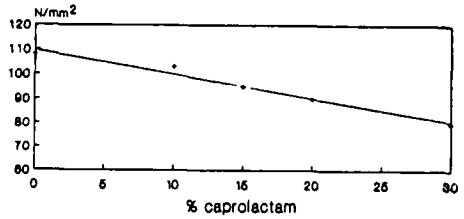

1) according to DIN 53455

picture 6

EMS

Dependence of water absorption 1) on the amount of caprolactam in Copolyamide 3

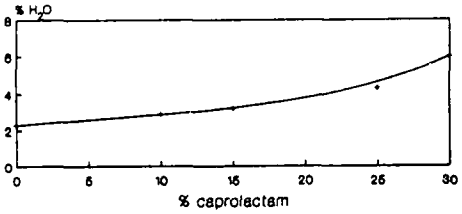

1) according to DIN 53495

picture 4

EMS

Dependence of melt viscosity 1) on the amount of laurolactam in Copolyamide 5

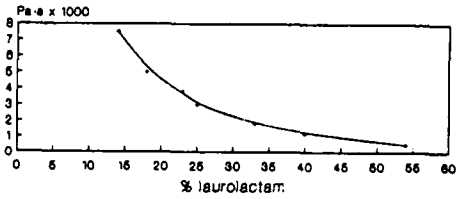

relative viscosity 1.45 (0.5% m-Kr)

1) according to DIN 53735

picture 7

EMS

Dependence of flexural modulus 1) on the amount of caprolactam in Copolyamide 3

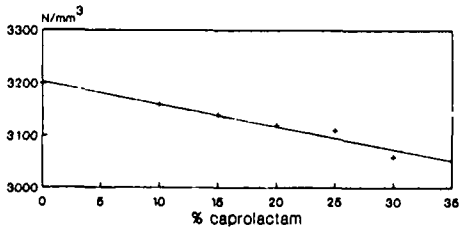

1) according to DIN 53452

picture 5

EMS

Dependence of glass transition temperature 1) on the amount of laurolactam in Copolyamide 5

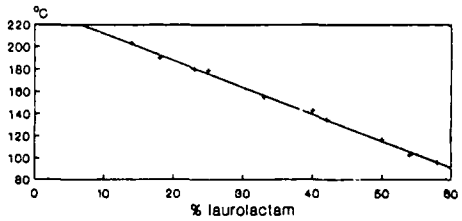

1) measured by DTA

picture 8

EMS

Dependence of water absorption 1) on the amount of laurolactam in Copolyamide 5

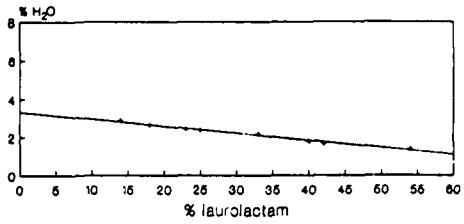

1) according to DIN 53495 picture 9

Dependence of flexural modulus 1) on the amount of laurolactam in Copolyamide 5

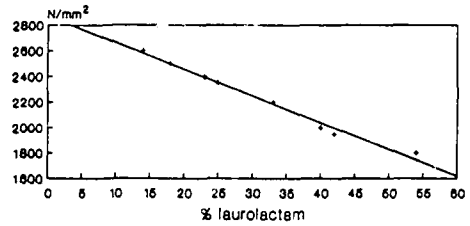

1) according to DIN 53452 picture 10

Dependence of notched impact resistance 1) on the amount of laurolactam in Copolyamide 5

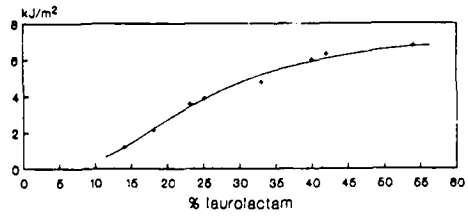

1) according to DIN 53453 picture 11

5. Polyamide blends

Some mechanical properties of copolyamides, such as crack and impact resistance or flexibility in copolyamides are rather weak. They can be substantially improved by blending these copolyamides with semi-crystalline polyamides like polyamide 6, 6.6, 6.10, 6.12, 11 or 12, which have good affinity to amorphous polyamides forming alloys with a stable block-copolymer structure. Heat distortion temperature and water absorption can also be influenced by forming these alloys.

These blend compositions differ enormously in their characteristics from the foregoing copolyamides, which may contain, for example, the same amount of polyamide 6 or 12 incorporated statistically as a lactam co-component in the polymer chain without obtaining the same improvements. Such blends partially combine the properties of linear crystalline polyamides (tenacity and chemical resistance) with those of the amorphous copolyamides (dimensional stability and independence of the rigidity from moisture content).
These blends are easily formed and processed using a simple heatable screw extruder. This operation may cause partially transamidation reaction depending on temperature and residence time, usually without affecting qualities.

The following two pictures (12-13) display some properties of two blend compositions:

Blend 9/8 and

Blend 5/4

The first represents a blend of Copolyamide 3 with Polyamide 6.6, and the second (Blend 5/4) demonstrates a mixture of Copolyamide 5 with Polyamide 12.

Picture 12

Blend 9/8

Property	Test Method	Unit	Value
Specific gravity	DIN 53479	g/cm^3	1.14
Refractive index	DIN 53491	°C	1.567
Melting point	DTA	°C	248
Glass transition temperature	DTA	°C	102
Heat distortion temp. B/A	ISO 75	°C	98/86
Coefficient of linear therm. expansion (-30 to +120°C)	DIN 52328	10^{-5}/K	5.8-6.8
Water absorption	DIN 53495	%	3.2
Tensile strength at yield	DIN 53455	N/mm²	105
Tensile strength at break	DIN 53455	N/mm²	65
Elongation at break	DIN 53455	%	50
Tensile modulus dry/cond.	DIN 53457	N/mm²	2500/2500
Flexural modulus dry/cond.	DIN 53452	N/mm²	3100/3100
Compressive strength	DIN 53454	N/mm²	100
Impact strength	DIN 53453	KJ/m²	n.b.
Notched impact strength (Charpy)	DIN 53453	KJ/m²	3
Shrinkage of a loose tube (Ø 1.2/2.0) after aging 24 hours at 100 °C		o/oo	~6
Crack resistance in methanol	test bars under load in 100 % methanol	N/mm²	110 very good

Picture 13

Blend 5/4

Property	Test Method	Unit	Value
Specific gravity	DIN 53479	g/cm^3	1.03
Melting point	DTA	°C	176
Glass transition temp.	DTA	°C	135
Heat distortion temp. B	ISO 75		130
Coefficient of lin. thermal expansion (-30°to 120°C)	VDE 0304/4	10^{-5}/K	7-8
Water absorption	DIN 53495	%	1.6
Tensile strength at yield	DIN 53455	N/mm²	80
Tensile strength at break	DIN 53455	N/mm²	60
Elongation at break	DIN 53455	%	100
Tensile modulus dry/cond.	DIN 53457	N/mm²	2300/2300
Flexural modulus dry/cond.	DIN 53452	N/mm²	2150/2150
Compressive strength	DIN 53454	N/mm²	98
Impact strength	DIN 53453	KJ/m²	n.b.
Notched impact strength (Charpy)	DIN 53453	KJ/m²	8
Shore hardness	DIN 53505		80
Shrinkage of a loose tube (Ø 1.2/2,0) after aging 24 hours at 100 °C		o/oo	0.4-0.6
Crack resistence in methanol	test bars under load in 100% methanol	N/mm²	~ 80 very good

Although the blend compositions present outstanding properties, a peculiar weakness (common to all kinds of polyamides) still persists - the ability to absorb water. However, these two copolyamides and the two blends displays this weakness to a lesser degree.

6. Dual loose tube

Long exposure to a water saturated environment results in reduction of certain properties of these copolyamides such as heat distortion temperature or dimensional stability.
Therefore an additional protective tube, consisting of resins with low water absorption (polybutylentherephthalate, but also polyolefines, polyvinylchlorides and fluoro polymers) is used as a barrier sheathing material around the first loose tube, forming a double tube (dual loose tube) construction. The outer and inner tubes should have comparable physical and mechanical properties to ensure good processability and compatibility. Coextrusion is an economically and suitable method for manufacturing dual loose tubes in one production step.

7. Polyamide blends for mono loose tube

Although the double tube around the optical fiber represents optimal protection for a long time, many efforts are currently under way to replace the dual tube with less expensive mono tube without reduction of the quality of protection for the optical fiber.

Polybutylentherephthalate has sometimes been proposed for this application, but is not being widely used, probably because of instability against hydrolysis and a insufficient compression resistance.

Since the mono loose tube must offer the combined properties of a dual loose system, an appropriate resin material must demonstrate, on one hand a remarkable stiffness, compressive strength and dimensional stability and on the other hand adequate flexibility, crack resistance and a greatly reduced water absorption faculty.

The foregoing copolyamides or polyamide blends may be additionally blended with compatible (but not similar) polymers like polystyrene, polyesters, polyoxyphenylenes, polyolefines (which are known to have poor tendencies to water absorption) resulting in materials for the mono loose tubing application with the above mentioned combined properties.

The next table shows some outstanding properties of a representative type of this new class of copolyamide blends: PA blend 57/15/10 (picture 14). According to the following picture (picture 15) this blend also presents high temperature stability of the polymer chain and a similar behaviour of the mechanical properties.

Picture 14

Polyamide blend 57/15/10

Property	Test Method	Unit	Values
Specific gravity	DIN 53479	g/cm^3	1.08
Melting point	DTA	°C	178
Glass transition	DTA	°C	142
Heat distortion temperature B	ISO 75/DIN 53461	°C	128
Coefficient of linear therm. expension	DIN 52328	K^{-1}	$7-8 \times 10^{-5}$
Water absorption 23°/50 % RH	DIN 53417	%	0.8
23° in water	DIN 53495	%	2.2
Tensile strength at yield	DIN 53455	N/mm^2	78
Tensile strength at break	DIN 53455	N/mm^2	69
Elongation at break	DIN 53455	%	117
Tensile modulus dry/cond.	DIN 53457	N/mm^2	2600/2600
Flexural modulus dry/cond.	DIN 53452	N/mm^2	2300/2300
Impact strength	DIN 53453	KJ/m^2	n.b.
Notched impact strength (Charpy)	DIN 53453/23°	KJ/m^2	18
Crack resistance in methanol	(tested under load in 100 % CH_3OH)	N/mm^2	very good ~ 86
Kinking resistance of a tube	nafrow slope with a tube of dimension O 1.2; 2.0 mm		very good ~ 10 mm
Shrinkage of a loose tube (O 1.2/2.0)after aging aging 24 hours at 100 °C		o,oo	~ 1.2

Picture 15

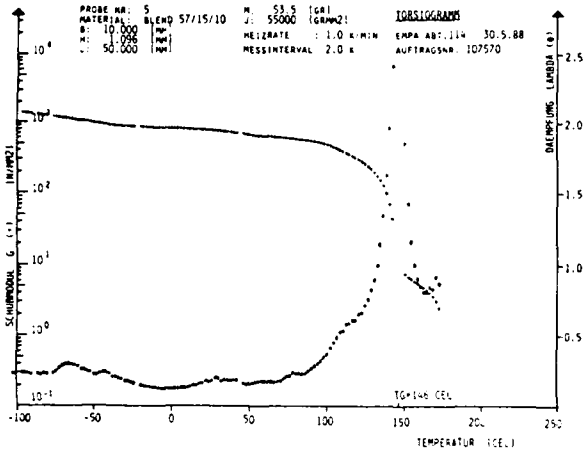

Conclusions

1. Copolyamides formed from rigid molecules like isophthalic acid, cycloaliphatic diamines and lactams show the kind of properties, which are needed in optic fiber dual loose jacketing materials.

2. By changing the ratio of lactam content the physical and mechanical properties can be adjusted to meet requirements of specific application.

3. Chemical resistance and flexibility can be improved by blending the copolyamides with linear polyamides.

4. Materials for mono loose jacketing are obtainable by blending the copolyamides with polymers which are poor in water absorption such as polystyrenes, polyesters, polyolefines.

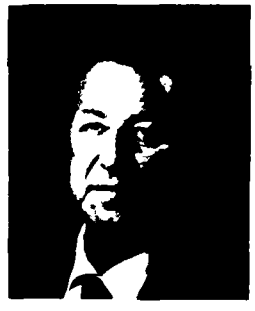

Biographical sketch

Hans H. Dalla Torre is member of the research staff of EMS-CHEMIE AG at Domat/Ems, Switzerland. He is currently responsible for the development of plastic materials for fiber optic purposes.

He holds a Ph. D. in chemistry from the university of Innsbruck, Austria.

Address: Dr. Hans H. Dalla Torre
EMS-CHEMIE AG

7013 Domat/Ems

Switzerland

SHIELDING EFFECTIVENESS OF SUPERCONDUCTIVE PARTICLES IN PLASTICS

Thomas Pienkowski, John Kincaid
Belden Wire & Cable
Technical Research Center
Geneva, Illinois

M.T. Lanagan, R.B. Poeppel, J.T. Dusek, Donglu Shi, K.C. Goretta
Argonne National Laboratory
Argonne, Illinois

Abstract

The ability to cool superconductors with liquid nitrogen instead of liquid helium has opened the door to a wide range of research. The well known Meissner effect, which states superconductors are perfectly diamagnetic, suggests shielding applications. One of the drawbacks to the new ceramic superconductors is the brittleness of the finished material. Because of this drawback any application which required flexibility (e.g. wire and cable) would be impractical. Therefore, this paper presents the results of a preliminary investigation into the shielding effectiveness of $YBa_2Cu_3O_{7-x}$ both as a composite and as a monolithic material. Shielding effectiveness was measured using two separate test methods. One tested the magnetic (near field) shielding and the other tested the electromagnetic (far field) shielding. No shielding was seen in the near field measurements on the composite samples, and only one heavily loaded sample showed some shielding in the far field. The monolithic samples showed a large amount of magnetic shielding.

Introduction

The recent advent of higher critical temperatures in superconductors has made it practical to investigate them for a wide range of applications. One application suggested by the Meissner effect is to use superconductors as a means of shielding. The Meissner effect simply states that a magnetic field is excluded from a superconductor. Thus, a monolithic superconductive shield would exclude magnetic interference as well as have infinite conductivity unlike copper shields. However, due to the brittleness of the ceramic high temperature superconductors, a cable shielded with this material would be impractical in most situations. An alternative might be to load a plastic with superconductive particles. This paper presents the results of a preliminary investigation into the far field electromagnetic shielding and the near field magnetic shielding of $YBa_2Cu_3O_{7-x}$ superconductors both mixed in a plastic matrix and as a pure ceramic.

Test Methods

Three different test methods were used, one testing far field shielding, one testing near field magnetic shielding, and the other testing for the presence of Meissner effect. A Superconducting Quantum Interference Device (SQUID) magnetometer was used to measure the flux expulsion or Meissner fraction.

A flanged coaxial holder design was selected for measuring electromagnetic shielding, and like many shielding effectiveness test methods, it is based on an insertion loss type measurement. Figure 1 shows a diagram of the fixture. A flanged coaxial fixture relies on displacement currents as opposed to conduction current. The disadvantage of this fixture is the extra measurement steps which must be taken to compensate for the perturbation of the transmission line caused by the insertion of the sample. This measurement method is usually used between 10 MHz and 1 GHz. The National Bureau of Standards (NBS) has proposed the standardization of this fixture and it is documented in several papers.[1,2]

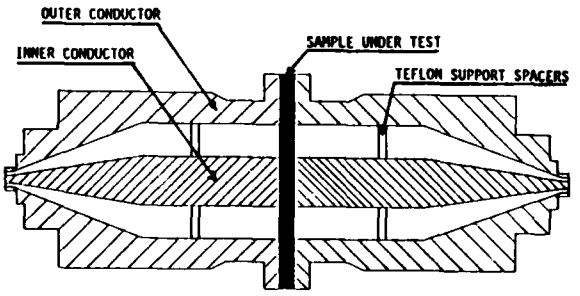

Figure 1. Flanged Coaxial Test Fixture

The NBS design for the flanged coaxial fixture was modified to allow for the liquid nitrogen cooling that is required. To allow for the boiling of the liquid nitrogen, small slots were cut through the outer conductor. This was also done in several other locations to ensure sufficient ventilation for the escaping nitrogen gas. The alternative to cutting slots in the outer conductor was to make the fixture "air tight". For safety reasons this was not attempted because of the large vapor pressure of liquid nitrogen.

The other major modification to the NBS design was to compensate for the liquid nitrogen dielectric. Liquid nitrogen has a relative dielectric constant of 1.45. To maintain a 50 ohm coaxial test fixture with this dielectric, the ratio of the inner to outer conductor was changed. It was decided to reduce the size of the inner conductor to maintain the 50 ohm impedance.

The magnetic shielding test apparatus is loosely based on the Helmholtz coil, ASTM A698 Vol. 3.04. It consists of a powered coil and a pick-up coil. The powered coil was driven by an amplifier and was swept in frequency from 10 Hz to 10 kHz. This coil produced a 22 gauss magnetic field. The pick-up coil was placed inside the powered coil and was centered for maximum output voltage. The shielding material was placed around the pick-up coil and was usually tube shaped. The ratio of the voltage generated by the shielded coil to the voltage generated by an unshielded coil is the shield effectiveness.

Processing of Samples

Composite Samples

The fabrication process begins with a well characterized $YBa_2Cu_3O_{7-x}$ (herein designated YBCO) powder. Powder synthesis may be carried out by a variety of methods, and the mixed oxide route was chosen in this study. Starting materials of $BaCO_3$, Y_2O_3, and CuO were mixed in stoichiometric amounts and pressed into disks for calcination (reaction at high temperatures). In this study, the calcination temperatures were between 900 and 950°C for durations of 16 to 48 hours, and the disks were crushed after firing. Powder calcination was a complex process due to low melting eutectics and residual $BaCO_3$, and several heat treatments were necessary to obtain the proper YBCO phase[3]. The procedure was repeated to produce a phase pure powder as judged by x-ray powder diffraction patterns. The final particle size and morphology will affect all of the subsequent processing operations. Milling operations were carried out to achieve the desired particle size and distribution. In this study, the calcined powder was milled to a median particle size in the 4-7 μm range.

The YBCO particles were then mixed with two different plastics, Ethylene-Vinyl Acetate (EVA) and Polychorotrifluordethylene (KEL-F). The KEL-F™ was selected for its low glass transition temperature and the EVA was selected because of its low processing temperature. Each plastic was loaded with superconductive particles on a plastics mill. The KEL-F processed at 450°F and the EVA at room temperature. However, due to the shearing stresses built up in the EVA during the milling, its temperature reached 150°F. The KEL-F samples were loaded to 10%, and 30% by weight and the EVA samples were loaded to 10%, 30% and 80% by weight. A fourth EVA sample was loaded with 70% YBCO and 9% carbon black. The addition of the carbon black increased the press temperature to 300°F. These samples were then pressed into .040" thick plates for testing in the flanged coaxial holder, and also rolled into tubes for the low frequency magnetic shielding test fixture.

Monolithic Tubes

Ceramic tube fabrication requires that the YBCO powder be mixed with a set of organics. A solvent provides the basic vehicle into which the oxide powder and other organics are placed. Care must be taken in selecting a solvent that is compatible with the YBCO powder and other organic constituents, and common solvents include methyl ethyl ketone, methanol, or xylene. Dispersants are utilized to deflocculate the inorganic particles in the solvent, and to assist in obtaining higher green (unfired) densities. Binders impart strength to the green body, and plasticizers allow for greater flexibility by reducing the glass transition temperature of the binder. In extrusion, the plastic mass was forced through a small aperture. Wire with radii between 0.3 and 1.5 mm have been manufactured in 12 to 20 cm lengths. In this study 6" long tubes were formed with a .190" inside diameter and a .040" wall. These tubes were used to measure shielding effectiveness in the near field test apparatus.

The heat treatment schedule for fabricated shapes is divided into three basic sections. Initially, a slow increase in temperature is required to remove organics from the green body. In this study, organics were volatilized below 350°C. During sintering a well calcined powder will have a liquid phase that has an onset temperature between 930 and 960°C[4]. The tubes were heated in oxygen to 950°C in order to sinter the powder to high density. The final step is an annealing procedure to incorporate oxygen into the YBCO lattice to form the superconducting phase. The relationship between oxygen content and phase transition to the superconducting orthorhombic phase has been studied extensively[5].

Monolithic Tapes

The tape casting process requires that the YBCO powder be mixed with a set of organics, which exactly parallels the ceramic tube fabrication. However, instead of being extruded, the tape cast samples were made by a doctor blade traversing over a glass plate to form a uniform layer. The tape was removed from the glass plate, and was very flexible in the unfired state owing to the

KEL-F is a Registered Trademark of 3M

organics incorporated in the cast material. The heat treatment schedule also parallels that of the tube fabrication including the final step of oxygen annealing to obtain the superconducting phase. The superconducting tapes were approximately 4" in diameter and .012" thick. These were used in the flanged coaxial test fixture for shielding measurements.

Results

Meissner Fraction

The Meissner fraction testing was performed on three composite samples and on the powder prior to mixing. The YBCO powder consistently showed a large Meissner effect. The three composites tested were the 10% and 30% samples loaded in KEL-F and the 80% sample loaded in EVA. The two KEL-F samples showed no Meissner effect. This is probably due to the lack of sensitivity in the SQUID and not due to the high processing temperature of the KEL-F.

The EVA sample which was loaded with 80% superconductive powder showed a large Meissner effect as seen in Figure 2. The horizontal scale is in °K and the vertical scale is in arbitrary units.

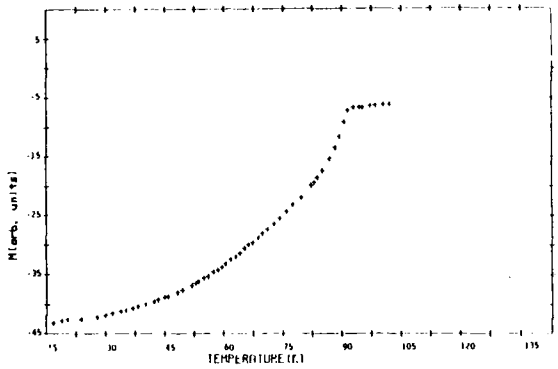

Figure 2. Meissner Fraction of 80% Loaded EVA

Magnetic Shielding Effectiveness

The magnetic shielding effectiveness testing showed no shielding from any of the composites. This might indicate that the plastics were not loaded heavily enough or that the particles were not properly aligned.

The shielding test on the monolithic superconductive tubes showed better than 60 dB of shielding in some frequency ranges. The shielding from 10 Hz to 20 kHz is shown in Figure 3. Shielding is in decibels and the horizontal frequency scale is logarithmic. Notice that the superconductor provided no shielding under 300 Hz. This shows that the field strength which causes the superconductor to become non-shielding is frequency dependent. Also shown in Figure 3 is the shielding obtained from a .048" wall copper pipe and a .066" wall steel pipe. (These two measurements were made at room temperature.) At this input power level the noise floor is around 60 dB. This implies that the shielding is actually better than 60 dB however more sensitive equipment is needed to determine it.

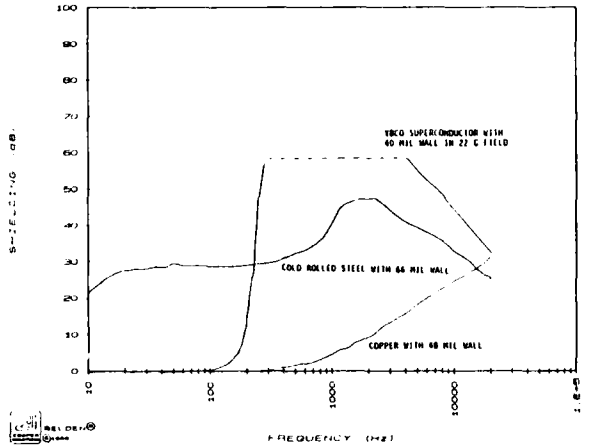

Figure 3. Magnetic Shielding Effectiveness for Copper, Cold Rolled Steel and YBCO Superconductor

As the input power level is decreased, the superconducting tube becomes superconductive at a lower frequency as seen in Figure 4. Unfortunately, as the power level is decreased, the noise floor is also decreased until only 30 dB of shielding can be seen. This, again, is not to say that this superconductive shield only provides 30 dB of shielding, it simply says the equipment is limited to 30 dB at this input power level. Figures 3 and 4 show the test results of a single tube of YBCO. Another tube has been tested and similar results were obtained.

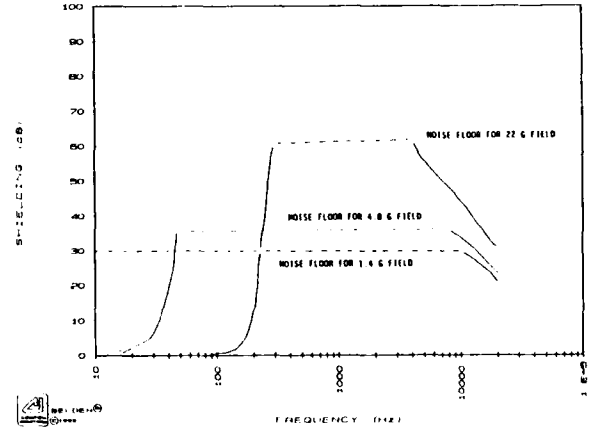

Figure 4. Minimum Magnetic Shielding of YBCO Superconductor in Different Field Strengths

Electromagnetic Shielding Effectiveness

The electromagnetic shielding measurements showed no shielding from any of the composite samples except the sample loaded with 70% superconductor and 9% carbon black. This sample's shielding effectiveness is shown in Figure 5. This meager 12 dB of shielding was first wrongfully attributed to the carbon black. An additional sample was loaded exclusively with carbon black in the same percent loading. This sample's shielding effectiveness was measured in liquid nitrogen and only 1 dB of shielding was seen. A large change in shielding was also seen when the 70% superconductive and 9% carbon black sample was cooled past its critical temperature. This also indicates superconductive shielding.

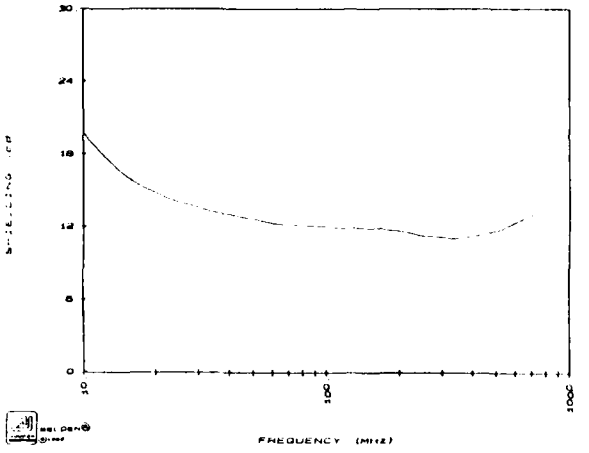

Figure 5. Shielding Effectiveness of a Sample of EVA Loaded with 70% Superconductive Powder and 9% Carbon Black

The pure YBCO tape cast sample was extremely difficult to mount in the flanged coaxial test fixture. Part of the mounting problem was due to the brittle nature of the superconductor. This problem is accentuated by the thinness of the sample. The other part of the mounting problem stems from the curved shape which the tape cast sample forms after firing. Because of this lack of "flatness" only an approximate shielding effectiveness measurement was attempted. This approximate method used a spacer ring to keep the flanges of the test fixture from crushing the sample. Unfortunately, the tape cast sample mounted in this manner showed no shielding. This result was somewhat unexpected given the relatively large amount of shielding seen by the magnetic shielding test fixture. Further work is presently being pursued to evaluate this apparent anomaly.

Conclusion

The monolithic YBCO superconductors provide a large amount of magnetic shielding. By weight or volume they provide more shielding than copper or cold rolled steel. The lack of electromagnetic shielding from the tape cast samples is as of yet unexplainable. Thicker test samples might allow direct mounting of the sample thus eliminating one source of error. There appears to be several problems with superconductive shields. One problem is the small critical magnetic field which the YBCO superconductors appear to have. Other problems include extreme brittleness and low critical temperatures. Shielding from composites with YBCO needs more development but should not be ruled out as a possible shielding material for the future.

Acknowledgements

The authors gratefully acknowledge Dave Johnson for his expertise in the manufacturing of the NBS test fixture. The work was supported by the U.S. Department of Energy, Office of Energy Storage and Distribution, and the BES-Materials Sciences, under Contract W-31-109-ENG-38.

References

1. Adams, J.W., Vanzura, E.J., Shielding Effectiveness Measurements of Plastics. National Bureau of Standards NBSIR 85-3035, 1986, January.

2. Ondrejka, A.R., Adams, J.W. Shielding Effectiveness (SE) Measurement Techniques. 1984 IEEE National Symposium on Electromagnetic Compatibility, San Antonio, Texas. 1984 April 24-26, 249-256.

3. S. Pejovnik. R.L. Porter, A.I. Kingon, T.M. Hare, and H. Palmour III, Proc. Int'l. Symp. on Sci. and Tech. of Sintering, Tokyo, Japan, Nov. 1987; Elsevier, (1988).

4. A.I. Kingon, S. Chevacharoenkul, S. Pejovnik, R. Velasquez, R.L. Porter, T.M. Hare, and H. Palmour III, Proc. Conf. on High T_c Superconductors, Chapel Hill, (1987).

5. H. Strauven, J.P. Loquet, O.B. Verbeke, and Y. Bruynseraede, Solid State Communications 65, pp. 293-296 (1988).

Biographies

Thomas Pienkowski
Belden Wire & Cable
Technical Research Center
2000 S. Batavia Avenue
Geneva, IL 60134

Thomas Pienkowski is presently working on the shielding effectiveness of superconductors and their applications. He received his MSEE from Ohio State University and his BSEE from Iowa State University. He is presently working as a Product Development Engineer with Belden's Electronic Division.

John Kincaid is Manager of Advanced Electronic Product Development at Belden's Technical Research Center in Geneva, Illinois. Mr. Kincaid is a member of the IEEE and is active in the EMC Society TC-4 Working Group on Shield Effectiveness. John Kincaid received the MSEE and BSEE degrees from the University of Oklahoma.

Dr. Michael T. Lanagan is an Assistant Ceramist at Argonne National Laboratory. His research interests include fabrication and electronic characterization of oxides. He received a BS in Ceramic Engineering at the University of Illinois at Urbana and a Ph.D. in Ceramic Science from Penn State University.

Dr. Roger B. Poeppel is a graduate of Cornell University, Ithaca, New York where he received a Bachelor of Engineering in Physics and a Ph.D. in Materials Science and Engineering. At Argonne National Laboratory, he is Manager of the Ceramics Section in the Materials and Components Technology Division. He is responsible for ceramic fabrication development and for the testing of ceramics for a wide variety of applications.

Joseph T. Dusek has worked in the field of ceramic processing and product development for nearly 50 years, the past 25 of which have been spent at Argonne National Laboratory. Prior to joining Argonne he held positions at the Armour Research Foundation and the IIT Research Institute.

Dr. Donglu Shi is a member of the Materials Science Division of Argonne National Laboratory. He received a Ph.D. in Materials Science from, and subsequently did post-graduate research at, the University of Massachusetts. He has concentrated on processing and properties high-T_c and A-15 superconductors.

Dr. Kenneth C. Goretta is an Assistant Ceramist in the Materials and Components Technology Division at Argonne National Laboratory. His research has focussed on the mechanical properties and fabrication of oxide ceramics. He received a BS in Metallurgical Engineering from the University of Illinois at Urbana and Ph.D. in Metallurgical Engineering from the Illinois Institute of Technology.

ELECTROMAGNETIC PROTECTION OF BURIED TELECOMMUNICATIONS CABLES BY USE OF A CONDUCTIVE SHEATH

Jean-Yves GODLOT & Dominique BERTIER
ACOME, 50140 MORTAIN, FRANCE

Guy BOUCHEZ
CNET, 22300, LANNION, FRANCE

SUMMARY

This paper describes a cable sheathing material suitable for used on buried telecommunications cables that maintains a low resistance to ground without sacrificing necessary mechanical properties.

Also developed is a conductive jelly filling compound to provide a low resistance path between the metallic shielding materials and the conductive jacket.

These materials have been extensively tested to confirm that the properties sought in the development endure in field installations. A 5-year test program in direct earth burial and a 6-months salt water immersion test have been passed successfully.

Cables have been manufactured using these conductive jackets and are in service on the French National Railways System where high circulating currents may be induced.

INTRODUCTION:

Buried cables often have metallic armor which provides good mechanical protection while being installed. A polymeric sheath applied over the armor prevents corrosion of the armor and also isolates it electrically from the earth. If induction effects occur, induced currents are produced within the metallic screens. Depending on the strength of the magnetic field in which the cables are located, very high potentials between screens and earth may appear and sometimes destroy the sheath by dielectric breakdown. Also, these high induced voltages can be dangerous to the personnel working on the cable system.

This phenomenon is very well known and became of more concern when the French highspeed railways were installed. Signal cables and telecommunications cables are buried near the rails and are parallel to the very high current power lines for long distances. Electric faults on these lines e.g., current surges, short circuits, train starting, etc. create high magnetic fields (typically from 10 to 500 A/m) including electromagnetic effects on these cables.

These problems may be avoided by minimizing the current circulating on the screens and the wires.

The first solution consists in grounding the metallic screens at regular intervals along the line (at about every mile). When the grounding is of good and stable quality (< 5 ohms) a solution to the noise appearing on the lines is the use of cables with reducing coefficient in which the shielding is acting as a lowering transformer for the wires. This perfect grounding is generally very hard to obtain. (Ref. 1)

Another well known solution that has not been widely used, is to keep the cable and the earth at the same potential through a good shield to earth continuity.

Many problems have to be solved when using this second approach:

...A semi-conductive jacket has to be used to protect the shielding against corrosion, its resistivity being, at most, equal to the resistivity of an average soil (10 to 1000 ohm. meter).

...The conductive properties must not be affected by current circulation. The jacket should be electrochemically stable.

...While the lowering of the electrical resistivity may be achieved by use of a high percentage of carbon black (Figure 1), these high concentrations lower the mechanical properties (Figure 2) and increase the melt viscosity to the point that extrusion becomes impossible on standard equipment (Figure 3) (Ref. 2).

...With most standard commercial grades of carbon black, concentrations of above 30% are required before the resistivity can be lowered below 10 ohms per meter.

...Similar observations have been made when trying to formulate semi-conductive jelly; the

higher the concentration of carbon black, the higher the viscosity.

These problems have been overcome as a result of this development.

MATERIALS DEVELOPMENT:

This project was undertaken with the following principal aims.

1. Development of a jacketing material meeting the requirement of a conventional sheathing compound; specifically:
   a. Having low resistivity, below 10 ohm. meter.
   b. Having tensile strength at break greater than 18MPa.
   c. Elongation at break over 400%.
   d. Being easy to extrude.
2. Maintain these essential characteristics in the jacket compound through the use of a low percentage of a carbon black additive, thus avoiding the deleterious effects on physical properties observed when high concentrations are employed.

To accomplish this, ACOME in cooperation with the French company TOTAL, identified a family of carbon blacks that could be used in concentrations of less than 10% and still achieve the low resistivity required to accomplish the objectives.

In addition to locating the preferred carbon blacks, the processing problems of assuring even dispersion of this reduced percentage of material withing the polymeric matrix was solved.

Materials with reproducible characteristics have been developed for both semi-conductive jacketing compounds and semi-conductive jelly filling compounds.

Table 1 contains the material characteristics obtained with these new compounds as compared to the requirements of the French telecommunications cable standards for jacketing materials.

Table 2 displays the principal characteristics of the semi-conductive jelly filling compound.

ELECTROCHEMICAL RESULTS:

The objective of this study was to check the stability of electrical properties of these new compounds while conducting an electrical current. The experimental device used is schematically described in Figure 4.

Polarization curves of studied samples are drawn versus a saturated calomel electrode (S. C. E.) which is the reference electrode. the pH of the KCl solution was maintained between pH = 2 and pH = 13. First we wanted to know the electrochemical behavior of the carbon blacks used and especially XE2 electrode and a platinum electrode in a 0.1 M KCl solution of pH 7. The result is shown in Figure 5.

The electrochemical window of XE2 carbon black extends from -1.5V to +1.5V versus the S. C. E. In this region no electronic exchanges can occur between carbon black and the solution (Current density is 0 A/m2) so XE2 carbon black can neither be reduced or oxidized. This window is larger than the platinum one (-1.1V to 1.4V versus S. C. E.).

Figure 6 represents relative positions of XE 2 polarization curves for different pH of the solution.

In the reduction region (negative voltages), these curves shift towards negative potentials as pH of the aqueous solution increases from pH = 2. The current observed in this region is due to the H_3O ions reduction i.e., the lower the pH is, the greater the H_3O ions concentration in the carbon black electrode vicinity is. So electronic exchanges between H_3O and electrode are easier and they appear at low negative potential for very acid pH.

In the oxidation domain (positive voltages), it is the O H ions oxidation which is involved to explain the current observed. With an interpretation identical to that described below, the polarization curves shift towards increasing potentials as the pH of the solution decreases.

This study shows that the only possible oxydo-reduction reactions at the interface between aqueous solutions and XE2 carbon black are oxidation or reduction of water; that can occur in an electrochemical domain more extended than the platinum one. Also, since there is no noticeable current in this region, XE2 carbon black is chemically pure.

Polarization curves of semi-conductive polyolefin compounds loaded with this XE2 carbon black have been established and a typical curve is represented in Figure 7. This curve is more difficult to interpret because the conductivity of the samples was too low. In this condition an ohmic component due to a potential gradient inside the electrode is added to the polarization characteristic. Even so, if we subtract this component, it seems that the semi-conductive electrochemical window is larger than the platinum one.

In conclusion, whatever the current density passing through the materials is, oxidation or reduction of the XE2 carbon black will not be possible and if these components are in aqueous solution, hydrolysis of water will be observed.

NOTE: Any trace of moisture in the materials is to be avoided either in the storage of the compounds or in the production process especially near the metallic screens. A study was done on the water

of carbon black loaded polymers (ref. 4). The total amount of water absorbed depends directly on the carbon black concentration. It is evident that having as low a concentration of carbon black as possible is absolutely necessary to obtain optimum electrical, mechanical and electrochemically stable jacketing materials.

RESULTS ON CABLE

Cables utilizing these newly developed materials were manufactured and tested to confirm the results obtained during the materials evaluation phase. Aging tests were performed on buried cable and cable immersed in salt water with the results reported in this paper.

Cable Structure:

Cables of 28, 56 and 112 pairs with .6mm copper wires were manufactured; see Figure 8. The construction is as follows:

- Ringed aluminum screen
- Semi-conductive waterproof jelly
- Intermediate semi-conductive polyolefin jacket
- Semi-conductive waterproof jelly
- Two steel tapes applied helically around the cable
- Semi-conductive waterproof jelly
- Semi-conductive polyolefin sheath.

Transverse Resistivity

The transverse resistivity was measured as this characterizes the grounding efficiency of these cables. An argent painting metallic contact is applied on about a 200mm length of the cable specimen. Measurements were performed according to the diagram as shown in Figure 9.

The resistance was measured between the aluminum screen and the argent paint contact. Since the cable is cylindrical, the following formula was used:

$$\rho = 2\pi \frac{L}{\ln\left(\frac{D}{D-2e}\right)} \cdot R_x$$

where L = length of the external contact
D = external diameter of the cable
e = thickness between aluminum screen and external contact
R_x = transverse resistance measured

Because of the multi-layer construction of the cable samples tested, there are many different materials of different conductivities in contact with each other. Each interface presents a contact resistance that varies according to current density (Figure 10). The resistivity varies from 70 ohm. meter to 700 ohm. meter depending on current density and cable type. These large variations are due to manufacturing variables. This measurement is a good method to determine contact quality on cables.

Natural variations in soil conditions fall within the same general intervals of resistivity.

Accelerated Aging of Cables in the Laboratory

Several 1.5 meter long cable specimens were immersed in salt water (40g of NaCl per liter of water) and subjected to a 50hz constant alternating current. The transverse resistivity of each sample has been monitored by measuring the transverse resistivity between the aluminum screen of the sample and an aluminum electrode in salt water.

After 6 months immersion with the cables subjected to two different current densities, 5 A/m² and 10 A/m² the resistance has remained stable after an initial decrease in the first few weeks. Hydrolysis of the water was observed during the entire length of the experiment (Figure 11).

Moreover, there was no noticeable corrosion of the metallic shielding materials on samples aged for 24 weeks. This structure is stable and waterproof so that it protects the screens from corrosion and ensures stable electrical properties of the shielding even for current densities up to 10 A/m².

Cables Buried in Earth

A sample of cable approximately 50 meters long was buried at about .8 meters in depth in soil of about 300 ohm/meter resistivity. The screens were discharging to earth with a current density of .4-.5 A/m² (this corresponds to a total amount of 2 amperes flowing to the earth over the 50 meter length). The earth to metallic screen resistance is measured with a tellurohmeter at regular time intervals. The results are plotted on Figure 12. Minor variations of resistance around a mean value of 10 ohms corresponds to climatic conditions, particularly the amount of moisture in the earth.

Earth resistance can be calculated using the formula for buried cables:

$$R = \frac{rho}{L}\left(\ln \frac{2L}{\sqrt{2\,r\,e}} - 1\right)$$

Where: Rho = earth resistivity in ohms/meter
L = length of the buried cable
2r = metallic screen diameter
e = depth in meters

The earth resistivity (rho) varies with the moisture in the soil. In Figure 12, resistance variations are represented versus earth resistivity from 50 ohm. meter to 1000 ohm. meter and length. This resistance tends towards an asymptotic value below 1 ohm for a 1 KM length and a 300 ohm/meter resistivity. Moreover, for a 50 meter length and a 300 ohm/meter resistivity, the calculated resistance (10 ohms) is very close to that measured in the experiment.

In conclusion, after this 5 years of aging, the earth resistance of buried cables remains stable. There is no significant variation of either the electrical or mechanical properties of the semi-conductive materials and no noticeable corrosion of the aluminum or steel screens. Finally, earth resistance below 1 ohm may be reached even when ground resistivity is as high as 1000 ohm.meter; this value being very difficult to obtain with standard grounds.

CONCLUSION

Electromagnetic protection of telecommunications cables needs not only an efficient screen structure but also low resistance earthing.

This latter point is difficult to obtain and continuous grounding through a conductive jacket has been known for a long time to be a promising technique.

Despite this, no commercially acceptable products were available heretofore, probably due to the poor mechanical and aging properties of the carbon filled compounds.

The new compounds developed by ACOME and TOTAL overcome these difficulties by using low concentrations of a highly conductive carbon black. In addition, these compounds achieve the same mechanical properties as conventional polyethylene sheathing materials. The long term suitability of this approach has been confirmed by a 5 year field test and a 6 month salt water immersion.

Larger scale tests are now underway with both the French Railway administration (SNCF) and French Telecom, the PTT.

ACKNOWLEDGEMENTS

The authors wish to thank the French Telecom and SNCF personnel who have contributed to this study.

REFERENCES

REF. 1: CCITT Documents: Directives concernant la protection des lignes de telecommunications contre les actions nuisibles des lignes electriques.

REF. 2: Communication BI - 3; P. 232-238
D. Bertier, J. Lemolton, B. Claude

REF. 3: Proc. 3rd International Conf. "Dieldectric Materials", Birmingham (GB), September 1979, P235.
J. C. Bobo, J. Schultz, E. Papirer, M. Prigent.

Guy Bouchez is the Deputy Manager for research and development of cables and accessories (both copper and optical) for CNET, "Centre National d'Etudes des Telecommunications". Previously, he was employed by the French PTT and was responsible for the local network in the Dijon area. He also was active on the coaxial intercities cable system after joining the PTT in 1953.

Dominique Bertier is a graduate of Ecole Centrale de Paris. His career began in 1971 with the French Research Center of Shell Oil. In 1976 he was appointed by ACOME as head of the irradiation cross linking activities and the polymer compound development program. His present position is Research Director for ACOME.

Jean-Yves Goblot was awarded his PHD from INSA de RENNES in France in 1984. His first position following graduation was as a researcher in organic chemistry of conductive materials for "Centre National d'Etudes des Telecommunications". He joined ACOME in 1986 and is assigned to continue research on these materials and on the design of telecommunications cables.

TABLE 1

CHARACTERISTICS OF SEMI CONDUCTIVE MATERIALS

CHARACTERISTICS	UNITS	REQUIRED	MATERIAL No. 1	MATERIAL No. 2
Tensile strength at break	MPa	≥ 18	21.3	[illegible]
Elongation at break	%	[illegible]	[illegible]	[illegible]
Mechanical characteristics after 240 hours ageing at 100 C				
Tensile strength at break	MPa		[illegible]	15.8
Variation of tensile strength	%	≤ 25	3	22
Elongation at break	%		55[illegible]	49
Variation of elongation	%	≤ 30	16	21
Melt index at 190 upon 21 kg	g/10 min	[illegible]	[illegible]	[illegible]
Shrinkage in boiling water	%	5	3 3.5	3.5-4
Oxidative induction time at 200 C	min			
aluminium holder		≥ 30	12[illegible]	115
copper holder			[illegible]	[illegible]
Oxidative induction time after [illegible] 3[illegible] minutes in boiling water on aluminium holder	min	≥ 15	66	65
Resistivity	Ω.m		0.5	1

All the properties mentioned in this table (except resistivity) are identical to those of conventional jacketing polyolefins. [illegible] was not a problem.

In the same time, a cooperation with [illegible] company allowed to develop a semi conductive jelly that coats the screens maintaining electrical continuity between the screens and the jacket and insuring watertightness. As seen in table 2, this product is consistent with French Telecom specifications.

TABLE 2

CHARACTERISTICS OF SEMI-CONDUCTIVE JELLY

CHARACTERISTICS	UNITS	MEASUREMENT METHOD	VALUE
Temperature of ball and ring	°C	NF T 66 008	>160
Dynamic viscosity (shear rate 13.3 s^{-1} and temperature 60 C)	c poises		70 900
Adhesion at low temperature	°C		- 10
Flash point	°C	NF T 60 118	266
Electrical resistivity	Ω.m		50

FIGURE 1 :CARBON BLACK FILLED POLYETHYLENE RESISTIVITY VERSUS DIFFERENT TYPES OF CARBON BLACKS

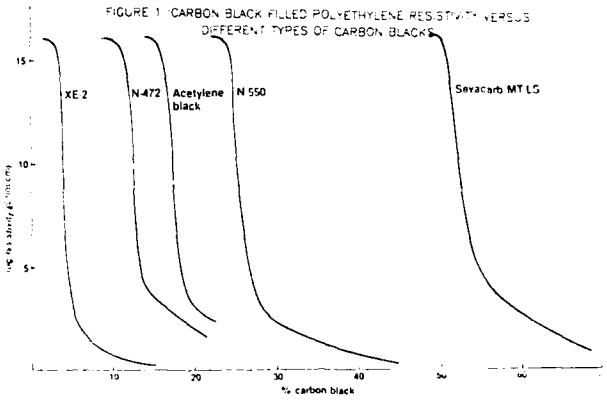

FIGURE 3 :MELT FLOW INDEX FOR DIFFERENT TYPES OF POLYETHYLENE VERSUS CARBON BLACK CONCENTRATION

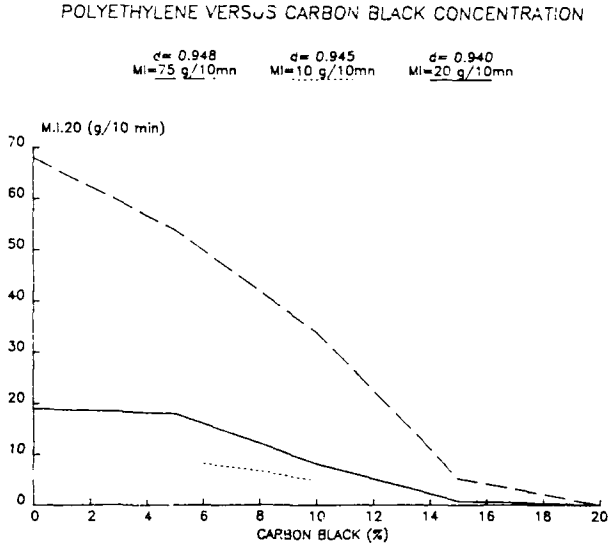

FIGURE 2 :MECHANICAL PROPERTIES FOR DIFFERENT TYPES OF POLYETHYLENE VERSUS CARBON BLACK CONCENTRATION

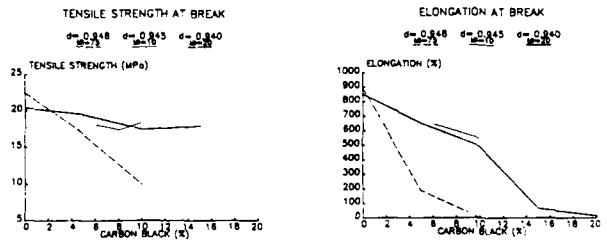

FIGURE 4 : EXPERIMENTAL DEVICE FOR ELECTROCHEMICAL STUDY

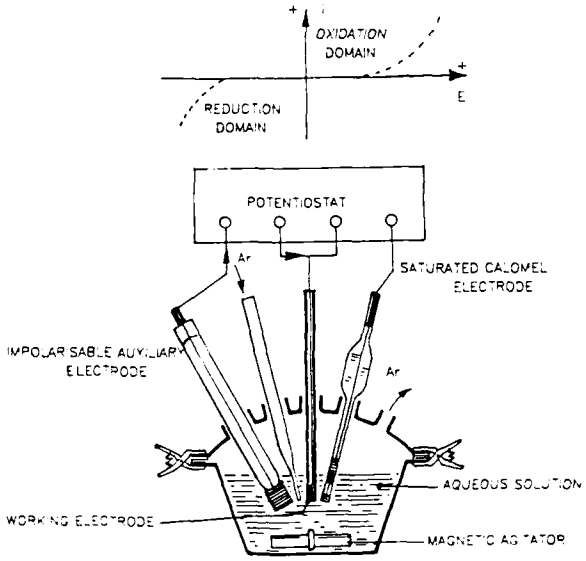

FIGURE 5 : POLARISATION CURVES COMPARISON BETWEEN XE2 CARBON BLACK ELECTRODE AND PLATINUM ELECTRODE (0.1M KCl SOLUTION pH=7)

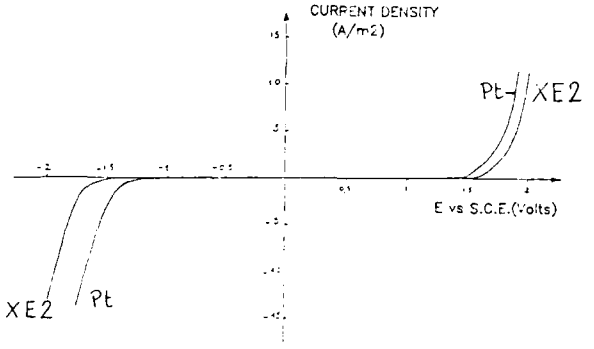

FIGURE 7 : POLARISATION CURVES OF SEMI-CONDUCTIVE JACKETING MATERIAL AND PLATINUM ELECTRODE (0.1M KCl SOLUTION pH=7)

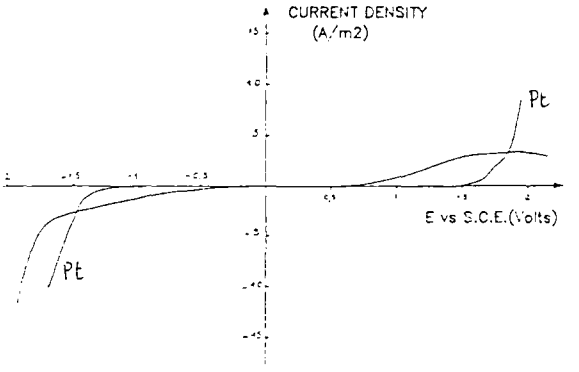

FIGURE 6 : POLARISATION CURVES OF XE2 CARBON BLACK ELECTRODE VERSUS pH OF AQUEOUS SOLUTION

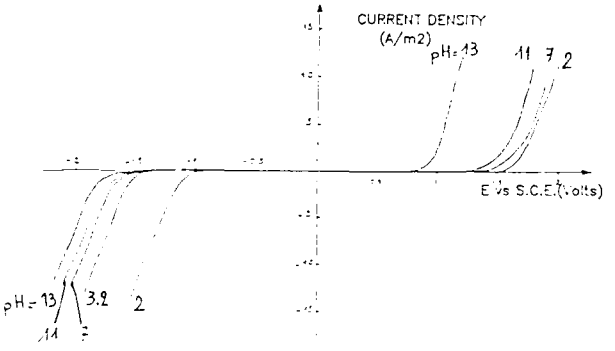

FIGURE 8 : CABLE STRUCTURE

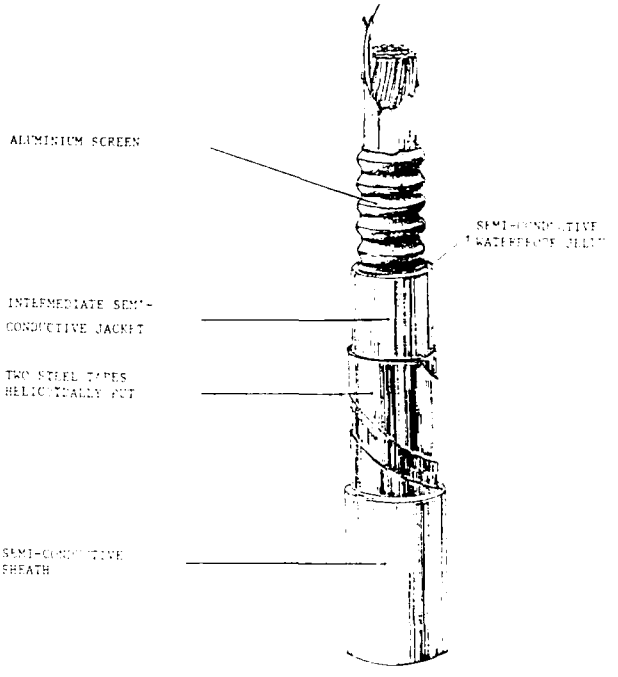

FIGURE 9 : TRANSVERSE RESISTIVITY MEASUREMENT DEVICE

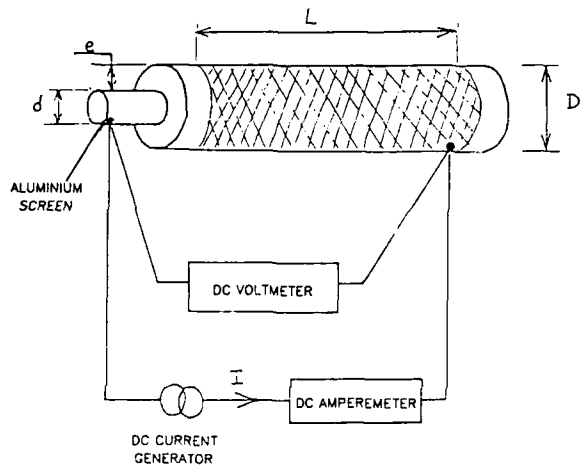

FIGURE 11: SCREEN TO WATER RESISTANCE VERSUS TIME FOR CABLE AGED IN SALT WATER

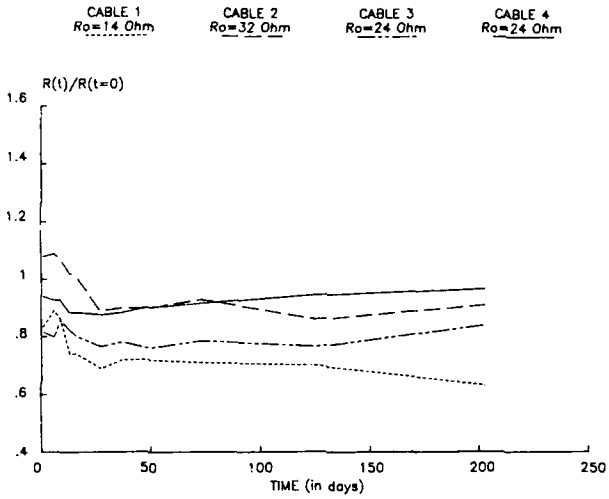

FIGURE 10 : TRANSVERSE ELECTRICAL RESISTIVITY VERSUS CURRENT DENSITY

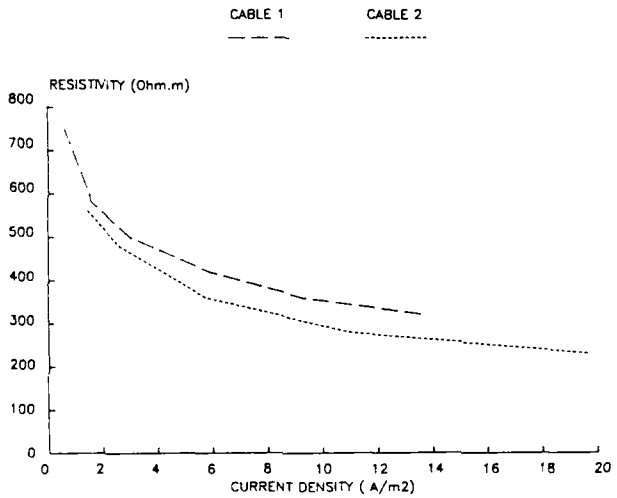

FIGURE 12 : EARTH RESISTANCE OF A CABLE BURIED (1 m DEPTH) VERSUS ITS LENGTH AND EARTH RESISTIVITY

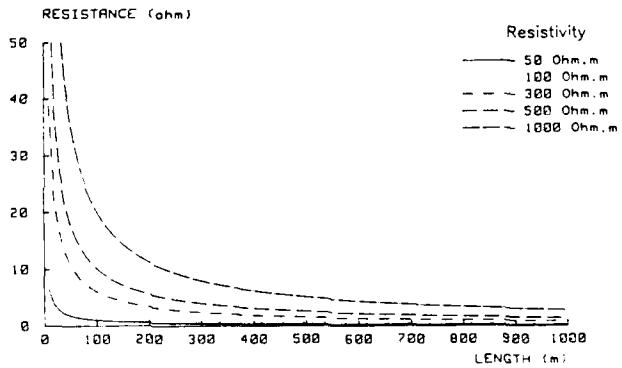

EVALUATION OF OPTICAL FIBER TERMINATING CABLES WITH FLAME-RETARDANT POLYURETHANE JACKETING

Susana CAMARA Carlos G. CORTINES Carlos BLANCO Miguel P. BUSTAMANTE

ALCATEL STANDARD ELECTRICA, S.A.
Maliano - Cantabria - Spain

ABSTRACT

To comply with International Standards for Indoor Telephone Exchanges, cables must be manufactured with fire-resistant and smoke suppressant materials. The materials used at present, such as polyethylene, PVC or polypropylene do not possess these properties. This was the reason for the study of a specially treated polyurethane which would possess the property of antiinflammability and at the same time display high flexibility.

In this paper the properties of this thermoplastic are shown, and a single-mode one fiber cable is described. Likewise, the paper shows the tests carried out for the qualification of the cable.

These cables can also be joined, if required, to optical connectors with insertion losses lower than 0.1 dB.

INTRODUCTION

The cables designed for indoor installations are usually cables for application in short and medium distances such as data transmission systems, instrumentation, CATV cables and terminals for the segregation of multi-fiber cables and connection to the transmission equipments. Since they are used inside buildings, they must meet a series of special requirements.

These special properties required by the different Administrations refer to the requirements which the cable must meet concerning flammability and the low-toxicity of gases given off when burning.

After profound studies the use of a specially treated polyurethane, possessing flame-retardance, was decided upon.

First the raw material was studied. Its mechanical properties: tensile strength at break, elongation at break, abrasion resistance, hardness, bending test at low temperature, cracking resistance, hot temperature deformation; its mechanical properties after submission to an accelerated ageing resistance to ultraviolet radiation, resistance to hydrolysis, electrical characteristics, thermal and flame behavior.

Then, a cable, Figure 1, having good transmission, properties was designed. Finally, it was manufactured.

After carrying out these steps, the parameters of the said cable were studied in detail: mechanical, electrical and thermal properties of the finished cable and, of course, its transmission features.

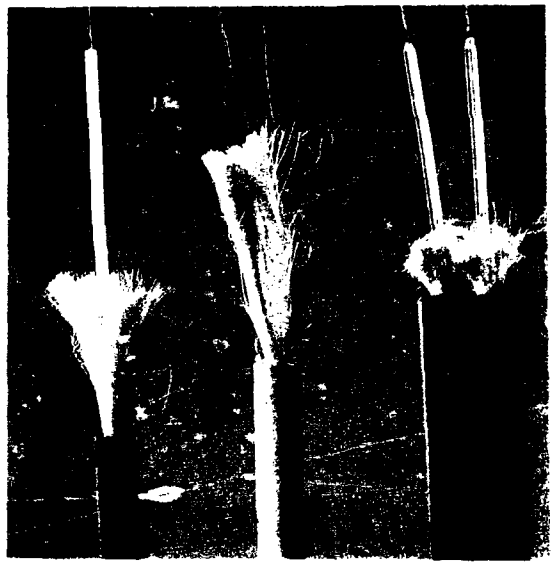

Figure 1

TESTS ON POLYURETHANE FOR JACKETINGS

The material used for sheathing the terminating cables was flame-retardant, thermoplastic and elastomeric polyure-

thane. It is one of the so called "lineal polyurethanes" and is a result of the reaction between aliphatic diisocianates and aliphatic glycols.

The group of lineal polyurethanes contains both non-crosslinking and partial crosslinking polyurethanes. For the design and manufacture of the terminal cable a virtually non-crosslinking polyurethane was used.

We would also like to point out that the manufacturers of this polyurethane use a special treatment so as to convert it into a flame-retardant material with a low content of halogens.

MECHANICAL, THERMIC AND ELECTRIC PROPERTY TESTS

In order to carry out the study of the properties of the above mentioned material, the raw material, in pellets, underwent treatment with a laboratory mill and press. From the strips obtained in this way we got the test pieces we needed. The mechanical properties studied are as follows:

1. Tensile strength at break.

The test was carried out following the ASTM D 638 Norm, the test temperature was 23 ± 2ºC with 50 ± 5 % relative humidity.

2. Elongation at yield and elongation at break.

Tests were made according to ASTM D 638, at the same temperature and relative humidity as in Test 1.

3. Environmental stress cracking.

Test was carried out following ASTM D 1693. The active agent used in this test was Igepal Co 630 at 10 % in water. The test temperature was 50 ± 0.5ºC.

4. Abrasion resistance.

The method followed was that of ASTM D 1242 Method A: Loose Abrasive.

5. Density.

The density was determined by the density gradient technique, and followed the ASTM D 1505 Norm. The gradient column was made with a mixture of water and calcium nitrate. The temperature was 23 ± 0.1ºC.

6. Bending test at low temperature.

The B.S. 6469 Norm was followed. The test temperature was -20 ± 2ºC for a period of two hours.

7. Hot deformation test.

The test was carried out in accordance with B.S. 6469, and on a 1.25 ± 0.15 mm thick strip. The material was kept at a temperature of 120 ± 1ºC for an hour. Then, without taking it out of the climatic cabinet, a 500 gramme perpendicular load was applied and kept on it, at the temperature mentioned above, for an hour.

8. Brittleness temperature by impact.

In accordance with ASTM D 746.

9. Dielectric constant and tag α .

The test was made following liquid displacement procedure as per ASTM D 1531.

10. Volume resistivity.

As per the Electrode Systems Method of ASTM D 257 Norm.

The results of these tests, made on 10 test pieces, displayed the average values shown in Table 1.

FLAME BEHAVIOR TEST

The manufacturers of this polyurethane achieved its special behavior by adding a compound mixture to it. Some of these additives include halogenated hydrocarbon and antimony trioxide. According to the manufacturers of the material the concentration of the antimony trioxide is higher than 1% and the concentration of chlorides is less than 10%.

The LOI of the polyurethane was also studied, in other words, the minimum oxygen concentration to support candle-like combustion, as per the ASTM D 2863 method. The value obtained was 31.5%.

So as to carry out a more detailed study of its behavior when faced with a flame we carried out the tests in accordance with ASTM D 1929 and we obtained the flash ignition temperature values and self-ignition temperature.

The flash ignition temperature which is the lowest initial temperature of air passing around the specimen at which a sufficient amount of combustible gas is evolved to be ignited by a smaller external pilot flame, is of about 300ºC for this type of polyurethane.

The self-ignition temperature is about 320ºC. By self-ignition temperature we mean the lowest initial temperature of air passing around the specimen at which, in the absence of an ignition source, the self-heating properties of the specimen lead to ignition.

TABLE 1

TEST VALUES OF MECHANICAL THERMIC AND ELECTRIC PROPERTIES

PROPERTY	UNIT	AVERAGE VALUE OBTAINED
Tensile strength at break	kg/cm^2	290
Elongation at break	%	625
Modulus of Young	kg/cm^2	55
Environmental stress cracking	F/10	0/10
Resistance to abrasion	cm^3	0.058
Density	g/cm^3	1.24
Bending test at low temperature	F/10	0/10
Hot deformation test	%	2
Brittleness temperature by impact	ºC	-68
Dielectric constant	-	5.63
Tag α	-	0.029
Volume resistivity	ohm.cm	1.10^{10}

THERMAL AGEING

The material underwent the following treatment: kept in a hot chamber with air conditioning at 70ºC for four weeks. Some test pieces were measured after a week's treatment and at the end of the cycle.

The variations observed in the above mentioned properties of the material are shown in Graphics 1, 2 and 3.

HYDROLISIS RESISTANCE

The polyurethane also underwent hydrolisis ageing. The material was kept in water at 70ºC for four weeks. The variations in mechanical properties (tensile strength at break, elongation, hardness) were studied.

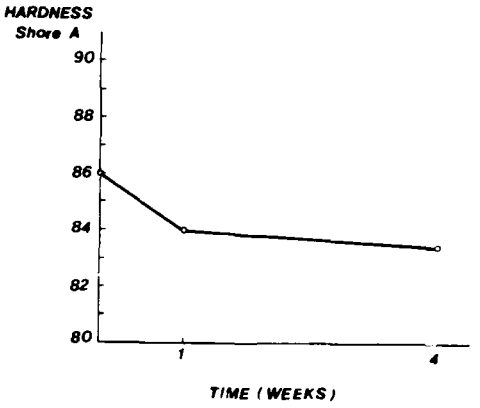

Graphic 1: THERMAL AGEING

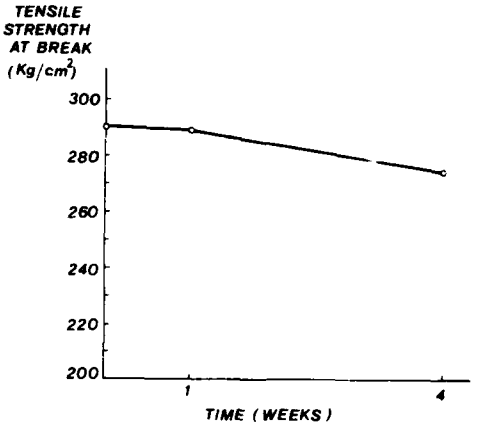

Graphic 2: THERMAL AGEING

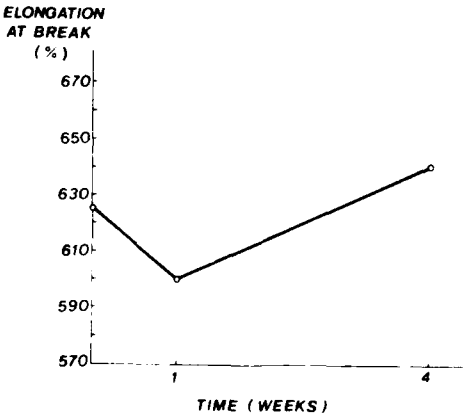

Graphic 3: THERMAL AGEING

Samples were taken at the end of the first week, also at the end of the second week and finally at the end of the cycle. The results can be seen in Graphics 4, 5 and 6.

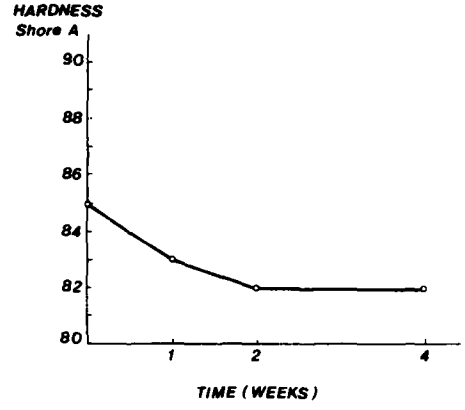

Graphic 4: HYDROLISIS RESISTANCE

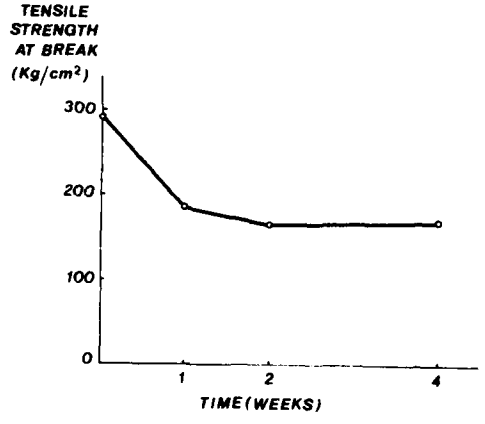

Graphic 5: HYDROLISIS RESISTANCE

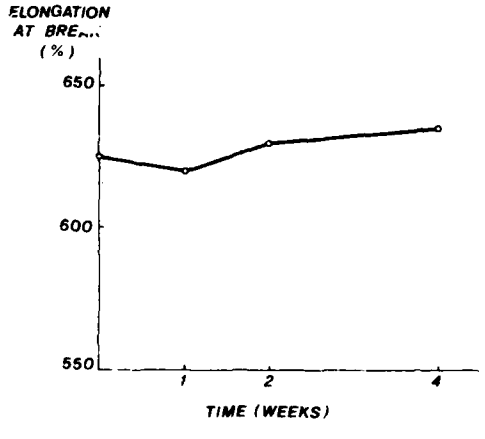

Graphic 6: HYDROLISIS RESISTANCE

LIGHT AGEING

The same as in the last two tests strips of polyurethane pigmented with special masterbatches for polyurthane were used. These strips underwent an Xenotest for 200 hours.

The masterbatches used for the test pieces were the same as those which were afterwards used for cable manufacture.

The colour of the test pieces suffered hardly any change.

As regards the mechanical properties, the variation which they displayed are those shown in Graphics 7, 8 and 9.

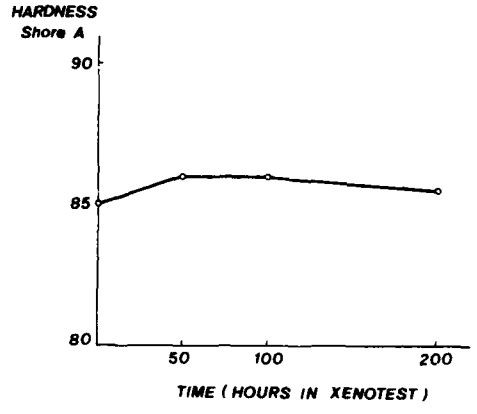

Graphic 7: LIGHT AGEING

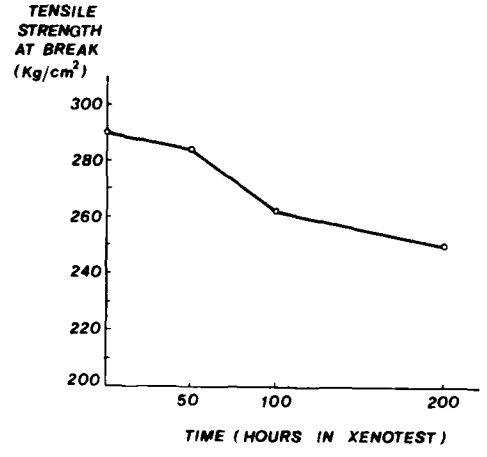

Graphic 8: LIGHT AGEING

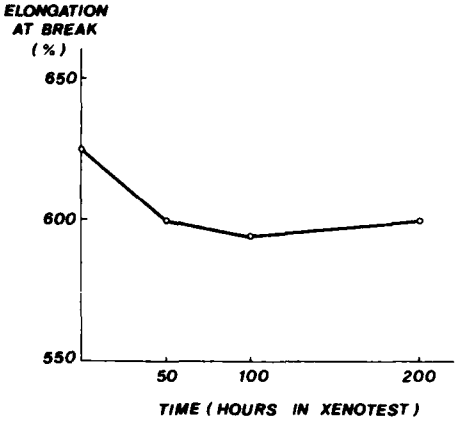

Graphic 9: LIGHT AGEING

CABLE CONSTRUCTION

The polyurethane studied was used for coating the monofiber cable described in Figures 2 and 3, the properties of which are shown in Table 2.

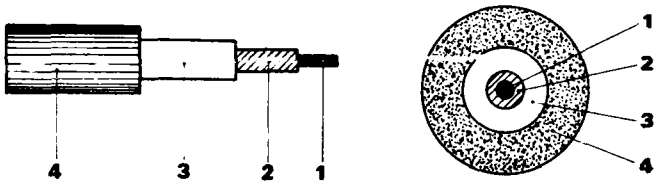

Figure 2 and 3:

1. **Optical fiber**
2. **Nylon coating**
3. **Aramid Yarns**
4. **Polyurethane jacket**

TABLE 2

CABLE PROPERTIES

	PROPERTY	UNIT	AVERAGE VALUE OBTAINED
MECHANICAL	Outer diameter, nominal	mm	3.0
	Weight	kg/km	8.0
	Bending radius	mm	30.0
	Tensile load	N	300
	Operating temperature	ºC	-20 to +70
TRANSMISSION	Fiber type		Single-mode
	Diameters core/clad	um	10/125
	Attenuation		
	λ = 1300 nm	dB/km	0.5
	λ = 1550 nm	dB/km	0.3
	Cromatic dispersion		
	λ = 1285 at 1300 nm	ps/km.nm	3.5
	λ = 1550 nm	ps/km.nm	20.0
	Numerical aperture	-	0.11

CONCLUSIONS

In view of the results shown, we can report that flame-retardant polyurethane is an ideal material for optical fiber indoor cables where suitable non-inflammable materials are required. The processability of this material, as well as its low financial cost make it feasible for optical-fiber cable manufacturers.

Although the studies were made on monomode fiber, no problem would be attached to using any other type of fiber, both monomode and multimode.

Of course, neither is there any problem attached to joining any optical connectors which may be required.

REFERENCES

1. P. Wright and A.P.C. Cumming, "Solid polyurethane elastomers", Maclaren and sons Ltd., London, 1969.

2. W.C. Kuryla and A.J. Papa, "Flame retardancy of Polimeric Materials", Marcel Dekker Inc, New York, 1973.

3. ASTM Standards.

4. Ellegast, K., Kallert, W. and Schultheir, H., "Preparation and Properties of Polyurethanes Elastomers" in Kunststoffe-Handbuch, Vol. 7. Eds. Viewig, R., and Hochtlen, A., Carl Hanser Verlag, Munich 1966.

SUSANA CAMARA received her Master Degree in Chemistry from Oviedo University in 1984, where she specialized in Organic Chemistry.

She joined ALCATEL STANDARD ELECTRICA in 1987 where she presently works in R & D Materials Department.

CARLOS G. CORTINES was born in 1944. In 1968 he graduated from Valladolid University with a Degree in Physics. He joined STANDARD ELECTRICA, ITT, today ALCATEL, and worked in the Engineering Department of the Telecommunication Cables Division. From 1982 he is the head of the Optical Fiber Development Group in ALCATEL STANDARD ELECTRICA, Cable Factory in Maliano-Cantabria.

CARLOS BLANCO received his Doctorate Degree in Telecommunications Engineering from Madrid University in 1972. He also received his Master Degree in Physics from Santander University in 1976. He joined ITT, STANDARD ELECTRICA in Spain in 1971 as R & D Manager of the Telephone Cable Division.

During 1982-1984 he joined ITT, ELECTRO OPTICAL PRODUCTS DIVISION in Roanoke, Virginia as Senior Scientist in the Optical Fiber R & D Department.

During 1987 he joined TELCOR (TELEFONICA CORNING GLASS) as Technical Director of the Optical Fiber Manufacturing Plant.

Since 1972 he has acted as part time Professor of the Electrical Engineering Department of the Santander University.

During 1983 he was nominated Adjunct Professor of the Electrical Engineering Department of the Virginia Politechnic Institute and State University, in Blacksburg, Virginia, lecturing on Optical Fibers and Optical Communications.

Presently, Dr. Blanco is with ALCATEL STANDARD ELECTRICA in Spain as Manager of the New Products Development Department.

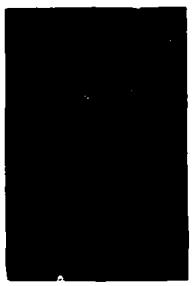

MIGUEL P. BUSTAMANTE received his Master Degree in Chemistry from Valladolid University in 1970, where he specialized in Industrial Chemistry.

He joined ALCATEL STANDARD ELECTRICA since 1971 in the Engineering Department of the Telecommunication Cable Division.

He is a member of the National Chemistry Association of Spain.

Presently, he is with ALCATEL STANDARD ELECTRICA in Spain as Manager of the Laboratory & Materials Development Department.

DEVELOPMENT OF SUPER RADIATION-RESISTANT CABLE

Kazumi Ito, Shin Yoshida, Fumio Aida, Enji Mada, Etsuo Hosokawa

Showa Electric Wire & Cable Co., Ltd. Kawasaki, Japan

ABSTRACT

With the advancement of the nuclear power industry, the construction of nuclear fuel recycling facilities is imperative. Since nuclear fuel recycling and related facilities contain much heavier radiation fields than nuclear power plants, the cables used in such facilities require extremely high radiation resistance. To meet this challenge, we have developed a new flame-retardant cable that retains sufficient flexibility even after exposure to doses of 10 MGy. This cable uses, as insulation, flame- retardant ethylene-propylene rubber which exhibits improved radiation resistance owing to special anti- radiation coagents. Further, it employs, as a sheath material, exceedingly radiation-resistant special thermoplastic urethane elastomer that has been modified through the addition of flame retardants and anti-radiation coagents.

INTRODUCTION

Nuclear fuel recycling and related facilities including radioactive waste disposal plants contain extremely heavy radioactive fields, so that high radiation resistance is required of systems and components used there. At present, the flame- retardant cables used in nuclear power plants are designed to maintain their ability to resist γ- irradiation of up to 2 MGy in terms of absorbed dose. Main materials of such cables, such as ethylene- propylene rubber (for insulation), chloroprene and chlorosulfonated polyethylene (for sheathes) [1] are degraded beyond use when exposed to radiation doses of more than 2 MGy. To overcome the disadvantages of these materials, we have not only improved the radiation resistance of ethylene propylene rubber by the addition of an anti-radiation coagent, but also selected a special urethane polymer as a sheath material in developing a super radiation-resistant cable. It is flame retardant and retains sufficient flexibility even after exposure to doses as high as 10 MGy.

This paper discusses the radiation resistance of different cable materials that have been screened to develop this cable and the effect of anti-radiation coagents used. Various tests including flexibility were also conducted to obtain corroborative evidence that this cable provides reliable service under various environmental conditions.

SELECTION OF MATERIALS

Base Polymers

With the increasing complexity of cable function, polymers as basic components of cables come in a great variety of kinds. Since the radiation resistance of these polymers depends largely on their chemical structures, much work has been done concerning this subject of inquiry. As a result, acceptable radiation doses for materials commonly used in such applications have been suggested [2]. Fig. 1 shows typical examples of such materials. As is clear from Fig. 1, ethylene- propylene rubber (EPR), chloroprene (CR), and chlorosulfonated polyethylene (CSM), currently used in cables for nuclear power plants, show relatively high radiation resistance. In order to select the base polymer for cables used in such places that have higher radiation hazards than conventional nuclear power plants do, typical polymer materials were investigated for radiation resistance. Seven kinds of polymers were tested for radiation resistance: ① cross-linked polyethylene (XLPE) and ② EPR for insulation, and ③ CSM, ④ thermoplastic urethane A (TPU-A), ⑤ TPU-B, ⑥ styrene butadiene rubber (SBR), and ⑦ acrylic rubber (AR) for sheathes.

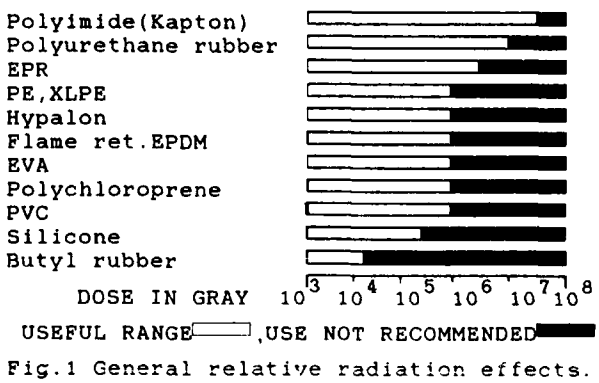

Fig.1 General relative radiation effects.

Specimens of these materials were pressed to a sheet 1 mm thick, and tensile tests were carried out after irradiation with γ-rays of cobalt 60 in the air. Fig. 2 indicates the test results, along with total doses computed, with a dose rate of about 15 KGy/h. *E/Eo* in Fig. 2 is the ratio of post-irradiation elongation (*E*) to original elongation (*Eo*) The results indicate that the materials which can be used at severe radiation doses as high as 10 MGy are EPR and TPU only. It was also found that the radiation resistance of TPU varies substantially with its polymer structure. This finding suggests that a slight modification of the polymer structure could have a considerable effect on the radiation resistance of materials.

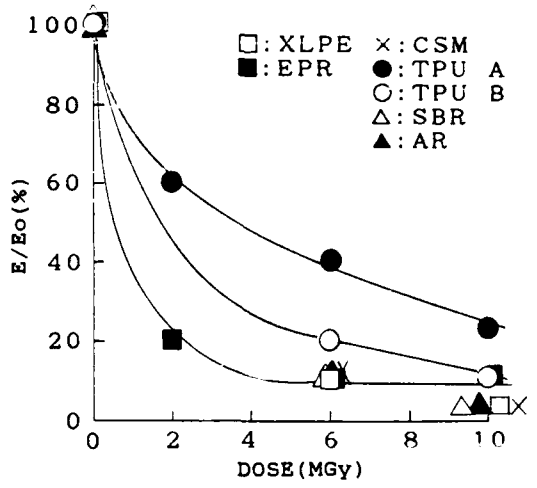

Fig.2 Dose effects on elongation at break.

Anti-radiation Coagent

As mentioned above, EPR and TPU which have superior radiation resistance to other kinds of cable materials are considered suitable for insulation and sheath materials, respectively. EPR retains the mechanical properties adequate to actual service even after the irradiation of 10 MGy. It has 20% retention to original elongation (70% as an absolute value) and 10% retention (35% ditto) at doses of 6 MGy and 10 MGy, respectively. However, if EPR is to be used as a cable component, its radiation resistance must be improved further. To achieve this objective, we attempted to improve the properties through the addition of anti-radiation coagents to EPR, a base polymer. For purposes of comparison, the effect on XLPE as a base polymer was also investigated. Four types of anti-radiation coagents were used: i.e., A-1) Amine antioxidant -1; A-2) Amine antioxidant -2; B) Benzophenon UV absorption coagent; and C) Benzotriazol UV absorption coagent. After irradiation at given doses, specimens with these anti-radiation coagents were subjected to tensile tests. The test results are presented in Fig. 3 and Fig. 4. These figures indicate that the addition of anti-radiation coagents will help moderate the tendency toward declines in percent elongation for both base polymers. The EPR has less reduction in percent elongation. This may be explained by the difference in radiation sensitivity between the base polymers themselves. The anti-radiation effect was more pronounced when EPR was used as a base material, and the specimens added with a UV absorption coagent had the percent elongation about twice obtained with no UV absorption coagent or with the addition of an antioxidant.

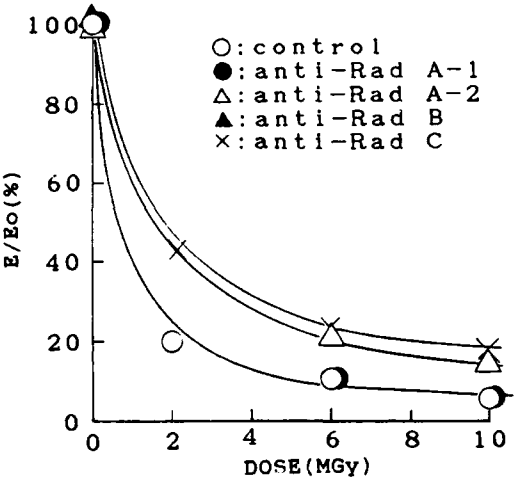

Fig.3 Anti-Rad effect on elongation of EPR

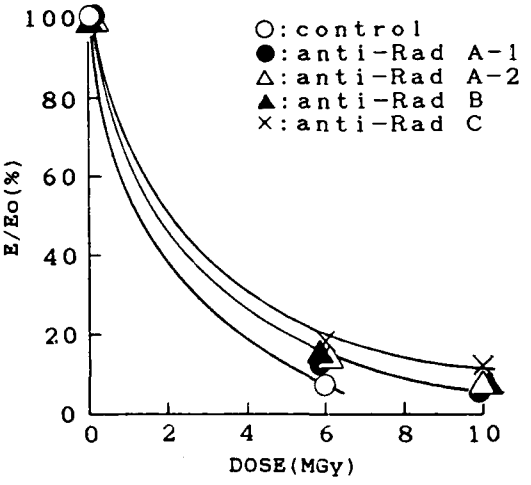

Fig.4 Anti-Rad effect on elongation of XLPE.

It has been known that much of degradation of a polymer by radiation is accounted for by oxidation [3]. In other words, when a polymer absorbs energy from radiation, oxidation occurs of itself, giving rise to alkyl-radicals and peroxi-radicals. These radicals act on the polymer in forming hydroperoxide. The hydroperoxide is decomposed to peroxi-radical and oxiradical again, thus promoting the degradation

of the polymer. Attempts were made in the present study to select suitable kinds of anti-radiation coagents from the standpoint of degradation prevention and energy absorption. The UV absorbing coagent exerts a greater effect than the antioxidant types, as shown in Fig. 3. The basic function of antioxidant is to capture active radicals, as shown in Eq. (1), thus providing the stability for auto-oxidation. On the other hand, the UV absorbing coagent absorbs energy of radiation rays through ring formation and releases it as heat energy, as shown in Eq. (2) Furthermore, the UV absorbing coagent helps decompose the peroxide to a more stable form. The results of the present study suggest that the energy absorption due to the aromatic structure by the UV absorbing coagent is more effective than the stabilization resulting from radical capture by the antioxidant. It should also be noted that whereas some anti-rads of the antioxidant type affected the degree of crosslinking and the electrical properties, the UV absorbing type was found having virtually no adverse effect on the physical properties.

$$R^{\cdot} + IH(AO^{*}) \rightarrow RH + I(\text{Non active})$$
$$ROO^{\cdot} + IH \rightarrow ROOH + I(\text{Non active}) \quad \text{Eq.(1)}$$

* Anti-oxidant

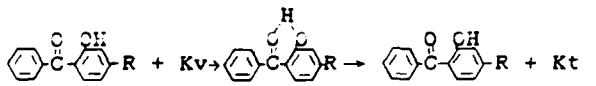

Eq.(2)

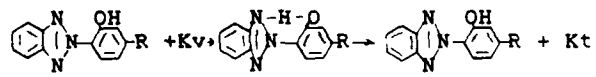

CABLE DESIGN

Component Materials

Insulation and Sheath Materials As is clear from the discussion above, it was found that EPR and TPU-A are suitable as base polymers for insulation and sheath, respectively and an anti-radiation coagent of the UV absorption type is ideal for obtaining excellent radiation resistance. When it comes to cable component materials, flame retardancy is no less essential than physical properties and radiation resistance. Since the oxygen index of TPU-A is 22, it still needs to have a much higher degree of flame retardancy to be an ideal material for a cable sheath. Commonly used flame retardants are not well miscible with TPU, thus posing such problems as improper dispersion, blooming, poor physical properties and low radiation resistance. As a result of our research, we have improved the flame retardancy of TPU (FR-TPU) without any compromise in physical or anti-radiation properties. Table 1 and Fig. 5 show its initial properties and radiation resistance characteristics, respectively.

TABLE 1 Initial properties of materials for sheath.

		TPU A	FR-TPU
Tensile strengh	kgf/mm²	6.4	3.2
Elongation	%	430	430
Hardness(A type)	-	82	83
Oxygen Index	-	22	31

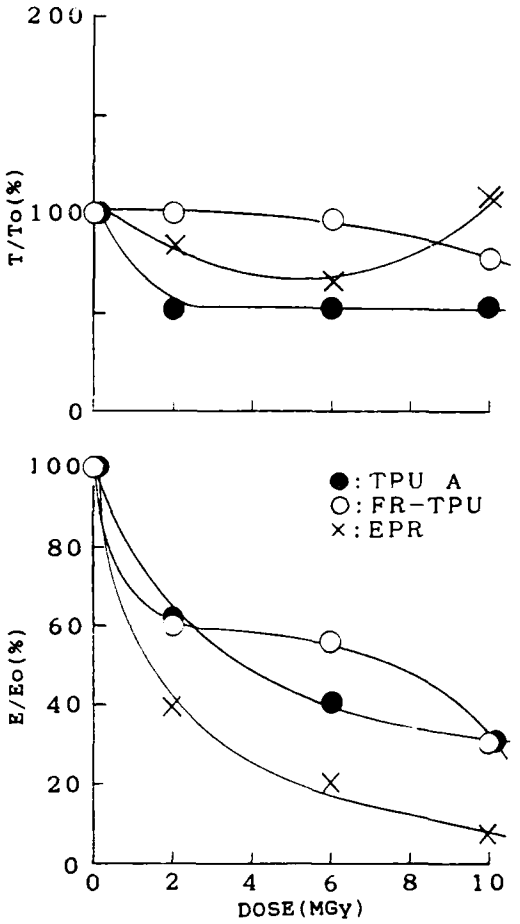

Fig.5 Dose effects on mechanical properties.

Other Components In order to improve the radiation resistance of a cable, not only insulation and sheath materials but also other materials such as binder tapes, fillers, and reinforcing tapes should be taken into account. For purposes of testing, the materials which are known to have good radiation resistance were selected to determine the effect of irradiation. Table 2 shows the test results.

Test Cable

The test cable was made using the most suitable materials in terms of radiation resistance and flexibility. Fig. 6 and Table 3 show a typical construction of the test cable and its initial properties, respectively.

TABLE 2 Radiation effects of other materials.

			Kevlar			PEEK			Kapton			Flame Cloth		
Size	W	mm	–			30			30			30		
	T	μm	–			50			50			50		
Dose		MGy	0	6	10	0	6	10	0	6	10	0	6	10
Tb		kgf/mm	–	–	–	9.5	9.6	8.6	23.6	22.5	24.8	3.1	1.6	1.0
Tb		kg f	70.4	66.8	60.3	–	–	–	–	–	–	–	–	–
Eb		%	18.0	16.4	17.5	83.5	95.8	75.2	29.5	24.7	36.3	7.7	2.3	1.4

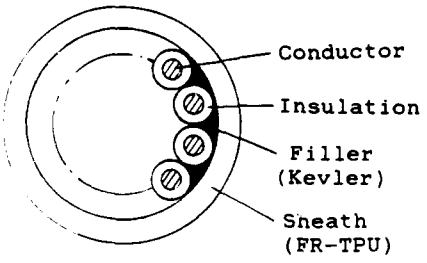

Fig.6 Construction of trial cable.

TABLE 3 Characteristics of new cable.

Conductor resistance	Ω/km	10
Insulation resistance	MΩkm	500
AC voltage test	v/min.	3000 OK
Insulation		
Modulus at 100%	kgf/mm²	0.23
Tensile strength	kgf/mm²	0.59
Elongation at break	%	620
AC breakdown test	kv	20
Sheath		
Modulus at 100%	kgf/mm²	0.23
Tensile strength	kgf/mm²	0.59
Elongation at break	%	620
Hardness(type A)	-	80
Brittleness temp.	°C	-50

EVALUATION OF TEST CABLE

Flame Retardancy

The flame resistance test was performed in accordance with IEEE std. 383 using a vertical tray. As is clear from Fig. 7 showing the test scene, the test cable exhibits such sufficient flame resistance that it meets the requirements in the IEEE standards.

Radiation Resistance

The test cable was wound in a bundle of 500 mm diameter, and irradiated with γ-rays at the specified dose. The dose rate used in this study was 8 KGy/h. After irradiation, general physical properties and flexibility were investigated. No abnormality was observed on the outer surface after irradiation up to 10 MGy.

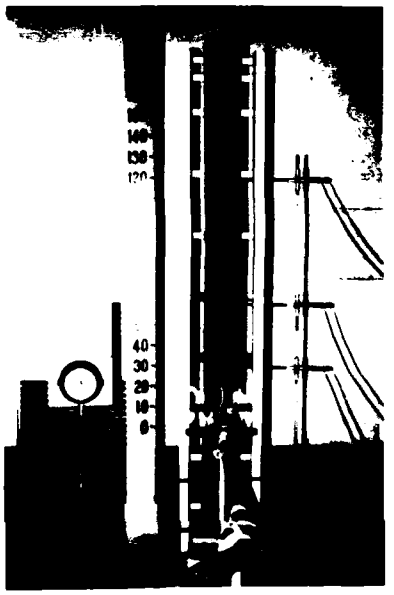

Fig.7 Flame test(IEEE std.383)

Physical Properties in General After irradiation with γ-rays at doses of 2, 6, and 10 MGy, the test cable was cut into test pieces to check the following physical properties.

(1) Tensile strength of insulation and sheath (see Fig. 8)

(2) Hardness of sheath (Durometer type A) (see Fig. 9)

(3) Short-term AC breakdown test (Fig. 10)

(4) Insulation winding test (Fig. 11)

As is obvious from the findings obtained in these tests, although the tensile elongation decreased to some extent with increasing dosage, the sheath hardness and the AC breakdown voltage showed only limited change, indicating that the cable has reasonably good properties. In the core winding test cracks occurred in winding of 2 and 2.5 times core's diameter when exposed to doses of 6 MGy and 10 MGy, respectively. On the other hand, in the cable winding test when wound around the mandrel of cable's own diameter, the cable remained intact after exposure to 10 MGy.

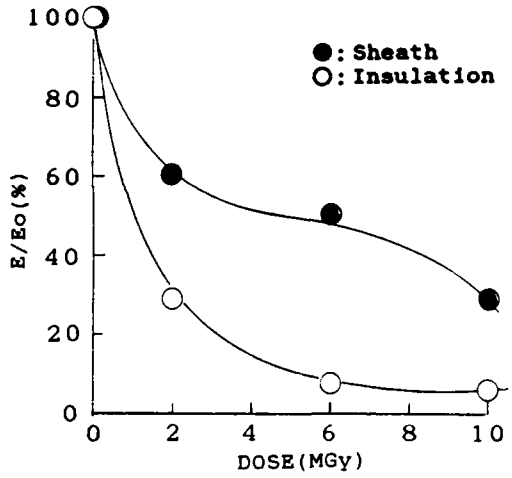

Fig.8 Dose effects on elongation of cable.

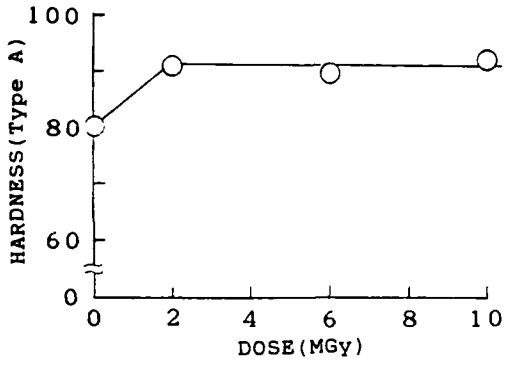

Fig.9 Dose effect on hardness of sheath.

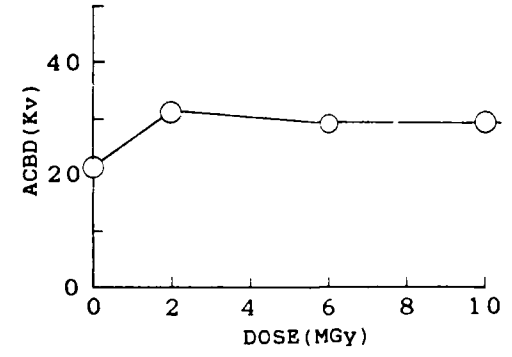

Fig.10 Dose effect on AC breakdown voltage of insulation.

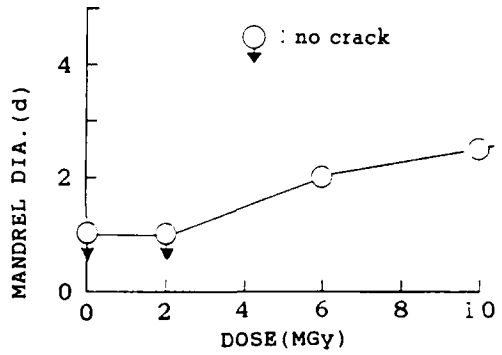

Fig.11 Dose effect on bending diameter on crack of insulation.

Flexibility Test It is an important consideration that a cable should retain its flexibility after irradiation and provide prolonged, trouble-free service in heavy radioactive fields. To determine the flexibility of a cable, the following three kinds of bending tests were conducted.

(1) Bending properties

The bending test was performed in accordance with JIS C 3005 29, then the test cable was carefully examined for inception of any cracks. Fig. 12 provides the outline of the test. In this test, the mandrel diameter was made six times larger the outer diameter of a cable. This is the minimum permissible bending radius for a mobile cable. The bending test was performed on two cables, one made of conventional materials (i.e., EPR as insulation/urethane as sheath) and another made of improved materials. The test results are presented in Fig. 13. After irradiation at a dose of 6 MGy, the conventional cable had a substantial reduction in flexibility. The newly developed cable, by contrast, suffered no loss of flexibility.

(2) U-bending test

In this test the cable was installed on the equipment shown in Fig. 14, and bent into a U-shape by moving up and down the plate on the moving side. It was then checked for failure or cracks in its sheath. Fig. 15 shows the test results. Unlike the conventional cable, the new one showed no loss of flexibility after exposure to doses of up to 6 MGy, and retained sufficient flexibility even when the dose was increased to 10 MGy.

(3) Reel-bending test

In this test the cable was installed on the equipment shown in Fig. 16, and reel winding was simulated over the small reel on the upper part of the equipment to find failure or cracks in its sheath. Fig. 17 shows the test results. It should be noted that prior to this reel-bending test the cable was subjected, after irradiation with γ-rays, to thermal degradation for five days at 105°C. The test results indicated that the

cable retained sufficient flexibility even under this extremely severe conditions.

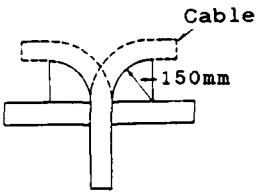

Fig.12 Method of bending test.

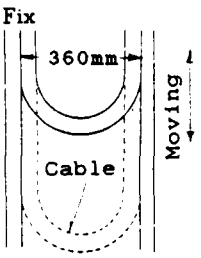

Fig.14 Method of U-bending test.

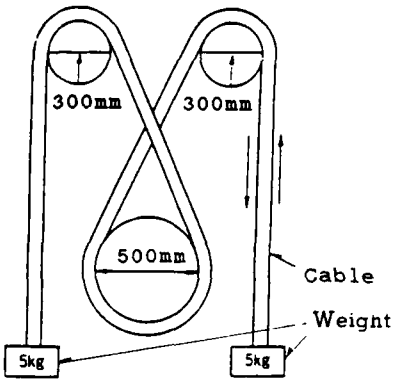

Fig.16 Method of reel bending test.

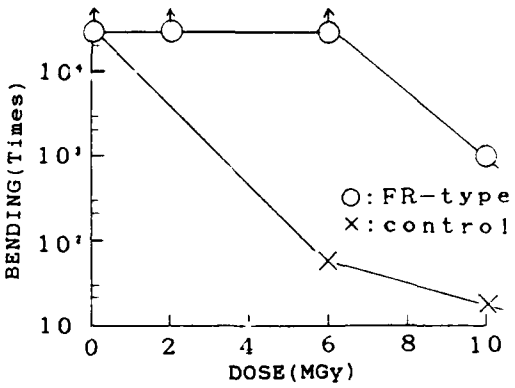

Fig.13 Bending test.

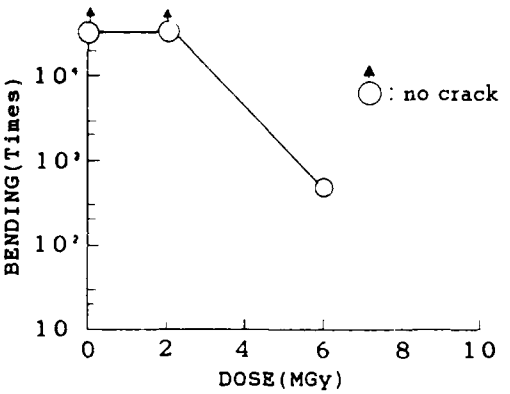

Fig.17 Reel bending test.

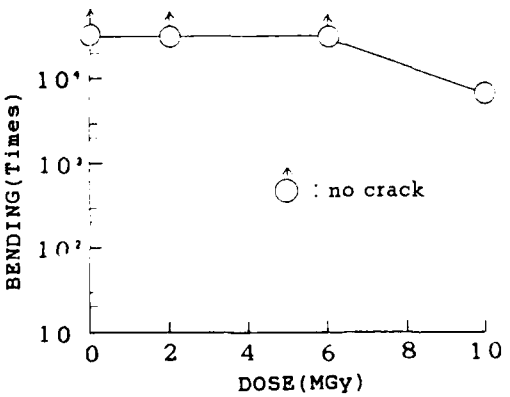

Fig.15 U-bending test.

Environmental Properties

In order to investigate potential application of this cable in light water reactor (LWR) power plants, environmental tests were performed using the profile shown in Fig. 18. Fig. 19 shows the scene of the LOCA (loss of coolant accident) simulation test that is in the final phase in the environmental test. The voltage endurance test was performed at the last stage of this test. After the cable was mounted on the mandrel, the specified voltage (2500 V) was applied in the water bath. Although slight damage such as swelling was found on the sheath, the cable withstood this voltage stress, showing no damage on its insulation layer. It is therefore suggested that it can be used for nuclear power plants.

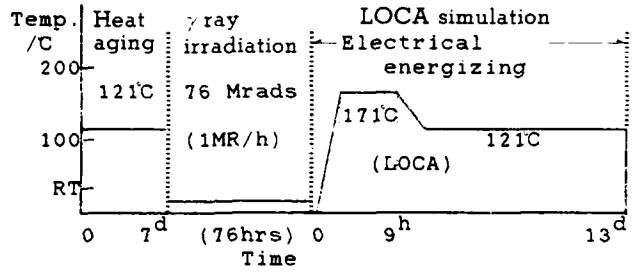

Fig.18 Sequential profile of environmental test.

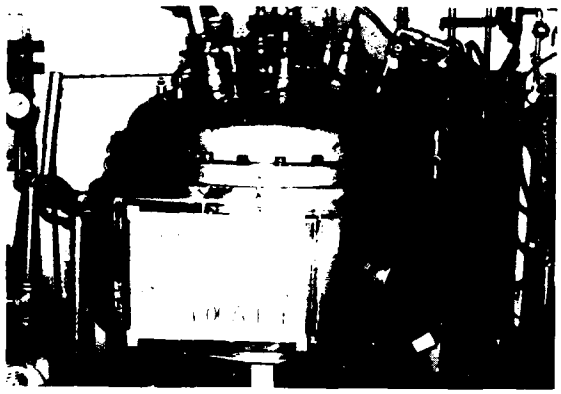

Fig.19 LOCA simulation test.

Summary

Our discussion has ranged from the selection of base polymers and anti-radiation coagents to the assessment of various kinds of cable. The findings obtained in this study are summarized below.

(1) The radiation tests were performed on seven kinds of polymers that are commonly considered to have good radiation resistance to doses of up to 10 MGy. The test results show that EPR and TPU alone can be subjected to post-irradiation tensile tests.

(2) The findings obtained with various types of anti- radiation coagents indicate that a UV absorbing coagent is most effective in imparting radiation resistance to EPR and TPU.

(3) The super radiation-resistant cable consisting of the radiation- and flame-resistant EPR insulation added with the anti-radiation coagent and the radiation- and flame-resistant urethane sheath exhibits no change in flexibility after irradiation at doses of up to 6 MGy, and may serve the purpose even when exposed to a dose of 10 MGy.

The results of our study provide evidence that the super radiation-resistant cable finds satisfactory use in applications that require high flexibility as in removal from site to site in radiation fields of 6 MGy or more and use with intelligent manipulators. Judging from its excellent characteristics, this cable is likely to find use in a variety of applications at sites of high radiation hazards.

Acknowledgements

The authors would like to thank Ms. T. Hasegawa and Mr. M. Yamada of Showa Wire and Cable Co., Ltd. for their assistance in this program.

REFERENCES

(1) P. Maier, A. Stolarz, CERN 83-08 (1983)

(2) P. Beynel, P. Maier and H. Schonbacher ***, CERN 82-10 (1982)

(3) Fukuji Kurihara, "Degradation of plastics" Daily Kogyo Shinbun Co.

Kazumi Ito
Showa Wire and Cable Co., Ltd.
2-1-1 Odasakae, Kawasaki, Japan

Mr Ito graduated from Suzuka College of Technology in 1973, where he majored in Industrial Chemistry. Then he joined Showa Wire and Cable Co., Ltd. and has been engaged in research and development of rubber and plastic materials for nuclear power cable.

Mr. Ito is now a member of the Research and Development Division of Showa Wire and Cable Co., Ltd.

Shin Yoshida
Showa Wire and Cable Co., Ltd.
2-1-1 Odasakae, Kawasaki, Japan

Shin Yoshida was born in 1960. He graduated from Nagoya University with a B.E. degree in synthetic chemistry in 1987. In the same year, he joined Showa Electric Wire and Cable Co., Ltd. and has been engaged in research and development of flame retardant cable and nuclear power plant cable.

Enji Mada
Showa Wire and Cable Co., Ltd.
4-1-1 Minamihashimoto, Sagamihara, Japan

Enji Mada was born in Beppu, Japan on 1946.

He received B.E. in Electrical Engineering from the Kyushu Institute of Technology in 1969.

He joined Showa Electric Wire & Cable Co., Ltd. in 1969 and has been engaged in the engineering of the insulated wires and cables.

He is a member of the Institute of Electrical engineers of Japan.

Fumio Aida
Showa Wire and Cable Co., Ltd.
2-1-1 Odasakae, Kawasaki, Japan

Fumio Aida was born in Tokyo, 1948. He received the B.S. degree in organic chemistry from Tokyo Metropolitan University in 1971.

Then, he joined Showa Electric Wire and Cable Company. His work has been in research and development of electrical insulating materials. Mr. Aida is a member of the Institute of Electrical Engineers of Japan.

Etsuo Hosokawa
Showa Wire and Cable Co., Ltd.
2-1-1 Odasakae, Kawasaki, Japan

Etsuo Hosokawa was born in Tokyo in 1935. He received the B.E. degree in chemical engineering from Yokohama National University in 1959.

Then he joined Showa Electric Wire and Cable Company. His work has been in research and development of insulation for magnet wires.

Currently he is a general manager of chemicals research department.

1-FIBER TACTICAL TETHER CABLE

Bernd D. Zimmermann
Dieter E. Kundis

Siecor Corporation
489 Siecor Park
Hickory, North Carolina 28603

ABSTRACT

The recent development of tactical platforms for reconnaissance and/or anti-armor purposes sponsored by the U.S. Army and Marine Corps have sparked needs for a single fiber, lightweight, small size, crush resistant optical fiber cable. This "tether" cable is to be used as a real time data link between the remotely guided platforms and their respective control consoles. The cable, to be payed off from these vehicle-like platforms, must be extremely rugged to allow proper operation during battlefield conditions. Passage of vehicles over the tether cable must not interrupt the signal transmission between the console and the vehicle. To meet these requirements an all-dielectric, 1.7 mm O.D., 3.1 kg/km cable was developed. It consists of a compositely-buffered 50 micron multimode fiber, stranded glass-reinforced polyester (GRP) rods, and a Nylon outer jacket. The cable shows negligible increases in attenuation across a -25°C to +80°C operating temperature range, superior crush performance in a simulated battlefield environment, and excellent bending performance.

1. INTRODUCTION

To date several types of fiber optic cables have been developed for tactical deployment applications. Most of these custom designed cables, however, were intended for dual channel transmission (i.e., 2 fibers) and did not require stringent size and weight characteristics [1, 2]. The outer diameter and weight of these cables have usually been on the order of 6 mm and 32 kg/km respectively. These cables are extremely rugged, but are not suitable for small size, mobile, tactical platforms [3, 4]. Such platforms require long length (4 - 30 km), single fiber cables, small enough to be spooled on light-weight, portable reels and light enough to be easily transported. Size and weight requirements for such cables in the order of 1.5 mm and 3.0 kg/km respectively, are not uncommon. Furthermore, the cables are to withstand the physical abuse typically encountered in tactical environments. This includes severe localized lateral loads due to heavy objects passing across the cable during deployment, operation, or retrieval. This paper will discuss the requirements, the cable design which attempts to meet these requirements, and testing results of prototype cables.

2. CABLE REQUIREMENTS

The requirements of a particular tele-operated vehicle manufacturer were used as initial design guidelines for this cable. Other similar applications may require different performance levels on specific cable characteristics. However, the overall design which evolved from these requirements should satisfy the needs of most tactical tele-operated vehicles. Important to note are the extremely low cable outer diameter (1.5 mm) and weight (3.0 kg/km) requirements. A specific requirement for resistance to lateral, localized loading was not included in these specifications, but was understood to be one of the most crucial characteristics of the cable. Other pertinent requirements include a small minimum bend radius (25 mm) which might be seen by the cable as it is payed off or retrieved across multiple sets of mandrels. The preliminary target requirements are summarized in Table 1.

3. CABLE DEVELOPMENT

The 1-fiber tactical tether cable was designed around the requirements in Table 1 knowing that cable outer diameter and weight characteristics might have to be sacrificed to achieve the all-important local crush resistance. Flame retardance was determined to be a secondary requirement which would be adressed in the future. Standard tight buffer cable designs (tightly buffered fiber, tensile yarns, outer jacket) could easily be processed and manufactured to meet the O.D. and weight requirements, but are known not to be very resistant to local crush. This fact is demonstrated in a later part of this paper, where different cable types were compared with respect to their resistance to these kinds of crushing forces. Cables which have shown extreme local crush resistance include single fiber undersea cables consisting of a compositely-buffered fiber, an "armor" of steel wires, and an abrasion-resistant outer jacket [5]. The steel wires which are stranded around the composite buffer have been found to form a protective shell around the fiber. The only drawback to these types of cables for tactical tether applications is their excessive weight. Even when their outer diameter is reduced to the required 1.5 mm, the weight of such cables is still 6.0 kg/km. Such a cable was manufactured and showed excellent performance during temperature cycling (<0.15 dB/km increases in attenuation from -25° to +80°C for SMF at 1550 nm). The cable also withstood 5000 N/cm loads in a modified crush test without experiencing any power losses. However, an alternate design approach was necessary to reduce the cable weight.

It was stipulated that not only the "shell effect" but also the "effective flexural modulus" of the cable played a roll in the cable's resistance to lateral, localized forces. Standard tight buffer cables lack both shell strength and possess low flexural modulus, and, have thus failed when exposed to real life field testing. Passage of HMMV type trucks over these cables on a gravel road resulted in fiber breakage and/or high (>10 dB) increases in attenuation. It was therefore necessary to design a cable which included light-weight strength members which could be stranded over the fiber without inducing attenuation increases, and which would provide shell strength and increase the effective flexural modulus. The strength members chosen consisted of Glass Reinforced Polyester (GRP) rods which have a flexural modulus of approximately 50,000 N/mm^2 and specific weight of 2.1 g/cm^3. This compares to the values of 190,000 N/mm^2 and 8.0 g/cm^3 for stainless steel. It was therefore anticipated that the cable would not be as strong as the steel wire cable, but would, on the other hand, show a drastic weight reduction.

As is the case with some of the above-mentioned undersea cables, the fiber buffering scheme of the new design was also based on a composite buffer. The buffer material was a tough, abrasion-resistant polyetherimide which would provide enough strength as a buffer when extruded with an extremely thin wall to an outer diameter of 0.54 mm. Notice that this is only 40 microns larger than the outer diameter of a typical, unbuffered 500 μm type fiber. The fiber was mechanically isolated from the buffer with a film of filling compound. This allowed stranding of the strength members directly over the buffer without inducing microbending losses in the fiber. Tolerances on the outer diameter of the composite buffer were held tightly to achieve the "shell" protection from the GRP rods. Furthermore, the outer nylon jacket would be pressure-extruded over the GRP rods to further enhance fiber protection. Minimal rod movement is allowed in this format during exposure to different types of mechanical abuse. The nominal outer diameter of the developed cable was 1.7 mm, slightly over the required 1.5 mm. The cable weight was 3.1 kg/km, 0.1 kg/km over the target. The cable cross-section is shown in Figure 1.

4. CABLE PERFORMANCE

The performance of the newly designed 1-fiber tactical tether cable was determined after rigorous environmental and mechanical testing of the cable and cable assembly (connectorized with ST compatible connectors). The test program included temperature cycling and testing for cable impact, flex, twist bend, modified crush, tensile and hot/cold bend performance. Connectorization losses and connector strength were measured on terminated samples. The test conditions and results are summarized in Table 2. Specifics were as follows:

- *Temperature Cycling:*
  A 3.5 km sample was temperature cycled from -25°C to +80°C at 1300 nm with overfilled launch conditions. 8 hour conditioning and 6 hour ramp times were used. The 50 micron fiber showed maximum increases in attenuation of 0.13 dB/km with an attenuation at room temperature of 2.42 (0.75) dB/km at 850 (1300) nm. No residual increases in attenuation were seen after five complete cycles (see Figure 2).

- *Cable Impact:*
  Samples were tested according to FOTP-25 with a 0.5 kg load being dropped from a 75 mm height. The fiber broke at an average (worst case) of 58 (28) cycles.

- *Cable Cyclic Flex:*
  Samples were tested according to FOTP-104 with a 2.0 kg load and a 25 mm bend radius. No damage was observed after 2000+ cycles and no changes in power occurred during testing.

- *Cable Twist Bend:*
  Samples were tested according to FOTP-91 with a 3.0 kg load and a 50 mm mandrel diameter. No damage was seen after 2000+ cycles and power levels during testing remained constant.

- *Modified Cable Crush:*
  A modified crush test was developed to simulate the localized lateral loads the cable could encounter in battlefield conditions. The test (see Figure 3) consisted of placing the cable samples across an ASTM #10 mesh sieve (simulating a gravel surface) and applying the crushing force with a padded steel plate (simulating the tire of a vehicle passing over the cable). The padding consisted of tire stock samples. Power was monitored as the crushing force was increased to 5,000 N/cm. At that load the 1-fiber tactical tether cable showed an average increase in attenuation of 3.4 dB. The average increase in attenuation for a standard 2.4 mm tight buffer cable was measured at 11.5 dB (see Figure 4). The steel wire undersea cable showed no significant increases in attenuation up to the maximum load.

- *Cable Tensile:*
  Cable Samples were tested for tensile performance according to FOTP-33. A maximum load of 150 N was applied while power, fiber strain, and cable strain were monitored. No attenuation increases were seen up to maximum load, and cable strain remained below 0.28%. The maximum short term load may be increased to 300 N if 100 Kpsi proof tested fibers are used in the design.

- *Cable Hot/Cold Bend:*
  Cable samples were tested at -25°C and 80°C for bending performance according to FOTP-37. A 50 mm diameter mandrel and 5 kg load were used for the test. After 4 hours of conditioning, the samples were wound across the mandrel over 10 turns, while power was monitored. A maximum increase of 0.62 dB at low and 0.69 dB at high temperatures respectively was observed. No residual power losses nor cable damage was noted after testing.

- *Cable Connectorization:*
  The cable was terminated with standard ST compatible connectors and showed a standard deviation/average excess loss of 0.021/0.036 dB 1300 nm per mated pair and withstood an average 110 N pull strength. The terminated cable is shown in Figure 5.

The cable without connector showing cable components is shown in Figure 6.

5. CONCLUSIONS/SUMMARY

A 1-fiber tactical tether cable has been developed for remotely controlled reconnaissance/anti-armor vehicles. The 1.7 mm O.D., 3.1 kg/km cable has exhibited excellent performance during environmental and mechanical testing. Using a 50 micron multimode fiber, the cable showed negligible increases in attenuation across a -25° to +80°C temperature range. Similar environmental performance is expected for single mode fibers. The cable also showed superior performance in all bending and flexing tests, where the cable was exposed to the minimum bend radius (25 mm) of the fiber. Modified crush testing indicates that the newly developed tether cable will outperform standard tight buffer type cables when exposed to localized lateral loads. Connectorization of the developed cable using ST compatible connectors is standard.

6. REFERENCES

[1] B. V. Darden et al, "Single Mode Tactical Fiber Optic Cable Assemblies", 1987 International Wire & Cable Symposium (IWCS) Proceedings, pp. 108 - 115.

[2] DOD-C-85045/8 (CR), "Military Specification Sheet: Cable, Fiber Optic, Ruggedized, Radiation Hardened (Metric)", July 15, 1987 Revision.

[3] G. Chamberlain, "Robot Warriors", Design News (Sept.'87), pp. 116 - 120.

[4] F. Quan, "The Fibered Battlefield", Laser Focus/Electro Optics (Aug. '87), pp. 102 - 106.

[5] Hydro Products,"Design Performance and Test Acceptance Specification: Ariadne Ocean Test Bed Production Cable (Reference SIECOR)", Nov. 19, 1985.

7. ACKNOWLEDGEMENTS

The authors acknowledge the help of all personnel involved with processing (M. Sigmon + Team) and testing (A. Garg + Team) of cable samples. Diane Kerley's help with the preparation of this manuscript is also greatly appreciated.

1-Fiber Tactical Tether Cable

Requirements

Fiber Type	50/125, Graded Index, 0.23 NA, < 4.0 (1.7) dB/Km at 850 (1300) nm.
Cable O. D.	1.5 +/- 0.1 mm
Cable Weight	< 3 Kg/Km
Connectors	ST compatible, < 1.0 dB pair loss
Cable Length	4 - 7 Km
Operating Temp.	-15 to +80 C
Flammability	DOD-STD-1678, Method 5010
Tensile Rating	320 N (short term)
Min. Bend Radius	25 mm (short term) 51 mm (long term)

TABLE 1

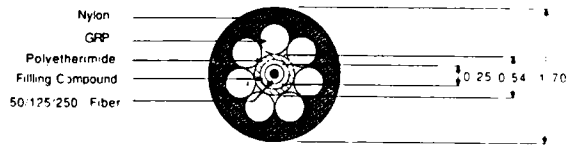

NOTE: All Dimensions in mm.

Figure 1: Cross-section of 1-Fiber Tactical Tether Cable

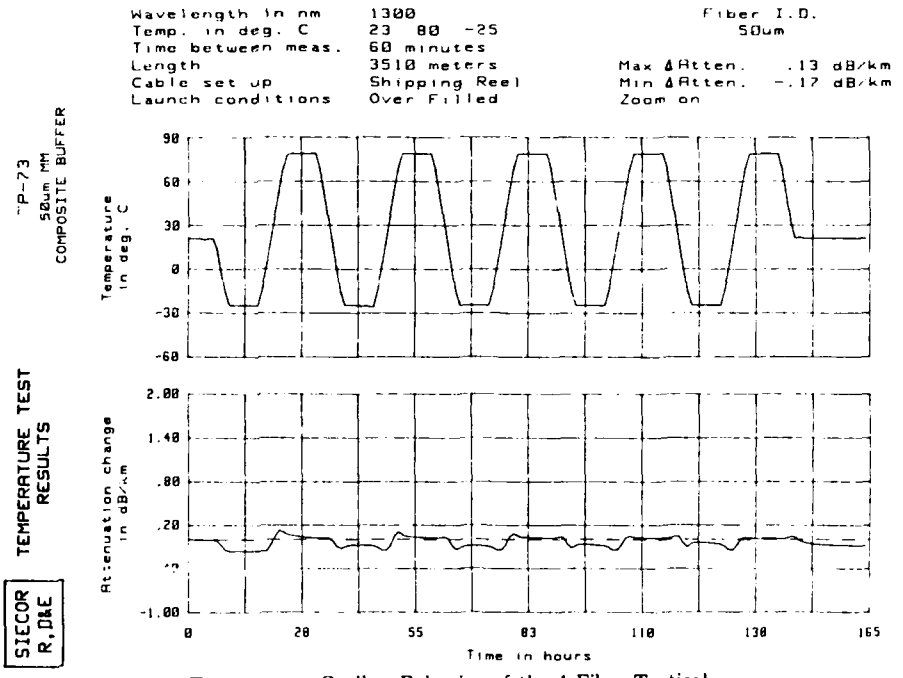

Figure 2: Temperature Cycling Behavior of the 1-Fiber Tactical Tether Cable

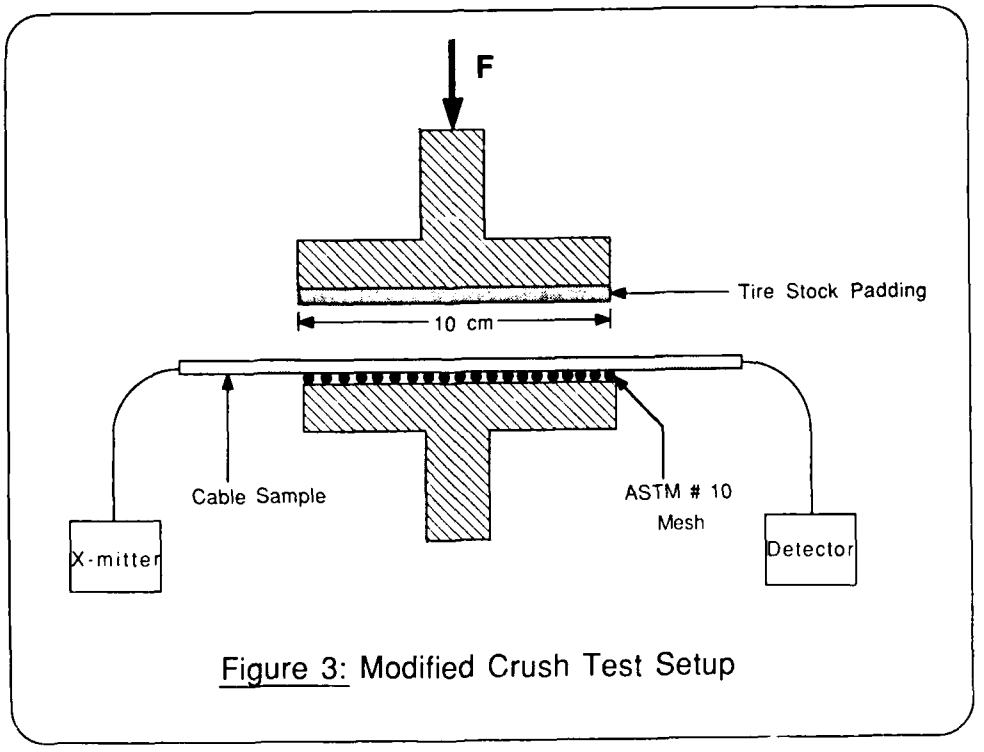

Figure 3: Modified Crush Test Setup

Figure 4: Modified Crush Test Results

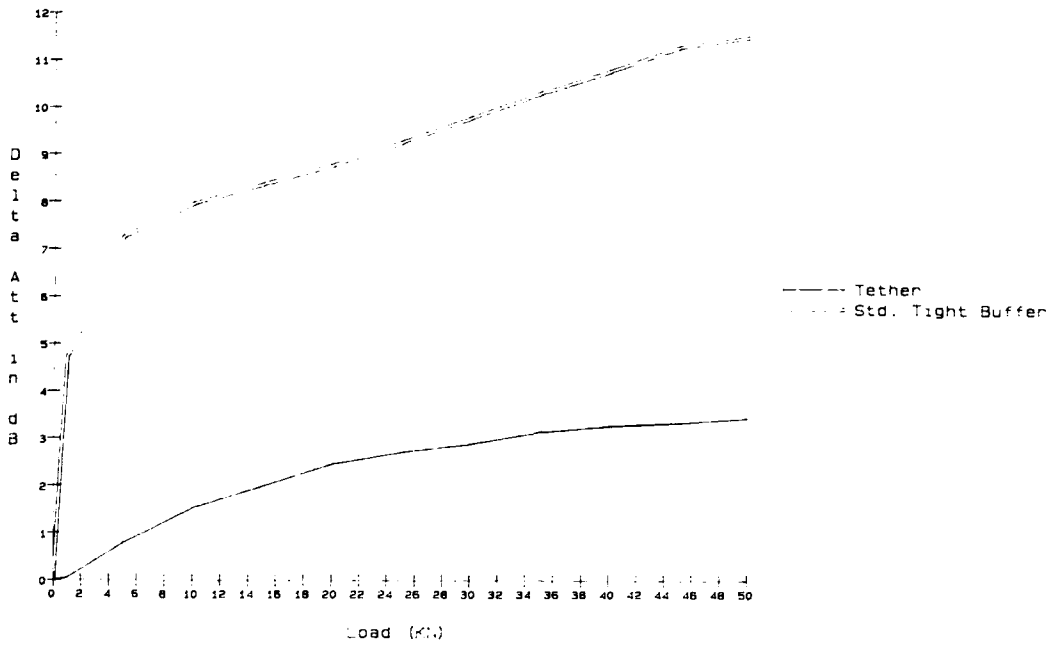

Figure 5: Connectorized 1-Fiber Tactical Tether Cable

Figure 6: 1-Fiber Tactical Tether Cable

1-Fiber Tactical Tether Cable:

Performance Summary

Temperature Range	-25 to + 80 C
Max Delta Attenuation	0.13 dB/km
R. T. Attenuation	2.42 (0.75) dB/km @ 850 (1300) nm
Nominal Cable O.D.	1.7 mm
Cable Weight	3.1 kg/km
Impact Resistance	M = 0.5 kg, H = 75 mm, > 28 cycles
Cyclic Flex	M = 2.0 kg, R = 25 mm, > 2000 cycles
Twist Bend	M = 3.0 kg, D = 50 mm, >2000 cycles
Modified Crush	< 3.4 dB Power Loss at 5000 N/cm
Tensile	L = 150 N, < 0.28 % strain, < 0.04 dB loss
Hot/Cold Bend	N = 10 turns, < 0.69 (0.62) dB loss
Connector Strength	110 N (t < 1 min)
Connector Loss	< 0.036 dB @ 1300 nm per mated pair

TABLE 2

Bernd D. Zimmermann
Virginia Polytechnic
Institute & State Univ.
Dept. of Electrical
Engineering
Blacksburg, VA 24061

Bernd D. Zimmermann was born in Lima/Peru in 1964. He holds a Bachelor's Degree in Electrical Engineering from Georgia Institute of Technology (1984) and a Master's Degree in Electrical Engineering from Virginia Polytechnic Institute & State University (VPI&SU, 1987). After working in the fiber optics field for three years, he is continuing with his graduate studies towards the PhD degree in Electrical Engineering at VPI&SU.

Dieter E. Kundis
Siecor Corporation
489 Siecor Park
Hickory, NC 28603

Dieter E. Kundis was born in 1959 in Munich, West Germany. In 1974 he graduated from High School and entered a 3 year apprenticeship as a Mechanical Technician at Siemens AG, Munich, West Germany. He received his degree in Mechanical Engineering from the Industrie- und Handelskammer in Munich in 1985. In 1977 he joined the Fiber Optic Cable Development Group at Siemens AG. In 1987 he came to Siecor Corporation where he is a Process Specialist.

LONG LENGTH MINIATURE OPTICAL FIBER CORD

Eric L. Buckland , P. Stephen Keith and John C. Rosko*

Sumitomo Electric Fiber Optics Corporation
Research Triangle Park, North Carolina, 27709

ABSTRACT

A long length miniature singlemode optical fiber cord has been developed for use in ground to ground and ground to air telerobotic systems. This cord was designed specifically to meet the requirements for use as a tether to a operations vehicle which is to be remotely controlled via video and data transfer over the optical fiber. Singlemode, tight buffer fiber is used for high bandwidth communications, providing excellent micro- and macro bend resistance. Aramid yarn strength members and a polyurethane jacket provide a high strength system in a compact and lightweight package (O.D. 2.1 mm, weight 5.2 kg/km) Rugged performance of the cord is verified through mechanical and environmental tests.

I. INTRODUCTION

A singlemode optical fiber cord has been developed for use in tactical applications such as military ground to ground and ground to air telerobotics. The cord is designed for use at either the 1.3 μm or 1.55 μm operating windows for singlemode fiber. The higher bandwidth of singlemode fibers over multimode counterparts allows for transmission of video as well as other voice or data signals.

Structurally, the cable was designed to exhibit low loss over long lengths, greater than 5 km. Its high strength design, including aramid yarn strength members and a durable jacket material is suitable for rugged applications. The cord has the added feature of exceptionally small size, less than 2.11 mm, and low weight, (5.2 kg/km).

This paper will detail design aspects of this cord, including fiber design, fiber coating, use of strength members and jacket material selection. Cord performance is verified through a battery of mechanical and environmental tests.

II. DESIGN

The cord was designed to be light weight, small in size and very strong and rugged for use in conditions requiring payoffs of long lengths of cable under difficult conditions. The basic design consists of a tight buffered singlemode fiber surrounded by aramid fiber strength members, and jacketed with a tough polyurethane coat to 2.11 mm, as shown below in Figure 1.

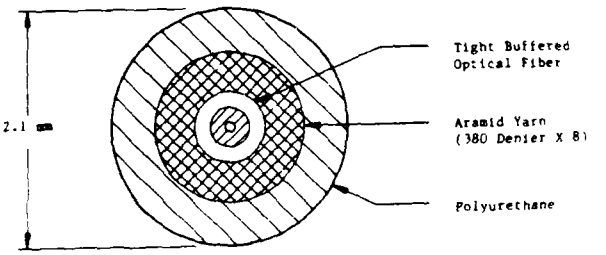

FIGURE 1. Miniature Optical Fiber Cord

A. Fiber selection

Singlemode fibers were chosen for this cord application because of the low optical loss and high bandwidth for video communications. In light of the potential abuse to the cord, the fiber needed to exhibit excellent bend resistance and

high tensile strength. The minimum optical requirements for the fiber are in Table 1.

Mode field Diameter	10 +- 1 μm
Cutoff wavelength	1190 to 1310 nm
Max. Attenuation	
@1300 nm	0.70 dB/km
@1550 nm	0.45 dB/km
Max. Dispersion	
@1300 nm	3.5 ps/nm/km
@1550 nm	25.0 ps/nm/km
Core/clad offset	< 1.0 μm
Proof test	100 kpsi

TABLE 1. Minimum fiber performance requirements

Small mode field diameter fibers (MFD = 9.0 μm nominal) were selected for optimum bending loss performance. A nylon jacketed tight buffer configuration was used for the fiber coating. This system provides good microbend resistance and low temperature performance.

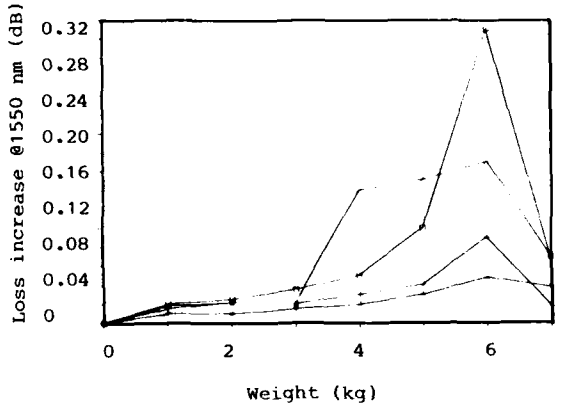

FIGURE 2. Microbend Resistance of Tight Buffer fibers

A selection of tight buffered fibers selected for cording was tested for microbend resistance using 36 grit sandpaper. Figure 2 shows loss increase at 1.55 μm as a function of applied load. The maximum loss increase under a 20 kg load was 0.32 dB. Residual loss after load removal was under 0.1 dB for all samples.

The same fiber set was subjected to a severe temperature cycle and monitored at 1.55 μm. The test regimen included three cycles with temperatures of 20C, -40C and +70C. The soak time at each temperature was at least two hours. Figure 3 is a plot of loss increase versus time and temperature. Even at -40C, maximum loss increase at 1.55 μm did not exceed 0.10 dB/km.

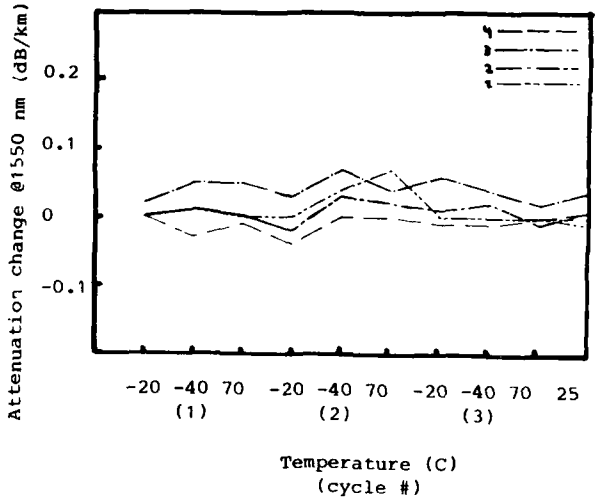

FIGURE 3. Temperature Cycling of Tight Buffer Fibers

B. Strength elements

To provide tensile strength to the cord structure, 8 strands of 380 denier aramid yarn were applied circumferentially around the fiber parallel to the fiber axis during the jacketing process. The ultimate tensile strength (UTS) of the yarns is 128 lbs (570 N).. The maximum elongation at break is 2.4%.

In order to decouple the cable elements and insure that the applied load is carried exclusively by the aramid yarns, the yarns were impregnated with a lubricating agent. Several flooding compounds were evaluated and a silicon oil compatible with the materials and existing equipment was selected for this application.

Payoff tension of the aramid yarns was initially high (450 gms) during processing trials. This was expected to equalize strain in the yarns and maintain a high system tensile strength. However, self-abrasion of the yarns at this tension was too high and resulted in reduced strength. Payoff tension was reduced and the resultant tensile strength was greater than 100 lbs (445 N), better than 81% of the design.

C. Outer jacket

The outer jacket material selected was a polyether-polyurethane compound, selected for its toughness and abrasion resistance. Pressure extrusion was desirable from the point of view of maintaining circularity of the cord and maintaining tight diameter tolerances. However, the pressure extrusion process over the soft core was found to cause shifting of the aramid yarns such that the optical fiber was not fully protected. This was abandoned in favor of a tubing set-up with excellent results.

Diameter control of the jacket was maintained at 2.11 mm to a tolerance of 0.05mm. Even with the tubed extrusion, the jacket formed a tight fit around the core, preventing any fiber kinking due to migration.

III. CABLE TYPE TESTING

TEST	GOAL
Impact	.25kg/150mm 100 strikes
Compressive Resistance	1,000 lbs. (4,454 N)
Cyclic Flex	20,000 cycles
Tensile strength	> 100 lbs (445 N)
Temperature Dependence of Attenuation	-30 C to +65 C

TABLE 2. Cord type test items

Once proper processing conditions were established, production length cords greater than 5 km were manufactured. In order to verify that design targets of cable performance were maintained during manufacturing, the cord was subjected to a battery of mechanical tests. Tests were conducted according to industry standards (EIA, DOD-STD 1678). A list of test items and performance goals is given above in Table 2.

A. Impact testing

The goal for the cord during impact testing was to maintain optical continuity after repeated strikes from a weight dropped onto the sample. The test apparatus consisted of a weighted hammer lifted to the desired height and released. The contact plate was a cylinder with a 1/2" radius of curvature for controlled transfer of energy from the hammer to the cord.

Ten samples were tested , five each using a 0.25 kg and 0.50 kg mass dropped from a height of 150 mm. At 0.25kg, 3 of the five tests experienced no fiber breakage or other power loss during 100 strikes. The remaining two samples withstood 60 and 70 strikes before fiber breakage.

With the 0.50 kg mass, all five samples maintained continuity for a minimum of 22 strikes. One sample resisted damage for the full 100 strikes.

B. Compressive resistance

The cord was subjected to compression testing between 10 cm plates using an Instron 4206 tensile/compressive loading machine. The load was applied at a rate of 2mm/min. Attenuation at 1.3 μm was monitored through the test. At the design limit of 1000 lbs. (4454 N), attenuation increased less than 0.05 dB. The load was increased to a maximum of 3300 lbs. (15000 N) Even at maximum load, the maximum increase in attenuation was 0.32 dB. There was full recovery upon release of load. Loss increase as a function of load is graphed in Figure 4.

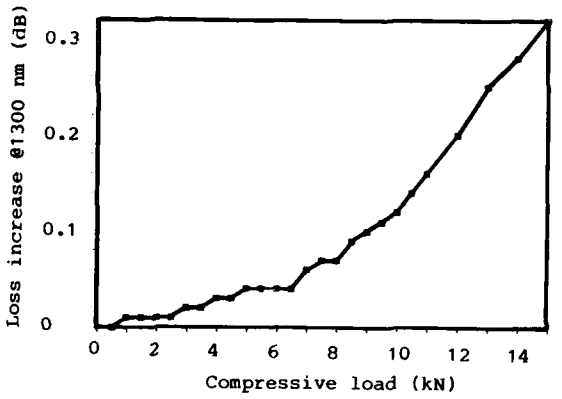

FIGURE 4. Compressive Resistance of Miniature Fiber Optic Cord

C. Cyclic flex

The cord was cycled 20,000 times at 30 cycles/min around 229 mm sheaves with no optical or physical damage.

D. Tensile Strength

Tensile strength was measured through processing trials to establish manufacturing conditions for the aramid fiber payoffs and again as a finished cable once optimum conditions were established. The Instron tensile machine was used for the testing with modified grips designed to eliminate damage to the cord as a result of improperly securing the cable for testing. The cord was wrapped around two 3" steel mandrels as shown in fig. so that a double strand of cord was tested. Friction between the cord and mandrels prevented the cord from slipping and provided repeatable test conditions. The break load was determined to be one-half the test load at which the fiber broke.

It is interesting first to note the effect of payoff conditions on ultimate cable strength. It was originally believed that higher payoff tensions were preferable from strength considerations. However, this proved not to be the case. Figure 5 shows the resulting cable strength versus payoff tension for a number of samples.

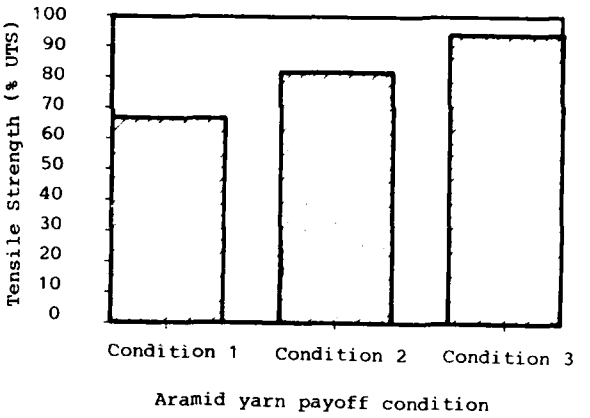

FIGURE 5. Cable strength versus processing conditions.

Cable strength as a percentage of Ultimate Tensile Strength (UTS) of aramid fibers.

Condition 1: 450 gram payoff tension trial 4 samples

Condition 2: 250 gram payoff tension trial 4 samples

Condition 3: 250 gram payoff tension production optimized 12 samples.

From the above results, the 250 gm payoff tension was chosen. The final cable strength after optimizing processing conditions was 120 lbs, (535 N) very nearly realizing the full potential of the aramid yarns.

E. Temperature Dependence of Attenuation

The cord was tested for attenuation change through the range -30 C to +65 C. Loss increase at 1300 nm was maintained below 0.10 db/km throughout this range.

IV. CONCLUSION

A small diameter cord designed to perform well under the strenuous conditions of tactical applications has been developed and manufactured in continuous long lengths greater than 5 km. The cord utilized singlemode fiber for high bandwidth communications. The fiber exhibits the superior bend resistance and high strength necessary for the application. Aramid yarn impregnated with a silicon oil lubricant was used for strength. An abrasion resistant polyurethane jacket was extrude above the fiber and yarn , maintaining a round concentric cord of just 2.11 mm. Proper tooling and processing allowed for full realization of the strength potential of this product. Type testing

of the manufactured cord demonstrates the rugged design of the cable with regard to impact and crush resistance and high tensile strength. This cord design should find use wherever a small, lightweight yet very durable fiber optic cord is desirable.

Eric L. Buckland obtained his B.S. degree in Physics in 1985 from North Carolina State University, where he is working part-time towards a Master's degree. Since joining Sumitomo Electric Fiber Optics Corp. in 1985, he has been engaged in the research and development of optical fibers and cables. He is currently involved with the development of all-dielectric self-supporting cables, singlemode fiber design and test method development. Mr. Buckland is a member of the Optical Society of America.

P. Stephen Keith graduated from Georgia Institute of Technology in 1968 with a B.S. degree in Physics and later did graduate work in Metallurgy at the same institution. His career has been in the wire and cable industry, previously being involved in materials development and the design and manufacturing of multi-conductor telephone and instrumentation cable. Prior to joining the Design Department of Sumitomo Electric Fiber Optics Corp. in 1986, Mr. Keith was associated with Superior Cable Corp. and National Wire and Cable Corp. He is presently Senior Process Engineer at Sumitomo Electric.

(Photo unavailable at this time)

John C. Rosko graduated with a BSEE from Union College in Schenectady, NY in 1974. He has held numerous positions in the cable industry including Times Wire and Cable co., Siecor Corporation, Phalo Corporation, and Sumitomo Electric Fiber Optics Corp. He is a member of the IEEE.

* Currently Mr. Rosko is Chief Engineer at Communications Cable, Inc. in Siler City, NC, where he is engaged in the development of electronic cable for data communication.

DESIGN AND PERFORMANCE OF TELECOMMUNICATION CABLES OPTIMIZED FOR LOW FIBER COUNTS

Martin C. Light, James A. Moses
Mark A. Sigmon, Christopher A. Story

Siecor Corporation - R,D&E, 489 Siecor Park
Hickory, NC 28603-0489

ABSTRACT

Until recently, fiber optic cables for outside environments typically used a common design for fiber counts ranging from 2 to 132. Recently, work was undertaken to design cables specifically for low fiber count applications, which offers the opportunity to design lightweight, compact cables with enhanced ease of installation.

An approach that has proven to be successful for low fiber count cables is the loose tube design, with the buffer tube positioned longitudinally in the cable surrounded by strength members and sheath. Important design parameters include the properties of the filling compound, the type and effectiveness of antibuckling elements, and the control of excess fiber length (EFL). These design parameters and their interactions are discussed here. In addition, a test method for determining the actual longitudinal cable shrinkage at low temperatures is presented.

Two experimental cables were produced and the mechanical and environmental performance was evaluated. The performance of these cables demonstrates the success of the design approach.

1.0 INTRODUCTION

Fiber optic cables for low fiber counts offer unique challenges to the cable designer. An attractive alternative for low fiber counts is the unstranded loose tube cable. This arrangement allows efficient use of materials and reduces the processing steps required. Special considerations are required in such areas as antibuckling methods and excess fiber length control. Two variations of this basic design are presented along with test results from each cable. The work presented is limited to single mode applications with performance targets aimed at conforming to the Bellcore TR-20 specification [1].

2.0 GENERAL DISCUSSION

2.1 Cable Design Considerations

Common to all cable design approaches is the requirement that the fibers within the cable be protected from the rigors of installation and service environment extremes. Specifically, the fibers must be isolated from excessive tensile strain and prevented from experiencing bends that would cause attenuation increases at operating wavelengths. In addition, it is desirable that the cables themselves be compact and lightweight, craft-friendly and readily produced on a large scale. Cable designs based on a longitudinal buffer tube fulfill the requirements above. Design mechanics are quite different from stranded loose tube cables, where the tensile and contraction windows are determined from the lay length of the stranded tubes and the radial distance of the tubes from the center of the cable. In cables where the tube is unstranded, the operating windows are achieved only through fiber movement within the tube.

Tensile Window - To achieve a "tensile window" where the cable is elongated under load and the fibers experience no strain, a certain amount of excess fiber length (EFL) must be incorporated into the buffer tube. The fibers ideally lay in a helix within the buffer tube as described in Equation 1 below. Note that several important construction parameters are included in the equation, including tube inner diameter, fiber diameter, the fiber bend radius and the fiber stacking factor. Fiber stacking factor is simply an empirically derived factor that is a measure of how fibers lie within the tube. The factor determines how much free space is available inside a buffer tube for a given fiber count and tube size, and is used to calculate the pitch circle diameter of the fiber helix.

$$EFL = \left(1 + \frac{(D_1 - F_s \cdot D_2)}{2R - (D_1 - F_s \cdot D_2)}\right)^{1/2} - 1 \qquad \text{[EQN. 1]}$$

where:

EFL = Excess fiber length in buffer tube
R = Minimum acceptable fiber bend radius (mm)
D_1 = Inner diameter of tube (mm)
F_s = Fiber stacking factor
D_2 = Fiber outer diameter (mm)

The magnitude of the EFL at room temperature determines directly how much the cable can be allowed to stretch before the fibers experience tensile strain. This allowable cable strain, in turn, determines the amount of strength member that must be incorporated into the cable.

Minimum Acceptable Bend Radius - The helical path of the fibers results in an induced bend whose radius is denoted as R in Equation 1. A great amount of effort has been spent to ensure that the bend radius does not fall below the desired minimum bend radius limits, which are determined from two considerations: long-term stress and attenuation increase.

Calculation of the stress induced by the helix is straightforward; however, determination of the stress level that is acceptable is not so simple. The probability of failure in static fatigue of fibers in bending is significantly less than fibers in uniform tension at the same maximum stress.[2] This, of course, is due to the fact that a smaller portion of the fiber surface is in tension, and only the very outer surface of the fiber experiences the maximum tensile stress. The common rule of thumb of limiting the long-term stress to 30% of the proof stress is based on fracture mechanics of individual flaws that survive the proof test.[3] For fibers with 125 micron cladding and proof test level of 50 kpsi, 30% of proof stress would be experienced with a bend radius of 45 mm.

Attenuation increases at 1300 nm and 1550 nm do not occur at bend radii greater than 25 mm to 30 mm in the most common, currently available commercial single mode fibers.[4,5] This implies that if the fiber bend radius is maintained above, say, 35 mm that the fiber will not exhibit attenuation increases due to the helix.

Of the two considerations affecting the minimum bend radius limit, the 45-mm limit imposed by long-term stress calculations is obviously the more restrictive. This value is regarded as an absolute limit and considerable safety factors are used. Realistic design targets typically range from 70 mm to 100 mm.

Low Temperature Performance - Because the cable shrinks with decreasing temperature, the tightest helix and subsequently the highest EFL and lowest fiber bend radius, will be experienced at the lowest service temperature of the cable. Given that the minimum bend radius occurs at −40°C, the effective thermal coefficient of expansion of the cable must be known in order to calculate the nominal room temperature value of EFL, which is used for the manufacturing target. The expansion coefficient of thermoplastic cabling materials is approximately two orders of magnitude greater than silica fibers, and it is necessary to incorporate antibuckling materials into the cable that limit the expansion of the cable. A computer model was used to iteratively calculate the antibuckling requirements for each design presented in this paper.

Practical Considerations - Two very important practical considerations complicate the production of cables and cause deviations from the cable behavior predicted by the design approach presented. One is that all techniques used to create EFL in buffer tubes result in a certain process tolerance or deviation from nominal targets. The resulting EFL range must be considered in the cable design with the minimum EFL determining the tensile requirement and the maximum EFL determining the antibuckling requirement.

The second practical consideration is the distribution of the EFL within the buffer tube. The helix equation assumes a uniform helix is created to accommodate the extra length of the fiber. In practice, any helix formed will be non-uniform to a certain extent, resulting in fiber bend radii smaller than those predicted by the helix equation. This phenomenon is closely related to cable material properties and process technology.

2.2 Filling Compound Selection

Filling Compound Functions - A buffer tube filling compound is used to prevent the intrusion of water and other liquids into the cable. A compound should be non-volatile, non-toxic, and chemically compatible with the optical fibers and other cable materials. The rheological behavior of a compound is also critical to the manufacture and installed performance of a longitudinal buffer tube cable. Rheological measurements are conducted by measuring the shear stress generated in a material as a function of temperature, time, and shear rate.

Rheological Characteristics - Ideally, the viscosity of a filling compound for an optical cable will be in the same order of magnitude at the high and low temperature extremes experienced by the cable. At low temperatures, the compound should be fluid enough to allow the optical fibers to move and remain stress-free; at high temperatures, the compound should be viscous enough to remain in the cable when tested according to compound flow tests (e.g., Bellcore 65°C drip test[1], R.E.A. 80°C drip test[6]). Figure 1 illustrates the rheological behavior of two filling compounds versus temperature: all other factors being equal, compound A would be the best choice for fiber optic cables.

The effect of shear rate on filling compound viscosity plays a key role in the successful manufacture of buffer tubes. Figure 2 shows a typical filling compound "flow curve": curve 1 is the shear stress versus shear rate curve for the compound from a shear rate of 0 sec^{-1} to 100 sec^{-1} (up ramp); curve 2 is the shear stress versus shear rate from 100 sec^{-1} to 0 sec^{-1} (down ramp). The area between curves 1 and 2 of Figure 2 is an indication of the amount of time-dependent shear effects - or thixotropy - of the filling compound. Figure 3 shows the viscosity versus shear rate for the two curves contained in Figure 2. Typically, the filling compound viscosity will drop with increasing shear rates, as seen in Figure 3.

In order to produce filled buffer tubes with the desired EFL and EFL tolerance, the effect of shearing caused by processing equipment on the filling compound viscosity must be measured, understood, and controlled. Fluctuations in processing conditions can result in wider EFL tolerances and uneven EFL distribution along the length of the buffer tube.

Time-dependent filling compound behavior also plays a role in the design and manufacture process. The rate at which a filling compound recovers its initial viscosity (if at all) after shearing affects the short-term and long-term optical and mechanical behavior of the fibers in the filled buffer tube.

Long-term Compound Stability - Most optical cable filling compounds are composed of blends of some of the following materials: waxes, natural and synthetic oils, polymers, silicone oils, petrolatum, gels, thickening agents, and thixotropic agents. These blended compounds have a tendency to separate into individual components over time, which can lead to major changes in the composition and viscosity of the filling compounds and result in unpredictable long-term cable performance.

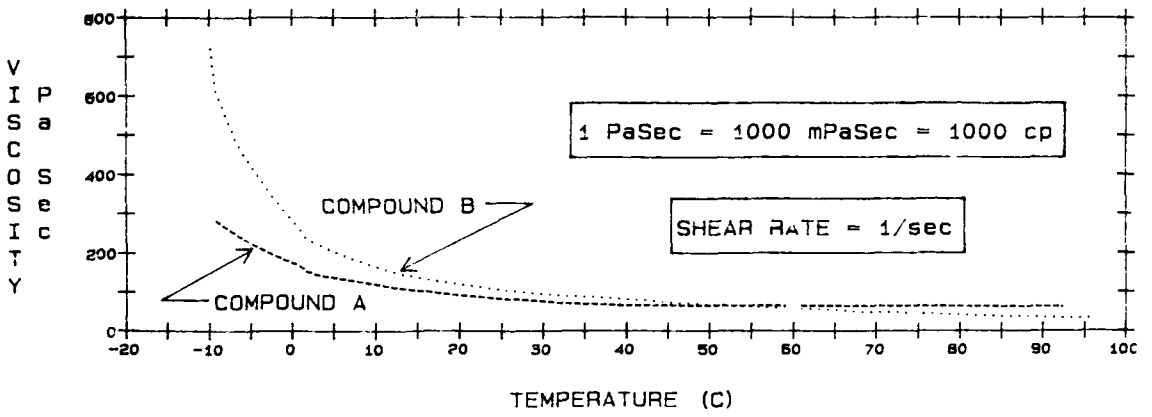

FIGURE 1 — Viscosity versus Temperature Graph

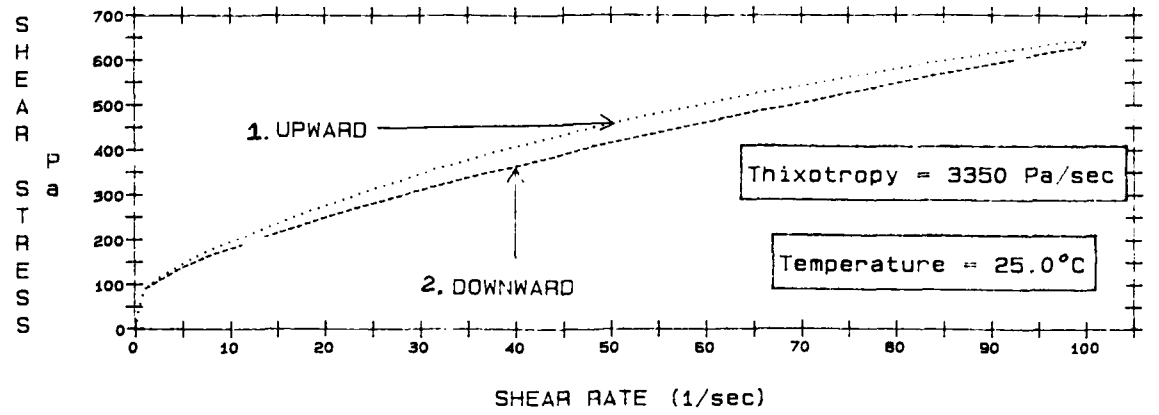

FIGURE 2 — Shear Stress versus Shear Rate Graph

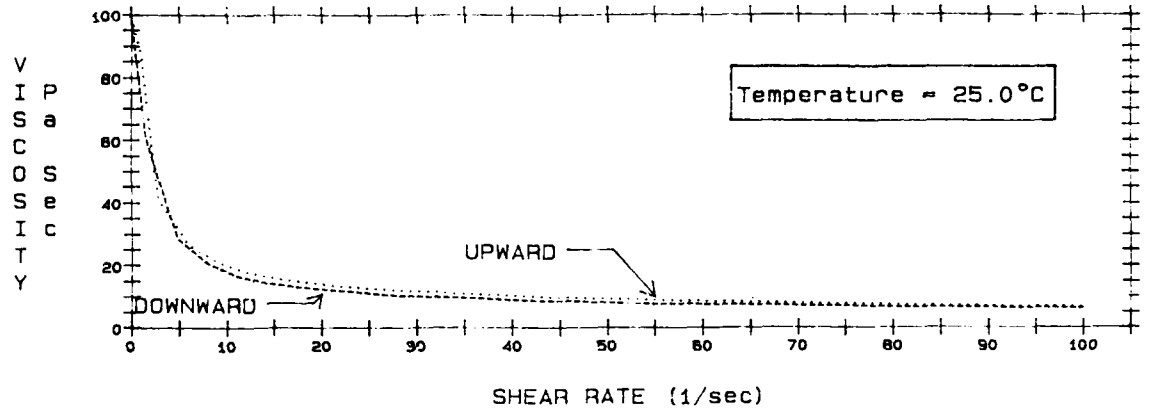

FIGURE 3 — Viscosity versus Shear Rate Graph

An oil separation test[7], originally developed to predict filling compound drip performance, can be used to predict the long-term physical stability of cable filling compounds. Based on evaluations of prototype cables, filling compounds with an 80°C oil separation value of 20% or less (total weight loss) can produce cables with good long-term stability.

2.3 Cable Antibuckling

Cable Contraction Theory - Cable shrinkage, caused by thermal contraction of polymeric cable materials, occurs as the cable is cooled. If cable shrinkage is great enough, the fibers will form a tighter helix, becoming compressed into smaller bend radii, and attenuation increases can result.

In order to reduce cable contraction, antibuckling elements are incorporated into the cable design. The antibuckling materials have thermal expansion coefficients (α) in the same order of magnitude as the glass optical fibers; they also possess high Young's modulus values (E), enabling them to withstand the shrinkage forces generated by the other materials.

Some cable designs use metallic wires or rods as antibuckling elements. Advantages of metallic antibuckling elements are relatively low costs and high modulus/area ratios. Other cable designs rely on glass/resin composite rods (GRP, FRP) with high glass-to-resin ratios. Advantages of GRP materials include no lightning, corrosion, or H_2 generation problems.

A new approach to achieving antibuckling in fiber optic cables is to use lightly-impregnated fiberglass rovings. These rovings are coupled to the cables through special processing techniques which take advantage of the high modulus and low shrinkage of the fiberglass. Advantages of this approach include more flexible cables, easier fiber access, and more space-effective cable designs.

Calculating Antibuckling Requirements - It is necessary to first calculate the antibuckling requirements of a cable design in order to determine the amount of antibuckling material to incorporate into the design. A number of methods have been previously discussed in the literature. The most common approach is calculating the effective cable thermal expansion coefficient and cable contraction strain with the rule-of-mixtures.[8]

In the rule-of-mixtures, the values for modulus and thermal expansion of all cable materials are selected at one specific temperature. These properties are highly temperature dependent. Using 23°C values for E and α for thermoplastics may cause strain predictions to be lower than what actually occurs. A more conservative approach is to use -40°C values for E and α, which will predict higher strain values. The most accurate approach should be to characterize the relationships of modulus and thermal expansion for each material over the entire temperature range of the cable.[9] Then, the E(T) and α(T) functions can be substituted into the rule-of-mixtures equation and integrated over the desired temperature range.

Measurement Technique - A procedure was developed to measure actual cable shrinkage using strain gages. Using the manufacturer's recommendations, a strain gage was glued onto the midpoint of a 30-meter cable sample with the gage aligned along the longitudinal axis of the cable segment. The strain gage was connected to an automated strain measurement system composed of a Wheatstone bridge circuit, thermocouples, and data acquisition unit (see Figures 4 and 5).

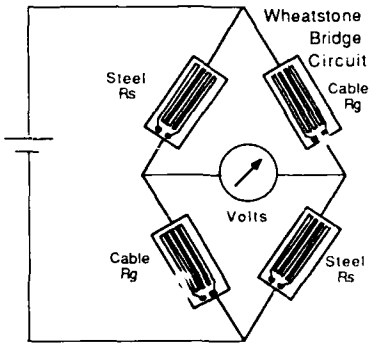

Rs Gages mounted on steel blocks
Rg Gages mounted on test cables

FIGURE 4 — Schematic Circuit for Strain Channels

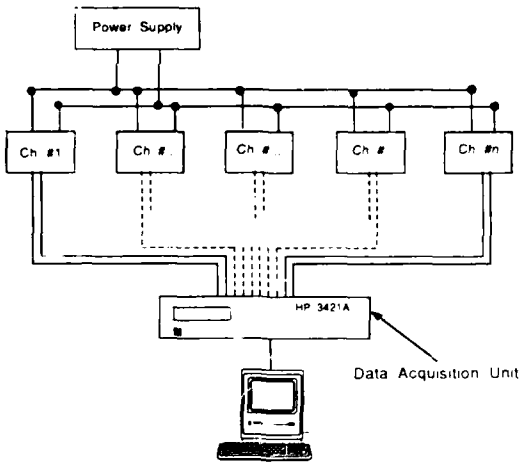

FIGURE 5 — Automated Multichannel Cable Strain Measurement System

The prepared cable segments were loosely coiled and placed in a temperature chamber programmed with the desired temperature cycle (room temperature to -40°C at a ramp of 2.5°C/hour). With the aid of a data analysis program, shrinkage and strain versus temperature graphs (Figure 6) were created.

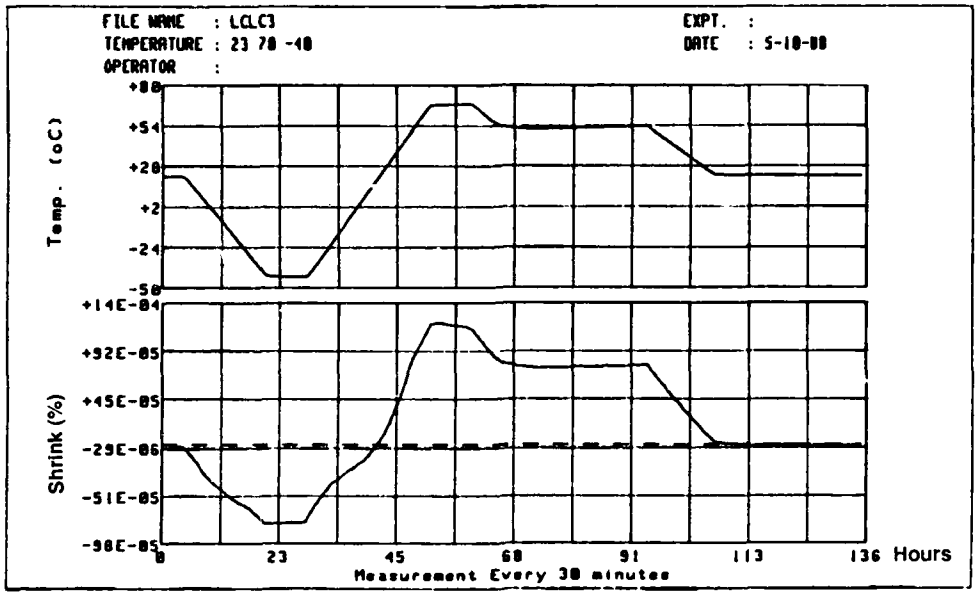

FIGURE 6 - Sample Cable Shrinkage Graph.

Predicted versus Actual Shrinkage - Table 1 shows predicted values of cable shrinkage for a number of different cable designs compared to the shrinkage measured with the strain gage technique detailed above. The predicted values were calculated with: 1) room temperature Young's modulus and thermal expansion values for cable materials; 2) -40°C E and α values; and 3) E(T) and α(T) functions integrated from 23°C to -40°C.

Cable #	Measured %Shrinkage	Predicted % Shrinkage: 23°C E & α	-40°C E & α	Integration of E(T) & α (T)
1	0.86	1.02	0.81	0.92
2	0.22	0.14	0.22	0.18
3	0.11	0.09	0.14	0.12
4	0.08	0.08	0.12	0.10

TABLE 1 — Cable Shrinkage Actual & Predicted Test Results

The predicted shrinkage values correlated very well with the actual shrinkage behavior of the four cable designs reported in Table 1. The table also indicates the wisdom of using conservative approaches to calculating the predicted shrinkage of cable designs. The predictions obtained from the calculations which used the -40°C E and α values were much closer to the actual measured values than the predictions made using 23°C E and values.

3.0 CABLE EXPERIMENTS

Two prototypes were produced to evaluate the design techniques presented here. Included are general descriptions of design parameters and the performance of each cable in key mechanical and environmental tests.

3.1 Cable A

Design - Cable A, intended for direct buried, duct and aerial applications, contains up to 12 single mode fibers. The color-coded fibers are packaged in a single, filled tube positioned longitudinally in the center of the cable. High strength yarns are stranded around the buffer tube providing the required tensile strength. The yarns are saturated with flooding compound ensuring the entire cable of being water-blocked. Corrugated steel tape is longitudinally applied around the core protecting the buffer tube. An adhesive is applied over the steel armor and is followed by an extruded polyethylene jacket. The outer diameter of the finished cable is 10.5 mm. A cross-sectional view of the cable is presented in Figure 7.

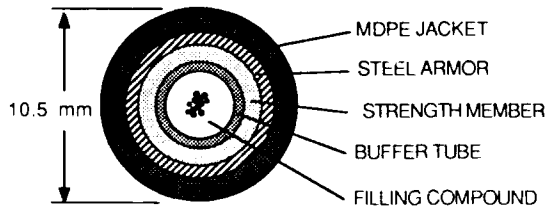

FIGURE 7- Cross-section of Cable A.

Tensile and contraction windows for the cable are achieved by assembling the fibers inside the buffer tube in a helical configuration as described earlier. This feature allows unrestricted fiber movement within the buffer tube, providing a tensile window. Likewise, at low temperatures, fiber movement accommodates cable shrinkage by decreasing the pitch of the fiber helix. Note that the armor provides the only antibuckling for this cable, and significant fiber movement is necessary to ensure good performance.

The success of this particular design relies on the accuracy with which the EFL is created and its distribution inside the buffer tube. Excess fiber length was measured using a mechanical excess length measuring device.[10] The measurements were then verified by performing a tensile test where fiber strain was determined using the time-of-flight method.

Performance - The cable exhibited excellent environmental and mechanical characteristics. In most cases, the prototype was tested beyond what the specifications called for to determine the integrity of the cable design. Test results are shown in Table 2 with typical temperature cycling performance displayed in Figure 8.

Test	Bellcore TR-20 Requirement	Result
Temp. Performance -40° C to +70° C	80 %<0.1 dB/km 20% <0.2 dB/km attn. change	<0.1 dB @ 1550 <0.1 dB @ 1300 all fibers
Tensile Strength	<0.1dB attn. change @ 2700 N load	pass
Impact	<0.2 db attn. change after 25 impacts	0 dB for 300+ impacts
Compressive Strength	<0.1 dB attn. change @ 440 N/cm	0 dB @ 440 N/cm
Cyclic Flexing	<0.1 dB attn. change after 25 cycles	0 dB for 500+ cycles
Cold/Hot Bend	<0.2 dB attn. change after 4 turns	0.10 dB cold 0.01 dB hot
Compound Drip	no drippage after 24 hrs @ 65° C	pass

TABLE 2 - Test Results of Cable A

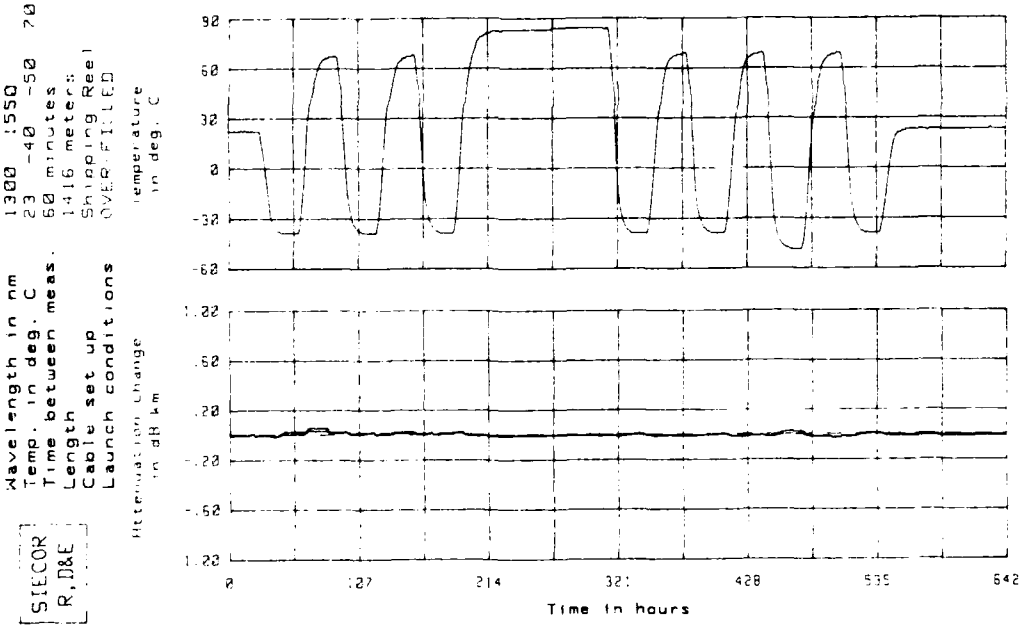

FIGURE 8- Attenuation During Temperature Cycling for Cable A.

3.2 Cable B

Design - This cable, like Cable A, was designed and tested with applications of 12 fibers or less in mind. The construction consists of a single, filled, loose tube containing the colored fibers. Around the tube are stranded high strength yarns; in this case, special lightly impregnated glass yarns along with conventional glass rovings. A flooding compound, corrugated steel tape and polyethylene jacket complete the construction. Figure 9 shows a cross-section of the cable.

Cables A and B are very similar in concept but represent different extremes with respect to design parameters. The purpose of producing this prototype was to demonstrate that a broad range of design parameters could result in successful cables given the proper process capability.

Cable B differs from the prototype first discussed in that a smaller tube with less EFL is used. In addition, because the smaller tube allows less room for the fiber helix to form, significantly greater antibuckling is required to minimize the cable contraction at low temperatures so that the fibers do not experience severe bends. The antibuckling is achieved through the use of the impregnated glass yarns mentioned earlier and through some contribution from the steel armor. Tensile requirements are fulfilled through the use of the impregnated yarns with the addition of conventional glass rovings to achieve the full 2700 N target rating.

Performance - As with Cable A, the performance of Cable B was excellent. Table 3 summarizes the test results and Figure 10 is a representative graph of the fiber attenuation during temperature cycling. The results of the temperature cycling were considered critical to the evaluation of the impregnated glass yarns as antibuckling members. The performance at -40°C after the 85°C heat soak demonstrates that the technique is successful.

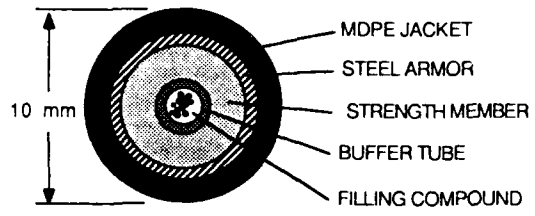

FIGURE 9- Cross-section of Cable B.

Test	Bellcore TR-20 Requirement	Result
Temp. Performance -40° C to +70° C	80 %<0.1 dB/km 20% <0.2 dB/km attn. change	<0.1 dB @ 1550 <0.1 dB @ 1300 all fibers
Tensile Strength	<0.1dB attn. change @ 2700 N load	pass
Impact	<0.2 db attn. change after 25 impacts	0 dB for 300+ impacts
Compressive Strength	<0.1 dB attn. change @ 440 N/cm	0 dB @ 800+ N/cm
Cyclic Flexing	<0.1 dB attn. change after 25 cycles	0 dB for 500+ cycles
Cold/Hot Bend	<0.1 dB attn. change after 4 turns	0 dB cold 0.03 dB hot
Compound Drip	no drippage after 24 hrs @ 65° C	pass

TABLE 3 - Test Results of Cable B

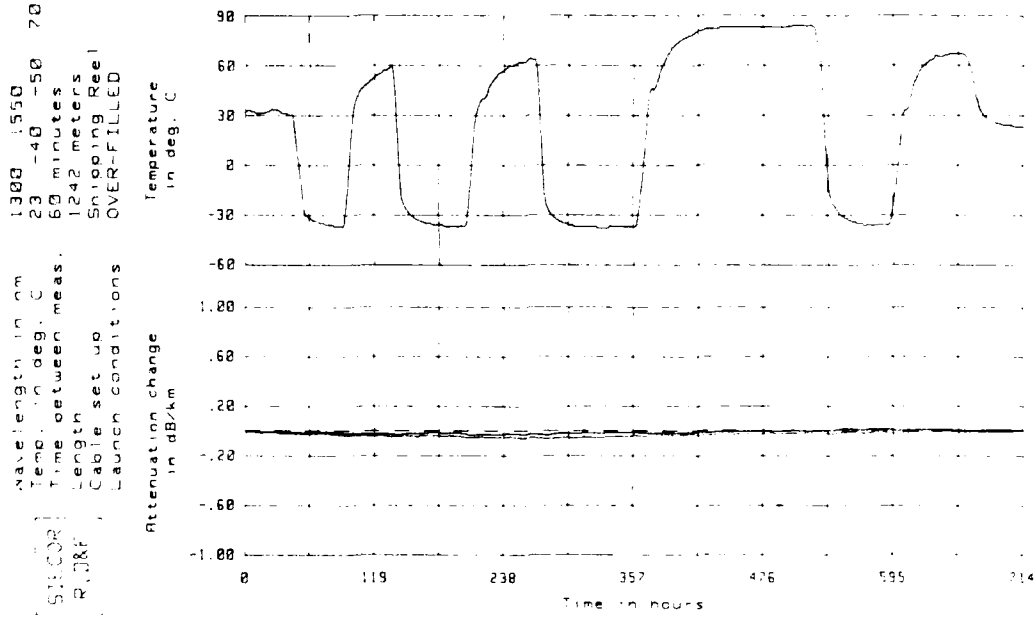

FIGURE 10- Attenuation During Temperature Cycling for Cable B.

4.0 CONCLUSION

A general discussion has been made of loose tube cable design, focusing on considerations for lower fiber count cables. Design equations have been presented based on the helix equation that models the distribution of fibers in a loose tube. Consideration has been given for choosing a filling compound for the buffer tubes, and several tests have been described for predicting performance of a filling compound in the finished cable. Various methods of achieving antibuckling have been examined, including a new, less expensive, lightly-impregnated fiberglass roving. A test has been devised to determine the exact antibuckling contribution of a given element.

Two separate classes of low fiber count cables have been designed, prototyped, and tested. The first of these, Cable A, used a large buffer tube with relatively high EFL, and was designed to allow fiber movement across temperature extremes. The second cable, Cable B, was designed with a philosophy of restricting fiber movement by using a large amount of antibuckling. Each of the prototypes tested well in comparison to Bellcore TR-20 specifications.

ACKNOWLEDGMENTS

The authors would like to acknowledge Avi Garg for developing the cable strain measurement system. Also, thanks to the groups in the Product Development Lab and Product Evaluation Lab. Special thanks to Diane Kerley for her help in preparing this manuscript.

REFERENCES

1. Bell Communications Research, Inc., "Generic Requirements for Optical Fiber and Optical Fiber Cable," Technical Reference TR-TSY-000020, Issue 3, December 1987.

2. P.D. Patel, H.C. Chandan, D. Kalish, "Failure Probability of Optical Fibers in Bending," 30th International Wire and Cable Symposium Proceedings, 1981, pp. 37-44.

3. R.D. Maurer, "Design Stress for Long Term Optical Waveguide Loads," Optical Communication Conference, Amsterdam, 1979, Post Deadline Papers, pp. 19.2-19.4.

4. J.A. Dixon, M.S. Giroux, A.R. Isser, R.V. Vandewoestine, "Bending and Microbending Performance of Single-Mode Optical Fibers," in Conference on Optical Fiber Communication/International Conference on Integrated Optics and Optical Fiber Communication Technical Digest Series 1987, Vol. 3 (Optical Society of America, Washington, DC, 1987) p. 40.

5. P.F. Glodis, C.H. Gartside III, J.S. Nobles, "Bending Loss Resistance in Single-Mode Fiber," in Conference on Optical Fiber Communication/International Conference on Integrated Optics and Optical Fiber Communication Technical Digest Series 1987, Vol. 3 (Optical Society of America, Washington, DC, 1987) p. 41.

6. Rural Electrification Administration, "Specification for Totally Filled Fiber Optic Cable - PE-90," May 28, 1986.

7. M.C. Light, Jr., "An Oil Separation Test to Predict Elevated-Temperature Drip Performance of Optical Cable Buffer Tube Filling Compounds," to be presented at the 37th International Wire and Cable Symposium Proceedings, 1988.

8. T.A. Lenahan, "Thermal Buckling of Dual-Coated Fiber," AT&T Technical Journal, Vol. 64, No. 7, September 1985, pp. 1570-1571.

9. S.M. Cooper, K.L. Coupe, B.D. Zimmermann, "The Effect of Temperature Dependent Materials Properties on Fiber Optic Cable Design," 35th International Wire and Cable Symposium Proceedings, 1986, pp. 148-158.

10. J.S. Barker, "A Device for Measuring Excess Fiber Length in Buffer Tubes," 36th International Wire and Cable Symposium Proceedings, 1987, pp. 175-178.

Martin C. Light, Jr.
Siecor Corporation
489 Siecor Park
Hickory, NC 28603-0489

Martin C. Light, Jr., was born in Lancaster, Pennsylvania, in 1963. He received his Bachelor of Science Degree in Ceramic Engineering from the Georgia Institute of Technology in 1985. Since then, he has been employed at Siecor Corporation as a Materials Engineer in the Research, Development and Engineering department.

James A. Moses
Siecor Corporation
489 Siecor Park
Hickory, NC 28603-0489

James A. Moses was born in Huntsville, Alabama, in 1963. He received his Bachelor of Science Degree in Mechanical Engineering from Vanderbilt University in 1985. He is currently employed as a Process Specialist in the Research, Development and Engineering department of Siecor Corporation.

Mark A. Sigmon
Siecor Corporation
489 Siecor Park
Hickory, NC 28603-0489

Mark A. Sigmon was born in Newton, North Carolina, in 1962. He received his Bachelor of Science Degree in Mechanical Engineering from North Carolina State University in 1985. Since then, he has worked as a Process Engineer for Siecor Corporation - Research, Development and Engineering department, and is currently Supervisor of the Product Development Lab.

Christopher A. Story
Siecor Corporation
489 Siecor Park
Hickory, NC 28603-0489

Christopher A. Story was born in Lincolnton, North Carolina in 1959. He received his Bachelor of Science Degree in Materials Engineering from North Carolina State University in 1981. Since graduation, he has been employed at Siecor Corporation in the Research, Development and Engineering Department. He has held positions as Materials Engineer, Process Engineer and is now Product Development Manager for cable products.

LXE – A FIBER-OPTIC CABLE SHEATH FAMILY with ENHANCED FIBER ACCESS

P. D. Patel and M. R. Reynolds

AT&T Bell Laboratories
Norcross, Georgia 30071

M. D. Kinard and A. J. Panuska

AT&T Network Systems
Norcross, Georgia 30071

1. ABSTRACT

As fiber-optic transmission penetrates the loop distribution network, frequent sheath entry for splicing into a tapered network will be required. A cable design maintaining strength-member continuity through the splice closure particularly suits applications with many branch splices. A new cable sheath family called LXE addresses this need by placing two opposed linear strength members outside the cable core in a plane passing through the neutral axis of the cable. Metallic and rodent-lightning armored constructions are presently available and a non-metallic construction is currently under development. These sheath designs are used with the proven Lightpack® cable core construction with up to 96 fibers and were evaluated with laboratory testing and field installations. Mechanical and optical performance is excellent, completely consistent with current industry standards for long-haul and trunk cables. The LXE Lightpack cable family offers standard performance and easy entry in a compact size suitable for underground, buried, and aerial applications.

2. INTRODUCTION

As fiber-optic transmission penetrates the loop distribution network, it appears that a tapered architecture similar to that for copper plant is evolving for fiber-optic cable. In this Serving Area Concept (SAC) approach, the dedicated channels for an individual customer extend from a Remote Terminal (RT) into a branching tapered network. The large fiber count backbone cables will branch into smaller count laterals which will in turn separate into single or multiple drops for businesses or residences, as illustrated in Figure 1. This tapered architecture results in many branching splice points. Therefore, frequent entry into the backbone and lateral cables will be common, with both end and mid-span splices.

A new Lightguide cable family addresses this need by combining the benefits of the Lightpack® cable core construction with a unique new sheath family called LXE. LXE Lightpack cables offer enhanced sheath entry combined with the easy fiber access of Lightpack cables.[1] Easy access to all of the cable's fibers while retaining the sheath's tensile strength is referred to as "Express Entry."

Linear strength members embedded in the jacket enhance sheath entry and maintain flexibility in a compact, rugged construction. LXE designs are offered with a standard 600-pound (2700-N) tensile rating and are intended for underground, buried, or aerial installation. With up to 96 fibers, LXE Lightpack cables are suitable for the backbone and lateral applications described above and offer excellent optical performance.

3. SHEATH DESIGN

3.1 Linear Strength Members

Fiber-optic cable designs must limit axial strain on the fibers during installation to insure their performance. While tensile loading strain is equal across the cable cross section, bending and torsional strains vary within the cable. For axisymmetric cable structures, pure bending and torsional strains increase from zero at the cable center to maximum values at the outside surface, with larger cables having higher strains under similar installation conditions. For example, when bent around a 10-inch radius, a 1-inch diameter cable experiences 5% maximum tensile strain at the outside of the bend, 2.5% strain halfway to the center, but zero strain at the center.

The original crossply cable design inherently minimized fiber strain by locating the fibers in a single, central core tube with strength members uniformly distributed on the outside.[2] Embedding strength members in the sheath layers rather than the cable center also provides a composite reinforced tube which results in a compact construction and enhances fiber protection. The strength members in the crossply and similar sheaths are helically applied within the jacket for flexibility and stability during bending, allowing a tight bend radius without kinking.

In keeping with these features, the LXE concept places parallel linear strength members aligned with the core on opposite sides to allow easy core access. Two opposing compressively-stiff strength members in the sheath are the minimum number to maintain the advantages of a single centrally located core tube. These two opposing rod-like members always force the neutral axis, the line of zero strain in pure bending to pass through their

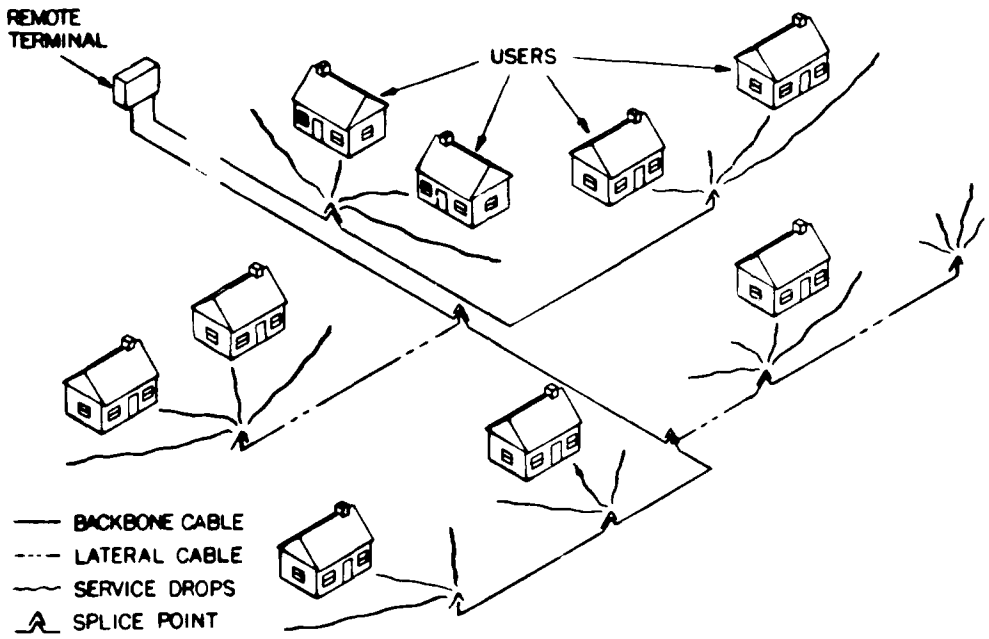

Figure 1. Potential Fiber-Optic Distribution Plant Architecture

centers and the core center. This bending behavior, restricted to a single plane, is called preferential bending and is illustrated in Figure 2. Rope-like elements adjacent to the rods can contribute to a higher tensile load rating.

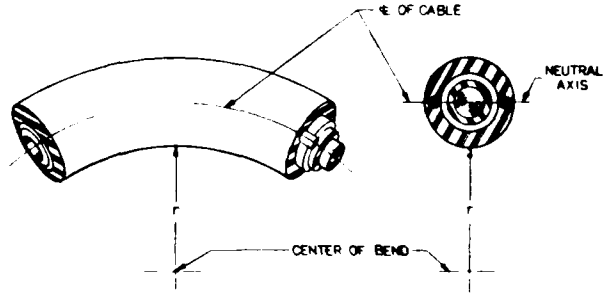

Figure 2. Neutral Axis of Bending

The LXE construction requires no helical lay since the strength member location causes preferential bending, minimizing strain and providing flexibility and stability. Preferential bending is accomplished by local twisting and is not apparent to the user, requiring no special handling procedures for any installation. Extensive testing has shown that regardless of the direction of the bend, under any combination of additional tensile and torsional loads, the cable will twist locally to maintain the neutral axis through the strength members and core, minimizing fiber strain. This testing is further discussed in the Mechanical Performance section, below.

Since there is no helical lay, the strength members have no tendency to twist the cable when under installation tension. Torsional stability against externally applied twisting during installation is provided by the cable's composite construction.

3.2 Armored LXE Description

Two types of metallic armored LXE sheaths are available: the standard LXE sheath (LXE-ME) and the rodent-lightning resistant LXE sheath (LXE-RL). Figures 3 and 4 are cross-sectional and three-dimensional views of the metallic LXE Lightpack cable designs. The standard LXE sheath incorporates the industry-standard 6-mil electrolytically-chrome-coated steel (ECCS) armor. The armor of the LXE-RL sheath is the AT&T bimetal of 3-mil 304 stainless steel bonded to 5-mil copper.[3] Both the ECCS and bimetal armors are bonded to the cable jacket with an adhesive for improved bending performance and increased strength[4] and, for the ECCS armor, to help retard corrosion.[5,6] Both are corrugated for flexibility and formed with a longitudinal overlapped seam. Under the armor are a rip cord to assist in sheath removal and a water-blocking core wrap surrounding the cable core.

Outside the armor lie the two linear steel strength members with tensile load capacity equal to the strength members in the crossply[2] or Primary Rodent/Lightning[3] sheaths. The armor and strength members are encapsulated by a high-density polyethylene jacket which bonds to the armor and completes the composite structure. Water blocking elements are also included under the jacket.

In this construction, the sheath components form a composite structure that responds mechanically as a single unit. The jacket-to-armor bond enhances hoop strength

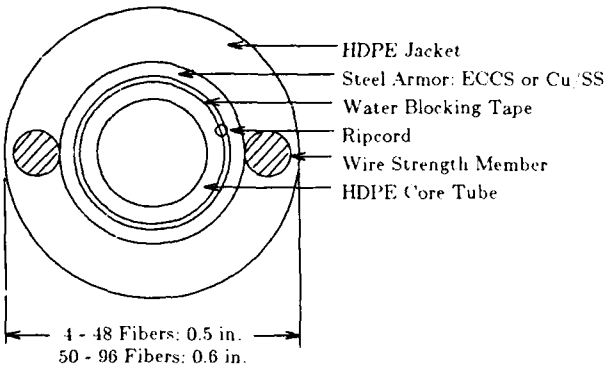

Figure 3. Armored LXE Lightpack® Cable

and evenly distributes bending and torsional strains.[4] Thus, the cable with either armor has good crush resistance and allows tight bends or twists without kinking or buckling.

3.3 Proposed Nonmetallic LXE Design

In the spirit of linear strength member design, two nonmetallic strength members would be simplest construction for a nonmetallic sheath. Size and economy considerations, however, may require a combination of rigid and flexible strength members.[7] This combination must provide the 600-pound (2700-N) load rating.

In a proposed nonmetallic design currently under development, an overlapping water-blocking tape is longitudinally applied over the core tube. Over that, two opposing rigid strength members are longitudinally applied alc ıg with rip cords. Additional tensile stiffness may be provided by flexible strength members adjacent to the rigid ones. The cable construction is completed with a high-density polyethylene jacket which encapsulates all the strength members and forms a composite structure.

The rigid rods preferentially locate the neutral plane to limit bending strain and to control bending flexibility. Rip cords are placed along the rods which guide the rip cords during sheath entry. The selection and placement of the strength members provide bending flexibility and ease of sheath entry along with mechanical integrity and tensile stiffness and strength.

This sheath design provides a compact and lightweight cable with enhanced fiber access. Since all strength members are coupled to the jacket, the entire sheath acts as a composite unit, facilitating handling during installation. The cable has good crush resistance and allows tight bends and twists without kinking or buckling. This design provides excellent water blocking both through the core and the jacket. Furthermore, the design is all dielectric and therefore well suited for lightning prone areas.

4. FEATURE ADVANTAGES

LXE Lightpack cables are comparable in size to their crossply cable counterparts and are considerably lighter and more compact than other cable designs for similar fiber counts. Both armored LXE Lightpack cables are available in same two sizes: 4 to 48 fibers in a 0.5-inch (12.7-mm) diameter cable and 50 to 96 fibers in a 0.6-inch (15.2-mm) diameter cable. Table I compares the size and weight of LXE Lightpack cable to common stranded fiber-optic cable designs.

Table I. LXE Lightpack® Cable Comparisons

Design	Fiber Count	OD (inch)	Weight (lb/kft)
Armored LXE Lightpack® Cable	48	0.49	105
	96	0.59	150
Armored Stranded Design	48	0.63	170
	96	0.74	230

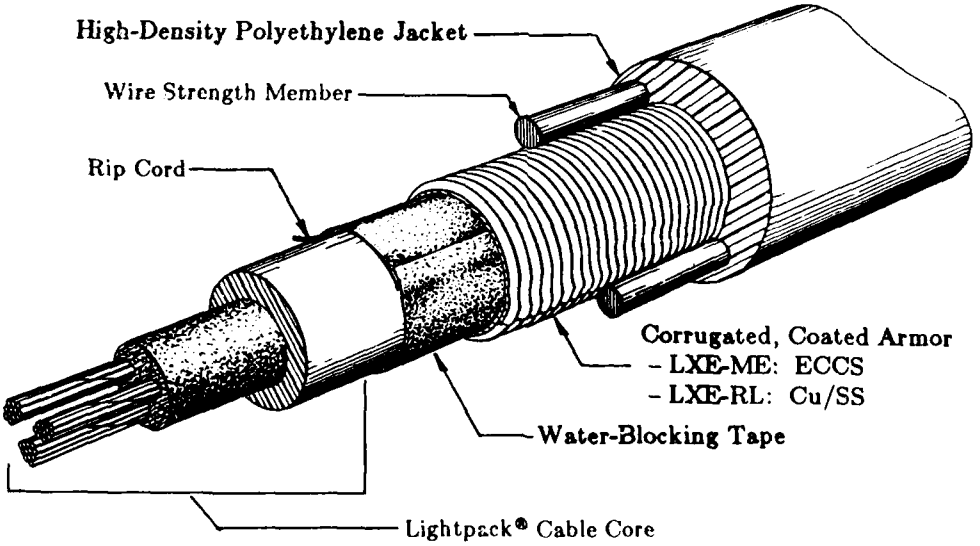

Figure 4. Armored LXE Lightpack® Cable Sheath

Smaller and lighter cables offer the advantages of longer aerial span lengths and longer pulls in urban ducts for traditional long-haul and trunk applications. The high-density polyethylene jacket also provides a low coefficient of friction for duct installations and protects the fibers in harsh chemical environments. Further advantages in loop distribution installations include easier handling and the availability of standard reels with long stock lengths which may be cut up into several runs.

The LXE sheath family was first developed with the Lightpack cable core construction because it is especially well suited to the multiple splices and mid-span entry aspects of the loop distribution environment. While LXE Lightpack cables currently offer fiber counts up to 96, ribbon core versions of the LXE cable sheath family are under development for higher fiber counts.

5. *SHEATH ENTRY*

As discussed above, fiber-optic transmission in the loop may adopt a tapered network similar to current copper plant, requiring frequent branch splicing and frequent sheath entry. LXE Lightpack cables were developed to address this need. The helically applied strength members in the crossply cable design have been integrated and moved to two locations on either side of the cable and rip cords are added. The result is a more readily accessible cable core for either end or mid-span entry. LXE sheath construction expidites sheath entry, reducing installation time in the field.

The armored LXE sheath designs allow taut-sheath mid-span entries as follows. The jacket is stripped away by first shaving it to expose the wire strength elements. The jacket halves are then peeled from the armor over the desired length, freeing the continuous wires. A small opening in the armor exposes the rip cord which slits the armor in two when pulled, releasing the cable core. The Lightpack cable core then provides direct access to all fibers which are enclosed in one large tube.

The nonmetallic LXE sheath under development allows taut-sheath mid-span entries without cutting the strength members as follows. The two rip cords located adjacent to the rigid rods are first exposed by shaving the outer jacket over the rods for about two inches. The rip cords are then pulled, guided by the rods, to cut the outer jacket into halves. The jacket halves, along with the water blocking tape, are peeled from the core tube, freeing all the continuous strength members. This exposes the Lightpack cable core, providing direct access to all the fibers.

Sheath entries at the cable end for all LXE sheaths require only a ring-cut opening through the sheath to expose the Lightpack cable core for one or two inches. After ringing the core tube as now practiced, the entire sheath construction, including the core tube, is slipped off the desired length of fiber.

6. *PERFORMANCE*

6.1 *Mechanical Performance*

LXE Lightpack cables were subjected to a variety of mechanical endurance tests to assure superior mechanical performance in the field. Table II summarizes the battery of standard tests performed on all outside plant cables. They are conducted according to both the Bell Communications Research[8] (Bellcore) and the Electronic Industries Association[9] (EIA) test procedures. LXE Lightpack cables meet or exceed all of the requirements. In addition, LXE Lightpack cables have passed all applicable mechanical and construction tests of the Bellcore generic cable specification.[8]

Table II. Mechanical Tests

Test	Specification[‡]	Requirement
Tensile Strength	FOTP-33 §5.3.5	600 lb_f Bend Radius = 20x Cable OD
Compressive Strength	FOTP-41 §5.3.4	1000 lb_f total load
Cable Twist	FOTP-85 §5.3.6	±180° Twist, 10 Cycles
Low and High Temperature Bend	FOTP-37 §5.3.2	Bend Radius = 15x Cable OD 4 Wraps ea. at -20° F, 140° F
Cyclic Flex	FOTP-104 §5.3.7	Bend Radius = 15x Cable OD
Impact Resistance	FOTP-25 §5.3.3	52 ft-lb_f Impact, 25 Cycles
External Freezing	FOTP-98 §5.3.8	1 hr. min freeze at -2° C

‡ FOTP's from EIA Std. RS-455. Section numbers from Bellcore TR-TSY-000020, Issue 3.

LXE Lightpack cables were also subjected to two destructive buried cable simulation tests in the laboratory: the sharp-edge test and the dynamic-squeeze test. These tests, which abuse the cables well beyond the normal load ratings, have become standard design capability tests for AT&T's outside plant lightguide cables since introduction with Lightpack cable in reference [1]. Both tests simulate improper and uncommon cable plow procedures during buried installations. In both tests, the LXE designs equaled or exceeded the performance of the crossply design.

Finally, as part of AT&T's standard design capability evaluation, test lengths of LXE Lightpack cables were subjected to a series of field installation handling and placing trials at the AT&T Bell Laboratories Chester Field Testing Laboratory. The trials included actual or simulated aerial, buried, and underground installations. The tests reproduce normal or extreme installation procedures and Table III summarizes the tests conducted for each installation environment.

Of particular interest for LXE Lightpack cables was the Cross (Perpendicular) Sheave Pull, which forces the cable to bend under maximum load around two small sheaves with perpendicular axes. During this test the cables undergo 90° twisting over approximately 8 inches to accommodate the bending about perpendicular axes, demonstrating how the linear strength members reorient the cable during bending, maintaining minimum strain on the fibers. During all testing, all fibers were monitored for loss and continuity. No adverse effects were observed during either standard installation procedures or abusive testing.

The mechanical test program showed that LXE Lightpack cables can withstand standard and abusive mechanical installation and extreme manual handling without sheath damage or optical loss increase.

6.2 Optical Performance

LXE Lightpack cables were designed to give the same optical performance characteristics as the crossply Lightpack cable. Figure 5 shows the optical loss distribution from recent production armored LXE Lightpack cables. These cables were manufactured to meet a maximum individual fiber loss requirement of 0.40 and 0.26 dB/km at 1310 and 1550 nm, respectively. The mean values for LXE are 0.35 dB/km at 1310 nm and 0.21 dB/km at 1550 nm which represent zero average added loss from cabling as with other AT&T cable designs.

In addition to room temperature optical loss, the environmental performance of LXE Lightpack cable was investigated. Figure 6 shows the performance of several LXE Lightpack cables for a standard Bellcore thermal cycle.[8] LXE cables exhibit the same excellent thermal stability as crossply and Primary RL Lightpack cables.

6.3 Rodent and Lightning Performance

Fiber-optic cables in loop distribution plant will be subject to rodent, lightning, and damage hazards similar to those faced by other outside plant cables, although less customer traffic is threatened in case of severe damage. The LXE Lightpack cable family offers three types of protection from these hazards.

Table III: Field Installation Testing

Aerial	• Max. Load Around 4 " dia. Snatch Block • Normal Installation Technique • Abusive Technique - High Tension from Heavy Reel - Bending from Reel Offset
Buried	• Crush Into Earth around 1" dia. Pin - approx. 1000 lb Peak Loads • Torture Run with Abusive Plow Technique - 20 ft. Radius "S" Turn - Raise/Lower Plow with Stationary Tractor - Jerk Starts
Underground	• Intermediate Assist Simulation - Maximum Load - Twisted Cable Racking • Cross (Perpendicular) Sheave Pulls at Maximum Load - 15" dia. Sheaves - C-Manhole Sheave and 9" dia. Sheave • Handpull with Backfeed Handling - "Figure 8" Storage - Free Loop Kink - Racetrack Storage • "Figure 8" Crushing by Line Truck • Excessive Tensile Load Retention with Wire Grip End Termination

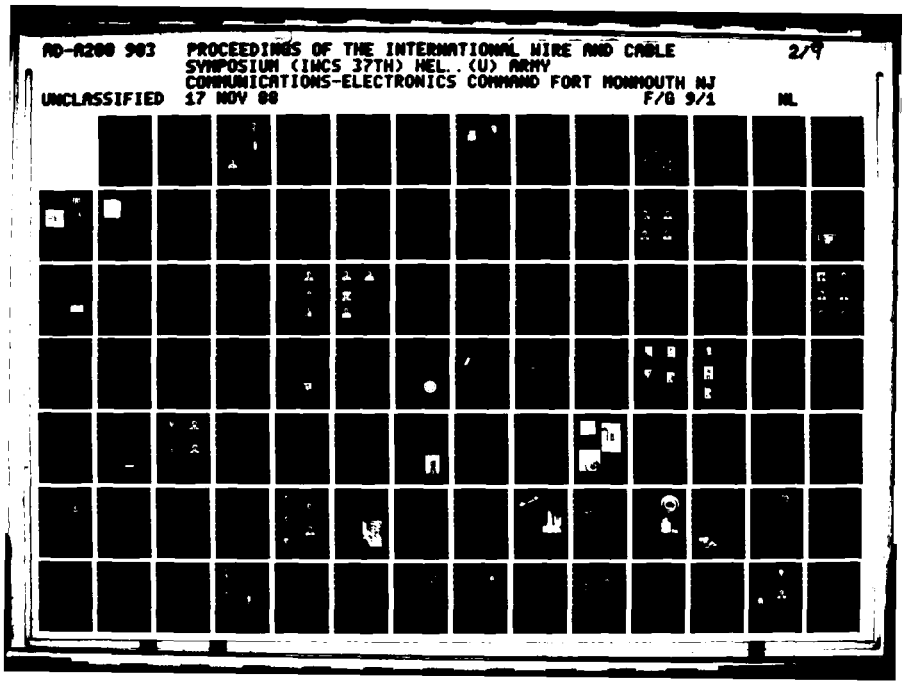
AD-A200 903 PROCEEDINGS OF THE INTERNATIONAL WIRE AND CABLE SYMPOSIUM (IWCS 37TH) HEL..(U) ARMY COMMUNICATIONS-ELECTRONICS COMMAND FORT MONMOUTH NJ
2/9
UNCLASSIFIED 17 NOV 88 F/G 9/1 NL

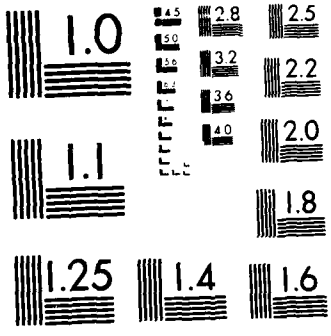

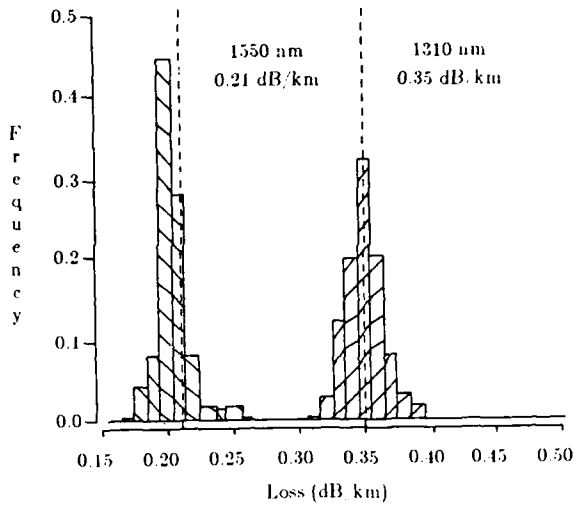

Figure 5. LXE Lightpack® Cable Optical Loss

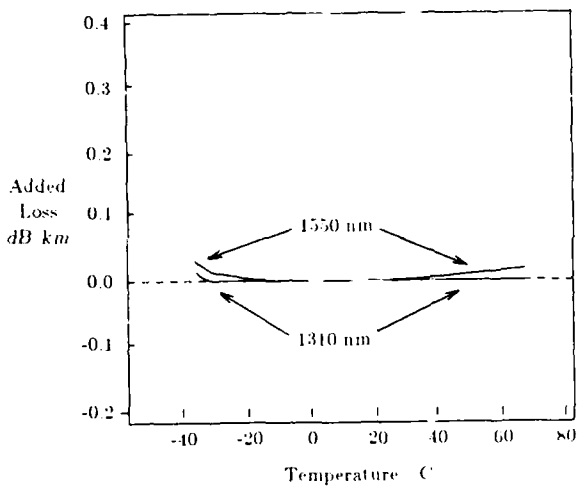

Figure 6. LXE Lightpack® Cable Thermal Cycle Performance

The two armored cables, LXE-ME and LXE-RL, offer a graded level of protection to both rodent and lightning hazards. Both have been evaluated with the standard rodent tests[10, 11] and with the emerging standard sandbox lightning simulation test.[12, 13] LXE-ME offers protection suitable to the lower capacity routes common in loop applications, using the same plastic-coated ECCS material for armor as is commonly used by many outside plant cables in the industry. It is rated at 2.0 (no armor or core penetration) in the rodent test and at 80 kA, Bellcore Level II,[8] for fiber counts up to 96 in the lightning test.

For applications where greater levels of lightning, rodent, or corrosion protection is desired, the LXE-RL Lightpack cable is available. It is also rated at 2.0 in the rodent test and features corrosion-resistant stainless steel armor. Due to its copper layer, it is rated higher in the lightning test at 105 kA, Bellcore Level I,[8] for fiber counts up to 96. Both armored cables may be oversheathed with AT&T's B-oversheath or extremely hazardous conditions.[14]

The *nonmetallic* LXE design *under development* is all-dielectric and therefore immune to direct lightning damage. In lightning-prone areas where rodent attack is not a threat, it will offer an excellent alternative.

7. *CONCLUSION*

The LXE linear strength member sheath family, combined with the proven Lightpack cable core, has been presented. Standard metallic and rodent-lightning resistant versions are presently available and a nonmetallic version is under development. LXE Lightpack cables are rugged, compact and flexible, featuring a composite sheath construction with a standard 600-pound load rating and allowing all common placing procedures. LXE cables retain many crossply sheath advantages while offering enhanced sheath entry tailored to the loop distribution environment.

8. *ACKNOWLEDGEMENTS*

The authors gratefully acknowledge the assistance and support of many people who were instrumental in the development and testing LXE Lightpack cables at AT&T Bell Laboratories and AT&T Network Systems.

REFERENCES

1. P. D. Patel and C. H. Gartside, III, "Compact Lightguide Cable Design," International Wire and Cable Symposium (IWCS), 1985.

2. P. F. Gagen and M. R. Santana, "Design and Performance of a Crossply Lightguide Cable Sheath," IWCS, 1979.

3. M. R. Reynolds, C. J. Arroyo, and M. D. Kinard, "Primary Rodent and Lightning Protective Sheath for Lightguide Cable," IWCS, 1986.

4. G. M. Yanizeski, E. L. Johnson, and R. G. Schneider, "Cable Sheath Buckling Studies and the Development of a Bonded Stalpeth Sheath," IWCS, 1980.

5. K. E. Bow and L. G. Colter, "Corrosion Studies on Shield Materials for Underground Telephone Cables, Part II: Corrosion Protection for Filled Cables", IWCS, 1976.

6. G. D. Schwank and K. E. Bow, "Galvanic Corrosion Studies of Aluminum and Steel Shielding Materials for Armored Telephone Cables", *Materials Performance*, vol. 17, no. 9, September 1978, pp. 25-30.

7. C. J. Arroyo, A. C. Jenkins, P. D. Patel, and A. J. Panuska, "A High Performance Nonmetallic Sheath for Lightguide Cables," IWCS, 1987.

8. *Generic Requirements for Optical Fiber and Optical Fiber Cable*, Bell Communications Research Technical Reference TR-TSY-000020, Issue 3, December 1987.

9. EIA Standard RS-455 and Addenda, *Standard Test Procedures for Fiber Optic Fibers, Cables, Transducers, Connecting and Terminating Devices*, Electronic Industries Association.

10. R. A. Connolly and N. J. Cogelia, "The Gopher and Buried Cable", *Bell Telephone Laboratories Record*, April 1970.

11. N. J. Cogelia, G. K. Lavoie, and J. F. Glahn, "Rodent Biting Pressure and Chewing Action and Their Effects on Wire and Cable Sheath", IWCS, 1976.

12. E. L. Fisher, E. C. Kelch, and W. F. Bishop, "The Effect of Lightning Arcing Currents on Telephone Cables", IWCS, 1971.

13. Lightning Capability Test Method, draft standards proposal (not numbered) of EIA FO-6.7.8 Task Group, outlined in a letter from C. J. Arroyo, AT&T Bell Laboratories, Member FO-6.7.8, to L. Levey, Bell Communications Research, Chairman FO-6.7.8, on 23 October 1987.

14. W. C. L. Weinraub, D. D. Davis, and M. D. Kinard, "A Rodent and Lighting Protective Sheath for Fiber Optic Cables," IWCS, 1983.

P. D. Patel is a Distinguished Member of Technical Staff at AT&T Bell Laboratories, Norcross, Georgia. He joined Bell Laboratories in North Andover, Massachusetts in 1969 after receiving degrees in Mechanical Engineering, including a B. E. from Maharaja Sayajirao University, India, and Engr. Sc. D. degrees from Columbia University. Since 1979 he has worked in the Lightguide Technology Department at Norcross and is currently working in the Exploratory Lightguide Cable Group. He is a member of the American Society of Mechanical Engineers.

Mickey R. Reynolds is Technical Supervisor of the Sheath Joining Group at AT&T Bell Laboratories, Norcross, Georgia. He joined AT&T Bell Laboratories in 1978 as a Member of Technical Staff after receiving BS and MS degrees in Engineering Mechanics from the Georgia Institute of Technology in 1978 and 1979. His most recent responsibilities included commercial and military fiber-optic cable design and development for the Fiber Optic Guided Missile (FOG-M). He earlier worked in single-mode fiber splicing and in copper cable mechanical characterization.

Michael D. Kinard is a Senior Development Engineer in the AT&T Technologies, Inc., Network Systems Media Division at Norcross, GA. He joined the Western Electric Company in 1979 as a Development Engineer. He has worked on the design, characterization and implementation of Bonded Sheath systems on copper and fiber optic cables. His prior experience was in thermal and heat transfer analysis and system design. He received his BS in Mechanical Engineering from Old Dominion University in 1974 and his MS in Mechanical Engineering from the Georgia Institute of Technology in 1986 and is a registered Professional Engineer.

Andrew J. Panuska is a Senior Development Engineer with AT&T Network Systems in Norcross, Georgia. He joined AT&T in 1963. He received B.S. Degrees in Mechanical Engineering and Civil Engineering from the Johns Hopkins University. Since 1979 he has worked in the Lightguide Cable Development department. He is presently responsible for the development of lightguide cable products and processes.

SELF-SUPPORTING DIELECTRIC FIBER OPTIC CABLES IN HIGH VOLTAGE LINES

Ulrich H.P. Oestreich
Siemens AG
Munich, West Germany

Hani M. Nassar
Siecor Corporation
Hickory, North Carolina

Abstract

Fully dielectric cables installed in parallel to conductors of super high voltage lines, i.e. with conductor-conductor voltages of higher than 132 kV suffer from tracking currents occuring at the surface or even inside the cable close to the towers if the cable is wet or semi-wet, e.g. under drying conditions. The minimum result is a slow abrasion of the jacket, the worst case the complete destruction of the cable.
The problem can be overcome even for very high voltages by a control of the electric field at the surface and in the cable interior. The control has to be made by a well defined resistor which is part of the cable construction.
The resistors consist of a highly compacted concentric layer of pretreated Aramid -yarn with a resistivity in the range of 1 to 10 MΩ cm. Experimental installations in 380-kV-lines prove the perfect behaviour of the concept.

The transmission of non disturbable information of any bandwidth along high voltage lines is beneficial not only for the utility companies operating the line, but for all who have the right to use such a transmission path. Optical glass fibers can do this job with almost no limitations for bandwidth or length of the connection. A lot of working fiber lines have been installed around the world, but almost all have been incorporated in ground wires (OPGW) installed in similar ways to ordinary ground wires.
Unfortunately these installations, in spite of satisfactory performance, leave several problems unresolved:

1. The installation of ground wires is not usual for medium voltages, and in some places not even in 230 kV-lines.
2. Ground wires with incorporated optical fibers should be larger and heavier than ordinary ground wires. In certain cases, where ground wires serve exclusively as lightning protectors, their cross-section is very small and cannot be replaced by larger and heavier products without causing mechanical problems for the poles or towers.
3. Although it is not a problem to provide new lines with optical ground wires, the installation of such connections in existing lines is difficult.
   Static and dynamic problems as well as de-energizing the wire may force the operating company to give up their intentions. Installation times, particularly in long super high voltage connections, can be extremely time consuming.

That is why the idea of a light weight, fully dielectric fiber optic cable installable in any line at any time without the necessity to de-energize the line is an old and well understood but not actually realized dream. In fact, there do exist some shorter installed cables in lines up to 132 kV. What they show in a positive sense is that the often addressed mechanical problems hardly exist. On the other hand, all trials to install such cables in lines of very high voltages have failed. The degree of destruction ranges from a slow erosion of the jacket surface to the complete burning down of the cable.

The simple reason is that any semiconducting part of the cable, e.g. a wet jacket surface or even just some humidity in a partially filled core, attracts electrical field lines. Consequently, it is loaded by a current that is dependent on the partial capacitance between the semiconducting path

and the high voltage system, as well as the ohmic resistance of this path.
A simplified model will give us the basis for a calculation.(Fig. 1)

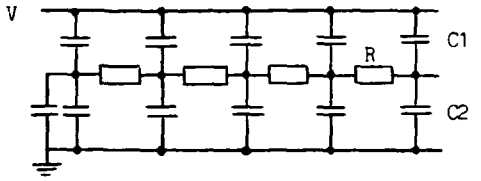

Fig.1: Electrical scheme of the current situation

Whatever position such a cable may have in the cross-section of a high voltage line, it will have a resulting capacitance to the system (C_1) and a capacitance to ground (C_2). The semiconducting path representing a longitudinal resistance (R) is definitly not homogeniously distributed but may be assumed to be. Inconsistencies will lead to steps in the voltage distribution and to bridging gas discharges if the resulting electrical stress at points of lower conductivity are high enough. While the calculation is boring the result is not.(Figs. 2 and 3)

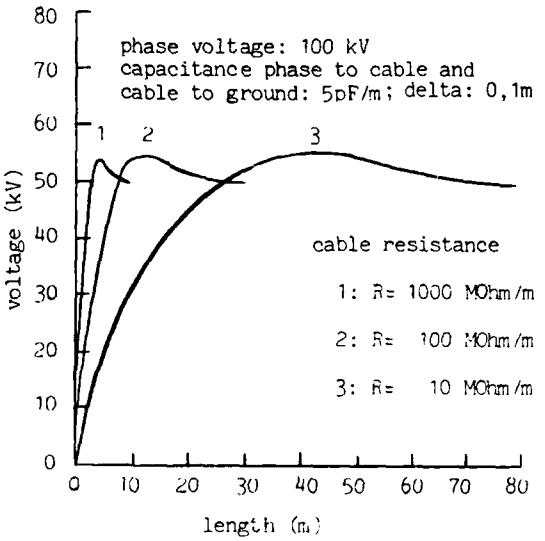

Fig. 2 voltage cable to ground

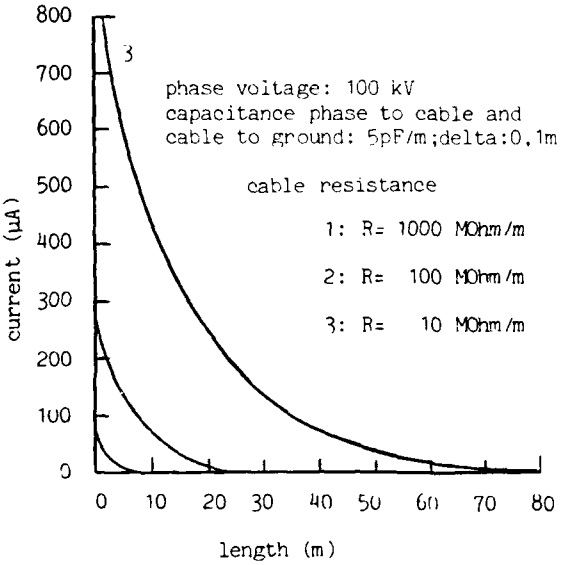

Fig. 3: Current on cable

What we see is a drastic fall of the absolute currents along a few meters and the voltage passing a maximum which enhances the electrical stress along the cable in certain regions. The slope of the fall and the distance of the voltage peak depend evidently on the resistance of the conducting path. If that resistance is sufficiently high, everything happens along a few centimeters; but as the currents in this case are very low, nothing happens with the cable. If the resistance is low, we need a long length of cable in order to make the current negligible. As the conductor in all cases is semiconductive, such high currents are dangerous for the cable and for people if such a cable should be installed in an energized line.
So the target is: make the longitudinal resistance of that cable as high as possible to give it the highest safety; but as a wet and dirty surface cannot be controlled by itself, a built-in element of high reliability is required. What kind of an element could that be?
Unfortunately we do not have many options. The element has to have a resistivity in the range of 10^5 - $10^7 \Omega \cdot cm$. If it has less, the minimum safe resistance of ca. $10^7 \Omega$ /m cannot be achieved. This number is given by the maximum voltage to ground - say 300 kV - and the minimum distance phase to ground - say 30 m, which for a safe current to ground of ca. 1 mA requires a value of the same order as above.

If we like to have a satisfactory control of the cable surface, the maximum value may not exceed 10^6 Ω /m. These values have to be stable, non aging and, most importantly, not dependant on electrical or mechanical stress. Up to this point in time, there is no non-exotic plastic material which will quarantee this to us. Available semiconductive materials have resistivities which are by far too low and are not stable enough for long term reliability. So, semiconductive jackets are out of the question. All what we can do is to use a material with a very large surface-to-volume ratio and to pretreat the surface so that the resulting conductivity can live up to the above requirements.

But as the semiconductive surface has to be loaded by currents in the order of 0.1 - 1 mA we have to provide the voltage controlling element with a giant surface what means the use of a large bundle of fine filaments.

It seems to be reasonable to combine the two basic requirements, semiconduction and high mechanical strength, in one element and to use Aramid yarn as the supporting element with the large pretreated surface. A cross-section of ca. 25 mm² provides us with a surface of 11.1 m²/m length. Theoretically other yarns could be considered also, e.g. glass or polyester. But neither has a satisfactory long term mechanical strength. Moreover, the Young's modulus is too low leading to high weights.

Therefore, we give the Aramid yarn a pretreatment with an ionogenic fluid which is chemically stable and neutral to bring it to the highest possible compactness. This causes it to behave like a solid semiconductive material without reducing all of the other important properties.

As far as we see there is no choice for this source of semiconductivity. We have now given the cable core the behavior of a reliable semiconductive resistor which gives the cable surface the needed voltage control. This excludes major irregularities in the electrical surface stress which are otherwise caused by droplets or separated conductive regions.

The electrical flow now gets a second path of conductivity R_2 which controls the inevitable and unreliable natural path R_1 of the cable surface. As any cable jacket has a certain capacitance C_3 between core and surface, the inside voltage control means a surface control as well.(Fig. 4)

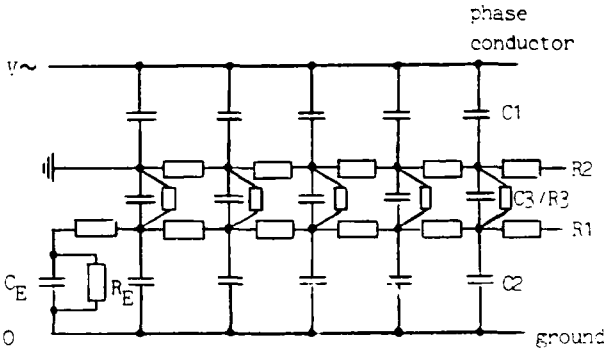

Fig. 4: control of the cable surface R_2 by an inner element R_1

The remaining question is what kind of a jacket material should we use? Generally and following the aforementioned statements, the jacket material could be freely chosen. Practically the choice is limited again. From an economic point of view a black Polyethylene should suffice. But if we keep in mind the risk of switchovers of any kind, the jacket should have a certain short term heat and flame resistance. Furthermore we should see that any control of the jacket surface by an interior element is limited by the value of the capacitance C_3 which is higher by a factor 20 - 40 than C_1 and C_2, but probably not always high enough for extreme conditions. This is particularly true if we do not ground the Aramid yarns at each tower, but rely on the grounding capacitance to the supporting helix (C_E, R_E in Fig. 4). Therefore it is recommended to give the jacket some track resistance, which points in the same direction as heat and flame resistance.

The final combination of all of that looks simple and is simple to handle.

A cable was first tested for its mechanical behavior as a self-supporting cable in several low voltage lines under most severe conditions for 8 years. The second step was to apply it to several lines in the range of 110 - 132 kV. The special applicability to very high voltages has been tested in a 220/380 kV system where it has been installed in a distance of 2 meters from a phase conductor which clearly gives higher C_1 values than normal. The result was a perfect long term behavior without remarkable effects on the jacket's surface.

We think we have a self-supporting cable which can be used up to 500 kV phase-to-phase and can be installed without switching off the line.

Dipl.-Ing. ULRICH H. P. OESTREICH
born 1928, has spent 35 years in development, manufacturing and testing of power and communication cables of all types.
As a senior director he is now responsible for development and testing of fiber optic cables in the Siemens Company, Munich, Germany.

HANI M. NASSAR, MSME
graduated from the Georgia Institute of Technology in 1981 with a Masters degree in Mechanical Engineering. He joined the R,D&E department of Siecor Corporation in 1982, where he was initially involved with the development of products for both the copper and fiber optic industry. His major projects included the development of hybrid cables, feeder cable systems, design and qualification of Fiber Optic Ground Wires and recently submarine cables and slotted core ribbon cables. He is a senior product development engineer for Siecor Corporation R,D&E, 1928 Main Ave SE, Hickory, North Carolina, 28601 and is currently assigned to the Siemens AG, Fiber Optic Research Center in Munich, West Germany.

Optical Ground Wire Design with a Minimum of Dielectrics

J.M. Schneider, J. Schmelter, R. Herff

Philips Kommunikations Industrie AG
Nachrichtenkabel und -anlagen
Schanzenstr. 30
D-5000 Koeln 80
Federal Republic of Germany

Summary

Most designs of self-supporting optical powerline ground wires (OPGW) contain a lot of of dielectric materials, such as loose plastic tubes, FRP-rods and plastic tapes.
This may lead to a large cable diameter and a heavy cable weight due to the surrounding metallic armouring wires.
In this paper a OPGW design is presented, which includes a minimum of dielectric materials by using steel tubes to enclose the optical fibres.
The use of steel tubes enables the design of an OPGW, which in its mechanical and geometrical properties is comparable to a normal ground wire.
Moreover, excellent optical performance can be achieved by using steel tubes.

1. Introduction

Self-supporting ground wires, which are used in overhead power lines are frequently modified into optical power line ground wires (OPGW) containing optical fibres for telecommunication applications.

Most OPGW designs include all-dielectric cable cores just as fibre optic ground cables.

The metallic armouring around the cable core determines not only the electrical conductivity, but also the tensile behaviour of the self-supporting cable. The tensile properties must be adopted to the cable weight.

The dielectric core leads to a large cable diameter and therefore to a heavy weight, as wind- and ice-load is a function of cable-diameter.

In this paper a different OPGW design is presented, which includes a minimum of dielectric materials leading to a cable with both, excellent ground wire properties and optical performance.

The main difference to a conventional OPGW is the use of steel tubes instead of plastic tubes to enclose optical fibres.

In the following, the advantages of steel tubes over plastic tubes for ground wire applications are discussed and the design of the steel tube containing OPGW is described.

The results of the first experiments with test cables of the new design are presented.

2. Comparison of steel tubes and plastic tubes

The optical performance of cabled fibres depends on the fibre curvature /1 /.

In usual loose tube cable designs /2,3/ this curvature is connected with the mechanical operation range of the cable due to the fibre excess length in relation to the tube length and due to the stranding of the tubes around a central member.
Moreover, also the radial clearance of the fibres in the tubes and the stranding radius of the tubes determine the mechanical operation range.

Self-supporting OPGWs usually need a large mechanical operation range of about 0.6 % .

Because the largest possible portion of the cable diameter is needed for mechanical strength and electrical conductivity the diameter of the dielectric cable core must be minimized.

This leads to both, small radial clearance of the fibres and small stranding radius of the plastic tubes, which on the other hand requires a short stranding lay length of the tubes to achieve the desired operation range.

Therefore, a minimized core diameter may lead to critical fibre curvature.

To avoid added loss or fibre strain in this case, every parameter must be of small tolerance and well suited to the special application.
While the fibre excess length is determined by loose tube manufacturing and tube stranding, the other above-mentioned parameters are determined by the geometrical tolerances of the tubes.

2.1 loose tube production

Plastic loose tubes are usually manufactured by an extrusion process, whereas steel tubes are manufactured by a steel tape forming and welding process (s.Fig.1).

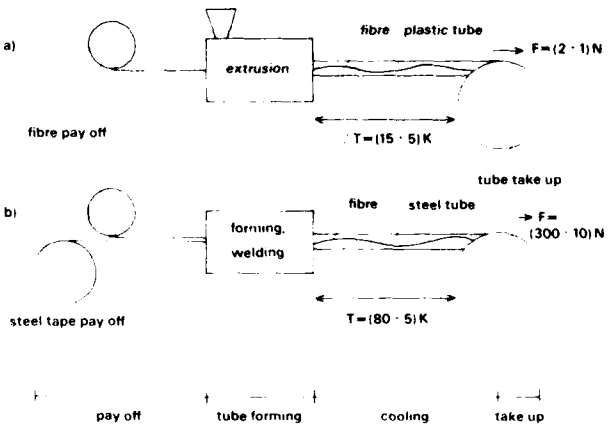

Fig.1 loose tube manufacturing

a. plastic tube extrusion
b. steel tube forming and welding

During the extrusion process as well as during the forming and welding process the tubes are exposed to temperature gradients due to cooling and due to longitudinal wind up forces.
Both may enlarge the excess length tolerance.

Therefore, the main tube material properties are the thermal expansion coefficient and the E-modulus.

The main process-parameters are temperature gradients and longitudinal pulling forces.
In Figs. 2 and 3 the contraction and elongation of the tubes are shown in relation to temperature gradients and applied longitudinal forces.

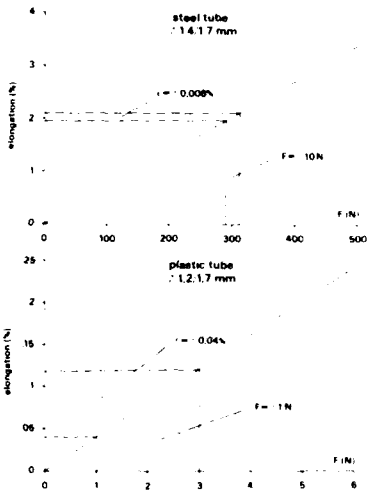

Fig.2 tube elongation due to winding up

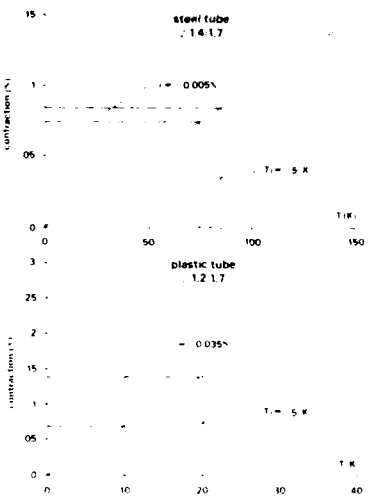

Fig.3 tube contraction during cooling

As can be seen from Fig.2 and Fig.3 a better excess length tolerance can be achieved with steel tubes than with plastic tubes.

In addition the shrinking of plastic tubes after production must be taken into account, which may enlarge the excess length.
A similar effect does not occur for steel tubes.

2.2 geometrical parameters

As stated above, the mechanical operation range of a loose tube cable depends strongly on the radial clearance of the fibres.
For a given cable design this clearance depends on the tube wall thickness.
Typical values for the tube wall thickness are between 0.1 and 0.3 mm.

The extrusion of plastic tubes with a very small wall thickness is a critical process, whereas steel tapes with a minimal thickness of 0.05 mm and excellent geometrical tolerances are easily available.

Fig.4 shows examples of the resulting tube cross sections.

Fig.4 cross section of steel tube 1.4/1.7 mm and of plastic tube 1.2/1.7 mm

Because of the smaller wall thicknes, steel tubes therefore enable a larger operation range for the same cable design with the same fibre curvature than plastic tubes.
This will be shown in the next section.

3. OPGW-design

The first step to a new OPGW-design is to modify a conventional design with an all-dielectric core.
An example for such a conventional design is the OPTOFLEX-cable, which is described in the following.

6 loose plastic tubes each containing 2 optical fibres are stranded around an FRP-rod.
The core is covered with a plastic sheath to keep the interstices of the core filled with a thixotropic gel.

The protection of the otical fibre core is provided by a multifunctional flexible hollow conductor made of 6 aluminum alloy (AA) profile wires.
It absorbs the radial and torque forces of the composite AA/AC-armour and contributes to its load bearing and conductive cross section.

The flexible hollow conductor design is important to avoid fatigue fractures often occuring on bending resistant solid aluminum pipes due to aeolian vibrations.
In addition to its rigidity the hollow conductor adds substantially to the self-damping properties of the cable by friction between the profile wires.

In the first step of modification, the dielectric elements are replaced by steel tubes and metal wires without altering the design of the outer armouring layers.

An example is shown in Fig.5.

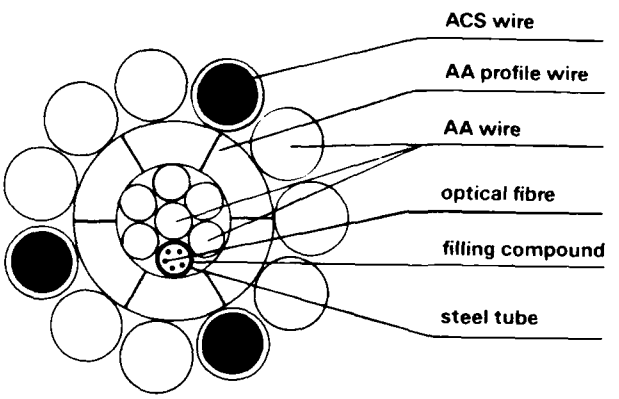

Fig.5 OPGW-design with a minimum of dielectrics

Independent of the outer armouring the cores of the two designs are compared in the following section.

3.1 comparison of the two different core designs

In order to compare the all-dielectric core with the metallic core, the corresponding operation ranges have been calculated.

The calculation is based on well known formulas /3 / and on the following assumptions

- in each case the tube is stranded around acentral member together with five dummies
- The sizes of the tubes are :
  plastic tube : 1,2/1,7 mm
  steel tube : 1,4/1,7 mm
- The stranding lay length is based on the mechanical operation range and the minimal radius of fibre curvature which is suited to the desired optical and mechanical requirements.
- The radius of curvature is 70 mm to avoid added loss at 1550 nm or 50 mm to avoid only critical fibre strain due to fibre curvature.
- each tube contains 2 fibres

The calculation was made for worst case conditions.

The results of the calculation are shown in Fig. 6.

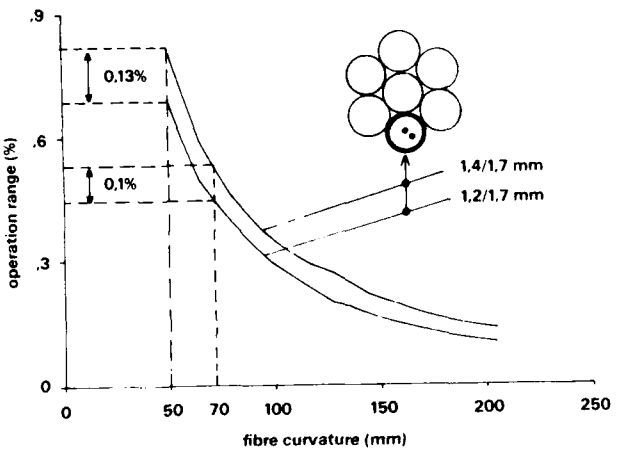

Fig.6 mechanical operation range for the two different OPGW-core designs

As follows from Fig.6, the decrease of the wall thickness of 0.1 mm leads to an increase of the operation range of about 0.1 %.

In addition, the calculation was made for core designs including different numbers of steel tubes with different outer diameters.
The core diameter is held constant in every case.

The results are shown in Tab.1.

Nr.	cable core	r mm	d_E mm	S_{1300} mm	S_{1550} mm	ϵ_{1300} o/oo	ϵ_{1550} o/oo
1	0 + 2	1,25	1,56	53	65	9,5	6,3
2	0 + 3	1,34	1,38	55	68	8,9	5,9
3	1 + 4	1,47	1,13	59	73	7,6	4,9
4	1 + 5	1,58	0,91	63	79	6,2	3,9
5	1 + 6	1,67	0,72	67	86	4,8	2,8
6	1 + 7	1,75	0,57	72	97	3,4	1,9

Moreover, because the radial fibre clearance decreases with the number of fibres in a tube, the mechanical operation range must be calculated for different numbers of fibres per tube.

To give an example, this calculation was made for the two different core designs Nr.1 and 5 of Tab.1.

The results are shown in Fig.7.

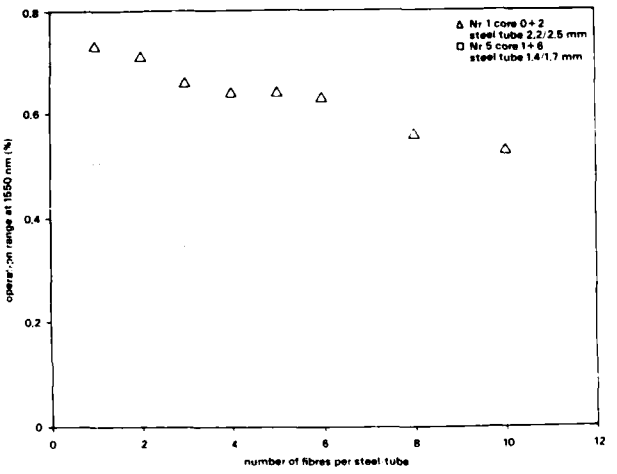

Fig.7 calculated mechanical operation range for different numbers of fibres in a tube

Based on the results of the calculations, an individual core design can be chosen for the special application.

3.2 measurement of the mechanical operation range

To proof the results of the calculation, the mechanical operation ranges of both, the conventional OPGW design and the corresponding new design (Nr.5) have been measured.

To be independent from the bending sensitivity of the fibres, the operation range in this case was not terminated by the loss increase but by the increase of fibre strain from zero.

The cable strain and the fibre strain were measured simultaneously during loading the cable with an increasing tensile force.

The results of the measurement are shown in Fig.8.

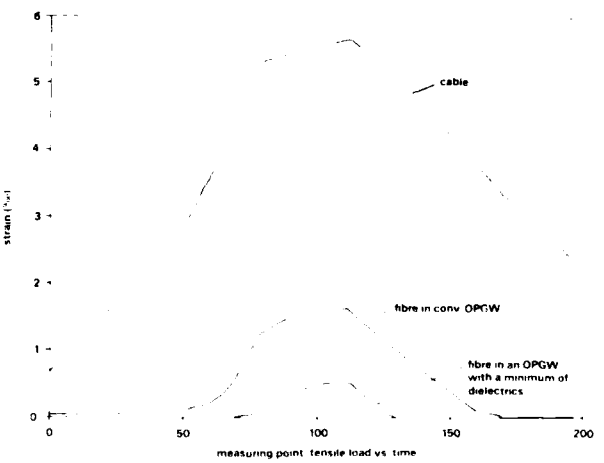

Fig.8 measured mechanical operation range for two different OPGW-designs

Fig.8 shows an operation range of 0.4 % for the conventional design and of 0.51 % for the new design.
This result is in good agreement with the calculation of sec.3.1 (Fig.6).

The results of this chapter show, that by replacing plastic tubes by steel tubes with a smaller wall thickness, the mechanical operation range or the number of fibres per tube can be increased.

4. Improved OPGW with a minimum of dielectrics

In the previous sections the improved optical performance of an OPGW containing steel tubes instead of plastic tubes was shown.

Mcreover, the use of steel tubes enables the improvement of the mechanical and electrical properties of the OPGW.

The aim of the development was a design of a cable which is comparable to a usual ground wire in its mechanical and electrical properties and which shows better optical performance than the conventional OPGW-design.

4.1 ground wire properties

A self-supporting ground wire consists of a core of galvanized steel wires serving mainly as tension elements and of an outer layer of aluminum wires serving mainly as electrical conductors.

In order to anchor a ground wire on the top of a tower, tension clamps are used which crush the outer aluminum layer to load the steel core.

In addition, to improve the behaviour against aeolian vibrations, damping clamps must be mounted onto the ground wire.

A ground wire must be characterized by the following main properties

- outer diameter
- weight
- ultimate tensile strength
- E-modulus
- electrical conductivity
- thermal expansion coefficient
- torque behaviour

4.2 Improved OPGW-design

At first sight, it seems to be an economic solution, to replace a steel or aluminium wire by a steel-tube enclosing optical fibres.

The manufacturing of such an OPGW would not be very different from a normal ground wire manufacturing.

While the mechanical and electrical properties of such a simple OPGW-design would be comparable to a ground wire, this type of cable shows the main technical disadvantage, that the steel tubes are deformed under the radial pressure of damper clamps and tension clamps.

In a crush test it could be shown, that this may lead to added loss, as can be seen in the following.
A steel tube containing fibres was crushed in radial direction by a stemple.
The tube deformation and the attenuation of the fibres were measured during the radial load was increased.

As can be seen from Fig.9, the fibres show strong increasing attenuation when a critical tube deformation is reached.

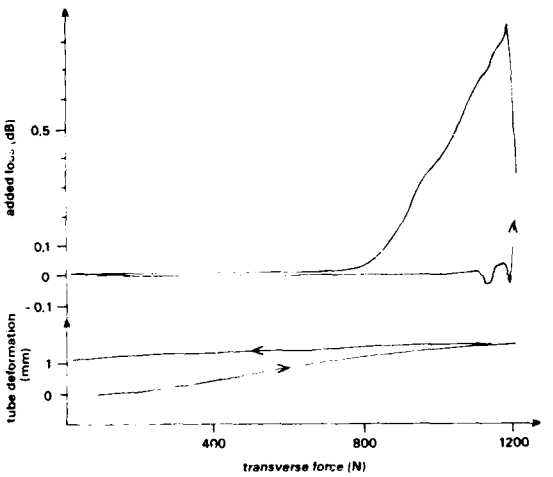

Fig.9 measured added loss due to radial steel tube deformation

So, to guarantee excellent optical performace under all expected conditions, the steel tubes in the improved OPGW-design must be protected against radial pressure.

To avoid tube deformation by tension clamps, the OPGW should be feasible to anchoring by spirals.

To protect the steel tubes against damper clamps, armouring by profile wires as shown in Fig.5 is necessary.

The OPGW-design which meets these requirements best is shown in Fig.10.

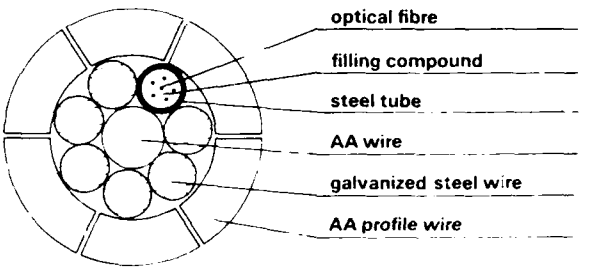

Fig.10 Improved OPGW-design with a minimum of dielectrics

The cable core includes a jelly filled steel tube containing the optical fibres, which is stranded around a central aluminum alloy wire together with six galvanized steel wires.
Around the core, aluminium-alloy wires of trapezoidal cross section are stranded in order to protect the steel tube against radial pressure and to guarantee anchoring by spirals instead of tension clamps.

The mechanical and electrical properties of this cable are comparable to a ground wire of corresponding diameter as can be seen from
Tab.2.

technical aerial cable data		ground wire 50/30	OPGW
cable diameter	mm	11,7	11,8
cable weight	kg/km	378	380
supporting cross-section	mm²	81	88,2
aluminium cross-section	mm²	51.2	65,4
steel cross-section	mm²	29,8	22,8
ultimate tensile strenght	kN	43,8	51,8
E-modulus	kN/mm²	107	78
nominal short time current (t_a=20°C)	kA,1s	5,1	6,1

In order to qualify the cable for ground wire applications, the following tests have been done on the improved OPGW :

4.3 Mechanical Tests

a.) clamp test

To test the influence of damper clamps on the steel tube in the OPGW-core, damper clamps were mounted onto the OPGW with a torque in the range of 46 Nm as shown in Fig.11.

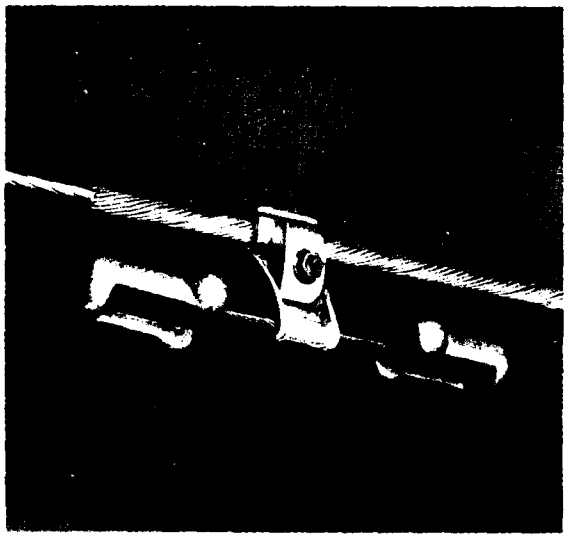

Fig.11 damper clamps mounted onto the OPGW

The attenuation of the fibres was measured after the clamps were mounted. After removing the clamps, the geometry of the steel tube was measured at the location of the clamps.

Neither a measurable added loss, nor a deformation of the steel tube due to the radial pressure was observed.
Therefore, the layer of aluminum profile wires over the core guarantees the protection of the steel tube against radial pressure of damper clamps.

b.) tension test

In order to test the anchoring behaviour, the OPGW was loaded with spirals as shown in Fig.12.

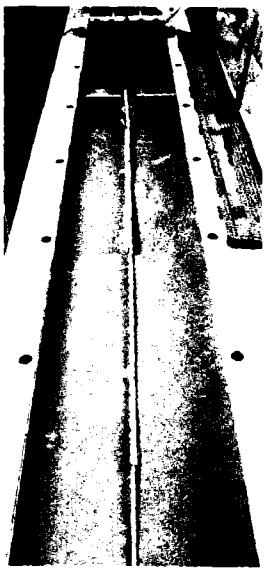

Fig.12 anchoring of the OPGW by spirals

While the cable was loaded up to the ultimate tensile strength, the cable strain was measured.
In addition the cable was loaded until break.

The results are shown in Tab.3 in comparison to corresponding results of a normal ground wire.

technical cable data	ground wire 50/30	OPGW calculated	OPGW measured
cable-ϕ mm	11,7	11,8	11,8
E-modulus kN/mm²	107	78	81
breaking load kN	43,8	51,8	54,4

When the breaking load was reached, all wires of the OPGW broke simultaneously between the anchor points in the middle of the span.
No slippage of the core inside the outer aluminum-layer was observed.

A typical break is shown in Fig. 13

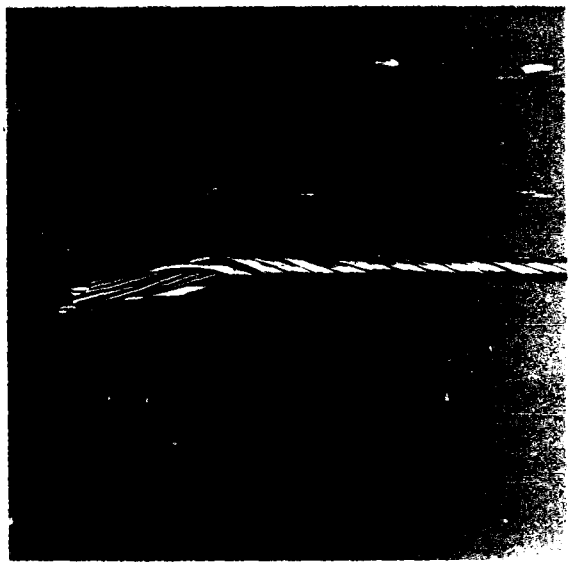

Fig.13 OPGW after breaking

This demonstrates, that the steel core of the OPGW can be loaded by anchoring spirals, so that no tension clamps are necessary.

c.) Torque behaviour

Due to the stranding of the armouring layers, an OPGW tends to twist during the laying procedure.
This may lead to a cable untwist and axial strain which exceeds the allowed value /4/.
For this reason, in most applications non-twist headboards are used to prevent the cable from twisting.
But, this leads to a complicated laying procedure.

To compare the torque behaviour of the new design in relation to the conventional OPGW, twist measurements have been done on both cables during a tensile test.

The results in Fig.14 show the improved torque behaviour of the new OPGW design.

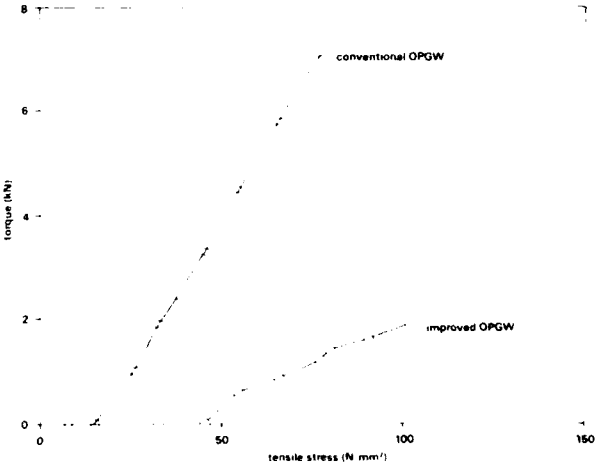

Fig.14 Torque behaviour of the conventional and the new OPGW

This improvement can be explained by the small cable diameter and the fact, that the steel wires are concentrated in the cable core.
So, no zero-twist headboards are necessary for the new OPGW.

4.4 Optical performance

All optical measurements on the improved OPGW have been done on singlemode fibres.
The attenuation after cabling and during tensile loading was measured at 1300 nm and 1550 nm.

a.) cabling

The attenuation was measured after every cabling step.

No added loss due to cabling was observed.
After cabling, the following attenuation values were measured :

$$\alpha_{1310\ nm} = 0.34 \pm 0.02\ dB/km$$

$$\alpha_{1550\ nm} = 0.21 \pm 0.02\ dB/km$$

b.) mechanical operation range

A test cable of the new OPGW design was loaded two times up to the maximum allowable load over a length of about 100m.
The attenuation was measured during increasing tensile force.

The results are shown in Fig.15.

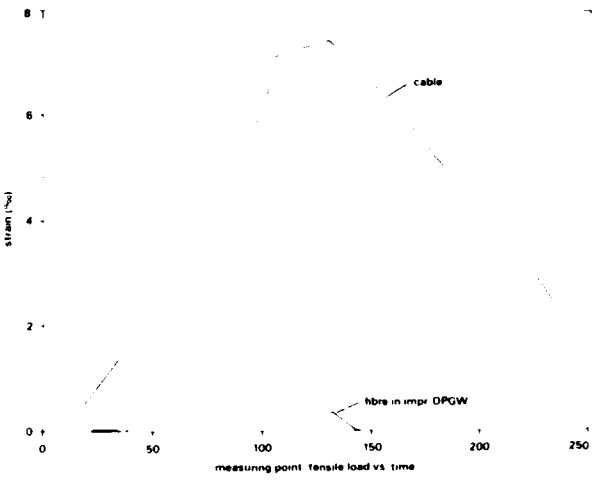

Fig.15 measurement of the mechanical operation range of the new OPGW

Fig.15 shows, that even at the highest load no increase in attenuation could be measured.

While the measuring accuracy of the attenuation depends strongly on the test length, the fibre strain can be measured by a phase shift method over a short test length with a high degree of accuracy.

Therefore, to find out the mechanical operation range of the cable, the strain method is preferred.

The results of the simultaneous measurement of the cable and fibre strain are shown in Fig.16.

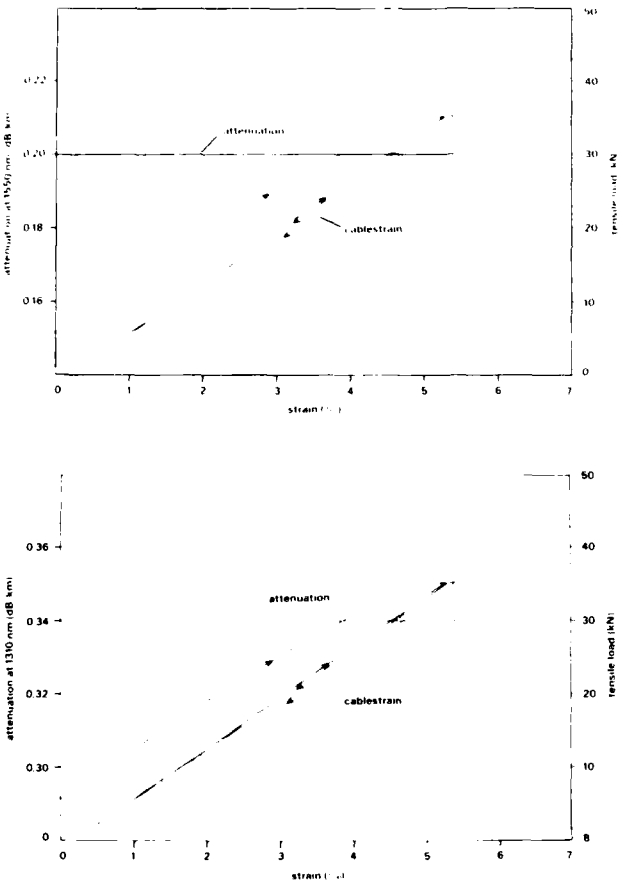

Fig.16 measured cable and fibre strain during cable loading

The results of the measurement are in good agreement with corresponding calculations and show the excellent behaviour of the new OPGW.

4.5 Further tests

The presented new OPGW design is now under study.
The most important tests are described above.
In our future development we expect further results for additional test conditions, such as

- lightning
- short current
- vibration
- temperature cycling

The results of these additional tests will be published in future.

5. conclusions

A new technique of loosely enclosing optical fibres into steel tubes has been presented in this paper.

This new type of loose tube enables the design of a new OPGW-generation with a minimum of dielectrics.
Due to the advantages of the steel tubes over plastic tubes, the new OPGW design is characterized by improved optical and mechanical properties.

The result of our development is an OPGW, which is comparable to a ground wire in its mechanical properties and to a conventional OPGW in its optical properties.

We are confident, that in future the cable will be used in overhead power lines.

Acknowledgements

The authors wish to express their thanks and acknowledge the contributions of Mr. H.-P. Dann, Mr. P. Koenig, Mr. F. Kurth, Mr. K.-H. Nolting and Mr. N. Wenzel.

References

/1/ P. Geittner, H. Lydtin, F. Weling, D.U. Wiechert
Proc. 13th ECOC, Helsinki 1987

/2/ H.G. Haag, W. Lackas, G. Zeidler
NTZ, 39 (1986), No. 7

/3/ U. Oestreich, G. Zeidler, P. Bark
Proc. 29th IWCS, Cherry Hill 1980

/4/ T.C. Cannon, M.R. Santana
Proc. 24th IWCS, Cherry Hill 1975

J.M. Schneider was born in 1954. He graduated from the University of Hannover in 1984 with a Dr.rer.nat. in Physics. From 1980 to 1984 he was a research and teaching assistant at the Institut für Plasmaphysik in Hannover where he worked on laser and plasma physics. He joined Philips Kommunikations Industrie AG in 1984.
Since 1987 he is head of the department for telecommunication cable development.

Jörg Schmelter was born in 1960. He studied at the college of Hagen and received the diplom degree in physical engineering in 1986.
From 1986 to 1987 he was testing engineer at the Bundesamt für Wehrtechnik in Munster where he worked on simulation of thermal radiation. Since 1987 he is with Philips Kommunikations Industrie AG where he is engaged in development of OPGWs.

Robert Herff is head of the project department of Philips Kommunikations Industrie AG, division communication cables and equipment, and he has been planning groundwire aerial cables for overhead power lines since 1970. After his study at the Köln polytechnic he headed some telecom cable projects both in Germany and abroad. Next he worked as planning engineer and took up his present post in 1978.

SUITABLE DESIGN AND CHARACTERISTICS OF OPTICAL GROUND WIRE FOR 1.55μm WAVELENGTH

M. Kawasaki S. Yamazaki T. Tokunaga K. Sanbonsugi

Hitachi Cable, Ltd.
Chiyoda Bldg., 2-1-2, Marunouchi, Chiyoda-ku, Tokyo 100, Japan

Abstract

Two types of Composite Fiber-Optic Overhead Ground Wire (OPGW) for 1.55μm wavelength at which silica based optical fibers have minimum optical attenuation have been developed.
One is the long distance type which consists of low attenuation type fiber and highly reliable "Sponge type" optical fiber unit.
The other is the large capacity type which consists of small dispersion type fiber and high-density "Spacer type" optical fiber unit.
Many tests have made it clear that both types of OPGW have satisfactory performances.

1. Introduction

Optical fiber telecommunication systems have major technical advantages in power utilities, such as low-attenuation, large-capacity and immunity of electromagnetic interference. Therefore Composite Fiber-Optic Overhead Ground Wire (OPGW), which is most reliable and suitable fiber-optic media along overhead power transmission lines, has been used widely in the world, containing 1.3μm SM fibers.
To fulfill recent demands for longer distance and larger capacity communication of power utilities, 1.55μm OPGW has been developed based on the fact that silica based optical fibers have minimum attenuation at 1.55μm wavelength.
But, when fibers designed for 1.3μm wavelength are used at 1.55μm wavelength, attenuation will be increased by microbending due to cabling and high temperature etc. especially for OPGW. Therefore it is necessary to design SM fibers for 1.55μm wavelength operation, but it is difficult to optimize both attenuation and dispersion at the same time. Then, we propose two types of 1.55μm SM fibers for this reason.
In addition, two types of Optical fiber unit (OP unit) were also designed for more usefull application of the above mentioned fibers.

2. Fiber design

The relationship among refractive index difference, cut-off wavelength, zero dispersion wavelength and core diameter is shown in Fig.1. Assuming that cut-off wavelength is 1.2μm and zero dispersion wavelength is 1.55μm, refractive index difference and core diameter should be about 1% and smaller than 4.5μm respectively.
In this case, attenuation will be large due to the increase of Rayleigh scattering.
On the other hand, when refractive index difference is smaller, attenuation will be small, but the bending loss and dispersion will be increased.
Furthermore, for the actual production, bending properties for cabling process and mode field diameter for easy splicing should be considered.
As a result of the above mentioned consideration, we designed two types of fibers having simple index profiles which are suitable for fully synthesized VAD (Vapor Phase Axial Deposition) methods;
One is low attenuation type which is optimized for attenuation properties, and the other is small dispersion type which is optimized for dispersion properties. As the profile of small dispersion type, we adopted the triangle index profile which has greater advantages than step index profile in low attenuation and large mode field diameter.
The characteristics of those two types of fibers are shown in Table 1.

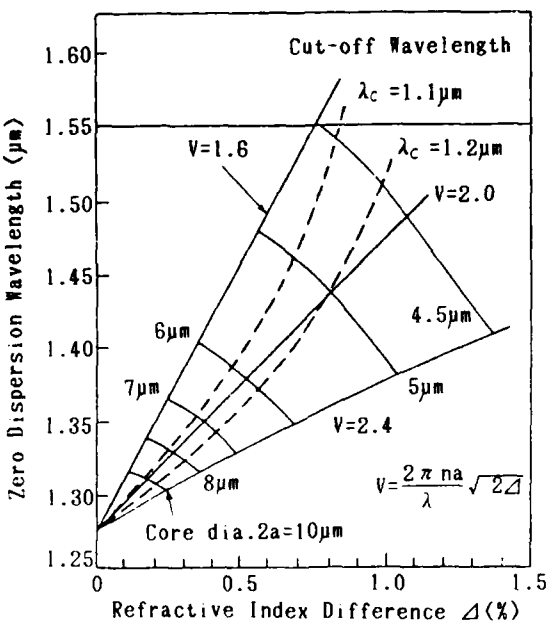

Fig.1 Parameters of Step Index Profile SM Fiber

Table 1 Characteristics of 1.55μm SM Fiber

Type of 1.55μm SM fiber	Low attenuation type	Small dispersion type
Refractive index profile	Step	Triangle
Refractive index difference	0.38%	0.85%
Mode field diameter *	10.5μm	7.7μm
Cladding diameter	125μm	125μm
Cut-off wavelength	1.45μm	0.98μm
Attenuation at 1.55μm wavelength	0.19dB/km	0.22dB/km
Dispersion at 1.55μm wavelength	18ps/nm.km	1.5ps/nm.km

* According to Petermann Ⅱ definition

3. Cable design

It is necessary for designing of optical fiber unit (OP unit) for OPGW to consider that optical fiber cores should be housed inside a small aluminum tube and the inside space of the tube should be utilized effectively.
Therefore, we concluded that the reliable "Sponge type" is suitable for a cable containing relatively small number of fibers and the high-density "Spacer type" is suitable for a cable containing relatively large number of fibers.
Both types of OP units containing 1.3μm SM fibers have been already adopted to OPGW both in Japan and abroad.
Every material to be used is selected to have heat resistance of 300°C.

(1) "Sponge type"

Fig.2 shows the cross-sectional view of "Sponge type" OPGW 70mm^2.
Each individual silicone coated fiber is jacketed by fluorocarbon polymer for easy handling and protection against heat and mechanical force.
The jacketed fibers are stranded onto a sponge core having FRP (Fiber Reinforced Plastic) tension member in the center of it, then covered by heat resistant glass tape, and covered with aluminum tube.
As shown in Fig.3, "Sponge type" OPGW is designed to reduce optical fiber strain.
When the OP unit is stretched together with the whole OPGW, each jacketed fiber compresses the cushion (sponge) layer and moves toward the center. Thus, the strain to each optical fiber is reduced considerably.

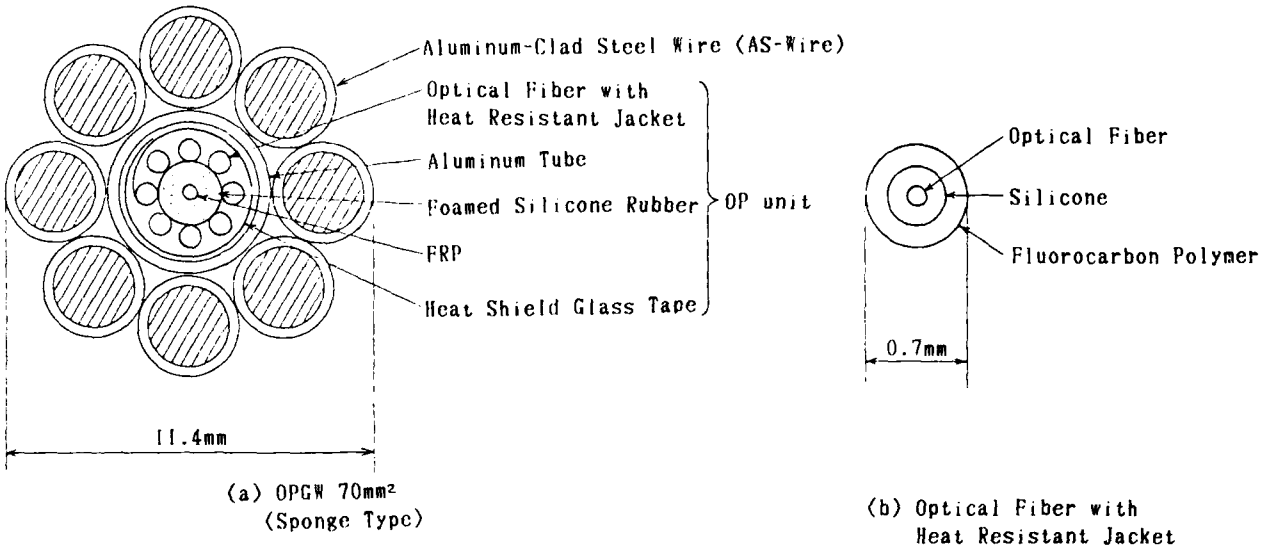

Fig.2 Construction of "Sponge Type" OPGW

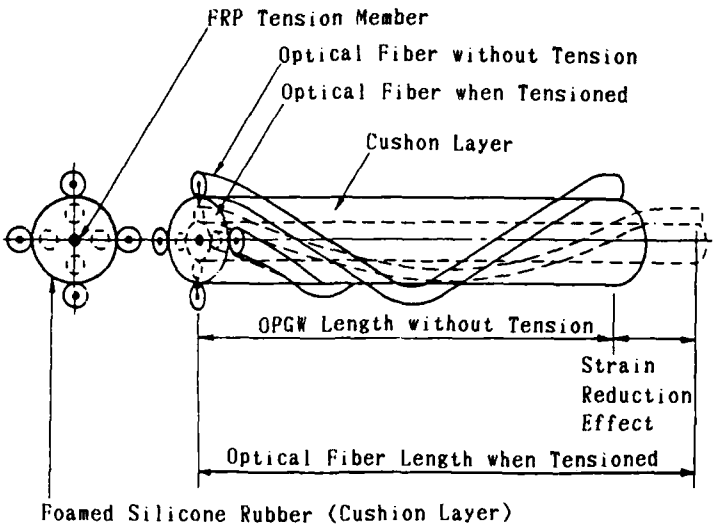

Fig.3 Strain Reduction Effect of "Sponge Type" OPGW

(II) "Spacer type"

Fig.4 shows the cross-sectional view of "Spacer type" OPGW 70mm^2. In order to save space, 6 fibers are formed into sub-unit and then settled inside the grooves of aluminum spacer.

The construction of sub-unit is that 6 silicone coated fibers are stranded around FRP core and wrapped with a thin heat resistant tape.
In this spacer type, the strain to the whole OPGW is directly transfered to each fiber. Therefore, it should be considered to increase the screening load to the fiber for reliable design.

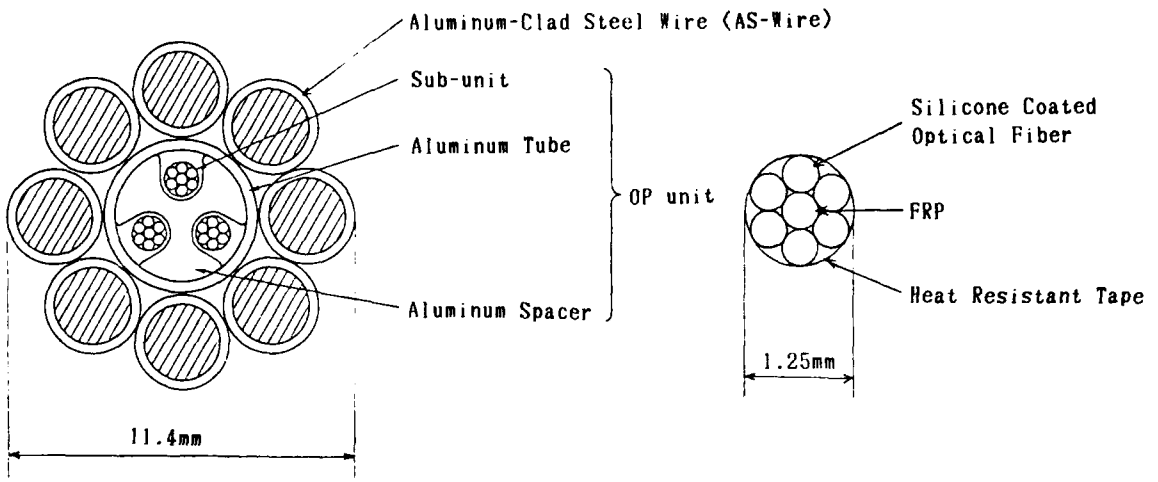

(a) OPGW 70mm^2 (Spacer Type)

(b) Sub-unit

Fig.4 Construction of "Spacer Type" OPGW

4. Cable characteristics

The evaluation was made on the following two types of OPGW.

A) OPGW combined low attenuation fibers and sponge type unit (OPGW.A)
——— long distance type

B) OPGW conbimed small dispersion fibers and spacer type unit (OPGW.B)
——— large capacity type

4.1 Optical fiber and fiber unit

In this paragraph, the characteristics of the low attenuation fiber jacketed by fluorocarbon polymer in OPGW.A and the small dispersion fiber in sub-unit of OPGW.B are evaluated.

(1) Heat cycle test

Fig.5 shows the attenuation change at 1.55μm wavelength under the heat cycle test. The applied temperature of -30°C to +150°C is considered based on the estimated low environment temperature and high temperature caused by induced current. The attenuation change showed a good result of within 0.03 dB/km in both types.

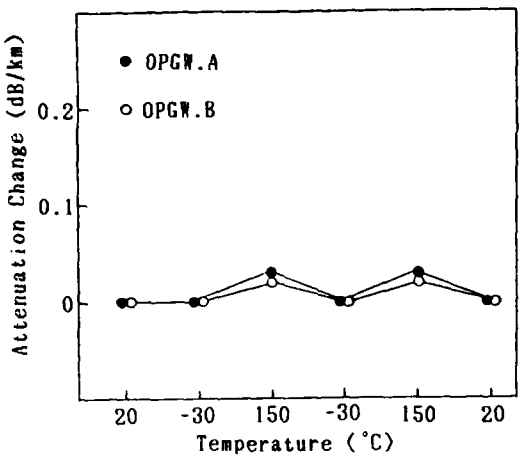

Fig.5 Optical Attenuation Change of 1.55μm Fiber under Heat Cycle (-30°C to +150°C)

(2) Continuous 150°C temperature test

The test result of attenuation increase under continuous 150°C environment was shown in Fig.6. The test condition of 150°C x 400 hours was considered as the accumulated heat of the temperature rise by induced current during summer seasons within the life cycle.
The result showed a good figure of the variation within 0.05 dB/km.

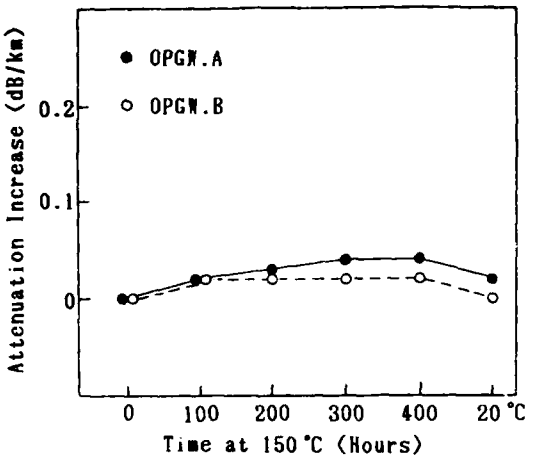

Fig.6 Optical Attenuation Increase of 1.55um Fiber under Continuous High Temperature (150°C)

(3) Heat shock test

Fig.7 shows the attenuation increase when 300°C is applied in short time. This test simulates the condition of short circuit failure. The attenuation change was within 0.03 dB/km in both types.

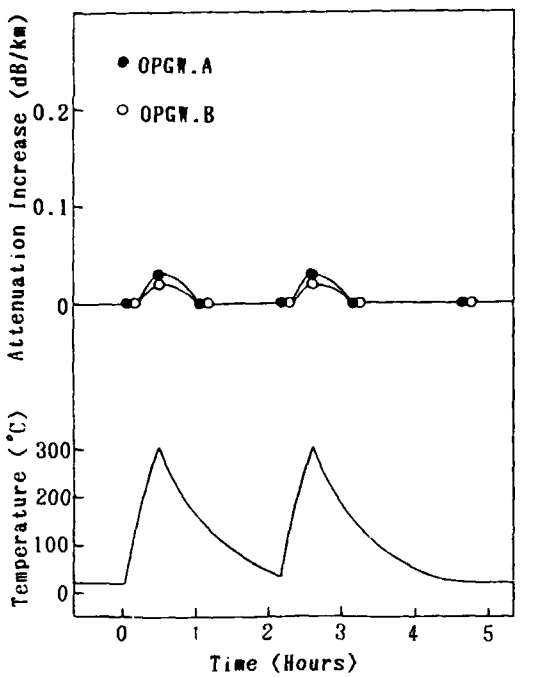

Fig.7 Optical Attenuation Increase of 1.55μm Fiber under Heat Shock (20°C to 300°C)

Through the above tests, the optical fibers and sub-units were proved their good characteristics under severe conditon of OPGW application.

4.2 OPGW

(1) Stretch test

Fig.8 shows the stretch-strain relations while monitoring optical attenuation. While the fiber within "Spacer type" receives the same strain as the whole OPGW, the strain of the fiber within "Sponge type" is approx. 60% of that of the whole OPGW. This shows the high reliability of "Sponge type". It is a remarkable characteristics of "Sponge type" that it has both high temperature resistivity and strain reduction effect.
Through this test, both types of OPGW showed no attenuation increase upto OPGW breakage.

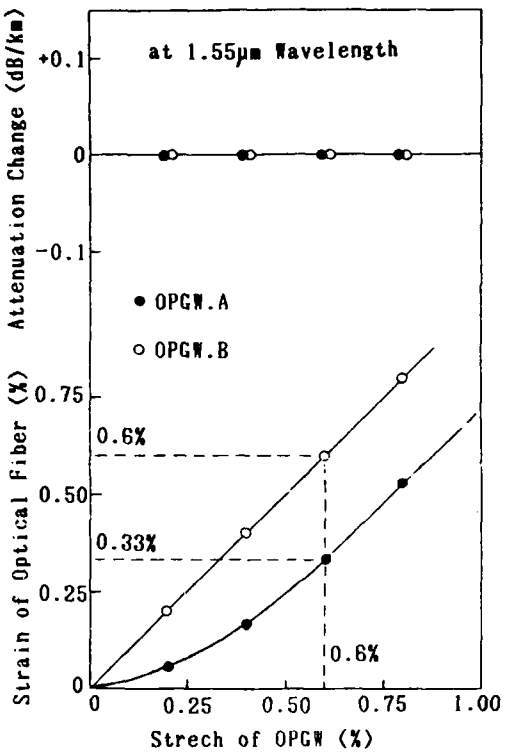

Fig.8 Strech Test of OPGW

(2) Continuous current test

Although the components of OP unit are of hydrogen free materials since the attenuation increase by H_2 is a serious matter to optical fibers, moisture within aluminum tube may react to aluminum and create H_2 gas when the electric current is rated to OPGW.

Therefore we confirmed the attenuation increase through the rated current test on OPGW.B.
Fig.9 shows the attenuation increase under rated current of 70°C to 160°C for 400 hours.
Although this test was aimed at the same condition as mentioned 4.1(2) continuous 150°C temperature test, the temperature varied from 70°C to 160°C according to environmental conditions in the actual outside fields.
The attenuation increase was considerably small of within 0.04 dB/km at 1.55μm wavelength.

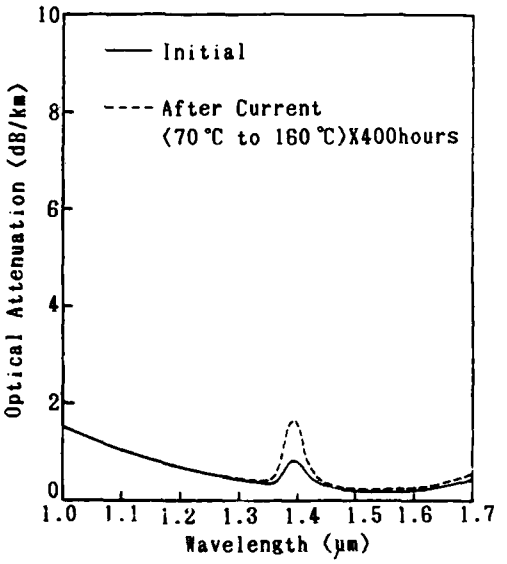

Fig.9 Continuous Current Test of OPGW.B

(3) General tests

Following tests were carried out on 1.55μm OPGW and the result was as good as that of the ordinary 1.3μm OPGW.

i) Bending

ii) Twist

iii) Vibration

iv) Compression

(4) Installation

i) Field application

The result of an actual field application of one type of OPGW.A is shown in Fig.10. The average attenuation value at 1.55μm wavelength among the three stages of optical fiber, OPGW and post-installation was 0.19dB/km to 0.20dB/km. We consider the values are very small and the change by installation is negligible in view of measuring conditions.

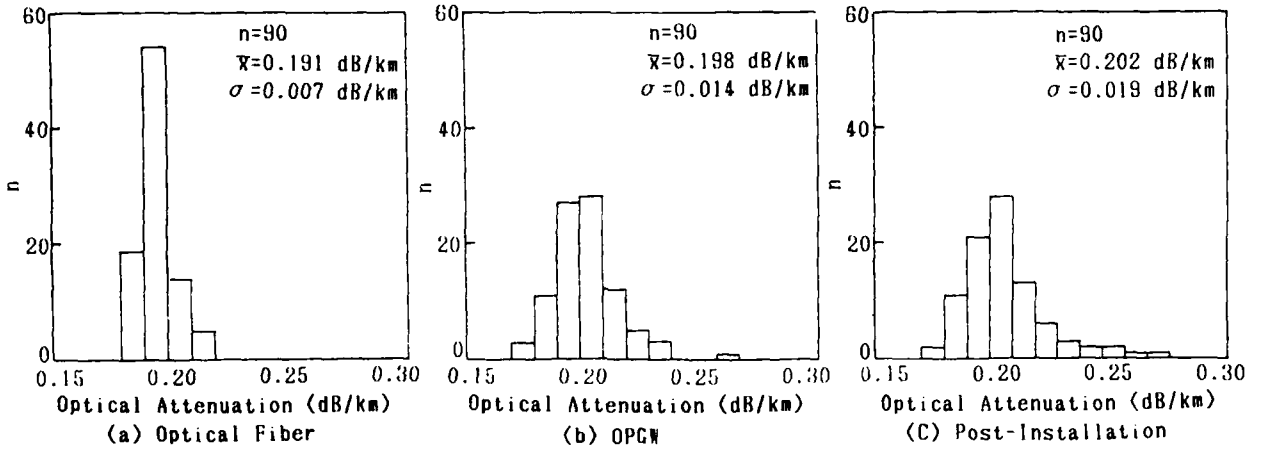

Fig.10 Optical Attenuation Histogram at 1.55μm wavelength (OPGW.A)

ii) Field test

OPGW.B was finally sagged in the test line shown in Fig.11 after three times of stringing process.

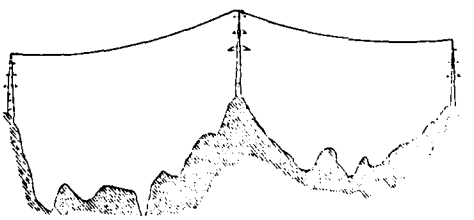

Tower No.	No.1	No.2	No.3
Span Length	534m	459m	
Height above the Sea	373m	394m	386m

Fig.11 Outline of the Test Line

Fig.12 shows the optical attenuation value of about 0.22dB/km. The result shows that OPGW.B has also stable characteristics for stringing and sagging.

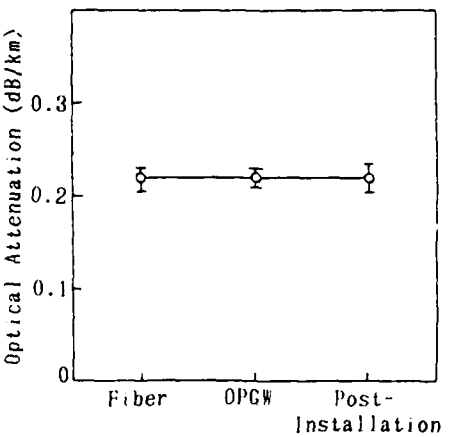

Fig.12 Optical Attenuation at 1.55μm Wavelength (OPGW.B)

5. Conclusion

For OPGW operated at 1.55μm wavelength, long distance (low attenuation and high reliability) type and large capacity (small dispersion and high density) type were developed and evaluated. Both types of OPGW showed good characteristics in various tests, and we are sure that those OPGW will contribute greatly to power utilities.

On the actual line, the long distance type having "Sponge type" OP unit was already installed and showed stable characteristics. Flexibility of OPGW selection depending on the requirement of transmission distance and capacity will be given by a suitable combination of SM fiber for 1.55μm wavelength and OP unit construction.

References

(1) D. Gloge, "Dispersion in Weakly Guiding Fibers", Appl. Opt., 10, No.11, P.2442, 1971

(2) Y. Takuma, et al., "Design Consideration on Bend Optimized 1.55μm Single-Mode Optical Fibers", First Optoelectronics Conference (OEC '86) Technical Digest, July 1986, Tokyo.

(3) S. Terada, et al., "Application of OPGW with Single Mode Optical Fiber in 360KV Large Scale Overhead Transmission Line", Hitachi Cable Review No.5 (August, 1986)

(4) T. Sato, et al., "Optimum Design of Composite Fiber-Optic Overhead Ground Wire (OPGW)", IEEE/CSEE Joint Conference on High Voltage Transmission Systems in China (October, 1987).

Makoto Kawasaki

Hitaka Works,
Hitachi Cable, Ltd.

5-1-1, Hitaka-cho,
Hitachi-shi, 319-14,
Japan

Makoto Kawasaki received his B.E. degree in Applied Physics from Waseda University in 1980. He then joined Hitachi Cable, Ltd. and has been engaged in design and development of optical cables.

Shojiro Yamazaki

Hitaka Works,
Hitachi Cable, Ltd.

5-1-1, Hitaka-cho,
Hitachi-shi, 319-14,
Japan

Shojiro Yamazaki received his B.E. degree in Electrical Engineering from the Osaka University in 1975. He then joined Hitachi Cable, Ltd. and is currently engaged in design of fiber optic communication systems with OPGW.

Toshihide Tokunaga

Cable Research Lab.,
Hitachi Cable, Ltd.

5-1-1, Hitaka-cho,
Hitachi-shi, 319-14
Japan

Toshihide Tokunaga received his B.S. and M.S. degrees in Chemistry from Kikkyo University in 1972, 1974. He then joined Hitachi Cable, Ltd. and has been engaged in research of optical fiber fabrication.

Kiyoshi Sanbonsugi

Toyoura works,
Hitachi Cable, Ltd.

1500, Kawajiri-cho,
Hitachi-shi, 319-14,
Japan

Kiyoshi Sanbonsugi received his B.E. degree in Mechanical Engineering from the Tohoku University in 1969. He then joined Hitachi Cable, Ltd. and is currently engaged in design and development of aluminum conductor for overhead transmission line.

MOVEMENT OF NON-METALLIC SELF-SUPPORTING OPTICAL FIBER CABLE UNDER WIND PRESSURE

Y. Ishihata*, K. Saito*, K. Nakadate*, H. Horima** K. Niikura**,
A. Kurosawa*** and T. Ohmori***

*Tohoku Electric Power Co., Inc. 3-7-1, Ichiban-cho, Sendai 980, Japan
**Sumitomo Electric Industries, Ltd. 1, Taya, Sakae-ku. Yokohama 244, Japan
***Kitanihon Electric Cable Co., Ltd. 1-2-1, Koriyama, Sendai 982, Japan

Abstract

Non-metallic self-supporting optical fiber cable has been developed for use as optical transmission line to be installed on steel pylons. When this optical fiber cable is installed on steel pylons with intervening long spans, the cable may be placed under severe conditions with higher wind pressure load. Therefore, it is important for the proper design of cable installation to determine clearly whether galloping vibration exists or not. Non-metallic self-supporting optical fiber cable was subjected to wind tunnel tests and an actual scale field test. Based on the test results it has now become possible to determine the most appropriate installation position of non-metallic self-supporting optical fiber cable on steel pylons.

1. Introduction

The authors have developed a non-metallic self-supporting optical fiber cable which can be installed on power transmission steel pylons in order to implement the flexible application of optical fiber cable. Furthermore, field testing has shown that this cable possesses the characteristics necessary for practical use.[1-3]

However, for installation of this non-metallic self-supporting optical fiber cable, the range of movement due to wind and other factors must be taken into consideration so that the optical fiber cable does not come in contact with the power transmission line. The results of wind tunnel tests and an actual scale field test with regards to range of movement and the presence/absence of galloping are herein reported.

2. Structure of non-metallic self-supporting optical fiber cable.

The structure of non-metallic self-supporting optical fiber cable is shown in Fig. 1. In order to prevent electromagnetic induction from the transmission line, glass fiber reinforced plastic (FRP) is used for the suspension line and the composition of the cable is completely non-metallic. The optical fiber cable is attached to the suspension line by polyethelene (PE) connectors with constant spacing so as to provide for catenary; i.e., the main body of the optical fiber cable is about 0.5% longer than the suspension line to which it is attached, midway between the plastic connecting bodies.
Since this composition does not result intension to the optical fiber cable itself until the suspension line is elongated by about 0.5%. Young's modulus of suspension line thus becomes 3-4 times that of conventional FRP rod in equivalent terms. Therefore the diameter of the FRP suspension line need not be enlarged, and small diameter and light weight of the entire cable are thus possible.

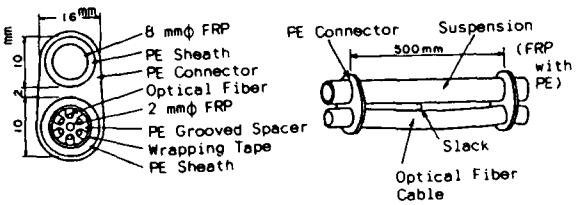

Fig. 1 Structure of non-metallic self-supporting optical fiber cable
(Note: cable weight is 0.21 Kg/m)

3. Summary of study

Wind tunnel tests and a field test were conducted in order to analyze the range of movement and the lateral deflection and galloping characteristics of non-metallic self-supporting optical fiber

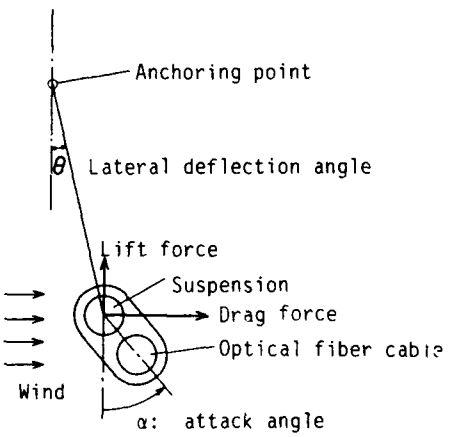

Fig. 3 Relationship between wind pressure force and lateral deflection angle

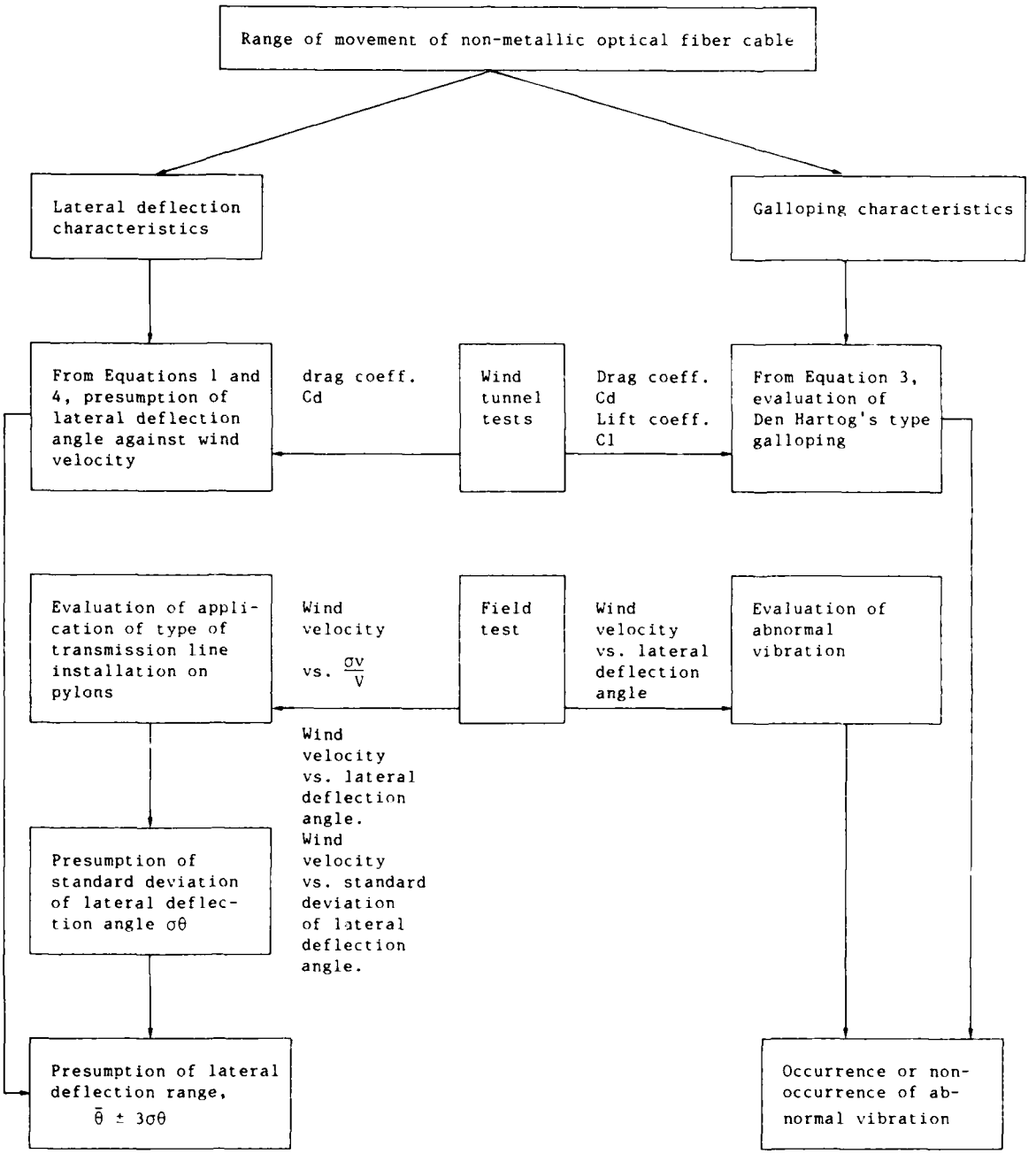

Fig. 2 Flow of analysis

cable. The flow of analysis is as shown in Fig. 2, and the definitions of lateral deflection angle, attack angle and wind pressure force (drag force and lift force) are as shown in Fig. 3.

4. Wind pressure characteristics

(1) Aerodynamic coefficient characteristics
As shown in Figs. 4 and 5, non-metallic optical fiber cable is fixed on a balance. This optical cable and the wind are set to obtain angle α (attack angle); wind velocity was changed and wind pressure force (drag, lift) were measured. Furthermore, the aerodynamic coefficients (drag coefficient Cd, lift coefficient Cl) were obtained from the following equations.

$$Pd = \frac{1}{2} \rho Cd\, DV^2 \qquad (1)$$

$$Pl = \frac{1}{2} \rho Cl\, DV^2 \qquad (2)$$

namely, Pd: drag force (Kgf/m)
Pl: lift force (Kgf/m)
ρ : air density (0.12 Kgf·sec^2/m^4)
D : equivalent outer diameter of optical cable (m)
V : wind velocity (m/sec)

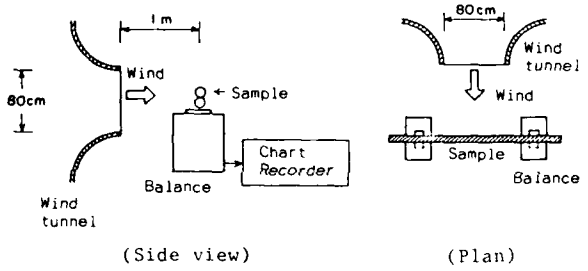

Fig. 4 Schematic of wind tunnel test equipment

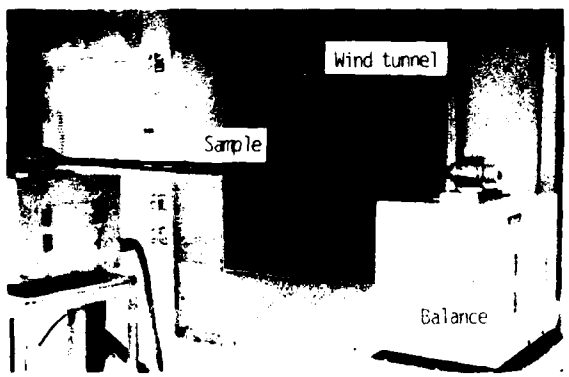

Fig. 5 View of wind tunnel test equipment

Also, equivalent cable outer diameter D was deemed to be the outer diameter of projection when the cable was at 45° inclination, setting a uniform diameter of 15.6mm (22mm × 1/√2). Test results regarding drag coefficient Cd and lift coefficient Cl are shown in Figs. 6 and 7.

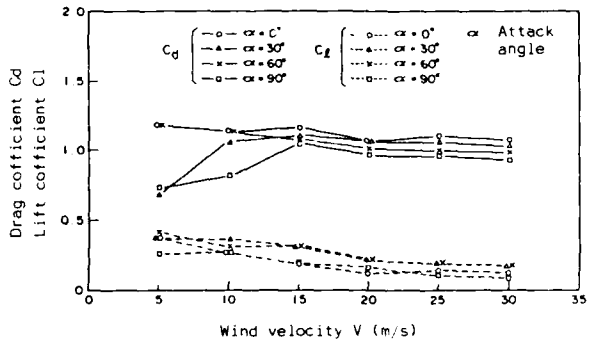

Fig. 6 Characteristics of aerodynamic coefficients of non-metallic optical fiber cable against wind velocity

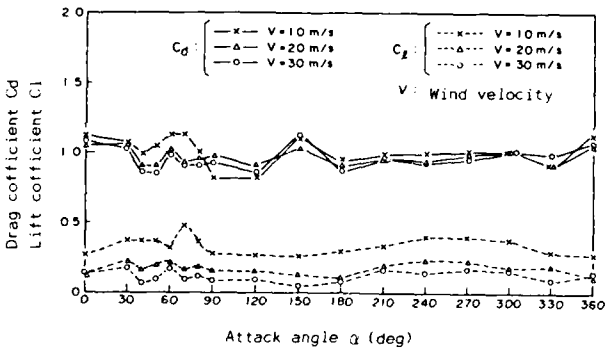

Fig. 7 Characteristics of non-metallic optical fiber cable against attack angle of aerodynamic coefficients

(2) Evaluation of Den Hartog's type galloping
Den Hartog's equation was used to determine whether or not galloping occurred.

$$(Cd+\frac{dCl}{d\alpha})\cos^2\phi - 2Cd + (Cl-\frac{dCd}{d\alpha})\sin\phi\cos\phi < 0 \qquad (3)$$

When the condition as per equation (3) is satisfied by inserting aerodynamic coefficients of respective attack angles into equation (3), galloping vibration of Den Hartog occurs. φ is the angle representing the vibration directions of optical cable. Since the vibration directions cannot be specifically determined from a stationary state, it was deemed that φ could be any value within 0-2π, following which aerodynamic characteristics of non-metallic optical cable was

inserted into Equation (3) to evaluate whether the Den Hartog's type galloping occured. It was found that aerodynamic coefficients of non-metallic optical fiber cable did not satisfy Equation (3) against respective wind velocities and attack angles. Therefore, it seems that this type of optical fiber cable is not conductive to Den Hartog's type galloping.

5. Field test of actual scope

To verify the range of movement of non-metallic optical fiber cable and the occurrence/non-occurrence of galloping, non-metallic optical cable was installed on actual scale steel pylons of the Mutsu test line of Tohoku Electric Power Co., Inc. as shown in Fig. 8. The field test was conducted over a period of 2.5 years (Feb. 1986 - July 1988).

(1) System composition

Information regarding the installation of non-metallic optical fiber cable is shown in Figs. 9 and 10, and composition of the test system is shown in Fig. 11.

Non-metallic optical fiber cable was installed on steel pylons of actual scale with a span of 285 m. Cable tension was measured using a load cell, and this measured result together with the values of wind direction and wind velocity were recorded by a data recorder and a multi-point dot printing strip chart recorder. Regarding the observation of behavior of cable, a target composed of reflection plate was fitted at the mid point of the span; the reflections, from the target, of sunlight during daytime and a lighting fixture from underheath of night were observed using an ITV camera and recorded by a VCR.

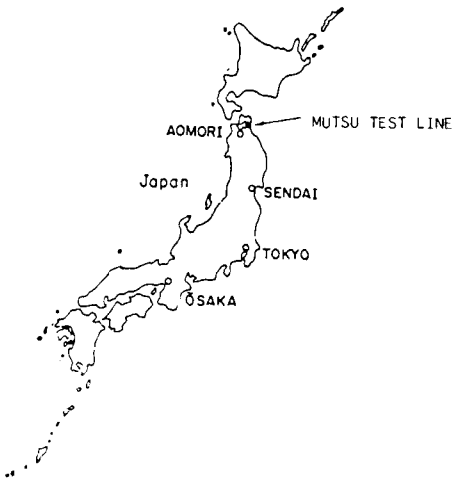

Fig. 8 Location of test line

Furthermore, the VCR and the data recorder were so controlled as to automatically activate when the wind velocity reached a certain point.

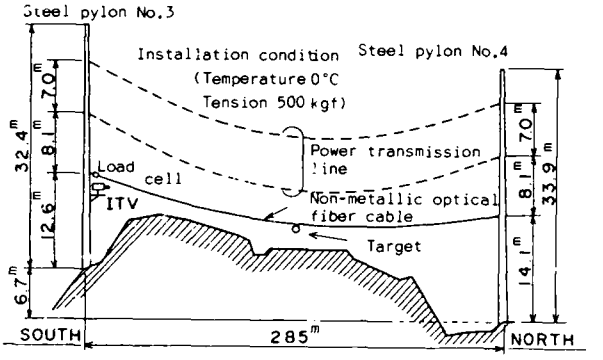

Fig. 9 Situation of installation of non-metallic optical cable

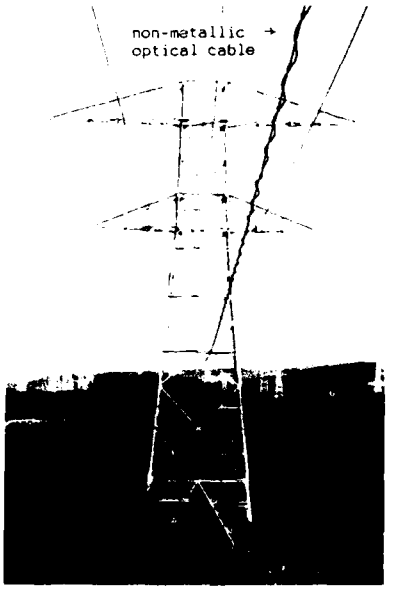

Fig. 10 View of non-metallic optical fiber cable installed on steel pylons

(2) Result of measurements

(a) Wind characteristics of the test environment

The relations between average wind velocity and gust rate (=maximum wind velocity/average wind velocity) and between average wind velocity) and intensity of wind disturbance (=standard deviation of wind velocity/average wind velocity) at the site during the field test are shown in Figs. 12 and 13. As shown in Fig. 12, gust rate is 1.2 - 1.6 in the high velocity band, equal to that reported elsewhere in general. This test line envi-

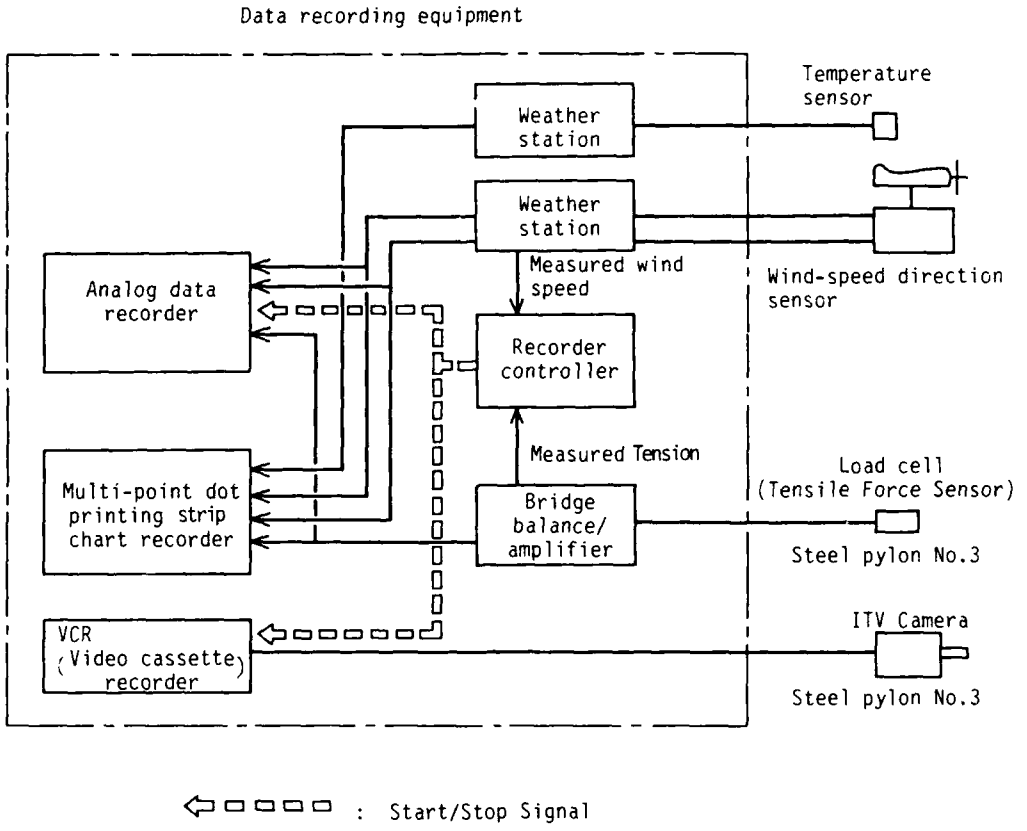

Fig. 11 Composition of test system

ronment is presumed to be typical, not special. Fig. 13 shows the intensity of wind disturbance used to calculate standard deviation of lateral deflection angle mentioned below. Based on this result, the intensity of wind disturbance in the high velocity band which poses a problem for the access of lateral deflection, was found to be 0.18.

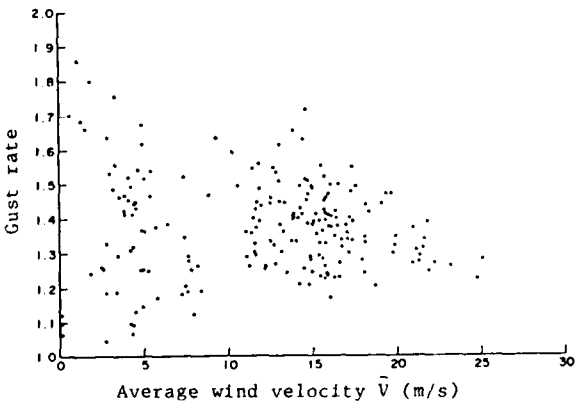

Fig. 12 Relation between wind velocity and gust rate

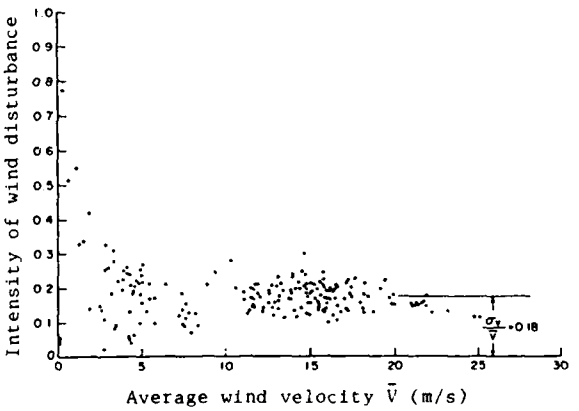

Fig. 13 Relation between wind velocity and intensity of wind disturbance

(b) Cable tension

The relations between average wind velocity and tension and between average wind velocity and maximum value of tension variation are shown in Figs. 14 and 15. From these figures, it was clarified that the maximum value of cable tension variation was less than 100 Kgf, which is less than 20% of installation tension, and that there was no occurrence of abnormal vibration such as galloping.

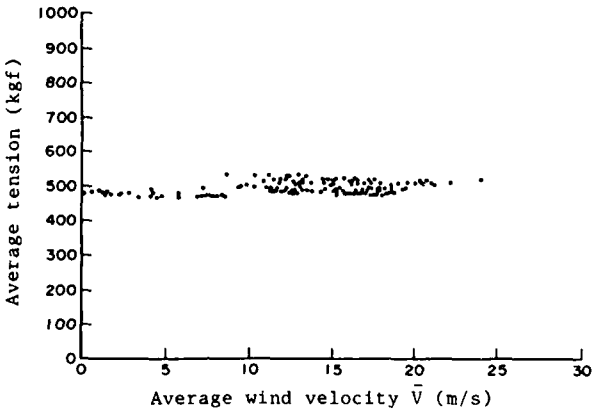

Fig. 14 Dependence of average tension on wind velocity

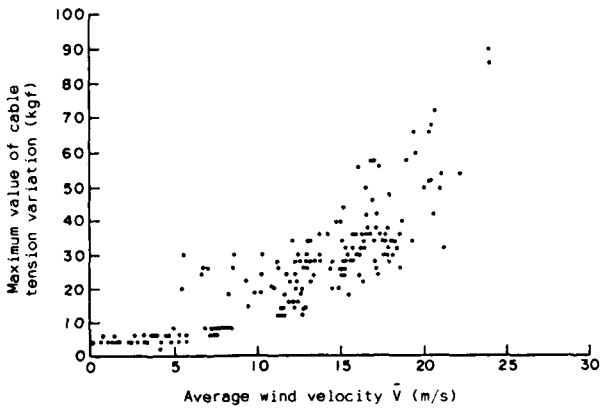

Fig. 15 Dependence of maximum value of tension variation on wind velocity

(c) Lateral deflection

An example of the locus of lateral deflection movement at the midpoint of the span of non-metallic optical fiber cable observed by ITV camera is shown in Fig. 16.

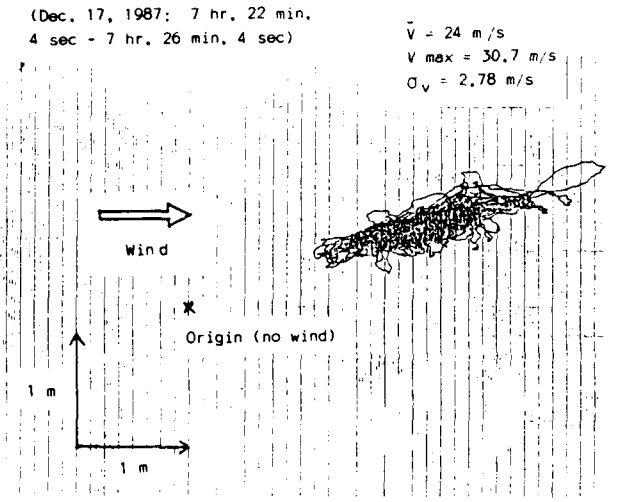

Fig. 16 Locus of lateral deflection movement (midpoint span)

Furthermore, the locus of lateral deflection movement recorded in VCR was subjected to AD conversion at the sample interval of 0.1 second. The average value and standard deviation of cable lateral deflection angle were calculated, and the relation to average wind velocity was obtained. The result is shown in Figs. 17 and 18. θ is given as follows:

$$\theta = \tan^{-1}\left(\frac{Pd}{W}\right) \qquad (4)$$

namely Pd: drag force (Kgf/m)
θ : lateral deflection angle (deg)
W : cable weight (0.21 Kg/m)

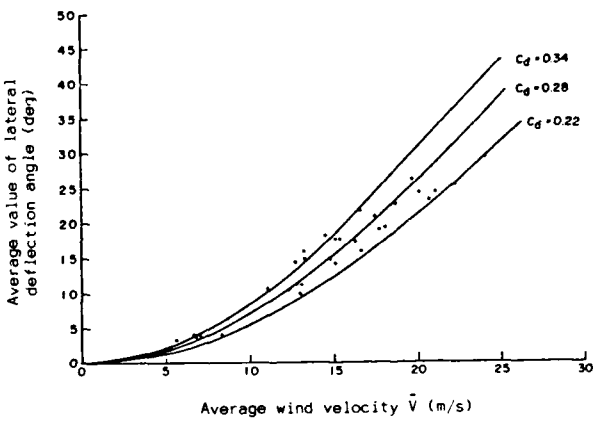

Fig. 17 Relation between average value of lateral deflection angle of cable and wind velocity

From the result of Fig. 17, theoretical value of Cd was calculated using Equations (1) and (4) and the value of Cd = 0.34 was obtained which was lower than the value (Cd = 1.12) obtained from the result of wind tunnel tests.

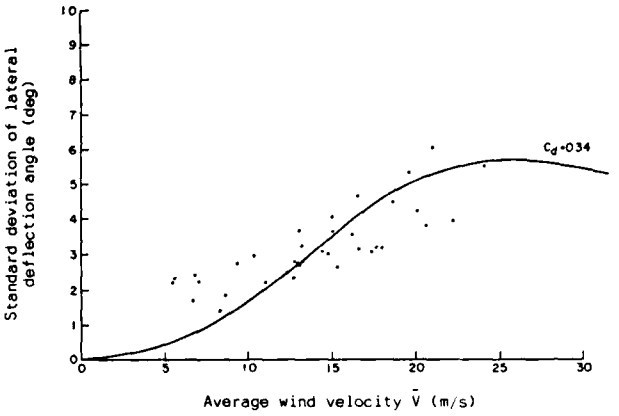

Fig. 18 Relation between standard deviation of lateral deflection angle of cable and wind velocity

It can be considered that the low Cd value was obtaine because of the drop of wind pressure force due to the difference of height between the position of the installed cable and the position of the wind velocity meter, and also due to the fluctuation of wind into different blocks in the direction longitudinal to the cable (size of air lump). Drag coefficient used when designing the installation of steel pylon was based on the result of wind tunnel tests that offered a high Cd value for purposes of safety. Also, as shown in Fig. 18, because the actual measured value coincided with the theoretical value obtained from Equation (5)[5], which has conventionally used to calculate standard deviation of lateral deflection for the designing of installation on steel pylons of power transmission lines, it was found that Equation (5) can also be applied to non-metallic optical fiber cable.

$$\sigma\theta = \mu \sin(2\bar{\theta}) \frac{\sigma v}{V} \times 1.1 \qquad (5)$$

namely μ: decremental coefficient

$$\mu^2 = 32\left\{\frac{1}{12ks} - \frac{1}{(ks)^3} + \frac{1}{(ks)^4} - \frac{1}{(ks)^4}\exp\left(-\frac{ks}{2}\right) + \frac{1}{(ks)^4}\exp(-ks)\right\}$$

$k = \frac{1}{L_x}$ L_x : size of air lump in line direction (= 30m)

S : span length (= 285m)

$\bar{\theta}$ = average lateral deflection angle (deg)

$\frac{\sigma v}{V}$ = intensity of wind disturbance

(0.18 from Fig. 13)

6. Study concerning range of movement of non-metallic optical fiber cable

For the designing of installation of non-metallic optical fiber cable on steel pylon, we used the method whereby the variation range of lateral deflection angle, with the average lateral deflection angle $\bar{\theta}$ as the central datum point, was expressed as standard deviations $\sigma\theta$ as shown in Fig. 19. $3\sigma\theta$ with occurence probability of 99.74% was used in the present study while $2\sigma\theta$ and $1\sigma\theta$ with occurrence probabilities of 95.44% and 68.26% respectivcly also fell within the range. Therefore, the lateral deflection angles against the respective wind velocities are as shown in Table 1 as based on Equations (1) (4) (5) and Cd = 1.12.

Table 1 Lateral deflection angle of non-metallic optical cable

V (m/s)	$\bar{\theta}$ (deg)	$\sigma\theta$ (deg)	$\bar{\theta}-3\sigma\theta$ (deg)	$\bar{\theta}+3\sigma\theta$ (deg)
5	7.11	1.41	2.88	11.3
10	26.5	4.58	12.8	40.2
15	48.3	5.69	31.2	65.4
20	63.4	4.59	49.6	77.2
25	72.2	3.33	62.2	82.2
30	77.5	2.42	70.2	84.8
35	80.7	1.83	75.2	86.2
40	82.9	1.41	78.7	87.1

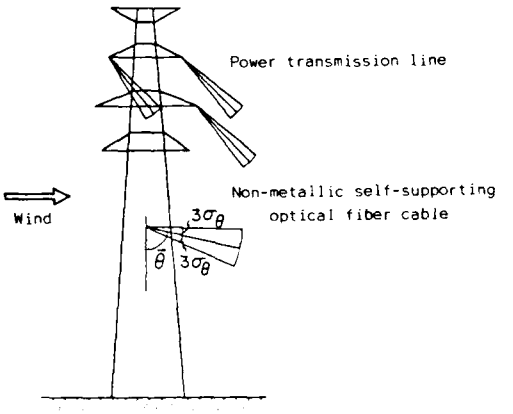

Fig. 19 Lateral deflection based on statical analysis of wind variation

7. Conclusion

Non-metallic self-supporting optical fiber cable was subjected to wind tunnel tests and an actual scale field test and the resulting data was applied to the design of installation of this cable on steel pylon.

Based on the result obtained on the aerodynamic coefficient characteristics, it was found that this non-metallic self-supporting type optical fiber cable is not conductive to Den Hartog's type galloping vibration. Furthermore, abnormal vibration of galloping was not observed during the field testing conducted over a period of 2.5 years.

Also, based on the result of the field test, it was shown that the equation of standard deviation of cable lateral deflection angle conventionally used in the design of transmission line installation on steel pylon could be applied. Using the equation of aerodynamic coefficients and equations of lateral deflection angle and standard deviation of lateral deflection angle, the guidelines as to the range of movement of non-metallic self-supporting optical fiber cable were obtained.

Based on the results mentioned above it has now become possible to determine the most appropriate installation position of non-metallic self-supporting optical fiber cable, with consideration given to the spacing between this optical fiber cable and the power transmission line, and to its height above ground surface.

References

(1) E. Hayasaka, F. Ohtsuka, M. Monma, S.. Ohira, H. Horima, K. Yamashita, M. Dazai and N. Abe, Non-metallic optical cable with optical fiber catenary for long span aerial application, IWCS, 1983.

(2) E. Hayasaka, Y. Ishihata, H. Horima, S. Hisano, T. Shishido and T. Ohmori, The clarification of movement of non-metallic self-supporting optical cable caused by wind and the design of its installation at steel pylon, IWCS, 1984.

(3) H. Takehara, Y. Ishihata, K. Saito, K. Niikura, H. Horima, A. Kurosawa, T. Takeda, T. Ohmori, Withstanding high voltage characteristics of non-metallic self-supporting optical cable, IWCS, 1987.

(4) M. Ito, Y. Fujino and H. Yamaguchi, Wind tunnel study on galloping oscillation of suspended figure-8 telecommunication cables, Proc. of JSCE, Structual Eng./Earthquake Eng., 2.1 (April 1985)

(5) K. Tsujimoto, O. Yoshioka, T. Okumura, K. Fujii, K. Shimojima, H. Kubokawa, Investigation of conductor swinging by wind and its application for design of compact transmission line, IEEE 82 WM 200-4.

Yoshinori Ishihata
Tohoku Electric
Power Co., Inc.
7-1, 3-chome
Ichibancho
Sendai 980, Japan

Yoshinori Ishihata received the M.S. degree in engineering from Tohoku University in 1979. He then joined Tohoku Electric Power Co., Inc., where he has been engaged in telecommunications and electronics engineering. He now serves as an engineer for the Integrated Communications Network Development Office and a member of the Institute of Electronics and Communication Engineers of Japan.

Kazunori Saito
Tohoku Electric
Power Co., Inc.
7-1, 3-chome
Ichibancho
Sendai 980, Japan

Kazunori Saito graduated from Fukushima Technical School in 1975. He then joined Tohoku Electric Power Co., Inc. and has been engaged in communications and electronics engineering. He is now an engineer for the Integrated Communications Network Development Office.

Katue Nakadate
Tohoku Electric
Power Co., Inc.
7-1, 3-chome
Ichibancho
Sendai 980, Japan

Katue Nakadate received the B.S. degree in engineering from Tokyo Denki College in 1957. He then joined Tohoku Electric Power Co., Inc., where he has been engaged in telecommunications and electronics engineering. He is now a Manager of the Integrated Communications Network Development Office and a member of the Institute of Electric Engineers of Japan.

Hiroaki Horima
Sumitomo Electric
Industries, Ltd.
1, Taya-cho
Sakae-ku
Yokohama 244, Japan

Hiroaki Horima received the M.S. degree in engineering from Osaka University in 1972. He then joined Sumitomo Electric Industries, Ltd. and worked on the development of CATV coaxial cables, multipair PEF-insulated junction cables and low loss unbalanced type cables. Thereafter, he concentrated on the development of optical fiber cables. He is now Section Manager of the Fiber Optics Division at Sumitomo Electric Industries, Ltd. He is a member of the Institute of Electronics and Communication Engineers of Japan.

Koji Niikura
Sumitomo Electric
Industries, Ltd.
1, Taya-cho
Sakae-ku
Yokohama 244, Japan

Koji Niikura received the B.S. degree in engineering from Waseda University in 1984 and joined Sumitomo Electric Industries, Ltd. He has been engaged in the development and design of optical fiber cables in the Fiber Optics Division.

Akira Kurosawa
Kitanihon Electric
Cable Co., Ltd.
1-2-1, Koriyama
Sendai 982, Japan

Akira Kurosawa received B.E. degree from Tohoku University in 1970. At Kitanihon Electric Cable Company, Ltd., he has been engaged in the design and development of communication cables. He is a member of the Institute of Electronics and Communication Engineers of Japan.

Toshiyuki Ohmori
Kitanihon Electric
Cable Co., Ltd.
1-2-1, Koriyama
Sendai 982, Japan

Toshiyuki Ohmori received the B.E. degree from Tohoku Gakuin University in 1966. At Kitanihon Electric Cable Co., Ltd., he has been engaged in research and development of communication cables, power cables and accessories for these cables. He is now a deputy manager of the Engineering Division. He is a member of the Institute of Electronics and Communication Engineers of Japan and the Institute of Electrical Engineers of Japan.

SZ-CABLED METAL-FREE OPTICAL CABLE FOR LONG SPAN AERIAL APPLICATION

H. Ishii[*1], N. Misono[*1], Y. Sugawara[*1], T. Hayakawa[*2], S. Suzuki[*3], K. Fujii[*3]

*1 Fujikura Ltd. Chiba, Japan
*2 Fujikura Ltd. Tokyo, Japan
*3 Chubu Electric Power Co., Inc. Nagoya, Japan

Abstract

A new type of metal-free self-supporting optical fiber cable was developed. This cable can be applied to long-span aerial power lines. The design of the cable is unique. Four optical fiber units with small diameter are SZ-cabled around a single rod FRP support member and fixed by two lashing wires.

The cable was evaluated in a laboratory and a test field. Results of various tests have verified that the cable has excellent transmission and mechanical characteristics.

1. Introduction

A power transmission network usually has very long power lines. So using existing towers, an optical transmission trunk line can be economically installed in the power transmission network.

One well-known cable which is already applied to power lines is OP-GW (Composite Overhead Ground Wire with Optical Fiber). Another is a metal-free self-supporting optical cable.

In designing OP-GW, heat resistant characteristics of an optical fiber must be taken into account in case of lightning and short circuit.

On the other hand, the metal-free self-supporting optical cable is free from induction. So heat resistant cable design is unnecessary. But the axial elongation of a metal-free self-supporting cable is larger than a metallic one, so that from the view point of life time of an optical fiber, it is very important to design the stress of the cable. One approach is an application of loose tube cable in which optical fibers have excess length. It has an advantage that the excess length of optical fibers can compensate the stress of the cable.

The newly designed self-supporting optical cable was developed through new technology. It consists of four tight buffered optical units with polyethylene outer jacket. These units are SZ-cabled around the FRP support member. This configuration gives optical units excess length.

2. Cable design

2-1. Design Criteria

The design criteria of the new cable are as follows.

(1) Metal-free configuration.
From the view point of safety, the new cable must be free from induction. So it must be composed of all dielectric materials.

(2) Maximum allowable fiber stress at maximum working tension.
A predicted life time of the cable is over 25 years. To achieve this target maximum allowable fiber stress is 0.2% using 0.5% screen test fiber.

(3) Maximum allowable stress of the support member at a maximum working tension.
For the dielectric support member, G-FRP(Glass Fiber Reinforced Plastic) and K-FRP (Kevlar-FRP) are available. Determining allowable tensile stress, the properties such as the time to break and the maximum creep strain have to be considered.
If the predicted failure probability of 10 Fit/100km is allowed during 25 years, 0.5% continuous tensile stress of G-FRP is allowed. The failure probability of K-FRP is less than that of G-FRP.
The maximum creep strain of K-FRP at 50% UTS(Ultimate Tensile Strength) is 0.1% during a life time of 25 years. The creep of G-FRP is less than that of K-FRP.

In actual working conditions, maximum tensile stress of supporting member is under 0.5%. Under this condition, the creep strain of K-FRP is negligible.
From the reason mentioned above, the maximum allowable stress of the supporting member is set to 0.5%.

(4) Maximum tower span of 500m.
Normal tower span is 200m through 250m. But longer installation for example crossing wide river is often required. So maximum allowable tower span of 500m is assumed.

(5) Aerodynamic characteristics.
From the view point of the life time of the fiber, the excess elongation of the cable induced by wind, galloping and ice load must be minimized. To minimize the susceptibility of the cable to wind load, the cable diameter must be as small as possible.

(6) Easy installation with high reliability.
To minimize the installation cost, the cable must have a capability to be laid and anchored quickly to tower structures.

(7) Fiber counts up to 20.

2-2. Structure

Fig.1 shows the cross section of the newly developed cable. Four tight optical units are SZ-cabled around a 10mm diameter FRP support member and fixed by two lashing wires. The lashing wires are made from Kevlar yarn and have a flat polyethylene sheath to minimize lateral pressure for optical units.

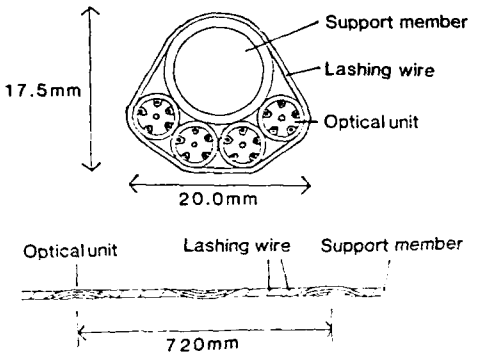

Fig.1 Cross-section of the cable

The tight buffered single mode fibers with 0.7mm nylon jacket are accommodated in a 4mm polyethylene slot. Each units can accommodate five fibers and have 5.5mm polyethylene outer sheath.

The tight buffered fiber has an advantage to be handled with ease. Because it has a suitable diameter and stiffness to be handled by installation technicians. And also it has a strong resistance to lateral force, so it can be accommodated in a splicing closure with ease and no trouble.

From the view point of aerodynamic characteristics, the optical cable is divided into four units to minimize the over all cable diameter resulting in low susceptibility to wind load. This structure also make it easy to branch any unit without shutting down another live units. Moreover the support member is separated from optical units, so it makes it easy to anchor the supporting member to the tower structures, resulting in less installation time.

The unit has slotted structure to protect the fibers from the large lateral force in case of installation. The tight buffered optical fibers are tightly stranded in the slotted core to make the unit diameter as small as possible.

In order to get excess length of optical fibers, the optical units are cabled around the supporting member by SZ-cabling method. The theoretical excess length depends on the cabling lay length and the reverse angle.

that is,

$$K = 1+\left(\frac{\pi \times R \times A}{4 \times P}\right)^2$$

where, K=ratio of excess length (%)
R=pitch diameter of the optical unit(mm)
A=reverse angle(rad)
P=lay length(mm)

But, because the optical units can not move freely due to the tension of the lashing wire, the effect of excess length is reduced. So the optimum lay length of the optical units was experimentally determined.

Fig.2 shows the relationship between the unit lay length and the optical fiber strain at the cable strain of 0.5%. Based upon this data, the lay length of 360mm was chosen as optimum to meet the allowable fiber strain requirement of 0.2%.

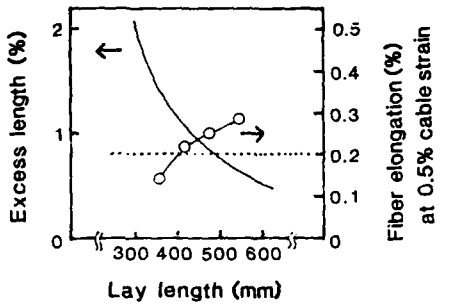

Fig. 2. Relationships between lay length of optical unit and excess length of optical unit and fiber elongation at 0.5% cable strain

The material of the support member is selected from G-FRP and K-FRP in accordance with an installation conditions such as tower span, sag, tension, wind load, ice load and temperature. Table.1 shows the characteristics of G-FRP and K-FRP.

Based upon the following conditions, we calculated the sag and the cable strain.

Maximum allowable cable strain=0.5%

Maximum allowable sag =4%

The results are shown in Table.2. In conclusion, the 10mm G-FRP can be applied up to 300m tower span. And the 10mm K-FRP can be applied up to 500m tower span.

Because we have the towers with 250m span, the experimental cable shown Fig.1 was made to be subjected to the field test using the 10mm G-FRP.

Table. 1 Data of support member

ITEM		G-FRP	K-FRP
Outer diameter of FRP	(mm)	10	10
Outer diameter of support member	(mm)	12	12
Weight per unit length	(kg/km)	193	138
Thermal coefficient of expansion	(1/K)	7×10^{-6}	-2×10^{-6}
Young's modulous	(kg/mm^2)	47	69
Breaking load	(kN)	69	98
Tension at 0.5% elongation strain	(kN)	19	27

Table. 2 Typical parameters of cable installation

Span	Support member	Condition A		Condition B		Condition C	
		sag.m	elong.%	sag.m	elong.%	sag.m	elong.%
100m	G-FRP	1.2	0.50	0.2	0.46	1.1	0.51
200m		4.8	0.50	1.1	0.35	4.4	0.49
300m		10.9	0.50	4.2	0.20	10.2	0.48
400m	K-FRP	13.5	0.50	3.8	0.22	12.8	0.47
500m		21.1	0.50	9.9	0.14	20.3	0.46

Condition A: Temp. 15c, Wind 40m/s, Ice no
B: 15c, no, no
C: -10c, 28m/s, 6mm thick

3. Characteristics

3-1. Tensile characteristics

The cable was subjected to tensile test to verify the stress level of the fiber. The optical attenuation was also monitored. Fig.3 shows the relationships between the tensile load and the fiber elongation and the cable elongation and the attenuation change at 1300nm wavelength. The test results show that the fiber elongation is less than 40% of the cable elongation at any tensile load. The fiber elongation is 0.14% in case of 0.5% cable elongation. The attenuation change was scarcely observed.

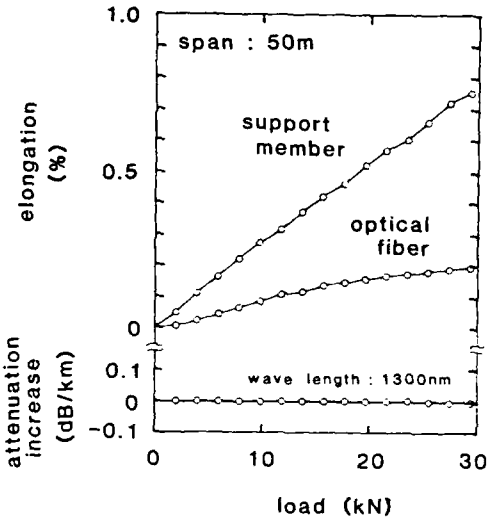

Fig. 3. Cable load versus strain

The cable was also subjected to the repetitive tensile test. Fig.4 shows the result of it. The cable was subjected to a 9.8kN load 50 times. The test result shows that the elongation of the optical fiber decreased and converged to 0.07% which is one fourth of the cable elongation. This means that the fiber elongation is assumed to be 0.13% at heavy load condition. It is small enough compare to the allowable continuous elongation of 0.2%.

The test verifies that the new cable satisfies the design criteria and has enough reliability in terms of life time.

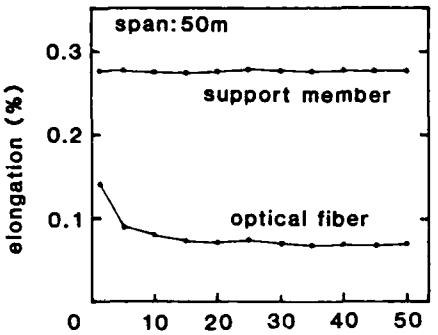

Fig.4 Repetitive load - strain test

3-2. Aerodynamic characteristics

Designing a self-supporting optical cable, aerodynamic and icing characteristics are the most important factors from the view point of the life time of the cable.

The new cable was subjected to the wind tunnel test to verify the excellent aerodynamic characteristics.

The important aerodynamic factors are a drag coefficient(Cd) and a lift coefficient(Cl).

Cd relates to the excess tensile load induced by wind load. Cl relates to the susceptibility to a galloping.

The wind pressure due to Cd and Cl, That is,

$$P=0.5CxdV^2$$

Where

P:the wind pressure (kg/m^2)
d:air density (kg/m^3)
V:the wind velocity (m/sec)
Cx:Cd or Cl

Fig.5 shows the test results of the wind tunnel test. Where, sample A is the support member with 12mm outer diameter; sample B is the newly designed cable. In case of figure-8 cable, it is well known that the number of Cd and Cl change depend on wind velocity. In general Cd has a trend of decrease and Cl has a trend of increase. This makes the cable unstable to the wind, resulting in galloping.

On the other hand, the newly developed cable has same trends as a support member with a round shape in terms of Cd and Cl.

The test results verified that the Cd of the new cable was improved about 20% by SZ configuration.

And it also verified that the new cable has less susceptibility to the wind pressure, resulting in rare possibility of galloping.

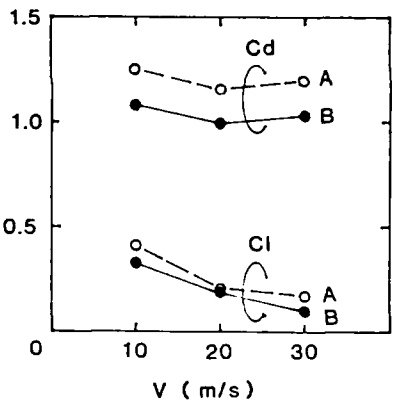

Fig. 5. Wind velocity versus aerodynamic coefficient

3-3. Attenuation in cable manufacturing process

Fig.6 shows the attenuation of optical fiber measured at each manufacturing process. The attenuation change through cabling was less than 0.02 dB/km.

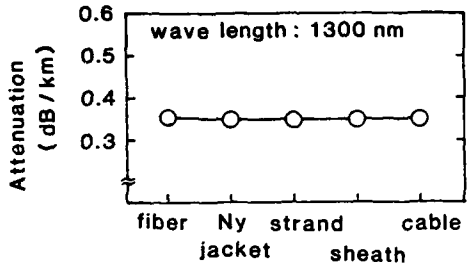

Fig. 6. Attenuation of optical fiber in cable manufacturing

3-4. Temperature Characteristics

The cable was subjected to the temperature cyclic test of ten cycles. The temperature range was -40c through +60c. Fig.7 shows the relationship between temperature change and attenuation change. The attenuation change was less than 0.01dB/km and the residual attenuation was scarcely observed after ten cycles.

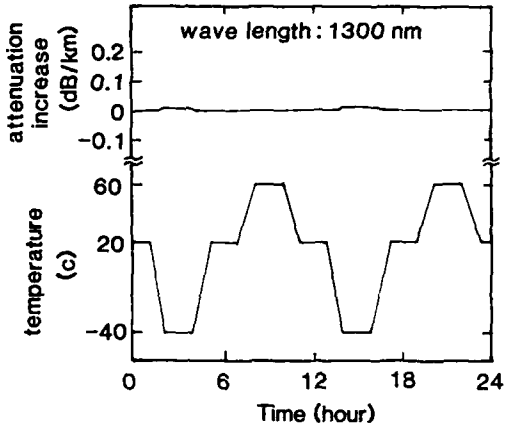

Fig.7. Temperature dependence of attenuation change

3-5. Vibration test

The optical cable was subjected to 2 tests; horizontal and 30 degrees inclined vibration test. The test condition was as follows. The span was 20m. The tensile load was 4kN (0.13% cable strain). The amplitude of vibration was ±6mm. The frequency was 40Hz. After vibration of 1×10^6 times, no attenuation change and no mechanical damage were observed.

3-6. A sheave wheel test

This test is to determine the maximum allowable pulling force during a cable installation. Fig.8 shows an outline of a sheave wheel test. Up to a cable tension of 4.9kN no attenuation change at 1300nm wavelength and no mechanical damage of the cable were observed. The attenuation change was observed from 5.9kN. The groove of polyethylene slot was deformed by lateral force to pinch the optical fiber, resulting in the attenuation increase. Therefore taking a safety margin of 2.0kN, 2.9kN was determined as a maximum allowable pulling force.

Since ordinary pulling force is under 1.0kN, 2.9kN is large enough as an allowable pulling force.

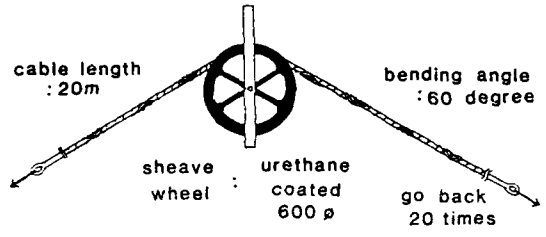

Fig. 8. Outline of sheave wheel test

3-7. Cable clamp

Fig.9 shows the structure of a cable clamp. From the view points of a reliability and a material and an installation cost, several methods to clamp the cable on the tower structure were investigated. We conclude that the following new method is the best one which can achieve a high reliability and a low cost.

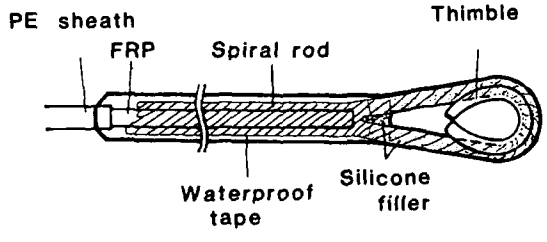

Fig. 9. Structure of cable clamp

The preformed spiral rod (grip) is wound around an unjacketted FRP rod. Then for the purpose of waterproof, they are covered with self-bonding tape, silicone sealant and vinyl tape. An advantage of this method is that special tools and materials are unnecessary.

A lot of sample were subjected to tensile test under several environmental conditions to verify the reliability.

Fig.10 shows the relationship between the grip length and the intrinsic tensile strength. Tensile strength is proportional to the grip length. Under 600mm of the grip length, the slip happens between the grip and the FRP. But over 600mm of it, the FRP breaks before slipping. So 600mm is chosen as a optimum clamp length.

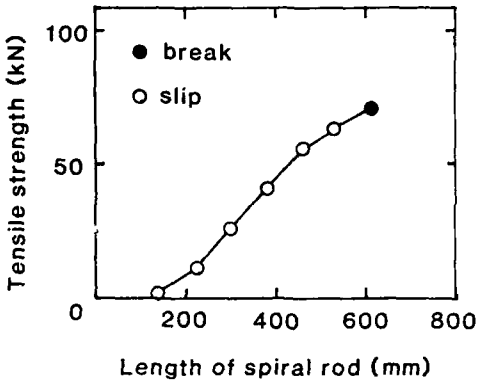

Fig. 10. Length of spiral rod versus tensile strength

After treatments such as vibration, water immersion, freezing and temperature cyclic, the clamp samples were subjected to the tensile test.

In case of the clamp with a waterproof treatment, the degradation of the tensile strength was scarcely observed at any treatment conditions.

The maximum tensile load at the heavy load condition is one fourth of the tensile strength of the clamp. So the reliability of the clamp is verified.

Table 3. Results of reliability tests on cable clamps

Item & Condition			Tensile Strength (kN) Without waterproof	With waterproof
VIBRATION				
Amplitude ± 5mm	20c	$1x10^6$ times	68.6	68.6
Frequency 10Hz		$1x10^7$ times	68.6	68.6
Tension 3.9kN	60c	$1x10^6$ times	69.6	69.6
		$1x10^7$ times	71.6	72.6
	-20c	$1x10^6$ times	69.6	69.6
		$1x10^7$ times	70.6	72.6
IN WATER				
In 60c water		10days	64.7	68.6
Tension free		1month	61.8	68.6
FREEZING				
In -20c ice Tension free		20days	68.6	68.6
HEAT CYCLE				
In 60c water x 1day		5 cycles	68.6	68.6
In -20c air x 1day In 60c air x 1day		10 cycles	71.6	73.5

4. Installation in the field

4-1. Stringing method

The optical cable has been strung on the towers with the spans of 248m and 148m by the carrier stringing method in the test field. Fig.11 shows the outline of this stringing method. A pilot rope with many suspended small pulleys and a messenger rope are pre-strung using a existing wire so as to minimize the tensile load of the cable and the sag during the installation. The measured pulling force in the test field was less than 0.5kN. This load is small enough compare to the allowable pulling force of 2.9kN. After installation any damage was scarcely observed on the cable.

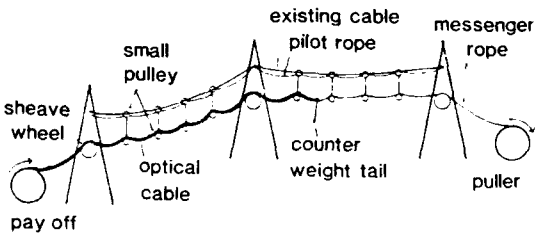

Fig. 11. Carrier method of stringing

4-2. Clamping and Jointing

Fig.12 shows the layout of the cable clamp and the joint box. The support member is fixed on the mid arm of each steel tower. Four optical units are branched at the cable clamp. These units are protected by the flexible plastic tube with a slit and guided to the joint box.

The necessary time to anchor the support member to the tower structure was about twenty minutes per one clamp in the field.

The necessary splicing time per one fiber was about eight minutes.

The field test verified that the new cable has a capability to be installed very fast.

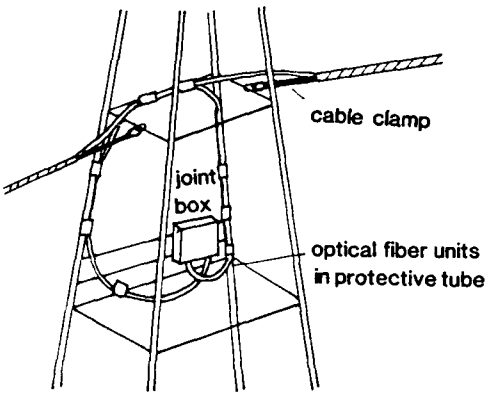

Fig. 12. Joint box location

4-3. Attenuation change after installation

An attenuation change at 1300nm wavelength after installation in the test field was less than 0.01dB/km(average of twenty fibers).

5. Conclusion

A newly designed metal-free self-supporting optical cable for long span application was developed. In this cable SZ-cabling configuration gives excess length to optical fibers. The test results in the laboratory and the test field verified that the new cable has superior transmission, mechanical, aerodynamic characteristics and the new clamping method has a high reliability to any environmental condition.

6. Reference

(1)N.Kuwabara,"High Reliability FRP Strength Member for Non-metallic Optical Fiber Cable",J71-B,5,pp626-632,1988, Transactions of IEICE Japan

(2)H.Takeshita,"Dip of Overhead Power Lines",1966

(3)T.S.Swiecicki,"Unit core cable structure for optical communication systems",pp656-660,Wire Industry, September,1979

(4)M.H.Horn et al.,"Strength and durability characteristics of ropes and cables from kevlar aramid fibers",MTS-IEEE 24E,OCEANS 1977

(5)"Creep and stress-rupture of kevlar ropes",Technical Documentation kevlar 29 - kevlar 49 aramid fibers

Hiroshi Ishii

Fujikura Ltd.

1440 Mutsuzaki,
Sakura, Chiba, 285,
Japan

Mr. Ishii was born in 1961. He joined Fujikura Ltd. after his graduation from Hirosaki University with a B.S. degree in 1983 and has been engaged in research and development of optical cables. He is now an engineer of optical cable section and a member of the Institute of Electronics, Information and Communication Engineers of Japan.

Toshiyuki Hayakawa

Fujikura Ltd.

1-5-1 kiba,
Koto-ku, Tokyo,
135, Japan

Mr. Hayakawa was born in 1948. He joined Fujikura Ltd. after his graduation from Yokohama National University with a B.E. degree in 1971 and has been in the development and design of coaxial cables, millimetric waveguides and optical cables. He is now a chief of fiber optic cable engineering section in telecommunication cable division and a member of the Institute of Electronics, Information and Communication Engineers of Japan.

Nobuyuki Misono

Fujikura Ltd.

1440 Mutsuzaki,
Sakura, Chiba, 285,
Japan

Mr. Misono was born in 1949. He joined Fujikura Ltd. after his graduation from Chiba University with a B.E. degree in 1973 and has been engaged in research and development of metallic cables and optical cables. He is now an assistant chief engineer of optical cable section and a member of the Institute of Electronics, Information and Communication Engineers of Japan.

Shinji Suzuki

Chubu Electric Power
Co., Inc.

1 Toshin-cho,
Higashi-ku, Nagoya,
461-91, Japan

Mr. Suzuki was born in 1953. He graduated from telecommunications course of Higashiyama Technical High School in 1972 and joined Chubu Electric Power Co., Inc.. He has been engaged in the research and development of telecommunication facilities for electric power systems. He is now a chief of telecommunications engineering section.

Yasuyuki Sugawara

Fujikura Ltd.

1440 Mutsuzaki,
Sakura, Chiba, 285,
Japan

Mr. Sugawara was born in 1947. He joined Fujikura Ltd. after his graduation from Tohoku University with a B.E. degree in 1969 and has been engaged in research and development of metallic cables and optical cables. He is now an chief engineer of optical cable section and a member of the Institute of Electronics, Information and Communication Engineers of Japan.

Katsuyuki Fujii

Chubu Electric Power
Co., Inc.

1 Toshin-cho,
Higashi-ku, Nagoya,
461-91, Japan

Mr. Fujii was born in 1941. He graduated from Tsu Technical High School in 1960 and joined Chubu Electric Power Co., Inc.. He has been engaged in the research and development of telecommunication facilities for electric power systems. He is now an assistant manager of telecommunications engineering section.

DRY BAND ELECTRICAL ACTIVITY ON OPTICAL CABLES SEPARATELY STRUNG ON OVERHEAD POWER LINES

C.N. CARTER

Central Electricity Research Laboratories, Leatherhead, United Kingdom

Summary

Several self-supporting optical cables strung on power transmission lines in Europe have suffered sheath failure after less than one year in service. Large scale capacitive coupling experiments have enabled electrical activity to be observed and recorded outdoors in natural wind and rain. They have shown that the main cause of failure is dry band arcing which occurs when a wet cable begins to dry. Degradation always occurs near a cable support because the currents flowing and voltages available are highest there. An analytical treatment allows judgement to be made on which particular power lines pose a threat and the optimum stringing positions to be determined for any given power line.

Introduction

There is a need for optical cables in the Electricity Supply Industry and the various cable types available for use on overhead lines have been reviewed[1]. Self-supporting, metal- free cables, developed originally in W. Germany and the Netherlands, have been in apparently successful use on power lines of up to 110 kV for some years. It has been demonstrated many times[2] that cable of this type satisfactorily meets the optical and mechanical requirements. However, the first attempts to instal cable on 220 kV lines was met by failure. After less than a year the cables fell down and on examination were found to have been damaged near to the supports, apparently by electrical activity.

Several theories were put forward as to why this had happened and several solutions were proposed. It was suggested[3] that near the earthed supports longitudinal components of the electric field drove currents along a wet and dirty cable sheath. If these cables were not earthed then the currents would not flow and degradation would be eliminated. Insulators were incorporated in the conductor fittings but to no avail; the damage appeared as before. Suggestions were made that, since the damage always occurred near to fittings, the problem was one of small radii metallic parts raising the local electric field. Several stress relieving devices were proposed and tried but no improvement was observed.

The cable manufacturers then turned to resisting rather than preventing the electrical activity. Several developed what they term track resistant sheaths. This approach has apparently worked well, although a suitable test regime which will accurately predict lifetime performance remains elusive.

Experimentally Induced Degradation

It has been found[4,5,6] that degradation apparently similar to that found in service can be produced on small (0.1 to 0.5 m long) cable samples sheathed with polyethylene, the original sheathing material, by exposing them to electric fields in the range 5-100 kV/m while the samples are wetted by salt fog or spray. In general the most damaging currents lie in the range 0.5-5 mA. Electrode effects can be dominant in these small scale tests and results on other materials are sometimes confusing.

In order to gain experience at more nearly the correct scale, an outdoor test facility was set up on a coastal site. A 10 m long, 275 kV (159 kV to ground) busbar was suspended horizontally by tension insulator strings between two vertical steel towers 16.75 m apart. Up to six cable samples could be suspended between these towers, parallel to the busbar and on an arc 1 m distant from it. Both ends of the cable samples were earthed. The calculated potential at the centre of the dry, insulating cables parallel to the 275 kV busbar was 75 kV.

Observation has revealed that electrical activity is confined to periods of heavy mist, drizzle, and drying after rainfall. No visible activity occurs when the cable is well wetted or when it is dry. After rainfall dry bands form more or less randomly along the end few metres of the cable and glow discharges run circumferentially around the ends of the cylinders of wetted surface. The two rings of discharge are separated by up to 50 mm of dry surface over which run thin serpentine unstable arcs. While damage to the sheaths which degraded (not all did) was heaviest near the cable ends, some damaged areas were bounded by undamaged cable. A metal electrode was not necessary for damage to occur.

To gain further insight into what happens in practical operation, two lengths of cable were joined and strung on one 308 m span of a double circuit 400 kV power line. One half of the resulting cable was sheathed in polyethylene and the other in a degradation resistant material. The end regions of the cable were examined by eye at monthly intervals. After exposure for four months the polyethylene sheath was noticeably degraded. The

form and course of the degradation was similar to that observed on the outdoor capacitively coupled rig and to that seen on some of the small scale laboratory experiments. Initially the material surface loses its hydrophobic nature. This is followed by the destructive phase which is essentially a melting and relaxation process that eventually exposes the cable core. After nine months exposure the polyethylene half span was so badly degraded that it was removed and replaced with a second degradation resistant cable. To date, after just over a year, the original degradation resistant cable has not suffered degradation.

Induced Voltages and Currents

The electric potential and the currents flowing at any point on an optical cable, strung on a power line separately from the conductors, are determined by the phase voltage and frequency, the conductance of the cable or the pollutants on it and the capacitive impedances from the cable to the line and ground. The capacitances per unit length to line and earth, C_1 and C_2, are broadly constant throughout the span and are governed by the geometry of the phase and earth conductors and the supports. Near to the supports the capacitance to ground rises sharply and there are minor variations along the span caused by sag, which itself varies with the weather.

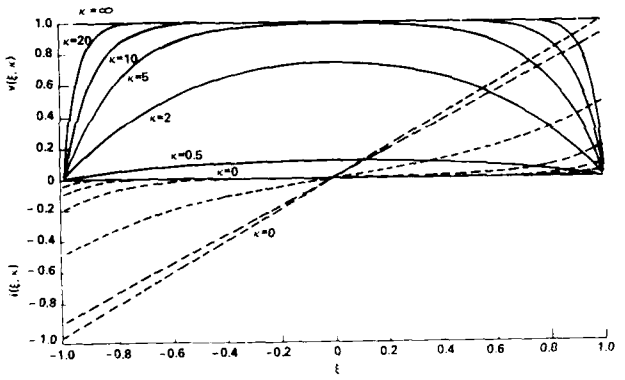

Figure 1 Normalized i-v characteristics

The analysis given in the Appendix, which assumes that capacitances and resistance per unit length are constant, shows how potential and current at any position on a cable vary over the full range of cable specific resistance, line voltage and constructional practice. The normalized plots shown in Fig. 1 are a convenient way to display the information. Current and voltage characteristics have been drawn for a range of values of κ, where κ^2 is the normalized cable resistance. When the cable has zero resistance it is at ground potential along its entire length. The current then builds linearly from zero at mid-span to a maximum at the support, determined by the line voltage and the capacitive impedance between the half-span and the line. When the cable resistance is infinite, the current flow along the cable is zero everywhere and the cable is at a constant potential determined by the ratio of the capacitive impedances to line and ground. For finite resistances the resistive impedance to ground falls as the support is approached. Hence the potential will also fall and the current rise in the manner illustrated by Fig. 1. To obtain current and potential values for a specific case it is necessary to assign values to the parameters I_0, V_0 and R, which together with κ are defined in the Appendix. The advantage of using these parameters, rather than the frequency and capacitances from which they can be derived, is that at least in principle they are measurable experimentally.

Most of the electrical activity is confined to a length of cable adjacent to the support. The concept of an active length, δ, is introduced and defined in the Appendix. It is dependent on only the line geometry, circuit status and cable resistance. When the active length is much shorter than the half-span, which is usually the case on power transmission lines, the earth leakage current is as though drawn from the line through a capacitor of value $C_1\delta$. Although the earth leakage current falls with δ, the heating per unit length at the support approaches an asymptote. In most practical cases heating will be at this asymptotic level, leading a wet cable to dry preferentially near the support. In general the effect of increased capacitance to ground near to the towers is a minor perturbation, which will only affect the characteristics of Fig. 1 significantly when the cable specific resistance is greater than about 10 MΩ/m and will act to limit the longitudinal field at the support.

Dry-band Formation

It is our experience that wet aged cable sheaths have resistances which vary widely in the range 1-100 MΩ/m. Drenching with simulated sea water decreases these values to around 100 kΩ/m but this is an unusual extreme. When dry, the aged cables have resistances of many gigohms per metre, which is high enough, when carrying the calculated currents, to sustain a surface field which would break down air. A wet cable suspended on a power line is likely to dry preferentially near the supports, partly because the cable slopes encouraging water to drain away, and partly because the current and hence the electrical heating is highest there. The exact site where crystallization of electrolye first occurs will be to some extent random, but at that site rapid drying will ensue. Heating in the surface film will rise as its resistance rises, creating an unstable runaway condition. In direct contrast, drying around the circumference of the cable at this site will be even because all current carrying paths are in parallel and heating will be highest in the path with the least resistance. Fig. 2 shows how the heating in, the voltage across and the current passing through the drying band vary with its resistance for a 400 kV case. It can be seen that the voltage developed across a drying band, likely to be initially of the order of the cable diameter in length, will rapidly reach that required to flash over the surface. The dry-band will then grow until its length just matches the voltage available to break down the gap. Figure 3 shows, for the same 400 kV case how the available potential difference

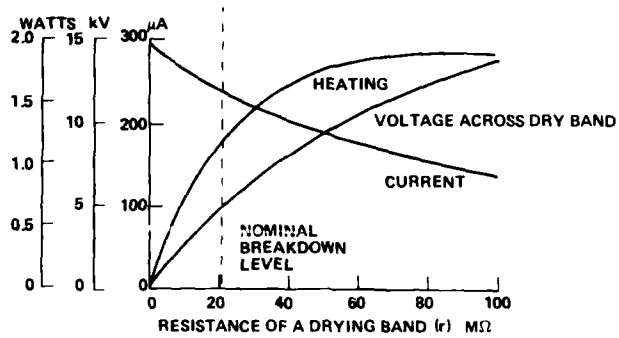

Figure 2 A developing dry-band

across a dry-band varies with position and sheath specific resistance. Photography has shown that this available voltage may be shared between two or more smaller dry-bands.

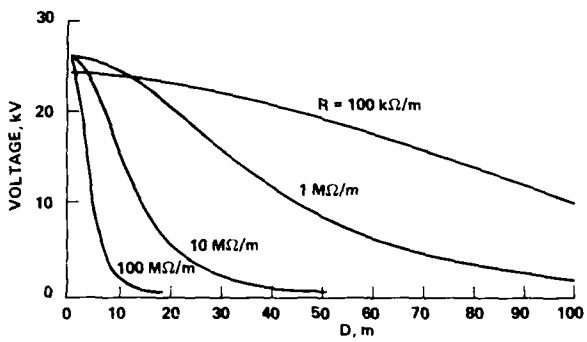

Figure 3 Voltage across a dry-band

Level of Degradation Threat

Although it has not been finally proved, it seems likely that sheath degradation is caused by arc-root heating. In that case the two important parameters in determining the heating are the arc striking voltage and the current flow or charge transfer, which are related. It can be seen from Fig. 3 that at the support the striking voltage is usually V_o. The current flow during dry-band arcing will be in bursts, of a frequency much higher than the power frequency, caused by repeated charging from the power line and discharging through the arc, of the capacitor formed by the optical cable and ground. It is not possible at this stage to analyse this complex dynamic situation, but it is probable that the maximum, power frequency, earth-leakage current I_o provides a measure of the arc current, however imperfect.

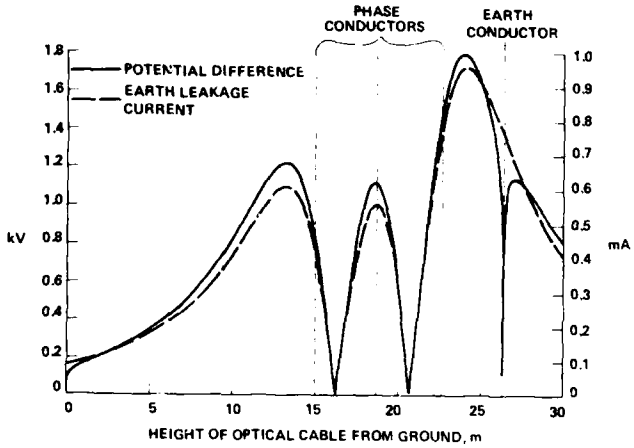

Figure 4 I_o and V_o for a 132 kV line

Fig. 4 shows how I_o and V_o vary with height on the centre line of a double circuit (both live) 132 kV line, a voltage at which no in-service degradation has been seen. The values are an order of magnitude lower than those calculated for a typical UK 400 kV line. Fig. 5 shows similarly how V_o varies with height on the centre line of a 400 kV line. In determining the optimum stringing position more than one case must be considered. On a double circuit line one or both circuits may be live. If only one circuit is live the other may be either earthed or floating. As if that were not enough, the relative phasing may vary from line to line; lines carrying more than two circuits are even more complex.

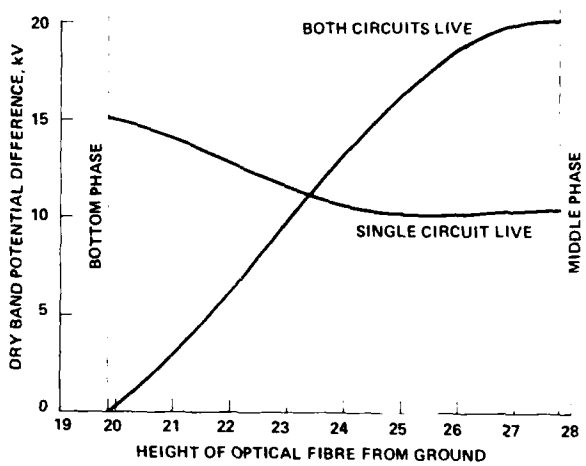

Figure 5 V_o for a 400 kV line

The voltage alone is not enough to determine the threat level. Geometry, which includes: conductor spacing and size, ground clearance, relative phasing, earthwire positions and subconductor spacings, is equally important. These complexities are not insurmountable, but they must be fully appreciated before self supporting optical

cables which are reliable can be designed and tested.

Discussion

We have shown theoretically that, as is found in practice, dry-banding, and the degradation caused by it, is confined to an active length of cable adjacent to the support. The crucial support feature which ensures this is the availability of a path for a modest current to flow to earth. Field shaping on cable fittings was ineffective in preventing degradation because stress raising was not the main degradation mechanism. Insulated fittings were equally ineffective. The insulators, which had relatively short creepage paths, and were as susceptible to pollution as the cable, were ineffective in preventing milliamp sized currents from flowing to earth. The rapid rise in the capacitance between cable and ground near to the supports, far from being a causative factor, is seen to be helpful in limiting longitudinal fields.

Conclusions

Large scale outdoor experiments have confirmed that dry-band arcing is the main mechanism causing sheath degradation in self supporting optical cable strung on power lines. Experimental and theoretical results show that the threat of damage will be confined to cable adjacent to the support positions. Analytical expressions have been derived for the voltages and currents induced on self supporting cables, and for the voltage available for dry-band arcing for any power line. These expressions can be used to assess the level of threat and the best stringing position for cable on a given power line.

Acknowledgement

The work described in this paper was carried out at the Central Electricity Research Laboratories and is published by permission of the Central Electricity Generating Board.

References

1. Bartlett, A.D., Carlton, G., Carter, C.N. and Nield, B., 1987, 'The development of optical communication systems in the UK electricity supply industry', Paper d12, CIRED 1987, Liege Belgium

2. Rowland, S.M., Craddock, K., Carter, C.N., Houghton, I. and Delme-Jones, 1987, 'The development of a metal-free, self-supporting, optical cable for use on long-span, high-voltage, overhead, power lines, IWCS Arlington, Va., Nov. 1987

3. Brüggendieck, S., Herff, R. and Mainka, M., 1984, "25 km optical aerial cable link on 110 kV overheadline", paper 35-09, CIGRE 1984 Session, Paris

4. Berkers, A.G.W.M. and Wetzer, J.M., 1988, 'Electric Stresses on a self-supporting, metal-free optical cable in high voltage networks', Fifth Dielectric Materials Measurements and Applications Conference, Canterbury, June 1988, pp 69-72

5. Wheeler, J.C.G. and Lissenburg, M.L., 1988, 'The development and testing of a track resistant sheathing material for aerial optical cables', Ibid., pp 73-76

6. Rowland, S.M. and Carter, C.N., 1988, 'The evaluation of sheathing materials for an all-dielectric, self-supporting communication cable for use on long-span, overhead, power lines', Ibid., pp 77-80

Appendix: Theoretical Analysis of Potentials and Currents on an Optical Cable

Consider an optical cable suspended between the supports of an overhead power line which carries one or more circuits. The capacitive coupling between the cable and the line will be made up of the sum of the capacitances to each of the phase conductors. The inductive coupling, which would dominate if the cable resistance were very low, is ignored. We will assume that the circuits are all synchronous. An equivalent capacitance per unit length between the optical cable and the line, whose terms are grouped by phase, can be written:

$$C_1 = \pi\epsilon\{(\alpha_1 + \alpha_2..) + \phi(\beta_1 + \beta_2..) + \phi^2(\gamma_1 + \gamma_2..)\} \quad \ldots (1)$$

where $\phi = -\frac{1}{2}(1 - j\sqrt{3})$ and α, β and γ are the geometric terms reflecting the relative positions and sizes of the optical cable and phase conductors of circuits 1, 2 .. n. We can then define the reference phase of the system voltage V_s to ground, such that C_1 will have no imaginary component. Similarly the capacitance per unit length of the cable to ground, C_2, is the sum of the capacitances to the ground plane, the earthwire and the conductors of any earthed circuits. If we assume that C_1, C_2 and R, the resistance per unit length of the cable, are independent of position the problem can be treated quite simply.

Consider the infinitesimal element shown below:

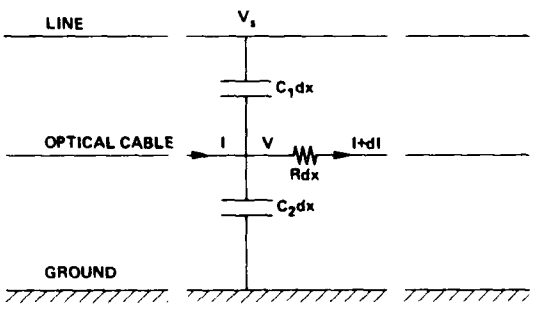

It is convenient to define normalized parameters for voltage, current, position and specific resistance which simplify the algebra and generalize the results. Thus:

$$v = \frac{V}{V_o}, \quad i = \frac{I}{I_o}, \quad \xi = \frac{x}{L} \text{ and } \kappa^2 = \frac{I_o RL}{V_o}$$

where: L is the half-span, V_o the cable potential when R tends to infinity, V_s the phase to ground system voltage, and I_o is the earth leakage current when R is zero.

By considering current continuity at the node and resistive potential drop along the element we can write:

$$v = 1 - \frac{di}{d\xi} \qquad \ldots (2)$$

and

$$\frac{dv}{d\xi} = - i\kappa^2 \qquad \ldots (3)$$

hence

$$\frac{d^2 i}{d\xi^2} = \kappa^2 i \qquad \ldots (4)$$

The cable is earthed at the support, so if we choose $\xi = 0$ at mid-span where i is zero, a solution for equation (4) is

$$i(\xi) = \frac{\sinh \kappa\xi}{\kappa \cosh \kappa} \qquad \ldots (5)$$

and the normalized earth leakage current

$$i(1) = \frac{\tanh \kappa}{\kappa} \qquad \ldots (5a)$$

and from (3):

$$v(\xi) = 1 - \frac{\cosh \kappa\xi}{\cosh \kappa} \qquad \ldots (6)$$

so the mid-span potential

$$v(o) = 1 - [\cosh \kappa]^{-1} \qquad \ldots (6a)$$

If a cut of infinite resistance is made in the cable a distance D (i.e. a proportion d = D/L) from the support then by analogy with (6a) the normalized voltage appearing across that cut is:

$$v(d) = [\cosh \kappa d]^{-1} - [\cosh \kappa(2-d)]^{-1} \qquad \ldots (7)$$

The parameter κ is complex.

Write $$\kappa = (1 + j)\frac{L}{\delta} \qquad \ldots (8)$$

where $$\delta^2 = \frac{2}{\omega R(C_1 + C_2)}$$

Here δ, which we will call the active length, represents the length of cable adjacent to the support along which most of the electrical activity occurs. When $L \gg \delta$, as will usually be the case, equation (5a) reduces to

$$i(1) = \frac{\delta}{2L}(1 - j) \qquad \ldots (9)$$

so the earth leakage current, for a uniformly resistive cable, will have the magnitude $I(L) = V_s \omega C_1 \delta$. The two ends of the cable will be independent of each other and of the span length; the earth leakage current will be as though drawn from the line through a capacitor of value $C_1\delta$.

Chris N. Carter
Central Electricity
Research Laboratories
Kelvin Avenue
LEATHERHEAD
KT22 7SE
England

Chris Carter graduated from the University of London with a B.Sc. Honours degree in Mathematics and Physics in 1963. He has since carried out research work for the CEGB on magnetohydrodynamic power generation, superconducting magnet design, ac loss measurements in superconductors, failure mechanisms in power cable stop joints and, since 1979, on the development of optical communications on power lines.

Optical Cable Broadband Subscriber Network

Georg Blume, Helmut Feilhauer, Friedrich Krahn, Norbert Lenge, Gerhard Olejak,
Bernd Sange, Hans-Gerd Zielinski

ANT Telecommunications
Backnang, West Germany

Abstract

A single-mode optical cable network is presented

- meeting all subscriber requirements for individual communication (conventional telephone, videophone, data exchange) and broadband distribution services (TV, stereo channels, data services)
- capable of being used without modifications for further services (i.e. HDTV) and new systems (i.e. coherent detection).

Cables based on high-fibre-density loose-tube design and containing up to 840 fibres have been developed, meeting all the requirements for the introduction of this network.

Introduction

Optical communication systems have reached a high technical and economical standard, proved by the fact that about 10 million kilometers of optical fibres have been cabled and installed up to now throughout the world.
Nevertheless, the introduction of optical communication systems considerably depends on the network level:
While mainly optical systems are installed instead of copper systems in trunk networks [1], in subscriber networks almost all the operating and even newly installed systems are based on copper cables (although the reliability and high performance of optical subscriber networks were demonstrated already long ago [2].

The reasons for this difference are well known:

- the existing symmetrical copper cables are sufficient and cost-effective for narrowband services (telephone, data transmission)
- coaxial cable systems are an economic and reliable solution for broadband distribution services (radio, TV)
- new services, especially those requiring a high bandwidth (videophone, videoconference), which can only be handled using optical systems are not yet used extensively.

Considering this situation, the installation of optical subscriber networks instead of copper networks will be enhanced (in addition to cost-effectiveness), depending on the following conditions:

- all existing subscriber requirements (conventional telephone, TV, stereo audio channels, data services) can be met
- transmission of future services (HDTV, videophone, high-speed data transmission) is possible without modification of the cable network
- application of new systems (i.e. coherent detection) is possible
- the same star network design is used as for the existing copper system (step-by-step-introduction of optical systems and replacement of copper by optical fibres)
- the same cable design and splicing technique is used as for existing optical cable systems (reliability, use of existing cables in an initial stage)

A network meeting all these requirements is presented here.

System

All services are transmitted on one single-mode fibre. The communication and distribution services, however, are independent and strictly separated using 2 different windows: the second window (1200 - 1330 nm) for communication, and the third window (1500 - 1600 nm) for distribution services [3].
A bi-directional transmission is used in both windows.
The separation of the 2 windows and of the forward and backward signals within each window is realized by means of wavelength division multiplexers (WDM).

This design allows a gradual introduction of new services and the corresponding terminal equipment:

- For broadband communication
  bi-directional transmission each at 150 Mbit/s for the forward and backward channel.
- For additional distribution services
  four 150 Mbit/s channels from centre to subscriber to be selected from an "unlimited" number of channels via a narrowband backward signal.
- For coherent systems
  n channels with m Mbit/s per channel where n and m do not have to be fixed, and so future requirements can always be met.

Both wavelength windows are easily combined and separated by existing components, i.e. taper couplers or interference multiplexers [4].

The separation of the forward and backward channel within each window is more critical [3]:
In order to minimize the WDM costs for the required low crosstalk a separation of more than 60 nm between the forward and backward channels is necessary, and therefore a wavelength range from 1200 to 1600 nm for single-mode operation is required.

Fibres and cables

The single-mode operational window of a cable system is given by

- modal noise (short wavelength limit) [5]
- microbending and macrobending losses of the fundamental mode (long wavelength limit).

In order to ensure the large single-mode wavelength range, the fibres to be cabled must have an adequate mode field diameter and cutoff wavelength; furthermore macrobendings and microbendings must be avoided as far as possible due to cable design and production.

The fibres used for the cables are standard matched cladding single-mode fibres. They have a mode field diameter of between 9,5 and 9,8 µm at 1300nm and cutoff wavelength λ_c of between 1230 and 1290 nm.

Theoretical calculations and experimental results carried out in the meantime have demonstrated that larger mode field and cutoff wavelength tolerances are possible.

Economical small-size high-fibre-density high-fibre-count cables are required for subscriber networks. Many cable designs meeting these requirements are possible [6]. However considering the fact that the loose tube design is well suited for minimizing microbends and that this cable type has been succesfully installed and proven its reliability in the networks of the Deutsche Bundespost [1] and in many other countries, we have also used this construction for our developments.

The cables are based on an improved loose tube design, each tube containing 1, 5, 10 or 20 fibres. A common basic unit contains six 20-fibre tubes. For purposes of identification, the fibres are colour-coded by 10 different colours and by additional black ring marking.
While conventional copper cables contain up to 2000 pairs, a maximum fibre count of about 800 seems to be sufficient for optical cables, because each subscriber is only supplied with one fibre, and one copper cable can be replaced by three optical cables by subdividing the existing cable ducts, if the cable diameter is sufficiently small.

The fibre count of the largest cable is 840. This cable consists of 7 basic units. The outer diameter of this cable is 35 mm, resulting in almost the same fibre density achieved by ribbon cables. A modular cable design and different fibre counts per tube ensure an optimum fitting to each requirement.

The cross-section of the 120-fibre basic unit of the 840-fibre cable and a view of the 120-fibre cable are given in the following figures:

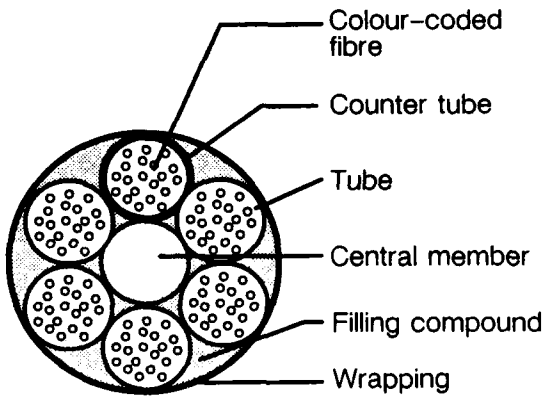

Fig.1 Cross section of 120-fibre basic unit

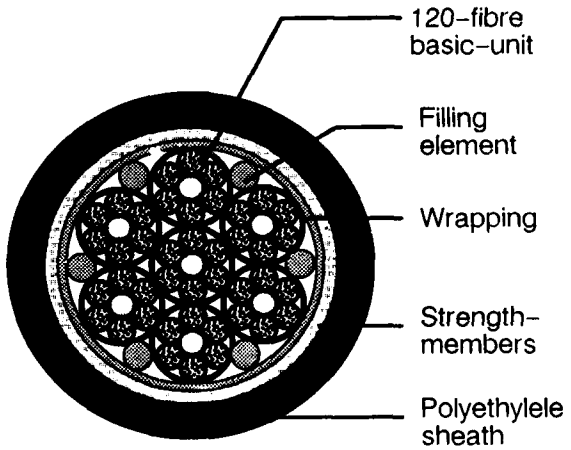

Fig.2 Cross section of 840-fibre cable

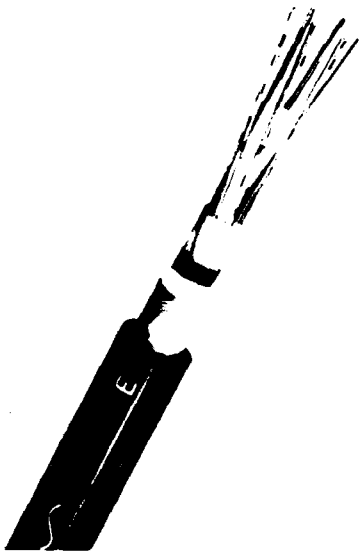

Fig.3 120-fibre cable

Cable production

The different cable production stages are as follows:

- colour coding
- tubing (secondary coating)
- stranding
- sheathing

The most critical step is tubing, because high-fibre density requires precise control of the excess fibre length in the tube; developments for speeding up this process are in progress.

Cable properties

Fig. 4 shows the spectral attenuation of the cabled fibres. Even at 1600 nm the attenuation is sufficiently small.

The cutoff wavelength λ_c of the fibres and λ_{cc} of the cabled fibres [6] were measured. The average values from 40 fibres are as follows:

$\bar{\lambda}_c$ = 1263 nm ± 8 nm

$\bar{\lambda}_{cc}$ = 1161 nm ± 15 nm

The difference between λ_c and λ_{cc} is ~100 nm, which complies with theoretical findings [7]. Taking into account the fact that matched cladding fibres are used, the cable cutoff wavelength is mainly given by the two 76 mm loops used in the arrangement for the λ_{cc} measurement.

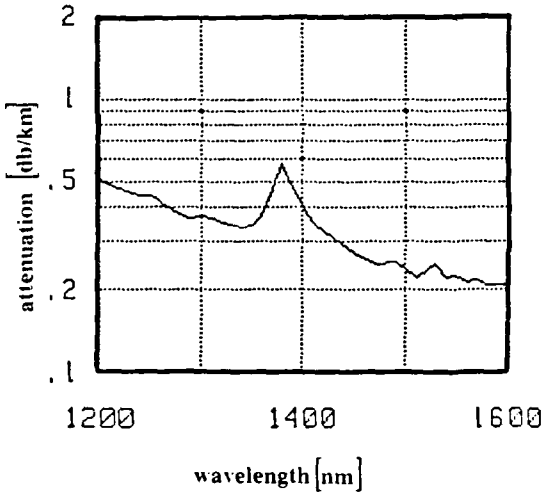

Fig.4 Spectral attenuation of cabled fibres

In order to ensure single-mode operation of the cable network even at 1200 nm, an additional 76mm loop is included close to the terminal equipment of the 1200 nm channel.

Furthermore, the behaviour of the fibres as a function of the cable tensile load was measured at the 120-fibre cable, as shown in Fig. 5.

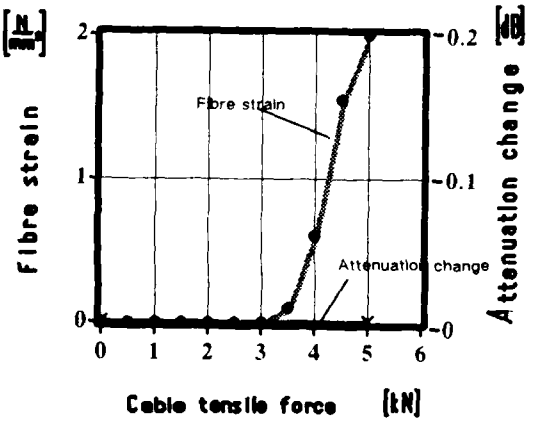

Fig.5 Fibre strain and attenuation change (at 1550 nm) vs cable tensile load

Conclusions:
- Fibres with and without ring marking have a similar behaviour.
- The excess fibre length has been well controlled. (The measured value of 0.35% exactly meets the theoretical value of 0.33%).
- The fibres in the cable are stress-free under standard operational conditions, and high reliability is thus ensured.

The temperature behaviour of the cabled fibre attenuation slightly depends on the colour coding (and naturally on the wavelength). Fig. 6 shows performance under worst-case conditions (ring marking, 1550 nm wavelength).

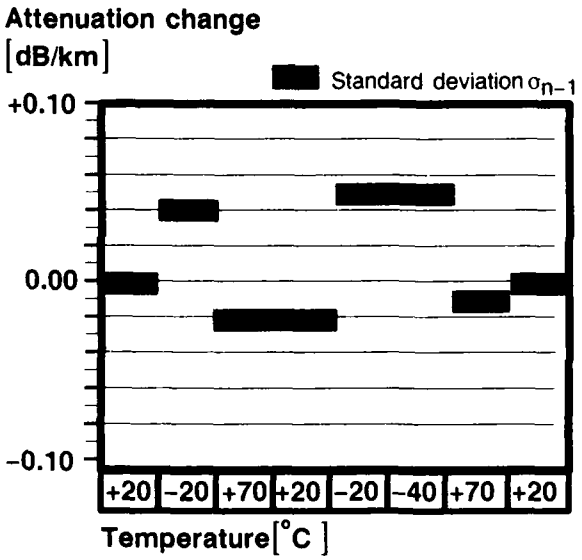

Fig.6 Attenuation change of cabled fibres vs temperature

The temperature behaviour of the attenuation is already sufficient. Additional improvements can be reached by better optimiziation of the tubing process.

Summarizing, it has been shown that a very high-fibre-density cable based on the loose tube design can be manufactured with a large single-mode operational window and good optical and mechanical properties.

Fibre splicing

Up to now, single-fibre splicing methods based on fusion methods or mechanical coupling methods have reached a high standard of reliability and practicability [9, 10, 11]. However, with the increasing number of fibres per cable required in subscriber networks, it is becoming more and more important for faster splicing methods to be available which are adapted to cable construction.

Analysing the particular steps of single-fiber splicing methods, it is conspicuous that it is not the splicing process itself, but preparation, fiber handling and mounting the splice protection which are the timeconsuming aspects of the splicing process. It is thus obvious that splicing time should be reduced by introducing multiple splicing techniques, where the timeconsuming stages can be effected simultaneously for several fibres.

The splicing technique is strictly related to the cable design.
The following table shows the advantages and disadvantages for the splicing technique of the loose tube cable design compared with the ribbon cable design, which is also suited for future subscriber networks [6].

Stages in splicing procedure	Loose tube unit	Ribbon unit
Removing the buffer-jelly	necessary	not necessary
Removing the buffer	simultaneously possible for several fibres	
Removing the primary coating	simultaneously possible for several fibres	
Simultaneous removing the primary coating and buffer	not possible	possible
Fibre sorting	necessary	not necessary
Fibre cutting	simultaneously possible for several fibres	
Subsequent axial adjustment of the fibres	possible	not possible
Subsequent switching of individual fibres	possible	not possible
Branching	easy	difficult

The comparison shows that both cable designs are nearly equivalent in their influence on the splicing technique. Ribbon cables allow slightly more economic features by simultaneously removing the primary coating and fibre buffer and sorting the fibres in the ribbon.
Loose buffer cables have advantages with regard to the possibilities of subsequent axial adjustment of the fibres thus allowing higher tolerances in the multiple cutting process and in subsequently switching and branching individual fibres.
Furthermore, it is possible to overcome the remaining disadvantages of fibre bundles by converting the fibres into a quasi-ribbon by means of additional tools.

Summarizing, loose tube cables have no disadvantages regarding splicing.

For subscriber networks, fusion splicing technique is favoured because of the following advantages when compared with mechanical splices:

- The self-allgning effect can be used for low

geometrical tolerance single-mode fibres.

- The longitudinal fibre offset and the quality of the fibre endfaces are less critical.

- Index matching materials for avoiding light reflections are not necessary.

- Longterm stability is ensured.

Furthermore, the fusion splicing technique has been used sucessfully in most cable networks all over the world.

ANT Telecommunications is one of the two splicing equipment suppliers for the Deutsche Bundespost (German PTT).

A "sandwich" has been developed for the splice protection, consisting of a V-grooved small aluminium plate covered by a permanently elastic material. Using a special tool, the splice can be easily positioned in the sandwich, and the plate is compressed. The whole procedure only involves a few seconds. The sandwich has already been introduced for single-fusion splicing by the Deutsche Bundespost since 1985. Further development for mass splicing can be achieved very easily by broadening the sandwich and modifying the fusion splice equipment.

Summarizing, fusion splicing is a favoured technique for broadband subscriber networks. For further economic progress, this technique can be enhanced for reliable multiple-fibre splicing.

Conclusion

A single-mode optical cable network has been presented meeting all the specifications required for present and future subscriber communication systems.
Particulary high-fibre-count cables based on a loose tube design have been developed which have the following features (not yet in production but in the laboratory)

- good optical and mechanical performance

- a large single-mode operational window (1200-1600 nm)

- high fibre density.

Because the network design is as far as possible the same as for existing copper and optical systems (star network, loose tube cables, fusion splicing technique), a gradual introduction of the optical subscriber network and a gradual replacement of copper by optical fibres can be easily achieved in accordance with current requirements.

References

[1] G. Schweiger; "Optical Fibre Cables in the Network of the Deutsche Bundespost"; ICWS Proceedings, 1986, pp 259 - 270

[2] F. Krahn; "Optical Cable Network for 150 Subscribers"; ICWS Proceedings, 1980, pp 418 - 423

[3] W. Bambach, G. Blume, F. Krahn, H.-G. Zielinski; "Weiterentwicklung in der Breitband-Kabeltechnik" Telematica Proceedings, 1988, Stuttgart

[4] D.Barth, G.Blume; "Passive Komponenten", ANT - Nachrichtentechnische Berichte 3 (1986), pp 79 - 89

[5] S. Heckmann; "Modal Noise in Single-Mode Fibres" Opt.Lett. 6 (1981), pp 201 - 203

[6] H. Muratai "Optical Fibre Cables and Accessories for Subscriber Networks", Proceedings of the OFC'88, p 190

[7] CCITT Recommendation G. 652, 1988

[8] F. Krahn, E. G. Neumann, B. Sange, Schwierz, J. Streckert, F. Wilczewski; "Cutoff Wavelength of Single-Mode Fibres: Definition, Measurements, Length and Curvature Dependance" to be published 1988/89

[9] C. M. Miller; "Mechanical Optical Fiber Splices", Journal of Lightwave Technology, Vol. LT-4, No. 8, August 1986

[10] G. Le Noane et al.;
"Successful Mass Splicing of Single-Mode Fibers: The Flat Design", Proceedings of ECOC 1985, pp 633 - 636

[11] N. Kashima, M. Tachikua, M. Hirai;
"Splicing and Connecting Techniques for Optical Sunscriber Cables" Review of the Electrical Communication Laboratories Vol. 32, No. 4, 1984

Georg Blume was born in 1954. He studied Electronics at the TH Darmstadt and received his diplom degree in 1980.
He joined ANT Telecommunications in 1980 and was first engaged in research and development of fiber optic measurement and splicing techniques.
Since 1988 he is responsible for the development of fiber optic systems in the telecommunication cable systems devision.

Helmut Feilhauer was born in Nördlingen, Germany, in 1958. He received the degree in electrical engineering from the Technical University Stuttgart in 1983.
In 1983 he joined ANT Telecommunications where he is working on the development of splicing equipments and on mearsurement techniques for optical fibre components within the telecommunication cable systems division.

Friedrich Krahn was born in 1939. He graduated from the University of Münster in 1970 with a Dr. rer. nat. in Physics. He then joined Felten & Guilleaume Carlswerk AG, now named Philips Kommunikations Industrie AG, and was first engaged in the field of innovation and diversification.
In 1973 he was appointed head of the department for fibre optics research and development.
In 1986 he joined ANT Telecommunications, and he is now responsible for the optical fibre cable development within the telecommunication cable systems division.

Norbert Lenge was born in 1956. After four years as research assistant at the Max-Planck-Institute in Stuttgart he graduated from the University of Stuttgart in 1984 with a Dr. rer. nat. in Physics. He then joined ANT Telecommunications and was first engaged in the field of polymer cross-linking.
Since 1987 he is responsible for progress engineering and construction of optical telecommunication cables within the telecommunication cable systems division.

Gerhard Olejak studied at the FH Düsseldorf and received the diplom degree in process-engineering in 1973.
From 1975 to 1985 he was engaged in the development of optical telecommunication cables at the Philips Kommunikations Industrie AG.
In 1986 he joined ANT Telecommunications, and he is now responsible for production of optical telecommunication cables.

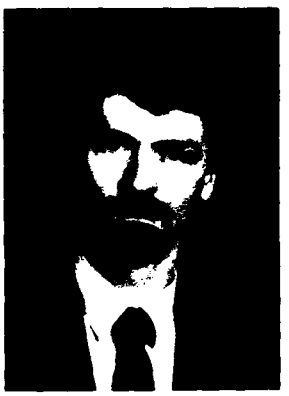

Bernd Sange studied at the Technical University of Berlin and received the diplom degree in Physics in 1980. He joined Philips Kommunikations Industrie AG in 1981, where he was engaged in R & D of optical fibre cables.
He moved to ANT Telecommunications in 1986 and he is now responsible for quality control and measurement of optical fibre cables within the telecommmunication cable systems division.

Hans-Gerd Zielinski was born in 1949. He studied Electrotechnics at the RWTH Aachen, and he received his diplom degree in 1975. He then joined ANT Telecommunications, and he was first engaged in the development of fibre optic splicing machines and connectors. In 1978 he became appointed head of the development of fibre optic passive components. From 1984 to 1988 he chaired the department of optical fibre cable systems, and now as head of the developments he is responsible for the cable system development within the telecommunication cable systems division.

The Architecture and Technology for the All-Fiber Loop

R. M. Huyler*, D. E. McGowan*, J. A. Stiles*, F. J. Horsey**

*AT&T Bell Laboratories, Whippany, New Jersey 07981, USA
**AT&T Network Systems, Newark, New Jersey 07102, USA

Summary

Since 1983, when high speed multiplexers operating over fiber feeder cables were first introduced, the race has been on to fiber the "last mile" of the telephone distribution network. This year several fiber distribution systems have been proposed. AT&T's system, the first in service in August 1988, is based on the SLC® Series 5 Digital Loop Carrier System, which has been extended to include the distribution plant. An all fiber network is completed by using DDM-1000 (DS3) or higher rate multiplexers in the feeder plant. This first Fiber-to-the-Home system will enable the Telephone Companies to prepare for future wideband services in an evolutionary and economical manner.

All Fiber Loop Architecture

The final barrier in the loop, the so called "last mile" has finally been breached. Since 1983, when high speed multiplexers operating over fiber feeder cables were first introduced into the network, the race has been on to complete the fiber picture with a fiber distribution network. With the introduction of fiber distribution and drop cables into the network this year, AT&T's system, using the SLC® Series 5 Digital Loop Carrier System, bridges the span from a copper network to an all fiber network. The SLC Series 5 Digital Loop Carrier System, in conjunction with the DDM-1000 in the feeder, is the first production all fiber network; see Figure 1. This all fiber network will enable the Telephone Companies to position themselves for future wideband services in an evolutionary and economical manner. Initially AT&T's system provides POTS (Plain Old Telephone Service) type services, with enhanced services following shortly thereafter.

Technology in the Loop

The architecture of this system is based on the SLC Series 5 Digital Loop Carrier System, which has been extended from a feeder only system to include the loop distribution. The basic system consists of a SLC Series 5 central office terminal connected to a SLC Series 5 remote terminal over a DDM-1000 Multiplexer in the feeder plant. The subscriber side of the remote terminal is connected to an optical shelf; fiber jumpers coming from this go to a fiber interconnect. The fiber interconnect terminates the fiber distribution cables, which run to the distant terminal, mounted on the outside of the customer premises. The following sections elaborate on these system components.

Central Office Terminal and Feeder Plant: The standard SLC Series 5 channel bank, with all the common plug-in units is the Central Office Terminal (COT) used in this system. The COT channel bank demultiplexes the DS1 signals to DS0 signals for switch input. Since the initial offering will be POTS service, standard POTS channel units will be used in the central office terminal.

The DDM-1000, operating at 45, 90, or 180 Mb/s in the feeder part of the loop, transports the DS1 (1.544 Mb/s) SLC® Series 5 signals between the central office and the remote terminal. Single-mode fiber cable is used in this feeder portion of the loop plant. If desired, higher rate systems, such as AT&T's FT Series G at 417 Mb/s, can also be used. The feeder part of the system is, in fact, no different from that used when SLC Series 5 serves conventional copper distribution. Copper feeder could even be used, but would be unusual with fiber distribution.

Remote Terminal: The remote terminal also uses the standard SLC Series 5 bank, and all the common plug-in units, but it has new channel units. These channel units are connected to optical units, in an optical shelf, by twisted pairs using standard 710 connectors. Four optical shelves, mounted under the SLC Series 5 banks can serve a maximum of 192 customers (two SLC Series 5 Dual Channel Banks); see Figure 2. The optical shelf is connected by fiber jumpers, with ST® connectors on each end, to a fiber

interconnect, which terminates the fiber distribution cable. The complete arrangement is housed in the initial trials in Controlled Environment Vaults (CEV). In 1989 deployment in smaller above ground enclosures will be available.

Channel Units

Two new RT channel units were developed for this fiber system. They fit into standard SLC Series 5 dual channel bank shelves, in place of the standard metallic channel units that would provide service over copper distribution pairs. The two units are functionally the same, except that one provides two POTS lines and occupies one channel unit slot, and the other provides four POTS lines and occupies two slots. Each channel unit serves one customer (unlike copper channel units, which provide two lines that may go to different customers). The initial service provided is standard two-wire analog, single party POTS with loop-start signaling and fast forward disconnect.

Fiber Interconnect: The fiber interconnect used in this system provides direct termination of the outside plant cables on ST connectors. The interconnect provides a flexible rearrangement point for connecting fiber jumpers from the optical shelf to the distribution plant, and access to the optical line for system turn-up and maintenance.

Optical Unit: The heart of the system is the optical unit. Two optical units are used for each loop, one located at the remote terminal in the optical shelf and the second in the distant terminal. The optical unit and the SLC Series 5 channel unit are connected via two twisted pairs through a 710 connector. The optical unit operates at a line rate of 1.544 Mb/s, and provides electrical-to-optical and optical-to-electrical signal conversion at each end of the fiber distribution loop. The optical unit receives DS1 signals from the channel unit and converts the electrical DS1 signal to an optical DS1 signal for transmission over the distribution fiber. A 1300 nm laser diode performs this transmission functionality. In addition, the optical unit receives the optical DS1 signal transmitted over the single-mode fiber and converts it into a DS1 electrical signal. A PIN (positive-intrinsic-negative) diode performs the receiver functionality in the optical unit. Transmit and receive signals are combined by an optical splitter, providing bidirectional transmission on a single distribution fiber. Single-mode fiber is used because of its superior transmission characteristics, while providing a wideband vehicle for future services.

Distant Terminal: The Distant Terminal (DT) is an outside plant closure mounted outside the customers premises. The DT contains an optical unit, channel unit, power converter unit, back up batteries and voice frequency terminals which are wired to a Network Interface Unit. See Figure 3 for a diagram of the DT. The DT's function in the receive (incoming) direction is to convert the 1.544 Mb/s (DS1) optical signal to a DS1 electrical signal and then convert the electrical signal to the standard telecommunication voice frequency signal. In the transmit (outgoing) direction the DT functions in the reverse fashion.

The DT channel unit also provides the "BORSCH" functions which are normally provided by the remote terminal channel unit in conventional copper distribution: battery feed, overvoltage protection, ringing, supervision, coding and decoding, and hybrid. Hence conventional telephones can be used by the customer. The distribution fiber, with an ST connector on it, terminates into the optical unit. The optical unit converts the DS1 optical signal to DS1 electrical signal or vice versa, depending on whether it is receiving or transmitting a signal.

The optical unit interfaces in the DT with the Channel Unit (CU). The CU provides from one to four lines to the customer, depending on the RT channel unit selection discussed earlier. The CU provides line mux, clock recovery, clock dividers, control, signaling and the BORSCH functions. Each of the line interfaces is provided with a current limited line feed.

The Power Converter Unit (PCU) provides battery charger, rectifier and ringing generator functions at the DT. The battery charger is a constant voltage charger and is used to maintain a charge on the backup batteries. The PCU monitors the incoming AC power and provides automatic transfer to battery backup if AC power fails. The backup battery pack contains six cells and is rated at 12 VDC, 5.0 Ah. The battery pack will provide a minimum of 8 hours of operation for the DT.

The AC power enters the DT enclosure into a sealed box for craft protection. The box contains a switch type circuit breaker and a line transformer which converts 120 VAC to 17.6 VAC. The AC line cord is three to four feet in length and is housed in waterproof flexible metallic tubing.

The DT enclosure also contains air vents on the bottom, grounding arrangements and an organizer to store any slack fiber.

Deployment in the Field

The SLC Series 5 Fiber-To-The-Home System

presently has multiple applications in various stages of deployment. Listed below are the sites of these deployments.

New Jersey Bell - South Brunswick: The first trial of this system was in New Jersey Bell. The first system was cut into service on August 5, with customers put in on a service order basis. Each customer will have a DT mounted on a stake designed by New Jersey Bell. The architecture used in NJ Bell consists of a SLC Series 5 Digital Loop Carrier remote terminal housed in a CEV. The entire outside plant is buried in conduit, including the drops.

Southwestern Bell - Leawood, Kansas: The Leawood site is the first application of the fiber-to-the-home feature utilizing production equipment. Subscribers will be provided with service over fiber commencing in October 1988. The distribution is LXE fiber with metallic shielding and terminates into above-ground pedestals. The drop cable is composite with two fibers and three metallic pairs.

South Central Bell - Memphis: South Central Bell's first fiber-to-the-home system is in a development in the eastern suburbs of Memphis, Tennessee. The feeder is optical and somewhat unusual in that it is at 417 Mb/s, using two stages of multiplexing (the first to DS3).

Distribution fiber cables (AT&T's LXE Lightpack®) are direct buried 36 inches deep, with direct burial of drop splice closures, also. Each drop closure serves up to four houses; drops for unbuilt houses are coiled in plastic boxes at the lot line. First customer service is scheduled for November 1988.

GTE: Cerritos, California is the Fiber-To-The-Home site selected by GTE. It is an existing community located in Southeast Los Angeles County. Homes in this community are already established and are currently served by a traditional copper architecture. Cerritos thus becomes the first site where a modernization situation is encountered.

GTE has established Cerritos as a test-bed whereby they can evaluate equipment and services from various vendors. Accordingly, Cerritos has been dissected into separate service areas to facilitate GTE's evaluation. Initial service is expected to be available in late December of 1988.

Contel: Contel's selection for a Fiber-To-The-Home site is a new subdivision within an existing community located in Ridgecrest, California. Ridgecrest is a community located in California's Mojave Desert near the U.S. Naval Weapons Center at China Lake.

Equipment for this site is initially designed to serve homes through the 1990 timeframe. All utility services will be provided through underground facilities. Distribution fiber has been planned for this area using the conventional single single-mode fiber per home. Initial service is expected to be available in late December of 1988.

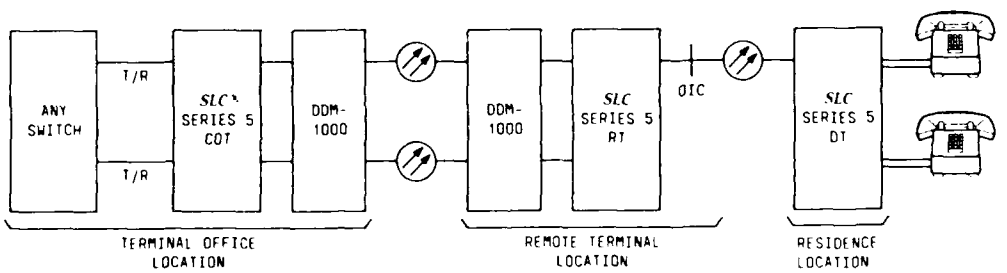

Figure 1 - SLC® Series 5 Carrier System Fiber-To-The-Home Universal Configuration

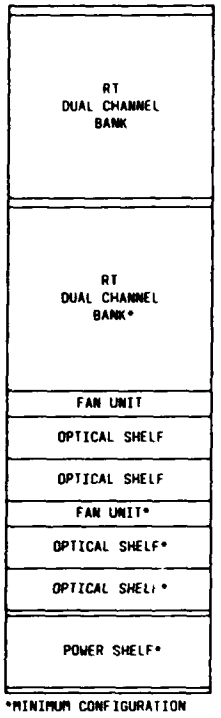

Figure 2 - Remote Terminal Bay Layout

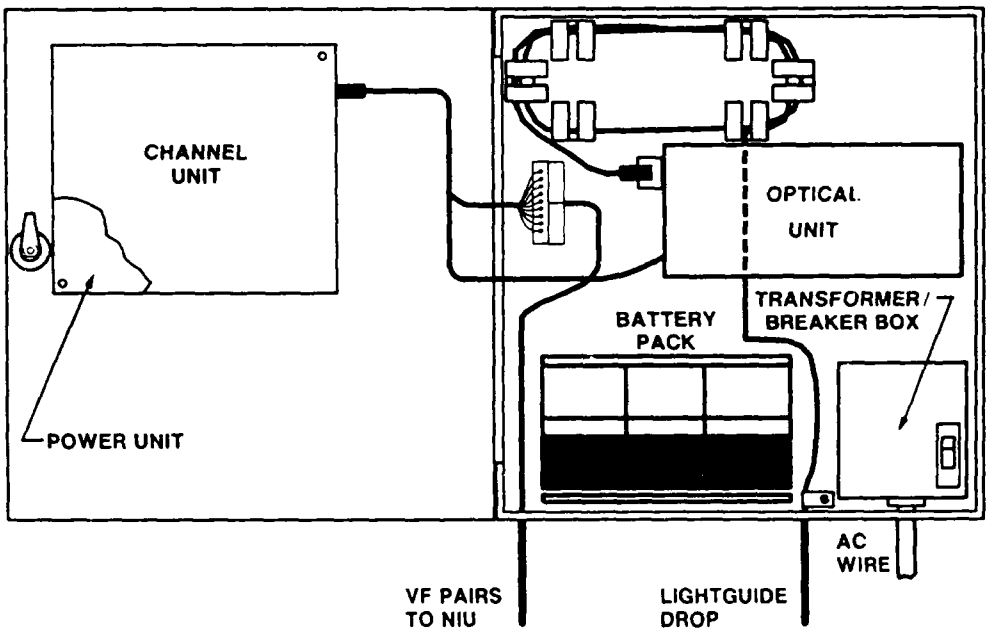

Figure 3 - Distant Terminal - Telephone Company Access

Raymond M. Huyler, Jr., is a Member of Technical Staff (MTS) with AT&T Bell Laboratories. Since joining the company December 24, 1950, he has worked in the Military Systems arena from 1950 through 1974 on Radar Tracking Systems. His next assignment was telephone loop transmission products from 1974 to 1978. From 1979 to the present his work is in systems engineering providing field support on the introduction of new products.

J. Anthony Stiles is a Member of Technical Staff at AT&T Bell Laboratories. He has a B.Sc. in Mathematics from Sydney University, Australia, and a Ph.D. in Automatic Control from Cambridge University, U.K. With a background in loop systems engineering, he is currently working on the SLC® Series 5 Fiber-To-The-Home System.

Dennis E. McGowan is a Distinguished Member of Technical Staff at AT&T Bell Laboratories. He worked in New York Telephone Company in the switching department for 17 years, before being transferred to AT&T Bell Laboratories. He has a BS and MS in Physics from Polytechnic Institute of New York. He is a Systems Engineer in the Loop Transmission Systems Laboratory at AT&T Bell Laboratories. He has extensive experience in integrated carrier systems and is currently working on the SLC® Series 5 Fiber-To-The-Home System.

Frank J. Horsey is a Senior Engineer for AT&T Network Systems (Customer Operations - Engineering Planning and Development) at Newark, New Jersey. Frank received his degree in Electronics Engineering from Spring Garden Institute in Philadelphia, Pennsylvania in 1964 and has been employed at AT&T since that time. He has worked in the area of project engineering and management for AT&T telecommunications programs involving various types of telephone central office switching and transmission systems for twenty-four years. He is currently in-residence at AT&T Bell Laboratories in Whippany, New Jersey for the SLC® Series 5 Carrier Fiber-To-The-Home Feature project.

LINE PLANT CONSIDERATIONS FOR PASSIVE OPTICAL NETWORKS FOR THE LOCAL LOOP

M.H. Reeve

British Telecom Research Laboratories, Martlesham, Ipswich,
Suffolk IP5 7RE, England

Abstract

Recent work at BTRL has concentrated on the introduction of single mode fibre in to the local loop against an initial use for telephony, whilst allowing later upgrade to broadband. In order to approach copper pair costs for telephony the fibre is shared amongst a number of users. One particular network studied at BTRL, the Telephony on Passive Optical Network (TPON), is a passive splitter approach. In this network a single fibre is fed from the exchange and fanned out via passive splitters at the cabinet and distribution point (DP) positions to feed a number of individual customers. This paper considers the line plant issues for such networks, including components design and maintenance and testing issues. A system model is developed to predict overall system losses. Finally a system demonstrator was installed on the BTRL site to test feasibility of the approach.

1.0 Introduction

Recently proposals have been made for passive optical networks for the local loop having the potential to cost in against copper pair for telephony use, and yet still have the potential for future wideband use. (1,2) In BT studies have concentrated exclusively on the use of single mode fibre for these networks.

One particular network studied at BTRL, the Telephony on Passive Optical Network (TPON), is a passive splitter approach. In this network a single fibre is fed from the exchange and fanned out via passive splitters at the cabinet and distribution point (DP) positions to feed a number of individual customers. A TDM signal is broadcast to all terminals from the exchange on a single wavelength, with the customer time accessing the particular bits meant for him. In the return direction data from the customer is inserted at a pre-determined time to arrive at the exchange in synchronism with other customer's data. Inclusion of an optical filter in the customer's terminal that passes only the TPON wavelength allows the later provision of new services on other wavelengths without disturbing the telephony transmission. A target maximum of a 128 way split operating at 20 Mb/s would allow the provision of basic rate ISDN to all customers.

In line plant terms the cable count near to the exchange is considerably reduced, with fibre and cable costs shared between many customers. In addition the exchange equipment is also shared by the splitting ratio, further reducing the cost per subscriber.

This paper examines the critical line plant issues for such networks, including likely overall losses using typical components, reflection problems in duplex working and maintenance and testing issues.

2.0 Basic Network

The basic network is shown in Fig 1. Two splitter points are assumed to model the flexibility points present in the existing copper network (streetside cabinets of up to 600 customers and distribution points (DP's) up to 15 customers) and thus most easily fit into the existing underground cable duct system. Typical lengths are shown with the average local loop being around 2 km total length in the BT network.

Table 1 shows a comparison of component numbers for various levels of split against a point to point system having one fibre to each customer. It is apparent that the passive splitter network typically has 10% of the fibre and half the number of splices and connectors.

In addition to the cost aspect the fibre sharing also removes the need for high-fibre count cables, removing the maintenance nightmare of damage to a cable containing many fibres.

3.0 Critical Components of the Splitter Network

Component issues important to the passive splitter based network are:-

-- Splitter arrays of up to 16 ways. Since it is likely that the initial telephony system will operate in the 1300 nm window, with broadband upgrade in the 1500 nm window the splitter arrays will need to be wavelength 'flat', with low loss and constant coupling ratio across a

wide band of wavelengths to avoid wavelength "steering" by the network.

-- Blocking filters to exclude later wavelengths from the customer's receiver.

-- Low fibre-count cables for cabinet and DP interconnect and customer's drop (overhead and underground) and internal applications.

-- Housings for splitter arrays and customer's equipment with adequate fibre management and testing facilities.

-- Testing and monitoring facilities that can be employed with the network "live". Since it is likely to be impractical to shut down service to up to 100 customers to test for a fault on one the network must be maintained whilst live.

-- If bi-directional working is used, (as in Fig 1) or reflection-sensitive systems (microwave subcarrier or coherent systems for example) are contemplated for future use then attention will need to be paid to reflection levels from splices, connectors and unused fibre outlets on splitter arrays. In this paper this is explored for the case of bi-directional working.

-- Low-cost components easily used by local network staff. In spite of the fibre sharing aspect it is unlikely that copper pair costs will be approached without a significant reduction in single mode fibre and component costs. To date fibres tend to have been installed in long haul networks by small numbers of highly skilled staff. In the local network it is likely that staff numbers will be higher and skill levels lower.

In order to study each of these aspects a system demonstrator has been built at BTRL, and an overall system model produced by consideration of individual component losses. In the following part of the paper the critical components and issues will be examined in more detail to produce an overall expected power budget for the system from the system model. This is then compared with results from the demonstrator.

4.0 Component Design

4.1 Splitter Arrays

At the present time the technology most suitable for making passive splitter arrays is that of the fused splitter, with planar ion-diffused glass and integrated optics (eg LiNbO3) likely to be contenders in the future. The work at BTRL has concentrated on the fused-splitter approach. In this approach a 2x2 splitter is made by fusing and tapering two fibres together. The wavelength dependance of the splitter can be reduced by altering one fibre slightly to ensure that the maximum available coupling between the two is at the 50% point. The splitter is then tapered to this point to produce a fairly flat wavelength response. Fig 2 shows the wavelength response for a single splitter, giving a deviation from the 3 dB or 50% split of up to 0.8 dB over the system wavelength range of 1270-1580 nm. Each curve corresponds to the output from one of the splitter legs.

Clearly any particular path through an array of splitters will exhibit a loss due to the summation of effects from each split. These may add or cancel, producing a variation in wavelength response from path to path (ref 3). Nevertheless, it is always the case that one path will exhibit the worst case response, leading to a loss given by multiplying the response of Fig 2 by the number of split levels. This loss is used in the system model.

In addition to the "loss" effect of coupling ratio, losses due to polarisation effects on coupling and splitter excess loss due to imperfections must be taken into account. Measured values for these effects across a typical batch of 20 splitters made at BTRL are shown in table 2 and later used in the system model.

The results shown are for individual 2x2 splitters spliced into arrays. Although this approach can give adequate performance it is unlikely to lead to low cost, and tends to produce large package sizes. A method of producing the splitter arrays by direct 'knitting' of the fibres without splicing is required, either by sequential or simultaneous manufacture of a number of splitters in one operation. Thus far prototype 4x4 arrays have been made at BTRL by simultaneous pulling of 4 splitters, although much work remains to be done to refine the process.

4.2 Customer's Blocking Filter

As previously explained a blocking filter is needed in the customer's telephony equipment to exclude later wavelengths from the receiver. Initial work at BTRL has attempted to reduce the amount of optical spectrum used for telephony to allow several extra wavelengths in the 1300 nm window. The result is a target for the blocking filter of 15 nm full width at half maximum, 1.5dB loss and essentially "top-hat" spectral shape, if it assumed that the exchange source is a DFB laser controlled to 1 nm.

Fig 3 shows a prototype device produced at BTRL. In this approach a multilayer dielectric filter is mounted in a slot in a conventional connector ferrule, with the connector ferrule providing fibre alignment to yield a low cost fibre-tailed device that can be spliced into the network. Fig 4 shows the response of the filters produced so far, with a performance of 16 nm FWHM and 1.5 dB loss.

4.3 Cabling

Interconnect of exchange to cabinet and cabinet to DP can use low fibre-count single-mode cables (either conventional or blown fibre) already in use in the network without significant development effort, with the existing specification of less than 0.5 dB/km in both windows.

For the subscriber drop and internal cables little is available and the area is technically challenging from both strain and bending aspects. With as much as 70% of subscriber drops on overhead cable in some areas it is likely that both overhead and underground solutions will be required. In the case of overhead drop cable termination methods are vitally important and often dictate cable design. Designs must be built to withstand ice and wind loadings of 5 mm radial thickness and 80 km/hour respectively, whilst still maintaining fibre strains below 0.15%.

Plate 1 shows prototype ruggedised blown-fibre tubes suitable for direct burial in underground drops and a prototype overhead drop cable in which the support member can be separated from the blowing tube and held using existing methods.

4.4 Cabinet and DP Housings

At cabinet and DP points, housings are required for the passive splitter arrays and associated splices. Important factors are:-

-- Maintenance of minimum bend criteria (35 mm) to avoid loss increases at 1550 nm.

-- Fibre management. Housings must allow rapid re-entry for addition of new subscribers without damage to existing fibres.

-- Test access. Provision must be made for clip-on or end-on access to each fibre.

-- Termination of spare fibre ends to prevent stray reflections.

Experience from the on-site demonstrator has shown the fibre management issue to be a critical one, with conventional approaches in which splice trays hold a number of fibres and splices being totally inadequate. An approach has been developed in which each splice and the associated fibre loops for splicing and clip-on are held in a novel single-splice holder having moveable components to release and contain the fibre loops. A prototype DP made in this way is shown in Plate 2.

4.5 Reflection Levels

The use of bi-directional working (as shown in Fig 1) has advantages in reducing the amount of plant in the ground, easing the fibre management problem at cabinet and DP points and of reducing the possibility of error in record keeping. (there is no chance of confusing go and return fibres). However, the network immediately becomes sensitive to reflections appearing back at the sending receiver in the form of crosstalk.

For the target transmitter and receiver performances of 0 dBm launch and -50 dBm receive reflection levels close to the system ends must be kept below 50 dB down on the incident signal (50dB return loss) if the signal to noise ratio of 5 dB required by the analysis of ref 5 is to be achieved. This applies to both splices and unterminated ends on splitter arrays. Since most mechanical splicing systems currently have return losses in the 30-40 dB range it is difficult to see how these can be used, restricting splicing to fusion.

5.0 System Model

The average local route length in the BT network is around 2 km, with 90% below 5 km. In order to assess likely overall losses of the TPON network a model was built of a 5 km system having a 128 way split and full duplex operation. This gives 9 levels of splitting (7 for 128 ways and 2 duplex).

Measured data for splitter arrays and other components such as splices, connectors and cables was gathered as shown in table 3.

The resulting spread of losses for the worst case path is shown in Fig 5 for 1300 nm. The resulting spectral loss is shown in Fig 6.

Losses up to 42 dB are expected for the worst case components and wavelength.

6.0 Testing Issues

Two approaches have been taken to testing the passive splitter network whilst live. The first involves the use of conventional OTDR equipment used at a test wavelength, with the blocking filters screening the test wavelength from the system receivers. Commercially available OTDR equipment currently has a dynamic range of around 23 dB, with the result that fibre can only be monitored over half of the split levels in a 128 way (9 split levels) network before losses become too great. This was overcome by monitoring from a mid-point in both directions through a demountable optical tap. The test wavelength used was 1550nm, with the system running at 1300 nm. The tap was made from a polished coupler (ref 6) designed to preferentially couple at 1550 nm. In this way the loss to the system due to the tap was 0.7 dB whilst coupled and 0.02 dB uncoupled, whilst the loss seen by the test equipment was around 3 dB. In this way a conventional OTDR trace could be obtained whilst the system was running without the need to terminate fibre ends.

Clearly when looking in to a splitter network light will be returned to the OTDR from several branches simultaneously, leading to problems of interpretation in determining in which branch a fault lies. A partial solution is to make use of customer's laser power monitoring normally employed by the system to determine which leg has developed a fault by looking for increased laser current to that subscriber.

In addition to the test wavelength approach a second test method was produced using optical "clip-on" to produce a low cost power meter, somewhat equivalent to the AVOmeter in use for copper pair. In this way a piece of test equipment was produced that would allow basic fault finding by each linesman.

The clip-on idea is based on using a small bend in the fibre to tap a small amount of light out. This light is collected and guided to a detector by a short waveguide to give the power meter operation. Careful choice of the bend radius can give an indication of power in the fibre to around 3 dB whilst adding less than 3 dB loss to the system with even the most bend sensitive fibre allowed by the fibre specification at the highest wavelength. A prototype instrument sensitive down to -30 dBm fibre core power is shown in plate 3.

7.0 Demonstration System

In order to test the various trade-offs inherent in the passive splitter network a demonstrator system was built at BTRL, as shown in Fig 7. Two exchange points and two DP's were interconnected via a passive splitter array mounted in a standard BT external cabinet to simulate a 128-way split. The total system length was around 1.5 km, with blown-fibre cable being used throughout. The measured loss of the system at 1300 nm was 35 dB, in comparison to a loss of 34 dB predicted by the system model.

Unused legs on the splitter arrays were terminated by a mandrel-wrap technique of introducing several turns at 3.4 mm radius to prevent reflections back into the network. Although effective it is unlikely to prove reliable in the long term and further work is necessary to produce a field termination for unused fibre ends.

As previously described the system could be tested with clip-on testers or by means of OTDR equipment launched via a demountable tap in the external cabinet.

8.0 Conclusions

Passive splitter approaches to fibre in the local network can enable initial deployment for telephony by means of fibre sharing amongst a number of customers. The result is a considerable reduction in the installed plant in the ground.

This paper has considered the problems of design, installation and testing presented to the optical plant by such a radical approach and has described the successful exploitation of prototype solutions in an on-site demonstrator at BTRL.

9.0 Acknowledgements

The author would like to thank his many colleagues who have contributed to the work presented in this paper, and the Director of Research and Technology for permission to publish the paper.

10.0 References

1. "Passive Optical Local Networks for Telephony Applications and Beyond", J.R. Stern et al, Elec Letts, Vol 23, No 24, pp 1255-1257.

2. "Southern Bell's Fiber-to-the-home projects", R. Berge n, OFC '88 New Orlea ns, Paper WK2.

3. "Wavelength-flattened 8x8 single-mode star coupler", D.B. Mortimore, Elec Letts, Vol 22, No 22, pp 1205-1206, 1986.

4. "Receiver penalty calculations in duplex optical systems", P. Rosher, Proc ICC 1987.

5. "Analysis of a tuneable single mode optical fibre coupler", M. Digonnet & H.J. Shaw, IEEE J Quantum Electronics, Vol QE-18, No 4, April 1982.

Biography

M.H. Reeve
British Telecom Research Laboratories,
Martlesham,
Ipswich,
Suffolk
IP5 7RE,
England.

M.H. Reeve is a section head at the British Telecom Research Labs (BTRL) concerned with research into optical networks. He has been with BTRL since 1973 and has worked on many aspects of optical fibre including modal properties, fibre strength, cable design and optical transmission systems. He gained a BSc in Applied Physics and Electronics from Durham University in 1973.

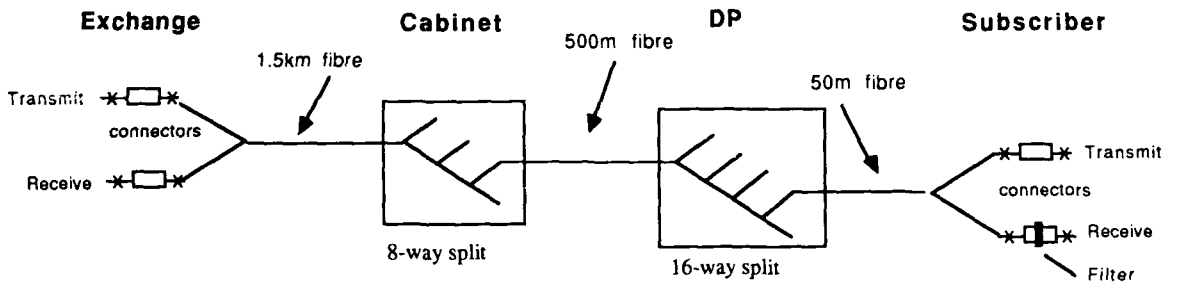

Fig 1. Basic Passive Splitter Network with Average Lengths.

Table 1. Plant per customer for the network of Fig 1.

Plant per customer =>	Fibre (m)	Splices	Connectors	Splitters
Point to Point Duplex	2050	6.00	4.00	2
TPON 128 way split	93	4.15	2.02	2
TPON 64 way split	105	4.17	2.03	2
TPON 32 way split	159	4.34	2.06	2
TPON 16 way split	206	4.44	2.13	2
TPON 8 way split	300	4.63	2.25	2

Table 2. Typical results for wavelength flattened splitters

	(MEAN AND STD. DEV)
FLATNESS (dB)	0.48±0.04
EXCESS LOSS @ 1300nm (dB)	0.05±0.01
EXCESS LOSS @ 1550nm (dB)	0.10±0.02
COUPLING RATIO @ 1300nm (%)	49.48±4.18
COUPLING RATIO @ 1550nm (%)	49.18±4.03
POLARISATION @ 1300nm (%)	0.94±0.56
POLARISATION @ 1550nm (%)	0.38±0.19

NB: POLARISATION CHANGES SHOWN ARE CHANGES IN COUPLING RATIO FOR ALL INPUT POLARISATION STATES

Fig 2. Wavelength response for a single splitter

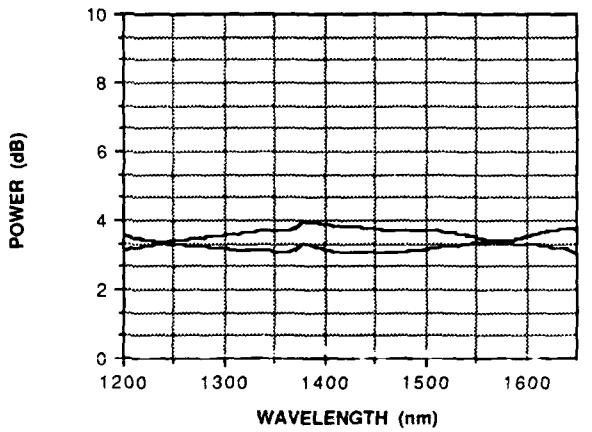

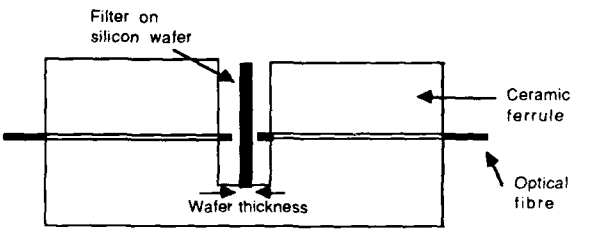

Fig 3. Prototype Optical Blocking Filter

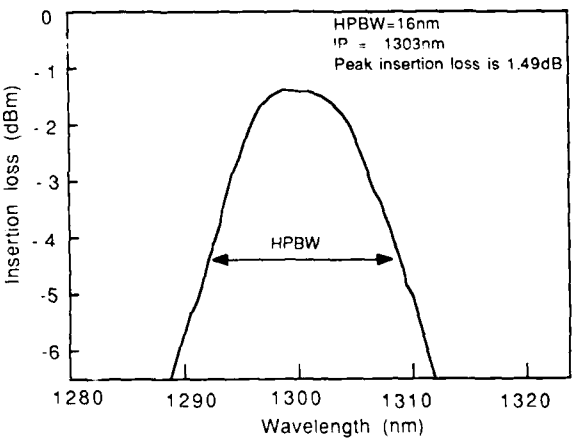

Fig 4. Wavelength Response of the Blocking Filter.

Table 3. Measured Data for Passive Network Components.

Device	Mean loss (db)	Standard deviation of loss (db)	Number used
Coupler Splitting ratio	3.18	0.29	9
Coupler excess loss	0.1	0.04	9
Connector loss	0.17	0.07	2
Splice loss	0.2	0.1	19
Fibre loss	0.4dB/km	0.05dB/km	5.6km
Filter loss	1.5	-	1
System	37.4	1.0	

Fig 5. Overall system loss distribution

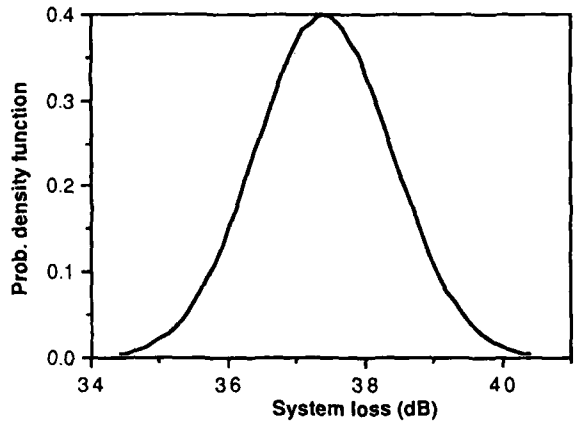

Fig 6. Overall System Loss Spectrum

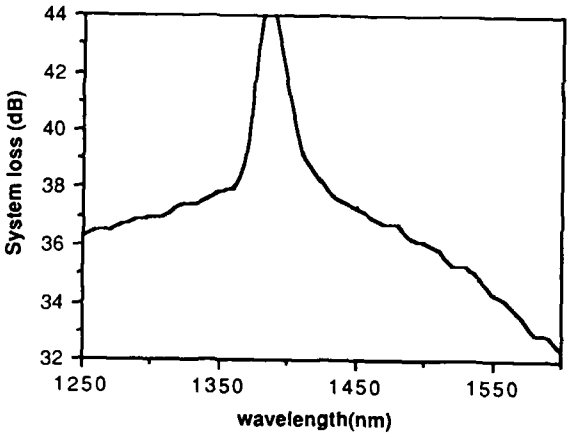

Fig 7. Schematic of the Passive Network Demonstrator

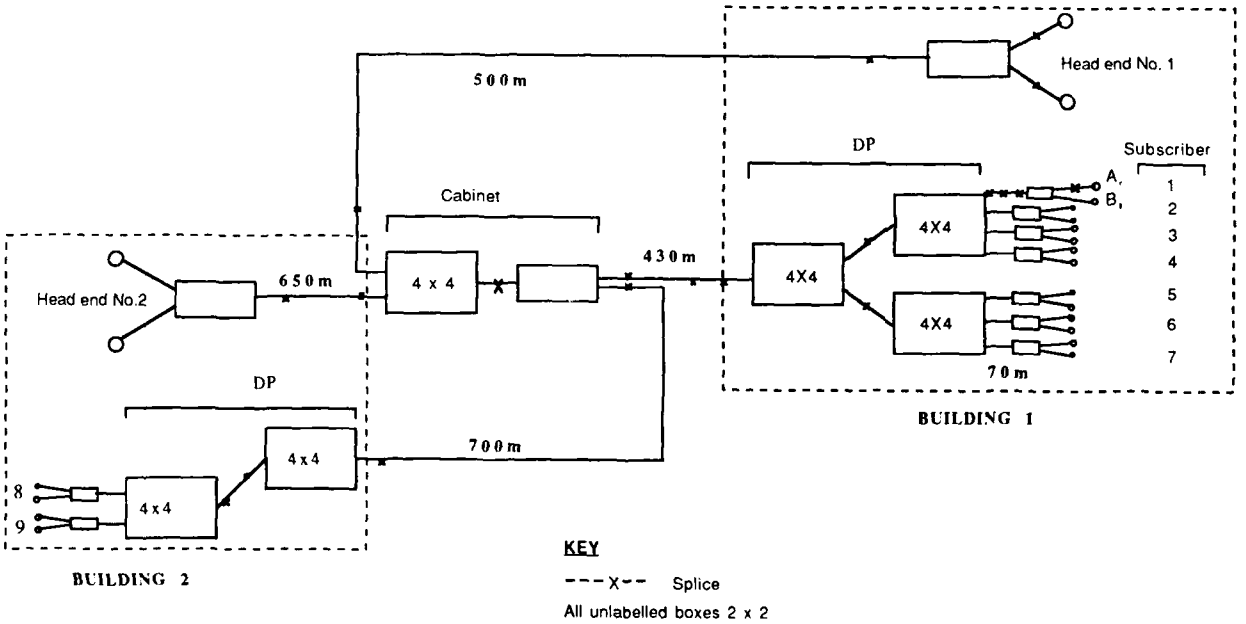

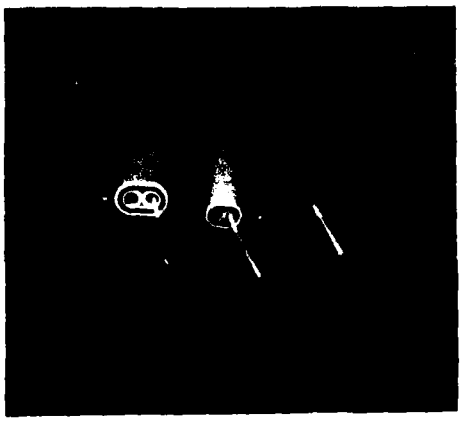

Plate 1. Prototype Subscribers Dropcables.

Plate 2. Prototype Subscribers Distribution Point.

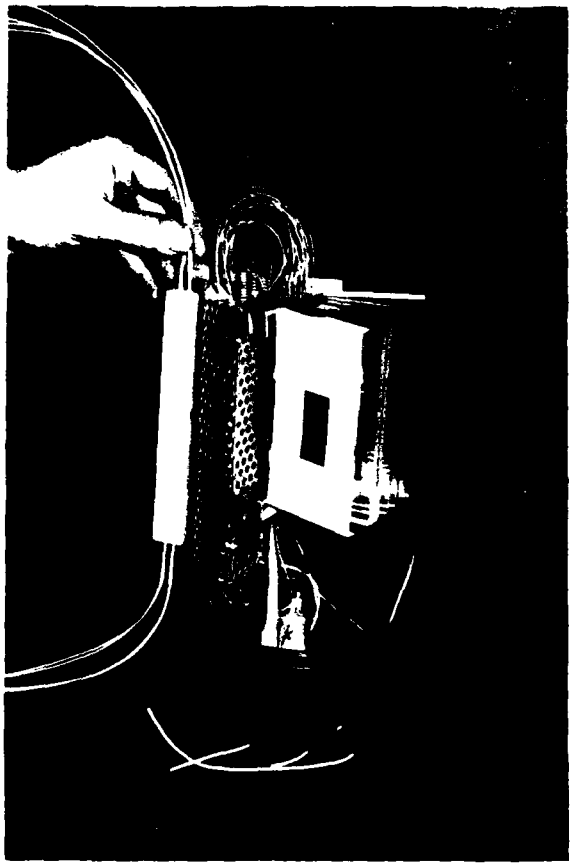

Plate 3. Clip-on Optical Power Meter.

Loop-Network Configuration For Subscriber Loops and Single-Mode Optical Fiber Ribbon Cable Technologies Suitable For Mid-Span Access

Masaaki KAWASE, Tatsuya FUCHIGAMI, Tadashi HAIBARA,
Shinji NAGASAWA and Seiji TAKASHIMA

NTT Network Systems Development Center
Tokai, Ibaraki, 319-11, Japan

ABSTRACT

This paper describes the loop-network configuration and high-fiber count, single-mode optical fiber ribbon cable technologies which enable a quick response to service demand, and offer high-reliability in the subscriber network.

A 1000-fiber cable composed of 8-fiber ribbons was developed. A mass-fusion splicing technique and a multifiber connector were developed for the fiber ribbon. Their performances were evaluated in an experimental line. It was found that these techniques were highly suitable for mid-span access which is indispensable for the fiber count nonreductional loop network.

1. Introduction

The introduction of fiber optics into telecommunications has enabled the construction of more economical, flexible telecommunications networks. Its high-speed, broadband services are superior to those of conventional metallic pair or coaxial cables. Initial efforts have invoked the introduction of optical fiber cable into trunk lines in telecommunications networks for commercial use. The current focus is the spread of optical fiber cable into nationwide subscriber networks. NTT has introduced Graded-Index optical fiber cable into subscriber networks to provide high-speed digital leased circuit services and video transmission services to meet business use demands over the past several years. In 1988, NTT started the INS service and the demand for high-digital services is rapidly growing. The optical fiber transmission system is suitable for these services because it can provide a very large capacity transmission line. Moreover, from the viewpoint of actual telecommunications plant installation and maintenance, it is essential that metallic cable be replaced by optical fiber cable because of the lack of underground conduits and premise pipe facilities especially in large cities. In order to construct optical fiber lines a wholly synthesized VAD[1] method, high count optical fiber cables[2] and a precise and efficient fiber jointing technique have been developed. These techniques allow the introduction of high performance and low cost SM (Single Mode) fiber into subscriber loops[3]. The star topology network configuration was adopted for metallic subscriber loops. In its early stages the demand for optical subscriber services varies and is very difficult to estimate. The fiber count nonreductional loop network configuration permits access at any point and to any number of fibers. Therefore, the loop configuration is suitable for optical fiber subscriber loops for business use in metropolitan areas. The above factors suggest that the single mode optical fiber and loop configuration subscriber network should be adopted as standard to achieve simple, high quality, high reliability optical subscriber loops over a wide area.

This paper describes the concept of the network configuration, and introduces single-mode optical fiber ribbon cable structure and jointing techniques suitable for mid-span access which is indispensable for the realization of the fiber count nonreductional loop network configuration.

2. Network configuration

2.1 Star and loop topology

The Features of the optical subscriber network are as follows.

(1) Demand variance ; In the early stages of the new service it is very difficult to predict the size and nature of the demand.

(2) Reliability ; The reliability of the broadband services should be higher than that of conventional telephone services. Therefore, it is desirable to have two transmission lines between the telephone office and each subscriber.

(3) Subscriber area ; Single-mode optical fiber has a very broad band and low loss performance, compared with metallic cable. As a result, the distance between the telephone office and the subscribers can be longer and the subscriber area can be wider.

The network configurations for the subscriber loops are illustrated in Fig.1 and Fig.2. For the conventional metallic pair subscriber network, NTT has adopted the fiber count successive diminution star topology as shown as Fig.1. It is an efficient network configuration for uniformly large demand such as conventional telephone services. Fiber count nonreductional loop topology is shown in Fig.2. It can be accessed by subscribers at any point by the mid-span access technique. Table 1 compares the features of the star and the loop network configurations.

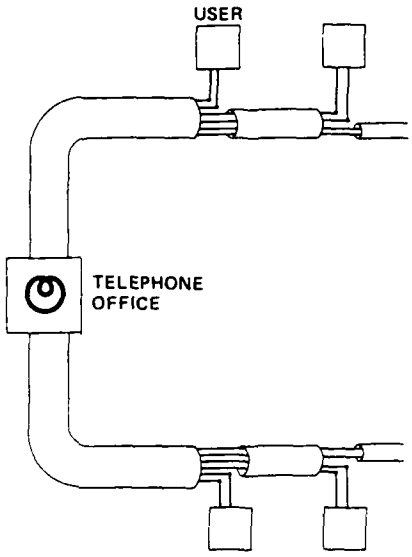

Figure 1. Star network configuration.

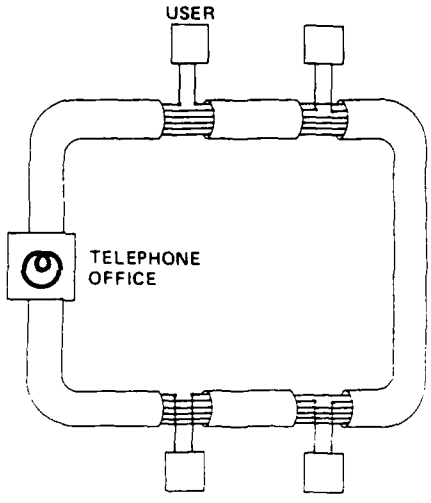

Figure 2. Loop network configuration.

Table 1 Features of the star and the loop network configuration.

Network configuration	Flexibility	Number of cable jointed point	Total route length	Multi routing
Non reductional loop	○	○	△	○
Successive diminution star	△	△	○	△

Taking the above conditions and the factors shown in Table 1 into consideration, the fiber count nonreductional loop topology is highly suitable for the optical fiber subscriber network in that it is more flexible and reliable than star topology especially in metropolitan areas.

2.2 Fiber count nonreductional loop configuration

Fiber jointing at drop points in the loop configuration was shown in Fig.1. Scheme of mid-span access is shown in Fig.3. In this cable

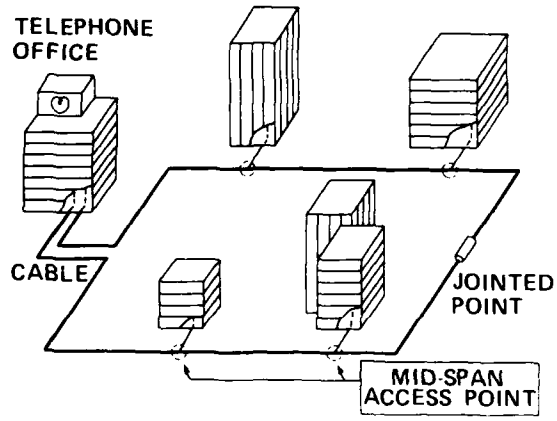

Figure 3. Scheme of mid-span access.

network configuration, any number of optical fibers can be dropped at any point along the cable by using a mid-span access technique, and the subscriber can access two directional routes in the cable loop. Accordingly, fiber usage flexibility can be improved. Furthermore, it is advantageous in that it improves network reliability since the circuits between the telephone office and subscriber are divided along two routes and a stand-by system can also be provided. A practical way to change the configuration is shown in Fig.4. The loop configuration can be realized by adding a path to the star configuration.

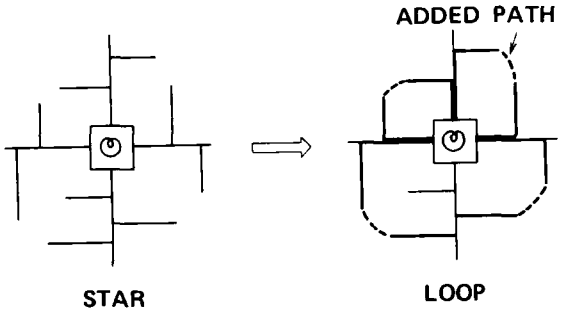

Figure 4. Practical way to change the configuration.

3. Cable, jointing and mid-span access

3.1 Requirements

Several hundred or more fiber cables are needed to construct a network in an area with several thousand subscribers. A high-fiber-count compact cable is advantageous in a metropolitan area where additional duct construction is difficult. At the mid-span access point, optical fibers must be able to be handled without causing optical power level changes in in-service optical fibers. In particular, loss changes caused by fiber bending while accommodating excess length of fiber into a closure should be suppressed. Therefore, the optical fiber parameters should be designed to decrease the excess loss due to fiber bending, and the coated fiber should be designed to make fiber handling easy. To joint high-fiber-count cables, it is necessary that the coated fiber structure is suitable for mass jointing techniques. Mass jointing techniques are required to increase the jointing work efficiency of high-fiber-count cable. At a mid-span access point, the length of fiber to be jointed with the distribution cable is not so long. Therefore, a technique for jointing short fibers is needed.

3.2 Cable

(1) Optical fiber parameters

When fibers are accessed in a closure or at any point along the cable, the optical power change caused by fiber bending must be kept to less than the allowable value. The optical loss changes while accessing the fibers in a closure were measured. From the relation between the measured values and the estimated values of optical fiber bending loss, the equivalent fiber bending radius during the handling of fibers in a closure was evaluated. As a result, it was found that the optical loss increase αr due to fiber bending should be less than 1 dB/1turn at a bending radius r of 15 mm in order not to affect the digital transmission signal at a wavelength of 1.55μm. As the 1.5 μm wavelength region will be used for WDM in the future and the performance at 1.55 μm was considered. The relation between MFD (Mode Field Diameter) and fiber bending loss is shown in Fig.5. To suppress the excess loss due to fiber bending, it is necessary to choose a small MFD and/or a high cutoff wavelength.

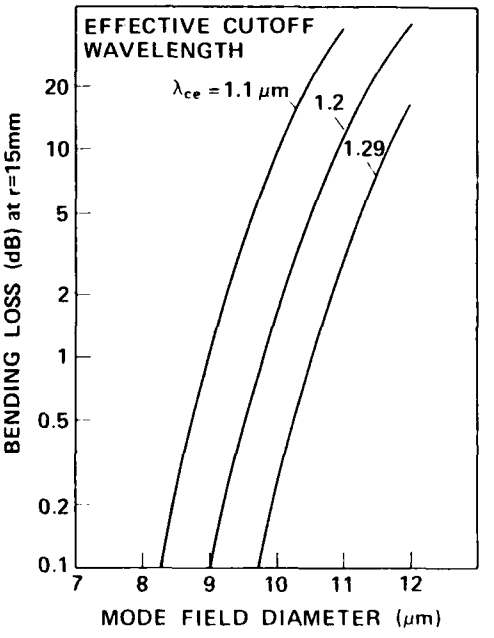

Figure 5. Calculated values of single-mode optical fiber bending loss at 1,55μm. λ_{ce} is an effective cutoff wavelength.

However, to reduce jointing loss, it is desirable to choose a large MFD. The calculated mean values of jointing loss are shown in Fig.6. For example, when level differences of transmission systems are 20 dB and the required transmission distance is 20 km, the optical loss α_L of the line is 1 dB/km. The mean optical loss of the optical fiber is 0.4 dB/km at 1.3 μm. Therefore, the total permissible jointing in a 1 km cable is less than 0.6 dB. When the transmission line has one connector and one fusion splice in each 1 km, an MFD more than 7.8 μm should be selected. As a result, fiber parameters were chosen in accordance with CCITT recommendations and are shown as the hatched area in Fig.7. The optimum range of MFD is from 8.5μm to 10.5μm. A fiber diameter tolerance of less than 2μm was chosen to minimize jointing loss.

(2) Optical fiber ribbon cable

A 4-fiber ribbon was developed for a cable of 600 fibers or less and 8-fiber ribbon was developed for a cable of 1000-fibers. The cross-sectional structures of the cables are shown in Fig.8. Optical fiber ribbon is superior in packaging density, handling ease and mass jointing. Cable diameters are 35 mm and 40mm for 600 and 1000-fiber cable, respectively. Slotted-rods are made of polyethylene, and five rectangular slots are shaped helically on the rod. The slot structure is an open structure for fiber accommodation, which allows easy access to the fibers after removing a part of the cable sheath. Fiber ribbons are accommodated tightly in each slot and stacked closely at the bottom of the slot. The tight structure makes the cable compact and also offers other important advantages[2]. Fiber strain is easily controlled during the insertion process. The stacked ribbons remain in regular order even when the cable is bent or vibrated. The tight structure does not prevent ribbon movement along the ribbon axis when the cable is bent. If the cable is bent and elongation and compression strains occur at the outer and inner parts of the cable, the ribbons move to cancel out these strains. A 4 fiber unit was selected as the most suitable for dropping to a subscriber considering the existing demand in metropolitan areas. Therefore, the 4-fiber unit is used to construct the cable. A 8-fiber ribbon is a combination of two 4-fiber ribbons and is better than a 4-fiber ribbon in terms of packaging density for high-fiber-count cables consisting of more than several hundred

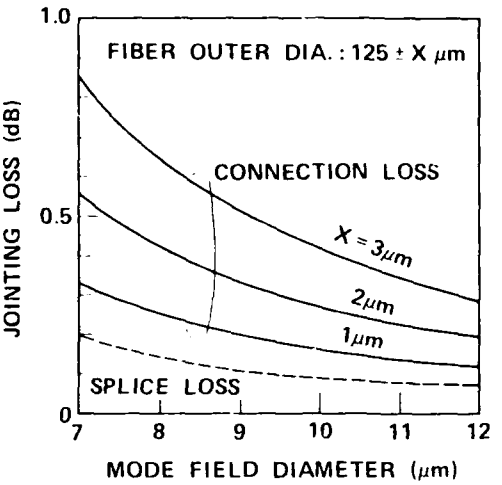

Figure 6. Calculated mean values of splice and connection loss.

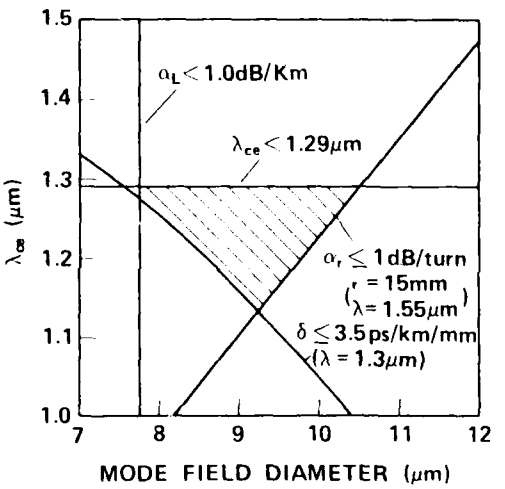

Figure 7. Design range of fiber parameters. Dispersion δ at 1.3μm was considered.

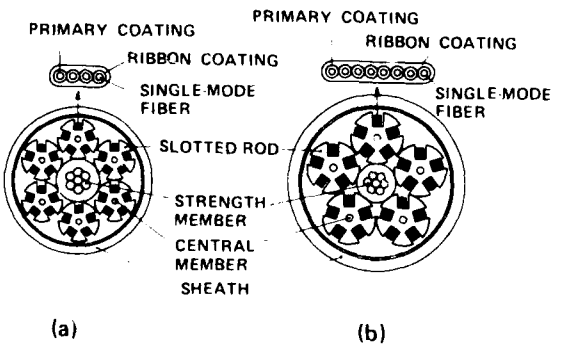

Figure 8. (a) A 600-fiber cable composed of 4-fiber ribbons, and (b) a 1000-fiber cable composed of 8-fiber ribbons.

fibers. For practical use, 4-fiber ribbon cables must be able to be jointed to, and also dropped from 8-fiber ribbon cables. Because of this, an 8-fiber ribbon which can be divided easily into two 4-fiber ribbons was investigated. An 8-fiber ribbon can be divided by the shearing force of a newly developed simple tool. All distances between adjacent fibers in a 4-fiber ribbon and an 8-fiber ribbon are the same. As a result, 4-fiber ribbons and 8-fiber ribbons can be jointed to each other by a common mass splicing machine or with common connectors and a 4-fiber ribbon can be branched from an 8-fiber ribbon cable.

3.3 Jointing techniques

In addition to the fiber cable cost, the reduction of the construction cost is an important factor in the introduction of optical fiber to subscriber loops. The establishment of multifiber splicing techniques to achieve high-splicing-efficiency are indispensable in the reduction of construction cost. Moreover, techniques for splicing very short length optical fibers are required in order to construct a subscriber loop network configuration. We have developed a mass-fusion splicing technique and a multifiber connection technique[4] by considering the following technical areas ;

a) reduction of splicing time by splicing a large number of fibers simultaneously.

b) reduction of splicing time and length by reducing the number of mis-splices.

c) miniaturization of the splice machine to reduce fiber length for jointing.

d) simplification of the connector structure for easy construction.

e) suppression of connection loss due to clearance between the ferrule hole and outer diameter of the fibers.

(1) Splicing

The problems relating to the mass-fusion splicing technique were the uniform heating of fibers to ensure the same temperature and the suppression of fiber end face variance. To achieve uniform heating, the fiber rows were offset from the electrode axis. The relation between the offset and the electrode was investigated, a uniform heating condition for a ribbon of up to 10 fibers was confirmed experimentally. On the other hand, a strongly bonded coat has been proposed to reduce fiber end face variance and a coat stripper with a heater has been developed to remove the coat easily. Maximum fiber end face variance is reduced to about 10um by using this tool and a fiber mass-cutting tool. As a result, the mass-fusion splice machine was made simpler and smaller than the conventional splice machine[4]. Figure 9 shows the mass-fusion splice machine. The size of the machine is 110x140x170 mm^3. A success rate of 80% was achieved during splicing procedures from coat stripping to fusion splicing.

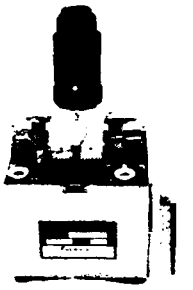

Figure 9. Mass-fusion splice machine.

Figure 10 shows the relation between the number of mass-splicing trials and the splice success rate. The cut length of fiber ribbon used in each trial is also indicated. The splice success rate exceeds 99% for three trials, where the usable fiber length is about 9cm. As the length from the inside of the closure to the splice machine is about 16cm, it is possible to splice an optical fiber ribbon of 25 cm in length.

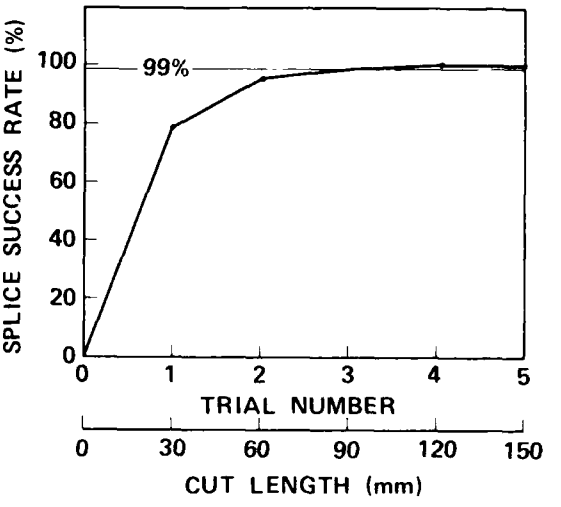

Figure 10. Relation between trial number of mass-fusion splicing and splice success rate.

(2) Connector

The structure of the multifiber connector for a 10-fiber ribbon is shown in Fig.11[4]. Ten fibers are positioned accurately between two guide-holes. The fibers to be connected can be easily aligned by two guide-holes and guide-pins. The connector component is made by a precision plastic molding technique for mass production. The connector loss is significantly affected by mis-alignment due to the clearance between the inner wall of the fiber hole and the outer diameter of the fiber. Therefore, to attain low splice loss it is important to suppress mis-alignment. By injecting adhesive into the fiber hole the fiber axis is aligned automatically. As a result, an average connector loss of 0.4 dB was attained. Moreover, this multifiber connector was easily assembled by using a heating machine to heat adhesive for fixing the fibers and a polishing machine to polish the ferrule ends. The size of the heating machine and the polishing machine are $100x100x120mm^3$ and $120x120x150mm^3$ respectively. The assembly time was about 20 minutes per ferrule.

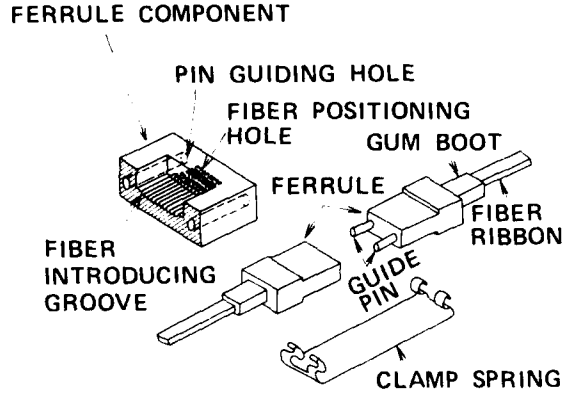

Figure 11. Multifiber connector structure for fiber ribbon.

3.4 Mid span access technique

It is necessary to establish a jointing technique for branching optical fibers from an arbitrary point on installed optical fiber cables. A fiber length of about 25cm is required in fiber splicing procedures to enable the above mentioned technique to be applied. Figure 12 shows the method for obtaining a fiber length of about 25cm for splicing. The procedure is as follows :

a) About 55cm of cable sheath is removed.

b) The slotted rods are separated by pushing the cable from either end a distance of about 5cm and the tension member is cut.

c) The branched fiber ribbons are removed from the slotted rods and the required slotted rods are cut.

d) The closure is attached to the part at which the cable sheath has been removed.

e) The fiber ribbons which are removed are cut at the center. The length of the fiber ribbons is about 25cm. Therefore, it is possible to branch the ribbon from an arbitrary point on the installed optical cable to another optical cable by applying the above splicing technique. The optical loss change at mid-span access was examined for single-mode optical fiber ribbons. While fiber ribbons were removed from or inserted into a closure, excess losses of the handled

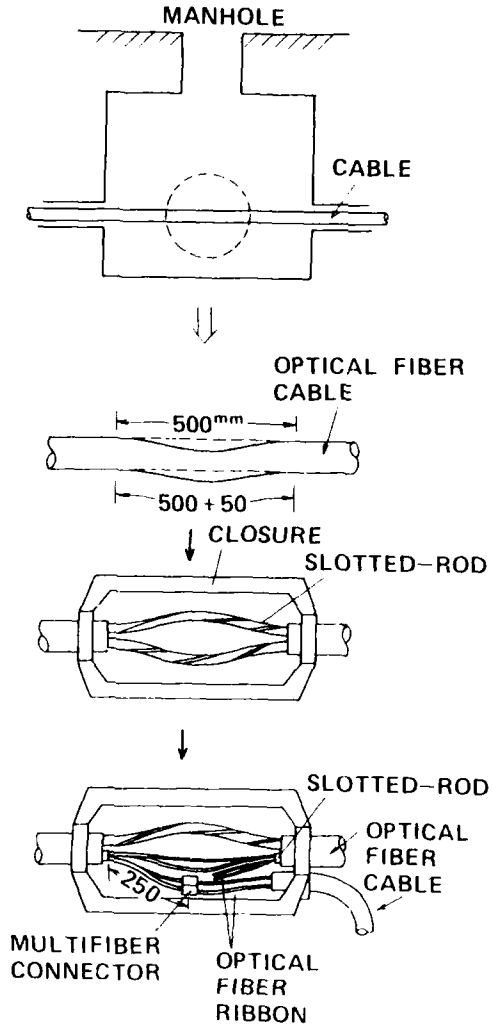

Figure 12. Procedure for attaining short length splice.

fibers were less than 2 dB at 1.55 μm. When an 8-fiber ribbon was divided by the shearing tool, the optical loss did not increase more than 1 dB at 1.55 μm. These results show that digital services at 1.3 μm are not interrupted by optical power level change while fiber ribbons are accessed at the cable jointing point and mid-span access point. These techniques were field tested and the results were found to be satisfactory. The details are described in section 4.

4. Experiments

The total performance of single-mode optical fiber ribbon techniques was examined. An experimental line was constructed in the area of Ibaraki Research and Development Center and included duct installation of the cables, splicing, and connection in manholes. Experimental routes are shown in Fig.13. The line consists of 3 underground cables and 2 short rising cables. The cables were jointed by mass-splicing and multi-fiber connectors. The route length was about 620 m. In order to confirm the practicality of single-mode optical fiber ribbon techniques for high-fiber-count cable, the experimental line was constructed by using cables consisting of 10-fiber ribbons. The underground cables have the same structure as the 1000-fiber cable shown in Fig.8. The loss change during cable installation was negligibly small at a wavelength of 1.55 μm.

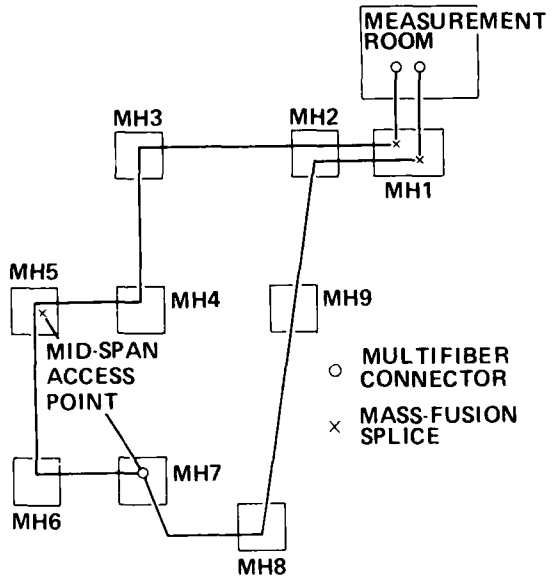

Figure 13. Experimental line consisting of single-mode optical fiber ribbon cable.

Mass-fusion splicing and a multifiber connector were evaluated in the experimental line. Figure 14 shows the splice loss distribution.

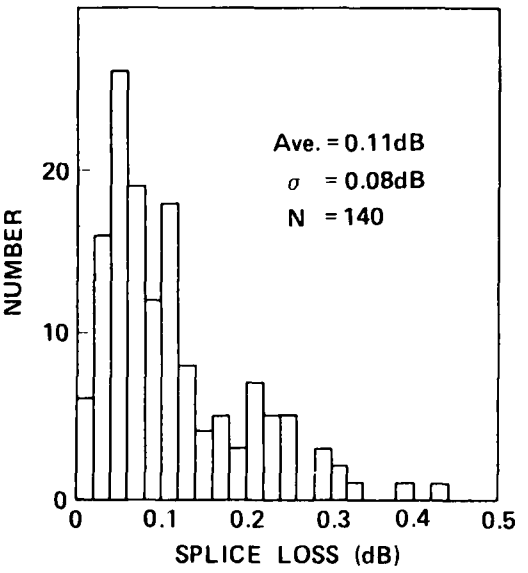

Figure 14. Splice loss distribution in field test.

The average loss was 0.11 dB. The total splicing time, required for splicing a 10-fiber ribbon in the field was 270 sec from start to finish. This means that the splicing time per fiber was only 27 sec, which is extremely short for high-density and high-fiber-count cables. Performances of the multifiber connectors constructed in the factory and in the field have also been evaluated in the experimental line. Figure 15 shows the connection loss between the field- and the factory-installed ferrules. The average connection loss was 0.42 dB. It took 20 minutes to assemble the ferrule in the field. These splicing and connection losses are found to be highly practical in the construction of subscriber lines. In the manhole (MH5), a part of the sheath was removed from the cable and several fiber ribbons were taken out by using the mid-span access technique as mentioned 3.4. During the mid-span access the optical loss changes of the accessed fibers were measured. No excess losses of more than 1 dB at 1.55 μm were observed.

As a result, it was found that these techniques were suitable for practical use.

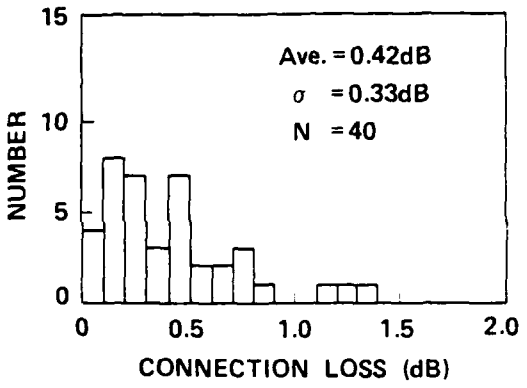

Figure 15. Connection loss distribution in field test.

5.Conclusion

The loop-network configuration which is constructed by the fiber count nonreductional distribution method was proposed. It was shown that the fiber count nonreductional loop topology is highly suitable for the optical fiber subscriber network in that it is more flexible and reliable than star topology. Single-mode optical fiber ribbon cable and jointing techniques were investigated to facilitate the construction of the loop-network. A 1000-fiber cable composed of 8-fiber ribbons was developed. A mass-fusion splicing technique and a multifiber connector were developed for the fiber ribbon. All aspects of the performance of these techniques was evaluated by constructing an experimental line. It was confirmed that these techniques were highly suitable for mid-span access which is indispensable for the fiber count nonreductional loop network.

Acknowledgment

The authors would like to thank Michito Matsumoto for helpful discussions and suggestions.

References

(1) H.Suda, S.Shibata and M.Nakahara, "High-rate fabrication of wholly synthesised fibre preforms by the multiflame VAD method using $SiHCl_3$ raw materials", Electron. Lett., 21, p.1123, 1985.

(2) S.Hatano, Y.Katsuyama, T.Kokubun and K.Hogari, "Multi-hundred-fiber cable composed of optical fiber ribbons inserted tightly into slots", 35th IWCS (Reno, USA), p.17, 1986.

(3) Y.Katsuyama, M.Miyauchi and N.Kashima, "Single-mode fiber cable and joining technologies for broadband networks", GLOBECOM'87 (Tokyo, Japan), p.1310, 1987.

(4) T.Haibara, S,Nagasawa and M.Matsumoto, "Single-mode multifiber jointing techniques for high-density high-count subscriber cables", 37th IWCS (Reno, USA), 1988.

Masaaki Kawase

NTT Network Systems
Development Center

Tokai, Ibaraki,
319-11, Japan

Masaaki Kawase received his B.E. and M.E. degrees in electrical engineering from Hokkaido University in 1970 and 1972, respectively. He joined NTT in 1972. He is engaged in development of subscriber optical transmission lines. He is Executive Engineer of the Fiber Optics Local Network Systems Project Group, NTT Network Systems Development Center, Ibaraki, Japan. Mr. Kawase is a member of the Institute of Electronics, Information and Communication Engineers of Japan.

Tatsuya Fuchigami

NTT Network Systems
Development Center

Tokai, Ibaraki,
319-11, Japan

Tatsuya Fuchigami received his B.E. and Ph.D. degrees in electronics engineering from Hokkaido University in 1975 and 1986, respectively. He joined NTT in 1975. He is engaged in development of optical fiber cables for subscriber network. He is Executive Engineer of the Fiber Optics Local Network Systems Project Group, NTT Network Systems Development Center, Ibaraki, Japan. Dr. Fuchigami is a member of the Institute of Electronics, Information and Communication Engineers of Japan.

Tadashi Haibara

NTT Network Systems
Development Center

Tokai, Ibaraki,
319-11, Japan

Tadashi Haibara received his B.E. and M.E. degrees in precision engineering from Hokkaido University in 1979 and 1981, respectively. He joined NTT in 1981. He is engaged in development of optical fiber splicing equipment. He is Senior Engineer of the Fiber Optics Local Network Systems Project Group, NTT Network Systems Development Center, Ibaraki, Japan. Mr. Haibara is a member of the Institute of Electronics, Information and Communication Engineers of Japan.

Shinji Nagasawa

NTT Network Systems
Development Center

Tokai, Ibaraki,
319-11, Japan

Shinji Nagasawa received his B.E. and M.E. degrees in electronics engineering from Chiba University in 1974 and 1976, respectively. He joined NTT in 1976. He is engaged in development of optical fiber connecting and splicing techniques. He is Senior Engineer of the Fiber Optics Local Network Systems Project Group, NTT Network Systems Development Center, Ibaraki, Japan. Mr. Nagasawa is a member of the Institute of Electronics, Information and Communication Engineers of Japan.

Seiji Takashima

NTT Network Systems
Development Center

Uchisaiwai-cho
Chiyoda-ku,
Tokyo, 100 Japan

Seiji Takashima received his B.E. and M.E. degrees in electrical engineering from Waseda University in 1967 and 1969, respectively. He also received M.S. degree in management from Massachusetts Institute of Technology in 1983. He joined NTT in 1969. He is Senior Manager in the Telecommunications Cable Systems & Outside Plant Project Group and Fiber Optics Local Network Systems Project Group in NTT Network Systems Development Center, Tokyo, Japan. He is a member of the Institute of Electronics, Information and Communication Engineers of Japan.

CITY FIBRE NETWORK ESTABLISHES LOCAL ACCESS OPTICAL PLANT

Ray Adcock

British Telecommunications, UK

SUMMARY

Early 1988 saw the opening of British Telecom's City Fibre Network as the first Flexible Access System with the latest single-mode optical fibre technology. A cable network involving several thousand business customer sites has been deployed in the City of London with equipment installed to handle initially some 10,000 analogue private circuits but which will also include digital private circuits. New external optical plant products were developed which provide for both 1300nm and 1550nm operation. 96 fibre fully-filled cables provide main spines to nodal jointing positions where Blown Fibre techniques or low fibre count cable connect customers for service. Future developments may lead to a new and refined network architecture where one single-mode fibre feeder will fan out from the exchange to several customers via passive optical splitters.

INTRODUCTION

Development of optical plant for use in the local network by British Telecom was first reported in 1986. By the end of that year, construction of the Flexible Access System (FAS) [1] optical network was well under way in the City of London where it serves the financial centre.

When this City Fibre Network was officially opened in January 1988, British Telecom said that the new FAS will provide 'future-proof' solutions for business customers with rapidly changing requirements. The immediate advantages were highlighted:

- fast supply of new circuits
- prompt circuit reconfigurations
- rapid maintenance and high reliability

Investments of over $200 million have already been made in the first operational systems. The total quantity of optical fibre installed by mid 1988 in the City Fibre Network is already substantial and now stands at around 35,000 fibre km direct to customers in the access network (local network for FAS). This compares with a total of about 350,000 fibre km installed in the core network, that is both trunk and junction. Already, one building providing a switch point node for the City Fibre Network has over 15,000 single-mode fibres terminating within it, see Fig 1.

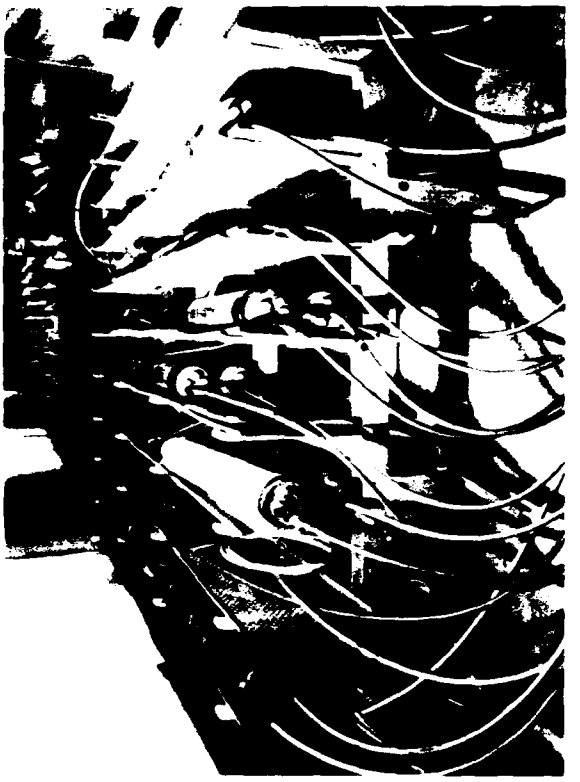

Fig 1 OPTICAL CABLES IN CABLE CHAMBER FOR SOME OF THE 15 000 FIBRES TERMINATED IN ONE SWITCH POINT NODE

There are three nodes in the City Fibre Network and this, the first FAS network is dimensioned to serve several thousand customer sites. FAS networks are currently being extended into Docklands, an adjacent area of London. This will be followed by other parts of London and other major cities. Within 6 years, it is intended to roll-out FAS to provide several million lines over optical fibre direct into all customer sites of 25 lines and over.

Initially, British Telecom has restricted optical fibre provided service to large and medium size businesses where there are significant operational benefits to be gained. In particular, the provision of an optical pipeline provides a single bearer over which all services can be provided. Fibre in the local network will enable restructuring to take place by node consolidation and hence reduce maintenance costs. British Telecom is seeking to reduce the price of optical line plant by increasing the volume required through network replacement.

An evolution plan has been devised which will lead to eventual provision of optical fibre for the single line residential customer site. For this to be economic, FAS network architecture will not be suitable and a new approach known as Telephony on Passive Optical Network (TPON) [2] is being considered by British Telecom.

The following sections deal first with some basic detail of the current FAS and future possibilities for TPON networks. The second section deals with development of optical cable and plant for the main infrastructure of the FAS Network and the third with Blown Fibre plant as a flexible system for service connection of a customer. The fourth section concludes with some developments for the future.

THE NETWORKS

Flexible Access System

FAS comprises of an intelligent multiplexer at the customer end in a Customer Service Module (CSM) which modulates the various customer inputs into a common format that is suitable for transmission over the network. The CSM includes opto-electronics, higher order multiplex and the appropriate number of primary multiplex (channel-banks). Automatic protection switching is provided at the 2Mbit/s level via duplicated fibre and transmission equipment. There are also standby batteries and line-testing aids. At the exchange end, opto-electronics and higher order multiplex demodulate the line systems back to 2Mbit/s, the various 2Mbit/s blocks are distributed to the appropriate functional networks. Higher bit rates can, of course, be provided for when required. Private analogue and digital circuits (the first to be available) are routed through automatic cross connect equipment known as a Service Access Switch (SAS) and the system is managed from a Service Access Control Centre (SACC), see Fig 2.

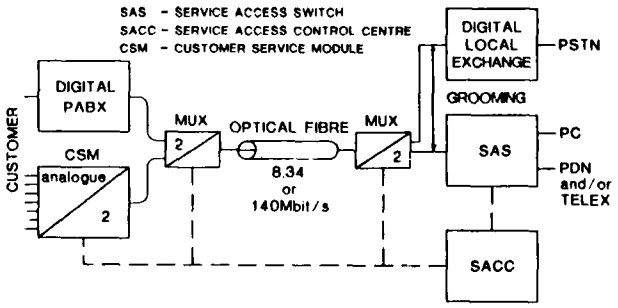

Fig.2 FLEXIBLE ACCESS SYSTEM

FAS provides a common bearer to make available a full range of services including ISDN telephony and analogue telephony. The latter requires a signalling system soon to be available which is known as Digital Access Signalling System 2 (DASS2). This is a high capability customer to network 64kbit/s common channel signalling system. Normally, both switched and private circuits will be separated at the 2Mbit/s level but there is potential for grooming where a single 2Mbit/s path is required to contain only a small number of private circuits as well as switched lines. The SACC provides for software control of the network allowing for a high degree of network management without the need for technican visits to customer sites. FAS will allow new circuits to be set up more speedily or to be reconfigured by a simple software change at the SACC, which can also monitor the status of any circuit ensuring high levels of reliability. Standby circuits switch in automatically should a fault be detected and centralised alarms will speed maintenance.

Telephony over Passive Optical Network

The future development of TPON presents one possibility to take fibre direct to residential customer sites using passive networks comprising single-mode fibres. These are fed from the exchange and fanned out via optical splitters at the joint box or cabinet and distribution point positions to feed a number of customers. For example, an arrangement giving 8 ways out at the cabinet and 16

ways at each distribution point would give capacity for 128 customers, each with a 144 kbit/s ISDN line. Downstream signals could be formed into a conventional time division multiplex at about 20Mbit/s, particular time slots being assigned to each customer. In the upstream direction converging traffic streams are passively multiplexed at DP and cabinet branching points, synchronisation being achieved by means of a timing handshake between customer and exchange.

The TPON structure may be evolved to carry broadband services such as CATV, HDTV and broadband ISDN as well as telephony services by using wavelength division multiplexing. This concept is termed Broadband Passive Optical Network (BPON). Each optical wavelength can be used to support a different service or provide a dedicated link to each customer. Possible configurations for TPON and BPON are shown in Fig 3.

A complementary paper [3] from British Telecommunications develops the detail of the architecture required for the TPON system.

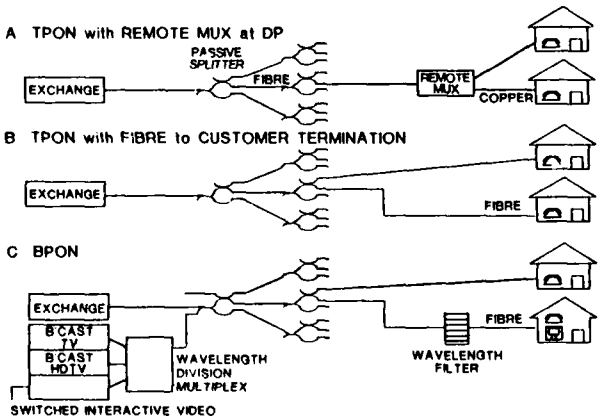

Fig 3 NETWORK CONFIGURATIONS FOR TPON (TELEPHONY ON PASSIVE OPTICAL NETWORK) AND BPON (BROADBAND PASSIVE OPTICAL NETWORK)

FAS NETWORK OUTSIDE PLANT

Cable

The design of filled single-mode optical fibre cable first described to IWCS in 1986 [4] is now well established and detail given then is not repeated in this paper. However, it is interesting to note that although British Telecom specifies optical cable in performance terms which allow a manufacturer considerable design choice, similar fibre in tube constructions have been design approved for all the suppliers. Ribbon constructions are not precluded but so far have not proved suitable for large fibre size cable. A range of fibre cable sizes based on units of 8 fibres has been chosen up to the current 96 fibre maximum. Although larger sizes have been considered, their use has so far not proved to be necessary despite the high density of fibre installed into the City Fibre Network. A factor here is the need to maximise reliability by providing diverse routing as far as is practicable, each customer is supplied by 4 fibres, a main and standby pair of go/return fibres. Consequently, it is desired that main and standby pairs are routed through separate 96 fibre cables.

The decision to specify both 1300nm and 1550nm operating wavelength has been fully justified by the achievement of 0.5dB/km maximum loss in both windows by all the cable manufacturers. A stringent program of design approval testing has been satisfied by all the suppliers.

The cable network for FAS is laid down with 96 fibre cable spines, these may be broken down through the range of 72, 48, 32, 24, 16 or 8 fibre cables as required, to a nodal joint from where a 4 fibre cable or Blown Fibre Bundle connection is made to the customer site.

Joints and Splices

It has been decided, initially at least, not to provide cabinets for flexibility but to arrange for this within the nodal joint. It is intended that flexibility is restricted to initial provision and not allowed for rearrangement purposes because of the risks that may be imposed on other working fibres. To provide the maximum number of cable entry ports to allow for all likely nodal joint configurations, including use of blown fibre microduct, an in line sheath closure design which is fully accessible has been adopted. Splice trays have been adapted to meet the needs of the FAS network, in terms of both flexibility for initial installation and access for maintenance. Self-contained trays with lids and which can be independently accessed are mounted within the sheath closure system. Each tray provides for separate routing of 24 fibres and their splices in such a manner that a tray may be entered to work on a single fibre without interference with any of the others. This may be for either maintenance purposes or connection of a new customer for service. A typical nodal joint is shown in Fig 4.

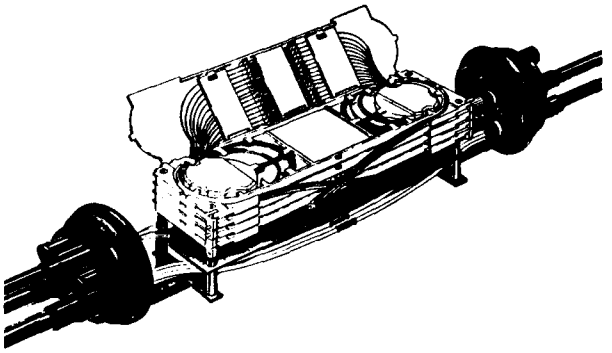

Fig.4 NODAL JOINT SHOWING ORGANISERS AND THROUGH CONNECTED BLOWN FIBRE MICRODUCT

A minimum bend radius of 40mm is applied to each fibre within the splice tray. This figure has been arrived at from considerations for both assessment of fibre lifetime limited by the probability of mechanical failure of the fibre and the need to maintain availability of the 1550nm window.

British Telecom continues to require fusion splicing to be used within outside network line plant and the current limit of 0.5dB per splice is met with ease. Although a tighter limit could be set which would be readily achievable, optical power budgets do not require this for the short route lengths employed on FAS and unnecessary remakes of splices are avoided. Because it was recognised that some situations arise where fusion splicing may not be practicable, a detailed program of evaluation of mechanical splices has been undertaken. However, all those which were short listed as likely to be suitable have shown some evidence of environmental temperature instability which has caused concern with regard to potential for long term use.

Return loss is of critical importance, in particular with regard to future exploitation of fibres for bi-directional working or wavelength division multiplex. Evidence has also been noted of variability of return loss of a particular mechanical splice in an experimental route due to Fabry-Perot effects. Consequently, use of mechanical splices is currently restricted to short term maintenance use only.

Flexibility and Termination in Exchange

The system reported on previously [4] has proven to be highly successful for the high density of single-mode fibres which have to be terminated in an exchange building. In this rack-mounted system shown in Fig 5, up to 24 splices are housed in jointing trays, each tray also containing sufficient spare fibre to enable re-connections to be made in future. With over 15,000 single-mode fibres already having been terminated in one building for the City Fibre Network, the economic need to restrict use of optical connectors to only the final connection into the terminating equipment is very obvious.

Fig.5 EXCHANGE TERMINATION SPLICE ORGANISER TRAYS

Consequently, connectorised patch panels have not been utilised and flexibility has been provided for by routing internal fibre through equipment racks of splice trays as follows. The external 96 fibre cables are jointed in the cable chamber to 24 fibre tight jacketed internal cable which is routed to the first rack of splice trays. A splice is made here to a single fibre ruggedised internal cable which is routed to a second rack of splice trays. This is, in turn, spliced to another 24 fibre cable routed to the final rack of splice trays serving the terminal equipment, here a single fibre ruggedised and pre-connectorised tail cable is spliced on ready for the final connection. Flexibility is obtained by re-routing and re-splicing the single fibre cables as required.

Although this system is operating very satisfactorily, it is desired to progress to a flexibility system that will allow a choice to be made between use of either connector or fusion splice to provide for flexibility. Such a design is now awaiting trial installation and is shown in Fig 6a and 6b. Each splice tray allows for independent access of any one fibre.

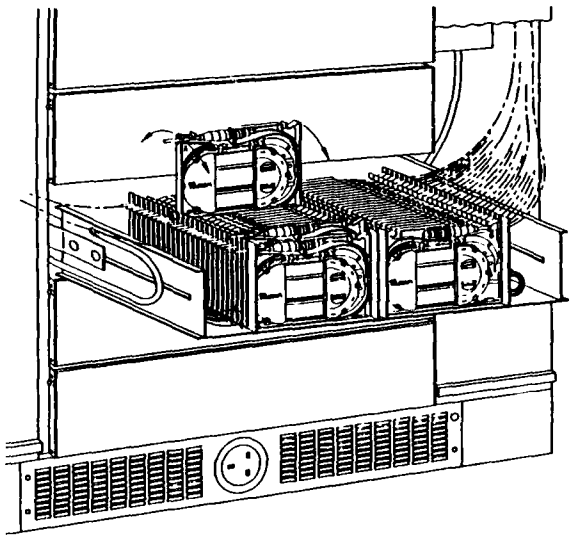

Fig 6a SPLICE ORGANISER SHELF, RACK MOUNTED

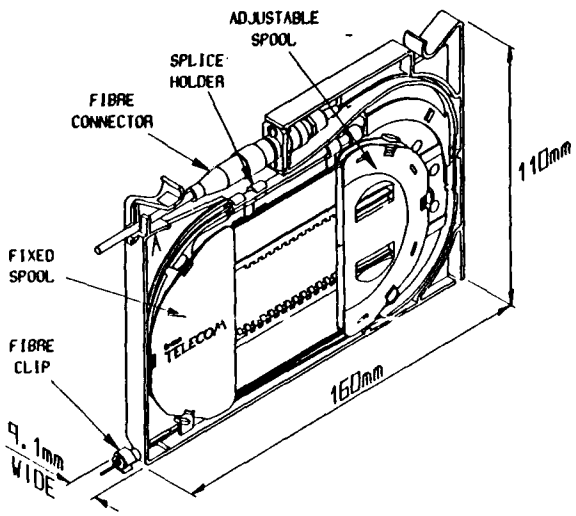

Fig 6b INDIVIDUAL SPLICE ORGANISER (FROM FIG 6a)

The mountings shown on the splice tray for a connector may be changed to ones which hold a splice protector and thus achieve the choice desired.

The NTT design of FC/PC connector has been chosen as the standard for use on single-mode fibre by British Telecom. Field termination is not yet deemed to be sufficiently practicable and reliable so pre-connectorised single fibre ruggedised cable tails are supplied for splicing on in the field. A 2.4mm diameter cable design was originally chosen but this has now been changed to the 2.5mm IEC standard.

Blown Fibre

This was reported on in 1986 and is now in full operational use by British Telecom. The first successful trial in Leeds, UK was completed mid 1985. Many of the final connections from the nodal joint in the City Fibre Network have been made using Blown Fibre. The attributes of the Blown Fibre system were dealt with in the earlier paper [4] and elsewhere [5] so the principle of operation is only briefly considered here. A fibre unit, currently 4 individually coloured and buffered fibres are held in a symmetrical unit, together with a ripcord to aid stripping, with a coating of foamed polyethylene.

Microduct is installed prior to provision of fibre, this is a small diameter tube, currently 6mm bore, extruded to provide a low friction static-free bore. Several of the microducts are bundled together (current sizes 2, 4, 7) and given an overall sheath of polyethylene or PVC. When required, the fibre unit is blown into the microduct using a blowing head shown schematically in Fig 7.

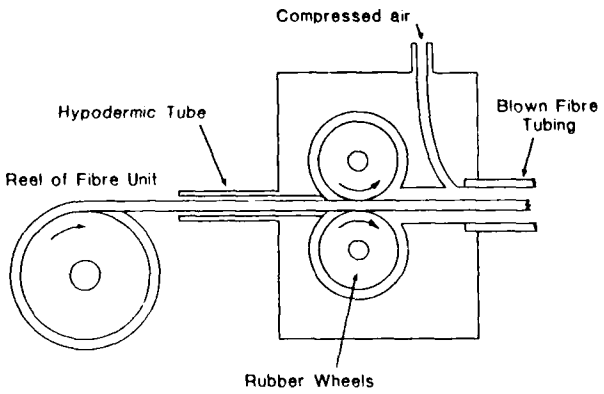

Fig 7 BLOWING HEAD FOR BLOWN FIBRE UNIT

Rubber driving wheels feed in the fibre unit which is then carried through the microduct tube by the viscous flow of air which distributes the applied forces along the whole length of the fibre unit.

The particular advantages of Blown Fibre are that it confers the ability to defer fibre provision allowing inexpensive microduct tubing to be installed at an early stage, possibly on a speculative basis. Also, the installation technique virtually eliminates any additional strain from being applied to the fibre unit and hence it is not necessary to include a strength member for strain relief. Blown fibre is of particular benefit within buildings enabling fibre to be re-routed by appropriate interconnection of microducts.

For initial installation into the City Fibre Network, a maximum planning limit of 600m for a single length blow has been adopted. However, range extending techniques have been developed which are in process of being introduced into field practice. [6] The planner and field installer will have available a choice of method most suited to a particular situation. Three are currently being made available:

- Mid Point Blowing. The fibre unit is supplied on reversible toroidal storage pans which give access to both ends, see Fig 8a. The fibre unit is first installed in one direction and then, after inverting the pan, in the other direction. Each loop within the pan is stored under torsion in such a manner that when dispensed the torsion is unwound.

- Tandem Blowing. By automating the blowing heads with fibre unit "buckle-detectors" on either side, a number of blowing positions can be set up in tandem for simultaneous blowing in of a theoretically unlimited length of fibre unit.

- End Loop Feeding (ELF). This uses an ELF machine, shown in Fig 8b, which receives fibre unit at the end of an up to 600m blow and re-stores it in a toroidal storage pan. The pan is then inverted as in the first method and the fibre unit can then be blown on for a further 600m.

Fig 8a TOROIDAL STORAGE PAN FOR BLOWN FIBRE UNIT

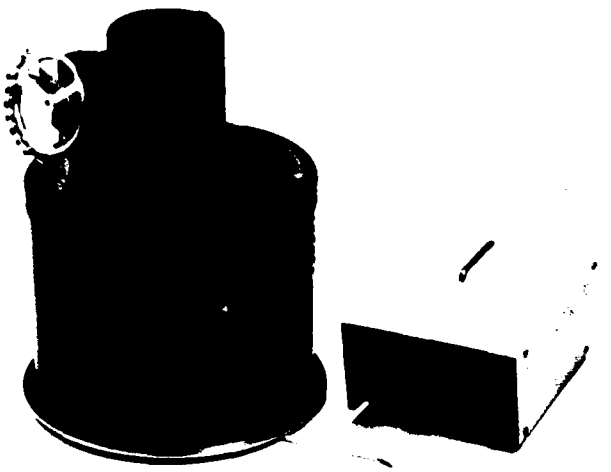

Fig 8b END LOOP FEEDER (ELF) MACHINE FOR BLOWN FIBRE UNIT

British Telecom sees great potential for Blown Fibre techniques as installation of optical fibre in the access network expands. Not only does the planner have an alternative to cable but also presented is the exciting prospect of spliceless networks for the future.

FUTURE DEVELOPMENTS

The establishment of FAS as a large scale access network with direct termination of optical fibre in customers premises has, initially, required an over generous deployment of fibre. Four individually dedicated fibres serve the customer all the way to the exchange while the future prospect of TPON requires only a single fibre which for most of the route from the exchange will be shared between many customers.

Intermediate between these extremes will be the introduction of couplers/splitters within the network to provide for both bi-directional working and wavelength division multiplex. Establishing a high integrity fibre network with commitment to fusion splicing to avoid restrictions due to return loss has been seen by British Telecom as an essential step in preparing for use of couplers/splitters, now successfully providing bi-directional working on core network routes.

British Telecom is actively pursuing non-instrusive fibre testing technology. In a novel instrument a controlled localised bend taps and a secondary waveguide efficiently collects a portion of the signal in a fibre. This "Clip-on" instrument generates little loss to the system, and therefore will not cause a disruption in the transmission to occur. "Clip on" technology will have several applications. Fig 9 shows a prototype "Clip-on" live fibre identifier/power meter. Fibres can also be actively identified [7], using a "Clip-on" instrument, by extracting and decoding unique identification codes incorporated into maintenance channels of a transmission system. An example of such a system is shown in Fig 10. "Clip-on" instruments will therefore be very useful in installing and maintaining a fibre-based local access network.

Fig 9 'CLIP-ON' LIVE FIBRE IDENTIFIER/POWER METER

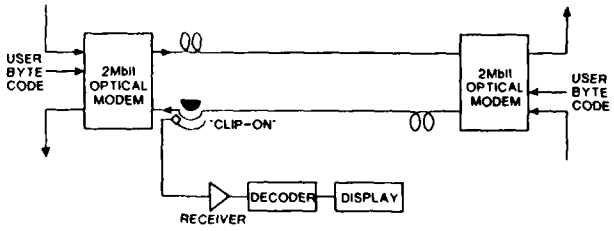

Fig 10 APPLICATION OF 'CLIP-ON' AS AN IDENTIFICATION DECODER

The large scale use of fibre in the exchange is making new demands on optical testing. In particular, where splices may be in close proximity, there is a need for OTDR's of much increased resolution of around 0.5m and decreased dead zone. The bulk of test results to be taken on commissioning also demands data bank storage and retrieval systems for maintenance purpose. These areas are all being pursued by British Telecom.

CONCLUSIONS

This paper has detailed the design and construction of a large single-mode optical fibre public network providing direct access for the customer, now fully operational and in service. Local access network requirements are driving forward development and economics of optical line plant, new horizons will enable telephone networks to evolve from the long serving copper pair local loop to fibre capable of providing a full range of services to every customer.

ACKNOWLEDGEMENTS

The author wishes to thank the many colleagues who have contributed towards the achievements reported in this paper and to the General Manager Network System Engineering (Transmission) for permission to publish.

REFERENCES

1 I Dufour, "Flexible Access Systems", Proceedings of International Symposium of Subscriber Loops and Services 1988.

2 K A Oakley, C G Taylor and J R Stern, "Passive Fibre Local Loop for Telephony with Broadband Upgrade", Proceedings of International Symposium of Subscriber Loops and Services 1988.

3 M H Reeve, "Line Plant Considerations for Passive Optical Networks for the Local Loop", IWCS this conference.

4 P Bridle, "Advances in Cables and Outside Plant for Cable Television and Optical Fibre Local Network", IWCS 1986.

5 M Howard, "Blown Fibre Experience in the Local Loop", Proceedings of International Symposium of Subscriber Loops and Services 1988.

6 R A Freeman, P D Jenkins, D J Stockton and B Wiltshire, "Advances in Blown Fibre Installation Methods", British Telecom Tehnol. J Vol 5 No 3 July 1987.

7 S James, "Non-instrusive optical fibre identification using a high efficiency macrobending "Clip-on" optical component". To be published, Electron. Lett. September 1988.

R C Adcock
British Telecom plc
UK Communications
Access Network Evolution Division
125 Shaftesbury Avenue
LONDON
WC2H 8BE
UK

Ray Adcock is Head of the Optical Fibre Engineering Group within UK Communications of British Telecom. He is responsible for the specification and approval of optical fibre cables together with their associated jointing techniques and practices. He joined the company (as the British Post Office) in 1963 and after a period in HQ dealing with requirements for early data transmission systems, he became a cable specialist in the External Plant Division. Early in 1983 he took charge of the Electrical Protection Group which involved considerable international committee work. From there, he joined the Access Network Evolution Division to co-ordinate optical plant requirements for the City Fibre Network before taking on his present role early in 1988.

INSTALLATION AND TESTING OF MULTISERVICE FIBER LINKS IN THE SUBSCRIBER LOOP: A CASE STUDY

F. A. Huszarik, R. Mariani, R. Yakimovich, J. Justice (NT)

Bell-Northern Research, P.O. Box 3511, Stn. C, Ottawa, Ontario, Canada K1Y 4H7
Northern Telecom Inc., 1 Ravinia Drive, NT Centre, Atlanta, Georgia, U.S.A. 30346

Abstract

The recent flurry of activity in deployment of fiber cables in the subscriber loop has produced considerable speculation as to the need for new for designs and test methods for optical cable and hardware. This paper reviews some of the early results from one such installation at Heathrow, near Orlando, Florida.

The design of residential fiber links in terms of link attenuation (loss) and optical reflections is analyzed. Also, we describe the design and operation of a loss and reflection test set custom-built for the Heathrow project. Finally, recognizing that the experience gained from these early fiber-to-the-home projects will provide valuable input to optical hardware suppliers, some of the current shortcomings are discussed.

Introduction

The shorter loop lengths associated with fiber-to-the-home systems have been considered to be an advantage in terms of fiber, splice, and connector losses. Consequently, it was generally assumed that subscriber loop installations could tolerate higher losses and, therefore, less expensive fiber, splices and connectors. In fact, practice has shown these assumptions to be incorrect. The profusion of splices and connectors in a 4 km subscriber link quickly depletes the available system margins, especially when passive optical devices such as power splitters or wave division multiplexers are used.

Most cost-effective fiber-to-the-home architectures planned for the future will probably rely on the multiplexing of either services and/or subscribers on a single fiber. To achieve this, optical splitters and/or wave division multiplexers (WDMs) will impose not only significant attenuations, as discussed above, but also new requirements for link testing and trouble-shooting. For example, bidirectional and to a lesser extent, multiwavelength transmission systems rely on low optical reflections for high performance operation. This requirement introduces a new parameter which needs to be qualified during link acceptance testing. Fortunately, the Heathrow experience has provided the impetus to design a field usable reflection test set. Also applied research into the measurement and analysis of reflections from concatenated fiber links is in progress.

Bidirectional transmission architectures also introduce a number of practical problems for outside plant and maintenance engineers. One of these problems, is the drop in productivity resulting from the need for fiber link acceptance testing in both upstream and downstream directions. The fiber-to-the-home project currently underway in Heathrow, Florida encompasses these issues, and others such as environmental performance of optical components, maintenance testing, and fault location, to name a few.

The Heathrow fiber link design uses optical splitters for bidirectional transmission at long wavelengths (1300 nm) as well as WDMs for bidirectional transmission at short wavelengths (780 nm and 890 nm). Furthermore, both long and short wavelengths go through a second stage of multiplexing onto a single fiber between the central office and the subscriber's residence.

The design, engineering, construction, and testing of these complex fiber links provide invaluable experience and data for next generation fiber-to-the-home architectures.

Fiber Link Test Set (FLINT)

The unique system design for Heathrow, using both short and long wavelength bidirectional transmission systems on single-mode fiber, required a test set capable of measuring both loss and reflections. Since no test equipment was commercially available Bell-Northern Research (BNR) engineers designed a custom Fiber Link Test set (FLINT) which enabled field personnel to fully characterize the fiber optic links.

The general features of the FLINT set may be summarized as follows:

- portable and rugged (hand carried in the field)
- multiple wavelength operation (820 nm, 1300 nm, 1550 nm)

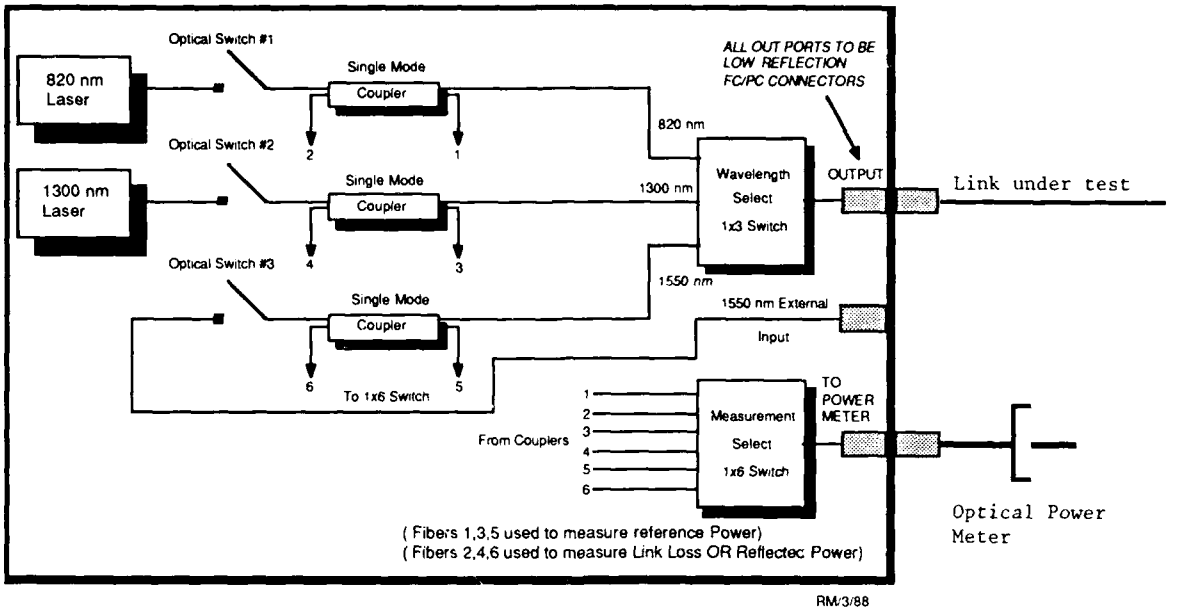

Figure 2: Fiber Link Test Set (FLINT) Optical Schematic

- multiple features
  - output power measurement
  - received power measurement
  - reflected power measurement
- optical stability
- simple operation

Normal fiber link acceptance testing consists of characterizing the installed fiber cable for optical loss to determine if design-loss budgets have been met. However, since Heathrow employs bidirectional transmission systems using a single fiber, another critical performance parameter optical reflection requires characterization.

In simple terms, reflections within a fiber link will cause electrical cross-talk in systems which employ optical power splitters for bidirectional transmission (Figure 1). In digital transmission systems, a signal to interference ratio (S/I) of less than 10 dB can result in significant transmission degradation.

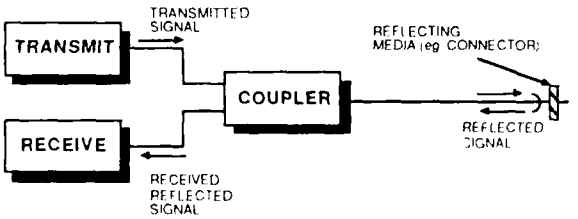

Figure 1: Optical Reflections

By selection of low reflection components within the test set, i.e. Anti-Reflection coated switches and low reflection, polished connectors, the total internal reflections within the test set are approximately -38 dB. This is sufficient for accurate fiber link characterization.

The schematic diagram in Figure 2 shows the functional arrangement of optical components which allow for simultaneous loss and reflection measurements when two test sets are used.

Fiber Link Design

Clear understanding of the loss and reflection performance of the link components is required for the successful operation of bidirectional and multi-wavelength transmission systems. Figure 3 describes the loss and reflection assumptions made during the design phase of the Heathrow links. These assumptions were based on a combination of factors:

- Advertised performance specifications from component suppliers (e.g., splices, connectors).
- Laboratory qualification tests; and
- Safety factors to account for influence of field environment and installation variability.

The rationale for this approach was to establish a compromise between losses required for practical outside plant construction and the system gain achievable with reasonably cost-effective optical transmitters and receivers.

	WORST CASE COMPONENT LOSS (dB)		
	1300nm	780nm	890nm
CABLED FIBER	0.5/km	3.2/km	2.7/km
CONNECTORS	0.7	1.0	1.0
SPLICES	0.2	0.2	0.2

Figure 3: Loss Design Criteria

Results of lab tests showed that although single-mode fiber is normally not tested at short wavelengths, its loss performance at 780 nm and 890 nm is well within the worst-case design criteria as shown in Figure 3, above. Various types of single-mode connectors were characterized for both loss and reflection performance. As expected, connector losses were approximately 0.3 dB higher at short wavelengths than at 1300 nm. Reflections of less than -40 dB were achievable with state-of-the-art PC polished connectors only. In general, single-mode connector performance has improved considerably over the last two years, however, the ability to mate connectors from different manufacturers and production in large quantities are two issues which need serious attention before large deployment of connectors in the subscriber loop is practical.

Unlike connectors, splices were expected to perform consistently at 0.2 dB loss, or better, over the entire range of wavelengths. Lab testing confirmed this to be true for both fusion and mechanical splices using index-matching fluid.

The Heathrow experience has shown that fusion splices consistently achieve reflection performances better than -40 dB. In fact, reflections from fusion splices are typically better than -50 dB and often too low to measure. Although more sensitive to installation methods and less repeatable, field test results from mechanical splices showed that -40 dB reflections are achievable only if they are properly polished and index-matched.

Using these component loss and reflection criteria, sectional and total link loss budgets can be calculated for acceptance testing. As an example, the calculated worst case loss for the feeder portion of the Heathrow fiber link which operates at 1300, 780 and 890 nm wavelengths is shown in Figure 4.

Field Test Results

A schematic description of the 'feeder' fibers at Heathrow is shown in Figure 5, below. Attenuation and reflection test results from 72 'feeder' fibers are analyzed below. Since the FLINT set was used to obtain these measurements, short wavelength data are shown for the 820 nm wavelength only. Consequently, component and total link loss must be interpolated from the 780 nm and 890 nm data shown in Figures 3 and 4.

LOSS DESIGN CRITERIA

	# IN LINK	LINK LOSS (dB)		
		1300nm	780nm	890nm
FIBER	1.8 km	0.9	5.8	4.9
CONNECTORS	2	1.4	2.0	2.0
SPLICES	2	0.4	0.4	0.4
ALLOWABLE TOTAL LOSS		2.7	8.2	7.3

Figure 4: Heathrow Feeder Link Budget

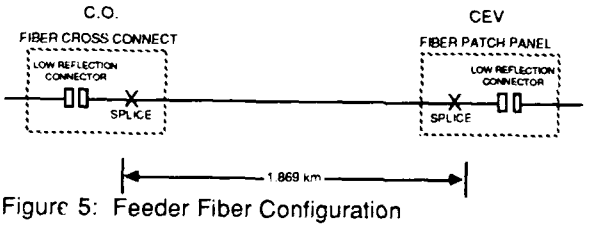

Figure 5: Feeder Fiber Configuration

Attenuation: A summary of the measured attenuation results for both 1300 nm and 820 nm (Figure 6) illustrates that the worst case design assumptions discussed above give a reasonable estimate of the losses achievable in the field. At 1300 nm the worst case design estimate was 2.7 dB. Statistical analysis of the measured results gives a mean of 1.4 dB. The spread between the minimum and maximum was 2.3 dB which reflects inconsistencies in materials and sensitivity to installation methods.

	LINK DESIGN ASSUMPTION (dB)	MEASURED	
		MEAN (dB)	MIN. - MAX. SPREAD (dB)
1300 nm	2.7	1.4	2.3
820 nm	7.5	5.0	3.4

Figure 6: Attenuation Results Summary

Similarly, at the 820 nm wavelength the worst case design assumption was 7.5 dB. By comparison, field test results give a mean of 5.0. The spread between minimum and maximum was 3.4 dB. The higher spread of the 820 nm data compared to the 1300 nm data can be attributed to the higher variability in the optical performance of long-wavelength components and fiber at the shorter wavelength. Although this variability was a major concern during the system design phase, these preliminary results give us a high degree of confidence that existing outside plant construction practices and long wavelength

components can be applied for short wavelength transmission.

The data shown in Figure 5 represents loss in only one direction. Since the link must support transmission in both directions an important analysis to consider is the impact of the bidirectionality on test methods. Attenuation measurements were performed in both the upstream and downstream direction on a number of Heathrow fiber links. As expected, the results show that loss can vary significantly depending on which direction is measured. Although the results at 1300 nm are more encouraging than those at 820 nm in terms of establishing a trend, we feel that there are insufficient data at this point to draw strong conclusions as to whether acceptance testing for bidirectional systems can be performed in one direction only. Further analysis of this issue is ongoing.

Reflections: A summary of the field-measured reflection results from the same 72 fibers is shown in Figure 7 for the downstream and upstream directions. The reflection specification for this fiber link configuration was -32 dB. Although the mean in each direction is quite good, i.e. -33.2 dB downstream and -34.2 dB upstream, the variation in results measured in the two different directions would seem to indicate that the primary, or larger, reflections exist at the near-end of the downstream measurement, or conversely at the far-end of the upstream measurement. This conclusion is drawn from the fact that reflections close to the source will attenuate less, whereas far-end reflections will be significantly attenuated before they reach the receiver. Since reflection measurements are a relatively new requirement for outside plant fiber links, there are limited data available from which to predict field performance. Total reflections are, of course, very much a function of individual component performance. Therefore, the ability of connectors and splices to achieve the discrete component spec of -40 dB is key to maintaining total link reflections at an acceptable level. Unlike link loss, where one bad splice can be compensated for by one better than average splice, several low reflecting splices will not compensate for one highly reflective splice. It is, therefore, critical to ensure all components in the link achieve high quality reflection characteristics, not only for bidirectional links but also for high speed (gigabit) links where laser performance can be degraded by high reflections. Again, further study of the reflection characteristics of installed links is ongoing and will be reported in subsequent papers.

Conclusions

The analysis of 72 field constructed fiber links shows that the design objectives for bidirectional loss and reflections are realistically achievable. State-of-the-art splicing and connector technology must be used combined with rigorous attention to quality of installation.

	LINK DESIGN ASSUMPTION (dB)	MEAN (dB)
UPSTREAM	-32	-33.2
DOWNSTREAM	-32	-34.2

Figure 7: 1300 nm Reflection Summary

Based on these early experiences in the construction and testing of bidirectional fiber-to-the-home links, a number of conclusions and recommendations for material improvements emerge:

1. Since short wavelength transmitters and receivers can offer significant price advantages in the near term, the performance of link components such as fiber, splices and connectors should be specified by manufacturers at these short wavelengths.

2. Future bidirectional and high speed fiber links will require low reflection characteristics to avoid optical cross-talk and laser performance degradations. Since connectors and splices are the primary sources of reflections, suppliers of these components must specify their reflection performance. Current experience indicates that a maximum reflection of -40 dB for individual components, either factory-installed or field installed, will provide adequate performance for most bidirectional fiber links.

3. Due to the lack of standards for low loss and low reflection connectors, the ability to mate connectors from different manufacturers is a major problem for system suppliers and the network operators. It is also clear that the volume supply of connectors for large scale fiber-to-the-home projects does not yet exist.

4. The development of cost-effective test sets capable of measuring individual component and fiber link reflections is required.

5. Research into the loss and reflection performance of bidirectional links at both long and short wavelengths is essential to establish practical and reasonably productive field test methods and equipment.

6. Results from the initial field tests showed that several Heathrow fiber links failed to meet the maximum specifications for loss and/or reflection. Although the faulty components in these links were subsequently replaced, this reinforces the need for high quality components and construction methods in order to meet subscriber loop link margins while maintaining a reasonable level of productivity.

Fred Huszarik
Bell-Northern Research
P.O. Box 3511, Stn. C
Ottawa, Ontario
Canada K1Y 4H7

Fred Huszarik received his Bachelors and Masters degress in Engineering from Queen's University at Kingston, Canada in 1972 and 1973 respectively. Since joining Bell-Northern Research in 1973, Fred has been responsible for research in both fiber and copper outside plant construction methods, tools and materials. Fred has been manager of BNR's Fiber Link Systems Design group since 1984 and currently holds Chief Designer responsibilities for Residential and Access Fiber Links, including Heathrow

R. Mariani, P.Eng.
Bell-Northern Research
P.O. Box 3511, Stn. C
Ottawa, Ontario
Canada K1Y 4H7

Renato Mariani received his Bachelor of Engineering degree in 1979 from Carleton University in Ottawa. Since joining Bell-Northern Reserach Ottawa R&D labs in 1981 as a member of scientific staff he has been involved in various research activities relating to outside plant technology in the field of cable splicing, installation products and methods, structures research and cable testing.

In 1984 he became actively involved in fiber installation and applications research for BNR's Fiber Link Systems Design group. Renato is presently manager of the Fiber Link Engineering group responsible for research on the deployment of advanced fiber systems to the residential subscriber.

Mr. Mariani holds several patents related to cable splicing and fiber testing technology.

Robert A. Yakimovich
Bell-Northern Research
P.O. Box 3511, Stn. C
Ottawa, Ontario
Canada K1Y 4H7

Robert A. Yakimovich received his Bachelor of Science degree in Electrical Engineering from the University of Alberta in Edmonton, Alberta in 1972. He has held various engineering positions in toll equipment, outside plant planning and rural multiplex development and implementation with British Columbia Telephone prior to joining Bell-Northern Research in 1981. There, he has been involved with the systems design of high bit-rate fiber systems and analytical work with fiber link technologies. He is presently member of scientific staff responsible for fiber testing issues in the deployment of advanced fiber systems to the residential subscriber.

Jim Justice
Northern Telecom Inc.
1 Ravinia Drive
NT Centre
Atlanta, Georgia 30346
U.S.A.

Jim Justice P.E. holds an Engineering Degree from Carleton University in Ottawa, Canada. He is currently the Marketing Manager for Northern Telecom's first fiber-to-the-home project at Heathrow, Florida. Over the past ten years he has been involved in the evolution of fiber optics hardware, software, and equipment in the telecommunications industry. After working in a variety of positions at Bell Canada in Toronto, he transferred to Atlanta with Northern Telecom and has since worked with Fiber - Transmission, Outside Plant and Switching Products.

SINGLE-MODE MEDIA AND APPARATUS FOR FIBER-TO-THE-HOME

J. B. Haber, D. Kalish, and J. J. Refi

AT&T Bell Laboratories
Norcross, Georgia 30071

ABSTRACT

Information Age technology has begun to appear in homes across the U.S. as several local exchange carriers, working closely with AT&T and other vendors, have begun placing fiber to residences in preselected upscale communities. AT&T has developed a complete line of single-mode fiber cables, splices, connectors, and closures to provide the media support for an all-fiber loop. The architecture used in current fiber-to-the-home applications is much like the architecture used in copper distribution. High fiber count backbone cables are spliced to lower fiber count laterals that branch out to the residences. Service drop cables are spliced in at subscriber property lines. Outside plant fibers are terminated in single-mode connectors. Easy entry cables, passively aligned splices, field-installable connectors, and reliable closures are all necessary components if fiber is to be deployed to the last mile of the loop on a widescale basis. All of these needs are met with AT&T's current line of fiber-to-the-home media products.

1. INTRODUCTION

Fiber optic technology has spread rapidly through the telephone network since its introduction in the late 1970s. Optical fiber has become the transmission medium of choice for long distance and metropolitan trunking networks; it is currently being deployed in more than fifty percent of new digital loop carrier installations; and now, in 1988, several Local Exchange Carriers in the U. S. are installing their first Fiber-to-the-Home service to residences in several preselected upscale communities. Many of these first applications, such as AT&T's SLC® Series 5 Carrier Fiber-to-the-Home Feature (Fig. 1.), use a dedicated single-mode fiber for each subscriber where each subscriber link requires its own optoelectronics.[1] Since the costs of the technology are not shared among many subscribers, the challenge to media and apparatus designers is to provide low cost, easily installable components to minimize the cost per subscriber. These objectives are met with AT&T's current line of fiber to the home media products.

2. MEDIA ARCHITECTURE

2.1 Similarities to Copper Distribution Design

The media architecture for AT&T's SLC Series 5 Fiber-to-the-Home feature is best described as a star emanating from a remote terminal (RT). The design requirements are similar to those used for copper distribution plant engineering. High fiber count backbone cables typically fan out from an RT and are spliced to lower fiber count lateral cables which run down side streets to bring the media to subscribers' front lot lines (for front lot feed) or backyard property lines (for rear lot feed). Figure 2 shows one spoke of a distribution network using a star-type architecture. Buried service lightguide or aerial drop cables are spliced to the lateral cables to complete the distribution to the subscriber.

FIGURE 1. **FIBER TO THE HOME FEATURE ON SLC® SERIES 5 CARRIER SYSTEM**

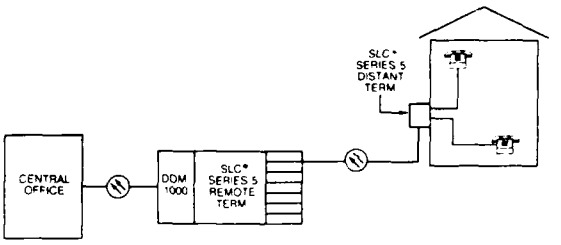

FIGURE 2. **LIGHTGUIDE DISTRIBUTION ARCHITECTURE**

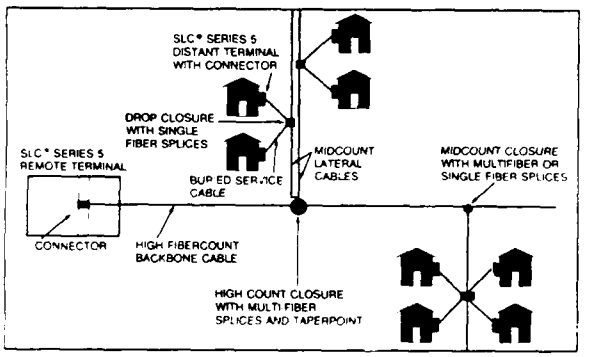

2.2 Differences from Copper Distribution Design

An architectural difference between fiber and copper distribution design is that the all-fiber design does not require a feeder distribution interface (FDI). This eliminates a craft access point and may help reduce outside plant maintenance costs.

The relative costs for splicing versus cable lead to some differences between fiber and metallic distribution design. Copper distribution designs, for example, rely heavily on tapering to reduce pair counts and minimize the expense of cut-dead-ahead, or unusable, copper pairs. Since copper splices are relatively inexpensive compared to copper cables, extensive tapering often results in significantly lower cost installations.

Fiber splicing, of course, is more expensive than copper splicing and costlier relative to cabled fiber, so fiber distribution area designs tend to use less tapering to minimize splicing costs. The savings in splicing costs often offset the cost of the cut-dead-ahead fiber, particularly for short distances.

Figures 3(a),(b), and (c) help to illustrate these differences between fiber and copper distribution area design. The plat for a new residential subdivision with 115 homes is shown in Figure 3(a). Figure 3(b) shows how this subdivision might be served from a subfeeder 800-pair copper cable, with tapering and branching on every street, and a total of seven splice points. A cost optimized fiber solution is shown in Figure 3(c). This fiber design uses only two distribution splice points and no tapering of the lateral cables from which the drops are made. The elimination of some splices was accomplished by using short runs of parallel cables. Several operating companies have reduced the costs on their first applications by using this approach with parallel cables.

FIGURE 3(a).

TYPICAL SUBDIVISION PLAN

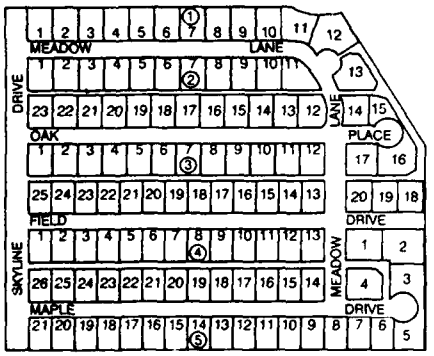

FIGURE 3(b).

COPPER DESIGN

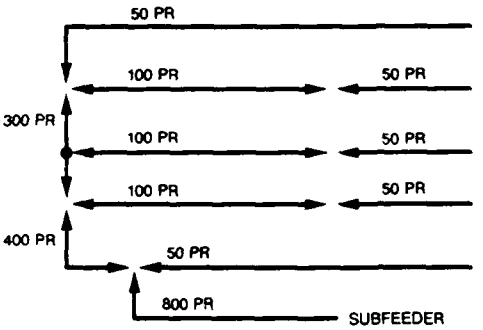

FIGURE 3(c).

FIBER DESIGN

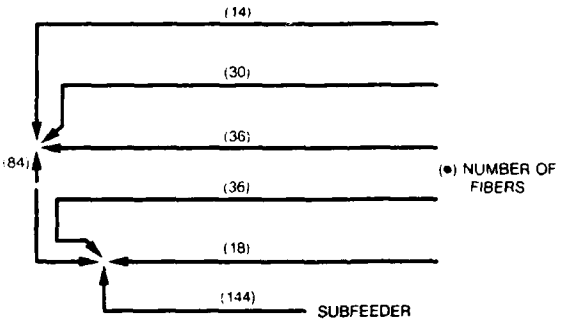

3. WHY SINGLE-MODE FIBER?

Over the past few years, there has been much discussion about whether to use multimode fiber (MMF) or single-mode fiber (SMF) in "the last mile" (the portion of the subscriber loop from the RT to the subscribers' homes). Just a short time ago, single-mode components were very expensive relative to multimode components; but, the gap in costs has narrowed. As the cost of single-mode technology has dropped, the arguments for SMF have become much stronger. SMF has less intrinsic loss than MMF, because it has less doping, and it is also more resistant to added loss due to bending and environmental fluctuations. The bandwidth of SMF is only limited by the optical characteristics of the laser or LED being used, whereas the bandwidth of MMF is restricted by the fiber itself. Finally, SMF is being used in most trunk and feeder routes and, furthermore, may be required for future advanced lightwave technologies like integrated optics and coherent transmission. For these reasons, AT&T's Fiber-to-the-Home offering is designed to use single-mode fiber.

4. CABLE AND APPARATUS DESIGNS

Distribution area lightguide cables and components must withstand a wide range of installation and environmental conditions. Cables are installed underground where temperature excursions are small, and aerially where temperatures can vary widely. Humidity extremes may be encountered because of seasonal climatic and geographical variations. Consistent, predictable performance under any environmental condition is required of all the lightguide media and apparatus used in carrying fiber to the home. The challenge to lightguide media and apparatus designers is clearly one of designing rugged, low loss components at a cost that will allow widescale use. Additionally, components should be easy to field install with a minimum of craft training and equipment.

4.1 Cable Options

Even with only moderate levels of tapering in fiber distribution area designs, cable sheaths must be entered frequently for both mid-span and end-splicing. Fibers must be readily accessible. Cables specifically designed for the last mile of the loop should incorporate both efficient core designs and easy sheath entry. AT&T has two lightguide cable core options and a new sheath design ideally suited for use in the distribution plant.

4.1.1 Core Structures

Ribbon Cores

The ribbon cable has a high fiber density core (Fig. 4a) with up to 144 fibers in a 0.6 inch diameter cable, using up to 12 ribbons. Each ribbon includes 12 individually color-coded fibers for easy identification. The histograms in Fig. 4(b) show the optical loss for production cables at 1310 nm and 1550 nm. The ribbon structure adds no loss to the fiber. Temperature cycling from -40°F to +190°F shows no added low temperature loss at 1310 nm and negligible added loss at -40°F for 1550 nm (Fig. 4c). The ribbon structure readily lends itself to mass splicing which can result in substantial reduction in installation times.

FIGURE 4(a). **RIBBON CABLE CORE**

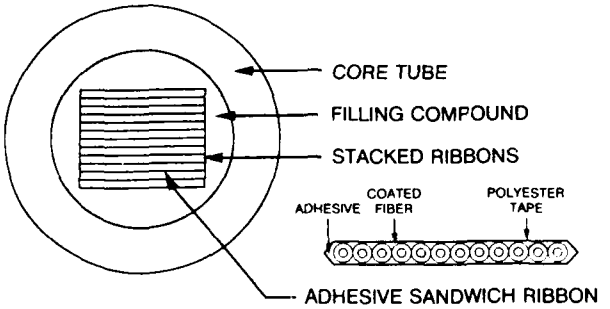

FIGURE 4(b).
RIBBON CABLE
OPTICAL PERFORMANCE - AMBIENT
(1065 FIBER KILOMETERS)

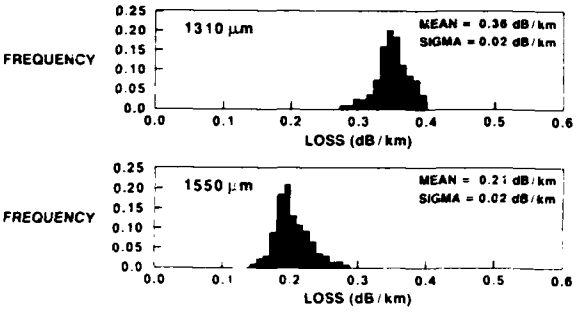

FIGURE 4(c).
RIBBON CABLE
ENVIRONMENTAL DATA

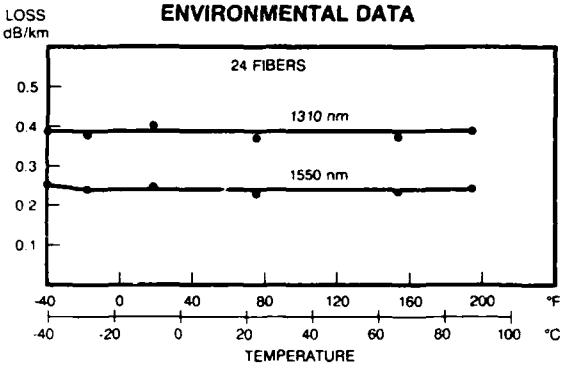

Lightpack® *Cable Cores*

AT&T's second option is the Lightpack core (Fig. 5) which contains up to 96 fibers within a 0.6 inch diameter sheath. The color coded fibers are bundled loosely with color-coded yarns for easy identification. There are up to 12 fibers per bundle. Fibers for this core option can be individually spliced or made into ribbons on the ends for mass splicing.

FIGURE 5. **LIGHTPACK® CABLE CORE**

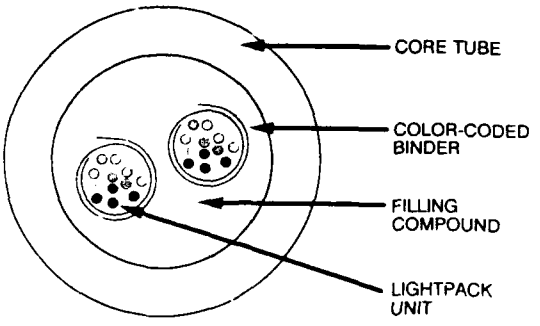

Both ribbon and Lightpack cores include a water-resistant filling compound to protect against water ingress.

4.1.2 Sheath Designs These core structures come in a variety of sheath options including standard configurations like metallic crossply, all-dielectric, and rodent and lightning protected. All AT&T cables are designed so that strength members are external to the core of the cable. This type of design provides protection against microbending losses in the fibers and insures optimum mechanical performance.

A new sheath option for the Lightpack core is the LXE, or "Lightguide Express Entry", sheath (Fig. 6).[2] This sheath, which was specifically designed for distribution cables, allows easy midspan entry for splicing service drops while the remainder of the fibers are expressed through. The Lightpack core tube is surrounded by a waterblocking tape and a steel armor. Two longitudinal steel wires provide tensile strength, and their placement opposite each other along the longitudinal axis of the sheath makes midsheath entry convenient, because sheath layers can be stripped away to expose the core while leaving the wires intact. A ripcord facilitates the removal of the steel armor.

FIGURE 6. LIGHTGUIDE EXPRESS ENTRY SHEATH

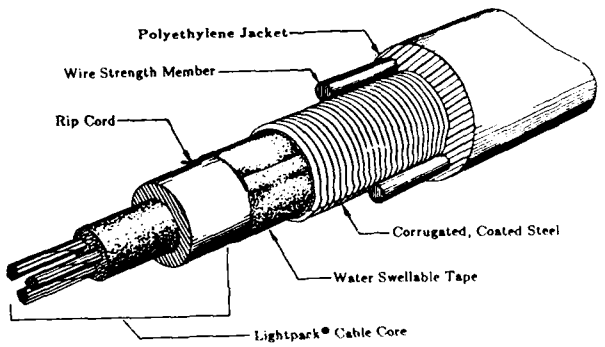

4.1.3 Drop Cables Either buried service or aerial drop cables are required to complete the distribution to the subscriber. Only one fiber per drop is required for bidirectional transmission systems like AT&T's SLC Series 5 Carrier Fiber-to-the-Home Feature.

AT&T's drop cables are available with either one or two color-coded, buffered fibers. Figure 7 shows a cross-sectional view of the two-fiber version of the

FIGURE 7.
BURIED SERVICE LIGHTGUIDE

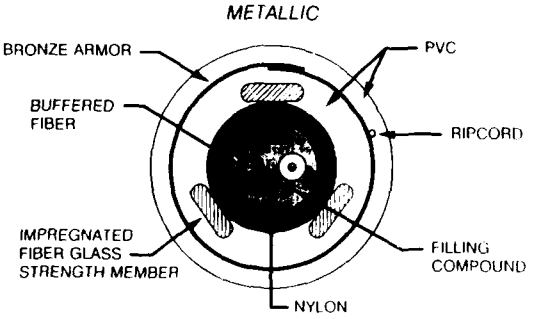

buried service lightguide cable with a metallic sheath. Buffering is required in the drops for protecting and handling the coated fibers. Buffering materials should perform well at low temperatures and should be easily strippable. Thermoplastic polyester buffers outperform PVCs in keeping added losses minimal at temperatures below -20 °C. Both thermoplastics and PVCs, however, can be difficult to strip at low temperatures. AT&T has chosen a thermoplastic polyester buffering material for its excellent low temperature (-40 °C) performance, and has introduced a new laboratory hand tool for stripping that has been successfully used on a trial basis by BOC craft.

A variety of sheath options is required for protecting drop cables, and AT&T currently offers a metallic option with a bronze armor, a non-metallic option, and a rodent and lightning protected version. Since the cables will run along the outside wall of the subscriber's home to the optoelectronics box, all drop cables have PVC jackets rather than polyethylene for fire retardancy, and all have filled cores confined within a nylon core tube.

5. SPLICES AND CONNECTORS

5.1 Mass and Single-Fiber Splicing Techniques

Splicing in fiber-to-the-home applications involves joining high fiber count backbone cables to lower count laterals and joining lateral to drop cables to complete the distribution. AT&T recommends mechanical splicing, because it can be done quickly with minimal equipment.

5.1.1 Array and Rapid Ribbon Splices Mass splicing techniques are preferred for joining high fiber count backbone cables to laterals and for any tapering of the laterals. Mass splicing can be accomplished by using factory-installed silicon chip array splices or field-installed rapid ribbon splices.

AT&T's silicon chip array splice can be applied to either ribbon or Lightpack fibers and allows cables to be joined very conveniently in the field. Field termination hardware protects the splices during shipment.

The single-mode rapid ribbon splice (Fig. 8a) is field-installable and ideally suited for mass splicing ribbons in the field.[3] It can be used directly on ribbon cables and also on Lightpack cables if the individual Lightpack fibers to be spliced are formed into ribbons, a procedure that requires roughly ten minutes to perform. Splicing two ribbons with the rapid ribbon splice requires about 25 minutes from the time the ribbons are accessed through the cable sheath opening. Laboratory and field splice loss measurements for AT&T's rapid ribbon splices show mean losses of less than 0.4 dB (Fig. 8b).

FIGURE 8(a).
SM RAPID RIBBON SPLICE

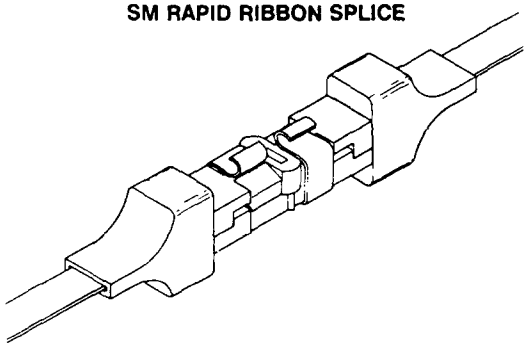

FIGURE 8(b).
SM RAPID RIBBON SPLICE PERFORMANCE

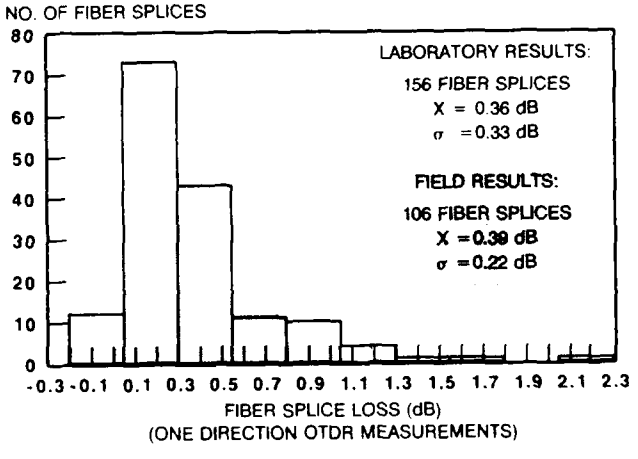

Temperature cycling between -40°F and +170°F shows loss changes less than 0.1 dB from the mean (Fig 8c).

FIGURE 8(c).
SM RAPID RIBBON SPLICE ENVIRONMENTAL TEST RESULTS

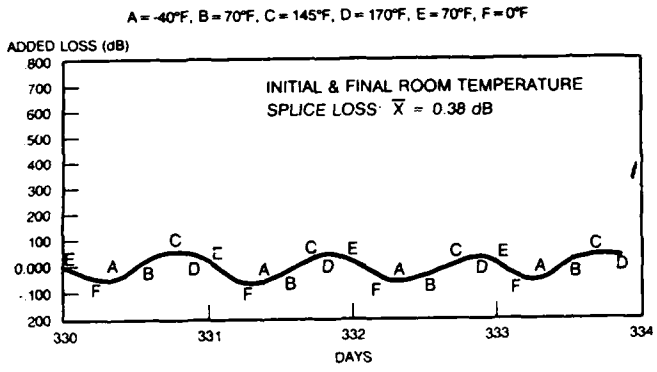

5.1.2 Enhanced Rotary Mechanical Splice Single-fiber splicing is required where drop cables are joined to laterals, for joining laterals (generally where the fiber counts are not integral multiples of twelve), and for repairs. AT&T's enhanced rotary mechanical splice (ERMS) (Fig 9a) is ideal for all of these applications, particularly since it requires no special equipment, active alignment, or testing.[4] The glass plugs for each splice are supplied as a continuous ferrule with a circumferential V-groove and alignment tabs. To make the splice, the mated plugs are snapped apart and installed on the two fibers. Simple passive alignment tools allow the fibers to be positioned with identical orientations inside the glass plugs and rotated to their original relative positions. The splice is then secured with a metal coupler sleeve. The entire procedure, from the time the fibers are exposed and made available for splicing to completion, with the splice ready to place in an

FIGURE 9(a).
ENHANCED ROTARY MECHANICAL SPLICE

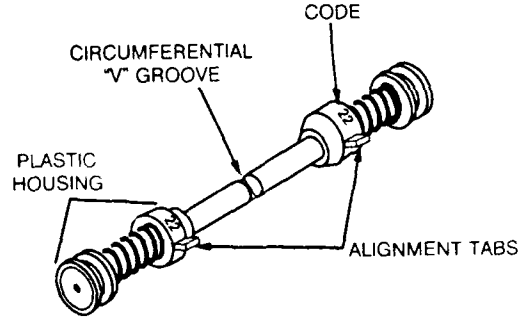

organizer tray, requires about 5 minutes. Average losses using this completely passive alignment procedure are roughly 0.2 dB. Blind splicing results by BOC craft confirm these low average losses (Fig. 9b). Even lower mean splice losses (0.1 dB or less) can be achieved by spending a few additional minutes actively tuning the splice. Temperature cycling between -40° F and +170° F for ERMS

FIGURE 9(b).
ALL BLIND-SPLICED BY BOC CRAFT ERMS PASSIVELY ALIGNED
BIDIRECTIONAL OTDR

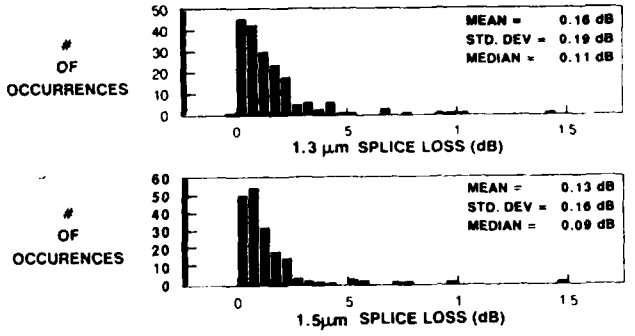

splices that were cycled for over nineteen months shows peak-to-peak loss variations of 0.03 dB or less (Fig 9c).

The distribution and drop cable splices must be stored and protected in closures, pedestals, or aerial terminals. These are discussed later in Section 6.

FIGURE 9(c).
ROTARY MECHANICAL SPLICE ENVIRONMENTAL TEST

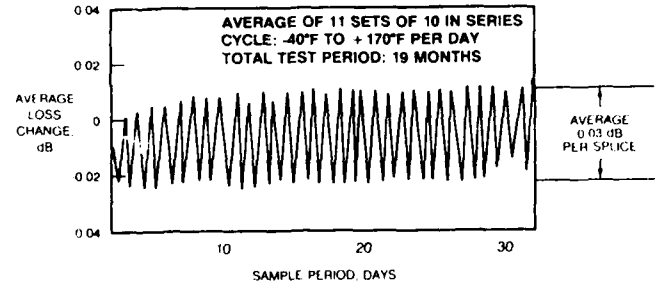

5.2 Connectors

The outside plant fibers for AT&T's Fiber-to-the-Home offering must be terminated at the RT and at a distant terminal (DT) on the outside of a subscriber's home with a single-mode connector. Single-mode connectors should exhibit low insertion and reflection losses and be easy to install in the field.

AT&T's single-mode ST® connector [5] (Fig. 10a) meets all of these requirements and is the connector recommended for the SLC Series 5 Carrier Fiber-to-the-Home Feature. The fibers are positioned in

FIGURE 10(a).
ST® Single Mode Lightguide Connector

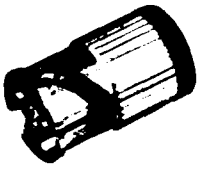

precision ceramic ferrules, alignment is provided by a split cylindrical sleeve, and the fiber ends are held in direct contact by the spring load of the coupling mechanism. The latching mechanism, which uses a ramped slot, is a twist-lock design that allows connections to be made easily. The ST connector can be factory or field-installed with a mean loss of less than 0.4 dB (Fig 10b). This loss is stable with temperature cycling between -40° C to +85° C with less than 0.1 dB added loss (Fig 10c).

FIGURE 10(b).

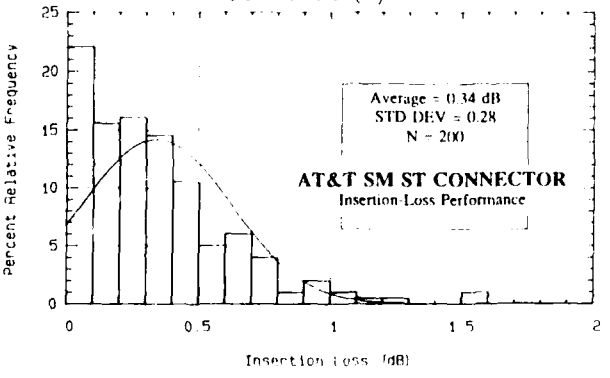

FIGURE 10(c).
PROFILES UNDER TEMPERATURE CYCLE TEST

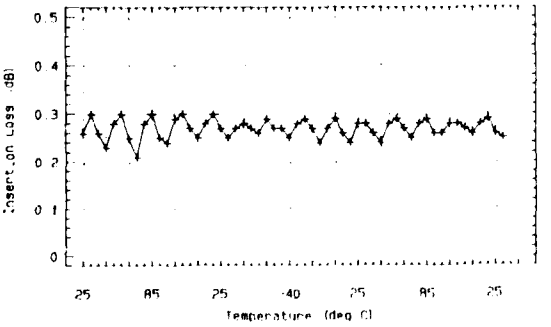

The distribution fibers in AT&T's Fiber-to-the-Home system are terminated in LGX (Lightguide Cross-Connect) distribution shelves at the remote terminal. The termination facility provides high density interconnect or cross-connect arrangements for the fibers.

6. CLOSURES

A variety of closures is required for deploying fiber in the loop distribution network. Where backbone cables are spliced to laterals, or where branching of lateral cables must be accomodated, closures or aerial terminals with several cable ports and multiple splice organizer trays are required. Lower splice capacity, multiple-port buried service closures, pedestal, and aerial drop terminals are required for storing splices (or possibly connectors) where drop cables are joined to laterals. Drop repair closures are required for handling repair splices in case the drop cables are cut. AT&T has a full line of closures to accommodate all of these needs.

6.1 Distribution Closures

The universal closure, which has been used for several years for lightguide applications, is a two-stage, re-enterable closure-within- a-closure. This 4-port closure is well-suited for handling branching from backbone or higher fiber count lateral cables and can accommodate both single-fiber and array-type splices. It can be used for in-line splicing as well as butt splicing arrangements.

A new, 6-port, re-enterable, midsize closure with molded plastic parts is available and is ideal for use where laterals are tapered or joined to backbone cables. This butt-type closure allows fibers to be spliced or unspliced fibers to be expressed through the closure.

6.2 Distribution/Drop and Pedestal Closures

A molded plastic, low count, buried distribution/drop closure designed to accommodate single-fiber splices can be used for low fiber count branching and drop cable splicing. It is re-enterable, requires no encapsulant, and can be used in either in-line or butt configurations.

An option to buried service closures in the drop is above ground pedestal closures, and AT&T has a lightguide pedestal closure which fits in most standard pedestals with at least a six-inch cross-sections. This allows fiber drop splices to be stored above ground for easy access.

AT&T is also developing a lightguide aerial drop terminal for use where aerial plant is preferred or required. This product is expected to be used extensively in rehabilitation areas where fiber will replace existing copper plant.

6.3 Drop Repair Closure

The AT&T drop repair closure is available to restore cables in the case of digups in service drop cables. It is quite small (only 18 inches long) and can accommodate up to four single-fiber splices.

7. FIBER TERMINATION FACILITIES

For the AT&T SLC Series 5 Carrier Fiber-to-the-Home Feature, the outside plant fibers must be terminated at a cross-connect or interconnect facility inside the RT and at the DT at the subscriber's home. At the RT end, the fibers, terminated with ST connectors, are housed in LGX (Lightguide Cross-Connect) shelves capable of handling up to 72 ST connectors each. The LGX equipment is co-located with the transmission equipment in a controlled environmental vault. At the DT, the drop cable fiber is terminated with an ST connector and plugged into the optical unit.

8. MEDIA DEPLOYMENT AND TESTING REQUIREMENTS

The typical sequence of steps for installation and testing of the outside plant lightguide cable are the following:

1. Cable Placement
2. Fiber Splicing
3. Connectorization
4. Completion Testing

Some general guidelines which are useful for deploying and testing fiber cables in distribution areas follow.

8.1 Cable Placement

No special precautions should have to be taken to place fiber cables in distribution areas. Standard practices used in the deployment of fiber feeder are also applicable in "the last mile". On-site inspectors should check to see that cable tension load ratings are not exceeded, that minimum bend radius requirements are not violated, that neither the maximum recommended number of turns nor the maximum pulling distances are exceeded, and that, in general, recommended deployment procedures are being followed. Cables received for placement have generally undergone extensive factory testing to insure quality, and if they are correctly handled, the cable integrity should be preserved. No special testing should be necessary to insure cable integrity.

8.2 Splice Testing

Splice testing can be handled several ways, depending upon the level of detail that the local construction crew is expected to acquire from their test measurements. The simplest test is a continuity test to merely insure that the splices pass light. A bare fiber adapter can be used to couple light from a source into one end of the fiber, and a fiber identifier can then be used to check for light on either side of the splice (Fig. 11a).

If an approximate path loss measurement is desired along with a continuity test, then a source could be coupled through a rotary splice on one end of the fiber, and a power meter could be used to take a measurement at the other end (Fig. 11b).

The most detailed level of splice testing would require an OTDR; this would allow continuity, path loss, and individual splice loss to be determined (Fig 11c). Multimode OTDRs can be used very effectively in this part of the loop, because the distances are short, and the narrow pulse widths allow better resolution of pulses.

FIGURE 11.
TESTING SEQUENCE

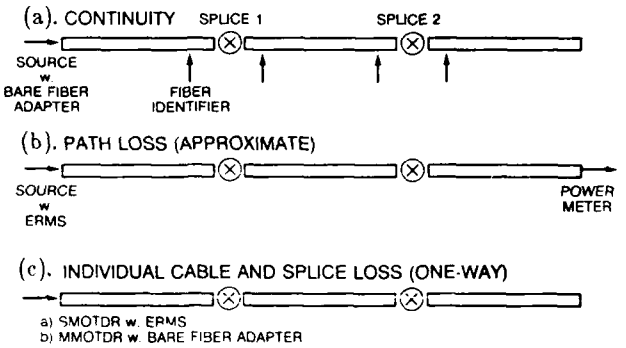

8.3 Completion Testing

Completion testing is performed when both ends of the outside plant fibers are terminated in connectors. This generally requires that the RT and DT be in place. For systems employing multiple wavelengths, completion testing is recommended at all expected operational wavelengths. Two-way path loss measurements should be taken with appropriately connectorized test leads on the instruments. This should result in an accurate end-to-end path loss measurement.

9. FIRST APPLICATIONS OF FIBER-TO-THE-HOME USING AT&T'S MEDIA AND OPTOELECTRONICS

AT&T has been working to support several operating companies, among them New Jersey Bell, South Central Bell, Southwest Bell, Contel, and GTE, in first applications where fiber-to-the-home is initially carrying POTS only services in 1988. The architecture is designed to allow a graceful upgrade to wideband services.

The experiences gained in working on these installations have allowed both AT&T and the operating companies to gain first-hand knowledge about fiber distribution area design, deployment and testing strategies, and desirable product features that will make fiber-to-the-home installations as economic and easy as possible. Installations have run relatively smoothly, schedules have been met, and subscribers whose homes are among the first to receive service over fiber have been watching the operations with enthusiasm.

10. CONCLUSIONS

Fiber optic technology has spread rapidly through the telephone network since its introduction in the late 1970s. Media and apparatus manufacturers have worked aggressively to reduce the costs of fiber optic components. If the rapid and widespread acceptance and deployment in earlier fiber markets is any indication, and if media and component manufacturers are able to further reduce the costs on the cable, apparatus, and hardware necessary to complete fiber distribution systems, it is likely that fiber will be deployed aggressively in residential areas. Subscribers are looking forward to new offerings, and operating companies are eager to be able to provide them. First applications, such as the ones currently underway in 1988, are just the beginning. The challenge to designers continues to be to design and construct fiber optic subscriber systems as economically as possible and to incorporate into the designs features that will minimize maintenance and operations expenses.

11. ACKNOWLEDGEMENTS

The authors would like to acknowledge the many members of the component design and testing groups in AT&T Bell Laboratories, Norcross, whose designs and advice made these first installations of fiber-to-the-home possible.

12. REFERENCES

[1] R. M. Huyler, D. E. McGowan, J. A. Stiles, "The Architecture and Technology for the All Fiber Loop," International Wire and Cable Symposium (IWCS), Reno, 1988.

[2] P. D. Patel, M. R. Reynolds, M. D. Kinard, and A. J. Panuska, "LXE - A Fiber Optic Cable Sheath Family with Enhanced Fiber Access," IWCS, Reno, 1988.

[3] N. E. Hardwick and S. T. Davies, "Single-Mode Rapid Ribbon Splice," IWCS, Reno, 1986.

[4] J. A. Aberson, G. F. DeVeau, K. M. Yasinski, "Enhanced Rotary Mechanical Splice with Fiber Positioning," 4th Annual Electrical Engineers Conference, New York, NY, April 1988.

[5] G. M. Alameel, A. W. Carlisle, "The Performance of the AT&T Single-Mode ST Connector and Its Latest Enhanced Features," SPIE International Symposium and Exhibition on Fiber Optics, Optoelectronics, and Laser Applications in Science and Engineering, Boston, MA, September 1988.

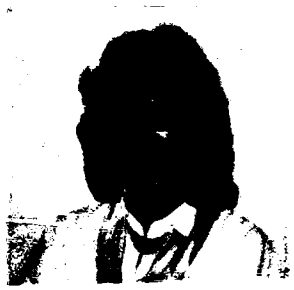

JANICE B. HABER
AT&T Bell Laboratories
Norcross, GA 30071

Janice B. Haber is a Member of Technical Staff at AT&T Bell Laboratories, Norcross, Georgia. Her current responsibilities in the Lightguide Systems and Applications Engineering Group include providing technical support for several fiber-to-the-home first applications across the U.S. and assessing lightguide system performance in ambient terrestrial and nuclear radiation environments. Janice holds a BSEE degree from the University of Maryland and an MSEE degree from the Georgia Institute of Technology.

DAVID KALISH
AT&T Bell Laboratories
Norcross, GA 30071

David Kalish is Technical Supervisor of the Lightguide Systems and Applications Engineering Group in AT&T Bell Laboratories, Norcross, Georgia. He joined Bell Laboratories in 1971 and has B.S., M.S., and Ph.D. degrees from M.I.T.

JAMES J. REFI
AT&T Bell Laboratories
Norcross,GA 30071

James J. Refi received the BSEE degree from Villanova University in 1966 and the MSEE degree from the Polytechnic University in 1968. He is a Distinguished Member of Technical Staff in the Lightguide Systems and Applications Engineering group at AT&T Bell Laboratories in Norcross, Georgia. Since joining Bell Laboratories in 1966, he has spent most of his career working on land coaxial and multipair cables - having authored papers on pair unbalance phenomena, lightning surges, and crosstalk. He began working on lightguide in 1982 and since then has obtained a patent and authored papers on field measurements, multimode bandwidth, and single-mode chromatic dispersion. Mr. Refi is currently responsible for several fiber-to-the-home applications. He is a member of the IEEE, the Optical Society of America, Tau Beta Pi, and Eta Kappa Nu.

A NEW INSTALLATION METHOD FOR CONVENTIONAL FIBRE OPTIC CABLES IN CONDUITS

W. Griffioen
PTT, dr. Neher Laboratories
Leidschendam
the Netherlands

Abstract

A new technique for the installation of conventional fibre optic cables in commonly used conduits using the viscous flow of air is decribed. Blowing experiments have been carried out, using different cables, conduits and lubricants. For better understanding also pulling experiments with conduits having different tortuosities and supporting laboratory experiments have been performed. The non linear pressure decay in the tube in which the cable is blown is experimentally verified. Furthermore a simple experiment for measuring the cable stiffness is described. With one installation unit 1 km fibre optic cable can be installed with speeds up to 1 m/s. Even 36 right angled curves in the conduit can be passed. In less than one hour a reel with 2100 m fibre optic cable can be installed using the installation units in cascade, without synchronisation problems. This means that longer cables can be installed in the future. The described method is very simple because for instance no pulling ropes have to be installed. Furthermore the cable strain can be kept low. Halfway 1988 1000 km fibre optic cable have been installed in the public network of the Netherlands using the described method, considerably saving man and time.

Introduction

The old installation method

In many countries fibre optic cables are pulled in pre-installed conduits. The pulling force is fully concentrated at the cable end there. It is well known that with this technique an exponential build up of the pulling force occurs due to the cable tension, especially on tortuous routes [1]. In some countries conduits with an inside diameter of only 26 mm (cheap!) are used. The only disadvantage of these conduits is the fact that without special precautions the windings give rise to a quick build up of the pulling force, necessary to install the cable (appendix 1). To reduce excessive forces on the cable, capstans are used for intermediate assistance. For the small diameter conduit, as are used in the Netherlands, the most economic distance between those capstans is 175 m for the installation of a reel of 2100 m fibre optic cable.

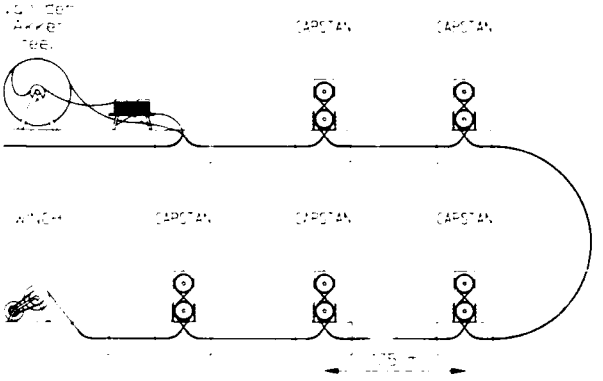

figure 1: pulling 1050 m of fibre optic cable with the help of capstans and a bufferreel (Netherlands PTT, before 1988)

In figure 1 the old installation method, as formerly used by the Netherlands PTT, is shown. The reel is placed halfway. In three 175 m sections the pulling rope is installed by means of a shuttle driven by compressed air. The cable is pulled with a winch assisted by two capstans. Next the winch is placed at the far end of the traject and the pulling rope is installed in the next three sections. Now the pulling takes place with the help of five capstans. When the first 1050 m is installed the rest of the reel is rewound on a special buffer ("van den Akker") reel. Now the next 1050 m can be installed in the same way as described above (this part of the installation is shown in figure 1).

It is clear that this installation method is man and time consuming. For this reason and for the need to install cable lengths longer than 2100 m in the future, another installation method is searched for.

The new installation method

The previously mentioned exponential build up of the pulling force can be prevented when the cable tension is kept low. This can be achieved when the friction between cable and conduit is compensated locally, i.e. when the pulling force is distributed along the whole cable length. In that case each conduit can be considered straigth for flexible cables. Cassidy et al. [2] have found an elegant method for reaching this. They blow very small, flexible and lightweight fibre members (designed for use inside buildings) into conduits

AD-A200 903 PROCEEDINGS OF THE INTERNATIONAL WIRE AND CABLE SYMPOSIUM (IWCS 37TH) HEL.. (U) ARMY COMMUNICATIONS-ELECTRONICS COMMAND FORT MONMOUTH NJ

UNCLASSIFIED 17 NOV 88 F/G 9/1 NL

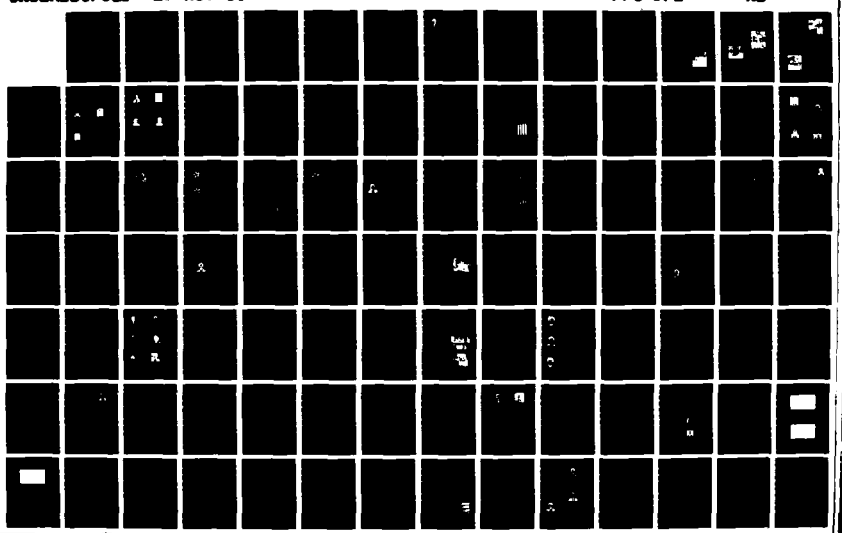

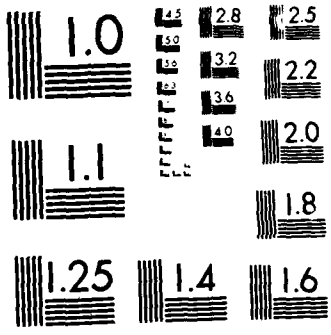

without the use of a shuttle at the cable end. The force F/l exercised on the cable per unit of length, when the pressure drop at the cable inlet is compensated mechanically, can be written as [2]

$$F/l = - \frac{dp}{dz} \cdot \pi \, r_{cab} \, r_{cond} \qquad (1)$$

where dp/dz is the pressure gradient along the conduit, and r_{cab} and r_{cond} are the outer radius of the cable and the inner radius of the conduit respectively.

In this contribution a scaling up of this method is described which can be used for conventional fibre optic cables. The cables do not need to be flexible, in fact a certain stiffness is advantageous. In that case the cables can be pushed over a certain distance which is a useful assistance because of a relatively low pressure gradient in the first part of the conduit [3]. In appendix 2 measurements have been carried out in order to verify the non linear pressure decay in the conduit. The stiffness of the cable must be such large that pushing of the cable causes not too much buckling. On the other hand the stiffness of the cable may not be too large because then the cable experiences too much friction with the conduit in curves and windings of the conduit. A good choice for the stiffness B of the cable can be derived [3].

$$\frac{8}{\pi^3} \cdot \frac{a(P/4)^2}{A} \cdot F_p \leq B \leq \frac{2}{3} \frac{W(P/4)^4}{A} \qquad (2)$$

where W is the cable weight per unit of length, A and P are the (estimated) amplitude and period of the (sine shaped assumed) windings in the conduit respectively, Fp is the pushing force and a is the half free radial space (r_{cond}-r_{cab}) of the cable in the conduit. This relationship has of course only sense when Fp may have values such that it effects the installation of the cable. Most fibre optic cables forfill inequalty 2. In appendix 3 a simple experiment for measuring the cable stiffness is described. It can be shown [3] that for a situation which is typical for the cable and duct combination of the Netherlands PTT, the additional pushing force can double the installation length that can be reached by cable blowing.

In figure 2 the new installation method is shown. The 2100 m reel is placed at one end of the traject. Four special developed dismountable cable injection units can operate in cascade with a most economic intermediate distance of 525 m and the whole cable reel is installed in this simple single operation, eliminating the installation of pulling ropes and the need for a bufferreel.

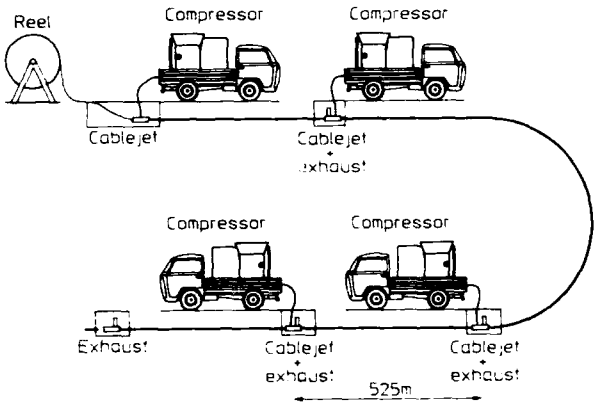

figure 2: Blowing 2100 m of fibre optic cable using the injection units in cascade (Netherlands PTT, after 1987)

The injection unit

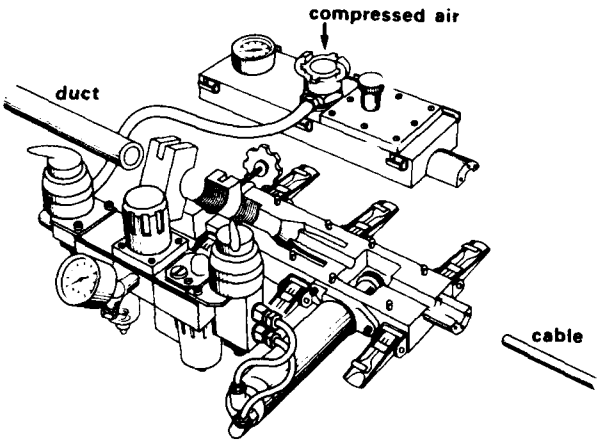

figure 3: The first prototype of the injection unit

A special cable injection unit [6] has been developed and is shown in figure 3. The airflow and all the other functions can be supplied by a simple compressor (75 l/s, 8 bars), which was formerly used for the installation of the pulling rope. The unit consists of two parts that can be mounted together in such a way that it will be possible to use several units in cascade. The compensation of the pressure drop along the cable inlet [2] and the additional pushing force [3] are supplied by grooved hollow wheels driven by a pneumatic motor. These wheels are pushed against the cable by means of pneumatic pistons (not shown in figure 3) so that small variations in cable diameter can be tolerated. The pneumatic motor can be stopped, just by holding the cable, also when lubricants are used. This is a great advantage when the cable injectors operate in cascade. The installation speed is controlled by the unit with the lowest setting of the pressure regulator for the pneumatic motor. For protection of the

injection units in cascade and for reasons of safety, a 'funnel' for the exhaust of the airflow (not shown in figure 3) has been developed for operation together with the injection units.

Results

It turned out to be possible to install cablelengths with a maximum of 1 km in conduits with an inner diameter of 26 mm using one single installation unit, while speeds up to 1 m/s were reached when using standard cables. Using cables with ribbons on their jackets or 40 mm inner diameter conduits the performance even increases. For the latter application a compressor with a maximum pressure of 8 bars and a capacity of 130 l/s is needed, while for smaller conduits smaller compressors are sufficient. The independency of curves and windings in the conduit is clearly shown during a test in an extremely tortuous circuit. In this circuit, which has a length of 420 m and in which there are 9 right angled curves and windings equivalent to 27 right angled curves, a cable is installed using the described method.

Several lubricants have been tested for the blowing method as a possible alternative for paraffine oil. The lubricants, two types 2 and one type 3 (see appendix 1), gave rise to foaming, were dried by the airflow or caused the cable to 'stick' to the conduit wall because of their high viscosities. Pipe 3 with lubricant 4 (see appendix 1) gave satisfactory results, however, only 800 m was available as a testlength. Until now paraffine oil is the best solution. It is sufficient to pour about one liter of the latter in the conduit before connecting the installation unit. The paraffine oil will be distributed through the conduit by the airflow and the cable doesn't need to be lubricated.

In an experiment in which 500 m of 26 mm inner diameter conduit was already filled with a cable, an attempt has been made to install a second cable using the blowing technique. This installation was possible in the first part of the conduit but stopped after 280 m.

In the public network 2100 m fible optic cable can be installed in less than one hour using four installation units in cascade. Occasionally also cables with a length of 3150 m have been installed using the blowing method. Halfway 1988 more than 1000 km of fibre optic cables have been installed in the public network of the Netherlands using the described method, considerably saving man and time. The old pulling method has now been abandoned.

Conclusions

The blowing technique for the installation of conventional fibre optic cables as is described in this contribution is a quick and simple method, eliminating the extra step of installing a pulling rope. The cable strain is kept low during installation. Long lengths can be installed per installation unit in both straight and tortuous routes so that cheap conduits can be used without paying special attention to reduce the windings during the installation of the conduits. For lubrication it is sufficient to pour a small amount of paraffine oil in the conduit before connecting the installation unit while the cable doesn't need to be lubricated. The installation units can be easily used in cascade with intermediate distances only dependent on the properties of the cable, conduit and lubricant used, and almost independent of curves and windings in the conduit sections. There are no synchronisation problems when several units are used in cascade. This means that there is no limit for the cablelength that can be installed, so that longer lengths and hence less splices in the future are possible. The possibilities of the described installation method can further increase when special cables (optimised for blowing instead of pulling) and lubricants are used. It is possible to install more than one cable in a conduit (not necessary in the same time) for short distances. This might add some applications to the described method, such as local networks and unforeseen expansions of the trunk network.

Acknowledgements

The author wishes to thank C.L. de Jong and K.F. Betcke for the construction of the injection units and J.C. Veenis with his crew members for assistance with the field experiments.

References

1. F.H. Buller, 'Pulling tension during cable installation in ducts or pipes', General Electric Review, pp.21-23, August 1949.

2. S.A. Cassidy and M.H. Reeve, 'A radically new approach to the installation of optical fibre using the viscous flow of air', Proc. IWCS, pp.250-253, November 1983.

3. W. Griffioen, 'The installation of conventional fibre optic cables in conduits using the viscous flow of air', To be published in Journal of Lightwave Technology.

4. A.L. Hale, 'The inelastica: The effect of internal friction on the shape and tension of a bent cable', Proc. IWCS, pp.237-243, November 1984.

5. H.M. Kemp, 'Procedure for the experimental determination of friction coefficient between a cable and a duct', Proc. IWCS, pp.557-563, November 1987.

6. W. Griffioen, C.L. de Jong; Patent pending.

Appendix 1: The effect of conduit windings on pulling force build up

In order to calculate the effect of windings in a duct traject Buller's formula [1] is used in combination with a formula that gives the effective angle per unit of length θ_{eff}/l for a given conduit geometry [3].

$$F_2 = WR \sinh [f\theta + \text{arcsinh} (F_1/WR)]$$

$$\theta_{eff}/l = 1/R_{eff} = 4\pi A/P^2 \qquad (3)$$

This formula gives the pulling force F_2 as a function of the force F_1 of the cable when entering the conduit at certain cableweight per unit of length W and bending radius of the conduit R. In the second part of the formula R_{eff} is an effective bending radius of a tortuous conduit with (sine shaped) windings of amplitude A and period P.

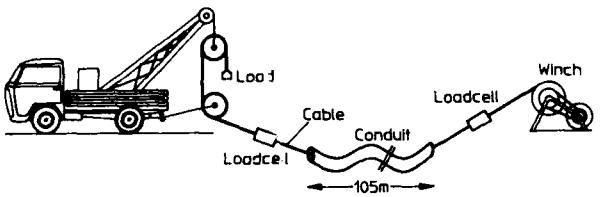

figure 4: Field experiment for measuring the effect of defined windings.

The formula which gives the effective tortuosity in an angle per unit of length has been verified in a field experiment with horizontally 'sine shaped' conduits (figure 4). Conduits with an inside diameter of 26 mm and a length of 105 m, having windings with amplitudes of 7.5 and 15 cm and periods of 2, 3 and 4 m were used. From the measured forces before and after the conduit in which the cable is pulled with a speed of about 20 m per min, the friction coefficients can be derived using formula 3.

P(m)	A(cm)	F(N) 10	20	30	40	50	100	150	200
4	7.5	0.46	0.42	0.40	0.34	0.34	0.31		0.24
3	7.5	0.38	0.35	0.31	0.31	0.28	0.24		
4	15	0.35	0.31	0.28	0.28	0.27	0.23		
3	15	0.27	0.24					0.24	

table 1: Friction coefficient f between cable and conduit, using paraffine oil as a lubricant, derived using formula 3. F is the load at the inlet side.

When the forces are low, not only the accuracy of the measured forces is low but also the cable stiffness plays an important role. This causes measured friction coefficients in that region that are higher than in reality, as can be seen in the left and upper part of table 1. Carrying these things in mind a friction coefficient of roughly 0.25 is found which is in agreement with the value derived from laboratory measurements.

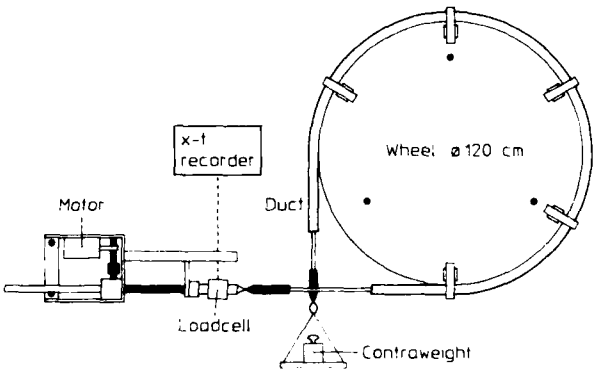

figure 5: Laboratory equipment for the determination of the friction coefficient between cable and conduit.

In figure 5 an equipment for the determination of the friction coefficient between cable and conduit is shown in which the cable is pulled through a 270 degrees section of a conduit around a 120 cm diameter wheel. The cable is pulled with a non controllable velocity of 12 cm per minute. The pulling force measured by a loadcell is monitored on a x/t-recorder. The cable is pulled with several contraweights attached at the other end. The friction coefficient is calculated using a formula which can be derived analogously to the formulas derived for vertical 90 degrees sections in [1].

$$F_2 = WR.[2f.e^{f.3/2\pi}-(1-f^2)]/(1+f^2) + F_1.e^{f.3/2\pi} \qquad (4)$$

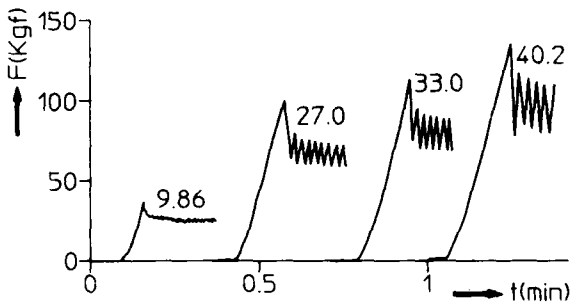

figure 6: Example of the measured force necessary to pull the cable through the conduit around the wheel as a function of time for different contraweights (represented by the numbers near the recorder traces in kgf).

In figure 6 a typical example of a recorder trace of a measurement of the friction coefficient is shown. The 'wiggles' in this recorder trace can be explained as a result of a combined effect of elasticity and inertia of the whole experimental setup [5]. The results shown in table 2 are obtained using the peak values of the recorder traces which can be considered to be the static friction coefficients. It is worth noting that not all the

recorder traces look the same, for instance the water based lubricant doesn't show 'wiggles'.

contraweight (kgF)	5.0	9.86	15.0	27.0	33.0	40.2
pipe 1, dry		0.29		0.29	0.30	0.29
pipe 2, dry		0.27		0.28	0.29	0.28
pipe 1, lubricant 1	0.28	0.28		0.27	0.26	0.25
pipe 2, lubricant 1	0.27	0.23		0.26	0.27	0.23
pipe 1, lubricant 2	0.16	0.17				
pipe 1, lubricant 3	0.20	0.21				
pipe 3, lubricant 4	0.23	0.22	0.21			

table 2: Measured (static) friction coefficients between cable (standard Netherlands PTT) and several conduits lubricated with several lubricants using formula 4. Pipe 1 and 2 are standard HDPE pipes wich an inner diameter of 26 mm, while pipe 3 has longitudinal ribbons. Lubricant 1 is ordinary paratfine oil, 2 is a water based lubricant, 3 is a lubricant based on triglycerine of eatable fat acid modificated by yellow amber acid and 4 is a mixture of a silicon based lubricant and microspheres.

Appendix 2: Measurements of the pressure decay along the conduit.

The pressure decay along the conduit is not linear because the flow cannot simply be considered incompressible in the pressure regime covering almost one order of magnitude. This pressure decay is calculated in [3]

$$p(x) = \sqrt{p_0^2 - (p_0^2 - p_1^2) \cdot \frac{x}{l}} \qquad (5)$$

with p(x) the (absolute) pressure at distance x from the air supply. The (absolute) pressures at the air supply side and at the exhaust side of the conduit with length l are p_o and p_1 respectively. In order to verify this formula measurements have been carried out using conduits with different tortuosity ranging from about 3 to 30 degrees per meter. The results in figure 7a are obtained by forcing an airflow through respectively 4, 5 and 7 pipes in cascade. These 26 mm inner diameter pipes are roughly 105 m long and measurements are carried out in the sequence of both increasing and decreasing tortuosity. The pressure is measured at the connections of the pipes.

The results shown in figure *7a* agree quite well with the calculated curve, bearing in mind the following things. After starting the compressor it took about one hour before equilibrium was reached. This can be caused by the warming-up of the compressor, the setting of a stationary temperature decay along the pipes (after some time the pipe right behind the compressor feels warm, while after 100 m underground it feels unchanged). Another cause can be the condensation and/or the evaporation of water in the expanding and cooling flow. All the mentioned effects as well as the effect of different tortuosities did not cause a significant

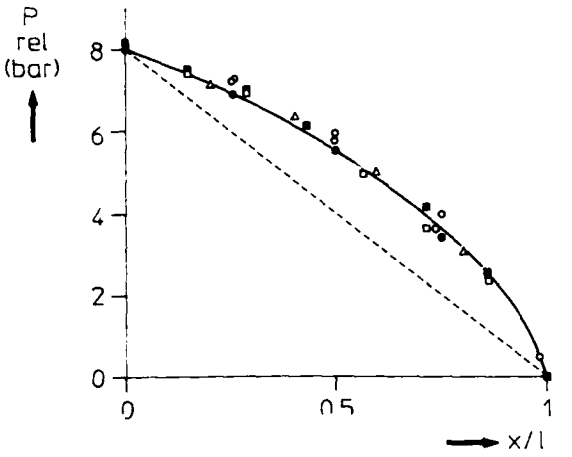

figure 7a: Pressure (relative to atmospheric pressure) p_{rel} as a function of the normalised distance x/l from the air supply. The solid curve is calculated for a (relative) pressure of 8.1 bars at the inlet side of the pipes using formula 5. The dashed line represents a linear pressure decay. The open circle, triangle and square symbols are measured at a total pipe length of 420, 525 and 735 m respectively with increasing tortuosity in the flow direction. The solid circle and square symbols have been obtained from measurements in the reversed direction at a total pipe length of 420 and 735 m respectively.

difference between measurements and theory.

The pressure gradient dp/dx can be derived from the calculated curve in figure *7a* and is shown in figure *7b*. In the first part of the pipe this pressure gradient, which is proportional to the force of the airflow acting on the cable, is almost twice as low as the pressure gradient for the case of a linear assumed pressure decay. In the last part of the pipe the pressure gradient is almost one order of magnitude larger than in the first part. Because in most duct routes (especially in tortuous ones) the 'overforce' at the exhaust side of the conduit can not reach the shortcoming at the airsupply side of the conduit, the cable blowing can be largely improved when an extra pushing force is applied at the cable by the injection unit.

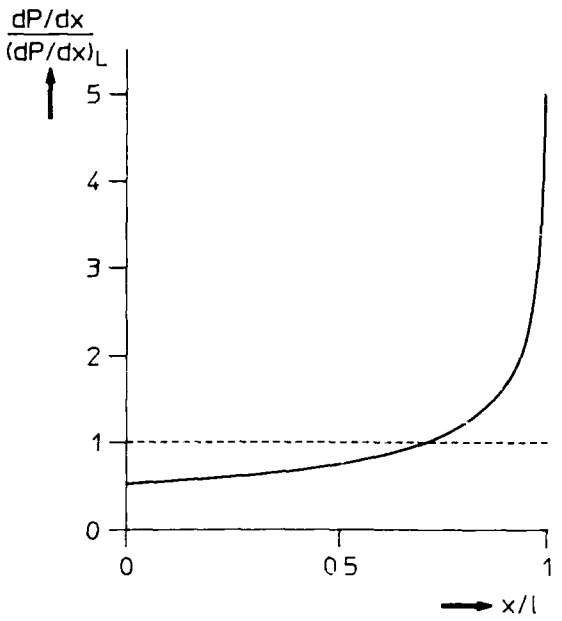

figure 7b: Quotient of the pressure gradient dp/dx, calculated using formula 5 for a (relative) pressure of 8.1 bar at the inlet side of the pipe, and the pressure gradient $(dp/dx)_l$ for a linear assumed pressure decay as a function of the normalised distance x/l from the air supply.

Appendix 3: A simple experiment for measuring the cable stiffness.

Applying a bending moment to, and measuring the curvature of a cable is a way in obtaining its stiffness. A much more simple method is measuring the sag of a clamped piece of cable as a function of the weight of the mass attached at the end of it.

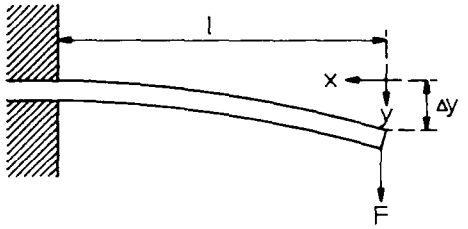

figure 8: Schematic view of the clamped piece of cable.

The sag is measured with the help of a displacement gauge. In order to eliminate the force on the piece of cable exercised by this displacement gauge (0.5-0.8 N) the situation of first electrical contact of the pin of the gauge and a piece of copperfoil, attached at the end of the cable, is measured.

The stiffness B is defined as the deriviate of the bending moment M with respect to the curvature k. For a small sag (y'<<1) this curvature is equal to y''. Using boundary conditions y(1)=y'(1)=0 this curvature can be expressed with the sag Δy=y(0) of the cable end

$$k = \frac{3\Delta y}{l^2} \cdot \frac{x}{l} \qquad (6)$$

Because in the case of an elastic cable k as well as M are proportional to x the value of B can be derived from the slope of M against k at for instance x=l. When the cable is not elastic but shows a behaviour as in [4] the transition from elastic to inelastic behaviour occurs first at x=l and translates to smaller x values when larger masses are attached to the piece of cable. This causes a smoothing of the mentioned transition. For the installation of the cable using the viscous flow of air only the elastic behaviour of the cable is of importance (worst case estimation [3]), so this smoothing causes no problems.

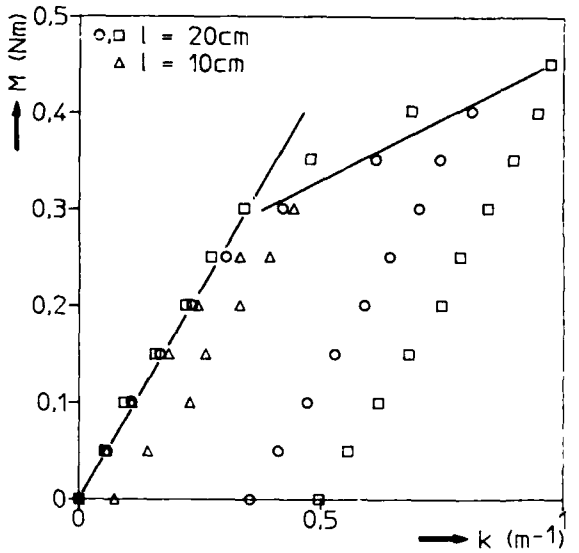

figure 9: Measured values of M against k for a standard Netherlands PTT fibre optic cable.

The measurements must be done using cable lengths and weights in such a way that y' remains much smaller than 1 and that the transition from elastic to inelastic behaviour is shown in the results. The results from the standard Netherlands PTT fibre optic cable (9.5 mm diameter, 6 fibres) are shown in figure 9. The transition from elastic to inelastic behaviour is clearly shown in measurements using a 20 cm piece of cable. For comparison measurements with a 10 cm piece of cable are shown resulting in the same slope in the elastic region. The cable stiffness B in this example can be found from figure 9 and is roughly 0.9 Nm^2 in the elastic region. This stiffness is mainly due to the aluminium waterbarrier of the cable.

Biography

Willem Griffioen was born in Oegstgeest, the Netherlands, on October 8, 1955. He received the B.S. and M.S. degrees in physics and mathematics from Leiden University, Leiden, the Netherlands, in 1978 and 1980. He worked at Leiden University from 1980 to 1984, where he investigated macroscopic quantum properties of liquid and solid $^3He/^4He$-mixtures at ultralow temperatures and in high magnetic fields. In 1984 he joined the Dr.Neher Laboratories of the Netherlands PTT, Postbus 421, 2260 AK Leidschendam, the Netherlands. His work includes research and development of fibre optic cables, installation techniques and reliability of optical fibres.

A NEW PROCESS : MULTIPULLING AND CABLING IN LINE OF OPTICAL FIBERS - TECHNICAL REALIZATION.

G. LE NOANE[1] - D. BOSCHER[1] - B. MISSOUT[2] - J.L. STRIEBIG[2]
P. TROMBERT[3] - P. CHERON[3] - B. INIZAN[4] - F. GALERNE[4]

1 FRANCE TELECOM CNET LANNION - FRANCE
2 SAT - PARIS - FRANCE.
3 SILEC - MONTEREAU - FRANCE.
4 Ets POURTIER - CHELLES - FRANCE.

1. ABSTRACT

Present optical fibers and cables industrial manufacturing conditions are mainly oriented according to long haul and trunk networks needs. Anticipated development of local video-communication broadband networks calls for new technical and economical progress in order to meet the low cost and mass production challenge presented. Multipulling and cabling in line process (MCL) brings one innovative contribution towards this goal. After prior feasability demonstration, the first real size prototype of an industrial MCL machine has been realized. The article describes its objectives and technical features enabling to perform in one step the simultaneous pulling and cabling, at speeds up to 100 m/min, of 5 fibers in a V-grooved structure, with possible extension to other types of fiber modules. Simple and reliable operation is granted by an original accumulation system allowing dynamic intermediate storage of several fiber kilometers. Resulting new approach concerning fibers and cable testing, quality control and yield is also discussed.

2. INTRODUCTION

Since the introduction of optical transmission technology more than 10 years ago, the goals and evolution process, as regards fibers performance, specifications and industrial organisation have been primarily guided by the needs of long haul or trunk networks. These have seen a continuous and fast increase of both transmission unreapetered spans and bit rates justified by communication requirements and new possibilities brought by the upgrading of fibers and other components. Presently some remarkable achievements have been reported[1].

In this respect a particular attention has been focused on transmission characteristics. First, with multimode fibers, development works have been largely applied to index profile and resulting bandwidth. Then, the orientation being shifted towards single mode fibers, the main fields of interest became optimisation of loss and dispersion[2] near theoretical limits, improvement of bending and microbending, together with mastering of geometrical tolerances in view of low loss splicing.

Furthermore, special efforts have been devoted to fibers mechanical strength[3], necessary when considering long term reliability level required for long haul terrestrial or submarine links representing strategic aspects for telco organizations.

One practical and important consequence of this evolution is the fact that present fiber manufacturing conditions are probably not economically optimized as regards production yield on a global basis.

Both requirements of top grade fibers and remaining limitations in technical possibilities of state of the art manufacturing and control processes result in a significant percentage of produced fibers being unsuitable for integration in long haul or trunk cables. Unfortunately, the present state of the market does not make it possible to use these lower grade fibers for less stringent applications which are not yet widely developed.

Furthermore, the efforts applied by fiber manufacturers in order to improve technico-economical efficiency are mainly leading to ever more sophisticated and high investment-consuming preform and drawing processes, justifying large scale and specialized production facilities.

However one can today seriously raise the question of whether the future of optical fibers needs a new approach in terms of types of applications, corresponding goals and industrial organization.

3. EVOLUTION OF OPTICAL FIBER APPLICATIONS

On one hand one may reckon that prospects in long haul and trunk networks are somehow limited, due to present state of completion and development rate of modern networks. On the opposite, most recent forecasting analyses agree to show that future boost in optical fiber needs will probably come from subscriber/videocommunication or broadband multiservice local networks[4].

In spite of important uncertainties remaining as regards for example political aspects, services offered, network architecture, implementation strategy, economics, advances in components other than fibers etc..., there is no doubt that the realization of such networks would result in huge quantitative needs.

On the other hand, it has to be considered that "subscriber fibers and cables" technical requirements will differ considerably from the present ones. Whether multimode or singlemode, the emphasis on transmission performance can be questioned when considering relatively limited link lengths and bit rates which will be used. Mechanical properties will have to be compatible with practical use in underground cables in most cases. Finally, a reasonable compromise can be expected between geometrical tolerances and connections suitable for subscriber link power budget.

As opposed to these aspects, the necessity of low cost fibers and cables, together with industrial conditions enabling mass production, will be of paramount importance with a view to ensuring credibility and rapid implementation of these new distribution networks.

Several ways of aiming at such targets are already well under consideration. Some of them focus on preforms, mainly in order to improve productivity by considerably increasing preform sizes, deposition rate and mass glass production, leading to development of new and promising third or forth generation technologies such as fully synthetizing[5], sol-gel[6] or plasma methods, especially POID[7]. In this last case, the economic progress is also expected to be accompanied by significant advantages as regards geometrical tolerances and mechanical strength.

Other works aim at introducing higher fiber drawing speeds such as reported already experimentally at 600 or 1000 m/min[8].

Finally studies are also being carried out concerning cable structures with the main objectives of achieving high cabling density, allowing cables with high fiber counts to be pulled in existing ducts, by means of modular designs aimed at reducing production as well as connection costs[9].

All these different research works, dealing with important topics and having ambitious goals are nevertheless somewhat restricted to one particular production step among the several ones leading from preform raw materials to completed cables.

An alternative and innovative approach has the ambition of combining and simplifying in an harmonious way several of these steps, ie the Multipulling - Cabling in Line process (MCL)[1], which is bound to drastically reduce optical cables manufacturing costs by avoiding many intermediate stages (fig. 1).

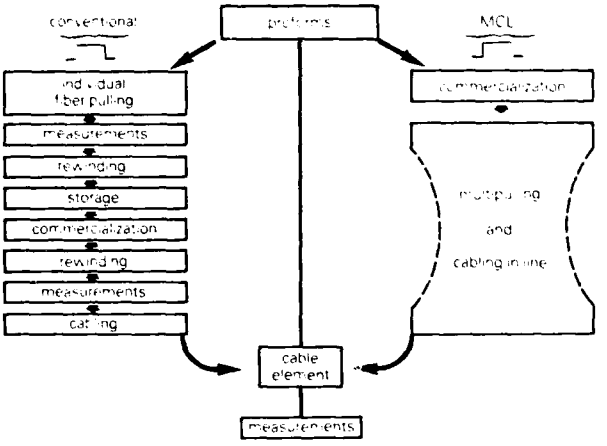

Fig 1 = Comparison between stages in conventional and MCL production

To some extent, several costly steps of the classical separated organization are not justified only by technical requirements but rather stem from present industrial and commercial conditions where preform pulling and fiber cabling are generally performed by separate companies or factories. The needs for these steps will naturally disappear in an integrated organization.

On another aspect, MCL will enable to take full advantage of progress made on preform manufacturing, drawing and cabling which are today well mastered techniques. One can for instance presently consider that preform yield is close to 100 % as far as subscriber network needs are concerned. Furthermore it must be noted that the simultaneous use by MCL of simple drawing lines running at moderate speed will actually compare to the speed performance offered by the most advanced and sophisticated single fiber pulling processes.

As a matter of fact, MCL concept shows some similarities with the reasoning having led in the past to integrate in one continuous operation copper drawing and wire insulating in the telecommunication copper cable manufacturing process.

4. INDUSTRIAL DEVELOPMENT OF MCL PROCESS

The initial concept of MCL was defined in 1980 and further technical feasability demonstrated by the French Telecom Research National Center CNET[10].

Considering the outstanding prospects resulting from this breakthrough, France Telecom promoted the development of an industrial MCL machine and a consortium of three French companies was put in charge of this task, with the following general objectives =

- Number of fibers = up to 5. This figure was primarily deducted as representative of the basic modularity used in future subscriber network architectures (for example the initial French videocom program was built with 5 fiber distribution boxes[11]), and also considering practical possibilities concerning multipulling and cabling of fiber modules. However the concept can be adapted to slightly different figures.

- Preform size up to 35 mm (either multimode or singlemode) and continuous cable manufacture length about 20 km, in order to take into account the anticipated evolution of preforms and the needs of cable mass production. These figures can also be expected to be increased in future developments.

- Line operation speed from 50 to 100 m/min, compatible with expected possibilities of both a medium-sized pulling machine and a fast cabling process. Operation of the machine by minimal staff number in order to minimize labor costs.

- Fiber characteristics (geometrical, mechanical, transmission) complying with the usual quality level presently available for use in video-communication networks, and with CCITT recommendations.

- Special emphasis on the industrial character of the machine, which has to be suited to usual scale, conditions and environment found in a cable factory. In this respect a reasonable compromise had to be found between simplicity (in view of installation, operation and maintenance) and some necessary sophistication (in terms of automatization, quality control and yield).

- Use of elementary equipment supplied, as far as possible, by French manufacturers.

In addition to these requirements, the general design of the machine has been greatly influenced by the fact that initial experiments showed the feasability of realizing large capacity fiber accumulators able to reliably store and deliver several fiber kilometers between the pulling and cabling operations. This breakthrough opened the way to extremely favorable possibilities as regards operation flexibility of the machine, which could then be designed, on the multipulling side, as several drawing lines able to be operated to some extent independently and at different speeds.

On the cabling side the machine has been designed for realization of fiber modules or low fiber count completed cables based on the cylindrical slotted core structure. This stemmed from the solid experience gained in FRANCE and several other countries on this type of design which offers many qualities[12] = reliability, industrial manufacture mastering, excellent temperature and mechanical behaviour, modularity enabling the construction of a full range of cables[11]. The cabling process had to be adapted to the speed objective stated by means of development of fast SZ cabling technique.

It should be noted however that the choice of the V-grooved structure for the first industrial machine does not preclude possibilities of MCL concept, which can be extended to produce other types of fiber modules such as ribbons, bundles etc... bound to be used in future high density cable designs.

Finally, as will be explained when describing the corresponding equipment, the industrial development of MCL concept has led to question the usual reasonings as regards continuous fiber mechanical testing and cable quality control and to propose radically new approaches.

5. TECHNICAL REALIZATION OF THE MCL MACHINE

Based on the above mentionned principles, the first real size prototype of an industrial MCL machine is now completed and being subjected to detailed evaluation test program.

We will describe hereunder its general outlay (fig. 2) and the new range of equipment specifically developed for its realization.

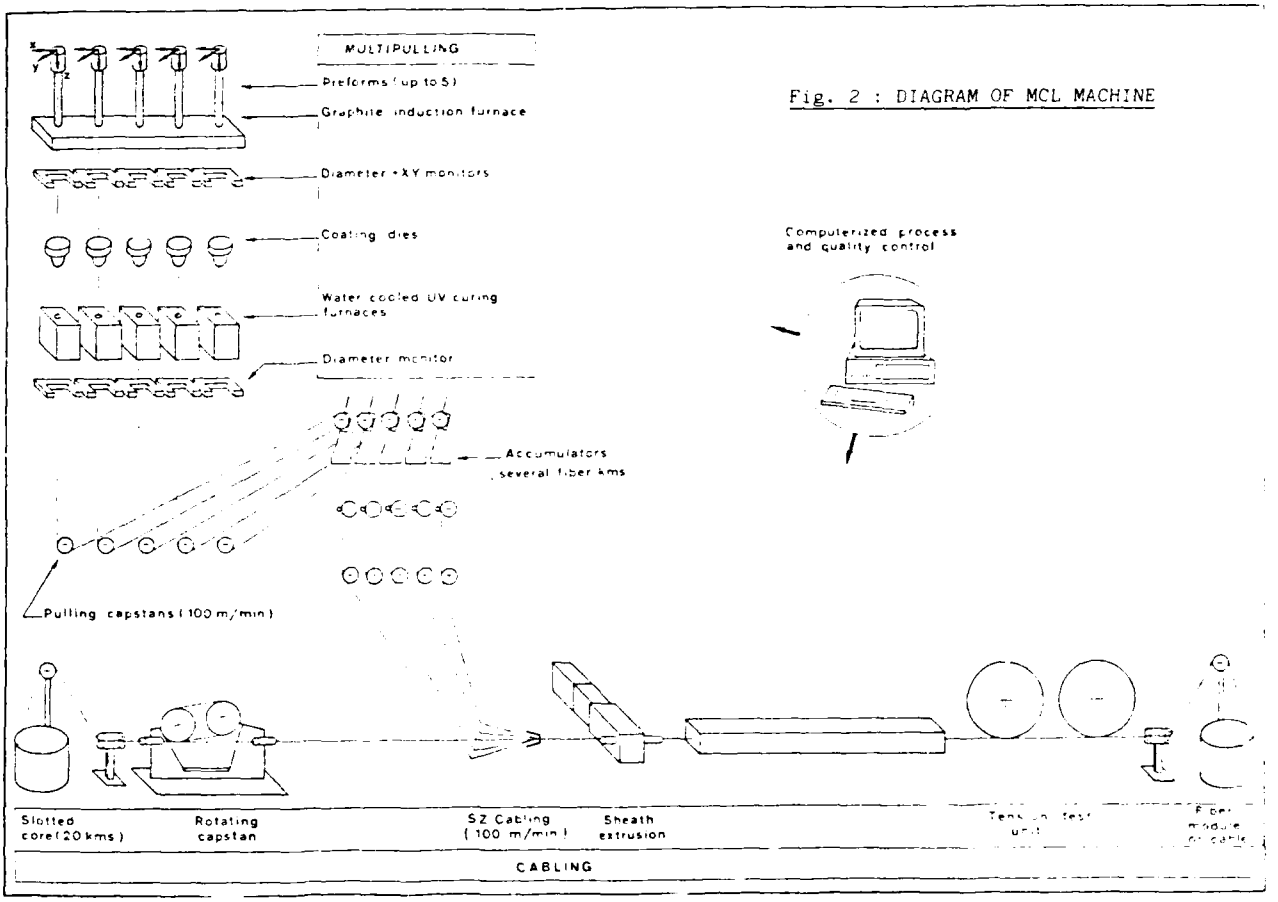

Fig. 2 : DIAGRAM OF MCL MACHINE

5.1. Multipulling tower.

Classically situated in an air conditionned clean room the tower has a frame made of steel modules bolted together (overall dimensions are height = 9 m ; floor area = 2.50x1.50 m). For start-up and possible adjustments during operation, a front lift running the full height of the tower is provided. The different equiment are mounted side by side on supports fixed onto a front vertical sliding rail (5 rails for preform feeding systems) with a 200 mm distance between axis of the 5 lines. This figure has been chosen as a result of equipment dimensions and ergonomic study of operation by one person situated in the facing lift.

The fusion furnace (fig. 3) is of graphite RF induction type. The 5 susceptors heated by 5 independently powered induction coils are situated in a common steel chamber containing necessary water cooling and argon gas circuits. Temperature is controlled by thermocouples encased in susceptor width, and can be adjusted with good precision and stability in each susceptor due to independent induction systems. However for future phases of MCL optimization a solution using a unique generator could also be considered.

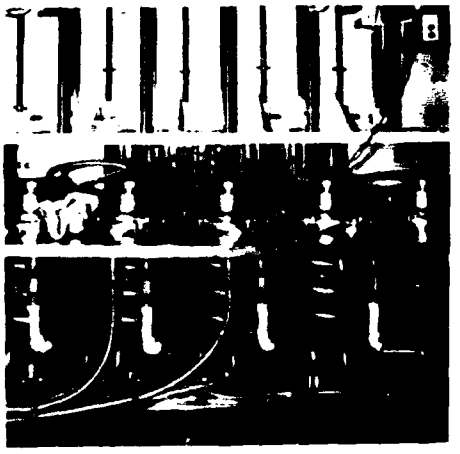

Fig. 3 : 5 cavities fusion furnace

The fiber diameter and XY position monitors are new compact and entirely static systems based on the principle of lighting the fiber along 2 perpendicular axis by LEDS and transmitting via microscopes the fiber image on photodiode detectors.
Information treatment is made by microprocessor ensuring high performance and flexibility to the system = accuracy of a few tenths of a micron ; output rate 300 Hz ; storage of measurements, statistic calculations and communication with the centralized process control system of the MCL line via analog and digital links.
A tube system for protection and helium cooling of fibers is provided.
The coating system (acrylate materials) is made classically of 2 pressurised dies per drawing line. For reasons of simplicity the 5 dies corresponding to each one of the two coating layers are fed by a common container and pressure system. However studies have been made to ensure the possibilities of pulling at different speeds, as featured by the MCL process.
The UV curing furnaces (2 per line) have been specifically developed and are characterized by water cooling, due to reasons of compactness and practical difficulties of providing in a small volume the important air flow required by 10 more conventional air cooled furnaces (fig. 4).

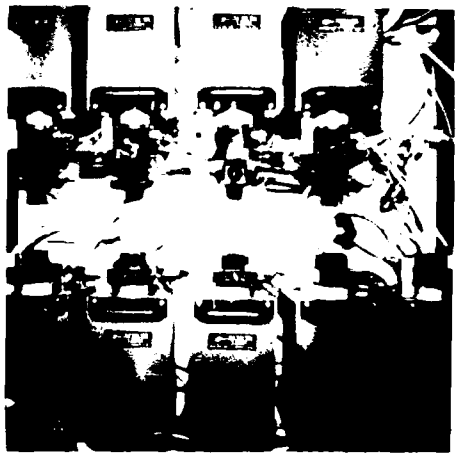

Fig. 4 : Water cooled UV curing furnaces.

At the base of the tower are situated the following equipment =
- coating diameter monitor, along one axis, based on principles similar to the fiber measurement systems ;
- pulling capstans with fiber tension control by load cell ,
- devices guiding the fibers either towards scrap containers (for start-up) or towards the accumulators, via tubes passing through the tower base.

5.2. Fiber accumulators (fig. 5)

The 5 accumulators are situated on a platform right above the insertion nozzle of the cabling machine. These innovative patented systems, which are a key element to the MCL line operation, ensure the feeding of the fiber down to a container where it is stored as overlapping coils. Due to the small weight of fiber, even in case of several kilometers storage, the smooth pulling of lower coils through the center of the container base is performed without disturbing the upper coil accumulation.

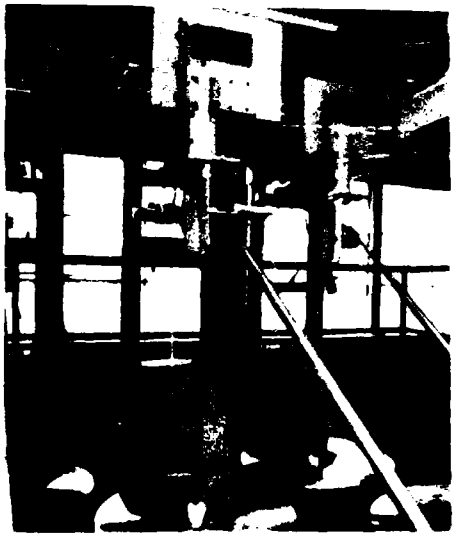

Fig. 5 : Large capacity fiber accumulators

The feeding and retrieving speeds are controlled according respectively to the pulling and cabling speeds. In normal operation these speeds are identical but the possibility to adjust them independently from a few to 100 m/min enables to solve in a very simple way the difficult problems raised by the integration in one single continuous process of the fiber drawing and cabling steps (start-up of the line ; changing of preforms or slotted core ; occurence of incidents or defects etc...). As an example, the capacity of the accumulators eases considerably the start-up sequence of the machine = after initial feeding down of the 5 preforms, the 5 lines are sequentially and independently adjusted at low speed up to the time when satisfactory fiber is present in each accumulator, when the cabling process is then started. The initial unbalance of fiber quantities stored in the accumulators can be further cancelled by pulling at variable speeds.

5.3. Cabling machine.

It is situated outside the environmentally controlled room containing the tower. Due to the speed and continuous cable length objectives not allowing use of conventional methods of cabling fibers in a cylindrical V-grooved structure (for example drum-twister), new equipment and techniques had to be developed :

- static slotted core pay-off and take-up stands, where the rod is stored in overlapping coils into containers (diameter 1600 mm x height 1000mm, accomodating more than 20 km of 4 mm diameter rod),

- rotating capstan ensuring slotted core elongation in order to provide the fiber overlength in the V-grooved structure,

- SZ insertion nozzle (fig. 6)able to efficiently and reliably operate at 100 m/min, and incorporating a device which optically detects the actual angular position of the rod with reference to its average position along the SZ pitch,

- in line compound filling and sheath extrusion

- in line cable tension testing unit prior to take up (fig. 7). Performed by means of 2 capstans, this test represents a new approach to mechanical testing of fibers and cables. Rather than providing the machine with on-line fiber screen-testing systems, whose both efficiency and significance can be questioned in an integrated production process such as MCL, the option has been taken of simulating the actual tensile stress and elongation which the fiber modules or cables as a whole are called to cope with in further stages of manufacturing, installation and operation.

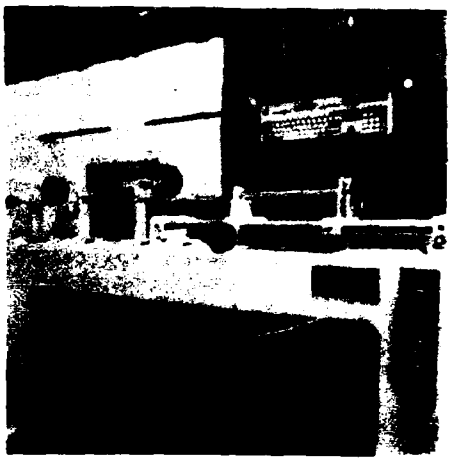

Fig. 6 : SZ cabling and computer

Fig. 7 : General view of the machine (seen from take up side)

5.4. Process control system.

The control and operation of the machine is assisted in a "user friendly" and flexible manner, by a fully computerized system built around 3 microcomputers situated respectively in the tower lift, in the tower room (priority between them being chosen depending on operational phases) and at the control desk of the cabling machine. This system performs the main following tasks :

- setting of all parameters necessary for running the machine, from either manually entered or preprogrammed data, and subsequent calculations on these parameters ;

- automatic sequencing of start-up and adjustment procedures on the different equipment and parts of the machine ;

- monitoring of the individual equipment electrical control systems, with outputs of alarms or safety commands in case of abnormal conditions ;

- monitoring and recording of quality control parameters. For each manufactured length a statistic data sheet is delivered (stating for instance diameters mean values and RMS). Furthermore, the defects detected as regards operation parameters or measurement results, together with their precise location are recorded and a mark printed onto cable sheath. This last feature is a new approach to quality control adapted to continuous and integrated process such as MCL. It enables to keep the machine running in case of localised occurence of defects, which are further eliminated in following manufacturing or conditioning stages. This is especially suitable for applications requiring supply and installation of relatively small or irregular cable lengths, as it will be the case in local networks.

6. EXPERIMENTATION AND YIELD

Due to largely independent design of the 5 pulling lines on one hand, and of the pulling and cabling machines on the other hand, enabled by the accumulators, a first representative experimental phase consisted in thoroughly testing the different equipment on a monofiber drawing tower prior to manufacturing of the complete sets and installation on the multipulling tower. In the same way the main operational conditions have been simulated. These detailed tests have proved all the equipment to be complying with the performance and industrial objectives.

As examples we can note =
- fusion furnace =
  . temperature stability better than 5°C
  . susceptor life duration of several hundred hours

- coating system = stability of coating diameter and concentricity, as well as complete curing in the whole range of speeds up to 100 m/min,

- transmission and mechanical characteristics of fibers comparable to commercially available fibers.

Besides, flexibility and reliability of fiber transportation and accumulation systems have been demonstrated on several hundred fiber kilometers at speeds varying from 20 to more than 100 m/min and accumulator filling up to 7 km.

Finally a few kilometers of cables have been produced with the cabling machine, showing results comparable to those achieved on traditional machines.

Presently a detailed program is being carried out as regards testing and assessment of the tandem zed process, with the aim of evaluating industrial yield on significant quantities of cables. In this respect it has to be emphasized that yield concept needs to be considered on a global basis.
Taking into account the practical yields of each of the pulling and cabling process, as known today, and theoretically combining them would lead to wrong and unrealistic final figures. One must rather reason in terms of global difference = total quantity of good fiber incorporated in the completed cables as compared to quantity potentially pullable in initial preforms. Due to industrial flexibility afforded by MCL design incorporating accumulators and by specific features of subscriber cable market ("low grade" fibers and short cable lengths) it is anticipated to reach high yield values making the MCL process particularly attractive. Furthermore one may even reasonably expect that the realization and performance of this first machine will prove suitable for other more stringent types of application.

7. CONCLUSION

The development of MCL concept takes place in a medium term context of preparing the ground for future subscriber/videocommunication networks which will require low cost and mass production of optical cables and justify new approaches on several technical and economical aspects.
The realization of the first industrial machine prototype has brought technical solutions to main questions raised by this innovative process integrating 2 presently separated techniques.
Evaluation phase is under way and expected to demonstrate the reliability and competitiveness of this technology which is complementary to research and development works carried out worldwide in the field of optical fibers and other components.
Prospects offered in terms of economic progress and new industrial organization will have to be thoroughly examined and deepened in view of potential returns at stake.

ACKNOWLEDGEMENTS.

We wish to gratefully acknowledge the very valuable contributions made to this project supported by FRANCE TELECOM by all members who have been participating in CNET, notably Mr. GROSSO and Mr. NOLF, and in the different companies involved.

References.

(1) R.A. LINKE = "Ultra high speed digital transmission system" Vol II p 126 ECOC 87 - HELSINKI.

(2) P.K. BACHMAN = "Dispersion flattened and dispersion shifted single mode fibers = worldwide status" vol II p 17 ECOC 86 - BARCELONA.

(3) C.R. DAY = "Recent advances in Silica-based fibers", p 387 IWCS 86 - RENO.

(4) L. LINNELL and D. SPEARS = "A broadband ISDN experimental prototype system" Vol II p 132 ECOC 87 - HELSINKI.

(5) A. WADA and al = "Fully synthesized single mode fiber fabrication by two-step VAD process using high rate cladding deposition burners" vol 1 p 159 ECOC 87 - HELSINKI.

(6) T.B. MAC CHESNEY = "Sol-gel and other fourth generation processes" vol II p 71 ECOC 87 - HELSINKI.

(7) G. LE NOANE = "Evolution of passive components for videocommunication networks" EFOC/LAN 88 - AMSTERDAM.

(8) U.C. PAEK and C.M. SCHROEDER = "Fiber drawing from 7.5 cm diameter preforms at high speed" OFC 88.

(9) H. MURATA and al = "Optical cables and connection technologies for multiservice subscriber systems" vol II p 79 ECOC 86 - BARCELONA.

(10)A. GOURONNEC and al = "Multipulling and cabling in line = a new process" p 316 IWCS 84 RENO.

(11)J.P. BOINET and al = "Fiber optic subscriber network using 85/125 fibers" p 534 IWCS 87 - ARLINGTON.

(12)G. LE NOANE and al = "Optical fiber cables using V-grooved cylindrical units = high performance cables". Fiber and integrated optics, vol 4, number 1, p 67...94, 01-1982.

Georges LE NOANE

FRANCE TELECOM
CNET LAB/OCM/FCO
Route de Tregastel
B P n° 40
22301 LANNION CEDEX
FRANCE

Georges LE NOANE, born in 1945, received his engineering degree from the Ecole Nationale Supérieure des Arts et Métiers and joined CNET in 1974. He began working on optical fiber connector techniques, then switched to cables. Since 1979, he has been responsible for the "Optical Fibers and Cables" Department at the CNET Lannion B Center.

Daniel BOSCHER

FRANCE TELECOM
CNET LAB/OCM/FCO
Route de Tregastel
B P n° 40
22301 LANNION CEDEX
FRANCE

Daniel BOSCHER, born in 1951, began working at CNET in 1973 after earning his engineering degree from the Ecole Nationale Supérieure des Arts et Métiers. Placed in charge of studies on the mechanical characteristics of circular waveguides, he was appointed in 1979 head of studies on passive components, cables, and connector/coupler systems within the "Optical Fibers and Cables" Department.

Bernard MISSOUT

Société Anonyme des
Télécommunications SAT
41 rue Cantagrel
75C31 PARIS CEDEX 13
FRANCE

Bernard MISSOUT graduated from the Ecole Nationale Supérieure des Arts et Métiers in 1971 and joined SAT in 1973. He has been in charge of special cables and associated machines development and studies, particularly optical fiber cables as deputy manager of SAT Cable Division.

Jean Louis STRIEBIG

Société Anonyme des
Télécommunications SAT
41 rue Cantagrel
75631 PARIS CEDEX 13
FRANCE

Jean Louis STRIEBIG was born in 1960. He graduated in 1982 from the Ecole Nationale Supérieure des Arts et Métiers. Since joining SAT in 1983 he worked successively for the Digital Switching Division and the Cable Division where he is presently engaged in optical fiber cables and machinery developments.

Philippe TROMBERT

Société Industrielle
de Liaisons Electriques
SILEC
B P n° 6
77871 MONTEREAU CEDEX
FRANCE

Philippe TROMBERT, born in 1949, graduated from Institut National Polytechnique de GRENOBLE in 1970. He joined SILEC in 1973 where he first held positions in the field of power cables. He was appointed in 1984 responsible for development and manufacturing of optical fiber cables.

Philippe CHERON

Société Industrielle
de Liaisons Electriques
SILEC
B P n° 6
77871 MONTEREAU CEDEX
FRANCE

Philippe CHERON, born in 1948, graduated from the Institut National des Sciences Appliquées de LYON in 1973. He joined the telecommunication cables division of SILEC in 1974 and has been engaged since 1979 in the development and manufacture of optical fiber cables.

Bernard INIZAN

Etablissements POURTIER
3 rue Gustave Eiffel
Zone Industrielle
77506 CHELLES CEDEX
FRANCE

Bernard INIZAN graduated from the Ecole Nationale Supérieure des Arts et Métiers in 1972.
Vice President and General Manager of POURTIER Co.

François GALERNE

Etablissements POURTIER
3 rue Gustave Eiffel
Zone industrielle
77506 CHELLES CEDEX
FRANCE

François GALERNE graduated from Conservatoire National des Arts et Métiers in 1968.
Technical Director of POURTIER Co., in charge of all engineering of machines for mechanics, electrics, electronics and process control.

Hydrogen Gas Effects on Installed Submarine Single-Mode Fiber Cables

W. T. Anderson, A. J. Johnson, J. P. Kilmer, and R. M. Kanen

Bell Communications Research
Morristown, NJ 07960-1910

Summary

Spectral attenuation measurements of installed submarine cables containing single-mode fibers exhibit increased attenuation due to the presence of molecular hydrogen. While the hydrogen levels are not presently high enough to impair operation of the 1310 nm systems operating on these cables, the levels are high enough to limit the future use of these cables at other wavelengths. The amounts of hydrogen observed are fairly well correlated to the average depth of the cable. Repeated measurements of one cable show that the amount of hydrogen is increasing slowly with time.

1. Introduction

Hydrogen gas increases the attenuation of optical fibers.[1,2] However, very few cases of hydrogen-induced attenuation increases for in-service cables have been reported[3,4], and these few involved high-phosphorus multimode fibers, which are known to be more susceptible to the effects of hydrogen. The use of single-mode fibers and a "proper" cable design (i.e., one which generates no hydrogen) are thought by many to be sufficient to prevent hydrogen problems based upon laboratory testing[5]. However, the effects of a corrosive and hostile environment on the materials in the cable are not easily simulated in the laboratory, and some users question whether hydrogen will present a limitation to the useful life of optical cables. Measurements of in-service cables can best answer these questions.

Two mechanisms for the generation of hydrogen have been studied extensively: chemical degradation of cable materials and the corrosion of metallic members in the cable structure. Evolution of hydrogen from cable materials can be quantified using a technique such as gas chromatography[6]. However, metallic corrosion is more difficult to test in the laboratory because the amount and nature of the corrosion depend upon the cable's environment, which is highly variable from one installation to another and difficult to characterize in general. In addition, there are several different types of corrosion that may lead to hydrogen evolution, such as galvanic corrosion of dissimilar metals, self-corrosion of galvanized steels, and biological corrosion by sulfate-reducing bacteria. Which, if any, of these corrosion mechanisms present a practical problem for installed optical cables containing metals is difficult to predict. Therefore, measurements of cables containing metals installed in hostile environments (that is, environments which are conducive to metallic corrosion) were performed to determine whether hydrogen is present in significant quantities.

One hostile environment of particular concern because of the high cost of installing and protecting the cable is the submarine environment. Submarine cables are typically used to cross rivers, lakes, and bays, which are often comprised of salt water. The possible presence of heavy marine traffic typically requires armoring the cable with one or more layers of armor wires, both for mechanical protection and to provide sufficient weight for the cable to rest securely on or in the bottom. This environment provides opportunities for all three of the above mechanisms for metallic

corrosion to take place.

The optical measurement which most conclusively identifies the presence of hydrogen is spectral attenuation. However, this measurement is not easily performed in a field environment, so a mobile test set was developed for this purpose, as will be described in the next section. Using this test set, three different submarine cables were measured. These cables are discussed in Sections 3 through 5 and are analyzed in Section 6. Finally, based upon these measurements, some conclusions are drawn and future work is suggested.

2. Spectral Attenuation Measurements

2.1 The Signature of Hydrogen

When hydrogen is generated in a cable, it diffuses readily into the glass fibers, taking approximately one week at room temperature to reach the core of a single-mode fiber. Once hydrogen is present in the glass, it may remain in a molecular state or may dissociate and chemically bond to the glass. In the molecular state, hydrogen causes a series of readily observable absorption peaks in the 1100 to 1600 nm region including one particularly strong, narrow peak at 1240 nm.[1,2] If the hydrogen chemically bonds to the glass, different absorption peaks appear, but at the relatively low temperatures encountered in the submarine environment, the extent of chemical bonding in single-mode fibers should be negligible[2].

Therefore, a spectral attenuation measurement of an installed cable to determine whether hydrogen is present should look for the characteristic molecular hydrogen absorption peaks, and especially for the pronounced peak at 1240 nm. These distinct peaks are unique to the molecular hydrogen effect and are unlikely to be confused with other loss-increasing mechanisms, such as microbending or macrobending, which have different spectral signatures. Furthermore, the height of the prominent 1240 nm peak is proportional to the partial pressure of hydrogen present so that a measurement of the height of this peak can be used to estimate the amount, or partial pressure, of hydrogen present. In principle, many of the other, smaller peaks in the 1100 to 1200 nm region could also be used for this purpose, but in practice these peaks are more difficult to measure since the fiber may support higher order modes in this wavelength region. The presence of higher order modes can lead to anomalous increases in the measured attenuation. Therefore, in this paper, all quantitative information will be derived from the 1240 nm peak. One atmosphere partial pressure of hydrogen produces an added loss at 1240 nm of approximately 7 dB/km. Using this relationship, a spectral measurement of an installed span gives both qualitative information (identification of hydrogen if present) and a quantitative measure which can be tracked over time or used to compare one cable design against another or one installation against another.

2.2 A Mobile Test Set

The measurement of the characteristic spectral signatures of hydrogen-affected installed fiber cable necessitated the construction of a field-portable, ruggedized spectral attenuation test set. Because of the urgent need to measure existing submarine cables, no major changes were made to the design of an existing laboratory system, with which the authors had several years of experience and had made numerous measurement comparisons with other laboratories. While this design does not result in a compact, easily transported system, it does give measurements which are traceable to an interlaboratory standard. One serious drawback to this expedient approach is that the launch and detect ends of the fiber must be located at the same end of the cable. This requires that two fibers be looped at the far end, and the result will be a measurement of the round-trip loss of these two concatenated fibers.

A high dynamic range (greater than 30 dB) is needed to measure 1240 nm hydrogen peak, which could be as large as several dB/km. Also, the test set must be stable over a wider range of temperatures than those encountered in the laboratory since the test set will sometimes be in

locations where there is little or no environmental control.

The details of the measurement system, which is very similar to many spectral systems in widespread usage, are as follows. The optical launch apparatus was arranged on a light weight, one by three foot optical breadboard. The light source was an optical feedback stablized tungsten-halogen lamp. Wavelength selection was provided by a grating monochromator which was driven by a stepper motor under computer control. The effect of the monochromator grating, slits, and fiber aperture is to reduce the spectral width to less than 10 nm. The launched light was chopped so that it can be synchronously detected using a lock-in amplifier. The lock-in amplifier readings are averaged for further signal-to-noise improvement. On the receive end, a 75 μm diameter pigtailed InGaAs PIN diode is coupled through the current-sensitive input of the lock-in.

In choosing a list of wavelengths to be measured, many points are desired in the 1100 to 1300 nm region where the distinctive hydrogen peaks are to be observed, and several points close to the important peak at 1240 nm are needed to fully resolve the height of the peak. However, as the number of points increases, the time required to perform the measurement also increases. As a compromise, 10 nm steps were used in the 1100 to 1300 nm region. Between 1300 and 1600 nm, step sizes of both 10 nm and 20 nm were used. The 1240 nm peak was fully resolved using 2 nm steps for one measurement of a fiber known to exhibit the hydrogen effect. This measured data was then used as a template to fit the routinely measured data, which had coarser wavelength resolution, over a wavelength range which included both the 1240 nm peak and the region near 1310 nm where there is little hydrogen effect. This fit contained three fitting parameters: a wavelength-independent attenuation (to account for differing splice and connector losses and measurement offset), a wavelength shift (to account for slight shifts in the monochromator central wavelength), and a multiplier from which the true peak height could be estimated. An example of the template and the more coarsely measured data is shown in Figure 1. The template is shown as a continuous line, while the measured data, from a different fiber measured at a different time, is shown as discrete data.

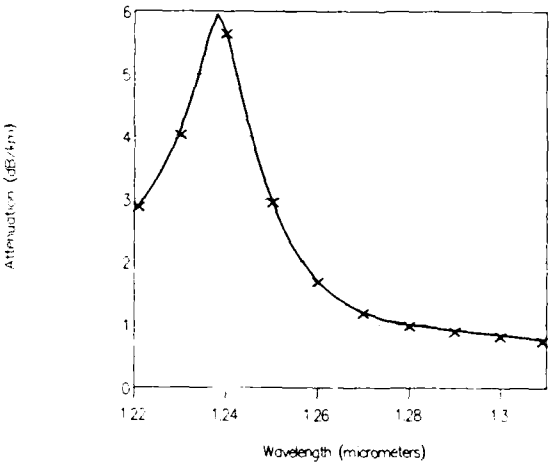

Figure 1. 1240 nm Fitting Template Applied to Measured Data

The correlation coefficient between the measured data and the template was always greater than 0.9 for all fibers, and when the 1240 nm peak was 2 dB/km or greater, the correlation always exceeded 0.99 which gives high confidence that the shape of the peak does not vary significantly from one fiber to another.

In most cases, a cutback attenuation measurement, which is destructive, was not possible. Instead, a reference measurement was obtained through a short piece of similar fiber using the attenuation by substitution, or insertion loss, technique. Care was taken in all cases to leave the launch conditions unchanged throughout both the reference and the unknown measurement. While attenuation by substitution measurements are less accurate than cutback measurements in an absolute sense, the uncertainty is limited to a "baseline" or "DC" attenuation that is approximately constant with wavelength. Therefore the spectral signature, and particularly the height of the 1240 nm peak above

the scattering baseline, can be measured with high precision.

The test set did not perform flawlessly. Since the equipment was originally intended for the well-controlled laboratory environment, it is hardly surprising that the performance of the system suffered when used in the field. For future measurements, an Optical Time Domain Reflectometer, or OTDR, with a measurement wavelength adjusted to match the 1240 nm hydrogen peak may be used. An OTDR permits not only end-to-end average estimates of the quantity of hydrogen present, but also gives a profile of the amount of hydrogen present along the length of the cable.

3. Submarine Cable Number 1

3.1 History

In the summer of 1985, two submarine optical fiber cables approximately 1.9 km long were installed across a tidal bay. The bay is fed by two rivers, which contain considerable bacterial matter emanating from several large metropolitan centers upstream. The maximum depth of this crossing is approximately 31 meters (100 feet), and the average depth is 18.3 meters (60 feet). The 1.9 km submarine cables comprise only a small part of the total 12.9 km span between central offices, with 8 km of terrestrial optical fiber cable to the east and 3 km of cable to the west.

The submarine cables each contain 100 single-mode fibers organized into ten units. The fibers are all of a conventional phosphorus-free matched-cladding single-mode design. The loose-tube units are stranded around a stainless steel central member and are surrounded by layers of aramid yarn, polyethylene, corrugated copolymer-coated high-carbon steel, and polyethylene from the inside out. To provide mechanical protection against dredging operations and other marine hazards, two layers of galvanized steel armor wires are added, and the entire structure is then covered with an asphalt jacket.

When the cables were placed in the summer of 1985, one cable was immediately placed in service while the second cable was considered a spare. 55 fibers in the service cable were spliced to 55 fiber terrestrial cables at the two manholes on either side of the submarine crossing. The spare cable was left unterminated at these manholes.

Post-construction measurements made by the cable supplier revealed anomalously high attenuation at 1550 nm for several of the fibers. While attempting to isolate the cause for this high attenuation during the following year, a gradual degradation at 1550 nm was observed. Because of the presence of dissimilar metals and bacterial matter, the telephone company was concerned that hydrogen-related problems may be responsible for this degradation. A diagnostic series of spectral attenuation measurements were initiated.

3.2 First Measurement- CO to CO

The easiest points to access on the route are the two ends- at the two central offices, or COs. At each CO, the cable was terminated in a connectorized panel, and fibers not yet placed in service could be easily connected to the test set. The test set was located at the eastern CO. A patch cord was used at the western CO to loop one test fiber onto another so that each measurement corresponded to the measurement of two fibers looped together at the far end. A reference power reading was obtained by connecting the source and detect connectorized patch cords together through a connector sleeve, and the power transmitted through the looped pair of fibers was compared to this reference level to determine the loss. The total measurement length, or twice the span length, was 25.8 km.

Connector losses were rather high, and OTDR measurements identified as much as 5 dB attenuation in the western CO where the patch cord was used to create the loop. Combined with the length of the round-trip path, this high loss connection gave total round-trip losses which approached, and occasionally exceeded, the dynamic range of the measurement system,

approximately 35 dB.

6 fiber pairs were measured, and two of these measurements which did not exceed the 35 dB dynamic range of the test set are shown in Figure 2. Three features suggest the presence of molecular hydrogen:

1. A sharp absorption peak at 1240 nm
2. A gradual loss increase above 1500 nm
3. A small absorption peak at 1590 nm

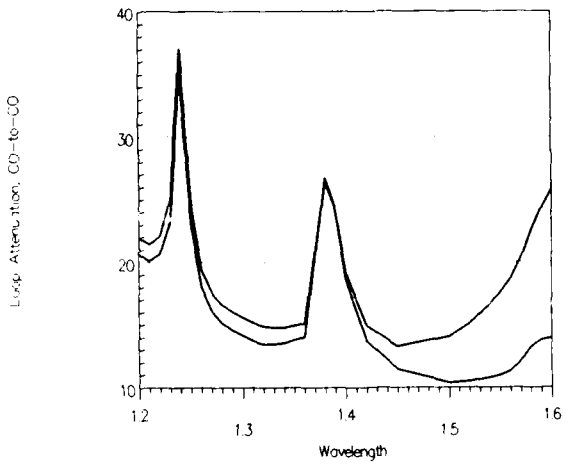

Figure 2. Spectral Attenuation Measurement- CO to CO

To better resolve these features, a second series of measurements were performed.

3.3 Second Measurement- the Spare Cable

Since the submarine cable represents only a small portion of the total span, the spare cable, which was not spliced to the terrestrial cables on either end, was measured. Accessing the spare cable was much more difficult since it was not terminated in a central office but rather was left unterminated in the manholes on either side of the submarine section. A splicing trailer, which provides some environmental control and a clean work environment, was provided by the telephone company at the manhole on the western end of the submarine section, and loop-back splices were performed on the eastern end of the spare cable. Two fibers in each unit were spliced together at the eastern end so that 10 fibers were available for measurement. Since the round-trip length is now only 3.8 km, the attenuation did not approach the dynamic range of the test set. Nine fiber loops were actually measured (the tenth had a high loss splice at the far end). The mean and the standard deviation of the nine spectral measurements are plotted in Figure 3.

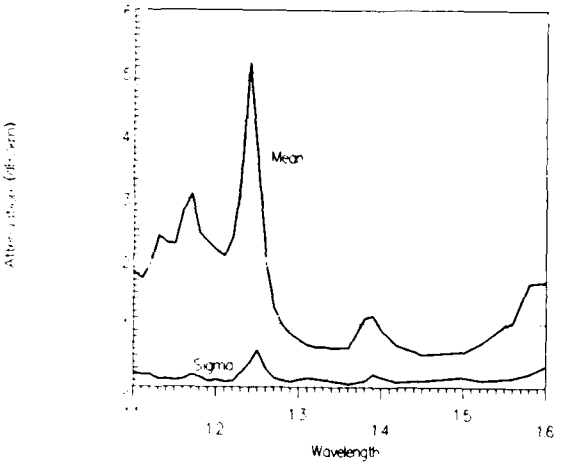

Figure 3. Spectral Attenuation Statistics- Spare Cable

3.4 Interpretation of the Measurement Data

The initial measurement of the entire span clearly showed a 1240 nm attenuation peak which is characteristic of molecular hydrogen. From Figure 2, the peak is estimated to be approximately 20 dB above the scattering loss. If this added attenuation is attributable exclusively to the 3.8 km submarine section (1.9 km, two passes), then the 1240 nm added loss in the submarine section is approximately 5 dB/km. Since one atmosphere of hydrogen produces approximately 7 dB/km added loss at 1240 nm, 0.7 atmospheres of hydrogen on average across the submarine section would be needed to produce the observed loss increases.

The measurements made on the spare cable gave better resolution of the many hydrogen peaks in

the 1100 to 1300 nm region and clearly demonstrated that hydrogen was present. Furthermore, the spare cable measurements more accurately resolved the 1240 nm peak. These measurements will be further analyzed in the next section.

These results were quite disturbing. A submarine cable, only two years old, has clearly degraded due to the presence of molecular hydrogen. While service had not yet been affected, it would be affected if the hydrogen levels increase significantly, and the significant loss increases at the longer wavelengths near 1550 nm may limit or preclude the future use of the cable in that wavelength region. To determine the rate at which the cable is degrading, repeated measurements of the cable were performed over the following year. These results are reported in the next two sections. Also, a theoretical worst-case value can be computed.

The cable structure cannot withstand pressurization, and the core of the cable is comprised of essentially incompressible materials (plastics and gel filling). Also, the filling materials do not readily flow. Therefore, the pressure in the cable core, including the space around the fiber, is the same as that of the surrounding water. The worst-case loss increase can be calculated from total pressure around the fiber, which can be found from the average depth of the cable, 18.3 meters. At this depth, there are 2.8 atmospheres of pressure on the cable. This pressure is the upper limit of the partial pressure of hydrogen. With 2.8 atmospheres of hydrogen present and in the absence of chemical bonding, the attenuation increases would be approximately 2.0 dB/km at 1270 nm, 0.8 dB/km at 1290 nm, 0.6 dB/km at 1310 nm, 1.4 dB/km at 1550 nm, and 2.2 dB/km at 1570 nm. These estimates are based upon the added loss due to molecular hydrogen presented in Reference 4.

8.5 Repeated Measurements of the Spare Cable-Time Dependence

To test for the time dependence of the loss increase, the spectral attenuation measurements of the spare cable were repeated three times- in October 1987, in May 1988, and in August 1988. The same test set was used, and the same nine fiber loops were measured in all four cases. All fibers measured clearly demonstrated the presence of molecular hydrogen, and the levels of hydrogen were slightly higher for each successive measurement.

To better analyze these measurements, a hydrogen indicator was calculated. This indicator was computed from the fitted 1240 nm attenuation peak, found by fitting the previously measured template to the measurement data and subtracting the baseline scattering, which is assumed to be of the form $a\,\lambda^{-4} + b$.

The hydrogen indicator computed for the four measurements of the spare cable are summarized statistically in Figure 4.

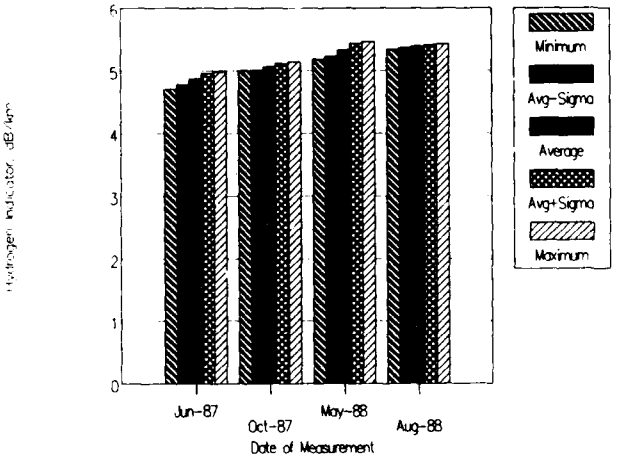

Figure 4. Summary of Four Measurements of Submarine Cable Number 1

The observed time dependence is well described by a power law fitting function with a zero intercept of the form $a\ time^{z}$ (since the hydrogen effect was assumed to be absent prior to installation), and an

exponent x c. 0.24 gave a correlation coefficient of 0.99. The average hydrogen indicator and the power law fit are plotted in Figure 5.

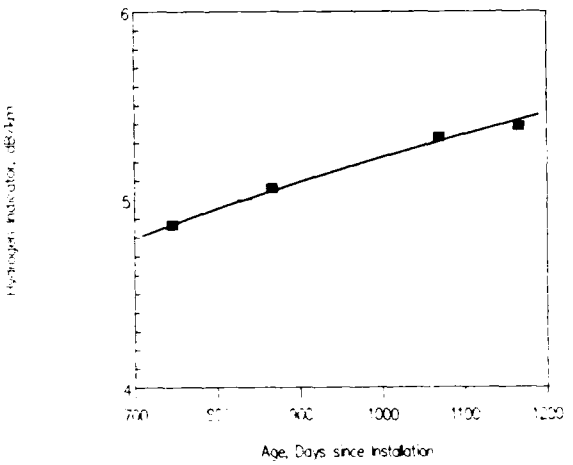

Figure 5. Time Dependence of the Hydrogen Indicator

Based upon these measurements, taken over a 14 month period, the hydrogen effect appears to be worsening slowly. Since the mechanism of hydrogen generation is not known, extrapolating this time dependence is risky, and the rate of hydrogen generation could either increase or decrease. However, it appears safe to conclude that, while hydrogen may limit the use of the cable both at longer wavelengths and for multichannel wavelength division multiplexing around 1300 nm, hydrogen does not pose an immediate threat to the operation of the 1310 nm systems presently in use on this cable.

4. Submarine Cable Number 2

Because of the presence of hydrogen detected in the first cable, other cable installations with a similar cable design and environment were chosen for measurement so that the effect of cable and fiber design and environment could be studied. The second installation was similar to the first installation, reported in the previous section, except that the depth was less but the distance was longer. Since this cable was located farther up a river from the ocean than the first cable, the salinity of the water was somewhat lower. The route depth varied from only one meter at one end to the maximum depth of 14 meters at the other end. This installation consists of two separate cables, each each containing 48 fibers, and the two cables follow a somewhat different route along the bottom, which accounts for the differing cable lengths- 6 and 6.5 km. The average depth of the two cables is approximately 4 meters.

The cable design was similar to that described in the first case except that the central member was dielectric rather than steel, and the cable was manufactured by a different cabler. The fiber used in this cable was of the same design as that used in the first cable- a matched cladding, phosphorus-free single-mode design.

The cables were accessed at a central office near one end of the submarine section. Relatively short terrestrial cables were used between the submarine cable and the central offices, so in this case an office-to-office measurement was appropriate since most of the measured loss was that in the submarine section. Twelve unused fibers within each cable were looped at the other central office near the opposite end of the submarine section to give six fiber loops in each cable. Access to the fiber was obtained at a patch panel using connectors on both ends.

The mean and standard deviation of the measurements made for these two cables are plotted in Figures 6 and 7. In spite of the fact that these two cables follow nearly identical routes and are identical in construction, the height of the 1240 nm hydrogen peak is significantly different in the two. The reason for this difference is not known. Since the two cables behaved significantly differently, they are plotted separately and will be analyzed separately.

These spectral attenuation measurements again clearly demonstrate the effects of hydrogen, although the magnitude of the attenuation increase is smaller in this installation. Further analysis will be performed later in this paper.

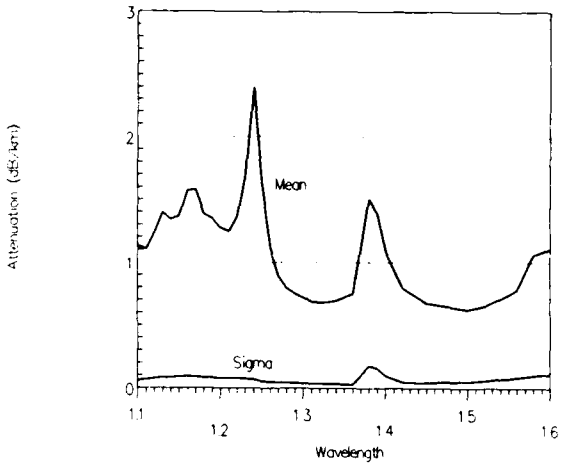

Figure 6. Measurement of Second Installation, First Cable

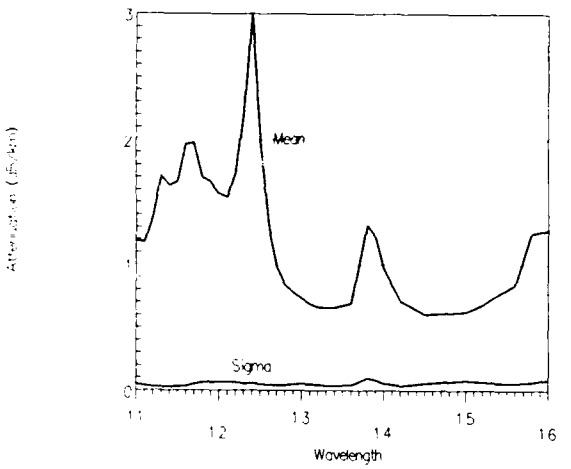

Figure 7. Measurement of Second Installation, Second Cable

5. Submarine Cable Number 3

A shorter and shallower installation using a different cable structure and fiber design was investigated. In this cable, a cable structure with steel wires in the sheath was used, and galvanized armor wires were applied over this sheath as in the other two cases. The fiber was a depressed-cladding design with a small amount of phosphorus in the cladding. The crossing was 1.4 km long with an average depth of approximately 8.5 meters. The cable was accessed at a manhole near one end of the submarine section, and fibers were spliced at the manhole on the other end of the submarine section to form twelve fiber loops. Measurements were again made in a splicing trailer.

The mean and standard deviation of the measurements on the 10 fibers are plotted in Figure 8.

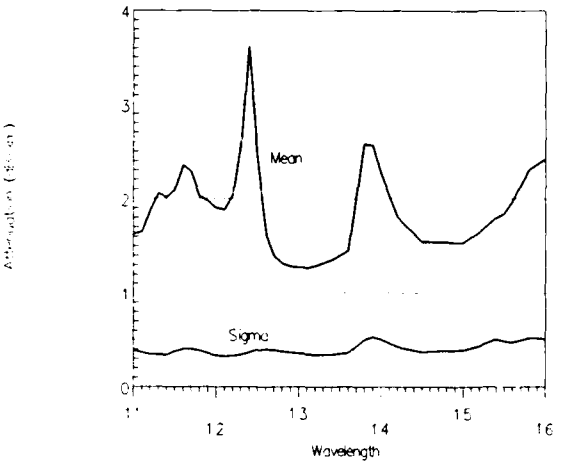

Figure 8. Spectral Attenuation Measurements-Third Installation

The spectral attenuation measurements again show the effects of molecular hydrogen. Other differences from the first two installations are apparent, such as an anomalous loss at long wavelengths, probably attributable to bend loss in splice cases or microbending. The measurements also are noisier, which is a result of the relatively short length of the cable. However, these features of the spectral attenuation are probably not hydrogen-related. All three installations will be analyzed further in the following section.

6. Comparison of the Three Cables

6.1 General Characteristics

Perhaps the most striking feature of the measurements made on the three submarine cables is their similarity. Even though the cable

structures were significantly different, the fibers were of different designs, and the environment in which the cables were laid was somewhat different, the unmistakable presence of molecular hydrogen is clear in all three cables. With these similarities in mind, common factors in the three installations should be considered.

First, all three cables were armored with layers of galvanized steel wires. These armor wires are the only metallic members common in all three designs. Also, a sample of a similar submarine cable which had been in operation for two years was physically examined, and the galvanized armor wires appeared to be significantly corroded. Second, all three cables were placed in a salt water environment, so galvanic corrosion is a possible source of hydrogen. Third, all three cables were buried in a soft bottom to provide additional protection from shipping and dredging operations. This would tend to reduce the rate of galvanic corrosion, which would be more pronounced if the cables were in free flowing water, but burial also ensures that the cables are in an anaerobic environment, which would permit sulfate-reducing bacteria to grow. Such bacteria can act on metals and generate hydrogen.

Telephone company engineers have reported to the authors that similar installations in fresh water have not shown increased attenuation at 1550 nm, while all three of these installations and several others in salt water have shown attenuation increases at this wavelength. This may indicate that salt water is a necessary ingredient for the generation of hydrogen by these and similar cables. Also, a restoration cable, identical in design to the cables used in the installation for which measurements were reported in section 3, has not yet been installed. Measurements of this cable by telephone company engineers show that there is no degradation, which would seem to rule out one of the possible mechanisms for hydrogen generation- the chemical degradation of cable materials- in favor of corrosion. However, with the information currently available, neither galvanic nor bacterial corrosion can be ruled out, and additional laboratory work and field measurements are planned.

6.2 Dependence upon Depth

The depth of these three installations appears to be an important factor in determining the amount of loss increase. The depth dependence is summarized in Figure 9. The two cables of the second installation are plotted separately. Two curves are plotted with the data. The first is a simple linear fit to the average hydrogen indicator, which appears to describe the depth dependence reasonably well. The second curve represents 25% of the computed worst-case hydrogen indicator as a function of depth, which bounds the observations.

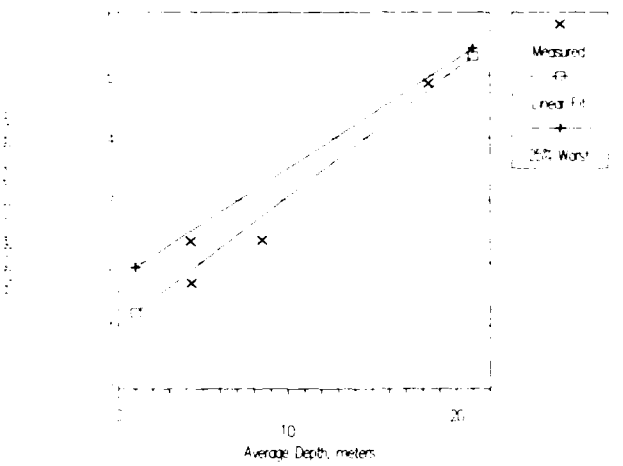

Figure 9. Dependence of Hydrogen Indicator on Depth

It is interesting to note that both of these two curves have a non-zero intercept at zero depth, which implies that cables at the surface could also be slightly affected by hydrogen if they are of similar construction (i.e., contain galvanized armor wires) and have a similar environment (i.e., anaerobic and saline). However, terrestrial cables are not typically armored, and no cases of hydrogen effects on terrestrial cables containing single-mode fibers have been identified.

7. Conclusions

A reasonable conclusion suggested by this work is that submarine cables constructed similarly to those described in this paper and installed in similar environments are likely to show attenuation increases attributable to hydrogen. For engineering purposes, the following worst-case increases should be considered when engineering submarine cables. Using the average depth d in meters and an underwater length L in kilometers, the maximum attenuation increase is given by

$$0.3\ L \left(\frac{d}{10} + 1 \right) \text{ dB in the 1300 nm region}$$

$$0.8\ L \left(\frac{d}{10} + 1 \right) \text{ dB in the 1550 nm region}$$

where the 1300 nm region is interpreted to mean 1290 to 1330 nm, and the 1550 region is interpreted to mean 1530 to 1570 nm. Attenuation increases of approximately 25% of the values computed above are expected to be reached within the first two years of operation.

For short or shallow installations, the worst-case attenuation increases computed above may be acceptable, and hydrogen-related loss increases at 1310 and 1550 nm may not present problems to operating systems. For the majority of cables of this construction, which are used for river and bay crossings which are usually short and/or shallow, hydrogen will probably not limit the life of the cable. However, for deep and long submarine installations, where the effects of hydrogen could be catastrophic, special precautions should be considered. These include all-dielectric cable constructions, to avoid corrosion; hermetic fiber coatings, to delay hydrogen entry into the glass; soldered, welded, or corrosion-resistant cable sheaths, to prevent the entry of water and hydrogen into the cable core; and hydrogen-absorbing filling and flooding materials. Investigations of the effectiveness of these precautions are continuing.

References

[1] K. Noguchi, Y. Murakami, and K, Ishihara, "Infrared Loss Spectrum of Hydrogen Molecules in a Silica Fiber," *Electronics Letters*, Vol. 19, No. 24, P. 1045, November 24, 1983.

[2] J. D. Rush, K. J. Beales, D. M. Cooper, W. J. Duncan, and N. H. Rabone, "Hydrogen Related Degradation in Optical Fibers-Implications and Practical Solutions," *Br. Telecom Technol. J.*, Vol. 2, No. 4, p. 84, September 1984.

[3] S. Hornung, S. A. Cassidy, and M. H. Reeve, "The Distribution of H_2 Gas Along an Inland Optical Fiber Cable," Technical Digest of the Symposium on Optical Fiber Measurements, 1984, NBS Special Publication 683.

[4] O. I. Szentesi, "Reliability of Optical Fibers, Cables, and Splices," *IEEE Journal on Selected Areas of Communications*, Vol. SAC-4, No. 9, p. 1502, December 1986.

[5] E. W. Mies, D. L. Philen, W. D. Reents, and D. A. Meade, "Hydrogen Susceptibility Studies Pertaining to Optical Fiber Cables," OFC'84, Postdeadline Paper WI3, January 23-25, 1984.

[6] I. Plitz and P. C. Warren, "Evaluation of Hydrogen Generation from Optical Fiber Cable," Proceedings of the 36th International Wire and Cable Symposium, p. 616, November 1987.

Authors

William T. Anderson was born in Buckhannon, West Virginia, in 1948. The received the B.S.E.E degree with Highest Honors from Georgia Institute of Technology in 1970, the M.S. degree in Electrical Engineering from Stanford University in 1971, and the Ph.D. degree in Electrical Engineering from Georgia Institute of Technology in 1979. He worked at Bell Telephone Laboratories from 1970 to 1983 in the areas of transmission and crosstalk in multipair cable and single-mode fiber measurement and design. In 1983, he joined Bell Communications Research, and is presently responsible for optical cable requirements and analysis. Dr. Anderson is a member of the Optical Society of America.

Aaron J. Johnson was born in Washington, DC, in 1958. He received the B.S. degree in Electrical Engineering and Economics from Carnegie-Mellon University in 1980 and the M.S. degree in Electrical Engineering from Georgia Institute of Technology in 1981. He worked for IIT Research Institute from 1982 to 1984, where he was engaged in electromagnetic compatibility analysis. Since 1984, he has been with Bell Communications Research where he has been developing novel optical fiber measurements and writing generic requirements for optical fibers and optical fiber cables. Mr. Johnson is a member of the Optical Society of America.

Joyce Kilmer was born in Pittsburgh, Pennsylvania, in 1958. He worked at the Noise Research Laboratory in the Electrical Engineering Department of the University of Florida for four years studying $1/f$ noise in solid-state devices before receiving the Ph.D. degree in Electrical Engineering in 1984. He joined Bell Communications Research in 1984 as the optical requirements engineer of the optical cables district. Since then, he has been involved in developing criteria and measurement methods for optical fibers and for optical fiber systems. Dr. Kilmer is a member of the Optical Society of America.

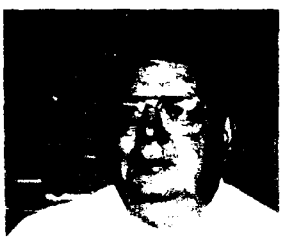

Robert M. Kanen was born in 1929. Prior to joining Bell Communications Research in 1986, he worked in the electronics technology area for 32

years for a number of companies, including ITT-Federal Electric, HRP-Singer, and R. H. Wagner, and served in Naval Electronics for 4 years. He has attended Champlain College and Worcester Polytechnic Institute. At Bellcore, he is responsible for operating and maintaining optical fiber and cable laboratory facilities and for the development and construction of optical test sets.

LIGHTNING DAMAGE SUSCEPTIBILITY OF FIBER OPTIC CABLES

Richard E. Clinage

Siecor Corporation
Hickory, North Carolina

ABSTRACT

One of the main reliability concerns today among Telco's is the optical cable's ability to withstand a lightning stroke. This paper presents a practical outlook on the lightning damage susceptibility of today's most common optical cable designs. The objective of this study was, if possible, to establish upper limits of performance for these designs. Hopefully, these results will give users valuable insight as to the long-term reliability aspects of installed cables and fiber optic systems. Conclusions are that dielectric cores and longitudinally applied (corrugated) copolymer coated steel armoring provide the optimum protection against lightning damage. Of those cables tested, double armored designs suffered less outer sheath damage than single armored designs. Results show that proper design and selection of materials provide alternatives to all-dielectric core designs. For the first time, results of testing performed to Bellcore TR-20 requirements at current levels as high as 229 kA are discussed.

BACKGROUND

Concerns began in the communications industry when statistics showed that many system breakdowns were due to lightning damage. In the copper world, cables suffered pair to pair and pair to ground faults. These electrical installations also contained very sensitive solid-state devices which were vulnerable to even low levels of surge current caused by lightning. The introduction of fiber optic cables has relieved some of these concerns; however, manufacturers have been unable to take full advantage of their all-dielectric nature. Faced with a lack of alternatives, fiber optic cable manufacturers often utilize metallic components to provide for low cost strength elements or optimum mechanical/rodent protection. As with copper cables, lightning is attracted to metal components because of their effective ground potential.

Cable lightning damage was originally expected to occur only in aerial cable installations; however, it was soon recognized that buried applications were not completely immune from lightning's harmful effects. In principle, lightning arcs to buried cable when the resistance of the soil is greater than the resistance of the cable system. The potential for lightning damage is expected to increase as the number of lightning strokes, the duration of the stroke, stroke current and soil resistivity increase.[1]

No decisive studies exist, to date, relating the depth at which the underground cables are placed and the resultant lightning protection. In fact, very few proven methods exist to prevent lightning discharges to buried objects. Predicting such occurrences is even more difficult. The effective cost of protection must always be considered relative to the risk of service loss, the frequency and severity of expected lightning discharges. In those instances where "more" lightning protection is required, options are direct burial of all-dielectric designs, installation of cables in concrete, steel or plastic ducts, or placement of shield wires above armored buried cables.

The single most important lightning parameter is the level of current discharged during a stroke. Most lightning discharges range from a few hundred amperes in strength up to several hundred thousand amperes (kA); however, in most buried environments the recorded occurrence for lightning strokes greater than 100 kA is too rare to be of any practical importance.[2]

The average lightning stroke is between 30 and 40 kA. Ninety-five percent (95%) of all lightning strokes occur at less than 100kA (Figure 1).[3,4,5]

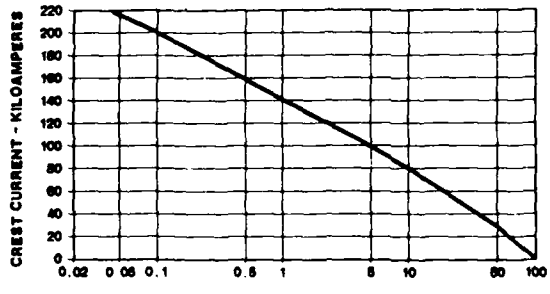

Distribution of Lightning Stroke Crest Currents to Buried Structures

Figure 1

A map of the most susceptible lightning areas across the United States is in Figure 2.[6,7]

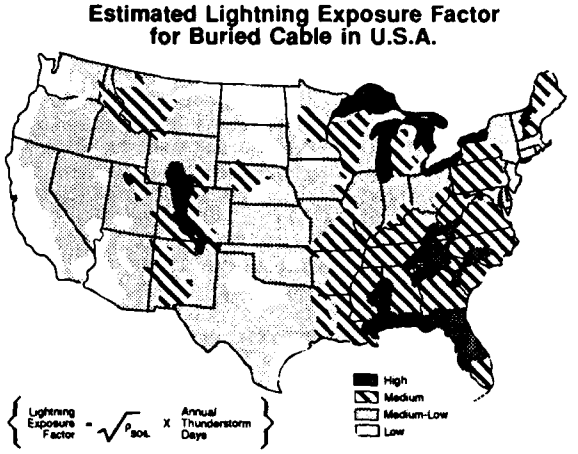

Figure 2

Based on this low percentage of lightning occurrences above 100 kA and the uncertainty of these strokes arcing to buried cables, the Bellcore established 105 kA performance requirement appears to be a very practical limit to characterize cable lightning damage susceptibility.

HISTORY OF CABLE LIGHTNING TESTING

For many years, numerous studies have been performed in an attempt to understand the fundamental behavior of lightning. To date, three methods have been developed to evaluate the performance of cable in buried environments. They are the magnetic crush test, the longitudinal current test and the arc discharge or "sand box" test.[8]

A review of the principles of these three tests yields two basic scenarios. Lightning damage occurs due to either a direct strike or by a strike in the vicinity of an object. Previous studies have shown that crushing and burning of buried cables can result from magnetic field effects caused by lightning. The magnetic crush test simulates a lightning strike in the vicinity of a cable, not a direct strike. The degree of physical damage to the cable is a function of the electrical and circumferential conductivity of the sheath and crush resistance of the cable core design. The higher the conductivity of the shield or armoring, the greater the crushing effects. The longitudinal current test simulates the ability of a cable (with metallic components) to withstand very high levels of surge current. The cable's ability to quickly dissipate this current following a lightning strike helps to minimize the damage caused by further arcing, burning or charring.[9] The arc discharge or "sand box" test simulates a direct lightning strike to buried cables. Both the cables' ability to withstand extremely high crushing forces and carry high levels of surge current are evaluated in this test. Although there is still much discussion as to the accuracy of these tests and how they relate to the real world, there has been a consensus in the cable industry that the proposed sand box test is the most difficult test to pass with even today's best cable designs. Based on this fact, the sand box test was chosen for our evaluation.

The sand box test was originally developed by Bell Laboratories in the 1960's. Since then, variations of this test have used different box sizes and cable grounding methods. Studies have shown that the only difference in results of these tests is dependent on the location of the cable ground. Typical placement of the ground is either inside[10,11,12] (in direct contact with the wet sand) or outside of the test box. Tests performed where the ground is located inside the box allow for some portion of the current to bypass the cable by flowing through the wet sand to ground. Results where cables were tested with the ground electrode inside the box show less damage than when the electrode is located outside of the test box. No significant difference in test results can be correlated to the size of the test box alone. Current Bellcore requirements and proposals for an EIA test method require cables to be grounded outside of the test box.

THE EXPERIMENT

The most common concerns today in buried cable environments are both lightning and mechanical/rodent protection. Field results have shown that the best rodent protection is provided by a steel tape armored cable design. Maximum mechanical and rodent protection is achieved by using a double steel tape armored cable design. Single jacketed all- dielectric "duct style" cables are usually not considered for direct buried applications because of their generally lower mechanical performance characteristics and vulnerability to attack by rodents.

The objective of this study was to evaluate currently available buried cable sheath constructions, and if possible, establish upper limits (maximum current levels) for their practical use. Today's most popular fiber optic cable sheath designs for direct buried applications are the cross ply with steel/copper armoring, the double jacket (polyethylene)/single steel tape armored, and the triple jacketed/double steel tape armored designs.

Previous lightning studies have been performed on all of the above listed cable types.[13,14,15,16] Maximum current discharge levels ranged from 50 kA to 145 kA. These results indicate that for lightning current levels above 110 kA, only dielectric core double jacketed steel armored and triple jacketed double steel armored cable designs prevent significant damage to the cable core. Based on this performance, these designs were selected for our study, Figures 3 and 4.

Siecor Single Armored Mini-Bundle Cable

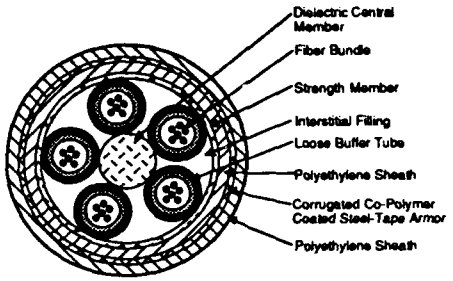

Note: This illustration is Not to Scale

Figure 3

Siecor Double Armored Mini-Bundle Cable

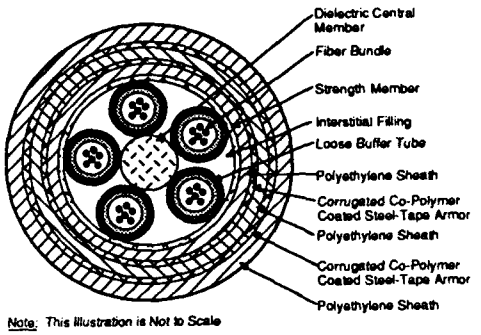

Note: This illustration is Not to Scale

Figure 4

The testing was performed at an independent laboratory capable of testing to currents in excess of 110 kA. A schematic of the test apparatus is in Figure 5.

Arc Discharge "Sand Box" Test

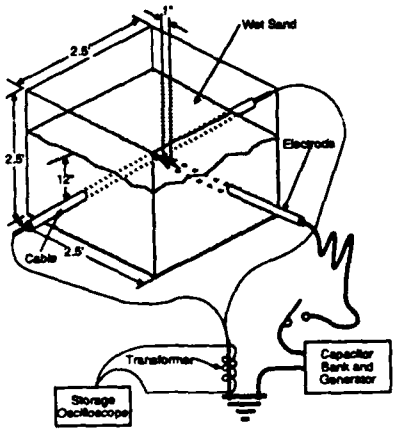

Figure 5

The Bellcore procedure and failure criteria for the sand box test were used to evaluate cable performance.[17] As specified, the test box was approximately 2.5 ft. (.76 m) square and was filled with 20 to 40 mesh wet sand. The depth of the electrode within the box, was approximately 12 inches (30 cm). The cable specimens were 3.5 ft. (1 m) in length. Both ends of each specimen were stripped back and all metallic components of the cable were electrically shorted to ground. The cables were placed horizontally within the box such that the end of the electrode (within the box) was approximately 1 inch from the cable sheath. A small pinhole was burned in the sheath to ensure that the arcing occurred at the point directly facing the electrode. A total of 14 tests were performed. Current levels ranged from 70 kA to 229 kA. The specific current levels and waveform data are listed in Table 1.

As noted, slight variations from the required time to half values were experienced and are attributed to the difficulty of controlling the water level within the sand. Deviations from Bellcore requirements were permitted only if the required crushing damage was obtained, as specified.

Single Armored Designs

Current (kA)	Frequency (kHz)	Time to Half Values (μs)
70	19.2	30
88	19.2	36
115	19.2	30
121	19.4	36
150	20.0	48
155	20.0	51
185	16.5	46
229	18.0	41

Double Armored Designs

Current (kA)	Frequency (kHz)	Time to Half Values (μs)
72	19.5	27
96	18.2	42
112	19.5	42
130	18.9	43
136	18.9	44
226	17.0	60

TABLE 1

RESULTS

Both single armored and double armored cable designs significantly exceeded the maximum Bellcore requirement of 105 kA for lightning damage susceptibility. Throughout all of the testing, 100% of the fibers remained continuous. As reported in previous studies, the damage mechanisms appeared to be a combination of minor crushing, charring, melting of the jacket, and vaporizing of the steel armor. These results are consistent with the informal surveys obtained from other researchers, cable maintenance crews and field damage reports.

SUMMARY OF LIGHTNING TEST RESULTS

Single Armored Designs

Current Levels	Results
70 kA	Minor abrasions to inner jacket, no fiber/core damage
115 kA	Minor abrasions to inner jacket, no fiber/core damage
150 kA	Slight melting and abrasions to inner jacket, no fiber/core damage
185 kA	Slight melting and pinhole in inner jacket, no fiber/core damage
229 kA	Abrasions and holes melted in inner jacket, no fiber/core damage

Double Armored Designs

Current Levels	Results
72 kA	No inner jacket damage, no fiber/core damage
112 kA	No inner jacket damage, no fiber/core damage
136 kA	Minor abrasions to inner jacket, no fiber/core damage
226 kA	Minor abrasions to inner jacket, no fiber/core damage

TABLE 2

Closer examination of the cable samples revealed that the damage was concentrated to the point where the current's energy was transferred to the steel armor. No physical damage, melting, or burning occurred away from this point. Surface damage to both the Siecor single and double armored sheath designs was the same for similar current levels. Also as expected, the damage to both designs became slightly worse as the current levels were increased.

For each sample tested, every layer of outer sheath (polyethylene jacket and armor) was removed and photographed following the strike. No significant damage occurred to the inner sheath or core on single or double armored cables tested up to 115 kA. Only the outer jackets and armor were penetrated on both the single and double armored sheath designs at current levels as high as 150 kA. At higher current levels, 229 kA, only minor damage occurred to the inner jacket on the single armored design. In all cases, the double armored design suffered less damage than the single armored design. None of the samples tested exhibited any significant damage to the cable core. Testing did not exceed 229 kA due to equipment limitations.

Justifiably, questions exist about the lightning damage performance of cables that employ more than one metallic element (for example, steel armor/steel central member or steel wire type armored cable constructions.[18]) In order to address these concerns and establish a formal baseline for further studies, a Siecor steel armored steel central member design, Figure 6, and a steel armored twisted pair design, Figure 7, were tested to the maximum Bellcore performance requirements. Results show only minor inner jacket abrasions and no core damage on cables tested at current levels as high as 112 kA. All designs tested performed equally well in comparison to their all-dielectric core counterparts. Based on the performance seen in these tests, we expect Siecor designs to withstand significantly higher levels of lightning discharge current. Double armored designs are expected to perform better than single armored designs.

Siecor Single Armored Mini-Bundle Cable with Steel Central Member

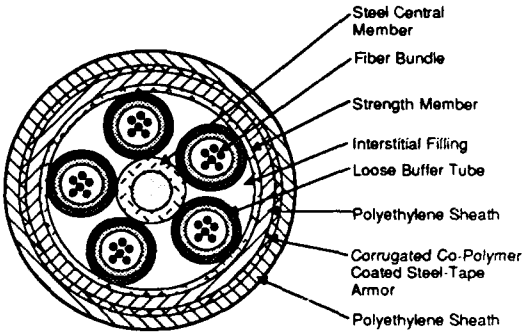

Note: This Illustration is Not to Scale

Figure 6

Siecor Single Armored Mini-Bundle Cable with Twisted Pair

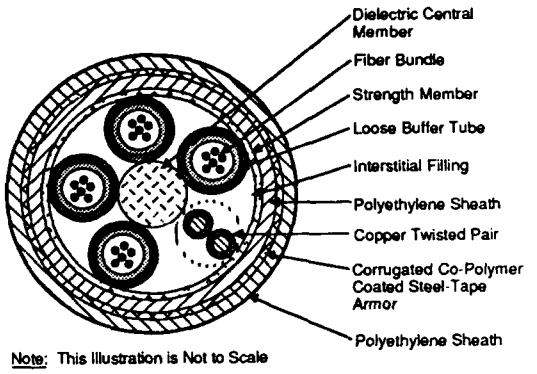

Note: This Illustration is Not to Scale

Figure 7

Most lightning studies have concentrated on the performance of outer cable sheath designs. Cables with longitudinally applied copolymer coated steel armor have consistently shown superior lightning performance to other sheath/armor options in all types of lightning test evaluations. As shown by our results, the dominant damage mechanisms of lightning strikes are both severe mechanical crushing and thermal effects. It is our belief that the crush resistance and thermal properties of the core materials are as important as the sheath design in providing cable lightning damage protection. Consequently, cable lightning performance can be improved by the selection of more crush resistant, higher temperature core materials.

CONCLUSIONS

Benefits of these results to the user are significant. It has been shown that many kilometers of currently installed Siecor single and double armored cable designs perform well in excess of the Bellcore TR-20 requirements. Furthermore, based on the superior performance of the double armored design, we expect Siecor double armored, triple jacket designs to perform well in excess of 230 kA without sustaining significant damage to the cable core. Under no circumstances did the current levels tested in this study induce cable damage that would cause system failure.

Major concerns in buried cable applications are lightning and mechanical/rodent protection. Given this, the results of this study show that Siecor double armored cable provides the optimum lightning and rodent protection for buried applications.

References

[1]H. M. Trueblood and E.D. Sunde, "Lightning Current Observations in Buried Cable," Bell System Technical Journal, 1948, pp. 278-302.

[2]The International Telegraph and Telephone Consultative Committee, "The Protection of Telecommunication Lines and Equipment Against Lightning Discharges," The International Telecommunication Union, 1974.

[3]David W. Bodie, Axel J. Ghazi, Moinuddin Syed, Ralph L. Woodside, "Characterization of the Electrical Environment," University of Toronto Press.

[4]N. Cianos and E. T. Pierce, "A Ground-Lightning Environment for Engineering Usage," Stanford Research Institute, August 1972.

[5]G. Sharick, "Grounding and Bonding," ABCs of Telephony," Volume 13, pp. 31-39.

[6]"Telecommunication Electrical Protection," Appendix 21, pp. 9, AT&T Technologies, Inc., 1985.

[7]REA Telephone Engineering and Construction Manual #801, Issue 4, Oct. '72, pp 10.

[8]K. E. Bow, Dow Chemical, Unpublished Work, 1986.

[9]D.A. Douglass, "Lightning Induced Current Surges on a Buried Multicoaxial Cable System," International Wire and Cable Symposium Proceedings 1971, pp. 293-308.

[10]W. C. L. Weinraub. D.D. Davis, M. D. Kinard, "A Rodent and Lightning Protective Sheath for Fiber Optic Cables," International Wire and Cable Symposium Proceedings 1983, pp. 243-249.

[11]M.R. Reynolds, C.J. Arroyo, M.D. Kinard, "Primary Rodent and Lightning Protective Sheath for Lightguide Cable," International Wire and Cable Symposium Proceedings 1986, pp. 455-463.

[12]G. McKay, W. Cousineau, B. Braham, J. Rowe, "Qualification Procedure for Fiber Optic Cable Design," International Wire and Cable Symposium Proceedings 1986, pp. 307-314.

[13]P.V. Bakhuru, K.E. Bow, D. Fisher, E. Schrom, "Crushing Metallic Shielded Telecommunications Cables With Dynamic Magnetic Field," International Wire and Cable Symposium Proceedings 1985, pp. 173-186.

[14]D. Fisher, K.E. Bow, W.F. Busch, E.C. Schrom, "Progress Towards the Development of Tests for Telecommunications Cables," International Wire and Cable Symposium Proceedings 1986.

[15]K.E. Bow, Dow Chemical, "Development of Lightning Tests for Fiber Optical Cable," 7/87, #870344.

[16]H. L. Blumsack, D. Fischer, "High Voltage Impulse Breakdown Between Metallic Central Strength Member and Metallic Armor of Valtec Fiberoptic Cables," Unpublished Work, December 1983.

[17]"Generic Requirements for Optical Fiber and Optical Fiber Cable", TR-TSY-000020, Issue 3, December 1987, Bell Communications Research.

[18]J.A. Olszewski, J.B. Masterson, "Lightning Considerations in Optical Cables Design," International Wire and Cable Symposium 1986, pp. 141-147.

Richard E. Clinage

Siecor Corporation
489 Siecor Park
Hickory, NC 28603

Richard Clinage received his B.S. degree in Mechanical Engineering from Texas A&M University in 1983. He joined Siecor Corporation in 1983 and has since held positions in Manufacturing and Applications Engineering. Currently, he is the Supervisor of the Marketing Support Group in Engineering Services responsible for Telephony, Government/Military, International and Utilities Applications.

PERFORMANCE OF OPTICAL FIBRE CABLES AND OPERATIONS AND MAINTENANCE PROCEDURES IN THE AUSTRALIAN TELECOMMUNICATIONS NETWORK

L. KISS

TELECOM AUSTRALIA, MELBOURNE, AUSTRALIA

ABSTRACT

Telecom Australia has turned to digital techniques for the development of its network. Optical fibre transmission systems form the high capacity backbone routes for the digital traffic.

With the advent of the new technology associated with the use of optical fibre systems and the strategic importance of these high capacity routes, specific procedures must be implemented to ensure the cable's effective operation and performance.

This paper briefly describes Telecom Australia's optical cable network and details its performance using the co-axial cable network as one basis for comparison. Details of the operations and maintenance philosophy currently being implemented throughout the network are also provided.

INTRODUCTION

Optical fibre cables have been in routine use in the Australian network for approximately four years, although, there were some early optical cable trial installations which were installed ten years ago,

During the introduction of these systems considerable effort was given to the development of external plant items, cable designs and installation practices. Success in these activities is confirmed with the satisfactory installation of approximatley 6,000 sheath kilometres (skm) of optical fibre cable.

In relation to the longer term aspects of the operation of fibre systems, operations and maintenance issues were not as well organised and only the immediate concern of emergency fault restoration had been addressed. To correct this situation a comprehensive operations and maintenance manual was prepared in 1987 and was nationally implemented early in 1988. The manual equips field management and supervisory staff with the necessary information to effectively operate and maintain these cable systems and react to emergency needs in the required time frame .

Fault statistics confirm that fibre cable is performing better than any other cable bearer. It also confirms Telecom Australia's decision to use a non-metallic cable for lightning immunity reasons. An analysis of the fault causes indicates that optical cables are following a similar pattern to other cables. Furthermore, if the optical cable's improved performance is to be maintained, acceptance and adoption of the practices detailed in the manual will have to be vigorously pursued.

THE AUSTRALIAN OPTICAL FIBRE CABLE NETWORK

Application of Optical Cables

Since 1984 the use of optical fibre cable systems in the Australian telecommunications network has increased at an explosive rate. This has been due to the reducing cost of singlemode optical fibre (SMOF) cable, the availability of suitable cable ploughing techniques and the need to economically satisfy the rapidly accelerating demand for digital bearers. Current applications for optical fibre cable in Telecom Australia's network are for:

- Inter-exchange routes, both short and long haul;
- The customer access network for wideband services; and
- Special applications.

Early installations were confined to metropolitan areas. However, since 1985 major long haul project work has comprised approximately 50% of the total usage of optical fibre cable. The remainder is shared between the major urban areas and minor rural trunk installations. Unless a major change occurs, such as optical fibre being routinely provided in the residential network, this pattern is expected to continue into the early 1990's. Annual quantities of optical fibre cable and the general areas of application are provided in Table 1.

Initially all optical fibre cable installations utilised MMOF in the urban area. With the push to higher bandwidths, the availability of suitable SMOF cable ploughing techniques in 1985 (Reference 1), and the ready availability of transmission equipment in 1986, a rapid changeover to SMOF was made; this is detailed in Table 2. A Central Business District application using MMOF was established in 1986 and has been previously reported, (Reference 2). A number of other CBD installations now utilise SMOF cable. The use of SMOF cable in the residential area is currently being investigated (Reference 3) and two trials are currently in progress in Melbourne and Sydney. In each trial area approximately 100 customers have been cabled with fibre to provide basic and enhanced telephone services. The next phase of the trial due to commence late in 1988 will include interactive broadband services and video services. Plans are also currently being finalised which may result in the routine use of fibre in significant quantities for an interactive video application.

Major Projects

It is planned that by the early 1990's all mainland capital cities in Australia will be linked with a high capacity single mode optical fibre network. Duplication of this inter capital network is planned for completion by the mid 1990's. This will provide Telecom Australia with an intercapital network capable of meeting both the expected interstate traffic growth well into the 1990's, and the route security needs of its key and major customers by route diversity. Details of major projects currently planned, under construction, or completed, are given in Table 3 and illustrated in Figure 1 and has been previously reported, (Reference 4).

TABLE 1 - OPTICAL FIBRE CABLE APPLICATIONS

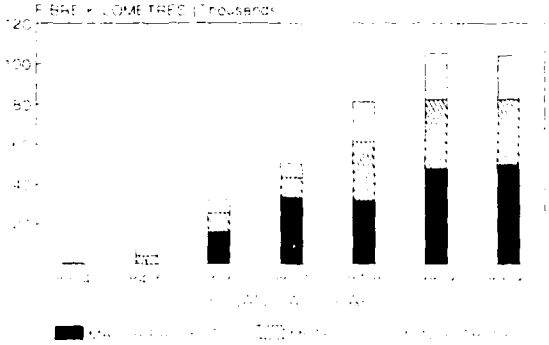

TABLE 2 - RELATIVE USE OF MMOF AND SMOF

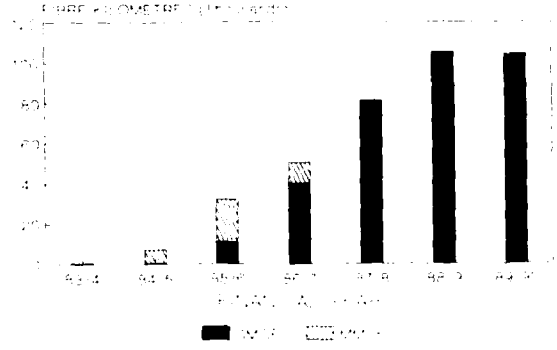

TABLE 3 - MAJOR SINGLE MODE PROJECTS IN AUSTRALIA

	Darwin-Katherine	Melbourne-Sydney	Tenant Creek-Adelaide	Perth-Adelaide	Adelaide-Melb-Sydney-Brisbane
Route Length (km)	330	1000	2100	2600	3100
Nominal Fibre Count	8	30	8	14	16
Fibre Kilometers (Fkm)	3000	32000	27500	37500	88000
Initial Capacity (Mbit/s)	140	140-565	140	565	565
In-Service Date	Oct 1986	Nov 1987	July 1988	Oct 1989	May 1991

PERFORMANCE OF THE NETWORK

Fault Recording and Categories

To monitor its external plant component of the optical fibre cable network Telecom Australia has implemented a system whereby specific reporting procedures are followed in the event of a cable fault. A report must be completed for any cable fault whether or not system outage occurs.

Faults are categorised on the basis of their cause and this information is used as an indicator of the suitability of the cable designs, installation techniques, training and effectiveness of Telecom Australia's operations and maintenance procedures. The broad classification of these fibre fault categories are: Outside Authority, Natural Causes, Manufacturer, Installation, Post-installation and Unknown.

FIG. 1. Inter Capital Network in Australia

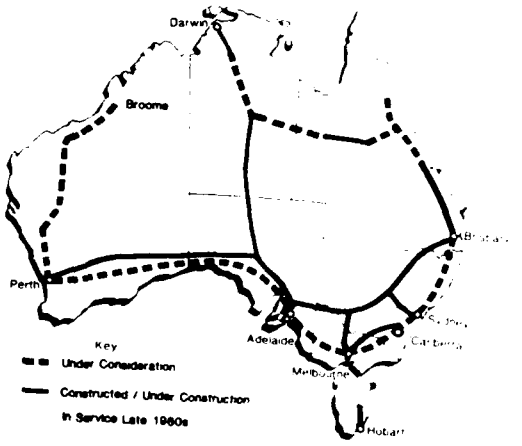

Optic Fibre Cable Comparative Performance

In attempting to quantify the performance of optical fibre cables, a comparison has been made with co-axial cable as these cables at the time of installation were the highest capacity cable bearers in use, are installed in similar areas of the network and were jointed by specialist groups displaying a high degree of care and expertise. A further feature of the co-axial cable network is its effective fault performance reporting system. Table 4 provides a comparison between these cables.

In analysing this comparative performance it should be noted that currently a low penetration of working fibres exist in most optical cables. Also extensive use is made of optical fibre cable protection systems which protect the operating system in case of both fibre cable and equipment faults. For these reasons both fibre faults and actual outages are considered. It is readily concluded from Table 4 that irrespective of whether actual outages or all fibre faults are considered, the current performance of optic fibre cable is most favourable when compared with the proven good performance of co-axial cable. Some allowance however could be made for the fact that the optical network is nowhere near as 'aged' as the co-axial cable network, however little evidence of this can be found from faults categorised under Natural Causes and Unknown

To explain this relatively good performance of optical fibre cables an analysis of the co-axial cable faults was performed. Findings indicate that the majority of co-axial cable faults are attributable to the 'human' element (65%) and the remainder to natural/undetermined causes. Current optic fibre experience, although limited, generally confirms this trend.

TABLE 4 - FAULT ANALYSIS; CO-AXIAL CABLE VS OPTICAL FIBRE CABLE
1985 TO JULY 1988

Av. Annual Skm (Operational)		Co-axial	Optical Fibre
		11,000	3057
Ratio of co-axial to optical fibre faults (Normalised)	actual outages	4.3:1	
	all faults	1.6:1	

Notes: 1 Normalised to their respective average Annual operational Skm.

2. All co-axial cable faults caused some outage whereas for fibre only 35% resulted in outages.

3. Co-axial cable is an 'aged' network compared to optical cable

4. Most optical systems have protection as well as spare fibres available.

The analysis also confirms Telecom Australia's decision to standardise upon the use of non-metallic optical fibre cable. The comparative fault rate of co-axial cable faults due to lightning is significantly higher than for optical cables even when allowing for the relative quantities of each cable in service.

As both co-axial and optical cables are installed under similar conditions, no practical difference between these categories of faults should exist. This is partly confirmed by the fact that the predominant fault cause for both cable types, the human element, is similar. Differences do however exist, and may be attributable to the difference in inherent material failures, in the actual installation techniques and/or to the possibility of a statistical 'abberation' caused by the significantly different sample size.

It is postulated that a correlation between the two cable types does exist. Unless the installation and operation and maintenance of optical fibre cable is improved beyond that performed on co-axial cable systems it can be expected that the performance of optical cable will tend to that of co-axial cables. It is therefore imperative that an improved operations and maintenance plan be adopted for optical fibre cables.

OPERATIONS AND MAINTENANCE PROCEDURES

Early Experience

Prior to 1987, Telecom Australia's cable designs and installation materials/ techniques were in a developmental stage. This was reflected in an ad hoc approach to the restoration of faulty cables. Various publications were prepared on specific issues of emergency repair, but no overall plan had been considered. Since then however, designs/techniques have been rationalised to the point where a meaningful nationwide Operations and Maintenance plan could be considered. With the rapid expansion in the use of optical cables, and their strategic importance in the digital network, an increasing need for an effective operations and maintenance plan became apparent.

Particular problems also arose from Telecom Australia's cable maintenance group who are generally non-specialist operational staff and are a different group to the optical cable installation staff. The installers become familiar through training and constant exposure to optical fibre technology whereas the maintenance staff receive only initial training with little or no continuing exposure. This situation in an emergency repair situation was further exacerbated with the cable testing staff being a separate group.

With the installation of the first major long-haul optical cable in the remote north Australian region the lack of any particular maintenance plan for this and other similar projects under construction also became obvious.

Because cable design and installation techniques were basically set, this, to a large extent, dictates the fault rate. It was therefore considered that to improve the plants' performance, effort was required to establish an effective plan which would ensure that service restoration times could be kept to a minimum. This was required to be achieved on both metropolitan and remote long-haul routes through effective planning and implementation by the available non-specialist maintenance staff.

National Plan

In late 1986 all of these issues together with the routine operations and surveillance issues were recognised. In 1987, they were addressed and a single comprehensive document detailing a complete plan for the external plant operations and maintenance requirements of optical fibre cables was prepared. In addition to the technical details required in restoring service, all other related issues are included such as organisational and support needs, restoration targets, ongoing training, strategic surveillance etc.

The 'targetted' user of the manual was identified as external plant managerial staff, field supervisors and in particular the individuals assigned the responsibility for fault restoration. A more practically oriented version was also prepared for all other maintenance field staff.

In early 1988 implementation was commenced by identifying all key personnel and instructing them of their resposibilities and familiarising them with the content of the manual.

The contents of the manual is detailed in Table 5. Some significant features included in the various sections of the manual are as follows:

- Local Organisation. Full details of all staff groups (including emergency telephone numbers) together with their resposibilities are provided for all fault repair work activites including, fault identification and reporting, emergency repair, transmission measurements and permanent repair.
- Restoration Targets. Minimum restoration times are provided as a guide to fault staff.
- Quality Assurance of Installation Practices. On the premise that 'no amount of maintenance effort can overcome inherent design and/or installation deficiencies' recommendations are provided on design details and installation standards for both initial and subsequent installations.
- Fault Notification and Action. Simplified flow diagrams, are provided for the procedures which should be followed during cable restoration. Action options available are also provided.
- Repair Techniques. Included in this section is a recommendation on the use of a (rapidly deployable) interuption cable for those instances where a difficult area/situation needs to be by-passed.
- Maintenance Equipment and Spares. Recommendations are provided for the holding and storage aspects of external plant material which must be held at strategic locations to enable the restoration of cable within the suggested times.
- Training. Both initial and ongoing training requirements are detailed. Ongoing training is most important as in zero/low fault incidence areas some skills may be lost as they are not utilised in routine day to day installation activities.
- Major Routes. Due to the importance and/or isolation of some routes, special operations and maintenance plans have been prepared for these routes. Details are provided and brought to the attention of the user.

Since the issue of the manual practical application has confirmed the satisfactory outcome and operation of the principles and organisational arrangements provided in it.

The manual has been well received and its effectiveness in containing faults on optical fibre cables to a low level will continue to be monitored.

TABLE 5 - CONTENTS NATIONAL EXTERNAL PLANT OPTICAL FIBRE CABLE OPERATIONS AND MAINTENANCE MANUAL

1 LOCAL ORGANISATION

2 RESTORATION TARGETS

3 QUALITY ASSURANCE OF INSTALLATION PRACTICES

4 ROUTINE MAINTENANCE AND RESPONSIBILITIES

5 ROUTE MARKINGS AND PLANS

6 FAULT NOTIFICATION AND ACTIONS

7 FAULT LOCATION

8 CABLE DESIGN

9 REPAIR TECHNIQUES AND OPTIONS

10 MAINTENANCE EQUIPMENT SPARES AND STORAGE

11 TRAINING

12 SAFETY ASPECTS

13 MAJOR ROUTES

Rapidly Deployable Cable

In providing cable for the temporary restoration of service, a number of alternatives are available. Depending upon the actual situation the following may be used :

- A spare length of conventional cable
- Rapidly deployable cable
- A length of fibre for 'piecing-in' at the repair joint.

The majority of requirements may be satisfied by the spare length of fibre or cable options but under certain conditions a specially designed rapidly deployable cable may be required to provide the optimum solution. A design for such a cable has been prepared and is available for use.

The cable design proposed has the following features :

- Lightweight; 20kg/km
- Small diameter; 6mm
- Robust, uncomplicated construction
- Non metallic
- 2km drumlength (handled by one person)

This cable is available in fibre counts of up to 10 fibres. Larger fibre count requirements are met by the use of more than one cable. Details of the design are provided in Fig. 2.

FIG. 2 - RAPIDLY DEPLOYABLE CABLE CROSS-SECTION

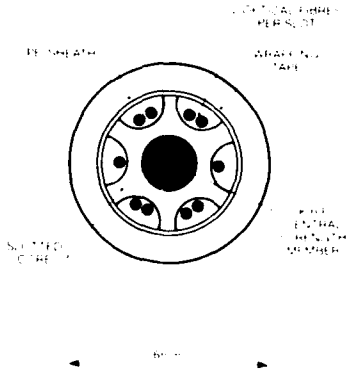

A more basic approach has been used by the use of single fibre cord. The fibre is used in a similar fashion to the 'piecing-in' procedure but as the fibre is protected it can be used in long lengths to temporarily by-pass a faulty section of cable. A major disadvantage of this approach is its high cost.

A practical application and assessment of the rapidly deployable cable has not occurred, as there have been no occurrences of mechanical damage requiring rapid restoration.

Conclusion

Telecom Australia's optical fibre cables are currently performing better than any other cable bearer used in its network. An analysis of the fault causes on optical fibre cables indicates that a similarity exists with co-axial cable. It is expected that, if left 'unchecked' optical fibre cables performance, will in time, tend to that of co-axial cables.

An analysis of lightning related faults has confimed the advantages of the previously reported decision by Telecom Australia to standardise upon the use of non-metallic cables. The largest contributor to cable faults however remains to be the human factor.

With the increasingly strategic importance of optical fibre cable in the digital network an innovative external plant operations and maintenance plan has been prepared by Telecom Australia to ensure that service restoration times will be minimised. The plan also provides for the continuing operations and surveillance requirements of the optical cables.

The plan is included in a single document and is applicable to both metropolitan and remote long-haul installations. With its recent implementation throughout Telecom Australia it is expected that the performance of optical fibre cables should be maintained at or below the current fault performance levels.

Acknowledgements

The author wishes to acknowledge the efforts of Mr. F. Pavanello for the analysis of optical fibre and co-axial cable faults. The permission of the Chief General Manager, Telecom Australia, to publish this paper is acknowledged.

References

1. Cable Design and Installation Technique for Direct Buried Non-Metallic Optical Cables -B.T. de Boer, R.W.A. Ayre, R.B. Schuster, 34th International Wire and Cable Symposium, Cherry Hill, New Jersey, November 1985.

2. Provision of Wideband Optical Fibre Cable Networks for Central Business Districts - L. de Valle, W.I. Harry, M. McKiterick, 36th International Wire and Cable Symposium, Arlington, Virginia, November 1982.

3. L. Kiss, D. Campbell and T. Wallis, "Optical Fibre Residential Pilot - External Plant Aspects" 12th Australian Conference on Optical Fibre Technology, Surfers Paradise, Queensland, December 1987.

4. Installation, Evaluation and Future Design of Optical Fibre Long Haul Routes in Australia - E. Johansen, B.M. Faulks, B.T. de Boer, 35th International Wire and Cable Symposium, Reno, Nevada, November 1986.

L. Kiss
Inter-Exchange
Networks Branch
Telecom Network
Engineering
Telecom Australia
29/570 Bourke Street
MELBOURNE VIC 3000
AUSTRALIA

Les Kiss is currently Manager of the Optical Installation and Maintenance Section of the Inter-Exchange Networks Branch, Telecom Australia. He joined Telecom Australia in 1971 after graduating in Mechanical Engineering at Melbourne University in Victoria, Australia. He has had extensive experience in the external plant area, in particular in cable design and specifications and in the installation of cable plant. He currently has full responsibility for the installation and maintenance of optical fibre cables in the inter-exchange network.

Reliability in Silica Based Optical Fibers

Dipak R. Biswas

Alcatel Cable Systems
Roanoke, Virginia

Abstract

The long-term reliability in silica based optical fibers is extremely important for the fiber optic system performance over its lifetime. The two major reliability issues are considered in this paper. The mechanical reliability which includes the strength and static fatigue and the radiation response on optical losses are discussed. The optical performance reliability and the hydrogen induced optical losses should also be considered for the total fiber optic system reliability.

1.0 Introduction

The reliability in silica based optical fiber is of great interest from the point of view of its applications in different environment. Two major areas of concern are the mechanical reliability and the radiation induced optical losses.

2.0 Mechanical Reliability

The mechanical reliability is mainly related to strength and static fatigue. The strength is important for mechanical reliability in cable construction, installation and services for telecommunication industries where the proof-test level (which can usually guarantee the minimum strength of entire length of optical fiber) is typically 50-80 kpsi. In military applications, where the proof-test level is in excess of 200 kpsi, the strength of fiber is important for high speed payout of optical fibers and for ruggedized cables. The static fatigue is important for long-term reliability of fibers in storage and services particularly in presence of moist environment. The initial high strength of optical fiber degrades under stress with time in presence of moisture due to static fatigue.

2.1 Strength

The tensile strength of glass fiber is mainly governed by the random distribution of small flaws on the surface and inside the fiber. The tension on the fiber enlarges the flaw to a critical size for failure. The theoretical strength of silica glass fiber is nearly 3 million psi. One to two million psi strength was measured in a dry liquid nitrogen environment. The average strength of silica based optical fiber is around 800 kpsi at room temperature and at ambient humidity. Lower strengths are reported when measured on longer length fibers. The variability in strength distribution can be explained by the Griffith's theory of brittle fracture. The strength is inversely proportional to the square root of flaw size. Typical flaw size for a 100 kpsi fiber strength is 0.8 micron, whereas for a 500 kpsi strong fiber, the flaw size is only 350 angstrom. The flaws are distributed randomly along the length of fiber. The probability of finding a larger flaw is greater in longer length of fiber. A typical strength distribution (Weibull plot) is shown in Figure 1.

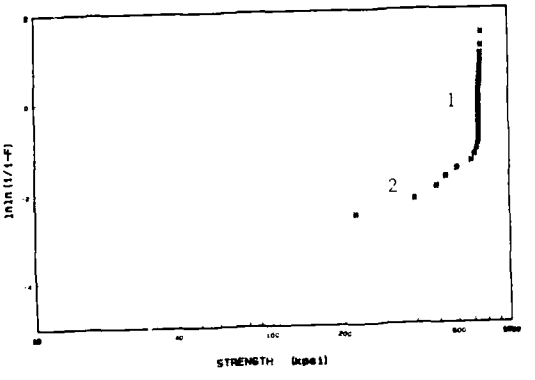

Figure 1. A Typical Weibull Plot

The slope of the probability vs strength plot gives the Weibull parameter (m-value). The step 1 portion of this bimodal strength distribution plot has considerably higher m-value than the step 2 portion. The higher m-value indicates the narrower flaw distribution. For a reliable product, the fibers with step 1 type strength distribution is preferable. The following four processes are mainly used to fabricate silica based optical fibers:

1) Outside vapor deposition (OVD)
2) Modified chemical vapor deposition (MCVD)
3) Vapor phase axial deposition (VAD)
4) Plasma chemical vapor deposition (PCVD)

Out of these, the MCVD process is relatively simpler and used extensively. In the MCVD process, glassy layers of doped silica are deposited inside a rotating high purity quartz tube. The cladding layers are first deposited followed by the core layers. After the deposition, the central hole of the tube is collapsed at a high temperature to a solid rod (called preform). Optical fibers are drawn from this preform. During the draw process, the bare glass is protected by using an uv-cured acrylate polymer.

To assure higher strength, the flaw sizes have to be very small. The flaws are mostly generated by the particles. The sources of these particles are:

* Quartz tube
* Environments for
  - deposition of glass layers and collapsing tube during preform fabrication
  - drawing and coating fibers
  - proof-testing, measurements and splicing fibers
* Unfiltered polymeric coating

Other types of flaws are bubbles, scratches and uncured coating. The following procedure can help in minimizing the number of flaws in fibers for a reliable high strength optical fiber product:

* High quality defect free quartz tubes
* Preform fabrication, drawing, coating, proof-testing, measurements and splicing in clean room environments
* Use of filtered polymers
* Use of right combination of uv-curing lamps for proper coating cure, and
* Minimize handling related damage on fibers

2.2 Proof-Testing

From the point of view of different optical fiber applications, minimum guaranteed strength in long length fibers, rather than strength in short length fibers is important. By proof-testing the entire length of fiber, one can guarantee the minimum strength. Proof-testing eliminates the flaws larger than the critical size corresponding to the proof-test level.

2.3 Static Fatigue

The initial strength after proof-testing is reduced due to long term stress. It is accelerated particularly in presence of moisture due to stress corrosion (static fatigue) by the interaction of water molecule with silica glass fiber surface (Si-O-Si + H-OH = 2SiOH). There are mainly three different ways to improve the static fatigue resistance of optical fibers:

1. By fabricating very high strength fiber containing only small flaws that will not grow to the critical level in an acceptable time under a desired stress level
2. By producing a surface compressive stress which will inhibit the flaw growth, and
3. By sealing the fiber surface from the surrounding environment with a hermetic coating.

Both metallic (such as Al, Ni, Sn, In, Sb) and dielectric hermetic coating materials (such as oxides, carbides, nitrides) are successfully applied on optical fibers. Recently there are considerable interests in carbon coating on optical glass fibers. Static fatigue parameter (n-value) which is a measure of fatigue resistance of carbon coated fiber is reported to be greater than 100 whereas the n-value of standard silica based optical fiber is only 20. After determining the static fatigue parameter, proof-test level (σ_p), the lifetime (t_{min}) can be calculated (1) from:

$$t_{min} = B\,\sigma_p^{n-2}\,\sigma_a^{-n}$$

$$\ln t = \ln B + (n-2)\ln\sigma_p - N\ln\sigma_a$$

Where B and n are constants, σ_a is the applied stress. Taking n=22, lnB=15 mPa^2.sec, σ_p=200kpsi, and σ_a=100kpsi, the lifetime can be calculated to be 82 days. When the applied stress is reduced to 84 kpsi, the lifetime can be as high as 10 years. The accurate determination of B and n-values are very important for predicting the lifetime of optical fibers. Therefore, to assure mechanical reliability, one should consider the strength, static fatigue test for short term and long term, design diagram of lifetime prediction, properties and performance of polymeric and hermetic coatings and the interaction of coatings with the service environments.

3.0 Radiation Induced Optical Losses

Optical losses increase when the fiber is exposed to nuclear radiation due to the formation of color centers in the core of the optical fiber. It is particularly significant when the fiber is placed in service at low temperatures due to slower recovery process at low temperature. The different parameters responsible for increased losses due to radiation exposure are mainly the glass composition, polymer material, temperature, dose rate, total dose, time of exposure, and operating wavelength. Figure 2 shows the induced loss vs the wavelength of different glass fiber composition when exposed to cobalt 60 source for one hour.

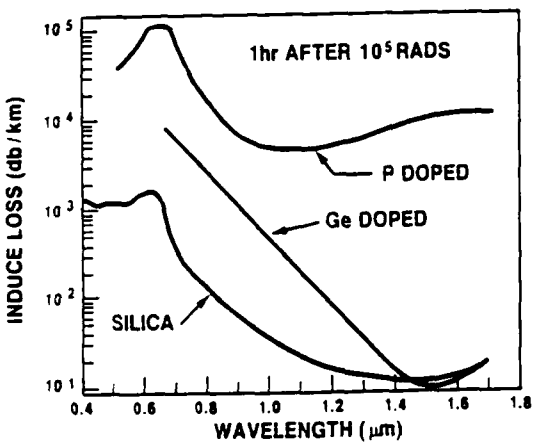

Figure 2. Radiation induced loss vs. wavelength of different glass composition (from re. 3).

Phosphorous doped silica fiber shows the highest loss whereas undoped silica and germania doped silica fibers show the lowest loss at 1.5 micron wavelength. Plastic clad silica fibers showed low radiation induced losses in many cases. In ultraviolet cured polymeric coating on glass fiber, the photoinitiators can absorb gamma radiation and optically damage the fiber. Several review articles (2-4) dealt with radiation effect on optical fibers. There are many variables that will affect the optical losses in different radiation environments and one should carefully consider those variables for determining the reliability of optical fibers.

4.0 Summary and Conclusions

For a reliable optical fiber product, one should consider the mechanical and optical reliability besides radiation and hydrogen induced optical losses. In mechanical reliability, the strength and static fatigue are very important. For uniform strength distribution in longer length of optical fibers, the processing and handling related defects should be minimized. To improve static fatigue resistance, hermetic coating on glass fiber is considered. Radiation induced optical losses can be minimized by improving mainly the glass and polymeric compositions and fiber processing parameters. Hydrogen induced losses (5-8) can be reduced by selecting the right organic materials in fibers and cables which do not release hydrogen, by reducing the metallic corrosion in cables, and by avoiding the exposure of fiber in hydrogen environment.

Acknowledgements:

The author would like to acknowledge Alcatel for granting permission to publish this paper.

References:

1. J.E. Ritter, Jr., et.al., J. Appl. Phys. 49(9) 4779(1978).
2. E.J. Freeble, et.al., SPIE Vol. 541, 70 (1985).
3. S.R. Nagel, SPIE, Vol. 717, 8 (1986).
4. R.H. West, J. Lightwave Tech., 6(2) 155 (1988).
5. R.J. Araujo, ibid., 197 (1988).
6. M. Ohmishi, ibid., 203 (1988).

Dipak R. Biswas received his Ph.D from the University of California, Berkeley in 1976. After working at Lawrence Berkeley Laboratory, University of Utah and Institute of Gas Technology, he joined ITT Electro-Optical Products Division. He worked on optical fiber strength and coating developments for different commercial and military applications. Currently, he is working at SpecTran Corporation (50 Hall Road, Sturbridge, MA 01566) as a Director of Research and Development in fiber optics.

HIGH STRAIN-RATE TESTING OF OPTICAL FIBERS

Torbjörn Svensson

Swedish Telecom, Technology Department
Material Laboratory
S-123 86 Farsta Sweden

ABSTRACT

The implementation of a new technique for lifetime estimation of optical fibers and fibers in cables required the development of an easily accessible method for determination of the fiber's inert strength. The method is based on the use of a newly developed instrument for high strain-rate tensile testing of optical fibers.

The features of the method are presented along with some Weibull statistics of fiber strength for a wide range of stress rates.

The method further advances the possibilities to map fiber properties in the early stages of fatigue in various environments. It appears to be a promising way to reduce the dependence of data generated in process of fiber drawing, thereby enhancing impartiality during a qualification process.

Introduction

The design of optical fiber cables and stated limits for their bending radii and pulling forces during installation are intimately related to the risk of failure due to fatigue cracking of the optical fibers.

At the Material Laboratory of the Swedish Telecommunications Administration, the base for such risk management is presently the Failure Frequency Technique, which has been applied for a couple of years by several cable manufacturers.[1] The technique has obvious advantages, but the customer is bound to the supplier's information, and has few possibilities to make an independent control of all the parameters which will determine the fiber's lifetime.

For this reason, a complementary technique was searched for at the Material Laboratory. The present paper is dedicated to the rebirth and implementation of the Inert Strength Technique.

Basic Assumptions

The basic assumptions made on the propagation of, and final fracture due to fatigue cracks in optical fibers are common for the two techniques of lifetime estimation which will be discussed later.

The stable growth of fatigue cracks in glass will follow Paris law. Under the major time of its growth, the change of the length of a crack will be due to $da/dt = AK^n$, where n is the crack growth resistance parameter.[2] The stress intensity factor, K, ahead of the crack's edge is $K = Y\sigma\sqrt{a}$. The value of Y is determined by the geometry and orientation of the crack, and σ is the load divided by the cross sectional area. When the applied stress, σ, is so high that K equals the fracture toughness, K_{Ic}, the terminating crack growth is unstable and the fiber will fracture.

From this can be shown that the time dependent change of the fiber's latent fracture stress, σ_f, is given by

$$\sigma_f^{n-2} = \sigma_i^{n-2} - B^{-1}\int_0^t \sigma^n dt$$

where σ_i is the inert strength and $B = 2/(AY^2(n-2)K_{Ic}^{n-2})$. From integration follows that the current fracture stress, σ_f, under static stress can be written

$$\sigma_f^{n-2} = \sigma_i^{n-2} - \sigma_s^n t_s/B \qquad ...(1)$$

where t_s is the duration of the static stress σ_s. Tensile testing at a constant stress-rate σ' yields the current strength

$$\sigma_f^{n-2} = \sigma_i^{n-2} - \sigma^{n+1}/(B(n+1)\sigma') \qquad ...(2)$$

To describe the strength of a long length of fiber, one has to consider also the variation of inert strength along the fiber. A useful description for optical fibers is the Weibull distribution of strength according to

$$N = (\sigma_i/\sigma_o)^m \qquad ...(3)$$

Hence, the survival probability S for an evenly loaded fiber with length L is given by the cumulative failure probability F as $S = 1 - F = \mathrm{Exp}(-L\cdot N) = \mathrm{Exp}(-L(\sigma_i/\sigma_c)^m)$.

It is commonly known that in optical fibers there are at least two types of failure modes. They represent failures caused by intrinsic flaws (significant for the failure of short-length fibers) and failures due to extrinsic flaws. The most severe extrinsic flaws are eliminated at the screen test which is routinely made on drawn fiber. Thus, an extended description of the survival probability of a screen tested fiber will be

$$1 - F = \mathrm{Exp}[-L((\sigma_f/\sigma_{oe})^{m_e} + (\sigma_f/\sigma_{oi})^{m_i} - (\sigma_p/\sigma_{oe})^{m_e})] \qquad ...(4)$$

where m_e and m_i are the shape parameters and σ_{oe} and σ_{oi} are the site parameters for the extrinsic and the intrinsic modes of failure. The variables are the fracture stresses, σ_f and σ_p, which depend on the stress history. At inert conditions they are constant.

This formula corresponds to the findings that when short lengths of fiber are stressed, failure most probably will be caused by intrinsic flaws. If the length of stressed fibers is largely increased, the probability for a single fiber to fracture at a low stress will increase significantly due to the extrinsic mode. Finally, when very long lengths of fiber are stressed, one has to consider the magnitude of the screen stress σ_p, which defines the lower limit of stress for which failure occurs.

Techniques for Lifetime Estimation

Two techniques for lifetime estimation of stressed fibers will be briefly reviewed in this chapter. The techniques can be used to estimate the failure probability of an arbitrary length of fiber, e.g the multikilometer lengths between repeaters. Both of the techniques require that a number of parameters be evaluated from tensile or static load testing of fiber. It will also be shown, that the application of their respective formulas yield similar results. In these respects, they are compatible tools for lifetime estimation.

However, if made available, the one presented here as the *inert strength technique* would offer such advantages as failure probability based on the cable's service environment (which can be different from the screen test environment) and also an independence of statistical data from the screen test of fiber.

Failure Frequency Technique

An extensively studied technique to estimate failure probability for long lengths of screen tested fiber was presented in the beginning of the eighties.[1,3] In this paper it is called "*failure frequency technique*", since it is mainly based on the failure frequency, N_p, by which the fiber will fracture at the screen test after drawing.

According to this technique, the time dependent cumulative failure probability F of screen tested fiber at static stress, σ_s, will be given by

$$1- F = \mathrm{Exp}\left\{-N_p \cdot L\left\{\left[\left(1+ (\sigma_s/\sigma_p)^n \cdot t_s/t_p\right)\left(1/(1+C)\right)\right]^{m_e/(n-2)} -1\right\}\right\} \quad ..(5)$$

and can be derived from the equations (1), (3) and (4) given in the chapter Basic Assumptions above. The duration of the stress at the proof- or screen test, σ_p, is t_p. Other parameters have their usual meaning. Use of this expression shows that the failure probability increases as the time, t_s, passes during static load. The failure probability versus time is shown in the familiar double logarithmic form below.[4]

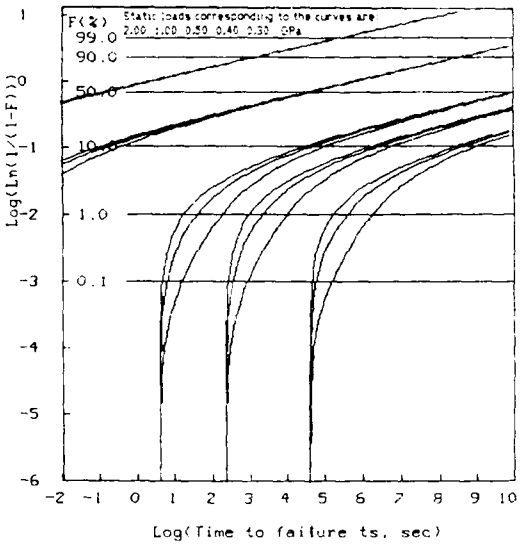

Increasing duration of the screen test displaces failure curves to the right: t_p for the curves are 0.01, 1 and 100 s.

The failure curves are computed by inserting the values of N_p and C in Eq. (5) using the substitutions

$$N_p = \left\{\left(\sigma_p^{n} \cdot t_p/B + \sigma_p^{n-2}\right)^{1/(n-2)}/\sigma_{oe}\right\}^{m_e} \text{ and } C = B/(\sigma_p^2 \cdot t_p)$$

The expression for N_p can be derived from Eq. (3) and Eq. (1) by setting $\sigma_f = \sigma_p$. The substitutions for N_p and C made here, enable the later comparison with the *inert strength technique*. The failure frequency at screen test N_p is only weakly dependent on B, but C is linearly proportional to B. The latter fact is an argument for the common assumption C = 0, which makes the life time estimation conservative. This ability to avoid the hard-to-measure parameter, B, is one of the advantages of the failure frequency technique.

Inert Strength Technique

Essentially the same static fatigue failure curves as from the application of failure frequency technique are obtained also from the use of *inert strength technique* with identical values on the basic parameters σ_{oe}, m_e, B and n. For static stresses smaller than the screen stress (σ_p = 0.5 GPa) both techniques yield identical results, provided that the screening time t_p is short. This can be clearly seen if the diagram below is compared with the previous one. In both diagrams the applied static stresses, σ_s, are 2, 1, 0.5, 0.4, and 0.3 GPa. The samples' length L is 20 m.

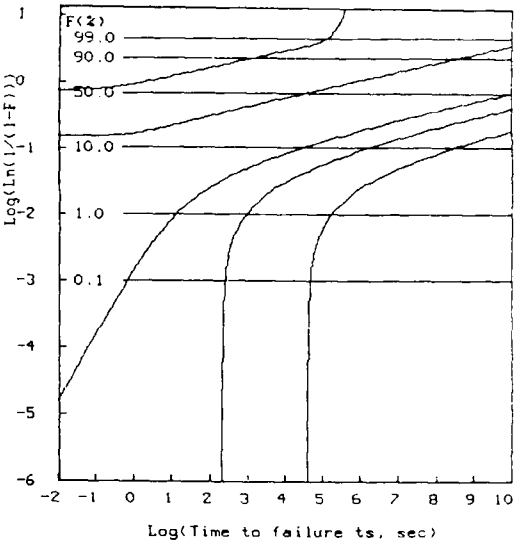

The times to failure using the two techniques were thus computed from *the same* inert strength distribution and fatigue parameters: σ_{oe} = 10 GPa, m_e = 2, B = 1 $(GPa)^2$s and n = 18. According to the inert strength technique, this distribution will be changed due to static fatigue causing the failure probability to read

$$1- F = \mathrm{Exp}\left[-L\left((\sigma_f/\sigma_{oe})^{m_e} + (\sigma_f/\sigma_{oi})^{m_i} - (\sigma_p/\sigma_{oe})^{m_e}\right)\right] \quad ...(6)$$

where $\sigma_f = \left(\sigma_i^{n-2} - \sigma_s^{n} t_s/B\right)^{1/(n-2)}$, which is Eq. (4) and Eq. (1) combined to the statical load case.

A comparison betwen the failure curves computed from Eq. (5) and (6) shows that, when differences exist between the failure frequency- and the inert strength technique, the inert strength technique is the more conservative, *i.e.* assigns the highest failure probability to the fiber. This conclusion is drawn also from studies on the variation of σ_p and B.

Measurement and Application The inert strength technique presented here is based on mapping the strength of an eventually prepared fiber over a wide range of strain rates. A strength saturation at high rates, if observed, would then reveal the inert strength, σ_i, by which the value of the B-parameter is calculated This can be done by extrapolating the fracture stress at low tensile speed with a slope 1/(n+1), until it intercepts the level of inert strength σ_i, at the stress rate σ';

$$B = \sigma_i^3/(\sigma'(n+1)) \qquad ...(7)$$

The expression can be derived from Eq. (2), since the term σ_i^{n-2} in Eq. (2) can be neglected at low stress rates, and by using the equality $\sigma_f = \sigma_i$ at the intercept.
Another method is to fit the Eq. (2) to the measured data by iteration. This is used in the forward chapter Experiments.

After evaluation of B, the lifetime at any level of failure probability for arbitrary lengths of fiber is available according to Eq. (6). When long lengths of multiple fiber cables are involved, the estimated failure probability often turns to be so extreme that it is not meaningful to quantify. In such cases the statistics are not very fruitful, but a simple formula as Eq. (8) below can be used as well.

The safe way is to replace in Eq. (6) the inert strength with the fiber load at screen test, and to use the values of B and n as determined in an environment significant for the fiber's future operation. This gives the time and load dependency of the weakest flaw in an arbitrary length of fiber, thus enabling to state the limits of failure-free operation. Knowing the value of B, the estimation of a minimum lifetime, t_{min}, at a static strain, e_s, will be made due to[5]

$$t_{min} = B\left((e_p/e_s)^{n-2} - 1\right)/(Ee_s)^2 \qquad ...(8)$$

with $e_p = \sigma_i/E$ where E is Young's modulus of the glass. The expression is derived from Eq. (6), by setting F = 0 and by using Hookes law $e = \sigma/E$. For a screen tested fiber, the minimum lifetime of the weakest part of the fiber is determined by inserting for e_p the value of the screen strain. Conversely, the maximal allowed static strain, e_s, for a given lifetime t_{min}, is given by

$$e_{s\ max} = \left\{B(e_p)^{n-2}/(E^2 t_{min})\right\}^{1/n}$$

Thus the "long length" statistics will be unnecessary and only information regarding the screen strain will be needed from the manufacturing process.

As pointed out before, a total description including allowable times for non-zero failure probability, is available from Eq. (6), but will of course require fracture statistics from long lengths of screen tested fiber.

Ways to the Inert Strength

To justify the use of the basic crack growth equations one has to clearly define the meaning of *inert strength*. As will be pointed out, this strength only occasionally corresponds to a maximally attainable fiber strength.

Strength in Inert Environment

Extremely high values of strength have been reported on fibers tested under inert conditions, i.e conditions presumed not to influence the fiber's strength by fatigue. Values found in the litterature on fracture strength of optical fibers are about 12.6 GPa, or 18% strain, measured in liquid nitrogen[6] and 8.6 GPa measured by tensile testing shortly after vacuum soaking of the fiber.[7] For freshly drawn silica glass, values as high as 24 GPa are stated.[8]

However, the applicability of these strength values for a mechanical equation of state for fiber fracture is obscure. When the inert strength of glass is searched for to enable evaluation of crack propagation parameters, it is necessary to consider any load supported by an eventual fiber coating. It is also obvious that crack-similar defects must exist, otherwise the simple crack-growth model will fail (in accordance with the chapter Basic Assumptions). If no cracks exist, almost any high level of fracture strength would be expected at short times of loading. When this is the case, some preparation of the fibers to induce crack-similar defects will be necessary to enable use of the inert strength technique.

Inert Strength when Cracks Prevail

Here, the use of the term *inert strength* applies to the strength of the fiber at the beginning of the tensile test, *at the moment when fatigue by stable crack propagation has just been initiated.* From the time when the nucleation of a fatigue crack is completed, the crack propagation is assumed to follow the growth laws given in the chapter Basic Assumptions.

Hence, an aged i.e strength degraded fiber has an inert strength as well as a freshly drawn fiber, though the latter's strength is considerably higher. So, when aiming at the value of the B-parameter, it does not matter whether the testing is done on aged fiber or a virgin fiber, as long as cracks prevail and the chemical and thermal environments are the same.

Inert Strength by Preparation

Since the B-parameter should be dependent only on the material and its environment, one would expect the strength saturation to occur at lower stress rates when the value of σ_i is lower, according to Equation (7). Observation of the saturation at tensile testing would then be simplified, i.e. lower stress rates would be required, if the value of σ_i could be suppressed by some ageing or static prestraining. Treatments based on chemical or mechanical attack on the glass surface are means by which the strength of optical fiber can be suppressed.[9,10]

A theoretical way to accelerate the nucleation and growth of truly crack-similar defects (in the respect of their growth-law

obeyancy) would be static load knock-down of a large number of parallell, equally loaded fibers.[11] When fractures start to occur, the load is decreased step-wise each time fibers fracture. The process can thus be regarded as a strength degrading screen test of fibers with unimodal strength. After a sufficient number of steps, a low strength level is reached on average, and the remaining fibers can be used for e.g. tensile testing. Due to the high load, most of the fibers then will contain the nucleated cracks required. In this way, an average low level of inert strength would quickly be achieved to simplify evaluation of the B-parameter searched for.

The figure below shows the initial and final strength distributions from a numerical simulation of strength knock-down.

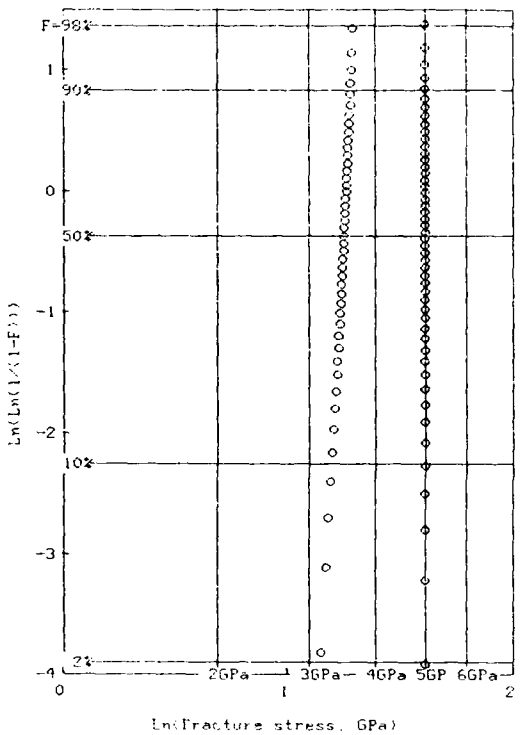

The figure shows how an initial Weibull distribution around 5 GPa with a shape parameter m = 10,000 is affected by 5 steps by 10% load reductions. The final distribution is centered around 3.5 GPa with m = 38. Cracks are assumed to prevail from the beginning. Assumed values of fatigue parameters are $B = 1\ (GPa)^2s$ and $n = 18$. One disadvantage is, that for more than a few steps, a very high value of the weibull shape parameter m (i.e. a very small scatter in strength) is required from the beginning, otherwise the strength of the remaining fibers will scatter too much to enable reliable evaluation of the fatigue parameters.

Owing to the difficulties above, the most straightforward way to obtain a measure on the inert strength seems to be, to increase considerably the stress rate at tensile testing.

Test Equipment

Tensile testing of the fibers is done in controlled atmosphere at a constant rate of strain, selectable within the range 10^{-3} to 10^{3} strain units per minute. The rates were chosen in decades with the lowest rates corresponding to the ones previously employed at testing at the Material Laboratory. Thereby, the new instrument's reliability could be checked and verified also by comparison with previous measurements on selected fibers.

The wide range of speed strived for was achieved by the instrument's unconventional design. Simpleness and easy maintenance did not allow the use of a gear box, so a stepping motor with a pulley mounted directly on the motor's axis was chosen. Above the pulley the load cell is adjustably mounted on a beam. The load cell consists of a rubber coated disc on which the torque from the wound-on fiber is measured by strain gauges located close to a low-noise DC amplifier with 125 kHz cut-off frequency.[12] The amplified signal is fed into a waveform recorder (Hewlett-Packard 5183) for analysis and storage.

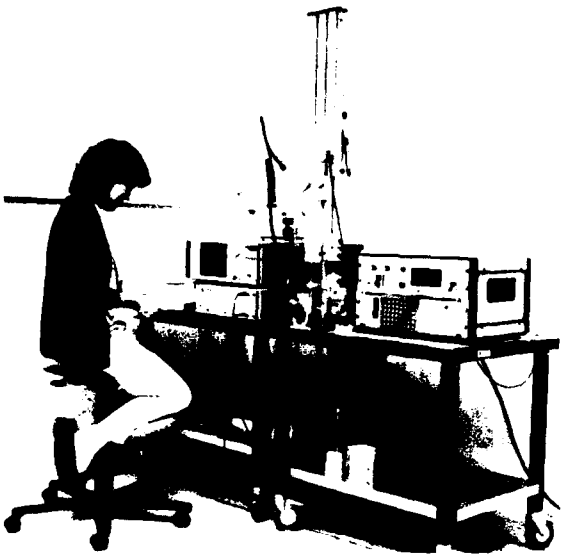

Instrumental properties

The measurement of tensile force on the fiber is influenced by the step-wise motion of the pulling axis at low speed and by the inertia of the load cell at highest speeds. Considerable effort has been made to secure accurate measurements.

Error sources

A 5-phase stepping motor with a resolution of 1,000 steps per turn will elongate the fiber step-wise with a resolution of 0.24 mm corresponding to 150-190 steps per load event. Hence, a frequency of 34 Hz moves the fiber with a velocity of 500 mm/min at the pulley end. The fully loaded length of fiber is 500 mm nominally, but is easily adjustable. An electronic driver is equipped with two oscillators which cover a frequency range of 0.03 Hz to 40 kHz.
Since the loaded length of fiber is not bound at 500 mm, the speed dependent errors have not been related to strain rate but to the frequency (Hz) by which the axis' position is stepped.

Low-speed errors. At 34 Hz and below, the motor in its original shape showed pronounced oscillations around its virtual poles. By adding a mass on the rear end of axis and a proper amount of viscous damping between the axis and the added mass, these vibrations were reduced to a negligible level.

However, the principle of the motion in distinct steps sets a limit to the accuracy by which fiber strength is measured. For an

average optical fiber the fracture strength is measured with an accuracy better than one percent.

At 340 Hz and above there are no measurable steps due to the inertia of the pulley.

High speed errors. The relatively high eigenfrequency of the load cell would not severely affect the load accuracy at 3.4 kHz, but at 34 kHz one has to consider the oscillations in the load cell's mass due to the rapid onset of motion of the fiber's pulled end. The load duration at the highest rate used here (34 kHz), corresponds to only 14 periods of free oscillation of the load cell with the fully loaded length of 500 mm of optical fiber.
If the load cell is modelled as a mass-spring system with internal damping, the deviation between measured load and load on the fiber can be studied as a function of time and loading rates. From this study it is possible to map the limits of the system's accuracy.

With reasonable accuracy, the model has been approximated with a mass on which the fiber force acts. On this mass a viscously damped spring is attached, which is rigidly coupled to a fixed environment in space. The displacement of the spring is assumed to be linearly proportional to the measured load F.

The displacement y with time t, of the mass m, from its unloaded equilibrium position is given by the differential equation

$$\frac{d^2y}{dt^2} + \frac{C}{m}\frac{dy}{dt} + \omega^2 y = \begin{cases} At/m & 0 \le t \le t_f \\ 0 & t > t_f \end{cases}$$

where C is the damping coefficient and ω is the undamped angular frequency (rad/s).

The load on the fiber is increasing linearly with time with a load rate, A, until fracture occurs at $t = t_f$ when the load vanishes.
To reduce the number of parameters, one will make the substitution $z = C/C_{cr}$ where C_{cr} is the value of the coefficient C at aperiodic, i.e. critical damping, and $B = \omega\sqrt{1-z^2}$.
With these substitutions, the assumptions made above and the boundary conditions $y(0) = 0$ and $y'(0) = 0$ one will find the solutions to the differential equation[13]:

$$F(t) = A\{t - 2z/\omega + [((2z^2-1)/B)\sin(Bt)+(2z/\omega)\cos(Bt)]e^{-z\omega t}\} \quad ..(9)$$

which is the measured load, i.e. the load on the spring, valid for any value $0 \le z < 1$, $0 \le t \le t_f$.
From the time, t_f, when the fiber fractures, the subsequent load is given by

$$F(t) = (\cos(Bt) + D\sin(Bt))Ce^{-z\omega t}$$

where

$$C = F(t_f)/[(\cos(Bt_f)+D\sin(Bt_f))e^{-z\omega t_f}] \quad \text{with } F(t_f) \text{ from Eq. (9)}$$

and

$$D = (B\sin(Bt_f)+z\omega\cos(Bt_f))/(B\cos(Bt_f)-z\omega\sin(Bt_f))$$

The relation between heights of two adjacent peaks of the same sign is equal to $\exp(2\pi z/\sqrt{1-z^2})$. This relation enables adjustment of the value of z to minimize the deviation between measured and applied load at fracture. No other entities are required except ω and z since B was given by $B = \omega\sqrt{1-z^2}$.
The value of ω is easily measured as $\omega = 2\pi/T$ where T is the period of undamped oscillations, and the value of z with the load cell in its damped state is calculated from the relation between peak heights after fiber fracture.

A close agreement between the measured and applied force at the moment of fracture is obtained for $z = 0.15$ due to the figure below, which is computed from the experimental value $\omega = 14{,}000$ rad/s.

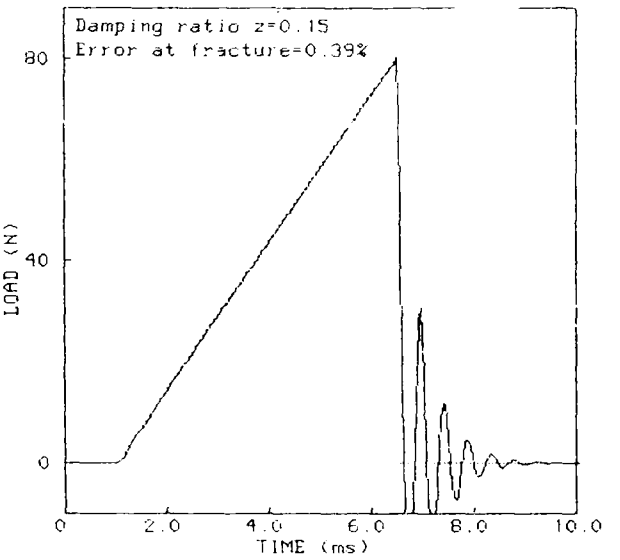

The duration of the linearly increasing load, 5.5 ms, is typical for tensile test of optical fiber at the highest rate used here.
The corresponding deviation between applied and measured load during the simulated tensile test is shown below. The ordinate is the underestimation, i.e. [1-(measured load/applied load)]·100 %.

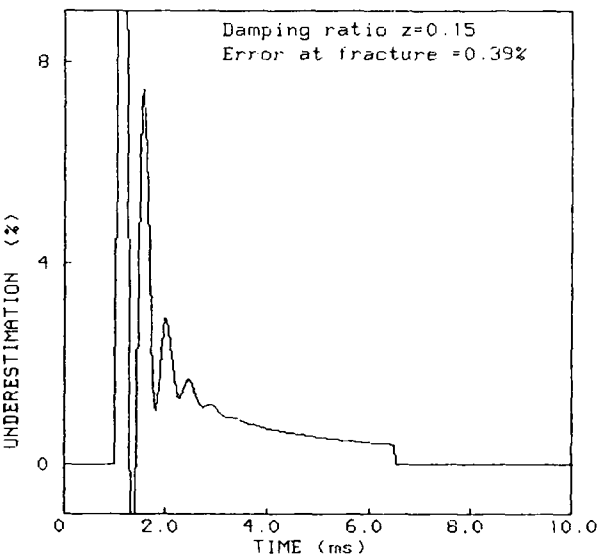

Thus, a reliable measure of the fracture strength at high loading rates is expected when the load cell is adequately damped.

However, due to the rapid onset of stress on the fiber, tensile waves will propagate along the fiber. Repeated wave reflection from the fiber's ends will be superimposed oscillation of the load

cell. This effect of variation of the fiber's load will not severely influence the measurement at the time of fracture, since the internal damping in the fiber's coating and the cyclic slip of the fiber ends on the grips, will cause the load oscillation to decline rapidly. At the moment of fracure, there is only second order oscillation, which is negligible besides the residual under-estimation of fiber load due to the load cell's damping. The figure below is typical for captures of high speed tensile testing.

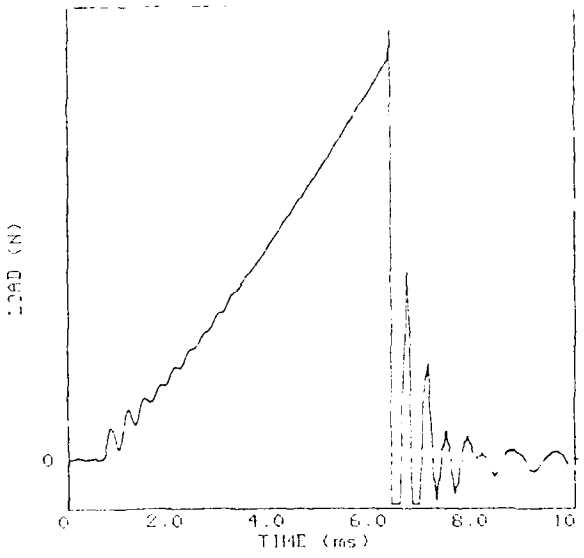

The fully loaded fiber length was 500 mm and the pulling speed was 8.3 m/s. As can be seen from the figure, the initial vibration is about three times as strong as predicted from ω and z for the load cell, but the deviation between the fiber load and the measured load at fracture, is essentialy determined by the damping of the load cell.

Thanks to the precautions taken, the accuracy of a single measurement of the fracture strength of an optical fiber is expected to be better than one percent for all rates of strain. The accuracy of the measured mean fracture strength of several equally strong fibers should be even better.

Experiments

The instrument's reliability has been checked in a series of tensile tests of preconditioned fiber. For this purpose single mode fused silica fiber coated with UV-hardened acrylate was used. Conditioning and tensile testing were made at 23°C, 55 %RH.

Measurements on stripped fiber indicated that the load supported by the coating at fracture, was only about 5% of the total load at low stress rates. The present experiments did not aim at the exact values of the fiber's fatigue parameters, so the fiber's fracture stress has been calculated roughly as the fracture load divided by the cross sectional area of the glass. Also, the samples were not randomly chosen prior to tensile testing, but the measurements are made on two independent series of fiber samples.

A number of samples were cut from the fiber drum and tested, beginning with five samples at the highest rate, $5{\cdot}10^5$ mm/min, next five samples at $5{\cdot}10^4$ mm/min and so on, including the lowest rate used, 0.5 mm/min. The procedure was repeated by taking five more samples to be tested at each rate. The resulting fracture stresses for virgin fiber is shown in the Weibull diagram below.

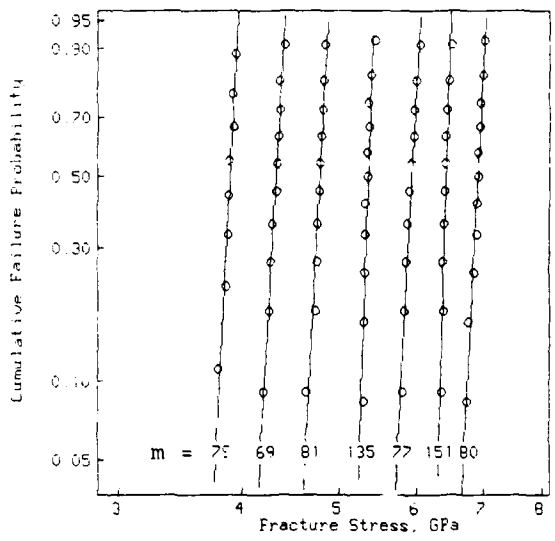

As can be seen from the steep slopes, the Weibull modulus, m, is high for all rates of strain, varying from 69 to 151. Thus, a good estimate of the average strength is obtained from the limited number of samples

The logarithm of median fracture stress plotted versus the logarithm of pulling speed shows a slight but significant deviation between the upper points and a straight line through the points at low rates of stress. Essentially the same shape is obtained when the median fracture stress is replaced by the site parameter σ_0. Applying the fatigue strength formula, Eq.(2), yields the curve fit shown below together with the median fracture stresses from tensile testing of virgin fiber. The curve fit corresponds to the parameter values σ_i = 7.0 GPa, n = 20.5 and B = 0.04 $(GPa)^2s$.

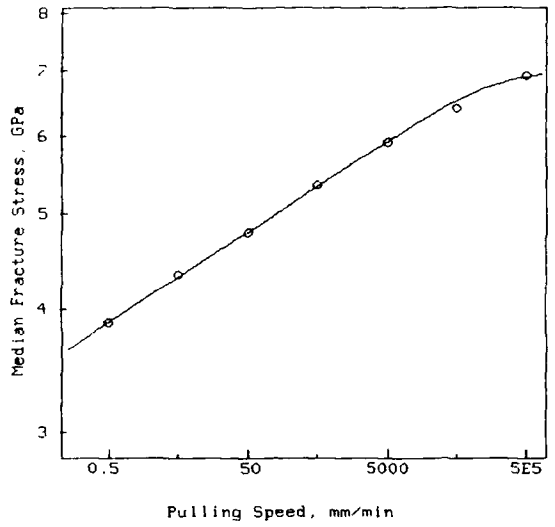

The theory predicts a sharper transition to the inert strength level, σ_i, than is obvious from the measured data. Deviation of the

distribution of data from the theoretical curve within the transitional region, could be the result of delayed crack initiation, which will lead to higher fracture stresses than anticipated from the simple crack-growth theory alone. Another possibiiity would be, that the crack-growth law is still valid at high stress rates, but with an increased value of n.

To check this hypothesis, a series of tensile tests were made on statically preloaded fiber. Due to the static stress, crack initiation was supposed to occur after a sufficient time. The specimens were stressed at a level equal to the median strength at the lowest rate at tensile testing, 0.5 mm/min. All specimens were kept at the same constant stress for 60 seconds. This duration was chosen experimentally to avoid extensive fiber fracture. Theoretically, the duration of static preload should not exceed a factor 1/n times the loading time to fracture at the slowest tensile test of virgin fiber, or about 200 seconds. Though the duration was quite short, some of the fibers fractured at the static preload. One reason for this was that the fiber slipped on the pulley, which caused the applied stress to vary a few percent.

As expected, the static fatigue reduced the Weibull modulus of the fiber's strength at the following tensile test, cf. chapter above on Inert Strength by Preparation. The values of m were reduced to 25-52. To obtain a reliable estimation of the fatigue parameters, a large number of samples would be required, but a rough estimate can be made from the present data which include about eight samples for each stress rate.

The resulting median fracture stresses at the tensile test of statically preloaded fibers are shown below.

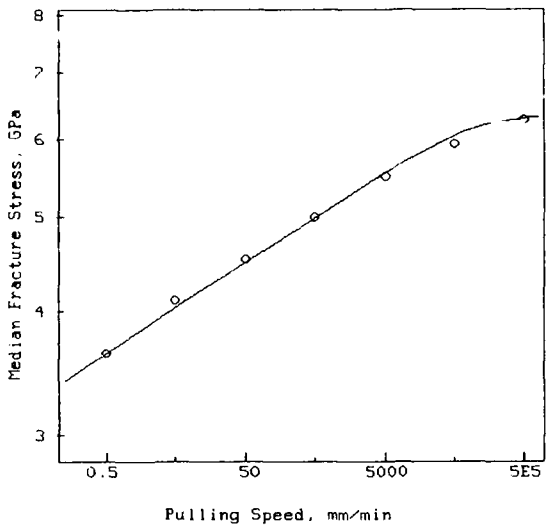

By analogy with the previous estimation of fatigue parameters the above curve fit yields the values σ_i = 6.35 GPa, n = 20.5 and B = 0.06 $(GPa)^2s$.

According to the present measurements, it seems doubtless that a saturation of the fiber's strength occurs at sufficiently high rates of strain. Extended testing of fiber with regard to the number of samples and their treatment for crack initiation before tensile testing will tell whether the basic crack-growth model is suitable for reliable lifetime estimation of optical fibers and cables.

Conclusions

The instrument for high strain rate testing described in this paper offers extended possibilities for the study of the mechanisms responsible for crack initiation and growth in optical fibers.

Tensile strength of acrylate coated, fused silica fiber has been studied at 23°C and 55 % RH. The present measurements give evidence of a saturation of the optical fiber's strength at high stress rates. Assuming that crack initiation is not suppressed at high stress rates, a close agreement between basic crack growth theory and measurements is obtained for the values of the crack growth parameters, n = 20.5 and B = 0.04-0.06 $(GPa)^2s$.

The inert strength of virgin fiber found in this study, 7 GPa, is significantly lower than the strength of optical fiber under inert condition, as stated in the litterature. This indicates that fatigue in high strength fiber may be caused by more than one single mechanism. Such strength degrading mechanisms are surface roughening due to corrosion, and the stress enhanced initiation and stable growth of cracks. When the initiation is suppressed, the fiber's strength will exceed the upper limit as given by the equations for growth of proper cracks only.

Acknowledgements

The author gratefully appreciates all the support given by Mr Laszlo Kőszegi, Head of Material Laboratory, and the skilful engineers at the workshop. The author owes special thanks to Mr Kurt Wilson and Mr Lars Carlsson for their accomplishment of the instrument, and to Miss Christina Norrback for her assistance with the experiments.

References

1. Y. Mitsunaga et al., "Reliability assurance for long-length optical fibre based on proof testing", *Electronics Letters* 17[16] (1981) p 567-68
2. S.M. Wiederhorn, "Subcritical crack growth in ceramics", *Symp. on Fracture Mechanics in Ceramics.* Vol II, N.Y., USA: Plenum (1974) p 613
3. Y. Miyajima, "Studies on high-tensile proof test of optical fibers", *J. of Lightwave Tech.* (LT-1) 2, june (1983) p 340-46
4. T. Svensson, "Failure probability of screen tested fiber. Choice of formulas and evaluation of parameters", *Televerket rapport Plm 86 233* (1986), internal report
5. J.E. Ritter et al., "Application of fracture mechanics theory to fatigue failure of optical glass fibers", *J.Appl.Phys.* 49[9] (1978) p 4779-82
6. W.J. Duncan, "Fatigue weakening of optical fiber", *J.Am.Ceram.Soc.*, 69[6] C-132-133 (1986)
7. T.S. Wei, "Effect of polymer coating on strength and fatigue properties of fused silica optical fibers", *Advanced Ceramic Materials* 1[3] (1986) p 237-41
8. Nabary-Szabo, J. Ladik, "Strength of silica glass", *Nature*, 188 [4746] october 15 (1960) p226-7
9. M..J. Matthewson, C.R. Kurkjian, "Environmental effects on the static fatigue of optical fiber", *J.Am.Ceram.Soc.* 71[3] (1988) p177-83
10. S.P. Craig et al., "The strength and fatigue of large flaws in silica optical fiber", *ECOC '82* (1982) p 205-08
11. T. Svensson, "Metod för uppskattning av optofibers B-parameter. Utmattning genom reglerad belastning", *Televerket rapport Plm 87 084* (1987), internal report (sw)
12. T. Svensson, "Snabb lastgivare för dragprovning av optofiber", *Televerket rapport Plm 88056* (1988), internal report (sw)
13. G. Smith, "Machine-dependent error sources at tensile testing of optical fibers" (to be published)

Torbjörn Svensson received his M.Sc. degree from the Royal Institute of Technology, Stockholm, Sweden in 1977. He joined the Dept of Physical Metallurgy at the RIT where he worked on mechanisms of plastic deformation of solids. In 1979 he joined the Dept of Materials at the National Defence Research Institute of Sweden, where he studied effects of shock wave propagation in solids and developed instruments for high strain rate testing of materials. In 1985 he joined the Material Laboratory at the Swedish Telecom Technology Dept where he is currently engaged in quality assurance and development of methods for testing of fibers and cables.

ALL SYNTHETIC VAD SINGLE MODE FIBER WITH DEPRESSED CLADDING

S. ENDO, T. KUWAHARA, Y. SUETSUGU, Y. KUBO, H. HONGO, J. OHTA

SUMITOMO ELECTRIC INDUSTRIES, LTD.
1 TAYA-CHO, SAKAE-KU, YOKOHAMA, 244 JAPAN

Abstract

Three types of depressed cladding single mode fiber were experimentally produced by the all synthetic VAD method. The micro and macro bending performance of these fibers was tested with the mandrel and the sandpaper methods.

The induced loss was 1.0dB/m ∿ 2.0dB/m at 1.55μm ,using a mandrel 20mm in diameter.

In order to confirm the fiber characteristics, the depressed cladding single mode fibers were manufactured by way of trial. These fibers had high strength, low attenuation, and low splicing loss just as the normal single mode fiber produced by the all synthetic VAD method.

From the results of the analysis of the macrobending performance of these fibers, it was clear that the MFD and the cutoff-wavelength had almost the same effect on induced loss during mandrel test.

1. Introduction

In order to provide longer and higher count single mode fiber cable, single mode fibers must exhibit the followings: long piece length, high strength, superior bending loss resistance and low splicing loss.

Recently, a high performance and high strength fiber produced through the all synthetic VAD process was introduced. (1)

The major advantage of the all synthetic VAD process can be found in the following typical characteristics: the median attenuation of 0.20dB/km at 1.55μm, the median length of 56km and 30km under 0.7% and 2.0% strain proof test, respectively.

Today, the development of flourine-doping technology has successfully accomplished production of the depressed cladding single mode fiber through the all synthetic VAD process.

In this paper,the characteristics of the fabricated depressed cladding single mode fibers will be discussed.

2. Bending performance

In order to evaluate the relationship between bending performance and depressing depth(Δ^-), three fibers, having three kinds of depressing depth were produced through the all synthetic VAD process ,using advanced flourine doping technology.

2-1. Fiber design

Fig.1 shows fiber construction. The outer portion of fiber(Ⅲ) consists of pure silica, the inner cladding(Ⅱ) is of F and SiO_2 glass and the core section(Ⅰ) consists of F,SiO_2 and GeO_2. The depressing depth(Δ^-) in each fiber was controlled by the doping the quantity of flourine and the total delta N(Δ^+), which realized the same MFD of 8.6μm for each type fiber, was adjusted by the addition of germanium.

The depressing depth(Δ^-) and the total delta N(Δ^+) are shown in Table 1.

Each fiber's cutoff-wavelength(λc) was about the same at 1.21μm.

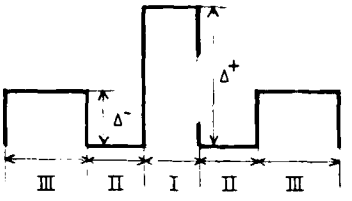

Fig.1 Fiber design

Table 1 Fiber construction

No.	Δ^+	Δ^-
a	0.40%	0%
b	0.42%	0.03%
c	0.44%	0.05%

2-2. Mandrel test

In order to evaluate the macrobending performance, the loss induced in a fiber section wrapped on mandrels at low tension was measured at 1.55μm.

Fig.2 shows the induced loss for each type of fiber wrapped on mandrels with diameters of 10, 15, 20, 25, 30, 35 and 40mm. The induced loss was linear with length of the fiber under bend, therefore, the results were reported in dB/m.

The induced loss of each fiber shows a similar increase in the mandrel's diameter of more than 25mm. However, at less than 25mm, the slope of the induced loss changed. The fiber, which had smaller depth depressed cladding, exhibited a smaller induced loss.

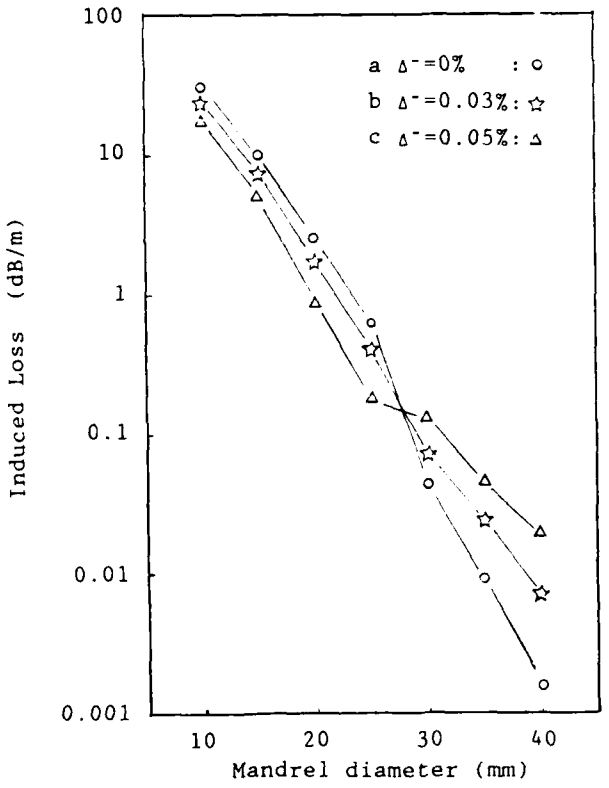

Fig.2 Macrobending loss at 1.55 μm induced by wrapping mandrel

2-3. Sandpaper test

The lateral load test is a way of measuring microbending performance.

The looped fiber shown in Fig.3 was placed between two square metal plates which has the size of 10cm x 10cm. The face of the lower plate is covered with 150-grit sandpaper, and that of the upper one is smooth. One or more weights were placed on the upper metal plate.

Fig.4 shows the induced loss was measured over a range of loads from 1.0g/mm to 8.0g/mm, using the three types of fiber. The deeper depressed cladding fiber exhibited smaller induced loss in this test.

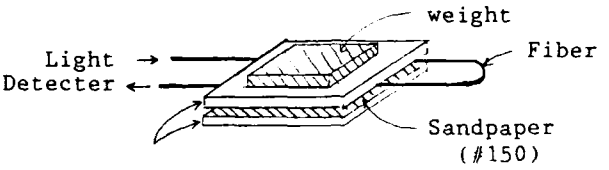

Fig.3 Rough sketching of Sandpaper test

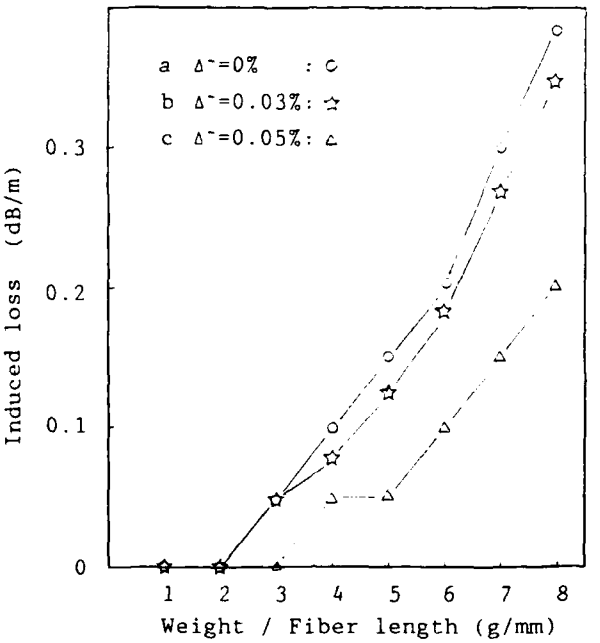

Fig.4 Macrobending loss at 1.55μm induced by sandpaper test

3. Trial manufacturing result

In order to evaluate the all synthetic depressed cladding single mode fiber, the fiber was manufactured by way of trial, having the Δ^- =0.02∿0.03%, the MFD=9.0 ∿ 10.0μm and the cutoff-wavelength(λ_c) 1.19 ∿ 1.33μm. These fibers had a 125μm outer cladding diameter and were dual-coated with UV curable materials.

3-1. Attenuation

The attenuation of these fibers was measured at the wavelength of 1.30μm and 1.55μm. The median value of all fibers was 0.347dB/km at 1.30μm, and 0.197dB/km at 1.55μm.

Fig.5 shows the spectral attenuation curve which was the lowest one of trial manufacturing fibers.

3-2. Fiber strength

The high strength was one advantage of the all synthetic VAD process. After those fibers were in-line proof-tested at 0.7% strain during drawing, the average length of the fibers were 56km.

After those fibers were re-tested at 2.0% strain , the average length was 30km.

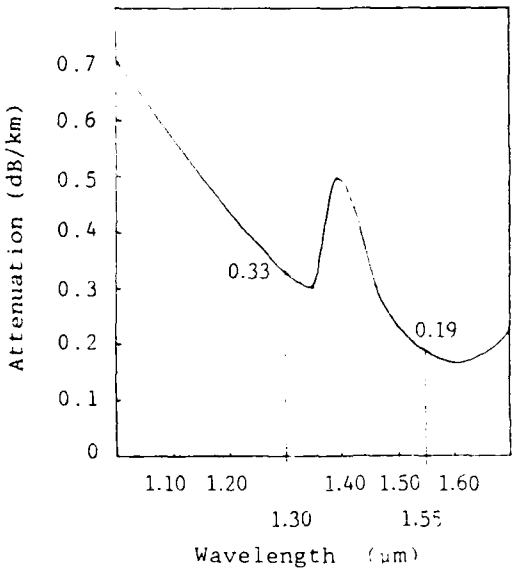

Fig.5 Spectal attenuation

3-3. Splicing loss

In order to realize low splicing loss, we have reduced the core eccentricity in the preform making process.

As a result,the median value of the core eccentricity became 0.16μm and the 0.038dB of average splicing loss was obtained by the self centering force splicing method.

Fig.6 shows the histogram of the splicing loss.

3-4. The influence of MFD and cutoff-wavelength on macrobending loss

The influence of MFD and refractive index profile design on macrobending loss was discussed in various reports.(2)(3)

It is well known that the cutoff-wavelength has much influence on macrobending loss. Therefore, the MFD and cutoff-wavelength effect on the macrobending performance of single mode fiber was analyzed by multiple regression analysis.

The analyzing method and results were described as follows.

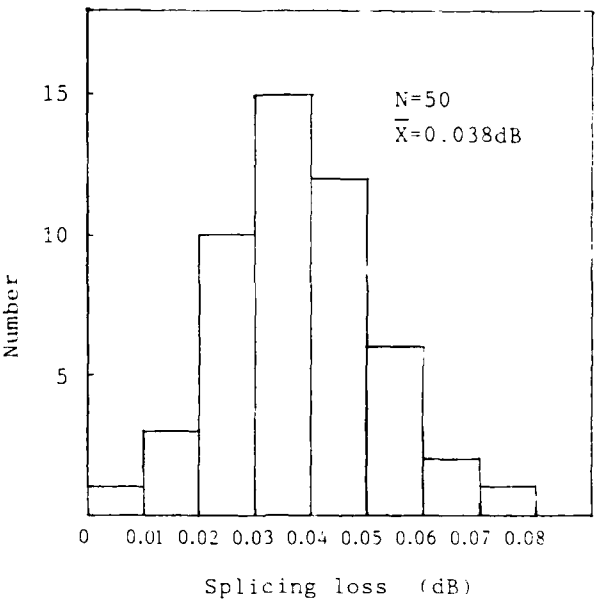

Fig.6 Splicing loss histogram

Those fibers were wrapped on mandrels, having 20mm diameters, and measured induced loss at 1.55μm as the same as 2-2. As usual, the induced loss during the mandrel test was described in log-scales.

Therefore, the induced loss data(dB/m) was calculated in accordance with following formula before analyzing:

$l = \log L$ L: Induced loss (dB/m)

As a result of analysis, the following multiple equation was obtained:

$$L = 10^{(0.899 + 1.09 \times MFD - 8.19 \times \lambda c)} \quad : r = 0.942$$

L: Induced loss (dB/m)
MFD: Mode field Diameter (μm)
λc: Cutoff-wavelength (μm)
r: Multiple correlation Coefficient

The 0.942 of r value was very close to one, therefore, the above equation explained the relationship between macrobending loss of single mode fiber and the MFD or the λc, very well.

The MFD and the λc range of those fibers were 1.0μm and 0.14μm, respectively.The induced loss range for 1.0μm of the MFD range was 12.3dB/m calculated with multipule equation and it for 0.14μm of λc range was 14.0dB/m.

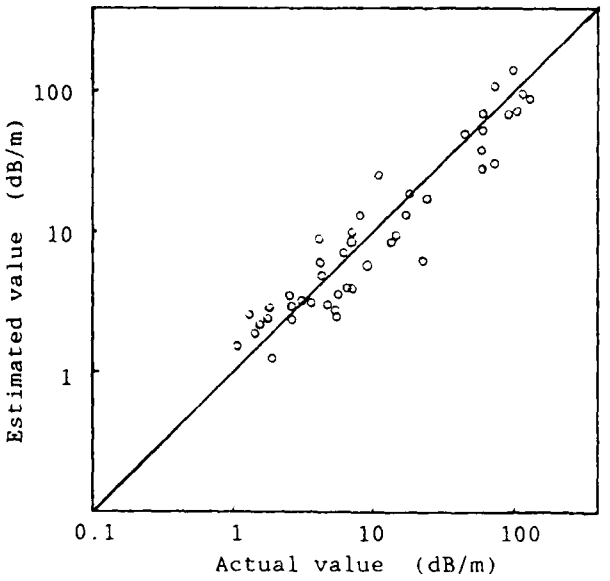

Fig.7 Multiple reguration scatter diagram

These induced loss ranges were almost same in mandrel wrapping test.

Therefore, the MFD and the cutoff-wavelength had almost the same effect on macrobending performance of single mode fiber.

Fig.7 shows the scatter diagram between the estimated value calculated with the multiple equation, and the actual value.

4. Conclusion

The depressed cladding single mode fiber was produced with the all synthetic VAD method. Those fibers exhibited excellent micro and macro bending performance.

The low attenuation of 0.197dB/km at 1.55μm, the high strength of 30km under 2.0% strain proof test, and the low core eccentricity of 0.16μm were confirmed as being the same as the all synthetic matched cladding single mode fiber, as a result of trial manufacturing.

Resulting from multiple regression analysis concerning the induced loss data of 20mm wrapping mandrel, it was confirmed that the MFD and the cutoff-wavelength had the same effect on the macrobending performance of single mode fiber.

5. Reference

(1) S.Ito,H.Sato,F.Mizutani,K.Tsuneishi and H.Kanamori,"Fabrication of long length, high strength single mode fiber by VAD process",IEEE J. of Lightwave Tech., Vol.LT-4,No.8,1986

(2) J.A.Dixon,M.S.Giroux,A.R.Isser, R.V.Vandwoestine,"Bending and performance of single mode optical fibers" ,OFC/IOOC '87 TUA2

(3) P.F.Glodis,C.H.Gartside,J.S.Nobeles, "Bending loss resistance in single-mode fiber",OFC/IOOC '87 TUA3

SHIGEKI ENDO

Mr. Endo received the B.S. degree for Electrical Engineering from Waseda University in 1976. He joined Sumitomo Electric Industries, Ltd. and worked on the production engineering of 9.5 and 4.4 coaxial cable. Thereafter he was engaged in the development of mother preform for optical fiber for more than 10 years. He is senior engineer of fiber optics production engineering section of fiber optics division.

YUJI KUBO

Mr. Kubo was born in 1963 and received the B.S. and the M.S. degrees from Hokkaido University in 1987. He joined the Sumitomo Electric Industries Ltd. in 1987, and has been engaged in research and development of optical fibers. He is a member of Institute of Electronics and Communication Engineers of Japan.

TOHRU KUWAHARA

Mr. Kuwahara was born in 1948 and received the M.S. degree from Tohoku University in 1973. He joined Sumitomo Electric Industries, Ltd. in 1973, and has been engaged in research and development of superconducting cables, milimeter waveguides, and optical fibers for more than ten years. He is a manager of fiber optics production engineering section of fiber optics division and is a member of the Institute of Electronics and Communications Engineers of Japan.

HITOYASU HONGO

Mr. Hongo was born in 1960 and received a M.S. degree from Tsukuba University in 1986. He joined Sumitomo Electric Industries, Ltd. in 1986, and has been engaged in development of manufacturing optical fiber. He belongs to fiber optics production engineering section.

YOSHIYUKI SUETSUGU

Mr. Suetsugu was born in 1961 and received the B.S. degree from Tsukuba University in 1984. He joined the Sumitomo Electric Industries Ltd. in 1984, and has been engaged in research and development of optical fibers and cables. He is a member of Institute of Electronics and Communication Engineers of Japan.

JUN-ICHI OHTA

Mr. Ohta received the M.S. degree from Tokyo Institute of Technology in 1987. He then joined Sumitomo Electric Industries and has engaged in research and development of optical fiber and cables. Mr. Ohta is a member of Communication R&D Department in Yokohama Research Laboratories, and a member of the Institute of Electronics & Communication Engineers of Japan.

Automated Optical Fiber Test Systems

Katsuya YAMASHITA, Mitsuhiro TATEDA and
Hiroaki AZUMA

NTT Transmission Systems Laboratories
Nippon Telegraph and Telephone Corporation
Tokai, Ibaraki, 319-11, Japan

ABSTRACT

Two types of an advanced automated measurement system have been developed. One is for measuring graded-index multimode(GI) fibers, and the other is for single-mode(SM) fibers. In order to attain the highest possible operation rate, two methodologies have been investigated. One is to speed up each measurement, and the other is to employ a fully multitask operation. Several measurement techniques, such as the side launch excitation technique for measuring structural parameters, are newly investigated to simplify measuring procedures and make these systems much faster than before. Multitask software has been developed enabling computer automation of almost all measuring procedures. By using multitask operation, we can assemble the arbitrary number of measuring setups into both systems without throughput decreasing. When one operator controls all the measuring procedures, both systems provide measuring rates of between 3 to 10 times greater than the rates of conventional methods, thus resulting in extremely low test cost optical fiber cables.

INTRODUCTION

More economical optical fiber cables have become neccessary in order to accelerate optical-fiber network development. Faster and more automated optical testing equipment is one prerequisit for reducing cable cost. Optical fiber testing procedures have been more time-consuming than metal cable measuring procedures. Various techniques and instruments have been developed to measure several optical characteristics. But, there has been insufficient consideration on constructing and unifying them into one system.

During optical fiber cable measurement, there are six basic procedures:

(1)fiber endface preparation
(2)fiber transportation to a measuring setup
(3)fiber axial alignment
(4)measurement
(5)fiber end transportation
(6)data processing/filing to mass storage systems

Here, we consider automation of procedures (2) to (6) in one system. All the procedures except for (4) are common for all automated systems for GI and SM fibers.

Items to be measured for GI fibers are loss, baseband frequency response and structural parameters (c · diameter, cladding diameter, etc.). Those for SM fibers are loss, cutoff wavelength, mode field diameter and structural parameters. In order to realize high throughput in automated systems, two methodologies have been investigated. One is to speed up the measuring rate for each item, and the other is to employ a fully multitask operation. High density optical fiber cable[1] testing should be applicable to optical fiber ribbons, which contain two to ten fibers. In this case, a ribbon-end remover[2] and a ribbon fiber cutter[3] are used to achieve higher measuring efficiency than that for a single fiber.

SYSTEM CLASSIFICATION

Three types of automated measuring setups are shown in **Fig.1.**

Type 1 has single pair of optical terminal (input and output)[4]. All measurements are sequentially done by optical switching for each measurement item. Advantages of this system are, as follows:
1)no fiber end transportation for any measuring item
2)only one time alignment for each fiber
3)easy software construction
Disadvantages are:
1)time-consumption due to sequential operation
2)a limited number of measurement items, which depend on optical switching device characteristics

Type 2 has a manipulator to enable transportation of several fiber ends at a time. There is the same number of optical terminal pairs as measuring items. Multitask operation can be introduced for each measurement. Transportation of all fiber ends at a stroke is carried out when all meaurements are finished. The advantage is:
1)n times greater operation rate than Type 1 if measuring time for each measurement item is the same, where n denotes the number of measuring items
Disadvantages are:
1)needs higher grade software than Type 1
2)it needs a reliable transportation system

Type 3 has a random transportation function, and can be constructed using almost the same hardware as for Type 2. This type requires a flexibly controllable manipulator.
The advantage is :

1)maximum operation rate
Even if there are especially time-consuming measuring items, Type 3 keeps a high operation rate by assembling two or more measuring setups into the system for the same item.

Disadvantages are:

1)significantly difficult software creation
2)needs a reliable manipulator
3)highly rigid structure protected from vibration caused by random manipulator transportation during measurements

This paper precisely describes the Type 2 system. To optimize Type 2, we tried to make each measurement measuring rate approximately the same. Hardware components between Type 2 and Type 3 systems are almost the same and a Type 3 system will be realized in the near future.

MEASUREMENT TECHNIQUES

GI and SM fibers measurement items are classified as shown in **Table 1**, in regard to measuring sample length.

Table 1. Measuring items and sample length

fibers	items	sample length
GI fibers	attenuation	long
	baseband response	long
	structural parameters	short
SM fibers	spectral attenuation	long
	cutoff wavelength	short
	mode-field diameter	short
	structural parameters	short
	(dispersion	short or long)

long : more than 50 m up to 20 km or more.
short: typically 2 m.

Here, much time is consumed in cutting a sample fiber and setting its endface in a holder. Therefore, reducing endface preparation time as far as possible is important for realizing fast throughput. From **Table 1**, it is found that long sample measurement is more common for GI fibers, whereas short sample measurement is more common for SM fibers. Thus, a side launch excitation technique (SLET)[5] was developed for GI fiber structural parameters measurement. This makes it possible to measure structural parameters in a long sample, thus rendering it needless to cut down a long fiber into a short piece by means of side launch using a fiber bend. If a reference fiber comparison method is employed for attenuation and baseband response measurement, then all measurement requires only one endface preparation.

For SM fibers, however, it is very difficult to measure all items on a long sample, so the

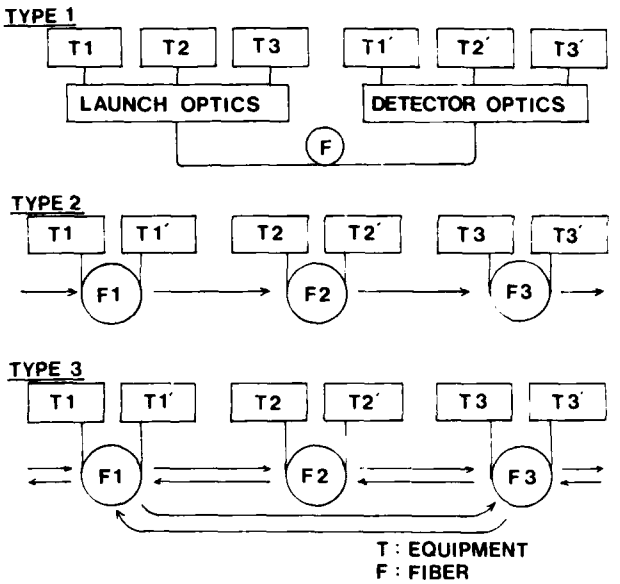

Fig.1 Basic constructions of the automated optical fiber test system.

cutback method is adopted for the loss spectrum measurement. This measurement occupies the most measuring time and requires the following sequential procedures:

1)long sample measurement
2)short sample measurement for attenuation evaluation
3)short sample measurement under bending for cutoff wavelength evaluation

To reduce each procedure's measurement time, fast and precise equipment was developed using Fourier Transform Spectroscopy.

Attenuation and Baseband response for GI fibers

These two items are measured by the reference fiber comparison technique (RFCT). Loss measurement setup for GI fibers consists of a 1.3 μm wavelength LED, an InGaAs photodiode, a 3D-alignment pulse stage pair and an A/D converter. Optical power is launched through a steady state GSG exciter[6], and is detected through an 80 μm core step-index fiber. Baseband frequency measurement setup consists of a 1.3 μm wavelength LD, a GeAPD, a 3-D alignment stage pair, a synthesized sweeper and a selective voltmeter. An SGS overfill-mode exciter[7] and an 80 μm core step-index detecting fiber were used.

To make systems much more suitable for automated operation, a spatial butting method is used for launching and detection, instead of fusion splice method or a matching oil filling method. In order to obtain high butting method precision, the most important point is to reduce the influence of the unstable launching condition between test-fiber endfaces and launch/detect fiber endfaces. Two methods were combined to combat this instability.

First, a precise non-contact endface gap sensor[8] was built in for automated alignment with high repeatability. Second, a spatial averaging technique was developed to reduce the influence of multi-reflection interference[9]. By varing the endface gap within a range of about six microns along the fiber axis, coupled optical power repeatability can be obtained below 0.02 dB. Practical power repeatability is governed by alignment repeatability, s_1, repeatability due to endface inclination distribution, s_2, and source power instability, s_3. Overall repeatability for automated alignment, s_{total}, is summarized in **Table 2** for loss measurement, where:

$$s_{total}^2 = s_1^2 + s_2^2 + s_3^2,$$

Table 2. Loss measurement reproducibility

Element	value	condition
s_1	0.02 dB	two endfaces
s_2	0.01	.6 degree inclination[10]
	0.05	2 degree inclination
s_3	0.01	
s_{total}	0.023 dB	.6 degree inclination
	0.056 dB	2 degree inclination

These reproducibilities are approximately the same as those of the conventional manual cutback method. Experimentally observed attenuation error of RFCT relative to the cutback method is shown in **Table 3.**

Table 3. RFCT attenuation error relative to the cutback method

Test fiber	RFCT L_r	cutback L_c	error $L_r - L_c$
1	.348 dB	.354 dB	-.006 dB
2	.172	.291	-.119
3	.523	.356	+.167
4	.368	.395	-.027
5	.216	.314	-.098
6	.717	.674	+.043
7	.897	.799	+.098
8	.824	.764	+.060
9	.677	.745	+.068
10	1.027	.982	-.045
average	-	-	+.014 dB

(NOTE) at 1.3 μm wavelength,
test fibers are 500 to 1,000 meters long.

Discrepancy from the conventional method is small enough on average. The small difference, which may become significant in some application, reflects the different structural parameters of the reference fiber and the test fiber. If necessary, deviation from the cutoff method can probably be diminished by a correction using structural parameters which are almost simultaneously measured by the automated system.

For baseband measurement, RFCT has been conventionally used. This automated system's reproducibility is almost the same as that in the conventional manual method. Within 0.10 dB reproducibility was obtained at 800 MHz at an endface inclination ranging from 0 to 2 degrees.

Structural Parameters for GI fibers

By the side launch excitation technique (SLET) shown in **Fig.2**, fast measurement of structural parameters can be done without cutting a short piece from the long fiber[5]. Core diameter reproducibility by SLET is compared to that of the conventional transmitted near-field technique (TNFT) in **Table 4.** Core diameter error in SLET relative to that in TNFT is also shown in **Fig.3.**

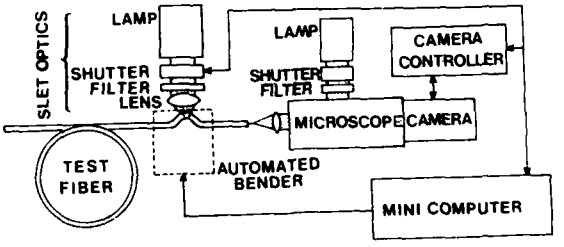

Fig.2 Structural parameter measurement diagram using the side launch excitation technique for GI fibers.

Table 4. SLET reproducibility compared with TNFT (core diameters standard deviation)

Sample #	SLET	TNFT
1	0.09 μm	0.07 μm
2	0.08	0.07
3	0.10	0.06
4	0.10	0.08
average	0.09 μm	0.07 μm

SLET reproducibility approximately equals TNFT reproducibility. Relative error is within 0.40 μm. These values are sufficiently small for core diameter measurement. Using this method reduces the time-consuming fiber-end preparation process.

Mode-Field Diameter Measurement for SM fibers

This item is measured by the scanning fiber probe technique(SFPT). A one-dimensional far-field technique is the easiest method for measuring the mode-field diameter of an SM fiber. A detector's practical sensitive area is much greater than typically specified diameter, hence endface separation must be large enough not to be influenced by the large diameter. Endface are conventionally separated by 80 to 120 milimeters. A relation between the Fraunhofer limit and detector surface sensitive area was investigated theoretically and experimentally. It is found that

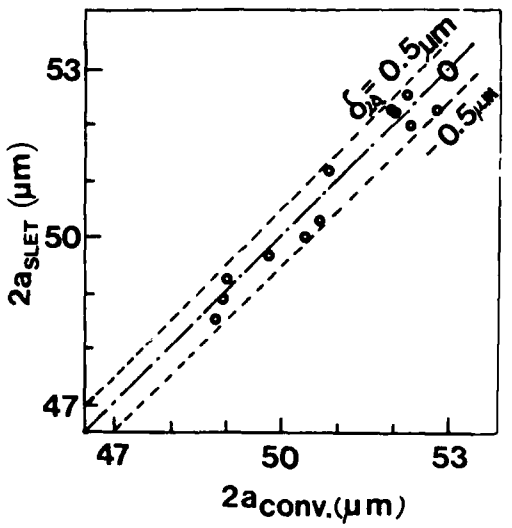

Fig.3 Measured core diameter comparison of SLET and TNFT for GI fibers.

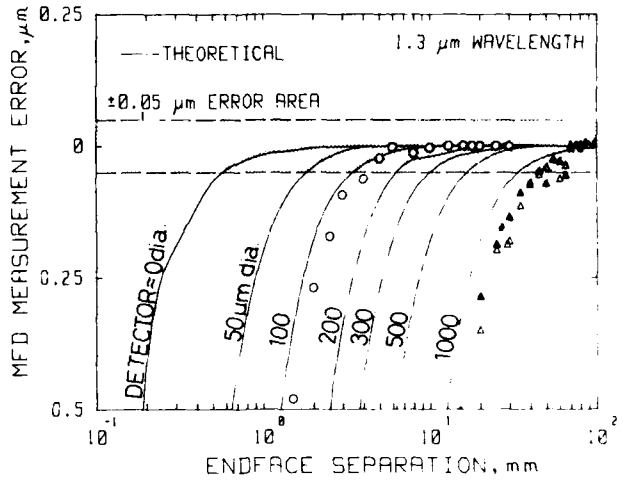

Fig.4 Mode-Field estimation errors as a function of endface separation between the fiber under testing and the detector(a probe fiber). Solid lines are computed results. Triangles ▲,▲are experimental results obtained by rotational scanning detector method. Circles are results obtained by a linear scanning fiber probe method.

endface separation between the test fiber and the detector surface can be reduced to several milimeters by using a fiber-probe coupled detector[11]. Calculation and experimental results are shown in **Fig.4.** According to these results, small-sized and faster measurement became possible because of reduced scanning range and a strong optical field.

Attenuation & Cutoff Wavelength Measurement for SM Fibers

A Fourier transform spectroscopy(FTS) using a Michelson interferometer was applied to the spectral attenuation and cutoff wavelength measurement, instead of conventional spectroscopy using a monochromator. This method is faster than the conventional one because an interferogram entirely constructed by light flux can be measured by short-distance mirror scanning. The final results of over the full spectrum range from 0.8 to 1.6 um are obtained in less than 0.5 second. In order to reduce noise influence, a time domain interferogram averaging method was developed, which is superior to the spectrum domain averaging method in signal-to-noise ratio enhancement effect. When using an InGaAs diode as a detector with 64 round averaging, the rms noise level can be reduced to less than -85dBm in about only 30 seconds. A reproducibility test sample is shown in **Fig.5(a),** Standard deviations, s_{av}, averaged in the range above cutoff wavelength (from 1.2 to 1.6 μm) are also shown in **Fig.5(b)** plotted as a function of the interferogram averaging number. 0.02 dB repeatability($3s_{av}$) can be obtained over just 16 rounds averaging in 8 seconds. This rapid measurement enables high total automated system throughput.

SYSTEM CONSTRUCTION

The basic construction of the automated test system is shown in **Fig.6.** The main hardware components are, as follows:

1)**3 to 5 pairs of three dimensional compact pulse stage** (40 milimeter width): Launch/detect optics are assembled on the xy stage and a sample fiber holder is transported on the z stage
2)**a common x shift stage suitable for measuring optical fiber ribbons including up to 10 fibers:** z stages are assembled on it
3)**a manipulator:** Up to 10 fiber holders can be transported at a stroke
4)**local controllers:** All stages and a manipulator can be controlled by the corresponding controllers
5)**measuring equipment for all measuring items:** For example, a halogen light source and an FTS michelson interferometer are assembled for spectral attenuation measurement
6)**a host computer:** It runs multitask programs, controls the local controllers and the measuring equipment, and processes data
7)**an SLET module:** It has fiber bend mechanisms and light sources (only for GI fibers)
8)**a bending machine:** It is added for cutoff wavelength (only for SM fibers)

Multitask softwares for the GI/SM systems are:

1)main controller-scheduler
2)loss/cutoff wavelength module controller
3)baseband/mode-field diameter module controller
4)structural parameter module controller
5)data processor-filer

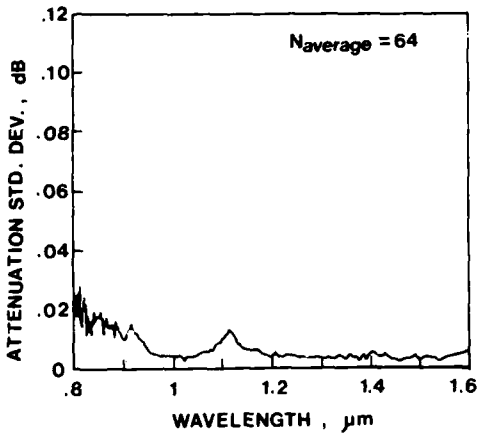

Fig.5(a) FTS measurement reproducibility, attenuation standard deviation to 10 rounds measurements, as a function of wavelength (when the averaging number is 64).

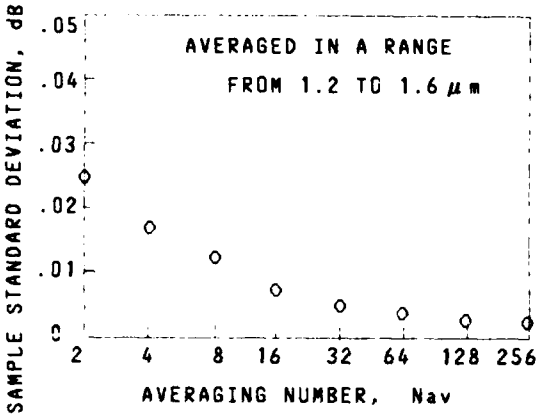

Fig.5(b) FTS measurement reproducibility, attenuation sample standard deviation to 10 rounds measurements, as a function of the interferogram averaging number.

These host programs are constructed on a Hewlett Packard 9020AS computer. These programs control module controllers by macro-commands through GPIB(IEEE488-1978 interface bus). Each module controller consists of an 8 bit CPU with each driver program's ROM.

The photos of these two systems are shown in Fig.7(a) and (b).

SYSTEM PERFORMANCE

The GI fiber system applied to single coated fibers has its performance summarized in **Table 5.** This result shows that the measurement rate for GI fibers is 8 to 10 times greater than that of the conventional manual measurements with equal reproducibility.

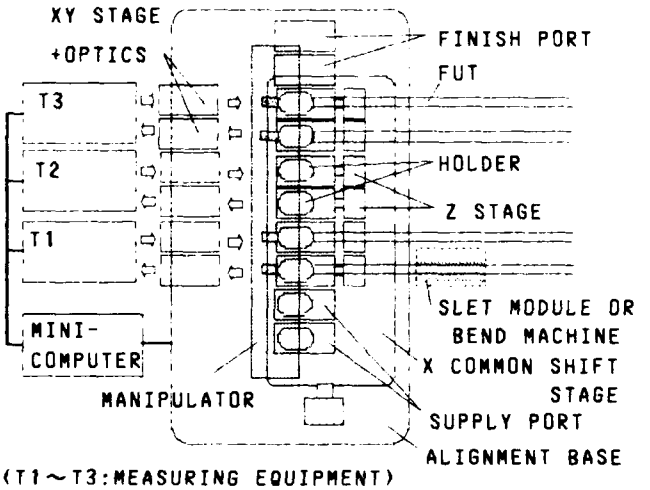

Fig.6 A block diagram of the constructed automated optical fiber test system.

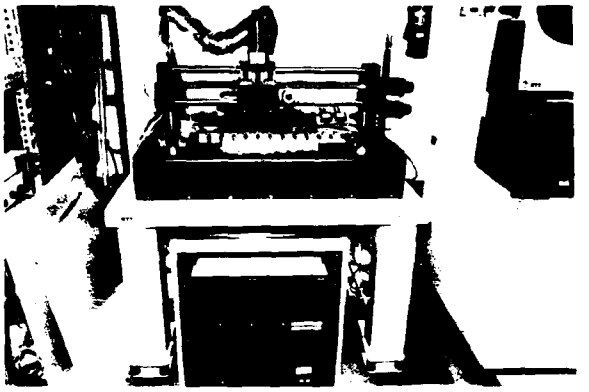

Fig.7(a) The system for GI fibers (alignment systems, a manipulator and local controllers).

Fig.7(b) The system for SM fibers.

Table 5. Performance of the GI fiber system

Items	method	time	repeatability
loss	RFCT	2 min.	±0.02 to 0.05dB
6dB frequency	RFCT	3 min.	2 to 10 %
structural parameters	SLET	3 min.	0.4 μm(core dia.) 0.2 μm(clad.dia.) 0.3 %(eccentricity) 0.005(N.A.) 0.3 %(noncircular.)
total time/fiber /all items		3min.45 sec	(with multitask & transportation)

(note) Each time includes automated alignment.

Performance shown in **Table 6** is of the SM fiber system applied to an optical fiber ribbon containing 10 SM fibers.

Table 6. Performance of the SM fiber system (applied to 10-fiber optical fiber ribbons)

Items	method	time	repeatability
loss spectrum & cutoff wavelength	FTS	<5 min.	±0.04 dB 2nm
mode field dia.	SFPT	2 min.	0.05 μm
structural parameters	TNFT	2 min.	0.1 μm(clad.dia.) 0.2 μm(eccentricity)
total time/fiber /all items		5 min.	(with multitask & transportation)

(note) Again, time contains automated alignment.

Similarly, these results also show that the measuring rate for SM fibers is 7 to 10 times faster than the conventional methods. A remarkable feature of these systems is that we can add one or two measuring items to these systems beyond those mentioned above, such as backscattered power and dispersion, and the throughput mentioned above remains nearly the same due to the system's multitask operation. Almost all operations for alignment and measurement are independently done by local controllers and measuring equipment.

CONCLUSION

Two types of all-in-one high-speed automated optical fiber test systems are developed, on which all specification items are measured under the control of only one operator. One type measures graded-index multimode fibers and the other measures single-mode fibers. Optical fiber ribbons containing up to 10 fibers can be directly measured by these systems without peeling off each fiber. The measuring rate is many times faster than the conventional semi-automated method.

ACKNOWLEDGEMENTS

The authors wish to thank Dr.F.Nihei, Mr.A.Sakamoto and Dr.Y.Koyamada for their useful suggestions and comments. The authors also would like to thank Dr.N.Kojima and Dr.N.Uchida for their encouragement throughout this work.

REFERENCES

1. Y.Katsuyama, S.Hatano, K.Hogari and T.Kokubun, "Higher-Density Single-Mode Optical Fiber Cables Than 1 Fiber/mm^2, Containing Hundreds of Fibers," Electron. Lett., Vol.23, No.10, pp.481-482,1987.

2. M.Hamada, K.Osaka, M.Fukuma and Y.Asano, "Development of a Coat Stripping Tool for Optical Fiber-Ribbon," Autumn National Conv.IEICE Japan, No.B-354,1988.

3. T.Haibara, "Design and Development of an Automatic Cutting Tool for Optical Fibers," IEEE J. Lightwave Technol., Vol.LT-4, No.9, pp.1434-1439, 1986.

4. Photon Kinetics Catalogue No.PN191,1988.

5. K.Yamashita, M.Tateda and H.Azuma, "Core Diameter Measurement of Graded-Index Multimode Fibers by the Side Launch Excitation Technique," IEEE J. Lightwave Technol., Vol.6, No.7, pp.1249-1255, 1988.

6. Y.Koyamada, T.Horiguchi, M.Tokuda and N.Uchida, "Theoretical Analysis of Optical Fiber Mode Exciters Constructed with Alternate Concatenation of Step-Index and Graded-Index Fibers," Trans. IECE Japan, Vol.J67-B, No.7, pp.722-729, 1984.

7. W.Love, "Novel Mode Scrambler for Use in Optical-Fiber Bandwidth Measurement," in Dig. Top. Meet. Optical Fiber Commun., Optical Society of America, Washington DC, 1979.

8. K.Yamashita, M.Yano, Y.Koyamada, "An Optical Fiber Gap Sensor," National Conv. IECE Japan, No.2201, 1986.

9. W.C.Young, L.Curtis, T.L.Williford and P.Kaiser, "Design and Performance of the Biconic Connector Used in the FT3 Lightwave System," 30th IWCS Proc., pp.411-417, 1981.

10. Y.Kato, S.Seikai, N.Shibata, S.Tachigami, Y.Toda and O.Watanabe, "Arc-Fusion Splice of Single-Mode Fibers 2: A Practical Splice Machine," Appl. Opt., Vol.21, No.11, pp.1916-1921, 1982.

11. K.Yamashita, M.Tateda, "Fiber Probe Far-Field Technique for Mode-Field Diameter Measurement of Single-Mode Fibers," Electron. Lett., Vol.24, No.2, pp.84-85, 1988.

Katsuya Yamashita

NTT Transmission Systems
Laboratories
Tokai, Ibaraki,319-11, Japan

Katsuya Yamashita graduated from the Kumamoto University, and he received B.S. degree in electrical engineering in 1975. He joined Electrical Communications Laboratories, NTT, in 1975, where he worked on development of submarine optical fiber cables. Since 1982, he has been engaged in research on test equipment for transmission characteristics on single-mode and mulimode optical fibers. He is a member of IEICE Japan.

Mitsuhiro Tateda

NTT Transmission Systems
Laboratories
Tokai, Ibaraki, 319-11, Japan

Mitsuhiro Tateda graduated from the University of Tokyo in physical engineering, in 1972, and received Dr of Science degree in 1982. After joining Electrical Communications Laboratories in 1974, he worked on the transmission characteristics of optical fibers, multimode graded-index, and single-mode fibers for the practical design of trunc-line optical cables. He worked also on optical integrated circuits for optical transmission systems. He is now Senior Research Engineer, Supervisor, Transmission Systems Laboratories, responsible for optical fiber cable measurement. He is a member of the OSA, and the IEICE Japan.

Hiroaki Azuma

NTT Transmission Systems
Laboratories
Tokai, Ibaraki, 319-11, Japan

Hiroaki Azuma graduated from the Fukuyama High School in 1979. He joined NTT in 1979. Since 1986, he joined Electrical Communications Laboratories, and he has been engaged in development of automated measurement systems for graded-index multimode fibers and single-mode fibers.

THE IMPORTANCE AND APPLICATION OF DISPERSION OF MULTIMODE FIBER IN LAN's AND ITS RELATION TO NA

M. J. Hackert

Corning Glass Works, SP-BN
Corning, New York 14831

Abstract

In the search for more cost effective solutions to communications needs, system designers are now giving more consideration to using wide spectral width sources such as LED's, performing wavelength division multiplexing (WDM), and increasing the system's operating frequency or bit rate. In these cases, chromatic dispersion of multimode fiber (MMF) can be very significant and should be a specified optical parameter to ensure proper system operation.

To save the system designer the expense of costly dispersion measurements which minimize the risk that the system will not meet specification, a simple means of accurately calculating the chromatic dispersion from MMF's numerical aperture (NA) fabricated by Corning's outside vapor deposition (OVD) process has been developed. Theory predicts that a relationship between dispersion and NA should exist. This paper presents the results of an experiment (Appendix 2) that characterized this dispersion versus NA relationship for all common MMF types and summarizes the means of applying the calculated dispersion to a given system design (Appendix 3).

Optical Fiber Dispersion

The information carrying capacity of optical fibers, both single-mode (SMF) and multimode (MMF), is limited by the temporal dispersion which occurs in a fiber. There are two main forms of dispersion which occur in optical fibers: chromatic dispersion and intermodal dispersion. Chromatic dispersion consists of two components - material or intramodal dispersion and waveguide dispersion.

Table 1 - Types of Dispersion

1) **Chromatic Dispersion**
   a) **Material or Intramodal Dispersion**
   b) **Waveguide Dispersion**

2) **Intermodal Dispersion**

Chromatic dispersion measurements typically give a value which is inclusive of its two parts. Intramodal dispersion, or within mode pulse broadening, is caused by the fact that light at different wavelengths propagates at different speeds due to the material characteristics of silica based glass. This effect can thus be minimized by using a source with a known central wavelength and a narrow enough spectral width so a pulse of light (being carried by one mode of the fiber) sees essentially one propagation delay.

Waveguide dispersion results from the fraction of the power in the highest order mode which propagates in the cladding changing as a function of wavelength. (This should not be confused with cladding modes which are undesirable and which typically are attenuated by the fiber's coating.) For multimode fiber, waveguide dispersion is negligible because the relative percentage of the cladding power is so small. However, for single-mode fiber, the percentage of the power carried outside of the core of the fiber is large enough to make it a contributing factor. In practice, one value for chromatic dispersion is reported because it is difficult to separate waveguide dispersion from intramodal or material dispersion. A bandwidth (chromatic bandwidth) can be calculated from the chromatic dispersion.

Intermodal pulse broadening occurs because all of the modes (rays of light) of a multimode fiber do not arrive at the output of the fiber at the same time. Although grading the index of the core improves the consistency of the modal delays[5], intermodal dispersion will still have an impact on multimode fiber information transmission, even for a theoretically ideal, graded-index profile. In order to measure the intermodal dispersion, a narrow spectral width source is chosen so that the impact of chromatic dispersion is less than 5%. The resulting measurement is usually called the bandwidth or intermodal bandwidth of the fiber and is the number typically specified for a fiber.

Importance of Chromatic Dispersion

In the search for more cost effective solutions to communications needs, system designers are now considering using wide spectral

width sources such as LED's and performing WDM to increase the number of channels per fiber. LED's usually provide lower cost and better reliability. However, they typically operate at 850 nm which is far from the zero dispersion wavelength (called Lambda 0 or λ_0) of the fiber. Two wavelength windows which are typically chosen for WDM operation are 850 nm and 1300 nm. Although the 1300 nm window is near to the fiber's zero dispersion wavelength, the 850 nm window is sufficiently far from lambda 0 that the fibers' chromatic dispersion is large and can degrade the bandwidth significantly.

Even near the zero dispersion wavelength of the fiber, chromatic dispersion can become significant as the transmission frequency or bit rate is increased. Increased bit rate is a viable upgrade scenario being considered for laser based systems already in the field. For these systems, the designer needs to know the fiber's dispersion relative to the system source's wavelength. This will permit the determination of whether or not the system will operate with the required signal-to-noise or bit-error ratio at the higher operation speed. For a system designer to take the fullest advantage of the fiber's capability to carry information and to provide the most cost effective communication system, the fiber's chromatic dispersion must be known.

There have traditionally been two common ways to minimize the impact of chromatic dispersion and avoid explicit consideration of it. One alternative is to use a narrow spectral width source such as a laser. A second alternative is to choose the operating wavelength corresponding to the fiber's zero dispersion wavelength (normally near 1300 nm). These alternatives may have been a viable design methodology in the past. However, in today's competitive market, they are losing commercial acceptability because of their inherent higher cost penalties.

Dispersion measurements (described later in Appendix 1) are relatively complex, are typically time consuming to perform, and require a large investment in capital equipment. This leads to a high cost for the measurement. Since the dispersion of the fiber does not change from the time of manufacture, a system designer should insist on manufacturer specifications for chromatic dispersion. Chromatic dispersion specification by the fiber manufacture provides the system designer with a vital piece of information which is required to remove some of the risk that the system will not operate at the needed bandwidth or bit rate.

Application of Dispersion

In order to estimate the system bandwidth, the chromatic dispersion of the fiber must be known. Some manufacturers provide a specified value of chromatic dispersion for their single-mode fiber similar to that provided for Corning's single-mode fiber or LNF™ 62.5 μm multimode fiber. The specification should bracket the fibers' zero dispersion wavelength with a certain range, and also should bracket the slope of dispersion versus wavelength at the zero dispersion wavelength. Such a specification is a minimum requirement for sound system design.

In some cases the system designer may desire an even more precise estimate of a specific fiber's chromatic dispersion. Traditionally, this required expensive and difficult measurements of the individual fiber. Recently, Corning has found a very strong empirical relation in its manufacturing process between fiber NA and chromatic dispersion (see Appendix 1 and 2). Since an individual fiber's NA measurement is easier to make than a dispersion measurement and is a normal production measurement on Corning fibers, this relationship allows precise calculation of a fiber's Chromatic dispersion (Equations 3, 7, and 8 in Appendix 1 and 2). Because of variations between fiber manufacturing processes, this empirical relation is only expected to apply to Corning fiber; other relations could also be derived for fiber from other manufacturing processes.

It was implied earlier that dispersion becomes more significant as the operating wavelength shifts further and further off the zero dispersion wavelength. This effect has been modeled using the equations for chromatic dispersion developed in Appendix 1 and 2, and translating the two dispersion factors (chromatic and intermodal) into system bandwidth (see Appendix 3).

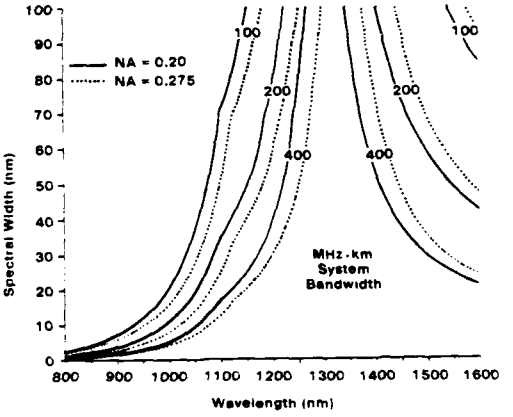

Maximum Spectral Width For A 10% Intermodal To System BW Error

Figure 1

The impact of spectral width as a function of wavelength is displayed in Figure 1. In Figure 1, the chromatic dispersion caused by the spectral width of the source, where the difference between the system bandwidth and the manufacturer's

specified intermodal bandwidth is 10%, is plotted as a function of wavelength. The NA used in the dispersion calculation was chosen to be 0.20 and 0.275, which corresponds to the nominal values of the more popular fiber sizes, 50 and 62.5 μm fiber, respectively. A range of system bandwidths were evaluated - in this case 100, 200, and 400 Mhz.km.

A number of key observations can be made from Figure 1. First, irrespective of system bandwidth and fiber NA, the allowable spectral width for a 10% degradation in the intermodal bandwidth at 850 nm is small (less than 5 nm). Next, at 1300 nm, the allowable wavelength region, over which the spectral width is insignificant, becomes much narrower as the expected system bandwidth increases. Thus, consideration should be given to how tightly the nominal wavelength of the source should be specified or traded off against a tighter spectral width restriction. Another observation is that NA tends to shift the curves to longer wavelengths as NA increases.

From the discussion to this point, it should be evident that dispersion has the ability to limit the maximum attainable bandwidth of a system. This is readily apparent in Figure 2. In Figure 2, the resultant system or link bandwidth is plotted versus the measured intermodal bandwidth at 850 nm. For the calculation of the chromatic bandwidth, a range of spectral widths were used - 25 nm, 50 nm, 75 nm, and 100 nm.

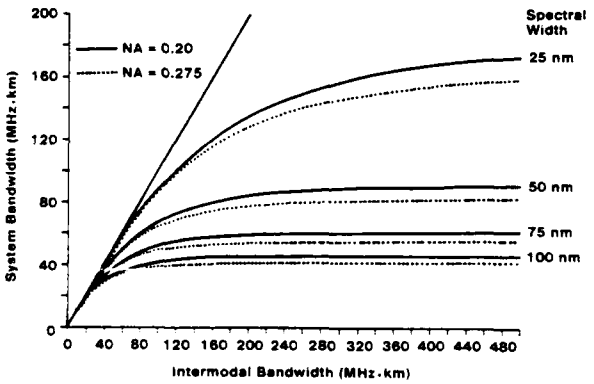

System Bandwidth At 850 nm For Various Spectral Width Sources

Figure 2

The impact of dispersion at 850 nm is very dramatic. The maximum system bandwidth approaches 170, 90, 60, and 45 Mhz.km for 25 nm, 50 nm, 75 nm, and 100 nm spectral width, respectively. These system bandwidths are reduced by 5 to 10 Mhz.km for 0.275 NA fiber as compared to the 0.20 NA fiber which has lower dispersion at 850 nm. Therefore, depending on the spectral width of the system source, choosing a fiber with a higher bandwidth may have little or no effect on increasing the end-to-end system bandwidth.

The degradation in the information carrying capacity of a link due to the spectral width of the source was demonstrated in Figure 1. First, the spectral width at which the chromatic dispersion causes the system bandwidth to be reduced by 10% from the fiber's bandwidth was plotted. At 850 nm, this spectral width is less than 5 nm. Figure 2 shows the asymptotic relation between system bandwidth and intermodal bandwidth for a range of common spectral widths. For a spectral width of 100 nm, the system bandwidth can not exceed 45 Mhz.km.

Conclusions

Chromatic dispersion for a multimode fiber can prevent a system from achieving the required information carrying capacity, irrespective of the bandwidth of the fiber used in the system, and should be evaluated prior to installation. Therefore, a system designer should insist on specifying chromatic dispersion when using wide spectral width sources at 850 nm such as LEDs. Also, by insisting on manufacturer specifications for chromatic dispersion, a system designer can save the added expense of costly measurements (both in time and in equipment).

Since it is not practical to measure dispersion on every fiber at every wavelength, a simple means of accurately predicting dispersion from NA over a range of 0.20 to 0.29 for fiber manufactured by Corning's OVD process has been developed and presented in this report. Thus, a system designer can use this algorithm to more precisely predict the information carrying capacity of the system prior to actual installation, and consequently optimize the system.

Appendix 1 - Measurement Overview

Chromatic dispersion is typically measured by the Electronic Industry Association's (EIA's) Fiber Optic Test Procedure (FOTP) number 168[1]. The technique described by FOTP 168 is relatively simple. The time-of-flight differences of different wavelength light pulses are measured. A centroid calculation is used to improve the precision of determining the pulse's delay.

Lasers are used to produce the pulses to obtain both temporally narrow (on the order of 400 psec or less) and spectrally narrow pulses (typically less than 10 nm). The narrow temporal width allows accurate and precise determination of the pulses' relative time-of-flight. The narrow spectral width produces limited chromatic broadening which could degrade the time-of-flight determination. The sources' wavelengths are

chosen between 800 nm and 1600 nm to achieve a range of delays. A modescrambler is used to produce a spatially and angularly overfilled launch. Figure 3 presents the block diagram of the apparatus.

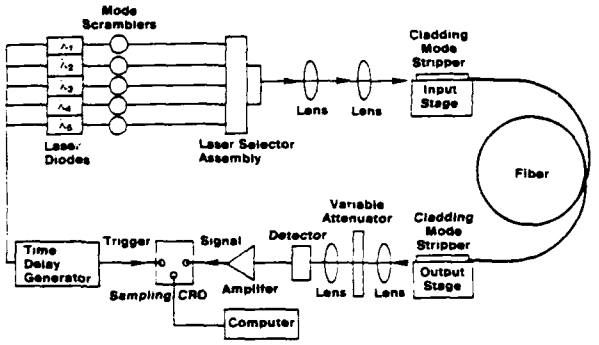

Multimode Fiber Chromatic Dispersion Measurement System

Figure 3

The delays are next fitted to equation 1 by a least-squares curve fitting routine.

$$[1] \quad \tau(\lambda) = A + (B * \lambda^2) + (C * \lambda^{-2})$$

where $\tau(\lambda)$ = relative time of flight
λ = wavelength
A, B, and C - fit coefficients

In order to convert the time delay into dispersion as a function of wavelength, equation 1 is differentiated to give equation 2.

$$[2] \quad D(\lambda) = (2 * B * \lambda) - (2 * C * \lambda^{-3})$$

where $D(\lambda)$ = dispersion

Equation 2 can then be modified to yield equation 3.

$$[3] \quad D(\lambda) = \frac{S_o * \lambda}{4} * \left[1 - \left(\frac{\lambda_o}{\lambda} \right)^4 \right]$$

where λ_o = zero dispersion wavelength
S_o = slope at zero dispersion wavelength

The zero dispersion wavelength and the slope at the zero dispersion wavelength fall directly out of equation 3. Because of their ability to completely describe the dispersion of a fiber, standards organizations have agreed to specify dispersion in terms of a range of zero dispersion wavelengths and a maximum value for the zero dispersion wavelength's slope. Thus, an accurate determination of the chromatic dispersion, which a source with a known spectral width will produce, can be made by a designer to ensure that the system will function as required.

Several additional, useful relationships between the fit coefficients B and C, and the zero dispersion wavelength and the slope at the zero dispersion wavelength are given in equations 4 and 5.

$$[4] \quad \lambda_o = \sqrt[4]{(C/B)}$$

$$[5] \quad S_o = (8 * B)$$

These equations allow a jump between the fit to the delay data and λ_o and S_o without having to actually perform a differentiation.

Appendix 2 - The Experiment

The fiber's dispersion results from the wavelength dependence of the propagation delay, or index of the glass, which makes up the fiber's core and cladding. The exact relationship between dispersion and index is complex and is outside the scope of this paper. However, it depends among other things on the NA of the fiber. This is intuitively acceptable since NA is also a function of index according to equation 6[2].

$$[6] \quad NA = \sqrt{(n_1^2 - n_2^2)}$$

where n_1 = core index
n_2 = clad index

Since theory predicts a relationship between dispersion and NA, approximately 50 fibers with NA's covering the range of the four standard MMF types (0.20, 0.26, 0.275, and 0.29) were selected and measured to specify the range of MMF dispersion. The results of the measurements are plotted in Figures 4 and 5. Figure 4 displays zero dispersion wavelength (λ_o) versus NA; and Figure 5 displays the slope at the zero dispersion wavelength (S_o) versus NA.

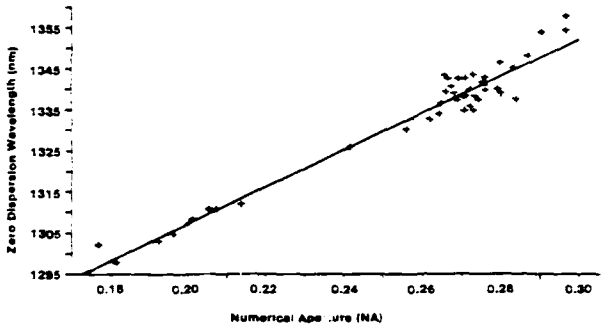

Multimode Fiber Chromatic Dispersion NA Regression Model

Figure 4

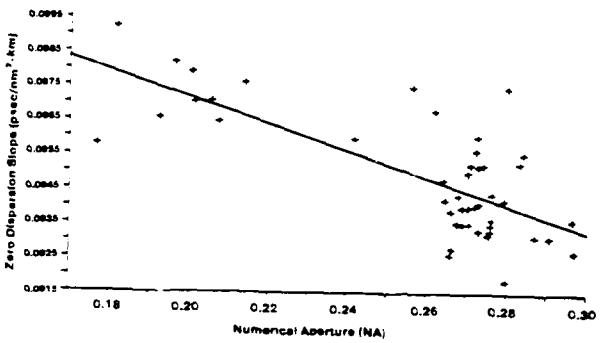

Multimode Fiber Chromatic Dispersion NA Regression Model

Figure 5

Conveniently, a linear relationship to NA accurately predicted the dispersion results. The regression model is included on both graphs and are given in equations 7 and 8.

$$[7] \quad \lambda_o = 1221.04 + (425.78 * NA)$$

$$[8] \quad S_o = 102.234 - (22.16 * NA)$$

For the zero dispersion wavelength, the correlation is visibly quite good over the range of NAs from .20 to .29 (Figure 4). In the case of the slope (Figure 5), the correlation is limited by the measurement error. The regression's root mean squared error (RSME or effectively the standard deviation of the error about the fit) is on the order of the measurement reproducibility of the dispersion measurement. Therefore, the relationship is as good as could be expected without making major improvements to the measurement system.

Appendix 3 - System Design Equation

Dispersion takes on real world meaning by use of a few simple system design equations. Because chromatic dispersion and intermodal dispersion are statistically independent, they can be added in quadrature as given in equation 9[3].

$$[9] \quad \frac{1}{BW^2_{system}} = \frac{1}{BW^2_{inter}} + \frac{1}{BW^2_{chrom}}$$

where BW_{inter} = intermodal bandwidth caused by the propagation delay differences of the different modes, multiplied by the system length

BW_{chrom} = chromatic or intramodal bandwidth resulting from material and waveguide dispersion, multiplied by the system length

The intermodal bandwidth is typically specified by the fiber manufacturer. The chromatic bandwidth needs to be calculated from the dispersion by equations 10 and 11[4].

$$[10] \quad BW_{chromatic} = \frac{187{,}000}{sigma_{chrom}} \quad \text{away from } \lambda_o$$

where $sigma_{chrom} = (.425 * \Delta\lambda * D(\lambda))$

$\Delta\lambda$ = full width half maximum (FWHM) spectral width

$$[11] \quad BW_{chromatic} = \frac{187{,}000}{sigma_{chrom}} \quad \text{near } \lambda_o$$

where $sigma_{chrom} = \{ (.425*\Delta\lambda*D(\lambda)^2) + (S_o^2 * (.425*\Delta\lambda)^4/2) \}^{1/2}$

Equation 10[2] applies to wavelengths far from the zero dispersion wavelength such as 850 nm. However, near the zero dispersion wavelength, this equation goes to zero although a wide spectral width source still experiences pulse broadening. Therefore, equation 11 includes second order effects and should be applied to wavelengths near the zero dispersion wavelength.

References

(1) Electronic Industries Association Fiber Optic Test Procedure 168, "Chromatic Dispersion Measurement of Multimode Graded-Index and Single-Mode Optical Fibers by Spectral Group Delay Measurement in the Time Domain", ANSI/EIA-455-168-1987, May 18, 1987.

(2) J. E. Midwinter, Optical Fibers for Transmission, New York, NY: John Wiley & Sons, 1979.

(3) J. Matthews, P. Reitz, "Measurement and Characterization of Optical Fiber Designed for Communication Systems with LED Sources", presented at the SPIE Fiber Optics Technical Symposium - 500, San Diego, California, August 21-22, 1984.

(4) D. Schicketanz, W. S. Jackman, "Effective Fiber Bandwidths in LED Based Systems", presented at the Symposium on Optical Fiber Measurements, 1986.

(5) Higher order modes modes, which tend to travel closer to the clad, have further to travel than lower order modes, which tend to travel closer to the center of the core. The graded index causes the higher order modes to propagate faster and arrive at the same time as the lower order modes.

Bibliography

Mr. Michael J. Hackert is a Sr. Electro-Optical Measurements Engineer at Corning Glass Works's Waveguide Product Engineering Lab in Corning, New York. He is responsible for developing and coordinating optical-fiber evaluation methodology, qualification tests, and selected customer measurement projects; and developing industry-wide test procedures that support standards activities. He came to Corning in 1982 after receiving his MSEE degree from Stanford University and a BSEE degree from Catholic University in 1980.

ACCURATELY PREDICTING CUTOFF WAVELENGTH OF CABLED SINGLE MODE FIBER

William H. Hatton and Masayuki Nishimura

Sumitomo Electric Fiber Optics Corporation,
Research Triangle Park, North Carolina, 27709

ABSTRACT

A new uncabled fiber deployment was developed to accurately simulate the cabling induced curvature effects on cabled fiber cutoff wavelength. Cable independent linear mapping routines were develo, experimentally for matched and depressed clad fiber. For typical effective bend diameters (curvature of fiber inside cable) of 100 mm to 200 mm, maximum cutoff wavelength shifts of 22 nm (depressed) and 50 nm (matched) were observed. Comparison between simulated and measured cable cutoff wavelength (FOTP-170) showed good correlation.

I. INTRODUCTION

The cutoff wavelength of the second order, LP_{11}, mode is an important parameter for characterizing single mode fiber because it is the wavelength above which single mode operation exists. Operation near or below the cutoff wavelength increases dispersion and produces modal noise (interference between the first and second order modes) both of which are undesirable from a system designer's point of view. The theoretical cutoff wavelength can be easily calculated from fiber design information (i.e. refractive index difference and core diameter), however, this parameter is of little importance because near cutoff wavelength both length and curvature effects substantially increases the attenuation of the LP_{11} mode. For this reason, an effective cutoff wavelength, determined from a fiber deployment which best simulates actual condition, must be utilized.

Accurate prediction of cutoff wavelength for cabled single mode fiber is desired because fibers which exhibit long theoretical cutoff wavelength (above operation wavelength) and possess improved performance (more resistance to micro/macro bending) can be used. To achieve this on a routine basis a measurement deployment that 1) simulates cabling effects precisely , 2) is not dependent on cable design, and 3) allows cabled fiber performance to be predicted from uncabled data must be developed.

The Electronic Industries Association (EIA) has adopted a test procedure (FOTP-170) [1] where cutoff wavelength is determined by measuring a 22 meter section of cabled fiber. This method produces results which best simulates worst case field conditions (typical minimum restoration length), however, routine measurements would be uneconomical from a cablers point of view and impossible for a fiber manufacturer.

To remove the economical drawback of the above method it has been suggested that a linear mapping function which maps uncabled fiber cutoff (FOTP-80)[2] into cabled fiber cutoff be experimentally determined [3]. This a beneficial

procedure, but without a complete knowledge of how cable structure effects cutoff, a different mapping would be required for each cable design and manufacturing process change (a very time consuming process)

It has also been suggested that the cable deployment conditions of FOTP-170 could be simulated by substituting the 20 meters of cable with 20 meters of uncabled fiber bent at a minimum bend radius of 140 mm [4]. This substitution is believed to be based on the facts that for matched clad fiber, the 76 mm bends would sufficiently strip the higher order modes (at the wavelengths of interest) and cabling effects would be inconsequential, and conversely, typical depressed clad fiber , being more resistance to bending induced losses [5], would exhibit only a length dependence.

These conclusions may be adequate for specific cable designs, but in most cases, the results would be extremely pessimistic due to an over exaggeration of fiber curvature (i.e. effective cabled fiber bend diameters of 100 mm to 200 mm are common). In this paper, a new method which utilizes both length and curvature effects to accurately simulate cabled fiber cutoff wavelength is introduced. In addition, the relationship between cabling induced bending and cutoff wavelength shift (uncabled - cabled) with focus on the development of a cable independent mapping routine is presented.

II. THEORETICAL BENDING LOSS OF LP_{11} MODE

The effective cutoff wavelength is the wavelength where the loss of the LP_{11} exceeds a required value. EIA/FOTP-170 specifies cutoff as the wavelength where the power contribution from the second order mode is 0.10 dB as referenced to the total power of the primary mode. Applying the basic loss equation to the above condition,

$$0.1\ dB = 10 * \log_{10} \frac{P_1 + P_2 e^{-\alpha}}{P_1} \qquad (1)$$

where P_1 and P_2 are the total power of the fundamental and second order modes respectively, and α is the attenuation coefficient of the second order mode, requires the total attenuation of the LP_{11} to be 19.38 dB at cutoff.

Cable cutoff wavelength can be determined theoretically by calculating the losses of the second order mode for the bending/deployment conditions of FOTP-170 (Figure 1)

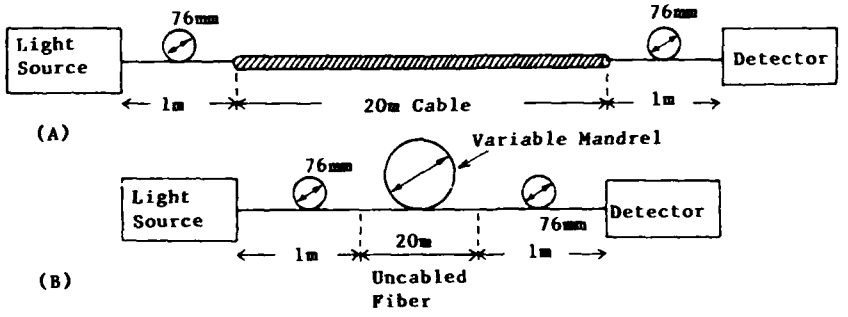

Figure 1 Schematic diagrams of A) deployment for cable cutoff per FOTP 170, and B) simulated cable cutoff

$$\alpha_{LP11} = 2 * L_{76} * \alpha_{76} + L * \alpha_{cable} = 19.36 \text{ dB} \quad (2)$$

where α_{76} is the attenuation due to the 76 mm mandrel, α_{cable} is the cabling induced bending losses calculated from an effective bend diameter, L_{76} is length of fiber around the 76 mm mandrel, and L is a compensation factor for cable length. The effective bend diameter can be derived mathematically for most cable structures, and Eq. (3) applies to the common loose tube, helical pitch design.

$$R_{effective} = \frac{D}{2} + \frac{P^2}{2\pi^2 D} \quad (3)$$

where D is the helix planar diameter, and P is the helix pitch length.

As stated earlier, it has been proposed, and currently in the ballot approval cycle of EIA, that 20 meters of uncabled fiber wrapped around a 280 mm mandrel could be used to simulate cabling effects. Table 1 summarizes the calculated shift in cabled fiber cutoff wavelength with respect to effective bend diameter as compared to the above recommended simulation. Both depressed and matched clad fibers were studied, and curvature loss calculations were based on the derivations presented in references [6,7,8].

Fiber Type	Effective Bend Diameter (mm)				
	250	200	160	120	80
Matched	0	0	2	11	40
Depressed	0	1	1	4	18

Table 1 Theoretical shift in cable cutoff wavelength with respect to effective bend diameter. All results are referenced to 280 mm simulation.

For both fiber types the 76 mm mandrels induced the most bending losses. For the spectrum of radii analyzed, matched clad, being more bend sensitive[5], showed the largest overall shift. In either case, these results suggested cabling effects are important and must be simulated if accurate predictions of cabled cutoff is to be achieved. To further understand this impact a new simulation technique was developed , and a battery of tests conducted.

III. EXPERIMENTAL STUDY

Figure 1 shows the cable deployment conditions specified by FOTP-170, and the fiber deployment developed to offer a variable scheme for simulating cabling effects on cutoff wavelength. With the addition of a variable mandrel, the 20 meters of uncabled fiber can be looped at a bend diameter equivalent to that occurring inside the cable. By adjusting the mandrel size, the relationship between cabling induced curvature effects and cutoff wavelength was modeled.

A collection of commercially available depressed and matched clad single mode fibers were analyzed. Each sample was 24 meters in length: 22 meters for cable cutoff simulations and 2 meters for fiber cutoff wavelength measurements. All fibers were subjected to mandrel diameters ranging between 80 mm to 280 mm, and cutoff was determined by comparing the spectral power transmitted through the simulated deployment to that when an additional smaller diameter mandrel (typically 30 mm) was introduced. For each test, the 20 meters of looped fiber was secured and removed from the mandrel to eliminate the possibility of introducing microbending. Uncabled fiber cutoff was determined by u ing FOTP-80 method A.

Because of the linearity of the measured results a linear least squares fit was used to

$$\lambda_{cs} = m * \lambda_{cf} + b \quad (4)$$

develop a relationship between uncabled and simulated cutoff wavelength. Figures 2A + B illustrates this relationship for matched and depressed clad fiber respectively.

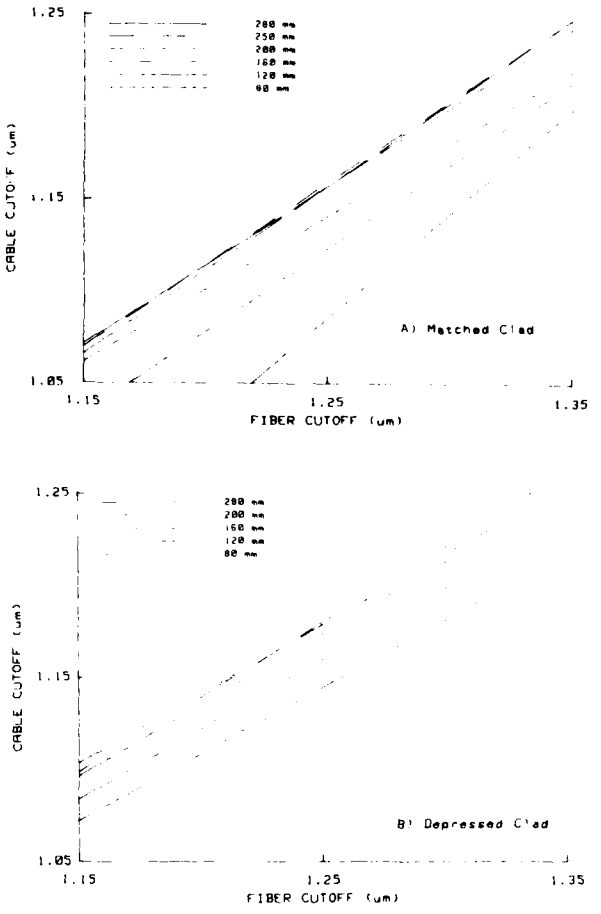

Figure 2 Relationship between simulated cable cutoff and uncabled cutoff for various effective bend diameters (A-matched clad, B-depressed clad)

For the most part, the slope of each curve as a function of bend diameter was constant, only the intercepts changed (i.e. relationship between fiber and simulated cutoff remained constant over the wavelength range of interest, only the magnitude of this relationship changed with respect to mandrel diameter). The small skewness observed was due to a narrow distribution of fiber cutoff wavelengths.

It is interesting to note that both fiber types possessed a critical effective bend diameter (200 mm for matched, 160 mm for depressed) where curvature effects become important.

To examine the above effects more closely the average shift in cutoff wavelength for each mandrel, as referenced to uncabled , was calculated. Figures 3A + B illustrates this relationship for both fiber types. Also shown are theoretically determined curves computed from equations (2) and (3). Both experimental and theoretical showed a comparable dependence. There was, however, a bias with respect to critical diameter implying more bending loss occurs at small bend diameters. This offset may be a function of nonuniformities in fiber structure (from ideal/theoretical) and/or coating induced bending losses. In any case, this additional loss would be present in cable form, and for typical bend diameters of 100 mm to 200 mm cutoff wavelength shifts of 22 nm (depressed) and 50 mm (matched) would occur.

The final step of the analysis was to verify the accuracy of this new simulation technique. Five loose tube/helical pitch cables with different effective bend diameters were measured for cutoff wavelength per FOTP-170. Each sample was 24 meters in length: 22 meters for cable cutoff deployment and 2 meters for fiber cutoff measurements (FOTP-80). Predicted cutoff was determined from fiber cutoff data utilizing the experimentally derived mapping functions. When the effective bend diameter fell between fitting

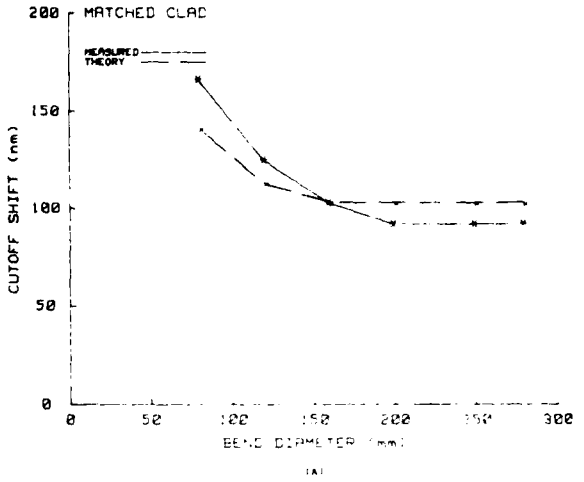

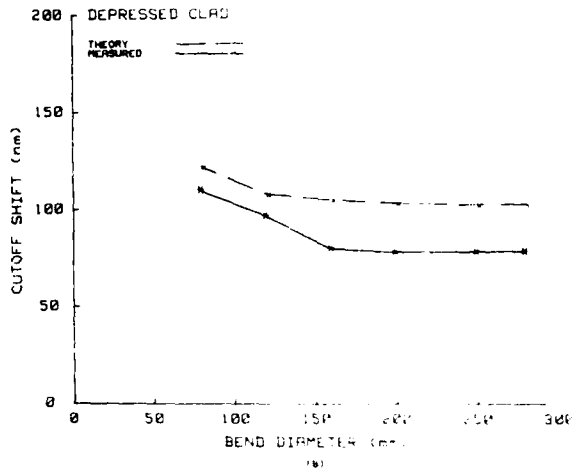

Figure 3 Relationship between effective bend diameter and cutoff shift (uncabled - simulated) for A) matched clad fiber and B) depressed clad

equations, interpolation was used. Table 2 summarizes the results. The average difference and standard deviation (1σ) between predicted and measured results were .25 nm and 3.2 nm respectively.

Fiber Type	Effective Bend Diameter (mm)	Cutoff wavelength Shift (nm)	
		Measured	Predicted
D	160	83	80
D	146	89	87
D	160	77	80
M	120	121	124
M	284	96	93

Table 2 Measured and predicted cabled fiber cutoff for various loose tube cable structures (D-depressed clad, M-matched clad).

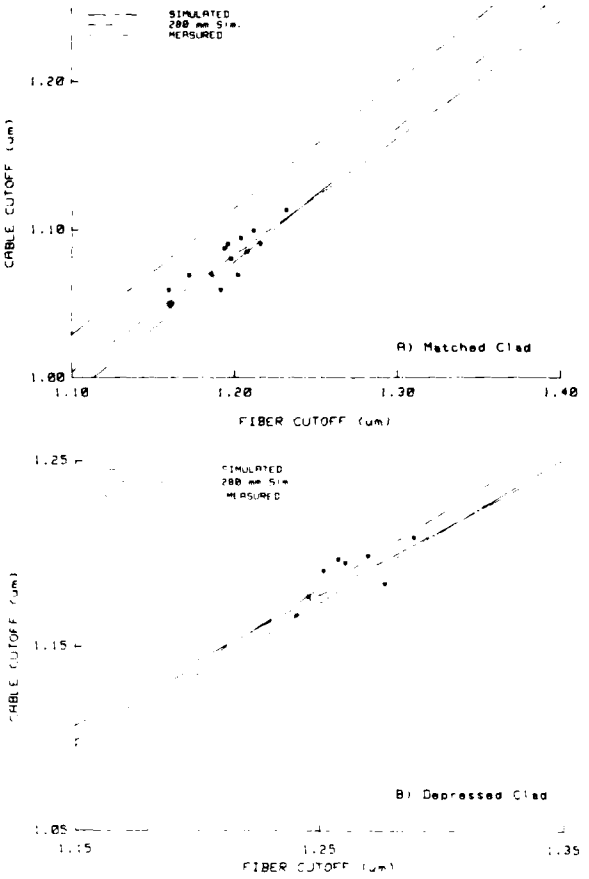

Figure 4 Comparison between predicted and measured cabled cutoff wavelength for A) matched clad and B) depressed clad. 280 mm mandrel simulation is shown for reference

Figures 4A + B compare predicted and measured data (linearly fitted) for two of the measured cables. In addition, results from a 280 mm mandrel simulation are shown for reference. The cable shown in Figure 4A contained depressed clad fiber and exhibited an effective bend diameter of 160 mm. Since this diameter exceeded the critical diameter for this fiber type, there was little to no difference between the two simulation techniques and the measured results. On the other hand, the cable shown in Figure 4B had an effective bend diameter of 120 mm, and contained matched clad fiber. In this example, the new simulation technique and measured results showed good correlation. The 280 mm mandrel simulation showed an offset of approximately 40nm. It is obvious from this condition, that if accurate prediction of cabled fiber cutoff wavelength is required cabling induced curvature effects must not be neglected.

IV. CONCLUSIONS

The cabling induced curvature effects on cabled fiber cutoff wavelength was examined. Both theoretical and experimental results showed cabled cutoff wavelength to be a function of the fiber's effective bend diameter inside the cable. For typical bend diameters ranging from 100 mm to 200 mm, cutoff wavelength shifts of 20 nm to 50 nm (depending on fiber design) would be observed. Neglecting curvature effects, or inadequate simulations (i.e. 20 m fiber/ fixed 280 mm mandrel) would significantly reduce the effectiveness of cable cutoff wavelength specifications.

A new uncabled fiber deployment was developed to accurately simulate both length and curvature effects on cutoff wavelength. This simulation is based on the ability to calculate the effective bend diameter. Experimentally developed linear mapping functions showed good correlation when compared to measured (FOTP-170). Knowing the relationship between effective bend diameter and cutoff wavelength allows cabled cutoff to be predicted for any cable design without the proliferation of numerous mapping routines.

REFERENCES

[1] EIA -455-170, "Cable Cutoff Wavelength of Single-Mode Fiber by Transmitted Power," Electronic Industries Association, Engineering Department, 2001 Eye St., N.W., Washington, DC.

[2] EIA -455-80, "Cutoff Wavelength of Uncabled Single-Mode Fiber by Transmitted Power," Electronic Industries Association, Engineering Department, 2001 Eye St., N.W., Washington, DC.

[3] J. P. Kilmer, W. T. Anderson, R. M. Kanen C. M. Connor Davenport, "Cabling Dependence of Optical Fiber Cutoff Wavelengths," IWCS Symposium Proceedings, pp. 49-56, Arlington, Va, (1987).

[4] D. W. Peckham, and F. M. Sears, "Relationship Between Fiber and Cable Cutoff Wavelength of Depressed-Cladding Fiber," in Technical Digest on Optical Fiber Communications (Optical Society of America, Washington DC, 1988), paper WE5.

[5] L. Wei, R. S. Lowe, and C. Saravanos, "Practical Upper Limits to Cutoff Wavelength for Different Single-Mode Fibers," J. Lightwave Technol., vol. LT-2, no. 9, pp. 1147-1155, 1987.

[6] D. Marcuse, " Curvature Loss Formula for Optical Fibers," J. Opt. Soc. Am.,vol. 66, no. 3, pp.216-220, 1976.

[7] D. Marcuse, "Influence of Curvature on the Losses of Doubly Clad Fibers," Appl. Opt., vol. 21, no. 23, pp. 4208-4213, 1982.

[8] V. Shah, " Curvature Dependence of the Effective Cutoff Wavelength in Single-Mode Fibers," J. Lightwave Technol.,vol. LT-5, no. 1, pp. 35-43, 1987.

William Hatton received the B.S. and M.S. degrees in Electrical Engineering from North Carolina State University in 1981 and 1983, respectively. He joined Sumitomo Electric Research Triangle Inc., in 1984 where he was engaged in optical fiber design, optical fiber characterization, and the development of new measurement techniques. In 1988 he was transferred to Sumitomo Electric Fiber Optic Corporation as a product design engineer and is currently involved in the mechanical and environmental characterization of optical fiber cables, and the research and development of new measurement techniques. Mr. Hatton is a member of the Optical Society of America.

Masayuki Nishimura was born in 1956 in Sapporo, Japan, and received the B.S. and M.S. degrees in electronics engineering from the University of Tokyo in 1979 and 1981 respectively. He joined Sumitomo Electric Industries, Ltd. in 1981 and moved to Sumitomo Electric Research Triangle Inc. in 1984. He was transferred to Sumitomo Electric Fiber Optic Corporation in 1988, and is currently manager of Product Design Engineering. Mr. Nishimura is a member of the Optical Society of America

STATUS OF REA-FINANCED RURAL SUBSCRIBER DISTRIBUTION PLANT

Gerald S. Schrage and Raymond E. Hitt

Rural Electrification Administration
Washington, D.C. 20250-1500

ABSTRACT

The future market for rural wire and cable plant is primarily influenced by three factors: 1. aging and obsolete cable plant, 2. subscriber growth, and 3. ultimate conversion to fiber optics. The current REA-financed rural loop plant is well designed and built using Feeder - Distribution Serving Area designs. This article examines the model of current loop plant using the 1986 REA loop study and investigates the paths for transitioning to the future loop plant.

THE LOOP STUDY

In 1986, the Rural Electrification Administration (REA) completed the data collection phase of a random 1,000 subscriber loop study. Since then we have translated this raw field data into an electronic data base model that we use to simulate and analyze rural telecommunications plant and facilities in the United States. This article will concentrate on the outside plant wire and cable aspects of the loop study.

The loop study data consisted of four categories of information: general interest, measured transmission values, circuit layout schematic, and associated switch information. This data was collected through on-site visits, route checks and record searches on each loop. The circuit layout schematic provided the data base for the wire and cable plant analysis. The 1,000 loops were chosen by a computerized random search routine from just over three million rural loops financed by REA. Therefore any specific numbers referred to in this article can be multiplied by 3,000 to statistically represent the total rural base financed by REA.

CURRENT STATUS OF REA-FINANCED OUTSIDE PLANT

Since 1976, REA Engineering Practices have officially endorsed the Feeder-Distribution Serving Area Design Concept using dual fine guage cables in rural telecommunications plant. The 1986 loop study has provided the first check on how well that design philosophy has been implemented by the telephone companies and their engineers. Figures 1 through 3 illustrate the composition of the current loop plant. Figure 1 (Gauge Sizes) demonstrates that up to about 60 kilofeet (kf) from the Central Office the dual fine gauge design of 24 plus 22 gauge has been followed rigorously. Beyond 60 kf the attenuation and resistance of the loop necessitates an increasing use of 19 gauge cable pairs. Interestingly, at about 70 kf we see an increasing use of the finer 24 gauge cable. This is the result of the use of remote digital switches where the availability of a new battery supply allows finer gauge cable pairs to be used at that distance from the host Central Office. Figure 2 (Cable Pair Sizes) is more subtle in its demonstration of the Serving Area Design Concept. Note the change in slope between the large (400 + pairs) cables and small (less than 100 pairs) cables. This illustrates the use of large pair count cables out a relatively short distance (generally under 20 kf) to a Serving Area Interface (SAI) point and small pair count cables predominately beyond that point. Figure 3 (Cable and Wire Types) does not illustrate Serving Area Design but, completes a picture of the cable composition. REA has recommended the use of buried cables for over 2 decades and over 90 percent of new construction is buried plant. Figure 3 demonstrates this policy has been effective and implemented as 60 to 70 percent of the total loop plant is now buried.

DISTRIBUTION MODEL OF SUBSCRIBERS AND CABLES

The physical layout of the feeder or distribution cables and distribution of the size and length of the cable segments are governed by the subscriber distribution, the natural terrain features and the physical infrastructure. As would be expected in a rural environment, the routes are characterized by low subscriber route density. The current average subscriber density in REA-financed plant is 5.7 subscribers per route mile. Figure 4 (Subscriber Distribution) gives a graphical picture of how rapidly the number of subscribers decreases with increasing distance from the central office switch. Exactly half of all rural subscribers are within 15 kf of the Central Office and over 75 percent are within 30 kf. An average REA-financed rural switch currently serves only 998 subscribers. Figure 5 (Segment Length Distribution) gives a perspective on how long a segment of cable can be placed before an obstacle is encountered that requires cutting the cable. Even in rural areas almost 50 percent of all cable segments are less than 1,000 feet long. The only exceptions to this natural distribution is caused by the use of load coils. REA has standardized on D-66 loading and a decided peak in segment length occurs at the 4,500 foot distance. There are some systems using H-88 loading as shown by the minor peak in segment length at 6,000 feet.

TOTAL RURAL WIRE AND CABLE MARKET

The rural wire and cable market is composed of different types of wire and cable construction in addition to the differences in pair size and gauge previously discussed. Table 1 (Type of Facility) lists 14 different types of wire and cable construction as sampled in the loop study. The total REA-financed rural market would be approximately 3,000 times larger because of the sampling ratio. The loop study data confirms that buried plant is predominant in REA-financed systems. Even so, there is still almost 30 percent of the plant in aerial construction.

The sheath length of the cables depends on their usage and how they are installed. Tip cables are the shortest and average only 37 feet long compared to buried filled cables averaging 2,603 feet. The fiber optic cables averaging 48,784 feet long really represent the span length from the Host Central Office to the Remote Switch. There are fiber optic splices in this span length, but that data was not collected. Average wire lengths are generally quite long ranging from 897 feet to 2,586 feet.

The average number of pairs in each cable also varies by the type of cable from 4 pairs for a buried drop cable to 1,206 pairs for a filled cable placed in underground conduit. Note the role reversal in cable pair size between air core and filled core cables. Filled core buired cables average 212 pairs and filled core aerial cables average 125 pairs. The equivalent air core cable sizes are approximately reversed in size. All of the fiber cables currently used in the loop plant are sized with 4 fibers.

In addition to the loop study data we also looked at the sheath miles under contract for 1987. In sheath miles 50 pair cables slightly exceeded the amount for the 25 pair size. Together, 25 and 50 pair cables made up 40 percent of all the total sheath miles contracted for in 1987. Also on a sheath mile basis over 90 percent of the contracted buried cables were 100 pair or smaller.

FUTURE RURAL WIRE AND CABLE MARKET

The future rural wire and cable market will be a product of at least three major factors. The immediate market will be a need to replace aging and deteriorating buried air core cables. A continuous market will be a result of subscriber growth in rural areas. A long range market will be the total replacement of all loop plant with fiber optic cables to accommodate subscriber services requiring bandwidths not practical or available with copper pair cables.

Let's look first at the buried air core cable rural market. From Table 1 and using our factor of 3,000 we estimate that there is 3.0 million sheath miles to be replaced in the near future. These cables are generally 15 or more years old. In addition they usually have some moisture content which prevents their usage for carrier based growth designs. An analysis of the location of the loops containing buried air core cables was performed. Figure 6 (Distribution of Sample Loops) is a map showing the number of loops sampled by state. The crosshatched states are those that loop survey data indicated that at least 1/3 of all loops tested

contain some buried air core segments and are candidates for early replacement.

Figure 7 (Cable Pair Sizes - Air Core Cable Only) is a graph similar to Figure 2. Notice the difference in the two graphs. Air core cables were installed during the period that the dedicated outside plant design concept was used. This resulted in larger pair size cables for longer distances. However, when these cables are replaced they will be replaced by a size distribution similar to Figure 2 resulting from a feeder - distribution design. This will produce an equivalent number of sheath miles but less conductor miles in the replacement plant.

Subscriber growth provides a continuous market for rural outside plant. Table 2 lists the rural growth for residence and business subscribers for the past 10 years in REA-financed systems. Except for the years 1985-86 most annual growth rates have been in the 2.0 to 5.0 percent range. The 10 year compounded annual rural growth rate for residence subscribers was 3.3 percent and for business subscribers 3.8 percent. In seven of the ten years, rural business growth rates exceeded the residential rates. Population growth in the South and West regions of the United States for this decade have far exceeded these rural rates. These trends are expected to continue and the rural cable market due to subscriber growth will be largest in the South and West.

Finally, in the long run, fiber optics will dominate the rural subscriber loop market. Already, as shown in Table 1, we have 55.4 miles of four fiber cable in the loop plant (1.3% of the total). So far this has been only to remote digital switches. Once economical electro-optical terminating equipment is developed it will begin to replace feeder routes to SAIs. It is expected that by the end of the next decade all new rural feeder routes will be fiber optic cables.

Our analysis of the 1987 construction contracts show that we are continuing to install fiber optic cables. At this time it is primarily for interoffice trunk routes. Last year we installed 2025 sheath-miles of fiber optic cable. These cables are being placed using the same construction methods as for copper cables. We are direct burying 89%, with 9% aerial, and 2% in underground conduit. The only exception to normal construction practices has been the depth of placement. Figure 8 (Cable Placement Depth) compares the placement depth of fiber optic cable versus copper cable. Because of the potential to disable a larger number of circuits, fiber optic cable is usually placed an extra six or more inches deeper than copper cable with 36 inches being the preferred depth.

FURTHER SUBSCRIBER LOOP PLANT INFORMATION

As a service to the telecommunications industry, REA has made the entire 1986 loop study data base publicly available in electronic form at a nominal charge. It is contained on five (5 1/4 inch) floppy disks organized in 11 files containing a total of 1,040 kilobytes of data. To use this data base all that is required is for the user to have LOTUS 1-2-3 Version 2.0 or better.

To purchase these disks, send a check for $25 payable to the "Rural Electrification Administration". Address your request to:

Gerald S. Schrage
Chief, Systems Engineering Branch
USDA/REA/TSD
Room 2832-S
Washington, D.C. 20250-1500

Gerald S. Schrage is a native of New York State. In 1960 he received a B.E.E. degree from Rensselaer Polytechnic Institute, in 1964 an advanced Communications Engineering Certificate from Cornell University and in 1976 a Masters Degree in Systems Engineering from Virginia Polytechnic Institute. He is a registered professional engineer.

Raymond E. Hill is a native of Iowa. Following WWII military service, he received the BS EE degree from the University of Denver, Colorado.

Since 1958, he has been associated with the Rural Electrification Administration, Washington, D.C., where he has been involved in a variety of electric and telephone engineering activities. He is a registered professional engineer. In 1960 he became a staff member of the Telecommunications Staff Division as a System Design Engineer.

TABLE 1
TYPE OF FACILITY

Cable or Wire Type	Quantity of Segments	Sheath-Miles	Conductor-Miles	Avg. Sheath Length (ft)	Avg. # of Pairs
Buried-Air Core	2,161	996.6	280,177.4	2,435	141
Aerial-Air Core	2,778	1,110.2	475,958.0	2,110	214
UDG-Air Core	945	101.4	214,993.8	567	1,060
Total-Air Core	5,884	2,208.2	971,129.2		
Buried-Filled	3,319	1,636.4	694,886.8	2,603	212
Aerial-Filled	251	101.3	25,329.1	2,130	125
UDG-Filled	349	37.1	8,946.5	561	1,206
Total-Filled	3,919	1,774.8	729,162.4		
Tip Cable	57	0.4	242.5	37	311
Buried Drop	1,116	48.7	369.2	230	4
Submarine	1	0.2	40.4	1,066	100
Fiber Optic	6	55.4	443.4*	48,784***	4**
Filled Wire	35	13.8	78.4	2,083	3
Dist Wire	80	13.6	124.6	897	5
Buried Wire	74	36.2	191.3	2,586	3
Open Wire	11	3.2	6.3	1,517	1
TOTAL	11,183	4,154.5	1,784,200.4	1,962	215

*Fiber-Miles
**Fibers
***Span Length

TABLE 2
RURAL SUBSCRIBER GROWTH

Year	Subscribers (000) Res.	Bus.	% Annual Growth Res.	Bus.
1987	4,383	621	3.4	4.9
1986	4,240	592	0.8	0.9
1985	4,205	587	1.0	0.3
1984	4,162	585	2.2	5.0
1983	4,071	557	1.8	1.6
1982	3,998	548	3.8	5.0
1981	3,852	522	2.6	3.0
1980	3,754	507	4.6	5.2
1979	3,589	482	5.5	2.3
1978	3,403	471	7.4	10.3
1977	3,169	427		
Ten Year Average			3.8	4.5

Gauge Sizes

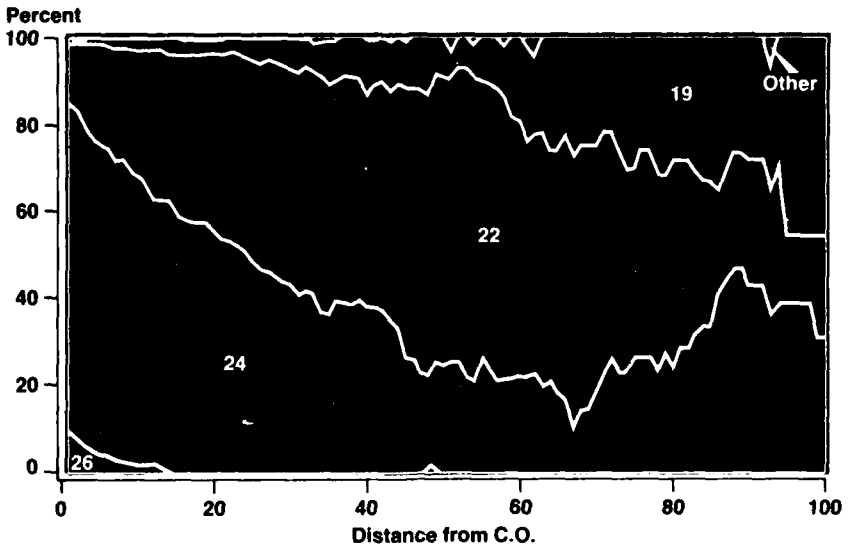

FIGURE 1

Cable Pair Sizes

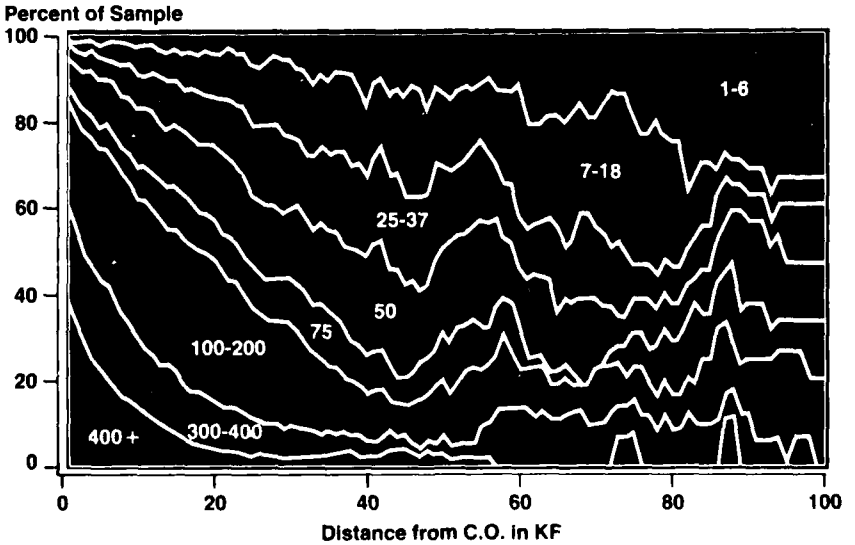

FIGURE 2

Cable and Wire Types

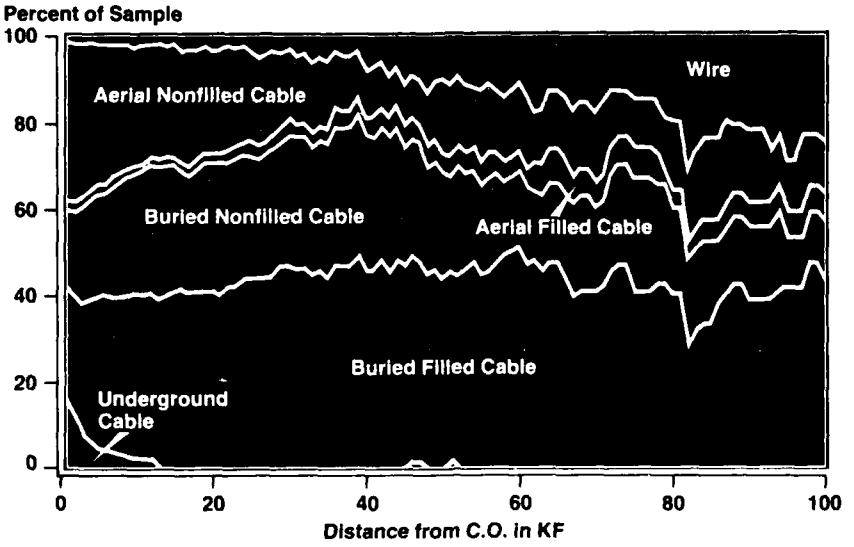

FIGURE 3

SUBSCRIBER DISTRIBUTION

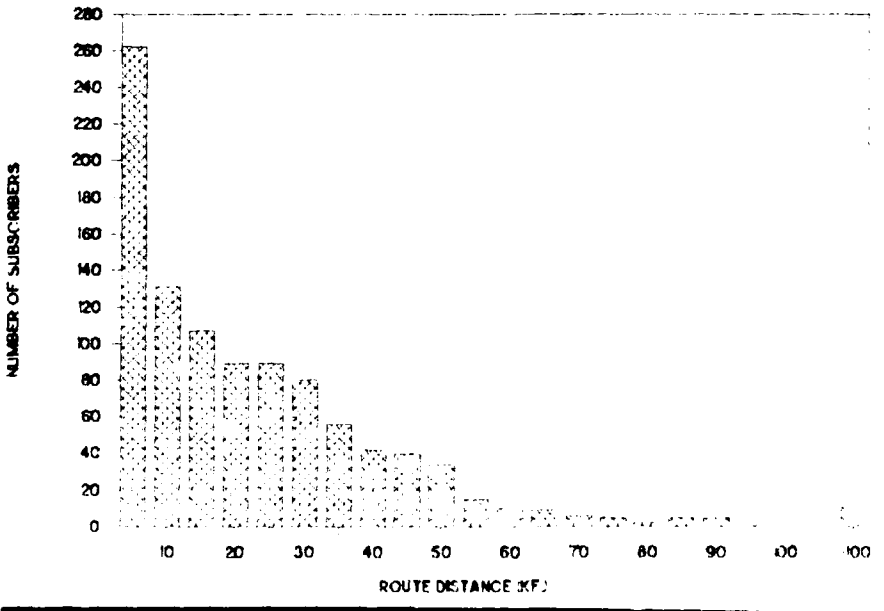

FIGURE 4

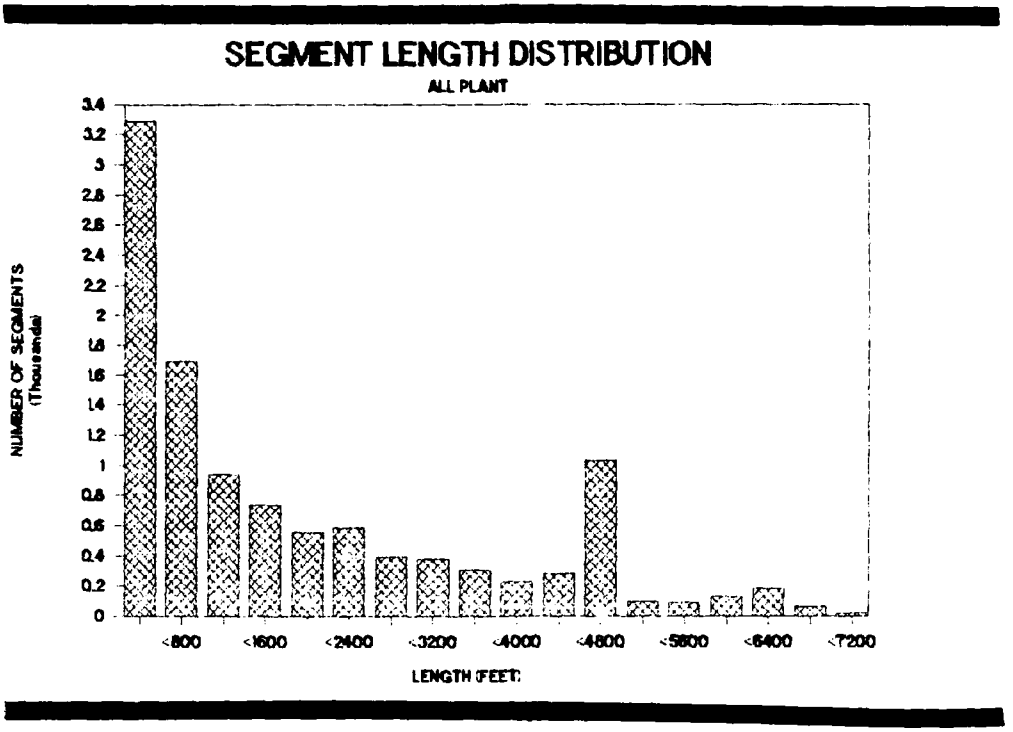

FIGURE 5

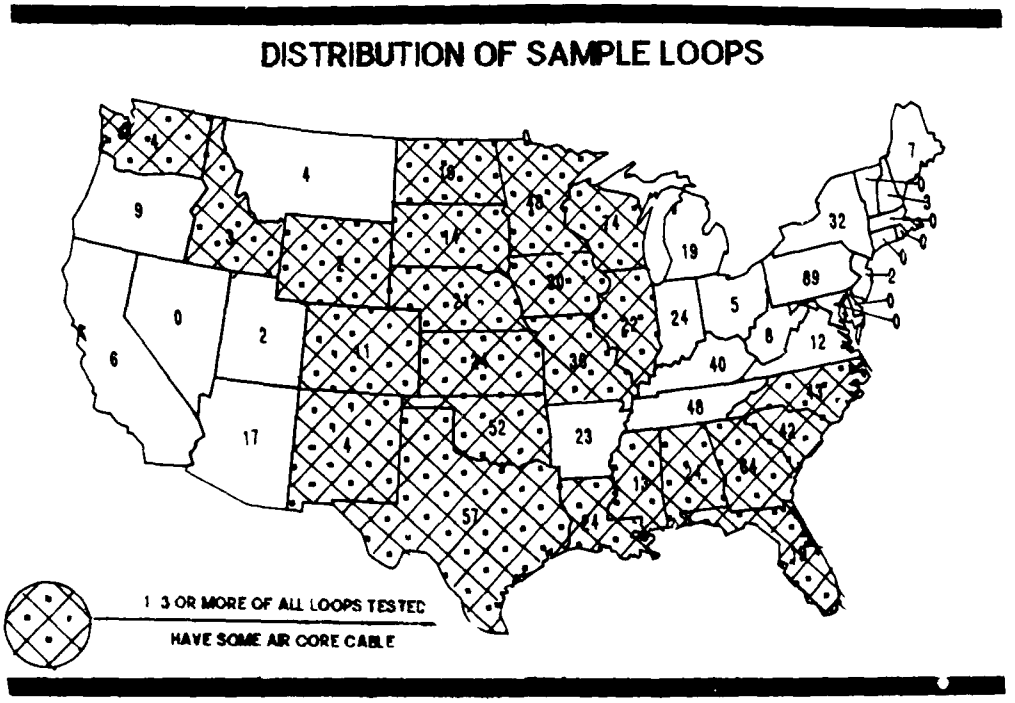

FIGURE 6

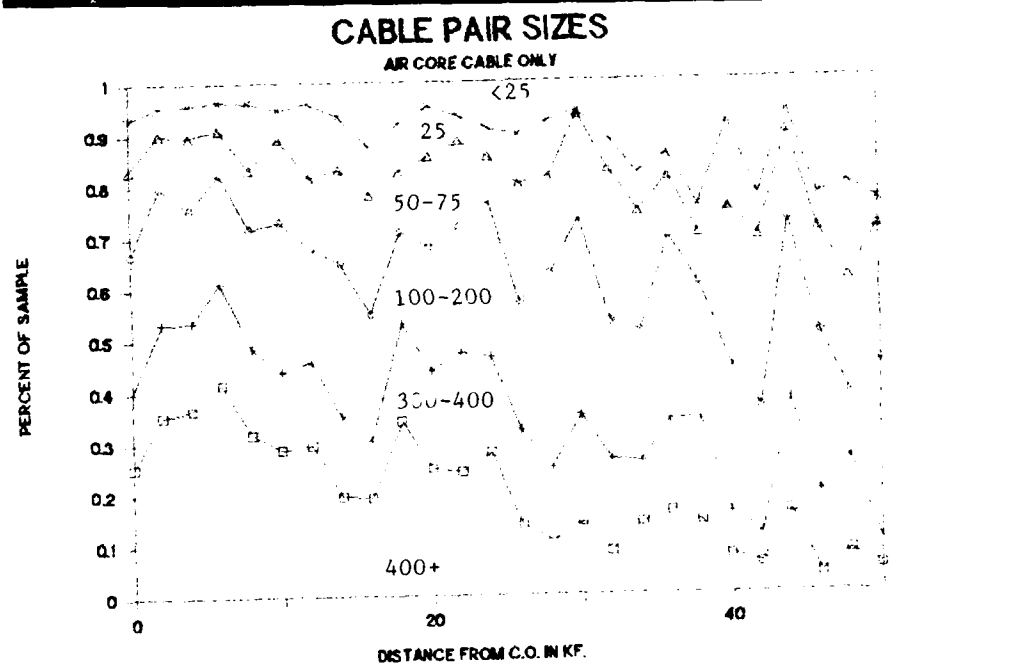

FIGURE 7

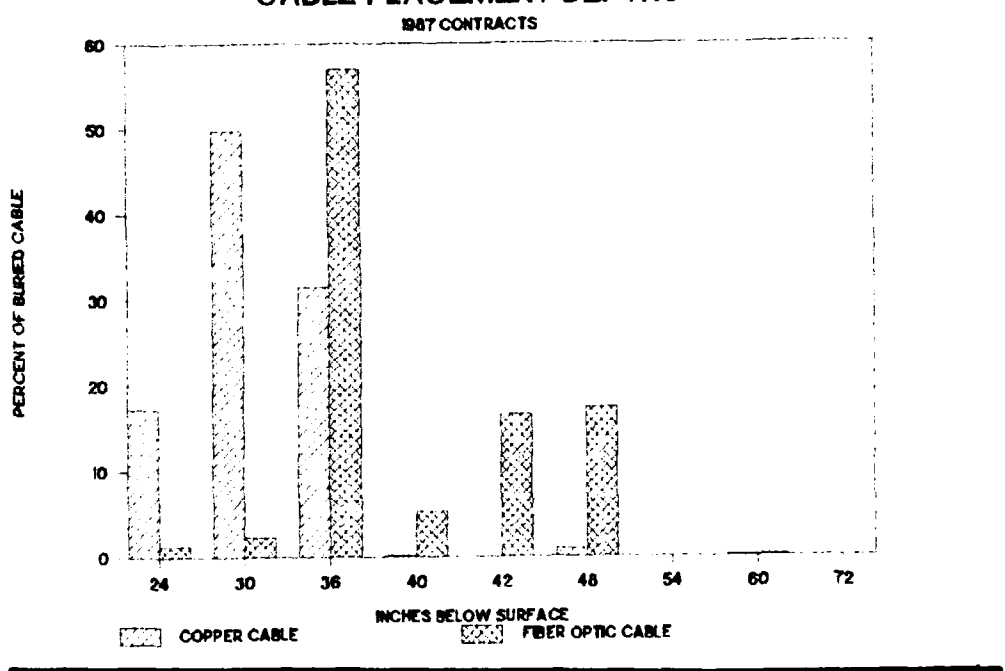

FIGURE 8

Final Approaches in Metallic Cable Technologies
— Improvement of Aerial Distribution Cable System —

Atsushi Matsuda, Koji Sakuda, Seiji Takashima

Nippon Telegraph & Telephone Corp.

Tokyo, Japan

1. Abstract

For the purpose of total cost reduction in aerial distribution cable systems, NTT has rearranged and drastically reduced the number of specifications. First, gauge integration from a 4 gauge method to a 2 gauge method has been achieved by adopting a foamed polyethylene insulation technique. But this type requires an improved wearing characteristic. The usual L.D.P.E. has thus been replaced by H.D.P.E. and a double layer structure. In addition, laminated aluminum polyethylene (LAP) structure is used for sheath. Second, cable structure integration from round type to self supporting (SS) type has been achieved. To expand the range of SS cable applications, a Zn-5%Al alloy messenger strand has been developed to counter vibration fatigue of the messenger strand due to wind and corrosion in coastral areas.

2. Background

The main subject in technological development has been shifted to the area of optical fiber cable from that of metallic cable. From the viewpoint of facility investment, however, metallic cable will continue to play an important role in our management.

For aerial distribution cables, NTT uses color coded polyethylene (CCP) insulated metallic cable. Specifications for this type of cable can vary according to gauge(0.4, 0.5, 0.65 and 0.9 mm), number of pairs(10, 30, 50, 100, 200 and 400), sheath structure(plain and laminated aluminum polyethylene) and cable structure(round type and self-supporting type).

On the other hand, since privatization in 1986, NTT has made an intense effort to implement cost-saving measures in plant engineering, the flow and storage of goods, and maintenance.

As one such measure, NTT has sought to drastically rearrange and reduce the specification variables of CCP cable as shown in Figure 1, by developing new materials, manufacturing techniques, and reliability assessments.

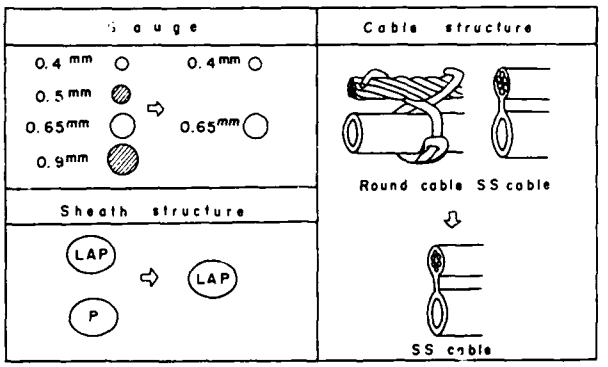

Figure 1 Cable integration

3. Integration of Gauge Diameter and Sheath Structure

3.1 Investigation of lowering line loss

For reducing kinds of specifications, the usage of larger gauge rusults in higher cost. Since the usage of finer gauge leads to loss increases, countermeasure, such as coil loading or two-way repeater installation, must be adopted to compensate. Furthermore, these measures cause other problems in that they take up considerable installation space at the central office and are restricted by the wider usage of frequencies in transmission lines that will be introduced with progress of digitalization.

In terms of electrical characteristics, it is effective to use a foamed polyethylene technique which is normally applied to underground cables such as jelly filled or multi-pair cables, based on the concept of keeping mutual capacitance (50nF/km) constant.

However, NTT requires 40nF/km mutual capacitance using a foamed polyethylene technique. Consequently, NTT realizes a line loss in the conventional 4 gauge method

of 0.4, 0.5, 0.65 and 0.9 mm by substituting 1-rank finer gauge. In other words, NTT has adopted a 2 gauge method in which 0.4-mm gauge is substituted in 0.5-mm gauge applications and 0.65-mm gauge in 0.9-mm gauge contexts.

3.2 Applying foamed insulation in aerial cable

Aerial cable is used in severe natural environments and release conditions[2]. Thus, applying a foamed polyethylene insulation technique to aerial cable requires measures to counteract the decline in mechanical and physical characteristics. First, high-density polyethylene (H.D.P.E.) is adopted in place of low-density polyethylene (L.D.P.E.) for its favorable physical characteristics. Second, a double layer insulation technique consisting of foamed core and solid skin is adopted. Third, laminated aluminum polyethylene (LAP) sheath is adopted for its excellent mechanical properties.

These countermeasures have made it possible to design an insulator that realizes 40nF/km mutual capacitance. 40nF/km is based on manufacturing ability of the present jelly-filled CCP cable whose characteristic is about 40nF/km removing the filling jelly. The foaming rate, thickness of the insulator and solid skin, which are the main structural parameters of the double layer insulator, are shown in Figure 2.

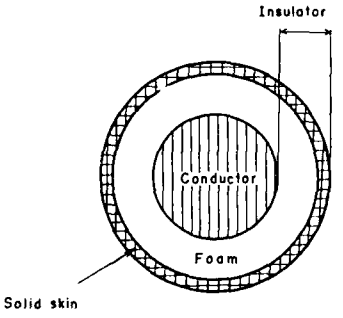

Figure 2 Double layer insulator

It is required that the maximum increase of thickness of the insulator be 10% more than that of the present cable, because the thickness relates closely to cable weight and outer diameter. The foaming rate and thickness of the solid skin, which depend on manufacturing ability, influence mechanical characteristics such as pin hole level. Therefore, the optimum design was sought by checking various patterns. Table 1 shows an example design of double layer insulator. Consequently, line loss is lowered as will be described in 3.3, and the area over which the finer gauge can be applied can be extended as shown in Figure 3.

Table 1 Design of double layor insulator

item	CCP-F	CCP	CCP-F	CCP
gauge diameter	0.4 mm		0.65 mm	
thickness of insulator	0.14 mm	0.13 mm	0.22 mm	0.20 mm
thickness of solid skin	0.03 mm		0.03 mm	
foaming rate	40 %		40 %	

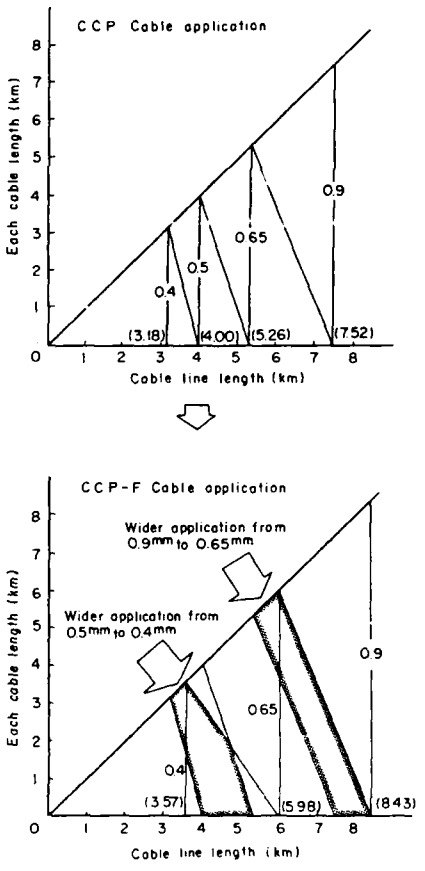

Figure 3 Wider application of finer gauge

New CCP cable having this double layer insulator and adopting the countermeasures described above is called CCP-F (Foamed) cable. CCP-F cable has a menu of 0.9-mm gauge as shown in Figure 3. However, this is a provisional measure for subscribers requiring high line loss compensating, since optical fiber cable will be substituted in the near future.

3.3 Characteristics of CCP-F cable

The characteristics of CCP-F cable are evaluated against conventional CCP cable (solid PE type) for aerial cable applications which require stringent mechanical requirements.

(1) Insulation characteristics

In terms of heat-oxidation inferiority, CCP-F cable has no problem because the oxidation inducing time of CCP-F cable is 31.8 minutes (9 data average) which is longer than that of CCP cable (more than 11 minutes). Briefly, the test method was as follows. After 400 hours, the heat disposition of film condition sample thickness in 160 $\pm$ 20 μm in 70 ℃ N_2 atmosphere, oxidation inducing time is measured at 200℃ by the DSC method.

The pin hole level is required to be less than that of conventional CCP cable which is 2 pin holes per 3000 m. CCP-F cable satisfies this target. The test method is briefly described below. After soaking 3000 m-long gauge in water for 1 month, a gauge whose insulate resistance is less than 50ω M Ω is selected as a poor insulator having pinholes.

The minimum breakdown voltage of insulation is 3.3 kV in 0.4-mm gauge and 3.5 kV in 0.65 mm. These values for CCP-F cable are smaller than those of CCP cable (by more than 10 kV). However, they satisfy the present CCP cable requirement; there is no problem by applying AC 350 V for 1 minute.

Though wide deviation was obtained for the wearing test, the wearing characteristic of CCP-F cable was similar to that of CCP cable, as shown in Figure 4. A NEMA wearing tester was used for the experiment and wearing times were measured at 23 ℃ for each applying weight such as 450, 500, 550 gf for 0.4-mm gauge and 800, 850, 900 gf for 0.65-mm gauge.

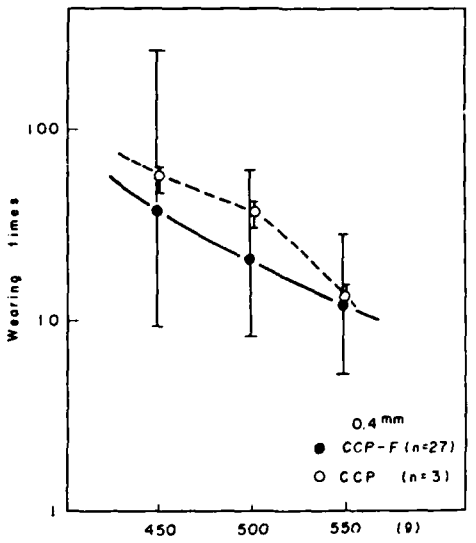

Figure 4 Wearing characteristic of 0.4 mm gauge

(2) cable characteristics

In terms of frequency characteristics of 0.4-mm CCP-F cable secondary constants, line loss at 1.5 kHz is 1.93 dB/km, which is 11% lower than that of the present CCP cable. On the other hand, characteristic impedance is 839 Ω at 1.5 kHz, which is 7% higher than the present CCP cable. But quality degradation such as increasing side-tone caused by impedance mismatching is apparently negligible.

The Far end cross-talk (FXT) frequency characteristics of 0.4mm CCP-F cable is 70dB/km. They satisfy the present CCP cable requirement (more than 55dB/km at 90% data, and 40dB/km at 100% data).

Change of mutual capacity was examined while subjecting the cable to bending, squeezing, and twisting. The maximum change in CCP-F cable is -1.74% after twisting and that of CCP cable is 3.32%. This indicates that the electrical characteristic is not affected by mechanical force. The heat shrinking test after squeezing, the cold proof test and the water proof test were also examined. Consequently, no problems were detected by the three test. Table 2 shows the mechanical test method.

From investigation of (1) and (2), it is confirmed that the foamed polyethylene technique can be applied to aerial cable.

Table 2 Mechanical test methods

Test	Test method	No.of times
bending test	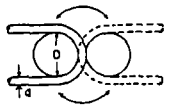 bending angle: ± 180 D = 6d	5 and 10 times
queezing test	 W: 150kgf (0.4 mm) 200kgf (0.65 mm)	10 and 15 times
twist test	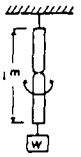 W:30kgf	1 twist

4.Integlation of Cable Structure

NTT uses both round and SS (self-supporting) aerial cable. The former is installed on a messenger strand with hanger rings. Since this method depends on manpower and includes overhead work, it is neither efficient nor safe. The latter method, on the other hand, employs a messenger strand attached directly above the cable. Therefore, regarding the cable structure, integration into self-supporting cable is desirable for both safety and cost savings in cable installation work. Measures must be adopted, however, to counter vibration fatigue of the supporting wire in strong wind areas and corrosion snapping in coastral areas.

4.1 Application in strong wind areas

Self-supporting cable has a critical defect in regard to easing vibrations; the so-called dancing phenomena that occurs in strong wind. In 1965, NTT had problems with the messenger wire being broken due to metal fatigue caused by this dancing phenomena. Thus, countermeasures, such as the adoption of larger size messenger and cable suspention method improvement, were taken to reduce the dynamic load due to the dancing phenomena. Although the problems experienced in 1965 have not reoccured, aluminum material fatigue on LAP sheath was found at their suspension clamp points. With this as a turning point, theoretical analysis and repeated observation were carried out at the Sakata experimental field station that can catch the full force of strong and transverse winds from the Sea of Japan. As a result, a messenger strand protection method was developed as shown in Figure 5, and a messenger guard, 2.15 mm in diameter and 500 mm long, minimizes the strain on the stranded messenger wire[3, 4].

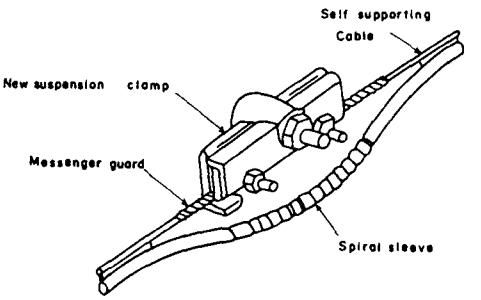

Figure 5 Messenger strand protection method

This method was first introduced in 1981. Application in strong wind areas has been avoided, however, out of consideration for worker safety. In addition, many strong wind areas in Japan overlap with intense metal corrosion areas. Corrosion resistance reliability assessment of the SS cable messenger strand and end grip has also been carried out. Based on 10 year-technical investigation in a particular geographical area as Sakata, the development of SS cable for high corrosion areas enables SS cable to be used in strong wind areas.

4.2 Application in corrosion areas

Present SS cable exposes a galvanized messenger strand at the cable's grip end. Galvanized messenger strand excels in corrosion resistance. After the galvanizing coming off, however, protection-less steel strand rusts rapidly and breaks. Corrosion in salty areas is conspicious, and the lifetime of strands is less than 10 years. For this reason, round cable and aluminum coated steel wire strand supporting with hanger rings is substituted for present SS cable in corrosive areas such as coastral, hot spring, and factory areas.

Application of SS cable in corrosive areas requires corrosion-proofing of the cable's grip end. A number of measures for accomplishing this are described below; (1)gripping onto the messenger strand directly without stripping the PE outer sheath, (2)the corrosion proving of the messenger strand partially where PE outer sheath is stripped, (3)using high corrosion resistance messenger strand. Since (1) and (2) proved to be inferior to (3) in reliability and economy, we concentrated our investigation on (3).

Development of a high corrosion resistance messenger strand, which is hereinafter referred to as CR messenger strand, requires such characteristics as corrosion resistance, bending fatigue and cost performance. At present, NTT judges Zn-5%Al alloy coated messenger strand to be a leading candidate for CR messenger strand, as will be described below in more detail.

4.2.1 Corrosion resistance characteristic

(1) Requirements

Messenger strand corrosion is divided into 2 parts; first, opening part corrosion where PE outer sheath is stripped, and second, corrosion under the PE covered part. On the other hand, messenger strand lifetime is defined as the time it takes to generate red rust. At the opning part, NTT requires a life of 15 years in strong corrosive areas. This requirement corresponds to experimental condition that no red rust generates after 1500 hours of salt spray test. This is thought to be analogy with galvanized messenger strand, because its life span is 5 years under the same conditions and generates red rusts after 500 hours of salt spray test.

Considering the difficulty of observing the corrosion under PE covered part, its local corrosion risk must be investigated. Corrosion factors applying to the PE covered part are described below, (1)long time in moisture conditions, (2)condensation of chlorine ions, (3)formation of differential aeration battery. Therefore, NTT requires that no local corrosion be present.

(2)Experiments and results

Corrosion resistance characteristics are examined by salt spray test (35 ℃, 5%Na-Cl solution) and intermittent salt spray test (8 hours salt spray test → water washing →16 hours in 35℃ and 90%RH→1 cycle/day). The aim of the intermittent test is to check the effect of chlorine-ion condensation on corrosion. The sample is a 450-mm-long Zn-5%Al alloy coated steel wire strand consisting of 7 wires 2.3mm in diameter, and partly coating with PE to simulate the messenger strand. Figure 6 shows the relationship between incidence of red rust at the opening part and time. This result indicates that there is no generation of red rust after 1500 hour of the salt spray test. Photo 1 shows the result of the intermittent salt spray test after 1500 hours. Salt water penetrates under the PE covered part, however, the corrosion speed of the PE covered parts is much slower than that at the opening part. This is the same results as was obtained in the salt spray test. For this reason, it is confirmed that there is no local corrosion of the PE covered parts.

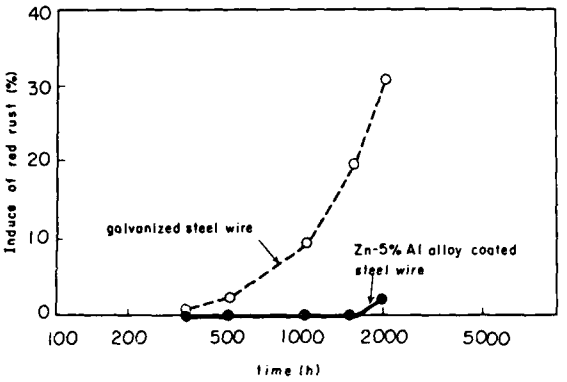

Figure 6 Corrosion resistance characteristics of Zn-5%Al alloy coated steel wire (salt spray test)

opening part under PE covered part

Photo 1 Result of the intermittent salt spray test

4.2.2 Bending fatigue characteristic

(1) Requirements

In corrosive areas, round cable has been supported by aluminum coated messenger strand for its anti corrosive characteristic with hanger rings. But field data shows that the bending fatigue characteristic of aluminum coated messenger strand is much inferior to that of galvanized messenger strand. On the other hand, there is no problem of bending fatigue in the case of galvanized messenger strand. Thus, for CR messenger strand, NTT requires bending fatigue characteristic equal to or greater than that of galvanized messenger strand.

(2)Experiments and results

The bending fatigue characteristic was examined by a strand bending fatigue tester constructed as shown in Figure 7.

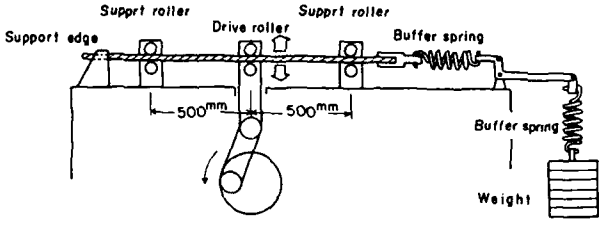

Figure 7 Bending fatigue tester

The settings of the tester are as follows: distance between two support rollers; 1000 mm, distance between support roller and drive roller; 500 mm, and diameter of support roller and drive roller; 87 mm. The test conditions were as follows: tension; 30% of the maximum standard tensile load of CR messenger strand, and repetition speed; 6 Hz. The sample was 7/2.3 Zn-5%Al alloy coated messenger strand and its mechanical characteristics are shown in Table 3.

Table 3 Mechanical characteristics of Zn-5%Al alloy coated messenger strand

wire diameter; 2.31 mm	number of torsion; 44 times
elongation ; 2.8%	deposit of coating; 330g/m²
tensile load; 160 kgf/mm²	

Figure 8 shows the result of the bending fatigue test. It is confirmed that the bending fatigue characteristic of Zn-5%Al alloy coated messenger strand is the same as that of galvanized messenger strand.

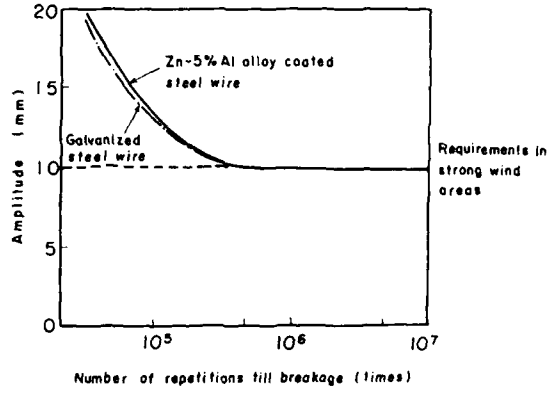

Figure 8 Fatigue characteristics of Zn-5% alloy coated steel wire

It is confirmed by the described experiments and cost considerations that SS cable can be applied to strong wind and corrosive areas by using Zn-5%Al alloy coated messenger strand.

5. Integration effect

By integrating gauge diameter and cable structure, the number of aerial distribution cables can be reduced from 80 to 17. These integrations raise the cost of production, but consequently, a total cost reduction of approximately $13 million a year is realized by cost savings in plant engineering, the flow and storage of goods and so on, as shown in figure 9

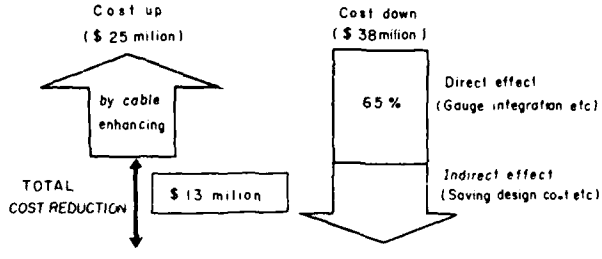

Figure 9 Economic effect by article reduction (a year)

6. Conclusion

A foamed polyethylene insulation technique has been applied to aerial distribution cable systems without filling compound, in order to compensate for line loss increase due to adoption of finer gauge conductor.

It is confirmed that a Zn-5%Al alloy coated messenger strand is the most suitable for application to self-supporting cables for aerial distribution systems from the viewpoints of cost saving, reliability and workability.

This newly developed CCP-F cable is now under commercial tests and will be widely introduced from 1989.

7. References

(1) D. M. Mitchell, "Material Savings by Design in Exchange and Trunk Telephone Cable, part1: Waterproof Cable with Dual Insulation", 23th IWCS, 1974.

(2) Gene R. Samuelson, "Evaluation of Foam-skin Cables for Aerial Applications", 32th IWCS, 1983.

(3) M. Iwazaki, K. Katagiri, A. Sekiguchi, S. Masaki, " Theoretical Analysis and Reductional Countermeasure of Dancing Phenomena on Self-Supporting Cable", 29th IWCS, 1980.

(4) H. Ishihara, K. Ishizaki, F. Takaesu, "New Self Supporting Cable for Overhead Subscriber Distribution Use", JTR april, 1980.

Atsushi Matsuda

NTT Network Systems
Development Center

2-1 Uchisaiwai-cho 1-chome
Chiyoda-ku, Tokyo 100 Japan

Atsushi Matsuda received his B.S. and M.S degree in civil engineering from Tokyo Institute of Technology in 1982 and 1984. He joined NTT in 1984. He is an engineer in the Telecommunication Cable Systems & Outside Plant Project Group in NTT Network Systems Development Center. He is a member of the Japan Society of Civil Engineers.

Koji Sakuda

NTT Network Systems
Development Center

2-1 Uchisaiwai-cho 1-chome
Chiyoda-ku, Tokyo 100 Japan

Koji Sakuda received his B.S. and M.S. degree in electrical engineering from Tokyo University in 1979 and 1981. He joined NTT in 1981. He is a senior engineer in the Telecomunications Cable systems & Outside Plant Project Group and Fiber Optics Local Network Systems Project Group in NTT Network Systems Development Center. He is a member of the Institute of Electronics, Information and Communication Engineers of Japan.

Seiji Takashima

NTT Network Systems
Development Center

2-1 Uchisaiwai-cho 1-chome
Chiyoda-ku, Tokyo 100 Japan

Seiji Takashima received his B.S. and M.S. degree in electrical engineering from Waseda University in 1967 and 1969. He also received M.S. in management from Massachusetts Institute of Technology in 1983. He joined NTT in 1969. He is a senior manager in the Telecomunications Cable systems & Outside Plant Project Group and Fiber Optics Local Network Systems Project Group in NTT Network Systems Development Center. He is a member of the Institute of Electronics, Information and Communication Engineers of Japan.

Development of Optical Composite Drop Wire

Kiyoyuki Isawa* Koichi Ishikawa* Masatoshi Suzuki*

Masayuki Niijima** Shintaro Sentsui** Takuzo Takahashi** Tetsu Sugisaki**

Tohoku Electric Power Co., Inc., Sendai-shi, JAPAN*

The Furukawa Electric Co., Ltd., Chiba, Japan**

Summary

The optical communication system is expected to be introduced to general subscribers. On that occasion, it is desirable to incorporate the optical fiber unit and electric wire into one-piece structure for the convenience of laying work and its good appearance. From this viewpoint, the authors have developed the optical composite drop wire, examined its electrical and optical properties to find it serves for this purpose.

1. Introduction

The optical communications system is considered to serve for domestic use in future as means of measurement and control of electrical facilities, wide band communication system, closed-circuit television and home automation. In Japan, the optical fiber cable will be dropped to the subscriber mostly through the aerial lead-in method in the same way as the electric wire. As separate drop of optical fiber cable and electric wire makes the laying work complicated and harms the appearance, supply of these in one-piece unit is desired. To answer this demand, we have developed the method of incorporating the optical fiber unit and electric wire in the optical composite drop wire. This is a report on this product.

2. Designing Conditions

The optical composite drop wire is used to drop the electric wire and optical fiber cable through one-piece unit from the service pole to each home. The concept diagram of the optical composite drop wire is given in Figure 1.

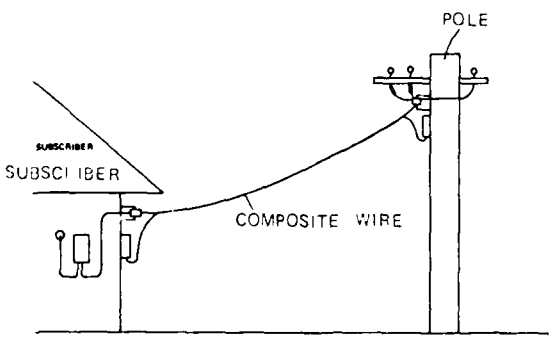

Figure 1 CONCEPT DIAGRAM

(1) The structure shall be of self-support type with electric wire to serve for suspension.

In consideration for laying work convenience and maintainability after completion, the self-support structure with the electric wire serving for suspension is employed. As for the electric wire, the same DV line as the existing drop wire (JIS C 3341 polyvinyl chloride insulated drop service wire, 8 mm^2 7/1.2) is used. The product is so designed as to allow the electric wire and optical fiber cable to be readily separated.

(2) The optical fiber shall be guaranteed for 20 years against fracture.

The optical fiber must be free from fracture in aerial lead-in state even when the tensile force is increased by fallen snow or wind pressure for 20 years.

(3) The optical fiber unit shall be of the structure resistible to electrical and mechanical influences from the electric wire.

The optical fiber unit employs non-metallic structure so as not to be affected by the electromagnetic induction from the electric wire and the optical unit is so designed as to be resistible to the influence of vibration.

On the basis of the above, we designed the optical unit and optical composite drop wire, produced it by way of trial and tested it. Description of each step follows.

3. Optical Fiber Unit

3.1 Designing

The optical fiber unit was designed as of spacer-type to house a maximum of 6 optical fibers, with FRP of 1.2 mm in diameter as core tension member of the spacer of 0.5 mm in groove diameter. This spacer houses optical fibers GI and SM of 0.25 mm in diameter, to be used within 0.2% of elongation strain of optical fiber on application of the maximum supposed load. In the same way as electric wire, the sheathing is made of PVC (Polyvinyl Chloride) of 1 mm in thickness for high weather resistance. The optical fiber unit of about 6 mm in external diameter, and 30 g/m in weight was prepared. The sectional appearance of the optical fiber unit is shown in Figure 2.

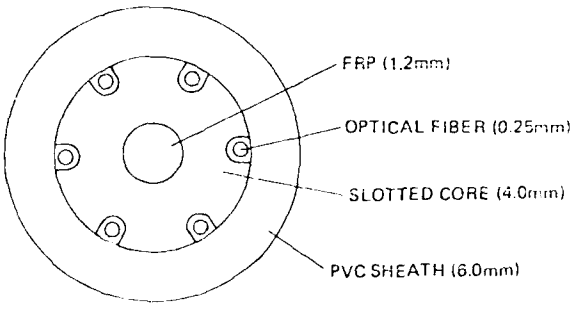

Figure 2 CROSS SECTION OF OPTICAL UNIT

3.2 Test Results

The optical fiber unit was manufactured as per 3.1 and a test was run to find nothing abnormal in optical loss variation between manufacturing steps, and temperature, tension and lateral pressure properties. The test results are shown in Table 1.

4. Optical Composite Drop Wire

4.1 Designing

For external configuration, the flat type, stranded type and bundle sheath type were selected taking into consideration the installation work convenience and appearance. The optical fiber unit was prepared as per section 3. For the electric wire, the hard-drawn copper conductor of 8 mm^2 in sectional area for two or three type was used. The sectional appearance of each type is shown in Figure 3.

The span length limit was determined for each type shown in Figure 3.

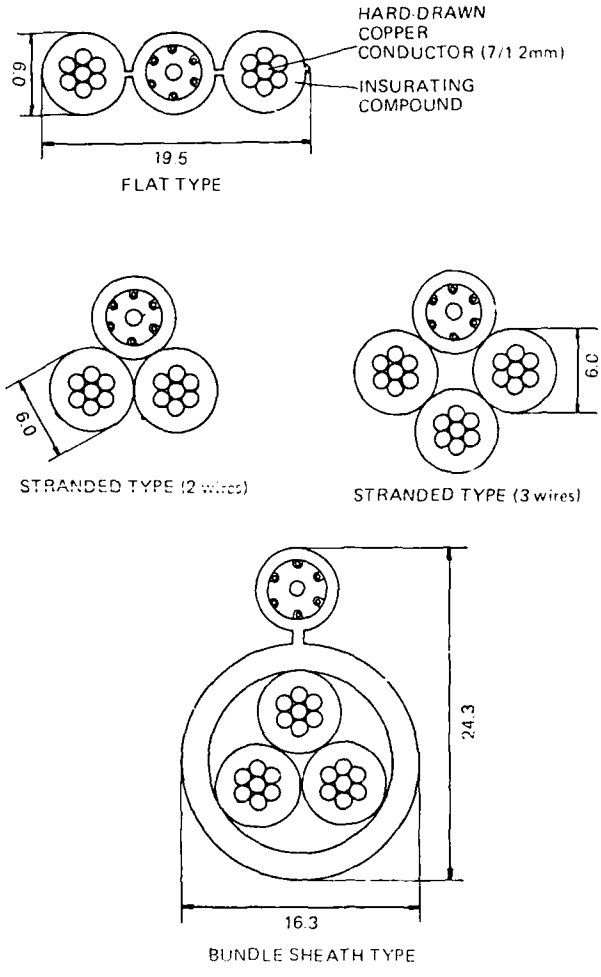

Figure 3 SECTIONAL APPEARANCE OF COMPOSITE WIRES

Table 1 Test Result (Optical Unit)

Item	Condition	Result
Optical Losses in Manufacturing Process	GI: λ=0.85 μm, 1.3 μm SM: λ=1.3 μm, 1.55 μm	The maximum loss change was less than 0.02 dB/km.
Temperature Characteristic	-20°C to +60°C	The maximum attenuation increase was less than 0.02 dB/km
Tensile Strength	Measuring length: 10 m	The tensile load corresponding to 0.2% fiber elongation was 15 kgf. The attenuation increase was recognized more than 40 kgf.
Lateral Pressure	50mm x 50 mm flat plate	The attenuation increase was recognized more than 200 kgf.

The limit is calculated to be 25 m for the flat type, 37 m for two core stranded type, 32 m for three core stranded type and 30 m for bundle sheath type. In any case, the span is reduced by the summer-time load. The data for span length limit obtained by calculation are given in Table 2.[1)]

Calculation conditions

Summer time: Wind speed at 40 m/sec
Winter time: Wind speed at 20 m/sec, and snow fall of 0.9 in specific gravity and 6 mm in depth
Fracturing load of electric wire: 326 kg/core
Safety factor: 2.5

The summer-time load was applied to determine the change of the elongation strain of the optical fiber and the tension of the lead-in wire caused by temperature change. The data obtained by calculation are given in Figure 4.

As the figure shows, the flat type exceeds the permissible value for the tension at low temperatures and that for the elongation strain of the optical fiber at high temperatures.

Calculation conditions

Summer time: Wind speed at 40 m/sec
Looseness : 2%
Span length: 30 m

As the data indicate, the span length of the lead-in wire should be 30 m at least. For this reason, the flat type was excluded from the objects of examination this time. It is also clear that the three core type can hold two core wire.

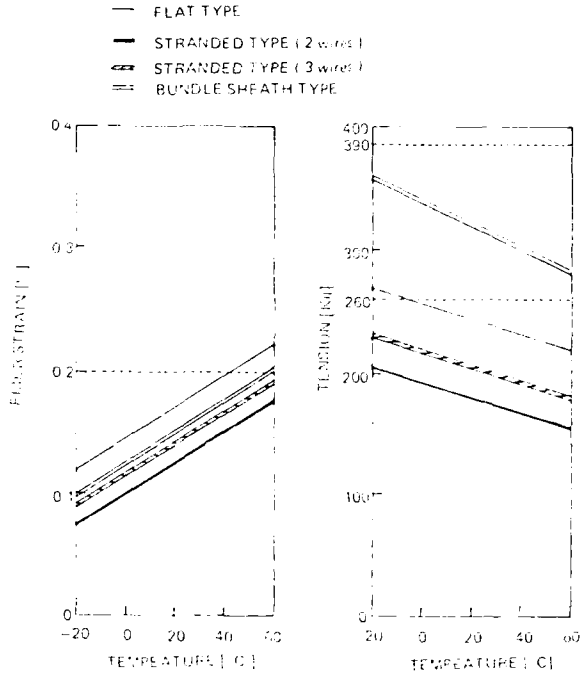

Figure 4 CALCULATED WIND PRESSURE AND ASSOCIATED ELONGATION OF THE COMPOSITE WIRES

Table 2 Limited Span Length

	In Summer				In Winter			
	Flat Type	Stranded Type (2 wires)	Stranded Type (3 wires)	Bundle Sheath Type	Flat Type	Stranded Type (2 wires)	Stranded Type (3 wires)	Bundle Sheath Type
Cable Weight [kg/m]	0.235	0.235	0.340	0.365	0.235	0.235	0.340	0.365
Cable Diameter [mm]	19.5	12.9	14.5	24.3	19.5	12.9	14.5	24.3
Allowable Tension [kg]	260	260	260	390	260	260	260	390
Limited Span Length [m]	25	37	32	30	33	39	34	39

4.2 Properties

The trial product of optical composite drop wire showed the voltage resistance, insulation resistance, tensile strength at the same level as existing DV wire, and no degeneration due to composition was detected in the properties.

Test results for electrical property are given in Table 3. The optical fiber unit in the optical composite drop wire is evaluated as follows. The optical transmission loss between manufacturing steps did not vary to ensure stable production. The elongation test indicated the relationship between the load and elongation almost as per the theory being kept within the elastic limit as far as the elongation was 0.2 % or under. This means the electric wire of hard-drawn copper conductor serves as the tension member for the optical fiber unit, the influence to the optical fiber unit is small even when the tensile load is increased, and the elongation strain of optical fiber can be kept low.

Measured optical transmission loss between manufacturing steps of the optical composite drop wire is shown in Figure 5. Values obtained by elongation test for the optical composite drop wire are given in Figure 6.

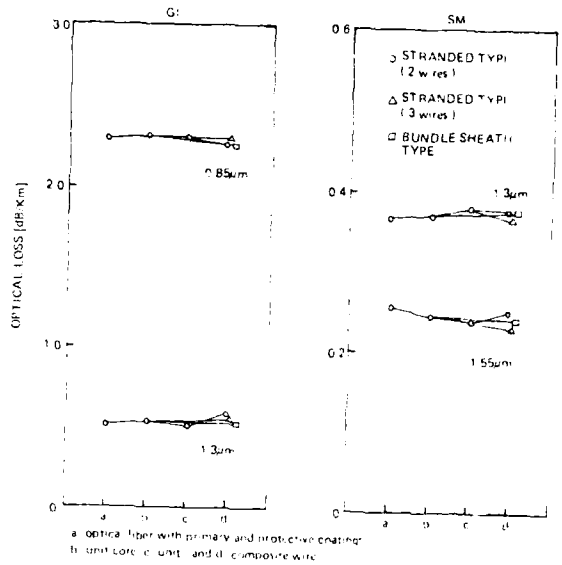

Figure 5 OPTICAL LOSSES IN MANUFACTURING PROCESS

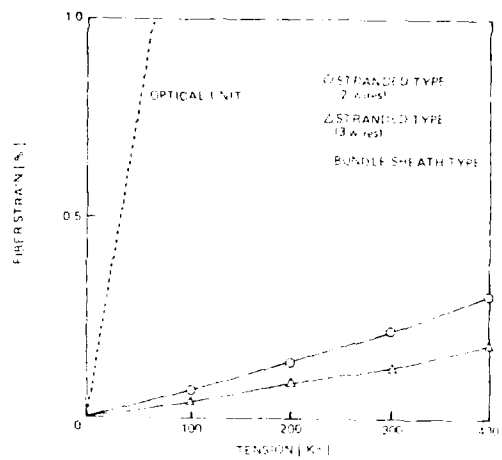

Figure 6 ELONGATION TEST RESULT

Table 4 Test Result

Item	Condition	Result: Stranded Type (2 wires)	Stranded Type (3 wires)	Bundle Sheath Type
Thermal Characteristic	-20 to +60°C	≤ 0.02 dB/km	≤ 0.02 dB/km	≤ 0.02 dB/km
Lateral Pressure	50 mm	≥ 200 kg	≥ 200 kg	≥ 200 kg
Bending Caring	± 180°	≤ 50 mm	≤ 50 mm	≤ 50 mm
Twist	Gauge length = m	≥ 2 times	≥ 2 times	≥ 2 times
Impact	Weight Diameter 25 mm	≥ 1 kg-m	≥ 2 kg-m	≥ 1 kg-m

Table 3 Electric Properties

Item	Specification	Stranded Type (2 wires)	Stranded Type (3 wires)	Bundle Sheath Type
Withstand Voltage Test	AC 1500 V, 1 min	good	good	good
Insulation Test	≥ 50 MΩ-km*	530 to 590	510 to 70	2020 to 2190
Conductor Resistance Test	≤ 2.18Ω-km*	2.18	2.22	2.19
Tensile Strength Test	326 kg	352 354	353 353 354	353 353 353

* at 20°C

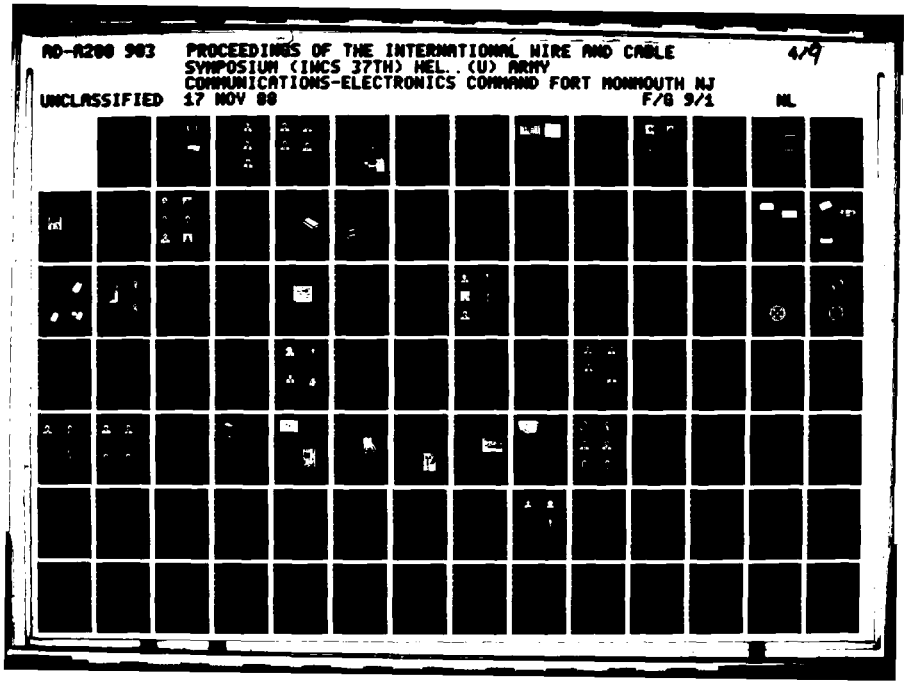
AD-A200 903
PROCEEDINGS OF THE INTERNATIONAL WIRE AND CABLE SYMPOSIUM (IWCS 37TH) HEL..(U) ARMY COMMUNICATIONS-ELECTRONICS COMMAND FORT MONMOUTH NJ
4/9
UNCLASSIFIED
17 NOV 88
F/G 9/1
NL

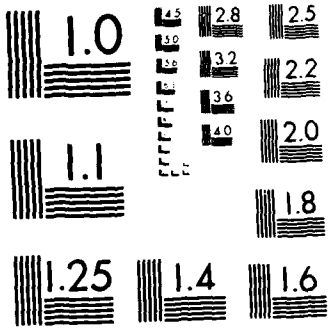

In order to determine the influence to the optical fiber in case an excessive current flowed to the electric wire of the optical composite wire, an excessive current test was run. The results are given in Table 5. In the test, the both ends of electric wire were fixed with span length of 5 m, and the conductor temperature was raised to 75°C and 120°C to measure the loss variation of the optical fiber, its elongation strain and the surface temperature of the optical fiber unit.

The conductor temperature of 120° C corresponded to supposed temperature rise caused by short-circuit, and the test indicated no transmission loss variation. The elongation strain of the optical fiber due to rise of electric wire temperature was kept within 0.05%, and the unit temperature was 60°C to remain in the permissible range.

5. Laying Test

A laying test was run for the optical composite drop wire we developed. For holding the lead-in, wire, the jig for the traditional DV wire is used. The jig used for the test is shown in the Photo 1. According to the cable structure, the drop wire insulator was used for the stranded type, and the shackle type strain insulator for the bundle sheath type. As the drop wire insulator could hold two electric wires only, two wires were held even in the case of three-line electric wire. The bundle sheath type required a jig for separation of the optical unit. However, the laying work could be carried out for either type in the same way as the case of electric wire only. The wire when laid is shown in Photo 2.

6. Transmission Loss Continuous Measurement

In order to determine the property variation of the optical composite drop wire thus laid, the transmission loss of the optical fiber was continuously measured. The measurement started in June 1988, and the results as favorable as 0.1 dB/km have been given for each type. This measurement is planned to be continued.

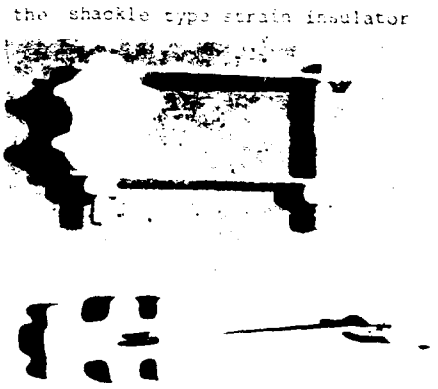

Photo 1 The jig used for the test

Photo 2

Table 5 Excessive current test result

Item \ Sample	Stranded Type (3 wires)		Bundle Sheath Type	
Conductor Temperature	75°C	120°C	75°C	120°C
Optical Loss [dB/km]	0	0	0	0
Fiber Strain [%]	0.022	0.045	0.020	0.045
Optical Unit Temperature [°C]	50	60	45	60

7. Conclusion

The optical composite drop wire was developed for the purpose of rationalization of laying work and improvement of appearance and evaluation tests were run. Each of the trial products of the two stranded types and one bundle sheath type proved successful in the test. In the laying test, the work progressed smoothly, and almost the same method as that of existing electric wire can be applied. For the laid optical composite drop wire, check of long-term reliability and observation of fallen snow will be carried out aiming at the practical use of this product.

Acknowledgments

Our most earnest thanks and appreciation are extended to Mr. S. Ohira of Tohoku Electric Power Co., Inc. and Mr. K. Okubo of Furukawa Electric Co., Ltd. who have supported this report with valuable advices.

Reference

1) Takamasa YASHIRO, "Thermal Characteristics of Aerial Cables with Plastic Sheath", IECE, JAPAN (SECTION tB), B66, 2, pp.215-222 (February 1983).

Kiyoyuki Isawa
Tohoku Electric
Power Co., Inc.
2-1, Nakayama 7-chome,
Sendai-shi, 981, JAPAN

Kiyoyuki Isawa received his B.E. degree from Chiba Institute of Technology in 1981. He then joined Tohoku Electric Power Co., Inc., where he has been engaged in telecommunications and electronics engineering. He is now a research worker for the applied technology research and development center and a member of the Institute of Electronics, Information and Communication Engineers of Japan.

Koichi Ishikawa
Tohoku Electric
Power Co., Inc.
2-1, Nakayama 7-chome,
Sendai-shi, 981, JAPAN

Koichi Ishikawa received his B.E. degree from Nihon University in 1982. He then joined Tohoku Electric Power Co., Inc., where he has been engaged in telecommunications and electronics engineering. He is now a research worker for the applied technology research and development center and a member of the Institute of Electronics, Information and Communication Engineers of Japan.

Masatoshi Suzuki
Tohoku Electric
Power Co., Inc.
7-1, Ichibancho 3-chome,
Sendai-shi, 980, JAPAN

Masatoshi Suzuki graduated from Aizu Technical School in 1974. He then joined Tohoku Electric Power Co., Inc., and has been engaged in communications and electronics engineering. He is now an engineer for the Integrated Communications Network Development Office. He is a member of the Institute of Electronics, Information and Communication Engineers of Japan, and the Institute of Television Engineers of Japan.

Masayuki Niijima
The Furukawa Electric Co., Ltd.
6 Yawata-Kaigandori, Ichihara, Chiba, 290 Japan

Mr. Niijima graduated from Waseda Univ. 1985 with a B.Ss. in electrical engineering. Then he joined the Furukawa Electric Co., Ltd. and has been engaged in development of optical fiber cables.
Mr. Niijima is now a staff engineer of Optical Fiber Transmission Group, Chiba Research Laboratory and Development Division at the Furukawa Electric Co., Ltd. and a member of Institute of Electronics, Information, and Communication Engineers of Japan.

Takuzo Takahashi
The Furukawa Electric Co., Ltd.
6-1, Marunouchi 2-chome, Chiyoda-ku, Tokyo, Japan

Mr. Takahashi received the B.Sc. in communications engineering from University of Electro Communications in 1974. Then he joined the Furukawa Electric Co., Ltd. and engaged in cable engineering and cable accessories.
Mr. Takahashi is now a manager of Optical Cable Systems Development Dept. at the Furukawa Electric Co., Ltd. He is a member of the Institute of Electronics, Information, and Communication Engineers of Japan.

Shintaro Sentsui
The Furukawa Electric Co., Ltd.
6 Yawata-kaigandori, Ichihara, Chiba, 290 Japan

Shintaro Sentsui received his B.S. degree in Physical Engineering from Tokyo University in 1970, and then joined the Furukawa Electric Co., Ltd.
He has been engaged in research and development of superconduction co-axial line, characterization and measurement of optical fiber.
He is now a manager of Optical Fiber Transmission, Chiba Research Laboratory, Research & Development Division.
He is a member of Institute of Electronics, Information, and Communication Engineers of Japan.

Tetsu Sugisaki
The Furukawa Electric Co., Ltd.
13-14,
Higashi-Shinagawa 4-chome, Shinagawa-ku, Tokyo, 140, Japan

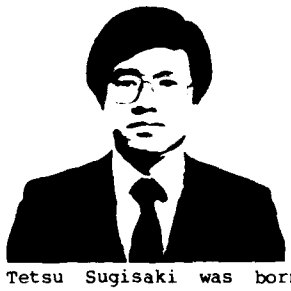

Tetsu Sugisaki was born in Yokohama, Japan, on February 19, 1951.
He graduated from Toin Technical College in 1971. In 1971, he joined the Furukawa Electric Co., Ltd. He has been engaged in the development, manufacture and design of distribution cables.
He is a member of the IEE of Japan.

REMOTE CONTROLLED CROSS CONNECTION FRAME USING PUSH-ON FIBER OPTIC CONNECTORS

M.OHSAWA H.HIRAO H.YOKOSUKA

Fujikura Ltd.
Opto-Electronics Labortory
1440, Mutsuzaki Sakura-shi Chiba-ken, Japan

1.SUMMARY

A new automatic cross connection frame using single-fiber push-on connectors has been developed for optical fiber networks. The cross connection frame system is divided into a connection frame and a control unit. The frame consists of connection boards, a multifunction arm, and a felt & cap holder plate. The 42 connector adaptors are arranged in two rows (21 for each) on the connection board. Two adaptors among them are used for the measurement of fiber loss and for the connection cap. The cross connection frame can accommodate a maximum of ten connection boards. The multifunction arm is used for connecting and disconnecting and cleaning of the connector with its precision positioning. These processes are controlled by a microcomputer in a control unit. One typical cycle requires ten seconds or less. On the average, the connection loss of this cross connection frame for multimode fibers is 0.2 dB. Various tests were conducted to ensure their long-term reliability.

2. INTRODUCTION

The optical subscriber cable networks using optical fiber connectors are easy to construct, as well as easy to connect and disconnect for maintenance and operation. Therefore, its use has been spreading especially in the subscriber loops. As its use has been spreaded, there has been an increasing demand to establish a remote controlled cross connection and measuring system for the fiber cables. The conventional optical cross connection frames have employed the thread fastening type connectors or the BNC type connectors. In order to simplify the connection and disconnection mechanism, the new cross connection frame developed. Fig.1 shows the connector. Its operation is as easy as in the case of the electric push-on connectors, so the operator can operate more quickly than in the case of conventional optical connectors. The new optical cross connection frame has obtained good connection characteristics with the components having high reliability. Fig.2 shows the optical cross connection frame. It is compact enough to be accommodated in a central exchange building. The maximum number of the lines that can be accomodated in the frame is 400.

3. CROSS CONNECTION FRAME

3.1 The basic Structure of the push-on Connector

The push-on connector connects the fiber end faces in the ferrules to each other by the hooks of an adaptor and the

Fig. 1

Single-fiber push-on connector

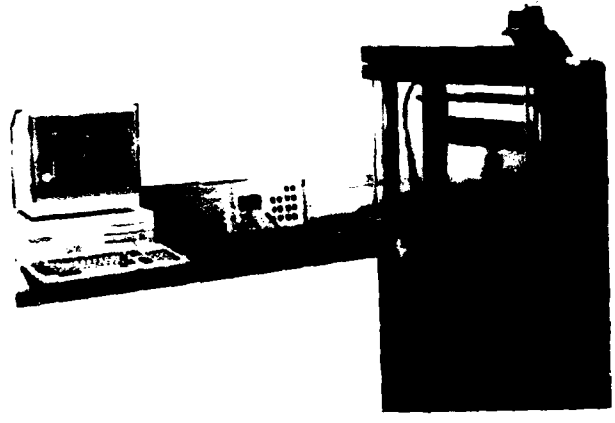

Fig. 2

Automatic cross connection frame system

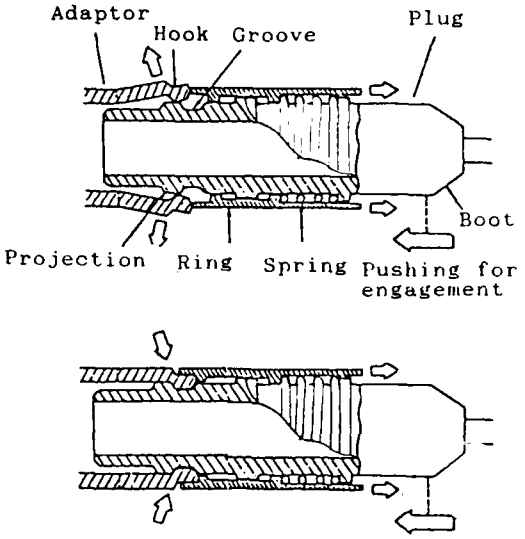

Fig. 3

The engagement of the push-on connector

grooves of a plug. Fig.3 shows the engagement between the connector plug and the adaptor.(1) In engaging, the plug is pushed into the adaptor by holding the rear part of the plug, and the hooks of the adaptor are secured in the grooves of the plug. The plug is pulled out from the adaptor by releasing the hooks from the ring holding the ring on the middle of the plug. The ferrules are made by precision plastics molding, and their top surfaces are polished to a spherical shape of 60 mm radius. The plug can accommodate a single-fiber cord of a sheath diameter not greater than 3 mm. Fig.4 shows the structure of the connector.(1) Normally, the connection loss of this cross connection frame for multimode fibers is 0.2 dB on the average, and the return loss is about 30dB.

3.2 Connection Board

The adaptors on the connection boards are used to connect single-fiber push-on connectors. On one connection board, 12 adaptors are arranged in two rows. The adaptors at the right ends of each row are used for the measurement of the characteristics of the connected fiber or for the connetion cap. A fiber guide plate is set on the connection board to accommodate the excess length of connected fibers and guide them to the cables. This cross connection frame can accommodate a maximum of 10 connection boards.

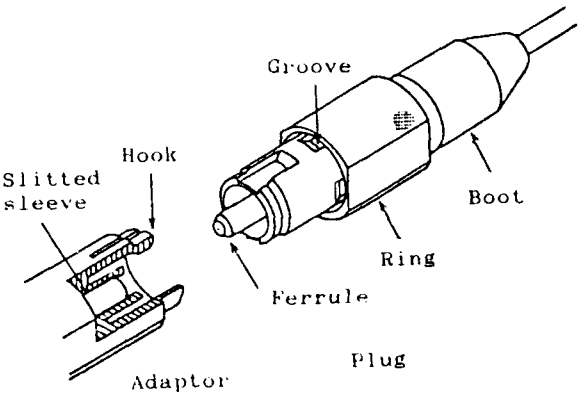

Fig. 4

The structure of the connector

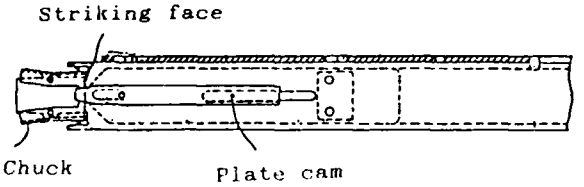

Fig. 5

Structure of multifunction arm

3.3 Multifunction Arm

The multifunction arm can move precisely so that it is used for connection and disconnection and cleaning of the connector. As mentioned above, the rear part of the plug is pushed to engage the hooks of the adaptor and the rings of the plug is pulled to open the hooks and to disconnect the plag. In order to realize such a function, the arm has been designed and manufactured. Fig.5 shows the structure of the arm. For example, in engaging a connector and a cap with an adaptor, the arm holds the rear part of plug and the plug is pushed in by the striking face in the arm. During this process, the plate cam stayed in a backward, and the chuck at the top of the arm is kept open. In pulling out, the arm is moved forward until the chuck reaches the connector coupling, and the plate cam is moved forward so that the chuck can grip the coupling.
To move the connector and the cap to any points for engagement, it is necessary to study the maximum allowable error when moving the connector to be moved to the adaptor to be connected, and to select a

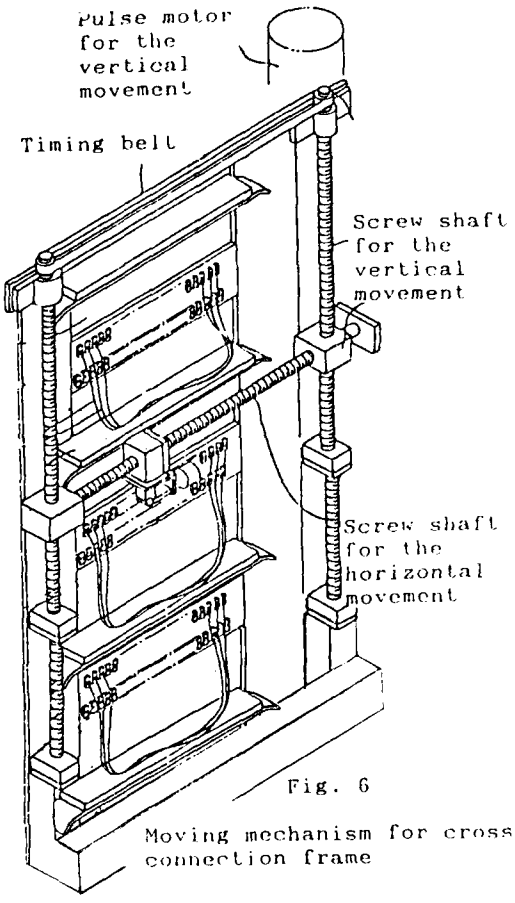

Fig. 6

Moving mechanism for cross connection frame

motor (servo, pulse motor, etc) of the specification to meet the maximum allowable error. Therefore, with respect to the single-fiber connector employed, the allowable error was studied using a magnescale (resolution is 10 um) and manipulator. Further the connection loss value was compared with that in the case of manual engagement, and it was confirmed that the difference was within the measurement error range. Table 1 shows the results. It was found that there is no special correlation between X and Y axis direction, and that the allowable error should be within 0.2 mm and the axial inclination should be within a degree.
Fig.6 shows the moving mechanism for connector to realize this error. In the system, the pulse motor for the vertical movement moves two vertical screw shafts synchronously with timing belt. The shaft for the horizontal movement is supported by two vertical ones. The other pulse motor for the horizontal movement moves the multi-function arm unit on the horizontal shaft. Therefore the multi-fuction arm unit can be moved to any adaptors on the connecting boards.

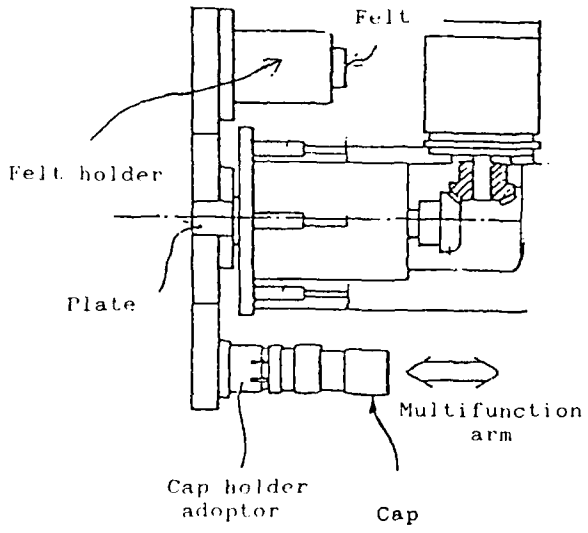

Fig. 7

The mechanism of the felt & cap holder plate

In addition, the motor moves the arm 1mm with 10 pulses, so the allowable errors shown in Table 1 can be satisfied. Further, the motor speed is as high as 50 mm/sec or over.

	Results	N
X-AXIS	0.2mm	5
Y-AXIS	0.2mm	5
Inclination	1 degree	5

Table 1

The maximum allowable error

3.1 Felt & Cap Holder Plate

To prevent the connecting loss increase caused by dust on the ferrule, the top of the ferrule is cleaned automatically by the felt on the plate during pulling out process.
Fig. 7 indicates the state where the arm has attached the cap in the cap holder adaptor. Connectors with fiber can also be engaged to the cap holder adapter, because the cap holder adopter has the same structure as that of the adaptor on the connection boards. The plate turns to 15 degrees in connecting or disconnecting process so as not to interfere with the course of the multi-function arm movement.
The method of cleaning the top of connector described below. After pulling

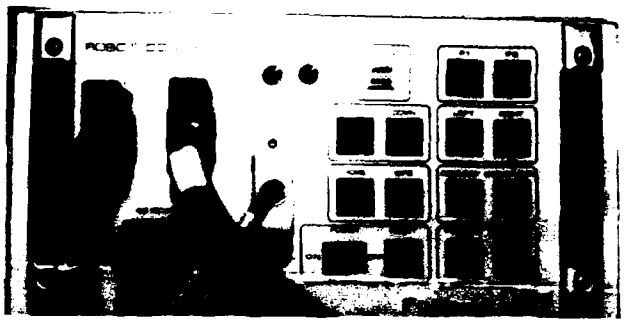

Fig. 8

The panel of cross connection frame controller

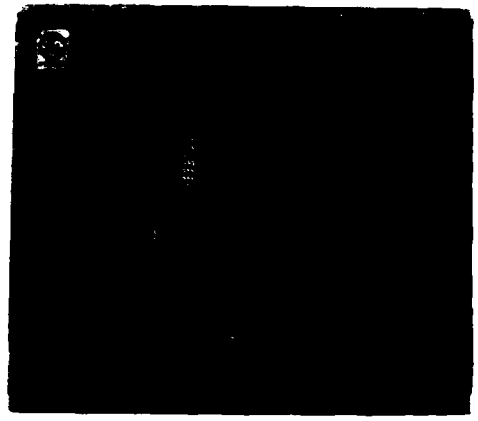

Fig. 10

The table form on the screen

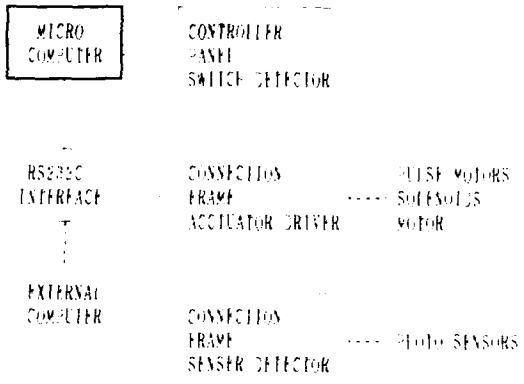

Fig. 9

Block diagram of control unit

out a connector on the cross connection frame, the multi-function arm is retracted and stopped at the position where the top of the ferrule makes minimum contact with the felt. The plate is turned so that the felt can pass over the top of connector and after passing, the plate is turned the other way so that the top of connector is cleaned twice by the felt.

4. CONTROL UNIT

4.1 Hardware

The solenoids, motors, sensors, and pulse motor in the cross connection frame are controlled by a controller connected with two interface cables. Fig.8 shows the control panel of the controller. The hardware of the controller is divided into the following blocks ; a microcomputer a connection frame actuator driver, a sensor detector,a panel switch detector, and RS232C interface for an external computer control. Fig.9 shows the block diagram of this hardware.

4.2 Software

Communication software, which permits the control of the multi-function arm (e.g. up, down, left, right, etc.) by operating the panel switches and the sequential control with an external computer, has been installed in the microcomputer in the controller. The software, which permits a operator to do sequential control of the motor for a desired period of time or desired number of pulses through the table form input using this communication software, has been created using a 16-bit personal computer. Fig.10 shows the examples of the table form on the screen. It is also possible to create software which permits an adapter at any position to be connected or disconnected. The time required for one typical cycle of connector movement is within 10 seconds from the start of pulling out to the completion of connection.

Testing Item	Condition	Result
Temperature cycling	From -30 °C to 60 °C 4 cycle/day	Less than 0.2 dB
High temperature	60 °C 100 H	Less than 0.1 dB
Low temperature	-30 °C 100 H	Less than 0.1 dB
Humidity	60°C X 95% RH 100H	Less than 0.1 dB
Repeatability	5000 times	Less than ±0.5 dB
Vibration	10 Hz amplitude 10 mm 2direction	Less than ±0.05 dB

LED (1.3um)
Steady state mode

Table 2

Reliability test

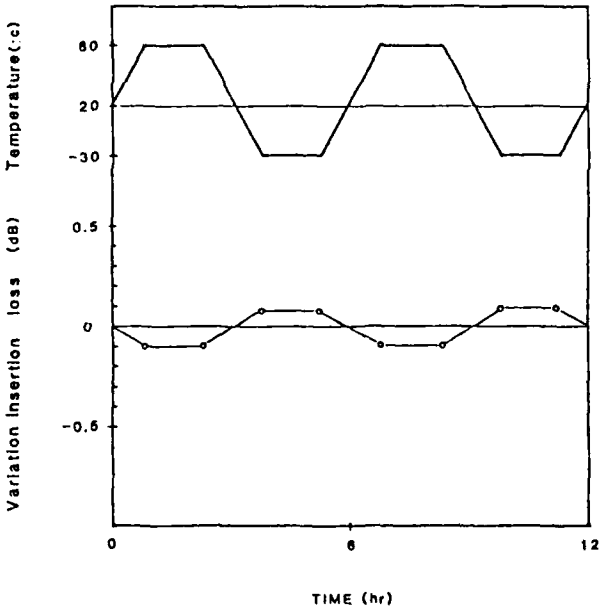

Fig. 11

Temperature cycling
(typical data)

5. RELIABILITY TEST

To confirm the long-term reliability, various tests such as vibration test, continuous connection and disconnection test, etc. on the connectors were conducted. The results are shown in Table 2. Fig.11 and 12 indicate the results of the temperature cycling test and the repeated connection and disconnection tests. The fluctuation of the connecting loss during the temperature

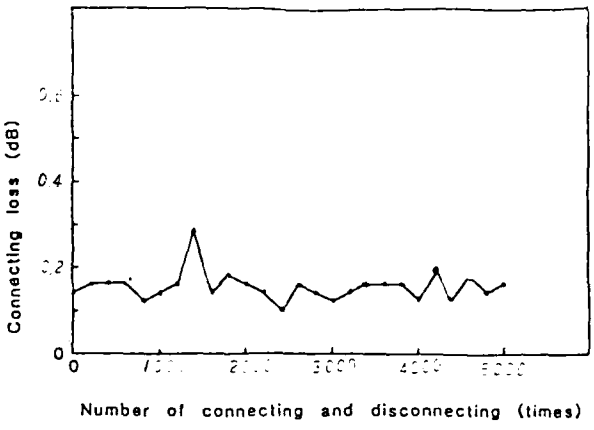

Fig. 12

Repeatability
(typical data)

cycling test was satisfactory small. All of the test results have proved that this cross connection frame has connection characteristics equivalent to those of ordinary connectors, and that it is satisfactorily suited to the practical use.

6. CONCLUSION

A new automatic cross connection frame have developed for the optical fiber networks using single-fiber push-on connectors. The cross connection can be made within 10 seconds for each fiber. This cross connection frame can lead in 20 fibers and lead out 20 fibers. The individual fibers to be led in can be automatically connected to specific fibers to be led out. The same connection characteristics as those in the case of the conventional manual cross connection flame have been obtained. It has been confirmed that this cross connection frame is suitable for the remote measuring and cross connection system in the fiber optic network.

7. REFERENCE

(1) S.NAGASAWA, I.SANKAWA, T.SATAKE and N.KASHIMA
" Small-size Push-on Type Optical Fiber Connector "
THE TRANSACTIONS OF THE IEICE VOL.E 70, NO.5 MAY 1987

(2) M.OHSAWA, H.HIRAO, H.YOKOSUKA and K.INADA
" Exchange Robot for Optical Push-on Connector "
in Proc. Nat. Meet. IEICE Japan 1988 paper B-605 pp.1-356

Makoto Ohsawa was born in 1960. He received the B.E.degree in electronics engineering in 1983 from Sophia University. He joined Fujikura Ltd. in 1983 and has been engaged in research and development in the Cable Accessory Section. Mr.Ohsawa is a member of the Institute of Electoronics, Information and Communication Engineers.

Hiroshi Yokosuka graduated in mechanical engineering from Tokyo metroporitan Technical Junior college in 1967. He has been engaged in development of telecommenication cables and accessories. He is now a Head of the Cable Accessory section. Mr. Yokosuka is a member of the Institute of Electoronics,Information and commenication Engineers of Japan.

Hideo Hirao was born in 1951. He received the B.A. degree in agricultural mechanical engineering in 1974 from Mie University. He joined Fujikura Ltd. in 1974 and has been engaged in research and development of telecommunication cables and accessories. He is now an Assistant Chief of the Cable Accessory Section.

LARGE CAPACITY AND COMPACT CROSS-CONNECTION CABINET FOR OPTICAL SUBSCRIBER NETWORK

Y. FUJII* T. HARA** H. TAYAMA*** S. GOTO**** S.MASE**** H. YOKOSUKA****

* KANSAI TELECOMMUNICATION TECHNOLOGY CORP. (OSAKA,JAPAN)
** OSAKA MEDIA PORT CORP. (OSAKA,JAPAN)
*** THE KANSAI ELECTRIC POWER CO.,INC. (OSAKA,JAPAN)
****FUJIKURA LTD. (TOKYO,JAPAN)

Abstract

This paper describes how one cross-connection cabinet can efficiently accomodate a high density communication network of optical fibers. With the current expansion of optical fiber cable networks, the number of optical fibers accommodated in cross connection cabinets is also increasing. Consequently, there is greater demand for the compact workable accommodation of optical fibers.

Now the accommodation density has been improved to about three times that of the conventional cabinets by designing the connector-adaptor panel into a movable type. The cross connection cabinet is capable of accommodating 400 optical fibers of feeder cable and 500 optical fibers of distribution cable by means of 500 connector-adaptors incorparated for this purpose.

1. Introduction

Optical fiber cable has already found an immense field of applications as a trunk cable, replacing metal cable. In Japan, this cable has been introduced not only into trunk lines but also into subscriber networks and is expected to find increasing applica tions in the field of ISDN.

Following such an expansion of optical fiber networks as cited above, the necessity for an efficient operating network (optical fibers) will come naturally. However, since, the previous scale of subscriber networks was so small, it scarcely required the consideration of a cabinet for accommodating a large number of optical fibers. Therefore no such cabinet has been developed until now. Under the above circumstances this research has led to the development of a cross connection cabinet with high-density accomodations. One is equipped to interface feeder cables and distribution cables and capable of that of the metal cable network.

2. Investigation Purpose

Fig. 1 shows a pattern of the communication network, which consists of a regional center, district center and an end office with cables installed to the subscribers. The cross connection cabinet is to be installed in each center and office, that is, in the office or in an outdoor hut or cubicle.

Since the installation space is often limited, the following points have been considered in investigating the structure of the cabinet:

1) Installation floor space should be comparatively small (compactness).

2) Work should be from the front of the cabinet alone (without using the rear or side space).

3) There should be flexibility toward the market trend.

4) The cabinet should be designed not to impair transmission characteristics.

3. Basic design conditions

The points which are shown in Table 1 were condsidered as basic conditions for the cabinet design.

The optical fibers in the cabinet have been designed to form a cord disregarding the increase in outside diameter, for fear of damage to the optical fiber itself when

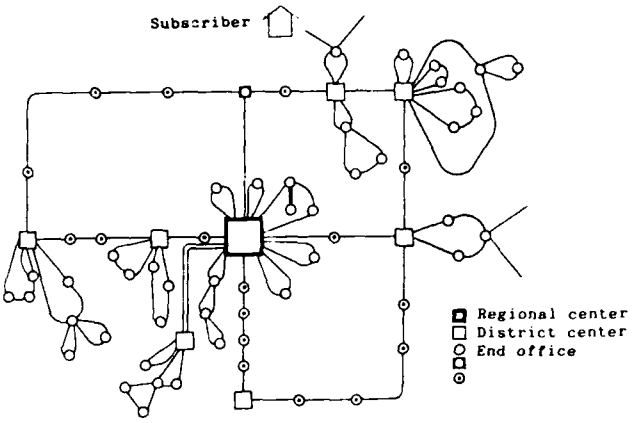

Fig. 1 Optical communication network

arranging the optical fiber in the cabinet. This design is also to prevent the instantaneous attenuation increase which may arise from contact by the operator or another fiber during the cross connecting operation.

The feeder cable uses a 5-fiber ribbon-type cable for the sake of high density and the distributon cable employs a mono-fiber cable for ease in distribution to the subscriber. It is therefore necessary that in the cabinet the ribbon fiber is converted to mono-fibers as necessary.

Table I Basic Design Condition

Feeder cable	5-fiber ribbon type cable (Multi mode)
Distribution cable	Mono-fiber type cable (Multi mode)
Connector	Push-on type connector
Accommodated number of fiber	Feeder cable : 400 fibers Distribution cable : 500 fibers Connector adapter : 500 pcs

4. Structure of cross connection cabinet

Photo. 1 shows the high-density accommodated cabinet which has recently been developed.

Fig. 2 illustrates the arrangment of high-density optical fibers in the cross connectionn cabinet.

The feeder cable enters the cabinet in the form of a five-fiber ribbon-type cable. It is spliced to the ribbon-mono fiber converting connectorized pig tail (Fig. 3), decreasing the number of optical fibers in the cabinet (400 fibers - 80 ribbons). Consequently, these pig tailes have been designed to form a cord with consideration focused on safety of the optical fiber during the threading arrangement.

The distribution cable uses a connecterized cable to make the cabinet compact and ease operation at the work site. The feeder cable and distribution cable are connected by means of a connector panel in the center of the cabinet.

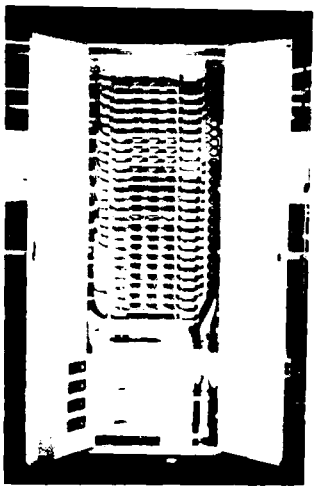

Photo. 1

Developed cross-connection cabinet

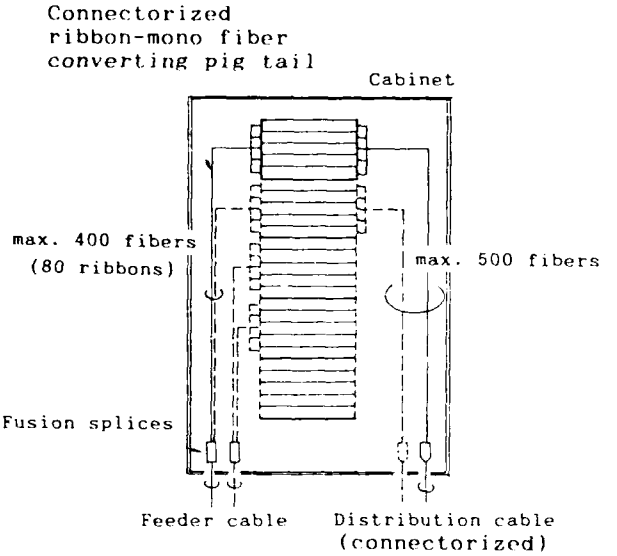

Fig. 2 Threading in the cabinet

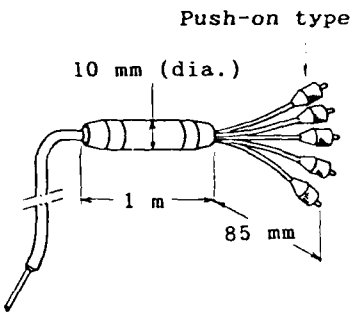

Fig. 3 5-fiber ribbon-mono fibers coverting pig tail

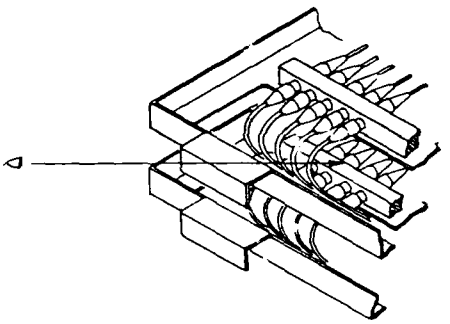

Fig. 5 Connector panel (2)

4.1 Structure of connector panel

To miniaturize the cross connection cabinet the structure of the connector panel connecting the distribution cable and feeder cable must be able to accomodate a high density of optical fiber cord and connectors.

It is further necessary to keep a reasonable operating space to allow for easy threading. In order to satisfy the above contradictive requirements, instead of keeping the operating space open all the time, a basic design was decided which reveals a cross connection cabinet in a constant state of high density. The operating space is provided only when the optical fibers are cross-connected.

Fig. 4 shows the structure of a connector panel. It is designed so that a connector panel contains 20 fibers which are epuivalent to 4 ribbon fibers of feeder cable. The slack of all excess fibers is set at the rear of the connector panel (particularly in the case of a distribution cable), so that the connector may be observed in a normal state, with the connector adapter located on the connector panel toward the front (Fig. 5).

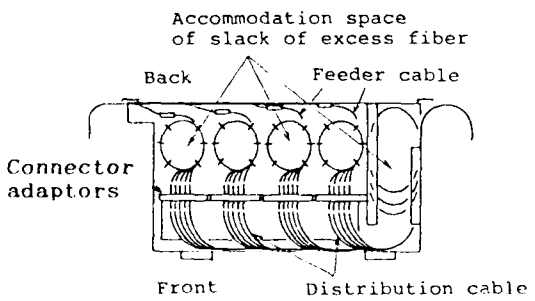

Fig. 4 Connector panel (1)

It is designed so that the slack fiber cord accomodation on the connector panel will maintain the fiber at a radius of 50 mm to ensuring that the optical fiber cannot be reduced below a radius of 30 mm.

To creating the space for threading or cross-connecting optical fibers in the cabinet, there are two methods as follows;

1) Connector panel rotation method
2) Connector panel drawing method

After investigating the above methods, the adopted connector panel rotation method was based on the following reason:

In the case for the drawing method, the excess fiber tightens during the forward movement and slackens during the backward movement of the connector panel and therefore it is difficult to maintain the optical fiber cord safety. During the operation, with the connector panel drawn out; the draw length represents the effective operating space. The space should be taken into consideration when another piece of equipment is installed near by.

On the other hand the connector panel rotation method is free of the drawbacks cited above in creating the operating space. In this method the connector panel normally rests in a half down-ward state (at 20) and the connector panel directly above the connector panel to be operated on is shifted upward by rotation to create the operating space. The connector panels in their natural state have a spacing of 63 mm, but an operating space of 195 mm is created when one is lifted to operate on another. (Fig. 6)

The photo. 2 shows that the space is enough to permit the operation. Four panels will be influenced by the rotation of a connector panel.

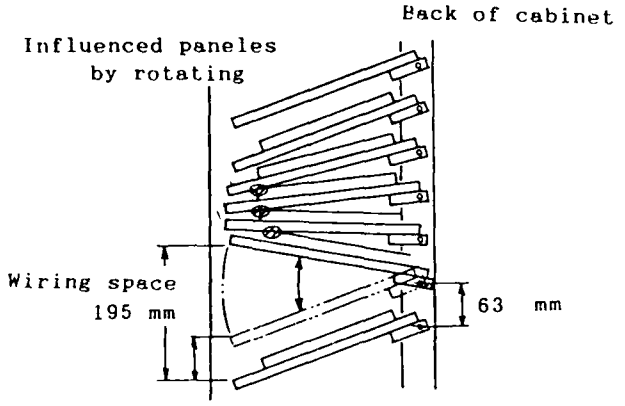

Fig. 6 Rotation of connector panel

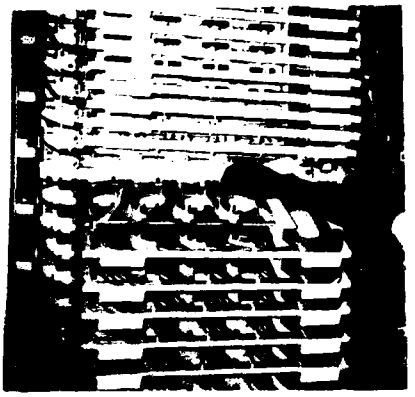

Photo.2 Space for threading or cross-connection operation

4-2. Fiber arrangement in the cross connection cabinet

Fig. 7 shows the fiber arrangement in the cabinet with the feeder cable and distribution cable passsing near the rotary shaft of the connector panel. The optical fiber cord is subjected to torsion alone but free from length variation (slack or tension of the optical fiber cord) in the connector panel movements. And Fig. 7 shows the pass of feeder cables in the cabinet. Excess length of fibers are adjusted by semicirculare guide.

It is possible for the prototype of the cross connector cabinet to accommodate 500 connector adaptors by arranging 20 connector adaptors per panel, with 25 vertically installed panels. Dimensions of this cabinet are 2300 mm (H) × 800 mm (W) × 320 mm (D).

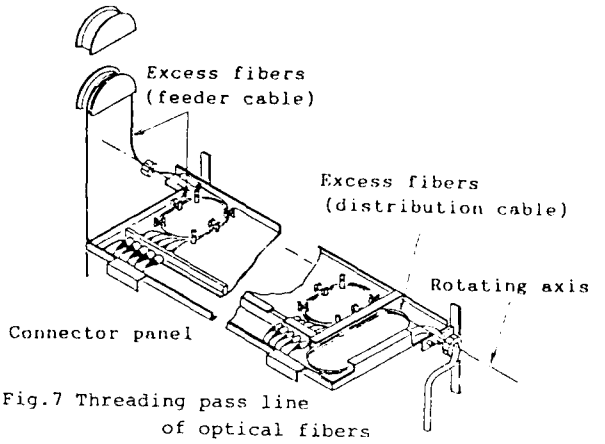

Fig.7 Threading pass line of optical fibers

5. Characteristics

Optical fiber losses are checked after accommodating excess length of fiber cords of feeder and subscriber cable into cabinet. Measuring procedures of fiber losses and results are shown in Fig. 8 and Table 2.

Fig. 9 Measuring procedures of fiber loss

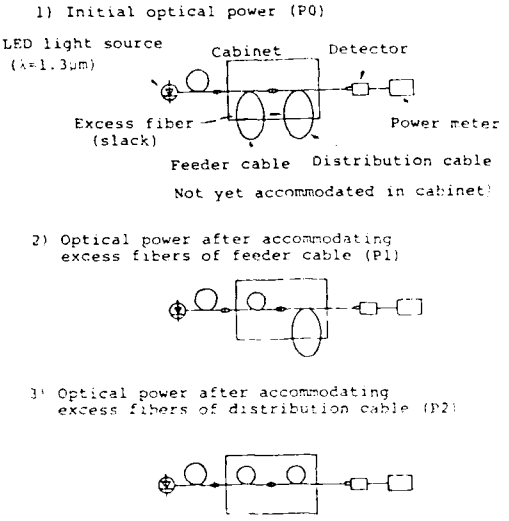

Table 2 Results

Number of fibers which are put into cabinet	400 fibers (80 ribbons)
Loss increase	Feeder cable (P0-P1) : below 0.02dB Distribution cable (P1-P2) : below 0.02dB

Conclusion

A high-density accommodated cross connection cabinet has been developed and confirmed. Occupied floor space is minimal. It is highly operable and does not impair transmission characteristics.

This cabinet has already been operated by Osaka Media Port Corp., a telecommunication company, and has proven it's effectiveness.

References

1. S. Goto et al.; B-601, '88 National Convention of IEICE of Japan.

Acknowledgements

The authors would like to thank all members of Kansai Telecommunication Technology Corp. and Fujikura Ltd. who have contributed to this development.

Yasuo Fujii

Kansai
Telecommunication
Corp.

3-20, Awaji-cho,
Higashi-ku,
Osaka, 541, Japan

Yasuo Fujii received M.Eng. degree from Osaka University and joined The Kansai Electric Power Co., Inc. in 1978. From 1986 he has engaged in R & D of telecommunication network system in Kansai Telecommunication Corp. He is now a assistant manager. He is a member of the Institute of Electronics, Information and Communication Engineers of Japan.

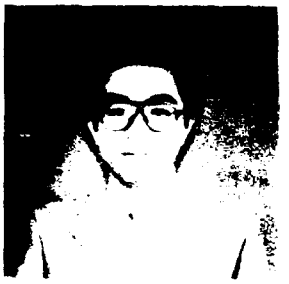

Shigenori Goto

Opt-Electronics
Laboratory
Fujikura Ltd.

1440, Mutsuzaki,
Sakura-shi,
Chiba, 285, Japan

Shigenori Goto received B.E. degree from Iwate University. He joined Fujikura Ltd. in 1974 and has been engaged in research and development of accessory for cable splicing. He is a member of the Institute of Electronics, Information and Communication Engineers of Japan.

Tadashi Hara

Osaka Media Port
Corp.

2-2-8, Nakanoshima,
Kita-ku,
Osaka, 541, Japan

Tadashi Hara received M.Eng. degree from Osaka University and joined The Kansai Electric Power Co., Inc. in 1975. In 1988 he belonged to Osaka Media Port Corp.. He is a manager of the network engineering section in the development depart. of telecommunication technologies. He is a member of the Institute of Electronics, Information and Communication Engineers of Japan.

Saburo Mase

Telecommunication
Cable Engineering
Dept.
Fujikura Ltd.

1-5-1, Kiba, Koto-ku,
Tokyo, 135, Japan

Saburo Mase received B.E. degree in Mechanical Engineering from Keio University in 1971 and has been engaged in engineering of cable accessaries. He is a member of the Society of Mechanical Engineers of Japan.

Hirofumi Tayama

The Kansai Electric
Power Co., Inc.

3-9-3, Honjohigashi,
Oyodo-ku,
Osaka, 531, Japan

Hirofumi Tayama received M.Eng. degree from Kyoto University and joined The Kansai Electric Power Co., Inc. in 1973. He is now a manager of the electric power distribution section in Osaka-kita branch office. During 1986 to 1988 he engaged in R & D of Telecommunication network system in Kansai Telecommunication Technology Corp..

He is a member of the Institute of Electrical Engineers of Japan.

Hiroshi Yokosuka

Opt Electronics
Laboratory
Fujikura Ltd.

1440, Mutsuzaki,
Sakura-shi,
Chiba, 285, Japan

Hiroshi Yokosuka joined Fujikura Ltd. in 1967 and has been engaged in research and development of automatic telephone cable splicing machines, joint closures and optical fiber connectors. He is now a chief of the fiber and cable accessory section in Opt-electronics Laboratory. He is a member of the Institute of Electronics, Information and Communication Engineers of Japan.

ACCESS METHODS FOR NON-INTRUSIVE OPTICAL FIBRE NETWORKS

G.J. Cannell, R.E. Epworth, P.G. Hale, T. Large, B. McDowell, A. Robinson, M.M. Ramsay, I.F. Scanlan, J.G. Titchmarsh & R.L. Williams

STC Technology Limited
London Road, Harlow, Essex CM17 9NA, England

Abstract

This paper discusses the design of an optical fibre local area network which uses a non-intrusive technique to access fibre at each network node. A demonstration system has been constructed which operates at 10 Mbits/s and has a capacity of 100 nodes. Practical aspects of a real system have been addressed, particularly implementation of a tapping method which can gain access to fibre through the sheath of a cable.

Introduction

Optical fibre is now accepted by the telecommunications community as the preferred technology for long haul point-to-point links, and is moving even closer to the end user. In order to give the user direct access to the bandwidth of fibre, a convenient and cost effective means of linking terminals and workstations to a fibre local area network is needed.

Current optical technology is based on point-to-point links, and for a true local area network is cumbersome in terms of both cable requirement and system organisation. The alternative approach - to use couplers and/or power splitters - requires a large investment in such components, generally limits the number of system nodes, and involves system downtime if the network is to be reconfigured or added to. To realise a practical fibre LAN, an approach is needed which can access the data carried in the fibre core in a non-intrusive way, and which uses cheap and readily available components.

Techniques for the local injection and detection (LID) of power in an optical fibre are already commonly used in the alignment of two cleaved ends prior to fusion splicing. Work has also been published which outlines the detection and extraction of real traffic[1,2]. The natural progression of this work is towards the use of LID to provide multiple access points on an optical fibre to provide a network, and such a system is outlined.

Whilst a rudimentary cable and access technique has been used for the demonstration system, non-intrusive networks give a host of new requirements to the cable designer. Simple cables can offer low cost solutions, but more complicated structures which incorporate some of the necessary tap features may be attractive; the trade-offs are considered here. Design details such as the effects of static fatigue and time-dependent deformation of fibre coatings are also discussed.

System Overview

Work at STL has centred on direct detection and injection with single mode fibres using a grating, a large area photodiode and a compact disc type diode laser. A system demonstration of one master node and four slave nodes operating at 10 Mbits/s has already been achieved with operating parameters which could allow up to 100 nodes on a single fibre ring. It uses 1 km of cable with taps which can be inserted anywhere along the cable length.

Many of the often quoted advantages of optical fibre transmission systems are applicable to non-intrusive networks - noise immunity and high bandwidth - but in this subset of systems, it is of course possible and practical to

insert or remove a node where desired and thus reconfigure. This may be of great utility in business premises, in industrial process plant, and on board ship. Cables specific to each environment will then be needed.

Optical Fibre Tap

A schematic diagram of the tap is shown in Figure 1, with the injected and collected light travelling in the same direction. The primary coated fibre is sandwiched between a grating of appropriate dimensions and a transparent block incorporating a lens system. A load is applied to the grating, perturbing the fibre so as to induce coupling between a core mode and one or more cladding modes. In order to extract light, the cladding power is transmitted across the boundary between the cladding and the protective primary coating, into the block, and is then collected and focussed by the lens onto a detector. Light injection is achieved similarly with an LED or laser replacing the detector. One of the useful features is that the coupling fraction between the core and cladding modes, which determines the maximum number of nodes in the system, can be controlled variably from zero to nearly 100% by simply adjusting the pressure on the grating.

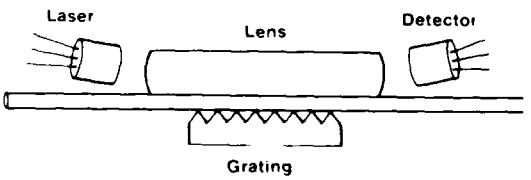

Figure 1: Tap Schematic

If a semiconductor laser is used for injection (as opposed to an LED) then aberrations in the imaging optics will need to be minimised, and the fibre/source alignment is critical. For collection, the active area of a semiconductor detector will typically be much larger than the emitting area of a laser, and less highly corrected optics and less stringent alignment is necessary.

Cable and Fibre Access

For the demonstration system, it was necessary to prove all aspects of a practical non-intrusive approach. Therefore, a practical and reliable cable and access method was needed. The system was required to operate in a real but relatively benign laboratory or business environment (rather than on a bench) which eased cable design, but all the essential features of a more hostile environment had to be considered.

The cable chosen (Figure 2) is a simple oval loose tube design strengthened with two pultruded dielectric strength members which allow moderate in-building installation forces to be withstood.

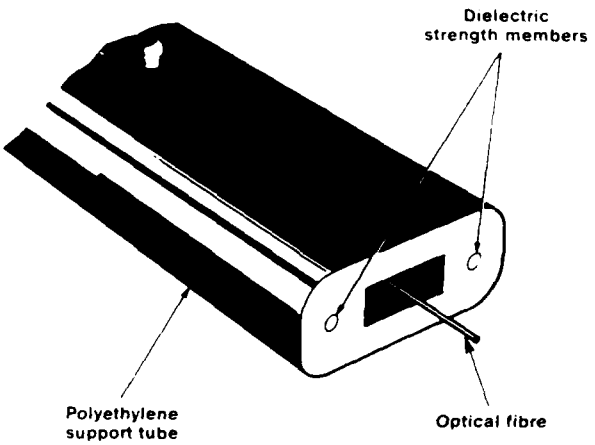

Figure 2: Non-intrusive Cable Prototype

Initially Kevlar 49 cords were used for strength, but these proved difficult to cut reliably when access was required. The current strength members provide a surprising amount of flexibility to the cable before break - a minimum bend radius of approximately 10 mm is achieved on the easy axis. Fibre access is gained by controlled cutting of the sheath within a jig which acts both as a cutting guide and as an 'exoskeleton', providing strength and protection when the fibre has been exposed. The tap may be easily mounted on the jig.

The cable is cheap to produce, involving only a single processing stage, and gives zero incremental loss over primary coated fibre. Full environmental and mechanical tests have yet to be carried out. Although currently a single fibre design, multiple fibres can be used, but in this case modifications to the access method will be needed. These have already been considered. A possible bonus of the access approach is that it should be directly applicable to the plastic loose tube packages widely used in the optical fibre cabling industry. Indeed, any cable where the sheath can be partially cut without damage to the fibre has potential for non-intrusive use.

Gaining access to the fibre does not involve system downtime, and has shown initial reliability. The principle is to use two opposed 'U' shaped pieces (Figure 3) which clamp onto the cable, the sheath of which is then cut in the manner described below. The double 'U' cable clamp and sheath removal method gives nearly 360° access to the fibre. This double sided access allows the grating to approach the fibre from one side, and the laser/photodiode package from the other.

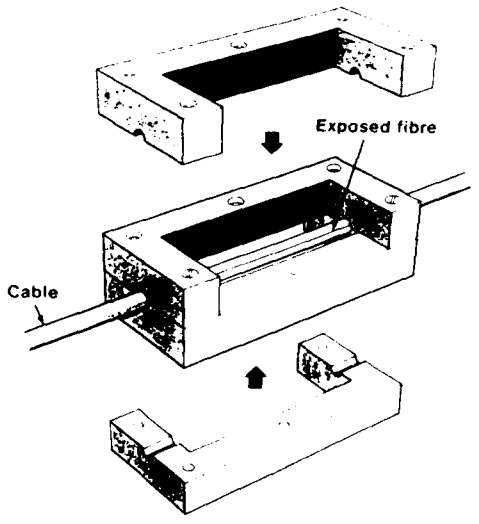

Figure 3: Tap Clamping Method

To facilitate access, the two 'U' shaped pieces are clamped to the cable sheath. A longitudinal cut which penetrates into the fibre space is then made along one edge of the sheath. It has been found experimentally that the fibre is not damaged, but moves out of the way of the blade reliably and repeatably. The jig is inverted and a similar cut made along the opposite edge. Then, transverse cuts are made across the sheath, half of which falls away; the jig is inverted again and similar transverse cuts made in the other half of the sheath which also falls away, exposing the fibre. Figure 4 shows the sequence of cutting. A small knife alignment mount has been found to considerably ease the cutting process. Note that the blade could be ultrasonically excited, or rotated (e.g. a dentist's drill); or a heated tool could be used which melts the cable sheath. Note also that the method is in principle applicable to structures with multiple fibres.

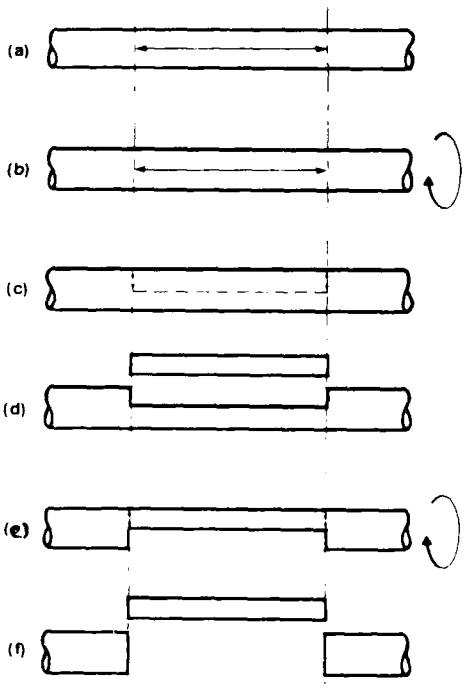

Figure 4: Cable Cutting Sequence

The fibre is now exposed between the 'U's' and is protected by the longitudinal parts of the clamp. Proper design allows the cable sheath to be gripped effectively. The 'U's' are also a convenient means of mounting a tap.

Demonstration System

The demonstration system comprises a master station plus four taps (slave nodes) working over a one kilometre ring of specially designed single mode fibre cable. The system is shown schematically in Figure 5. Both fibre ends are connected to a master station which can launch and receive directly into and from the fibre without loss. This master station is used as a regenerator and allows downstream taps to communicate upstream. The experimental network uses desktop computers as the slave node devices and a data rate of 10 Mbits/s was chosen to be compatible with other standards such as Ethernet. This data rate is the total channel capacity for all the taps, and so a suitable multi-access protocol must be chosen to share the resource.

Copper Ethernet uses TDMA (time division multiple access) with carrier sense and collision detection. Collision detection is more difficult in an optical system and so a simpler technique was required for the demonstration system. Unlike Ethernet networks with distributed intelligence, the master station naturally lends itself to a central control approach (and can also be used as a gateway to other networks) so a polling protocol was adopted with the master controlling allocation of the channel based on requests from taps for channel usage.

A standard telecommunications type laser emitting at 1300 nm, and with a launch power of 1 mW was used as the master source. To be economically viable, it is essential to use cheaper components at the tap and restrict any more expensive components that may be required to the one master site. The (cheap) laser used in compact disc players was the ideal choice for the tap injection source emitting at 790 nm. At this wavelength, conventional telecommunications fibre can support more than one mode, and in order to prevent modal noise problems, the laser is modulated at 250 MHz to reduce its coherence. A silicon

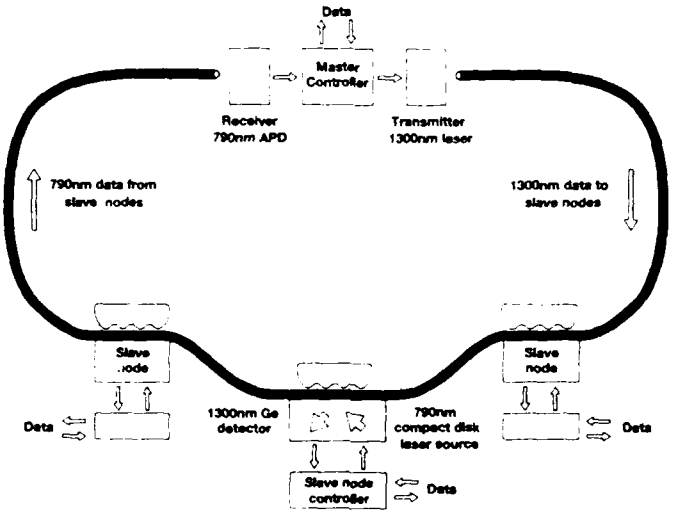

Figure 5: Prototype System Schematic

Wavelength	790	1300	nm
Fibre loss	3.5	0.2	dB
Source power	-5	0	dBm
Receiver sensitivity	-62	-45	dBm
Peak/mean ratio	3	3	dB
Injection loss	22	--	dB
Tapping loss	--	10	dB
Coupling fraction	17	17	dB
Total node loss	5	5	dB
Total loss	50.5	35.2	dB
Operating margin	6.5	9.8	dB

Figure 6. Power Budget for 50 node, 1 km system

avalanche photodiode was used at the master receiver where its high sensitivity could usefully be employed to offset the tap injection losses. Relatively cheap germanium photodiodes were used as tap receiver detectors, the efficient light collection process obviating the need for an expensive APD to realise a workable sensitivity. The tapping fraction was adjusted at each slave node to be representative of a fifty node system, but economic considerations did not allow for fifty taps to be constructed.

The demonstration system power budget is shown in Figure 6.

Cabling Techniques

The concept of an installation based on non-intrusive techniques presents some novel cable requirements to engineers. They are used to designing cables which protect the fibre by making it difficult to access. They are now asked to cable it in such a way that it gives quick and easy access to, and anchorage for, the tap, while still providing adequate protection.

By using a complicated cable structure, convenient features can be built in, such as a measure of fibre/tap alignment, but at a cost. Take two examples. The first is a cable in which a coated fibre is held on the cable neutral axis by a lightly foamed elastomer which is extruded with a permanent split to its centre, achieved by the use of a web in the extruder crosshead. In the cable construction, this split is arranged to correspond with an easy split line in the sheath. This line is marked during sheath extrusion by a different coloured plastic inserted by a small 'piggy back' extruder. When a tap is required, the cable can be easily split down this line, and a wedge shape tap inserted. Positive tap alignment can be achieved.

The second example is a cable with a sheath which is made in two identical halves. Whilst manufacturing the halves, periodic stampings are made which indent the sheath to provide knock-out panels which ease removal (in the manner of a soft drink can lid with ring-pull). The cable is then put together by glueing or oversheathing.

Whilst elegant, both of these designs lead to multi-stage production processes, with inevitable drop in yield and rise in cost.

Other cable structures which aid tapping can be envisaged. For example, the grating itself can be incorporated during manufacture, (e.g. by the stamping process described above) and designed to be used only when a tap is required - although this may be somewhat dangerous if the cable is bent. Alternatively, 'zip-like' like features could be included in the cable sheath.

However, such additions will increase cabling costs, and will only be used in fields where the simpler tapping procedures compensate for this increased cost. Simplicity will be of the essence, to keep costs down in what are likely to be very competitive and cost-conscious markets.

System Reliability

From the overall system view, a properly designed non-intrusive optical network will be no less reliable than a conventional point-to-point link, as they both use similar optoelectronic components. There are, however, two important additional aspects of the technique which merit special consideration. These, both concerning the tap itself, are static fatigue and long-term deformation of fibre coatings.

Static fatigue must be considered because the tap subjects the fibre to bending strain. One of the advantages of using a grating rather than a simple bend to tap light is that the bending strain is much lower[1]. Using classical bending beam theory, the shape of the bent fibre has been described by means of a Fourier series[3]. The crucial result of this, as far as static fatigue is concerned, is the maximum surface tensile strain. This is slightly different for injection and detection, as two different gratings are used. The maximum tensile strain for injection is 0.15%, and for collection 0.12%.

The inert fibre strength required to survive a 0.15% strain for ten years service life was calculated using standard static fatigue theory, assuming an N value of 25 for an indoor environment and a B value of $10^{10}Pa^2s$. In terms of strain this inert strength is 0.645%. This is comparable with the 0.5% proof test level used for standard telecommunications fibre, so it can already be seen that fatigue will not be a major problem. When it is realised that only a very small surface area of the fibre is exposed to this strain, a large safety margin is seen to exist.

In the demonstration system tap, the length of fibre under strain totals 13.6 mm. In order to obtain a conservative estimate of failure probability, the following assumptions were made. Firstly, the entire 13.6 mm was considered to be under the maximum 0.15% strain, and secondly, the entire fibre surface was also considered to be at this maximum surface strain. In actuality, only the extreme outside of the bend is at this strain. The probability of failure was then calculated using data obtained from longer length tensile strength experiments on commercial fibre[4]. This is less than 10^{-10} over the ten year period and is thus negligible.

The second aspect of long term reliability, creep of fibre coatings due to loading by the gratings over the system lifetime, has also been addressed. Any such deformation would result in drift in the amount of light collected or injected. A theoretical analysis of the problem is difficult, since it is not clear which model of deformation applies to the coatings. Each model predicts a different behaviour in the long term, ranging from continual flow leading to breakdown, to the eventual establishment of an equilibrium distortion.

A simple approach was adopted measurement of coating movement under simulated service conditions. The experimental configuration is shown in Figure 7. The two bare fibres simulate two bars of the grating and the fibres are loaded by applying a weight to the top plate. This is a mechanically stable configuration where the load on an intersection can be calculated. Coating deformation may be measured by monitoring the capacitance between the metallic plates. The area of the formed capacitor is large enough to ignore changes in dielectric constant at the crossovers.

At room temperature, 90% of the coating distortion was complete during the first few minutes from loading, after which exponentially decreasing movement was observed. Extrapolation of results made over a month (Figure 8) suggests that after some 80 microns of flow (66% coating deformation), a stable condition was reached. Indeed, many centuries would pass before complete penetration of the 120 m primary coating.

Further experiments, also shown in Figure 8, were conducted at elevated temperatures to 70°C and showed no evidence of catastrophic breakdown to (ductile) failure. The apparent inconsistency between the results at 40°C and 50°C can be explained by the fact that there is a glass

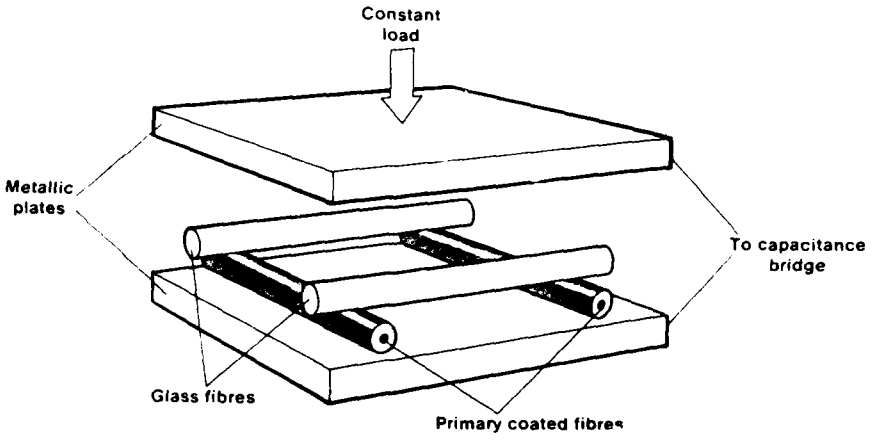

Figure 7: Creep Experiment Schematic

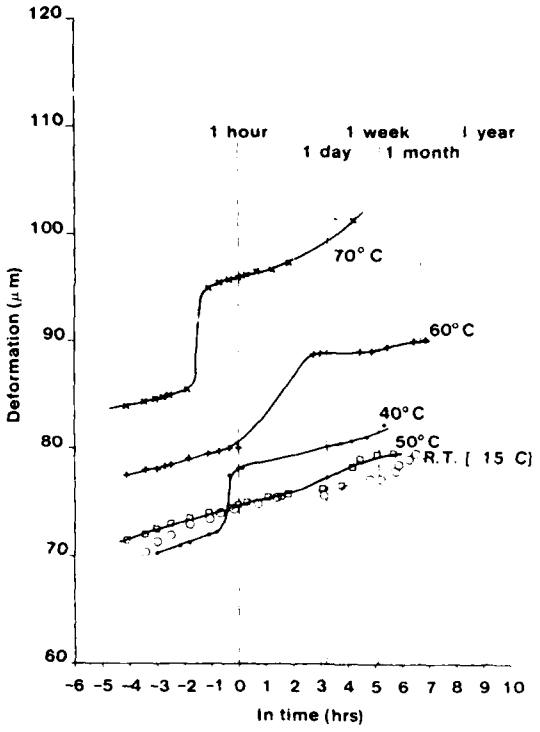

Figure 8: Primary Coating Deformation With Respect To Time

transition of the acrylate used at approximately 39°C.

The results of the analyses of both static fatigue and polymer coating distortion leave us confident that a system designed on the principles thus far adopted would have a service life of more than 10 years.

Summary and Conclusions

This paper has presented the implementation of a non-intrusive optical fibre network. It has shown that such techniques are fundamentally practical, and have the potential to operate reliably over extended periods of time.

Acknowledgements

The authors thank the directors of STC Technology Ltd for their permission to publish this paper. The work is the result of the collaboration between many STL colleagues; to name some would be unjust, and to name them all would be impractical.

References

1. Aberson & White, OFC/IOOC '87, TUQ12.

2. Plessey, Sunday Times, 18/10/87.

3. A. Robinson, private communication.

4. Scanlan, et al, IEE Coll, June 1984.

George J. Cannell received a B.Sc. honours degree in Electronics, and an M.Sc. degree in Electrical Materials Technology from the University College of North Wales, Bangor, in 1963 and 1964 respectively. He joined STL in 1973 and has been primarily engaged on research into optical fibre design and propagation, and on the development of new measurement techniques. His more recent work includes the application of fibres in networks and network components.

Richard Epworth received a B.Sc. degree in Electrical Engineering from the University of Manchester in 1966. He then joined STL where he worked on a variety of projects including radar signature recognition, intruder detection systems, and an instrument landing system. Since 1973 he has worked almost exclusively on various aspects of optical fibre communication and sensors, particularly modal noise and coherent systems. He is now working on eye-movement controlled technology.

Dr. Peter G. Hale graduated with an honours degree in Engineering Science and Economics from the University of Oxford in 1973. After a short period with Instron Ltd., he returned to the University of Oxford where he gained a D.Phil. in 1979, on the subject of the metal coating of optical fibres. He joined STL in 1980 as a Research Fellow in the Optical Fibre Cable Group, has worked on many different aspects of optical fibre cables and sensors, and is currently involved in advanced optical fibre cabling techniques.

Timothy Large graduated from Cambridge University in 1985 with a degree in Natural Sciences. After a year of research into scanning optical microscopy at the Cavendish Laboratory, he joined STL where he has worked on various aspects of optical technology including laser evaluation and coherent transmission systems.

Boyd S. McDowell graduated from Birmingham University in 1987 with an honours degree in Metallurgy and Materials Science. He joined STL in the same year as a Research Engineer in the Cable and Materials Engineering Department.

M. Murray Ramsay obtained a B.Sc. from University College, London in 1952. He is a Chartered Physicist and a Fellow of the Institute of Physics. He joined STL after graduating and was a founder member of the team set up in 1958 to study optical communication systems. He acted as consultant to ITT-EOPD Roanoke in 1973 when work on optical communication systems started there. He later returned to STL and is currently Chief Research Engineer for optical fibre cables.

Alan Robinson graduated with honours in physics from the University of Cambridge in 1973, where he subsequently studied metal fatigue in the Department of Physics. On joining STL in 1977, he worked on optical fibre preform fabrication by plasma deposition, on the design, fabrication and evaluation of nuclear radiation resistant fibres, and is currently investigating waveguide modelling and fibre based components.

Ian F. Scanlan gained an honours degree in Physics from Nottingham University in 1964 and then joined STL. He has worked on electronic switching processes in glass and on high frequency transistors for submerged repeaters. More recently, he has specialised in the theory of static fatigue in, and reliability of optical fibre.

Jim G. Titchmarsh obtained a B.Sc. in Physics from Bristol University in 1964, and an M.Sc. in Solid State Electronics from Manchester University in 1966. He then joined STL to work on thin film deposition techniques. After a period studying plasma panel displays, he started work in optical fibre, and is responsible for technology development in the Cable and Materials Engineering Department.

Roy L. Williams gained his B.Sc. from Queen Mary College, University of London in 1967, when he joined STL. He has worked on many analogue and digital systems including magnetic printing, aircraft instrument landing, videotext, point-of-sale terminals, and ISDN. He became involved in optical communications in 1987.

CABLE ACCESSORIES FOR OPTICAL FIBRE RIBBON CABLES IN SUBSCRIBER LOOP NETWORKS

P. Deußer, J. A. Becker

Philips Kommunikations Industrie AG
Nachrichtenkabel und -anlagen
Schanzenstr. 30; D-5000 Köln 80
Federal Republic of Germany

Abstract

Techniques so far developed for optical telecommunication trunk line networks do not fulfil the requirements of future subscriber loop networks. Based on the optical fibre ribbon cable, multiple splicing techniques and the plastic connector a full range of cable accessories has been developed.
New type splice organizers assure orderly storage of ribbon-to-ribbon connections and splicing lengths in both existing and future splice closures. The splicing lenghts of fibre ribbons are stored prior to the splicing process. They are to be pulled out of the organizer for the splicing procedure and pushed back when the splice is finished.
Modular constructed cable terminals employing the recently developed plastic connector [1] and pre-connectorized jumper fibres are the main elements of optical cross connecting cabinets and main distribution frames.

1. Introduction

Optical telecommunication techniques are succesful used in trunk line networks for several years. The next step of development will be the introduction of fibre optic techniques into subscriber loop networks. Techniques, equipment and procedures developed so far for telecommunication networks therefore fulfil the requirements of trunk line applications but are hardly the appropriate approach of the subscriber loop networks of the future.

Key element of the subscriber loop network is the optical fibre ribbon cable, which offers the combined advantage of high fibre density and multiple fusion splicing of the fibres.

Based on this cable and splicing approach the principles of a complete range of cable accessories for subscriber loop networks have been developed including a new splice organizer for fibre ribbons.

In addition to permanent ribbon-to-ribbon connections subscriber loop networks also require detachable fibre connections for cable terminals in cross connecting cabinets and main distribution frames. A new technological approach to cables terminals is the subscriber loop connector employing precision thermoplastic moulding technologies and fibre adjustment in v-grooves [1]. Together with the above mentioned splice organizer this plastic connector is the main element of terminal units in modular constructed terminals for fibre ribbon cables.

2. Splice Organizer for Fibre Ribbon Connections

The main problem of cable accessories for optical fibre ribbon cables is to store the ribbon-to-ribbon connections and the appropriate splicing- and repair lengths well arranged in an easy and time saving procedure. Due to the rectangular shape of the fibre ribbon these lenghts cannot be stored in simple loops after completing the splice procedure as it is done with single fibres.

Special splice organizers for optical fibre ribbons have been developed. In these organizers the splicing- and repair lenghts of the ribbons to be connected are stored in separated storage chambers prior to the splicing procedure. Before the splicing procedure is started the ends of the already stored fibre ribbons have to be pulled out of the storage chambers of the splice organizer. When the splicing procedure is finished the ribbons are pushed back into the storage chambers.

2.1 One-chamber splice organizer

The one-chamber splice organizer is made up by two cylindrical storage chambers for fibre ribbons as shown in Fig. 1.

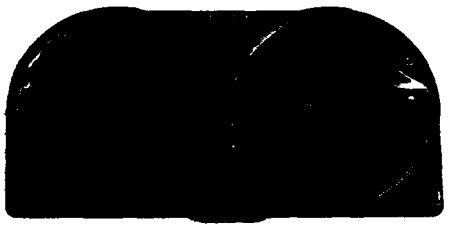

Fig.1 One-chamber splice organizer

The fibre ribbons to be stored are introduced through guiding channels into the organizer. Before they reach the interior of the storage chambers they are turned into upright position. Thus the ribbon lenghts to be stored are inserted into the storage chambers through slotted holders loop by loop. The ends of the fibre ribbons are led out through ports in the outer walls of the storage chambers. Normally all layers of the ribbons are close to the outer walls due to their stiffness. The ends of fibre ribbons are to be pulled out of the storage chambers before the splicing procedure is started, the coils of ribbon layers are drawn together and ribbon length is gained to lead the ribbon ends to the splicing machine. When the splicing procedure is finished the ribbons are pushed back into the storage chambers and the protected splice is fixed in the space between both storage chambers.

The one-chamber splice organizer fulfils all requirements for the storage of ribbon-to-ribbon connections including the appropriate splicing- and repair lenghts. But the splice organizer cannot be taken out of the splice closure to bring it close to the splicing machine without providing further unprotected lenghts of fibre ribbon remaining unarranged in the splice closure.

2.2 Two-chamber splice organizer

The two-chamber splice organizer should be used in all cases where it is required to take the splice organizer out of the cable accessory and bring it close to the splicing machine.

In contrary to the one-chamber splice organizer the storage chambers are subdivided into two zones by a separating wall. In the interior zone of the storage chamber that part of the ribbon length is stored, which is necessary to bring the organizer close to the splicing machine. The splicing- and repair length is stored in the outer zone. The two-chamber organizer is shown in Fig. 2.

FIG.2 Two-chamber splice organizer

To prepare the two-chamber splice organizer for the splicing procedure the fibre ribbon is inserted into the interior zone first and then is changed over into the exterior zone. At the separating wall between both zones the fibre ribbon is fixed by a clamping device. All other mounting steps are the same as described in the case of the one-chamber splice organizer.

Due to its construction it is possible to take the two-chamber splice organizer out of the splice closure whereby the ribbon portions stored in the interior zones are used; to get the ribbon ends to the splicing device the stored lengths in the exterior zones are used. When the two-chamber organizer is placed back into the splice closure after the splicing procedure both fibre ribbon lengths are stored well protected within the splice organizer.

3. Support for Splice Organizer

The supports as shown in Fig. 3 serve for screwless fixing of both type of splice organizers in cable accessories. The supports are provided with slots for the organizers to be pushed in. Every slot is able to carry one organizer in horizontal position or two organizers standing upright. According to the modular construction long rows of supports can be formed.

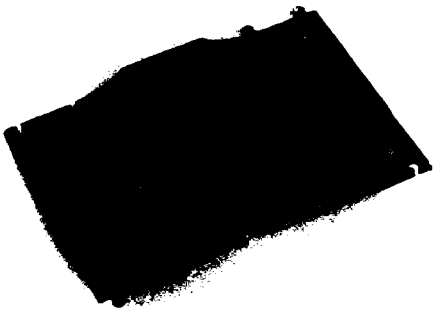

FIG. 3 Support for splice organizer

4. Splice Closures for Optical Ribbon Cables

The described splice organizers are designed for both existing and future types of splice closures. In the initial stage of optical subscriber loop networks probably proven types of splice closures will be used, e. g. the well known TK-closures of screwed- and clamping type.

Due to their dimensions the closures TSK 100-4 and TK 95-64 are only suitable for one-chamber splice organizers. Fig. 4 shows the splice closure TSK 100-4 equipped with 5 one-chamber splice organizers to store the splices of 5 fibre ribbons.

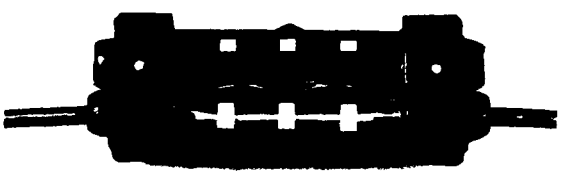

FIG. 4 TSK 100-4 equipped with 5 one-chamber splice organizers

Two-chamber splice organizers can be used beginning with the size TK 120-80. This closure is able to take up 20 two-chamber organizers for 200 fibre splices. It is shown in Fig. 5. One of the two-chamber organizers has been taken out for splicing.

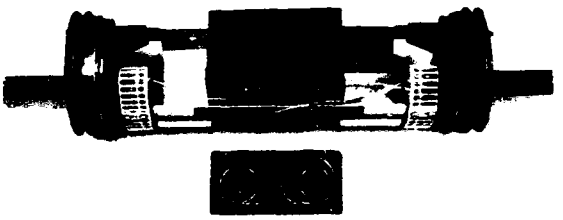

FIG. 5 TK 120-80 equipped with 20 two-chamber splice organizers, one taken out for splicing

The closures TK 155-100 and TK 155-100L are able to take up 50 or 80 two-chamber splice organizers respectively. Table 1 surveys the dimensions and the fibre/ ribbon capacity of the complete TK-closure family equipped with one- and two- chamber splice organizers.

One chamber organizer			
Type	Dimension (mm)	Capacity	
		organizer	fibres
TSK 100-4	86 x 114 x 207	5	50
TK 95 64	Ø155 x 430	15	150
Two chamber organizer			
Type	Dimension (mm)	Capacity	
		organizer	fibres
TK 120-80	Ø181 x 585	20	200
TK 155-100	Ø214 x 675	50	500
TK 155-100 L	Ø210 x 925	80	800

Table 1: Dimension and fibre capacity of TK-closures

The further progress in building out optical subscriber loop networks will require the development of a new closure family especially designed to the requirements of fibre ribbon cables. In Table 2 the possible range of a future closure family with main dimensions and fibre capacity is shown.

Size	Capacity		Dimension (mm)
	organizer	fibres	
1	10	100	120 x 170 x 385
2	25	250	170 x 230 x 375
3	50	500	170 x 230 x 550
4	100	1000	170 x 230 x 850
5	200	2000	270 x 275 x 850

Table 2: Possible capacity and dimensions of a future closure family

5. Switching Units for Fibre Ribbon Cables

Based on the above mentioned plastic connector for subscriber loop network applications [1] a new type of optical cable terminal was developed to provide detachable connections in cross connecting cabinets and main distribution frames.

This cable terminal allows termination of 100 fibres. It is modular constructed and made up of plug-in units to terminate one fibre ribbon each.

A complete mounted plug-in unit is shown in Fig. 6.

FIG. 6 Plug-in unit completely mounted

On its bottom side it is provided with modified splice organizers and a tenfold connector port. One fibre ribbon of the outside plant cable is spliced to single fibre pigtails of the plastic connectors. Both splicing lengths of the fibre ribbon and the pigtails are stored in separate storage chambers see Fig. 7.

FIG. 7 Plug-in unit, bottom view

On the upper side of the terminal unit a stack of storage disks for pre-connectorized jumper fibres is arranged. These disks are needed to store the overlengths of pre-fabricated jumper fibres, see Fig. 8.

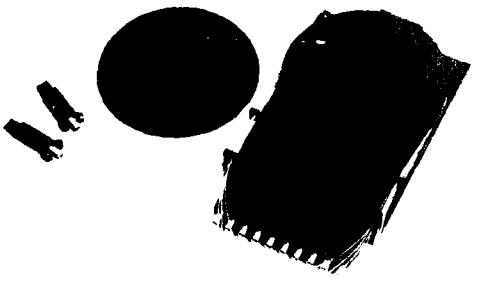

FIG. 8 Plug-in unit; top view with storage disk and pre-connectorized jumper fibre

Switching units are built up by at least one pair of terminal blocks but only one stack of storage disks per terminal is needed. Therefore a second type of terminal unit, without storage disks was taken into account.

Cross connecting cabinets and main distribution frames built up with described cable terminals are comparatively small units. They offer the advantage of time saving switching operations. Fig. 9 shows the first model of a column of terminal units for use in cross connecting cabinets. Simular structions can be built up for main distribution frames.

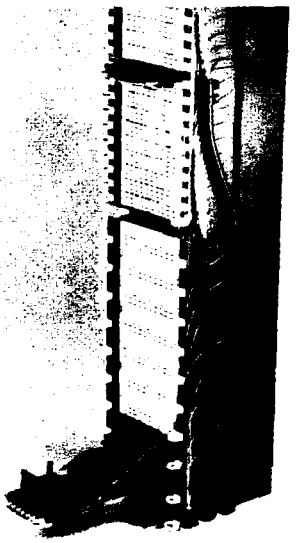

Fig. 9 Cable terminal units for fibre ribbon cables in cross connecting cabinets

6. Conclusion

The basic principles for a complete range of cable accessories for optical fibre ribbon cables have been developed which fulfil the very special requirements of subscriber loop networks.

One- and two-chamber splice organizers assure easy storage of ribbon-to-ribbon splices in splice closures.

Cable terminals built up by plug-in units provide detachable fibre connections.They also provide well organized arrangement of pre-connectorized jumper fibres in cross connecting cabinets and main distribution frames.

References

[1] W. Eutin, U. Grzesik, E. Schürmann, "New Plastic Single Mode Fibre Connector For Subscriber Networks", presented at this conference

Peter Deußer was born in Ellwürden, West Germany, in 1946. He received the degree Dipl.-Ing. in electrical engineering in 1971 from the Fachhochschule Wilhelmshaven, W. Germany.
In 1974 he joined the Philips Kommunikations Industrie AG where he is now responsible for the development and design of cable accessories.

Johann A. Becker was born in Rheinberg, West Germany, in 1944. He received the degree of Dipl.-Ing. in electrical engineering in 1969, and the degree of Dr.-Ing. in 1973, from the Rheinisch-Westfälische Technische Hochschule Aachen, W. Germany.
In 1974 he joined the Philips Kommunikations Industrie AG where he is now responsible for the development of Interconnection Technology.

OPTICAL FIBER CORD FOR AIRPLANE APPLICATION

*Y. Masuda, *J. Ohta, *J. Ohsugi

*Sumitomo Electric Industries, Ltd.

**Luis J. Lazaro, **Ai D. Tu and **Deffie Coy

**Boeing Commercial Airplane Co.

ABSTRACT

A new small diameter, light weight optical fiber cord with good optical and mechanical performances was developed for airplane application by overcoming microbending and jacket shrinkage problmes. The fiber has 208μm core and 250μm cladding. The transmission loss is less than 8.0dB/km at 0.85μm in the temperature range from -65°C to +150°C. This temperature range would be applicable to a relatively large area of the airplane.

1. Introduction

Among various features of optical fiber cable, the compactness, lightness and immunity to electromagnetic interference are the most attractive aspects for its application to airplanes. Optical fiber cable used in airplanes is required to function properly over a very wide range of temperatures about from -65°C to +150°C. An optical fiber cord (single fiber cable) has usually no anti-bucking elements. Therefore it shows a very large increase in optical loss at temperature below -50°C due to thermal shrinkage of the cord jacket material and its relaxation of residual strain of extrusion after being exposed at high temperature. This problem has to be solved. In addition, extremely high mechanical reliability, flexibility, lightness and low loss optical transmission property are required for an airborne optical fiber cord. This paper reports the development of an optical fiber cord to meet the abovementioned severe requirements.

2. Cable specification

The airborne optical fiber cable is very different from other application cables in the following ways.

i) It must have much better reliability.

ii) The cable must withstand a very wide temperature range, from -65°C to +150°C or more.

iii) The fiber must transmit as much optical power as possible due to the vast amount of branching necessary.

Based on these requirements, the specification for optical fiber cord described in Table 1 was set. The reason for a very high N.A. (=0.35) is to make the fiber very resistant to microbending loss, since microbending loss is proportional to Δn^{-3} or Δn^{-5} [1],[2]. Δn is the refractive index difference between the core and the cladding and is related to N A as follows: $NA=n\sqrt{2\Delta n}$, where Δn is the refractive index of core. A large size core (=208μm) was chosen due to above requirement iii).

3. Cable technology

To get a cable that meets the specifications in Table 1, the cable as shown in Fig.1 was designed. The following new concepts and techniques were developed and applied to the cable;

① A very high index difference fiber (Δn=3.6%) was made by doping a large quantity of germanium in the core as well as in the fluorine in the cladding. An example of an actual refractive index profile is shown in Fig.2.

Table 1 Specification of optical fiber cord

Item	Requirement
A. Optical performance	
1 Attenuation	Less than 15dB/km from -65°C to +150°C
2 Numerical aperture	0.35 ± 0.03
3 Light susceptibility	Less than 150 nanowatt/km for 3000 foot candles
B. Mechanical/Physical characteristics	
1 Eccentricity	Less than 6% for core/cladding and cladding/jacket
2 Tensile strength and elongation	Less than 3% elongation for 80kg load
3 Flexibility	Flex torgue is less than 650k·cm, 875k·cm for bending 90°, 180° respectively
4 Impact	Less than 0.5dB for 50 cycles of 37.5kgfm impact
5 Weight and diameter	Weight; 4kg/km max., O/D; 1.8mm max.
C. Environmental requirements	
1 Accelerated aging	No cracks for 120 hours at 200°C
2 Cold bend	Loss increase less than 0.5dB for 8 turns on 50mmφ mandrel
3 Flammability	Self-extingishing within 30 sec after flame removed
4 Flexure endurance	Loss increase less than 0.5dB for 2000 cycles of flexing with 50mmφ mandrel
5 Scrape abrasion resistance	Strength member shall not be exposed for specified brade
6 Thermal shock resistance	Shrinkage of any layer is less than 3.5mm for rapid temp. change from +150°C to -65°C
7 Shrinkage or elongation of layers	Less than 3.5mm for aging for 6 hours at 150°C
8 Wicking	Less than 3.5mm for ink immersion test

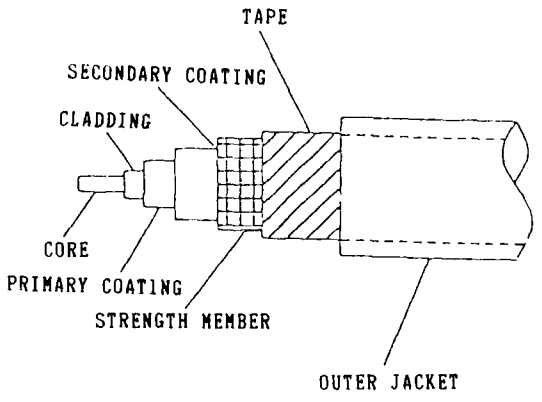

Fig. 1 Optical fiber cord

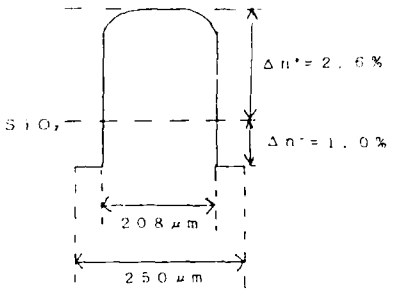

Fig. 2 Refractive index profile

② Fluorocarbon polymer in which 3.8% of inorganic wiskers were added was used for the outer jacket. The reason for this is as follows: Plastic generally used for a jacket of optical fiber cord degenerates at a high temperature (+150°C). Though fluorocarbon polymer can withstand this temperature, it adversely affects fibers due to thermal shrinkage and relaxation fo extrusion stress. To reduce this problem, wiskers were added into the fluorocarbon polymer. We selected $K_2O \cdot 6TiO$ as wisker because it was able to withstand the extrusion temperature of the fluorocarbon polymer. Wiskers in the polymer were oriented in an axial direction during the extrusion process as shown in Fig.3 which suppressed the polymer shrinking.

By adding wiskers,

i) Thermal shrinkage can be reduced to 40 ∿ 60% of the original value (Fig.4).

ii) Young modulus at high temperature is as twice as the original value of the fluorocarbon polymer. This increases the mechanical strength of the cord at high temperatures (Fig.5).

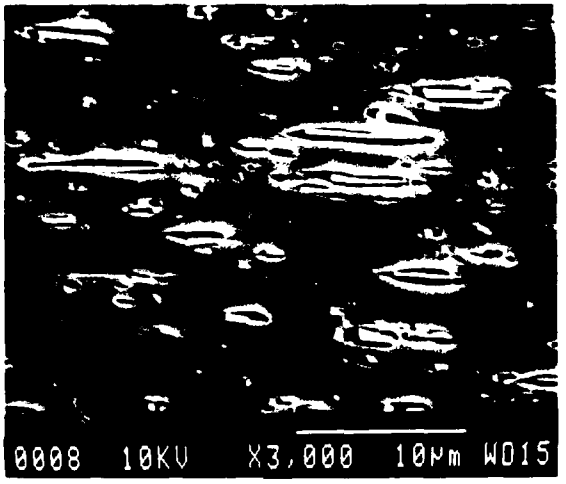

Fig.3 Magnification of the outer jacket showing orientation of wiskers in axial direction

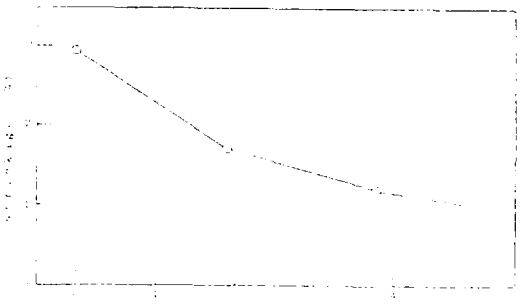

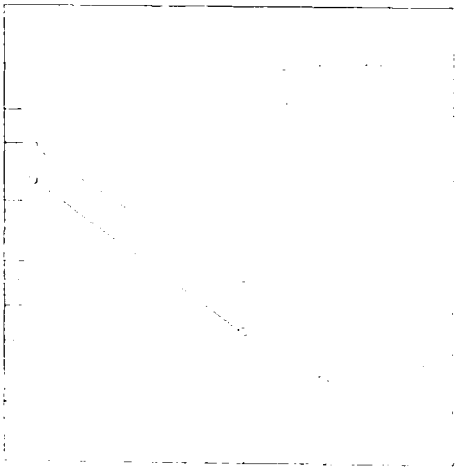

③ A slipping tape was applied beneath the outer jacket layer in order to achieve uniform lengthwise jacket contraction. This costruction served to reduce the increase of transmission loss.

4. Property of the finished optical cord

1) Construction of finished optical core

Construction of finished optical cord is shown in Table 2.

Table 2 Construction of finished optical cord

Items		Construction
Fiber	Core diameter	208μm
	Clad diameter	250μm
	N.A.	0.35 ± 0.02
	Index profile	ΔN^{+}= 2.6% (Gr doped silica) ΔN^{-}=-1.0% (F doped silica)
Primary coating	Diameter	0.45mm
Secondary coating	Diameter	0.5 mm
Outer jacket	Diameter	1.7 mm
Total weight	———	3.2g/m

2) Attenuation

The attenuation loss measured at room temperature is shown in Fig.6 and loss change at 0.85μm against temperature from -65°C to +150°C is shown in Fig.7. From these results the attenuation of this optical cord is less than 8dB/km over the temperature range from -65°C to +150°C.

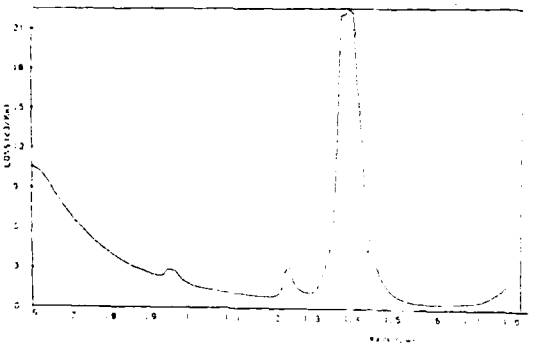

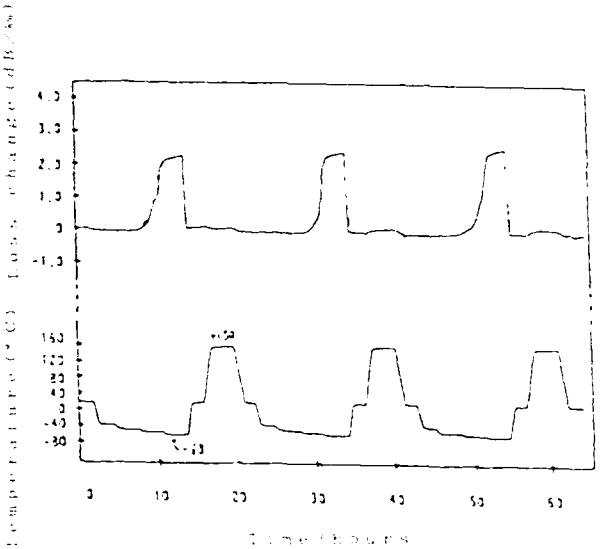

3) Tensile strength

Fig.8 shows the elongation of the cord when tensile load was applied. This cord showed no breakage till 130kgf since all the constituting materials had breaking elongation at more than 2%.

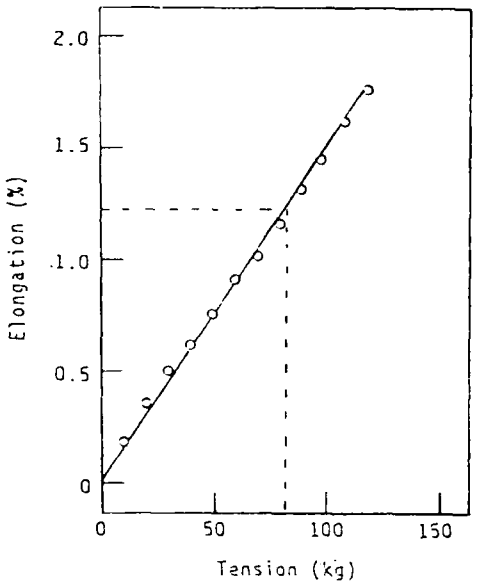

Fig. 8 Elongation against Tension

4) Other mechanical properties

Some mechanical properties are shown in Table 3. All other properties listed in the specification (Table 1) are satisfied.

5. Conclusion

A new small diameter, light weight optical fiber cord with good mechanical performance was developed for airplane application. The transmission loss is less than 8.0dB/km at 0.85μm in the temperature range from -65°C to +150°C. This temperature range would be applicable to a relatively large area of the airplane.

References

[1] K. Olshansky, "Mode Coupling Effects in Graded-Index Optical Fibers", Appl. Opt., 14, 4, pp.935~945 (1975).

[2] E.G. Hanson, "Origin of Temperature Dependence of Microbending Attenuation in Fiber Optic Cables", Fiber and Integrated Optics, 3, 2-3, pp.113~148 (1980).

Table 3 Mechanical properties of a developed optical fiber cord

Items	Test condition	Loss change
Impact	The hanmer of 0.25g weight was dropped from 150mm height for 50 cycles	Less than 0.1dB
Cold bend	6m length specimen was wound 8 turns on 50mm diameter mandrel at -65°C	Less than 0.1dB
Flexure endurance	The specimen was bent through 180°C using mandrel with 50mm diameter at a rate 15 cycle/min.	Less than 0.05dB
Scrape abrasion resistance	The specimen was subjected to 30 cycles of scraping using blade with a 0.5kg applied weight	Less than 0.05dB
Twist	250mm specimen with a load of 2kg weight was twisted through 180° in either direction for 200 cycles	Less than 0.05dB

Yuichi Masuda received his M.S. degree in Electrical Engineering from Kyoto Univ. in 1970. He then joined Sumitomo Electric Industries and has been engaged in development and sales of optical fiber and cables. Mr. Masuda is now a chief research associate of R&D Group, and a member of the Institute of Electronics & Communication Engineers of Japan.

Junichi Ohta received a M.S. degree from Tokyo Institute of Technology in 1987. He then joined Sumitomo Electric Industries and has engaged in research and development of optical fiber and cables. Mr. Ohta is a member of Communication R&D Department in Yokohama Research Laboratories, and a member of the Institute of Electronics & Communication Engineers of Japan.

Tetsuya Ohsugi received his B.S. degree in physical engineering from science university of Tokyo in 1984. He then joined Sumitomo Electric Industries and has been engaged in Analytical Characterization Center Basic High Technology Laboratories R&D Group.

Luis J. Lazaro, Jr. received his B.S. degree in Electrical Engineering from Mapua Institute of Technology in Manila in 1965. He then joined the Boeing Commercial Airplane Company in 1968 and has been engaged in various manufacturing research and development programs. Mr. Lazaro presently is the lead engineer in the Fiber Optic group engaged in the development of aircraft quality optical fibers and cable, connectors and splices.

Ai D. Tu, Boeing Commercial Airplane, Seattle, Washington. Ai Tu received his B.S. degree in Mechanical Engineering from University of Washington in 1984. Mr. Tu then joined Boeing and has been engaged in the development of optical fiber and cables.

Deffie Coy, Boeing Commercial Airplane, Seattle, Washington.

FIBER-OPTIC CABLE FOR SHIPBOARD SYSTEMS

K. Kathiresan, M. W. Shute, Sr., M. R. Gotthardt, C. J. Arroyo, B. A. Khorramian, and J. W. Shea
AT&T Bell Laboratories, Norcross, Georgia 30071

J. B. Fluevog and J. W. Baumgart, AT&T Network Systems, Norcross, Georgia 30071

ABSTRACT

Application of fiber-optic technology can significantly enhance the operational capability of a ship. Ship designers and builders have already placed fiber-optic systems aboard ships to take advantage of the inherent attributes of fiber-optic technology. A fiber-optic cable's small size allows for substantial weight reduction and increases usable interior space. The characteristic of optical fiber provides for very high bandwidth, low noise-to-signal ratio, and immunity to EMP/EMI/RFI radiation. Early trials aboard ships used large core 100/140 μm core/cladding fiber. However, the present trend is towards radiation-hardened 62.5/125 μm graded index multimode and single-mode fibers to take advantage of these fibers' characteristics. In any case, the impressive features of fiber-optic systems when matched to shipboard requirements, not only enhance system performance, but also increase system reliability and survivability. This paper describes a shipboard fiber-optic cable design and presents some test results.

INTRODUCTION

Fiber-optic technology can take a place among other great technologies such as radio, radar, transistor, laser, etc. Even in its infancy this technology caused the restructuring of the entire national long distance network. In its subsequent growing age, fiber optics progressed and reached beyond the telephone loop plant into serving areas, office buildings, and finally residences. Today, the technology has reached a more mature stage, and the military is actively engaged in extending fiber optics into weapons systems, sensor systems, control systems, and combined computer and telecommunications systems.

The U.S. Navy has numerous programs underway to efficiently integrate fiber optics into both shore facilities and shipboard systems. With regard to shipboard systems, the U.S. Navy has recognized the overwhelming advantages fiber optic systems can provide to enhance a ship's operational capability. It should be noted that fiber optics affords the opportunity:

- to remove tens of thousands of pounds from a ship's weight and reduce cable space requirements by providing cables that are light in weight and have small diameters (volume), yet increase the information carrying capability compared to present copper cable systems, thereby enhancing the ship's operational capability
- to integrate all of a ship's systems and sub-systems, i.e., control (machinery), sensors, alarms, weapons, surveillance, telecommunications, administration, video, etc., into a single survivable network aboard a ship
- to be assured that this network is capable of sustaining technological and capacity growth, and that the components are designed to last for the life of the ship
- to implement a cable plant that provides immunity against electromagnetic pulse (EMP), electromagnetic interference (EMI), and radio frequency interference (RFI) and requires no sheath grounding
- to achieve cost effectiveness when compared to similar functional systems and to enhance the overall reliability, survivability, and capability of a new class of warships

As the Navy moved to integrate fiber-optics technology with naval shipboard requirements,[1] programs were started to produce standards and specifications for marine shipboard fiber-optic components. The intent of these specifications is to avoid a proliferation of designs and acquire an inventory of marine-qualified components. These components would be available for use in several new systems being developed for shipboard installation. For example, the Fiber Distributed Data Interface (ANSI X3T9.5) system and the SAE AE-9B system are two commercial Local Area Network (LAN) standards that are either fiber based or enhanced through the use of fiber. These commercial systems, based on multimode fiber, are being studied as base-line models for conversion to military systems including shipboard applications. Military qualified fiber-optic hardware designed for shipboard use provides the necessary compliance to naval requirements to support the implementation of these systems aboard ships. In a further effort, the Navy is also developing a shipboard fiber optic distribution system to provide both high and low speed data transport for the various systems aboard ships. Based on single-mode fiber, this distribution system will have excellent throughput and latency characteristics with data rates in the upper gigabit ranges. System survivability and network integrity is assured by bypass

mechanisms, distributed switching, and redundant path features. It should be noted that systems of this type could not have been considered without the application of fiber optic technology with its inherent low loss and extremely high bandwidth characteristics.

In ships today, copper coaxial cables are used extensively to connect radar and other surveillance systems to a ship's main computers and processors distributed throughout the ship. Figure 1 illustrates typical system locations aboard a ship. Most of the sensory equipment is generally interconnected and clustered in the superstructure while the computers and displays are located below decks. This causes a high concentration of copper cable weight in the superstructure which must be balanced by ballast below. Since modern ships no longer have heavy boilers, piping, etc. below decks (lighter weight gas turbines are the main propulsion units), the added compensating ballast reduces the weight advantage originally gained by installing gas turbines. Fiber-optic cable can drastically reduce the weight of the transmission media aboard a ship and restore some of the weight reductions sought. It is estimated that a 75% or higher weight reduction of transmission media can be achieved by replacing copper cables with fiber-optic cables. Furthermore, because the volume of the fiber cables is less than their copper counterparts, usable space inside a ship is increased.

Recently, several trials and shipboard tests of fiber-optic components have been successfully completed. These trials consisted mainly of point to point data links and embedded system applications. Nevertheless, the success of these trials and experimentation, the recent ongoing development of fiber-optic shipboard component specifications, and the publishing of a first draft standard for a shipboard LAN using fiber-optic technology (SAFENET)[2] [3] attest to the high level of activity surrounding the placement of fiber-optic components and systems aboard ships.

In summary, fiber-optic technology can provide the means to achieve weapons platforms with a high degree of survivability, ship systems that are more reliable, flexible, and secure, and a ship that has a substantially increased operational capability. This paper presents preliminary information on a new fiber-optic cable design for shipboard applications. The following sections describe the fiber, the cable structure and some early optical, chemical, mechanical and environmental performances of the cable.

FIBER FOR SHIPBOARD APPLICATIONS

The 62.5/125 μm fiber is becoming the *standard* multimode fiber for LAN and other premises applications, and is ideal for many shipboard system applications. Early trials aboard ships used 100/140 μm multimode fiber. However, the present trend is towards radiation-hardened 62.5/125 μm graded index multimode fiber. It offers the best combination of low loss, low microbending and macrobending loss sensitivity, good source-to-fiber coupling efficiency, and high bandwidth as well as compatibility with existing connectorization and splicing technologies and components. In the future, as data transmission capacity requirements increase, it appears that single mode fibers will find more applications in shipboard fiber-optic systems.

The standard 62.5/125 μm fiber has a typical attenuation coefficient of 0.8 dB/km at 1300 nm and a bandwidth of up to 1000 MHz-km at 1300 nm. Table I shows a relative performance comparison of three other multimode fiber designs with the 62.5/125 μm fiber. The source-to-fiber coupling efficiency increases with core diameter and refractive index difference. However, bending loss sensitivity increases as the core diameter increases or as the refractive index difference decreases. Bandwidth performance is inversely related to the

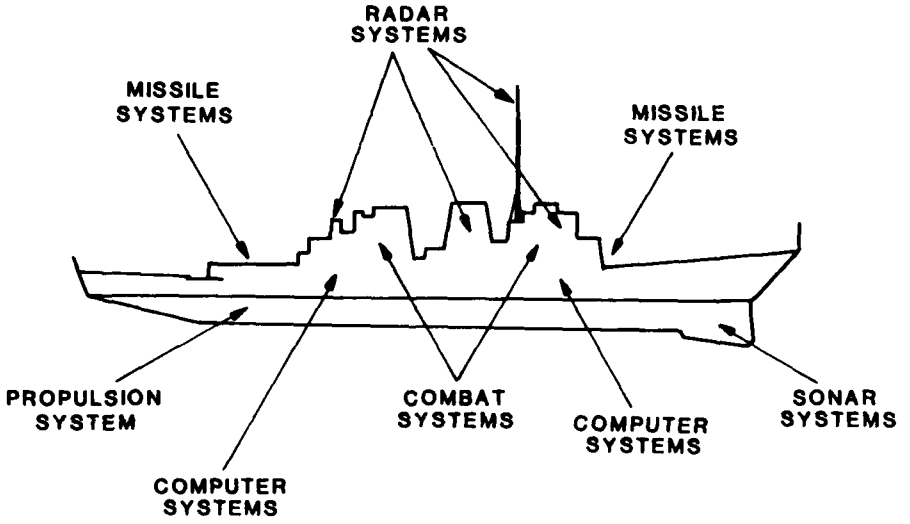

Figure 1. Typical System Locations Aboard a Navy ship

TABLE I. RELATIVE PERFORMANCE COMPARISON OF PREVALENT MULTIMODE FIBERS

Core/Cladding Diameter (μm)	Index Difference (%)	Numerical Aperture NA	Relative Source-to-Fiber Coupling (dB)	Relative Microbending Loss (dB/km)	Relative Macrobending Loss (dB/loop)
50/125	1.1	.21	-3.8	2.5	1.5
50/125	1.3	.23	-3.2	1.5	1.2
62.5/125	2.0	.29	0	1.0	1.0
100/140	2.2	.31	3.0	2.5	1.5

refractive index difference, i.e., an increase in the index difference results in a decrease in the bandwidth of the fiber. The typical bandwidth of the 62.5/125 μm fiber is 700 MHz-km at 1300 μm. The 62.5/125 μm fiber is well-suited for applications in a shipboard environment because of its low bending loss sensitivity and high bandwidth.

In military applications, particularly shipboard and tactical applications, the survivability of a fiber-optic communication system after exposure to nuclear radiation is of extreme importance. One of the most susceptible components in the system is the fiber itself. Radiation from a nuclear event causes darkening or transmittance loss, scintillation effects, dispersion, and several other effects in optical fibers. Scintillation effects from Cerenkov radiation produce noise in a fiber-optic transmission system and generally do not last very long. Dispersion effects are due to radiation-induced changes to the refractive index of the fiber. The primary mechanism for radiation-induced loss in optical fibers is absorption at the common operating wavelengths for fiber-optic transmission systems of 0.85, 1.3, and 1.5 μm. This absorption is caused by trapped carriers, which are generated by the ionizing radiation, at defect sites in the glass matrix.[4] The fiber composition, particularly the type and concentration of the dopants, has a significant effect on the radiation sensitivity of a fiber. It has been shown that the radiation sensitivity is strongly dependent on the concentration of the phosphorous in the core.[5] [6] Many other factors govern the severity of radiation damage in an optical fiber such as the total ionizing radiation dose, dose rate, temperature, operating wavelength, processing conditions, and photobleaching effects due to transmitted and ambient light. In order to improve the nuclear radiation survivability of the 62.5/125 μm fiber, a radiation-hardened (rad-hard) version of the 62.5/125 μm fiber has been developed and optimized for operation at 1300 nm. While standard 62.5/125 μm fiber has both germanium and phosphorous in the core, the rad-hard 62.5/125 μm fiber has no phosphorous. The typical attenuation coefficient of the rad-hard 62.5/125 μm fiber is 0.8 dB/km at 1300 nm and the bandwidth is 400 MHz-km at 1300 nm. The low dose rate, room temperature sensitivities, measured with gamma radiation from a Cs^{137} source at 5 rad/hr for approximately 100 rads total dose, of standard and rad-hard 62.5/125 μm multimode fibers are shown in Table II.[7] The high dose rate sensitivities, measured with gamma radiation from a Co^{60} source at 200 rad/s for approximately 62,000 rads total dose, at room temperature and -55 C are shown in Tables III and IV. The radiation sensitivities, expressed in mdB/km/rad, were determined by dividing the peak induced loss by the total dose and do not imply that the induced loss is linearly related to the total dose received by the fiber; the radiation sensitivities are used for comparative purposes only. Figures 2 and 3 show the radiation responses for the standard and rad-hard 62.5/125 μm fiber at room temperature and -55 °C. The rad-hard 62.5/125 μm fiber is suitable for shipboard applications requiring nuclear radiation survivability because of the lower induced losses and enhanced recovery after exposure to nuclear radiation.

SHIPBOARD CABLE SPECIFICATIONS

Currently, there are two military specifications, namely DOD-C-85045C and PMS-400-XYZ-1, which can govern the shipboard cable design. The DOD-C-85045C specification is used at present for tactical cable designs. This specification also includes requirements pertinent to shipboard cable designs. However, this specification is not currently being used for shipboard cables. PMS-400-XYZ-1 is the specification which is being used at present for shipboard cable designs. These specifications are currently being reviewed by the U. S. Navy and a new specification or modification to the existing specifications may result. Due to this reason, the performance of the cable described later has been evaluated from a general and diverse shipboard test requirements basis, instead of evaluating the cable to any specific specification.

TABLE II. LOW DOSE RATE, ROOM TEMPERATURE RADIATION SENSITIVITIES (mdB/km/rad) OF 62.5/125 μm MULTIMODE FIBERS

Wavelength (μm)	Standard Design	Radiation Hardened
0.85	8.7	0.98
1.3	3.4	0.05

TABLE III. HIGH DOSE RATE, ROOM TEMPERATURE RADIATION SENSITIVITIES (mdB/km/rad) OF 62.5/125 μm MULTIMODE FIBERS

Wavelength (μm)	Standard Design	Radiation Hardened
0.85	20.1	2.64
1.3	5.7	0.39
1.5	7.9	0.30

TABLE IV. HIGH DOSE RATE, -55 ° C RADIATION SENSITIVITIES (mdB/km/rad) OF 62.5/125 μm MULTIMODE FIBERS

Wavelength (μm)	Standard Design	Radiation Hardened
0.85	18.8	38.8
1.3	15.5	5.2
1.5	22.1	2.9

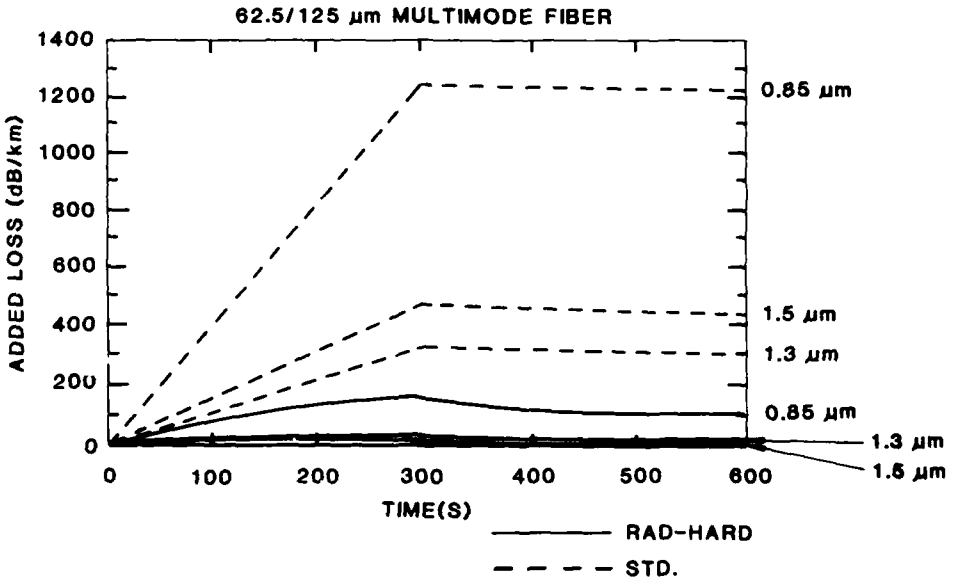

Figure 2. Optical Fiber Radiation Response at 25 ° C

These specifications, in general, require that the cables have low toxicity, contain low or no halogen, generate low smoke and acid gas, be flame retardant, operate under extreme operating and storage temperature ranges, withstand stringent mechanical requirements and very high water pressure, survive hostile fluids at high temperature, and meet other demanding criteria. All the above requirements, individually and in most combinations thereof, can be met with appropriate material selection and cable design features. Meeting all of the requirements simultaneously without any exceptions may be very difficult and/or may result in quite expensive cables. For example, meeting the high temperature fluid exposure requirement may call for radiation crosslinking or continuous vulcanization of jacketing materials. There are some thermoplastic materials available which will meet the fluid requirements, but are too stiff for shipboard applications. These aspects make the design and development of shipboard cables most difficult and challenging. Design and development of cables for shipboard applications are currently underway. In the following, such a preliminary cable design and test results are presented.

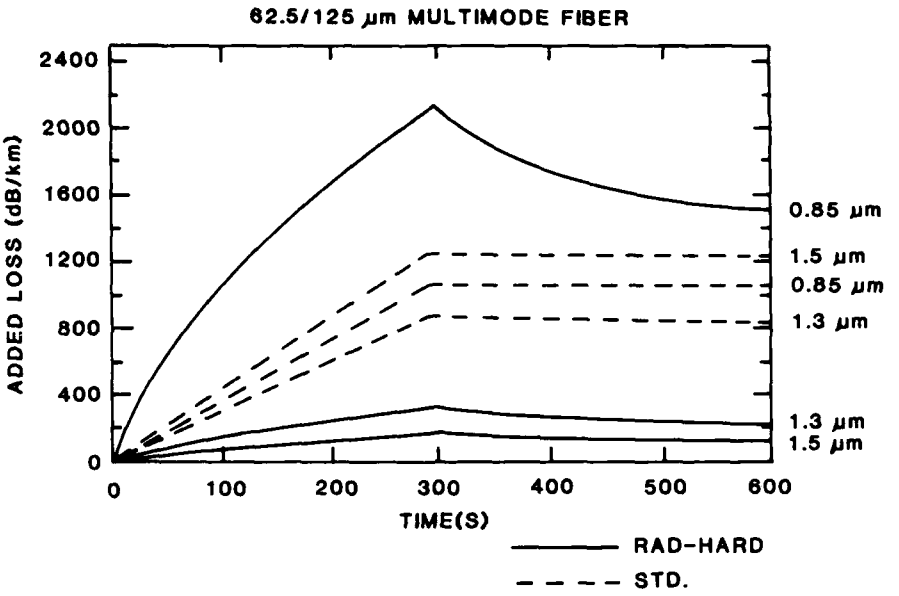

Figure 3. Optical Fiber Radiation Response at -55 ° C

CABLE DESIGN

Preliminary development of a four fiber shipboard cable has been completed. The cable cross-section is presented in Figure 4, and an isometric view is presented in Figure 5. The cable uses radiation-hardened 62.5/125 μm multimode fiber. The cable consists of a central waterblocking yarn with four optical fiber cable components (OFCC) stranded over it along with waterblocking yarn. The cross-section of the OFCC is given in Figure 6. The OFCC contains a 900 μm polyester elastomer buffered fiber, surrounded by Kevlar® yarn and a low halogen jacket. Over the OFCC units, two layers of Kevlar® yarn strength members are stranded in opposing lays. These Kevlar® yarn strength members are treated with polymers which are water swellable, eliminating the need for separate waterblocking members. The use of such waterblocking Kevlar® yarn also minimizes the cable size, in addition to providing a uniform waterblocking structure. A low

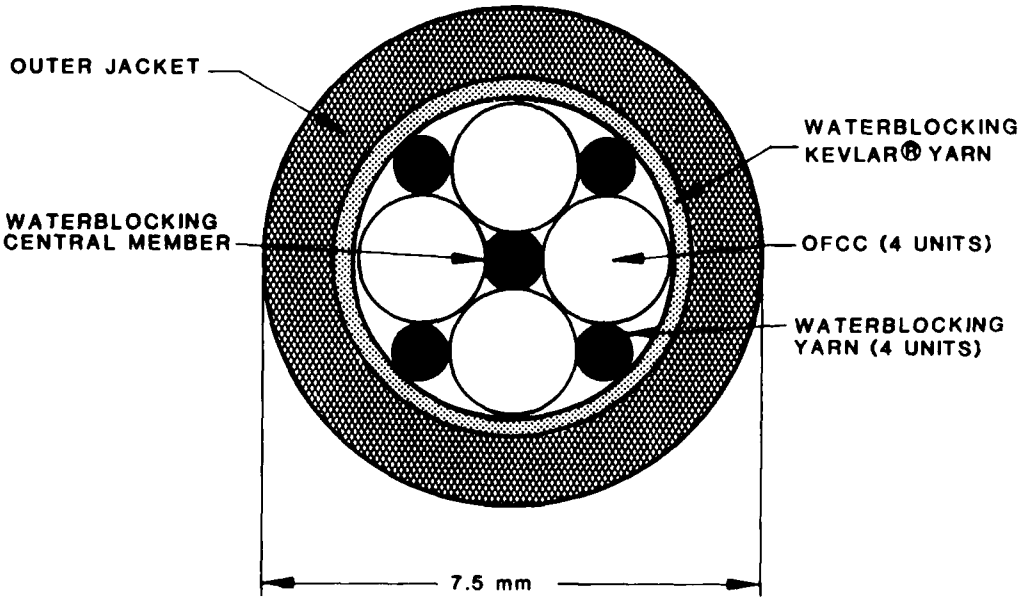

Figure 4. Cross-Section of 4-OFCC Shipboard Cable

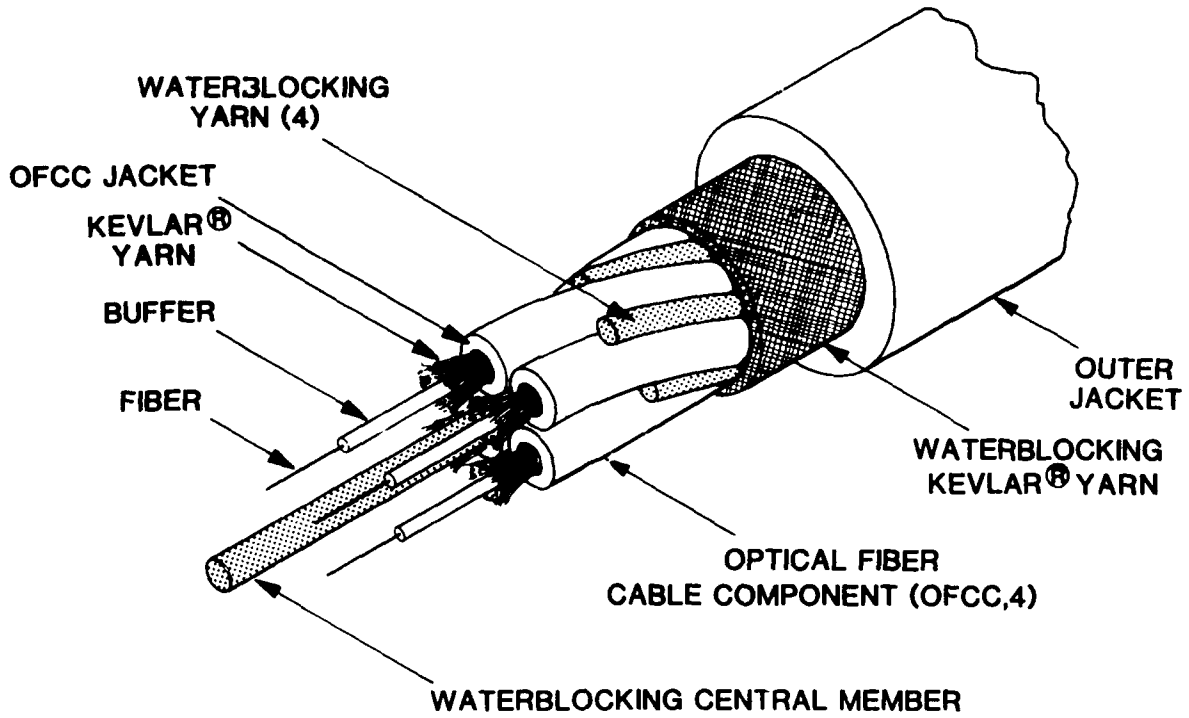

Figure 5. Isometric View of 4-OFCC Shipboard Cable

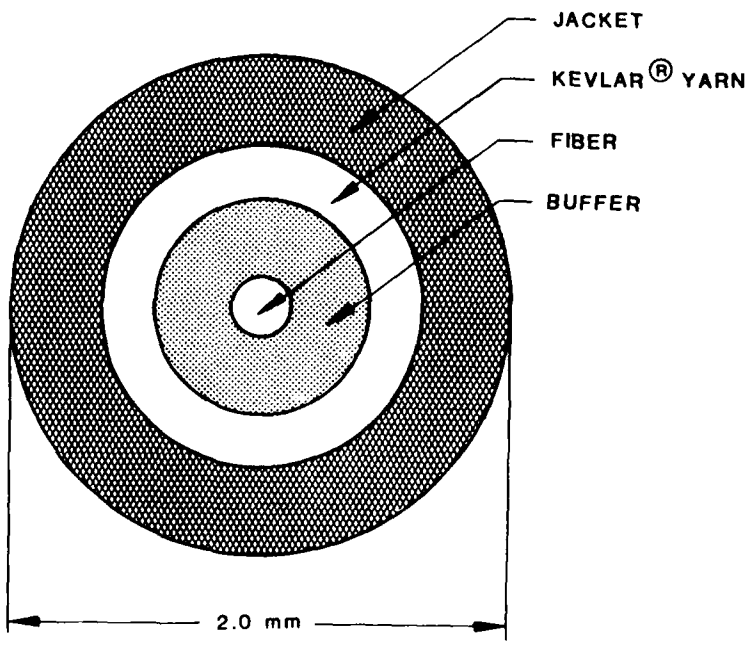

Figure 6. Cross-Section of Optical Fiber Cable Component (OFCC)

halogen outer jacket is then extruded over the Kevlar® yarn strength members. The waterblocking features, the central member, waterblocking yarns and the waterblocking Kevlar® yarn, incorporated in the cable design and the use of flexible elements for the central member ensure that the cable is very flexible, compact and meets the waterblocking requirement more than adequately.

CABLE PERFORMANCE

The shipboard cable performance evaluation consists of optical, chemical, environmental and mechanical tests. Optical properties of attenuation rate, bandwidth and numerical aperture along with numerous other dimensional and mechanical requirements are checked at the fiber stage, and fibers which meet all the specifications are then used for cabling. Fibers used were proof tested to 690 MPa. The mean attenuations of the finished cable at 850 nm and 1300 nm were 4.3 dB/km and 1.4 dB/km, respectively.

The chemical tests consist of acid gas generation, halogen content, toxicity index, and fire and smoke properties. The results of these tests and the requirements are presented in Table V. The finished cable meets the acid gas generation, halogen content, and toxicity index requirements with good margin. The halogen content results correspond to the total of the four halogens, namely fluorine, chlorine, bromine and iodine.

The cable passes the required IEEE-383 flame test. In addition, the cable was also evaluated for flame propagation and smoke generation using the UL-910 test. Note that the shipboard cable is not required to meet this stringent plenum cable test. However, the employment of this test is being considered with the following partial modification to the requirement. The cable is required to meet the standard UL-910 smoke requirements of 0.15 and 0.5 average and maximum optical density values, respectively. With respect to flame propagation, the modified requirement under consideration is that the flame travel time product value for the cable for the first ten minutes of the test using the ASTM-E-84 procedure should not be greater than 27.5 m-min. The finished cable also meets the above requirements under consideration. The standard flame propagation requirement is that it should not be greater than 1.5 m within the test duration of 20 minutes. For the 4-fiber shipboard cable, the flame traveled the 5.9 m full test length of the tunnel in 10 to 15 minutes of the test.

Three of the most important environmental tests are temperature cycling at ambient and high humidities, and accelerated aging. For shipboard cable evaluation, the temperature cycling at ambient and high humidities have been combined to a temperature-humidity (95%RH above 20°C and uncontrolled below 20°C) cycling as shown in Figure 7. The first three cycles correspond to the required temperature range of -28°C to 65°C. In the next two cycles, the cables were evaluated for an extended cold temperature of -55°C. The result of the temperature-humidity cycling performance of the cable is given in Figure 8. In the accelerated aging test, the cables were subjected to a constant temperature of 100°C for 240 hours. The result of the accelerated aging performance of the cable is given in Figure 9. The cable meets and surpasses the requirements for these environmental tests showing excellent performance.

The cables were then subjected to a battery of other mechanical and environmental tests. The results of these tests along with the specified requirements are given in Table VI. The cable's mechanical and environmental performance exceeds that of the specification requirements in terms of test loading,

TABLE V. CHEMICAL AND FIRE PROPERTIES OF SHIPBOARD CABLE

Test	Requirement	Cable Performance
Acid Gas Generation	$\leq 2.0\%$	$=0.19\%$
Halogen Content	$\leq 0.2\%$	$=0.04\%$
Toxicity Index	NES 713 ≤ 5.0	$=3.02$
Flame Propagation and Smoke Generation	IEEE-383, Flame Spread $\leq$ 2.4 m	Maximum Flame Spread = 1.3 m
	UL-910 Average Optical Density $\leq$ 0.15 Maximum Optical Density $\leq$ 0.5 Flame Spread Time Product for First 10 Minutes $\leq$ 27.5 m.min	Average Optical Density = 0.11 Maximum Optical Density = 0.5 Flame Spread Time Product for First 10 Minutes = 12.8 m.min.

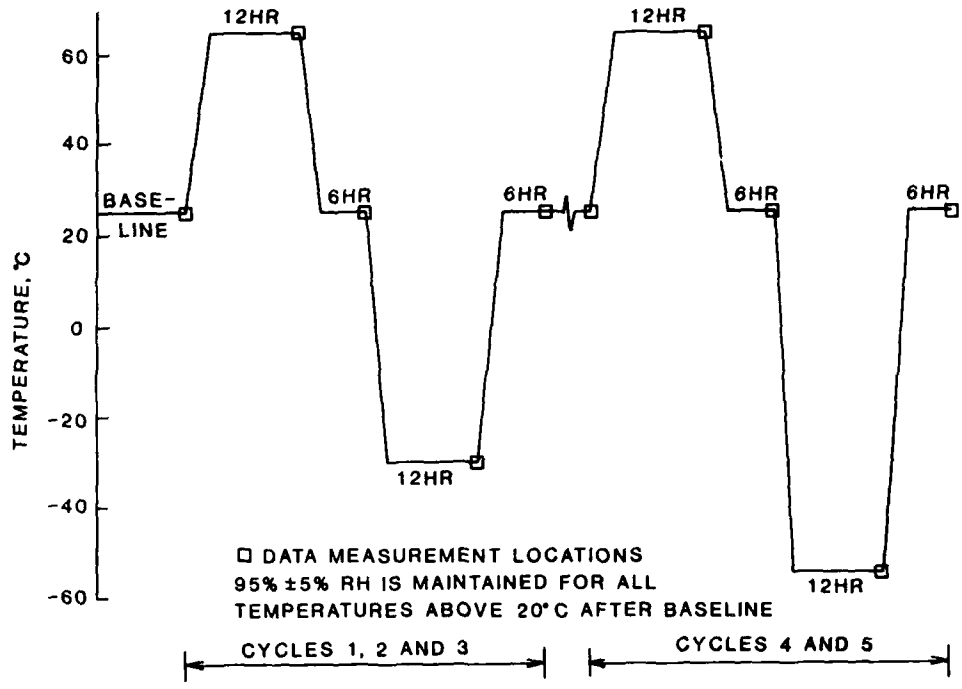

Figure 7. Temperature-Humidity Cycle for Shipboard Cable

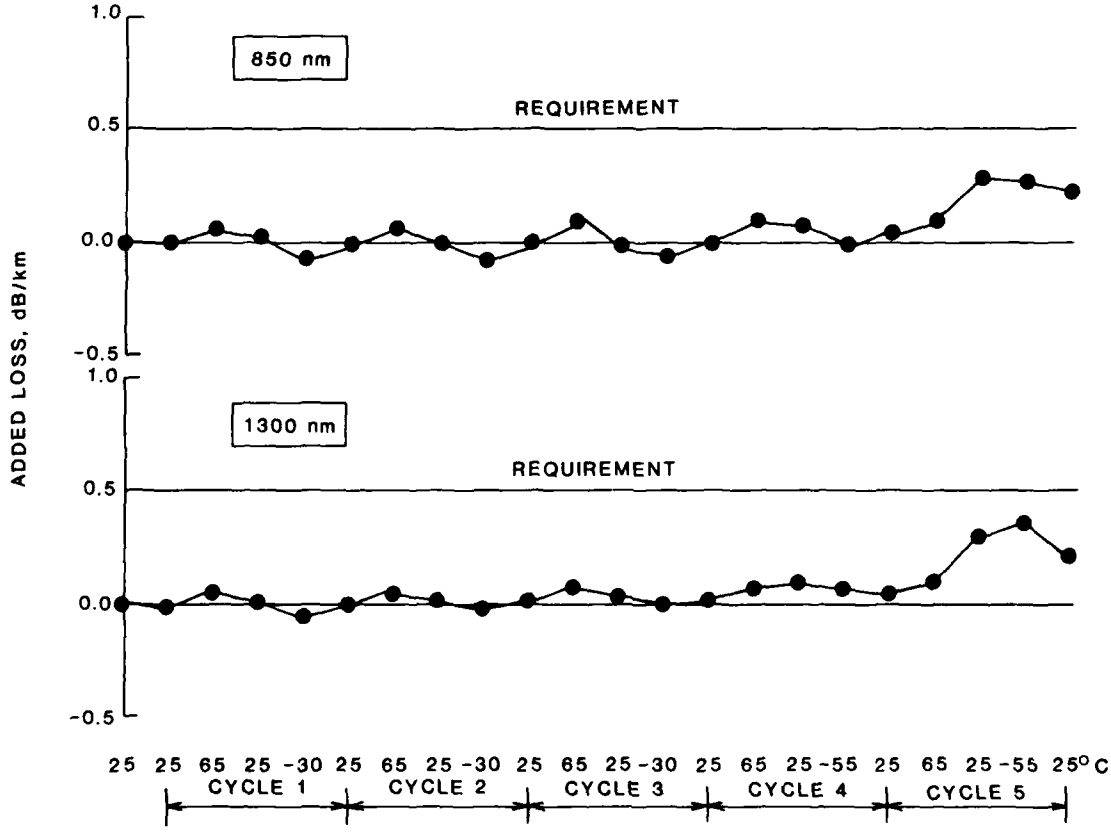

Figure 8. Temperature-Humidity Cycling Test Result for Shipboard Cable

TABLE VI. MECHANICAL AND ENVIRONMENTAL PROPERTIES OF SHIPBOARD CABLE

Test	Requirement	Cable Performance
Tensile Loading	EIA-455-33 150 m Length $\geq$ 1875 N @ 0.67% Strain $\Delta^* \leq$ 0.5 dB	AT&T Bell Laboratories 1.8 m (Short Length) = 1920 N @ 0.67% Strain Δ = 0.08 dB
Cyclic Flexing	EIA-455-104, 4.5 kg, 8x** 500 Cycles $\Delta \leq$ 0.5 dB	10.0 kg 2000 Cycles Δ = 0.05 dB
Torsion	EIA-455-63, 10 Cycles $\Delta \leq$ 0.5 dB	30 Cycles Δ = 0.03 dB
Cold Bend	EIA-455-65, 8x**, -28 ° C, 3 Turns $\Delta \leq$ 0.5 dB for OFCC No Δ Requirement for Cable	Δ = 0.03 dB for OFCC Δ = 0.29 dB for Cable
Twist Bend	EIA-455-91, 4.5 kg, 8x** 500 Cycles $\Delta \leq$ 0.5 dB	10.0 kg 2000 Cycles Δ = 0.10 dB
Crush	EIA-455-41, $\geq$ 1500 N $\Delta \leq$ 0.5 dB	Δ = 0.04 dB
Impact	EIA-455-25, 1.0 kg, 100 Cycles $\Delta \leq$ 0.5 dB	2.0 kg Δ = 0.04 dB
Corner Bend	5x**, $\geq$ 375 N $\Delta \leq$ 0.5 dB	Δ = 0.03 dB
Dripping	FED-STD-228, 150 ° C, 6 hrs No Drip	No Drip
Waterblocking	0.175 MPa, 6hrs Leakage $\leq$ 33 ml	Leakage = 18 ml
Jacket Material Tensile Strength and Elongation	FED-STD-228 $\geq$ 900 N/cm^2 $\geq$ 180%	= 1134 N/cm^2 = 142%
Cable Shrinkage	150 ° C, 6 hrs $\leq$ 0.63 cm	= 0.13 cm
Gas Flame	EIA-455-99 $\Delta \leq$ 0.5 dB	Δ = 0.14 dB
Salt Spray	EIA-455-16, 35 ° C, 96 hrs No Damage	No Damage
Jacket Self-Adhesion	EIA-455-84, 71 ° C, 48 hrs No Adhesion	No Adhesion

* Δ - Increase in Attenuation
** Mandrel diameter to cable outer diameter ratio

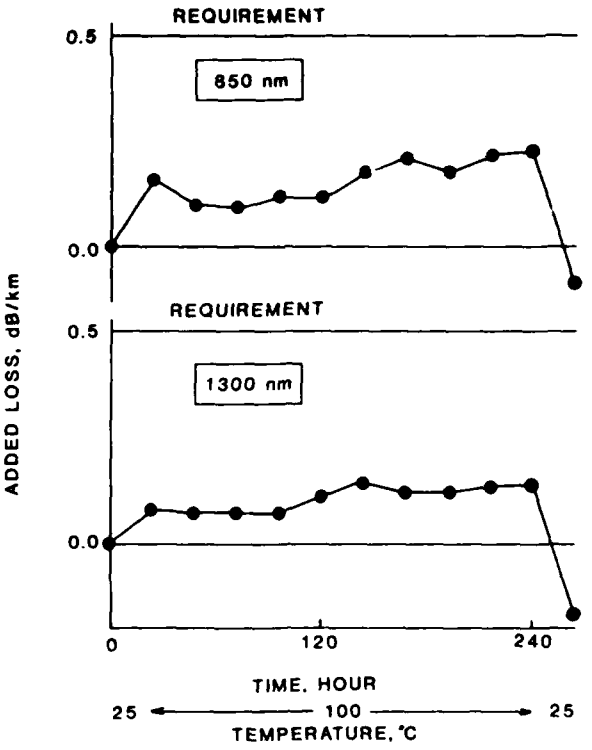

Figure 9. Accelerated Aging Test Result for Shipboard Cable

number of cycles, and/or attenuation change. During these tests, two of the fibers were monitored at 850 nm wavelength, and the other two fibers at 1300 nm. The increase in attenuation (Δ) reported in Table VI corresponds to the maximum of the four fiber values.

CONCLUSIONS

The preliminary design, development, and performance evaluation of fiber-optic cable for shipboard systems were presented. The cable either meets or surpasses the requirements in the tests conducted thus far. Further evaluation of the cable against the remaining PMS-400-XYZ-1 and other specification requirements are underway and a complete evaluation will be presented in the future.

ACKNOWLEDGEMENTS

The authors gratefully acknowledge the support and contribution of J. E. Andrews, G. H. Campbell, S. P. Gentry, L. C. Hotchkiss, M. R. Santana, L. R. Sherrets, R. W. Tarwater, A. G. Vedejs and several other members of AT&T Bell Laboratories and AT&T Network Systems.

REFERENCES

1. R. M. Morais, "Implementation of Fiber Optic Technology in Naval Combatants," *Marine Technology Magazine*, (1987)
2. M. M. Poland, and R. A. Buddenburg, "SAFENET Survivable Fiber Optic Embedded Network," Washington D.C., (1988)
3. R. Bailly, "Militarized Vehicular LANs," *Fiber Optics Magazine*, (1988)
4. E. J. Friebele, C. G. Askins, M. E. Gingerich, and K. J. Long, "Optical Fiber Waveguides in Radiation Environments II," *Nucl. Instr. Meth. Phys. Res.B1*, 355, (1984).
5. E. W. Mies and L. Soto, "Characterization of the Radiation Sensitivity of Single Mode Optical Fibers," *European Conference on Optical Communications (ECOC)*, Venice, Italy, (1985).
6. E. J. Friebele, M. E. Gingerich, and K. J. Long, "Recovery (?) of Radiation Damage in Single-Mode and Multimode Optical Fiber Waveguides," *Technical Digest of OFC '82 Topical Meeting on Optical Fiber Communications*, paper WAA7, Phoenix, Arizona, (1982).
7. J. B. Haber, E. Mies, J. R. Simpson, and S. Wong, "Assessment of Radiation-Induced Loss for AT&T Fiber-Optic Transmission Systems in the Terrestrial Environment," *J. Lightwave Tech.*, **LT-6** 150, (1988).

Kris Kathiresan is a Member of Technical Staff in the Lightguide Technology Department at AT&T Bell Laboratories in Norcross, Georgia. He is responsible for the design and development of specialty cables, including military applications.

Dr. Kathiresan joined AT&T Bell Laboratories in 1985. He has a B. E. Hons in Mechanical Engineering from University of Madras, India, an M. E. in Aerospace Engineering from Indian Institute of Science, India, and a Ph. D. in Engineering Science and Mechanics from Georgia Institute of Technology, Atlanta, Georgia.

Dr. Kathiresan is a Senior Member of American Institute of Aeronautics and Astronautics and a Member of American Society of Mechanical Engineers. He is a registered Professional Engineer (Mechanical) in States of Georgia and Florida.

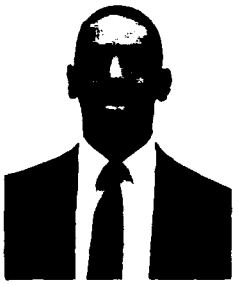

Marcus W. Shute, Sr. joined the Materials Engineering and Chemistry Department of AT&T Bell Laboratories, Norcross, Georgia, in 1986. Initially, he was involved in the evaluation of fiber properties and characterization of various optical fiber designs, including specialty fibers such as polarization-maintaining fibers. Presently, his interests are radiation effects in optical fibers, fiber optic guided vehicles, and fiber optic sensors.

Mr. Shute received his B. S. Degree in Mechanical Engineering from Tennessee State University in 1984, and S. M. Degree in Materials Science and Engineering from Massachusetts Institute of Technology in 1986. He is currently pursuing the Ph. D. Degree in Georgia Institute of Technology.

He is a member of the Optical Society of America, Society of Photo-Optical Instrumentation Engineers, National Society of Black Engineers, American Society of Mechanical Engineers, Tau Beta Pi, and Omega Psi Phi Fraternity, Inc.

Manfred R. Gotthardt is a Member of Technical Staff in Local Area Network Systems and Engineering Group at AT&T Bell Laboratories, Norcross, Georgia, where he has been a project manager for several Task Groups responsible for developing military and commercial fiber optic specification and standards. He is also a technical consultant for the application and integration of fiber optics into military systems. His earlier work was in integrated circuit design, fiber optic apparatus development, and circuit design and software development for the initial #1 Electronic Switching System.

Mr. Gotthardt graduated from Northern Illinois University with a B. S. Degree in Industrial Engineering. He has also done graduate work at Northern Illinois University, Georgia State University, and Air War College, Air University, U. S. Air Force. He has been granted two patents and two more pending. He is a member of the IEEE.

C. John Arroyo is a Member of Technical Staff at AT&T Bell Laboratories, Norcross, Georgia. He joined Bell Laboratories in 1969 and worked in Fire Research Technology. Since 1972 he has been a member of Lightguide Cable Group engaged in sheath design, rodent-lightning protection and cable development.

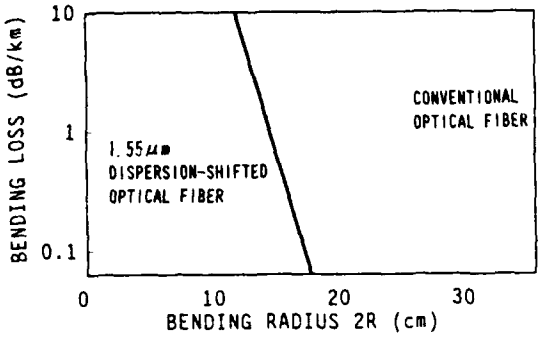

Fig.2 Bending Characteristics

3. Cable Design

3.1 Submarine Optical Fiber Cable

The 1.55 μm submarine optical fiber cable structure is shown in Fig.3. This structure is the same as that for the 1.3 μm submarine optical fiber cable. Double-layer pressure-resistant pipes are used to protect optical fibers at 8,000 meters below sea level. The pipes are made of aluminum to reduce cable weight. This results in lower tensile strength when the cable is lifted from the sea bottom. The space between the pipes and the fiber is filled with a special compound to prevent water infiltration.

3.2 Terrestrial Optical Fiber Cable

The 1.55 μm terrestrial optical fiber cable structure consists of four optical fiber ribbons accommodated in slotted rods. This structure results in lower cable cost and improved space efficiency (Fig.4). Cable diameter and cable weight are 14 mm and is 200 kg/km respectively.

This structure is also the same as the 1.3 μm single-mode optical fiber cables, which enables the use of conventional transmission route construction techniques, including installation equipment and splicing closures.

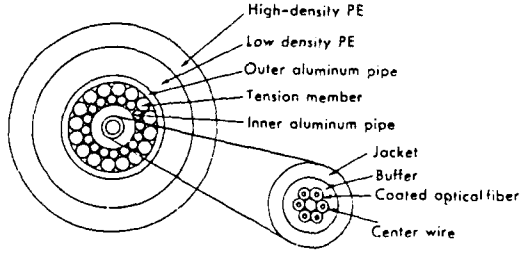

Fig.3 Submarine Optical Fiber Cable

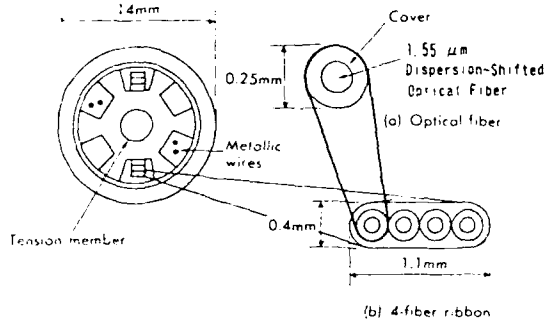

Fig.4 Terrestial Optical Fiber Cable

4. Commercial Test Outline

4.1 Commercial Test Routes

The 1.55 μm dispersion-sifted optical fiber cable have been introduced in three sections in Japan (Fig.5). These routes are Hiroshima to Matsuyama(69 Km), Matsuyama to Oita(120 Km), and Nagasaki to Fukue(108 Km). As can be seen from the map, all three routes include a submarine section, which as summarised in Fig.5, are 30 Km, 111 Km, and 93Km, respectivery. There are 12 optical fibers per cable for the Hiroshima to Matsuyama and Matsuyama to Oita routes, and 8 optical fibers for the Nagasaki to Fukue route.

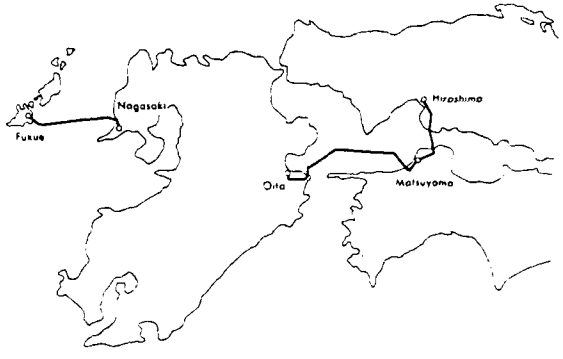

Route	Route length (Submarine Portion)	System
Hiroshima-Matsuyama	69km (30km)	F-400M
Matsuyama-Oita	120km (111km)	F-400M
Nagasaki - Fukue	108km (93km)	F-100M

Fig.5 Commercial Test Routes

In the factory, 1.55 μm dispersion-shifted optical fibers are spliced together to withstand the high-strain proof test and a 47 km maximum piece length is achieved.

4.2 Trasnsmission System

Maximum repeater spacing for the F-400M transmision system is 120 km.[3] This is three times long than that for the conventional system using 1.3 μm fibers. Moreover, as traffic increases, it will be possible to switch over to the F-1.6G system, which has a 23,040 telephone channel capacity, [4] simply by replacing the transmission equipment in telephone offices.

The system employs a 1.55 μm DFB (Distributed Feedback) laser diode for the optical source and a InGaAsP-APD for the detector.

5. Commercial Test Results

5.1 Optical fiber Cable

(1) Optical Loss Characteristics

The commercially introduced (Matsuyama-Oita) 1.55μm dispersion-shifted optical fiber cables show excellent optical loss characteristics, as indicated in Fig.6. Average loss is 0.22 dB/km.

(2) Dispersion Characteristics

Dispersion Characteristics for the 1.55 μm dispersion-shifted optical fiber in cable are shown in Fig.7. Maximum dispersion coefficients at 1.53 μm and 1.57 μm are 3.24 ps/km/nm and 3.50 ps/km/nm, respectively. These values are almost equal to the characteristics for conventional single-mode optical fiber in the 1.3 μm wavelength region.

5.2 Section Characteristics

Optical characteristics of the Matsuyama-Oita for the 1.55 μm dispersion-sifted optical fiber cable after burying are as follows.

(1) Optical Loss Characteristics

Overall length for the Matsuyama-Oita route is 120 Km of which 9 Km is overland. The average piece length of the terrestrial section is about 2 Km. The optical loss is shown in Fig.8. Average loss is 0.225 dB/Km which represents optimum optical loss Characteristics.

(2) Dispersion Characteristics

Average dispersion coefficients at 1.53μm and 1.57μm are -1.38 ps/km/nm and 1.21 ps/km/nm, respectively. On the other hand maximum dispersion coefficients are -1.86 ps/km/nm and 1.51 ps/km/nm. These are shown in Fig.9.

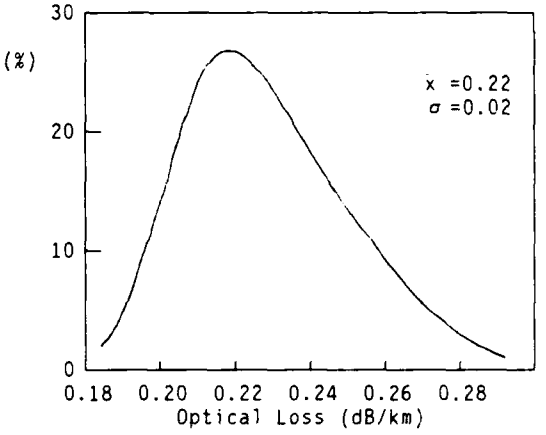

Fig.6 Histogram of Optical Loss (Optical Fiber Cable)

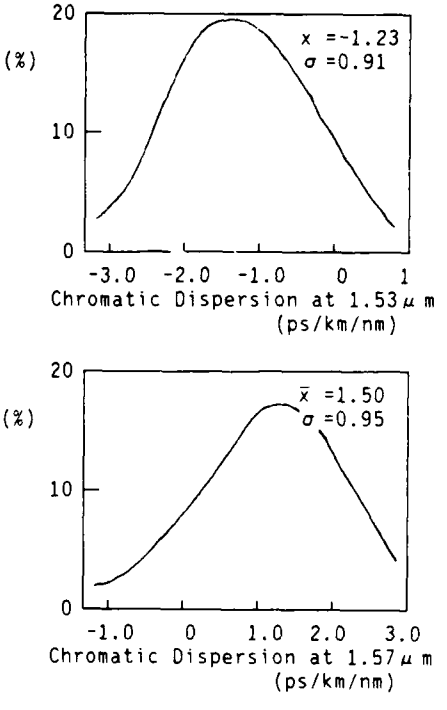

Fig.7 Histogram of Chromatic Dispersion (Optical Fiber Cable)

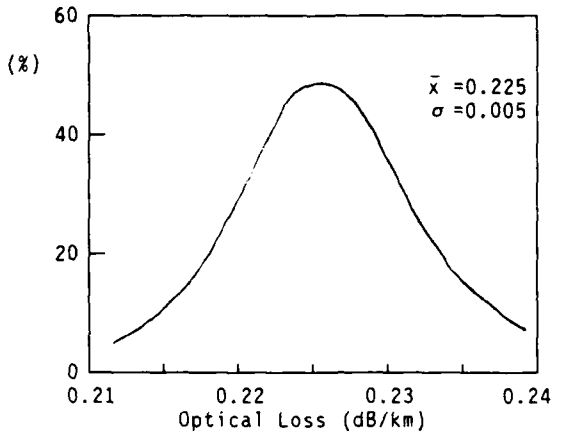

Fig.8 Histogram of Optical Loss (Section Characteristics)

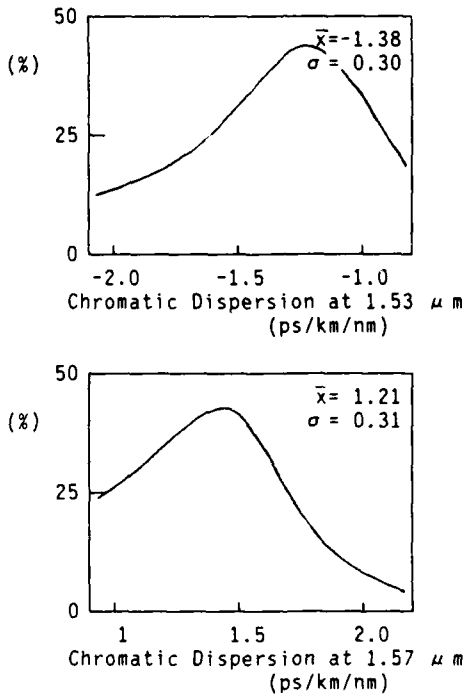

Fig.9 Histogram of Chromatic Dispersion (Section Characteristics)

5.3 Splicing

NTT uses a direct core-alignment method for conventional single-mode optical fiber. The same method was also applied in the commercial tests on the 1.55 μm dispersion-shifted optical fiber.

The nominal mode field diameter for 1.3 μm single-mode optical fiber is 10 μm, while that for 1.55 μm dispersion-shifted optical fiber is 8 μm.

In principle, the same misalignment should cause 1.6 times greater loss in 1.55 μm dispersion-shifted optical fiber than in conventional optical fiber.

Figure 10 shows splicing loss characteristics for 1.55 μm dispersion-shifted optical fiber. Average splicing loss is 0.09 dB which is almost the same as the splicing loss for 1.3 μm single-mode optical fiber. It was also clarified that there is no significant loss increase due to core-end misalignment.

In addition, a mass-fusion splicing machine was used, which was develcped for conventional single-mode optical fiber. The mass-fusion splicing loss characteristics for 1.55 μm dispersion-shifted optical fiber is shown in fig.11. Average splicing loss is 0.10 dB. These values are almost equal to the caracteristics for conventional fiber. This machine drastically reduces the number of splicing operations and makes full use of the advantages of ribbon optical fiber.

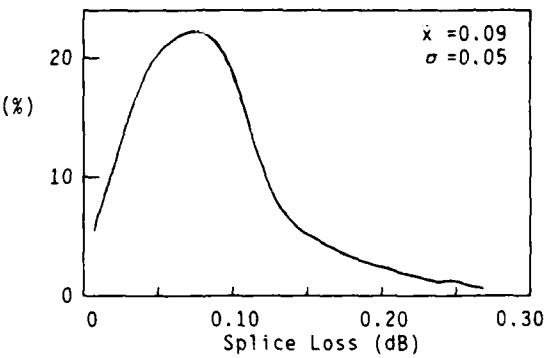

Fig.10 Histogram of Splice Loss

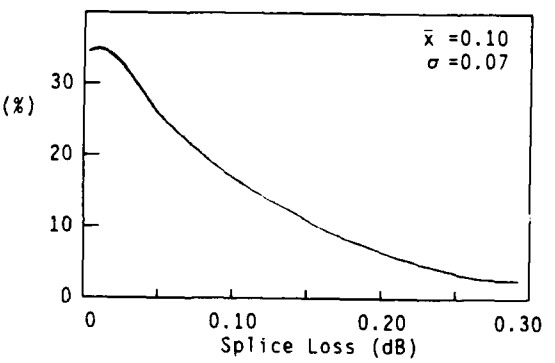

Fig.11 Histogram of Splice Loss (Mass-fusion Splicing Machine)

5.4. Submarine Optical Fiber Cable Laying Technology

In shallow sea areas, submarine cables must be buried in the sea bed to prevent damage from fishing gear or from ship anchors. In coventional submarine optical fiber cable laying technology in NTT, armored-cable is buried with the Mark IV (P-4) submarine cable burying plow, which can withstand a strong side force while the cable is being buried.

In the commercial introduction of 1.55 μm dispersion-shifted optical fiber submarine cable, non-armored cables are buried without significant loss increases (Fig.12) . The maximum burying depth is 130 cm.

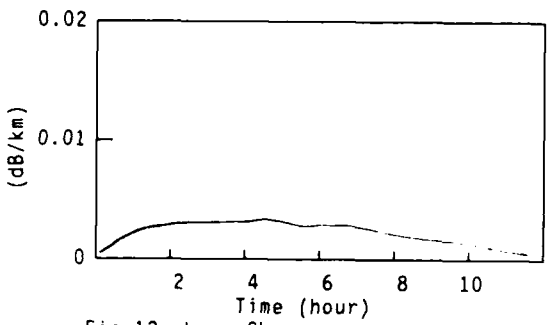

Fig.12 Loss Change

6. Conclusion

This paper has described NTT's 1.55 μm dispersion-shifted optical fiber cable technologies, and has provided the first commercial test resultus for this cable. Introduction of these technologies in large-capacity, longhaul transmission systems will at least doubie the repeater spacing, reduse total cost and improve reliability for the systems. 1.55 μm dispersion-shifted optical fiber cable technologies will greatly advance optical transmission systems.

The authors wish to acknowledge the support of many people and organizations.

References

(1) S. Takashima: "Promising Developments in Optical Fiber Cable Technology" Japan Tech.Rev., Vol.29, No.4,pp.26-32,1987.

(2) M.Ohashi,N.kuwaki,C.Tanaka,N.Uesugi,Y.Negishi:"BEND-OPTIMISED DISPERSION-SHIFTED STEP-SHAPED-INDEX(SSI) FIBERS"ELECTRONICS LETTERS.,Vol.22,No.24,pp.1285-1286.9

(3) K. Aida,K.Nakayama and Y. Negishi: "New F 400M Transmission System Version"E. C. L. Tech. Jour. NTT,Japan Vol.36,No.3,pp.315-322,1987.

(4) K. Aoyama:"1.6Gps Very Large Capacity OpticalFiber Transmission System" Japan Tech. Rev. Vol.30,No.3,pp. 16-20,1987.

Katsuya Uema is a Engineer, Trunk Transmission Network Project Group in Network Systems Development Center of NTT. He received his B.S. degree in electrical engineering from Ryukyu University in 1985.
He joind NTT in 1985 and has been engaged in development of trunk optical fiber cable system.

Kiminori Sato is a Senior Engineer, Trunk Transmission Network Project Group in Network Systems Development Center of NTT. He received his B.S. degree in electrical engineering from Kyoto University in1980.
He joind NTT in 1980 and has been engaged in development of subscriber optical fiber and trunk optical fiber cable systems. He is a member of Institute of Electrical and Electronics Engineers, and Institute of Electronics, Information and Communication Engineers of Japan.

Seiji Takashima is a General Manager, both Fiber Optics Local Network Systems Project Group and Telecommunication Cable Systems & Outside Plant Project Group in Network Systems Development Center of NTT. Hereceived his B.S. and M.S. degrees in electrical engineering from Waseda University in Japan in 1967 and 1969, respectivery. He also received M.S. in Management from Massachusetts Institute of Technology in 1983.
He joined NTT in 1969 and has been engaged in development both of subscriber optical fiber network systems, and whole range of copper telecommunication cable systems and outside plant technologies. He is a member of Institute of Electrical and Electronics Engineers, and Institute of Electronics, Information and Communication Engineers of Japan.

Hiroyuki Kasai is a General Manager,Trank Transmission Network Project Group in Network Systems Development Center of NTT. He received his B.S and M.S degerees in electronics engineering from Yamanashi University in Japan in 1966 and 1968,respectivry and D.E.degrees from Tokyo Institute of Technology in 1983.
In 1968, he joined NTT Laboratories, Yokosuka, Japan. He was engaged in reserch on mainly PCM wave equalization over coaxial cables and high speed mulutiplexing system. He is presently engaged in development of trank transmission network system. Dr.Kasai received The Achivement Award of the Institute of Electrpnics,Information and Communication Engineers of Japan in 1978. He is a member of Institute of Electrical and Electronics Engineers, and Institute of Electronics, Information and Communication Engineers of Japan.

LONG LENGTH OPTICAL FIBER COMPOSITE POWER SUBMARINE CABLE

M. IIZUMI, Y. ASABA, A. TAKASE, H. INOUE, H. ISHIKURA, M. IWAYA, K. SUZUKI, Y. MIYAJIMA

The FURUKAWA ELECTRIC CO., LTD.
No.6 Yawata Kaigan Dori, Ichihara, Chiba, 290 Japan

Abstract

Long length optical fiber composite power submarine cable has been developed.

The key factor was the development of the joint method of the fiber unit in the cabling process of the composite cable.

This novel method, which we call factory joint, enabled the production of 31km long composite submarine cable.

Various mechanical tests were conducted on the factory joint and the cable and high reliability was confirmed.

This cable will be installed this fall.

Introduction

Optical fiber has superior characteristics such as immunity from electro magnetic induction, wide band width and long repeater spacing.

Optical fiber composite power cables have been developed because of the advantages of the fiber as mentioned above and the reduction of manufacturing and installation cost by integrating two types of cables.

Many of such cables have been actually used as terrestrial cables. They are short in length, however, because of the transportation and installation limitations.

For the submarine cable application, where manufacturing and installation cost is high, the merit of the integration is even greater. Transportation and installation no longer limits the cable length because of the usage of ship.

The production of the composite cable is quite difficult because of the complex manufacturing processes, large diameter, and heavy weight. Thus the maximum cable length was limited to a few kilometer.

We have developed a method of making a strandable optical fiber unit joint in the factory. This method is called F.J or Factory Joint method and enabled us to make a long length optical fiber composite power submarine cable.

We have produced about 31km long composite cable for Turkish Electricity Authority.

The characteristics and manufacturing results of F.J are mentioned below.

Requirements

Manufacturing and installation techniques for terrestrial composite cables have been well established after much experience. Here are mentioned the special requirements for composite submarine cables.

The submarine cables are steel armored to withstand the large installation tension and to avoid damage by ship's anchors. Thus optical unit must withstand the lateral force given by the steel wires during the armoring process.

The cable must be chemically stable against salt water and must withstand the water pressure of max. 100 meter deep.

The cable must withstand the tensile force during pulling up the cable for remedy in case of accident.

The long composite cable can no longer be wound on a drum and it must be coiled. In the coiling operation, the cable is twisted once every turn. The characteristics of fiber must remain unchanged during the coiling operation.

Another important requirement for fiber unit F. J is that it can be stranded in the same position as the unit itself.

Cable Construction

The fiber unit is placed in the gap of three power cable core strand in order to protect it from external force and to minimize the cable diameter. The constructions of fiber unit, composite cable and F. J of fiber unit are discribed below.

1. Fiber Unit

The structure of eight fiber unit was determined from our past experiences with composite cables.

Single mode fibers made by fully synthesized VAD method were used because of their high resistance against hydrogen attack and good mechanical strength.

The Construction and Properties of optical fiber is listed in Table 1.

The fibers are protected in P.E. Slotted core from direct application of outer force and uneven pressure. In order to minimize the hydrogen generation, copper plated steel tension member and laminated copper tape were used.

The cable is jelly filled to prevent water penetration. The reliability is enhanced by lead sheath and perfect water-proof characteristic was achieved. The cross section of fiber unit is shown in Fig. 1.

Table 1 Construction and properties of optical fiber unit

Item		Specification
Core	Material	Doped silica
	Diameter	Nom. 9μm
Cladding	Material	Silica
	Diameter	125 ± 3μm
Primary coating	Material	UV curable resin
	Diameter	Approx. 0.4mm
Secondary coating	Material	Nylon
	Diameter	0.9 ± 0.1mm
Concentricity error		Max. 1μm
Cladding non-circularity		2% or less
Mode field diameter		10 ± 1μm
Dispersion		Less than 3.5ps/nm/km at 1285 ~ 1330nm
Attenuation		Max. 0.55dB/km at 1300nm

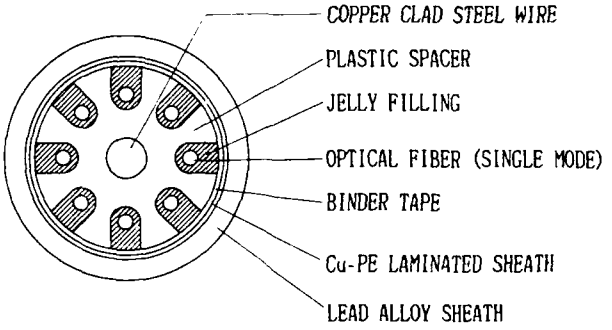

Fig. 1 Cross Sectional View of Optical Fiber Unit

2. Composite Cable

Three cores of 34.5kV XLPE insulated lead sheath power cable and fiber unit were stranded and protected by a single layer of 6mm steel wire armour.

The O.D. is 110mm and the weitht is 30ton/km. The cross section of the composite cable is shown in Fig. 2.

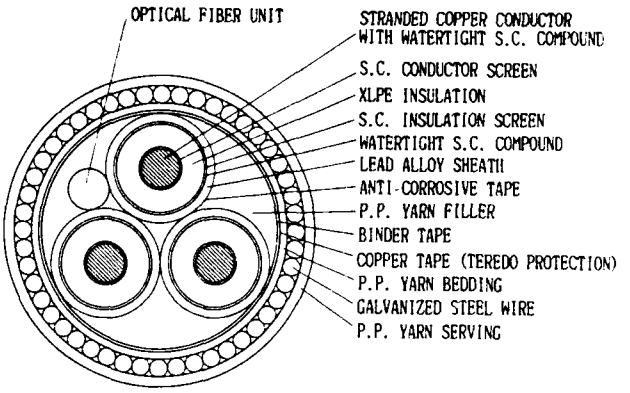

Note S.C. : Semi-conducting

Fig. 2 Cross Sectional View of Composite Cable

3. F.J of fiber unit

The factory joint (F.J) of fiber unit must be also placed in the gap of three power cable cores.

Thus the following conditions must be satisfied by the joint.

1) Diameter almost as small as the unit itself to allow stranding.
2) Structure allowing re splice in case of splice failure.
3) Good water proof characteristic.
4) Good flexibility
5) Good mechanical characteristic for cabling and installation.

The construction of F.J is Shown in Fig. 3. The joint is protected against lateral force and water pressure by a flexibel protective tube around it. The lead tube is applied on the protective tube to prevent water penetration. The F.J is also jelly filled to achieve the continuity of unit structure and to avoid water run at the time of accident.

Characteristics

1. F.J of fiber unit

Various tests were conducted on F.J and the results are listed in Table 2. The test conditions are determined considering the various forces which could be applied to the joint during manufacturing and installation. No loss increase was observed.

Table 2 Characteristics of Factory Joint

Item	Testing condition	Result
Heat cycle test	Temperature range : −30 ~ 60℃	No loss increase after test
Lateral force test	Compression length : 50mm compression load : 100kg	No loss increase No deformation
Bending test	Bending dia. : 2 m Bendig angle : ±130° Bending time : 5 times	No loss increase after test No deformation
Twist test	Sample length : 18m Optical fiber unit including Factory Joint Twist angle : 360°	No loss increase after test
Tensile test	Tensile strength : 130kg	No loss increase after test
Tensile bending test	Bending dia. : 3 m Tensile strength : 18kg 3 times repeat	No loss increase after test No deformation
Water pressure test	Pressure : 20atm time : 2 weeks	No loss increase No deformation

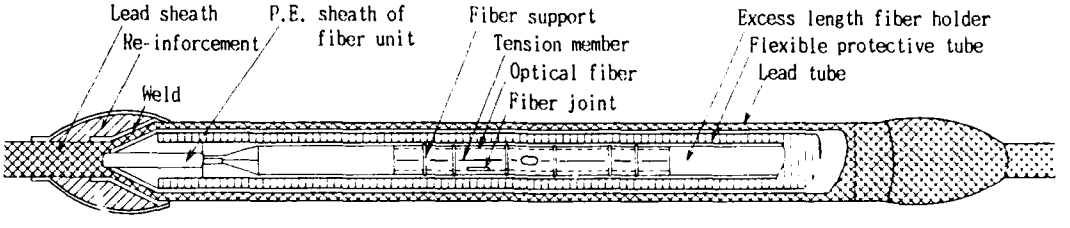

Fig. 3 Schematic Diagram of Factory Joint

2. Composite Cable

The composite submarine cable with F.J of fiber unit was coiled and then tested under the condition simulating installation. The results are shown in Table 3. No loss increase was observed. After these tests, F.J was observed very carefully. No visible damage was given to the appearance and fibers inside F.J.

From these tests of F.J itself and composite cable with F.J, we observed that they possess sufficient characteristics to be used in the field.

Table 3 Characteristics of composite cable including Factory Joint

Item	Testing condition	result
Coiling test	Coiling dia. : 6 m	no loss increase after test
Tensile bending test	Bending dia. : 7 m Tensile strength: 7ton 3 times repeat	no loss increase after test

Manufacturing

Based on the results above, we manufactured a long composite cable to be actually installed.

All the processes from the production of fiber, fiber unit, and power cable core, stranding, steel wire armouring to the final loading to the ship were done within the same site.

F.J of fiber unit was made between the stranding and steel armouring processes.

For F.J, a simple clean room was set up in which all the process from fusion splice of the fiber to the completion of F.J was done.

The change of attenuation at every process is shown in Fig. 4. The attenuation includes the splice loss after steel armour process. No loss increase was observed during the manufacturing process. The fusion splice loss at F.J was average of 0.07dB and it did not change up to the loading of the cable on the ship.

a : fiber
b : fiber unit
c : composite cable stranding
d : steel armouring (including F.J)
e : loading on the ship (including F.J)

Fig. 4 Loss Change during Manufacturing

Conclusion

We have tested and demonstrated that F.J and the composite cable with F.J possess sufficient characteristics for the practical use. The development of J.F enabled us to make long length optical fiber composite power submarine cable and we have actually made a 31km composite cable for practical use.

Masahiro IIZUMI
The Furukawa Electric Co., Ltd.
No.6 Yawata Kaigan Dori
Ichihara, Chiba, 290
Japan

Mr. Iizumi received the B.S. degree in electric engineering from Iokai Univ. in 1986. In 1986 he joined the Furukawa Electric Co., Ltd.

He has been a stuff engineer of energy transmission research section of power cable.

Atsuo TAKASE
The Furukawa Electric Co., Ltd.
No.6 Yawata Kaigan Dori
Ichihara, Chiba, 290
Japan

Mr. Takase graduated from Nagoya Univ. in 1984 with a B.Sc. in electric engineering then joined The Furukawa Electric Co., Ltd. and has been engaged in development of the optical fiber cable.

Mr. Takase is now a staff engineer of the Production
Engineering Section of Optical Fiber Telecommunication Division.

Yoshihisa ASADA
The Furukawa Electric Co., Ltd.
No.6 Yawata Kaigan Dori
Ichihara, Chiba, 290
Japan

Mr. Asada was born in Tokyo in January, 1949.

He received the B.S. and M.S. degrees in electrical engineering from Waseda University in 1970 and 1972, respectively.

In 1972 he joined the Furukawa Electric Co., Ltd., where he was assigned the Research and Development Section. He has been engaged mainly in the development of high voltage XLPE cables and high pressurized SF_6 gas insulated cables since 1972.

At present, he is primarily concerned with dielectric and mechanical testing on high voltage XLPE cables of 275KV class and above.

Hideo INOUE
Power Cable Engineering Dept.
The Furukawa Electric Co., Ltd.
4-13-14, Higashishinagawa,
shinagawa-ku, Tokyo 140,
Japan

Mr. Inoue graduated from Akita Technical college, electrical engineering in 1970 and the joined the Furukawa Electric. Currently, engaged in the design of XLPE insulate power cables.

Shigeru ISHIKURA
Power Cable Production Dept.
The Furukawa Electric Co., Ltd.
No.6 Yawata Kaigan Dori
Ichihara, Chiba, 290
Japan

Mr. Ishikura graduated from Tomakomai Technical College, Industrial Chemistry in 1970 and the joined The Furukawa Electric Co., Ltd. and has been engaged in Development of power cables.

Mr. Ishikura is now deputy manager of the Production Engineering Section of Power Cable Division.

Katsuaki SUZUKI
The Furukawa Electric Co., Ltd.
No.6 Yawata Kaigan Dori
Ichihara, Chiba, 290
Japan

Mr. Suzuki graduated from Yamanashi Univ. in 1987 with a B. Sc. in electric engineering then joined The Furukawa Electric Co., Ltd. and has been engaged in Development of optical fiber cables.

Mr. Suzuki is now a staff engineer of the Production Engineering Section of Optical Fiber and Telecommunication Division.

Masanori IWANA
The Furukawa Electric Co., Ltd.
No.6 Yawata Kaigan Dori
Ichihara, Chiba, 290
Japan

Masanori Iwana received the B.E. degree in electrical engineering from Ibaraki University in 1975.

He joined the Furukawa Electric Co., Ltd. in 1975 and engaged in development of the high voltage power cable and accessories.

Since 1984 he has been engaged in the quality assurance of high voltage power cable and power optic fiber composite cable.

Yukio MIYAJIMA
The Furukawa Electric Co., Ltd.
No.6 Yawata Kaigan Dori
Ichihara, Chiba, 290
Japan

Mr. Miyajima graduated from Tokyo Institute of Technology in 1983 with a B.Sc. in production engineering then joined The Furukawa Electric Co., Ltd. and has been engaged in Development of optical fiber cables.

Mr. Miyajima is now a staff engineer of the Production Engineering Section of Optical Fiber and Telecommunication Division.

DEVELOPMENT OF OPTICAL FIBER/POWER COMPOSITE TETHER CABLE FOR DEEP SEA UNMANNED VEHICLES

Y.SHINGO, T.KAMIJYO, K.KANEKO, Y.URABE, A.MOGI, M.NARUSE

FUJIKURA Ltd.
TOKYO,JAPAN

Summary

Scientific and technical interest in deep seabed to survey oceanic resources have been rising. Japan Marine Science and Technology Center (JAMSTEC) has been developing many kinds of seabed survey systems for that purpose.
Shinkai 2000, a manned deep submergence vehicle that can dive to a depth of 2000m, has been in operation to bring valuable information to us from the seabed.
The Dolphin 3K system, a new unmanned deep submergence vehicle capable of diving to a depth of 3300m was developed to survey the seabed where it is too dangerous for manned deep submergence vehicles to approach, and where the depth exceeds 2000m, the maximum capability of Shinkai 2000.
A 5000m long optical fiber/power composite tether cable is used for electric power and signal transmission for control the vehicle. It comprises a compact, optical fiber/power composite, underwater connector and a compact mechanical cable termination for the Dolphin 3K system.
This tether cable system is required to be highly reliable under a water pressure of up to 376kg/cm², side-wall pressure of 2tons/m, and high tensile strength of 16.5tons and have high bending endurance properties.
The cable system is installed in Dolphin 3K, supported by a mother ship, and sea trials to a depth of 3400m have been satisfactorily conducted.

1. Introduction

Interest in deep seabed to surveys of oceanic resources has been rising in Japan, a resourceless country surrounded by the sea.
Objects of such surveys include hydro thermal deposits, manganese nodules at depths from 1000m to 6000m, and seabed research to predict earthquakes, as well as surveys of fishery resources on continental shelves. Interest is centered not only on resources, but also on technical and scientific aspects.
Interest in Japan declined in the 1960s because of insufficient technical support and social demand.
But interest re-emerged with the appearance and availability of new techniques of optical fibers providing light weight, small diameter, low transmission loss, and no interference from electric fields and for aramid fibers for tension members providing light weight and high tensile strength. A highly reliable tether cable is needed, capable of supplying electric power to drive the vehicle, and sending a large quantity of signals from high resolution colour TVs and other instruments mounted on the vehicle to survey the condition of the seabed.
It is difficult to develop a long tether cable of 5000m if it is designed by conventional cable techniques such as those applied for some coaxial transmission cables, and some high tension steel wires for tension members.
Shinkai 2000 , a manned deep submergence vehicle capable of diving to a depth of 2000m was developed by JAMSTEC for surveying oceanic resources, structures for marine use and for oceanography and geophysics research. The system is now in use. In order to conduct surveys and perform research safely and effectively using it, the Dolphin 3K system was developed for the following purposes:

- Presurvey before the Shinkai 2000 dives.
- Surveys of seabeds with complicated topography that are dangerous for the Shinkai 2000 to perform.
- Rescuing the Shinkai 2000 in an emergency.

The development of this system started in 1983 and delivery was made in 1987. The vehicle and control equipment of the system were developed and constructed by Mitui Engineering and Shipbuildings Co. Ltd.(MES).
Sea trials started since Feburary 1987 were conducted satisfactorily. Details of the development results are given in this report.

2. Construction and Requirements of the Dolphin 3K System

2.1 Abstract on Dolphin 3K System

Fig.1 shows the composition of the Dolphin 3K system.
The system, a direct-shot type system, consists of a control station, vehicle, tether cable, winch, tensioner and acoustic navigation equipment.
The abstract of the system is as follows:

Dimensions	(m)	: 3 (L) × 2 (W) × 2 (H)
Weight	(kg)	: 3700 (in air) and -10 (in water)
Max.Operation Depth	(m)	: 3300
Speed	(knot)	: 3 (forward), 2 (reverse), 1 (up and down)
Thrusters		: Electro-hydraulic servo motor
Navigation equipment		: sonars, gyrocompass, depthometer, velocimeter, altitude sensor, etc.
Instrumentation		: High-resolution color T.V. etc. Manipulator Grabber and cutter

Two mother ships are available to support this system.

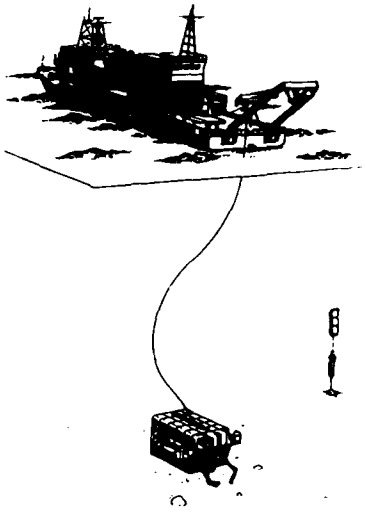

Fig.1 Dolphin 3K System

2.2 Requirement for Tether Cable

As shown in Fig.1, the vehicle is suspended by a tether cable through many sheaves from a cable winch on the supporting mother ship.

High tension and high side wall pressure is applied repeatedly to the cable, so toughness and bending durability are required of the cable's design.

Furthermore, a small diameter, low weight and flexibility are also required of the cable to prevent reduced movility of the vehicle in water and to reduce drifting in a tidal current.

To prevent the cable from being tangled in the water, it must have a small degree of self-rotation.

Furthermore, a water-tight structure, in other words a dry structure, is required of the cable to prevent optical transmission fiber from suffering a deterioration of tensile strength caused by direct contact with the sea water.

Main specification of the tether cable is as follows:

(1) Supply voltage and power : 2500V 3ϕ 70KVA
(2) Overall diameter : 30mm
(3) Cable length : 5000m
(4) Breaking Tensile Strength : 16.5tons or more
(5) Optical fiber : 4 fibers, G.I.type
(6) Water pressure resistance (Transmission loss of optical fibers) : 1.0 dB/km or less at wave length of 0.85μm, under water pressure of 376kg/cm^2
(7) Transmission loss in optical fibers : 1.0 dB/km or less at wave length of 1.3μm
3.0 dB/km or less at wave length of 0.85μm

Band width in optical fibers: 400 Mbps. 5km or more

3. Development of Tether Cable

3.1 Construction of Tether Cable

Cross-sectional shape and construction of the developed tether cable are shown in Fig.2 and Table 1, respectively.

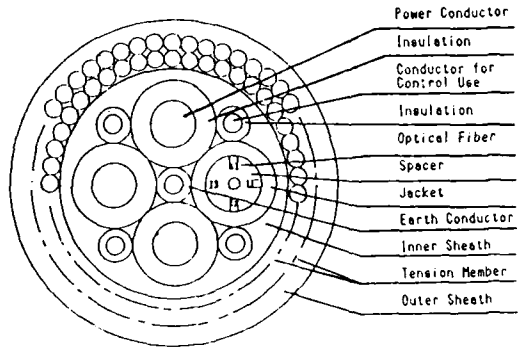

Fig.2 Cross Sectional Structure of Tether Cable

Table 1. Construction of Tether Cable

		Power conductor	Control conductor	Optical Fiber	Eeath conducter
No. of cores		3	4	4	1
Conductor Size (mm^2)		6	0.7	—	1.4
Optical Fiber	Type	—	—	G.I.	—
	Material of Spacer	—	—	Engineering plastics	—
Tension Member	Material	polyamide covered rod type aramid fiber			
	Construction	1.9ϕDia. 2layers, contrahelically			
Overall Diameter(mm)		approx. 30			
Weight (kg/km)		approx. 850			

Three power cores, 4 control cores and optical fiber unit containing 4 fibers, are laid around a earth core.

The metal cores are all insulated with closs-linked polyethylene and fibers are inserted into a spacer made of engineering plastics and covered with the same material.

Optical fibers used are made of 50/125μm graded index type silica, have secondary coat of UV-cured resin and have been subjected to a proof strain test of 2% elongation.

The laid cores are sheathed with a solid extrusion of closs-linked polyethylene to prevent the deterioration of the tensile strength of optical fibers in water, and to give a uniform bedding for two layers of contrahelically wound tension members.

Rod-type aramid resin fiber (Kevlar ®) impregnated with unsaturated polyester resin and covered with polyamide resin, is applied to the tension member.

Attension was paied to the design of the double-layered tension member, such as the ratio of the numbers of tension member in each layer and the lay angle of each layer, to prevent it from rotating when torsional balance is affected by tension.

And a solid extrusion of the overall sheath made from specially formulated EP rubber, covers the tension member to provide protection from mechanical deterioration such as abrasion (Fig.2, Fig.3).

Abrasion of tension member caused when passing through the sheaves many times, causes a deterioration of the tensile strength of the cable.

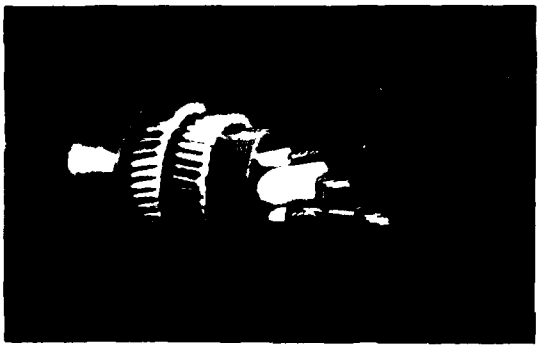

Fig.3 Tether cable

3.2 Water Pressure Property of Tether Cable

Some profiles of water pressure tests were conducted on the developed cable and transmission loss from the optical fiber etc. were measured.

(1) Short-term water pressure test

A short-term but high water pressure test up to 600kg/cm² was conducted on 1.5m long cable specimen. The increment of water pressure was approximately 100kg/cm² per minute.

The test results are shown in Fig.4 and Fig.5. No change of transmission loss was observed, not only at specified water pressure of 376kg/cm², but also at 600kg/cm².

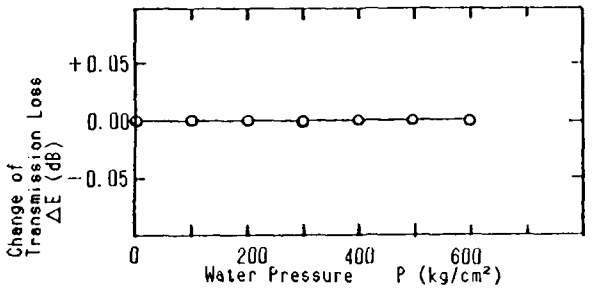

Fig.4 Relation Between Water Pressure and Transmission Loss

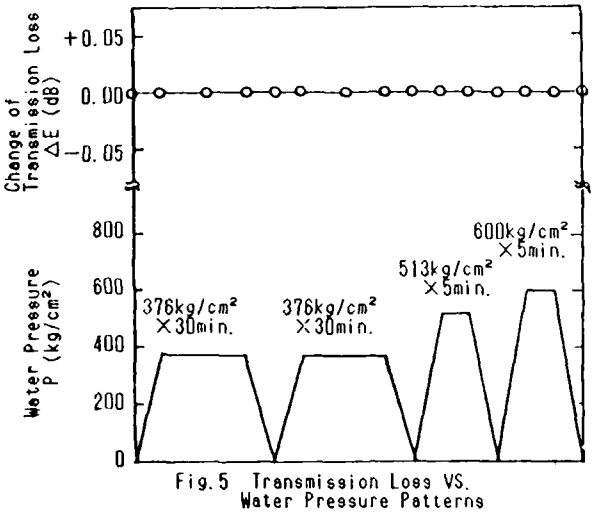

Fig.5 Transmission Loss VS. Water Pressure Patterns

(2) Long-term water pressure test

A specified water pressure of 376kg/cm² was applied for 10 days continuously to the cable specimen; same as item (1). As shown in Fig.6, no change in transmission loss of optical fiber was observed. The normal submergence operation of the vehicle will only be several hours.

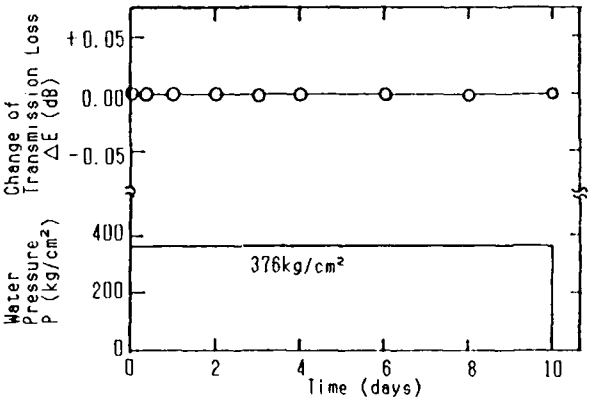

Fig.6 Relation Between Pressurized time and Transmission Loss

(3) Water pressure test with a large vessel

A water pressure test was conducted at 2 times 376kg/cm² for 30min. on 20m long cable specimen(approx. 80m long fiber core) in a large water pressure test vessel (1.4m int.dia., 3m high, maximum pressure 1560kg/cm²) at JAMSTEC.

No change of transmission loss was observed.

Test vessel are shown in Fig.7.

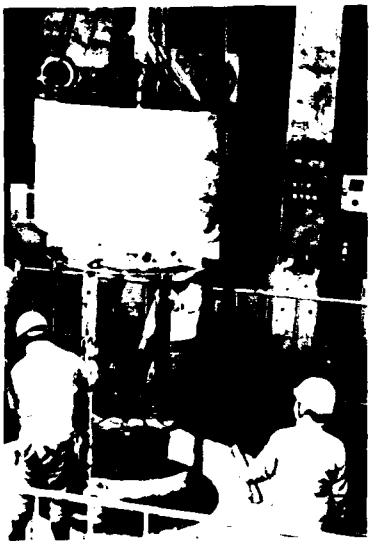

Fig.7 Water Pressure Vessel (Courtesy of JAMSTEC)

(4) Cyclic water pressure test

A test under 200 times cyclic water pressure, from 0kg/cm² to 376kg/cm², was conducted on a cable specimen; same as item (1).

The holding time at 376kg/cm² was 5 min. and it took approx. 8 min. each for pressurization and depressurization.

The pressure-time profile and the test results are shown in Fig.8 and no change of transmission loss was observed.

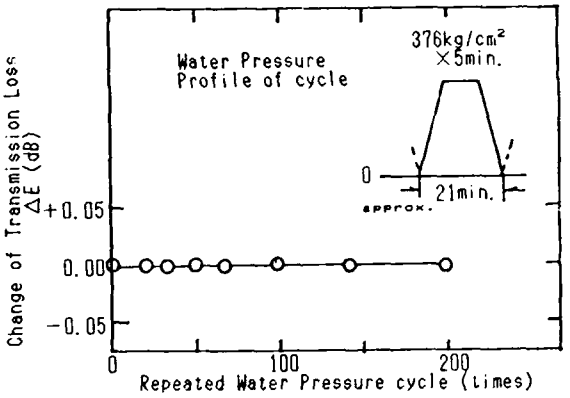

Fig.8 Relation Between Repeated Water Pressure cycles and Transmission Loss

3.3 Mechanical properties of tether cable

(1) Flexibility test

Flexibility of the cable was measured by a supported beam deflection test using a 1m long cable specimen.

The test results are shown in Fig.9; the deflection of the cable was almost the same as one for a common low voltage CV power cable (XLPE insulation, PVC sheath) having the same overall diameter. It shows us that the cable will be flexible enough and easy to handle.

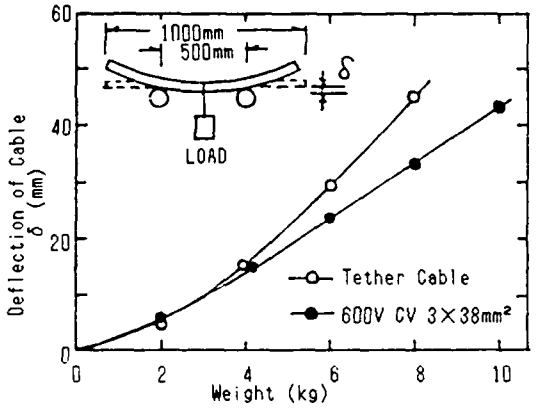

Fig.9 Relation Between Weight and Deflection of Cable

(2) Tensile property test

Elongation of cable and transmission loss of optical fibers were measured by appling tension of 15tons repeatedly using 100tons horizontal Amsler tensile tester. The test was conducted using an 8m long cable specimen with a pulling speed of about 15mm/min, and the tension was released immediately the peak tension of 15tons was reached.

The test results are shown in Fig.10. The test facility is also shown in Fig.11.

The elongation of a cable saturated to 0.5% at a normal operating tension of 1ton, 1.8% at 15tons respectively in a few tensioning cycles.

And little change of transmission loss was observed in the optical fiber.

Finally, the cable specimen was broken at 17.4tons.

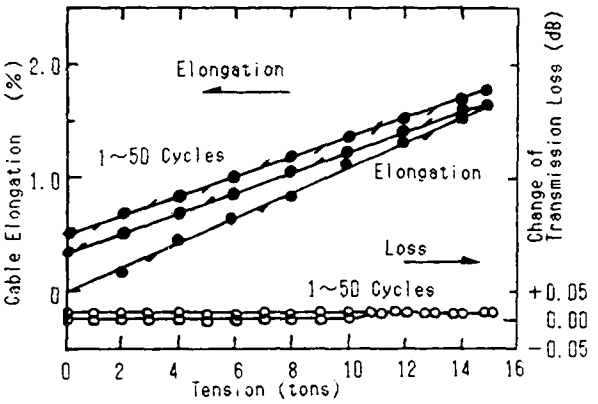

Fig.10 Relation Between Cyclic Tension and Cable Elongation

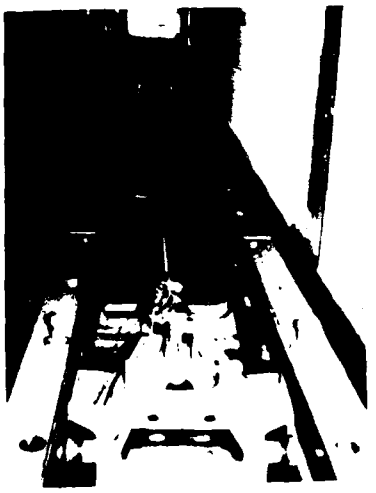

Fig.11 Tensile Tester

(3) Self-rotation test

The self-rotation property of cable was measured by applying a tention of upto 2tons using the same test equipment and same length of cable as in item (2).

The test results are shown in Fig.12 and the angle of self-rotation was about 3°/m, the torque was about 0.6kg-m at normal operating tension.

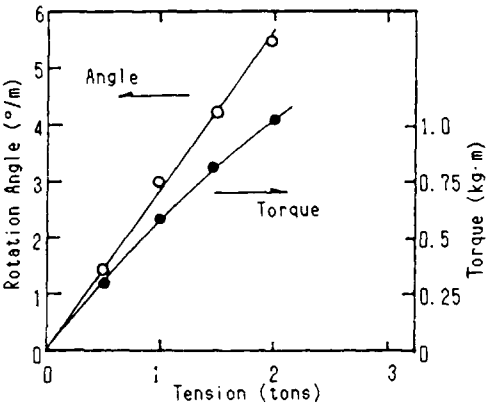

Fig.12 Relation Between Tension and Rotation Angle

(4) *Tensile strength test*

As shown in Fig.13, the tensile strength when the cable specimen broke was high enough for the specified value of 16.5tons. The test conducted was almost same as that in item (2). The transmission loss of optical fibers and continuity of insulated metal conductors were also monitored in this test. As shown in Fig.14, the optical and insulated metal conductors broke at the same time as the cable broke. The maximum elongation of the cable is considered to be approximately 2%.

The mechanical cable termination used in these tests is shown in item 4.

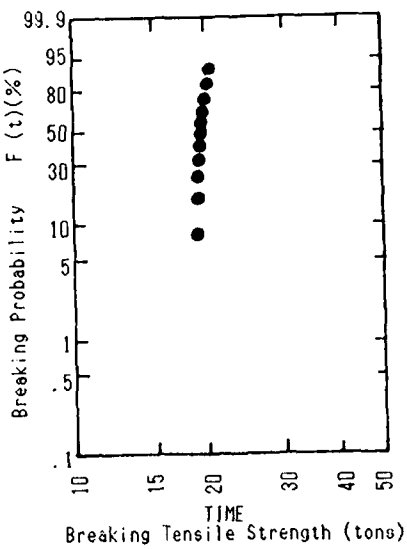

Fig. 13 Weibull Probability Plot of Tether Cable

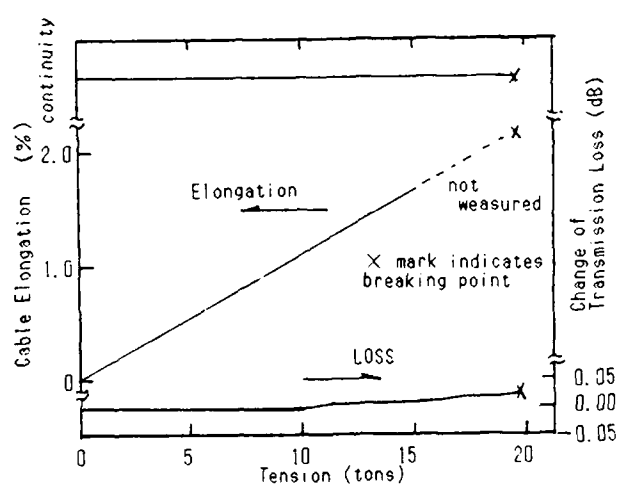

Fig. 14 Tension VS. Transmission Loss, Elongation and continuity of conductors

(5) *Small radius bending test*

A test was conducted to evaluate the resistance of small radius bend such as a kink. A streight cable specimen was gradually bent to a smaller radius, and the transmission loss of the optical fiber was monitored during bending.

As shown in Fig.15, specimen was bent to a radius of 75mm, no change of transmission loss in the optical fiber untill a radius of 75mm was observed. And no break, no change of insulated metal conductor, tension member rods and optical fiber were also observed after the test.

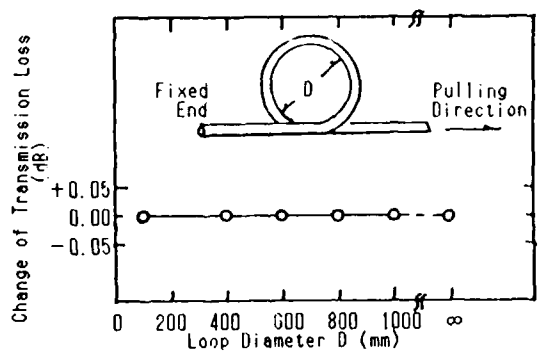

Fig. 15 Relation Between Transmission Loss and Loop Diameter

(6) Side-wall pressure test

To estimate the life of the cable, up to approx. 8 times the side wall pressure under normal operation were applied to a 10m long cable specimen and the continuity of insulated metal conductors, transmission loss of optical fibers were monitored.

Fig.16, shows the test equipment.

Fig.16 Side Wall Pressure Test Facility

As shown in Fig.17, the life under normal operation is considered to be one million times or more.

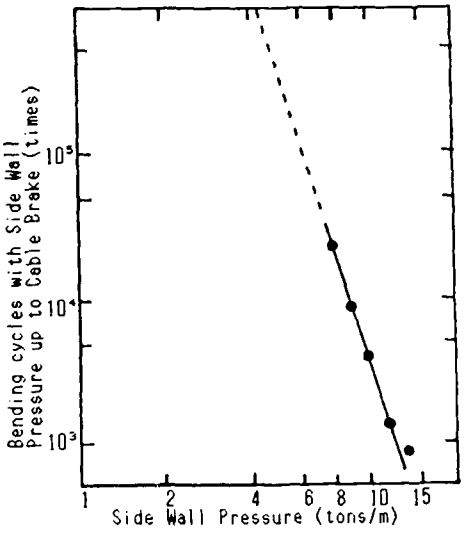

Fig.17 Relation Between Side Wall Pressure and Bending Life

(7) Twisting durability test

The twisting durability of the cable was also evaluated at a twist rate of ±45°/m, 30 times/min, using a 1m long cable specimen.

After twisting 10,000 times, no change of cable appearance, optical fibers or insulated metal conductors was observed.

4. Mechanical Cable Termination

A suspension ability of 16.5 tons or more, which is equal to the specified tensile strength of the cable, is required of the mechanical cable termination because the tether cable has the role not only of supplying electric power and exchanging signals, but also of tying the vehicle to a mother ship, as shown in Fig.1. Flexibility is required so as not to disturb the mobility of vehicle on and in the sea, as well as suitable tensile strength and bending durability.

A polyamide covering of rod-type tension member was removed from the end of the cable, then a termination block made of titanium alloy was inserted into the end of the cable. Tension was applied uniformly to each rod after being arranged in an orderly way, and epoxy resin was casted inside the termination block.

The breaking tensile strength has already been shown in Fig.13, and the suspension ability would be 20 tons or more. No change of transmission loss in optical fibers, continuity and insulation resistance of insulated metal conductors were observed after 3000 bending cycles at 50kg and after 150 cycles at 200kg with a G-FRP bell-mouth.

The compact, light-weight and highly reliable mechanical cable termination that was developed is shown in Fig.18,19.

5. Optical/Power Composite Underwater Connector

A one-body type, optical fiber/power conductor, composite connector was developed for the electricity supply and signal transmission from the mother ship to the vehicle.

It is not difficult to develop connectors only for an optical fiber and a power conductor individually, because water pressure affects them concentrically (radially), and the pushing force on their smaller cross-sectional area is also smaller.

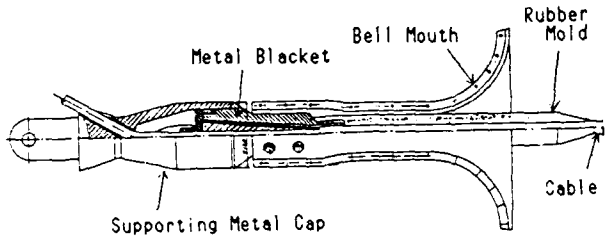

Fig.18 Cross Sectional Structure of Mechanical Cable Termination

Fig.19 Mechanical Cable Termination

A large space is required on a small vehicle if connectors are prepared for 4 optical fibers, 7 insulated conductors of the tether cable individually. This constitutes a big problem regarding convenience and reliability.

A one-touch connection, one body type, compact, light-weight, optical/power composite under water connector was developed as shown in Fig.20 and 21.

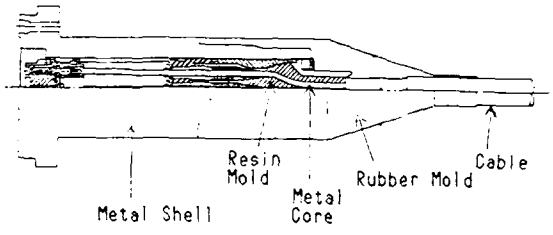

Fig.20 Cross Sectional Structure of Composite Under Water Connecter

Fig.21 Composite Under Water Connector

A water pressure test was conducted at 2 times 376kg/cm² for 30 min., and no change in the transmission loss of optical fibers, continuity and insulation resistance of insulated metal conductors were observed, nor was a water leak. Furthermore, in a cyclic water pressure test, conducted at 100 times of 376kg/cm² for 5 min., by the same method as in item 3.2.(4), little change was observed. The test result is shown in Fig.22.

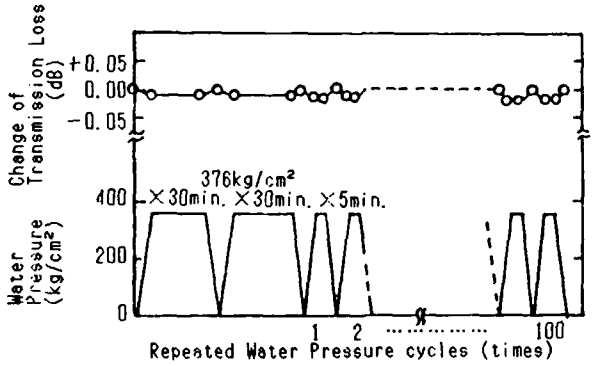

Fig. 22 Relation Between Repeated Water Pressure cycles and Transmission Loss

In addition, water pressure tests of 513kg/cm² for 30min.on the feed through elements of optical fiber and insulated metal conductor were also conducted satisfactorily.

6. Sea Trial

The Dolphin 3K system was equipped on a supporting mother ship and over 30 sea trials have been satisfactorily conducted in SAGAMI BAY by JAMSTEC, since last 1987, including a maximum dive to a depth of 3429m.

A large quantity of valuable information including images of the seabed and living creatures and samples of water, rocks were collected from the deep seabed.

The benefits of an unmanned deep submergence vehicle are that images and living creatures on the seabed are observed in realtime by many people on the mother ship via a high quality colour TV. monitor.

7. Conclusion

From the results of many sea trials conducted since last 1987, it has been proved that Dolphin 3K system with a tether cable, a mechanical cable termination and a optical/power composite underwater connector, are of sufficient quality and reliability for regular applications, including joint use with Shinkai 2000.

The speed of recent technical innovation has been remarkable, and the development of unmanned deep-water submergence vehicles capable of operating at a depth of 10,000m using an approximately 13km long cables without a repeater for optical fibers and higher voltage electricity is now under consideration.

In the future, the authors will approach more difficult themes by applying knowledge and techniques gained from the development of Dolphin 3K including the development of this new system.

The authors wish to acknowledge the joint developers, the members of Japan Marine Science and Technology Center (JAMSTEC) and also member of Mitsui Engineering and Ship Building Co. Ltd. (MES).

Yoshioki Shingo

Fujikura Ltd.
9-1 Futaba-cho,
Numazu City,
Shizuoka 410, Japan

Yoshioki Shingo was born in 1941 and graduated from Chiba University with a B.E. degree in electrical engineering in 1965. He jointed Fujikura Ltd. in 1965 and has been engaged in development and manufacturing of insulated wires and cables. He is now a maneger of manufacturing department in Numazu plant.

Tetsuya Kamijyo

Fujikura Ltd.
1-5-1 Kiba Koto-ku
Tokyo 135, Japan

Tetsuya Kamijyo was born in 1943. He jointed Fujikura Ltd. after his graduation from Waseda University with B.E. degree in electrical engineering in 1968 and has been engaged in design of insulated cables. He is now an engineer of oceanic cable development department.

Kiichi Kaneko

Fujikura Ltd.
1-5-1 Kiba Koto-ku
Tokyo 135, Japan

Yiichi Kaneko was born in 1952. He jointed Fujikura Ltd. after his graduation from Kyusyu Institute of Technology with B.E. degree in electrical engineering in 1974 and has been engaged in design of insulated cables. He is now an engineer of insulated cable engineering section.

Yuji Urabe

Fujikura Ltd.
1-5-1 Kiba Koto-ku
Tokyo 135, Japan

Yuji Urabe was born in 1951. He jointed Fujikura Ltd. after his graduation from Ibaraki University with B.E. degree in electrical engineering in 1974 and has been engaged in design of electric power distribution systems. He is now an engineer of distribution system engineering department.

Akio Mogi

Fujikura Ltd.
1440 Mutsuzaki,
Sakura,
Chiba 285, Japan

Akio Mogi was born in 1946. He jointed Fujikura Ltd. after his graduation from Haneda Institute High School in 1967 and has been engaged in reseach and development of the matalic cables and optical cable. He is now an engineer of optical fiber and cable section and member of the IECE of Japan.

Mineaki Naruse

Fujikura Ltd.
9-1 Futaba-cho,
Numazu City,
Shizuoka 410, Japan

Mineaki Naruse was born in 1955 and graduated from Iwate University with a B.E. degree in electronical Engineering in 1982. He jointed Fujikura Ltd. in 1982 and has been engaged in development and manufacturing of insulated wires and cables. He is now an engineer of oceanic cable development department.

A MICROCOAXIAL CABLE FOR HIGHLY PACKED HIGH BIT RATES DIGITAL MULTIPLEXERS

Carlos BLANCO Susana CAMARA Carlos G. CORTINES

ALCATEL STANDARD ELECTRICA, S.A.
Maliaño, Cantabria, Spain

SUMMARY

The use of microelectronics in Digital Multiplexers has increased its packing density. It has been necessary to develop a minicoaxial cable which maintains a high quality in its transmission parameters; special attention has been given to the cable return loss, far end cross talk and transfer impedance. The insulation process has been controlled very carefully to obtain a uniform diameter and expansion degree of the dielectric and a low return loss figure. The addition of a thin foil of aluminium polyester has improved significantly the far end cross talk figure of the cable.

INTRODUCTION

In central telephone exchanges digital multiplexer devices are connected to transmission line equipment by means of flexible coaxial cables which are grouped together in rather large bundles. Within these bundles, the coaxial cables run parallel to each other along distances that range from 30 to 100 m.

The electronic devices are grouped together in racks and, at the moment, each rack contains four digital multiplexers.

As each multiplexer needs a total of 10 cables outputs, the total number of cables is 40 per rack.

With the application of LSI techniques to the construction of digital multiplexers, its packing density has been increased up to 16 multiplexers per rack. This means that the total number of cables in the bundles is 160 per rack.

With conventional coaxial cables, used till now, the access to the new multiplexer outputs is virtually impossible due to the fact that they are crammed into a very small space.

Therefore it has been necessary to develop a miniature flexible coaxial cable having transmission characteristics able to support digital rates of up to 8 Mbits.

As the new cables must run parallel to each other along the same distances as the conventional ones, no change must be made to their transmission characteristics except for the attenuation which must obviously be higher due to the smaller size of the new cable.

A parameter that has been found to be critical in high speed digital transmission is the return loss of the whole system. In order to maintain this loss at the specified level, a stringent requirement has been imposed to the cable intrinsic structural return loss.

Another parameter that has been necessary to control carefully is the transfer of energy between cables running parallel to each other for a long distance. This leakage of energy is regulated by the cable transfer impedance. However, an alternate approach to the evaluation of this influence is the measurement of the Far End Cross Talk between two short lengths of cables bound together as in a real installation.

From the mechanical construction point of view it has been necessary to design the cable with a maximum outer diameter of 3.3 mm in order to adapt it to the connectors used at the inputs and outputs of the digital multiplexer and transmission line equipment.

It has also been necessary to design the cable incorporating a drain wire to facilitate the soldering of the outer conductor of the cable to the body of the connector.

A final consideration concerning the cable jacket is that it has been chosen with good flame retardant and abrasion resistance properties since the cable is intended for indoor installations.

CABLE DESIGN

Two different approaches have been followed to design the cable. In both of them bare copper was used for the central conductor. As the diameter of the cable is small it is not necessary to use a stranded conductor. Also common to both alternatives is the use of foamed polyethylene as dielectric.

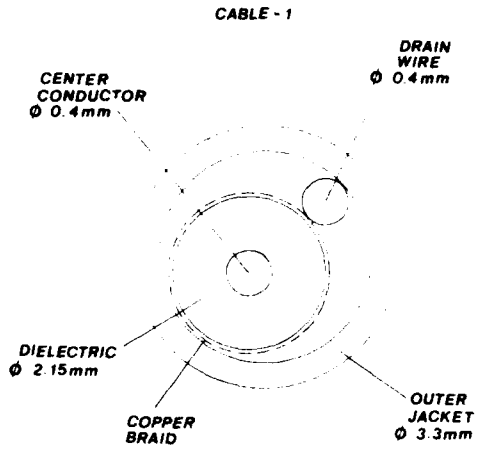

FIG. 1: Cross section of cable 1

The distinctive element between the two cables is the outer conductor.

The first approach incorporates a tinned copper braid, of a high covering factor, applied over the dielectric and the drain wire. Fig. 1.

The second approach has an outer conductor made of a thin film of a polyester-aluminium laminate overlapped and longitudinally applied over the dielectric. Fig. 2.

Over it a tinned copper braid, of a lower covering factor, has been applied. The drain wire is placed between the aluminium-polyester foil and the copper braid.

In both types of cable, the jacketing material used was PVC which is a good compromise between reasonable flame retardant properties and low cost.

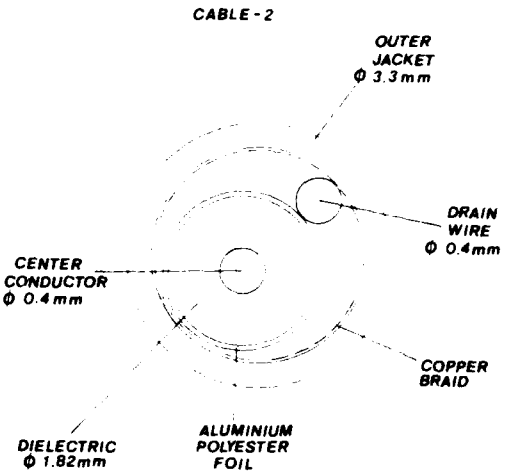

FIG. 2: CROSS SECTION OF CABLE 2

Because of the similarities between the two cable constructions the analysis that follows will only be applied to the first prototype.

The characteristic impedance of the cable was determined by that of the multiplexer whose value is 75 ohm.

Based on the well-known expression of the impedance of a braided coaxial cable.

$$Z_o = \frac{138.2}{\sqrt{\varepsilon_r}} \log_{10} \frac{D_1 + 1.5\, d_w}{k_1 d} \quad (1)$$

where:

ε_r = Relative permitivity of dielectric

D_1 = Diameter over dielectric

d = Over-all diameter of inner conductor

k_1 = Effective diameter factor ($k_1 = 1$ for bare conductors)

The following geometrical design was used

$$D_1 = 2.15 \text{ mm}$$

$$d = 0.4 \text{ mm}$$

$$d_w = 0.13 \text{ mm}$$

Using the above expression of the impedance the resultant permittivity is

$$\sqrt{\varepsilon_r} = 1.415 \text{ hence } \varepsilon_r = 2.00$$

As the permittivity of solid polyethylene is 2.28 this indicates that the insulation requires a certain degree of expansion.

The resultant mutual capacitance of the cable is obtained from the expression

$$C = \frac{\sqrt{\varepsilon_r}}{c\ Z_o} \qquad (2)$$

where: $c = 3\ 10^8$ m/sec.

Entering into this expression the values obtained previously we get for the mutual capacitance the figure of **C = 63 nF/km.**

A requirement imposed by the transmission equipment is that the cable attenuation at 4 Mhz must be kept below 4 dB/100 m.

To verify that this requirement can be adequately met with the dimensions and values used in the design the following expression was used[1].

$$\alpha = \alpha_{c1} + \alpha_{c2} + \alpha_{c3} =$$

$$= \frac{2.2870\ \ 10^{-3}\ \sqrt{\varepsilon_r}\ f}{\log_{10} \frac{D_1}{k_1\ d}} \left[\frac{k_3\ k_t \sqrt{C_1}}{d} + \frac{k_b\ k_t \sqrt{C_2}}{D_1} \right] +$$

$$+ 1.0470\ \ 10^{-4} \sqrt{\varepsilon_r}\ f\ \ \text{tg}\ \delta \text{ (nep/cm)} \qquad (3)$$

where:

f = Frequency in Mhz

k_3 = Voltage gradient factor (k_3 = 1 for bare conductors)

k_t = Coating factor (k_t = 1 for pure copper)

k_b = Braiding factor (it is a function of the diameter of the dielectric. (For D_1 = 2.15 mm, k_b = 1.7).

C_1 = Resistivity of inner conductor

C_2 = Resistivity of outer conductor

tg δ = Tangent of loss angle of dielectric

Using the values of

$C_1 = C_2 = 1.7241\ 10^{-6}$ ohm/cm (pure copper)

tg $\delta = 5\ 10^{-4}$ (slightly foamed polyethylene)

The resultant attenuation is $3.85\ 10^{-5}$ nep/cm or its equivalent 3.35 dB/100 m, which is lower than the especified value.

To determine the expansion degree of the polyethylene that must be extruded to form the dielectric of the cable, the following formula was used

$$B\ (\%) = 100 \left(1 - \frac{\varepsilon_r - 1}{1.28} \right) \qquad (4)$$

This expression takes into account the different specific gravities of both foamed and solid polyethylene.

Entering into expression **(4)** the relative permittivity obtained above, we can determine the expansion degree that must be given to the polyethylene by the extrusion line. The figure obtained is 22 %.

As mentioned previously a critical parameter that must be controlled very carefully in a high data rate link between a digital multiplexer and its corresponding transmission line equipment, is the return loss. In order to maintain this parameter as low as possible, the cable joining both devices must also have a very low structural return loss figure.

It is a very well-known fact that the impedance regularity of a coaxial cable (return loss) is directly related to the extrusion uniformity of its dielectric. Even small variations in the insulating material diameter or expansion degree can have detrimental effects on the final cable return loss, specially if these variations are regularly spaced.

In consequence, if we want to maintain the final return loss of the cable below a certain level, it is of primary importance to evaluate the maximum deviation allowed to the diameter and expansion degree of the dielectric.

In evaluating this parameter what concerns us are the highest peaks which are obtained at a certain number of critical frequencies and their corresponding overtones.

At these frequencies the return loss of a coaxial cable is given by the following expression[2,3]

$$PR = -20 \log_{10}\left\{ \rho_{12}\, e^{-2\alpha L_1} \cdot \sqrt{\sin^2 2\pi t_2 + \left[\cos 2\pi t_2 - (1-\rho_{12}^2)\, e^{-2\alpha L_2}\right]^2} \cdot \frac{1-\left[(1-\rho_{12}^2)\, e^{-\alpha(L_1+L_2)}\right]^{2n}}{1-\left[(1-\rho_{12}^2)\, e^{-\alpha(L_1+L_2)}\right]^2} \right\} \quad (5)$$

where:

ρ_{12} = Reflection coeffient between two irregularities

L_1, L_2 = Physical length of each irregularity

t_1, t_2 = Propagation times in the irregularities

n = Number of irregularities in a certain length of cable

If there is perfect symmetry of the irregularity and if $\rho_{12} \ll 1$, we can express the reflection coefficient at the critical frequency as follows[3]

$$\rho_{12} = \frac{(1 - e^{-\alpha L})\, 10^{-PR/20}}{e^{-\alpha L}\,(1 - e^{-2\alpha Ln})} \quad (6)$$

Using the expression of the impedance given by equation (1) we can express the differential variation of the diameter of the dielectric as follows

$$dD_1 = \frac{D_1 + 1.5\, d_w}{60.02} \sqrt{\varepsilon_r}\; dZ_o \quad (7)$$

Finally, based on the relation between the differential impedance variation and the reflection coefficient of an irregularity we obtain[3]

$$dD_1 = \frac{D_1 + 1.5\, d_w}{60.02} \sqrt{\varepsilon_r}\; 2Z_o \frac{(1-e^{-\alpha L})\, 10^{-PR/20}}{e^{-\alpha L}\,(1 - e^{-2\alpha Ln})} \quad (8)$$

This expression shows that the differential variation of the diameter of the dielectric is a function of frequency and if we, therefore, wish to obtain the worst return loss peak, calculations must be carried out in a complete range of frequencies.

Assuming critical frequencies of 10 and 100 Mhz respectively and a cable return loss figure greater than 20 dB in 100 m, table I shows the tolerance allowed in the diameter of the coaxial cable insulation at these critical frequencies.

TABLE 1

Frequency (Mhz)	Cable Attenuation (nep/m)	Cable RL (dB)	dD_1 (mm)
10	0.0060	20	0.070
100	0.023	20	0.020

In other words, when the operating frequency increases and if a certain value of return in the cable is to be met, a stricter control of the extruded diameter of the insulation must be maintained.

The other parameter that is controlled during the extrusion process of the dielectric is the uniformity of the dielectric permittivity, which in turn, is controlled through the coaxial capacitance of the insulated wire.

If we combine equations (1) and (2) we can obtain[3]

$$d\varepsilon_r = \frac{(\sqrt{\varepsilon_r})^3}{(-\tfrac{1}{2})\, 138 \log_{10} \frac{D_1 + 1.5\, d_w}{k_1 d}}\, dZ_o \quad (9)$$

and

$$dC = -2\, \frac{\sqrt{\varepsilon_r}}{c Z_o^2}\, dZ_o \quad (10)$$

Using now the relation between the differential impedance variation and the reflection coefficient, the differential variation of the coaxial capacitance of the dielectric is expressed as follows[3]

$$dC = 4 \frac{\sqrt{\varepsilon_r}}{cZ_o} \frac{(1 - e^{-\alpha L})\ 10^{-PR/20}}{e^{-\alpha L}\ (1 - e^{-2\alpha Ln})} \qquad (11)$$

Using the values obtained previously for the reflection coefficient at frequencies of 10 and 100 Mhz to get a minimum return loss of 20 dB in 100 meters we obtain

TABLE II

Frequency (Mhz	Cable RL (dB)	dC (pF)
10	20	2.36
100	20	0.65

These results indicate that, the same as in the case of the control of the diameter of the insulation, the higher the operational frequency, the smaller the tolerance that can be allowed to the coaxial capacitance of the extruded material.

Fig. 3 is a chart of the continuous monitoring carried out on this parameter during the extrusion manufacturing process.

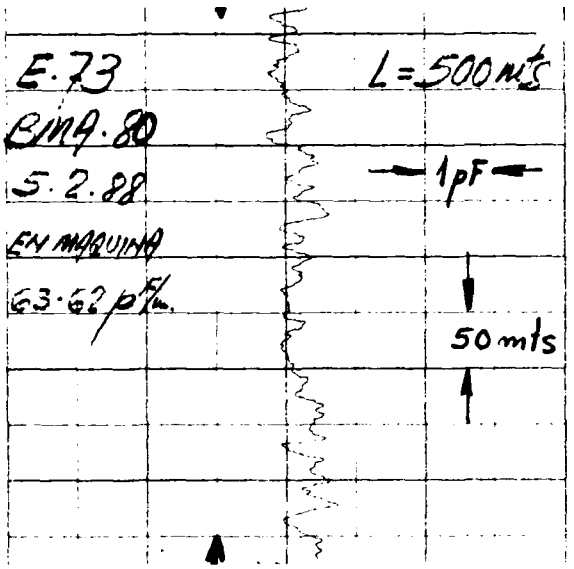

Fig. 3: CONTINUOUS COAXIAL CAPACITANCE. MONITORING

Due to the small diameter of the cable there are two parameters which might be considered as a cause of concern, i.e. the r.m.s. voltage under continuous operation and the maximum power rating the cable has to withstand.

When specifying dimensions and the type of material used as dielectric, 2000 volts was the minimum r.m.s. voltage allowed for continuous operation.

To prove that the selected cable design really conforms to the safe r.m.s. value mentioned above, the following equation can be used

$$U = \frac{0.081\ Ed}{k_2} \log_{10} \frac{D_1}{k_1 d} \text{ (kV)} \qquad (12)$$

where:

E = Voltage gradient at inner conductor (peak value) in kV/cm.

Taking the figure of 100 kV/cm for E, as corresponds to a low expanded polyethylene, we obtain

$$U = 2{,}36 \text{ kV}$$

which is well over the required limit.

The second critical parameter to consider is the maximum power rating to be transmitted. Although the cable is not intended to be used immediately after the transmission line equipment, where the output power is maximum, a figure of 100 watts is considered as a safe minimum at ambient temperatures of 40ºC.

Taking the expression of the total temperature rise of inner conductor above ambient temperature we get[4]

$$T_c = H_o \left\{ \frac{\alpha c_1 + \frac{1}{2}\alpha c_3}{\alpha} \frac{G_d}{2\pi} \text{Ln} \frac{D_1}{k_1 d} + \frac{G_c}{2\pi} \text{Ln} \frac{D_s}{D_o} \right\}^{4/5} + \left\{ \frac{H_o}{10\pi D_s k_h} \right\} \qquad (13)$$

where:

G_d, G_c = Thermal resistivities of dielectric and sheath

D_o and D_s = Inner and outer diameter of the jacket

k_h = Thermal dissipation constant for cable surface exposed in air

(For a cable of a diameter of 3,4 mm, k_h is equal to 8 10^{-4} W/ºCm^2)

Entering into this expression the values used for the cable design we obtain

$$\alpha_{c1} = 0{,}0399 \text{ dB/km}$$
$$\alpha_{c2} = 0{,}0126 \text{ "}$$
$$\alpha_{c3} = 0{,}000643 \text{ "}$$

The expression for T_c is

$$T_c = 0.9568 \; H_o + \left(\frac{H_o}{0.0854}\right)^{4/5} \qquad (14)$$

Using a value of 45ºC for the total temperature rise over an ambient temperature of 40ºC, the dissipation factor obtained is

$$H_o = 8 \text{ watts/m}$$

The maximum power rating is related to the dissipation factor by the expression

$$P_o = 8.686 \frac{H_o}{2 \alpha_{T_c}} \qquad (15)$$

where:

α_{T_c} = Cable attenuation at T_c with a temperature coefficient of 0.20 % per degree celsius.

Using this expression we obtain for the maximum power rating the value of

$$P_o = 532 \text{ watts}$$

which is well over the required safe minimum of 100 watts.

Finally, the cut-off frequency for the excitation of higher modes, different to the TEM's, is not important to this cable due to its small dimensions. The calculated cut-off frequency is in the order of 50 Ghz well in excess of the range of the utilization of the cable.

Based on the design considerations seen so far, Table III summarizes the details of the construction of both cables.

TABLE III

	Cable 1	Cable 2
1. CENTER CONDUCTOR		
. Material	Plain-Cu	Plain-Cu
. Diameter (mm)	0.4	0.4
2. DIELECTRIC		
. Material	Foam-PE	Foam-PE
. Expansion degree (%)	22	36
. Tolerance of the coaxial capacitance (pF)	± 0.6	± 0.6
. Diameter (mm)	2.15	1.82
. Tolerance of the diameter of the dielectric (mm)	± 0.02	± 0.02
3. OUTER CONDUCTOR		
3.1. Foil tape		
. Material	-	Aluminium polyester
. Width (mm)	-	10
. Thickness (mm)	-	0.031
3.2. Braid		
. Material	Tinned Cu	Tinned Cu
. Groups	16	16
. Wires/group	4	5
. Wire diameter	0.13	0.1
. Lay length (mm)	9	20
. Coverage	92 %	88 %
3.3. Drain wire		
. Material	Tinned Cu	Tinned Cu
. Diameter (mm)	0.4	0.4
4. OUTER JACKET		
. Material	PVC	PVC
. Outer diameter (mm)	3.3	3.3

As can be seen, cable no. 2 has a smaller dielectric diameter than cable no. 1 in order to accomodate the additional aluminium-polyester foil. However, as both cables must have equivalent transmission characteristics, this smaller diameter is compensated with a larger expansion degree of the polyethylene.

Table IV summarizes the electrical and mechanical requirements that the cable must comply with, and that have been used as references in the cable design process.

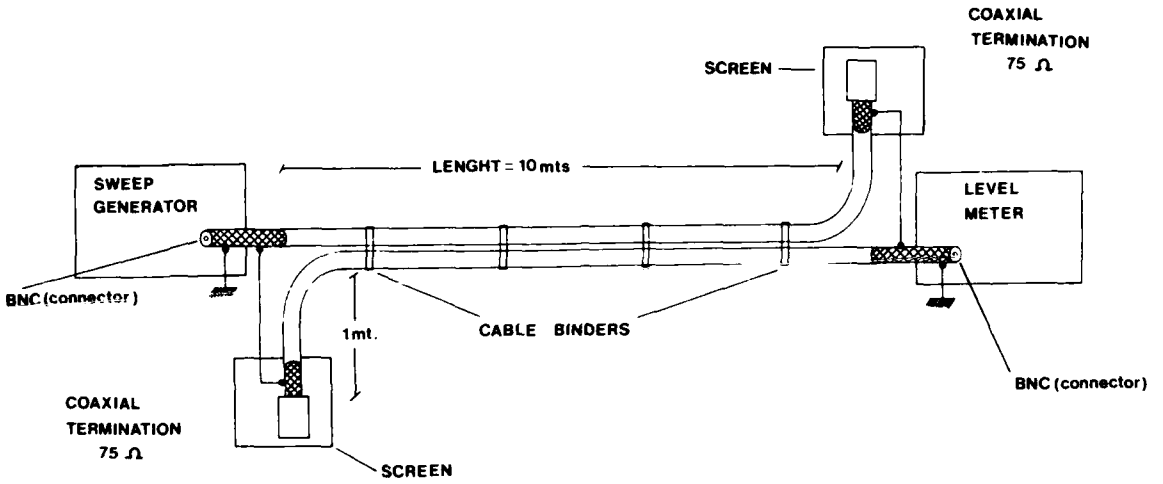

Fig. 4: FAR END CROSS TALK MEASUREMENT SEP UP

TABLE IV

PARAMETERS (at 20ºC)	Value
1. Characteristic impedance	75 ohms
2. Mutual capacitance	< 65 nF/km
3. Dielectric strength (r.m.s.) (1 minute, 50 Hz)	> 2 kV
4. Attenuation. (Min. length 100 m) (f=4 Mhz)	< 4 dB/100 m
5. Structural Return Loss. Frequency range 1 Mhz-100 Mhz (Length 100 m)	> 20 dB
6. Minimum power rating	100 watts
7. Far End Cross Talk Frequency range 1 Mhz - 100 Mhz (Length 10 m)	> 90 dB
8. Elongation at break	
. Center conductor	10 % min.
. Jacket (Not aged)	200 % min.
. Jacket (Aged 5 days, 100ºC)	150 % min.
9. Tensile strength	
. Jacket (Not aged)	125 kg/cm^2 min.
. Jacket (Aged 5 days, 100ºC)	94 kg/cm^2 min.

CABLE MEASUREMENTS

In order to verify the performance of both cable types a measurements program was set up. All measurements were carried out using standard equipment and none of it required any special arrangement.

As mentioned before, the installation of these cables is carried out in bundles that run along lengths that can be as long as 50 m. Taking into account the braiding construction of the outer conductor a parameter of concern is the leaking of energy from two cables which run one beside the other. This is the aim of specifying a value for the Far End Cross Talk between two cable lengths running parallel to each other.

The required test consisted in a standard End Cross Talk measurement in which the two coaxial cables were bound together in a length of 10 m and in which the braids in both cables were connected to each other and to the earth of the equipment.

Fig. 4 shows a sketch of the measurement set up.

In order to avoid the influence of pigtail and connecting pins both cable ends were directly soldered to the test equipment connectors.

The coaxial terminating loads were also soldered to the free cable ends and screened from outer interferences.

Both testing devices were placed back-to-back and at some distance apart.

The dynamic range of the test equipments is up to 130 dB and the frequency range from 10 Mhz to 1 Ghz.

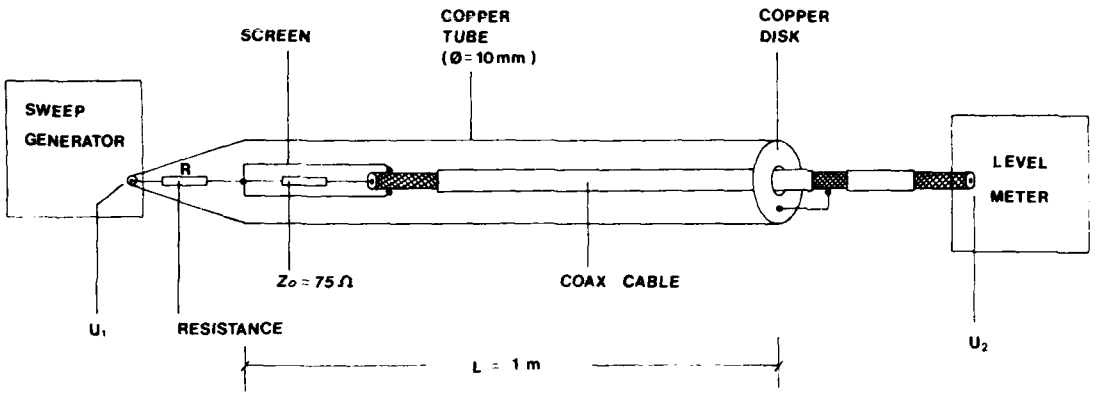

Fig. 5: TRANSFER IMPEDANCE MEASUREMENT SET UP

An alternative approach to measure the energy leak out of a coaxial cable is by means of the measurement of its transfer impedance.

The corresponding set up is shown in Fig. 5.

The principle of this measurement is to create a double coaxial structure. The outer structure (the one which causes the interference) consists of a copper tube and the braid of the coaxial cable. The inner structure (the one which receives the interference) is the coaxial cable actually being tested.

The signal which causes the interference is fed into the outer structure via a small resistance (R). This coaxial structure is terminated at the other end by a copper disc that acts as a short-circuit.

The signal induced into the coaxial cable under test is directly received by the level meter, and the far end of this structure is duly terminated with its characteristic impedance and conveniently screened to avoid picking up any unwanted signal.

The short-circuiting disc of the outer copper tube is connected to the coaxial cable braid and as in the Far End Cross Talk measurements, the coaxial cable end is directly soldered to the connectors of the test equipment.

The following equation gives the modulus of the transfer impedance[5]

$$Z_T = \left(\frac{2R}{L}\right) \cdot \left(\frac{U_2}{U_1}\right) \cdot \frac{(1-n^2)\, u \sqrt{\cos^2 u + m^2 \sin^2 u}}{\sqrt{n^2 (\cos u - \cos nu)^2 + (\sin u - n \sin nu)^2}} \qquad (16)$$

where:

$m = \frac{1}{R}$ (Impedance of the outer structure)

$n = \frac{\lambda_1}{\lambda_2}$

$u = \frac{2 \pi L}{\lambda_1}$

λ_1, λ_2 = Wavelengths of the outer and inner structures

In order to avoid any standing wave phenomena, the system must not be used with wavelengths smaller than 10 L, where L is the copper tube length.

Experience has demostrated that a suitable value for parameter m should be more or less 0.7.

Parameter n can be calculated as follows

$$n = \frac{\lambda_1}{\lambda_2} = \frac{c/\sqrt{\varepsilon_1}}{c/\sqrt{\varepsilon_2}} = \frac{\sqrt{\varepsilon_2}}{\sqrt{\varepsilon_1}}$$

where, ε_2 and ε_1 are the relative permittivity of the dielectrics of the inner and outer structures.

An approximate value for Z_1, is

$$Z_1 = \frac{138}{\sqrt{\varepsilon_1}} \log_{10} \frac{\text{ø copper tube}}{\text{ø over braid}} \qquad (17)$$

Using the numerical values seen in Fig. 5 we obtain

$$Z_1 = 63 \text{ ohms}$$

$$R = 88 \text{ ohms}$$

$$n = 1.4$$

$$u = \frac{2\pi f(\text{Mhz})}{300}$$

It can be demostrated that the expression

$$\frac{(1-n^2)\, u \sqrt{\cos^2 u + m^2 \sin^2 u}}{\sqrt{n^2 (\cos u - \cos nu)^2 + (\sin u - n \sin nu)^2}}$$

takes a value close to one for frequencies ranging from 0.05 Mhz up to 50 Mhz.

Based on the above considerations, the test frequency should not be increased beyond the frequency corresponding to:

$$0.1\, \lambda_1 = 1 \text{ m}$$

$$\lambda_1 = 10 \text{ m} \qquad f_1 = 30 \text{ Mhz}$$

RESULTS

Table V and Fig. 6 to 15 summarize the results obtained on the tests carried out on both cables.

TABLE V

	Cable 1	Cable 2
1. Characteristic impedance (ohms)	Fig. 6	Fig. 7
2. D.C. Resistance (ohms/km)		
. Inner conductor	129	131
. Outer conductor	15	23
3. Mutual capacitance (nF/km)	65	65
4. Dielectric Strength (kV) (1 min, 50 Hz)	2.5	2.3
5. Insulation resistance (Mohms/km) (1 min, 500 V_{DC})	100,000	90,000
6. Attenuation	Fig. 8	Fig. 9
7. Return Loss (L = 100 m)	Fig. 10	Fig. 11
8. Far End Cross Talk (L = 10 m)	Fig. 12	Fig. 13
9. Transfer impedance	Fig. 14	Fig. 15
10. Elongation at break (%)		
. Center conductor	13 %	13 %
. Jacket (Not aged)	200 %	200 %
. Jacket (Aged)	170 %	170 %
11. Tensile strength (kg/cm^2)		
. Jacket (Not aged)	186	190
. Jacket (Aged)	150	160

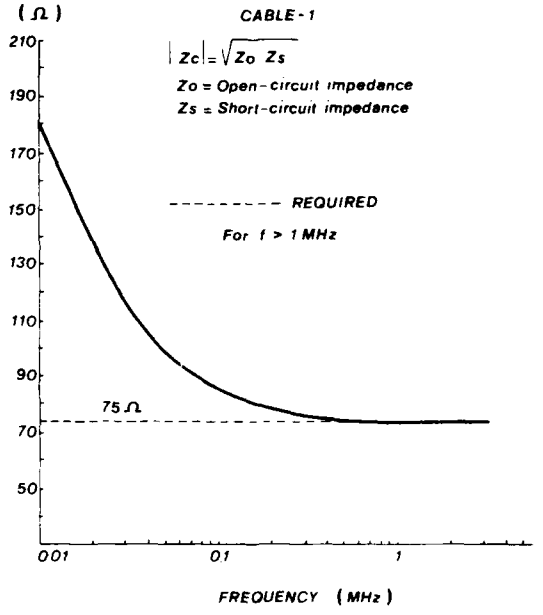

Fig. 6: CHARACTERISTIC IMPEDANCE OF CABLE TYPE 1

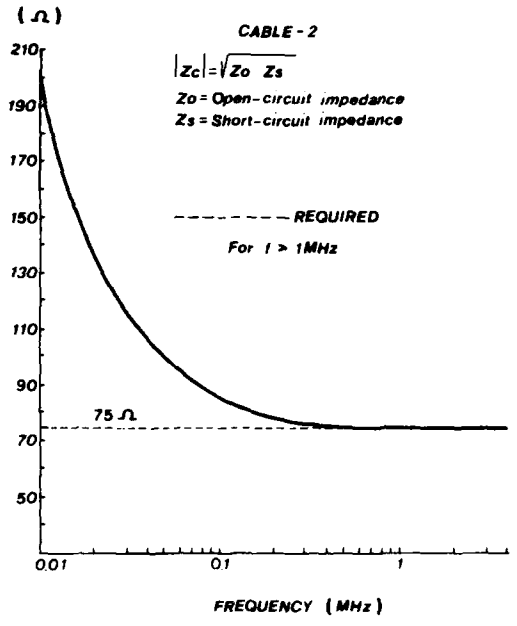

Fig. 7: CHARACTERISTIC IMPEDANCE OF CABLE TYPE 2

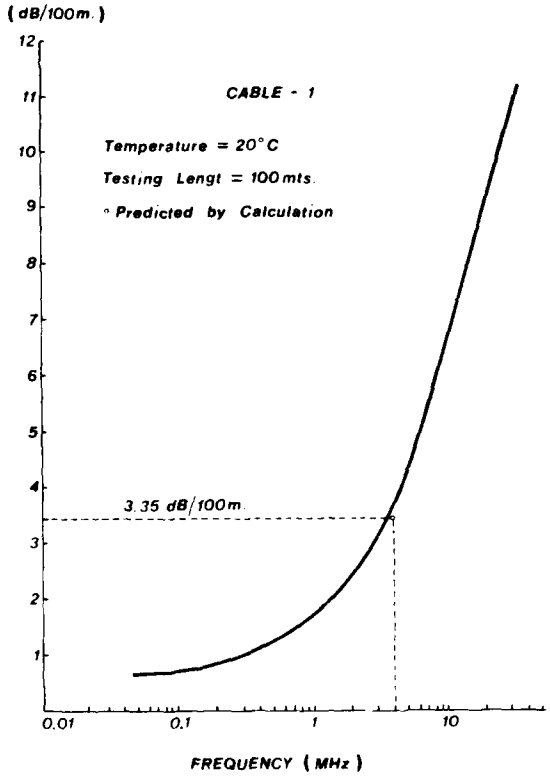

Fig. 8: ATTENUATION OF CABLE TYPE 1

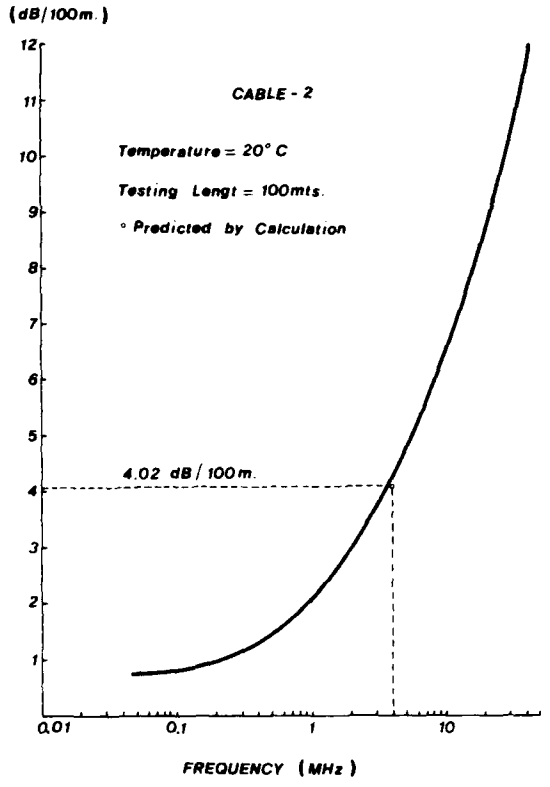

Fig. 9: ATTENUATION OF CABLE TYPE 2

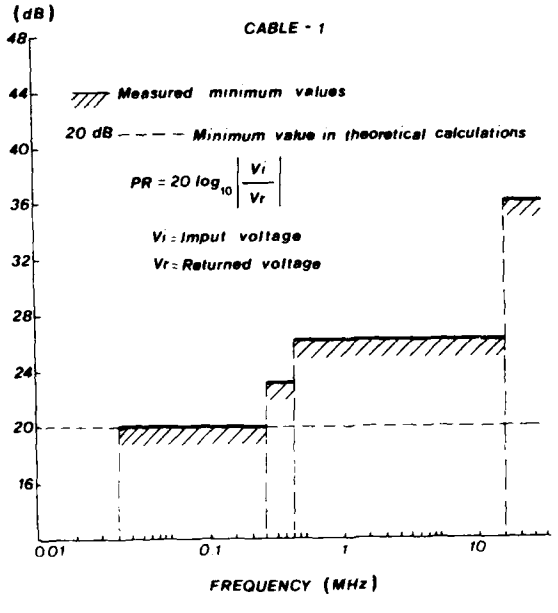

Fig. 10: MINIMUM RETURN LOSS VALUES ON CABLE TYPE 1

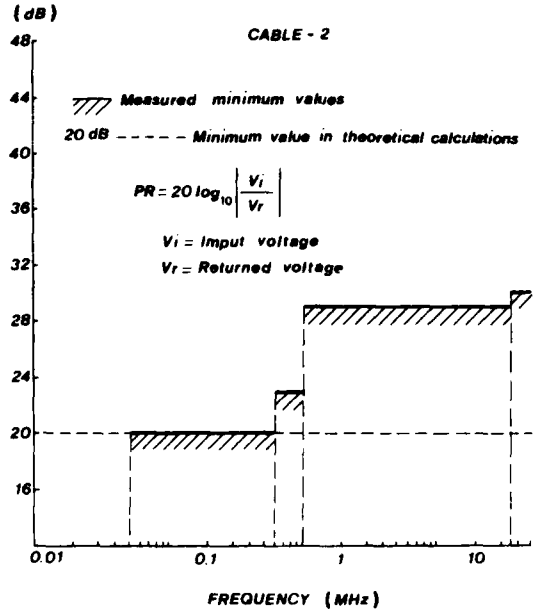

Fig. 11: MINIMUM RETURN LOSS VALUES ON CABLE TYPE 2

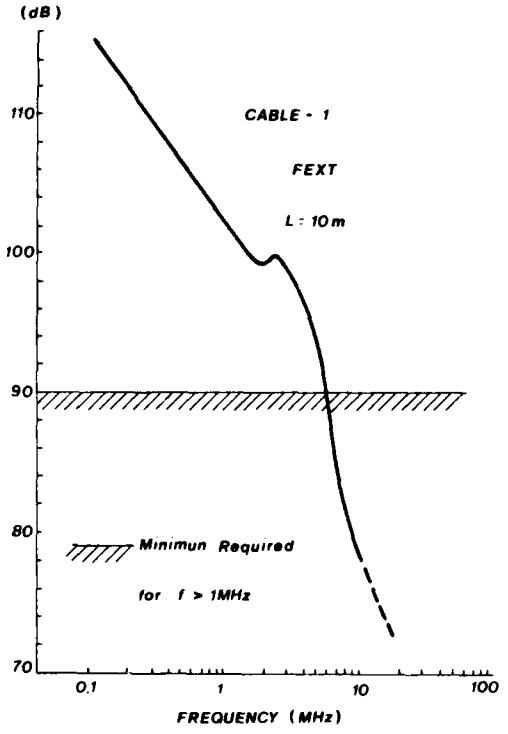

Fig. 12: FAR END CROSS TALK ON CABLE 1

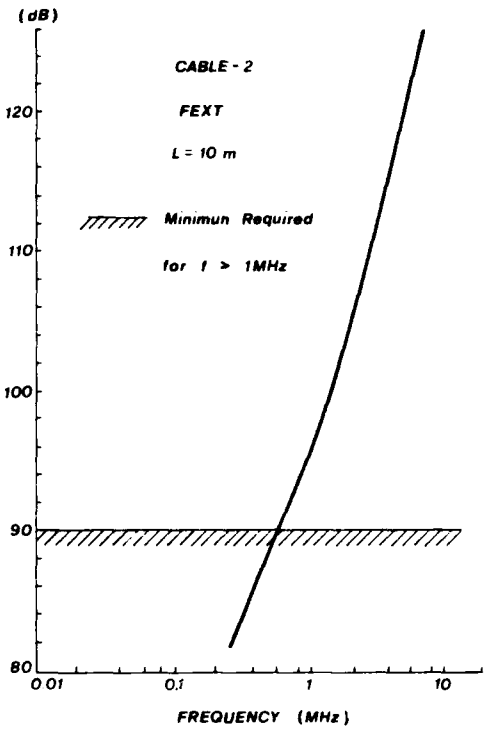

Fig. 13: FAR END CROSS TALK ON CABLE 2

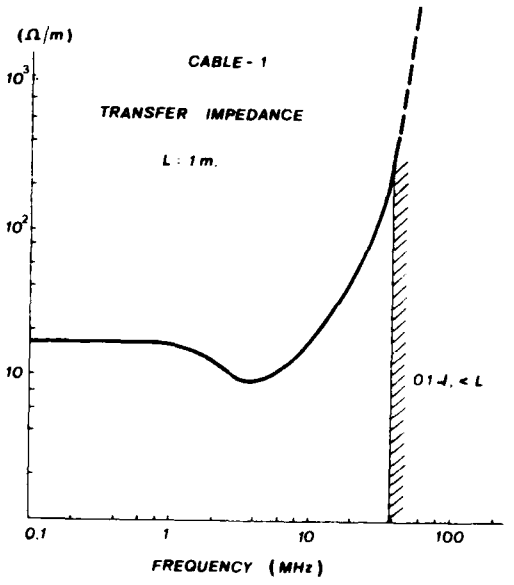

Fig. 14: TRANSFER IMPEDANCE ON CABLE 1

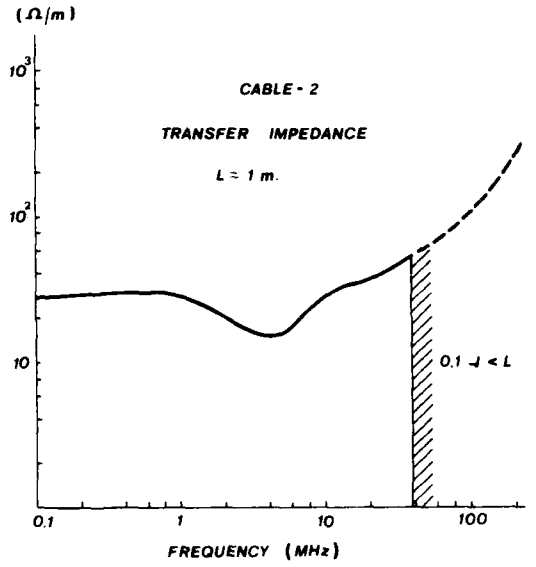

Fig. 15: TRANSFER IMPEDANCE ON CABLE 2

CONCLUSIONS

The analysis of the results obtained after the evaluation of both cables provides us with some conclusions of interest.

As we can see on Fig. 10 and 11 the return loss of the cable which has a dielectric with a lower expansion degree (cable 1) is significantly better than that of the other cable which has a dielectric with a larger expansion degree.

This was anticipated in the theoretical analysis made on the cable design section. As mentioned there, maintaining the uniformity of the characteristics of the dielectric is absolutely essential if a good return loss figure is to be obtained. Due to the inherent difficulty in maintaining the uniformity of both the diameter and the expansion degree, in a foamed insulating material, its performance is appreciably inferior to the corresponding solid version.

From Fig. 12 and Fig. 13 we can see that the effect of adding a thin foil tape to the copper braid to form the outer conductor has a dramatic effect on the Far End Cross Talk performance of the cable. Actually cable 1 was unable to meet the required FEXT figure of 90 dB for frequencies higher than 10 Mhz.

Moreover, the behaviour of both curves vs. frequency is completely different ie. while in cable 2 the FEXT figure increases from 1 up to 10 Mhz, the behaviour of cable 1 is the exact opposite. The values obtained beyond the frequency of 10 Mhz cannot be taken into consideration because of the effect of standing waves in the short length of cable under study.

This conclusion is consistent with the results obtained in Fig. 14 and Fig. 15 for the transfer impedance of both cables. The addition of a laminated aluminium foil to the copper braid, closes the loopholes of the outer conductor to electromagnetic radiation, providing a much lower transfer impedance than that of the cable which only has a single copper braid.

REFERENCES

R.1 R.C. Mildner. Journal of the Institute of Electrical Engineers No. 93, III (24) July 1946.

R.2 J.A. Olszewsky and H. Lubars. "SRL phenomenon in coaxial cables". Proceedings of the IEEE. Vol. 58 No. 7, July 1979, pp. 1036-1050.

R.3 C. Blanco. "Perturbations in a wide band transmission over coaxial cable due to regularly spaced irregularities". E.T.S.I.T. Madrid 1972.

R.4 R.C. Mildner. Transaction of the American Institute of Electrical Engineers, 68 I 289, 1948.

R.5 IEC Recommendation No. 96-1 Screening Efficiency 5.2.2. Test procedures.

CARLOS BLANCO received his Doctorate Degree in Telecommunications Engineering from Madrid University in 1972. He also received his Master Degree in Physics from Santander University in 1976. He joined ITT, STANDARD ELECTRICA in Spain in 1971 as R & D Manager of the Telephone Cable Division.

During 1982-1984 he joined ITT, ELECTRO OPTICAL PRODUCTS DIVISION in Roanoke, Virginia as Senior Scientist in the Optical Fiber R & D Department.

During 1987 he joined TELCOR (TELEFONICA CORNING GLASS) as Technical Director of the Optical Fiber Manufacturing Plant.

Since 1972 he has acted as part time Professor of the Electrical Engineering Department of the Santander University.

During 1983 he was nominated Adjunct Professor of the Electrical Engineering Department of the Virginia Politechnic Institute and State University, in Blacksburg, Virginia, lecturing on Optical Fibers and Optical Communications.

Presently, Dr. Blanco is with ALCATEL STANDARD ELECTRICA in Spain as Manager of the New Products Development Department.

SUSANA CAMARA received her Master Degree in Chemistry from Oviedo University in 1984, where she specialized in Organic Chemistry.

She joined ALCATEL STANDARD ELECTRICA in 1987 where she presently works in R & D Materials Department.

CARLOS G. CORTINES was born in 1944. In 1968 he graduated from Valladolid University with a Degree in Physics. He joined STANDARD ELECTRICA, ITT, today ALCATEL, and worked in the Engineering Department of the Telecommunication Cables Division. From 1982 he is the head of the Optical Fiber Development Group in ALCATEL STANDARD ELECTRICA, Cable Factory in Maliano-Cantabria.

MINI QUAD THE WAY FORWARD FOR SUBMARINE TOWED ARRAY CABLE

Dr. Trevor R. Smith

STC Cable Systems Division, Newport, Gwent, NP9 OWS, U.K.

Abstract

Current submarine tow cable systems are usually based on a standard quad core design, or a coaxial cable, which are encased in cellular material to achieve a neutral buoyancy. However, cellular materials are compressible and under pressure will be compacted and thus the neutral buoyancy can be affected. This can significantly influence operating parameters.

From a systems analysis of existing towed array cable, it becomes apparent that it was feasible to design a new generation of thin line hard wire cables which met the signals requirement and were neutrally buoyant. The reduction in copper cross-section area and the use of Kevlar fibres, reduced the overall diameter, without the need to introduce cellular foam, and enhanced the operational performance of the cable system. It also allowed existing handling equipment to be used.

The paper describes the design aspects of an operational 37 quad submarine tow cable referencing test programmes and towing at sea.

Introduction

Current submarine tow cable systems are usually based on a standard quad core design, or a coaxial cable, to a similar design as that used for surface ship applications. However for submarine application it is necessary to have the cable system designed for neutral buoyancy so that the cable remains in a horizontal position behind the submarine and does not tend to float or sink. This is particularly important since the density of sea water can vary and sudden change of isotherms can occur, both of which can have a significant impact on operational performance of the submarine whether it be a hunter or a target.

Since most of the conventional cable systems would be too dense, it is usual to encase the core in a cellular material to achieve the neutral buoyancy. However cellular materials are compressible and under pressure will be compacted thereby affecting the buoyancy. It was considered that the use of aramid fibre reinforcement in place of steel armour wire could reduce or even eliminate the use of the cellular material.

As a result of a reappraisal of the problem a new and novel solution was developed based on a Mini Quad concept.

Systems Analysis

All tow cables have to be designed to meet a data transmission capability, limitations on cross talk and be capable of withstanding the mechanical loading associated with towing a body/array at speed.

It was quickly realised that a surface ships tow cable has to be longer than that for a submarine because of the need to get the cable down to an appropriate depth. As a consequence of the shorter length for submarine application the electrical parameters such as attenuation can be relaxed but still meet the overall systems requirement. Similarly the shorter length reduces the flow induced drag and therefore the mechanical loads are reduced.

Thus having established new parameters to be achieved, it was necessary to consider the design of the electric centre. Various forms of cables based on quads or pairs were theoretically appraised and compared with single and multi coaxial cables.

In order for a coaxial cable to replace a pair it is required to work at twice the data rate. For a coaxial pair to replace four quads then the coaxial system would have to operate at 8 times the quad frequency. Increasing the frequency increases the attenuation losses. Provided the power feeding and telemetry is capable of handling the data rates then a coaxial cable is a feasible solution in terms of electrical parameters. However, the system is vulnerable as one component failure leads to a total loss of transmission. There are also design problems associated with flexible coaxials pairs of conventional constructions in a tow cable configuration, namely inter pair crosstalk and fatigue failure in the outer conductors and in particular, the braided construction. Armoured tow cables have been successfully designed to survive fatigue endurance

testing and these usually have been based on a copper tape outer conductor.

However, in the case in question it was determined that systems vulnerability was a key operational factor and therefore the system dictated that a quad type construction should be used.

Mini Quad Design

In addressing the design of the cores it was realised that conventional quads were over designed for the operating requirements and that a reduced size of quad cable - so called Mini Quad would be adequate. There was only two problems. How could a fine wire quadded core be built which extended the manufacturing technology to its limits and would such a system withstand the mechanical loading?

A considerable amount of effort went into determining the process parameters evaluating materials to come to a satisfactory conclusion. Early attempts were not all successful due to a tendency for the wire to break during the stranding operation but all the problems were gradually overcome and a quad with a nominal diameter 1.35 mm produced. This can be compared with the standard quad with a nominal diameter of 2.79 mm (Figure 1)

Having established the size of the cores, a design of a 37 quad was established. This design utilised aramid fibre strength members in place of steel wires since aramid fibre has a much higher specific strength capability which was essential for the achievement of a neutrally buoyant cable.

It was found that the fretting and abrasion of the aramid fibre would be a long term problem for this type of cable and therefore consideration was given to the use of a resin impregnated aramid fibre, which is available as round or strip sections. These were successfully incorporated in the cable design. An oversheath of polyethylene was considered necessary to avoid problems of ultra-violet light degradation.

The final design for a 37 quad cable, illustrated in figure 2, produced a cable of 24.6 mm diameter compared with the standard cable design of 44.0 mm diameter.

The reduction in the amount of copper and the elimination of the steel armouring created a cable design which is neutrally buoyant and which does not suffer from the problem of compression affecting its density and hence its position relative to the submarine.

One of the spin off benefits from the design of the electric centre is the fact that it is a very flexible unit and it is now being considered for use in wiring harnesses for tow-bodies where space and accessibility are at a premium. The size and weight reductions in this cable system can improve the overall operational capability of the platform.

Termination

From the onset it was decided that the termination must be compatible with existing units and to meet the current operational characteristics. Fundamentally there were no problems from a design point of view. In order to achieve a full water blocking termination a glass to metal seal was adapted within a termination housing. It was more difficult to develop the processes and procedures from the practical point of view. It was necessary to develop the skills for handling small size conductors and specialist techniques had to be developed for taking the end loading. Techniques used for "potting" armour wire could not be readily used with the resin impregnated aramid fibre. An outline design is illustrated in Figure 3.

All these challenges were met and a satisfactory termination developed.

Trials

The proof of any system is in the physical performance and a major programme of evaluation was undertaken by the U.K. Ministry of Defence.

The following series of tests were undertaken.

(1) Tensile testing
(2) Torque balance evaluation under load
(3) Vibration testing
(4) Cyclic loading (Tension - Tension)
(5) Reeling tests
(6) Sea trials

Many of these tests were undertaken on equipment similar to that described in a paper by Smith and Carter at the 36th IWCS. (Ref. 1)

Obviously, the full data cannot be revealed but it is sufficient to report that the new Mini Quad system met all the land based test requirements and two systems were evaluated at sea to investigate the Mini Quad ability to perform under different operational circumstances. Again then trials were successful and the new cable system is being introduced into fleet service. The trials showed that the cable system could be used in place of all other submarine towed array cable systems and is compatible with existing cable handling facilities.

Conclusions

A novel design of submarine towed array cable has been developed having met all the system and operational requirements. This Mini Quad system is now being introduced into the fleet operation as an alternative to existing cable systems.

Reference 1 T. R. Smith and D. R. Carter. Fibre optics in dynamic strain cables, 36th IWCS, November 1987.

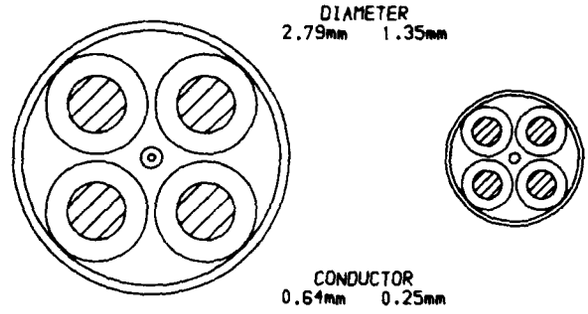

COMPARISON OF STANDARD AND MINI QUAD CORES

Figure 1

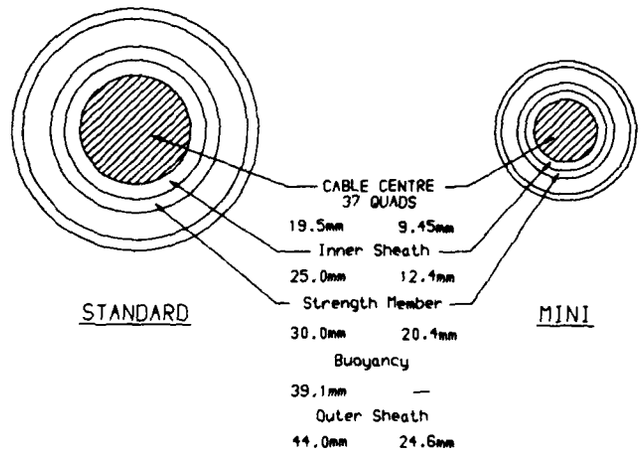

COMPARISON OF STANDARD AND MINI QUAD CABLES WITH 37 QUAD CENTRES

Figure 2

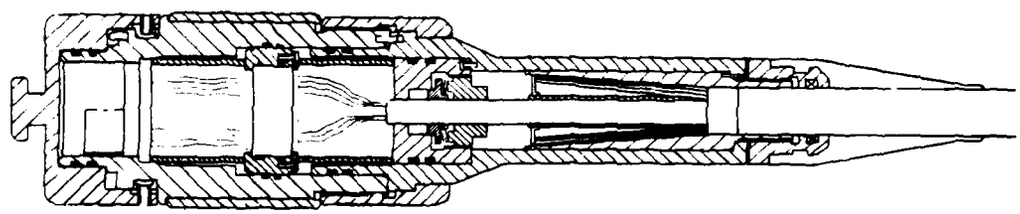

TERMINATION OF MINI QUAD CABLE

Figure 3

MAGNETIC MATERIALS IN TRANSMISSION LINES: THE MAGIC REDUCTION OF RESISTANCE AT HIGH FREQUENCIES

Simos D. Dadakarides

Department of Electrical Engineering
Stamford University
POB 10291, Stamford, CA 94309

ABSTRACT

A major new finding, a striking at a first sight phenomenon, is presented. In transmission lines with small amounts of magnetic material incorporated in their insulation losses at high frequencies are substantially reduced. In light of the marginal inductance increase, this behavior is attributed to the decrease of the induced eddy currents within the conductors. The incorporation of low-loss ferrites leads to optimized designs. Heavy doping provides advantageous distributed inductive loading but light doping is also beneficial. In both cases the formed hollow magnetic cylinders surrounding each conductor guide the magnetic field of adjacent current carrying elements. The reduction of the flux intercepting the conductors translates into reduced eddy currents, particularly at high frequencies. Nearly optimum operating condition is accomplished with low loss ferrites when mixture permeability is 10. Lightly doped cables still exhibit reduced losses, while all the other transmission characteristics, including impedance, remain practically unchanged. They can be used in new or old systems without terminal modifications. The light doping does not require major manufacturing process changes or speed reduction, which can be a drawback for heavily loaded cables. Experimental twinaxial cables with AWG20 stranded conductors show half the attenuation in the MHz's region, but no other major change.

INTRODUCTION

Information transmission systems can be divided into wired and wireless. For a number of years most of the attention and progress has been focused on wireless transmission, with the latest major achievement being communications satellites. At the same time wired systems have made little progress, with the exception of optical fibers which tend to revolutionize this field. Conventional metallic cables have reached a level of apparent perfection which advances only marginally. It seems as if metallic cables are destined to disappear. However, this pseudo-optimum is the limit for metallic cables which utilize conductors and insulators to transmit electromagnetic energy. A vital component is missing from these conventional cables and this is magnetic materials.

Transmission lines with much improved properties have been designed by incorporating low loss magnetic materials in the cable structure. Part of the insulation is occupied by a mixture of preferrably ferrite powder embeded in a suitable nonconducting matrix. Even though the permeability of the compound material is substantially lower than that of the ferrite used, for practical doping levels, it is adequate to result in much improved properties of the transmission line. The magnetic material acts in two distinctly different ways. It provides additional inductance, which compensates the insulation capacitance, and it modifies the current distribution over the conductors cross section. The first action, along with the desired properties of the magnetic material used, has been described by Dadakarides et.al[7]. The investigation of the second action, which is supported by experimental results, is the purpose of the present treatment. It starts with a short overview of key design guidelines which apply to all magnetically doped cables. Additional and new ones focus on the individualities of cable designs which aim at utilizing only the action of the magnetic material that modifies the current distribution.

Following this overview, is a referral to the theoretical and experimental studies on the skin and proximity effects of current carring conductors. The importance of the proximity effect at high frequencies is pointed out. This establishes the value of any design which minimizes this effect and, consequently, results in improved performance transmission lines. The section concludes with the presentation of a formalization which is valid for any TEM (Transversal Electric Magnetic Field) transmission line. At the same time, this formalization provides the boundary between the inductive action and the proximity minimization action of the magnetic material incorporated in the cable insulation.

Concludingthe theoretical support is a section on the effect of magnetic fields. It is shown that even relatively magnetically weak walls provide effective paths for the external magnetic field lines. This fact and the power distribution over the cross section of a twinaxial transmission line explain the important experimental findings that follow. These experimental findings are expressed in terms of the primary and secondary properties of twinaxial cables. Their careful examination reveals the major performance differences between the inductively loaded and the proximity reduced cables. They also suggest the respective potential applications of each cable type.

The presentation concludes with a discussion which attempts to identify the relative "pros" and "cons" of the two cable types and their relation to other, competing, transmission media.

PART I: THEORETICAL SUPPORT

A) Magneti Materials in Cables

Soft magnetic materials, which have linear characteristics, are traditionally used for transformer cores. The primary property of interest in that case is the strong permeability which provides adequate induction to the secondary circuits. Losses associated with the magnetic material are of secondary importance. For that reason these materials are optimized with respect to permeability and only very compact ones, in the case of powder cores, are of interest to transformer designers. It is well known that small voids in the magnetic material, particularly those located inside the grains composing the powder, result in strong demagnetizing fields and substantial reduction of the permeability. (See for Example Wohlfarth[8]). When the volume occupied by the non-magnetic substance, air-void or other material, is comparable to the volume occupied by the magnetic material the permeability reduction is very sharp and nonlinear with respect to the relative volumes of magnetic and non-magnetic substances of the composite material (Dadakarides[9]). This is a very undesirable effect for materials used in transformer cores.

On the contrary, this nonlinearity does not constitute a disadvantage for materials used in transmission lines. Manufacturing speed and mechanical flexibility dictate the maximum amount of magnetic material in the insulation wall. For commercially available insulating materials the maximum doping level is around 50-60% per volume. Even with these doping levels many polymeric insulations become fragile. Experiments have shown that there exists at least one insulator which keeps its elasticity at these doping levels[9]. Theoretical predictions by Dadakarides[9] and experimental results have shown that insulators doped with 50% per volume ferrite result in mixtures that have relative permeability close to 5.0. This value is nearly independent of the relative permeability of the pure ferrite, as long as the latter is much higher than unity. The strong demagnetization which reduces the mixture permeability reduces the magnetic losses as well.

Even though these values are clearly unacceptably low for transformer cores, they are perfectly acceptable for cable structures. The primary property for magnetic materials used in cables is low magnetic losses, while the value of permeability is of secondary importance. This condition is the opposite from that which is necessary for transformer cores. The requirement for low losses and the insensitivity of the mixture permeability to that of the pure ferrite act in a synergestic way.

There is an inherent trade-off for any magnetic material: the higherits permeability, the lower its cut-off frequency. The cut-off frequency is defined as that at which the D.C. permeability drops by 50% and at the same time the magnetic losses reach a maximum. The synergy lies in the fact that one can utilize ferrites with low permeability, hence low losses at high frequencies, without sacrificing the mixture permeability in the doping level range of interest, that is below 50-60% per volume. For doping levels in the upper part of this range the cable is inductively loaded and is here defined as Magnetically Loaded Cable (MLC). The low magnetic cost requirement dictates the use of Nickel-Zinc ferrites and possibly Nickle Manganese-Zinc ferrites, for lower frequencies. A large variety of compositions for these families of materials

exist and many of them incorporate minute quantities of other additives which improve their performance. A fairly extensive referral to these materials and their properties was presented by Dadakarides et.al[7].

A number of observations and rules of thumb have been included in the same reference. Two of most relevance to the present treatment is the description of the basic "cable cell" and the behavior of MLC at different frequencies. The "cable cell" is composed of the conductor which is covered by the insulation. Part of the insulation is occupied by the composite magnetic-nonmagnetic mixture, which in effect constitutes a cylindrical wall that surrounds the conductor. The best location for this wall is right next to the conductor. Also, it is preferrable to have a thinner and heavily doped wall rather than a thicker and lightly doped wall for a given amount of available magnetic material.

The MLC cable performance over a frequency band starting from D.C is divided in two sub-bands by the "critical frequency". Below the critical frequency the MLC exhibits improved performance with respect to the unloaded cable, while above this frequency the MLC exhibits worse performance. The critical frequency is closely related to the cut-off frequency of the ferrite used and denotes the point at which the magnetic losses of the ferrite start to dominate. This frequency is also closely related to the amount of the ferrite used. If the doping level is substantially lower than 50% per volume the sharp reversal from improved to degraded performance is not present because conductor losses dominate even at high frequencies when good quality ferrites are used.

When the doping level is substantially lower than 50% per volume the inductive loading is almost negligible. However, the presence of the magnetic material still modifies, to a lesser extend, the magnetic field. The guidance of the field by the magnetic wall results in a reduction of the number of field lines that cross the adjacent conductor. Consequently, the current distribution over the conductor cross section changes. The net result is a decrease of the induced eddy currents.

When good quality ferrites are used this action of the lightly doped insulation, which is also present in MLC's, offers the advantage of reduced eddy losses without the disadvantage of performance degradation beyond a critical frequency. The complementary rule of thumb, to those for MLC's, states that: low doping levels still result in improved performance via a phenomenon which is not related only to the insulation but to the conductors as well. For reasons which will become apparent these cables are called Reduced Proximity Cables (RPC). The peculiarity of RPC's rests on the fact that modifications in the insulation leave its properties virtually unaltered but change the apparent properties of the otherwise unaltered conductors. The nature of this action is as such that cylindrically symmetric structures, like coaxial cables, do not experience it while asymmmetric ones, such as twinaxial cables, do experience it.

B) High Frequency Resistance of Conductors

The most significant element of a conventional metallic transmision line is the current carrying conductors. Ironically, this is also the element of least perfection, the one that introduces most of the losses when good quality insulators are used. Ideally, at D.C. the current is uniformly distributed over the cross section of conductors with smooth surfaces. When edges are present there are some local disturbances of this uniformity near the edges. On the contrary, alternating currents create time varying magnetic fields which induce voltages that destroy the uniform distribution of current in any type of conductor.

When the origin of the induced voltage lies within the same conductor, where the induction takes place, the phenomenon is called "skin effect". It forces the current to redistribute in such a way that most of it concentrates near the conductor surface. Alternatively, when the origin lies within another conductor, located at a finite distance from the conductor where the induction takes place, the phenomenon is called "proximity effect". The current redistribution depends on the relative positions of the two interacting conductors, the intensity and the direction of the currents. In stranded and twisted conductors a third and similar phenomenon, the "spirality effect", introduces an additional current disturbance, Kennelly et.al[12]. In that case the helical path of each strand introduces a longitudinal magnetic field component. Since the magnetic material of the insulation reshapes only the transversal field components, only the skin and the proximity effects, and particularly the latter, is of importance in this treatment.

I) Skin Effect: Metallic conductors and phenomena associated with the conduction of current attracted the attention of most of the great names in Electrical Engineering. A partial list includes Maxwell[1], Heaviside[4], Poynting[5], Rayleigh[22], and Kelvin[3]. During their period, which ends around 1915, a broad definition of skin effect included the proximity effect as well, even though most of the treatments appear to concentrate on the self-induction associated with the pure skin effect as this is defined in this treatment. The expression for the narrowly defined skin effect, which utilizes the ber and bei Bessel functions with complex arguments, which is used until our days, was introduced by Kelvin in 1889. Fundamental experimental and theoretical investigations were conducted by Kennelly et.al [16]. Extensive research was conducted by Dwight in [9,10,11], among other, who also introduced a clear differentiation between skin and proximity effects and the "similitude principle". An interesting and different approach, more suitable to numerical solution, was presented by Silvester[23,24]. It utilizes the concept of modal theory to calculate the skin effect of conductors with complex shapes.

The skin effect, and along with it the losses originating within the conductors, becomes more profound as frequency increases. An absolute indicator is the "penetration depth" δ which is defined as:

$$\delta = (\pi f \mu \sigma)^{-\frac{1}{2}} \qquad (1)$$

where: f is the frequency in Herz
μ is the permeability of the conductor
σ is the conductivity of the conductor

The penetration depth is a physically meaningful quantity. It is the thickness of a layer, with infinite dimensions and radius of curvature, which carries a uniformly distributed current that causes the same losses as the real distribution of current carried by the conductor under examination per unit. The surface materials of the layer and the real conductor have the same electromagnetic properties.

For practical conductors with finite dimensions and curvature a relative indicator is more helpful than the penetration depth. The similitude principle states that: for conductors with arbitrary but proportionate shape the skin effect is the same as long as the conductors are isolated and the normalized frequency:

$$p = \left(\frac{f}{R_{DC}}\right)^{\frac{1}{2}} \sim (\sigma . f)^{\frac{1}{2}} \qquad (2)$$

is the same. Rdc is the D.C. resistance of the conductor. The relative indicator p is proportional to the product $(\sigma f)^{1/2}$ within a geometric constant. A more generalized indicator q can be used which incorporates the magnetic properties of the conductor as well. It is defined as:

$$q = \frac{r}{\delta} \sim (\sigma f \mu)^{\frac{1}{2}} \qquad (3)$$

where r is the conductor radius of curvature. The indicator q is proportial to $(\sigma f \mu)^{1/2}$ within a geometric constant. There are two "soft boundaries" for q which define the low, intermediate and high frequency ranges as seen from the conductor size and conductor properties point of view. The intermediate range is defined by the inequality:

$$1.4 < q < 5 \qquad (4)$$

For values of q smaller than 1.4 the current is almost uniformly distributed over the conductor cross section, which is said to operate in the low frequency range. When q is larger than 5 the current occupies a thin layer close to the conductor surface, the conductor operates in the high frequency range and the strong skin effect increases the resistance markedly above its D.C. value. In the intermediate range the skin effect is moderate, strong and the current, even nonuniformly distributed, occupies all of the conductor cross section.

In the case of pure skin effect, which is present only when the conductor is isolated and at infinite distance from other current carrying elements, the circular symmetry of conductors is maintained in the current distribution. In the contrary, this symmetry is not present when proximity effects are non-negligible.

II) Proximity Effect: The assumption of an isolated conductor is unrealistic because the return path experiences always at a finite distance. This coupled system of go-and-return paths experiences a generalization of the skin effect, as far as the magnetic induction phenomena are concerned. The initial studies appear to have focused on the pure skin effect because at the low operating frequencies of that time the proximity effect is almost unobservable. Physically, the two phenomena are of the same nature, namely magnetic induction. The decisive difference is the origin of the inducing magnetic field. Two avenues for generalization of the skin effect were followed. One led to researches on complex shapes of isolated conductors and the other to researches on the real proximity effect in systems of conductors. Dwight in [9,10] and Silvester in [23,24], follow the first avenue, while Dwight in [9,10] and Kennelly et.al. in [16], Carson[6], Butterworth[2] follow the second. Both types of generalizations require the use of higher order Bessel functions, for cylindrical symmetry, or other complicated functions of the complex arguments. A close look at the arguments reveals that these have the form of normalized depth of penetration similar to indicator q. This verifies the value of q as an indicator of induction and mathematically confirms the already stated physical equivalence of the skin and proximity effects.

When alternating currents flow in conductors located within close proximity, each one of them lies within its own magnetic field and the one created by its neighbors. According to Faraday's law the time varying magnetic flux that intersects a conductor creates an inductive voltage which generates currents. These eddy currents redistribute the primary current of the conductor in a way that increases the losses beyond the level corresponding to skin effect. The increased losses are described by a increased effective resistance. Physically, the current occupies a smaller part of the conductor cross section, part of which is left practically unutilized. Since the resistance is inversely

proportional to the utilized conductor cross section, its effective value increases. Butterworth[5] observed that this current squeeze is stronger when the interacting conductors carry currents that flow in opposite directions, compared to the case of codirectional flow. In practical transmission lines the interacting magnetic fields are non-uniform and the qualitative description of the proximity effect is obscured by the complex mathematical expressions. The basic characteristics of this phenomenon are identified if the simplified case of uniform magnetic field acting on a conductor is analytically treated.

Suppose a circular solid conductor lies within the space occupied by a uniform magnetic field normal to the conductor axis. By carrying out an integration over the conductor cross section of the induced voltage, it turns out that the losses generated within the conductor by the inducing magnetic field, per unit length, are:

$$W = \frac{1}{4}(\pi a^2).a^2\sigma\,\omega^2 B^2 \sim \frac{1}{\sigma}.(a^2\mu)^2.H^2 = \frac{1}{\sigma}.q^4.H^2 \qquad (5)$$

where: a is the conductor radius
$\omega = 2\pi f$ is the angular frequency of the inducing magnetic field
B is the rms value of the flux density of the field
$H = B/\mu$ is the intensity of the inducing field.

For a given conductor the eddy losses are proportional to the square of the magnetic field intensity. This behavior, characteristic of eddy currents independently of geometrical or field configurations, shows the seriousness of the problem of increased losses at high frequencies.

The orthonormal basis of Bessel functions, necessary to expand the fields created by any system of conductors with basic circular symmetries, incorporates the q indicator in the argument of the functions. The behavior of the series of Bessels as the value of q changes is totally obscured in all, but the limiting cases. On the contrary, by using (5) it is shown that eddy losses vary as the fourth power of this indicator which is a very strong dependence on frequency, conductivity and permeability of the conductor. The incorporation of permeability assumes a simplified model that neglects any phase lag phenomena associated with magnetic - conducting materials. It has been attempted because the resulting equation includes q explicitely and becomes helpful in comparisons. The dependence of eddy losses on the square of the external magnetic field intensity is also of fundamental importance. In practical systems, where the conductors are in close proximity, the intensity is inversely proportional to the distance from the generating conductor. Therefore, the eddy losses vary approximately as the square of the separation between the conductors. The dependence on the conductor cross section area is also strong and dictates the use of thinner conductors for high frequency applications. All these dependencies can be expressed by an extension of the similitude principle given by Dwight [illegible], that states: for a given go-and-return circuit shape, the proximity effect is constant as long as the q indicator and the ratios t/a and s/a are held constant. In the general case t is the thickness of a hollow conductor, a is its radius (inner or outer) and s is the axial separation between the go and return conductors. This principle can be extended to any number of conductors, as long as the shape of the system is held constant in all cases. Also, results that refer to cylindrical conductors can be used for other shapes as well, as indicative and qualitative information.

The findings about the effect of the relative direction of flow of the interacting currents and the relative strength of the skin and proximity effects are of importance for the design of stranded conductors. Mechanical reasons and minimization of the skin effect, among others, dictate the use of stranded instead of solid conductors. Interaction between the go-and-return conductors causes an increased interproximity effect, due to the opposite directions of the two currents. At the same time the fine strands suffer from less skin effect but introduce a strong intra-proximity effect because of their minimum separation. Measurements performed by Kennelly et.al. [illegible] with thick conductors, [illegible] 1.168 cm diameter, up to 5 kHz confirmed the strong dependence of the proximity effect of solid conductors on their separation. Other measurements by Kennelly et.al. [illegible] up to 100 kHz confirmed the theoretical predictions about the intra-proximity between strands, when the strands are in ideal contact with each other the overall skin and proximity effect is the same as that of the equivalent solid conductor. However, even a small separation between the strands reduces the overall effect markedly.

In terms of [illegible] Kennelly et.al. [illegible] [illegible]

The effort to minimize the overall losses [illegible] stranded conductors is effective only over a frequency range which depends on the number of strands, and on the respective solid conductor size. Measurements performed by Green et.al. [illegible] showed that a conductor comprised of [illegible] strands had higher losses above 1MHz than the equivalent solid one, while one with 271 strands had even higher losses. Also, the rate of loss increase with frequency of the second case was higher than that of the first

case. This denotes a total proximity effect that depends on the number of strands.

All these measurements which were performed over a limited frequency band can be used as calibration for any size of conductors and operating frequency by using the similitude principle and its extension. There is only one variable, that describes the degree of contact between strands, which may not be calculable with satisfactory accuracy. Arnold indicated that experimental results showed that the ratio of resistance along the strands to the resistance across the strands varies between 0.45 and 0.5, the exact value depending on the type and tightness of stranding.

Theoretically, there are three ways to attack the problem of high frequency resistance of a set of conductors. One is based on a mathematical treatment by Mannebach [20] who considers the basic case of an infinitesimal conductor located in the vicinity of a finite conductor. The real problem is solved by dividing a conductor into a large number of infinitesimal conductors and by integrating their fields. This method involves difficult integrals of Bessel functions. Another method, used by Butterworth [5], and Carson [6], makes use of the Poynting vector to calculate the dissipation in the conductors and to derive the effective alternating current resistance. A third one, used by Belevitch [3,4] and Groenendaal et.al.[13], makes use of the scalar electrical and vector magnetic potentials and appropriate boundary conditions. All end up with infinite series of Bessel functions with complex arguments. Belevitch's approach seems more elegant and the linear system which provides the coefficients describing the proximity effect is presented for the sake of completeness. It can be applied to any system of conductors. In the case of a go-and-return circuit the proximity impedance is given by the infinite series:

$$Z_{prox} = \frac{j\omega\mu}{\pi}\sum_{n=1} A_n \qquad (6)$$

where A_n are the solutions of the infinite linear system

$$\sum_{m=1} T_{nm}A_m + \frac{V_n A_n}{\beta^{2n}} = 1 \qquad n=1,2,3,\ldots \qquad (7)$$

The various constants are defined as follows:

$$T_{nm} = \frac{(m+n-1)!}{(n-1)!\,(m-1)!} \qquad (8)$$

$$V_n = -n\,\frac{J_{n-1}(ka)}{J_{n+1}(ka)} \qquad (9)$$

$$\beta = \frac{a}{s} \qquad (10)$$

and $k = \sqrt{-j\omega\mu\sigma}$ [illegible], taken with negative real part
a is the conductor radius
s is the axis-to-axis separation of the conductors.

The mathematical elegance of the solution is not accompanied by an equivalent "practical" elegance. Even in the case of two conductors the necessary number of factors is large and increases fast with normalized frequency. When the conductors are more than two the system practical size becomes quickly "large", the theoretical being always infinite. The irrational variation of the high order Bessel functions having large arguments provides no insight into the redistribution of current. Furthermore, the large number of factors renders this analytic solution equivalent to a numerical one with finite accuracy. In that sense these solutions can be considered as approximations of the real one. In effect using 3-4 factors of the infinite series, following Butterworth's Poynting approach, resulted in substantial inaccuracies in the calculation of the high frequency resistance for AWG20 solid conductors above the Megahertz region.

In order to avoid the complexity of the high order Bessels, a number of approximations have been proposed. Dwight [illegible] did extensive work on the subject but it seems that the best approximate formulas were proposed by Arnold [1,2] for solid and hollow conductors. Owing to its wide acceptance and good accuracy, less than 1% inaccuracy over a wide frequency band, Arnold's basic approximation for the inter-proximity between two solid conductors is presented:

$$[illegible] \qquad (11)$$

where [illegible]

[illegible]

closed and symmetric ones, like coaxial cables. The outer conductor of the coaxial cables, even though it lies in the magnetic field of the core conductor, is too thin to experience high eddy losses.

It is impractical to design transmission lines with large separation between the go-and-return conductors or to design conductors with complex shape. Therefore, a viable alternative is to design lines in such a way as to decrease the interception of conductors by the transversal magnetic field. The definition of the TEM transmission line implies that the longitudinal and transversal field problems can be solved independently. This is expressed by the following condition, which is derived after a manipulation of Maxwell equations for a TEM case:

$$|(\mathrm{Re}(\gamma).D)\cdot(D/\lambda)|^{\frac{1}{2}} \ll 1 \qquad (12)$$

where: Re is the attenuation, defined as the real part of the propagation constant
D is the maximum transversal dimension of the cable
λ is the wavelength of operation

Therefore, the effect of the magnetic material incorporated in the insulation on the transversal magnetic field can be treated independently.

C) Magnetic Conduction

The primary property of every non-conducting magnetic material is the guidance of external magnetic field lines. This can be compared to the conduction of current by conductors or the conduction of electric field lines by dielectric materials. In that respect, and by the substitution of current density by magnetic flux density, a proper arrangement of magnetic elements forms a magnetic circuit. Its magnetic resistance, not related to losses but to easiness of conduction, is small in the volume occupied by magnetic material and large in gaps and in the volume occupied by nonmagnetic substances. The second correspondence, between electric and magnetic non-conducting materials, has physical origin. Since the magnetic field is a dual representation of the electric field, a magnetic field-material interaction can be modelled in a way similar to an electric field-material interaction. Both fields satisfy a Laplacian, when no sources or sinks of charges exist, which in the case of magnetic field has the form:

$$\nabla^2\bar{A} = 0 \qquad (13)$$

with A being the vector magnetic potential. The correct application of the boundary condition at the interfaces between different materials defines the exact shape of the field. The magnetic flux density B is derived from the equation:

$$\nabla \times \bar{A} = \bar{B} = \mu H \qquad (14)$$

where: μ is the permeability at the given point
H is the magnetic field intensity

According to the previous section the magnetic field of a twinaxial transmission line is nonuniform. However, a uniform approximation gives a good estimate of the effect of the magnetic material on the field. Figure 1 shows the direction of the field lines when a cylindrical tube of magnetic material is uniform field.

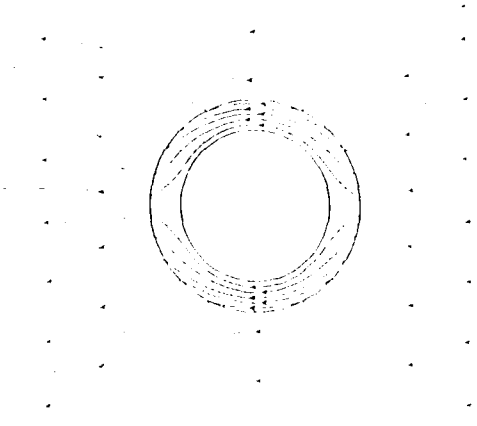

FIGURE 1

It is apparent that field lines prefer to flow through the magnetic tube leaving its interior free of magnetic field. This is a rather limiting case in which the relative permeability of the tube is much higher than unity. Practically, when the relative permeability is higher than 10 the wall provides strong guidance to the external magnetic field, provided that the ratio of the wall thickness to its inner radius is not much smaller than unity. Under this condition, the intensity of the magnetic field inside the tube is substantially weaker than the intensity of the external field.

As showed before, the proximity effect losses vary as the square of the magnetic field intensity intercepted on the conductor. In cables which incorporate magnetic material in the insulation the conductors occupy the hollow region. Suppose that the ratio of the magnetic field intensity in the hollow region to that when no tube is present is S_r. Then, proximity losses vary as S_r^2. Figure 2 is a parametric plot of S_r^2 for a number of thickness-to-inner radius ratios when the external magnetic field is uniform.

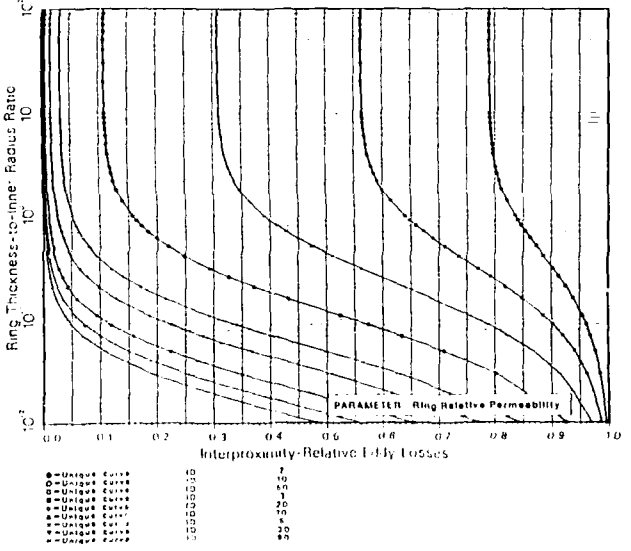

FIGURE 2

It becomes apparent that even weak magnetic materials having relative permeabilities between 3 and 5 decrease the proximity effect losses considerably for reasonable wall thickness. This is very important because these permeability values correspond to mixtures that are easily and inexpensively manufacturable. Reading from this plot a wall with relative permeability 10 decreases the eddy losses by more than 80% when its thickness is more than half of the conductor radius. The impressive effectiveness of this wall, in guiding the field lines, deserves particular attention because the practical upper doping level of 55% or so, with available technology, results in mixtures with permeability in the vicinity of 10. Hence, even with the imposed limitation on the doping level of matrices, the magnetic wall field guiding capability is utilized very efficiently.

In real twinaxial cables the intercepting fields are not uniform and the wall becomes even more effective. Therefore, in twinaxial cables, the proximity reduction is more profound than that predicted by the plot in Figure 2 for a given wall geometry and relative permeability. Also, the wall becomes more effective when it is located right next surrounding the conductor because most of the transmitted power lies in the vicinity of the conductors as Figure 3 from Kraus et.al [4] shows.

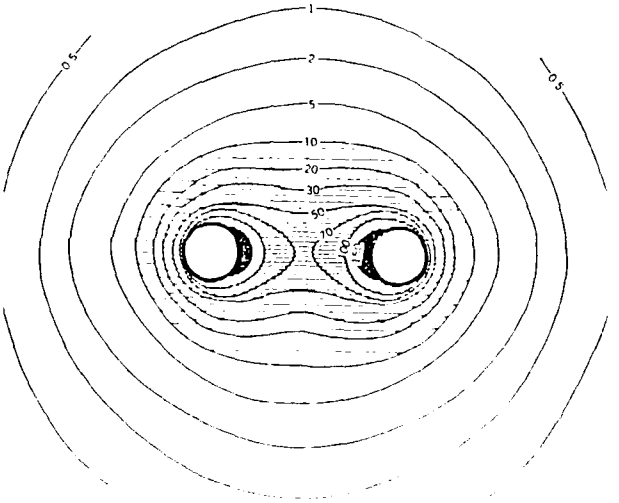

FIGURE 3

The following experimental results prove the capability of magnetic walls to reduce overall losses, provided that the magnetic losses introduced by the magnetic material itself are very low.

PART II : EXPERIMENTAL FINDINGS

Experimental twinaxial cables were built [29] and their measured performance characteristics are presented. The conductor is copper AWG20 composed of seven strands AWG32 and the insulation is standard polyethylene. Approximately one half of the insulation wall is doped with a good quality ferrite which comprises 16% of the ferrite-insulation mixture volume. The low doping level is chosen so the inductance increase is very small and any substantial performance differentiation, with respect to the undoped cable, can not be attributed to the distributed inductive loading.

The cable characteristics are divided in primary and secondary ones. The primary are independent of each other and are the capacitance,the inductance, the conductor resistance and the electric and magnetic loss elements of the compound insulation. The secondary are the characteristic impedance and the propagation constant which is expressed by its attenuation and phase velocity components. All the following plots present the respective property of the cable without magnetic material, called "unloaded", with dotted curve,and the same property of the one with magnetic material, with solid curve. Even though the generic terms "loaded" and"unloaded" are used, the cable is a RPC (Reduced Proximity Cable).

I) **Capacitance**: Figure 4 shows the cable capacitance over the frequency band extending from 1KHz to 10MHz

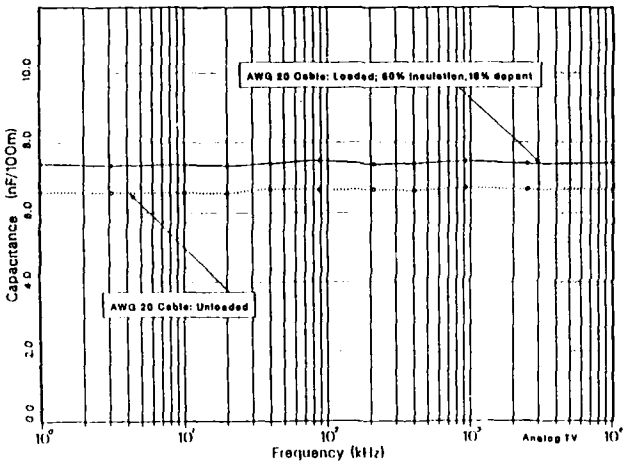

FIGURE 4

The relative dielectric constant of ferrite was not measured, but it is known that its value is much higher than unity. Judging from published values for a number of ferrites, its value in the upper part of the frequency band is estimated to lie between 10 and 16. In the lower part it can be substantially higher. However, the light doping makes the dielectric properties of the mixture insensitive to the value of the ferrite dielectric constant. Over the frequency band, the estimated relative dielectric constant of the mixture lies between 3.5 and 3.6, Kharadly et.al.[18] Since only part of the insulation is doped and the capacitance dependence on the magnetic wall thickness is almost logarithmic, its increase is only 12%, as the measurements show, and constant over the frequency band.

II) **Inductance**: Figure 5 shows the cable total inductance over the same frequency band, 1KHz to 10MHz. Part of it is the inherent inductance of the conductors, but the main element is the mutual inductance between the go-and-return circuits.

The ferrite used has relative permeability 1300 at D.C. and an estimated cut-off frequency of 3.5 MHz. Beyond this point,where the D.C. value drops to 650,permeability decreases linearly with frequency,at a comparable rate. Therefore, it is substantially higher than unity throughout the frequency range of interest.According to the theoretical predictions, which have been verified experimentally, the mixture has relative permeability approximately 1.6.

The mutual inductance depends almost logarithmically on the magnetic wall thickness, but linearly on the wall permeability.The light doping increases the overall inductance approximately 18% at D.C. and 30% at 10MHz because as the frequency increases the influence of the inherent inductance decreases.The skin and proximity effects squeeze the current which occupies only a thin ring and thin rings have very small inherent

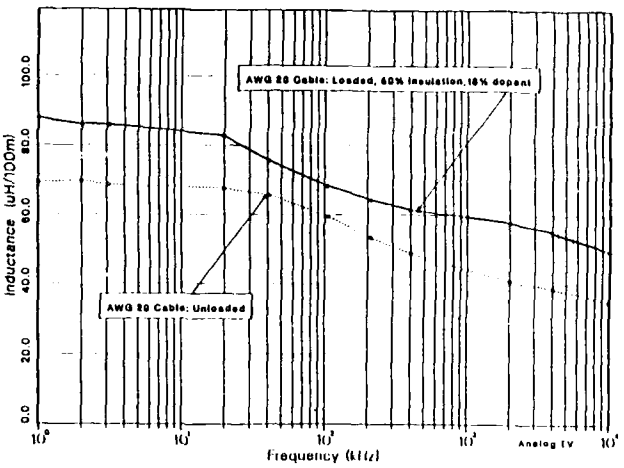

FIGURE 5

inductance. The parallel curves prove the insensitivity of the inherent inductance to the existence of the magnetic wall and the insensitivity of the mixture properties to the variation of the ferrite permeability. The sizeable deviation from parallelism at intermediate frequencies has no apparent physical explanation and may be due to measuring conditions. The total inductance value at 10MHz, where the inherent is negligible, is equal to the mutual inductance of the line for both cables.

III) **Loop Resistance**: Figure 6 shows the loop resistance of the two cables over the same frequency band. Below 100KHz the cable with magnetic doping has slightly higher resistance. At these frequencies the penetration depth for copper is more than 200 μm and the thin (AWG32) strands experience negligible skin and very low proximity effect. Hence, the slight increase of the resistance in the cable with magnetic doping is attributed to the small additional losses introduced by the magnetic material. The Q indicator at these frequencies is very small, denoting an almost uniform distribution of the current over the strand cross section. However, as frequency increases skin and later proximity effects become strong and the AC conductor loop resistance increases quickly.

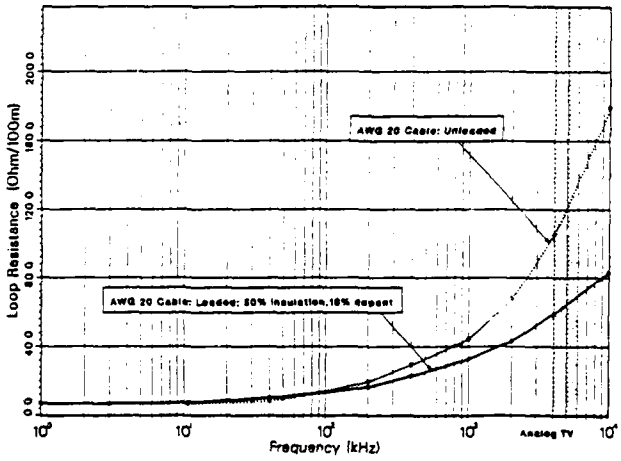

FIGURE 6

Magnetic losses increase as well. However, since the magnetic particles are not in full contact within the mixture at such low doping levels, strong demagnetizing forces are developped within each particle and the effective magnetic flux within the mixture volume is not strong. This results in low mixture permeability and low magnetic losses.Consequently magnetic losses do not increase fast with frequency and the actual effective resistive element in the doped cable, besides conductor ohmic resistance, is small.

Proximity losses are lower in the cable with magnetic doping. The wall guides a large portion of the magnetic field lines, which do not intercept the conductor, and this way it reduces the additional losses.Reading from the parametric plot of Figure 7,the wall reduces the inter-proximity losses by 15% when the external field is uniform. In the experimental twinaxial cable the reduction is more substantial. This reduction is

complemented by an intra-proximity reduction. The magnetic field of each one of the seven strands comprising each conductor intercepts the other strands and generates eddy currents. When the insulation incorporates magnetic materials part of the field lines of the outer strands are guided by and close through the magnetic wall which is in contact with their surface. This results in a reduction of the intra-proximity effect.

The loop resistance reduction, which becomes stronger at high frequencies and reaches 50% at 10MHz in the experimental cable, is the net outcome of the slow increase of the low, newly introduced, magnetic losses and the sharp reduction of the total proximity losses.

IV) Characteristic Impedance: The combined effect of the capacitance, inductance and loop resistance variation is reflected in the change of the secondary characteristics of the line. Figure 7 shows the magnitude of the characteristic impedance of the two cables over the 1KHz to 10MHz range. Throughout this frequency band they have almost the same impedance. A closer examination reveals the reasons for the shown relative positions of the two curves.

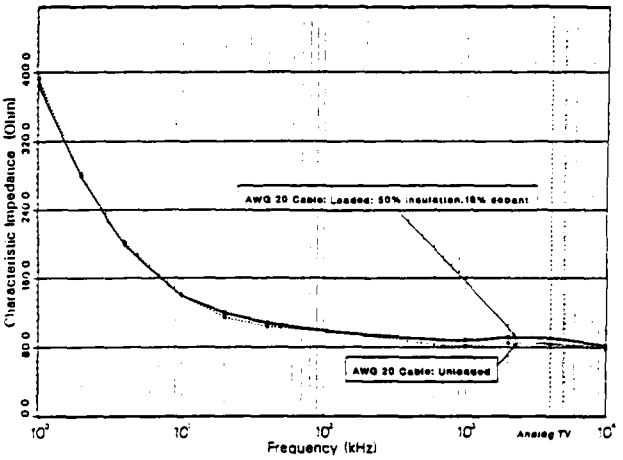

FIGURE 7

Characteristic impedance is given by:

$$Z_{ch} = \left(\frac{R+j\omega L}{G+j\omega C}\right)^{1/2} \qquad (15)$$

where: R is the total loop resistance, including the magnetic losses
L is the inductance
C is the capacitance
G is the insulation conductance
ω is the radial frequency

All quantities refer to a unit-length cable. At low frequencies the role of ωL is minor in both cables. Therefore the PPC has lower impedance because its capacitance, and its ωL factor, is higher. At intermediate frequencies R and ωL are comparable but at high frequencies inductive ωL dominates and the characteristic impedance value is close to $(L/C)^{1/2}$. Since the relative inductance increase is a little higher than the relative capacitance increase in the doped cable its impedance is slightly higher. However, the difference is very small and, in practical terms, the two cables have nominally the same impedance. This is of particular interest because cables with lightly doped insulation can be used with existing terminal equipment without creating impedance mismatch problems. Their advantage is lower attenuation or, equivalently, higher capacity, as the following figure shows.

V) Attenuation: Attenuation characteristics, shown in Figure 8, resemble those of total loop resistance. The relative increase in capacitance and inductance is approximately the same in the magnetically doped cable. Therefore, the net effect of the magnetic wall on quantities depending on transversal fields is very small. The propagation constant differentiation is the result of loop resistance changes, hence the similarity between the resistance and attenuation curves.

VI) Propagation Velocity: Propagation velocity, which is the normalized reciprocal part of the propagation constant, is consistently lower in cables incorporating magnetic materials than in the corresponding undoped ones. The measured values of the experimental cables are presented in Figure 9 over the 1Hz to 10MHz frequency band. Neglecting the effects of losses, phase velocity is given by $1/(LC)^{1/2}$.

Magnetic doping increases both quantities and decelerates propagation. At low frequencies the influence of ωL is weak and the resistive element R, which is practically the same in both cables, dominates and propagation velocity is almost the same for the magnetically doped and the

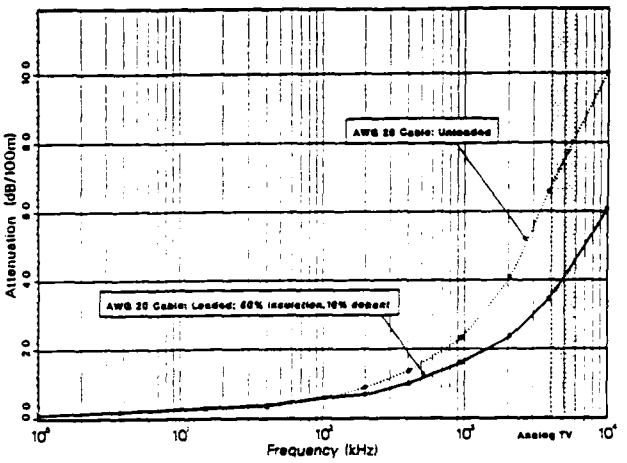

FIGURE 8

corresponding undoped cables. As frequency increases the influence of ωL increases and is more profound in the doped cable. Consequently, the propagation velocity curves diverge as frequency increases but the relative difference remains within 10-15%. The rate of divergence of the curves decreases at higher frequencies if the permeability of the doping ferrite is still much higher than unity, typically higher than 50-100. The resulting stabilization of the relative positions of the two curves in that case is the result of the frequency independent mixture permeability and of the negligible influence of the conductor intrinsic inductance. Therefore, PPC experience little propagation deceleration with respect to their undoped counterparts throughout any frequency range of practical interest. The low deceleration, in conjunction with the reduced attenuation of PPC, makes them very useful for delay sensitive applications, like computer networks.

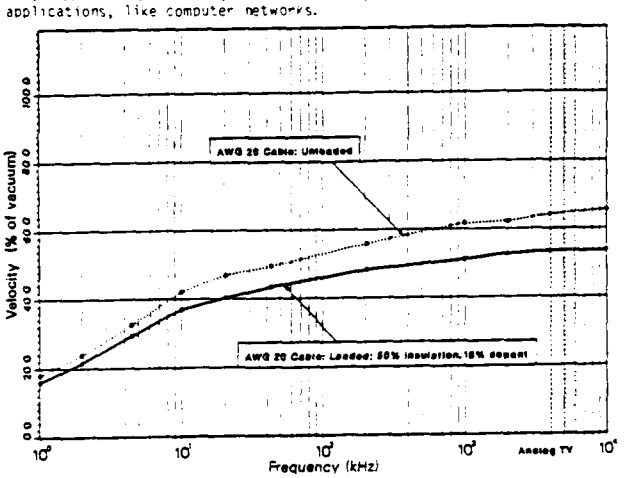

FIGURE 9

PART III : REMARKS

A) Discussion

The incorporation of magnetic materials in cable structures introduces an additional, independent variable in the design of metallic transmission lines. The position of the magnetically doped section of the insulation and the level of doping influence the transmission characteristics considerably. One can distinguish two distinct phenomena which shape the line performance, namely inductive loading and proximity reduction.

When the doping is heavy, as in MPC's, inductance increases substantially. The inductive reactance has opposite sign from the capacitive one and the line tends to become an ideal R line with ohmic characteristic impedance. The physical explanation is that electric energy, stored in the capacitance, and magnetic energy, stored in the inductance, are both tender balanced in every point along the line. There is little need for an out of phase current, with respect to the voltage across the conductors, to feed unbalanced reactance. As a result, almost all the power is real because the imaginary, oscillating component is proportional to the out of phase current. The ohmic losses depend on the total current carried by the conductor, the drastic decrease of the out of phase current

in MLC's results in decreased total flowing current,hence decreased losses.

The behavior of MLC's is discussed more extensively in Dadakarides et.al[7]. The important observation is that all the characteristics of the MLC cable are different than those of the corresponding unloaded one. There is a critical frequency, which depends on the cable architecture and on the ferrite used.At lower than critical frequencies the transmission performance improves when the cable is loaded, while at higher than critical performance degrades. The distributed inductance increases substantially, independently of the cable architecture as long as the doping level is relatively heavy. For manufacturing and mechanical reasons the heaviest possible doping,with present technology and materials and for practical cables, is approximately 55-60% per volume. The dopant permeability influences mixture properties weakly, if it is much higher than that of vacuum.Magnetic losses may be a serious drawback and the advantage of increased inductance is maintained only if the ferrites have very low losses. Major characteristics of MLC's are higher, stable and nearly ohmic characteristic impedance, lower attenuation and phase velocity,all being as such below the critical frequency.

The second phenomenon, besides distributed inductive loading, is proximity reduction due to the guidance of magnetic lines,generated by adjacent currents, by the magnetic wall surrounding the conductors.The important property is the unchanged propagation characteristics of the cable, besides attenuation, when the doping is light. This proximity reduction is present in heavily loaded structures as well as in lightly doped ones.The relative advantage of the latter is that ferrite losses, as long as they are low, influence the cable resistance less drastically. Also,for light doping, mixture properties are virtually independent of ferrite electromagnetic characteristics.

In both designs, MLC and RPC, and particularly for light doping, the insensitivity of the mixture properties permits the efficient use of low permeability ferrites without compromising the magnetic strength of the mixture. This is important because there is an inherent trade-off between permeability and losses in every magnetic material. The higher the permeability the higher the losses over the usable frequency band. Since practical transmission lines must have very low losses and a reasonable inductance is effective at high frequencies, the proper use of low permeability,low loss, ferrites offers nearly optimum operating conditions.

The fundamental difference between inductive loading and proximity reduction is that the former is present in every heavily doped structure while the latter is sizeable only in asymmetric structures like pairs of cables. Coaxial lines do not suffer from proximity losses and if their insulation is lightly doped their performance does not change appreciably.

B) Conclusion

The major, unexpected at a first sight, finding is that modifications of the insulation structure can change the apparent properties of the conducting elements. The incorporation of proper magnetic materials perturbes the transversal magnetic field in such a way that ohmic losses decrease. The investigation of the cause of this behavior leads to induction effects in conducting bodies. Skin effects, even though not responsible for this unexpected behavior, forms the basis of a long and wide theoretical and experimental treatment on induction. Analysis of simplified structures provides a theoretical background which is used to explain the findings of a set of measurements.

The light doping of the investigated RPC proves the general usefulness of magnetically doped cables, beyond the practical inductive loading of the MLCs. As the measurements show, RPC have the advantage over MLC that all the propagation characteristics besides attenuation remain almost the same as those of the undoped cables.

Applications for RPC include a variety of old and new systems. The invariability of the characteristic impedance makes the RPC attractive for old systems where terminal equipment must not change. Major applications envisioned are smart-home, high bandwidth wired systems, high capacity subscriber loops, computer or other modules interconnections, buses or drop cables for local area networks, wirings serving PABX installations and other.

Reviewing the available wired transmission media for medium distance-bandwidth applications one finds three major representatives:pair cables, coaxials and optical fibers. In terms of attractiveness small coaxials seem to face fierce competition from optical fibers. However, fiber optics is not an inexpensive alternative for these applications because of the hidden costs of optoelectronic transducers, connectors and the extra care that their delicate nature requires. In many cases they are used, even though grossly underutilized, due to a lack of a viable alternative. Conventional pairs, on the other part of the spectrum, offer limited services.

The incorporation of magnetic doping improves the performance of the pair cables and makes them prime candidates for these applications. They offer the simplicity of a pair and almost the behavior of a small coaxial at a lower cost than optical fibers. The increased attention that conventional pairs have attracted recently in local area networks, after the realization of the practical limitations of optical fibers, provides an independent verification of the potential of RPC or MLC.

A hidden advantage of the proposed cables is that in all efforts only commercially available ferrites were used.These are optimized for maximum permeability, which presents almost a worst case scenario when cable doping is considered. It is expected that the development of new ferrites, optimized for minimum losses, will be very beneficial to RPC and MLC cables.

BIBLIOGRAPHY

1. **Arnold, A.H.M.** : "Proximity Effect in Solid and Hollow Round Conductors". J.IEE,Vol.88,1941, pp.349.
2. **Arnold, A.H.M.** : "Eddy-Current Losses in Single-Conductor Paper-Insulaited Lead-Covered Unarmored Cables for a Single-Phase Circuit". J.IEE, Vol.89, 1942, pp.636.
3. **Belevitch, V.** : "Theory of the Proximity Effect in Multiwire Cables", Part I, Philips Res. Repts., vol. 32, 1977, pp.16.
4. **Belevitch, V.** : "Theory of the Proximity Effect in Multiwire Cables", Part II, Philips Res. Repts., vol. 32, 1977, pp.96.
5. **Butterworth, S.** : "Eddy-Current Losses in Cylindrical Conductors with Special Applications to the Alternating Current Resistances of Short Coils", Royal Soc. Phil. Trans, vol. 222, May 1922, pp.57.
6. **Carson, J.R.** : "Wave propagation over Parallel Wires:The Proximity Effect", The Philosophical Magazine, April 1921, pp. 607.
7. **Dadakarides, S.D. Lusignan, B.B.**: "Magnetically Loaded Cables", Proceedings of the 35th IWCS, 1986, pp.368
8. **Dwight, H.B.** : "Skin Effect and Proximity Effect in Tubular Conductors", Trans.of AIEE,Feb.1922, pp.189
9. **Dwight, H.B.** : "Proximity Effect in Wires and Thin Tubes", Trans. of AIEE, June 1923, p.p. 850.
10. **Dwight, H.B.** : "A Precise Method of Calculation of Skin Effect in Isolated Tubes", Trans. of AIEE, Aug. 1923, pp. 827.
11. **Dwight, H.B.** : "Reactance and Skin Effect of Concentric Tubular Conductors", Trans. of AIEE, July 1942, pp. 513.
12. **Green, E.I.; Leike, F.A; Curtis, H.E.** : "The Proportioning of Shielded Circuits for Minimum High Frequency Attenuation", Bell System Tech. J., vol. 15, 1936, pp.248.
13. **Groenendaal, G. C; Wilson, R.R; Belevitch, V.**: "Calculation of The Proximity Effect in a Screened Pair and Quad", Philips Res. Repts., vol. 32, 1977, pp. 412.
14. **Heaviside, O.** : "Effective Resistance and Inductance of a Round Wire", The Electrician, 1884, pp.58.
15. **Lord Kelvin** : "Journal Soc. of Tel. Eng., vol. 18, 1889 pp. 36, Mathematical and Physical Papers, vol. III, 1889, pp. 491.
16. **Kennelly, A.E; Affel H.A.**: "Skin-Effect Resistance Measurements of Conductors at Radio Frequencies up to 100, 000 cycles per second", Proc. of the Inst. Radio Eng., May 1916, pp. 523.
17. **Kennelly, A.E; Laws, F.A; Pierce, P.H.** : "Experimental Researches on Skin Effect in Conductors", Trans. of AIEE, vol. XXXIV, Part II, 1915, pp. 1953.
18. **Kharadly, M.M.Z; Jackson, W.** : "The properties of Artificial Dielectrics", Proc. Inst. Electr. Eng., vol. 100, 1953, pp. 199.
19. **Kraus,D.I; Carver,K.R.**: "Electromagnetics", 2nd edition, McGraw Hill
20. **Mannebeck, C.** : "An Integral Equation for Skin Effect in Parallel Conductors", Journal of Math. and Phy., April 1922.
21. **Maxwell, J.C.** : "A Treatise on Electricity and Magnetism",Oxford Univ. Press., vol. II, 1873.
22. **Poynting, J.H.** : "Philosophical Transactions 1884, 1905.
23. **Lord Rayleigh** : "On The Self Induction and Resistance of Straight Conductors", Philosophical Magazine, vol. 21, 1886, pp. 381.
24. **Silvester, P.** : "AC Resistance and Reactance of Isolated Rectangular Conductors", IEEE Trans.on PASS-86, no.6, June 1967, pp. 770.
25. **Silvester P.** : "The Accurate Calculation of Skin Effect in Conductors of Complicated Shape", IEEE Trans. on PAS-87, no.3, March 1968, pp.735.
26. **Stratton, J.A.** : "Electromagnetic Theory", McGraw Hill, 1941.
27. **Wohlfarth, E.P.-Editor** : "Ferromagnetic Materials", vol.3, North Holland Publishing Co., 1982.
28. **Dadakarides, S.** : Unpublished
29. **Private Communication**

Dadakarides Simos D: He was born in Greece, where he received the "Diploma" in Electrical Engineering from the "Aristotelian University of Thessaloniki". He continued graduate studies at Stamford, received the MSEE in 1984 and is currently working towards the completion of Ph.D-EE. He has done research on Scattering from Dielectric Cylinders (undergraduate thesis), on incorporation of magnetic materials in transmission lines and on design of optical fiber networks (graduate). In addition to his purely academic activities he did consulting in the cable industry. Among a number of various honors, he received the 35th IWCS "Outstanding Technical Paper", 1986 award. He has two patents pending in the U.S.A. and abroad.Besides his technical interests on magnetic materials, transmission systems and optical communications, he has a keen interest in creating infrastructures for teaching optical communications and the process of innovating.

HIGH SPEED TRANSMISSION THROUGH TWISTED PAIR WIRE

LAL M. HORE AND V. THURAISAMY

Bellcore - New Jersey, USA

ABSTRACT

High speed transmission through twisted copper pairs in the presence of crosstalk and other impairments, is discussed. A fundamental transmission model for premises wiring is developed and it considers both crosstalk and loss characterization. The model for premises wiring parallels the transmission model used for outside plant cable. For various desired levels of confidence, the trade-off between signal frequency and transmission distance is investigated. However, in digital applications one must be cautious in relating bit rate to frequency. Near-end crosstalk (NEXT) is assumed to be the limiting factor and all derivations are based on this assumption.

In addition, bridged tap causes increased signal attenuation which may result in reducing the range significantly. For example, with the critical quarter wavelength of about 210 feet of 24 gauge bridged tap, at 772 KHz the acceptable distance may be reduced by as much as 1200 feet. Results are based on measurements carried out on several vendors' cables, and further insight is derived from extensive computer simulation and theoretical analyses performed in connection with the development of standards for the ISDN Basic Access Digital Subscriber Line.

INTRODUCTION

In the telecommunications world, the copper plant was designed and engineered initially to provide analog voice-band transmission. With the advent of digital transmission, and with advances in signal processing technologies, these same twisted pairs of copper wire have been successfully utilized for transmitting an increased volume of data. While transmission of multi-megaherz frequencies will require other media, twisted pair copper wires will continue to play a crucial role for telecommunications in the distribution portion of the loop plant and in the building wire environment.

The loop plant imposes severe constraints on a transmission system in meeting performance objectives. The loop includes outside plant cable, central office wiring and also customer premises wiring. The outside plant transmission facilities include aerial, buried and underground cables, with a multiplicity of wire gauges, pair counts and bridged taps. Any design of a bidirectional transmission facility must accommodate the wide disparity of cable compositions, bridged tap configurations and highly variable impedances of the loop. It is not practical to specify the transmission parameters of the particular loop to which a given system may be connected.

Objective and Overview

Extensive transmission models exist for outside plant cables.[1] The main question we are attempting to answer here is: What is the maximum transmission rate possible on a twisted pair of copper wires used in premises wiring? Clearly, the answer will depend on a number of factors and requirements. We shall discuss these factors in detail in the process of defining the problem and deriving approximate solutions.

Based on OSP cable model, the feasibility of using the existing non-loaded copper wire loops, without preconditioning, to provide Integrated Services Digital Network (ISDN) Basic Access has recently been established.[2] To estimate performance limits, it was necessary not only to characterize the loop plant, but also to investigate optimum design criteria of the transmitter and receiver components. This involved an extensive search for the best possible methods in transmission technology, line code, filter techniques, echo removal, equalizer design, timing recovery and jitter control mechanisms, noise minimization etc. E.g., the echo cancelling method (as opposed to Time Compression Multiplexing) proved to be the winning technology and the 2B1Q line code was adopted as the standard.[3]

The performance of inside wiring cables has received less attention in past due to lack of premises wiring transmission models. Thus we develop such a model in order to study the transmission characteristics of inside wiring cables. A complete answer to our question cannot be given even with such detailed studies as for the ISDN Basic Access. Our discussions here will concentrate on the loop transmission capability in a generic sense, and in particular the trade-off of transmission rate and

range without reference to any particular technology, line code etc.

To set the stage for the discussion of the work entailed here, a brief review of the relevant factors affecting digital transmission is presented in Section 2. Performance measures and associated quantities are described in Section 3. The studies carried out to derive our premises wiring model are detailed in Section 4. The results are collected in Section 5 and our discussion of our findings are presented in Section 6.

Results are based on measurements carried out on several vendors' cables, and further insight is derived from extensive computer simulation and theoretical analyses performed in connection with the development of standards for the ISDN Basic Access Digital Subscriber Line.[4] The main results show a premises wiring transmission model useful for considering the trade-off between maximum distance (range) and rate of transmission. The data and models are for 25 pair 24 gauge cables where all pairs are deployed with the same type of system. Thus there are 24 disturbers crosstalking into each receiver. For example, the transmission rate-distance model shows with a typical allowance for the unknown and uncertain sources of noise, an Alternate Mark Inversion (AMI) system operating at 772 KHz (1.544 kbps) and an error ratio of one in 10^7 to have a NEXT-limited range of about 2800 feet, while at 6 MHz the distance is less than 400 feet.

IMPAIRMENTS

The principal contributors to noise resulting in limiting the high speed transmission over telephone loops are inductive noise, echoes, intersymbol interference, impulse noise, and crosstalk.

Inductive noise is caused by power lines in the vicinity of the telephone cable, consisting of 60 Hz and its harmonics. It is not a serious problem for most high speed transmission, but may require a high-pass filter.

Echoes can be a very serious problem in full duplex high speed transmission on a balanced pair of copper wires. Because of the echoes from bridged taps and the associated wide variation of impedances from loop to loop and because of the high suppression of echoes required, simple balance networks as with voice circuits are totally inadequate. Echoes can overwhelm a relatively weak received signal on long loops. In the following, we assume that adaptive echo canceling techniques are generally adequate to reduce echo noise to a tolerable level.

Intersymbol interference (ISI) is the phenomenon where some of the energy from a pulse spills over into the neighboring time slots. As with echoes, adaptive techniques for equalizers are required to effectively reduce intersymbol interference to permissible levels.

Impulse noise, by definition, has a high peak relative to typical peaks of the background noise and is generally of short duration. The switching system in the wire center is believed to be a significant contributor to impulse noise, but significant impulse noise has also been observed at customer premises.

Since crosstalk has been a problem for voice circuits, it has been studied extensively at voice frequencies and for transmission of T-1 signals. Indeed the many aspects of the design and manufacture of cables, such as the twist lay of the pairs, the bundling in groups to form high capacity cables were influenced by the need to minimize crosstalk.[5]

SIGNAL-TO-NOISE RATIO AND MARGINS

Having reviewed the contributors to potential bit errors, we are ready to consider reasonable requirements in the form of signal-to-noise ratios for acceptable data transmission. From the customer's point of view viable digital transmission may be measured in terms of its Bit Error Ratio (BER). For digital transmission a BER of one error in ten million (10^{-7}) is our desired goal. This can be translated to Signal-to-Noise Ratio (SNR), which relates closely to the system equipment capabilities and the wire transmission characteristics. In a digital transmission system, the value of SNR required to achieve a given BER varies with many details, including the number of different symbols (levels) transmitted. Increasing the received signal strength with respect to noise will clearly be an advantage but certain noise components such as near-end crosstalk will increase proportionately. That is, when noise components like self or similar system near-end crosstalk dominate, the SNR is not affected by the (common) transmit level. Furthermore, spectrum management considerations and device constraints may limit signal amplitudes of certain systems.

The SNR's required to achieve 10^{-7} BER for some typical digital transmission schemes are presented in Table 1.[8] The values in Table 1 are based on the assumption that the total interference is characterized as Gaussian. Note that the four level code 2B1Q requires a SNR of 24.0 dB compared to a binary code requirement of only 14.3 dB. The greatly reduced bandwidth required for 2B1Q results in much lower signal attenuation, while at the same time the crosstalk loss is much higher. That is, while the received signal strength S has gone up, the noise N has come down so that the much larger S/N requirement for the 4-level code can still be met more easily than that for the simpler binary code.

All the impairments discussed earlier may contribute to the noise N. However, there are several sources

of noise that cannot be easily quantified, or are uncertain or unknown. Thus it is customary to allow a margin in addition to the theoretical SNR requirement in deriving performance criteria. We shall not dwell on the details here. Suffice it to say that based on engineering judgment and by consensus, a margin of 12 dB against theoretical calculations based primarily on NEXT and ISI, was accepted for ISDN Basic Access.[9] We shall use this as the basis for our discussion. In what follows S/N will be replaced by S/NEXT, to emphasize the fact that NEXT is assumed to be the dominant source of interference.

LOOP PREMISES WIRING CHARACTERIZATION

For both outside plant cables and premises wiring, three important attributes of a transmission system are crosstalk compatibility and range. As discussed above, we assume that the most significant factor determining the maximum bit rate to distance relationship is NEXT. So far we have assumed that the disturbing pairs in a cable are serving the same type of systems as the disturbed pair. When this is the case, we speak of self-NEXT and compatibility will imply their ability to coexist. Often, different types of systems are deployed on twisted pairs within the same cable. In such cases NEXT is also important, and assuring compatibility among systems, usually referred to as spectrum management, is a major concern of systems designers and transmission engineers. In this paper we shall consider only self-NEXT.

The range of a system is the maximum distance over which the system will operate satisfactorily. The measure of the available signal-to-noise ratio at the input to the signal receiver, in turn depends on the attenuation of the transmitted signal and the level of noise, including crosstalk from other systems. An ideal loop would be one of uniform characteristics from the transmitter to the receiver. But in general loops have more complicated makeup with not only different gauge pairs spliced together, but may also have one or more bridged taps of varying lengths and locations. These taps contribute significantly to the loss of the loop. Thus for our purposes, it is more appropriate to think of range in terms of loop loss than in terms of actual loop length.

In any application, the bit rate versus range capability depends not only on the transmission medium but also depends strongly on transmit and receive electronics. Also the bit rate on the line may differ from the customer data rate. For example, reference[2] discusses the effects of different line codes (with associated optimum equalizing etc) in achieving maximum coverage of the non-loaded loop plant for ISDN Basic Access. Among the factors affecting the performance of each code are its S/NEXT requirements (Table 1) and the degree to which it

Table 1

REQUIRED PEAK SIGNAL TO RMS NOISE IN dB

CODE	VOLTAGE LEVELS	PROB	NOISE	ERROR PROB	S/N FOR 10^{-7}
BINARY	V -V	5 5	N	$\phi\left(\frac{V}{N}\right)$	14 32 dB
TERNARY*	V 0 -V	33 33 33	N	$1\ 33\phi\left(\frac{V}{2N}\right)$	20 43 dB
TERNARY**	V 0 -V	25 5 25	N	$1\ 5\phi\left(\frac{V}{2N}\right)$	20 46 dB
QUATERNARY	$V\ \frac{V}{3}\ -\frac{V}{3}\ -V$	25 25 25 25	N	$1\ 5\phi\left(\frac{V}{3N}\right)$	23 99 dB

* Represents a typical 4B3T or 2B2T block code

** Represents a typical AMI code that ignores pulse polarity

Source R A McDonald, "Signal to Noise Requirements for 2B1Q Line Code," ANSI/ECSA Contribution T1D1 3/86-212, Oct 1986

takes advantage of the cable loss and crosstalk characteristics through bandwidth reduction. Our goal here is to define a process whereby we can give a reasonable idea of the bit rate capability of twisted wire pairs without specific reference to any specific system. Therefore we shall concentrate on NEXT with the assumption that improvements possible from the transmit and receive electronics are all in place.

Outside Plant

The plot designated OSP, the third from the top in Figure 1 is a NEXT model for outside plant cable.[6] (Other curves and points represent premises wiring cables and are discussed in Section 5.) The OSP plot was derived from a computer simulation of a lumped parameter model. The model was calibrated at 772 KHz, a frequency for which extensive field measurement data were available.[7] This calibration allowed the definition of the lumped parameters of the computer model. Simulation at several selected frequencies then facilitated the derivation of the plot. The plot represents the 1% worst power sum NEXT points when the disturbers are single frequency sources. The 1% point here means that 99% of the simulated NEXT power sum values were better (i.e., have higher loss) than this value. Any individual cable at any given frequency may have better or worse NEXT performance than given by the model.

The model also assumes colocation of up to 49 disturbing transmitters with the disturbed receiver, in a 50-pair binder group over a long enough common route in the cable to approach essentially maximum crosstalk coupling. The model is based on termination of individual pairs with approximately their characteristic impedance. The model does not represent crosstalk loss between individual pairs in a

cable. The crosstalk losses differ from one to another and have different shapes versus frequency. Note that NEXT loss decreases with frequency at about 14 dB per decade.[6] These are consistent with theoretical predictions and field measurements.

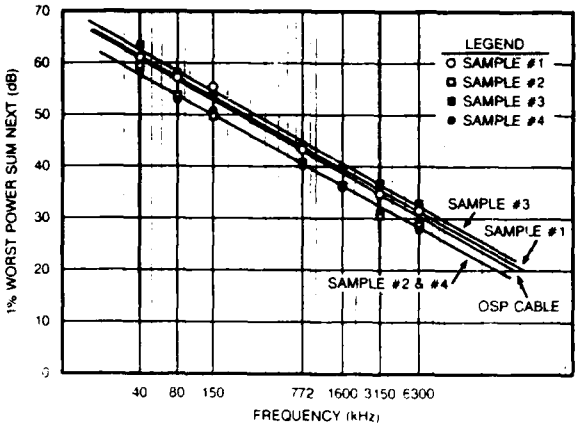

Figure 1: NEXT Models For Inside Wire And Outside Plant Cable

Recent NEXT measurements made on loops that included significant amounts of central office wiring generally agree with the model but show a little less crosstalk loss. The measurements may indicate that central office wire and wiring practices need further review. As a first step in investigating the question, we performed some measurements of building wire.

Inside Wiring Cable

The contribution to the NEXT power sum at the end point of a cable from coupling at distant points drops off rapidly for increasing distance.[5] Figure 2 illustrates the importance of careful look at inside wiring. The plots in Figure 2 display the percentage of NEXT (power) as a function of exposure length for selected frequencies. It is clear from these plots that, at high bit rates, the bulk of NEXT contributed by a loop may occur within the building wiring, especially in a campus-like environment, high rise buildings, or a large or multi-story central office where the switch may be some distance from the main distributing frame. (At the 80% point of a curve, the NEXT is about 1 dB less than the 100% value (asymptotic or converged NEXT.)

The physical characteristics of inside wiring cables are different from those of the outside plant cable. Inside wire and cable designs require special materials to meet the fire safety criteria. Polyvinyl chloride (PVC) insulation is the most often used insulation for inside wiring and cable since it provides protection against fire hazard. In situations where more stringent fire resistance requirements apply, fluoropolymers are often used.

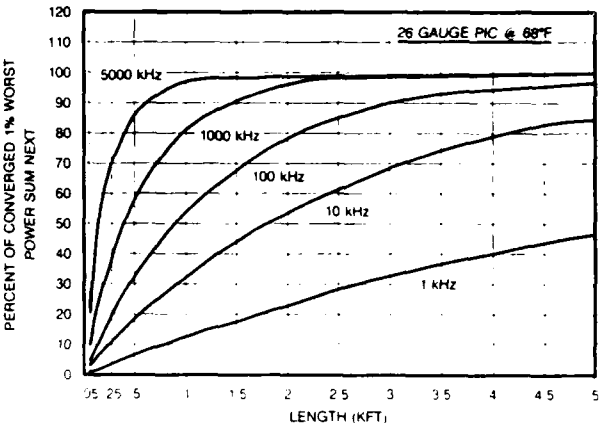

Figure 2: 1% Worst Power Sum NEXT By Exposure Length

Samples of inside wiring cables from four different vendors were used in our measurements to characterize inside wiring cables. Attenuation and crosstalk were measured using a DCM model CMS-2PCX Computerized Automatic Cable Measuring System. The measurement technique can be summarized by stating that the attenuation is measured directly in dB by a signal analyzer subsystem that consists basically of a single or dual channel narrow-band signal detector, a stable signal oscillator to stimulate the cable under test, and interface switching for control of the drive and receive signal paths.

Near-end crosstalk loss is measured by applying an oscillator to one pair and a detector to another. The cable pairs under test are driven and terminated in stable circuit impedances that closely approximate their characteristic impedance at carrier frequencies. Since telephone cable pairs are used in the balanced mode, the single-ended output of the oscillator and detector test signal input are impedance matched using precision broad-band balancing transformers.

RESULTS

Table 2 summarizes the diameter over dielectric (DOD), the coaxial and mutual capacitance and the dielectric constant data of the four inside wiring cable samples used for this characterization. In estimating range of transmitted distance versus bit rates, NEXT and attenuation are the two key factors. The effect of splicing on crosstalk and attenuation was measured on one cable group and found to be negligible for good splices. Next, the effect of bridged tap was measured. Table 3 is a summary of the measured values for cable sample #1. The total length of the cable was 897 feet. A bridged tap of length 315 feet was placed at the transmitting end (column VI); 300 feet from the transmitting end (column V); or at 600 feet from the

Table 2.

25/24 D INSIDE WIRE

Sample	DOD Avg. Ins	Coaxial Capacitance (μF/kft)	Mutual Capacitance nF/mile	Dielectric Const. ϵ_m
1	0.032	0.124	122	3.4
2	0.031	0.120	107	3.1
3	0.033	0.118	115	3.5
4	0.032	0.134	116	3.7

Table 3

Attenuation and Power Sum (PS) NEXT of Sample 1 (25/24 D Inside Wire) With or Without a Bridge Tap (B.T.)

	I				II				III			
Freq (kHz)	Att. (dB) Avg	PS NEXT (dB) Avg	Worst	σ	Att. (dB) Avg	PS NEXT (dB) Avg	Worst	σ	Att. (dB) Avg	PS NEXT (dB) Avg	Worst	σ
40	1.97	72.6	63.5	3.7	2.03	74.0	65.4	3.9	1.93	73.9	64.9	3.9
80	2.30	67.3	58.3	3.4	2.34	68.7	58.0	3.5	2.29	67.1	58.2	3.5
150	3.47	62.9	58.0	2.8	2.97	61.7	53.3	3.1	3.05	61.8	53.3	3.1
772	6.41	51.0	45.6	3.1	6.32	51.4	43.6	3.2	6.29	51.3	43.7	3.2
1600	9.88	45.0	35.7	3.5	9.69	46.3	39.8	3.1	9.71	46.2	39.7	3.1
3150	14.57	42.2	36.0	3.1	14.29	42.4	34.5	3.8	14.25	42.4	34.5	3.7
6300	21.26	37.9	32.9	2.8	21.20	38.3	34.9	2.4	21.17	38.1	34.5	2.4
Test Configuration	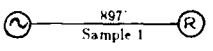				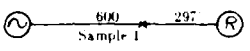				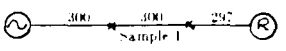			

Table 3 (Continued)

	IV				V				VI			
Freq (kHz)	Att. (dB) Avg	PS NEXT (dB) Avg	Worst	σ	Att. (dB) Avg	PS NEXT (dB) Avg	Worst	σ	Att. (dB) Avg	PS NEXT (dB) Avg	Worst	σ
40	2.04	70.2	63.2	2.9	2.03	71.1	63.9	2.9	2.04	72.4	64.9	3.1
80	2.78	65.4	58.5	2.6	2.73	66.0	58.7	2.6	2.69	66.4	59.0	2.8
150	4.13	61.1	55.0	2.2	4.16	60.5	53.4	2.5	3.79	60.8	53.5	2.7
772	7.69	50.9	45.5	2.4	7.74	50.9	43.3	3.1	7.90	51.1	43.0	3.2
1600	13.22	45.3	41.1	2.4	13.22	46.1	40.6	2.9	14.05	45.9	39.7	3.1
3150	16.91	42.2	35.6	3.4	17.01	42.5	34.7	3.8	17.30	42.4	34.6	3.8
6300	25.02	38.3	34.6	2.3	25.01	38.4	34.7	2.5	25.55	38.1	34.3	2.5
Test Configuration	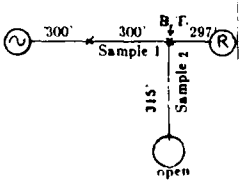				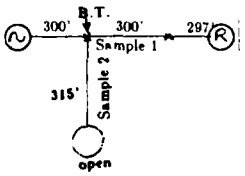				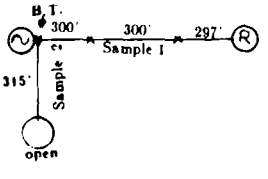			

transmitting end (column IV). The attenuation, the average crosstalk, the standard deviation and the worst crosstalk (of all the 24 possible values) for all these cases are given in Table 3 for a set of frequencies from 40 KHz to 6.3 MHz. The effect of bridged tap on the attenuation of the cable sample was evident at all frequencies, resulting in an attenuation increase with frequency. At 6.3 MHz the attenuation increase was as much as 3.8 to 4.4 dB. Also, the location of the bridged tap was significant (as expected). It was observed that the bridged tap nearest to the transmit end produced higher loss than at other locations, especially at higher frequencies. No appreciable difference in NEXT (or FEXT) was observed with the bridged tap at any of the locations.

It is known from theoretical estimates that the worst effect of a bridged tap is generally felt when its length is of quarter wavelength; therefore, additional measurements at 772 KHz and 1.6 MHz were made with bridged taps having approximate quarter

wavelengths of 210 feet and 102 feet, respectively. These taps were cut from cable sample 2. Table 4 displays the details of these measurements. As expected, the attenuation increased significantly with these bridged taps for each case. At 772 KHz it increased from 7.15 dB to 16.71 dB when the 210 foot bridged tap was placed at the signaling end. These results are an indication of the need for extra caution when bridged taps are present. Note that one of the principal contributors to increased loss was impedance effect of the bridged tap.

Table 5 summarizes the measurements made on the four premises cable samples. The automatic test set computes the attenuation and the NEXT values both in dB/kft from the measured values. The correction factor for computation of NEXT in dB/kft can be found in reference[10] and also in Table 5 along with other equations for "Total Average NEXT" and "1% NEXT." Using the corrected value for NEXT in dB/kft in the equation for Total Average NEXT, the 1% NEXT is calculated.

Example: Sample #1 - 897 ft.
At 772 kHz,
Measured Avg. Attenuation = 7.15 dB/kft.
Measured Avg. Power Sum NEXT = 51.04 dB
Computed Standard Deviation σ = 3.1 dB

$$\text{Computed Avg. NEXT}_m = \text{next} + 10 \log \left[\frac{1-10^{-\alpha \frac{\ell}{5}}}{1-10^{-\frac{\alpha}{5}}} \right]$$

$$= 51.04 + 10 \log \left[\frac{1-10^{-7.15 \times \frac{0.897}{5}}}{1-10^{\frac{-7.15}{5}}} \right]$$

$$= 51.0 \text{ dB/kft.}$$

$$\text{Computed Total Avg. NEXT} = \text{NEXT}_m - 10 \log \left(\frac{1}{1-10^{-\frac{\alpha}{5}}} \right)$$

$$= 51.0 - 0.16 = 50.8 \text{ dB}$$

1% NEXT = Total Avg. NEXT - 2.33 σ
= 50.8 - 2.33 x 3.1
= 43.6 dB

Table 4

Attenuation and Power Sum (PS) NEXT of Sample 1 (25/24 D Inside Wire) *Including* a Bridge Tap (B.T.) With a Quarter Wavelength Sample

(A) Freq = 772 kHz

	I			II			III			IV		
	Att (dB) Avg	PS NEXT (dB) Avg	Worst	Att (dB) Avg	PS NEXT (dB) Avg	Worst	Att (dB) Avg	PS NEXT (dB) Avg	Worst	Att (dB) Avg	PS NEXT (dB) Avg	Worst
	6.41	51.2	43.1	14.43	47.7	44.5	14.62	48.9	42.0	14.98	49.6	41.9

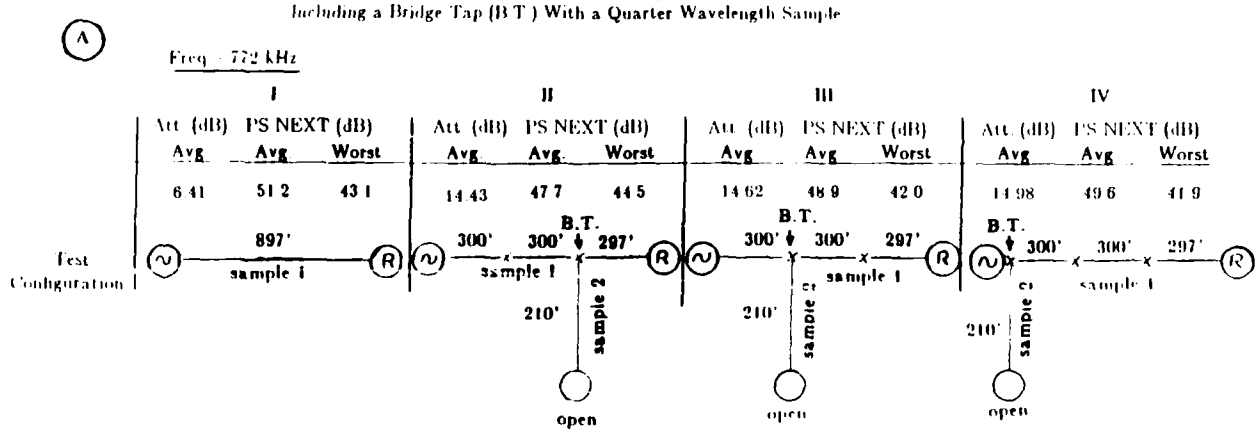

(B) Freq = 1600 kHz

	I			II			III			IV		
	Att (dB) Avg	PS NEXT (dB) Avg	Worst	Att (dB) Avg	PS NEXT (dB) Avg	Worst	Att (dB) Avg	PS NEXT (dB) Avg	Worst	Att (dB) Avg	PS NEXT (dB) Avg	Worst
	9.88	46.4	40.3	19.08	43.7	40.5	19.20	45.7	42.2	20.10	45.7	40.8

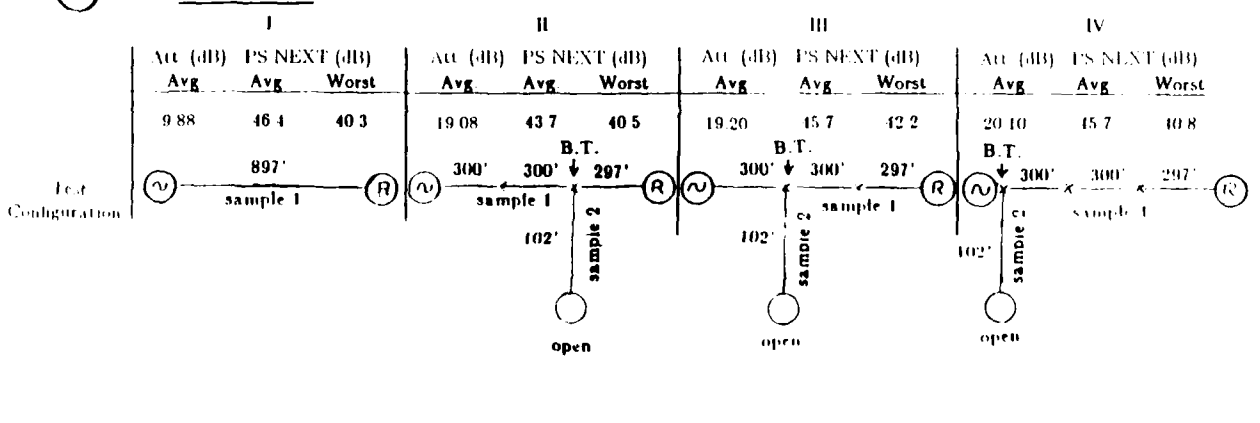

Table 5.

Transmission Characteristics of 25/24 D Inside Wire

	Sample 1			Sample 2			Sample 3			Sample 4		
Freq. (kHz)	Att. dB/kft	$NEXT_m$ dB/kft	1%NEXT dB	Att. dB/kft	$NEXT_m$ dB/kft	1%NEXT dB	Att. (dB/kt)	$NEXT_m$ (dB/kft)	1%NEXT (dB)	Att. (dB/kft)	$NEXT_m$ (dB/kft)	1%NEXT (dB)
40	$\bar{x}$ - 2.19	$\bar{x}$ - 72.3 worst-63.3 σ - 3.7	61.2	$\bar{x}$ - 2.14	$\bar{x}$ - 66.8 worst-63.1 σ - 2.5	59.4	$\bar{x}$ 2.27	$\bar{x}$ - 70.8 worst-67.6 σ - 2.3	63.9	$\bar{x}$ - 2.38	$\bar{x}$ - 64.0 worst-60.5 σ - 1.6	58.5
80	$\bar{x}$ - 2.56	$\bar{x}$ - 67.0 worst-58.1 σ - 3.4	57.5	$\bar{x}$ - 2.47	$\bar{x}$ - 60.8 worst-57.2 σ - 2.3	53.7	$\bar{x}$ - 2.63	$\bar{x}$ - 64.6 worst-61.6 σ - 2.2	58.0	$\bar{x}$ - 2.62	$\bar{x}$ - 58.0 worst-54.7 σ - 1.5	53.0
150	$\bar{x}$ - 3.87	$\bar{x}$ - 62.7 worst-57.8 σ - 2.8	55.4	$\bar{x}$ - 3.32	$\bar{x}$ - 56.2 worst-52.9 σ - 2.2	50.0	$\bar{x}$ - 3.53	$\bar{x}$ - 59.7 worst-56.8 σ - 2.0	54.0	$\bar{x}$ - 3.79	$\bar{x}$ - 54.3 worst-51.9 σ - 1.1	50.9
772	$\bar{x}$ - 7.15	$\bar{x}$ - 51.0 worst-45.5 σ - 3.1	43.6	$\bar{x}$ - 6.63	$\bar{x}$ - 45.0 worst-42.2 σ - 1.9	40.4	$\bar{x}$ - 7.10	$\bar{x}$ - 48.4 worst-45.5 σ - 1.7	44.2	$\bar{x}$ - 7.08	$\bar{x}$ - 42.9 worst-40.9 σ - 1.1	40.1
1600	$\bar{x}$ - 11.01	$\bar{x}$ - 45.0 worst-35.7 σ - 3.5	36.8	$\bar{x}$ - 10.07	$\bar{x}$ - 40.7 worst-37.7 σ - 1.8	36.5	$\bar{x}$ - 10.74	$\bar{x}$ - 44.9 worst-40.7 σ - 2.2	39.8	$\bar{x}$ - 10.94	$\bar{x}$ - 38.6 worst-36.9 σ - 1.1	36.0
3150	$\bar{x}$ - 16.25	$\bar{x}$ - 42.2 worst-36.0 σ - 3.1	35.0	$\bar{x}$ - 14.84	$\bar{x}$ - 36.5 worst-33.9 σ - 2.4	30.9	$\bar{x}$ - 15.79	$\bar{x}$ - 40.2 worst-37.8 σ - 1.4	36.9	$\bar{x}$ - 16.17	$\bar{x}$ - 34.7 worst-32.9 σ - 1.3	31.7
6300	$\bar{x}$ - 23.71	$\bar{x}$ - 37.9 worst-32.9 σ - 2.8	31.4	$\bar{x}$ - 21.92	$\bar{x}$ - 32.5 worst-30.1 σ - 1.7	28.5	$\bar{x}$ - 23.18	$\bar{x}$ - 36.6 worst-34.0 σ - 1.6	32.9	$\bar{x}$ - 24.21	$\bar{x}$ - 30.9 worst-28.4 σ - 1.1	28.3

NOTE:

$$NEXT_m(dB/kft) = \textbf{next} + 10 \log \left[\frac{1-10^{-\alpha\frac{\ell}{6}}}{1-10^{-\frac{\alpha}{6}}} \right]$$

$$Total\ Avg.\ NEXT\ (dB) = NEXT_m - 10 \log \left(\frac{1}{1-10^{-\frac{\alpha}{6}}} \right)$$

1% NEXT (dB) = Total Avg. NEXT - 2.33 σ

where,

next = Measured value of NEXT in dB
α = Average attenuation in dB/kft
$\bar{x}$ = Average value of 25 pairs
σ = Standard Deviation
ℓ = Length of cable

The individual 1% NEXT values for each sample were then derived from computed total average NEXT and the standard deviation as shown above. For each of the four samples, the 1% NEXT values were plotted as shown in Figure 1. The plots for samples #1 and #3 indicate better crosstalk characteristics than that displayed by the outside plant (OSP) model. But the plots for samples #2 and #4, which are almost identical, are consistently about 2 dB below the OSP model. To be on the conservative side, the NEXT model for inside wiring was estimated from samples #2 and #4 and is displayed in Figure 3. It is important to note that this model does not take into consideration the effects of bridged taps or gauge changes.

The NEXT model can now be used to estimate the bit rate versus range values. The bottom three plots in Figure 3 are for signal loss (not crosstalk loss) required to achieve the required S/NEXT at the given frequency for binary transmission with margins of 6 dB, 12 dB and 18 dB respectively. As discussed earlier, a margin of 12 dB is considered to be a conservative allowance for all the unknowns etc. However, we saw above that, bridged taps may add significantly to loss and therefore must either be added to the loss considerations or be included in the margin. In the latter case, a margin of 18 dB may not be far-fetched. Furthermore, the frequency in Figure 3 is not directly translatable into bit rate because any digital signal covers a band of frequencies rather than just one.

DISCUSSION

From the plots of Figure 3 a corresponding set of curves have been drawn and displayed in Figure 4 for use as a model for considering the trade-off of transmission rate versus transmission distance for premises wiring. We emphasize that these curves should not be applied to any individual system. As suggested earlier, for digital systems there is in general no simple relationship between bit rate and frequency. We saw that the crosstalk loss worsens and the loss increases rapidly with frequency. Thus a system may be designed, for example, to increase the low frequency components and filter the relatively strong high frequency components. For such a system, the practice of taking the center frequency (e.g., 772 KHz for the 1.544 mbps AMI digital system) to represent the system and use the plots from Figure 4 will yield results that are too pessimistic. Noise and signal must be considered as a whole over the signal bandwidth to obtain accurate signal to noise ratios. Our purpose was to obtain a simplified model that does not depend on details of system design. Therefore, further work is needed before this result can be applicable to any specific system design.

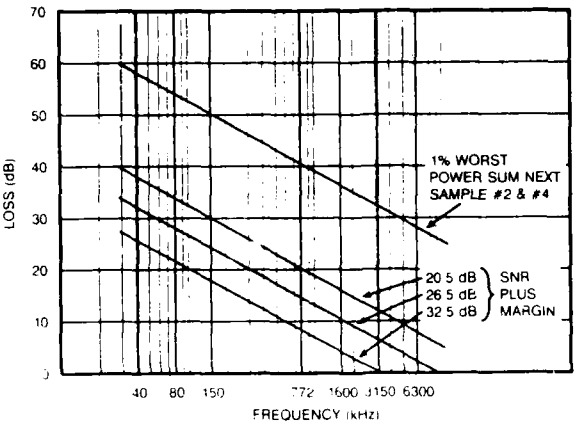

Figure 3: NEXT Model And SNR Plus Margins For Inside Wires

In summary, these plots are useful indicators in estimating the trends of transmission rate versus distance with applications in areas such as cable manufacturing, office wire planning for telecommunications and high speed data transmission.

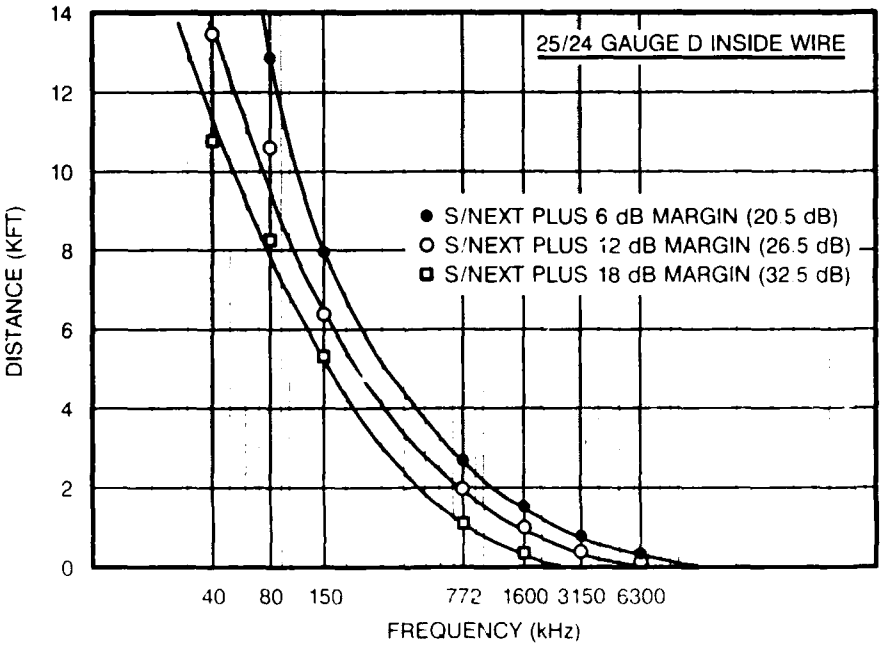

Figure 4: Distance Vs. Frequency

AD-A200 903 PROCEEDINGS OF THE INTERNATIONAL WIRE AND CABLE SYMPOSIUM (IWCS 37TH) HEL..(U) ARMY COMMUNICATIONS-ELECTRONICS COMMAND FORT MONMOUTH NJ

5/9

UNCLASSIFIED 17 NOV 88 F/G 9/1 NL

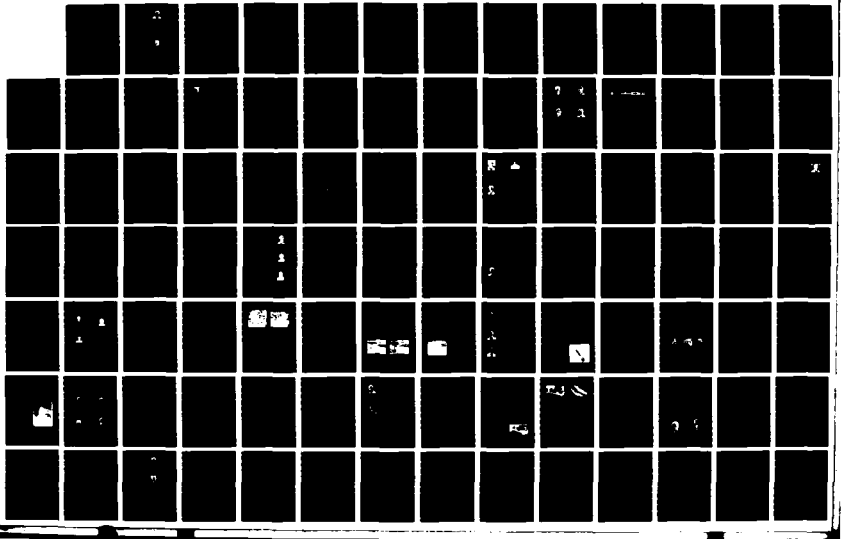

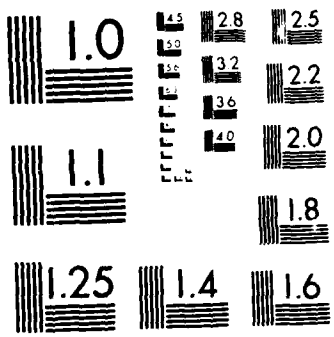

ACKNOWLEDGEMENTS

Authors would like to thank Dr. R. A. McDonald for his valuable advice and Mr. A. J. Gambardella for his help in performing the tests.

REFERENCES

1. Bell Communications Research, Inc., "I-MATCH.1 Loop Characterization Data Base," Special Report SR-TSY-000231, Issue 1, June 1985.
2. J. W. Lechleider and R. A. McDonald, "Capability of Telephone Loop Plant for ISDN Basic Access," ISSLS 1986, p156.
3. Bell Communications Research, "ISDN Basic Access Digital Subscriber Lines," TR-TSY-000393, May 1988.
4. American National Standard for Telecommunications, "Integrated Services for Digital Network - Basic Access Interface for use on Metallic Loops for Application on the Network Side of the NT - Layer 1 Specification," ANSI T1.XXX-188Y.
5. H. Cravis and T. V. Crater, "Engineering of T1 Carrier System Repeatered Lines," BSTJ, March 1963.
6. J. H. W. Unger, "Near-End Crosstalk Model for Line Code Studies," T1D1.3/85-244, November 12, 1985.
7. S. H. Lin, "Statistical Behavior of Multipair Crosstalk, Bell System Technical J., 59, No. 6, July 1980, pp955-974.
8. R. A. McDonald, "Signal to Noise Requirements for 2B1Q Line Code," ANSI/ECSA Contribution T1D1.3/86-212, Oct. 1986.
9. R. A. McDonald, "Common Definitions for Use in Comparing Alternative Line Code Proposals," ANSI/ECSA Contribution T1D1.3/85-241, November 18, 1985.
10. Bellcore "Generic Requirements for Metallic Tele- communication Cables," Technical Reference TR-TSY-000421, Issue 2, June 1988.

Lal M. Hore

Bellcore
445 South Street
Rm. MRE-2K171
Morristown, NJ 07960

Lal M. Hore received the B.Sc.(Hons.) degree with Physics major, M.Sc. (Tech.) degree in Applied Physics, both from the University of Calcutta and Dr. Tech. degree from the Technical University of Budapest in Electrical Engineering. He was with Bell Northern Research, Canada as Member of R&D staff in design and development of communications cables from 1970 to 1972 and next with General Cable Company's Telecommunications Cable Division from 1972 to 1987 - first eight years in the R&D Laboratories as Research Section Manager and next as Staff Project Manager in the Applications Engineering. Currently, as a Member of Technical Staff of Bellcore, he is responsible for the preparation of Technical References for Outside Plant Cables and also the development of transmission requirements of all wire products for high speed transmission.

Dr. Hore has authored ten technical papers on dielectric properties of electrical insulation materials and telecommunications cables. He holds three patents on coaxial and other cable products.

V.Thuraisamy

Bellcore
445 South Street
Morristown, NJ 07960

V. Thuraisamy received the B.Sc(hons) degree from the University of Ceylon, the M.A. from the University of Massachusetts in 1963 and the Ph.D. from the University of Maryland in 1967, all in mathematics. From 1967 to 1972 he was with Bellcomm participating in the Apollo and Skylab programs of NASA. From 1972 to 1983 he was with AT&T Bell Labs performing network optimization and analysis of nonlinear signaling systems. Since the Bell System divestiture he has been with Bell Communications Research, Inc. working on noise cancellation and other related aspects of high speed data transmission at the exchange level. He received the 1987 Bellcore Award of Excellence for his contributions to the ISDN project. His interests are in numerical analysis and computer simulation of systems.

Dr. Thuraisamy is a Distinguished Member of Technical Staff at Bellcore and is a member of the Society for Industrial and Applied Mathematics.

Transmission and Shielding Considerations in Communication Cables

J. W. LEVENGOOD

AT&T Technologies

1. INTRODUCTION

Shielding of various types have been used on paired cables for many years. Many papers have been written on this subject, but they usually only investigate the degree of shielding. What we propose to do in this paper is to provide information (test results) on shielding effectiveness of various shield materials (thin foils, thicker foils, dual foils, braids, and hybrid shields of both foil and braid). The edge preparation is considered in that both flat foil and "Z" foil shields are used in the samples. The method of application of these shields is considered in that samples were made with the shields applied in the twisting operation using both a single twist as well as a double twist machine. Representatives of each shield type was made up into single pair cables, two pair cables and twelve pair cables. In the last two cases overall shield samples were also included. The transmission parameters on each of these cables as well as the crosstalk on the twelve pair cables was measured and is presented

2. SAMPLE PREPARATION

There are a total of 28 cables that were made for the shielding study. There are seven one pair cables, nine two pair cables, and twelve twelve pair cables.

All wires of a given color were made in a continuous operation. All pairs of a given color were made on the same equipment in a continuous operation except where noted. These steps were used in order to minimize the effect of wire or pair differencies. In the cases where individually shielded pairs were used each pair was treated the same (and manufactured) and placed into the appropriate cable whether single pair, two pair, or twelve pair. The twist length of each pair color was maintained the same in all cables and the twist length scheme was such that there were few if any repeats in a cable. In each set of cables, at least one cable was not shielded so it could be used as a reference.

For the single pair cables the following list gives the pertinent data.

TABLE 1. SINGLE PAIR CABLES

CABLE	SHIELD TREATMENT
XA01	No shield.
XA02	0.0003 inch aluminum shield on a polyester film applied longitudinally with a flat fold during the twisting operation using a single twist machine.
XA03	0.0003 inch aluminum shield on a polyester film applied longitudinally with a flat fold during the twisting operation using a double twist machine.
XA04	0.0003 inch aluminum shield on a polyester film applied longitudinally with a "Z" fold during the twisting operation using a single twist machine.
XA05	0.0003 inch aluminum shield on a polyester film applied longitudinally with a "Z" fold during the twisting operation using a double twist machine.
XA06	0.001 inch aluminum shield on a polyester film applied longitudinally with a flat fold during the twisting operation.
XA07	90% (actual coverage 88%) braid shield.

TABLE 2. TWO PAIR CABLES

CABLE	SHIELD TREATMENT
XB01	No shield.
XB02	Individual 0.0003 inch aluminum shield on a polyester film applied longitudinally with a flat fold during the twisting operation.
XB03	Individual 0.0003 inch aluminum shield on a polyester film applied longitudinally with a "Z" fold during the twisting operation.
XB04	Individual 0.001 inch aluminum shield on a polyester film applied longitudinally with a flat fold during the twisting operation.
XB05	Individual braided shield (88% coverage).
XB06	Individual 0.001 inch aluminum shield on a polyester film applied longitudinally with a flat fold during the twisting operation with an overall braided shield (88% coverage).
XB07	Overall 0.001 inch aluminum shield on a polyester film applied longitudinally with a flat fold seam

CABLE	SHIELD TREATMENT
XB08	Dual overall 0.001 inch aluminum shields on a polyester film applied longitudinally with opposite flat fold seams. Inner shield with aluminum out and outer shield with aluminum in and drain between shields.
XB09	Hybrid overall 0.001 inch aluminum shield on a polyester film applied longitudinally with a flat fold seam with a 88% coverage braid.

TABLE 3. TWELVE PAIR CABLES

CABLE	SHIELD TREATMENT
XC01	No shield. This cable had core with a 15 inch lay.
XC02	Individual 0.0003 inch aluminum shield on a polyester film applied longitudinally with a flat fold during the twisting operation.
XC03	Individual 0.0003 inch aluminum shield on a polyester film applied longitudinally with a "Z" fold during the twisting operation.
XC04	Individual 0.001 inch aluminum shield on a polyester film applied longitudinally with a flat fold during the twisting operation.
XC05	Individual braided shield (88% coverage).
XC06	Overall 0.001 inch aluminum shield on a polyester film applied longitudinally with a flat fold seam. This cable had a layless core.
XC07	Overall 0.001 inch aluminum shield on a polyester film applied longitudinally with a flat fold seam. This cable had core with a 15 inch lay.
XC08	No shield. This cable had core with a 15 inch lay using an oscillating face plate.
XC09	Dual overall 0.01 inch aluminum shields on a polyester film applied longitudinally with opposite flat fold seams. Inner shield with aluminum out and outer shield with aluminum in and drain between shields. This cable had core with a 15 inch lay.
XC10	Overall braided shield (88% coverage). This cable had core with a 15 inch lay.
XC11	Hybrid overall 0.001 inch aluminum shield on a polyester film applied longitudinally with a flat fold seam with a 70% coverage braid. This cable had core with a 15 inch lay.
XC12	Hybrid overall 0.001 inch aluminum shield on a polyester film applied longitudinally with a flat fold seam with a 88% coverage braid. This cable had core with a 15 inch lay.

3. DISCUSSION

3.1 TRANSMISSION LINE

The equations of transmission lines have been developed by many authors using different methods. We do not propose to develop these equations here but to use those available from the literature. The following work is based upon the work by Dr. Chipman[1].

A transmission line may be modeled many ways, but from an engineering standpoint the simpler the model the better as long as it is adequate to define what is happening.

IN THE FREQUENCY DOMAIN

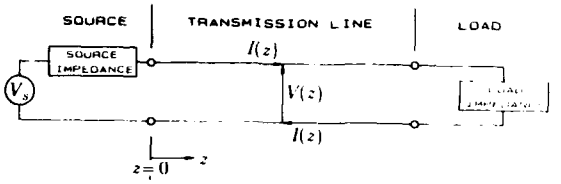

FREQUENCY DOMAIN

Figure 1. TRANSMISSION LINE

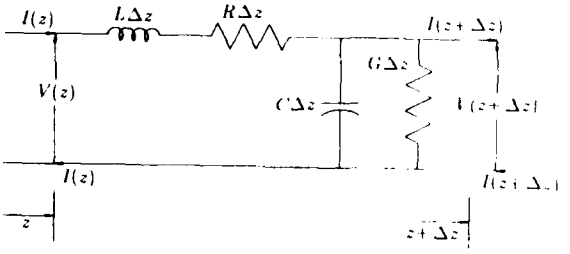

Figure 2. SEGMENT OF TRANSMISSION LINE

Figures 1 and 2 show a transmission line and a segment of that transmission line at a position z. Using the distributed parameters shown in that segment the equations for the transmission of a signal along the line can be developed.

$$\begin{aligned}\Delta V(z) &= V(z+\Delta z) - V(z) \\ &= -R\,\Delta z\, I(z) - j\,\omega\, L\,\Delta z\, I(z)\end{aligned} \tag{1}$$

$$\begin{aligned}\Delta I(z) &= I(z+\Delta z) - I(z) \\ &= -G\,\Delta z\, V(z) - j\,\omega\, C\,\Delta z\, V(z)\end{aligned} \tag{2}$$

$$\lim_{\Delta z \to \infty} \frac{\Delta V(z)}{\Delta z} = \frac{dI(z)}{dz} = -R\, I(z) - i\omega L\, I(z) \tag{3}$$

$$\lim_{\Delta z \to \infty} \frac{\Delta I(z)}{\Delta z} = \frac{dI(z)}{dz} = -G\, V(z) - i\omega C\, V(z) \tag{4}$$

$$\frac{dV(z)}{dz} = -(R + i\omega L)\, I(z) \tag{5}$$

$$\frac{dI(z)}{dz} = -(G + i\omega C)\, V(z) \tag{6}$$

Differentiating both sides we obtain:

$$\frac{d^2 V(z)}{dz^2} = -(R + i\omega L)\frac{dI(z)}{dz} \tag{7}$$

$$\frac{d^2 I(z)}{dz^2} = -(G + i\omega C)\frac{dV(z)}{dz} \tag{8}$$

Solving for $\frac{dI(z)}{dz}$ from equation (7) and substituting back into equation (6) we get:

$$\frac{d^2V(z)}{dz^2} - (R + j\omega L)(G + j\omega C)V(z) = 0 \quad (9)$$

Solving for $\frac{dV(z)}{dz}$ from equation (8) and substituting back into equation (5) we get:

$$\frac{d^2I(z)}{dz^2} - (R + j\omega L)(G + j\omega C)I(z) = 0 \quad (10)$$

where:

$$\gamma^2 = (R + j\omega L)(G + j\omega C) \quad (11)$$

$$\gamma = \sqrt{(R + j\omega L)(G + j\omega C)} \quad (12)$$

$$\frac{d^2V(z)}{dz^2} - \gamma^2 V(z) = 0 \quad (13)$$

$$\frac{d^2I(z)}{dz^2} - \gamma^2 I(z) = 0 \quad (14)$$

These are linear, homogeneous second order equations which have solutions of the form of:*

$$y = C_1 e^{m_1 x} + C_2 e^{m_2 x}$$

Therefore:

$$V(z) = V_1 e^{-\gamma z} + V_2 e^{\gamma z} \quad (15)$$

$$I(z) = I_1 e^{-\gamma z} + I_2 e^{\gamma z} \quad (16)$$

The equations show two signals one traveling in the +z direction and one in the -z direction. The first would be derived from the source and the second if it exists would be due to reflections from the load.

If we consider a system where there are no reflected waves then:

$$V(z) = V_1 e^{-\gamma z} \quad (17)$$
$$I(z) = I_1 e^{-\gamma z} \quad (18)$$

Since gamma is a complex variable we can define:

$$\gamma = \alpha + j\beta \quad (19)$$

and

$$V(z) = V_1 e^{-\alpha z} e^{-j\beta z} \quad (20)$$
$$I(z) = I_1 e^{-\alpha z} e^{-j\beta z} \quad (21)$$

Where:

$$\alpha + j\beta = \sqrt{(R + j\omega L)(G + j\omega C)} \quad (22)$$

The characteristic impedance of the line can be determined by differentiating equation (17):

$$\frac{dV(z)}{dz} = V_1 (-\gamma) e^{-\gamma z} \quad (23)$$

and substituting into equation (5).

$$-V_1 \gamma e^{-\gamma z} = -(R + j\omega L)I(z) \quad (24)$$

Obtaining the value of $I(z)$ from equation (18) we get:

$$V_1 \gamma e^{-\gamma z} = (R + j\omega L)I_1 e^{-\gamma z} \quad (25)$$

Solving for $\frac{V_1}{I_1}$ and substituting from equation (12) for γ we get:

$$\frac{V_1}{I_1} = \frac{(R + j\omega L)}{\sqrt{(R + j\omega L)(G + j\omega C)}} \quad (26)$$

or,

$$Z_o = \frac{V_1}{I_1} \quad (27)$$

$$Z_o = \left[\frac{(R + j\omega L)}{(G + j\omega C)}\right]^{1/2} \quad (28)$$

The equations for γ and Z_o lend themselves to simplification in certain regions of the frequency domain depending on the relative value of the elements involved. At frequencies such that $R >> \omega L$ (usually below 10 KHz) and $\omega C >> G$ (generally for all frequencies):

$$\gamma = \sqrt{j\omega CR} = \sqrt{\omega CR} \text{ at an angle of } \frac{\pi}{4} \quad (29)$$

$$Z_o = \left[\frac{R}{j\omega C}\right]^{1/2} = \left[\frac{R}{\omega C}\right]^{1/2} \text{ at an angle of } -\frac{\pi}{4} \quad (30)$$

At frequencies such that $\omega L >> R$ (usually above 100 KHz) and $\omega C >> G$:

$$\gamma = j\omega\sqrt{LC} = \beta \quad (31)$$

$$Z_o = \left[\frac{L}{C}\right]^{1/2} \quad (32)$$

However, even though alpha will be small compared to beta it is still important and can be found by expanding the expression for γ in a binomial series and retaining only the low order terms. Therefore:

$$\alpha = \frac{R}{2}\left[\frac{C}{L}\right]^{1/2} + \frac{G}{2}\left[\frac{L}{C}\right]^{1/2} \quad (33)$$

3.2 EQUIVALENT CIRCUIT PARAMETERS

The equivalent circuit parameters of a transmission line (see Figure 2) are the distributed resistance, inductance, capacitance, and conductance. These values are functions of the mechanical positioning of the various elements of the line and the electrical characteristics of the materials involved in the line. Resistance and inductance are also functions of frequency.

3.2.1 RESISTANCE The parameter of resistance will vary with frequency, but is also effected by all parts of the transmission line around it. We can consider three regions of interest with respect to frequency. They are:

* "CRC MATHEMATICAL TABLES", 26th EDITION, CRC PRESS, BOCA RATON, FLORIDA

Low Frequency

$$R = 2\,R_e + R_{s1} \tag{34}$$

Intermediate Frequency

$$R = 2\,R_e + R_{s2} \tag{35}$$

High Frequency

$$R = 2\,R_e + 2\,\delta_1\,R_e + R_{s3} \tag{36}$$

where:

R_e = *resistance in space of a single conductor with a coaxial return.*

R_{s1} = *proximity effect of the shield at low frequencies.*

R_{s2} = *proximity effect of the shield at intermediate frequencies.*

R_{s3} = *proximity effect of the shield at high frequencies.*

$2\,\delta_1\,R_e$ = *proximity effect of the two conductors on each other.*

3.2.2 INDUCTANCE The parameter of inductance will also vary with frequency and is also effected by all parts of the transmission line around it. We can consider three regions of interest with respect to frequency. They are:

Low Frequency

$$L = L_{space} + 2\,L_i + L_{s1} \tag{37}$$

Intermediate Frequency

$$L = L_{space} + 2\,L_i + L_{s2} \tag{38}$$

High Frequency

$$L = L_{space} + 2\,(\delta_1 + 1)\,L_i + L_{s3} \tag{39}$$

where:

L_{space} = *external inductance in space of the two conductors of a pair.*

L_i = *internal inductance of a single conductor in space.*

L_{s1} = *proximity effect of the shield at low frequencies.*

L_{s2} = *proximity effect of the shield at intermediate frequencies.*

L_{s3} = *proximity effect of the shield at high frequencies.*

$2\delta_1 L_i$ = *proximity effect of the two conductors on each other.*

3.2.3 CAPACITANCE The mutual capacitance (C) does not vary with frequency if the dielectric constant of the insulation material is constant with frequency. A thorough discussion of the capacitance of a shielded balanced pair is covered in the literature.[2]

$$C = C_{12} + \frac{C_{1g} \times C_{2g}}{C_{1g} + C_{2g}} \tag{40}$$

where:

C_{12} = *direct capacitance of the two wires in a pair.*

C_{1g} = *capacitance on wire 1 to the rest of the world.*

C_{2g} = *capacitance on wire 2 to the rest of the world.*

3.2.4 CONDUCTANCE For most materials used in the modern transmission lines the value of mutual conductance (G) is small (*i.e.* $G \ll j\omega C$) and may be determined from the power factor (PF) of the dielectric constant as follows:

$$G = 2\,\pi\,f_{kHz}\,C\,PF \tag{41}$$

3.3 CROSSTALK

If the signals are transmitted in only one direction in a cable then only far end crosstalk (FEXT) is of importance, however, if signals go both ways in a cable then near end crosstalk (NEXT) must also be considered.

Crosstalk in a cable or transmission system is defined as the intrusion into the cable or transmission system of unwanted signals from other sources. This could be the intrusion of signals from another pair in the same cable or from other cables or sources. Shields are used to reduce crosstalk in cables and between cables. Crosstalk can therefore be used as a measure of the value of various shields.

There are several measures of crosstalk used. They are:
Mean:

$$MEAN = \frac{\sum_{i=1}^{N} XT(i)}{N} \tag{42}$$

RMS:

$$RMS = -20 \times \log \left[\frac{\left(\sum_{i=1}^{N} \left(10^{\frac{-XT(i)}{20}} \right)^2 \right)}{N} \right]^{\frac{1}{2}} \tag{43}$$

MINIMUM VALUE (MV):

$$MV = MIN\ \ OF\ XT(i),\ for\ all\ i,\ 1 \le i \le N \tag{44}$$

POWER SUM (PS):

$$PS = -20 \times \log \left[\sum_{i=1}^{N} \left(10^{\frac{-XT(i)}{20}} \right)^2 \right]^{\frac{1}{2}} \tag{45}$$

In order to compare the crosstalk of different length cables the following two equations may be used to convert the measured values to values referenced to a specific length.

$$NEXT_K = NEXT_{MEAS} + 10 \times \log \left[\frac{\left(1 - e^{\frac{-4AK}{n}} \right)}{\left(1 - e^{\frac{-4AL}{n}} \right)} \right] \tag{46}$$

$$FEXT_K = FEXT_{MEAS} + \left[-10 \times \log\left(\frac{K}{L}\right)\right] \quad (47)$$

It is usually best to convert the FEXT measurement to an equal level measurement in order to have the signals at the far end referenced to the same levels. This is accomplished by first subtracting the insertion loss (IL) at the measured length and then converting the FEXT to the referenced length.

The IL may be converted to the referenced length by:

$$INSERTION\ LOSS_K = IL_{MEAS} \times \left(\frac{K}{L}\right) \quad (48)$$

where:

XT = *a pair to pair crosstalk value in dB*
N = *total number of crosstalk values*
M = *total number of send pairs*
A = *average insertion loss per foot*
L = *length of cable in feet*
K = 1000 *feet*
n = 8.68588

3.4 SHIELDING EFFECTIVENESS

The shielding effect can be measured using the transverse impedance method. In this method a current is generated on the inner surface of the shield and the resulting voltage on the outer surface of the shield is measured. The ratio of these two quantities is an impedance called the transverse impedance ($Z_{\alpha\beta}$).[4] In general the lower the value of the transverse impedance the "better" the shield.

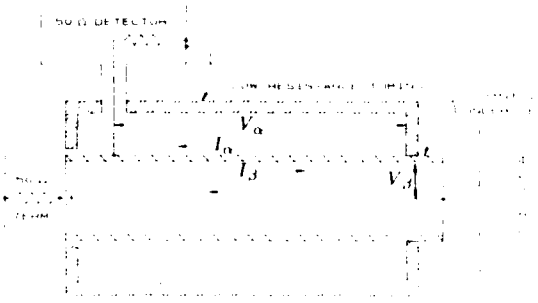

Figure 3. $Z_{\alpha\beta}$ TEST CIRCUIT

Figure 3 presents the test circuit for the tests. The generator develops a voltage between the selected wire in the cable and the shield which drives a current (I_β) through the 50 ohm resistor. The voltage on the outer surface of the shield is detected (V_α). Care must be taken in connecting the cable to the end terminations to insure that the leakage due to these terminations does not effect the test results.

$$Z_{\alpha\beta} = \frac{V_\alpha}{I_\beta} \quad (49)$$

[4] Unpublished memorandum; "A Cable Shielding Effectiveness Measurement Setup", October 19, 1981; T. P. Bursh

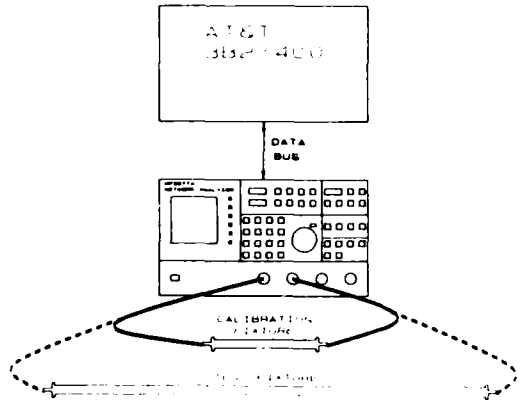

Figure 4. $Z_{\alpha\beta}$ TEST SETUP

Figure 4 presents the actual test setup showing the source and receiver (HP-3577A NETWORK ANALYZER) under the control of an AT&T 3B2/400 computer using an IEEE-488 data bus. The program that controls the measurements calculates 32 frequencies per decade on a geometric basis and is set up to take readings from 1 KHz to 100 MHz or 160 readings per sample. A calibration fixture is always measured first and that data is stored in order to calibrate the readings.

4. TEST RESULTS

4.1 TRANSMISSION RESULTS

The transmission parameters measured are presented in a set of figures of resistance, inductive reactance, capacitance, alpha, beta, and characteristic impedance.

Figure 5. SINGLE PAIR CABLES (XA) (1/3 mil foil shields)

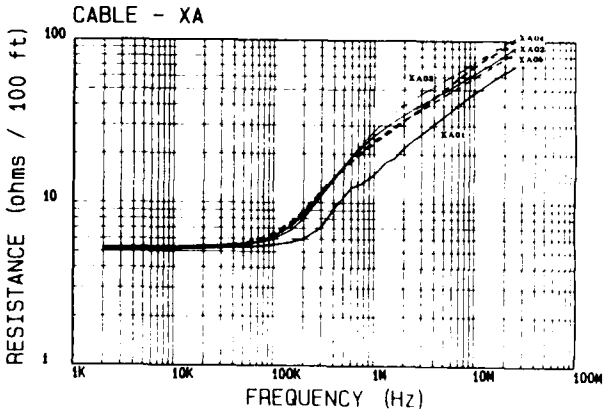

Figure 5a RESISTANCE

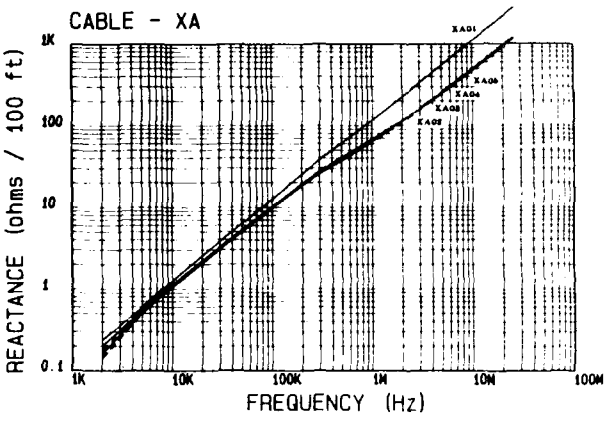

Figure 5b INDUCTIVE REACTANCE

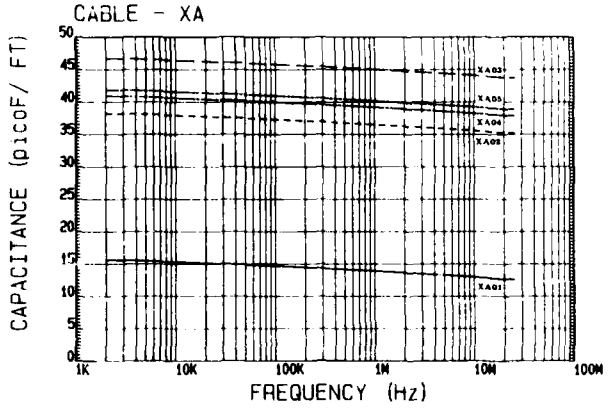

Figure 5c CAPACITANCE

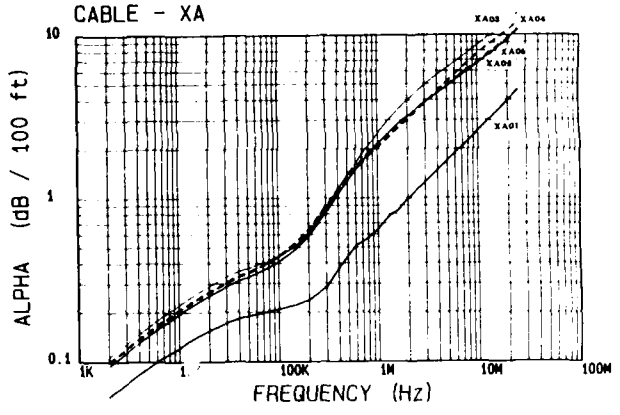

Figure 5d ATTENUATION

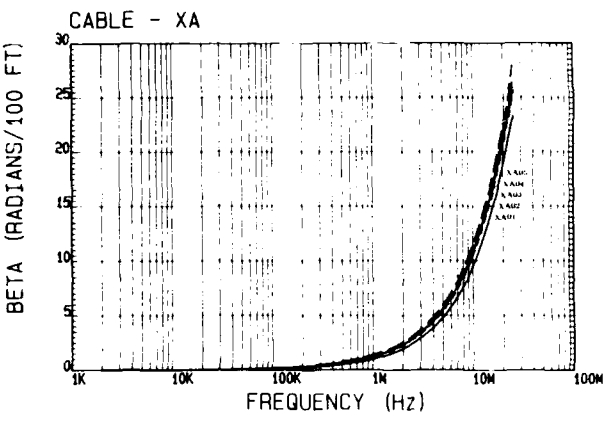

Figure 5e PHASE

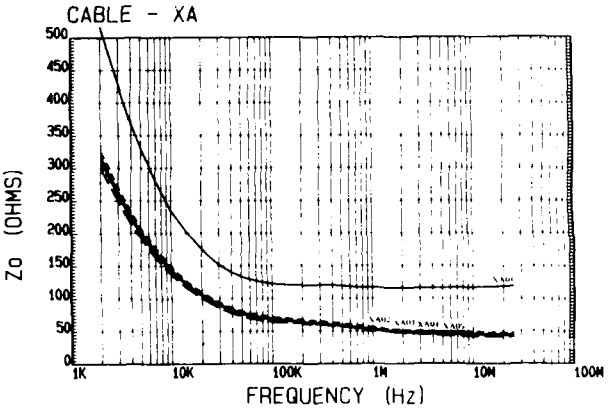

Figure 5f CHARACTERISTIC IMPEDANCE

Figure 5 (a, b, c, d, e, and f) presents the resistance, inductive reactance, capacitance, attenuation (α), phase (β), and characteristic impedance (Z_o) of five of the seven single pair cables. These cables (XA02, XA03, XA04, and XA05) all have 1/3 mil aluminum shields except for XA01 which has no shield.

Figure 5a is a plot of the resistance versus frequency of the cables. At low frequencies (below 10 KHz) all traces are together and essentially flat. Above 1 MHz the traces are separated but parallel and are increasing at a $\sqrt{f}$ rate.

Figure 5b is a plot of the inductive reactance ($j\omega L$) versus frequency of the cables. The traces cross the 5 ohm/100 ft level between 40 KHz and 80 KHz (i.e. $r \approx j\omega L$). Below 10 KHz the low frequencies equations (29 and 30) are valid. The trace of inductive reactance is increasing as a function of frequency (ωL) and the trace of resistance is increasing as a function of $\sqrt{f}$. Above 1 MHz the high frequency equations (31, 32, and 33) are valid.

Figure 5c is a plot of the capacitance versus frequency of the cables. Generally these traces would be flat, how-

ever, the insulation in this case is SR-PVC and the dielectric constant has a slight reduction in value with respect to frequency. The effect of the shield is very apparent and in one case the capacitance value is increased by over 300 pf.

Figure 5d is a plot of attenuation versus frequency of the cables. The traces of the shielded cables all exhibit a slope of $\sqrt{f}$ above about 1 MHz. The trace of the unshielded cable has a slightly greater slope than the $\sqrt{f}$ of the unshielded cables.

Figure 5e is a plot of phase (β) versus frequency of the cables. The traces of the shielded cables and the unshielded cable all merge into one trace at the higher frequencies.

Figure 5f is a plot of magnitude of the characteristic impedance (Z_o) versus frequency of the cables. The value of the characteristic impedance at high frequencies shown dramatically shows the effect of the addition of the shields. Characteristic impedance is reduced by some 60 to 70 pf.

Figure 6. SINGLE PAIR CABLES (XA)

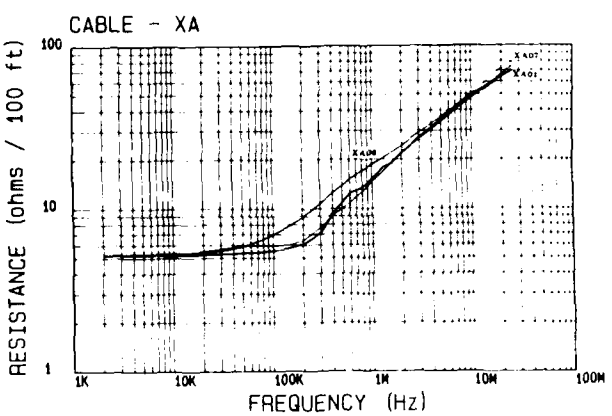

Figure 6a RESISTANCE

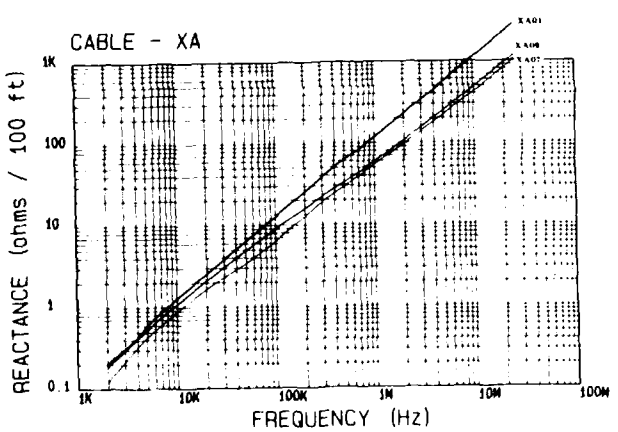

Figure 6b INDUCTIVE REACTANCE

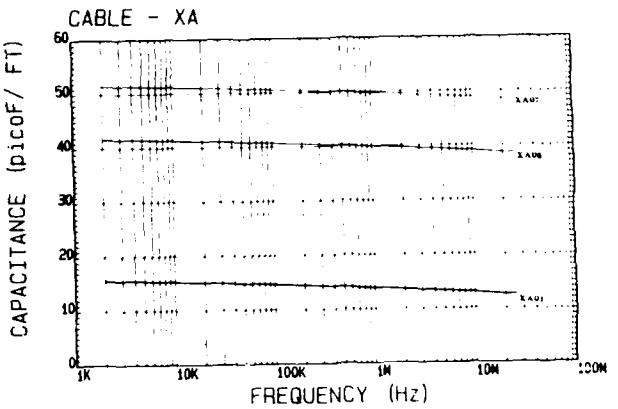

Figure 6c CAPACITANCE

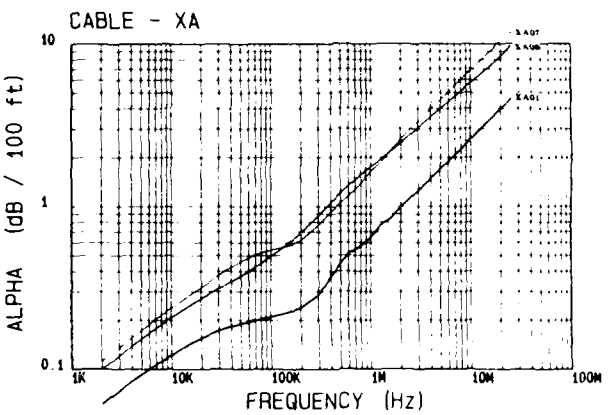

Figure 6d ATTENUATION

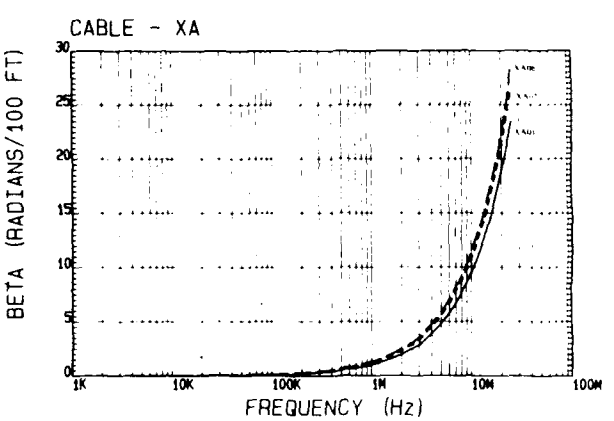

Figure 6e PHASE

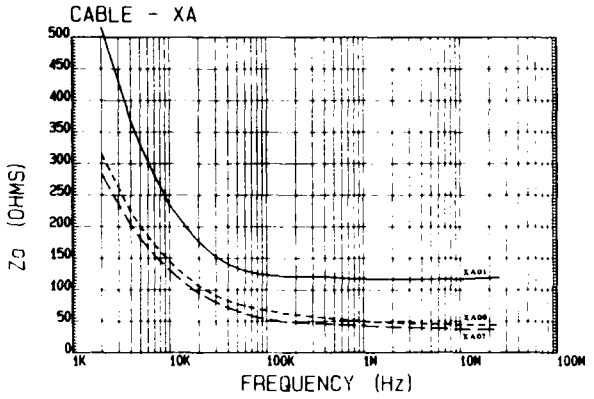

Figure 6f CHARACTERISTIC IMPEDANCE

Figure 6 (a, b, c, d, e, and f) presents the resistance, inductive reactance, capacitance, attenuation (α), phase (β), and characteristic impedance (Z_o) of three (XA01, XA06 and XA07) of the seven single pair cables.

Figure 7. TWO PAIR CABLES (XB) (INDIVIDUAL SHIELDS)

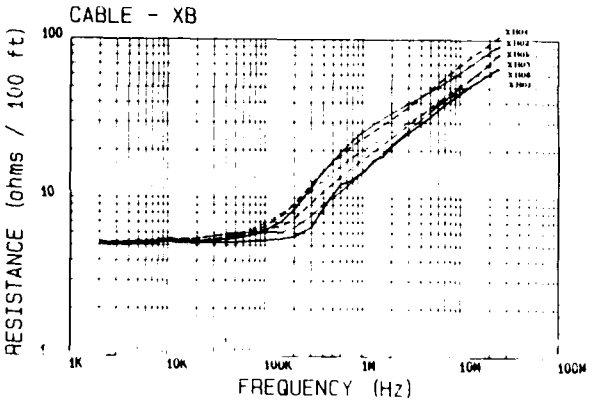

Figure 7a RESISTANCE

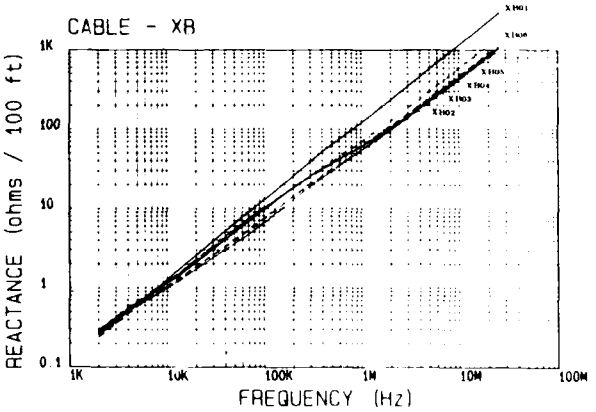

Figure 7b INDUCTIVE REACTANCE

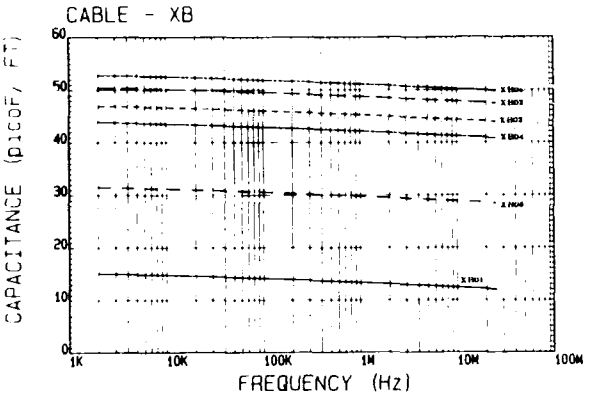

Figure 7c CAPACITANCE

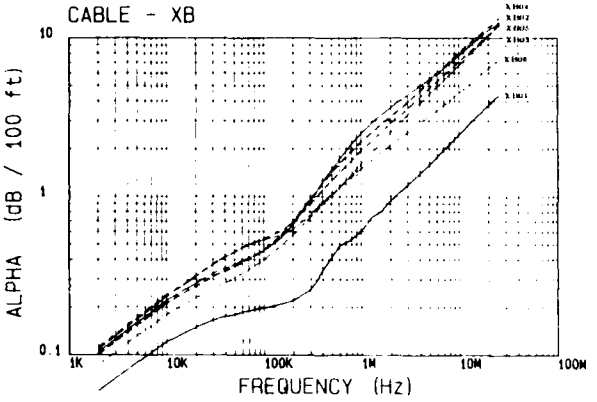

Figure 7d ATTENUATION

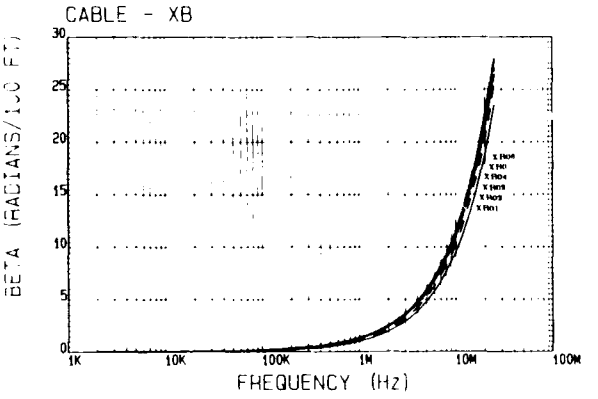

Figure 7e PHASE

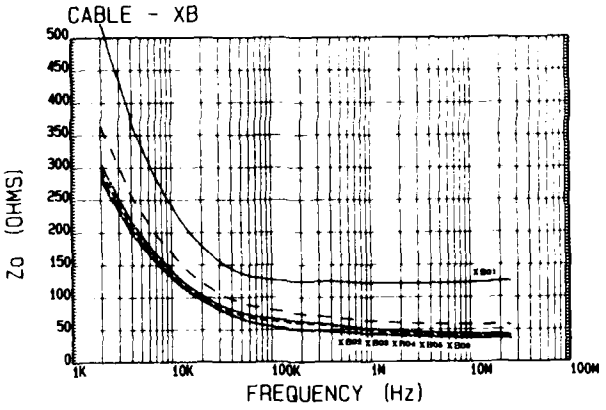

Figure 7f CHARACTERISTIC IMPEDANCE

Figure 7 (a, b, c, d, e, and f) presents the resistance, inductive reactance, capacitance, attenuation (α), phase (β), and characteristic impedance (Z_o) of six of the nine two pair cables. All of the cables with individual shields (XB02, XB03, XB04, XB05, and XB06) and XB01.

Figure 8. TWO PAIR CABLES (XB) (OVERALL SHIELDS)

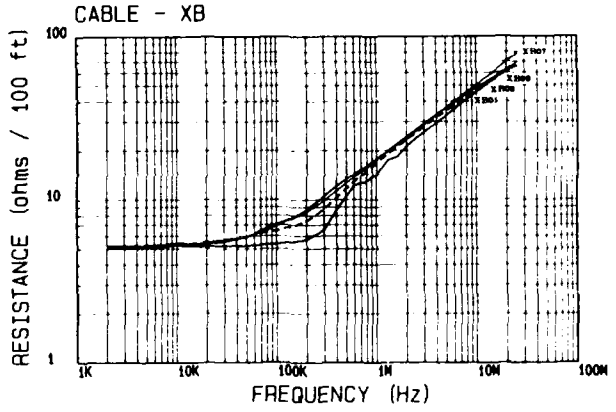

Figure 8a RESISTANCE

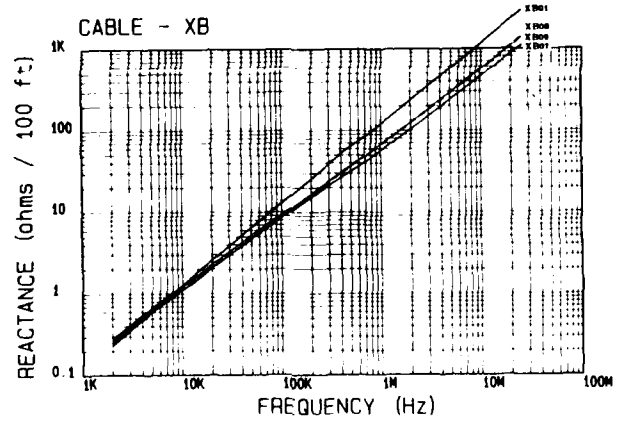

Figure 8b INDUCTIVE REACTANCE

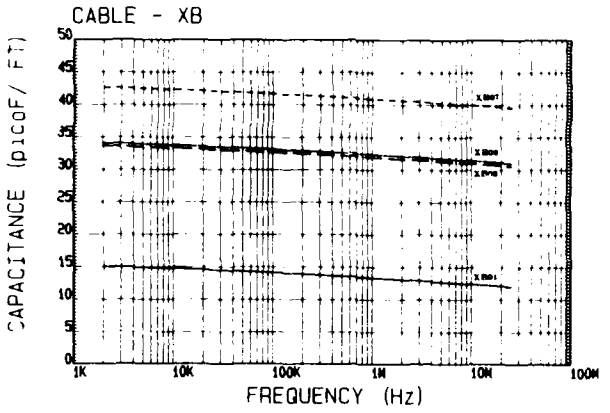

Figure 8c CAPACITANCE

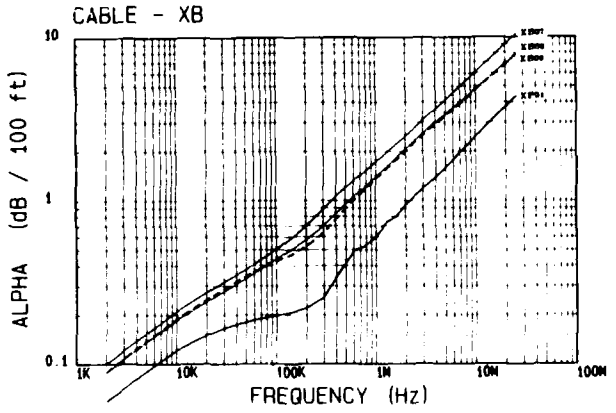

Figure 8d ATTENUATION

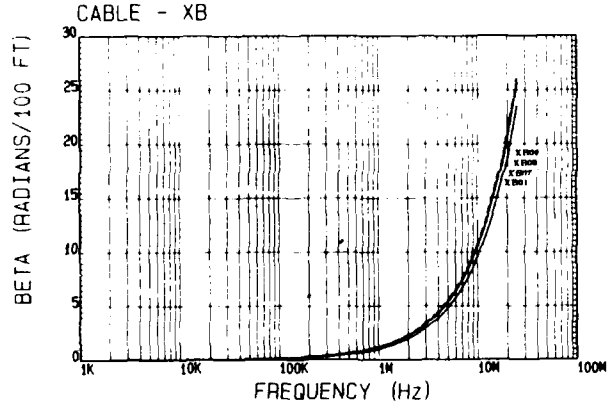

Figure 8e PHASE

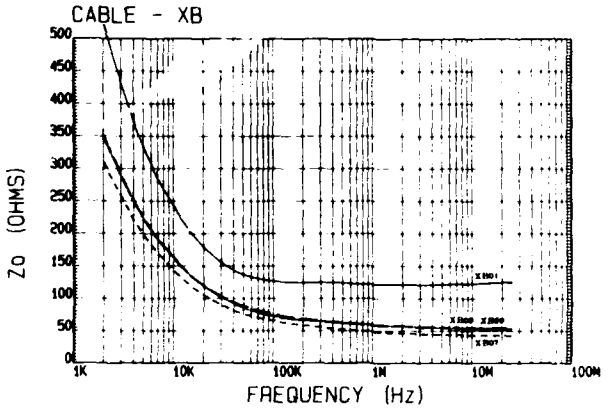

Figure 8f CHARACTERISTIC IMPEDANCE

Figure 8 (a, b, c, d, e, and f) presents the resistance, inductive reactance, capacitance, attenuation (α), phase (β), and characteristic impedance (Z_o) of four of the nine two pair cables. All of the cables with overall shields (XB07, XB08, and XB09) and XB01.

Figure 9. TWELVE PAIR CABLES (XC) (INDIVIDUAL SHIELDS)

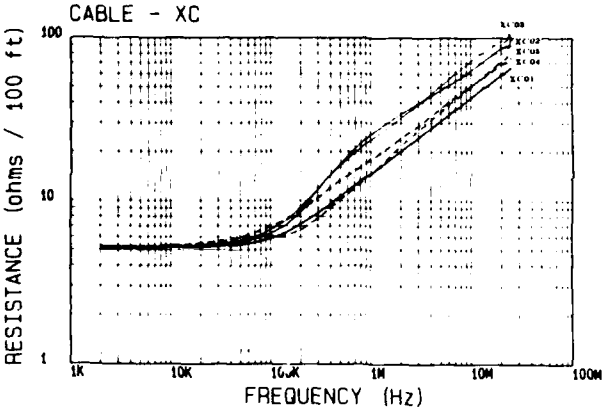

Figure 9a RESISTANCE

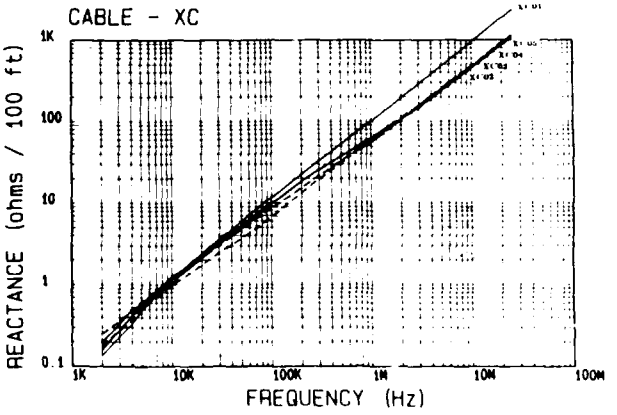

Figure 9b INDUCTIVE REACTANCE

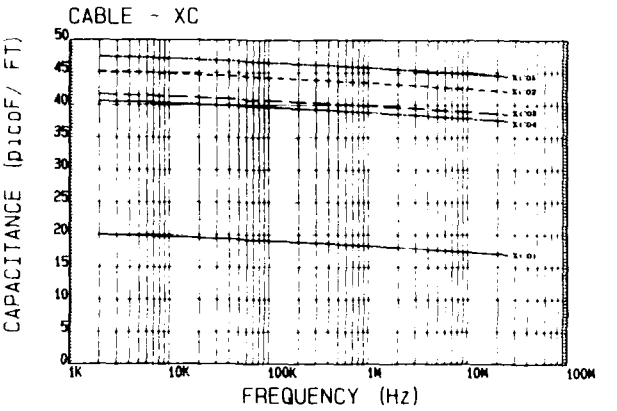

Figure 9c CAPACITANCE

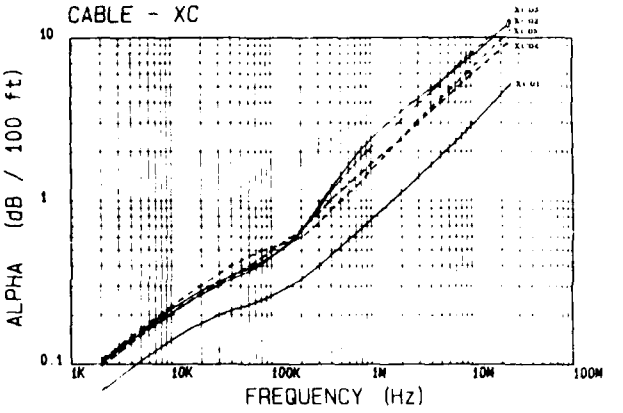

Figure 9d ATTENUATION

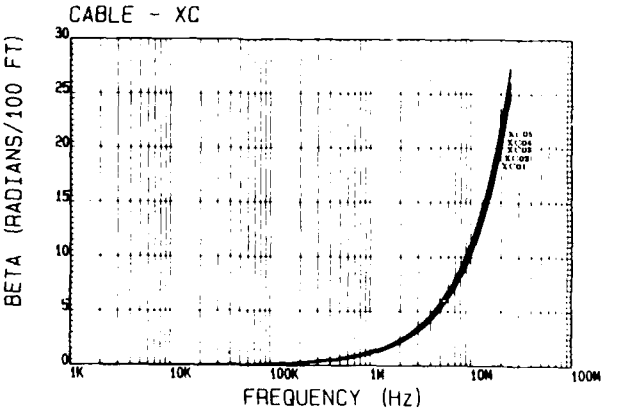

Figure 9e PHASE

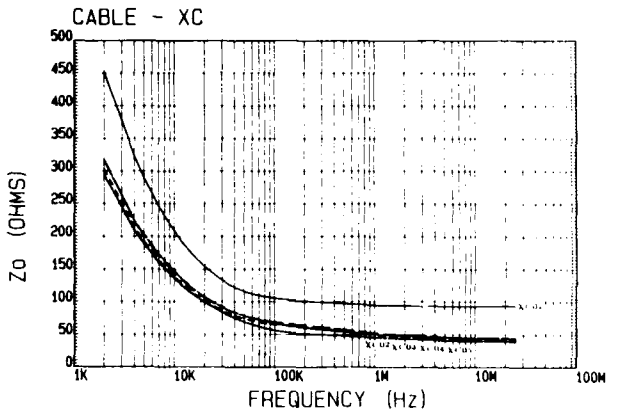

Figure 9f CHARACTERISTIC IMPEDANCE

Figure 9 (a, b, c, d, e, and f) presents the resistance, inductive reactance, capacitance, attenuation (α), phase (β), and characteristic impedance (Z_o) of five of the twelve twelve pair cables. All of the cables with individual shields (XC02, XC03, XC04 and XC05) and XC01.

Figure 10. TWELVE PAIR CABLES (XC) (OVERALL SHIELDS)

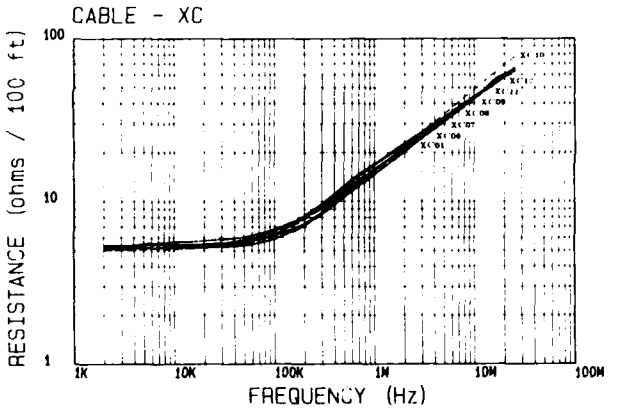

Figure 10a RESISTANCE

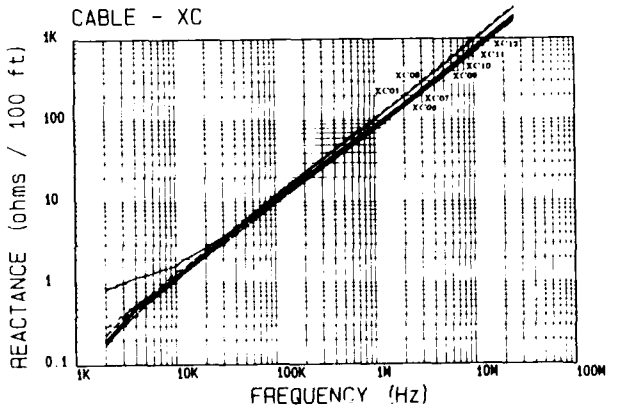

Figure 10b INDUCTIVE REACTANCE

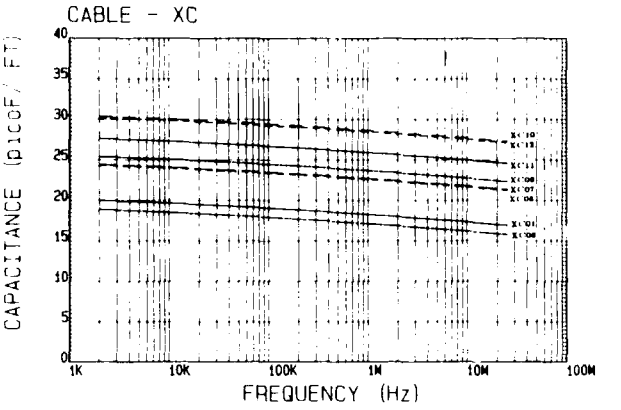

Figure 10c CAPACITANCE

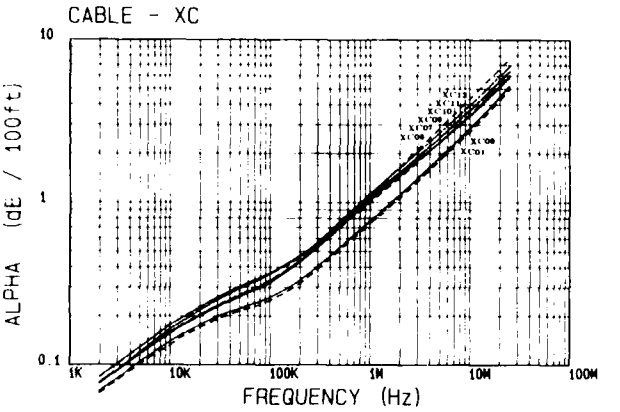

Figure 10d ATTENUATION

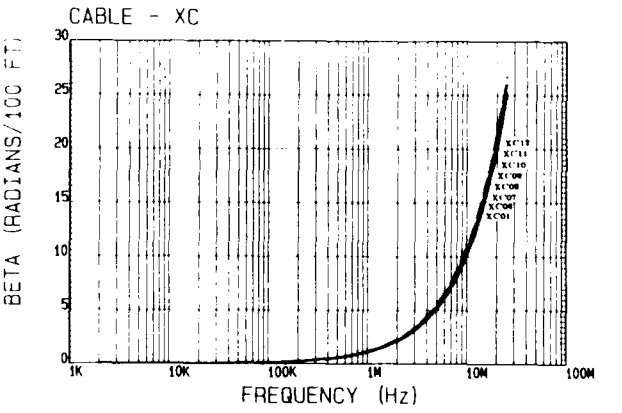

Figure 10e PHASE

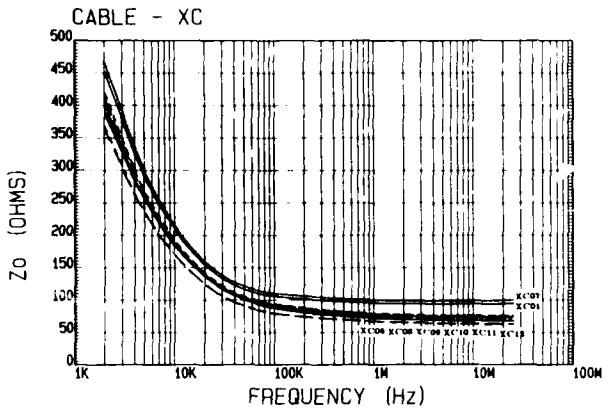

Figure 10f CHARACTERISTIC IMPEDANCE

Figure 10 (a, b, c, d, e, and f) presents the resistance, inductive reactance, capacitance, attenuation (α), phase (β), and characteristic impedance (Z_o) of eight of the twelve twelve pair cables. All of the cables with overall shields (XC06, XC07, XC09, XC10, XC11, and XC12) and the two unshielded cables (XC01 and XC08).

The discussions associated with Figure 5 can be made for all the set of figures (Figures 5 - 10). The effect of the individual shields have the greatest effect on the parameters, however, the overall shields and multiple pairs in a cable also effect the parameters. For unshielded cables increasing the number of pairs in the cable will increase the resistance, capacitance, attenuation and phase while the inductance and characteristic impedance will be decreased. For shielded cables increasing the number of pairs under the shield in the cable will decrease the resistance, capacitance, attenuation and phase while the inductance and characteristic impedance will be increased.

4.2 CROSSTALK RESULTS

The crosstalk of the twelve twelve pair cables was measured. Both equal level far end crosstalk (FEXT) and near end crosstalk (NEXT) was computed.

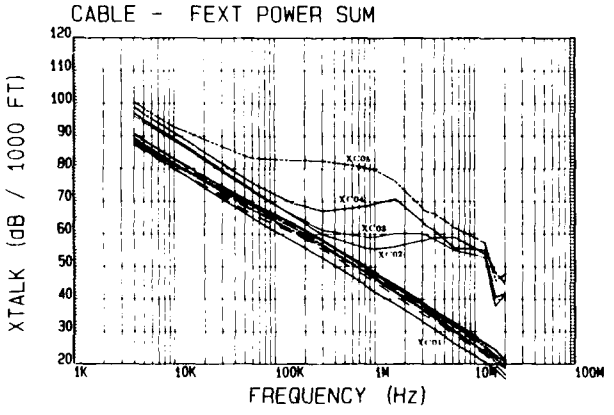

Figure 11. FEXT POWER SUM

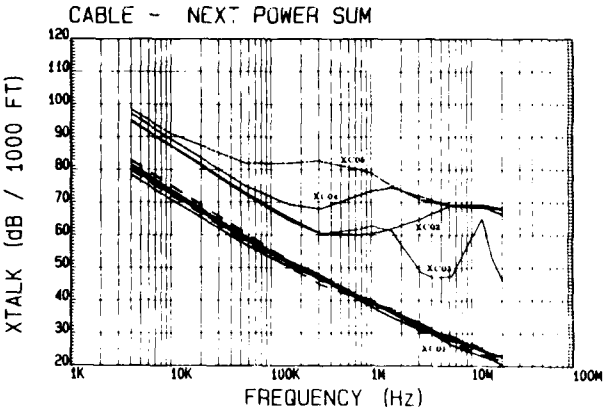

Figure 12. NEXT POWER SUM

Figures 11 and 12 presents the crosstalk for all the twelve pair cables. There is at least a ten dB margin over the unshielded case for all individually shielded cables (XC02, XC03, XC04 and XC05) at all measured frequencies. The more material in the shield the better the job it does in providing isolation between pairs. The edge treatment does not seem to have a large effect.

4.3 SHIELDING EFFECTIVENESS RESULTS

The results of the test is presented as a plot of impedance per length versus frequency.

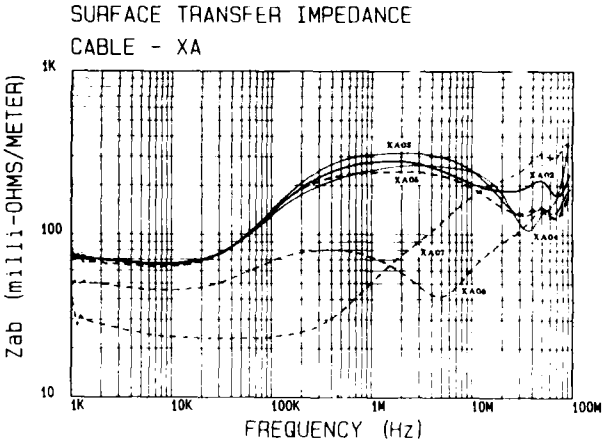

Figure 13. SINGLE PAIR CABLES

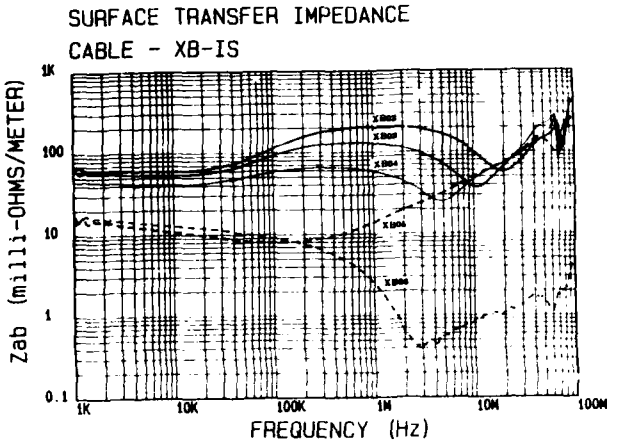

Figure 14. INDIVIDUALLY SHIELDED TWO PAIR CABLES

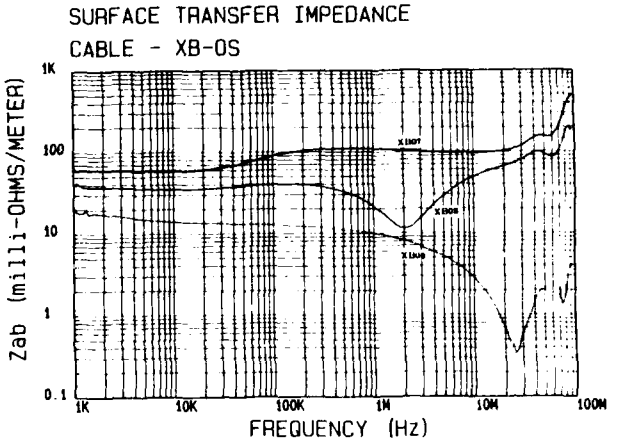

Figure 15. OVERALL SHIELDED TWO PAIR CABLES

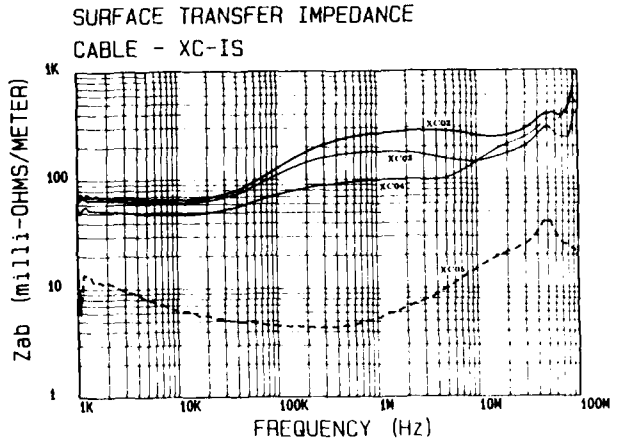

Figure 16. INDIVIDUALLY SHIELDED TWELVE PAIR CABLES

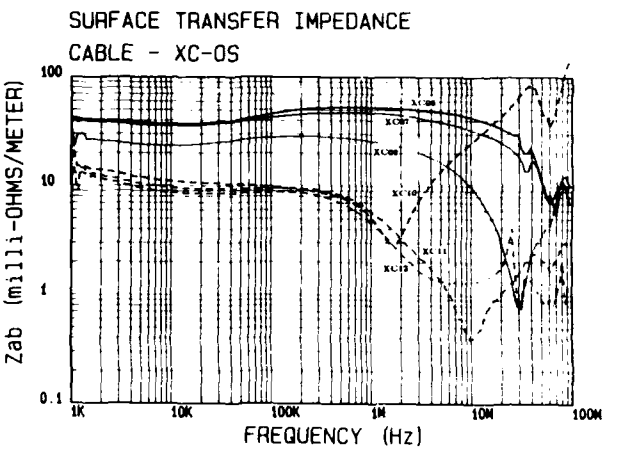

Figure 17. OVERALL SHIELDED TWELVE PAIR CABLES

5. SUMMARY

5.1 TRANSMISSION

The resistance curves, Figures 5a, 6a, 7a, 8a, 9a, and 10a, all have similar shapes. They all start out at low frequencies with little if any slope to the curve. At high frequencies they have a slope of approximately $\sqrt{f}$. Between these two regions they bend to mesh the slopes from the two regions.

The reactance ($j\omega L$) curves, Figures 5b, 6b, 7b, 8b, 9b, and 10b, have similar shapes. The ω accounts for the general slope, however, the value of inductance (L) at low frequencies is larger than the value at high frequencies. The value of reactance for the unshielded cable is greater than the values for the shielded cases.

The capacitance (C) curves, Figures 5c, 6c, 7c, 8c, 9c, and 10c, have a slight downward slope due to the material (PVC) used to insulate the conductors. Most noticeable though is the large separation between the curves of the various individual cables. There is a difference of between 200% and 300% within the various cable configurations from the unshielded to shielded case.

The attenuation (α) curves, Figures 5d, 6d, 7d, 8d, 9d, and 10d, have a slope of $\sqrt{f}$ at low frequencies and again a slope of $\sqrt{f}$ at high frequencies with a knee in between. The low frequency slope can be accounted for by observing the equation for attenuation at low frequencies (equation number 29); Similarly, the slope at high frequencies can be accounted for by investigating equation 33. Observing that by neglecting G and that since both L and C are nearly constant, the slope is then due to the slope of resistance (R) which was shown above to be approximately the $\sqrt{f}$.

The phase (β) curves, Figures 5e, 6e, 7e, 8e, 9e, and 10e, are the same as the attenuation curves at low frequencies (equation 29) and have a slope that is a function of frequency at high frequencies (equation 31). The magni-

tude of the individual curves increases with shielding since C will increase much greater than L will decrease. The phase velocity is $V_p = \frac{\omega}{\beta}$ and will decrease in value with the addition of shielding.

The characteristic impedance (Z_o) curves, Figures 5f, 6f, 7f, 8f, 9f, and 10f, show that the value of Z_o decreases with frequency. This can be shown, for the low frequency case by observing equation 30. Both R and C are approximately constant, therefore, the magnitude of the characteristic impedance will decrease as a function of $\frac{1}{f}$. For the high frequency case the near constant value is shown by equation 32 since both L and C are approximately constant in value.

5.2 CROSSTALK

The power sum equal level far end crosstalk (FEXT) results are shown in Figure 11. The top curve is XC05 followed by XC04, XC03, XC02, and then all the remaining (XC01, XC06, XC07, XC08, XC09, XC10, XC11, and XC12). The bottom curve is XC01.

The power sum near end crosstalk (NEXT) results are shown in Figure 12. The top curve is XC05 followed by XC04, XC03, XC02, and then all the remaining (XC01, XC06, XC07, XC08, XC09, XC10, XC11, and XC12).

These results seem to indicate that the more material in the shield the better the shield from a crosstalk standpoint. The largest effect was at the higher frequencies however there were measurable effects at all frequencies.

5.3 SHIELDING EFFECTIVENESS

The shielding effectiveness results are presented in Figures 13, 14, 15, 16, and 17. Figure 13 shows the transfer impedance for cables XA02, XA03, XA04, and XA05. XA02, XA03, XA04, and XA05 were included in order to investigate the effect of edge treatment (flat fold versus "Z" fold) and of machine selection (single twist versus double twist) on the transfer impedance.

Figure 14 presents the $Z_{\alpha\beta}$ results for individually shielded two pair cables. Cables XB02 and XB03 again compare the shielding effectiveness of the flat fold versus the "Z" fold. Cable XB01 has a 1 mil aluminum foil shield. Cable XB05 has a 88% copper braid shield. Cable XB06 has a hybrid shield of 1 mil aluminum foil and 88% coverage copper braid.

Figure 15 presents the $Z_{\alpha\beta}$ results for overall shielded two pair cables. Again the effectiveness is a function of the bulk of the material in the shield.

The individually shielded twelve pair cables displayed in Figure 16 show an advantage to the "Z" fold seam over flat fold seam (XC03 versus XC02). The other two shields are 1 mil flat fold aluminum foil (XC04) and braid (XC05).

Figure 17 presents the $Z_{\alpha\beta}$ for the overall shielded twelve pair cables. The levels again loosely follow the amount of material in the shield. The two cables XC06 and XC07 both have a 1 mil flat fold aluminum foil shield with the cable having a core that was layless where as XC07 had a core with a 15 inch lay. Cable XC09 had a dual 1 mil aluminum foil shield. Cable XC10 had a 88% copper braided shield. Cables XC11 and XC12 both have hybrid shields, braid with aluminum foil, but on XC11 the braid was only 70% where as XC12 had a 88% braid.

6. CONCLUSIONS

In the introduction we proposed to provide information for comparing various shield materials, shield configurations, edge treatment on foils, and methods of application with respect to shielding effectiveness, transmission parameters on all of the cables and crosstalk on the twelve pair cables. The selection of cable size, shield types, shield materials and manufacturing methods have yielded data on these subjects. This is presented as the $Z_{\alpha\beta}$ of each cable, plots of resistance, inductive reactance, capacitance, attenuation, phase, and characteristic impedance of each cable, and graphs of both the FEXT and NEXT of each of the twelve pair cables.

These data can be used to compare the relative worth of various shields for a particular application considering both transmission parameters and $Z_{\alpha\beta}$ as well as the crosstalk performance of various shields.

ACKNOWLEDGMENTS

The author wishes to thank Mr. R. D. Beggs of AT&T Technologies for his help in the design of this experiment. Thanks is due to Messrs D. E. Geller and T. G. Hardin of AT&T Technologies for their help in manufacturing of the cable samples. The work of Messrs B. McNeal and M. J. Thomas was helpful in preparing and testing samples. The contributions of Mr. P. H. Ward of Bell Laboratories for his testing of cables for transmission parameters and crosstalk are much appreciated. Thanks is also due to Mr. H. W. Friesen of Bell Laboratories for discussions on certain aspects of this work.

REFERENCES

[1] Chipman, Robert A., Ph.D.: "*Transmissions Lines*"; Schaum's Outline Series; McGraw-Hill Book Company; 1968.

[2] Miller, C. M.; "*Capacitance of a Shielded Balanced-Pair Transmission Line*"; Bell System Technical Journal, Vol. 51, No. 3, March 1972.

[3] Skilling, H. H.; "*Electric Transmission Lines*"; McGraw-Hill Book Company, Inc.; New York, 1951.

[4] Johnson, W. C.; "*Transmission Lines and Networks*"; McGraw-Hill Book Company, Inc.; New York, 1950.

John W. Levengood holds a BEE degree from the University of Florida (1959), and a MEE degree from New York University (1961). He joined Bell Laboratories in 1959 and transferred to Western Electric Company in 1970. He presently works for AT&T Technologies, Inc. in the Electronic Wire and Cable Development Department in Atlanta.

THE EFFECT OF ALTERNATING CURRENT ON CORROSION OF CABLE SHIELDING MATERIALS IN SOILS

Robert Baboian
Texas Instruments Inc.
Attleboro, MA 02703

Gregory Hessler
REA-Outside Plant Branch
Washington, DC 20250

Kenneth Bow
Dow Chemical USA
Granville, OH 43023

Gardner Haynes
Texas Instruments Inc.
Attleboro, MA 02703

The impact of corrosion on buried telephone cable shielding materials has been demonstrated over the last thirty years in a wide range of laboratory and soil burial tests sponsored by the Rural Electrification Administration (REA) and conducted by the National Bureau of Standards (NBS) and Industrial Organizations.[1-16] These tests were conducted on electrically isolated lengths of cable with intentionally damaged jackets which exposed metal shields in a controlled manner. The comparative behavior of idle cable versus cable carrying alternating current, as it does in actual service, was not evaluated in the NBS-REA tests.

Since it has been established that alternating current may affect the corrosion of metals such as copper, steel, and aluminum in soils, a soil burial study was conducted to determine the corrosion behavior and the associated effects of alternating current on commonly used shielding materials.[17-20] This paper evaluates the results of the six year program giving special attention to the comparative behavior of six types of commonly used shields in buried static and active cables.

Introduction

The metallic sheath in telecommunications cables provides an important line of defense with electrical and mechanical protection. The properties required of the sheath in order to provide proper protection include:

Electrical Protection from Noise

- Conductivity
- Connectability
- Magnetic Properties
- Corrosion Resistance

Electrical Protection from Lightning

- Conductivity
- Connectability
- Heat Transfer
- Heat Capacity
- Temperature Limits
- Crush Resistance
- Corrosion Resistance

Mechanical Protection from Rodents

- Tensile Strength
- Puncture Resistance
- Abrasion Resistance
- Corrosion Resistance

Mechanical Protection from Installation Damage

- Mechanical properties to prevent Kinking, Tearing, Puncturing
- Crush Resistance
- Corrosion Resistance

In each of these protection categories, the sheath corrosion resistance plays an important role. When corrosion of the sheath occurs, the result is an increase in electrical resistance and a decrease in mechanical protection.

The importance of sheath integrity in telecommunications cable is demonstrated by the extensive literature available which documents results of accelerated, field, and service tests. These studies include the effect of shielding design and material, and the effect of the environment. The most extensive tests were conducted jointly by the National Bureau of Standards (NBS) and the Rural Electrification Administration (REA).[1-8] These soil burial studies included cables with over 120 different shielding materials and/or designs located at six sites representing various environmental aggressivities. The electrically isolated lengths of buried cable had damage sites in the outer jacket (rings and windows) which exposed the shielding to the soil environment. The characteristics of the soils at the six test sites and the corrosion behavior of the shielding in the test cables has been well documented. Results showed that shielding corrosion behavior is strongly dependent on materials, design, and soil environment. For example, bare aluminum and bare steel were corrosive in most soil sites while stainless steels were corrosion resistant. Copper was susceptible in acid and sulfide containing soils but corrosion resistant in others. In some cases, organic or metallic coating designs provided increased corrosion resistance.

Although the corrosion behavior of metallic sheaths in electrically isolated cable (static) has been studied extensively, very little testing on active cable carrying alternating current, as in actual service, has been conducted. Since it has been established that alternating current can affect the rate of corrosion of metals such as aluminum, steel, and copper in soils, a cooperative study was undertaken by REA, Horry Telephone Cooperative, The Dow Chemical USA, Contel Corporation and Texas Instruments Incorporated. Its purpose was to compare the corrosion behavior and the associated effects of alternating current on commonly used shielding materials in static and active buried cable.

Test Program and Conditions

The commercially available shielding materials included in the test program are listed in Table I. They were chosen because they include the commonly used metals, aluminum, steel and copper. They also incorporate current sheath designs including the clad metal configuration and organic coatings.

The shielding materials were fabricated into twenty-five pair polyethylene jacketed telephone cable according to REA specifications. Continuous five hundred foot lengths of cable (prepared by cable manufacturers) with damage sites at 30 foot intervals (active test) as well as individual two and one-half foot lengths of cable with damage sites (static test) were prepared by the shielding manufacturers. The damage site pattern (Figure 1) was intended to simulate possible installation, lightning or rodent damage to the cable's outer jacket. Windows and circumferential rings were made by cutting the polyethylene jacket to within 0.010 inches of the shield with a single edge razor blade in a depth controlled fixture. The polyethylene jacket was then peeled away taking care not to damage the shield. The window was designed to simulate shield damage during installation. The ring was designed to simulate gopher damage. The pinholes were designed to simulate lightning damage. Holes were made by drilling to within 0.10 inches of the shield with a collared drill and then removing the remaining jacket by hand with an end mill. The ends of the individual lengths of static cable were sealed with vinyl tape and wax. This type specimen allows comparison of the amount of corrosion at the windows and holes to that occurring where the complete circumference is exposed.

In March of 1980 the five hundred foot lengths of cable were buried in a test site under the jurisdiction of Horry Telephone Cooperative in Conway, S.C. A trenching machine was used to dig a 4 inch wide 3 foot deep trench and the cables were laid in by hand. Markers were placed on the nearby road to facilitate location of the test area for retrieval. The cables were electrically connected (active) in series to each other and in parallel to an existing cable which had a high level of induced AC shield current. The electrically isolated (static) specimens were buried at the same depth as the cable six feet away from each area with damage sites so that a pair of active and static specimens could be easily obtained at each retrieval. The test program called for retrieval of a control cable (static) and a section of test cable (active) of each type of shielding at intervals over the course of years. Electrical continuity was maintained by splicing the cables each time a specimen was removed.

During installation, soil samples were obtained at the bottom of the trench at the midpoint of each cable. The soil samples were sealed in plastic bags for transportation back to the laboratory. The pH and resistivity of the soils were measured within 24 hours after collecting the samples. The pH was measured according to ASTM G51-77, Standard Test method for pH of Soil for Use in Corrosion Testing. The values were measured in the laboratory using an Orion Model 801 pH meter. Resistivity values were measured in the laboratory according to ASTM G57-78, Standard Method for Field Measurement of Soil Resistivity Using the Wenner Four-Electrode Method. A Miller soil box and a Nilsoon Model 400 soil resistance meter were used to measure the "as-received" and "saturated" soil resistivities.

Preparation of soil water extracts was conducted using the techniques established by NBS-REA in previous studies. A suspension of soil and distilled water in the ratio of 1:5 was shaken mechanically on a ball mill at intervals (8 hours on, 16 hours off) for a period of 72 hours. The extract was decanted and filtered through 45 micron filters prior to analysis.

Qualitative analysis of the extracts was conducted using DC-Plasma emission spectroscopy and a series of anionic specific methods. The primary chemical constituents were then quantitatively determined by the methods listed in Table II. EPA water quality standards were used as an external check on the methods employed.

The properties of the soil at the Conway test site are shown in Table III. The resistivity values for the "as received" soil samples are listed in parenthesis and range from a low of 11,000 to a high of 110,000 ohm-cm. The "saturated" resistivity values ranged from 7,000 to 34,000 ohm-cm. As stated in G57, these values should be considered a worst-case situation.

The pH values indicate that the soils are nearly neutral. As indicated by the high resistivity values, very low concentrations of soluble salts were found in all of the soils including aggressive anions such as chloride, which accelerate corrosion.

An evaluation of the data in Table III when compared to data from other test sites, indicates that the soil properties at the Conway, S.C. test site in this program are similar to those for Hagerstown loam, a test site of the National Bureau of Standards. Results of the REA-NBS study have shown that this NBS site is comparatively mild with regards to corrosivity.[1-8] However, other effects such as drainage, aeration, and electrical factors play an important role in corrosion reactions and

therefore can introduce unique characteristics at a particular test site.

During installation, seepage of ground water into the trench at the three foot level indicated that the cables were below the water table. However, at various times during subsequent retrievals, the cables were above the water table. A rising and falling water table provides aeration at the cable depth. Also the presence of alternating current in the active test cable was confirmed by measurement at the end of the six year exposure period. These data is shown in Table IV.

Retrievals of each type of specimen were made after 0.5, 1, 2.5, 4 and 6 years.

After retrieval, the polyethylene jackets were removed from the specimens and the flooding compound was dissolved in kerosene taking care not to remove corrosion products so that the extent of corrosion could be evaluated. The specimens were then rated by consensus by a panel using the rating system in Table V. The panel consisted of representatives from REA, Contel Corporation, The Dow Chemical Company and Texas Instruments Incorporated. The rating system had a scale of 0 to 10 with 10 being no indication of corrosion and 0 being electrical discontinuity due to corrosion.

Results

The program consisted of six different shielding materials and cable designs and six retrievals (duplicate retrievals were made after the six year exposure period). The performance ratings for the 1, 4 and 6 year exposure periods are listed in Tables VI through XI. The window, ring, holes and under jacket ratings for static and active specimens are included. For ASP, CASP and CACSP cable constructions, the ratings are for the steel and aluminum. For copper clad steel, the copper outer, steel center, and copper inner are rated. For aluminum clad steel, the aluminum outer, steel center, and aluminum inner are rated. Due to the complexity of the shielding and cable designs, explanatory notes are required to interpret the results and these are listed in Table XII.

A convenient way to evaluate the data in this program is through the use of bar charts as shown in Figure 2 (data for the 6th year retrieval are averaged). Since each metal in the multi-component shieldings was rated, the performance of the materials systems and the comparative behavior of the various systems in static and active cables can be easily observed for this ring area on the cables (where ring ratings were not available, window ratings were used).

Overall, the corrosion ratings of bare steel in the static cables were very poor. However the coated steel ratings were very good during the six years of static exposure. The steel in the copper clad configuration had a good rating after six years (static) and the steel in the bare or coated aluminum clad configuration under similar conditions had a very good to excellent rating. These static results for steel are in agreement with those obtained at similar sites in the REA/NBS tests.[1-8]

The behavior of steel in active cables was quite different when compared to the static results. Here, the steel in the active cables corroded more rapidly whether bare, coated or clad with aluminum. However, a significant reduction in corrosion of the steel in the copper clad configuration was observed in the active cables.

In general, the site was a mild one for aluminum since the ratings ranged from fair to excellent. Corrosion was observed with bare aluminum after four years, but not with coated aluminum (except in the aluminum clad steel configuration).

The effect of AC on aluminum corrosion was not well defined in this study. Bare monolithic aluminum had more corrosion in the static cables. However, in the clad configuration, the active cables had more aluminum corrosion when it was coated and the behavior was mixed in the uncoated clad aluminum. Where corrosion was observed, the outer aluminum layer in the clad was affected more than the inner.

The outer copper (in copper clad steel) was rated very good to excellent for all exposure periods. Superficial corrosion took place uniformly providing an adherent layer over the outer surface. The inner copper was almost unaffected by corrosion after the six year exposure period. There was virtually no difference in corrosion behavior of copper in static and active cables.

Discussion

The corrosion behavior of aluminum, steel and copper in the cable configurations (see Table I for constructions) of this investigation and under static conditions is in agreement with previous studies in similar soil environments. The Conway, S.C. site environment is a mild one compared to other sites. However, the presence of AC in the active cables has produced corrosion effects which can play an important role in the performance of metallic shieldings in cables.

In ASP and CASP shielded cables, the performance rating of bare steel is reduced from fair (static) to very poor (active) after one year. At the end of six years all bare steel shieldings are very poor. With CACSP, the effect of AC is to reduce the ratings from very good to poor after six years for the coated steel but there is an improvement with this coated steel over uncoated. Since aluminum did not corrode appreciably in this program, it is difficult to assess the various

affects. However, bare aluminum corrosion was observed in some static ASP cables while no corrosion was observed for coated aluminum in CASP and CACSP. Overall, the order of shielding corrosion resistance for these cable constructions in these tests is as follows for static conditions:

$$ASP < CASP < CACSP$$

for active conditions it is

$$ASP = CASP < CACSP$$

In both bare and coated aluminum clad steel (Al/St/Al), the steel ratings were good to excellent with the higher ratings in static cables. These shields behaved similarly to CACSP except that some aluminum corrosion was observed. The galvanic interaction between the steel and aluminum may play a role in the corrosion behavior of these shields since both steel and aluminum corrosion were affected by the presence of AC. After six years, the bare outer aluminum ratings in the clad dropped from good (static) to fair (active) and the coated aluminum ratings in the clad dropped from excellent (static) to fair (active). The overall order of shielding corrosion resistance for these cable constructions in these tests is as follows for static conditions:

$$Al/St/Al < CAl/St/CAl$$

and for active conditions it is:

$$Al/St/Al = CAl/St/CAl$$

The copper clad steel (Cu/St/Cu) behavior under static conditions was similar to results of previous tests in similar environments. Copper ratings were excellent after six years while some edge corrosion of the steel occurred due to galvanic effects. Interestingly, both the copper and steel received excellent ratings in the active test cables after six years exposure. This increase in steel corrosion resistance in the copper clad configuration while under the influence of AC in active cable tests is in sharp contrast to the reduction in steel corrosion resistance in all other shielding configurations in this program under the influence of AC.

Although an increase in steel corrosion under the influence of AC can be explained by the discharge of the AC current where it is exposed, no explanation exists for the increase in steel corrosion resistance under the influence of AC in the copper clad steel configuration. However, discharge of the AC current from the large copper surface would essentially eliminate any effect at the steel edge (but this would not explain the increased corrosion resistance).

The effect of AC on coated steel is to concentrate the discharge at edges and at damage sites in the coating. The same effect can occur when steel is clad with aluminum due to the insulating properties of the oxide layer on aluminum.

The varying behavior of aluminum under static and active conditions cannot be explained at this time. This site was mild for aluminum and therefore it is difficult to draw significant conclusions.

Summary

The effect of alternating current on the corrosion behavior of metallic cable shielding materials has been studied in a burial study at Conway, S.C. The test site has been characterized as comparatively mild with regards to soil chemistry and resistivity. Although the effects of the varying water table and aeration could not be quantified, the presence of AC did influence the corrosivity and therefore significant effects have been observed and reported in this study.

Results of field testing of 6 different metallic shielding materials in cables indicate that there is an effect of AC in active cables when compared to isolated static cables. The most significant effects were observed with steel. Although the corrosion resistance was improved by plastic coating, aluminum cladding and copper cladding, the presence of AC reduced the corrosion resistance of steel except in copper clad steel where it improved. The results with aluminum were mixed in this mild environment. In the presence of AC, the corrosion resistance of bare monolithic aluminum was improved. The effect of AC on coated aluminum could not be assessed in the absence of corrosion and the corrosion resistance decreased in the aluminum clad configuration. Copper in the clad configuration was not affected by the presence of AC.

Considering the performance ratings for all shield configurations in this program, the overall order of increasing corrosion resistance under static conditions is:

$$ASP < CASP < Al/St/Al < CACSP = Cu/St/Cu < CAl/St/CAl$$

and for active conditions it is

$$ASP = CASP < Al/St/Al < CAl/St/CAl = CACSP < Cu/St/Cu$$

Acknowledgement

The authors wished to express their appreciation to Horry Telephone Cooperative for installing and retrieving specimens.

References

1. Lohsl, G.A., Romanoff, M., Corrosion Evaluation of Shielding Materials for Direct Burial Telephone Cables, paper presented at the 17th International Wire and Cable Symposium, Atlantic City, NJ, 1968.

2. Lohsl, G.A., Romanoff, M., Progress Report on Corrosion Evaluation of Shielding Materials for Direct Burial Telephone Cables, paper presented at the 18th International Wire and Cable Symposium, Atlantic City, NJ, 1969.

3. Gerhold, W.F., McCann, J.P., Corrosion Evaluation of Underground Telephone Cable Shielding Materials, Paper No. 31, presented at the NACE Annual Conference, Houston, TX, 1976.

4. Gerhold, W.F., Fink, J.L., Corrosion Evaluation of Underground Telephone Cable Shielding Materials, NBSIR81-2243. Prepared for the Rural Electrification Administration; National Bureau of Standards; April, 1981.

5. Gerhold, W.F., Escalante, E., and Fink, J.L., Corrosion Evaluation of Underground Telephone Cable Shielding Materials, NBSIR 82-2509. Prepared for the Rural Electrification Administration; National Burea of Standards; June, 1982.

6. Fink, J.L., and Escalente, E., Corrosion Evaluation of Underground Telephone Cable Shielding Materials, NBSIR83-2702, prepared for the Rural Electrification Administration; National Bureau of Standards; May 1983.

7. Fink, J.L. and Escalante, E., Performance Evaluation of Telephone Cable Pedestals in Underground and Atmospheric Environments, NBSIR84-2810. Prepared for the Rural Electrification Administration; National Bureau of Standards; January, 1984.

8. Fink, J.L., Mathews, D., Hessler, G. and Speed, E., Corrosion Evaluation of Underground Telephone Cable Shielding Materials, NBSIR87-3546. Prepared for the Rural Electrification Administration; National Bureau of Standards, January, 1988.

9. Baboian, R., Corrosion Barrier Shielding Materials for Buried Wire and Cable, Paper No. 81, NACE Annual Conference, Anaheim, CA, 1973.

10. Baboian, R., Haynes, G.S., Corrosion Resistance of Copper Clad Stainless Steel Cable Shielding Materials, Materials Performance, Vol. 14, No. 8, p 16, 1975.

11. Haynes, G.S., Baboian, R., Corrosion Barrier Materials for the Communications Industry, Materials Performance, Vol. 16, No. 9, p 30, 1977.

12. Haynes, G.S. and Baboian, R., A Comparative Study of the Corrosion Resistance of Cable Shielding Materials, Materials Performance, Vol. 18, No. 2, p 45, 1979.

13. Baboian, R., Hartley, S.R., and Hyman, E.D., High Strength, Corrosion Resistant Clad Metal Shielding for Telephone Wire and Cable, paper presented at the 23rd International Wire and Cable Symposium, Atlantic City, NJ, 1974.

14. Schick, G., Effect of Inhibitors on Aluminum Shield in Telephone Cable Sheaths, Paper 107, National Association of Corrosion Engineers, St. Louis, MO, March, 1972.

15. Cox, C.L., Tingley, T.E., Webster, H.A., Problems of Water in PIC Cable, 17th International Wire and Cable Symposium, Atlantic City, NJ, December, 1968.

16. Schwank, G.D., and Bow, K.E., Galvanic Corrosion Studies of Aluminum and Steel Shielding Materials for Armored Telephone Cables, Materials Performance, Vol. 17, No. 9, September, 1978.

17. Compton, K.G., The Underground Corrosion of Copper and the Effects of A.C. on Concentric Neutrals of URD Cable, Paper No. 145, NACE Annual Conference, Toronto, 1981.

18. Moore, W.M., Chen, C. and Shirn, G.A., A Voltametric Investigation of AC Corrosion Phenomena at an Aluminum Electrode in Hydrochloric Acid, Corrosion, Vol. 40, No. 12, p 644, 1984.

19. Jones, D.A. and Wide, B.E., Corrosion, Vol. 43, No. 2, p 66, 1987.

20. Williams, J.F., Corrosion of Metals Under the Influence of Alternating Current, Materials Protection, Vol. 5, No. 2, p 52, 1966.

BIOGRAPHIES

Robert Baboian is a TI Principal Fellow and Head of the Electrochemical and Corrosion Laboratory of Texas Instruments Inc. He received his PH.D. degree from Rensselaer Polytechnic Institute in 1964 and his B.S. degree from Suffolk University in 1959. He has edited 6 books and authored 110 technical publications in the field of electrochemistry and corrosion. Dr. Baboian served as Chairman of the Board of ASTM in 1987 and received the Frank Newman Speller award for outstanding contributions to Corrosion Engineering from the National Association of Corrosion Engineers in 1988.

Kenneth E. Bow is a Senior Associate Development Scientist with Dow Chemical USA, Granville, Ohio. He has been involved in the research and development of materials for the wire and cable industry for over 20 years. He is currently the Manager of the Coated Metals Technical Center and responsible for the global development of coated metal shielding and armoring tapes for applications in cables. Mr. Bow graduated with a B.S. E.E. degree from Michigan State University in 1962.

Gregory Hessler is a Communications Specialist in the Outside Plant Branch of the Rural Electrification Administration an Agency within the United States Department of Agriculture. His responsibilities include developing standards for copper wire cable products, fiber optic cable products, outside plant hardware products, and the evaluation of such products for REA acceptance. Prior to joining REA, Mr. Hessler was a member of the Wire Media Group of Bell Telephone Laboratories, Norcross, Georgia. Mr. Hessler received an Associate of Arts Degree in Electronics from the Community College of Baltimore in 1969.

Gardner Haynes is currently a Member Group Technical Staff of the Electrochemical and Corrosion Laboratory of Texas Instruments Inc. He received his Bachelor's Degree in Mechanical Engineering Technology from Northeastern University in 1974. He has been active in the field of corrosion for 20 years and has published many papers, edited one book, and holds 7 patents. His professional activities include chairmanship of numerous groups in both the American Society for Testing and Materials and the National Association of Corrosion Engineers. His career has been dedicated to the development of materials systems and devices for corrosion control.

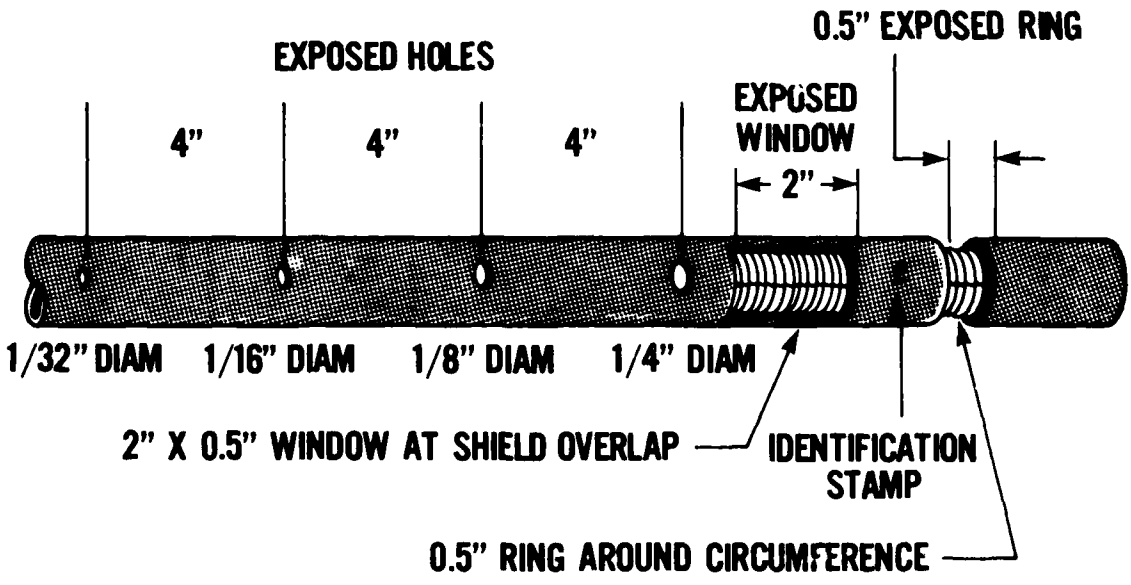

FIGURE 1 - PATTERN OF DAMAGE SITES FOR ISOLATED LENGTHS AND CONTINUOUS CABLE

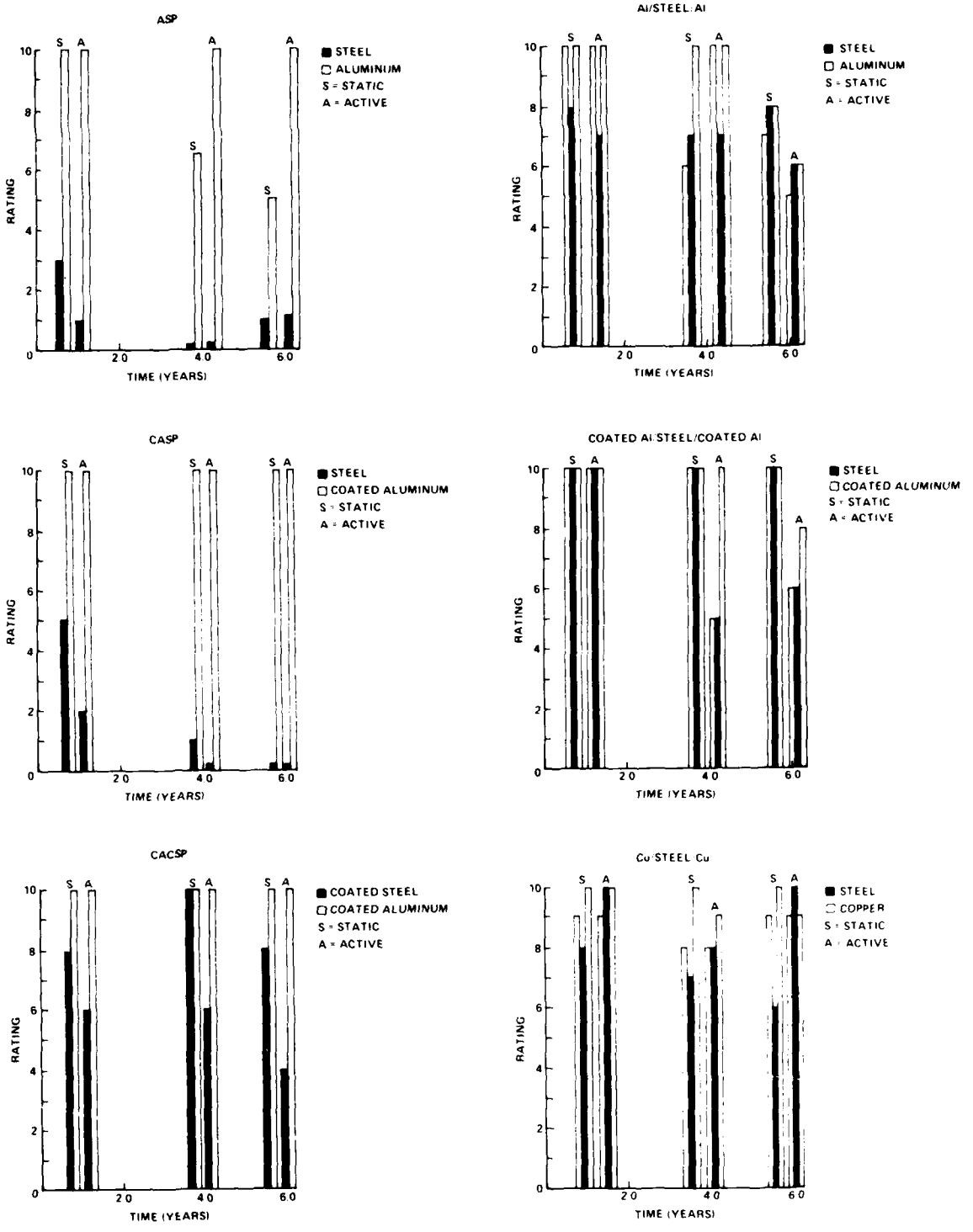

FIGURE 2 - PERFORMANCE OF SHIELDS AT RINGS

TABLE I

SHIELDING MATERIALS IN TEST PROGRAM[1]

ASP ..... (bare 8 mil aluminum/bare 6 mil tin plated steel)

CASP..... (coated 8 mil aluminum/bare 6 mil tin plated steel)

CACSP ..... (plastic coated 8 mil aluminum/plastic coated 6 mil tin plated steel)

Al/ST/Al .... (aluminum clad steel clad aluminum 0.008/0.003/0.005)

CAl/ST/CAl... (coated aluminum clad steel clad coated aluminum - 0.008/0.003/0.005)

Cu/ST/Cu..... (copper clad steel clad copper 0.0004/0.002/0.0036)

NOTE: 1 - Sheath interfaces were fully flooded with atactic polypropylene based floodant and the cable core was filled with petrolatum based filler.

TABLE II

ANALYTIC TECHNIQUES FOR SOIL WATER EXTRACTS

SPECIES	TECHNIQUE EMPLOYED
Na^+	Atomic Absorption Spectroscopy
Ca^{++}	Atomic Absorption Spectroscopy
K^+	Atomic Absorption Spectroscopy
Mg^{++}	Atomic Absorption Spectroscopy
Cl^-	Ion Selective Electrode
NO_3^-	Ion Selective Electrode
$SO_4^=$	UV-Visible Spectroscopy
HCO_3^-	Titrimetry
$CO_3^=$	Titrimetry

TABLE IV

AC CURRENT IN SHIELDS OF TEST CABLES

SHIELD TYPE	SHIELD CURRENT AT BEGINNING OF TEST CABLE (ma)	SHIELD CURRENT AT END OF TEST CABLE (ma)
ASP	100	180
CASP	180	130
CACSP	130	205
Cu/ST/Cu	205	215
Al/ST/Al	215	200
CAl/ST/CAl	200	150

TABLE III

PROPERTIES OF SOILS AT CONWAY, S.C. TEST SITE

SHIELD	RESISTIVITY (ohm-cm)	pH	COMPOSITION OF WATER EXTRACT (parts per million)							
			Ca	Mg	Na	CO_3	HCO_3	SO_4	Cl	NO_3
CASP	9500 (16000)	5.47	0.6	0.4	7.2	nil	0.18	3	0.1	3
ASP	34000 (110000)	5.40	1.9	0.4	5.4	nil	0.11	6	0.1	2
CACSP	11000 (29000)	5.81	5.9	0.6	3.6	nil	0.10	15	0.1	8
Al-ST-Al	7000 (11000)	5.55	3.1	0.8	10.8	nil	0.26	3	0.1	20
Cu-ST-Cu	11000 (19000)	5.45	2.5	0.6	6.3	nil	0.13	4	0.1	16
CAl-ST-CAl	8000 (13000)	5.40	3.4	0.7	9.4	nil	0.13	5	1.0	21

TABLE V

RATING CODE FOR THE EVALUATION OF SHIELDS IN CABLE SPECIMENS

Rating	Performance	Degree of Corrosion
10	Excellent	Unaffected - no indication of corrosion.
9	Excellent	Superficial rust or etching on surface.
8	Very good	Uniform metal attack, rust, and/or slight localized pitting.
7	Good	Appreciable pitting over the surface, but no perforations through metal shield. Some minor delamination or dissipation of metallurgically or plastic-bonded metals leaving cathodic metal intact.
6+	Good	Localized pitting: only one perforation in shield by pitting.
6	Good	Localized pitting: 2 to 5 perforations in shield by pitting
5	Fair	Many localized pits causing perforation of shield <5% of shield dissipated by corrosion; extensive delamination of metallurgically bonded metals.
4	Poor	Severe corrosion: pitting to perforation of shield; 5 to 10% of shield dissipated by corrosion; severe corrosion of anodic part of metallurgically bonded metals.
3	Poor	Severe corrosion: pitting to perforation of shield; 10 to 25% of shield dissipated by corrosion.
2	Very poor	Severe corrosion: more than 25% of shield dissipated by corrosion; shield still has electrical continuity along the cable.
1	Very poor	Severe corrosion: shield is close to electrical discontinuity (ELD) due to perforation in shield and dissipation of metal by corrosion.
0	Very poor	Severe corrosion: shield is electrically discontinuous (ELD) due to dissipation of metal by corrosion

TABLE VI
PERFORMANCE RATINGS FOR ASP IN CONWAY BURIAL TESTS

EXPOSURE TIME (YEARS)	PASSIVE	ACTIVE	WINDOW	RING	HOLES				UNDER JACKET
					1/4	1/8	1/16	1/32	
1.0	STEEL		3	3	6[1]	-	-	-	8
	AL		(10)	(10)	(10)	(10)	(10)	(10)	(10)
		STEEL	2	1	7	10	10	10	7
		AL	(10)	(10)	(10)	(10)	(10)	(10)	(10)
4.0	STEEL		0	0	-	-	-	-	5
	AL		(10)	(6+)	(10)	(10)	(10)	(10)	(10)
		STEEL	1	0	0	0	-	-	7
		AL	(10)	(10)	(10)	(10)	(10)	(10)	(10)
6.0	STEEL		0	1	0	0	0	10	7
	AL		(6)	(5)	(10)	(10)	(10)	(10)	(5)
		STEEL	1	1	3	10	10	10	9
		AL	(10)	(10)	(10)	(10)	(10)	(10)	(10)
	STEEL		1	1	3	0	10	10	7
	AL		(5)	(5)	(3)	(10)	(0)	(10)	(5)
		STEEL	1	1	0	1	10	10	9
		AL	(10)	(10)	(10)	(10)	(10)	(10)	(10)
	STEEL		0	0	1	4	9	3	7
	AL		(9)	(3)	(10)	(10)	(10)	(10)	(8)

SEE TABLE XII FOR EXPLANATION OF FOOTNOTES

TABLE VII

PERFORMANCE RATINGS FOR CASP IN CONWAY BURIAL TESTS

EXPOSURE TIME (YEARS)	PASSIVE	ACTIVE	WINDOW	RING	HOLES				UNDER JACKET
					1/4	1/8	1/16	1/32	
1.0	STEEL		5[1]	5[1]	5[1]	6+	10	10	8
	AL		(10)	(10)	(10)	(10)	(10)	(10)	(10)
		STEEL	3[1]	2[1]	0[1]	0[1]	-[5]	-[5]	8
		AL	(10)	(10)	(10)	(10)	(-)	(-)	(10)
4.0	STEEL		1	1	0	6+	-	-	6
	AL		(10)	(10)	(10)	(10)	(10)	(10)	(10)
		STEEL	0	0	0	0	0	-	5
		AL	(10)	(10)	(10)	(10)	(10)	(10)	(10)
6.0		STEEL	0	0	0	0	0	0	5
		AL	(10)	(10)	(10)	(10)	(10)	(10)	(10)
	STEEL		0	0	0	0	0	0	5
	AL		(10)	(10)	(10)	(10)	(10)	(10)	(10)
		STEEL	0	0	0	0	0	0	5
		AL	(10)	(10)	(10)	(10)	(10)	(10)	(10)

SEE TABLE XII FOR EXPLANATION OF FOOTNOTES

TABLE VIII

PERFORMANCE RATINGS FOR CACSP IN CONWAY BURIAL TESTS

EXPOSURE TIME (YEARS)	PASSIVE	ACTIVE	WINDOW	RING	HOLES				UNDER JACKET
					1/4	1/8	1/16	1/32	
1.0	STEEL		8[1]	8[1]	-[7]	6[1]	7[1]	7[1]	10,7
	AL		(10)	(10)	(10)	(10)	(10)	(10)	(10)
		STEEL	5[1,6]	6[1]	8[1]	.[7]	5[1]	0[1]	10,7
		AL	(10)	(10)	(10)	(10)	(10)	(10)	(10)
4.0	STEEL		10	10	10	10	10	10	10
	AL		(10)	(10)	(10)	(10)	(10)	(10)	(10)
		STEEL	8[10]	6[10]	-	0	0	0	9[10],7[8]
		AL	(10)	(10)	(10)	(10)	(10)	(10)	(10)
6.0	STEEL*		10	10	0	0	0	0	10
	AL*		(10)	(10)	(10)	(10)	(10)	(10)	(10)
		STEEL	4[10]	1	3	10	10	10	5[10]
		AL	(10)	(10)	(10)	(10)	(10)	(10)	(10)
	STEEL		6[10]	6	1	1	1	1	10
	AL		(10)	(10)	(10)	(10)	(10)	(10)	(10)
		STEEL	5	7[8]	8[10]	9	10	10	10
		AL	(10)	(10)	(10)	(10)	(10)	(10)	(10)

* Unearthed by CATV Company and reburied

SEE TABLE XII FOR EXPLANATION OF FOOTNOTES

TABLE IX

PERFORMANCE RATINGS FOR CU/STEEL/CU IN CONWAY BURIAL TESTS

EXPOSURE TIME (YEARS)	STATIC	ACTIVE	WINDOW	RING	HOLES				UNDER JACKET
					1/4	1/8	1/16	1/32	
1.0	CU		9	9	-[7]	10	10	10	10
	ST		8	-	-	-	-	-	-
	CU		(10)	(10)	(-)[7]	(10)	(10)	(10)	(9)
		CU	9	9	-[7]	9	9	10	9
		ST	10	-	-	-	-	-	-
		CU	(10)	(10)	(10)	(10)	(10)	(10)	(10)
4.0	CU		8[9]	8	9	9	9	9	9
	ST		7	7	-	-	-	9	9,7[8]
	CU		(10)	(10)	(10)	(10)	(10)	(10)	(10)
		CU	8	8	8[2]	8[2]	8[2]	8[2]	9
		ST	8	8	-	-	-	-	9
		CU	(8)	(9)	(10)	(10)	(10)	(10)	(10)
6.0	CU		9	9	9	9	9	)	10
	ST		5[8]	7[8]	-	-	-	-	-
	CU		(10)	(10)	(10)	(10)	(10)	(10)	(10)
		CU	9	9	9	9	9	9	10
		ST	9	-	-	-	-	-	-
		CU	(9)	(9)	(10)	(10)	(10)	(10)	(10)
	CU		9	9	9	9	9	9	10
	ST		5[8]	5[8]	-	5	-	-	-
	CU		(10)	(10)	(10)	(10)	(10)	(10)	(10)
		CU	9	9	9	9	9	9	10
		ST	10	10	-	-	-	-	-
		CU	(9)	(9)	(10)	(10)	(10)	(10)	(10)

SEE TABLE XII FOR EXPLANATION OF FOOTNOTES

TABLE X

PERFORMANCE RATINGS FOR AL/STEEL/AL IN CONWAY BURIAL TESTS

EXPOSURE TIME (YEARS)	STATIC	ACTIVE	WINDOW	RING	HOLES				UNDER JACKET
					1/4	1/8	1/16	1/32	
1.0	AL		10	10	-[7]	10	10	10	10
	ST		8	-	-	-	-	-	-
	AL		(10)	(10)	(-[7])	(10)	(10)	(10)	(10)
		AL	10	10	(-[7])	10	10	10	10
		ST	7	-	-	-	-	-	-
		AL	(10)	(10)	(-[7])	(10)	(10)	(10)	(10)
4.0	AL		6+	6	10	10	10	10	10
	ST		7[8]	7[8]	10	10	10	10	9,7[8]
	AL		(10)	(10)	(6+)	(10)	(10)	(10)	(10)
		AL	10	10	10	10	10	10	10
		ST	7[8]	7[8]	10	10	10	10	9,9[8]
		AL	(10)	(10)	(10)	(10)	(10)	(10)	(10)
6.0	AL		6	6	8[2]	10	10	10	6+
	ST		10	6	-	-	-	-	-
	AL		(8)	(6)	(10)	(10)	(10)	(10)	(10)
		AL	3	4	9	9	9	9	7
		ST	5	6+	-	-	-	-	-
		AL	(5)	(5)	(10)	(10)	(10)	(10)	(7)
	AL		8	8	10	10	10	10	10
	ST		10	10	-	-	-	-	-
	AL		(9)	(10)	(10)	(10)	(10)	(10)	(10)
		AL	6	6	4	6+	8[2]	10	7
		ST	6	6	4	4	8	-	-
		AL	(6)	(6)	(6+)	(10)	(10)	(10)	(7)

SEE TABLE XII FOR EXPLANATION OF FOOTNOTES

TABLE XI

PERFORMANCE RATINGS FOR CAL/STEEL/CAL IN CONWAY BURIAL TESTS

EXPOSURE TIME (YEARS)	STATIC	ACTIVE	WINDOW	RING	HOLES				UNDER JACKET
					1/4	1/8	1/16	1/32	
1.0	AL		10	10	-[7]	10	10	10	10
	ST		10	-	-	-	-	-	-
	AL		(10)	(10)	(-[7])	(10)	(10)	(10)	(10)
		AL	10	10	-[7]	10	10	10	10
		ST	10	-	-	-	-	-	-
		AL	(10)	(10)	(-[7])	(10)	(10)	(10)	(10)
4.0	AL		10	10	10	10	10	10	10
	ST		10	10	10	10	10	10	10
	AL		(10)	(10)	(10)	(10)	(10)	(10)	(10)
		AL	6	5	10	10	10	0[2]	10
		ST	6	5	10	10	10	0[2]	9[8]
		AL	(10)	(10)	(10)	(10)	(10)	(10)	(10)
6.0		AL	6	6	10	10	10	10	10
		ST	6	6	-	-	-	-	-
		AL	(6+[8])	(6+[9])	(10)	(10)	(10)	(10)	(10)
	AL		6[10]	10[2]	10	10	10	10	10
	ST		8	10[2]	-	-	-	-	-
	AL		(10)	(10[2])	(10)	(10)	(10)	(10)	(10)
		AL	5	5	10	10	10	10	10
		ST	6+	6+	-	-	-	-	-
		AL	(7)	(9)	(10)	(10)	(10)	(10)	(10)

SEE TABLE XII FOR EXPLANATION OF FOOTNOTES

TABLE XII

EXPLANATORY NOTES

1. Corrosion at or along line where shield was touched by punch or cutting tool.
2. Mechanical damage.
3. Coating torn.
4. NBSIR 81-2243, 4/81
5. Sample area missing probably due to preparation of holes with punch.
6. One perforation not initiated by mechanical damage.
7. Removed for metallurgical analysis by TI prior to exam by panel.
8. Extensive corrosion from the edge
9. Mechanical deformation (dimple) caused by internal corrosion products.
10. Filliform corrosion observed.

- Inner jacket evaluation indicted by ( ).
- Blanks indicate inability to evaluate.
- Where dual ratings are given, the second rating is for edge effects.
- Evaluations are based on exposed area only.

OPTIMIZATION OF RETURN LOSS AND INSERTION LOSS PERFORMANCE OF SINGLE-MODE FIBER MECHANICAL SPLICES

W.C. Young, V.S. Shah, and L. Curtis

Bellcore, Red Bank, New Jersey

SUMMARY

Single-mode fibers having oblique endfaces can be used in conjunction with index-matching material to achieve mechanical splices (both single and multiple fiber splices) that exhibit high return loss performance without significantly affecting insertion loss performance. Furthermore, this improvement in performance does not require any additional alignment complexities. In cases where oblique endfaces are used without index-matching material, high return losses can still be realized, however, this may result in degraded insertion loss performance and/or increased complexity in terms of the relative orientation of the oblique fiber endfaces. This technique of incorporating small faceted endface angles and index-matching materials can also be used to upgrade some of the existing mechanical splices in installed fiber cables, if future lightwave systems require higher-performance splices. Upgrading the splices in this manner would only require a simple polishing procedure and would yield splices having high return loss characteristics over wide environmental and climatic conditions. For example, we have demonstrated that by applying 10 degree endface angles, with random relative orientation within the joint, the return loss of an index-matched mechanical splice was increased from 24dB to more than 60dB, while maintaining an insertion loss of 0.2dB.

INTRODUCTION

Optical feedback from reflections caused by connectors and splices can generate intensity noise in lasers[1] and introduce power penalties in digital transmission systems[2]. It was recently reported, that multiple reflections between fiber joints can cause the conversion of laser phase noise into intensity noise that can severely degrade both high-speed direct-detection and coherent lightwave systems[3], even when isolators are used. Unlike fusion splices, that typically exhibit reflection characteristics greater than 60dB, present mechanical splices usually exhibit reflections ranging between 20 and 50dB in return loss, even when index-matching material is used. Furthermore, as a result of multiple beam interference, even in cases where index-matching is employed, climatic and environmental changes can cause large fluctuations in return loss while only exhibiting negligible changes in insertion loss. In this paper, we report on a novel technique of mechanical splicing that optimizes both return loss and insertion loss performance of mechanical joints by simultaneously using oblique fiber endfaces and index-matching material. This novel technique can be used with single and multiple fiber mechanical joints employing either multimode or single-mode fibers, and can be used to upgrade the return loss characteristics of existing mechanical splices without degrading their insertion loss performance, provided index-matching material is used.

DISCUSSION

Various methods can be used to realize high return loss and/or low insertion loss fiber joints such as physical contact between adjacent

fibers[4], index-matching materials between adjacent fibers[5], and angled endfaces[6]. In the following we will describe how the optimization of high return loss and low insertion loss performance can be achieved by using, in combination, oblique fiber endfaces and index-matching material. These oblique endfaces decouple, from the fiber, the power reflected from the endface, and the index-matching material reduces both the amplitude of the reflective power component and the beam deflection angle caused by the oblique endfaces. This combination, as explained below, yields single-mode fiber joints that exhibit high return loss without degrading insertion loss performance.

The return loss of a single-ended single-mode fiber, having various endface angles was investigated both theoretically and experimentally. Since it is assumed that the oblique endfaces would more than likely be applied by employing a polishing technique, and that practical techniques of polishing fiber endfaces have been shown to produce non-flat and scratched surfaces, index-matching material was used in this study. Furthermore, since this type of simple polishing can also produce a high-index-layer (about n=1.6) due to compaction[7], a matching oil having an index of 1.6 was selected to reduce the effects caused by these departures from ideal flat and smooth endfaces. It should be noted, that although the index oil reduces the reflection occurring between the high-index layer and air, the residual intrinsic reflection occurring between the bulk fiber material and the compacted layer (1.46/1.6) remains. It is this boundary that limits the return loss performance of this type of polished endface to a value of about 35dB for perpendicular endfaces. Furthermore, although the index-matching oil minimizes the effect from the surfaces of non-flat endfaces due to polishing, it has no effect on the non-flat boundary between the bulk material and high-index layer, that we assume has also taken a similar shape as the endface. Investigations of the non-flatness of these endfaces usually reveals a concave surface caused by the radial dependence of the fiber's hardness. The results of our theoretical and experimental study of the single oblique endface are shown in Figure 1.

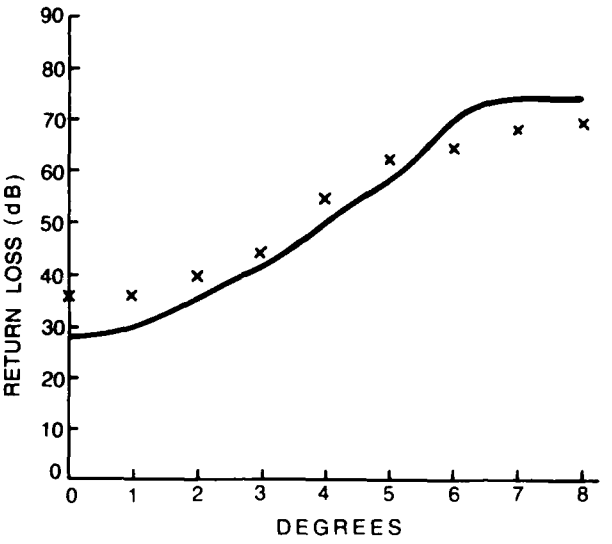

Fig. 1 - Theoretical and experimental return loss versus endface angle (polished endfaces of single-ended, single-mode fiber, immersed in index-matching oil(n=1.6).

The theoretical curve[8] assumes a spherical concave surface across the core with a radius of 250 microns, and the crosses are experimental values of return loss. As can be seen in this figure, when the oblique angle is greater than 5 degrees, the return loss of endfaces polished with this type of simple procedure (dry polishing with 1 micron aluminum-oxide coated polyester sheet on a hard flat surface) increases much less rapidly than that of perfectly flat and smooth cleaved endfaces.

As shown above, oblique endfaces exhibit high return loss characteristics, but this type of endface also causes deflection of the emitted beam resulting in a transverse offset as shown in Figure 2, even though the fiber axes may be perfectly aligned.

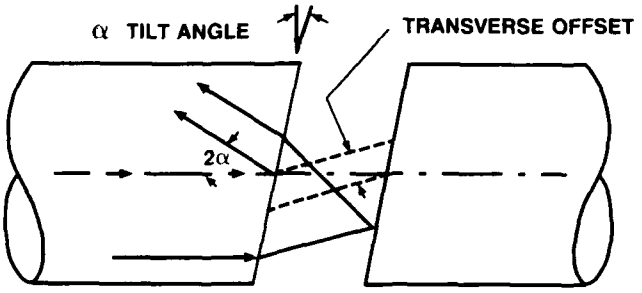

Fig. 2 - Schematic of a butt-joint of two single-mode fibers having oblique endfaces.

It can be shown that the magnitude of this offset is a function of the fiber endface angle and the deflection angle of the emitted beam. By orienting the fiber endfaces parallel to each other, to minimize the angular misalignment, and by establishing and controlling the longitudinal separation and transverse offset of the fiber axes, good coupling efficiency of the transmitted beam (low insertion loss performance) can be achieved. To ensure high return loss performance we have shown that an angle of at least 5 degrees is required for a single-ended single-mode fiber. When the second endface of a joint is considered, the return loss performance of two parallel endfaces having the same angle is only slightly less than the singled-ended case. But, in cases where the second endface is not parallel, due to the presence of a relative rotational displacement of the two fibers, the beam reflected from the second endface can have a smaller angle within the first fiber, resulting in increased returned power (i.e. degraded return loss performance). Therefore, in this case, larger endface angles must be used to maintain similar return loss performance. However, insertion loss performance will suffer because of the larger angular misalignment present. In this study, we have found that by using index-matching material, the deflection angle can be reduced to a very small value. The insertion loss is then significantly improved because of the very small angular misalignment, and the return loss is also improved because the beam reflected from the second endface enters the first fiber at an angle very close to twice the oblique angle (same as parallel endfaces). Thus, the use of index-matching material allows the random orientation of the two fiber endfaces with only negligible degradation in either insertion loss or return loss performance compared to the case of parallel orientation. It should be noted that the index-matching material for the case of perpendicular endfaces also reduces the reflective power component from the fiber endfaces, however, the residual reflection from the interface between the bulk fiber material and the polishing-induced high-index layer is not reduced. But in the case of the oblique endface, the resulting angular interface between the bulk fiber material and the compacted layer of the endface, greatly reduces the coupling of this reflected power component (1.46/1.6). Therefore, high-return-loss, low-insertion-loss mechanical splices can be realized by simultaneously using oblique fiber endfaces (greater than 5 degree endface angle) and index-matching material. Furthermore, this approach permits random relative orientation of the oblique endfaces without degrading performance.

RESULTS

A v-groove splice with index-matching oil was used to confirm the above conclusions. First, 40 splices were assembled using cleaved single-mode fibers having endface angles less than 1

degree, and their return losses and insertion losses were measured using a 1300 nanometer OTDR. Next, 100 splices were assembled using polished single-mode fiber endfaces having a 10 degree endface angle. The polishing was done dry, using 1 micron aluminum-oxide coated polyester sheets on a flat glass plate. Each end was polished by hand, requiring less than 1 minute, and no inspection was made of the endfaces. The splices were then assembled without regard to their relative endface orientation, and their return loss and insertion loss were also measured with the OTDR. Figures 3 and 4 compare the return loss and insertion loss performance of these two types of splices, respectively.

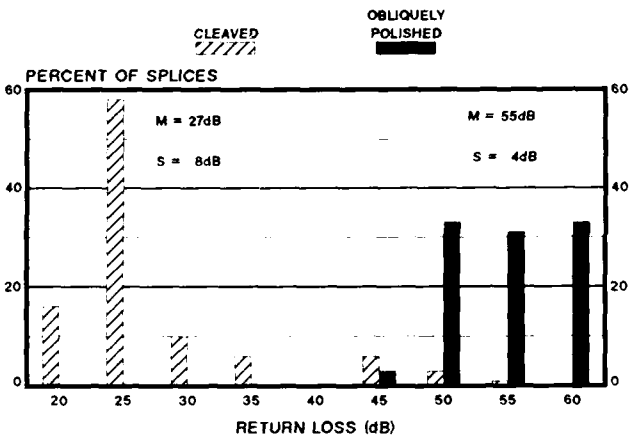

Fig. 3 - Histogram of return loss for 40 splices having perpendicular, cleaved endfaces and 100 splices having obliquely polished endfaces.

As shown in Figure 3, the cleaved perpendicular (less than 1 degree) endfaces have values ranging between 20 and 55dB (mean of 27db and standard deviation of 8dB), while the return loss performance for the splices having oblique endfaces show significant improvement (mean of 55dB and standard deviation of 4 dB).

In addition, since in practice index-matching is generally not perfect, resulting multiple beam interference causes any longitudinal movement of the fibers to change the return loss. For the case of perpendicular endfaces the minimum return loss can be very low as seen in this study (20dB), where as for the case of oblique endfaces the minimum value is greater than 45dB. Contrary to the large difference in return loss performance of splices having oblique and perpendicular endfaces, the insertion loss performance, even with the presence of the relatively large oblique angle of 10 degrees, was similar for both types of splices, as can be seen in Figure 4.

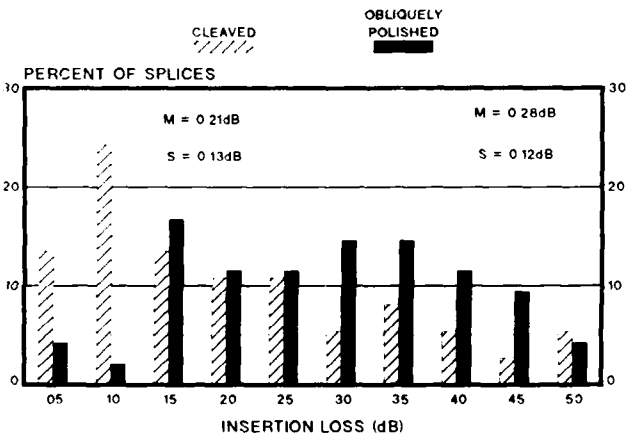

Fig. 4 - Histogram of insertion loss for 40 splices having perpendicular, cleaved endfaces and 100 splices having obliquely polished endfaces.

The mean and standard deviation for splices having perpendicular endfaces was 0.21 and 0.13dB and for splices having oblique endfaces was 0.28 and 0.12dB, respectively.

To evaluate this technique in the case of multiple fiber splices and to confirm that six degree endface angles are large enough to

provide excellent return loss characteristics, an eight-fiber-array splice was modified by polishing an angled facet (6 degrees) across the endface of the array, as shown in Figure 5.

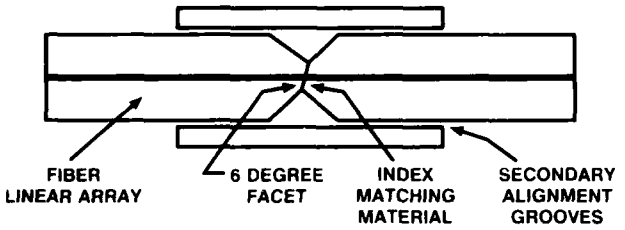

Fig. 5 - Schematic of a linear fiber array splice.

Fiber	Return Loss (dB)	Insertion Loss (dB)	Insertion Loss (dB) (Initial)
1	57*	0.19**	0.00
2	60	0.20	0.00
3	57	0.08	0.06
4	57	0.20	0.14
5	58	0.10	0.00
6	61	0.03	0.07
7	62	0.03	0.05
8	56	0.34	0.34

* 46dB (Air-Gap) ** 0.58dB (Air-Gap)

Table 1 - Return losses and insertion losses for an 8 fiber array splice having oblique endfaces.

Due to the relatively large thickness of the array (1.5 mm), compared to an uncoated fiber (125 microns), a small facet was used to minimize the longitudinal separation between the fibers, since any mismatch in endface angle would have caused a larger separation than the one occurring in just fiber-to-fiber interfaces. Although not a necessity, parallel orientation of the two opposing facets was controlled by the design characteristics of the linear-array splice. For the previously mentioned reasons, index-matching oil ($n = 1.6$) was also used in assembling these particular splices. Table 1 shows the measured values of return losses and insertion losses of the eight-fiber-array measured at a wavelength of 1539 nanometers. As shown in the table, return losses of greater than 55dB were achieved when index-matching oil was used, and no significant increase in insertion loss occurred when compared to measurements made before modification of the endfaces.

To evaluate cases where poor index-matching and/or migration (from between the fiber endfaces) of the index-matching material occurs, the return loss and insertion loss of one fiber path was measured when the splice was assembled without index-matching material. In this case, due to the presence of an air-gap and the resulting increase in reflection, the insertion loss increased from 0.19 to 0.58dB while the return loss decreased from 57 to 46dB,as detailed in Table 1. This measurement shows that, if preferred, the splice can be assembled without index-matching material and still have good return loss characteristics. However, due to the increase in reflection from the endfaces, the insertion loss performance is degraded accordingly.

The splice was also assembled such that the two opposing facets formed a 12 degree angle. In this case, the insertion loss was 0.80dB and the return loss was 55dB when index-matching material was used, and 5.4dB and 25dB, respectively, without index-matching material.

It is noteworthy, that even when the splice is assembled with the opposing faces not parallel, with index-matching, the return loss characteristics are about the same as in the parallel-endface arrangement. Furthermore, caution should be used in comparing the insertion loss value of 0.80dB with those in Table 1, since in this latter case the fiber-to-fiber interfaces were not the same as any of the previous ones reported on in the table, and the 0.80dB value is well within the expected value for this particular type of single-mode, multiple-fiber-array splice.

CONCLUSIONS

We have shown that the return loss and insertion loss characteristics of single-mode fiber mechanical splices can be optimized by using oblique fiber endfaces (greater than 5 degree endface angles) in combination with index-matching material. Using this combination, splices can be assembled without regard to the relative orientation of the oblique endfaces and still exhibit return losses of greater than 55dB without degrading insertion loss. Furthermore, even when index-matching is imperfect, the minimum value of return loss is still very high, thereby ensuring excellent return loss performance over wide environmental and climatic conditions. We have also shown that this technique can be used to upgrade existing splices in installed single-mode fiber cables, if higher-performance splices are required by higher bit-rate systems. Besides requiring access to the splices, this upgrade would involve a simple polishing procedure and would yield splices having high return loss characteristics and comparable insertion loss performance.

REFERENCES

1. Hirota,O. Suematsu,Y. and Kwok, K.S. : "Properties of intensity noises of laser diodes due to reflected waves from single-mode optical fibers and its reduction", IEEE J. Quantum Electron., QE-17,1024(1980).

2. Mazurczyk,V.J.:"Sensitivity of single-mode buried heterostructure lasers to reflected power at 274 Mbit/s", Electron. Lett. 17, 143 (1981).

3. Choy,M.M., Gimlett,J.L., Welter,R., Kazovsky, L.G., and Cheung,N.K.: "Interferometric conversion of laser phase noise by single-mode fiber-optic components", Electron. Lett. 23, 1151(1987).

4. Young,W.C., Curtis,L., and Kaiser,P.:"A transfer molded biconic connector with insertion losses below 0.3dB without index match", Sixth ECOC, York, UK, paper PD5, (1980).

5. Miller,C.M.:"A fiber-optic-cable connector", Bell Syst. Tech. J., 54: 1547, (1975).

6. Suzuki,N., and Nagano,O.:"Low insertion loss- and high return-loss optical connectors for use in analog video transmission", IOOC'83, 30A3-5, (1983).

7. Shah,V.S., Young,W.C., and Curtis,L.:"Large fluctuations in transmitted power at fiber joints with polished endfaces", OFC/IOOC'87, TuF4, (1987).

8. Shah,V., Young,W.C., and Curtis,L.:"Return loss studies of a single-ended single-mode fiber: effect of the nonflat fiber endface", NBS Symp. on Optical Fiber Measurements, Boulder, CO., (1988).

L.CURTIS
Bellcore
331 Newman Springs Rd
Box 7030
Red Bank, NJ 07701

Mr. L. Curtis is a Member of the Technical Staff in the Lightguide Technology Group. Since 1975 he has been associated with the development of optical connectors and has received three patents and co-authored several papers in this area.

W.C. YOUNG
Bellcore
331 Newman Springs Rd
Box 7030
Red Bank, NJ 07701

Bill Young is District Manager of Bellcore's Lightguide Technology Research District. His main areas of interest include fiber and fiber-based component research, as documented by patents and publications. Related to these interests Mr. Young is Chairman of Sub-Committee 86B, "Fiber Optic Interconnecting Devices and Passive Components", of the International Electrotechnical Commission.

V. SHAH
Bellcore
331 Newman Springs Rd
Box 7030
Red Bank, NJ 07701

Viren Shah was born in Bombay, India. He received his B.S. degree in electrical engineering from the University of Bombay and M.S. and Ph.D degrees in electro-physics from Polytechnic Institute of New York in 1973, 1976 and 1982, respectively.

He joined the satellite communications lab of AT&T Bell Laboratories, Holmdel, in 1982. Since 1984, he has been with Bellcore, where he is engaged in propagation studies in optical fiber waveguides.

LOSS AT DISSIMILAR FIBER SPLICES

R. Raman

Contel Laboratories
Norcross, Georgia 30092

ABSTRACT

The purpose of this paper is to determine the factors that contribute to excessive loss at dissimilar fiber splices and derive a maximum limit for acceptable loss.

Despite variations in alignment techniques, fusion, V-groove, and rotary splices, all yield extremely low losses. This means that mechanical misalignments, as well as fiber intrinsic factors, are eliminated. Comparison of the experimental and theoretical loss values for various combinations of matched cladding and depressed cladding fibers indicates that the effects of mode field diameter mismatch are negligible.

If a transmission method of measurement is used, an acceptable maximum level of 0.15 dB can be set. Assuming that there are no extraneous errors, a splice loss in excess of this value must be attributed to manufacturing deficiencies of the mechanical splices.

When an OTDR is used, factors such as group velocity and variations of scattering contribute to measurement deviations. Therefore, when specifying loss values, allowances must be made to account for the inherent experimental inaccuracies.

INTRODUCTION

General

In recent years there have been significant improvements in single mode fiber manufacturing tolerances and splicing techniques. Some mechanical splices perform so well that loss and strength approaching those of fusion splices can be achieved. This would imply that errors due to fiber geometry variations and fiber misalignment are virtually eliminated. However, under field conditions, high losses are still encountered. In view of this, the question is whether we can establish precisely an acceptable level of splice loss objective.

In a paper published in 1987, Hopiavuori, Matthews, and DeVito have reported results of a detailed investigation of fusion splicing of matched cladding and depressed cladding fibers[1]. Their conclusion is that mode field diameter (MFD) mismatch and lateral offset of the cores contribute less to the splice loss than the end angle. Only fusion splices using fibers cleaved precisely and tests using OTDR are considered.

The purpose of this paper is to determine various factors that contribute to the excess loss and derive a maximum acceptable limit. Excess loss becomes increasingly significant when dissimilar fibers are involved, or when early vintage fibers are joined with present day fibers.

Fiber Dimensional Tolerances

The main fiber variations are in the core size, cladding diameter, ellipticity, and core-cladding eccentricity. In recent years, fiber manufacturers have tightened fiber geometry specifications. Computer-controlled processes now enable the manufacturer to achieve great dimensional precision, repeatability, and uniformity. For example, core-cladding offset less than 1 micron and a noncircularity less than 2 percent have become routine. At the present time, standard deviations for core size (MFD) and cladding diameter are 0.15 micron and 0.6 micron, respectively[2]. The precision is so high that one manufacturer describes the process as "cloning". However, one variability which is unavoidable is the index profile, which reflects the deposition process.

Splicing Techniques

All splicing methods involve V-groove(s). In the fusion process, the two fiber ends are located in two V-grooves on either side of the arc electrodes. This arrangement permits movement of the fiber in three mutually perpendicular directions. Sometimes there is a provision for fiber rotation. High precision and repeatability are attained by microprocessor control.

Most mechanical splices feature a continuous V-groove. One exception is the rotary splice. The elastomeric splice consists of two half-

hexagonal pieces, one with a V-groove. The triangular interstitial space formed by the two pieces is smaller than the fiber size. This enables equal distortion of all three sides so that the fibers are concentric to one another. The core contains an index matching gel. Variations of the design include four-rod arrangement (PSI) and a V-groove with a flat plate on top (Mekconlite). In addition to longitudinal alignment, the fibers can also be rotated. This, coupled with the fact that active alignment (LID) is used, permits elimination of most of the misalignment problems.

To achieve high precision, the V-groove must be smooth and straight. As stated by Cannon and Williford, the offset ϵ between the two fiber centers differing in radii by an amount Δ is:

$$\epsilon = \frac{\Delta}{\sin \alpha/2}$$

where α is the angle of the V-groove[3]. The minimum attainable offset occurs where $\alpha/2 = 90^0$ or a flat plate. It gets worse as the angle gets smaller. The usual angle is 45^0. The reliability of a V-groove depends on the fiber outside diameter (O.D.). If the fiber diameters vary greatly, it will not be possible to obtain satisfactory alignment.

In the rotary technique, the fibers are held rigidly in two ferrules, which are then inserted into a discontinuous V-groove formed by three glass rods contained in a triangular metal sleeve[4]. Built-in eccentricities of the bore within the glass ferrules and the offset in the sleeve allow relatively large rotational movements and small movement of the cores relative to one another. Active alignment involves injecting light into the core at one end and detecting scattered light at the splice point.

A comparison of the various methods shows that fusion represents the ideal case. Losses as low as 0.01 or 0.02 dB are easily obtained. The rotary technique approaches this level, especially when similar fibers are used. In contrast, the precision possible with a V-groove splice is considered somewhat lower.

Extraneous Factors

The two extraneous factors that contribute to excess loss are craft errors and measurement inaccuracies.

There are three tangible elements that influence craft errors: inadequate training, alignment difficulties, and unsatisfactory cleave angle. One intangible element is the degree of skill. However, the alignment difficulties and inadequate training can be corrected by systematic mastering of the technique. Although cleaving tool defects will yield large end angles, in general an operator repeats the cleaving step at least three times. The use of index gel can often compensate for nonuniformity of the ends. Many microprocessor controlled fusion splicers will not function if end angles are larger than 3^0. One way to eliminate end angle problems is to polish the fiber ends, as is the case with the rotary splice.

Measurement Inaccuracies

A transmission method is often suggested for the determination of splice loss. However, when cut fibers or discontinuous cables are used, this method is not accurate because of the need to use a cutback technique. Similarly, the detector in a LID system provides only an estimate of the splice loss.

At Contel Labs, we have developed a technique for accurately measuring loss at dissimilar splice points[5]. However, this method is not feasible in the field.

In most field situations, an OTDR is employed. In applying an OTDR, it is important that the trace is interpreted correctly[6]. First of all, bidirectional measurement is required with the actual loss being the average of the two values. Furthermore, factors such as mode field diameter mismatch, group velocity, and variations of backscattering must also be considered[7,8].

SAMPLES

A large number of splices (V-groove, rotary, and fusion) were prepared using various combinations of the following dissimilar fibers representing different vendors:

FIBER	TYPE	MODE FIELD DIA., μm	CLADDING DIA., μm
A	Depressed Cladding	9.00	124.89
B	Depressed Cladding	9.04	125.00
C	Matched Cladding	9.45	125.20
D	Matched Cladding	10.27	124.70
E	Depressed Cladding	9.78	125.10

A microprocessor-controlled fuser was utilized to fuse fibers. Two cleaving tools were used to prepare fiber ends. End angles were not measured. However, previous tests have shown that cleaver I typically yields an average end angle of 0.99^0 (sigma = 0.27) and that cleaver II provides 2.1^0 (sigma = 1.25). The rotary splice was optimized using an Anritsu source and a detector operating at 1300 nm.

The splices featured 3 to 10-foot fiber sections except when an OTDR was used to optimize during sample preparation. Only a limited number of rotary and V-groove splices were available. However, the V-groove devices were reused a number of times.

MEASUREMENTS

Splice loss was determined using the experimental technique described in a previous paper[5].

The procedure is a modified version of the traditional transmission measurement and includes cutback and substitution steps. The errors introduced when the fiber ends of a test splice are removed and reinserted at the interconnection points are calculated based on the known values of control splices.

Initial loss is measured by connecting a long section of fiber between two test points (laboratory splices). The fiber end at the detector side is removed, and a third laboratory splice is inserted. Finally, the test splice is introduced between the third splice and the second splice.

The total loss is composed of three components:

$$\text{Loss} = L_T + L_3 + B$$

where, L_T = Loss at Test Splice

L_3 = Loss at Splice No. 3

B = Correction Factor.

The correction factor is determined using control splices, the absolute loss values of which are known.

The correction factor was 0.01 dB.

RESULTS

The data are contained in Tables I and II, and Figures 1 through 4, and represent the three types of splicing, namely fusion, V-groove, and rotary. Table II contains splice loss for three rotary splices optimized and tested using a Laser Precision TD-9950 OTDR.

The average splice loss for fusion is 0.043 dB when a depressed cladding fiber is joined to a matched cladding fiber. The worst case is 0.14 dB. The V-groove yields an average of 0.046 dB. The performance of the rotary splice approaches that of fusion splices. A low value of 0.02 dB is obtained even when a fiber with a low MFD (9.04) is coupled with a fiber having a high MFD (10.27). These low values demonstrate the precision that can be achieved in installing a mechanical splice.

The results confirm that almost all of the factors contributing to excess splice loss can be eliminated. In the tests performed in a controlled environment, craft errors can be taken as negligible. Experimental inaccuracies are also quite small, especially in the transmission method. The high technology of alignment process eliminates misalignments. Data published in the industry indicate that even a 2-micron lateral offset contributes only approximately 0.01 dB to the splice loss[1].

The effect of mode field diameter mismatch on splice losses has been discussed by a number of authors[7,8,9]. If $2w_1$ and $2w_2$ represent the mode diameters of the two fibers, the resulting mismatch loss can be calculated based on R. R is defined as the ratio of the mode diameter difference divided by the mode diameter average.

$$R = 2\,(w_1 - w_2)/(w_1 + w_2)$$

$$\text{Loss} = dB(R) = 20 \log_{10} \left(0.5 \left[(w_1/w_2) + (w_2/w_1)\right]\right)$$

$$\simeq 4.343\, R^2 \text{ for } |R| < 0.8$$

If we consider the worst case condition of two fibers having MFDs 10.27 μm and 9.04 μm, the loss contribution is 0.02 dB. In several instances losses equal to or less than this value are observed. Therefore, the mode field diameter mismatch has only a marginal significance.

In the OTDR test (Table II) the difference between the transmission loss and the OTDR loss average ranges from 0.06 dB (Samples 5 and 6) to 0.21 dB (Samples 1, 2, 3, and 7). One way loss is still higher, thus accounting for the effect of loss or gain in the backscattered power. The measured backscattered power shown in Table II is the difference between a one-way OTDR value and the average of the bidirectional values. It can also be calculated theoretically as follows:[7,8]

$$\text{Backscattered Power (Both Directions)} = -10 \log \left[\frac{1/2\ MFD_1}{1/2\ MFD_2}\right]^2$$

MFD_1 and MFD_2 are respective mode field diameters of the two fibers.

The calculated and measured values agree except in the case of Sample 8. Samples were prepared by optimizing in one direction. Because backscattering loss is almost equal to the average loss (Table II), it is hard to compute the actual loss. It is interesting to note that preparation using an OTDR tends to yield higher values.

All three modes of splicing yield identical results. Even a simple V-groove can provide extremely low losses. Therefore, the acceptable maximum can be set as low as 0.15 dB. However, when an OTDR is employed, it is difficult to specify a low value.

CONCLUSIONS

All three types of splicing, namely fusion, V-groove, and rotary, provide extremely low losses. This implies that mechanical misalignments as well as fiber intrinsic factors are eliminated. Comparison of the experimental and theoretical loss values for various combinations of matched cladding and depressed cladding fibers shows that mode field diameter mismatch has only marginal significance.

The results demonstrate that it is possible to set an acceptable maximum loss as low as 0.15 dB. A loss in excess of this value must be attributed to manufacturing deficiencies of the mechanical splices.

Large measurement deviations are possible when an OTDR is used. This is because other factors such as group velocity and variations of back-scattering must be taken into account. Therefore, when specifying loss values, allowances must be made to account for the inherent measurement inaccuracies.

TABLE I.
ROTARY SPLICE LOSS - TRANSMISSION METHOD

SAMPLE	FIBER MFD, μm	LOSS, dB		
		A	B	AVG.
1	10.27/9.78	0.06	0.01	0.04
2	10.27/9.78	0.01	0.02	0.02
3	10.27/9.78	0.02	0.04	0.03
4	10.27/9.04	0.01	0.02	0.02
5	9.00/9.45	0.05	0.06	0.06

TABLE II.
ROTARY SPLICE LOSS - OTDR METHOD

SAMPLE	FIBER MFD, μm	LOSS, dB			BACK SCATTERING LOSS, dB	
		A	B	AVG.	MEAS.	THEOR.
6	9.04/9.45	-0.03	0.26	0.12	0.14	0.18
7	10.27/9.78	0.26	0.01	0.14	0.21	0.10
8	9.00/9.04	0.19	0.02	0.11	0.08	0.01

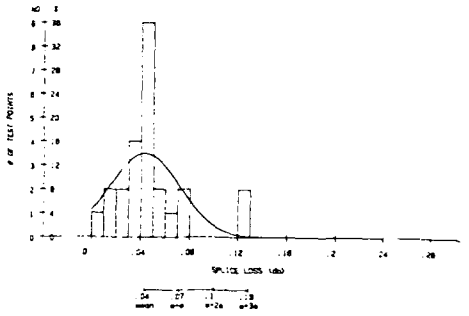

FIGURE 1. HISTOGRAM OF SPLICE LOSS
FIBER B (9.04 micron) TO FIBER D (10.27 micron)
FUSION

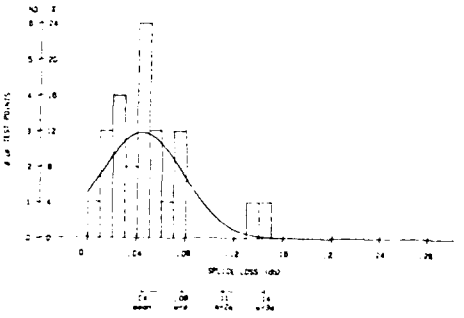

FIGURE 2. HISTOGRAM OF SPLICE LOSS
FIBER D (10.27 micron) TO FIBER B (9.04 micron)
FUSION

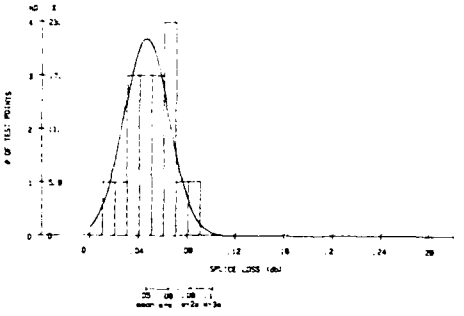

FIGURE 3. HISTOGRAM OF SPLICE LOSS
FIBER B (9.04 micron) TO FIBER D (10.27 micron)
V-GROOVE

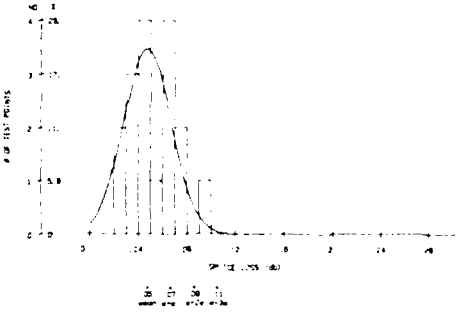

FIGURE 4. HISTOGRAM OF SPLICE LOSS
FIBER D (10.27 micron) TO FIBER B (9.04 micron)
V-GROOVE

ACKNOWLEDGMENTS

The author wishes to thank Dr. R. Gerdes for helpful suggestions and J. Boyles for performing numerous measurements.

REFERENCES

1. E. M. Hopiavuori, J. Matthews, and A. DeVito, "Study on Arc-Fusion Splicing Ge-Doped Silica Single-Mode Fibers Manufactured by Outside and Inside Vapor Deposition Processes", Proceedings of the 36th IWCS, (1987), pp. 392-398.

2. Based on information from several cable vendors.

3. T. C. Cannon and T. L. Williford, "High Technology at the Submicron Level", Telephony, (November 18, 1985), pp. 72-79.

4. C. M. Miller, G. F. DeVeau, and M. Y. Smith, "Single-Mode Fiber Splicing", Telephony, (March 4, 1985), pp. 61-62.

5. R. Raman, "Continuous Monitoring of the Loss of Large Numbers of Fiber Optic Splices", Proceedings of the 36th IWCS, (1987), pp. 63-70.

6. J. Lidh, "Splice Losses: How Measurements Can Mislead", Lightwave, (June 1986), pp. 43-47.

7. W. L. Smith, "Factors Affecting Splice Loss Measurements Using the OTDR", National Fiber Optic Engineering Conference, (May 5-7, 1987).

8. F. Kapron, et al, "Mode Field Diameter Effects on OTDR Splice Measurements", Symposium on Optical Fiber Measurements, NBS Special Publication 720, (1986), pp. 81-84.

9. W. T. Anderson, et al, "Fusion Splicing of Dissimilar Fibers - A Comparison of Mode Field Diameter and Cross-Correlation Loss Predictions with Experimental Results", Symposium on Optical Fiber Measurements, NBS Special Publication 720, (1986), pp. 65-68.

R. Raman
Contel Laboratories
270 Scientific Drive, Suite 10
Technology Park/Atlanta
Norcross, GA 30092

R. Raman joined Contel Laboratories in 1978. He is currently Senior Materials Evaluation Engineer.

He holds two Ph.D. degrees, one from the Indian Institute of Science, Bangalore, India, and the second from the University of Nottingham, England, specializing in dielectric materials, photoconductivity, and polymer applications. He is engaged in the evaluation of cables and cable components, lightguide splices and connectors, fiber optic closures, organizers, and terminals.

EVALUATION OF FIBER END FACE TILTS DURING AUTOMATIC FUSION SPLICING OF SINGLE-MODE FIBERS

T. Eder, W. Lieber

Siemens AG,
Munich, West Germany

M. Heier

RXS GmbH,
Hagen, West Germany

Abstract

Local injection and detection (LID) systems allow the loss measurement of single-mode fiber splices using the "air gap method" by monitoring the transmitted power while aligning and fusing the fiber ends. However insufficiently prepared end faces, particularly tilted end faces increase both measurement error and loss of the fusion splice. This paper reports a new technique for measuring the mutual end angle in a single-mode fiber air splice and investigates its influence on local splice loss measurement error. The analysis is based on the physics of the Fabry-Perot resonator formed by the fiber end faces and the air gap. A theoretical model for interference effects in a single-mode fiber air splice is developed and experimentally verified. This concept has been implemented in a microprocessor controlled fusion splicer and allows the automatic rejection of unsatisfactorily prepared fiber ends. In this way a maximum error of +/- 0.05 dB in determining the splice loss can be guaranteed and an increase in splice loss due to end face defects is avoided.

Introduction

Field experience has proven that accurate local splice loss estimation is an important feature involved in optical fiber splicing. Two different methods for local loss estimation in fusion splicers are commonly used. The accuracy of both methods is restricted due to various deficiencies. The "core monitoring" method uses the digitized video signal of the splice point to calculate the splice loss from the detected lateral core offset and the tilt of the core axes /1/. For this the wavelength dependent spotsize of the fibers to be spliced has to be known. A deviation from the assumed spotsize can lead to a significant measurement error. Moreover, core bending or other splice defects like dirt, bubbles etc. are not taken into account.

A more reliable method is to determine the splice loss from the transmitted power levels P_b and P_a which are measured e.g. by means of a LID system after optimal alignment of the fiber cores before fusing and after the fusion process, respectively /2,3,4/. It is shown in /2/ that using the measured power levels P_b and P_a the splice loss a_s can be determined from

$$a_s = 10 \log \frac{P_b}{P_a} + a_b \qquad (1)$$

where a_b is the loss of the optimally aligned splice before fusing. If an index matching liquid is used between the fiber ends during the alignment the attenuation component a_b disappears almost completely. With this socalled "wet method" the error in estimating the loss is as low as +/- 0.01 dB /4/. A disadvantage of this method is that additional hardware is required for applying the immersion drop to the fiber ends. The "dry method" or "air gap method" can be implemented without additional hardware. However, data aquisition is more complex due to interference effects in the air gap /5/. The accuracy of this method depends on the quality of the fiber end faces, i.e. on the air splice loss a_b. Particularly tilted end faces cause a significant error in splice loss estimation.

Therefore this paper investigates the transmission properties of a single-mode fiber air splice. Especially the influence of end face tilts on splice loss and measurement error of the "air gap method" is discussed. It is shown that the oscillation amplitude of the loss of a single-mode fiber air splice, which is observed while moving the fiber ends in axial direction, is directly related to an effective tilt angle of the fiber end faces. A new method is described for automatically evaluating the end face quality of the fibers to be spliced which guarantees a maximum error of +/- 0.05 dB by rejecting unsatisfactorily prepared fiber ends.

Theory

The loss of a single-mode fiber air splice is caused by Fresnel reflection, lateral offset, axial offset, tilt of fiber axes, tilted fiber end faces versus the fiber axes, curved fiber end faces, surface roughness, dirt and mode mismatch. After optimal fiber alignment the loss of an air splice is essentially influenced by the surface

quality of the end faces. The most important loss factor involved in fiber cleaving and fusion splicing is the end face tilt particularly in the light guiding core region.

In the worst case the total tilt angle Ψ is given by the sum of the angles of cleave Ψ_1 and Ψ_2 of the transmitting fiber 1 and the receiving fiber 2, respectively (Fig. 1). The electromagnetic

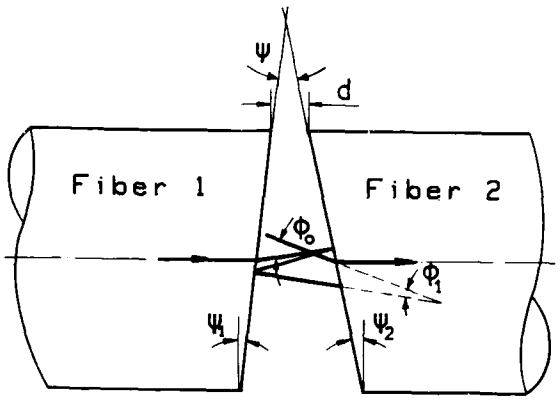

Fig. 1 Multiple beam interference in a single-mode fiber air splice

field radiated from fiber 1 is multiply reflected in the air gap at the glass/air interfaces /5/. From theory the coupling efficiency or loss of the air splice is calculated by superimposing the phase shifted fundamental modes which are excited in the receiving fiber 2 by the 2n-fold reflected fields. Due to the small reflectivity R=0.034 at a wavelength of 1.3 μm, a good approximation of the coupling efficiency is obtained by superimposing only the first two fundamental modes. This step is equivalent to approximating the multiple-beam interference by a two-beam interference. Thus, assuming a strictly monochromatic light source the coupling efficiency η of an air splice can be expressed in terms of the complex coupling coefficients C_0 and C_1

$$\eta = (1-R)^2[|C_0|^2+R^2|C_1|^2+2R|C_0||C_1|\cos\delta] \quad (2)$$

$$\delta = \arg\{C_0\} - \arg\{C_1\} .$$

where the coupling efficiency η is related to the splice loss a_b by

$$a_b = -10 \log \eta \quad (3)$$

In equation (2) the reflectivity for oblique incidence is well approximated by the reflectivity for normal incidence which causes a negligible error for angles less than 10°. For this a distinction between parallel and orthogonal polarisation of the incident wave is not necessary. C_0 and C_1 are determined by solving the overlap integral /6,7/ for the directly transmitted and twice reflected field, respectively.

We assumed gaussian shaped fundamental modes and therefore the radiated fields in the gap are gaussian beams. Applying the method described in /8/ the solution of the overlap integral for mismatched and misaligned gaussian beams can be written as

$$C = \frac{2\, w_1\, w_2}{\sqrt{(w_1^2+w_2^2)^2 + (z_0\lambda/\pi)^2}}\; e^{-(X + jY)} \quad (4)$$

$$X = \{(w_1^2+w_2^2)[x_0^2+y_0^2+(\pi/\lambda w_1 w_2 \sin\Phi)^2]+z_0 w_2^2$$
$$(z_0 \sin^2\Phi+2x_0\sin\Phi)\}/[(w_1^2+w_2^2)^2+(z_0\lambda/\pi)^2]$$

$$Y = \{z_0\lambda/\pi[x_0^2+y_0^2+(\pi/\lambda w_1 w_2 \sin\Phi)^2]-\pi/\lambda w_2^2$$
$$(w_1^2+w_2^2)(z_0\sin^2\Phi+2x_0\sin\Phi)\}/[(w_1^2+w_2^2)^2+$$
$$+(z_0\lambda/\pi)^2]+2\pi/\lambda z_0 - \arctan[\lambda z_0/\pi/(w_1^2+w_2^2)]$$

where the optical mismatch is characterized by the mode field radii w_1 and w_2 of fiber 1 and fiber 2, respectively. λ is the wavelength and the parameters Φ, x_0, y_0, z_0 define the geometrical misalignment (Fig. 2) of the beams. Taking into

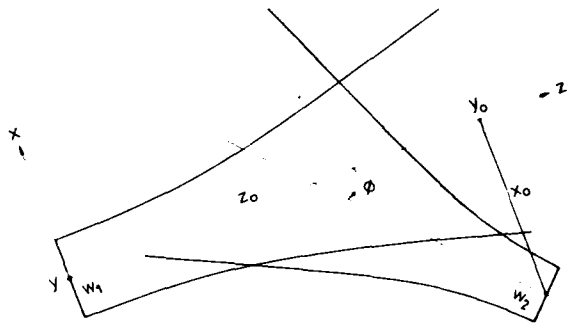

Fig. 2 Coupling of mismatched and misaligned gaussian beams

account the refraction and the 2n-fold reflection of the radiated fields at the glass/air interfaces the angular misalignments Φ_0 and Φ_1 for the coupling of the corresponding gaussian beams according to Fig. 1 are given by

$$\Phi_i = |(2i+1)\Psi - \sin^{-1}(n\sin\Psi_1) - \sin^{-1}(n\sin\Psi_2)|$$
$$\approx |[(2i+1)-n]\Psi| , \qquad i = 0,1 \quad (5)$$

where the refractive index of air has been set to

l and n is the refractive index of the fiber core. The transverse offset x_0, y_0 and the axial offset z_0 is determined by solving the simple geometrical problem for the coupling of the directly transmitted and 2-fold reflected beam of fiber 1 with the exited beam of fiber 2 (Fig. 1, 2).

Experimental Verification

High resolution measurements of the coupling efficiency were made as a function of the gap width for varying end angles Ψ. To eliminate the influence of the azimuthal orientation of the fiber ends an end face perpendicular to the fiber axis was used for the transmitting fiber 1 ($\Psi_1 < 0.1°$). The end angles were measured with an error of less than 0.1° using a Mireau-Interferometer.

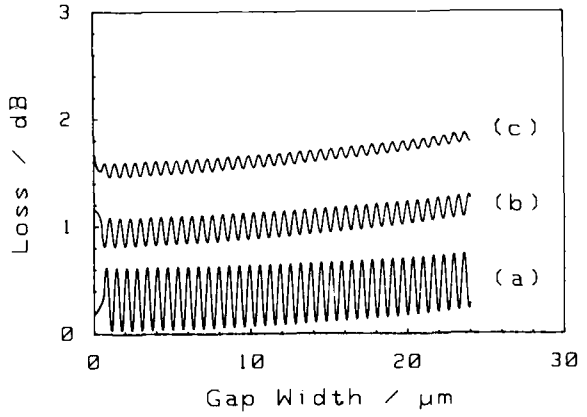

Fig. 3 Measured loss of a single-mode fiber air splice vs. the gap width d for total tilt angles Ψ=0.1° (a), Ψ=3.9° and Ψ=5.5° using a quasi-monochromatic light source (λ=1.3 µm, $\Delta\lambda$=4 nm)

Fig. 3 reveals the measured loss of a single-mode fiber air splice for two identical fibers ($w_1 = w_2 = 4.98$ µm) vs. the end face separation d (Fig. 1) for different total tilt angles. White light and a monochromator was used as a narrow bandwidth light source (λ=1.3 µm, $\Delta\lambda$=4 nm). The observed period length is half the operating wavelength. Fig. 4 shows the results for a broadband light source. For this an edge-emitting LED with a center wavelength of 1.293 µm and a spectral half width of 71 nm was used. It should be noted that the slight decrease in the oscillation amplitude with increasing gap width in Fig. 3 is due to diffraction of the radiated fundamental mode. In contrast the decrease in oscillation in Fig. 4 is mainly caused by the small coherence length of the LED (l_c=24 µm). A large number of experiments was carried out for end angles covering the range from 0° to 10°. The peak-to-peak (p-p) amplitude was determined using the 3rd and 4th extremum of the coupling

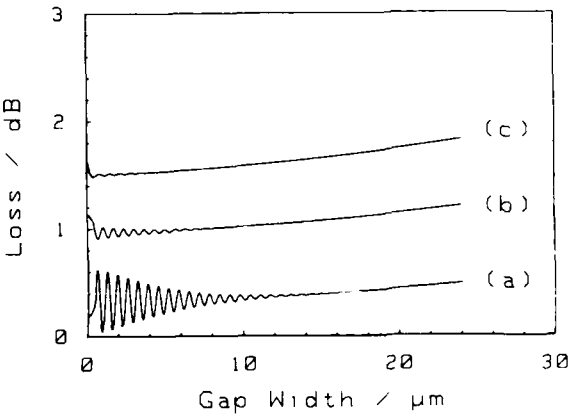

Fig. 4 Measured loss of a single-mode fiber air splice vs. the gap width d for total tilt angles Ψ=0.1° (a), Ψ=3.9° and Ψ=5.5° using an edge-emitting LED (λ=1.293 µm, $\Delta\lambda$=71 nm)

efficiency or the loss of the air splice before the point of contact. As can be seen from Fig. 5 the short coherence length of the LED results in a stronger decrease of the p-p oscillation amplitude as compared to the narrow bandwidth source. The solid curve represents the calculated p-p amplitude for monochromatic light and shows good agreement with the measured results for the narrow bandwidth light source.

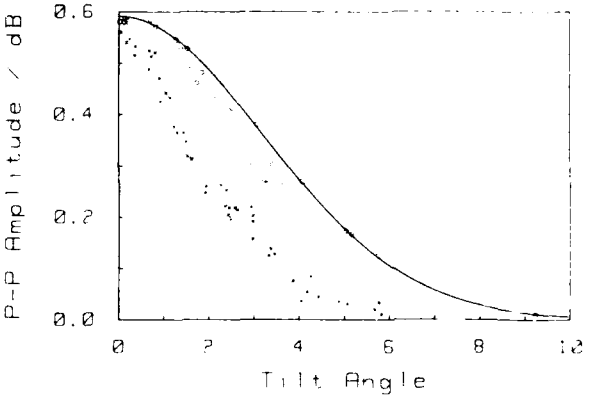

Fig. 5 Peak-to-peak (p-p) oscillation amplitude of the air gap loss vs. the total tilt angle Ψ.

— theoretically calculated for monochromatic light (λ=1.3 µm)
o measured using a quasi-monochromatic light source (λ=1.3 µm, $\Delta\lambda$=4 nm)
x measured using an edge-emitting LED (λ=1.293 µm, $\Delta\lambda$=71 nm)

Application

As mentionend above the loss of an arc-fusion splice can be estimated using the "air gap method" by measuring the transmitted power levels P_b and P_a before and after the fusion process e.g by means of a LID system. It is a prerequisite for high precision loss estimation to measure the power levels at the operating wavelength of the fiber link since there is no strict relation-ship between the losses at different wavelengths. Particularly LID systems operating at 850 nm are not appropriate for precision loss estimation. Therefore a LID system at 1.3 μm has been built into a microprocessor controlled fusion splicer which is the basis for the successful implementation of the "air gap method".

Since the relative power level P_b begins to oscillate for gap widths below half the coherence length of the LED the best way to measure P_b is to average the data over a certain number of periods at a gap width of some microns. As can be seen from eq. (2) this is equivalent to neglecting the interference term, i.e P_b measured in this way is equal to the power level that would be measured in case of completely incoherent light. For this case Fig. 6 shows the loss of a single-mode fiber air

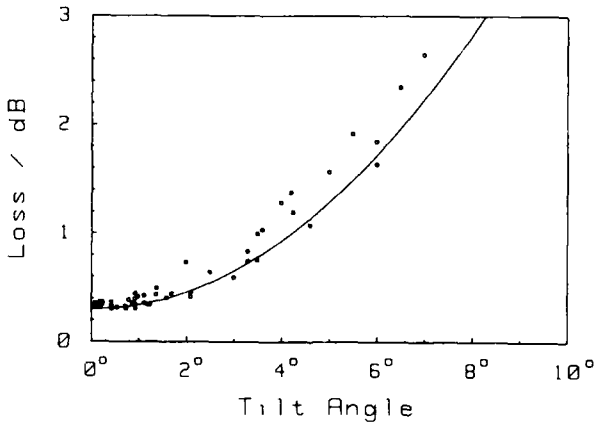

Fig.6 Measured (o) and theoretical (—) loss of a single-mode fiber air splice vs. the total tilt angle Ψ for a gap width d=0 neglecting the interference effect

splice vs. the total tilt angle Ψ, where P_0 is the relative power just before the splice /2/. For ideal end faces (Ψ=0) the loss of an air splice is 0.30 dB. It is evident from Fig. 6 and eq. (1) that the loss of a fusion splice can be estimated with an error of +/- 0.05 dB if a_b is set to 0.35 dB and P_b is measured in the way explained above where only total tilt angles less than 1.6° are permitted. Therefore the operator has to decide whether the end faces meet this requirement.

Our solution to this problem is to measure the p-p oscillation amplitude while aligning the fibers in axial direction. For this a high resolution axial movement of the fiber ends has to be performed. To measure the oscillation amplitude with an error of less than 0.02 dB a resolution better than 50 nm is required which is achieved by using a piezo driven z axis. Fig. 5 shows that the oscillation amplitude for total tilt angles Ψ<1.6° is greater than 0.30 dB. In this way the fusion splicer is able to perform an automatic check of the end face quality of the fibers to be spliced. This guarantees a maximum splice loss estimation error of +/- 0.05 dB and an increase in splice loss caused by unsatisfactorily prepared fiber ends is avoided.

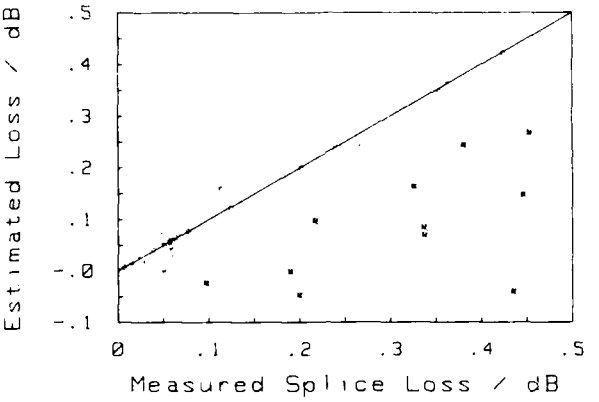

Fig. 7 Correlation between estimated and measured splice loss using the "air gap method"

Fig. 7 shows the correlation between the estimated and measured splice loss using the "air gap method". The data points which are out of the +/- 0.05 dB tolerance (■) were achieved by splicing fiber ends with total tilt angles Ψ>1.6°. Almost all these data points were detected using the proposed oscillation amplitude criterion. It must be mentioned that the data points which show good correlation and high splice loss were intentionally produced by using inadequate fusing parameters to show the good correlation over the whole loss range.

Conclusion

A new method for measuring the mutual end face tilt in a single-mode fiber air splice is theoretically derived and experimentally verified. A practical criterion is proposed in order to provide accurate splice loss estimation using the "air gap method". This concept has been successfully implemented in a microprocessor controlled fusion splicer and guarantees a maximum splice loss estimation error of +/- 0.05 dB. Furthermore an increase in splice loss caused by end face tilts is avoided and the automatically performed end face check makes the splice results even more independent of the operator's carefulness.

References

/1/ T. Haibara, M. Matsumoto, T. Tanifuji, M. Tokuda, "Monitoring method for axis alignment of single-mode optical fiber and splice-loss estimation", Optics Letters, Vol 8, No. 4, April 1983, pp. 235-237

/2/ T. Eder, R. Engel, "Einmodenspleiße automatisch messen und herstellen", Nachrichtentechnische Zeitschrift, Vol. 41, No. 4, April 1988, pp. 230-233

/3/ Y. Kato, S. Seikai, T. Tanifuji, "Arc-fusion splicing of single-mode fibers: an apparatus with an automatic core-axis alignment mechanism and its field trial results", Journal of Lightwave Technology, Vol. LT-2, No. 4, Aug. 1984, pp. 442-447

/4/ Y. Kato, T. Tanifuji, M. Tokuda, N. Uchida, "New optical monitoring method for arc-fusion splice of single-mode fibers and high precision estimation of splice loss", Electronics Letters, Vol. 18, No. 22, Oct. 1982, pp. 972-973

/5/ R. Wagner, C. Sandahl, "Interference Effects in Optical Fiber Connections", Applied Optics, Vol. 21, No. 8, April 1982, pp. 1381-1385

/6/ D. Marcuse, "Loss Analysis of Single-Mode Fiber Splices", Bell System Technical Journal, Vol. 56, No. 5, June 1977

/7/ H. Kogelnik, "Coupling and Conversion Coefficients for Optical Modes",Microw. Res. Inst. Symp. Series,Vol.14,1964

/8/ F. Bayer-Helms, "Ableitung der Kopplungskoeffizienten für die Eigenfunktionen eines sphärischen optischen Resonators bei Fehlanpassung und Fehljustierung der einfallenden Welle", Physikalisch-Technische Bundesanstalt, Me-43, Braunschweig, Feb. 1983

Thomas Eder received his diploma degree in electrical engineering from the Technical University of Munich, West Germany, in 1984. Since then he has been employed at Siemens AG, Munich, where he at first worked on optical measurement techniques. Since 1986 he has been working on the development of fusion splicing equipment and on the process for localized attenuation measurements.

Winfried Lieber received his diploma degree and Ph. D degree in electrical engineering from the University of Kaiserslautern, West Germany, in 1983 and 1987, respectively. His work was concerned with group delay time measurements, cutoff phenomena and optical time domain reflectometry. Since 1987 he has been emloyed at Siemens AG, Munich, West Germany. He is responsible for the development of fusion splicing equipment.

After studying electrical engineering and business administration, Manfred Heier joined Siemens AG, Munich, West Germany, in 1968. Since then he has been active in the field of telecommunication cables. From 1974 to 1976 Manfred Heier worked as a sales manager for Siemens in the Republic of South Africa. He then resumed his work for Siemens in Munich until 1985 he joined RXS Schrumpftechnik-Garnituren GmbH, Hagen, West Germany as Joint Managing Director.

Automated Field Spectral Attenuation Measurement Unit for Single Mode and Multimode Optical Fibers

Avinash Garg

Siecor Corporation
489 Siecor Park (RD)
Hickory, NC 28603-0489

ABSTRACT

Fiber optic cables are measured for attenuation at various wavelengths using spectral attenuation measurement equipment designed for laboratory use. These systems can be quite large, highly sophisticated, and require critical alignment procedures making them essentially non-transportable. If relocated, then extreme care must be taken with respect to alignment of optics, temperature conditions and other environmental and mechanical factors which could influence the accuracy of subsequent measurements. However, there is often a need to make attenuation measurements in the field on fiber optic cable which is about to be installed or which has already been placed. An Automated Field Spectral Attenuation Measurement System has been developed which is capable of measuring spectral attenuation of installed or on-reel fiber optic cable for wavelengths from 850 nm to 1700 nm with equal accuracy. In addition, the unit can measure pre-connectorized or bare fiber. The system is small, quite portable and can be easily carried and operated by a single person. It utilizes a tungsten halogen bulb as a light source instead of lasers, thereby significantly reducing its cost. At the same time, it maintains a high measurement accuracy without laborious calibrations or optical alignments after relocation, and does not require expensive environmental conditioning units for reliable operation.

INTRODUCTION

The measurement parameters of an installed fiber optic cable/link are dictated by the need for the measurements and include post-installation checks, routine system maintenance and troubleshooting transmission problems due to attenuation increases. Attenuation increases may be caused by hydrogen absorption, microbending or macrobending effects, and point defects or damage to the cables incurred during installation, to name a few. In solving transmission problems, spectral attenuation studies are preferred, as it is difficult to differentiate among potential problems when the measurements are made at a limited set of discrete wavelengths. Field spectral attenuation studies require measurement equipment capable of generating and measuring a broad range of wavelengths.

Multiple wavelength attenuation measurement devices have traditionally been complicated, cumbersome and costly units. Most commercially available units contain multiple lasers (which multiplies the cost by the number of wavelengths being measured) or else contain optical components requiring critical alignment and tightly controlled environmental conditions with respect to temperature and humidity fluctuations. Most of these units, by virtue of their complexity, are essentially non-transportable.

This paper describes a field spectral attenuation measurement device developed at Siecor R,D&E. It is capable of making spectral attenuation measurements on installed optical fiber cables. The unit is small and portable, completely automated by virtue of a hand-held computer, and needs no special handling, even after transporting to the field site. The system is capable of accurate and repeatable measurements comparable to those recorded under laboratory conditions or by the much larger attenuation measurement units discussed previously. There are no requirements for specific controlled environments, eliminating the need for air-conditioned vans at the test site.

SYSTEM

The system is designed primarily for evaluation of relative rather than absolute spectral attenuation. Absolute attenuation at any wavelength may be calculated using one OTDR measurement at 1300 nm. The system measures by insertion loss technique; however, if bare fibers are being measured, cutback technique is easily possible with this unit.

The system consists of two separable sections: a source unit and a receive unit. The spectral attenuation of an installed cable or fiber section between two separate locations is measured without needing a fiber loop-back at the remote end. The units are capable of coupling and/or receiving light from either a bare fiber or a connectorized fiber (as in installed systems).

The schematic of the complete system (source and receive units) is depicted in Figure 1. The source unit consists of a 10 watt tungsten-halogen lamp (white light) mounted in a Kohler optic configuration along with a long-pass filter and lenses for focusing the light onto the launch-end pigtail or fiber. The receive-end is completely automated. The receive pigtail or fiber enters a Spex monochromator which not only splits the incoming signal into various wavelengths, but also converts the incoming DC light into an AC signal. The AC light is then fed into an InGaAsP photodiode and further amplified using a synchronous detection amplifier. The monochromator, the

synchronous detection amplifier and a 3.25 inch Disc Drive are all hooked to a computer via an HPIL loop.

Automation of the field unit is made possible by a hand held Hewlett Packard 71B computer. The data is stored in an ASCII format on a diskette and can be retrieved later and analyzed by any computer having an IEEE 488 or RS 232 interface.

The field unit itself has limited computing capability and writes all the data to a floppy disk. Field computations are limited to attenuation at specified wavelengths; however, a bigger computer (i.e., HP 9816 or IBM PC) can easily retrieve and analyze the data and graph the spectral curves.

MEASUREMENT TECHNIQUE

Although the unit is capable of operating over a broad range of wavelengths from 850 nm to 1700 nm in steps as small as 2 nm, it is normally programmed for 1000 nm to 1700 nm in increments of 10 nm.

Before starting measurements each day, the source pigtail is connected to the receive pigtail using a short jumper pigtail of a similar fiber type. This forms the reference system. The reference system has the same number of mechanical connectors in the loop as the final installed system (not including the splices/connectors used to make up the installed system). A spectral scan of the reference pigtail/fiber is made and stored on the diskette for later analysis. The source unit is then moved to the remote location housing the launch end of the cable system under evaluation. Once the transmitting and receiving electronics are hooked onto the transmit and receive ends of the cable, the computer performs another spectral scan of the system and stores the scan on the computer diskette. The transmitter can then be moved to the second system and so on.

After the final measurements or at end of the day, the transmitter is moved back to the receive end where a second reference scan is made. The two reference scans are then compared to evaluate any drifts in the launch optics for which the analysis of the measurements can later compensate. Spectral attenuation values at 1300, 1550 and 1650 nm can be calculated and displayed on the spot using the HP 71B.

Since the data is on the diskette and is in a format that is easily accessible; data analysis, graphing, etc. may be performed later with any microcomputer or PC (e.g. HP 9816 or IBM PS/2).

SYSTEM EVALUATION

The system has been successfully used at various field locations. A sample measurement is presented in Figure 2. It has been noted that variability over a four-hour period is well below 0.04 dB, which translates to less than 0.004 dB/Km for a 10 Km span. This variability is highly dependent on the types of connectors used in the system.

A curve depicting the drift in the reference scans obtained by the field unit from morning to evening is shown in Figure 3.

The measurement system offers a high dynamic range of 35 dB for multimode optical fibers and 32 dB for single-mode fibers. The accuracy of the relative attenuation values is better than 0.02 dB/Km. If a cutback technique is used for bare fibers, the absolute accuracy of the system is better than +/- 0.02 dB/Km. The automation of the spectral system makes it relatively operator-independent and greatly reduces measurement time. A typical spectral scan from 1000 nm to 1700 nm in steps of 10 nm requires less than 10 minutes.

SUMMARY

A field spectral attenuation measurement system has been developed at Siecor R,D&E which is capable of accurately measuring spectral attenuation of installed optical fiber cables with connectorized or bare fiber ends. The system is portable and does not require special environmental conditions or on-site alignment of optics. The unit does not require a skilled operator or any special precautions during its operation.

ACKNOWLEDGMENTS

The author would like to thank J. E. Matthews III, S. L. Saikkonen and M. Robinson of Corning for their help in collecting the data.

REFERENCES

1) A. O. Garg, "Field Spectral Attenuation Measurement Unit", FOCLAN '85, Sept. 19 '85, San Francisco, California.

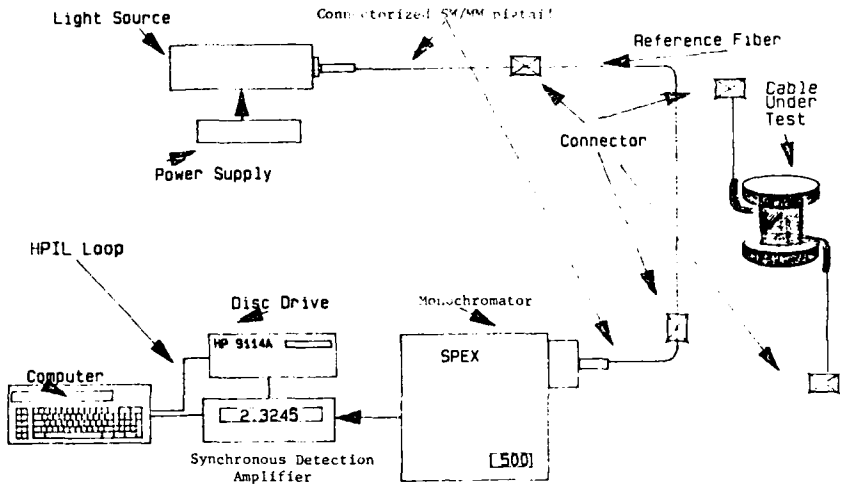

Fig. 1. Schematic of Automated Field Spectral Unit

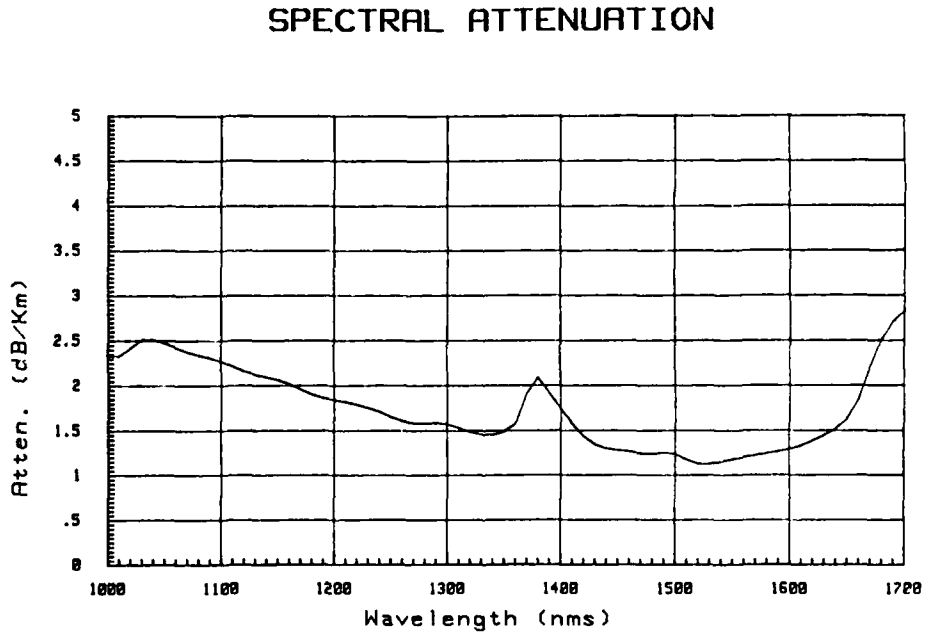

Figure 2: Spectral Scan of an Installed System

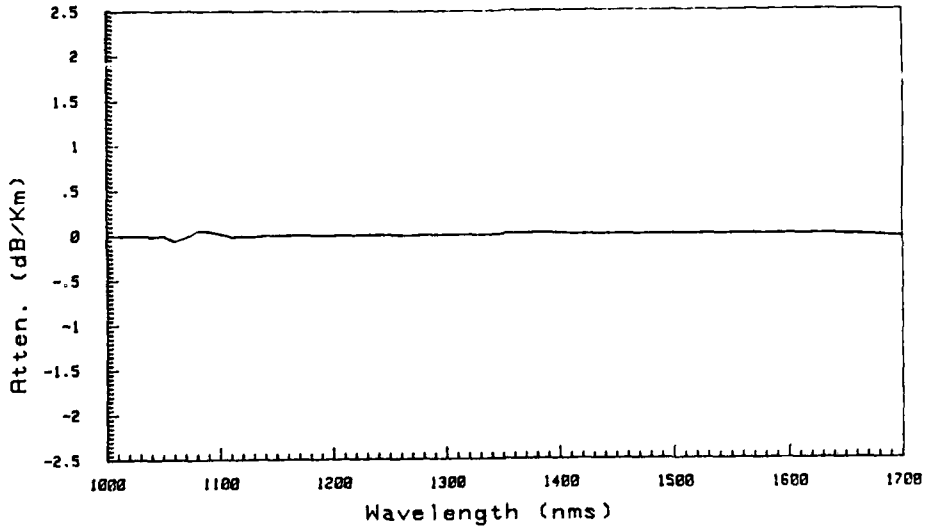

Figure 3: Comparison of Morning and Evening Reference Scans

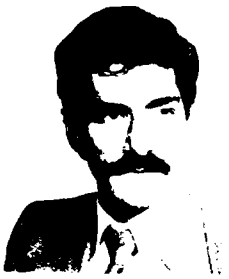

Avinash O. Garg

Siecor Corporation
489 Siecor Park
Hickory, NC 28603-0489

Avinash Garg received his B.S. degree in Physics from University of Bombay, Bombay, India. From 1981 to 1982 he worked as a graduate research assistant with Dr. R. O. Claus at Virginia Tech, Blacksburg, VA. He was granted a M.S degree in Electrical Engineering from that University for his work on systems for nondestructive testing and evaluation using acousto-optic, interferometry and fiber optics.

Since 1982, he has been employed by Siecor Corporation where he is now Supervisor of the Product Evaluation Lab at Research, Development & Engineering. He is responsible for designing and building optical and electro-optical measurement systems and maintaining the lab with its state of the art measurement capability.

METAL-FREE SINGLE-MODE OPTICAL FIBER CABLE WITH HIGH MECHANICAL PROPERTIES

Carlos G. CORTINES Carlos BLANCO Susana CAMARA

ALCATEL STANDARD ELECTRICA, S.A.
Maliano, Cantabria, Spain

ABSTRACT

The cable described is made up of 8 S.M. optical fibers 10/125 with attenuation $\leq$ 0.37 dB/km and Modal Dispersion $\leq$ 3.5 ps/km.nm, both parameters in 1330 nm window. The remaining characteristics in the fiber are in accordance with the limits established by the CCITT G.652 Recommendation.

The cable consists of a central strength member suitably treated so as to prevent kinking.

The optical fibers are loose in tubes (1 fiber per tube). These tubes, or fiber buffer, are filled with a thysotropic compound.

A detailed description is given regarding cable design, characteristics of the materials used, as well as all the tests made in the cable plus the results.

1. INTRODUCTION

During the last ten years, the development and progress in Optical Communication Technology and the parallel evolution in microelectronics, have made it possible to have at our disposal communication systems of great capacity and reliability. Because of their enormous technical, economic and social repercussions, these systems constitute the great technological challenge of our times. An important factor in this technological panorama is the means of transmission, in other words the Optical Fiber Cable.

There are, at the moment, thousands of kilometres of optical fiber cables being used all over the world. All of them are functioning very well, all of them were designed to withstand any kind of installation and future maintenance.

After the problem of the increase in attenuation of aged fibers arose, due to the absorption of H_2, and the causes of the generation of H_2 verified, the fiber manufacturers as well as cable manufacturers very quicky eliminated the sources of generation of H_2 from their cables. In the subject which interests us, ie. cables, it has been demonstrated how metals, aluminium, steel and above all, a combination of them, is a high factor of risk. Traditionally however, the above mentioned metals have been the base for designing cable of high mechanical properties.

The aim of this paper is to prevent a wholly dielectric monomode optical fiber cable which possesses mechanical properties comparable to those of conventional cables with metallic protection. Among the different designs of present day optical fiber cables, such as the slotted cable, ribbon type cable or cables with a central strength member around which fibers are stranded -tight, loose or bundle coated- Spanish manufacturers opted for the latter design: ie. central strength member with fibers stranded around it. Obviously, if circumstances were to require it the possibility of manufacturing any other type of cable is always possible, since each design has its pros and cons, according to the conditions of installation and future service required.

2. CABLE DESIGN

In Figure 1 the transversal section of the cable is shown. As can be seen, the cable is made up of the following materials:

CENTRAL STRENGTH MEMBER

Rod of reinforcing fibers of strictly unidirectional orientation combined with thermosetting epoxy resin. Aprox. 83 % by wt. high modulus glass and 17 % by wt. epoxy resin.

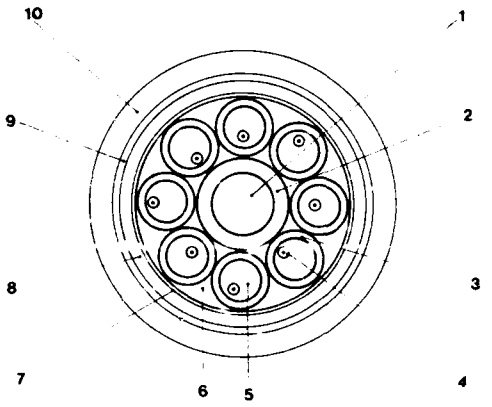

Fig. 1: TRANSVERSAL SECTION

1 Central strength member	**7 Wrapping tapes**
2 Coating of C.S.M.	**8 Low density PE**
3 Loose tubes	**9 Aramid fibers**
4 Optical fibers	**10 High density PE**
5,6 Filling compound	

CENTRAL MEMBER COATING

Low density polyethylene. This coating is applied so as to increase the diameter of the central strength member to the size necessary so that in the stranding operation, the loose tubes which contain the fibers will adapt to it. Owing to the high cost of the tensile strength members, the one which complies with the mechanical properties required is used and is coated with polyethylene until it possesses the diameter required by the loose tubes. Financially, the cost of coating a smaller diameter tensile strength member is lower than the cost of not having to coat a tensile strength member which has a diameter larger than necessary.

LOOSE TUBES

Eight polyester tubes are stranded around the central strength member. Inside each tube there is an optical fiber, with its corresponding overlength. Inside the tube there is a filling compound, which is put into it together with the fiber, during the loose tube extrusion process.

FILLING COMPOUND

During stranding, the empty spaces between tubes and also those between the tubes and the central strength member, are filled with a compound which prevents the penetration and/or circulation of water into the core if the coating suffered a breakage.

WRAPPING TAPES

At the same time as the stranding operation, two polyester-polyuretane-polyester tapes are wrapped around the core and are laid helicoidally and overlapped. These tapes, as well as acting as a thermal barrier, also absorb, and prevent the transmission of the kinking of the polyethylene of the coatings to the fiber core, which takes place both when the coatings are applied and later on, due to temperature changes.

These tapes, together with the central strength member, act as anti-kinkers for the fiber core.

PRIMARY COATING

Layer of low density extruded polyethylene.

MECHANICAL PROTECTION

Two layers of aramid fibers, laid helicoidally from right to left and from left to right, are applied over the primary polyethylene coating. Each one of the layers completely covers the surface being coated. These fibers, as well as withstanding tensile loads, are calculated to act as longitudinal mechanical protection, above all for aerial cables which require high shot gun resistance.

FINAL COATING

A layer of high density extruded polyethylene.

3. PROPERTIES OF THE OPTICAL FIBER MATERIALS

Up till now the optical fibers used for telecommunications have not been manufactured in Spain, therefore imported fibers are used for all cables.

The fibers used for the cable under discussion were manufactured following the VAD method.

The properties which this fiber possesses are as follows (Table 1).

As mentioned before each of these fibers was inserted into a loose tube together with the filling compound. The properties possessed by the loose tubes and filling compound are shown in Table 2.

The extrusion line used to manufacture the loose tube allows the fiber to be inserted with enough overlength to absorb the tensions caused during the unwinding

of the tube or those caused by changes of temperature. In this case the overlength given to the fiber was around 0.6 %.

The filling compound inside the tubes, the viscosity and platic properties of which are shown in Table 2, is a soft jelly, based on suitable formulas of SiO_2 and synthetic oils free from scattered hydrogens.

TABLA 1

OPTICAL FIBERS PROPERTIES

OPTICAL PROPERTIES	Attenuation at 1330 nm (dB/km)	≤ 0.37
	Attenuation over range 1285-1330 nm (dB/km)	≤ 0.40
	Attenuation at 1550 nm (dB/km)	≤ 0.25
	Attenuation over range 1475-1575 nm (dB/km)	≤ 0.30
	Mode-field diameter (μm)	9.75 ± 0.5
	Cut-off wavelength (nm)	1180 - 1280
	Dispersion (ps/nm.km)	
	1285 - 1330 nm	≤ 3.5
	1270 - 1350 nm	≤ 6.0
	1550 nm	≤ 19.0
GEOMETRICAL PROPERTIES	Reference surface diameter (μm)	125 ± 2
	Glass concentricity error (μm)	≤ 0.8
		Median ≤ 0.4
	Glass non-circularity (%)	
	Core	≤ 6
	Reference surface	2
	Coating diameter (μm)	
	Primary	205 ± 15
	Overall	250 ± 15
	Coating concentricity error (%)	≤ 10
	Coating non-circularity (%)	≤ 11
MECHANICAL PROPERTIES	Bend test (60 mm diameter mandrel, 100 turns, loss at 1550 nm in dB/m)	≤ 0.01
	Proof test (%)	0.75

TABLE 2

PROPERTIES OF THE LOOSE TUBES AND FILLING COMPOUND

LOOSE TUBES		
Material:	Polybuthylene-Terephtalate (PBTP)	
Inner diameter	mm	0.90 ± 0.02
Outer diameter	mm	1.80 ± 0.02
Tensile strength	kg/mm^2	≥ 4
Elasticity modulus	kg/mm^2	≥ 210
Thermal exp. coefficient	$°K^{-1}$	10^{-4}
Filling compound:		
- Haake viscosity	P	500 - 800 at -30°C
	P	15 - 75 at +70°C
- Plasticity	dmm	200 - 260 at -30°C
	dmm	300 - 360 at +70°C

STRANDING MATERIALS

The eight tubes containing the optical fibers are stranded around the central strength member with a 130 mm coil lay. The whole is filled with a filling compound similar to that used for the filling of the inside of the loose tubes. The stranding machine then wraps the core with two tapes, laid in tight coils or loops and overlapped.

The properties possessed by the central strength member and by the wrapping tapes are shown in Tables 3 and 4.

TABLE 3

PROPERTIES OF THE CENTRAL MEMBER

CENTRAL STRENGTH MEMBER		
Material:	Glass epoxy resin	
Diameter	mm	2.20 ± 0.07
Weigth per m	g	7.7
Strength at 0.5 % elongation	N	1.210
Breaking load	N	10,200
Minimum bending radius at 1 % edge strain	mm	110
Elasticity modulus	N/mm^2	60,000
Tensile strength	N/mm^2	2,300
Elongation at break	%	3.4
Thermal exp. coefficient	$°C^{-1}$	4.4×10^{-6}

TABLE 4

PROPERTIES OF WRAPPING TAPES

WRAPPING TAPES

Material:	Foam polyurethane coated with polyester in the two sides	
Thickness		
- Foam polyurethane	mm	0.4 - 0.6
- Polyester tapes	mm	12 ± 1 each
Weight	g/m^2	60 - 65
Breaking load	N	≥ 45
Elongation at break	%	≥ 40
Thermal conductivity	$W\ m^{-1}\ ºK^{-1}$	0.040

SHEATING MATERIALS

Our aim was to develop a totally dielectric optical fiber cable with mechanical properties comparable to conventional cables with metallic protection. The coating was, therefore, a decisive factor in the cable design.

Several prototypes were made and then underwent both shot gun and temperature tests. As will be seen later on the tests demonstrated that the cable which displayed the mechanical resistance required, has a double coating of polyethylene with a reinforcement of fibers between the two coats and is, therefore, the one being presented. The first layer of PE, laid over the cable core, was extruded black, low density PE, with 0.8 mm radial thickness. The outside layer of PE, also black plus extruded was of high density.

The reason for using high density PE for the outer coating is because when it is a question of installations in subducts, as these are of high density PE, the friction coefficient between duct and cable is better when both of them -duct and cable- possess high density, than when the duct has high density but the cable possesses low density.

Between the outer and inner PE coatings mechanical protection was applied. This protection consists of two layers of aramid fibers laid helicoidally, first around from right to left then around from left to right. In this way the surface of the cable is completely and totally covered.

The properties of these fibers are shown in Table 5.

TABLE 5

MECHANICAL PROTECTION OF THE COATING

PROPERTIES

Material:	Aromatic polyamide fibers	
No. of yarn		24 per layer, Total 48
Characteristics of each yarn		
- Weight of 10 km	(g) dtex	1580
- Yarn dia.	mm	0.45
- Fill factor	%	70
Breaking strength min.	N	280
ave.	N	330
Tensile strength	N/mm^2	2,650
Young modulus	N/mm^2	127,500
Elongation at break	%	2.4
Density	g/cm^3	1.45

4. LABORATORY TEST

PERFORMANCE OF SINGLE MODE FIBERS IN HYDROGEN.

According to the data and studies carried out by the fiber manufacturer-supplier, single mode fiber contains no phosphorous dopants. Results after an exposure of 16,775 hours (nearly 2 years) in 0.25 atmospheres of hydrogen are shown in Figure 2.

The total attenuation increase due to interstitial and permanent effects after 25 years at the above hydrogen partial pressure, and a temperature range of -10ºC to +30ºC is predicted to be less than 0.003 dB/km over the wavelength range 1275 nm - 1325 nm and 0.006 dB/km over the wavelength range 1525 nm-1575 nm. These very small attenuation effects are not expected to affect system performances over the fiber lifetime but can, if necessary, be included in system budget calculations.

In our laboratory a cable was put into a climatic device at 120ºC in the following way: so as to bring about the generation of H_2 a length of 30 m was put into an aluminium pipe. We kept a continuous control of the attenuation at 1300 nm. During the 30 days'test no variation in the initial values of fiber attenuation was observed.

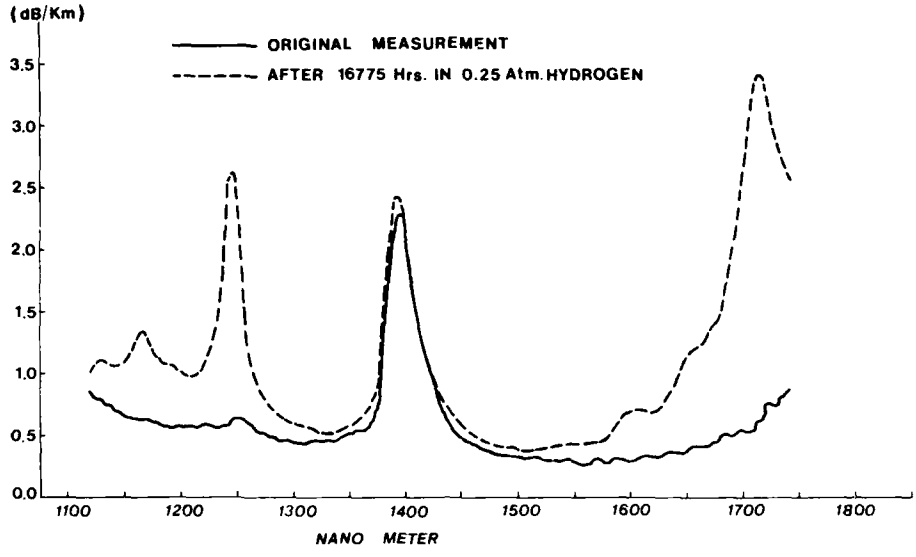

Fig. 2: PERFORMANCE OF SINGLE-MODE FIBERS IN HYDROGEN

SHOT GUN RESISTANCE TEST

Another issue dealt with in this study was shot gun resistance. We wanted to develop a design which could be used for aerial cables. The test was designed to evaluate the effects of shot gun blasts. The cables used as targets were approximately 50 cm long with a 13.3 mm outer diameter. A 12 gauge shot gun was used to fire at the cables as this appears to be the most powerful shot gun used by the majority of hunters. The shot gun loads fired in each test 1 1/4 oz No. 4 (1 1/4 oz weight of the pellets in a cartridge). Shots were fired from distances of 8, 15, 20, 25 and 30 m, and the 5 cables (one for each distance) were mounted on a wooden frame ie. the target. The results of the tests are shown in the Table 6.

TABLE 6

SHOT GUN RESISTANCE TESTS

Distance (m)	No. of pellets hitting target	Location of pellet in cable			
		In outer PE	In aramid fibers	In inner PE	In fiber core
8	17	4	10	3	-
15	12	1	9	2	-
20	10	-	10	-	-
25	7	2	5	-	-
30	5	1	4	-	-

Since it is highly improbable that aerial cable would be installed at less than 8 m from the ground, tests at distances of less than 8 m were not carried out. It is obvious, however, that the best way to protect aerial cables from shot gun blasts at distances of less than 8 m, would be by increasing the amount of aramid fibers, a very expensive solution which should only be applied when absolutely necessary.

THERMIC CYCLES

This test allowed us to study the behaviour of the cable in temperatures ranging from -20ºC to +60ºC. The cable was put into a climatic device and tested using the following thermic cycle (Figure 3).

The attenuation at 1300 nm of each one of the fibers was tested at 20ºC. Then the temperature was raised to 60ºC, reached in 40 minutes. The climatic device was kept at 60ºC for 12 hours, enough time for the whole cable to reach this temperature. At the end of the 12 hours the fibers were measured again. After measuring the fibers the temperature was lowered to -20ºC, reached in 90 minutes. The climatic device was left at -20ºC for 12 hours, at the end of which time the attenuation of the 8 fibers was measured again. Then the temperature of the climatic device was raised to 20ºC again. After the cable had been subjected to this temperature for 3 hours, the attenuation tests were carried out again.

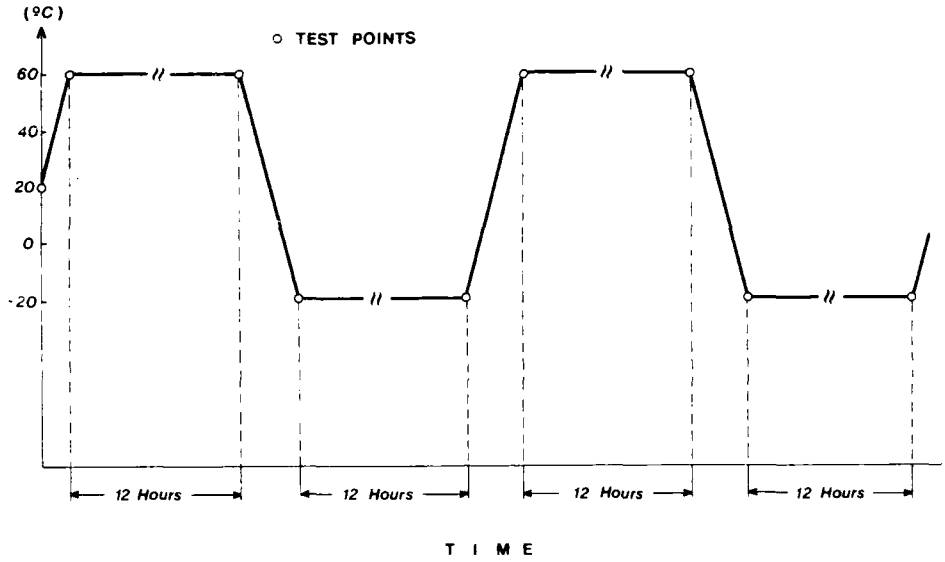

Fig. 3: THERMIC CYCLES

The whole cycle was repeated a second time. There were no significative variations in fiber attenuation in any of the partial measurements nor at the end of the cycle.

FINAL PROPERTIES OF THE CABLE

Besides the properties, already shown, of all the materials which make up the cable and the results of the specific tests carried out, the following general properties of the cable can be added:

Attenuation at 1300 nm.	Ave.	0.36 dB/km
	Max.	0.38 dB/km
Attenuation at 1550 nm.	Ave.	0.24 dB/km
	Max.	0.25 dB/km

The rest of the properties, for the fiber as raw material, have already been shown.

Outer diameter:	13.3 ± 0.1 mm
Weight:	127 ± 5 kg/km
Bending Radius:	150 mm
Tensile strength:	2500 N

The cable is also suitable for both aerial and duct installation.

5. CONCLUSIONS

We have presented a totally dielectric monomode optical fiber cable which possesses mechanical properties comparable to those of conventional cables with metallic protection and strength members.

It is our intention to obtain the homologation of this cable by the Spanish Railways Network as well as its use in Electric Companies, in the version of cable lashed to the ground-wire of high tension lines.

Even though the development has been carried out with an 8 optical fiber prototype, if a fewer or greater number of fibers are required, this could be done with slight modifications in the design. The modifications would only be slight due to the arrangement of the fibers which are loose in tubes.

6. REFERENCES

- Cable design, testing and installation, by P.R. Berk and others. Fiber Optical Communications, 1983.
- OPTICAL FIBERS: Single-mode fiber SM-02-R and The Optimisation of Single-mode fiber. Application notes. October 1987.
- OPTICAL FIBERS: Performance of single-mode and multimode fibers in hydrogen. Application note AN 10, March 1988.

- FIGURE 2: Reproduced from S. Stannard-Powell (BICC).

- Shot gun resistance of various sheaths used in telephone cables, by John W. Smith, October 1986.

CARLOS G. CORTINES was born in 1944. In 1968 he graduated from Valladolid University with a degree in Physics. He joined STANDARD ELECTRICA, ITT, today ALCATEL, and worked in the Engineering Department of the Telecommunication Cables Division. From 1982 he is the head of the Optical Fiber Development Group in ALCATEL STANDARD ELECTRICA, Cable Factory in Maliano-Cantabria.

CARLOS BLANCO received his Doctorate Degree in Telecommunications Engineering from Madrid University in 1972. He also received his Master Degree in Physics from Santander University in 1976. He joined ITT, STANDARD ELECTRICA in Spain in 1971 as R & D Manager of the Telephone Cable Division.

During 1982-1984 he joined ITT, ELECTRO OPTICAL PRODUCTS DIVISION in Roanoke, Virginia as Senior Scientist in the Optical Fiber R & D Department.

During 1987 he joined TELCOR (TELEFONICA CORNING GLASS) as Technical Director of the Optical Fiber Manufacturing Plant.

Since 1972 he has acted as part time Professor of the Electrical Engineering Department of the Santander University.

During 1983 he was nominated Adjunct Professor of the Electrical Engineering Department of the Virginia Politechnic Institute and State University, in Blacksburg, Virginia, lecturing on Optical Fibers and Optical Communications.

Presently, Dr. Blanco is with ALCATEL STANDARD ELECTRICA in Spain as Manager of the New Products Development Department.

SUSANA CAMARA received her Master Degree in Chemistry from Oviedo University in 1984, where she specialized in Organic Chemistry.

She joined ALCATEL STANDARD ELECTRICA in 1987 where she presently works in R & D Materials Department.

CONTINUOUS MOLDING EQUIPMENT FOR SELF-SUPPORTING PRE-HANGER TYPE OPTICAL FIBER CABLE WITH CATENARY

T. Koseki, S. Yamaki, F. Onodera

Kitanihon Electric Cable Co., Ltd.
1-2-1 Koriyama, Sendai, 982, Japan

Summary

In 1982, we developed a non-metallic self-supporting pre-hanger type optical fiber cable (SPOF cable)[1,2,3,4] to be used for steel pylon suspension type optical fiber transmission line. This type of cable has been marketed and used with successful results. Although the manufacture of this cable has been conducted so far by intermittent pre-hanger molding equipment, manufacturing equipment of greater efficiency and the ability to produce cable of consistent quality has become necessary. To replace conventional intermittent pre-hanger molding equipment, we have succeeded in developing new high-performance continuous pre-hanger type molding equipment, which can produce SPOF cable of better quality at a higher speed.

Introduction

Figure 1 shows the structure of SPOF cable. Continuous pre-hanger molding equipment conducts the molding of the pre-hanger part (PE Connection) while imparting catenary to the main fiber cable.

This equipment is such that plural numbers of catenary setting guides and metal dies for molding (attached with an opening and closing mechanism) are fixed alternately on the outer circumference of a round rotating table, which serves simultaneously as a take-up unit. An injection molding machine is incorporated in the unit to provide compact design. The take-up of cable, the provision of catenary and the molding of the pre-hanger part are conducted by a single unit simultaneously and continuously, without stopping the flow of cable.

Catenary is automatically imparted by guiding the cable so that a difference is provided between the length of the support line and the main fiber cable between the metal dies. By using these mechanisms, a stable catenary can be imparted with high speed.

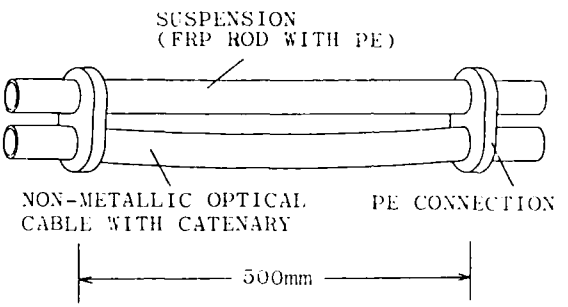

Fig. 1 Structure of SPOF cable

Outline of Continuous Pre-hanger Molding Line

As shown in Fig. 2, the line consists of a supply stand for main cable and support line, continuous pre-hanger molding equipment, a trimmer, shape identifier and take-up unit.

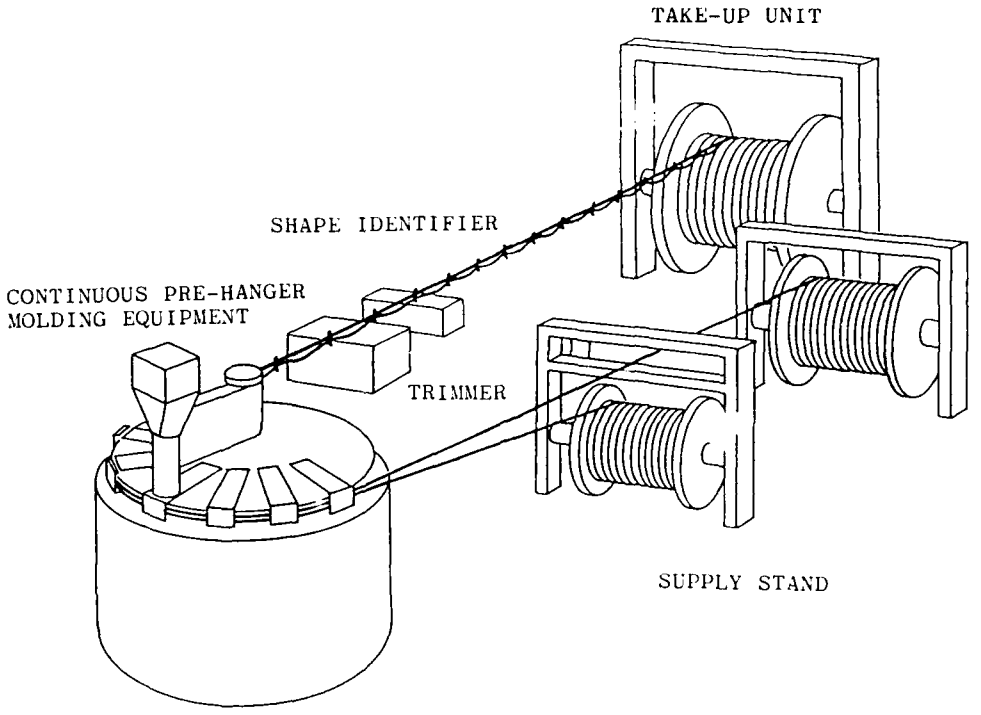

Fig. 2
Continuous pre-hanger molding line

Continuous Pre-hanger Molding Equipment

As shown in Figs. 3 and 4, (photographs) plural numbers of metal dies for molding, each with an opening/closing mechanism, and catenary setting guides are fixed alternately on the outer circumference of a round rotating table, with the center of the table serving as an axis. Thus, with rotation, pre-hanger molding is conducted by the injection molding machine which moves reciprocally and synchronously with the opening and closing of the metal dies, while continuously providing catenary.

Specification of Equipment

Diameter of table:	1830 mm
Height of machine:	1600 mm
Height of pass line:	1000 mm
Cable bending diameter:	1591.6 mm
Fitting pitch of metal dies:	500 mm
Catenary setting:	0 - 2%
Nos. of metal dies fitted:	10 pcs
Nos. of catonary guides fitted:	10 pcs
Injection molding machine:	Max.11g/shot
Production capacity:	over 75 Km/month

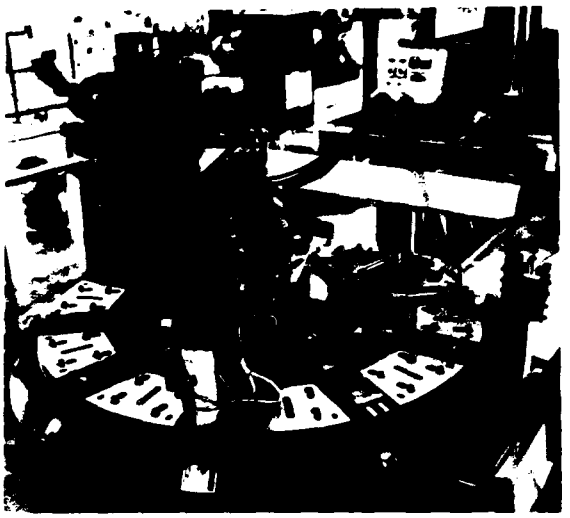

Fig. 3
Continuous pre-hanger molding line

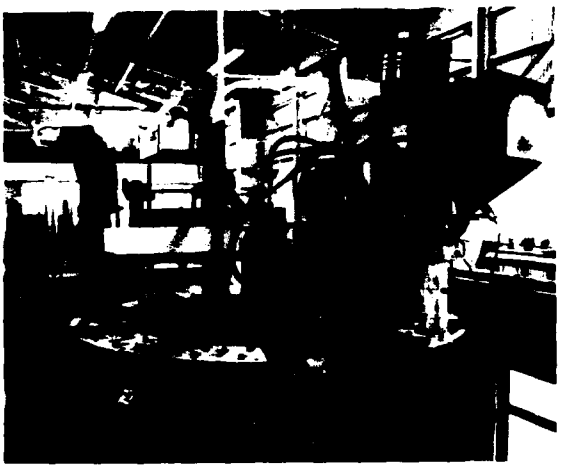

Fig. 4
Continuous pre-hanger molding equipment

Movement

As shown in Fig. 5, the incoming suspension line and the main fiber cable are led to the catenary setting guides, metal dies are closed and resin is injected. After the cooling of the resin, the metal dies are opened and the support line and main fiber cable are led out.

Figure 6 shows the range of reciprocating movement of the injection molding machine and the opening and closing range of the metal molding dies.

Figure 7 (photograph) shows the open position of the metal dies.

Figure 8 (photograph) shows the closed position of the metal dies.

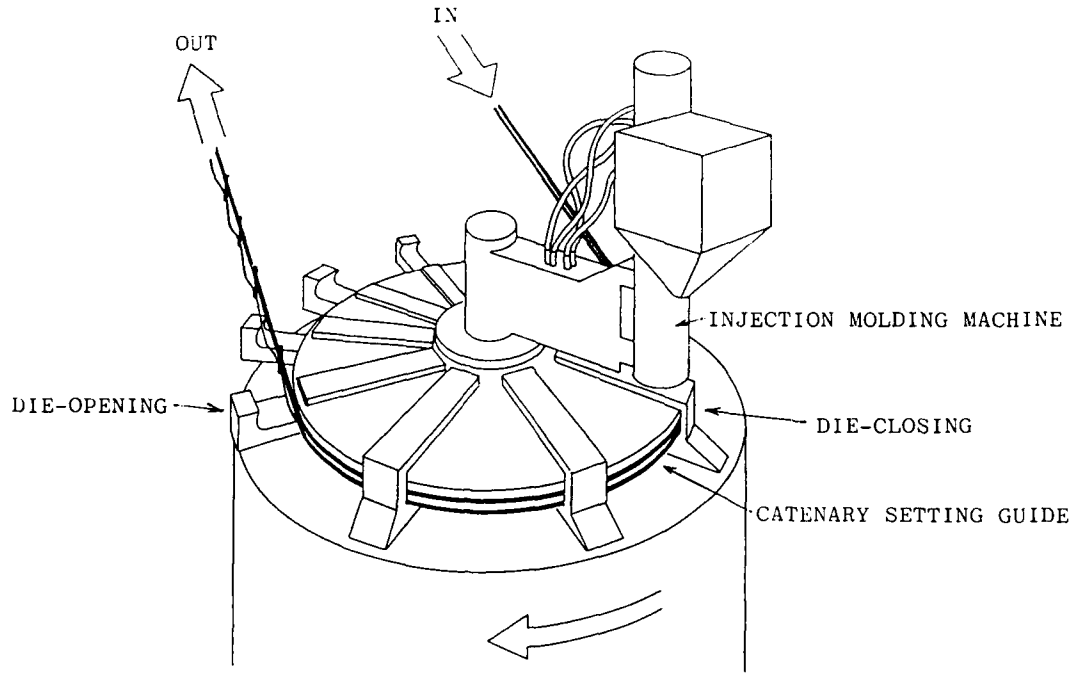

INJECTION MOLDING MACHINE

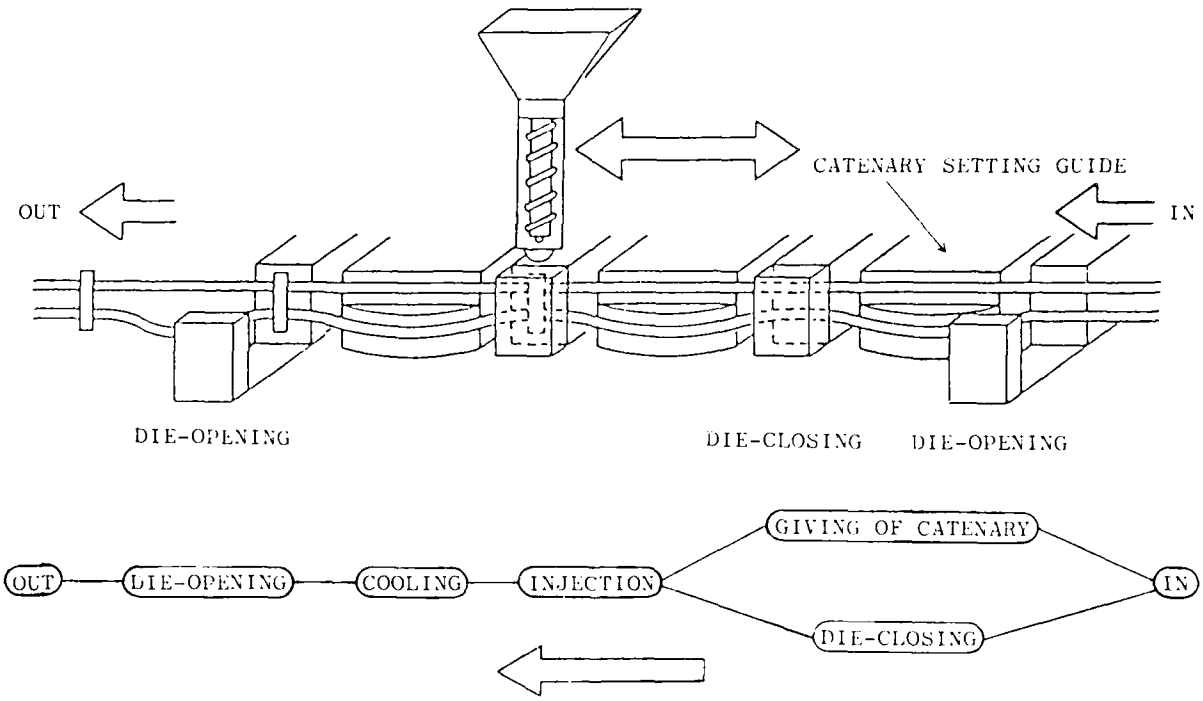

Fig. 5
Continuous pre-hanger molding equipment and its operational process

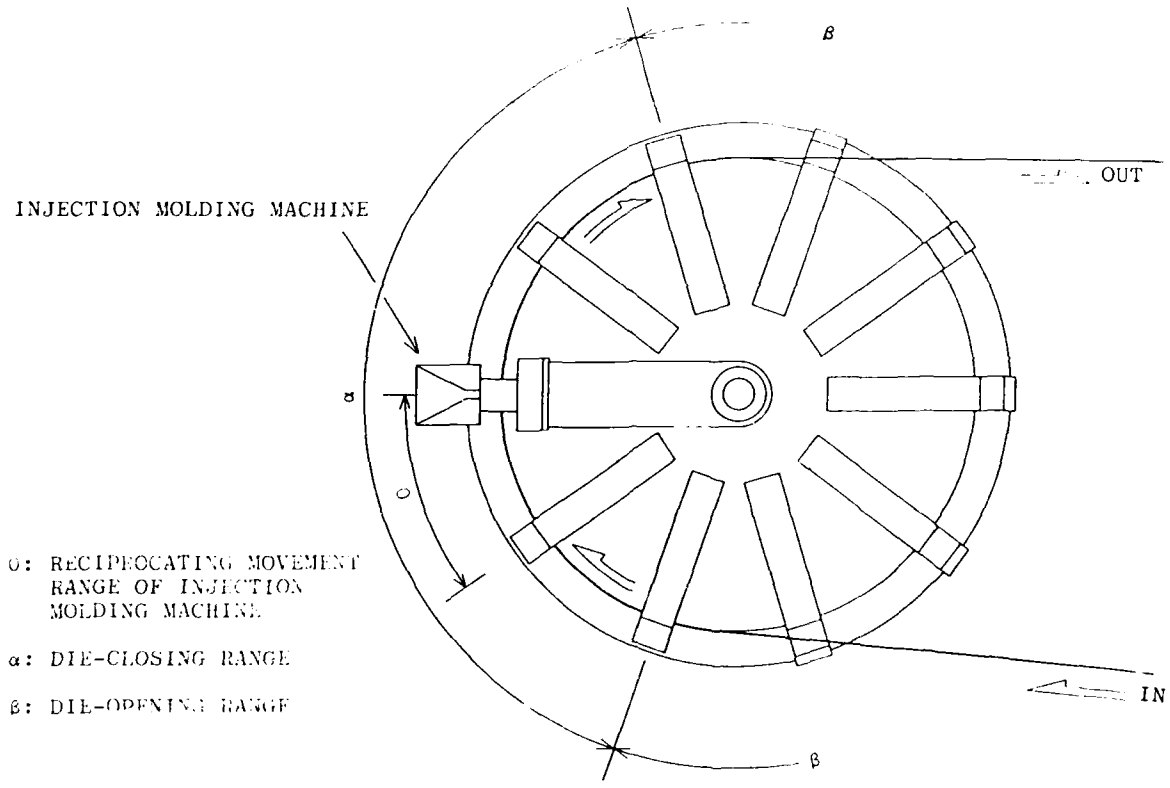

Fig. 6 Operating principle

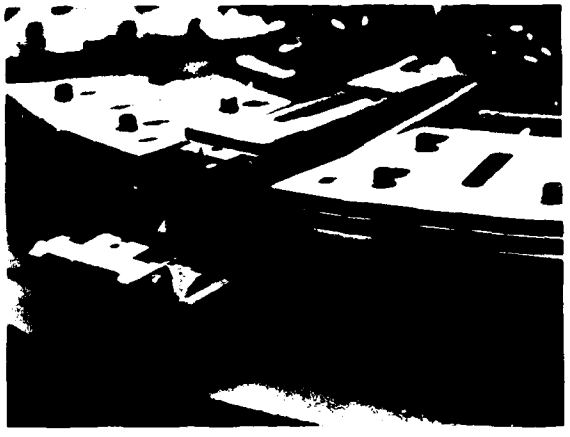

Fig. 7 Metal dies (open)

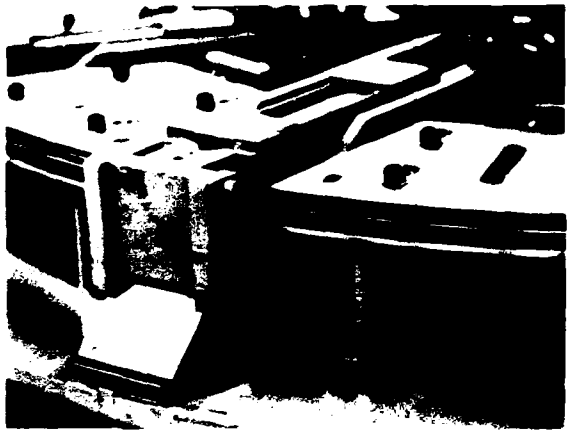

Fig. 8 Metal dies (closed)

Provision of Catenary

Catenary is automatically provided by catenary setting guides as shown in Fig. 9 (photograph). These are fan-shaped guides with grooves and each consists of two parts, one for the suspension line and the other for the main cable. These guides can slide in a radial direction on the table. By leading the main cable along these guides towards the periphery of the table, the length of the line between the pre-hangers becomes longer in the main cable than in the suspension line.

Resin is injected into the metal dies. After the resin has cooled, and the cable being guided out of the molding equipment has straightened, the difference in length is accounted for by the catenary of the main fiber cable.

This procedure provides the cable with a well-balanced and uniform catenary. Since the catenary setting guides are arranged alternately with the dies, catenary is provided continuously and automatically with the rotation of the table and a series of molding movements.

Fig. 9 Catenary setting guide

Conclusion

With the development of this manufacturing equipment, productivity of SPOF cables at our plant has shown remarkable improvement, and we are now producing cables of better quality at higher speed.

References

1. E. Hayasaka et al.: "Non-Metallic Optical Fiber Catenary for Long Span Aerial application," IWCS, 1983.
2. E. Hayasaka et al.: "The Clarification of Movement of Non-Metallic Self-supporting Optical Cable Caused by Wind and the Design of Its Installation at Steel Pylons," IWCS, 1984.
3. H. Takehara et al.: "Withstanding High-Voltage Characteristics of Non-Metallic Self-supporting Optical Cable," IWCS, 1987.
4. Y. Ishihata et al.: "Improvement of Fiber Reliability in Splice Enclosures Resulting from the Reduction of Relative Movement between Cable Core and Sheath," 1984.

Authors

Toshio Koseki
Kitanihon Electric
Cable Co., Ltd.
1-2-1, Koriyama
Sendai 982, Japan

Toshio Koseki received his B.E. degree from Tohoku University in 1975. At Kitanihon Electric Cable Co., Ltd., he has been engaged in the development and design of plants for power cables and communication cables. He is now the chief engineer of the engineering section. He is a member of the Japan society of Precision Engineering.

Shigenori Yamaki
Kitanihon Electric
Cable Co., Ltd.
1-2-1, Koriyama
Sendai 982, Japan

Shigenori Yamaki joined the Kitanihon Electric Cable Co., Ltd., in 1962 and has been engaged in the development and design of plants for power cables and communication cables. He is now the manager of the engineering section.

Fumio Onodera
Kitanihon Electric
Cable Co., Ltd.
1-2-1, Koriyama
Sendai 982, Japan

Fumio Onodera joined the Kitanihon Electric Cable Co., Ltd., in 1958 and has been engaged in the development and design of plants for power cables and communication cables. He is now the manager of the technical department.

AN OPTICAL FIBRE CABLE WITH HEAT EXPANDABLE TAPE AS A CUSHIONING

Anders Larsson, Karin Nygård-Skalman
Thomas Norlund, Nils-Erik Grip

ERICSSON CABLES, BOX 457 , HUDIKSVALL , SWEDEN

ABSTRACT

The design of a dielectric optical fibre cable with high crush resistance is presented. The cable has a double sheath with a Heat Expandable Tape, as a cushioning between inner and outer sheath.

The HET wrapping is applied unexposed on the inner sheath of the cable. When applying the outer sheath the heat from the extrudate will expand the HET and the thickness of the tape will increase. Cables with Heat Expandable Tape as a cushioning has been tested and proved to be suitable for direct burial by ploughing. In some applications this cable is an alternative to steel tape or wire armoured cables, when armouring is used only as mechanical protection.

Cables with HET can also be used as an alternative to duct installation.

INTRODUCTION

To make optical fibre cables mechanically strong and rigid enough for direct burial, the cables often are made with a steel tape or wire armouring. However, a metal armouring is not always wanted. One way to make dielectric optical fibre cables more rigid is to have a cable construction with a thick sheath. Unfortunatly an optical fibre cable with a too thick sheath, will have bad temperature performance. This is due to the high temperature coefficient of the polymeric material in the sheath.One solution to this problem is to make a cable with a spacing between inner and outer sheath. The spacing can be unfilled or filled with jelly. A tape can also be used to fill the space. Using a tape, the tape acts as a bedding for the outer sheath.

To apply a tape in a sheating line, regular extrusion lines can be used. Applying a tape longitudionally on a cable in a sheating line is a very simple process. However, if the tape is thick, a few mm, some practical problems will occure. For example a tape pad with a 2 mm thick and 1000 m tape length will have a diameter of 1.5 m. Other practical problems can also be present when folding a too thick tape around a cable with a small diameter.

In solving the practical problems, how to apply a thick tape on a cable, a newly developed cable wrapping can been used. The new wrapping is a Heat Expandable Tape, HET. This tape expands when heated and gives a very good bedding for the outer sheath. The HET acts as a cushioning and will protect the inner cable. In figure 1.is a cable is shown where the HET is visable under the sheath.

The development of the tape and the process how to apply it on a cable, has been going on for about 2 years. Much work has been done to optimize the expansion of the tape and the process how to apply it in an extrusion line.

To verify the possibilities in using the HET in cable construction a dielectric optical fibre cable has been made. The new cable is called Tube Jacket Cable.

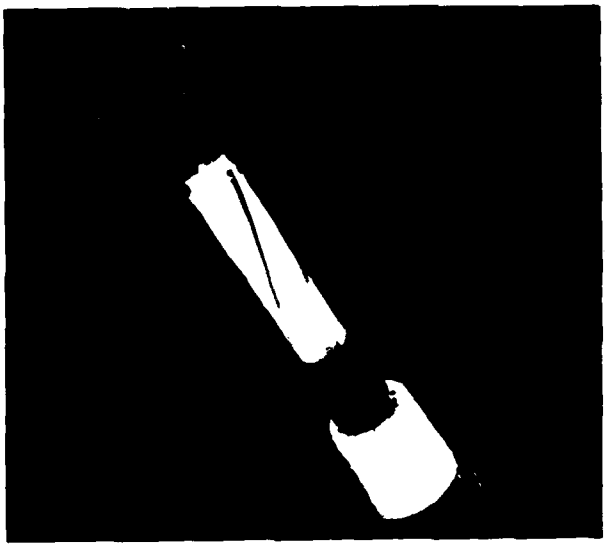

Fig.1 A Tube Jacket Cable, where the HET can be seen under the outer sheath.

CABLE CONSTRUCTION

To verify that a cable with a HET wrapping as a cushioning is suitable for installation by ploughing, a cable for duct installation has been used as the cable core in the tube jacket cable.

A crosssection of the tube jacket cable is shown in Fig.2. The cable is a slotted core design with a central strength member of FRP, fibre reinforced plastic. The slots are made of polyethene and produced in an extrusion line with a rotating head.Inside the slots,there are secondary tubes with four fibers in each tube. The cable core is filled with petroleum jelly, to prevent water penetration. Linear low density polyethene, LLDPE is used as a sheath on the inner cable. This inner cable is normally used for installation in ducts.

The tube jacket cable has a heat expandable tape applied on the outside of the cable core toghether with a sheath of high density polyethene, HDPE. The HET is expanded to a thickness of 2.5 mm. The tape acts as a support for the sheating process and as a cushion for the cable core.The outer sheath of high density polyethylene act as a conduit. The HDPE was selected for its good mechanical properties.

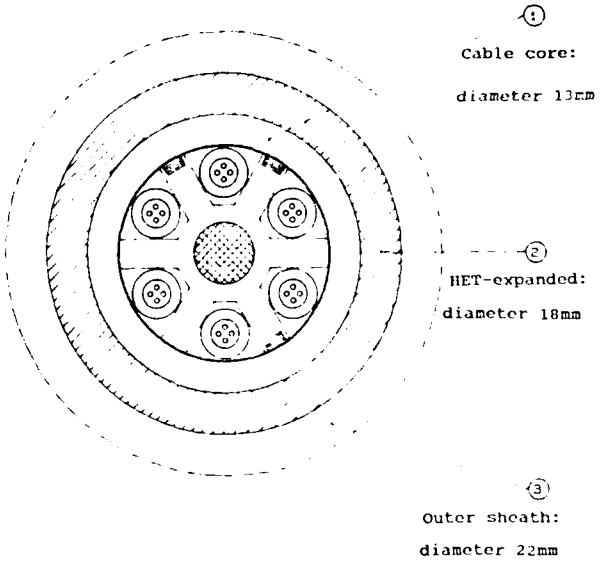

Fig.2 Construction of the Tube Jacket Cable.

The main design requirements of the Tube Jacket Cable are:

Crush strenght with 100 mm plates,in accordance with IEC-794-1-E3: > 6000N
Bending radius
> 15 x cable diameter

The fibre parameters are in accordance with the recommadation G 652 of CCITT:

The inner cable is specified to meet the following temperature requirements:

Temperature range,
operation -30° -+70°C
Temperature range,
storage -40° -+70°C
Temperature range,
installation -10° -+50°C

Heat Expandable Tape

Heat Expandable Tape, HET is a non-woven tape on which heat expanding microspheres are bonded with a bonding agent.

Microspheres are spherically formed particles, which consist of a polymeric shell with an enclosed blowing agent. The shell is an acrylonitrile-vinylidenchloride copolymer and the enclosed blowing agent is isobutane.

The characteristic property of HET is the expansion, which defines the final thickness of the tape. Expansion takes place in the temperature range 90°- 120°C depending on the tape design and type of microspheres. It is possible to make a tape for a special application as there are microspheres expanding at different temperatures. It is also possible to have, in the same tape, seperate layers of microspheres that expands at different temperatures.

One advantage of HET is that a thin tape, can give a thick bedding for the outer sheath. When the tape expands, the isobutane in the microspheres absorb heat from the extrudate. This is a positive effect which enables the use of material with high extrusion temperature.

Expansion of the tape is approximatively ten times the original thickness. HET should not be exposed to extremly high temperatures for too long, due to the risk for cracking of the microspheres. If the microspheres crack the thickness of the expanded tape decreases rapidly.

Figure 3 shows the depandance of the tape thickness to time at a temperature

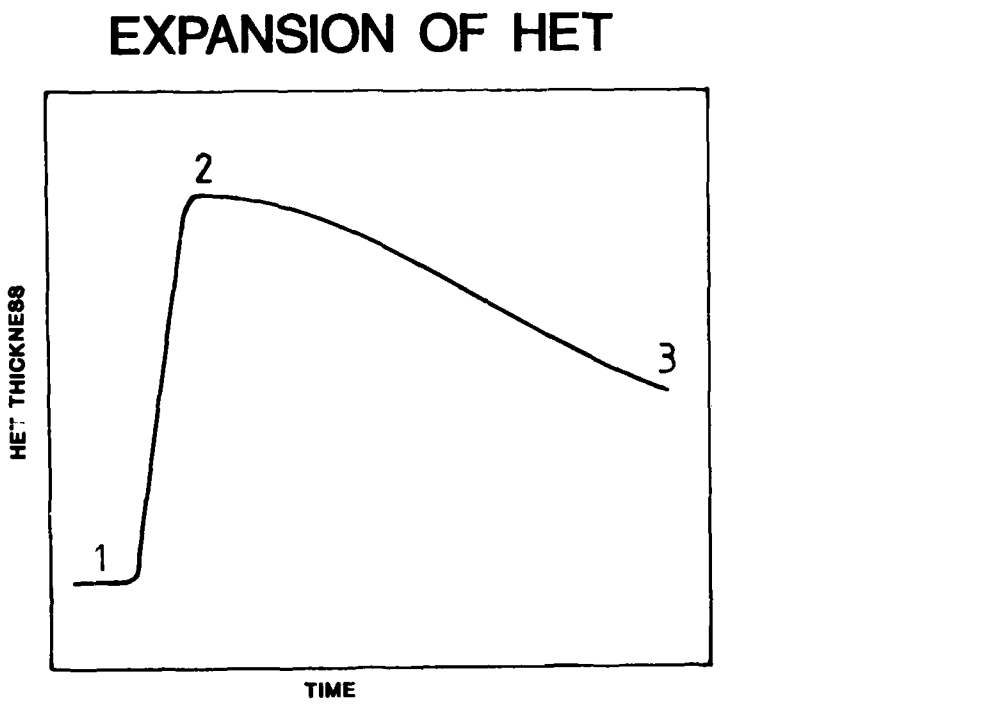

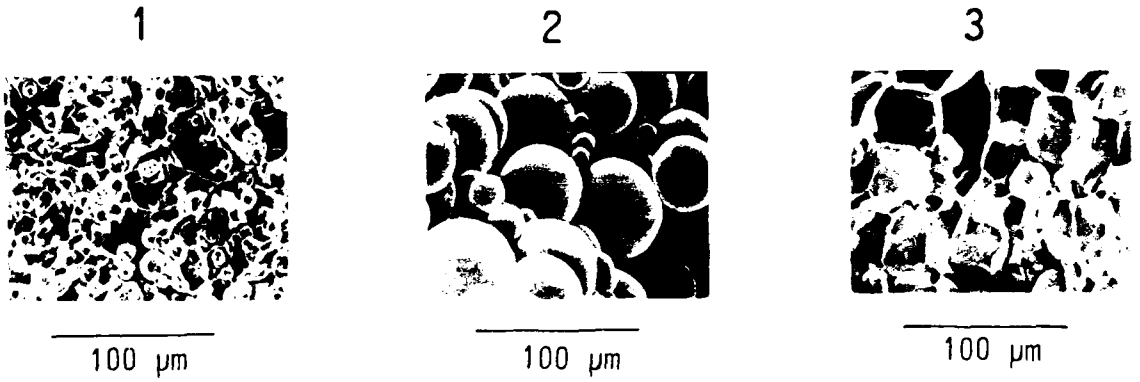

Fig.3 Expansion height as a function of time at constant temperature.

above expansion temperature
HET before expansion is showed in picture 1. Fully expanded HET in picture 2. In picture 3 some of the microspheres are cracked.

PROCESSING

The main task in developing a process for using Heat Expandable Tape, has been to make the use of the tape as simple as possible. In order to find a simple process, it has been necessary to modify the HET to fit the process parameters in a sheating line. After optimizing the HET the tape is suitable for a wide range of cables and sheating materials.
The Heat Expandable Tape is applied longitudionally on the cable, and folded around the cable in a guide tube. The guide tube is located at the inlet of the extruder head in the sheating line.

Passing through the extruder head, the

Deformation is measured as the inpact on the outer cable diameter.
The test is in accordance with IEC 794-1-E3.

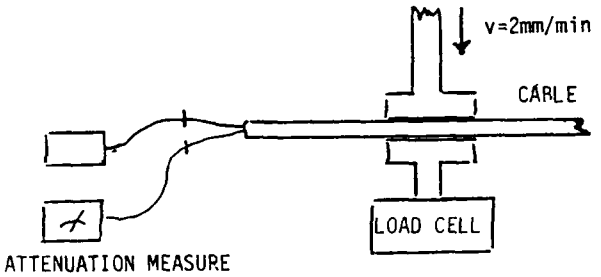

ATTENUATION MEASURE SET UP

Fig.4 Crush strenght measurement setup.

Results:

In fig.5 the attenuation change and the deformation as a function of the compressive force is shown.The attenuation reaches 0.1 dB at a load of about 6.5 kN. A comparision is done in fig 6. between a cable for duct installation (fig 7,type 1), a tube jacket cable (fig 1) and an armoured cable (fig 7,type 2) .

Fig 6 shows the attenuation change at 1550 nm as a function of the compressive force.

The most sensitive cable to compression is the ductcable.
The armoured cable has a very steep increase in attenuation versus compression at a load of about 8 kN. The tube jacket cable shows notable increase in attenuation above 6 kN, however the increase in attenuation is still at 14 kN below 0.8 dB.

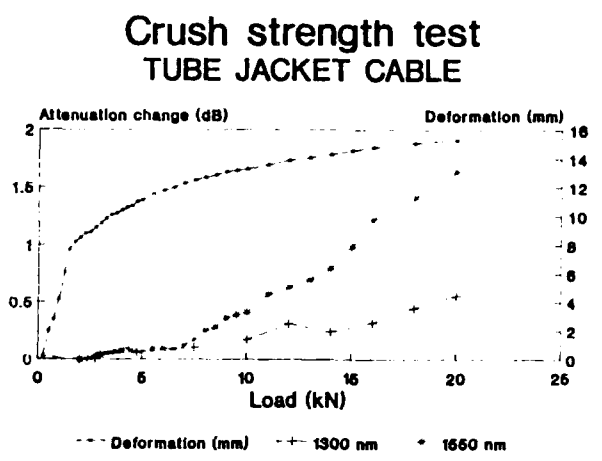

Fig.5 The attenuation change and deformation as a function of crush load.

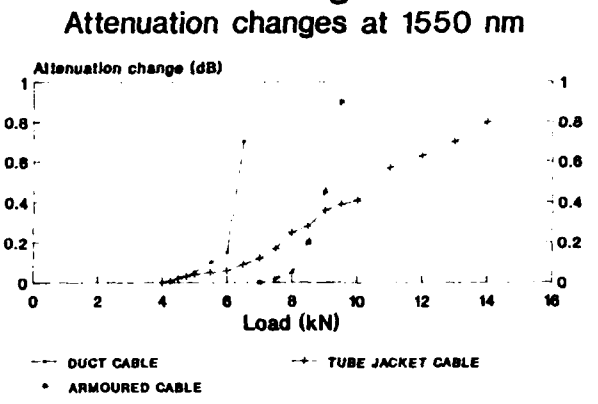

Fig.6 A comparision between three types of cables regarding crush resistance. The attenuation was measured at 1550 nm.

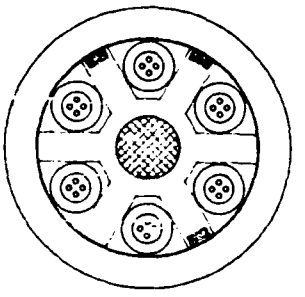

Type 1 - duct cable

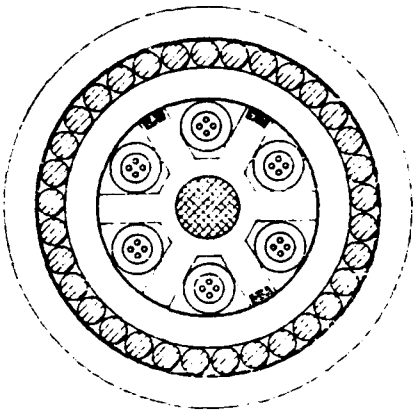

Type 2 - armoured cable

Fig.7 Cable for duct installation, type 1 and a wire armoured cable, type 2.

Tensile load test

Test procedure: 25 m of cable is tested under tension.The cable is terminated at one end by winding 5 turns round a fixed wooden mandrell.On the other end the tension load is increased in steps of 250 N.

The elongation of the outer sheath is measured at the cable grip where the tension is applied. The slip between the outer sheath and the cable core is also measured.

Results: The strain and the slippage of the cable as a function of the load is shown in fig 8. The cable can withstand a load on the outer sheath of 2,0 kN without too much slippage. When the load is removed the slippage will return to almost zero.

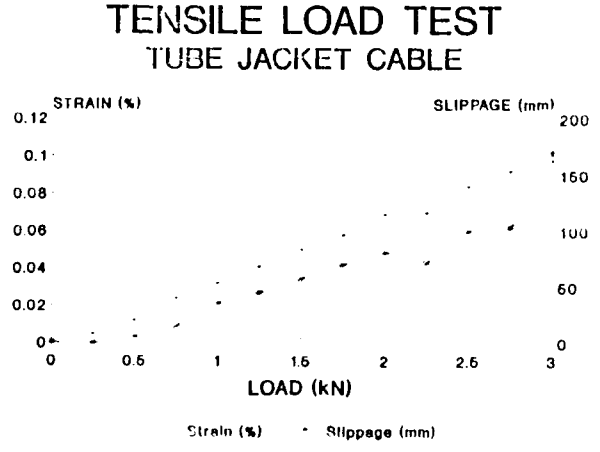

Fig.8 Tensile load test of the tube jacket cable.

Freezing test

Test procedure: The cable was put into a steel tube, 2.5 m in lenght, filled with water. Four holes with a diameter of 6 mm were drilled in the outer sheath. The holes was 0.5 m apart. This was made to simulate water leakage between the sheaths. The temperature around the cable was brought down below freezing point, for 24 hours.

The attenuation was measured, both at 1300 nm and at 1550 nm.

Results: The attenuation did not change at neither 1300 nm nor at 1550 nm during temperature cycling. In some places the microspheres were slightly deformed but not cracked.

PILOT INSTALLATION

In december 1987 a pilot installation was done.The attenuation has been measured continously for eight months.During that time the temperature has varied between -5° to +20°C. The cable is installed into ground at 80 cm depth. The installation was carried out in accordance with the Swedish PTT specification for installation of armoured cable.

The cable installed has 12 fibres and it is 700 m in lenght.

Measurement: The 12 fibres were looped toghether and the attenuation was measured with a backscatter. During installation the attenuation change was measured continously. From then on, the attenuations measurement have been made regulary over the period.

Results: The plot in figure 9, shows the attenuation change as a function of time. The measurements are made before, and after installation. In figure 10 the attenuation change is plotted as a function of temperature.

The results from the pilot installation shows that the cable does not change attenuation during installation. During the testing period of 8 months, no significant change in attenuation, due to temperature variations was observed.

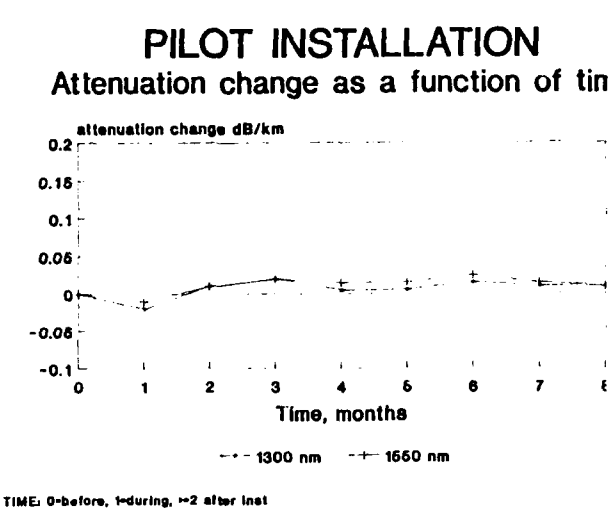

Fig.9 Attenuation change as a function of time

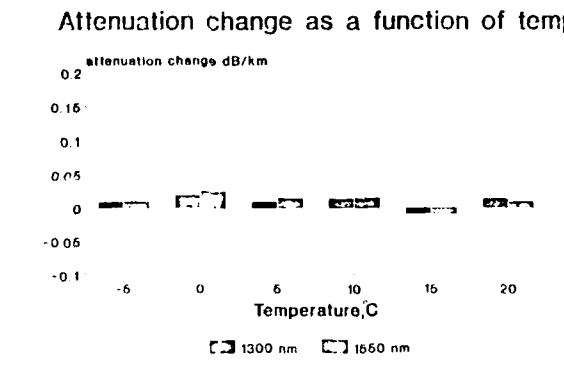

Fig.10 Attenuation change at different temperatures.

CONCLUSIONS FROM TESTING AND PILOT INSTALLATION

The tube jacket cable fullfill our design requirements. The cable is rigid enough to withstand mechanical forces that occurs when the cable is ploughed directly into ground. A tube jacket cable is comparable to a wire armoured cable regarding the resistance against

REFERENCE INSTALLATION

Some 100 km tube jacket optical fibre cable have been installed in 1988 by the Swedish Railway Authorities.
The cable was installed by ploughing, toghether with two other cables directly into the railway embankment. The cables had been laid out along the railroad before installation.

The experience from these installations is that tube jacket cable with HET as a cushioning can be ploughed directly into ground.

The dielectric cable is easy to handle and well suited for installation close to electrified railways.

Fig.11 Installation of the Tube Jacket Cable by the Swedish Railway Authorities.

ACKNOWLEDGMENT

The authors wish to thank the technical and research staff at Lantor / Firet, who has been envolved in the development of the Heat Expandable Tape, for their good work on the HET and their help in our work to develop the process how to apply the HET on the cable.

AUTHOR'S ABSTRACT

Authors

Mr Anders Larsson recieved his M.Sc. in Electrical Engineering from the Royal Institute of Technology, Stockholm, in 1973. He has been working in the cable industry and with cable machinery since 1975. Since 1985 he is Technical Manager at Ericsson Cable Telecom Cable Division.

Mr Thomas Norlund recieved his B.Sc. in Chemistry from Uppsala university in 1981. He joined Ericsson Cable Telecom Cable Division in 1985. At present he is working with material development for telecom cables.

Mrs Karin Nygård Skalman recieved her M.Sc. in Chemical Engineering at the Royal Institute of Technology, Stockholm, in 1982. She has been working at Ericsson Cable Telecom Cable Division since 1984. At present she is responsible for development of optical fibre cables.

Mr Nils Erik Grip joined Ericsson Cable Telecom Cable Division in 1982. He has been working as a process and production engineer and is at present mainly working with product and process development in extrusion lines.

BLASTING NEAR FIBER OPTIC CABLE

Mark A. Setman, Max J. Brandtner

Siecor Corporation
Hickory, North Carolina

I. ABSTRACT

Questions have arisen relative to the safety of blasting near fiber optic cable. These questions occur when a contractor is attempting to place another utility line, be it water, sewer, gas or power, along the same right of way as a fiber optic cable. If the contractor encounters rock along the right of way, he is often forbidden to blast in any "reasonable" vicinity of the fiber optic cable. This situation can cause great additional expense for the contractor in terms of time and increased mechanical excavation equipment costs. Changing the route to avoid the fiber optic cable is normally cost prohibitive or nearly impossible. The questions posed are: "Are fiber optic cables adversely affected by blasting?" and "Must the data transmission be rerouted during the blast?". This experiment showed that Siecor's single armor, loose tube design experienced no damage within the severe blasting environment.

II. BACKGROUND

Contractors placing new utility lines along highway right of ways where fiber optic cables have been previously placed face tough alternatives. There is normally only five to twenty five feet of right of way along the road and when other utilities are already in place, even less space is available. If there is an existing fiber optic cable in place, the Telco is often very nervous when contractors start digging up the area near their cable. Severing a cable can be very expensive in terms of lost revenues. The Telco normally gets very upset at the mere thought of using explosives when the contractor encounters rock requiring blasting. The Telco will often do whatever they can to stop a contractor from blasting anywhere near their cable. Mechanical extraction of solid rock is often extremely expensive and time consuming, and it is normally unacceptable to the contractor.

Is fiber optic cable tough enough to withstand the effects of excavation using explosives in the immediate vicinity of the cable? A positive answer to this question would certainly ease the tensions and concerns for both the contractors and the Telcos. At face value it may appear that fiber optic cable is a fragile entity. However, Siecor fiber optic cable construction is designed to protect the fiber from harsh physical and environmental effects. Within the cable industry, standards define the physical requirements for the cable. Rigorous physical tests have been performed on Siecor fiber optic cables with excellent results. Tests performed under laboratory conditions may yield very good indications of the probable success of blasting near fiber optic cable. However, unless cable is tested in the actual field blasting conditions, there may still be many doubts. It was for these reasons that a local excavation contractor and Siecor decided to share resources and expertise in conducting a test that would replicate typical and worst case scenarios for blasting near fiber optic cables.

III. EXPERIMENT

The plan employed typical blasting techniques near direct buried fiber optic cable and involved the direct burial of single armored fiber optic cable in a bed of shale using a vibratory plow. A series of blasts were detonated at varying distances from the cable. The blast patterns employed were designed to simulate what would typically be required for placing a water main eight foot below the ground, near the fiber optic cable. See Figure A for the plan view of the experiment.

Fifty meters of cable were buried with the remaining cable running above ground to the electronic monitoring equipment safely located 50 meters away. Optical fiber was spliced at the cable ends to create over two hundred meters of an optical fiber run in a fifty meter cable. This situation made the cable more sensitive to blasting effects since more fiber was subject to the blast.

Blasting Experiment Plan View

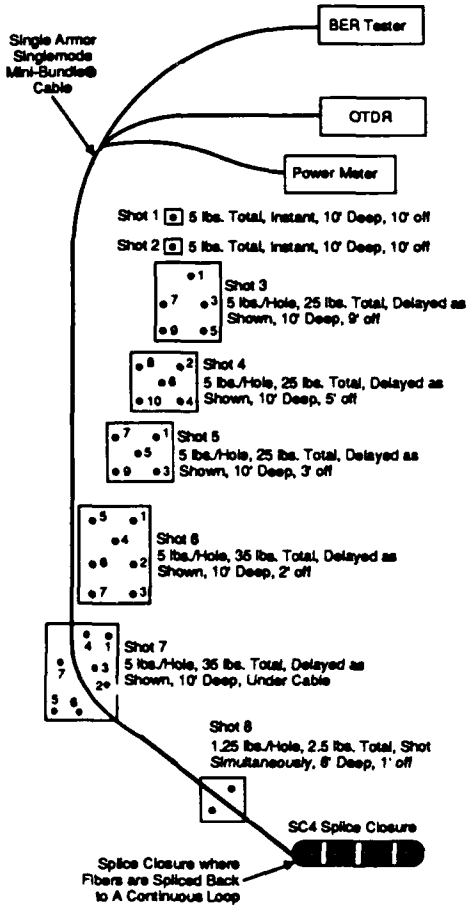

Note:
The Number Associated with Each Hole Signifying the Blasting Cap Delay. A Number 1 Indicates that there is a 25 Millisecond Delay, A Number 2 has 2 X 25 or 50 Millisecond and so on. No Number Indicates No Delay and was Used on Single or Simultaneous Blasts.

Figure A

The fiber optic cable employed was Siecor's single armor loose tube design. This design is a gel filled, double layer loose tube construction that utilizes aramid yarn and fiberglass strength members, multiple polyethylene jackets and longitudinally applied corrugated steel armoring. This design is typically recommended for direct buried applications since it provides the physical protection required for vibratory plow installations and potential rodent or lightning exposure. See Figure B for the cable cross section.

SIECOR 30-Fiber
Loose Tube Mini-Bundle®
Single Armor

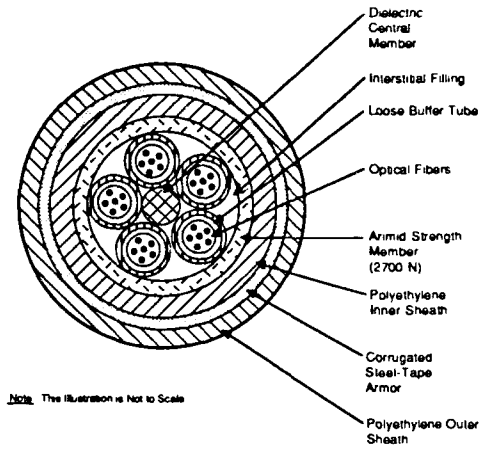

Figure B

To measure the transient effects of the blasts the cable was monitored by a Bit-Error-Rate (BER) tester operating at a bit rate of 500 MBits per second. Using this device and an optical attenuator, the bit errors per bits transmitted were kept at a level of 0.5×10^{-9} between blasts, which resulted in an average of one error per four seconds and represented the highest BER typically accepted in a system. During the blasts, the BER tester was switched to display the actual number of errors counted. If errors were recorded during the blast beyond the normal rate, the BER tester would indicate that transmission may have been adversely affected. Figure C illustrates the layout of the BER test device. An Optical Time Domain Reflectometer, (OTDR), was used to locate any possible anomalies in the fiber caused by the blast. Additionally, a power meter was employed to measure any changes in attenuation before and after each blast.

Bit Error Rate
Measurement Set-Up

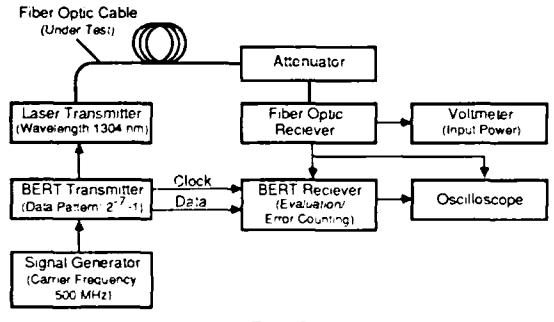

Figure C

Every effort was made to achieve realistic field conditions. The area used was primarily shale rock with a few inches of loose top soil. The dust produced by the rock drill was mostly white indicating hard shale, with a few occasional bursts of dark brown indicating soft shale. Across most of the test area the plow could easily install the cable to the desired twenty four inch depth even though it occasionally brought five to twenty five pound chunks of shale to the surface. Over one area of the test, the plow hammered on top of a layer of hard material at a depth of about twenty inches. In all probability, a cable installation contractor would have laid the cable the same way, right on top of the rock. This area was also used for the most severe test of blasting under and beside the cable. If the ground had been much harder, the cable would have been trenched in and probably surrounded by a few inches of protective material such as sand thereby making the plow-in scenario worst case. The likelihood of shearing or crushing the cable was greater than if the cable had been trenched in through harder rock and back filled with softer material (sand).

The explosive used was a nitroglycerine based dynamite, which had an absolute energy (bulk strength) of 1400 cal/cc, a relative energy of 190 (using Ammonium Nitrate-Fuel Oil, ANFO=100 as a bench mark), and a velocity of 16,000 feet per second. Electric time delay caps were used to detonate the dynamite. The holes were stemmed with #67 stone. When multiple charges were fixed, they were covered with a weighted sled (for safety reasons) to eliminate flying rock.

The experiment was started with one charge of five pounds, (2 each 2"x16" sticks) placed ten feet from the test cable and ten feet deep as per Figure A. This places the explosive at about eleven feet from the cable. The shot raised the ground about six inches. No additional errors were recorded by the BER tester and no increase in attenuation was measured by the power meter.

Shot #2 was basically the same with the BER tester set to be more sensitive (BER of $0.5x10^{-9}$). The results were identical to the first shot.

Shot #3 was made with a five hole pattern as per Figure A. Each hole was loaded with five pounds of explosive giving a total load of twenty five pounds. This shot was covered with the sled to protect observers from flying debris. As normal blasting practice dictates, the delay on the caps were designed so that the closest hole to the cable would be the last to fire. This shot picked the sled up about six inches, humped the area about one foot and cracked the ground in all directions. This shot probably displaced the cable slightly. No additional errors or increases in attenuation were seen.

Shot #4 was the same as #3 except the pattern was varied slightly and was now five feet from the cable as per Figure A. The results were identical to #3.

Shot #5 was also similar to #3 and #4 except the two closest holes were drilled about three feet from the cable. The results were identical to #3 and #4. The cable was probably displaced a few inches by this shot. Again, no additional errors were detected and no increases in attenuation were observed.

Shot #6 was a seven hole pattern containing thirty five pounds total dynamite, with the closest holes being two feet from the cable. The ground was raised about a foot and the cable was probably displaced more than six inches, but again, no additional errors were recorded on the BER tester.

Shot #7 was a seven hole pattern as per Figure A, which actually crossed under the cable. It is doubtful that a contractor would attempt this shot in an actual job situation with a live cable, but, given the way cable is often installed around an obstruction, there is an excellent chance that such a blast could occur without prior knowledge that the cable was within the hole pattern. This shot occurred in the area where the cable was installed right on top of the rock layer. The seven hole pattern contained thirty five pounds of explosive, all within ten feet of the cable. The closest explosive was about six feet from the cable. This shot picked the sled up more than a foot, humped the area about a foot, and probably displaced the cable about one foot. No additional bit errors or cable damage were found, nor was an increase in attenuation noted.

Shot #8 was designed to be representative of an "accidental" shot for a water line trench. Holes were drilled a foot on each side of the cable and six feet feet deep. Each was loaded with one half stick of 2"x16" dynamite which placed the explosive at about four feet from the cable. This shot was rather loud and disturbed the ground in the same manner as the other shots due to the shallow depth. As we had hoped, this shot also caused no increase in bit errors, nor any increase in cable attenuation.

IV. ANALYSIS

None of the blasting shots caused an increase in attenuation as measured by the power meter and no increase in bit errors as measured by the BER tester. No additional bit errors were observed indicating that no transient effects were witnessed by the cable. The instantaneous shock provided by the blast did not adversely affect the data stream. The cables were excavated at the most severe blast areas and showed only insignificant cosmetic scratches on the outer

jacket. These scratches are most likely a result of their contact with the rock either during direct burial or during the blast and are not considered to be any factor in the short term or long term performance of the cable. What is most significant is that the cable showed no signs of deformation. The cables were still round, showed no flattened or oval areas indicating no significant physical damage.

This experiment was designed to replicate most commonly used blasting techniques used in the industry. The parameters in the test were either considered typical or "worst case". There are many variables that can enter into this type of experiment: rock type and density, cable depth and placement method, cable type or construction, blasting methods, shot pattern, blast hole depth, explosive type and quantity used, and the sensitivity of the electronic equipment employed. Our intent was to keep most of these constant or at least to quantify the variables in order to collect the most meaningful data possible. Different parameters or assumptions may alter the testing results. However, using typical and worst case parameters should help to justify the results of this test relative to many other less harsh blasting situations.

Specifically, we chose to use a vibratory plow to place the cable into the shale rock bed as a worst case scenario because the vibratory plow vibrates the plow blade to fracture and move the rock aside, laying the cable in this new path. This method may cause the newly fractured rock to damage the cable if the blast is severe enough. This scenario also keeps the ground homogeneous enough to allow the highest propagation of the shock wave. Normal trenching burial procedures provide a change in density of material in the ground around the cable since the backfill material around the cable is normally sand or a "softer", less dense material. This procedure would tend to protect the cable from protruding rock fragments and also reduce the effect of the shock wave. The shale rock bed was chosen because it is the hardest material that would be plowed through with a vibratory plow. If a material like granite was encountered, then it is most likely that the cable would be trenched in and have that extra protection as was previously described.

The blasting materials and techniques described were used because they are considered typical for the type of rock encountered. The depth of the blasts and hole pattern employed are typical for the scenario of a water or sewer main going in eight feet below the ground and would replicate a typical large excavation that would occur along a highway or railroad right of way. Another variable that was introduced into this experiment was the cable design. Since the experiment was performed with Siecor's single armored loose tube cable, one should not assume that other cable designs will produce the same positive results.

V. CONCLUSION

Unchanged attenuation measurements, as measured by the power meter, both before and after each blast indicated that no increase in attenuation occurred because of the blast. No increase in bit errors, as measured by the BER tester, indicated that no measurable transient fluctuations occurred during blasting. The OTDR scan makes it obvious that no breaks in the fiber occurred. The conclusion that can be drawn from the readings taken during this test is that these Siecor fiber optic cables were not adversely affected by the blasts. No significant physical damage was done to the cable, as subsequent inspection showed no damage short of cosmetic scratches. This indicates that no long term failure due to blasting is expected.

The cables in this experiment held up quite well through the rigors of blasting. Even with charges within one foot (plan view) and two to eight feet below the cable (side view), no detrimental effects were observed. Some concerns have been expressed about the crush resistance of fiber optic cables. These test results show excellent protection in worst case situations.

The results of our experiment indicate that excavation utilizing explosives and blasting techniques standard to the industry performed by excavation experts should be relatively safe when employing reasonable charges and at reasonable distances from Siecor loose tube fiber optic cable that employs steel tape armor. This experiment indicates that the rerouting of data should not be necessary; however, each company should weigh this risk based on the sensitivity of the data being transmitted and the severity of their respective excavation requirements before blasting.

VI. ACKNOWLEDGEMENTS

Thanks should be extended to Brad Barringer of B.R.S. for providing the site, blasting materials and related excavation equipment.

Mark A. Setman

Siecor Corporation
489 Siecor Park
Hickory, NC 28603

Mark A. Setman received his B.S. degree in Civil Engineering from Bucknell University, Lewisburg, PA in 1978 and his M.S. in Engineering Management from the University of Missouri in 1982. He worked for four years as an Engineer Officer in the U.S. Army before joining Siecor Corp. in 1982. At Siecor, he held various engineering and staff positions supporting copper and fiber optic cable manufacturing. For the last three years, he worked as a Senior Applications Engineer.

Max J. Brandtner

Siemens AG
Hofmannstrasse 51
8000 Muenchen 70
West Germany

Max Brandtner received his M.S. degree in Electrical Engineering from the Fachhochschule in Munich in 1979. For two years, he was employed in the Sales Department of the Communication Cable Division of Siemens Corporation as a Sales Engineer. Beginning in 1981, he worked in the design and implementation of fiber optic test equipment. Max co-authored this paper during his time with Siecor Corporation working as the Supervisor of Measurement Systems from 1986 to 1988. He has recently returned to Siemens AG, Munich, West Germany as a Supervisor of Technical Sales for LAN products.

"A METHOD FOR EVALUATING OXIDATIVE STABILITY AND PERFORMANCE OF POLYOLEFIN INSULATIONS FOR FILLED TELEPHONE CABLES."

H.S. Aitken and V.B. Mascarenhas

Canada Wire and Cable Limited, Toronto, Canada.

ABSTRACT

There is conclusive evidence both from our prior studies and published data that, in filled cable, depletion of the stabilization system in polyolefin insulation occurs as a result of the manufacturing processes, the storage environment of the cable and the service environment of the cable. A long term programme was initiated to develop an accelerated laboratory scale test, to simulate these aging conditions and to predict the performance of different insulating materials and filling compounds in service. A material test procedure has been developed for evaluating the aging performance of polyolefin insulation systems. This procedure involves the simulation of processing, storage, and service parameters, using the components of filled cable systems, and is a meaningful laboratory scale test which does not require the use of completed cables. In addition, the study demonstrates the correlation between residual antioxidant activity and physical integrity of the insulation. Prediction of life expectancy of the insulation system, following depletion of the antioxidant, may be possible.

The information obtained from almost two years of evaluations using this technique advances the understanding of the behaviour of filled cable insulation systems and provides a basis for reliably predicting the performance and the life expectancy of filled cable systems.

INTRODUCTION

Since the introduction of fully filled telecommunications cables over 25 years ago, there has been an ongoing concern about the effect of cable filling on the life expectancy of polymeric insulations in current use.

When one scans previously published papers on this subject, some fifty odd papers presented at previous symposia alone, there seems to be general agreement by manufacturers as well as users of filled cables, that there is an undesirable interaction between the insulation and petrolatum filling compounds, however, at the service conditions, generally the effect is such that it does not significantly alter the overall service performance of the cable. Reports on performance of filled cables after some years of service suggest that indeed the cables are doing well[1,2].

Much of the work done prior to accepting a filled cable system for commercial cables has been done through accelerated aging tests. Canada Wire laboratories have been involved in this type of work since the late 1960's and is continually upgrading the evaluation techniques used in qualifying filled cable components. From earlier studies on polyolefins, it was confirmed that accelerated aging temperatures of 70°C or higher are to be avoided so that the results of the experiments would not be complicated by the second order transition point of medium density polyethylene (69-70°C) which was one of the materials under study. 55°C, 60°C and 65°C were the selected temperatures for this study, results of which formed a part of an IWCS paper[3]. 65°C is the upper aging temperature for the current program results of which are reported here. The program will continue to study and report on the filled cable system at lower temperatures.

Results of aging under exaggerated test conditions have shown that in time the stabilizing additives are depleted. Laboratory data has suggested that for buried cable this could be greater than 100 years and for aerial cable the depletion is understandably in less time. What happens to the insulation after complete depletion of stabilizing system? How long does the integrity of the insulation remain intact in the cable and at the terminals? It is hoped that information generated in this program will be helpful in confirming the life predicted for filled cables or provide evidence for further improvements of the system.

TEST PROGRAMME

Conductors insulated with commercially available cellular high density polyethylene, cellular medium density polyethylene and solid polyprorylene (ethylene/propylene copolymer) were selected for this work. The filling compounds selected were petrolatum type commonly used in the industry.

The insulated conductors were treated with hot filling compounds at a temperature and duration simulating the filling operation (105°C). They were then aged in the filling compounds at 65°C for predetermined intervals of time, followed by removal from the filling compounds and further aging in an air oven at 65°C. While the insulations were subjected to the above processes, the depletion of the antioxidant system was monitored by determining the Residual Antioxidant Activity using well established Thermal Analytical Techniques. Slightly different techniques were required for cellular insulations (REA Specification PE 89) and solid insulations (REA Specification PE 39). Simultaneously, the above samples were also tested for dimensional change, and flexibility/dielectric strength. Dielectric test is used to determine the onset of cracking, since physical examination alone is not reliable for detecting the appearance of minute cracks which form as a result of embrittlement due to oxidation. This represents a major deviation from the methods used in other studies and is the leading reason for the enhanced accuracy of results and prediction of service life.

The Residual Antioxidant Activity data in conjunction with other test data allows for a more precise evaluation of compatibility and integrity of filled cable systems and promotes a more reliable prediction for the life of the insulation. An extension of this study was to determine the remaining life of the insulation after complete depletion of the stabilizer system, through aging of stressed (pigtailed) samples.

TEST METHOD

Apparatus

1. Forced Draft Oven: Any forced draft circulating air oven capable of maintaining the test temperature within ± 1°C and having inside dimensions large enough to accommodate several immersion trays. For this study, a Blue M Model Number POM2530C-1 (Internal Dimensions: Height 20", Width 24", Depth 30" and a Blue M Model Number POM2050 (Internal Dimensions: Height 14", Width 19", Depth 18", were used. Both

ovens were maintained at 200 air changes/hour.

2. Immersion Trays: Glass or Enamelled trays of a size which will allow for the immersion of specimens of insulated conductors of at least 18 inches in length once the tray has been filled with cable filling compound. For this study, enamelled tray with internal dimensions of 15½ inches in length, 9 inches in width and 2½ inches in depth were used.

3. Thermal Analyzer: Any thermal analyzer with a Differential Scanning Calorimeter capable of determining the Oxidation Induction Time of polyolefin insulations as described in RRA Specification PR 89 (Residual Antioxidant Activity after Processing). For this study a DuPont Series 99 Thermal Analyzer with a DuPont 910 Differential Scanning Calorimeter was used.

4. Dielectric Strength Tester: An apparatus capable of providing an AC potential (voltage) sufficient to cause dielectric failure in the insulation under test. The apparatus shall also be capable of applying the AC potential at a predetermined fixed rise of 500V AC per second. For this study, a Hipotronics AC Dielectric Test Set Model 760-5/10340 and an AC Dielectric Test Set designed and built in house were used.

5. Microscope/Magnifying Glass: An apparatus (magnifying glass or microscope) capable of providing 5 times magnification, for visual examination of insulated conductor. A hand held magnifying glass approximately 2½" in diameter was used here.

6. Micrometer: A micrometer capable of measuring the diameter of insulated conductors to the nearest 0.001 inches.

Materials Under Evaluation

1. Insulations

1. Cellular High Density Polyethylene (HDPE): #24 AWG Soft Bare Copper (SBC) conductor (insulation density: 0.640 g/cm³; insulation thickness: 0.008 inches nominal). The base resin conforming to ASTM D 1248, Type III, Class A, Category 4, Grade B9.

2. Cellular Medium Density Polyethylene (MDPE): #24 AWG (SBC) conductor (insulation density: 0.651 g/cm³; insulation thickness: 0.008 inches nominal). The base resin conforming to ASTM D 1248, Type II, Class A, Category 4, Grade B4.

3. Solid Polypropylene PP: #24 AWG (SBC) conductor (insulation thickness: 0.011 inches nominal). Ethylene/propylene copolymer conforming to ASTM D 4101, Class PP 200 B 40003 E 11.

2. Cable Filling Compounds

The two cable filling compounds are commercial grade petrolatum type compounds: Compound A is designed to meet RRA PR89 (Residual Antioxidant Activity and 80°C Compound Flow Test). Compound B is designed to meet 65°C Compound Flow Test and is formulated with only sufficient antioxidant to provide stability of the compound during processing. The typical properties of both filling compounds are given in Table I.

Sample Preparation

1. A plurality of 2 foot long specimens of each insulation type and colour to be studied were prepared. Based on previous studies sufficient specimens were prepared to allow for the evaluation of 2 specimens per month for a period of 3 years (plus 10% for potential retests, etc.). Specimens are aged in 2 grades of filling compound and in air, therefore, 238, 2 foot specimens were prepared for each insulation type and colour.

TABLE I

Typical Properties of Cable Filling Compounds

Property	Compound A	Compound B
Drop Melting Point, °C (ASTM D 127)	97	93
Cone Penetration @ 25°C, 1/10 mm (ASTM D 937)	43	45
Cone Penetration @ 65°C, 1/10 mm (ASTM D 937)	140	160
Dissipation Factor @ 1 MHz/25°C (ASTM D 924)	0.001	0.001
Dielectric Constant @ 1 MHz/25°C (ASTM D 924)	2.10	2.10
Volume Resistivity @ 100°C, ohm-cm (ASTM D1169)	1×10^{13}	5×10^{12}
Oxidation Induction Time @ 190°C Alum Pan, minutes	50	5

2. Specimens of each insulation are placed lengthwise in an empty sample tray such that the ends of each specimen extend approximately 3 inches beyond the sides of the tray. The trays containing the specimens are then filled with cable filling compound at a temperature equal to that used in cable production (105°C). After the compound has cooled and equilibrated to ambient temperature (about 25°C) two specimens of each type are removed from the compound for evaluation. The tray containing the remainder of the specimens is then placed in a circulating air oven which is maintained at 65°C. Two colours (Blue and Brown) for each of three insulation types (MDPE Cellular, HDPE Cellular and Solid Polypropylene) are immersed in two petrolatum type cable filling compounds (Type A with an antioxidant and Type B without an antioxidant). Specimens of each insulation type and colour are removed from both of the cable filling compounds at regular intervals (2 weeks, 1 month, 2 months... and late in 2 month intervals) for evaluation.

3. Untreated Specimens of each type and colour are also placed in empty trays and aged in air at 65°C and used as control samples. Specimens are taken and evaluated at the same intervals as those aged in cable filling compounds.

Fig. 1. Specimens prior to immersion in Cable Filling Compound.

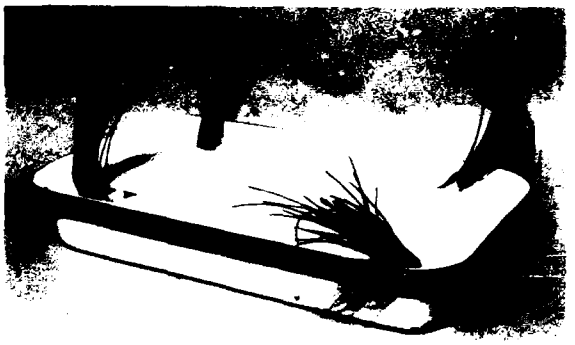

Fig. 2. Insulated Conductors Immersed in Cable Filling Compound.

Specimen Evaluation

Each specimen is evaluated for Residual Antioxidant Activity; Dimensional Change; Flexibility/Dielectric Strength; and Cracking of Pigtailed Specimens after Depletion of Antioxidant (when applicable).

Evaluation Procedures

1. Residual Antioxidant Activity: The Residual Antioxidant Activity of each specimen is measured as per REA Specification PE-89 for the cellular insulations and as per REA PE-39 for the solid insulation, except the cable conditioning (8h @ 68°C) is waved.

2. Dimensional Change: The diameter (D) is measured to the nearest 0.001 inches using a hand held dial micrometer, the mean average of 5 measurements is taken as the diameter.

3. Flexibility/Dielectric Strength: The dielectric breakdown voltage of each specimen is measured between the conductor and ground. The specimen is wiped carefully using a soft tissue, to remove any filling compound or foreign material from the insulation surface, then wound into a "pigtail". The "pigtail" is formed by making a one-inch loop in the centre of the specimen such that one end of the specimen crosses over the other end at approximately 90° and is wound six complete turns around the insulation (adjacent turns touching). See Fig. 3 below. Each specimen is examined for cracks at 5 times magnification. The "pigtailed" specimens are then placed in a solution of 5% (w/w) of Sodium Chloride in water, with the leads extending far enough above the solution such that flashover does not occur. The Dielectric Strength (breakdown voltage) of each specimen is measured in turn (voltage increased at a rate of 500V AC per second).

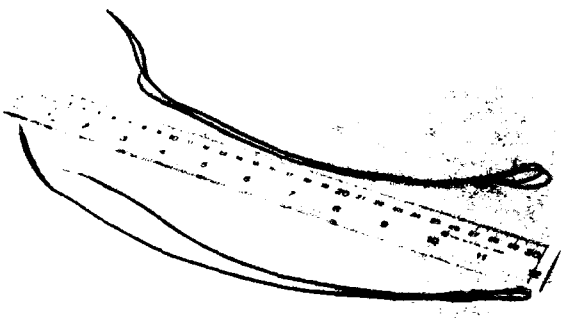

Fig. 3. Pigtailed Specimens.

Fig. 4. Pigtailed Specimens after Dielectric Strength Test. (Note blows occur in the stressed area of the insulation.)

4. Cracking of "Pigtail" Specimens after Depletion of Antioxidant (AO): When the Residual Antioxidant Activity (O.I.T.) of the insulating materials becomes one minute or less and the AO is considered depleted, 3 specimens of the appropriate insulating material are formed into pigtails and aged in this configuration, in air at 65°C. The pigtailed specimens are examined weekly for cracks at 5 times magnification, if no cracks are observed the specimens are returned to the oven for further aging.

RESULTS

1. Residual Antioxidant Activity (O.I.T.) - Refer to Figures A thru I in Appendix 1.

HDPE Cellular

Aged in Air @ 65°C: The O.I.T. of HDPE aged in air at 65°C decreases gradually with time. After 20 months an O.I.T. of 10 minutes for both the Blue and Brown insulations indicates that the AO is still active and offers the insulating material protection against oxidative degradation.

Aged in Cable Filling Compound A @ 65°C: The O.I.T. of HDPE aged in compound A decreases dramatically during the first 2 weeks of aging at 65°C, after 2 weeks the reduction in O.I.T. is very gradual and after 20 months the AO would appear to be still active. It is noteworthy that the much of reduction in O.I.T. during the first 2 weeks is the result of the simulated filling operation (exposure of the insulating material to the cable filling compound at 105°C). Prior to the simulated filling operation, the Blue HDPE Cellular insulation had an O.I.T. of 80 minutes and the Brown 100 minutes, after the simulation of the filling operation, the Blue had an O.I.T. of 48 minutes and the Brown 46 minutes. No O.I.T.'s of 1 minute or less have been observed after 20 months of aging and therefore aging of pigtailed specimens has not been initiated so far.

Aged in Cable Filling Compound B at 65°C: The observations made for Compound B are generally the same as for Compound A, including the dramatic effect of the simulated filling operation on the O.I.T. of both the Blue and Brown insulation. The most significant difference in the behaviour of HDPE Cellular in Compound B versus Compound A, is the earlier depletion of AO in specimens removed from Compound B (Brown specimens at 10 and 12 months).

Specimens of the HDPE cellular aged in Compound B, pigtailed and further aged in Air (Cracking of Pigtailed Specimens after Depletion of Antioxidant) show no evidence of failure after 8 months at 65°C.

MDPE Cellular

Aged in Air @ 65°C: The O.I.T. of MDPE aged in air at 65°C decreases gradually with time. After 20 months O.I.T.'s of 9 minutes for Blue and 5 minutes for Brown indicates that the AO is still active and offers the insulating material protection against oxidative degradation.

Aged in Cable Filling Compound A @ 65°C: As is the case when HDPE is aged in Compound A a dramatic reduction in O.I.T. of the insulation occurs during the first 2 weeks, after which the reduction in O.I.T. is very gradual. Again as with HDPE the filling operation is most responsible for reduction of O.I.T., the Blue had an O.I.T. of 91 minutes prior to the filling operation and the Brown 92 minutes, filling reduced the O.I.T. to 55 and 65 minutes respectively. After 20 months O.I.T.'s of 7 minutes for the Blue insulation and 9 minutes for the Brown insulation, suggests that the AO is still active.

Aged in Cable Filling Compound B @ 65°C: Observations made for samples aged in Compound B are generally the same as those for Compound A, excepting that the O.I.T. of the Brown insulation after 18 months had reached zero minutes.

Specimens of Brown MDPE cellular aged in Compound B, pigtailed and further aged in Air (Cracking of Pigtailed Specimens after Depletion of Antioxidant) show no evidence of failure after 2 months at 95°C in Air.

Solid Polypropylene

Aged in Air @ 65°C: The O.I.T. of Solid Polypropylene aged in air at 65°C decreases gradually. After 20 months the O.I.T. of 19 and 21 minutes for the Blue and Brown insulations receptively indicates that the AO is still active.

Aged in Cable Filling Compound A @ 65°C: As noted above in the cases of HDPE and MDPE rapid reduction in the O.I.T. of PP occurs during the first 2 weeks of exposure to Compound A. O.I.T. data indicates that the filling operation has less effect on solid PP versus the cellular materials. The O.I.T. for PP prior to filling is 86 minutes for Blue insulation and 87 minutes for Brown insulation, after filling the O.I.T. is 71 minutes and 64 minutes for the Blue and Brown respectively. The O.I.T. of PP aged in Compound A has remained essentially constant between 2 weeks and 20 months exposure time at 65°C. O.I.T.'s of 5 minutes and 4 minutes for Blue and Brown PP insulation respectively indicates that the AO is still active and offers the insulations protection against oxidative degradation.

Aged in Cable Filling Compound B @ 65°C: The observations made for compound B are generally the same as for compound A. The most noticeable difference in the behaviour of PP insulation in Compound B versus Compound A is the earlier depletion of AO as a result of aging in Compound B (both Blue and Brown specimens exhibit O.I.T.'s of less than 1 minute after only 7 months in Compound B at 65°C).

Specimens of Solid PP aged in Compound B, pigtailed and further aged in Air, show no evidence of failure after 13 months at 65°C.

2. Dimensional Change

The change in the diameter of the insulated conductors is measured at regular intervals during the aging period. Diameter changes observed on specimens aged in Air was considered insignificant and within normal variation for products manufactured on a high speed insulating line. Diameter changes observed on specimens aged in both Compound A and Compound B, are small, but significant, indicating that the filling compounds or components of the filling compounds are absorbed by the insulation materials. Results are given in Table II.

3. Flexibility/Dielectric Strength

HDPE Cellular: HDPE Cellular insulation, both Blue and Brown, exhibits excellent retention of Dielectric Strength even after 20 months at 65°C in Air, Compound A and Compound B. This excellent retention of Dielectric Strength suggests that the flexibility of HDPE Cellular remains essentially unaffected after 20 months. Refer to Figures J, K and L in Appendix 2.

MDPE Cellular: The comments made for HDPE Cellular Insulation above, hold true for MDPE Cellular. See Figures M, N and O in Appendix 2.

Solid PP: Solid PP insulation, both Blue and Brown exhibits excellent retention of Dielectric Strength even after 20 months at 65°C in Air, Compound A and Compound B, in fact insulation aged in Compound A & B, show a large increase in Dielectric Strength. This excellent retention of Dielectric Strength suggests that the flexibility of Solid PP does not deteriorate after 20 months. Refer to Figures P, Q and R in Appendix 2.

4. Cracking of "Pigtail" Specimens after Depletion of Antioxidant (AO)

Specimens of insulated conductors which have reached complete depletion of antioxidant were "pigtailed" and are being aged in air at 65°C, very limited data is available at this stage. At this writing no cracking of the insulations being aged after depletion of antioxidant has been observed. The data is summarized in Table III.

TABLE II

	Cellular HDPE		Cellular MDPE		Solid PP	
	Blue	Brown	Blue	Brown	Blue	Brown
Initial Dia. (inches)	0.037	0.036	0.038	0.036	0.043	0.043
Dia. after 20 months in Air @ 65°C (inches)	0.036	0.036	0.038	0.036	0.044	0.044
Dia. after 20 months in Compound A @ 65°C (inches)	0.038	0.038	0.040	0.040	0.045	0.045
Dia. after 20 months in Compound B @ 65°C (inches)	0.038	0.037	0.040	0.038	0.045	0.045

TABLE III

Insulation Type	*Cellular HDPE* Blue	Brown	*Cellular MDPE* Blue	Brown	*Solid PP* Blue	Brown
Aged in Air	1	1	1	1	1	1
Aged in Compound A	1	1	1	1	1	1
Aged in Compound B	1	2	1	3	4	4

1 = Tests not started, complete depletion of AO has not been reached.

2 = No cracking after 8 months, test continuing.

3 = No cracking after 2 months, test continuing.

4 = No cracking after 13 months, test continuing.

CONCLUSION:

A method for evaluating stability and performance of polyolefin insulations in filled cable systems has been developed. This method does not require the use of completed cables and is useful for qualification of insulations and filling compounds or their combinations. The use of dielectric strength failure to determine the onset of crack formation in the insulation enhances the accuracy of determination of failure point and will provide a more realistic prediction of service life of the system. Aging of insulations after depletion of antioxidant is continuing, results so far suggest that there is indeed life after complete depletion of the antioxidant.

REFERENCES

1. Pritchett, J., Mather, B.L. and Verne, S., "Fully-Filled Cable with Cellular Polyethylene Insulation after 10 years Service" 24th IWCS, 1975.

2. Englehart, W.H. and Hayes, R.D., "An Analysis of Field Performance of Cellular Insulated Filled Telephone Cable after a Decade of Service", 35th IWCS, 1986.

3. Boll, C.R., "The Aging of Filled Cable with Cellular Insulation", 27th IWCS, 1978.

Hal S. Aitken graduated from Centennial College of Applied Arts and Technology in 1976. He joined Canada Wire and Cable Limited, Toronto, Ontario, Canada in 1977 and is currently Senior Engineering Technologist (Chemical).

Vieney B. Mascarenhas received his MSc degree in Chemistry from the University of Bombay (India) in 1960. He worked for a total of nine years in cable manufacturing plants in India. He joined Canada Wire and Cable Limited, Toronto, Ontario, Canada, as a member of Corporate Materials Development Laboratory in 1969 and is currently Supervisor of the Laboratory. He is first Vice-President of Communications Section of the Insulated Cable Engineers Association (ICEA).

APPENDIX I

Fig. A
HDPE CELLULAR

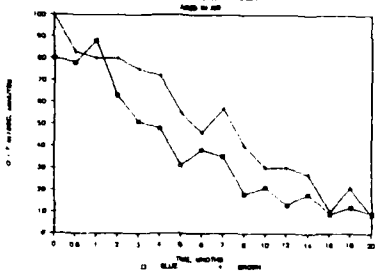

Fig. B
HDPE CELLULAR

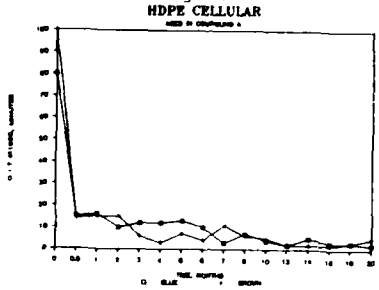

Fig. C
HDPE CELLULAR

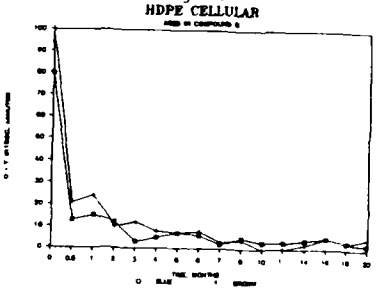

Fig. D
MDPE CELLULAR

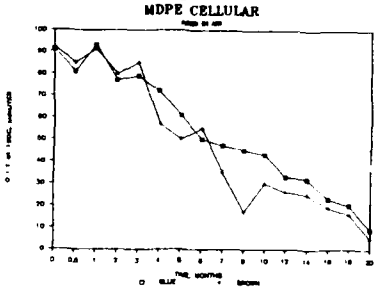

Fig. E
MDPE CELLULAR

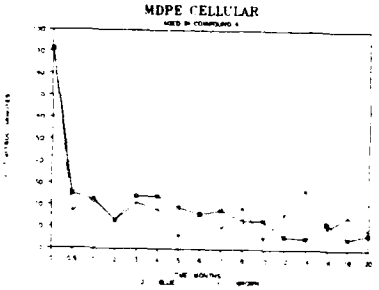

Fig. F
MDPE CELLULAR

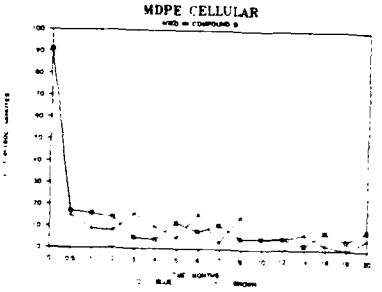

Fig. G
SOLID POLYPROPYLENE

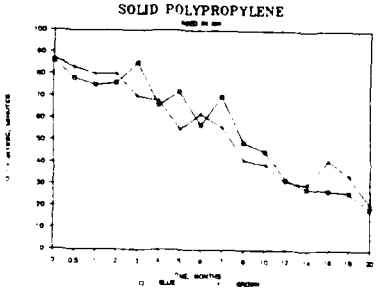

Fig. H
SOLID POLYPROPYLENE

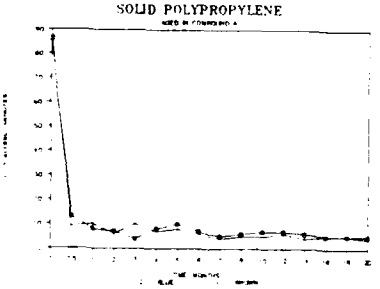

Fig. I
SOLID POLYPROPYLENE

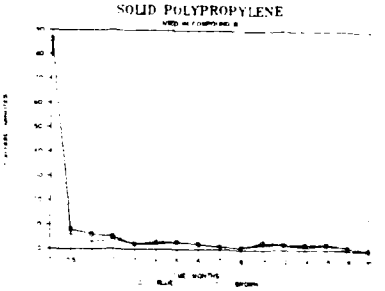

APPENDIX II

Fig. J
HDPE CELLULAR

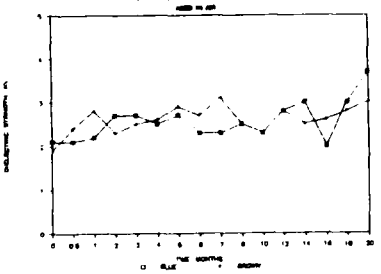

Fig. K
HDPE CELLULAR

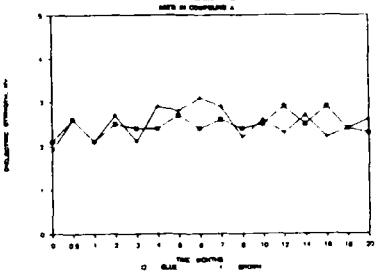

Fig. L
HDPE CELLULAR

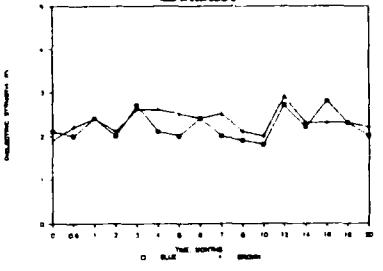

Fig. M
MDPE CELLULAR

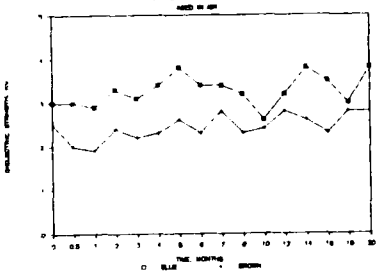

Fig. N
MDPE CELLULAR

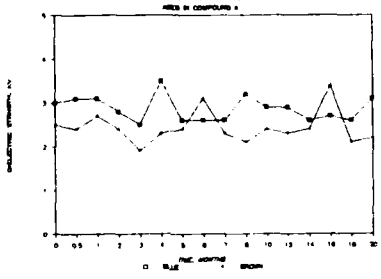

Fig. O
MDPE CELLULAR

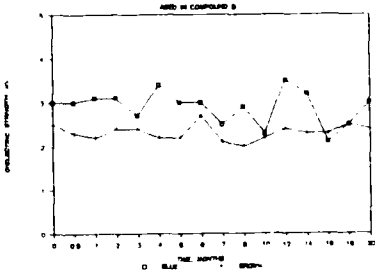

Fig. P
SOLID POLYPROPYLENE

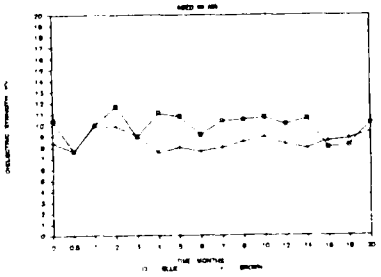

Fig. Q
SOLID POLYPROPYLENE

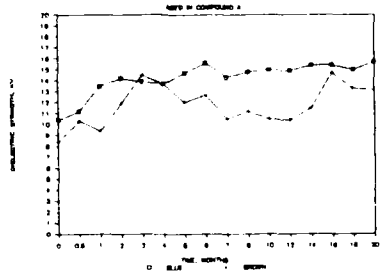

Fig. P
SOLID POLYPROPYLENE

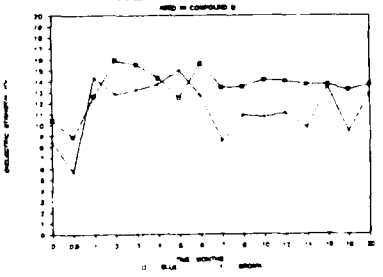

INVESTIGATION ON THE RHEOLOGICAL CHARACTERISTICS OF FILLING COMPOUNDS FOR OPTICAL FIBRE CABLES

R.W.Corne, J.Broad

DUSSEK CAMPBELL LIMITED,

THAMES ROAD, CRAYFORD,KENT DA1 4QJ,ENGLAND

Abstract

The use of a controlled stress rheometer to characterise nine optical fibre transmission cable tube filling compounds. The properties investigated include flow, low shear flow, thixotropic recovery and compliance.

The use of the rheometer highlights how much information is missed when conventional techniques alone are used to characterise filling compounds(eg cone penetration).

Introduction

In Europe and the UK the current trend is for softer and softer compounds for use as tube fillers in optical fibre transmission cables. The result of this trend is that conventional techniques for the characterisation of the compounds are no longer effective. We believe that far more information can be obtained on these compounds by the use of a controlled stress rheometer. This instrument allows the measurement of parameters that not only fully characterise but also predict the processing and "in tube" performance of very soft filling compounds.

Rheological measurements using a controlled stress rheometer with a parallel plate measuring configuration have been made on nine soft tube filling type compounds. These being based on three different oils with three gelling mechanisms as shown in Table 1.

Method

Flow

The flow investigation was carried out using a "flow curve" technique. Stress is applied to the sample, increasing linearly over a known time period, in this case, one minute. The angular velocity of the measuring head is sampled one hundred times during the run. From these values a graph of viscosity against shear rate is produced.

Measurements were made initially on the three base oils over the range of shear rate from 10 to 1000 sec^{-1}. The results are presented in Fig 1. Whilst the mineral oil and polybutene behave as a Newtonian Fluid, the polyalphaolefin shows a slight viscosity change over the range of shear rate.

The flow curve for a typical gel shown in Fig 1. shows a far more significant change in viscosity, reduced by a factor of 100 by the shearing action. At high shear rates, the gel viscosity approaches that of the base oil. In fact, one would not expect the gel viscosity to reach the base oil viscosity due to the thickening effect of an inert particulate filler.

Flow curves for the silica gelled compounds and the associated base oils are shown in Fig.3. It is noted that whilst the mineral oil and polybutene based gels show parallel curves, the gelled polyalphaolefin curve has a steeper gradient, indicating a greater sensitivity to shear.

A possible cause for this effect is that both mineral oil and polybutene contain at a wide distribution of carbon numbers, whereas polyalphaolefin is a'very narrow cut' material, which may interact differently with the silica gellant.

The flow curve technique can be taken a stage further by applying linearly reducing stress. Again, the angular velocity is sampled on hundred times over a further one minute time period to produce information on the recovery characteristics of the material. A flow and associated recovery curve is shown in Fig 4. If viscosity were solely dependant on shear, i.e: pseudoplastic, the recovery curve would be superimposed on the flow curve. Here, the recovery characteristic has the additional element of time dependency. This time dependant, pseudoplastic nature is known as thixotropy.

Flow and recovery curves for the silica gelled compounds are shown in Fig 5. All show a similar, partial recovery effect.

The second gelling system investigated was the combination of pyrogenic silica with a thixotropy modifier. A comparison of a modified gel with its unmodified version and base oil shown in Fig 6. The two systems show parallel flow curves suggesting that the sensitivity to shear has not been affected. However, the modified system shows a lower overall viscosity, and under the conditions of this experiment (i.e. controlled stress reduction) shows no recovery. In fact the material does recover but not within the timescale of this experiment. Recovery characteristics are examined in more detail in a later experiment.

The complete series of modified gels is presented in Fig 7. All flow curves show a similar gradient to the unmodified gels, indicating no change in shear sensitivity but the recovery curves all show a significant increase in the time dependant factor.

The third gelling mechanism investigated was produced by gelling the base oils with a small percentage of low density polyethylene. This type of gel is designed to be processed at around 120°C and therefore flow measurements made at ambient temperature do not, in this case, represent processing conditions, but have been included to show the characteristics of the material. Flow and recovery properties are shown in Fig 8. All three gels behave in a similar manner showing a reduction in viscosity on shearing and a small degree of recovery. A further experiment was carried out on this group of materials in which the sample was applied at 120°C and allowed to cool in contact with the measuring head. Flow curves produced by this method are presented in Fig 9. A higher initial viscosity and a greater degree of shear thinning was evident along with greater recovery. These findings support the theory that the rheological properties of this type of material are highly dependant on the shear history of the sample and can be reconstituted on heating above the melting point.

2. Recovery

The information on recovery properties generated by the previous technique is very limited. There are alternative techniques for assessing recovery, one such is described here. The sample was pre-sheared at a high shear rate (1000 sec^{-1}) until a constant viscosity reading was obtained. At this point the stress was removed, and the measuring head allowed to reach equilibrium (i.e. stationary). As soon as equilibrium was reached (after about 15 seconds) a very low constant stress was applied and the angular velocity of the measuring head recorded over an extended time period.

From these results, a graph of viscosity building with time was plotted. An example of this is shown in Fig 10. In this example, taking the time for a ten fold viscosity increase, the recovery time for the modified silica gelled system is doubled, compared to silica only analogue. This technique was found to have two limitations. Firstly, some materials tested recovered within the 15 second equilibriating period, and therefore no absolute measurements could be made. Secondly, the need to apply some shear, however small, may delay or inhibit recovery of particularly shear sensitive materials. Further results are shown in Fig 11 on a modified time base scale to include the delay period. The limitations are highlighted by the polyalphaolefin based gels recovering within 15 seconds and the modified silica gelled mineral oil showing, as in previous experiments, no recovery under stress.

Owing to the shear history phenomena experienced with the polyethylene gelled systems it was felt beyond the scope of this paper to include them in this experiment.

3. Low Shear Rate

Investigation of flow at relatively high shear rates and of recovery within a relatively short time period were an attempt to assess the processing characteristics of the filling compound.

A further investigation was required to assess the characteristics of the filling compound under service conditions. The object of loose tube construction is to allow free movement of the fibre in the event of the cable being distorted. To achieve free movement, the filling compound must exhibit little resistance to cut through or exhibit a high compliance.

Measurements of very low shear rates were made by means of a creep technique. A series of 10 stress levels was applied to the sample in turn, each after an equilibriating period. These stress levels were in fact below the measured yield stress of the material. A deviation of the measuring head with time was recorded for each stress level. On compiling this data a graph of viscosity against shear rate was produced. An example of such is shown in Fig 12. Such measurements are beyond the scope of conventional equipment.

Fig 13 shows a graph of the combined low shear and high shear results and demonstrates a very good agreement between the two methods.

Fig 14 and Fig 15 show the results obtained from low shear measurements on the modified silica gels and the polymer gels. Although not in as great detail, the general trend is evident that all types of gel examined here exhibit extremely high viscosities at low shear rates.

At very low shear rates such as may be incurred by thermal expansion of the cable it is likely that the fibre doesn't actually cut through these types of gel, but instead is held firmly in place. Some would agree this an advantage in that the fibre remains buffered while others would suggest this is a disadvantage in that the fibre has restraining forces exerted on it.

4. Creep

Until this point we have examined the viscous properties of the material. If we are to suppose that at low shear rates the fibre does not cut through the gel but is allowed to move by temporary deformation, then we must examine the elastic properties of the gel.

One technique for measuring such properties is called Creep in which a constant known stress is applied to the material under test and the resultant strain measured. The strain is measured by monitoring angular displacement. In practice a plot of compliance, which is the ratio of strain to stress, against time is obtained. Fig 16 shows a compliance curve one would expect for a material that exhibits a viscoelastic response at low stress. As can be seen when the stress is removed there is a partial recovery back to the original state.

Fig 17 shows a compilation of the compliance curves obtained on the materials, as can be seen the majority show classic viscoelastic behaviour at low stress. The significance of these results to the cable maker and the performance of an optical fibre cable is difficult to assess and is beyond the scope of this paper.

Conclusions

The flow data obtained for each of the nine compounds gives a more reliable and detailed characterisation of very soft tube filling compound than cone penetration.

To fully utilise the low shear rate and compliance data generated by the controlled stress rheometer more work is required to assess the levels of shear stress and shear rate fibres exert on compounds during the normal service of an optical fibre cable.

References

1. "Rheology" by F Walter (Chapman and Hall).

2. "Rheology: Industrial Applications" Ed. by P [illegible] (Wiley and Sons).

3. "[illegible]" by P W Atkins, W H Freeman [illegible].

4. "[illegible]" by P W Bamm, [illegible]

ROB CORNE
DUSSEK CAMPBELL LTD
THAMES ROAD
CRAYFORD, KENT DA1 4QJ
ENGLAND

Rob Corne is Chief Chemist of the Cable Products Development Laboratory at Dussek Campbell UK Ltd. Prior to joining Dussek Campbell, he worked on the development of cable filling compounds at BICC. Rob has an HNC in Applied Physics and is a Graduate of the Plastics and Rubber Institute.

JOHN BROAD
DUSSEK CAMPBELL LTD
THAMES ROAD
CRAYFORD, KENT DA1 4QJ
ENGLAND

John Broad is a Senior Development Chemist in the Cable Products Development Laboratory at Dussek Campbell UK Ltd. He is engaged in the development of filling compounds for optical transmission cables. John is a Chartered Chemist and a Member of The Royal Society of Chemistry.

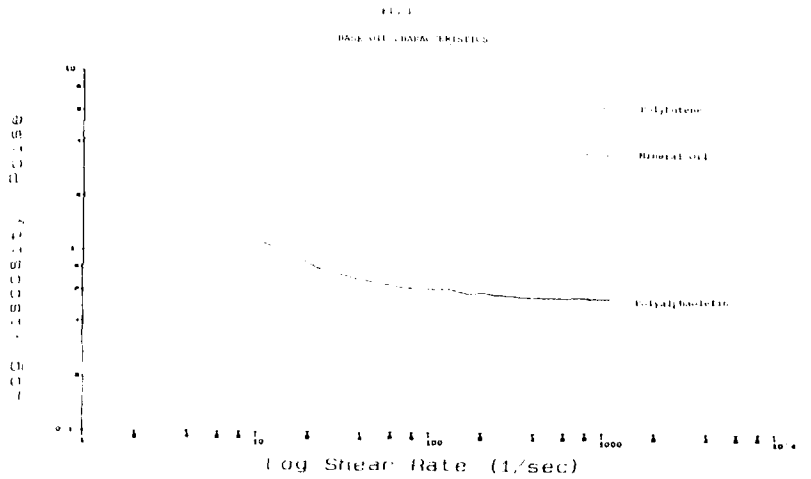
Log Shear Rate (1/sec)

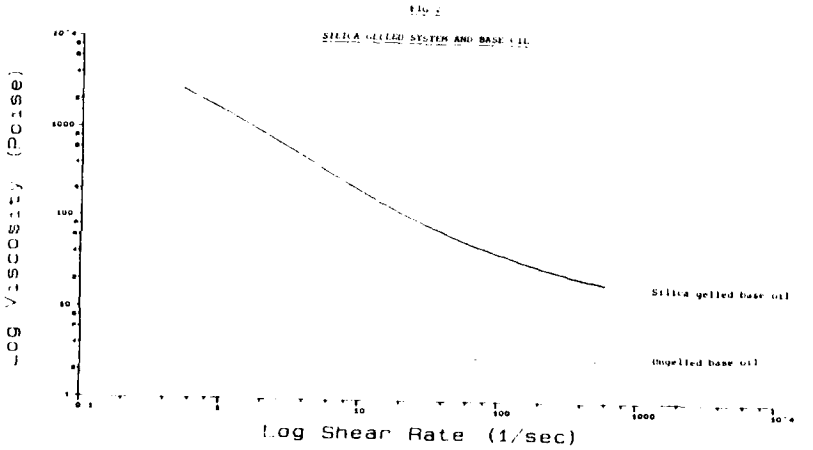
Log Viscosity (Poise)
Silica gelled base oil
Ungelled base oil
Log Shear Rate (1/sec)

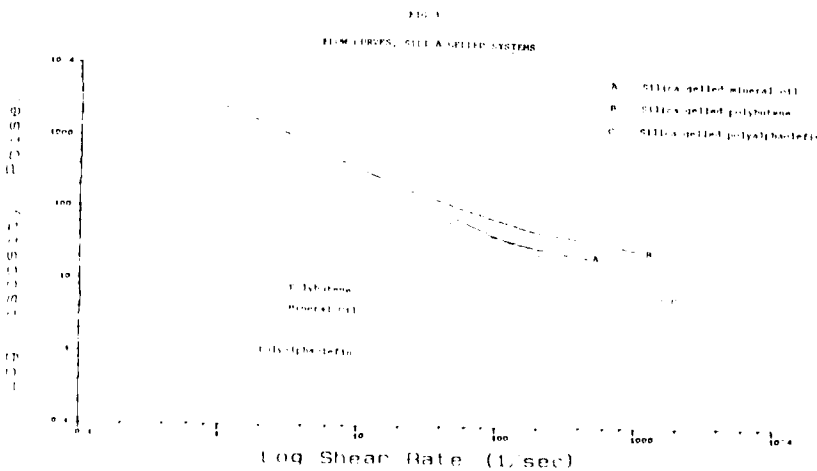
Log Viscosity (Poise)
Log Shear Rate (1/sec)

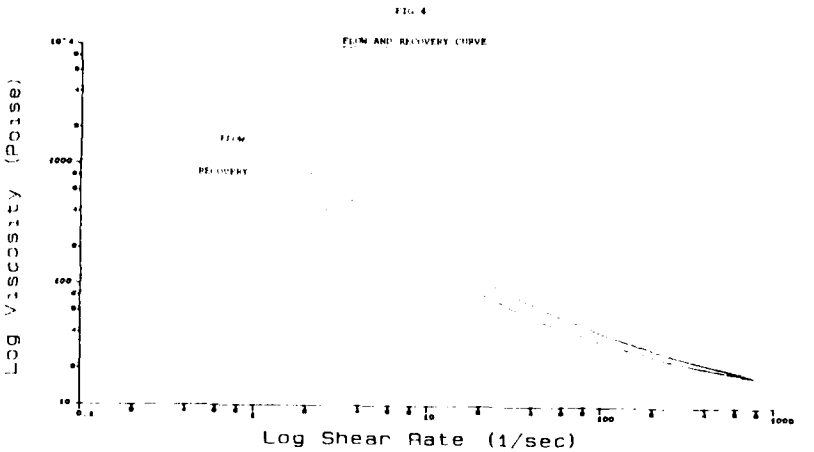
Log Viscosity (Poise)
Log Shear Rate (1/sec)

FIG 5

FLOW AND RECOVERY CURVES SILICA GELLED SYSTEMS

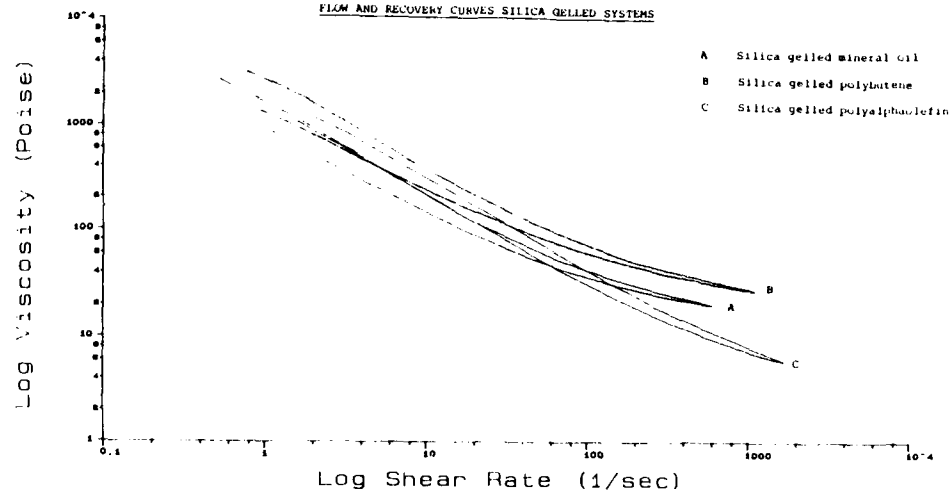

FIG 6

EFFECT OF THIXOTROPY MODIFIER

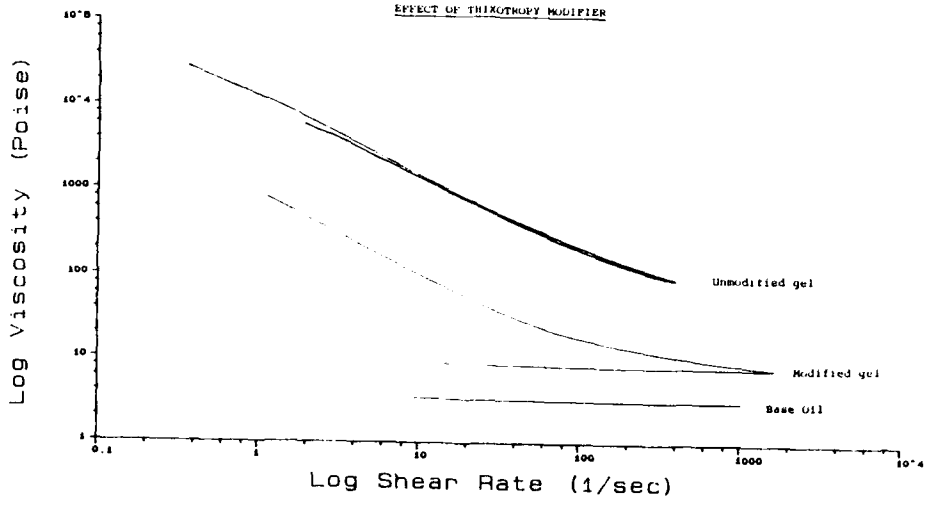

FIG 7

FLOW AND RECOVERY CURVES, MODIFIED SILICA GELLED SYSTEMS

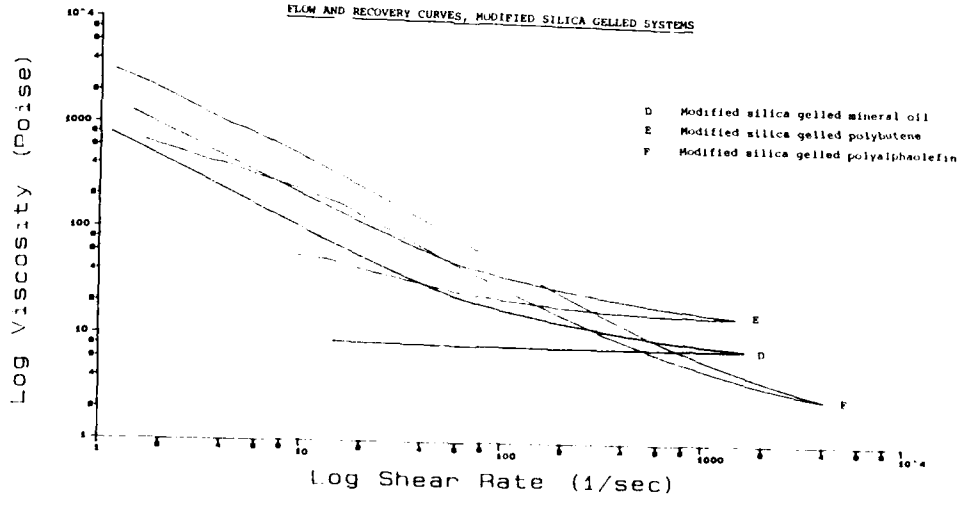

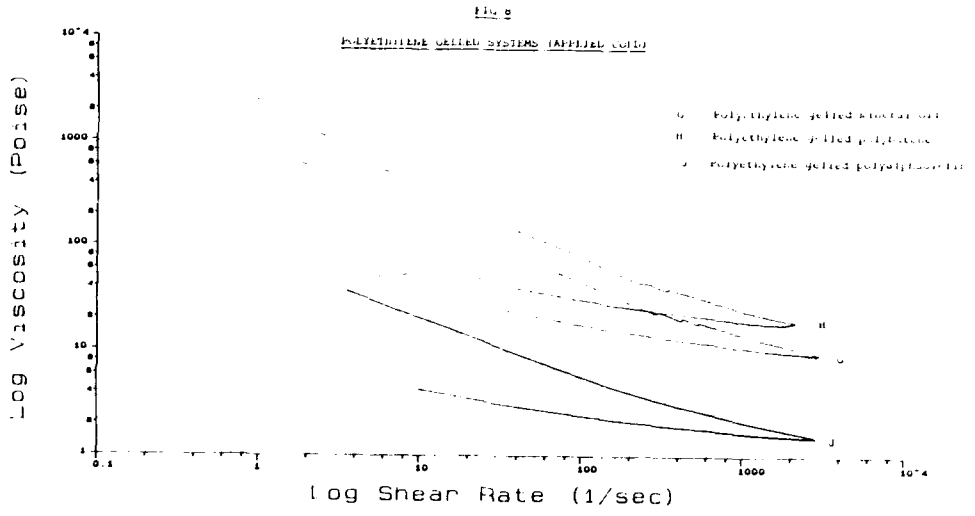
Log Viscosity (Poise)
Log Shear Rate (1/sec)

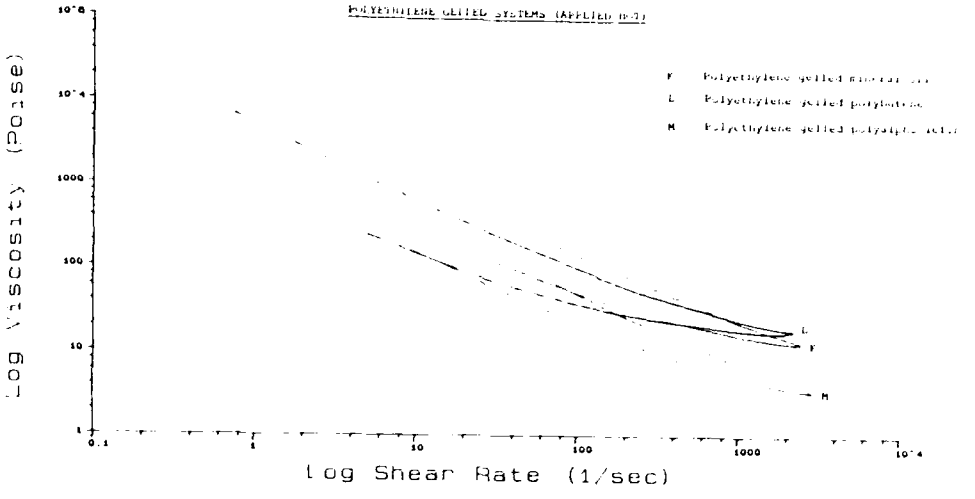
Log Viscosity (Poise)
Log Shear Rate (1/sec)

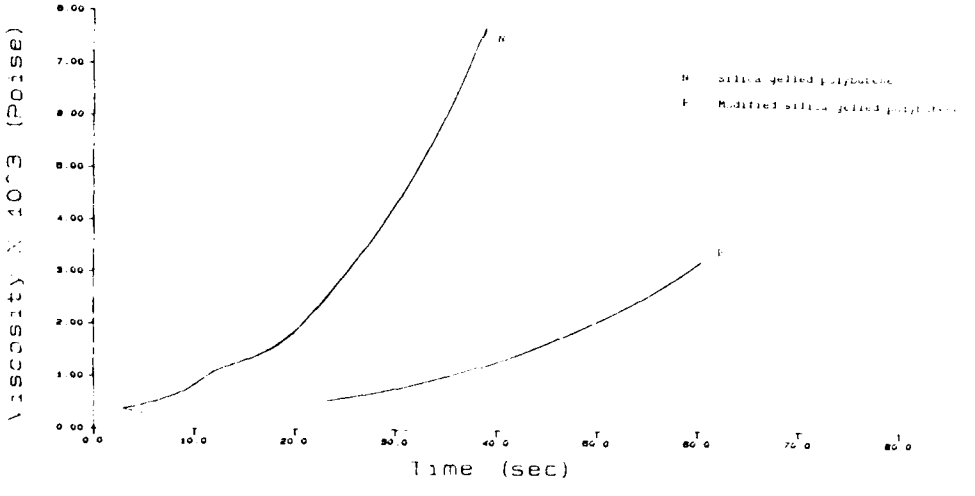
Viscosity x 10^3 (Poise)
Time (sec)

FIG 11

RECOVERY CHARACTERISTICS

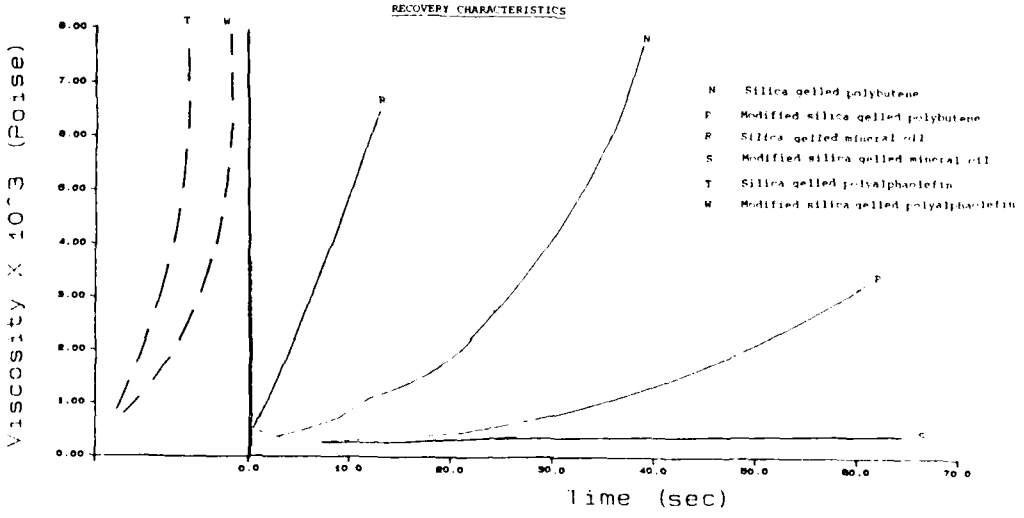

FIG 12

LOW SHEAR RATE

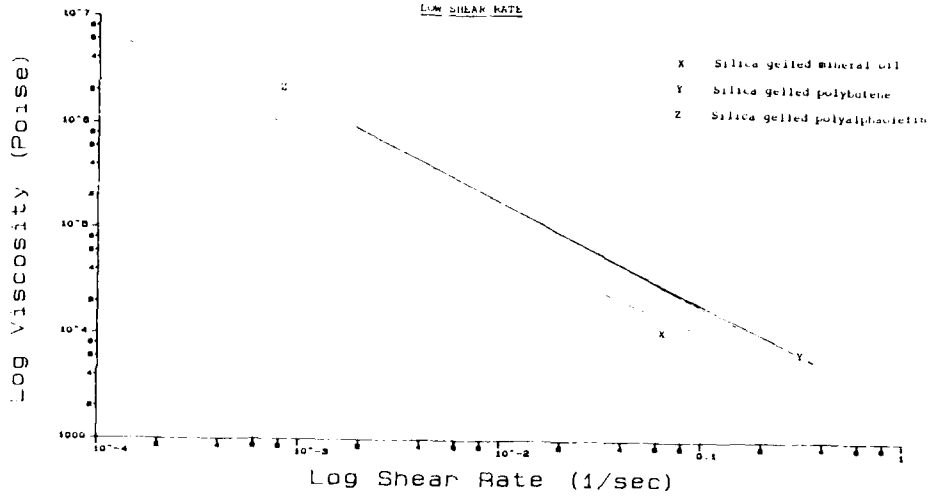

FIG 13

COMBINED HIGH AND LOW SHEAR RATE, SILICA GELLED SYSTEMS

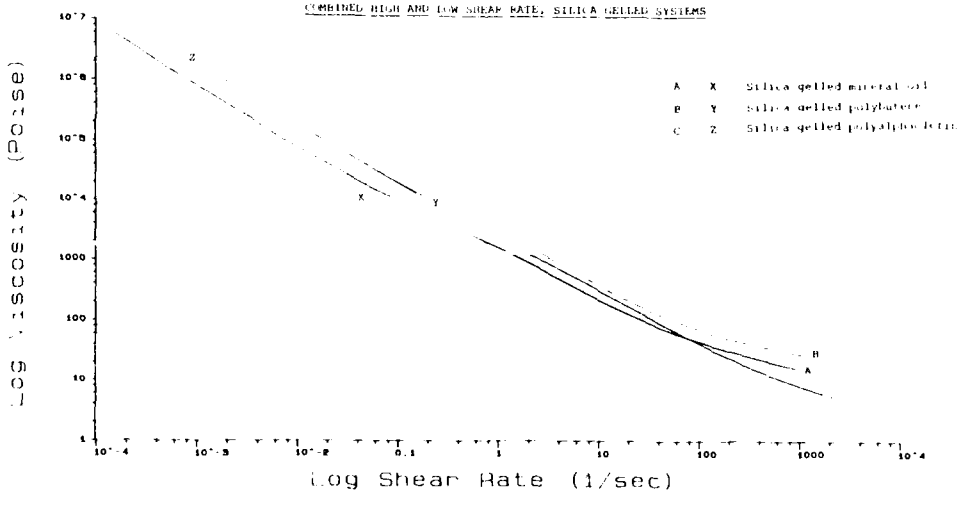

FIG 14

COMBINED HIGH AND LOW SHEAR RATES, MODIFIED SILICA GELLED SYSTEMS

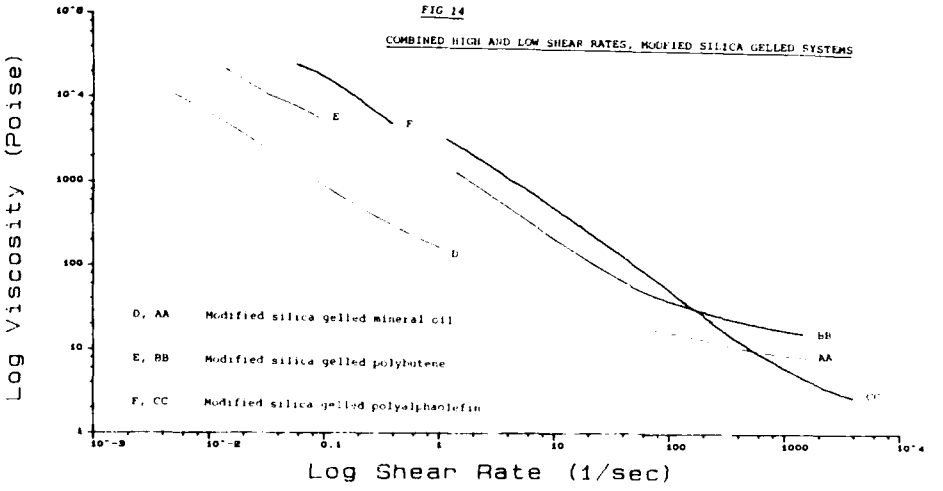

FIG 15

COMBINED HIGH AND LOW SHEAR RATES, POLYETHYLENE GELLED SYSTEM

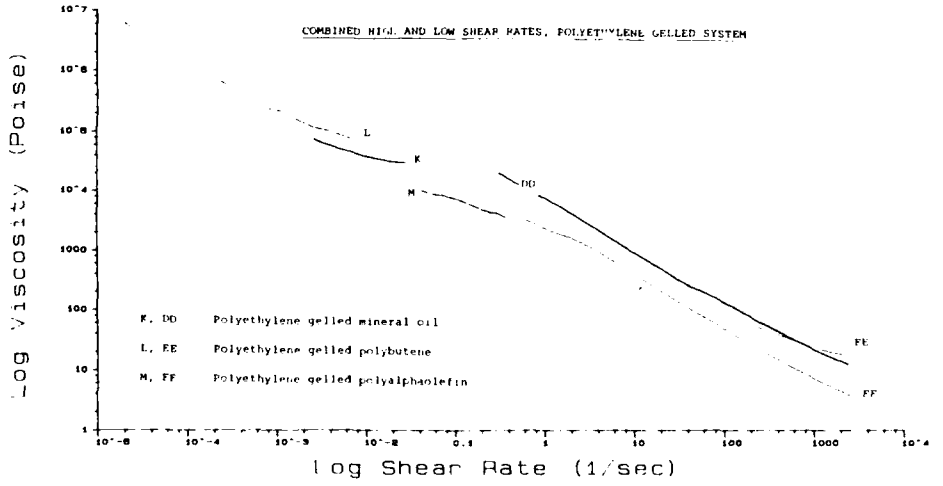

FIG 16

COMPLIANCE CURVE FOR A MODEL VISCOELASTIC MATERIAL

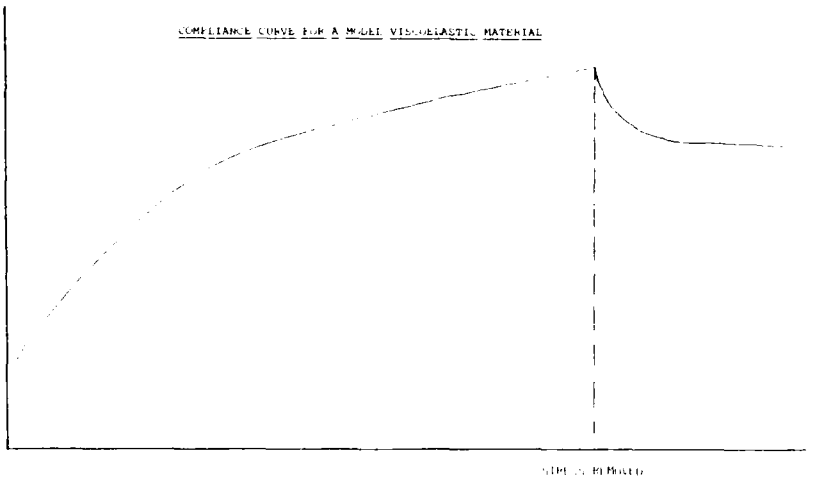

FIG 17

COMPLIANCE CURVE FOR COMPOUNDS IN MATRIX

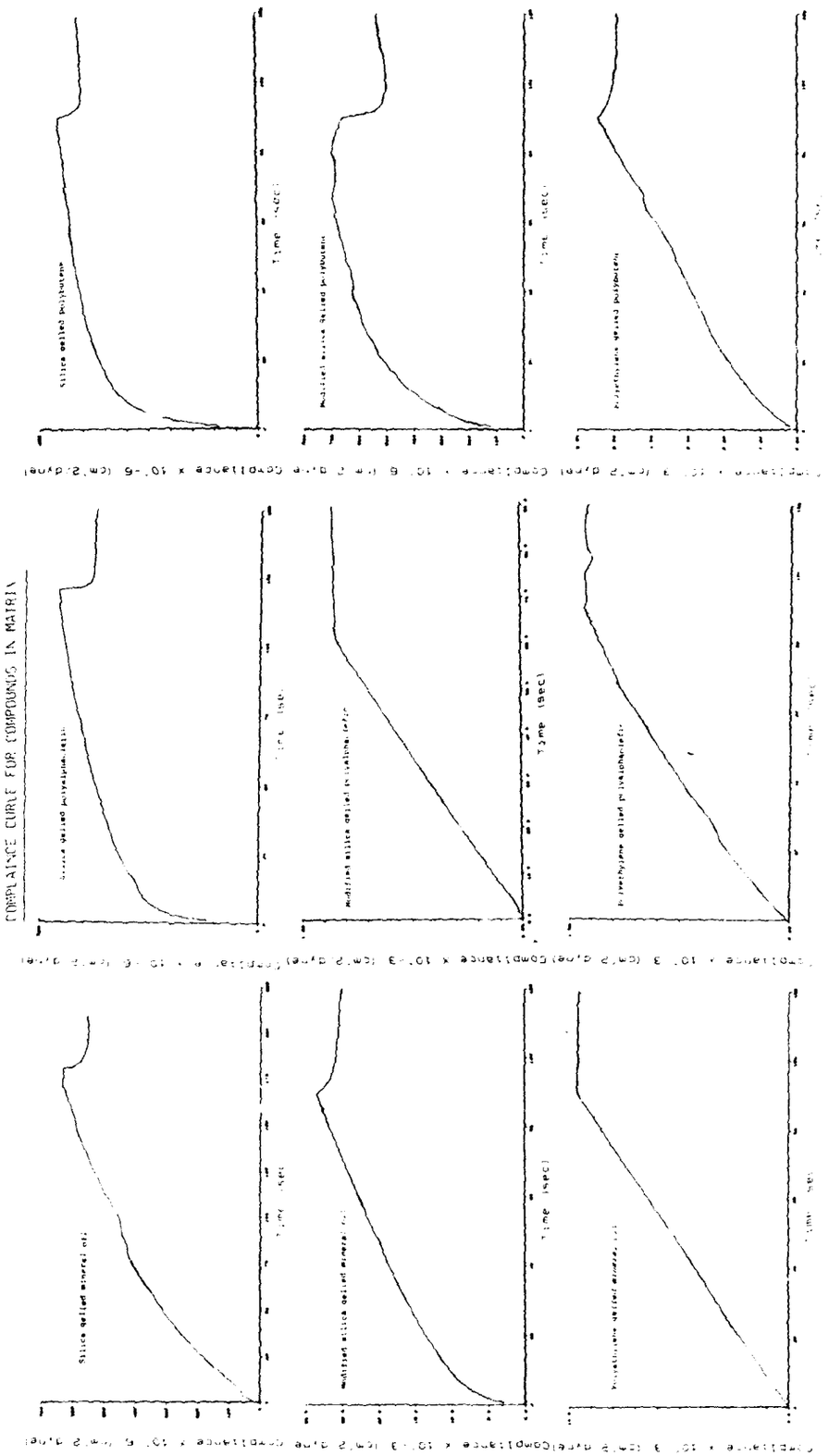

TABLE 1

	Pyrogenic Silica	Pyrogenic Silica +Thixtropy Modifier	Low Density Polyethylene
Mineral Oil	✓	✓	✓
Polybutene	✓	✓	✓
Polyal-phaolefin	✓	✓	✓

TABLE 2

Table 2 gives the physical characteristics normally available on compounds of this type.

TEST	Mineral Oil + Silica	Polybutene + Silica	P.A.O. + Silica	Mineral Oil + Silica + Modifier	Polybutene + Silica + Modifier	P.A.O. + Silica Modifier	Mineral Oil + LDPE	Polybutene + LDPE	P.A.O. + LDPE
Cone Penetration @ -40°C	74	218	278	70	180	300	45	151	380
Cone Penetration @ -30°C	111	278	289	162	305	334	-	-	-
Cone Penetration @ -20°C	267	329	308	205	314	337	-	-	-
Cone Penetration @ -10°C	>350	334	321	300	>350	>350	-	-	-
Melting Point °C	Non-Melting	Non-Melting	Non-Melting	Non-Melting	Non-Melting	Non-Melting	92	93	92

AN OIL SEPARATION TEST TO PREDICT ELEVATED-TEMPERATURE DRIP PERFORMANCE OF OPTICAL CABLE BUFFER TUBE FILLING COMPOUNDS

Martin C. Light, Jr.
Siecor Corporation, 489 Siecor Park — RD&E, Hickory, NC 28603

1. ABSTRACT

A simple, repeatable test method to measure filling compound oil separation and predict cable drip performance was developed. The results of room temperature and elevated temperature oil separation testing on 11 filling compounds showed high correlation with drip test results. Threshold values of oil separation above which loose tube cable drip failures will likely occur were found to be 2% separation at 23°C, and 15% separation at 65°C and 80°C. Coupled with other rheological testing, this oil separation test can greatly aid in the understanding of filling compound behavior and the development of improved compounds and cables.

2. INTRODUCTION

2.1 BACKGROUND

A key component of loose tube optical cable designs is the filling compound (also referred to as the flooding or waterblocking compound). Most optical cable filling compounds are composed of blends of some of the following materials: natural or synthetic oils, petrolatum, waxes, gels, polymers, silicone oils, thickening agents, and thixotropic agents. Filling compounds should act to prevent the intrusion of water and other liquids into the cable, be non-volatile and non-reactive with cable materials, and be relatively stable across the cable operating temperature range.

Since filling compounds in fiber optic cables are composed of waxes, oils, and relatively low-molecular-weight polymers which can change consistency quickly at different temperatures – and since optical cables are often required to perform at temperatures above 60°C – cables are required to pass filling compound drip (or flow) tests. In tests of this type, segments of optical cables (30 cm to 50 cm) are vertically suspended in circulating-air ovens at elevated temperatures for a period of time and monitored for filling compound flow: *any* amount of filling compound dripping from the cable samples constitutes a failure in these tests.

2.2 CABLE DRIP TESTING DETAILS

While many cable compound flow or drip tests are used in the optical cable industry, three of the most widely used— Bell Communications Research (Bellcore)[1,2], GTE[3], and Rural Electrification Administration (REA)[4] — are detailed in Table 1. Prepared cable test segments are displayed in Figure 1. The highest test temperature encountered was the 80°C specified in *REA PE-90*.

FIGURE 1 — CABLE DRIP SAMPLES

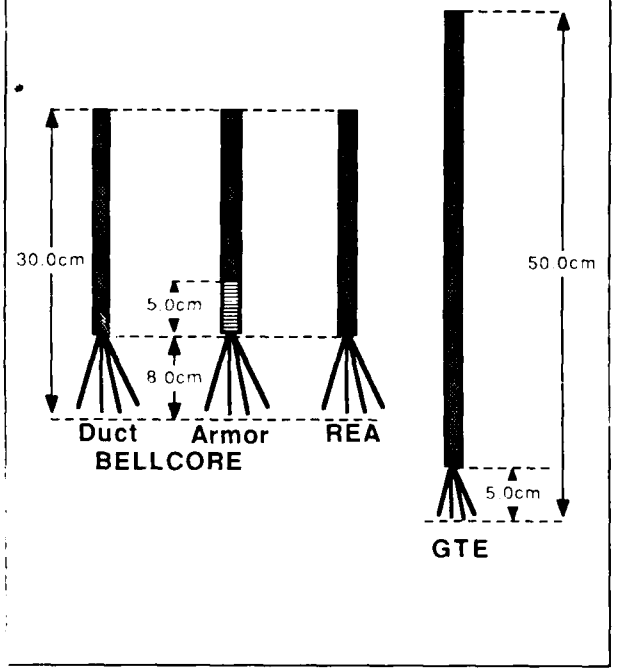

2.3 RATIONALE FOR A DRIP SCREEN TEST

Because of time and resource considerations, it is difficult to justify manufacturing lengths of fiber optic cable for the sole purpose of drip testing a new filling compound. It is desirable to establish a high probability that a given filling compound will pass all required drip tests before optimizing the many other processing variables needed to produce a high quality fiber optic cable. Thus, a number of test procedures have been developed to eliminate from consideration those compounds likely to fail when tested in cabled form.

Testing unjacketed, filling-compound-containing cable components — rather than segments of jacketed cables — is one way to screen filling compounds for drip test performance. These samples can be prepared and tested per the procedures detailed above; results are very similar to finished cable samples tested in the same manner. However, producing buffer tubes or cable core units still requires a significant amount of processing time and materials cost. A more suitable screening procedure would test some measurable filling compound characteristic which could be correlated to actual cable drip performance.

A test procedure based on ASTM D-1742, *"Oil Separation from Lubricating Grease During Storage"* [5], was reported in the 1987 IWCS proceedings.[6] In this procedure, a small container holding a sieve-strainer full of compound is placed under pressure at an elevated temperature. The amount of oil separating from the bulk of the material is weighed after the test completion. A high correlation was reported between results of this test and cable compound flow tests; however, this one-sample-at-a-time procedure was designed for copper cable filling compounds.

Another test procedure cited by filling compound manufacturers is the "cone bleed" test. In this test, a 100-ml filling compound sample is placed in a cone-shaped sieve, initially weighed, and subjected to an elevated temperature. The apparatus is cooled and reweighed, and the weight difference is reported as percent of the initial weight; the volume of oil collected under the cone can also be measured and reported. The results of this one-sample-at-a-time test are very dependent on the method used to fill the cone. Also, the sieve-cone can retain some oils more than others, contributing to misleading results.

The oil separation test described in the following sections is a simple, repeatable test which can be performed on fiber optic cable filling compounds with common laboratory equipment. Sample preparation consists of obtaining and dispensing a blended, deaired sample of filling compound. The test can be conducted at a variety of elevated temperatures and many samples can be tested simultaneously. Results are obtained within 48 hours.

3. EXPERIMENTAL PROCEDURES

3.1 OIL SEPARATION TEST DETAILS

Equipment — In addition to a thoroughly mixed and deaired sample of the filling compound tested, the following equipment was used to conduct oil separation tests: 10-ml disposable syringes, 11-cm diameter Type I Whatman filter paper, Pyrex watchglasses (12-cm diameter), 600-ml Pyrex beakers, lab spatula, analytical balance (accurate to ±0.0001

TABLE 1: DRIP TEST PROCEDURES

TEST CONDITION	BELLCORE	GTE	REA
Sample Length:	30 cm	50 cm	≥30 cm
Exposed Core Length:	13 cm (unarmored) 8 cm (armored)	5 cm	8 cm
Number of Samples:	Not specified	Not specified	3
Cap Unprepared End?:	Optional	No caps	Optional
Test Temperature:	65°C ± 2°C	60°C ± 2°C (tube filling) 70°C ± 2°C (core flooding)	80 C ± 1 C
Preconditioning Time:	72 hours (optional)	None	None
Test Time:	24 hours	24 hours	24 hours
Failure Criteria:	No drips (<1% wt. in preconditioning)	No drips	No drips

gram), tweezers, scissors, and circulating-air ovens set to the test temperature (± 1°C).

Procedure — The mixed and deaired filling compound was loaded into a syringe with a lab spatula. Care was taken to prevent introducing air bubbles into the compound. After the syringe was filled, the plunger was replaced and slowly depressed until compound flowed from the syringe.

One 11-cm circle of filter paper was weighed on the analytical balance (all weights to ± 0.0001 gram) and placed onto a labeled Pyrex watchglass.

A number of 2.6-cm (± 0.1 cm) squares were cut from another piece of filter paper with scissors. One of the 2.6-cm squares was weighed on the analytical balance. After the weight was recorded, 1 ml of filling compound was applied from the syringe onto the center of the square (in a circular dab with approximately a 0.5-cm space between the sample and any edge). The 1-ml volume dispensed was measured by reading the graduations printed on the syringe. Using tweezers, the sample-containing square was weighed. Care was taken to prevent moisture, skin oils, and other foreign particles from contaminating the sample and affecting the results.

Immediately after the sample-containing square was weighed, it was placed in the center of the filter paper circle, which had been previously weighed and put on the watchglass. The watchglass was then covered with an inverted 600-ml beaker and remained at room temperature (23°C ± 1°C) for 24 hours.

If additional samples were to be tested concurrently, they were prepared in the manner described above. It was found that one-at-a-time sample preparation enhanced test repeatability when compared to "assembly line" sample preparation. A minimum of 4 samples of each compound were prepared for each test temperature.

At the end of 24 hours at room temperature, the beaker was removed and the sample-containing square and the filter paper circle were separately weighed. After the weights were recorded, both were replaced on the watchglass and the apparatus was transferred to a preheated circulating-air oven at the desired temperature. The watchglass was again covered with the 600-ml beaker and left undisturbed for 24 additional hours in the oven.

At the end of the additional 24 hours, the watchglass assembly was removed from the oven and allowed to cool on a marble surface for approximately 5 minutes. The sample-containing square and filter paper circle were again separately weighed, and the results recorded. After noting any unusual visible changes in the sample, the sample and filter paper were discarded. The watchglass and beaker were cleaned with a solvent prior to any future testing.

Calculations — During the course of the test procedure, sample identification and analytical balance weights were recorded in a laboratory notebook. Upon completion of a test, this information was then entered into a spreadsheet program running on a minicomputer to facilitate data analysis. The following designations were used for the weighing results:

WT 1 = filter paper square weight
WT 2 = initial weight of sample-containing square
WT 3 = initial weight of filter paper circle
WT 2A = post 24 hrs at 23°C sample-square weight
WT 3A = post 24 hrs at 23°C filter paper circle weight
WT 2B = sample-square wt. after 24 hrs at elevated temperature
WT 3B = filter paper circle wt. after 24 hrs at elevated temperature

The following calculations were made for each sample using the weights as listed above (bracketed numbers are used to indicate the value of previous calculations — *e.g.* [1.1] refers to the numeric result of equation 1.1 below). All calculated results were reported to the nearest 0.1% separation.

1.1 Initial Sample Weight = (WT 2) – (WT 1)
1.2 23°C Sample Weight Loss = (WT 2) – (WT 2A)
1.3 % Weight Loss at 23°C = [1.2] · 100 ÷ [1.1]
1.4 23°C Filter Paper Circle Weight Gain = (WT 3A) – (WT 3)
1.5 23°C Volatile Weight Loss = [1.2] – [1.4] if > 0
23°C Volatile Weight Loss = 0 if [1.2] – [1.4] ≤ 0
1.6 % Volatile Weight Loss at 23°C = [1.5] · 100 ÷ [1.1]
1.7 % Nonvolatile Weight Loss at 23°C = [1.3] – [1.6]
1.8 T°C Sample Weight Loss = (WT 2) – (WT 2B)
1.9 % Weight Loss at T°C = [1.8] · 100 ÷ [1.1]
1.10 T°C Filter Paper Circle Weight Gain = (WT 3B) – (WT 3)
1.11 T°C Volatile Weight Loss = [1.8] – [1.10] if > 0
T°C Volatile Weight Loss = 0 if [1.8] – [1.10] ≤ 0
1.12 % Volatile Weight Loss at T°C = [1.11] · 100 ÷ [1.1]
1.13 % Nonvolatile Weight Loss at T°C = [1.9] – [1.12]
(In 1.8 to 1.13, 'T' indicates the elevated test temperature.)

3.2 BUFFER TUBE DRIP TEST DETAILS

Sample Preparation — Buffer tube samples were produced with standard tube materials on standard equipment. The tube inner diameter was 2.0 mm. The tubes were filled in the standard method with filling compound and 12 colored fibers.

Procedure — After a 100-meter length of filled buffer tube was produced, samples were prepared by cutting the tube into 30-cm segments. These segments were vertically suspended over glass dishes in a circulating-air oven; the samples were secured near the bottom to prevent them from excessive motion caused by the oven fan. Two sets of samples were prepared for each filling compound — one set was tested according to the Bellcore 65°C drip procedure, the other according to the REA 80°C procedure. No preconditioning cycles were used, and failures were determined as outlined in the test procedures.

4. EXPERIMENTAL RESULTS

4.1 RESULTS OF VARIOUS COMPOUNDS

The test results for 11 different filling compounds are displayed in Table 2. All oil separation results are for total separation (including volatiles) and are reported as a percent of the initial sample weight. The drip test results are reported as the percent of all buffer tube samples which failed the respective drip test.

4.2 CORRELATION OF TESTS

Table 3 contains the results of correlation calculations performed on the data shown in Table 2. The relatively high degree of correlation indicates that oil separation test results can be used to predict drip test results with good success.

TABLE 3: CORRELATION OF OIL SEPARATION RESULTS TO DRIP TEST RESULTS

CORRELATION COEFFICIENTS	
65°C Oil Separation & 65°C Drip Failures:	0.90
80°C Oil Separation & 80°C Drip Failures:	0.86
23°C Oil Separation & 65°C Drip Failures:	0.76
23°C Oil Separation & 80°C Drip Failures:	0.69
23°C Oil Separation & 65°C Oil Separation:	0.88
23°C Oil Separation & 80°C Oil Separation:	0.79

TABLE 2: RESULTS OF 65°C OIL SEPARATION & BUFFER TUBE DRIP TESTING

FILLING COMPOUND	23°C % SEP.	65°C % SEP.	65°C DRIP % FAILURE	80°C % SEP.	80°C DRIP % FAILURE
A	0.0	0.0	0	0.0	0
B	0.4	1.0	0	0.0	0
C	0.4	8.0	0	11.4	0
D	0.8	5.6	0	16.4	0
E	2.0	10.8	0	14.3	27
F	1.7	18.8	20	36.4	40
G	2.4	17.6	67	20.7	73
H	6.0	32.0	100	34.0	100
I	12.1	22.0	25	23.0	35
J	13.1	41.4	90	45.0	100
K	28.5	50.0	100	54.2	100

All drip tests conducted on 12-fiber tubes of 2.0-mm inner diameter; no caps/preconditioning

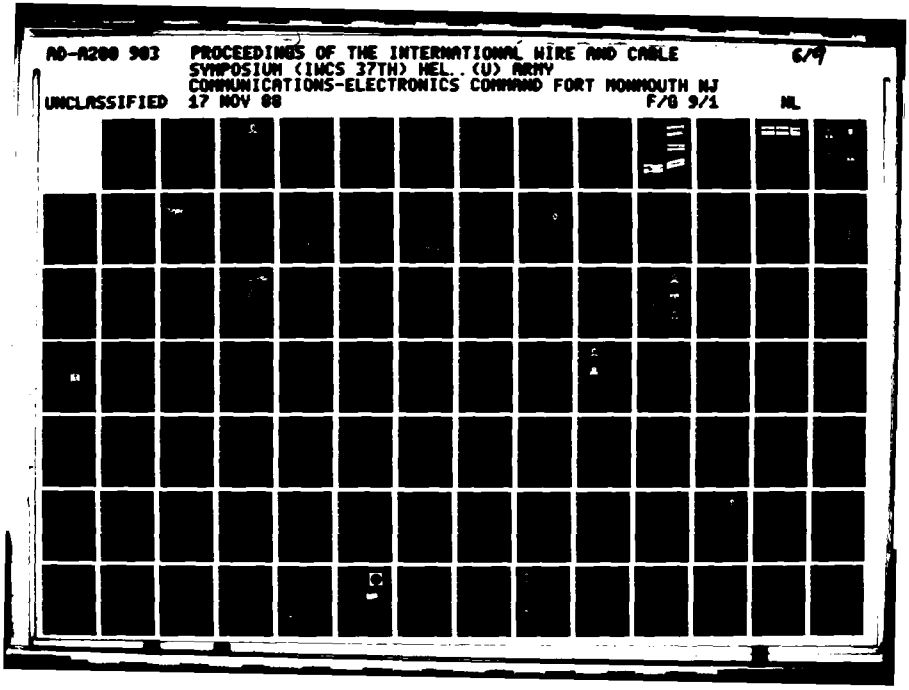
AD-A200 903 PROCEEDINGS OF THE INTERNATIONAL WIRE AND CABLE SYMPOSIUM (IWCS 37TH) HEL.. (U) ARMY COMMUNICATIONS-ELECTRONICS COMMAND FORT MONMOUTH NJ
6/9
UNCLASSIFIED 17 NOV 88 F/G 9/1 NL

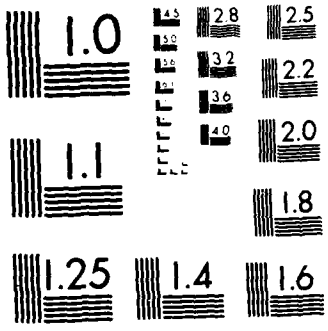

4.3 TEST REPEATABILITY

Based on studies of the same filling compounds in the same lab with the same operator at different times, the test repeatability was determined to be within ± 12% of the separation value. The greater the total amount of separation was for a compound, the greater was the variability in test repetitions — this may reflect the fact that compounds which tend to separate to a greater degree are inherently less stable and can be greatly affected by slight handling differences.

4.4 TEST REPRODUCIBILITY

At this time, no round robin laboratory studies have been undertaken to calculate the reproducibility of the oil separation test. However, non-statistical comparisons of data obtained from in-house and from filling compound suppliers have shown similar results for a given filling compound.

5. DISCUSSION OF RESULTS

5.1 GENERAL

The purpose of the experimental work detailed above was to develop a simple, reliable, and repeatable screening test for cable filling compound drip tests. Based on the correlation coefficients contained in Table 3, it can be concluded that the oil separation test can be used to accurately predict the drip performance of loose tube fiber optic cables. The highest degree of correlation — 0.88 average for both elevated temperatures — was obtained when the oil separation test was conducted at the same temperature as the cable drip test. A 0.70 degree of correlation was obtained when the 23°C oil separation value was used to predict elevated temperature drip performance.

The high degree of correlation is especially notable when the diverse nature of the filling compounds tested in this study is considered. The variety of compounds ranged from silicone-based systems to polyisobutylene-based blends to petrolatums to metallic soap compounds.

Based on the test results reported in Table 1, two threshold values were derived as upper limits for an oil separation screening test. Compounds which separated less than 2% at room temperature and less than 15% at 65°C or 80°C were most likely to pass the buffer tube compound drip tests with a low incidence of drip failures.

5.2 LIMITATIONS OF TEST

The oil separation test results are dependent on the handling of the filling compound prior to and during the execution of the procedure. Care should be taken to mix and de-aerate all filling compounds to be tested and compared in a similar manner. Also, the area of the compound touching the small filter paper square should be similar for each sample.

When predicting the drip performance of filling compounds in a loose tube cable, it is important to note that oil separation is only one mechanism by which a compound may fail a drip test. A compound with a low viscosity or one that melts near the drip test temperature may not exhibit a great deal of separation and still fail a compound drip test. The cable designer must consider the total chemical, physical, and rheological aspects of a filling compound's behavior in order to produce the highest quality fiber optic cables.

5.3 RECOMMENDATIONS

It is recommended that further work be done to quantify the reproducibility of the oil separation test procedure. Additionally, investigating the effects of shear and temperature history on the oil separation of filling compounds may also lead to a better understanding of long-term filling compound behavior.

Predicting drip performance of filling compounds is complicated by the wide variety of test procedures currently in use. The adoption of an industry-wide compound drip procedure, with performance requirements closely tied to actual and measurable cable field requirements, could simplify and legitimize the entire issue of cable drip.

6. CONCLUSIONS

An oil separation test procedure was developed which can be used to predict the filling compound drip test performance of loose tube fiber optic cables with a high degree of correlation. The test is simple, repeatable, uses ordinary laboratory equipment, yields results in 48 hours, can be conducted on a large number of samples simultaneously, and was designed to test optical cable filling compounds.

7. ACKNOWLEDGEMENTS

The author would like to acknowledge the contributions of the following individuals: Drew Dodd, Kelly Coupe and Dr. Chris Eoll, for valuable input; Catherine Topping and Kitty Tedder, for conducting the tests; and Ron Bailey and Phil Miller, for producing the buffer tube samples.

8. REFERENCES

1) Bell Communications Research, Inc., *"Generic Requirements for Optical Fiber and Optical Fiber Cable"*, Technical Reference TR-TSY-000020, Issue 3, December 1987.

2) Electronic Industries Association, *"FOTP-81: Compound Flow Test for Filled Fiber Optic Cable"*, EIA-455-81, March 1985.

3) GTE, *"Specification GTS 8542 for Aerial, Buried, and Underground Multimode and Single-mode Optical Fiber Communication Cables"*, Issue 2, Revision 2, 12/14/84.

4) Rural Electrification Administration, *"Specification for Totally Filled Fiber Optic Cable — PE-90"*, May 28, 1986.

5) American Society for Testing and Materials, *"Standard Test Method for Oil Separation from Lubricating Grease During Storage"*, ASTM D-1742-83, 1983.

6) G. J. Hughes, *"Development of a Compound Flow Test Method for Predicting Drip Performance of Filling Compounds in Finished Cables"*, 36th IWCS Proceedings, 1987.

Martin C. Light, Jr.
Siecor Corporation
489 Siecor Park — RD&E
Hickory, NC 28603

Martin C. Light, Jr., was born in Lancaster, Pennsylvania, in 1963. He received his Bachelor of Science Degree in Ceramic Engineering from the Georgia Institute of Technology in 1985. Since then, he has been employed at Siecor Corporation as a Materials Engineer in the Research, Development and Engineering department.

DEVELOPMENT OF A WATERTIGHT BURIED CLOSURE SYSTEM

John A. Loken, David H. Proffer, Mark J. Stanek

SIGMAFORM CORPORATION
Santa Clara, CA

SUMMARY

The problem of water ingress into direct buried telephone plant is reviewed from a historical viewpoint. Unsuccessful attempts to solve the problems are discussed and a summary of the different ways in which water can enter into the buried plant are outlined. The four main leakage paths are: 1) Permeation, 2) Leakage through the closure to cable seal, 3) Condensation and flooding in above ground pedestals, 4) Leakage through cable and service wires. The solutions to these four problems are presented and combine the following components: 1) Service Wire Dams, 2) Service Wire Splices, 3) Forced Encapsulation, 4) Heat Shrinkable Outer Sleeves, 5) Heat Shrinkable Splice Caps for Pedestal Closures. Combinations of these components can provide a highly watertight system for any type of direct buried plant.

INTRODUCTION

When "out of sight plant" was first conceived as a method for communities to beautify their areas by removing unsightly overhead telephone cables, the telephone companies were still using pulp insulated lead and plastic sheathed cables. Since this type cable had performed well in the aerial and underground environments, it was assumed by the phone companies that they could also be direct buried.

THE PROBLEM

Unfortunately, direct burial of pulp insulated cables created many serious problems for both maintenance and construction crews. The overwhelming majority of these problems were caused by water entering the cable and splices and saturating the pulp insulation. The water changed the dielectric properties of the insulation creating problems with noise and ultimately dead shorts.

With the development of Plastic Insulated Conductor (PIC) cables, the pulp cables were replaced and it was assumed this would solve the problem since the dielectric properties of polyethylene are unaffected by moisture. However, the problems persisted even though there was some improvement. At this point, it was realized by the telephone companies that substantial changes in existing practices would be necessary to bring about more significant improvement.

The first major change was introduction of filled cable, but while filling compounds reduced the flow of water in the cable, the splices continued to accumulate water in the wet areas where they were direct buried.

The next step was to attempt to prevent water entry into the splice. Three methods were used:

1) Petroleum jelly was injected into the closure.
2) Re-enterable polyurethane encapsulants were gravity poured into the closures and allowed to cure.
3) The splice was removed from the buried environment and placed in an above ground pedestal.

This latter method had the further advantage of making splices more readily accessible while still maintaining the aesthetic advantage of eliminating overhead plant.

Despite these precautions, however, a high rate of trouble due to ingress of water into the direct buried closures and even the pedestal closures continued to be a problem. Product troubles added to the overall problem and created other difficulties.

A detailed analysis of the problems led to several pertinent conclusions. Water can enter the closure by a number of different paths:

1) Permeation through the closure.
2) Leakage through the seal between the closure and cable.
3) Through condensation, leaking or flooding into the above ground pedestals.
4) Leakage through the cable and service wires.

THE SOLUTION

1) The permeation problem is not a significant factor and as a precautionary matter, a metalfoil permeation barrier is almost always included as part of a non-metallic closure to insure that water does not enter through the closure itself.

2) Leakage through the seal between the closure and the cable is one of the major sources of water entry into the closures. The advent of heatshrink technology has provided the most reliable and versatile cable to closure sealing method and virtually eliminated this problem. The combination of a shrinkable outer sleeve in combination with the hot melt adhesive coated onto the sleeve which melts and bonds to the cable during installation provides an effective and long lasting seal.

3) The solution to the pedestal closure problem also can be found in the use of a heatshrinkable system. Butt Closures in the form of a long cap with a shrinkable lower part can be placed over the splice bundle inside the pedestal. When the lower portion of the cap is shrunk onto the jacket of the entering cables, an effective seal against condensation, leaking, flooding, UV and oxidative degradation is affected again by means of hot melt adhesives coated onto the shrinkable portion of the cap. These caps can be reentered and reused.

4) Finally, the problem of leakage through the cables itself is addressed by use of the technique known as forced encapsulation. In this technique, a re-enterable polyurethane encapsulant is contained in a plastic bag which is placed around the splice bundle and sealed onto the opposite ends of the cable opening. This bag is then compressed by means of an outer wrapping technique which squeezes the encapsulant around the conductors and connectors into the core of the splice and even into the cable core and most importantly between the terneplate and the outer jacket. This added pressure forcing the encapsulant into all voids is the solution to the problem which occurs in all gravity poured closures.

While the previous methods provide solutions to the problem of entry of water into the main cable and splices in buried plant, there is one further entry path into buried plant: the service wire.

A study has been conducted on this source of water entry. Both shielded and unshielded service wires were investigated. The shielded service wires all leaked water when subjected to a static waterhead. A majority of unshielded service wires leaked also. Details of this testing are available.

Sources of water entry into the service wire are:

1) Damage to the sheath
2) Service Wire Splices

A solution to this problem with service wires has been to develop a service wire dam and service wire splice based on a specially designed hot melt adhesive in combination with heatshrink components which results in a "flooding" and complete damming of sources of water entry into service wires and service wire splices. The dam is applied at the source of entry of the service wire to the main cable while the splice can be installed easily where the service wire leading to the house is spliced.

Sigmaform's Research and Development activities indicate that combinations of the following components can provide a highly reliable watertight system for any type of direct buried plant:

1) Service Wire Dams
2) Service Wire Splices
3) Forced Encapsulation
4) Heat Shrinkable Outer Sleeves
5) Heat Shrinkable Splice Caps for Pedestal Closures. This combination provides a highly reliable watertight system for any type of direct buried plant.

ZIPPERING FAILURES IN TELECOMMUNICATIONS CABLE JACKETS

O.S. Cebizlioglu, P.B. Grimado, C.T. Avant and E.J. Biron

Bellcore
New Jersey, U.S.A.

ABSTRACT

During underground installation of telecommunications cables, polyethylene jacket that is bonded to the steel shield may zipper, i.e., rip open along and above the shield overlap. The torsion test was developed by the cable manufacturers and users to assess the risk of zippering. In this investigation, the mechanics of torsion was studied and related to observed failure patterns. Two cable parameters were found to be important: 1) the unbonded zone width divided by the jacket thickness, b/t_p, and 2) the diameter-to-sheath thickness ratio, D/t_s. For $b/t_p < 5$, the well-known torsional buckling is observed. For $b/t_p > 5$, cables appear to exhibit localized buckling of the unbonded portion of the jacket over the shield overlap and may eventually zipper.

I. INTRODUCTION

Telecommunications cables with plastic jackets may exhibit jacket damage during underground installation. In jackets bonded to the steel shield, the failure appears in the form of sheath buckling and/or "zippering", a tearing of the jacket along the shield overlap.

A typical cable sheath consists of a polyethylene jacket bonded to a corrugated steel shield. For an average cable diameter (over core wrap) of 32.8 mm, a minimum jacket thickness of 1.0 mm is required[1]. For cables of average diameter greater than 76mm, a minimum 1.4 mm is required. The maximum thickness at any cross section is restricted to 155 % of the minimum thickness. Figure I-1 presents a schematic representation of a cable cross section. Underlying and overlying edges of the shield overlap are not bonded; the overlying edge is formed inwards to minimize sawing action on the jacket. To further minimize injury to the jacket, a tape may be placed on the shield overlap[2]. This cable sheath design yields a bonded polyethylene jacket of high torsional stiffness combined with a narrow longitudinal unbonded portion over the shield overlap.

The polyethylene jacket is bonded to the steel shield to improve the buckling resistance of the sheath[3]. However, the incidence of zippering has greatly increased with the use of bonded jacket. Currently three tests are used to predict zippering. These are notch, sheath adherence and torsion tests[1]. The notch and sheath adherence tests are used as indicators of the effects of damage on the jacket by the edge of the shield overlap, and the bond strength between the jacket and the steel shield, respectively. Hence, they do not provide a measure of cable sheath performance under the forces which may operate in the field installation. The torsion test, on the other hand, subjects a cable specimen to a shear deformation, and the response of the cable sheath approximates buckling and zippering damage observed in the field.

During installation into duct, cable from the reel is fed through a C-bend or an S-bend. In each case, the cable sheath is subjected to tensile and/or shear forces. The damage patterns from the field specimens clearly indicate that the intense shearing on the jacket along the shield overlap initiates the failure. Moreover, the field failure patterns closely match the failure patterns on torsion test specimens. Maguire and Rossi[2] also report that their torsion test results on 5 foot-cable specimens were statistically consistent with installation failures in the field.

In this presentation, we discuss the deformation of a thin cable jacket bonded to a steel shield and the relationship of testing stresses to buckling and failure patterns in torsion. In section II, we describe: (1) our detailed observations of damage patterns, (2) their relationship to the state of bonding of the jacket to the shield overlap, and (3) major deformation mechanisms of the jacket. In section III, we develop an experimental shear stress-twist angle relationship and use it with the buckling criteria of section II to predict the failure pattern for a test cable.

II. TORSION TEST

A torsion test on cables with polyethylene jacket bonded to steel shield is a procedure for evaluating resistance to zippering and other

deleterious deformations such as large buckles or kinks that can hinder cable installation. The test is applied to a 1.5 meter (60 inch) length of cable. The free end is rotated in the direction opposite to the overlap portion of the steel sheath. Bonded cables under 2 inches outside diameter are rotated 540 degrees; cables of larger outside diameter are rotated 360 degrees.

Torsion tests performed on cables from several vendors showed four diverse patterns of cable sheath deformation. The first pattern consisted of screw-type buckles of varying radial displacement helically wrapped around the cable at a 45 degree angle, shown in Figure II-1. These represent well-known torsional buckling modes of thin-walled tubes of circular cross-section[4]. It is worthy to note that the buckling pattern does not follow the jacket seam. The second mode involves local buckling of the cable sheath in the vicinity of the shield overlap, shown in Figure II-2. These buckles form a periodic pattern oriented, at least initially, at 45 degrees to the cable axis and evenly spaced along the length of the cable.

The third and fourth deformation modes involve zippering of the cable jacket. The third mode is merely a terminal state of mode II. When buckling occurs during the early stages of torque application, the buckled surfaces tend to behave like a series of diagonal tension members upon subsequent load increases[4]. Zippering can then occur by tearing of the jacket along lines normal to the buckles, i.e., in the direction of the diagonal tension field shown in Figure II-3. The ruptures or tears on the jacket occur along the peaks of the ripples while the valleys remain intact. The fourth pattern is illustrated in Figure II-4. In this mode, cable sheath deformations are not noticeable near the tear which occurs along the shield overlap. The tear resembles a knife cut. This type of failure is precipitated by cutting of the polyethylene jacket by the sharp edge of the steel shield because of faulty forming during manufacture.

Cable deformation modes I and II do not appear together and therefore compete. Mode I is described as torsional buckling of thin-walled cylinders. The critical shear stress for buckling is given by the expression[4]

$$(\tau_c)_c = K\,(EE_t)^{0.5}\,(t_s/D)^{1.5} \qquad \text{(II-1)}$$

where K = 0.73, E and E_t are modulus of elasticity (or Young's modulus) and tangent modulus of the polyethylene-steel shield composite, respectively; t_s is the thickness of the composite, and D is the outside diameter of the cable.

In many instances, the polyethylene jacket is not completely bonded to the corrugated steel shield. The unbonded portion spans the shield overlap as depicted in Figure II-5a. When the cable is twisted, an out-of-plane displacement or warping of the cross-section ensues similar to that of a split ring. This deformation imposes shear stresses on the segment of unbonded jacket as described in Figure II-5b. For a sufficiently large shear stress, the mode II buckling pattern of Figure II-2 can result. This mode resembles shear buckling of flat plates[4,5]. The critical shear stress for buckling is given by the equation[4,5]

$$(\tau_c)_p = K\,(EE_t)^{0.5}\,(t_p/b)^2 \qquad \text{(II-2)}$$

where K = 5.85 for a simply supported plate; E is the modulus of elasticity; E_t is the tangent modulus of polyethylene, i.e., the slope of the uniaxial tensile stress-strain curve, and t_p and b are the jacket thickness and unbonded zone width, respectively.

It is expected that the mode with the lower critical stress will dominate, i.e., $(\tau_c)_c < (\tau_c)_p$ for mode I and, conversely, $(\tau_c)_p < (\tau_c)_c$ for mode II. The buckling curves of these modes plotted against the characteristic ratios, i.e., b/t_p and D/t_s appear in Figure II-6. The tangent moduli required for this calculation were obtained from our tensile tests performed on samples of polyethylene jacket and steel-bonded polyethylene.

Table II-1 summarizes the results of torsion tests performed at room temperature on bonded cables. Cables with the same diameter listed in this table were taken from the same reel. There was a large variation in the dimensions of the cables and especially in the width of the unbonded portion. For instance, measurements taken over a 3 inch-length of the cable revealed a two hundred percent variance in unbonded width. Nevertheless, from the buckling curves of Figure II-6 and Table II-1, several trends are evident. First, when the width of the unbonded zone is small, $b/t_p < 5$, screw-type (mode I, Figure II-1) buckling of the cable seems to dominate. The test results on cables 1-3, 7, 8, 12, 13 support this observation. When the mode I pattern occurs to this extent, it will obviously hinder the cable placement. Second, from Figure II-6 and the experimental data of Table II-1, it appears that when $b/t_p > 5^*$, local shear buckling (mode II) near the unbonded region takes place and is followed, in most instances, by zippering failure (modes III or IV). The test results on cables 4-6 and 9-11 corroborate this conclusion.

Some discrepancies observed on cables such as 4, 10 and 11 are attributed to the broad distribution of the unbonded zone width along the cable length previously noted. An alternative explanation may be that an initially bonded area can become unbonded during the testing if the shear strength of the bond between the steel and polyethylene jacket is exceeded. When $b/t_p > 5$, it does not necessarily mean that zippering failure is imminent, i.e., cables 5, 10, 11. However, this

* This ratio varies with D/t_s. For the cables tested, $5 < b/t_p < 6.5$. The lower limit is conservatively adopted.

indicates a potential zippering failure since mode II buckling must always precede zippering.

TABLE II-1

Torsion Test Summary

Cable	Outside Diameter (cm)	D/t_s	b/t_p	Failure Mode
1	5.97	22	3.54-4.16	I
2	5.97	22	2.33-2.76	I
3	5.97	22	2.03-2.85	I
4	7.87	28	2.40-3.28	III
5	7.87	28	5.76-6.11	II
6	7.87	28	3.27-5.94	III
7	7.62	31	0.0	I
8	7.62	31	0.0	I
9	6.35	20	5.23-6.72	IV
10	6.35	20	0.0	II
11	6.35	20	3.34-3.89	II
12	8.38	25.0	1.07-1.24	I
13	8.38	25.0	0.0	I

III. EXPERIMENTAL STRESS ANALYSIS

In the preceding section, two buckling patterns (mode I and mode II) were described in the torsion of a cable sheath consisting of a polyethylene jacket bonded to a steel shield. For prediction of failure patterns, one needs to determine the maximum shear stress on the cable jacket as a function of the angle of twist in the torsion test and compare it with the critical shear stress defined in section II for buckling. This critical stress can be established by using cable parameter ratios in conjunction with the buckling curves of Fig.II-6.

In this section, we determine maximum shear stress as a function of the twist angle in two steps. First, we develop the maximum shear strain-twist angle relationship. In the second part, we derive the maximum shear stress-strain curve for polyethylene jacket. Thus, we arrive at an experimental maximum shear stress-twist angle relationship.

(a) Maximum Shear Strain-Twist Angle Relationship

When the cable is subjected to a torque at one end, say at z=0 (where z is the direction of the cable axis), in addition to a twist of angle θ (Figure II-5a), an out-of-plane displacement or warping takes place[6,7]. It is this warping of the cross section that precipitates zippering of the unbonded portion of the jacket.

Considering the bonded cable sheath to be a thin-walled split cylinder, shown in Figure II-5a, $U_\theta(z)$ and $U_z(\theta)$ are defined as the two components of the displacement vector and are shown in Figure III-1. The total shear strain, at a given angle of twist, has also two components that are related to those of the displacement vector. Γ_g is the global strain due to twisting. It is measured as $\Delta U_\theta/\Delta z$, shown in Figure III-1a. Γ_l is the local strain on the unbonded portion of the jacket. It is related to the second component of the displacement vector and defined as $\Delta U_z/h$. ΔU_θ and ΔU_z refer to changes, due to twisting, in components of the displacement vector, U_θ and U_z, respectively; Δz and h are defined in Figure III-1. Thus, the total strain is obtained from the expression

$$\Gamma_{tot} = \Gamma_g + \Gamma_l \qquad \text{(III-1)}$$

$$\Gamma_{tot} = (\Delta U_\theta/\Delta z) + (\Delta U_z/h)$$

One can determine $\Delta U_\theta/\Delta z$ by measuring the arc length AB, Figure III-1a, and dividing it by the length of the cable between the torsion grips at a selected angle-of-twist. The local shear strain, Γ_l, on the unbonded portion of the jacket over the shield overlap is determined by following the deformation of the rectangle depicted in Figure III-1b with increasing twist angle. Figure III-2a shows the rectangle drawn on the unbonded portion of the jacket at zero twist angle. Figures III-2b and III-2c display the deformation of the rectangle at 15 degrees and 60 degrees, respectively. The local shear strain is obtained by dividing the axial displacement ΔU_z by h, shown in Figure III-1b. Figure III-3 shows a plot of total shear strain against the angle-of-twist for one of the cables tested.

(b) Maximum Shear Stress-Shear Strain Relationship

The maximum shear stress-strain relationship for the polyethylene jacket is obtained from the uniaxial tensile stress-strain curve of a representative cable jacket material. The tensile stress measured in uniaxial tension is also the principal stress[6], and the maximum shear stress is one half of the principal stress. Similarly, maximum shear strain is calculated from tensile strain. However, in this case, one must consider two components of the tensile strain field, tensile strain in the direction of the principal stress, and strain at 90 degrees to the tensile stress. Hence, maximum shear strain is given by the following expression[6], for a Poisson's ratio of 0.5

$$\Gamma_{max} = 0.75\ \epsilon_{max} \qquad \text{(III-2)}$$

where ϵ_{max} is the tensile strain in the direction of tensile stress. Figure III-4 shows the maximum shear stress-strain relationship for polyethylene.

(c) Prediction of Failure Patterns

Having established the maximum shear stress-twist angle relationship for a representative cable, we can attempt to predict the buckling pattern observed in the torsion test sample.

Step I: One reads the total shear strain from Figure III-3 for the angle-of-twist at which the buckling pattern appears. With the total shear strain, we then determine the maximum shear stress on the unbonded portion of the jacket from Figure III-4

Step II: We measure the characteristic ratio D/t_s for the cable and read the corresponding critical shear stress $(\tau_c)_c$ from Figure II-6. If the shear stress determined in Step I is lower than $(\tau_c)_c$, then mode II buckling is confirmed.

For example, one of the test cables exhibited a critical angle-of-twist for buckling of about 45 degrees. From Figure III-3, a total strain of 0.36 is found. At this value of total strain, we read a maximum shear stress of 6.2 MPa from Figure III-3. The measured value of D/t_s, for this cable, is 28. The corresponding critical stress for buckling, $(\tau_c)_c$, from Figure II-6, is 6.7 MPa. Since shear stress on the jacket is lower than the critical shear stress, we conclude that mode II buckling will occur. This result is consistent with our observations listed for cables 4, 5 and 6 in Table II-1, and it appears to be in good agreement with the buckling pattern-cable parameter relationships observed.

SUMMARY AND CONCLUSIONS

The mechanics of a torsion test for telecommunications cables containing a polyethylene jacket bonded to a steel shield has been investigated analytically and experimentally. The objective of this study was to identify the most significant cable parameters which could be used to predict zippering during cable placement.

Four torsional deformation modes were identified: overall screw-type buckling, Figure II-1; local buckling about the overlap seam, Figure II-2; and two cable sheath failures, Figures II-3 and II-4. In a typical cable construction, the polyethylene jacket is not bonded over a small segment along the shield overlap. Therefore two characteristic buckling conditions are evident: (1) the torsional buckling of the cable sheath, which can be treated as a thin-walled tube, and (2) the localized shear plate buckling of the unbonded portion of the polyethylene jacket. It is determined that the latter buckling mode occurs for the unbonded width-to-jacket thickness ratios greater than five, i.e., $b/t_p > 5$. This has been shown to agree with test results presented in Table II-1 and the buckling curves of Figure II-6.

Although post-buckling behavior was not addressed in this analysis, it is possible that when $b/t_p > 5$, the cable jacket can exhibit zippering since this failure is preceded by large localized deformations of the unbonded portion of the jacket about the shield overlap. Work still in progress is aimed at the prediction of failure patterns by measuring torque and shear stress on the cable jacket.

Acknowledgement

The authors would like to thank Mr. F.Ricker for his assistance in extensive testing of cable samples required for this study.

REFERENCES

1. Bellcore Technical Reference TR-TSY-000421 Issue 2, June 1988

2. C.V. Maguire and R. Rossi, "Cable Sheathing Design and Performance Criteria", Proceedings of the 36th International Wire and Cable Symposium, 1987, p 327.

3. G.M. Yanizeski, E.L. Johnson and R.G. Schneider, "Cable Sheath Buckling Studies and the Development of a Bonded Stalpeth Sheath", Proceedings of the 29th International Wire and Cable Symposium, 1980, p 48.

4. F.R. Shanley, "Strength of Materials", McGraw-Hill, 1957, p622

5. F. Bleich, "Buckling Strength of Metal Structures", McGraw-Hill, 1952, pp 390-399

6. E.P. Popov, "Mechanics of Materials", Prentice-Hall, 1976, p 60.99

7. W. Flugge, "Handbook of Engineering Mechanics", McGraw-Hill, 1962, p36-5

Fig. II-2

Local buckling of the unbonded zone in a bonded cable

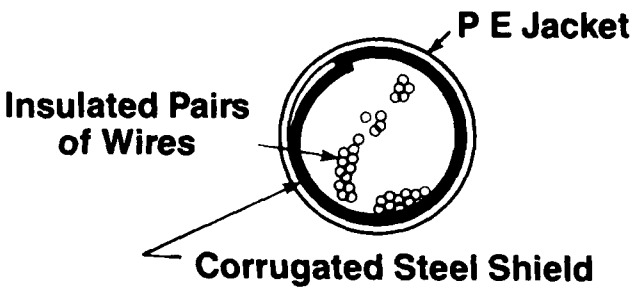

Fig. I-1

Cross-sectional view of a cable

Fig. II-3

Zippering failure in a buckled unbonded zone

Fig. II-1

Torsional buckling in a bonded cable sheath

Fig. II-4

Zippering failure by the sawing action of the shield edge

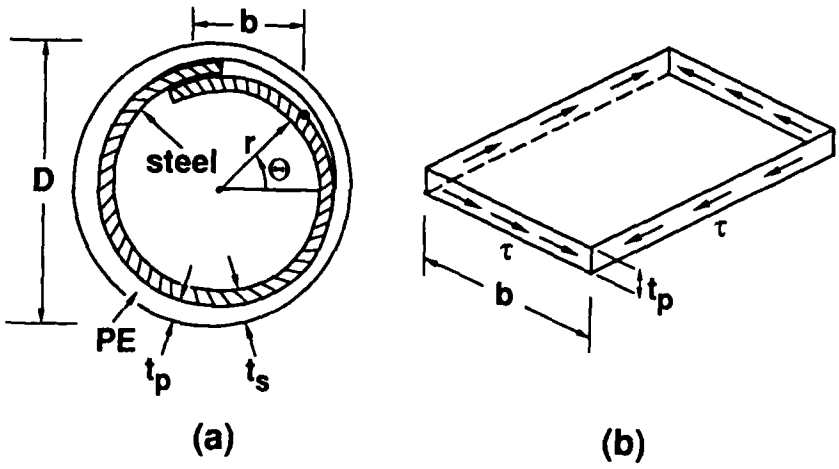

Fig. II-5

a) A schematic representation of the thin-walled split cylinder

b) The state of stress in a bonded cable jacket

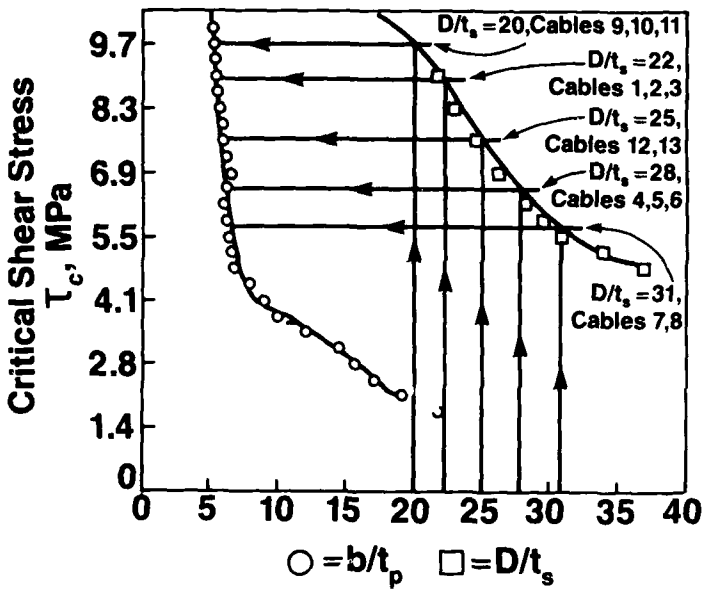

Fig. II-6

Buckling curves for shear plate and thin-walled cylinder

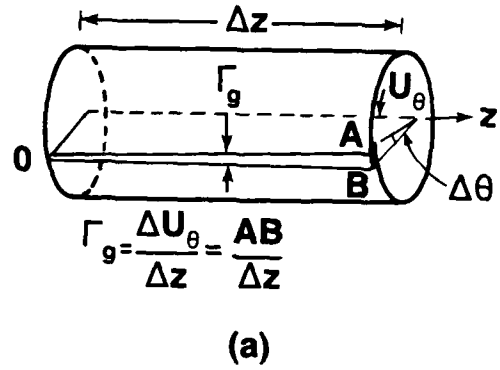

Fig. III-1

a) Torsional strain in a thin-walled cylinder

b) Local strain in the unbonded zone of the jacket

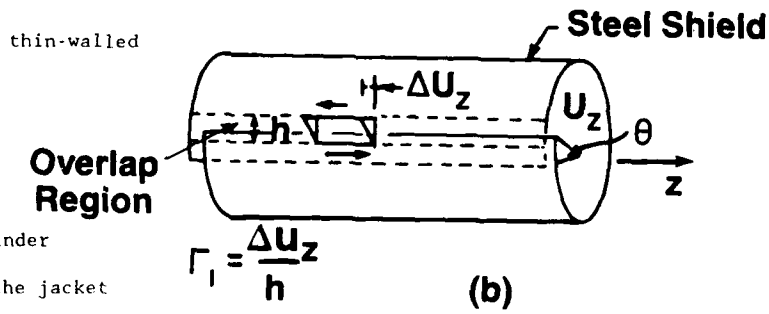

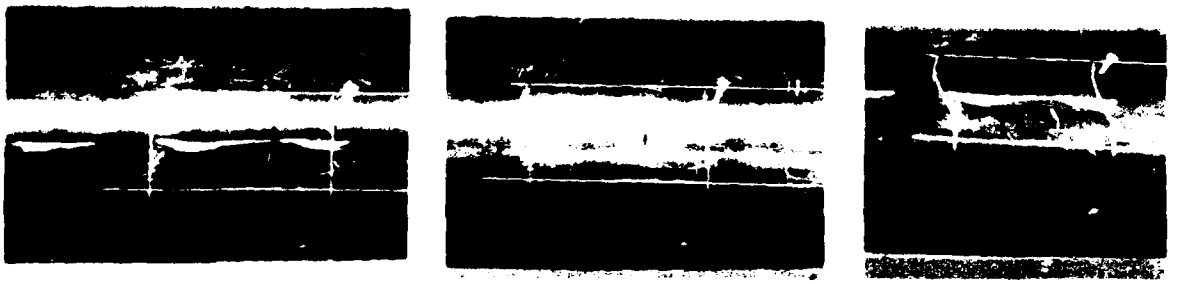

Fig. III-2

Deformation of the unbonded portion of the jacket at a twist angle of a) 0 degrees
b) 15 degrees
c) 60 degrees

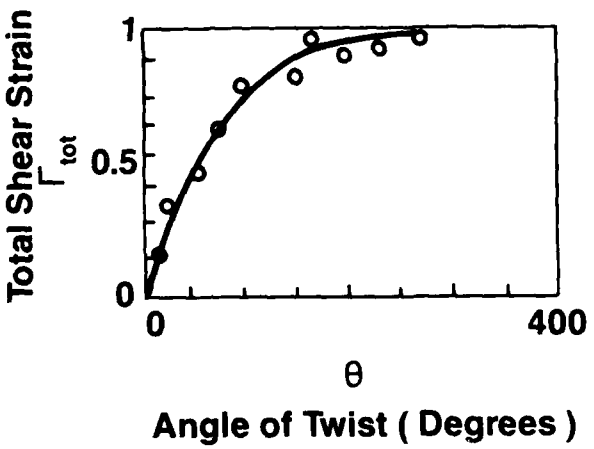

Fig. III-3

A plot of total shear strain in the unbonded zone against the angle-of-twist

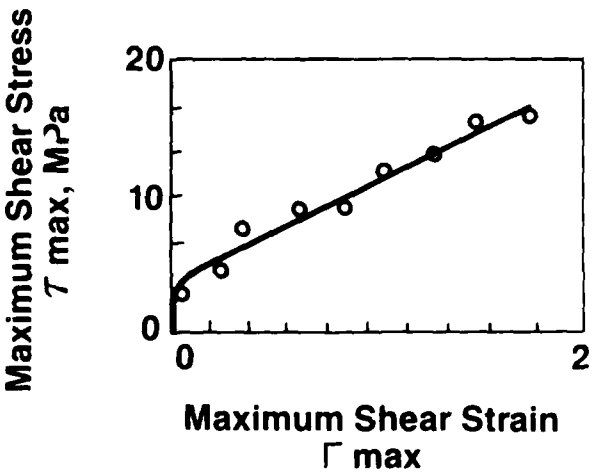

Fig. III-4

Maximum shear stress-shear strain curve for polyethylene jacket

Osman S. Gebizlioglu is a member of the Polymer Chemistry and Engineering Research group in Bellcore, Red Bank, New Jersey. After receiving his Ph.D in Chemical Engineering from Princeton University, he pursued research in physics of toughening of glassy polymers at M.I.T. (Cambridge, Mass.). He joined Bellcore in 1987. His research interests include the morphology and mechanical behavior of heterogeneous polymers and composites.

Philip B. Grimado, B.S. (Civil Engineering, 1961), City University of New York; M.S. (1962) and Ph.D (1968) in Applied Mechanics, Columbia University. He was in the Staff of Bell Laboratories from 1968 to 1983. His responsibilities included vulnerability studies of antiballistic missile systems, fire risk analyses for telecommunications equipment and optimal control of environmental equipment. Presently, he is in the Distribution Technology Research group at Bellcore, Morristown, New Jersey.

Charles T. Avant is a Distinguished Member of Professional Staff in the Metallic Media/Wire Analysis group at Bellcore, Morristown, New Jersey. He received his B.S. degree in 1962 from Mississippi State University and M.S. degree from the University of New Mexico. He worked at Sandia Corporation (1962-1970), Albuquerque, New Mexico; Western Electric Company (1970-1983), and in the public telephone area (1983-1986).

Ernest J. Biron is a Member of Technical Staff in the Metallic Media Analysis group at Bellcore, Morristown, New Jersey. He earned certificates in Tool and Machine Design at Newark College of Engineering and Fairleigh Dickinson University. He worked at Western Electric in wire and cable design. Currently, he is involved in analysis and requirement writing on outside plant products.

CRACKING OF FOAM-SKIN POLYETHYLENE INSULATIONS IN PEDESTALS

T. N. Bowmer

Bellcore
Red Bank, New Jersey 07701 U.S.A.

ABSTRACT

Foam-skin HDPE insulations have been found to be susceptible to thermal oxidation and cracking after less than a decade in the field. These insulations are used in the latest design of water resistant PIC (polyolefin insulated conductor) cables. The problem is attributed to inadequate stabilizer design for the pedestal environment, not poor quality control during manufacture. The residual stability of field insulations, measured for selected sites in the U.S.A. depended on the climatic factors, primarily temperature. The extent of cracked insulations and vulnerable plant was high in the hot southwest but decreased on moving to cooler climates. Cracking patterns were predicted using results from laboratory aging of field samples as well as the history of cracked LDPE insulations.

INTRODUCTION

Multipair telecommunications cables consist of polyolefin insulated conductors (PIC) grouped into color coded pairs that are protected by metallic and plastic sheaths. Over the last two decades PIC cable insulations have experienced varying degrees of degradation inside above-ground, ready-access closures. Buried cables are brought into pedestals where the protective sheaths are removed and the insulated copper conductors exposed for splicing and terminations. Temperatures greater than 130 F can be reached inside such pedestals when heated by direct sunlight[1,2]. Thermally-induced oxidation of the insulation eventually produces microscopic defects and crazes, which slowly grow in length and concentration until visible cracks develop leading to noisy transmission and interrupted service. The insulations are affected by humidity, rodents, flood, lightning, dust, sunlight, pollutants and other environmental factors, but high temperatures and physical stress are believed to be the major factors that determine insulation lifetime.

Polyolefins are durable outdoor materials provided they are protected against thermal oxidation by chemical additives (eg., hindered phenols or secondary amines)[3]. Well stabilized polyethylene can last many years, as seen by the longevity of black polyethylene cable jackets. These stabilizers can react or be lost by migration and evaporation, whereupon oxidation can occur at susceptible sites in the polymer molecule such as labile C-Hs at chain branch points or allylic positions. The peroxy radicals ($RO_2^{\bullet}$) produced will propagate the oxidation reaction by abstracting hydrogens atoms and create more free radicals and or cause main chain cleavage producing unsaturation, keto-compounds, organic acids and other oxidation products[3].

In the 1960-70s, catastrophic cracking occurred in low density polyethylene (LDPE) insulations. Such deterioration occurred in as little as 3-4 years in the southwestern United States. Extensive work showed that not only was stabilizer loss and oxidation accelerated by high temperatures, but also the copper conductor catalyzed the oxidation[1,2,4-11]. Consequently, the insulation material was changed to high density polyethylene (HDPE), a less volatile antioxidant was used and a metal deactivator added. The procedures developed during this time form the basis of the stability requirements for today's cable[2,12-14].

Concomitant with these material changes, water-resistant PIC cable was introduced into the buried plant environment in 1972. This involved filling the cables with a waxy hydrocarbon material. Polypropylene (PP) insulations were initially used in these cables, but were replaced by a foam-skin HDPE design in 1976 that incorporated an inner coating of foamed HDPE with a outer coating of solid HDPE. These insulations were expected, from previous research[15], to last greater than 40 years in the pedestal environment without trouble, although some accelerated testing results predicted only a 10-15 year lifetime[16].

Foam-skin HDPE insulations placed in 1976-80, have begun to crack in closures in southern Arizona and New Mexico[17]. There have even been reports of cracking in cables of later vintage in Phoenix. The concern is that such failures are again caused by stabilizer depletion. Based on the LDPE experience[15], the southwest is a harbinger on what can be expected in the rest of the

country, since the high temperatures and long summers of the southwest greatly accelerate thermal oxidation and stabilizer loss inside pedestal closures. These concerns are further magnified by the quantities of foam-skin insulations that have accumulated in the field over the last 12 years.

Insulation samples were collected from pedestals and cabinets in different geographical and climatic regions. Their stability was measured as a function of material type, cable age and physical location (i.e., buried underground, inside cable sheath, or inside a pedestal). Cable lifetimes and cracking patterns around the country were predicted from accelerated aging tests.

EXPERIMENTAL

Insulations were sampled randomly from pedestals in Arizona, New Mexico, Utah, Nebraska, Iowa, South Dakota, Minnesota and Louisiana. At three selected sites, cable sections were taken from the connector in the pedestal to a point in the buried cable, 12-15 feet distant and ~30 inches underground. Stability profiles were obtained by analyzing insulations from the same wire at regular intervals along this section.

Insulations were stripped from their copper conductors and their Oxidative Induction Times (OIT) at 200°C measured with a DuPont 990 thermal analyzer. A sample of insulation (~4 mg) is placed in an aluminum DSC pan with a loose fitting aluminum cap or screen. The cap or screen helps maintain a uniform and reproducible temperature in the sample while allowing oxygen ready access to the sample. After heating the sample to 200°C in nitrogen, the atmosphere is switched to oxygen. Degradation is observed as an exothermic reaction in the calorimetric trace and the time between the admission of oxygen and the onset of degradation is the OIT value. Although OIT values are not reliable for predicting lifetimes in the field, they are useful for (1) following loss of stability in given a polyolefin composition, (2) identifying insulations devoid of stabilizer (OIT $\cong$ 0) and (3) characterizing the chemical structure of the polyolefin.

Samples with low OIT values were selected for accelerated aging tests, in which the insulated wires were held at temperatures between 60 and 100°C until they cracked. Representative samples were chosen to cover different insulation designs and materials as well as different climates around the country. The top twelve inches of a standard six-inch square, four foot pedestal was heated with a 260 Watt Glas-Col heating mantle while the internal temperature was controlled (±1°C) by a Omega Model CN-310-RTD-C controller. The samples were routinely removed and examined for cracks with an eyeglass. This apparatus has been used routinely for oxidative stability testing of wire insulations[19].

Infrared spectroscopy was used to confirm material identification and detect oxidation products. Oxidation of polyethylene forms C=O and C-O moeities that have infrared resonances at ~1800 cm^{-1} and ~1100 cm^{-1} respectively. The spectra were recorded with a Nicolet Fourier Transform Infrared spectrometer using a Attenuated Totally Reflectance (ATR) accessory.

FIELD OBSERVATIONS

Cracks in foam-skin HDPE insulations have been found in southern Arizona and New Mexico[17]. Damage is confined to exposed insulations in ready-access pedestals and is usually seen near wire bends, loops or twists. This latest cracking phenomenon is different from that seen in LDPE and PP materials during 1960-70s, in that the inner foam coating is more susceptible to abrasion and peeling than those solid insulations which tended to mainly crack[20-22]. The solid HDPE skin protects the soft foam polyethylene underneath but once this outer skin is cracked, the soft inner coating will easily peel back and expose the bare copper conductor.

Several field observations are worthy of note: (1) cracks appear preferentially at bends or stress points in insulations, (2) all colors crack with similar frequency, which is different from the LDPE cracking case where reds and whites cracked sooner than all other colors and black insulations rarely cracked, (3) sunlight heats the pedestal and accelerates the degradation and (4) insulations on 26 gauge wire crack more often than insulation on other larger wires.

LDPE REVISITED

To understand why there is a higher incidence of cracking and insulations with low OIT values in the southwest, it is useful to review the history of LDPE cracking. Link[18](1971) examined over a thousand pedestals around the country looking for cracked LDPE insulations and his results are shown in Figure 1. By regression analysis of the cracking pattern, he concluded that the climatic factors of importance were the average maximum temperature and the number of days that the temperature exceeded 90°F (Figure 2). The degradation rate increased exponentially with temperature.

Fig.1 LDPE CRACKING PATTERN (1970)

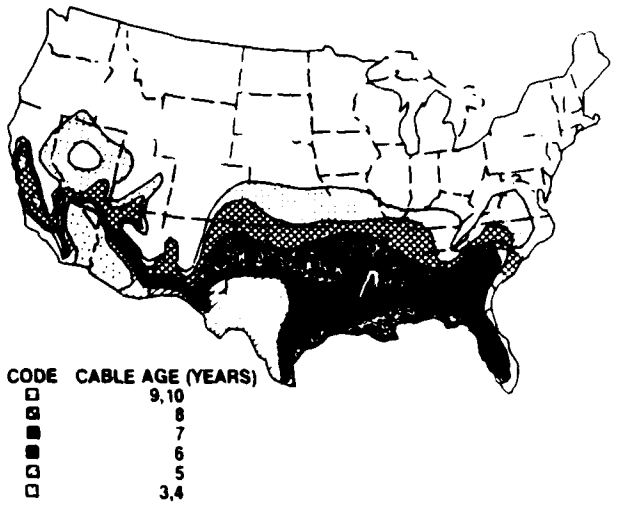

Fig.2 CRACKED LDPE INSULATIONS

(Data from Table 1, ● and Ref.18, ○)

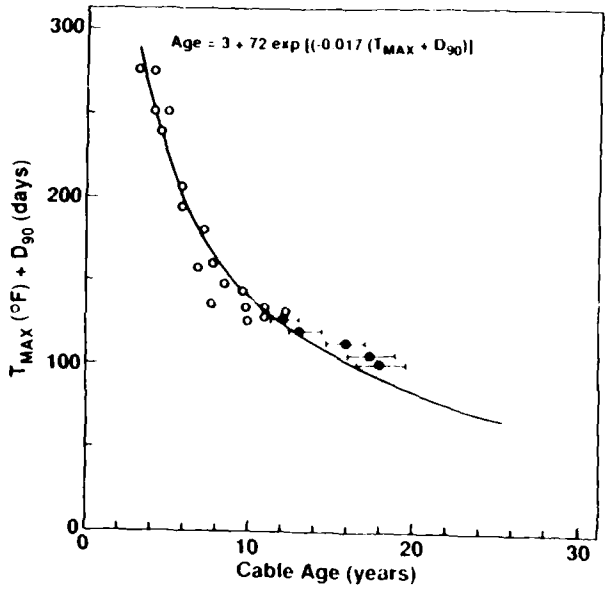

LDPE insulations installed two decades ago, and which cracked within 3-5 years of installation in the southwest, have now begun to crack in the cooler sections of the country. This more recent data was combined with Link's 1970 data and correlations with various climatic factors were considered. Link's[18] basic conclusion was confirmed and the best empirical fit of the cable age to climate factors was found to be:

$$AGE = 3.0 + 72 \exp[-0.017(T_{MAX} + D_{90})]$$

where,

AGE = Cable age at first cracking

T_{MAX} = Average Maximum Temperature (June-August)

D_{90} = Days per year with temperatures > 90°F

An accelerated aging test ("Pedestal Test") was developed to evaluate different materials as replacements for the LDPE[2]. For this test, an Arrhenius relationship between reaction rate and temperature was assumed :

$$Rate = A_0 \exp\{-E_{act}\ kT\}$$

where,

Rate = reaction rate, expected to be ∝ time to crack

A_0 = pre-exponential factor, constant

E_{act} = activation energy

k = Boltzmann's Constant

T = temperature (°K)

It follows that extrapolations to field lifetimes is best done by plotting log(time to crack) against the reciprocal of the temperature since this should give a linear relationship. In Figure 3, LDPE laboratory and field failure data from 1974[22] are combined with the additional results shown in Table I. The test data and the field results are consistent, forming a single curve. The deviation from linearity implies that the activation energy is temperature dependent. The temperature used on the Y-axis for the field locations is an effective temperature, T_{eff} , calculated by taking into account the day night temperature cycles, the exponential increase in reaction rate with increasing temperature[23] and the 15-30°F higher temperatures that can be found inside a pedestal in direct

TABLE I. LDPE CRACKING REVISITED

REPRESENTATIVE LOCATIONS	INITIAL CRACKING YEAR	CABLE AGE (years)	T_{eff} in PEDESTAL (°C)
ARIZONA - Tucson,Yuma,Phoenix	1965-70	3.4	40
CALIFORNIA - El Centro	1965-70	4.5	40
TEXAS - San Antonio,El Paso	1967-70	5.6	38
LOUISIANA - New Orleans,Lafayette	1968-70	7	35
FLORIDA - Miami	1968-70	6.7	33
TENNESSEE - Nashville	1970	8	32
NEBRASKA - Omaha	1978-82	12-15	30 ± 2
MINNESOTA - Minneapolis	1980-82	15-20	30 ± 2

sunlight[1]. Table 1 list the field data for representative locations across the country. The 1974 aging data for solid HDPE insulations from aircore cables, predicted at least 40 troublefree years of use (Figure 3). The unexpected failure of the foam-skin HDPE insulations implies that stabilizer is being reacted and or lost at a faster rate than expected from the solid HDPE data. The

Fig.3 ARRHENIUS PLOTS FOR SOLID LDPE AND SOLID HDPE INSULATIONS (AIRCORE CABLES)

(Data from Table 1, • and Ref.21, ○,□)

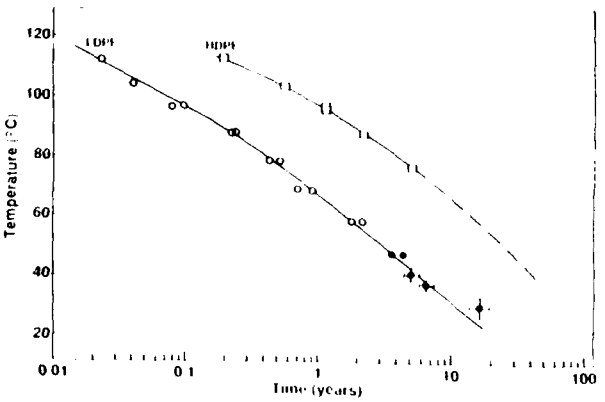

foam-skin design, pedestal design, stabilizer extraction by the filling compounds and or interactions with other components of the cable may contribute to this enhance rate of loss[24-30].

FIELD SURVEY

Various insulations were sampled and are listed in Table 2 as a function of material formulation, design, and geographical location. These samples represent the current status of buried plant that was installed from 1969 to 1983. The remaining stabilizer activity for each sample was measured using the OIT test.

Table 2. INSULATIONS TESTED

MATERIAL & DESIGN	TOTAL	NUMBER FROM*		
		SOUTHWEST	SOUTH	MIDWEST
LDPE	55	5	-	50
PP	70	30	15	25
HDPE(solid)	55	15	10	30
HDPE(foam-skin)	140	100	20	20

* SOUTHWEST = Arizona, New Mexico
SOUTH = Louisiana
MIDWEST = Minnesota, Nebraska, Iowa, South Dakota, Utah

Several of these insulations had already cracked and were characterized by OIT values of 0-0.4 minutes and infrared spectra that showed oxidation products were present. These facts confirm that thermal oxidation is the primary degradation mechanism responsible for cracking in LDPE, PP and now foam-skin HDPE insulations.

Although OIT values cannot reliably predict cable lifetimes, some general ranges can be defined. An OIT value of 0-2 minutes implies that the material has little or no stabilizer remaining and is vulnerable ("at risk") to oxidation and cracking. For example, all cracked insulations had OIT values less than 0.4 minutes. A 2-10 minute value reflects depletion of stabilizers, but it is difficult to generalize about the lifetime remaining of such insulation, for it depends not only on insulation type and stabilizer system, but also local environmental conditions (eg., sun exposure, craft activity in pedestal). Insulations with 10-20 minute OIT values are of little concern unless the cable was installed recently which may imply inadequate stabilization during manufacture. Times of greater than 20 minutes indicate a well stabilized material. New insulations for example may have OIT values up to 150 minutes.

All LDPE insulations tested had low OIT values (< 2 minutes) and most showed evidence of cracking. The PP insulations tested were manufactured during 1972-76 and showed a wide range of OIT values (0.6 to 100 minutes). PP insulated wires could be found cracked with an OIT of 0.6 minutes, while other PP insulations installed in the same year in the same city could appear like new with OIT values of 70-80 minutes. Without detailed investigation, it is unclear whether this wide range of behavior arose from variations in the local pedestal environment or inconsistent quality of insulations (eg. stabilizer not well dispersed[31]).

Significant fractions of foam-skin HDPE insulations placed in pedestals since 1976 have low OIT values (i.e., less than 2 minutes). Table 3 and Figure 4 show the distribution of OIT values for HDPE foam-skin insulations for the three geographical areas sampled. In the southwest, 60% of the HDPE foam-skin insulations examined had OIT values less than 2 minutes and had either cracked or were "at risk" of cracking. In the cooler climates of the south and further north, the percentage of vulnerable insulations was found to be 25% and 15%, respectively.

TABLE 3. DISTRIBUTION OF OIT VALUES

OIT VALUE (MINUTES)	PERCENT OF HDPE INSULATIONS TESTED		
	MIDWEST	SOUTHWEST	SOUTH
0-2	15	60	25
2-10	25	30	35
10-20	20	5	35
20-30	25	4	5
> 30	15	1	-

The loss of stabilizer from the insulation could reflect either low stabilizer loadings (a manufacturing problem) or poor stabilizer design for the operating environment (a technology problem). The OIT value of the product when it was initially installed is required to differentiate between these two possibilities. While it is not possible to measure this OIT value for insulations installed many years ago, it seems reasonable to assume that insulations underneath the ground, several feet back from the pedestal, should have OIT values similar to when they were initially installed. This cable section has not been exposed to the elevated temperatures found inside pedestals. The OIT value of insulations when installed will be at least that found for these buried insulations.

Accordingly, the stability profiles of three cables installed in 1977-79 were measured as a function of position inside the pedestal and buried sections (Figures 5 and 6). Measurements of OIT values of individual insulations measured at varying intervals from the connector inside the pedestal to 12-15 feet back into the cable indicated that within the buried portion, the insulations were well stabilized (OIT > 35 minutes) and of uniform quality (±2%). These measurements show that the original stabilizers are not only well dispersed but also are present in concentrations comparable to levels typical of insulations produced in the 1970's. Such measurements imply that there has been no significant extraction of stabilizer into the filling compound.

As seen in Figures 5 and 6, there is a dramatic decrease in insulation stability where the insulated wires emerge from the cable inside the pedestal. This result coupled with the previous measurements on buried sections of cable confirm that it is loss of stabilizer, not poor quality control, that is the progenitor of cracking. That is not to say that poor quality control can be completely ignored. Studies of six other buried cables, located next to pedestals containing foam-skin HDPE insulations with low OIT values, revealed OIT values in the buried sections of 10 and 12 minutes in two of the six cases. For these two cables sufficient stabilizers may not have been added during manufacture or alternatively stabilizers may have lost during manufacture and or storage. In such cases, cracking may occur considerably earlier than what would otherwise occur with a normally stabilized insulation. Insulations from the buried sections of the other four cables all had OIT values greater than 20 minutes.

Fig.4 DISTRIBUTION OF VULNERABLE INSULATIONS

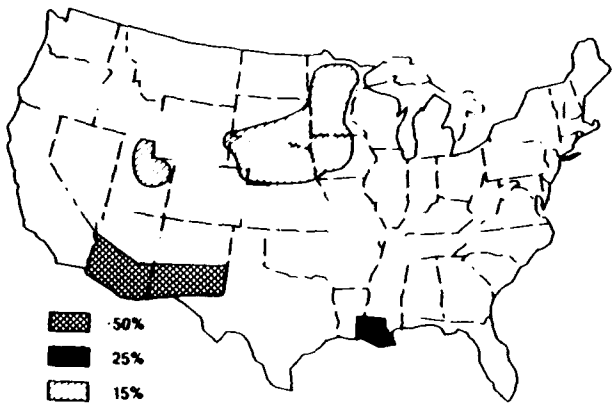

Fig.5 TYPICAL STABILITY PROFILE

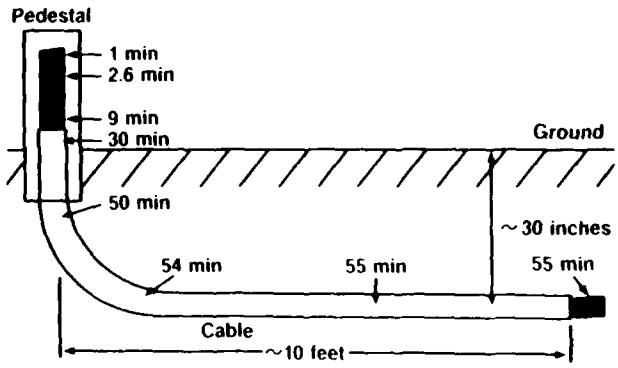

After the stabilizers are lost, oxidation of the polyolefin begins. Changes in the chemical structure lead to physical stresses and craze formation. Physical defects and/or voids in the insulation act as initiation sites for crazes to grow in size and concentration until visible cracks are formed. It is difficult to theoretically predict the time between the onset of oxidation and when the first cracks are seen. This latency period is determined by the defect concentration and the physical stresses on the insulation. This interval can be determined by empirical studies of insulations.

Fig.6 INSULATION OIT VALUES VERSUS DISTANCE FROM CONNECTOR

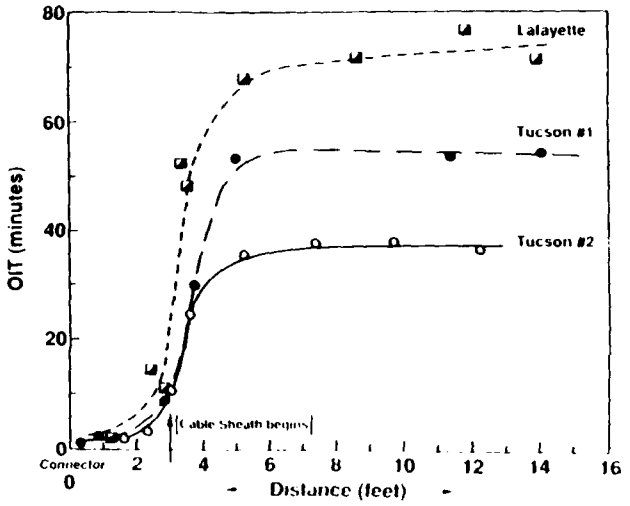

Accelerated aging experiments were performed to predict lifetime remaining for those insulations found to be "at risk". As with LDPE, log(time to crack) was plotted versus the reciprocal of the temperature for a selection of "at risk" insulations. A typical plot is shown in Figure 7 for foam-skin insulations from Arizona, which predicts cracking will occur within a further 1-3 years. Similar aging experiments were done on field samples from the three geographic zones and the remaining lifetime was determined to be as low as 1-3 years in the southwest, 3-6 years in the south, and 5-7 years in the midwest. For each sample tested, the remaining lifetime found was added to the time since installation to obtain the cable age at which cracking may begin. This turns out to 8-10 years in the southwest, 14-18 years in the south and 16-20 years in the midwest. These predictions are consistent with extrapolations based on LDPE cracking that began in the 1960s (Figure 8).

Fig.7 ARRHENIUS PLOT FOR PREDICTION OF LIFETIME REMAINING

(○, ●, ■ = 3 different insulations)

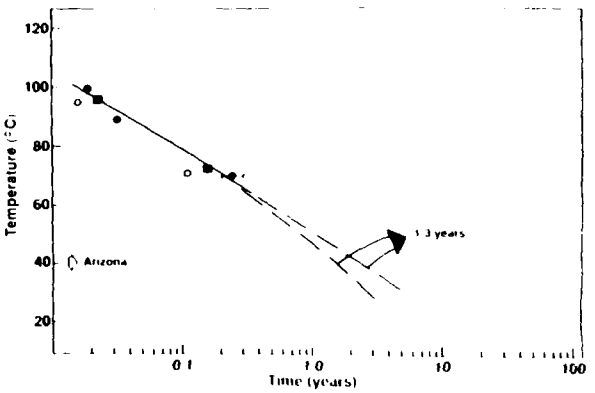

The predicted cable ages for cracking are for insulations in ready-access pedestals that experience regular activity and full sun exposure. High activity in a pedestal increases stress on the insulations which increases their degradation rate. High temperatures accelerate the degradation and are determined by the climate of the geographic area and the sun exposure of the pedestal.

Fig.8 PREDICTIONS FOR FOAM-SKIN HDPE BASED ON LDPE HISTORY

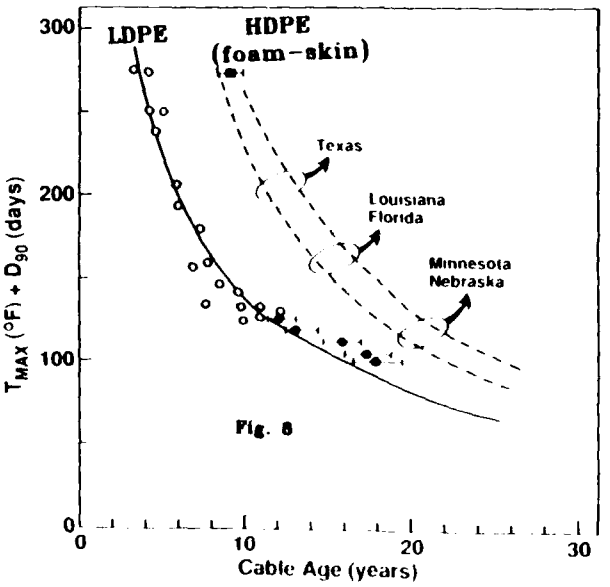

Predictions of the onset of cracking and cable lifetimes for representative locations around the country are shown in Table 4.

TABLE 4. PREDICTIONS FOR FOAM-SKIN HDPE INSULATIONS

LOCATION	AVERAGE T_{MAX} (JUNE-AUGUST) °F	DAYS/YEAR WITH > 90°F	FIRST CRACKS YEAR & CABLE AGE (years)		CABLE LIFETIME (years)[a]
Phoenix, AZ.	108	170	1985	8-10	10-15
Tucson,Yuma AZ.	105	150	1985	8-10	10-15
El Centro, CAL.	100	150	1987	10-12	10-15
San Antonio, TEX.	95	110	1988 +	12-14	12-17
El Paso, TEX.	95	101	1988 +	12-14	12-17
New Orleans, LA.	90	69	1990 +	14-18	15-20
Miami, FL.	90	67	1990 +	14-18	15-20
Nashville, TENN.	88-90	60	1990 +	14-18	15-20
Omaha, NEB.	90-92	40	1992 +	16-20	> 20
Minneapolis, MINN.	83	15	1992 +	16-20	> 20
Portland, MAINE	76	5	1995 +	20 +	> 25
Seattle, WASH.	70-74	2	1995 +	20 +	> 25

(a) Cable Lifetime = Cable age when 20-25% percentage of insulations in a pedestal have cracked.

The spread of the cracking around the country is expected to follow the same pattern as was seen in the LDPE case, since the same fundamental mechanism is occurring; i.e, thermal oxidation of polyethylene. The years when cracking can be expected in various parts of the country are summarized in Figure 9. The number in parenthesis equals the expected cable lifetime which is defined as the cable age when 20-25% of the insulations inside a pedestal have cracked. Extensive remedial action would be needed for insulated wires in such a pedestal.

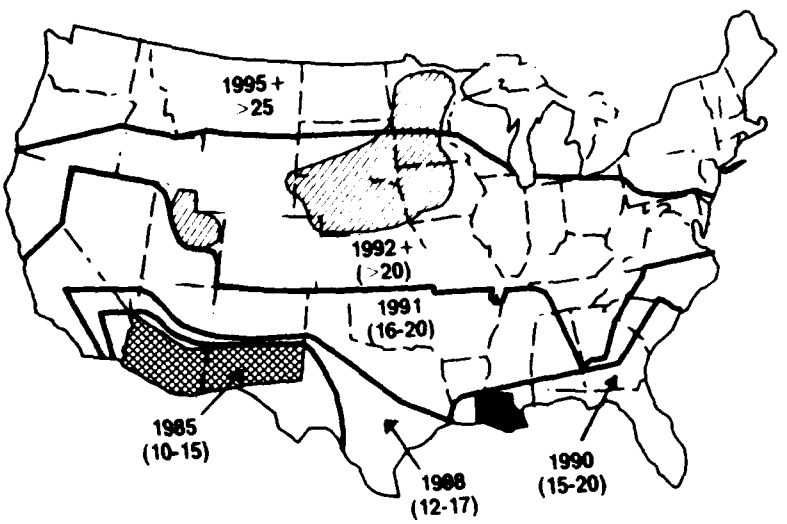

Fig.9 PREDICTIONS FOR U.S.A.
(This map is for illustration and should not be used to predict lifetimes for specific location. Local variations can greatly affect T_{MAX} and D_{90}.)

REMEDIAL ACTIONS

The remedial action selected for existing pedestal plant depends on whether the insulation is in category (1) already cracked, (2) "at risk" of cracking or (3) in no danger of cracking for many years. Cracked insulations have been irreversibly damaged and cannot be rejuvenated. Rehabilitative insulating varnish sprayed on wires should be regarded only as a temporary fix because it does not adhere well to the insulation surface which is usually contaminated with filling compound or dirt. Permanent repair requires replacement of the damaged wires.

Antioxidant booster sprays and pucks are concentrated reservoirs of stabilizer that are placed in the pedestals on the principle that volatile stabilizer will migrate from the reservoir to vulnerable insulations. However, stabilizer will also migrate to all other parts of the pedestal, out of the pedestal and out of the insulation. Sprays are available to coat the insulated wires directly with a varnish-like coating. They do retard the degradation rate, however, they make the insulations tacky and spraying needs to be repeated every year or so. Such sprays do not appear to regenerate the insulations, since samples of such coated insulations were examined and the underlying insulations had OIT values of ~0.4 minutes. The urethane coating sealed the insulation and reduced further oxidation. The coating is brittle and will eventually crack, exposing the underlying insulation to the environment once again.

It is impossible to determine whether insulations are in category (2) or (3) without laboratory analysis. However, the history of cracking in low density polyethylene insulations in the 1960-70s, coupled with this field survey, allows susceptible geographic areas to be identified (Figure 9). For those insulations "at risk", steps can be taken to slow deterioration. The temporary fixes noted above may last for years in milder climates. The best repair, short of replacement, consists of an internal airtight closure that minimizes oxygen infiltration and stabilizer evaporation. These closures should protect the insulation like a cable sheath which prevents stabilizer loss even inside a hot pedestal (Figures 5 and 6). Such closures may also act as a heat sink that reduces the temperature extremes seen by the insulation and lowers the T_{eff}. A reduction of 10°C in T_{eff} should double the insulation life. The final option is to cut back into the sheathed cable and re-splice (or add jumper cabling) which will replace the vulnerable insulation with well stabilized insulated wires. In any case, minimizing activity in the pedestal will delay the onset or extent of failures, since stress accelerates both crack formation and propagation.

CONCLUSIONS

This survey has confirmed that foam-skin HDPE insulations are susceptible to thermal oxidation and cracking after less than a decade in the field. Such insulations are used in the latest design of water resistant PIC (polyolefin insulated conductor) cables. The problem is attributed to inadequate stabilizer design for the pedestal environment, not poor quality control during manufacture. The residual stability of field insulations was measured for selected sites in the U.S.A. and depended on climatic factors, primarily temperature. The incidence of cracked insulations and vulnerable plant was high in the hot southwest but decreased on moving to cooler climates. Cracking patterns were predicted using results from laboratory aging of field samples as well as the history of cracked LDPE insulations.

ACKNOWLEDGEMENTS

The author is indebted to C.Moser, B.Havens, F.Zimmerman, T.Cox, T.Clarke, M.McManus, R.Munson, and A.Perry of U S WEST Communications; J.Blaszczynski, D.Wilmont, D.Whitley of BellSouth; G.Woodward and H.Barnard of South Central Bell for their aid in sample selection and collection. R.J.Miner is thanked for assisting in OIT measurements. P.A.Link is thanked for sharing and discussing his previous surveys. R.J.Gabel (U S WEST Communications), P.C.Warren and I.M. Pfitz are thanked for discussions and suggestions throughout this study. P.C. Warren and M.J. Bowden are thanked for their suggestions on the manuscript.

REFERENCES

1. J.Howard, Proceed. 21st Int. Wire Cable Symp. 329, 1972.
2. H.Gilroy, Proceed. 23rd Int. Wire Cable Symp. 42, 1974.
3. W.L.Hawkins, "Polymer Degradation and Stabilization" , Springer-Verlag, Berlin , 1984.
4. L.H.Lee, C.L.Stacy and R.G.Engel; J. Appl. Polym. Sci.,**10**, 1699, 1966.
5. H.S.Laver, "Developments in Polymer Stabilization - 1", Chap. 5 (Ed. G.Scott) Appl. Sci. Pub.; London, 1979.
6. W.L.Hawkins, M.G.Chan and G.L.Link; Polym. Eng. Sci., **11**(5), 377, 1971.
7. D.L.Allara and M.G.Chan; J. Polym. Sci., Polym. Chem. Ed., **14**, 1857, 1976.
8. M.G.Chan, H.M.Gilroy, J.Johnson, and W.M.Martin; Proceed. 27th Int. Wire Cable Symp., 99, 1978.
9. M.G.Chan and R.A.Powers, Soc. Plast. Eng., Tech. Pap.,**21**, 292, 1975.
10. M.G.Chan, Proceed. 23rd Int. Wire Cable Symp., 34, 1974.
11. K.D.Kiss and E.G.Malawer, Proceed. 26th Int. Wire Cable Symp., 68, 1977.
12. H.E.Bair, Chap. 9 of "Thermal Characterization of Polymeric Materials", ed. E.A.Turi, Academic Press, New York, 1981.
13. E.T.Kokta, Proceed. 24th Int. Wire Cable Symp., 220, 1975.
14. M.G.Chan, H.M.Gilroy, I.P.Heyward, L.Johnson and W.M.Martin; Soc. Plast. Eng., Tech. Pap., **24**, 381, 1978.
15. L.D.Loan, Proceed. Golden Jubilee Conference on *Polyethylenes 1933-83 (June 1983) London.*
16. B.D.Gesner, J.W.Shea and F.R.Wight, Proceed. 32nd Int. Wire Cable Symp. 7 (1973)
17. B.Havens, Outside Plant, 19, Jan-Feb. 1988.
18. P.A.Link, private communication
19. BELLCORE Technical Requirements - TR-TSY-000421 - "Generic Requirements for Metallic *Telecommunications* Cable" 1987.
20. D.D.O'Rell and A.Patel, Proceed. 24th Int. Wire Cable Symp., 231, 1975.
21. B.B.Pusey, Proceed. 10th Int. Wire Cable Symp., 1961.
22. J.J.Helbing and R.A.Houben, Can. Plast., **31**, 18,1973.
23. G.Link, private communication.
24. G.D.Brown, Proceed. 36th Int. Wire Cable Symp., 337, 1987.
25. L.E.Davis, Proceed. 36th Int. Wire Cable Symp., 475, 1987.
26. G.D.Brown and L.E.Davis, Proceed. 36th Int. Wire Cable Symp., 734, 1987.
27. H.J.Ruddell, D.J.Adams and B.A.Chisholm, "Plastics in Telecommunications III, Plastics and Rubber Inst., London, Eng. 8 1-21, 1982.; and Aust. Telecommu. Res., **6**(2), 57, 1982.
28. B.L.Board and H.J.Ruddell, Proceed. 32nd Int. Wire Cable Symp., 300, 1982.
29. H.J.Ruddell, D.J.Adams, P.Latoszynski and B.T.de Boer; Proceed. 33rd Int. Wire Cable Symp., 104, 1983.
30. G.A.Schmidt, Proceed. 26th Int. Wire Cable Symp., 161 (1977)
31. R.H.Hansen, T.DeBendictis and W.M.Martin; Polym. Eng. Sci., **5**(4), 3, 1965.

Trevor N. Bowmer is a member of the Polymer Chemistry and Engineering Research Group in Bellcore, Red Bank N.J. He received his Ph.D. in chemistry from the University of Queensland, Australia, where he studied radiation chemistry of polymers. Joining Bell laboratories in 1980, he investigated radiation cured systems and lithographic materials. In 1984, he came to his present position where his interests include degradation mechanisms and characterization of polymeric materials used in telecommunications applications.

Improved Life Expectancy Testing for PIC Cable Insulation

Lawrence E. Davis

Superior Cable

ABSTRACT

Due to the work of several companies, the stabilization package for insulation has been changed within the last two years to correct premature failure of cellular insulation installed in the warmer regions of the country. The response of organizations to improve quality control test procedures has understandably been proceeding at a slower pace. Areas of concern include preaging of cable, maximum insulation test temperature, test chamber, and formation of stress within the insulation under test. Comparative laboratory evaluation of new test procedures will need to be conducted to establish repeatability and compliance by manufacturers before new requirements can be incorporated into industry specifications. Work under an ICEA advisory committee is being conducted to resolve problems and concerns associated with the current specification requirements and improve test methods.

INTRODUCTION

The stabilization package for foam and foam skin insulation has been recognized to be less effective than the same stabilization package in solid insulation. This is reflected in the oxidation induction time (OIT) test and requirements for cellular and solid insulation when the material was accepted by the industry. Foam skin insulation has an OIT requirement one half as stringent as solid insulation. This is accomplished by removing the catalytic action of copper from the foam skin OIT test. Two additional changes in the OIT test from the REA PE-39 to the REA PE-89 specifications effectively cancel the other. The end point requirement is doubled while the test temperature is reduced, cutting the oxidation rate in half (Table I). Cellular insulation was never claimed to be the equivalent of solid insulation in terms of oxidation stability or physical toughness; foam and foam skin were only claimed to be "good enough". In retrospect the claim appears to be invalid with respect to aging requirements. Recent improvements in the stabilization package have been incorporated to improve life expectancy of celular insulation (Table II).

Changes in the stabilization package resulted from field failures and laboratory oven aging test. The current quality assurance and quality control tests do not indicate the need to increase the stabilization of foam skin insulation.

TABLE I

OIT Test Condition And Requirment

Document	Requirment (minutes)	Temperture Deg C	Pan	Oxygen flow rate (ml/minute)
TR-TSY 000421 solid	20	200	copper	200
TR-TSY 000421 foamskin	20	200	aluminum	200
REA PE-39 solid	15	199	copper	50
REA PE-89 foamskin	30	190	aluminum	50

TABLE II

STABLIZATION PACKAGE RANGE CHANGE
(percent)

YEAR	SOLID		FOAM	
	ANTIOXIDANT	COPPER INHIBITOR	ANTIOXIDANT	COPPER INHIBITOR
1978	0.08-0.15	0.08-0.15	0.08-0.12	0.08-0.12
1979	0.11-0.20	0.10-0.18	0.08-0.12	0.08-0.12
1985	0.18-0.26	0.10-0.18	0.08-0.12	0.08-0.12
1986	0.18-0.26	0.10-0.18	0.12-0.18	0.12-0.18
1987	0.18-0.26	0.18-0.26	0.15-0.21	0.15-0.21

LABORATORY WORK

Early in the use of foam skin Superior Cable recognized that filling compounds rapidly leached antioxidants from the insulation, reducing Oxidation Induction Times (OIT) to low values. Tests conducted in 1979 show significant OIT reductions after one week at 70 degrees C. Similar studies had previously indicated reduced stability of cellular insulates. Refer to Oxidation Stability Studies on Cellular High Density Polyolefin Insulation for Communications Wire by O'Rell, D.O., and Patel, A., International Wire and Cable Symposium, 1975.

TABLE III

Oxidation Induction Time Of Foamskin

CABLE	UNAGED REA PE-39	AGED 1 WEEK AT 70°C REA PE-39
1	47.6	11.25
2	24.1	2.8
3	34	4.8

NOTE. Values are an average of ten readings and are in minutes.

The data in Table III was presented to a material supplier who quietly canvassed the industry to determine if an increase in antioxidant was needed since Superior Cable desired an increase. Unfortunately, the industry concensus did not agree with Superior and little change in the stabilization package was made in 1979 since an independent cable supplier could not cost effectively obtain an alternate material. There were several reasons why more attention was not given to the aged OIT data. First, OIT data did not have good extrapolation or correlation with field failure. Secondly, the industry was operating in the "its good enough" mode, and finally the quality assurance test in the specifications did not indicate any long term problem.

By 1982 Superior Cable began development of an oven aging test which incorporated preaging of the insulation in filled cable to simulate reel storage. Initial data extrapolation indicated some foam skin stress crack failure would occur in approximately 10 years in the warmer regions of the country. The oven aging test was continued for several years as part of a joint effort by Union Carbide and Superior Cable to develop a foam skin product with improved life expectancy. The results of the joint effort were reported in three papers presented at the 1987 International Wire and Cable Symposium and established the need to increase the stabilization package for foam skin. Concurrent with this work, reports of field failure of foam skin insulation began to be received in 1985 substantiating the validity of the oven aging test.

As a result of the field failures, AT&T and Bellcore began a series of laboratory work to determine the cause of the failure. AT&T and Bellcore laboratory work also indicated a need to increase the stabilization package for the foam skin insulation. The net result of the laboratory work was to increase the antioxidant and copper inhibitor in the polyethylene insulation in 1986 and 1987. While improvement in the life expectancy of the foam skin insulation has been obtained by increasing the stabilization package, the inadequacy of the specification test to provide safe guards that insure reasonable life expectancy is still being addressed.

TEST IMPROVEMENT

The industry does recognize the need for an improved quality assurance test for insuring the long term performance of foam skin insulation. Numerous opinions as to the pros and cons of different approaches have been expressed. Two test methods are currently undergoing evaluation to provide a standard for judging the quality of commercial products. They are a modification of the oven test employed by Superior Cable to predict field problems and a modification of the pedestal aging test provided by Bellcore. Table IV provides a summary of the differences and proposed changes of the two tests. To determine the relevance and to delineate the differences between the test methods a criteria must be established against which the procedures can be judged. The following points should be considered in evaluating the two test methods:

- The test method when used to evaluate material with a 1978 to 1985 stabilization package should predict early failure commensurate with field failure.
- The test has to be repeatable when conducted by different laboratories.
- Accelerated aging should not alter the physical state or crystallinity of the materials under evaluation. (above that which may occur in the field)
- Test time should be reasonable for a qualification test.
- Test method must be capable of detecting all failure modes which might occur.
- Test should be easy to conduct.
- Test should evaluate the worst case field condition that may occur due to manufacture, storage, and installation which can be reasonably controlled in the laboratory.

The oven aging test developed by Superior Cable is capable of meeting these requirements. Oven aging data predicted field problems before they occurred.

Moderate temperatures, 80° C, or less are used to maintain the material below the major transition range of high density polyethylene which are not encountered in application of the product. Exceeding the transition temperature of polyethylene will alter the rate of deterioration caused by a number of degradation processes.

A total test time of seven months is required to insure a 30 year life expectancy, using the oven test. Seven months is a reasonable test time for a qualification test.

The oven procedure uses the introduction of stress to the sample at scheduled times to evaluate the degree of thermal embrittlement and solvent cracking, as well as exposure to hot air to evaluate oxidation. While oxidation is the primary form of degradation for currently used high density compounds, other forms of deterioration must be evaluated since the introduction of new material may have different synergistic effects or weakness.

The oven procedure does not require special controllers, heating mantels, or containers not found in wire and cable plants, and is easy to conduct.

By using preaging of the insulated conductors in the cable and the formation of pigtails in the test wires, the worst case condition of reel storage and induced stress due to installation and maintenance are incorporated into the oven aging procedure. The air movement in a forced draft oven also accelerates the oxidation.

Repeatability concerns appear to be the cause of reluctance to accept the oven test in specifications. The main elements of the procedure have been repeated by Superior Cable on a number of different cables and found to be repeatable within the expected distribution of cable samples from different suppliers. Currently, a round-robin test is being conducted to establish the repeatability of a modified method at various laboratories under ICEA sponsorship. The round-robin test should confirm the desirability of using the oven aging method of evaluating life expectancy for communication cable insulation.

The ICEA working committee has modified the oven test from the procedure used in the work presented last year. The main features of the test have not been altered, including the preaging of cable for 4 weeks at 70° C, formation of periodically controlled stress in the sample, and the uses of 80° C or less test temperature in a forced draft oven. The modifications are the addition of additional stress after 20 weeks in the oven (due to longer life expectancy resulting from higher stabilization package) and the use of a mandrel instead of the insulated wire as the core around which the wire is stressed. To aid in repeatability, an oven capable of complying with ASTM E 145-68 is specified and minor clarifications have also been included. The "Long Term Stability of Solid, Foam, and Foam Skin Insulation Round Robin Test" is provided below for the readers:

LONG TERM STABILITY OF SOLID, FOAM AND FOAM SKIN INSULATION

A. OUTLINE OF METHOD

Insulated conductors from communications wire or cable are exposed to elevated temperature conditioning in the finished product, then removed from the wire or cable and subjected to controlled stresses at elevated temperatures in a forced draft over. Additional controlled stresses are placed in the insulated conductors, at periodic intervals, during oven aging. End points are determined from the initial stressed (coil) insulation failure.

B. APPARATUS

1. Forced Draft Oven: A circulating air oven conforming to ASTM E 145, Type IIB, and having a minimum internal height of 15 inches.

2. Support Bracket: Any device which will allow the test samples to hang free in the oven. Material in contact with the insulation should not act as a catalyst to oxidize the insulation.

3. Temperature Monitoring System: Any system capable of monitoring the oven temperature.

4. Mandrel: Smooth, round steel (piano wire, drill bit, etc.) with a diameter equal to that of the insulated wire being evaluated and having a surface which is free of burrs and rough edges.

C. PROCEDURE:

1. Sample Preparation:

1.1 From completed wire or cable, cut sufficient samples 24 inches long, so that the samples contain a minimum of 30 insulated conductors.

1.2 Seal the ends of the wire or cable samples with cable caps.

1.3 Precondition the sealed wire or cable samples, for 4 weeks, in an oven stabilized at 70° ± 1° C.

1.4 At the end of 4 weeks, remove from oven, stabilize at room temperature (overnight) and then remove the insulated conductors from the sealed wire or cable samples.

1.5 Separate twisted pairs into single insulated conductors.

1.6 If the finished product contained filling compound, remove the compound from the insulation by wiping with a clean dry tissue or clean soft cloth. DO NOT USE SOLVENTS.

1.7 Form a loop or hook in one end of an insulated conductor to allow for hanging the sample. (see Figure I). The loop or hook should be approximately one inch in diameter. Make a "coil" in the insulated conductor (1 1/2" below the loop or hook) by wrapping around the appropriate mandrel for ten close, tight turns.

CAUTION: USE FORCE SUFFICIENT TO FORM A CLOSE, COMPACT SERIES OF TURNS ON THE WIRE WITHOUT CRUSHING THE UNDERLYING INSULATION. BE CAREFUL NOT TO

DAMAGE THE INSULATION WITH FINGERNAILS. A PAIR OF THIN, COTTON GLOVES MAY BE WORN TO ENSURE THAT THE INSULATION IS NOT DAMAGED BY FINGERNAILS.

1.8 Repeat Step 1.7 until 30 specimens (3 of each color, if 10 colors are available) have been prepared.

2. Aging:

2.1 Hang the 30 insulated conductor specimens on a support bracket in a forced draft oven maintained at 80° ± 1° C. Insulated conductor samples from different types of wire or cable should not be aged in the same oven. In this case "different" means different insulating materials, stabilization packages or filling compounds.

2.2 If extrapolation of results to field conditions is desired, a second set of samples shall be placed in a forced draft oven maintained at 70° ± 1° C. This condition is not required for insuring adequate stabilization.

2.3 At the end of 8 weeks of oven aging form a second "coil" approximately one inch below the first "coil".

2.4 At this point begin inspecting specimens for "coil" cracking every two weeks and record the percentage of "coil" cracking for the first and second "coils".

NOTE: Cracks may occur in the loop or hook due to handling, weight of the specimen or oxidation at the point of contact with the support bracket. For this test, cracks in the loop or hook are not counted.

2.5 At the end of 20 weeks of oven aging form a third "coil" in each specimen and continue to record the percentage of "coil" cracks every two weeks for first, second and third " coils".

NOTE: For qualification testing purposes, the test may be terminated when a 50% failure of the first coil occurs. For investigation into the type of insulation failure, proceed with Steps 2.6 and 2.7.

2.6 When 50% of the first "coils" fail, form a fourth "coil" in each of the specimens and record the percentage of fourth "coils"which crack during formation.

2.7 When 100% of the first "coils" fail, form a fifth "coil" and record the percentage of fifth "coils" which crack during formation. Formation of fifth "coils" terminates the oven aging.

D. REQUIREMENT:

If more than 5% of the first or second "coils" crack on or before the 26th week, it shall be considered that the insulation is inadequately stabilized for the composite construction of the communication product or that processing conditions have compromised the life expectancy of the material.

E. INTERPRETATION

1. The time to failure of the first "coils" provides a measure of life expectancy for the worst case condition of the product as received by a customer for any of the failure modes for insulation.

2. The second and third "coils" provide information as to the susceptibility of the insulation to thermal embrittlement. Early failure of the second or third "coils" relative to the first "coil" indicates degradation of the insulation prior to formation of the additional "coil" stresses.

3. The fourth and fifth "coils" aid in determining the type of insulation failure occurring for the first "coil".

PEDESTALS IN THE LABORATORY

A comparison as to over all relevance of oven versus pedestal test methods is inappropriate since modification and development of both procedures are currently being conducted. Indeed, Bellcore has suggested changes in the Pedestal test which incorporate many of the features of the oven test (preaging and addition of stress). The differences in the proposed methods, therefore, are much closer together than the original two tests. However, a few comments are in order as to the use of a pedestal as a test chamber. There is a misconception that the operating environment is more closely simulated by using a pedestal in the laboratory. When one examines the facts it becomes apparent that the use of the pedestal in a laboratory test does not simulate the field environment better than ovens.

Cable access in the field may not even be in a pedestal. There are several different kinds of housings in which cable may be spliced, such as hand holes, cross connect boxes, pedestal of different kinds, and even ready access closures in the air. The environment in each of the kinds of housing and even various models of pedestals may be considerably different. In fact, operating practices may alter the conditions within a particular model of pedestal by the use of ped caps, polyethyelene bags containing antioxidants, and other modifications to the pedestal that an operating company may use.

The location of pedestals in a given run of cable may also affect the environment within the pedestal. The pedestal could be located at the top of a hill in an open field, or in a ditch, or along a creek bank which may periodically flood, or be located in a hedge row that provides continuous shade. On a broader scale, pedestals may be placed in swamp conditions subjecting the wire to decay products such as hydrogen sulfide, sulfur dioxide,

swamp gas, etc. or be placed in salt air conditions along a coast, or exposed to air borne pollutants in industrial cities, or exposed to agricultural chemicals beside farm land, or exposed to relatively clean air in open country. The exposure of the pedestal to temperature cycles and humidity cycles will be widely different. Some pedestals will have biological waste products form invading wasps, ants or other insects leading to the use of insecticide in some pedestals.

From the above discussion, it can safely be assumed that neither a pedestal nor an oven totally simulate field conditions. Then why has the use of a pedestal been incorporated into specification test? As one advocate, of pedestals, said: "The pedestal is a cheap static air oven". If the pedestal is used as an oven, lets examine what makes a good oven.

Ovens are used in the laboratory to provide accelerated aging conditions which can be controlled to close tolerances and that are repeatable from test to test and location to location. If the proper conditions are chosen and maintained then laboratory testing can provide a means of insuring a reasonable life expectancy for cable and wire systems. The determination of using pedestals needs to be made with regard to the ability of the housing to function as a test oven.

Technicians conducting pedestal aging test have noted variations in results dependent on the placement of wire within the pedestal, particularly rapid deterioration of material results if contact with the metal sides occurs. More recently Bellcore mapped the temperature distribution in a pedestal and found significant gradients horizontally and vertically. Therefore, the placement of samples within a pedestal as well as the placement of the measurement and control thermocouple relative to the samples are critical. Also, problems with temperature over-shoot at start-up and pedestal reentry have been noted. These temperature variations make it difficult to maintain reliability and repeatability when using pedestals. Since the pedestal has a restricted volume of usable temperature controlled space it is difficult or impossible to employ repeated stressing of the insulation which may be required to insure life expectancy or determine failure modes. For providing controlled, repeatable test temperature and convenient work space, pedestals do not compare with modern ovens which meet ASTM requirements for temperature and air exchange rates. There is an inertia, however,to keep the pedestal as a test oven in order to maintain the historical record. Maintenance of a historical record is not justification to continue using an inferior test chamber.

The selection of the type of oven to be used to accelerate aging then depends on the desirability of maintaining a uniform temperature within the oven and whether the air is to be stagnant or moving. Pedestals in the field do not have a stagnant environment. Air is exchanged due to thermal convection and wind disturbance. A forced air oven will exchange the air surrounding the wire more frequently than occurs in a field installed pedestal. This aids in accelerating the oxidation rate and reduces cross contamination between samples. When using a pedestal as a static air oven, the air movement is restricted by the heating mantel, temperature gradients and lack of wind in the laboratory environment as opposed to actual use conditions. To insure repeatability forced air ovens complying with ASTM E145 Type IIB should be employed for artificially aging wire.

QUALITY CONTROL TEST FOR STABILIZER

As previously noted, the oxidation induction time procedures used for quality control purposes are different for solid and foam skin insulation. The differences are related to the inability of the insufficiently stabilized foam skin insulation to comply with the original solid insulation requirements rather than with the level of stabilizer needed to provide adequate service. Logically the test requirement for foam skin insulation should be the same as that required for solid material. While the capabilities may be different for the two products, the end use expectation is not. OIT test procedures also need to be reviewed by REA, Bellcore, ICEA and other organizations concerned with specifications.

CONCLUSION

The need to revise the quality assurance test has been generally recognized by the industry and an effective dialogue for developing a consensus for a new test has been established. Ultimately, the selection of a universal test procedure will depend upon the effectiveness of the test and its reproducibility.

Lawrence E. Davis is the Senior Engineer for Materials/Processing for Superior Cable Corporation. He received his B.S. degree in physics from the Appalachian State University in 1969 and graduated with a Master's degree in physics from the University of Wisconsin, Milwaukee in 1974. Prior to joining Superior Cable, Mr. Davis was the Materials Engineering Manager for Technical Staff, Siecor Corporation and was formerly a Materials Engineer for Continental Telephone Laboratories.

Table IV
Comparison Of Test Methods

Method	Chamber	Preaging	Stress	Type Of (3) Stress	Temperture Deg. C
Globle Test (oven test)	Forced Draft Oven	4 Weeks At 70 C	Initial 8 Weeks (2) 50% of Initial 100 % of Initial	Pigtail	80
ICEA Modified Oven	ASTM Type II (1) Oven	4 Weeks At 70 C	Initial 8 Weeks 20 Weeks 50% of Initial 100% of Initial	Coil	80
Thermal Oxidation Stability (pedestal)	Pedestal 6 Inch Square By 16 or 24 or 48 Inches	None	End Of Test Period	Coil	90
Modifide Pedestal	Pedestal 6 Inch Square By At Least 16 Inches	2 Weeks At 70 C	Initial	Coil	90

NOTE: 1. Control temperture and air flow.
2. For the ICEA round robin test the stress formed after 50% and 100% failure of the first pigtail are considerd as research tools and may be eliminated for purposes of quality assurance.
3. Pigtails are formed by wrapping the insulated conductor around itself. Coils are formed by wrapping the insulated conductor around a steel mandral with the same diameter as the insulated wire.

STABILITY OF POLYETHYLENE INSULATIONS IN THE FIELD AND LABORATORY

T.N.Bowmer, E.P. Hjorth, R.J. Miner and O.S. Gebizlioglu

Bellcore
New Jersey, U.S.A.

ABSTRACT

The latest design of polyolefin insulations used for copper telecommunication wires cracked after less than a decade in the field. We have compared insulations aged in the field with those subjected to accelerated aging tests in the laboratory. The thermal stability tests currently used in U.S.A. cable requirements were shown to be inadequate for ensuring the desired 40 year lifetime in the field environment. The effects of physical stress and stabilizer extraction on the aging of cable insulations were examined. Insulated wires stressed into tight wrapped coils were found to degrade 3-4 times faster than straight unstressed wires. In addition, extraction of stabilizers by the filling compound increased degradation rates by another factor of 3-4. Filling compounds extracted the stabilizers equally efficiently from both solid and foam-skin insulation designs.

INTRODUCTION

A large percentage of telecommunication cables consist of polyolefin insulated conductors (PIC) grouped into color coded pairs and protected by metallic and plastic sheaths. The latest design of PIC cable utilizes insulations of high density polyethylene (HDPE) consisting of an inner coating of foamed HDPE with an outer skin of solid HDPE. Foam-skin HDPE insulations began to be deployed around 1976 and were expected to last 40 years. However insulations have cracked inside pedestals after less than a decade in the hot southwest of the U.S.A.[1]. Clearly, the test procedures used to evaluate these insulations did not simulate the operating environment.

The insulations are affected by many environmental factors but the two most important are believed to be temperature and physical stress. High temperatures accelerate the rate of both oxidation of the polyolefin and stabilizer loss by extraction and evaporation. Since 1972, buried cables have been filled with a waxy hydrocarbon compound to make them water resistant. These filling compounds have been reported however to extract stabilizer from the insulation particularly when the cable reel is exposed to the sun during storage and or transport before installation[2-4]. Once buried, temperatures are cooler and extraction of further stabilizer is assumed to be minimal. Physical stress accelerates craze formation and crack propagation. It is important therefore that test procedures designed to screen cable insulations for long term applications take these factors into account.

The Oxidative Induction Time (OIT) test and the EPIC (Experimental Pedestal Installation Complex) pedestal test[5] have been used to evaluate the stability of PIC insulations. The OIT test determines the time for oxidative degradation to begin at high temperatures (typically 200 C) in pure oxygen. This test is excellent both for screening materials and for quality control since relative changes in OIT values represent changes in stability and or stabilizer concentrations. The absolute OIT value is less important since it can not be used reliably to forecast insulation lifetime. However, very low OIT values of 0-2 minutes imply that little or no stabilizer is present.

In the pedestal test, insulated wires are heated in laboratory pedestals at various elevated temperatures. The times at which the insulations crack are noted and lifetime predictions are then made by extrapolating to field temperatures. The pedestal test has proved reliable for predicting failures in LDPE insulations[1,5,6].

Monitoring degradation inside forced-air ovens is an alternative accelerated aging technique, but previous studies[7,8] suffered from large variations in results between laboratories. These variations probably resulted from inadequate temperature control from oven to oven since different ovens may have different air exchanges, temperature tolerances and inside temperature profiles.

Current PIC cable insulations in the United States are required to have a minimum OIT value of 20 minutes and survive pedestal tests of 45 days at 110 C and 1 year at 90°C [9]. These test conditions were expected to ensure a 40 year life[6] although some aging results[2,10] predicted cracks may occur in foamed and foam-skin polyethylene insulations after only 10-15 years in the field. The current

pedestal test involves placing loops of insulated wires inside a heated pedestal, whereas field wires are typically twisted together for easy identification, and folded coiled to make maximum use of the pedestal space. Therefore stress should be applied to the insulated wires in the accelerated aging test to obtain an accurate field simulation.

There are two approaches to slow the degradation of polyolefin insulations (a) modify the operating environment or (b) improve the insulation material. The former may involve deploying stabilizer boosters, lowering temperatures inside closures through use of protective shields and reflective coatings, using secondary enclosures or even elimination of the ready-access plant in favor of closed plant. Improvement of the insulation material through better stabilizers, more stable resins or better filling compounds also represents a viable approach but requires an improved stability test that simulates the operating environment.

This paper examines the effects of stress and stabilizer extraction on the aging of PIC cable insulations. Cables that were manufactured in 1985 and 1987, but never installed, were examined along with cables recovered from the field after 8-10 years service. Calibration of laboratory testing to real field experience was achieved by accelerated aging of these cable insulations in ovens and pedestals. Such calibration of the accelerated test is essential for (1) accurate field lifetime predictions, (2) evaluating stability of new insulations and (3) quantitative assessment of remedial actions for insulations already installed.

TABLE 1 - WIRE AND CABLE SAMPLES

CODE	SAMPLE
A	Foam-skin HDPE insulation, filled cable, 1987
B	Foam-skin HDPE insulation, filled cable, 1987
C	Solid HDPE insulation, filled cable, 1987
D	Foam-skin HDPE insulation, filled cable, 1978 (stored outside for years in New Jersey)
E	Solid HDPE insulation, aircore cable, 1985
F	Solid HDPE insulation, aircore cable, 1987
G	Solid HDPE insulation, aircore cable, 1987
H	Uncabled wire insulated with solid HDPE (1987) (never exposed to filling compound)
I	Uncabled wire insulated with foam-skin HDPE (1987) (never exposed to filling compound)
X1	Buried section from in-service cable (Tucson, Arizona) Foam-skin insulation, filled cable, 1977
X2	Buried section from in-service cable (Tucson, Arizona) Foam-skin insulation, filled cable, 1979
X3	Buried section from in-service cable (Lafayette, Louisiana) Foam-skin insulation, filled cable, 1979

EXPERIMENTAL

The cable and wire samples used in this study are shown in Table 1. We have examined foam-skin insulated wires in filled cables and solid insulated wires in both aircore cables and filled cables. Table 2 lists the various test procedures used in the thermal testing of PIC cable insulations.

TABLE 2 - TEST PROCEDURES

TEST	PRECONDITIONING	SAMPLE	OVEN TYPE	CONDITIONS
OIT	--	INSULATION	CALORIMETER	200°C in O_2
CURRENT PEDESTAL	none	LOOP	PEDESTAL ("static oven")	110°C, 45days or 90°C, 1 year
MODIFIED PEDESTAL #1	none	COIL	PEDESTAL	110°C or 90°C
MODIFIED PEDESTAL #2	70°C 4 Weeks	COIL	PEDESTAL	110°C or 90°C
OVEN #1	none	LOOP	ASTM HB	80°C
OVEN #2	none	COIL	ASTM HB	80°C
OVEN #3	70°C, 2 Weeks	COIL	ASTM HB	80°C
OVEN #4	70°C, 4 Weeks	COIL	ASTM HB	80°C

Standard PC-6 (6x6x48 inch) pedestals from Kisco Company or Champion Metal Products were used. Accessories such as the terminal plates, plastic liners, grounding straps and support frames were removed before testing. Glas-Col Apparatus Company supplied 260 Watt heating mantles to fit closely over the top 12 inches of the pedestal. Temperatures of 110 or 90°C (±1°C) were maintained at the sample position using Omega Model CN-310-RTD-C or Glas-Col Model #PL612 proportional controllers. For better temperature control, the thermocouple was attached to the pedestal wall close to the heat source (Figure 1). An I^2R model OTP-30A protection probe was used to ensure that heat surges did not expose the insulations to high temperatures, which contribute disproportionately to the degradation.

The isothermal profiles generated in a heated pedestal are shown in Figure 2 as a 2-dimensional view through the center of the pedestal. If viewed in 3-dimensions, dome-shaped isotherms are seen. Temperatures increased rapidly as one moved up the pedestal and towards the wall. It is critical to keep the samples close to the apex of the profile otherwise the acceleration factor and predicted lifetime will be greatly altered. The sample temperature was monitored with thermocouples positioned at the height of the topmost insulated wire. Similar gradients are probably found in field pedestals.

Blue M model OV-510A-2 ovens (ASTM type IIB[11]) were used at 70 or 80°C (±1°C) with 150-180 air exchanges per hour. Insulated conductors from different cables were suspended 6 inches apart to allow an unrestricted flow of air over the samples and avoid cross-contamination. Preconditioning of cables was done by heating sealed cable sections at 70°C for periods up to 6 weeks.

For accelerated aging tests in pedestals and ovens, the insulations were removed from the cable sheaths, the filling compound wiped off with a dry cotton cloth, and the insulations stressed as outlined below. Typically, 25 or 50 insulated wires were selected with all colors represented. Oxygen Induction Times (OIT) were measured in aluminum pans at 200°C on insulations stripped from the conductors as described elsewhere[1].

Fig.1 PEDESTAL TEST

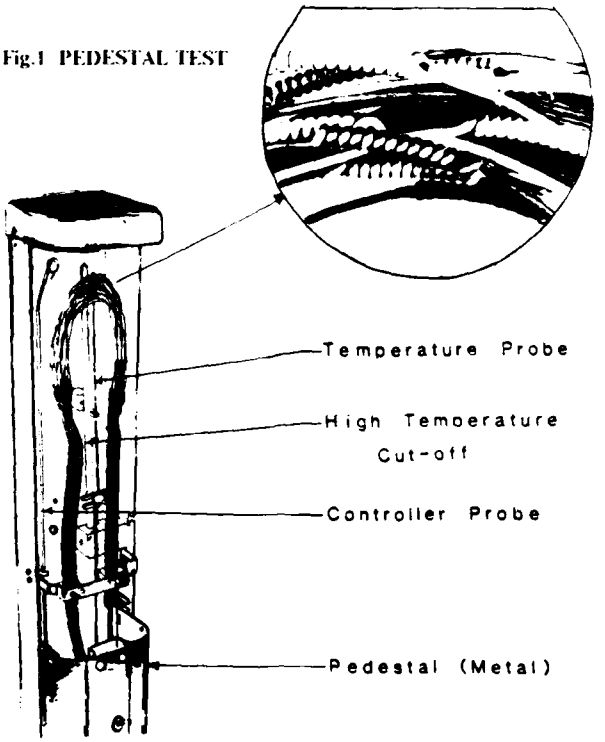

Fig.2 ISOTHERMS INSIDE HEATED PEDESTAL

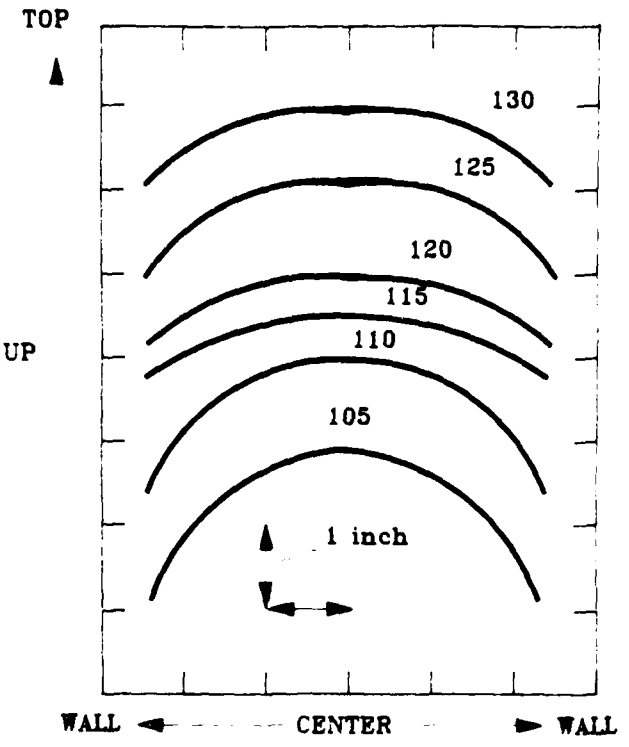

RESULTS AND DISCUSSION

Current Pedestal Test

The current pedestal test criteria was developed from aging studies of solid HDPE insulations from aircore cables[6,5,9], the assumption being made that the same test conditions would simulate forty years in the field for foam-skin insulations. The buried field cables (X1,X2) recovered after 8-10 years underground were tested and found to pass the current test. Insulations from these buried cables had OIT values of 40-60 minutes. Since these insulations were protected by cable sheaths in a cool environment, they are assumed to have at least the oxidative stability of the insulations when installed. For these buried samples, cracks were first seen after 120-140 days in a pedestal at 110°C. From the current test as written (i.e., 45 test days → 40 year life), one would surmise that these insulations would last

$$\frac{\text{40 years x 130 test days to failure}}{\text{45 day test minimum}} = 115 \text{ years}$$

However, insulations in the pedestal adjacent to this cable had OIT values of ~1 minute which implied little or no stabilizer remains. These insulations should begin to crack in another 1-3 years[1], giving an insulation lifetime of ~10 years.

The purpose of the pedestal test is to simulate the field behavior and predict a minimum lifetime that can be expected from an insulation. The analysis of the field samples shows that the pedestal test as currently written in the product requirements[9] clearly falls short of this objective.

Stress

One factor missing in the current test is adequate simulation of the mechanical stresses on the insulation during cable installation, splicing operations, terminations and routine maintenance activities that occur during the insulation's lifetime. Previous work on LDPE had shown that when accelerated aging was performed in pedestals with insulations twisted in pigtails or coils[5,6], the tests predicted the field cracking times of LDPE insulations.

In the current study, stress was applied by wrapping the insulated wire 10 close turns around a mandrel whose diameter equals the DOD (diameter over dielectric) of the insulated wire. For example, a 1.0 mm diameter mandrel was used for a 24 AWG gauge wire that is typically covered by 0.2 mm of insulation. The mandrel was removed leaving free standing coils which typically have an outer diameter of 3 mm and 1-2 mm between coils (Figure 1). Other stress configurations used were (1) elongated coils, where the helix coils are 10-20 mm apart but the outer diameter is still 3 mm, (2) large coils with a diameter of 10 mm and ~5mm between coils, and (3) insulated wires twisted around one another to form a double helix. These different stressing techniques change the direction and absolute magnitude of the stresses as well as the relative degree of tensile, compressive and shear stresses[12] applied to the insulation

Linear elastic stress analysis[12] predicted the relative stresses shown in Table 3 for the different sample configurations. Close wrapped coils have high tensile stresses directed along the axial direction of the wire which will lead to craze formation perpendicular to the wire and annular cracking. Elongated coils are under lower overall stress than close wrapped coils, and the stress pattern is much more complex with significant contributions from tensile, compressive and shear stresses. The stress magnitude and direction is more

TABLE 3 - LINEAR ELASTIC STRESS ANALYSIS

SAMPLE FORM	RELATIVE STRESSES			
	TENSILE		COMPRESSIVE	SHEAR
	Stress	Angle*		
Close Wrapped Coils	100	10	2	40
Elongated Coils	30-50	65-50	15	25-30
Large Coils	25	5	0.5	15
Loop	5	85	5	5

* Angle between maximum tensile stress direction and wire axis.

sensitive to the distance between the coils in elongated coils than in close wrapped coils. The elongated coils are therefore expected to crack later than the close wrapped coils and produce cracks at a 25-40 degree angle to the wire axis. The large coils will behave like close wrapped coils (i.e., annular cracks) but with a much slower degradation rate since the stresses are ~4 times smaller. The loop in the current pedestal test has stresses less than 0.1 of the stresses found in the close wrapped coils and therefore will take considerably longer to crack.

These conclusions were confirmed by experiments with samples A,B,X1 and X2. The results for X2 in various test and sample configurations are shown in

Table 4. Our samples showed that as the stress on the insulation increased the time to crack decreased. The degradation rate is at least doubled on going from the elongated coils to the close wrapped mandrel coils. The order of cracking is close wrapped coils > elongated coils ≅ twists > large coils > loops ≅ straight wires. In addition, the predicted pattern of annular cracks in close wrapped coils and loops, and angular cracks along the insulation in the elongated coils, was also found.

TABLE 4 - EFFECT OF STRESS ON AGING OF SAMPLE X2

SAMPLE		DAYS TO FIRST CRACK	
Conditions	Form	Pedestal,110°C	Oven,80°C
NO	Loops	115	-
PRECONDITIONING	Close Wrapped Coils	60	70
PRECONDITIONED	Loops	-	> 70
AT	Close Wrapped Coils	24	25
70°C FOR	Elongated Coils	-	45
4 WEEKS	Large Coils	-	> 70

The close wrapped coil configuration is preferred because it accelerates the degradation at a faster rate than the other configurations and shortens the test time. In addition, the type and magnitude of the stress is easy to reproduce and there is minimal handling of the insulated wires. Fingernail pressure and or a tight grip on the insulation can cause defects that can initiate cracks prematurely. These defects are reduced in the mandrel wrapped coils where the stress is taken up smoothly by the polished surface of the mandrel and the coiled region rarely needs to be handled. Using the elongated coils it is difficult to reproduce stresses and hence variable rates of cracking will occur. Large coils and loops are low stress configurations that increase the test time.

Stabilizer Extraction

Brown and Davis[4] have suggested that heating a sealed cable at 70°C for 4 weeks simulates the environmental effects experienced by a cable sitting in a hot reel yard. Figure 3 and Table 5 show the effect of aging at 70°C on the OIT values of the insulations. The OIT value, and therefore the effective stabilizer concentration in the insulation, decreases in a two step process. The OIT value decreased by 50-60% over the first two weeks, after which the rate of loss slowed to ~5% per week, i.e., one half of the stabilizer package was easily lost while the remainder was strongly retained. The long term stability and field lifetime of the cable should thus be determined by these strongly held stabilizers. During heating of the cable, the OIT value of the adjacent filling compound first increased and then decreased after ~1 week suggesting that the stabilizers moved from the insulation to the adjacent filling compound, and then diffused throughout the rest of the filling compound and cable components.

OIT values are shown in Table 5 as a function of time at 70°C for foam-skin and solid insulations that have been (a) never exposed to filling compounds, (b) exposed to filling compounds in sealed jars, (c) exposed to filling compounds as part of the normal manufacturing procedure, or (d) recovered from the field after being buried for 8-10 years. In the absence of filling compounds, the OIT values for foam-skin and solid insulations decreased by less than 20% after 4 weeks at 70°C. When filling compounds were present, large reductions (>50%) in OIT values were observed in both foam-skin and solid insulations.

Fig.3 70°C AGING

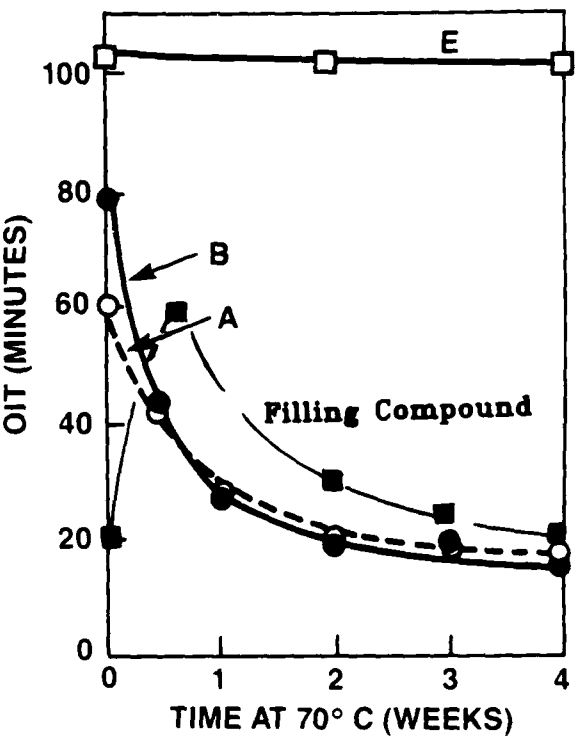

Insulations from cable manufactured in 1987 that was preconditioned, i.e., heated at 70°C for 4 weeks, has 50-70% lower OIT values than the 8-10 year old cable insulations that were manufactured, stored and buried in the Phoenix/Tucson area of Arizona. The area's climate is known to be hostile for PIC insulations since the first reports of LDPE cracking in the 1960s, of polypropylenes in the 1970s and now foam-skin HDPE insulations in the 1980s all originated there. Furthermore, preconditioning the buried cables reduced the OIT values of their insulations by 75%. These results imply that aging cables for 4 weeks at 70°C may be too severe, since it results in a much greater loss of stabilizer than has been seen in the field.

TABLE 5 - OIT VALUES AFTER 70°C AGING

SAMPLE (see Table 1)	FILLING COMPOUND PRESENT*	OIT (mins) OF INSULATION			% REDUCTION AFTER 4 WEEKS
		INITIAL	2 WEEKS	4 WEEKS	
SOLID					
H	none	120	110	100	15
H	EPR	120	15	9	90
E	none	100	-	100	0
E	none	150	-	120	20
E	EPR	150	21	18	90
E	PE/PJ	150	46	29	80
C	EPR	80	-	18	80
FOAM-SKIN					
I	none	94	76	76	20
I	EPR	94	6	5	95
D	PE/PJ	76	-	38	50
A	EPR	60	-	30	50
B	EPR	84	-	24	70
X1	PE/PJ	50	-	15	70
X2	PE/PJ	37	-	12	70

* EPR - Extended ThermoPlastic Rubber
PE/PJ - Petrolatum Jelly/Polyethylene

Accelerated Aging Tests

Accelerated aging at elevated temperatures may be carried out in laboratory pedestals or ovens to simulate the thermal oxidation of PIC cable insulations in the field. Table 6 lists the advantages and disadvantages for each. The pedestal test has the advantages that the test apparatus is similar to pedestals used in the field and the test has a successful record in predicting LDPE cracking. However, it not only takes a long time (45 days, 1 year) at high temperatures (90 C, 110 C), but also there are large temperature variations inside the heated pedestal

TABLE 6 - PEDESTAL VERSUS OVEN

TEST	ADVANTAGES	DISADVANTAGES
PEDESTAL	Field Equipment	Non-uniform Temperature Profile
	Successful LDPE Predictions	Long Test (1 month → 1 year)
	History of Use by Industry	High Temperatures (90°C, 110°C)
OVEN	Uniform Temperature Profile	Laboratory Equipment
	Shorter Test Times at Lower test temperatures	Possible Cross Contamination between Samples
	Airflow accelerates stabilizer evaporation	Non-uniform Airflows can give non-uniform degradation

(Figure 2). The advantages of ovens include uniform temperature control, an enhanced airflow to accelerate evaporation of stabilizers from the insulations, and shorter test times at lower temperatures. Although the airflow facilitates shorter test times, prediction errors may occur since the extrapolation from forced-air oven to field closure may be inaccurate. No adequate correlation between oven test time and field lifetime is available.

We subsequently tested field samples and "as manufactured" insulations by both pedestal and oven tests. Cross correlations between oven testing, pedestal testing, field aged samples and newly made insulations should enable selection of the test procedure that best simulates the field environment and will predict the field lifetime of insulations.

Pedestal

The results of pedestal testing are summarized in Figure 4 and Table 7. The OIT values of the insulations dropped exponentially, reaching values of 0.3-0.6 minutes in less than 40 days for all samples; i.e., little or no stabilizer remained. This decay occurred ~ 3 times faster for insulations that were preconditioned. Cracking began 15-40 days after the OIT value reached these low values. This latency period was determined by the growth rate of crazes which is determined by applied stress on, and defect concentration in, the insulation[1,13].

Fig.4 PEDESTAL TEST RESULTS AT 110°C

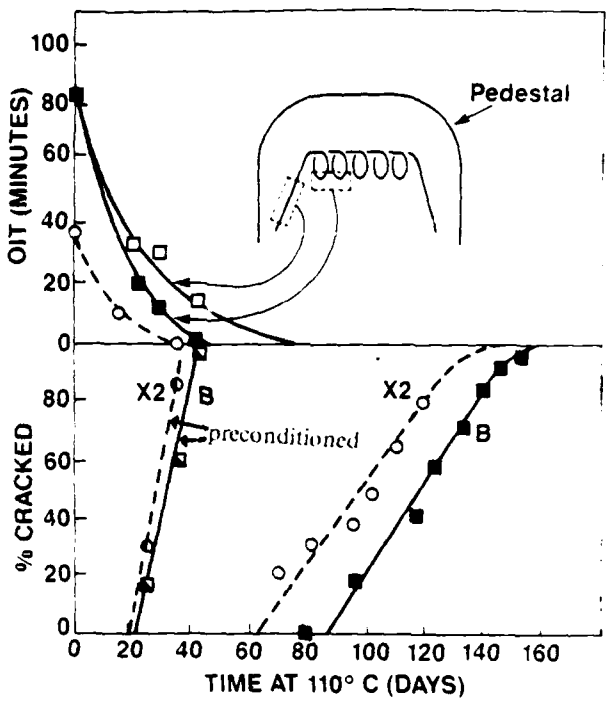

TABLE 7 - PEDESTAL TEST RESULTS

SAMPLE (see Table 1)	PEDESTAL TEST (see Table 2) TYPE	TEMP.	NUMBER OF DAYS UNTIL Initial Cracks	25% Cracked	50% Cracked	RATE[a] % per day
A	current	110°C	200			
A	modified #1	110°C	110			
A	modified #2	110°C	36	42	50	4
A	current	90°C	> 200			
A	modified #1	90°C	> 150			
A	modified #2	90°C	45	62	70	2.5
B	current	110°C	> 200			
B	modified #1	110°C	90	105	120	1.7
B	modified #2	110°C	22	26	32	5
B	current	90°C	> 200			
B	modified #1	90°C	> 140			
B	modified #2	90°C	80	95	~ 120	1.5
X1	current	110°C	> 150			
X1	modified #1	110°C	130	155		
X1	modified #2	110°C	10-15	~ 15	~ 20	~ 7
X2	current	110°C	115	125	137	~ 7
X2	modified #1	110°C	60	80	100	~ 2
X2	modified #2	110°C	24	28	32	~ 8

(a) Rate = Slope of lines in Figure 4

An effect of the temperature variations in the pedestal is shown in Figure 4. For example, the OIT of insulation from a coil of sample B situated at the apex of the 110°C isotherm, was reduced to < 1 minute in ~ 40 days. It took ~ 65 days for insulation from the same wire situated 2-3 inches lower in the pedestal and therefore exposed to cooler temperatures, to reach the same value. Sample configuration did not affect OIT loss since similar measurements inside an oven showed the same OIT values for coiled and straight portions of the insulated wire. Stress reduced the latency period between stabilizer loss (OIT ≅ 0) and visible crack formation. Therefore, it is believed that stress decreased this time for crack formation by increasing craze production and crack propagation rates and not by enhancing stabilizer loss.

After 2-4 weeks in the pedestal test, crystals were observed on all parts of the insulated wire in the heated zone. Stabilizer has apparently migrated to the surface of the insulation and formed crystals. In oven testing, no crystals were seen since evaporation rates were high.

After the latency period, the insulations cracked linearly with time and at comparable rates for all colors except white which cracked ~ 10-15% sooner than all the other colors. This is in contrast to the 1960's LDPE case where reds and whites cracked much earlier than other colors and black insulations never cracked[5,14]. This is probably a result of improved understanding of pigment chemistry, stability and dispersion by manufacturers.

Two 1987 cable insulations from different manufacturers showed similar aging behavior in terms of time to crack and slope (% per day) values. When these insulations were preconditioned at 70°C for 4 weeks, cracking was observed after 36 and 22 days at 110°C at a rate of 4 and 5% per day respectively. Without preconditioning, the same cable insulations survived more than 90 days before they started to crack at a rate of 1.5-2% per day. The field samples from 1977 and 1979, i.e., insulations recovered from the buried portion of an in-service cable, began to crack ~ 30% sooner than the new cables and at higher rates, see Table 7.

Based on these pedestal results, cables manufactured in 1987 would appear to be ~ 1.5 times more stable than the field samples (X1 and X2). Even so, they would still not survive the desired 40 year lifetime, but should crack after ~ 15 years in similar environments as X1 and X2.

Insulations from preconditioned 1987 cables cracked 2-3 times faster than insulations aged 10 years in the field further substantiating the conclusions drawn from OIT measurements that preconditioning cables at 70°C for 4 weeks is excessive.

Oven Testing

Oven testing results at 80°C are summarized in Figures 5-6 and Table 8 and are in general agreement with the pedestal testing results in that:

- Coiled insulation cracked first.
- All colors cracked.
- Preconditioning increased degradation rates.
- Preconditioned modern (1987) cable insulations cracked 2-3 times faster than 10 year old field samples.
- OIT values decreased exponentially long before cracking occurred.
- There was always a latency period of 10-40 days between stabilizer depletion and onset of cracking.
- The 1977 and 1979 field insulations were 1.3-1.7 times less stable than the modern 1987 cables.

Fig.5 OVEN AGING RESULTS AT 80°C
Effect of Preconditioning

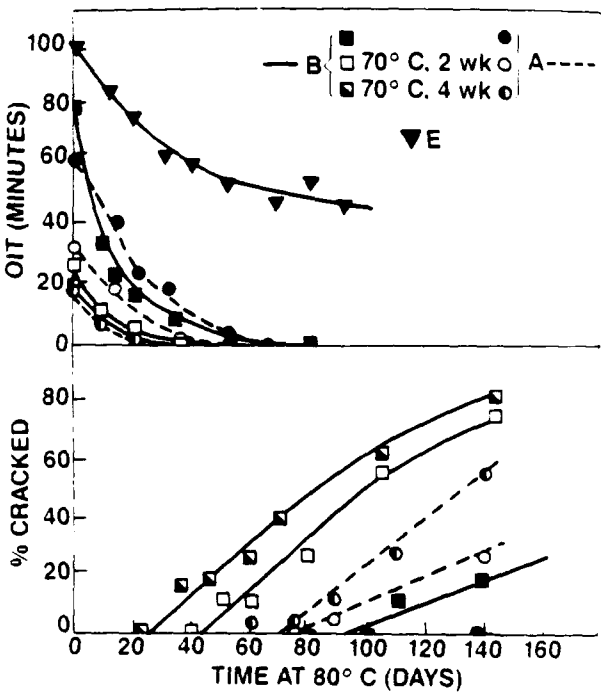

The effects of different preconditioning conditions on the 1987 cables (A and B) periods are shown in Figure 5. These conditions were (1) not preconditioned, (2) preconditioned for 2 weeks at 70°C, and (3) preconditioned for 4 weeks at 70°C. As expected from the OIT data in Figure 3, the first two weeks of preconditioning at 70°C had a disproportionate effect on the lifetime of the insulation. For example, preconditioning insulation A for 2 weeks at 70°C reduced the time to crack by more than 50% (> 70 days) during 80°C aging. Preconditioning for 4 weeks only decreased the time to crack by a further 20-25% (10-15 days).

Solid HDPE insulations from aircore cables (samples E,F and G) have not cracked after 200 days and the OIT value for sample E is still greater than 30 minutes. However when these insulations were exposed to filling compounds before oven testing, then they cracked quickly. For example, a three inch section of cable F was filled with an Extended ThermoPlastic Rubber (ETPR) compound and preconditioned for 4 weeks at 70°C. These insulations cracked after 32 days aging at 80°C. Such preliminary data suggests that solid insulations are susceptible to stabilizer extraction similar to foam-skin insulations with the resultant decrease in lifetimes.

Fig.6 OVEN AGING RESULTS AT 80°C
Field Samples and 1987 Cables

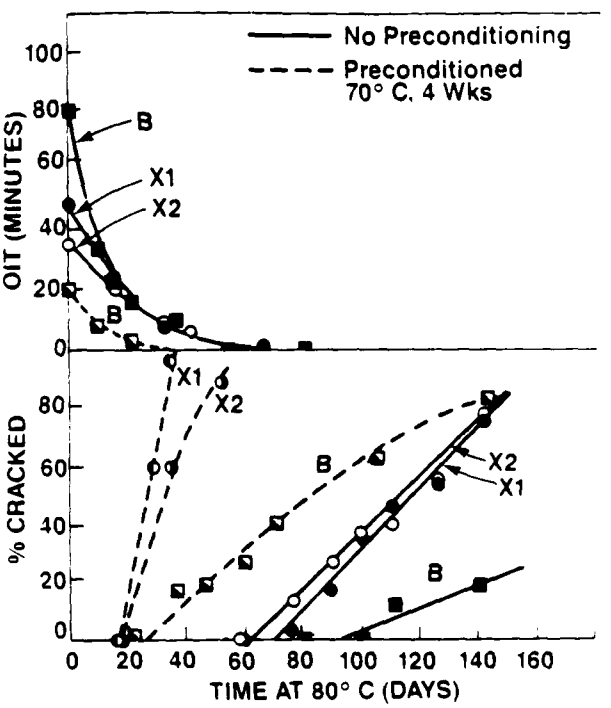

TABLE 8 - 80°C OVEN TESTING RESULTS

SAMPLE (see Table 1)	OVEN TEST # (see Table 2)	NUMBER OF DAYS UNTIL Initial Crack	25% Cracked	50% Cracked	RATE[a] (% per day)
A	1	> 150			
A	2	> 150			
A	3	65	> 100		
A	4	50-55	85	~ 125	0.5
B	1	> 150			
B	2	100			
B	3	50	75	105	0.5
B	4	30	40-45	80	0.5
X1	1	> 100			
X1	2	75	95	120	2
X1	4	20	24	28	~ 7
X2	1				
X2	2	70	90	120	2
X2	4	25	30	35	~ 6
D	1	> 150			
D	2	60	75	90	2

(a) Rate = slope of lines in Figures 5 & 6.

SUMMARY

The current thermal stability tests for cable deployed in the U.S.A. do not guarantee a 40 year life for the insulation in a pedestal environment. Cable insulations that meet these current test requirements are known to fail after less than a decade in hot parts of the country. Either the pedestal closures should be redesigned or else the test requirements improved to better simulate the field experience.

Although today's cables are ~1.5 times more stable than cables installed 10 years ago, they will still not last the desired 40 years. Improved cable formulations may improve these lifetimes by changing the resin, the stabilizers and or filling compounds. These formulations are complex mixtures and therefore compatibility between components needs to be considered early in the design process to avoid deleterious interactions and seek advantageous synergies.

An accurate accelerated aging test requires the insulations to be stressed and possibly preconditioned. Stress simulates physical activity during installation, maintenance and repair. Coiled insulations prepared on a mandrel are best since they (1) are simple to make and examine, (2) have minimal defects introduced during handling, and (3) stress the insulations uniformly and consistently. Preconditioning was expected to simulate stabilizer extraction by filling compounds that can occur before the cable is installed. However, preconditioning at *70 C for 4 weeks appears too severe.* Such conditions may simulate cables exposed to high temperatures (110°F+) for many months or years in a reel yard, but they do not correlate with measurements on cable that has already been in the field for 10 years in hot climates, eg. Arizona.

Both pedestal and oven tests are useful as accelerated aging tests, but more data is needed on reproducibility and extrapolation to field lifetimes. The tolerances in parameters such as temperature control, airflow rates, *preconditioning times and temperatures,* and applied stresses need to be evaluated further. Our preliminary studies show that consistent cracking results are obtained if temperature is maintained at ±1-2°C and close wrapped coils are used. With these procedures, 10 years in the field is equivalent to 60-70 days in a pedestal at 110 C or 60-70 days in a forced-air oven at 80°C. If the cables are preconditioned at 70°C for 4 weeks, 10 years in the field becomes equivalent to ~20 days in either a pedestal at 110 C or an oven at 80 C. Accelerated aging of preconditioned samples may represent a worst case scenario where cables are exposed to the hot sun for a long time before installation, used in ready access plant and where the pedestal enclosure has full sun exposure. The intrinsic variations that occur in insulation manufacture, the test procedure and the laboratory-to-field correlation need to be assessed before the test can be applied to all cables from all manufacturers. Tests on a wide selection of cables, at a variety of temperatures and in different laboratories are in progress to optimize the test conditions and procedures.

ACKNOWLEDGEMENTS

We would like to thank P.C.Warren, I.M.Plitz, E.Hershkowitz, L.E.Davis, and G.Brown for discussions and comments throughout this study. R.J.Schmieder is thanked for supplying and programming the HP 5300 Data Acquisition System for automatic temperature monitoring.

REFERENCES

1. T.N.Bowmer, Proceed. 37th Int. Wire Cable Symp. (1988)
2. L.E.Davis, Proceed. 36th Int. Wire Cable Symp., 475 (1987)
3. G.D.Brown, Proceed. 36th Int. Wire Cable Symp., 337 (1987)
4. G.D.Brown and L.E.Davis, Proceed. 36th Int. Wire Cable Symp., 734 (1987)
5. H.Gilroy, Proceed. 23rd Int. Wire Cable Symp. p42 (1974)
6. L.D.Loan, Proceed. Golden Jubilee Conference on Polyethylenes 1933-83 (June 1983) London.
7. G.A.Schmidt, Proceed. 22nd Int. Wire Cable Symp., 11 (1973)
8. G.A.Schmidt, Proceed. 26th Int. Wire Cable Symp., 161 (1977)
9. Bellcore Technical Requirements - TR-TSY-000421 - "Generic Requirements for Metallic Telecommunications Cable" 1987
10. B.D.Gesner, J.W.Shea and F.R.Wight, Proceed. 22nd Wire Cable Symp. 7 (1973)
11. ASTM Method #E 145-68 (Reapproved in 1981)
12. O.S.Gebizlioglu, private communication
13. I.M.Ward, "Mechanical Properties of Solid Polymers", 2nd Edition, Chap 12, Wiley Pub. (1983)
14. J.Howard, Proceed. 21st Int. Wire Cable Symp., 329 (1972)

E. Paul Hjorth is District Manager of the Metallic Media Requirements and Analysis group at Bellcore, Morristown, N.J. After receiving a BSIE degree from University of Alabama, he joined Western Electric as a cable engineer and worked on numerous projects including the Submarine Cable Rigid Repeater. In 1957, he received a MSIE degree from Stevens Institute of Technology. In 1962, he became a Department Chief whose assignments included introduction of new apparatus and equipment designs, exchange cable sheathing and inspection, and outside plant products. He attained his present position in 1984 and his interests center on requirements and analysis of metallic cable and wire products.

Trevor N. Bowmer is a member of the Polymer Chemistry and Engineering Research Group in Bellcore, Red Bank N.J. He received his Ph.D. in chemistry from the University of Queensland, Australia, where he studied radiation chemistry of polymers. Joining Bell laboratories in 1980, he investigated radiation cured systems and lithographic materials. In 1984, he came to his present position where his interests include degradation mechanisms and characterization of polymeric materials used in telecommunications applications.

Russell J. Miner has been a Member of the Technical Staff at Bellcore since 1984. Before that he was with Bell Telephone Laboratories from 1961 and worked in the Plastics Development and Applied Research Department. He has studied the effects of soil burial, electron irradiation, outdoor aging, heat and fire on the plastics materials used by telecommunications companies.

Osman S. Gebizlioglu is a member of the Polymer Chemistry and Engineering Research group in Bellcore, Red Bank, N.J. After receiving his Ph.D. in Chemical Engineering from Princeton University, he investigated the mechanical and chemical engineering of polymeric systems at M.I.T. (Cambridge, Mass.). He joined Bellcore in 1987 where his research interests include the morphology and mechanical behavior of heterogeneous polymers and composites.

THE EFFECT OF FILLING COMPOUND ON THE CAPACITANCE OF FOAM-SKIN INSULATION LABORATORY SIMULATION VS. CABLE PERFORMANCE

D. M. Mitchell

AT&T TECHNOLOGIES, INC.
PHOENIX, ARIZONA

ABSTRACT

Capacitance measurements have been made periodically at 60-degrees C and at room temperature on individual pairs of conductors with foam-skin insulation, encapsulated in ETPR-type cable filling compounds. Results from the laboratory method have been compared with data obtained from completed cable when held at constant 60-degrees C and with cables exposed to atmospheric temperature changes in aerial and buried environments. The results show that the increase in capacitance observed for individual pairs when immersed in excess compound can be significantly greater than that for the same combination of filling compound and insulated conductors in cable. ETPR compounds have been formulated that minimize capacitance increase while retaining desirable properties for filled cable.

INTRODUCTION

The advantages of foam or foam-skin insulations for use in filled, multipair, telephone cables - and the considerations related to their use - have been identified and discussed previously (1-3). Indeed, the pertinent literature has become quite extensive and in referencing selected papers, we have no intention to overlook other contributors. The References in the papers cited are an archive for the interested reviewer. It is of historic interest to note that a British patent issued in 1930 anticipated the expansion of insulating materials for improvement of dielectric properties (4) and the application to filled cable was proposed by Dean in 1968 (1).

Interaction phenomena between filling compounds and plastic insulation materials were recognized at an early stage in filled cable development (5, 6). Reports by other investigators have followed (7, 8), providing additional insight and reflecting changes in cable design, materials, and test methods. Investigation of cell structure, per se, in the presence of filling compound has been of particular interest.

A variety of compounds and methods for application have been suggested (9, 10) for the treatment of cable cores to resist or mitigate the effects of water entry. Sabia (11) has provided a comprehensive review of representative classes of materials. Compounds consisting of petrolatum and selected additives, PE/PJs, or of thermoplastic rubbers (11) extended in mineral oil, ETPRs, are currently in general use in the United States, and their relative effects on cable transmission properties are understandably of interest. Stratton, Foessing, and Burkhard (12) have monitored the electrical capacitance vs. time of short lengths of foam-skin insulated conductors encapsulated in bulk quantities of PE/PJ or of ETPR type compounds, at 70 degrees C and at room temperature.

It is the purpose of this paper to compare other experimental data with that reported by Stratton, et al. In addition, results obtained for short lengths of conductors encapsulated in bulk compound are compared with measurements made on electrically long sections of filled cable.

Field Observations

ETPR-1 filling compound, was developed for use in buried multipair telephone cable; however, its properties (11) prompted an interest in the evaluation of an aerial section. An important objective was the observation of cable handling and performance under conditions as close as possible to the maximum environmental temperature to which cable can be subjected within the Continental United States. A site in the low desert of Arizona was selected to install 50-pair, 22 gauge cable containing ETPR-1 filling compound and having an ASP sheath. The foam-skin insulation is designed for 83 nf/mi nominal mutual capacitance.

The field trial was designed to permit direct comparison of the performance of aerial and buried cable sections. A 4178-foot aerial section

was directly connected to 2483 feet of buried cable. Terminal cabinets were provided at ground level at each end of the aerial portion, for periodic transmission measurements. Mutual capacitance has been monitored over an eight-year period and is reported below.

Experimental Procedure

Data obtained from the above cable have been compared with measurements of mutual capacitance made on approximately 1000 feet of 200-pair, 22 gauge cable with ETPR-1 filling compound and ASP sheath, coiled on a reel and held at constant 60-degree C for an extended time period. The comparison is completed with results obtained from 22-gauge twisted pair, approximately 100-feet long, coiled, encapsulated in bulk ETPR-1 filling compound and held at constant 60-degree C. Figure 1 shows the relative changes in capacitance with time for each configuration.

Throughout this report, the term "encapsulated" describes short lengths of twisted pairs or single conductors immersed in excess filling compound. Twenty-six gauge, foam-skin insulated conductor designed for 83 nf/mi nominal capacitance has been used, unless otherwise noted.

The effect of a modified filling compound, ETPR-2, on the capacitance of foam-skin insulation has been included for comparison with ETPR-1 filling compound and ETPR-3 compound (12). Figure 2 compares ETPR-2 filling compound on 26 gauge wire at 60-degrees C with the results reported (12) on 24 gauge wire at 70-degrees C. Figure 3 shows the relative time-dependent capacitance change in separate ETPR compounds at 60-degrees C, of 26 gauge, foam-skin insulated, twisted pairs. Figure 4 compares the capacitance change in 26-gauge cable at 60-degrees C for the same two compounds. Capacitance vs. time has also been measured at room temperature for 26 gauge foam-skin twisted pairs encapsulated in PE/PJ, ETPR-1 filling compound, and ETPR-2, filling compound respectively; the results are shown in Table 1.

Discussion

From Figure 1 it is seen that the change in capacitance resulting from the exposure of a short length of twisted pair encapsulated in bulk filling compound is substantially greater than that observed for comparable filled cable at the same continuous temperature. The aerial cable has approached a limiting change in mutual capacitance after 8 years, at the same level approached by the test cable in 6 months. The latter result can be explained by the difference between exposure to a constant high temperature and to atmospheric variations. Although the explanation is less clear for the difference in capacitance change between the isolated pair and the completed cable at the same constant temperature, the result is experimentally repeatable. We have considered the remarks of Eoll (13) and Tenzer and of Olszewski (14) with respect to this observation. Notwithstanding the change observed for the encapsulated pair, the mutual capacitance of the buried section has not changed significantly during the 8-year period. This is particularly noteworthy since cable containing ETPR-1 filling compound was developed for buried service.

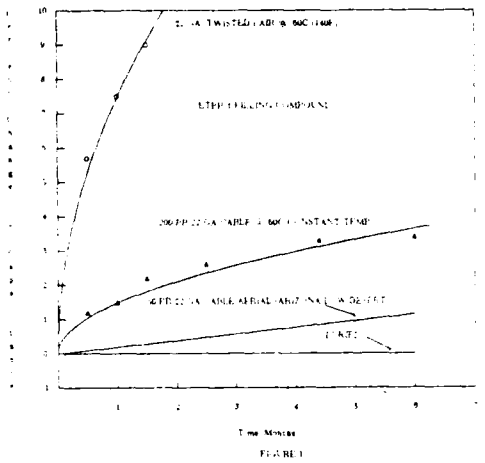

FIGURE 1

Figure 2 provides a qualified comparison of the performance of foam-skin insulated conductors in ETPR type compounds. Stratton et al. (12) tested ten feet of 24-gauge single conductor at 70-degrees C, whereas our data are based on approximately 100-feet of 26-gauge twisted pair at 60-degrees C. Since the results include two ETPR type compounds under somewhat comparable conditions, there is an indication that significantly different effects can result for different formulations within the same generic class.

Figure 3 presents data for short lengths of twisted pairs of 26 gauge foam-skin insulated conductors encapsulated in ETPR-1 and ETPR-2 filling compounds respectively, and held at 60-degrees C. This comparison indicates that ETPR-2 filling compound should demonstrate less change in capacitance when tested in cable. That indication is confirmed by the data displayed in Figure 4. It will be noted, however, that in each case the change in cable is significantly less than that obtained for isolated pairs.

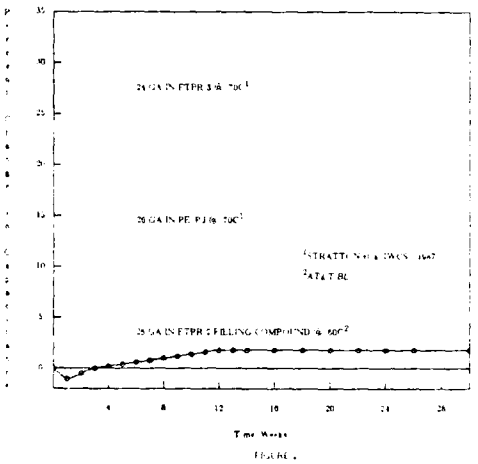

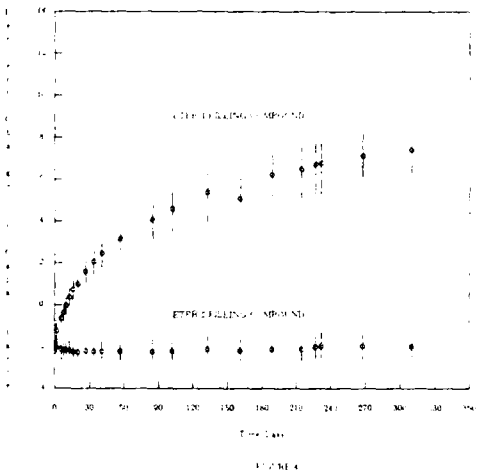

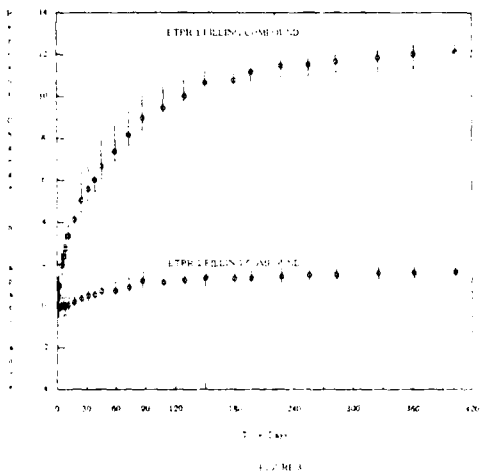

Twisted pairs of 26 gauge foam-skin insulated conductors have been encapsulated in ETPR-1 and ETPR-2 compounds and PE-/PJ and held at room temperature for 5-1/2 months. Capacitance has been monitored during that period and is reported in Table 1. The changes indicated thus far are significantly less than those reported by Stratton, et al. (12) for an ETPR type compound; the work is continuing and will be compared with long term data from the outdoor exposure of finished cable.

PERCENT CHANGE IN CAPACITANCE

FILLING COMPOUND

Date	ETPR-1			ETPR-2			PE/PJ		
2/8	----------			---- (start)			----------		
2/15	----------			---- 0.0			----------		
2/17	---- (start)			----------			----------		
2/19	----------			----------			---- (start)		
2/22	---- 0.0	----	----	0.0	----	----	0.0	----	
2/29	---- 0.0	----	----	0.2	----	----	0.0	----	
3/9	---- 0.0	----	----	0.2	----	----	0.0	----	
3/16	---- 0.3	----	----	0.5	----	----	0.2	----	
3/22	---- 0.3	----	----	0.2	----	----	0.2	----	
3/30	---- 0.3	----	----	0.2	----	----	0.2	----	
4/12	---- 0.3	----	----	0.5	----	----	0.2	----	
4/27	---- 0.3	----	----	0.5	----	----	0.2	----	
5/5	---- 0.3	----	----	0.5	----	----	0.2	----	
5/13	---- 0.3	----	----	0.2	----	----	0.2	----	
6/22	---- 0.3	----	----	0.2	----	----	0.2	----	
8/4	---- 0.3	----	----	0.2	----	----	0.2	----	

TABLE I - ENCAPSULATED TWISTED PAIRS, 26 GA. FOAM-SKIN AGED @ ROOM TEMPERATURE

Conclusion

As pointed out by others (13, 14), the testing of short lengths of insulated conductors in bulk filling compound is convenient and economical for the preliminary evaluation of electrical compatibility between insulating and filling materials. The results reported here confirm the validity of the method for that purpose; however, it must be noted that indications obtained by testing in bulk compound do not necessarily predict quantitatively the performance in finished cable. Furthermore, the experimental results indicate a significant difference in the effect of different ETPR type compounds on foam-skin insulations.

A standardized test method is essential for the critical comparison of results.

Acknowledgement

The assistance of P. H. Ward, AT&T Bell Laboratories, and of K. R. Einstein, AT&T Network Systems, in the preparation of this report is very much appreciated.

References

1. Dean, N. S., "The Development of Fully Filled Cables for The Telephone Distribution Network", 17th IWCS, 1968.

2. Mitchell, D. M., "Material Savings by Design in Exchange and Truck Telephone Cable", 23rd IWCS, 1974.

3. Tyler, J. S., "The Case for a Lower Cost, Watertight Cable", Telephony, Oct. 21, 1974.

4. Windeler, A. S. "Polyethylene Insulated Telephone Cable, Bell System Technical Journal, Sept. 1953.

5. Biskeborn, M. C., and Dobbin, D. P., "Waterproof Plastic Insulated Multipair Telephone Cable", 17th IWCS, 1968.

6. Dean, N. S., Wardley, B. J. and Walters, J. R., "A Report on the Further Progress Made in the Application of Cellular Plastics to Telephone Cable Design and Manufacture", 18th IWCS, 1969.

7. Garmon, J. P. and Davis, L. E., "A Comparison of the Properties of Foam and Foam-Skin Insulation in Filled Cables", 28th IWCS, 1979.

8. Englehard, W., and Hayes, R., "An Analysis of Field Performance of Cellular Insulated Filled Telephone Cable After a Decade of Service", 35th IWCS, 1986.

9. Kreuger, F. H., and Gorissen, H. L., "A New Type of Longitudinally Waterproof Cable", 24th IWCS, 1975.

10. McManus, T. K., and Beveridge, R. A., "A New Generation of Filled Core Cable". 26th IWCS, 1977

11. Mitchell, D. M. and Sabia, R., "Development, Characterization, and Performance of an Improved Cable Filling Compound", 29th IWCS, 1980.

12. Stratton, A. W., Roessing, T. J., and Burkhard, J. D., "A Comparative Stability Study Related to the Performance of PE/PJ and ETPR Filling Compounds", 36th IWCS, 1987.

13. Eoll, C. K., "The Aging of Filled Cable with Cellular Insulation", 27th IWCS, 1978.

14. Tenzer, M., Olszewski, J. A., "Analysis of Long Term Stability of Expanded Insulations in Filled Cables", 28th IWCS, 1979.

D. M. Mitchell
AT&T Network Systems
645 N. 51st Avenue
P. O. Box 13369
Phoenix, Arizona 85002-3369

David M. Mitchell is a Senior Engineer with AT&T Network Systems in Phoenix, Arizona. He is a graduate of Newark College of Engineering (now New Jersey Institute of Technology), BS-ME. Mr. Mitchell joined Bell Laboratories in 1954 as a Member of Technical Staff and worked on various cable design and development projects until transferring to his present position in 1987. He is currently a member of the Strategic Engineering and Planning Group at AT&T's cable manufacturing location in Phoenix.

IN-SERVICE CAPACITANCE STABILITY PREDICTION OF FILLED CABLES BASED ON 70°C LABORATORY AGING

J. A. Olszewski and J. J. Woods

General Cable Company
Woodbridge, New Jersey

ABSTRACT

Accelerated aging of solid and foam-skin insulated filled telephone cable samples at 70°c and their resultant mutual capacitance changes, to be more meaningful to the cable user or the cable manufacturer, have to be related to the temperature that the cables will experience during their anticipated service life of 20 to 40 years. This study makes an attempt to establish such a correlation using an assumption that the Arrhenius relationship obtained in time-temperature studies of embrittlement of insulations is also applicable to the kinetics causing capacitance changes in 70°C agirg. It becomes clear that low geographic latitudes, with their high temperatures, represent the most severe global environment, and consequently, the maximum possible deviation of mutual capacitance from nominal. For the same reasons, aerial installations constitute the most severe operating environment. The study shows, however, that both solid and foam-skin HDPE insulated filled telephone cables should have sufficiently stable transmission characteristics under practically any climatic condition. An acceleation factor is developed which relates days of 70°C aging to years of service life. The use of this technique indicates that the mutual capacitance change of well designed filled telephone cables should not exceed 3 percent over their expected service life under the most extreme global environments.

INTRODUCTION

Most transmission stability studies conducted on filled cables by the cable industry have employed oven aging and insulation weight gain versus time or capacitance changes of cable samples versus time (1)(2)(3)(4)(5). Publications dealing with actual field performance are few, cover insufficient times of exposure to the operating environment, or describe results obtained in the underground environment and/or temperate climate, such as that of Great Britain(6). The most significant discussions cover foam-skin filled cables in aerial links located in subtropical areas, i.e. Florida(7) and Phoenix, Arizona(8), and the observed mutual capacitance changes ranged from +0.9 to about +4.0% respectively in 8 years of operation.

While the transmission stability versus time of filled telephone cables in a given operating environment is unquestionably a function of the insulation/filler system, its prediction for the expected service life of up to 40 years has to rely on accelerated aging, commonly conducted at 70°C, and the correlation of these results to the actual operating conditions and time spans. The work contained herein attempts this correlation using a basic assumption that the modified Arrhenius relationship obtained in temperature-time to embrittlement studies on insulations is applicable to the kinetics responsible for capacitance changes.

AGING AS A FUNCTION OF TEMPERATURE

General Cable Laboratory studies of 1000 Hz mutual capacitance stability of selected insulation/filler systems in oven aging at 70°C are shown in Figure 1.

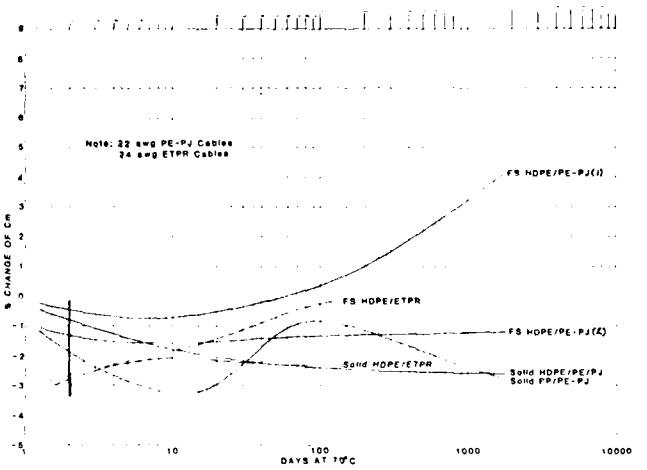

FIGURE 1

In Figure 1 attention is drawn to the following:

i. All the insulations shown are HDPE type and are either solid or foam-skin. Lower density polyethylenes were eliminated as insufficiently stable while plain foam constructions some time ago were judged to be unsuitable for filled cable designs.

ii. The bulk of the experimental data is on PE-PJ filled type cables for a period of about 5 years. The ETPR filler type cables at the time of writing, had less than 200 days of aging, but appear to have similar stability to PE-PJ filler type cables. This tends to contradict conclusions and findings reported by Stratton, et al (9). The greater initial drop in mutual capacitance on exposure to the 70°C test temperature has to be attributed to the higher oil content of the ETPR compounds.

iii. All the capacitance stability curves show the basic effect of initial measurements made at about 20°C versus subsequent measurements on samples exposed to 70°C temperature. The two-day data points most probably reflect elevation of relatively short cable samples to the 70°C test temperature, augmented by varying degrees of insulation swelling which depend on the insulation/filler system. In view of the foregoing, the two-day normalized data points were considered to be a "zero reference".

iv. The critical importance of cell structure in the foam-skin HDPE/PE-PJ cables is illustrated by the disparity between the curves marked (1) and (2). The former was recorded on an earlier vintage foam-skin design which was characterized by an overblown foam layer which exhibited large interconnecting gas cells. Curve (2) illustrates a state-of-the-art design and exhibits a minimum deviation from initial conditions.

v. Solid insulations in general exhibit negative capacitance changes due to oil migration and swelling of solid HDPE matrices, except that PP (propylene-ethylene copolymer) insulations tend to go through a maximum, typically caused by lack of adhesion to conductors or gaps at the conductor surfaces where oils migrate and collect.

The air oven insulation aging data to embrittlement are shown in Figure 1 (10). This study was undertaken primarily to determine if a classical Arrhenius plot relationship, of twice the reaction rate per 10°C increase in temperature holds, and therefore, can be used for insulation life prediction at much lower operating temperatures. The plot shows clearly that 2x/10°C holds roughly for 90°C and higher temperatures. Between 70 and 90°C the rate increases to about 2.4x/10°C, while below 70°C the rate is uncertain as no failures were obtained after 1320 days at 60°C, but is at least 2.9x/10°C. Additional uncertainty is also contributed by test data scatter.

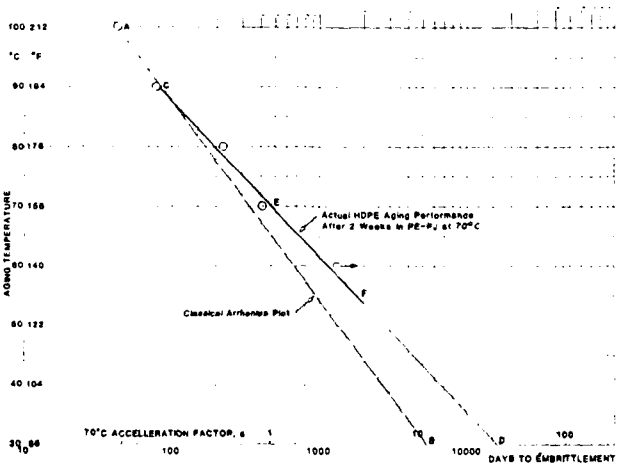

FIGURE 2

The actual performance indicated in Figure 2 for HDPE insulation with its inflection points at C (90°C) and possibly at E (70°C) was expected due to the characteristic composition of the PE-PJ filling compound in which the insulations were conditioned for 2 weeks at 70°C before aging at 100, 90, 80, 70 and 60°C. At a temperature of 115 to 120°C the filler is liquid, but its individual components undergo a phase change, or begin to solidify, as the temperature decreases. This reduces the kinetics, and slows down the physical aspects of aging.

The aging performance above about 80°C is not of particular interest from the point of view of this study, since filled cables are not expected to operate at such high temperatures and because the transmission stability studies in accelerated aging (see Figure 1) are typically conducted at 70°C.

The small break in the curve at E, or about 70°C, is most probably an indication of some transition in the PE component. ETPR filling compounds can be expected to undergo a similar change due to the presence of PE wax.

No aging tests were conducted at temperatures below 60°C because of the anticipated extremely long times to failure. In the case of PE-PJ filler additional performance inflection points are expected. One should take place around 50°C since at this temperature microcrystalline wax components are expected to crystallize. Thus, at temperatures of 50°C and below, the aging processes can be expected to diminish further, reflecting in a decreased slope of the aging

performance curve of Figure 2. The rubber and the crystallization of waxes encapsulate the most mobile oil constituents. It should be realized that while PE-PJ compounds typically constitute 10 to 15 percent oils, ETPR compounds utilize oils in the range of 90%.

Assuming that the kinetics responsible for the aging performance depicted in Figure 2 are also responsible for mutual capacitance changes in aging depicted in Figure 1, and taking a conservative approach, or slope of line CD, the aging acceleration factor "a" represented by 70°C transmisison (capacitance) stability studies becomes

$$a = 1 \quad \text{.....(1)}$$

for cables operating at the same 70°C (158°F) temperature, while for any other operating temperature T, the equation becomes

$$a = 486e^{-.0884T} \quad \text{.....(2)}$$

where T is in °C

or,

$$a = 2339e^{-.0491T} \quad \text{.....(3)}$$

where T is in °F

Outside plant cables however, never operate in the constant temperature environment and therefore modifying for times t at different temperatures, the combined effective acceleration factor A_f represented by 70°C aging becomes

$$A_f = \frac{1}{\frac{t_1}{a_1} + \frac{t_2}{a_2} + \ldots + \frac{t_n}{a_n}} \quad \text{.....(4)}$$

where $(t_1 + t_2 + \ldots + t_n) = 1$, or one year operating cycle. Thus, if monthly temperature statistics are used, then $(t_1 = t_2 = \ldots = t_n) = 1/12 = .0833$, etc.

In general, it should be realized that the finer the time-temperature intervals, the more accurate will be the approximation of the actual aging effects.

AGING AND OUTSIDE PLANT OPERATING ENVIRONMENT

It is well known that from the point of view of temperature extremes the aerial operating environment is the most severe, while the tropics encompass the regions of the highest temperature climates. As far as the U.S.A. is concerned, the country spans wide latitudes from subtropics to polar regions with corresponding variations in climate. A scan of the climatic statistics by the U.S. Department of Commerce, National Oceanic and Atmospheric Administration (11) reveals substantial swings in temperatues for a given northern latitude location, but any given outside plant cable has to be designed for the worst possible location. The U.S. weather statistics for high population locations indicates that Phoenix, Arizona at 33.5° N. latitude has higher summer temperatures than Honolulu, Hawaii located in the tropics at about 21.8° N. latitude. For this reason the Phoenix area is a good cable test site. Other important factors, such as year round temperatures (11), daylight durations (12) (Figure 3), and percentages of possible sunshine (11), cannot be overlooked.

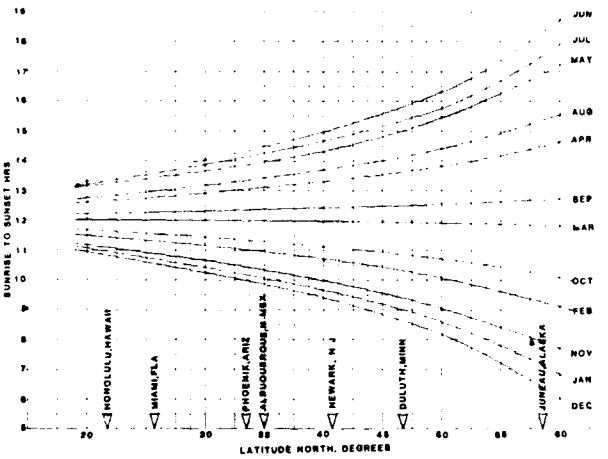

FIGURE 3

The issue of sunshine is critically important since aerial cable temperatures can be substantially higher than ambient. A General Cable-Lenkurt Electric study of an aerial filled cable experimental link in Albuquerque, New Mexico (13), showed 38.8°F higher cable temperature than ambient with zero cloud coverage, and 28.6°F higher than ambient cable temperature with 10 or complete cloud coverage. Heat absorption by "black body" jacketed cable and infrared radiation respectively are the responsible phenomena. The parameters of equation 4 should take into account the above discussed phenomena applicable to aerial cable links.

Using Phoenix, Arizona and Honolulu, Hawaii monthly weather data as a basis, the acceleration factors, represented by 70°C cable aging per Figure 1, were estimated as shown in Tables 1A and 2A. These factors were estimated to be 15.1 and 15.5 respectively, showing that Phoenix aerial environment, in spite of colder winters, is slightly more severe than that of Honolulu, Hawaii. These values of A_f also imply that 40

year aerial service in Phoenix and Honolulu are equivalent to 40/15.1 = 2.65 years (970 days) and 40/15.5 = 2.58 years (940 days) aging at 70°C, respectively.

Utilizing the results shown in Figure 1, the earlier vintage foam-skin HDPE/PE-PJ cables would be expected to exhibit an increase of 3.6 and 3.5 percent in mutual capacitance, in Phoenix and Honolulu, respectively. Present day foam-skin and solid HDPE/PE-PJ designs would be expected to show changes of approximately -0.1 and +1.8 percent, respectively, under the aforementioned service conditions.

The situation improves dramatically for higher northern latitudes, as shown in Table 3A for Juneau, Alaska and in Figure 4A for Duluth, Minnesota. In the case of these two northern locations, the 70°C aging acceleration factors come to 84.2 and 63.6 respectively, making the time of aging at 70°C equivalent to 0.48 years (175 days) and 0.63 years (230 days) respectively for 40 years service life of aerial cables. In this case the expected average mutual capacitance changes, for the same cable designs cited above, come to :

+1.3 and +1.6% for the foam-skin HDPE/PE-PJ (1) cable design

and

-1.6 and -1.7% for the solid HDPE/PE-PJ cable design

The situation with buried installations, as stated at the outset, is not nearly as severe, because of lack of exposure to sunlight and lower soil temperatures in general. Buried cables are typically placed at 36 inches below ground level, and the main difficulty that has to be faced for purposes of prediction, is lack of published soil temperatures. Over the years, however, General Cable has conducted a fair number of field trials where soil temperatures at this cable depth were monitored with a series of thermocouples. Taking the most severe trial site, Joshua Tree, in the California desert, the lowest temperature measured in winter was 48°F, while the highest was 85.1°F, the latter not during peak summer heat. Therefore, taking once more a pessimistic approach of 48 and 90°F ground temperature extremes, the rough estimate of the acceleration factor comes to

$$A_f = \frac{1}{\frac{0.5}{2338e^{-.0491 \times 90}} + \frac{0.5}{2339e^{-.0491 \times 48}}}$$

$$= \frac{1}{.017745 + .002257}$$

$$= 50.0$$

or roughly equivalent to aerial operation in Duluth, Minnesota.

Worst case underground duct installation temperatures are not known to the writers, but lack of contact with the earth is expected to yield somewhat higher maximum yearly temperatures than those in the worst case buried installations. Therefore, 100°F maximum is possible as considered by some standard transmission engineering practices(14). These temperatures though will never present as severe an environment as that seen by the aerial cables.

YARD CABLE STORAGE

General Cable's study of temperatures reached by cables on reels stored in the open yard showed rough agreement with the reference (13) study, i.e. about 30 and 40°F cable temperature increase over the ambient for full cloud coverage and no cloud coverage respectively, but these temperatures were limited to the outer layer winding. Black polyethylene jacket surface temperatures were on occasion about 60°F over the ambient, while the inner cable windings were much cooler, lagged behind the ambient changes, and thus can be represented by the daily mean temperatures for the storage location. Considering the fact that storage of a cable reel in the open yard is of limited duration, yard storage has a limited bearing on the overall aging considerations. Installation rigors on overheated jackets remains the most important possible problem area.

Our study of mutual capacitance change on reels in open yard storage of about 5 years duration in central New Jersey - see Figure 4 - shows that 70°C oven aging represents two orders of magnitude faster aging, or an acceleration factor of about 100. This observation applies to minima exhibited by foam-skin cables and stabilization after the decrease exhibited by solid HDPE insulated cables.

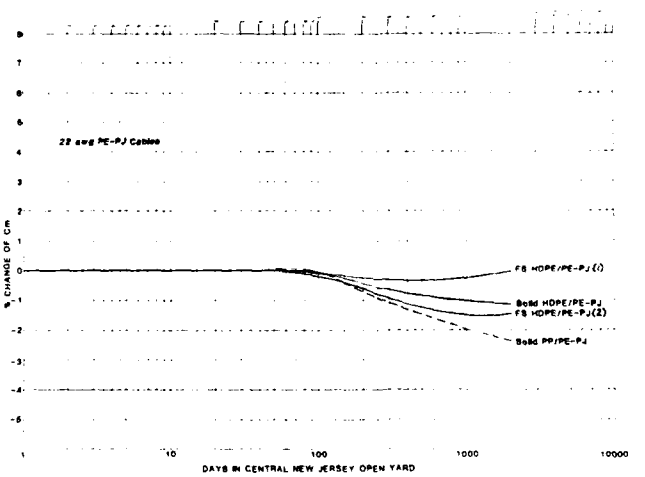

FIGURE 4

The treatment in Table 5A shows almost perfect agreement with computed A_f of 103 and thus implies correctness of the approach. The differences in magnitudes of capacitance changes in yard and 70°C agings are due to the difference in temperature during measurements in these two environments.

CONCLUSIONS

The study described herein shows that the transmission stability of modern day filled telephone cables, be they solid or foam-skin HDPE insulated, is sufficient to warrant their use in buried, duct or aerial installations, in any geographical location. Mutual capacitance changes in cables of reasonable design should not exceed 3% during their 40 year service life. Since the attenuation, both at voice and carrier frequencies, is directly proportional to the square root of capacitance, its maximum change should be limited to about 1.5%. This is less than half the expected excursion of individual pair attenuations in a newly manufactured telephone cable, based on allowable deviations of conductor resistance and mutual capacitance from their specified averages.

SUMMARY

This paper presents a method of relating 70°C accelerated aging performance of filled telephone cables to actual service performance. Using an acceleration factor and climatic statistics allows for a prediction of mutual capacitance change over the service life of a cable.

The analysis confines itself to a static scenario for conditions of installation. The effects of convective air currents on aerial cables and the flooding conditions of underground duct systems have not been considered. On the other hand, the mechanical behavior of installed cables has not been examined. Aerial cables are subject to wind induced vibrations and variations of sags and tensions with time, while buried cables are exposed to varying longitudinal stresses and earth compaction. These physical phenomena can serve to modify the predictions of capacitance change presented herein and could be the basis for further studies.

Good correlation between calculated predictions and long term monitoring of cables in a reel yard was obtained, and verifies the method of analysis. It is expected that this will allow for more rapid evaluations of proposed insulation/filler systems based on minimum 70°C aging times.

REFERENCES

1. S. Verne, R. T. Puckowski and A. A. Pinching, "Long Term Stability of Polyethylene Insulated Fully-Filled Telephone Distribution Cables", 20th International Wire and Cable Symposium, Proceedings, November 1971.

2. C. K. Eoll, "The Aging of Filled Cable with Cellular Insulation", 27th International Wire and Cable Symposium, Proceedings, November 1978.

3. J. P. Gamon and L. E. Davis, "A Comparison of the Properties of Foam and Foam-Skin Insulation in Filled Cables", 28th International Wire and Cable Symposium, Proceedings, November 1979.

4. M. Tenzer and J. A. Olszewski, "Analysis of Long Term Stability of Expanded Insulations in Filled Cables", 28th International Wire and Cable Symposium, Proceedings, November 1979.

5. D. M. Mitchell and R. Sabia, "Development, Characterization, and Performance of an Improved Cable Filling Compound", 29th International Wire and Cable Symposium, Proceedings, November 1980.

6. J. Pritchett, E. L. Mather and S. Verne, "Fully-Filled Telephone Cable with Cellular Polyethylene Insulation After 10 Years Service", 24th International Wire and Cable Symposium, Proceedings, November 1975.

7. W. Englehart and R. Hayes, "An Analysis of Field Performance of Cellular Insulated Filled Telephone Cable After a Decade of Service", 35th International Symposium, Proceedings, November 1986.

8. W. G. Nutt, R. Sabia, F. J. Mullin and D. M. Mitchell, 36th International Wire and Cable Symposium, Poster Paper, November 1987.

9. A. W. Stratton, T. J. Roessing and J. D. Burkhard, "A Comparative Stability Study Related to the Performance of PE/PJ and ETPR Filling Compounds", 36th International Wire and Cable Symposium, Proceedings, November 1987.

10. G. A. Schmidt, "Insulation-Filling Compound Systems", 1st CANTV Cable Symposium, Proceedings, Caracas, Venezuela, November 1983.

11. "Statistical Abstract of the United States - 1981" 102d Edition, National Data Book and Guide to Sources, U.S. Department of Commerce, Bureau of Census.

12. The World Almanac and Book of Facts - 1988.

13. E. Mushall, "Cable Temperature As a Function of Ambient Temperature", General Cable Laboratory Report No. 36122, dated 11/21/85.

14. GTE Practices, Engineering Plant Series, Section 836-910-073, Issue 3, "9102A - 48 Channel Repeatered Line Equipment Transmission Engineering Considerations", April 1979.

TABLE 1A

Phoenix, Arizona
Aerial Installation

Month	Daily Mean Temp, °F	Average % Possible Sunshine	Average Daylight Hours	Average, Fraction of 24 Hr. Day				Average, Fraction of Year, t			"Adjusted" Mean Cable Temp., °F			a			t/a		
				Daylight	Night	Sunshine	Cloudy	Night	Sunshine	Cloudy	Night	Sunshine	Cloudy	Night	Sunshine	Cloudy	Night	Sunshine	Cloudy
Jan.	51.2	78	10.2	.425	.575	.332	.093	.0479	.0277	.0078	51.2	90.0	79.8	189.3	28.18	46.49	.000253	.000983	.000168
Feb.	55.1	80	11.0	.458	.542	.366	.092	.0452	.0305	.0077	55.1	93.9	87.3	156.3	23.27	32.17	.000289	.001311	.000239
Mar.	59.7	83	12.0	.500	.500	.415	.085	.0417	.0346	.0071	59.7	98.5	88.3	124.7	18.56	30.63	.000334	.001864	.000232
Apr.	67.7	38	13.1	.546	.454	.481	.065	.0378	.0401	.0054	67.7	106.5	96.3	84.22	12.53	20.68	.000449	.003200	.000261
May	76.3	93	13.9	.579	.421	.539	.040	.0351	.0449	.0033	76.3	115.1	104.9	55.21	8.216	13.56	.000636	.005465	.000243
June	84.6	94	14.4	.600	.400	.564	.036	.0333	.0470	.0030	84.6	123.4	113.2	36.75	5.468	9.023	.000906	.008595	.000332
July	91.2	85	14.1	.588	.412	.500	.088	.0343	.0417	.0073	91.2	130.0	119.8	26.58	3.955	6.526	.001291	.010544	.001119
Aug.	89.1	86	13.3	.554	.446	.471	.083	.0372	.0393	.0069	89.1	127.9	117.7	29.46	4.384	7.234	.001263	.008964	.000954
Sept.	83.8	89	12.4	.517	.483	.460	.057	.0403	.0383	.0048	83.8	122.6	112.4	38.22	5.685	9.381	.001054	.006737	.000512
Oct.	72.2	88	11.3	.471	.521	.415	.056	.0434	.0346	.0047	72.2	111.0	100.8	67.52	10.05	16.58	.000643	.003443	.000283
Nov.	59.8	84	10.4	.433	.567	.364	.069	.0473	.0303	.0058	59.8	98.6	88.4	124.1	18.47	30.48	.000381	.001640	.000190
Dec.	52.5	77	10.0	.417	.583	.321	.096	.0486	.0268	.0080	52.5	91.3	81.1	177.6	26.43	43.62	.000274	.001014	.000183

$\Sigma t/a = .066249$

$Af = 1/\Sigma t/a = 15.09$

TABLE 2A

Honolulu, Hawaii
Aerial Installation

Month	Daily Mean Temp, °F	Average % Possible Sunshine	Average Daylight Hours	Average, Fraction of 24 Hr. Day				Average, Fraction of Year, t			"Adjusted" Mean Cable Temp., °F			a			t/a		
				Daylight	Night	Sunshine	Cloudy	Night	Sunshine	Cloudy	Night	Sunshine	Cloudy	Night	Sunshine	Cloudy	Night	Sunshine	Cloudy
Jan.	72.3	63	11.0	.458	.542	.289	.169	.0452	.0241	.0141	72.3	111.1	100.9	67.19	10.00	16.50	.000673	.002410	.000855
Feb.	72.3	64	11.4	.475	.525	.304	.171	.0438	.0253	.0143	72.3	111.1	100.9	67.19	10.00	16.50	.000652	.002530	.000867
Mar.	73.0	68	12.0	.500	.500	.340	.160	.0417	.0283	.0133	73.0	111.8	101.6	64.92	9.66	15.94	.000642	.002929	.000834
Apr.	74.8	67	12.6	.525	.475	.352	.173	.0396	.0293	.0144	74.8	113.6	103.4	59.43	8.844	14.59	.000666	.003313	.000987
May	76.9	69	13.2	.550	.450	.380	.170	.0375	.0317	.0142	76.9	115.7	105.5	53.61	7.977	13.16	.000700	.003974	.001079
June	78.9	70	13.4	.558	.442	.391	.167	.0368	.0326	.0139	78.9	117.7	107.5	48.59	7.231	11.93	.000757	.004508	.001165
July	80.1	74	13.3	.554	.446	.410	.144	.0372	.0342	.0120	80.1	118.9	108.7	45.81	6.817	11.25	.000812	.005017	.001067
Aug.	80.7	75	12.8	.533	.467	.400	.133	.0389	.0333	.0111	80.7	119.5	109.3	44.48	6.620	10.92	.000874	.005031	.001016
Sept.	80.4	75	12.2	.508	.492	.381	.127	.0410	.0318	.0106	80.4	119.2	109.0	45.14	6.718	11.08	.000908	.004734	.000956
Oct.	78.9	68	11.6	.483	.517	.328	.155	.0431	.0273	.0129	78.9	117.7	107.5	48.59	7.231	11.93	.000887	.003775	.001081
Nov.	76.5	60	11.1	.463	.537	.278	.185	.0448	.0232	.0154	76.5	115.3	105.1	54.67	8.136	13.42	.000819	.002852	.001147
Dec.	73.7	59	10.8	.450	.550	.266	.184	.0458	.0222	.0153	73.7	112.5	102.3	62.73	9.335	15.40	.000730	.002378	.000993

$\Sigma t/a = .064618$

$A_f = 1/\Sigma t/a = 15.48$

TABLE 3A

Juneau, Alaska
Aerial Installation

Month	Daily Mean Temp., °f	Average Possible Sunshine	Average Daylight Hours	Average, Fraction of 24 Hr. Day				Average Fraction of Year, t			"Adjusted" Mean Cable Temp., °F			a			t/a		
				Daylight	Night	Sunshine	Cloudy	Night	Sunshine	Cloudy	Night	Sunshine	Cloudy	Night	Sunshine	Cloudy	Night	Sunshine	Cloudy
Jan.	23.5	32	7.1	.296	.704	.095	.201	.0587	.0079	.0168	23.5	62.3	52.1	737.8	109.8	181.2	.000080	.000072	.000093
Feb.	28.0	32	9.3	.388	.612	.124	.264	.0510	.0103	.0220	28.0	66.8	56.6	591.5	88.02	145.2	.000086	.000117	.000151
Mar.	31.9	37	11.8	.492	.508	.182	.310	.0423	.0152	.0258	31.9	70.7	60.5	488.4	72.68	119.9	.000087	.000209	.000215
Apr.	38.9	39	14.5	.604	.396	.236	.368	.0330	.0197	.0307	38.9	77.7	67.5	346.4	51.54	85.05	.000095	.000382	.000361
May	46.8	39	16.9	.704	.296	.275	.429	.0247	.0229	.0358	46.8	85.6	75.4	235.0	34.97	57.70	.000105	.000655	.000620
June	53.2	34	18.3	.763	.237	.259	.504	.0198	.0216	.0420	53.2	92.0	81.8	171.6	25.54	42.14	.000115	.000846	.000997
July	55.7	31	17.5	.729	.271	.226	.503	.0226	.0188	.0419	55.7	94.5	84.3	151.8	22.59	37.28	.000149	.000832	.001124
Aug.	54.3	32	15.4	.642	.358	.205	.437	.0298	.0171	.0364	54.3	93.1	82.9	162.6	24.20	39.93	.000183	.000707	.000912
Sept.	49.2	26	12.2	.508	.492	.132	.476	.0410	.0110	.0397	49.2	88.0	77.8	208.9	31.08	51.29	.000196	.000354	.000774
Oct.	41.8	19	10.2	.425	.575	.081	.344	.0479	.0068	.0287	41.8	80.6	70.4	300.4	44.70	73.76	.000159	.000152	.000389
Nov.	32.5	23	7.9	.329	.671	.076	.253	.0559	.0063	.0211	32.5	71.3	61.1	474.2	70.57	116.5	.000118	.000089	.000181
Dec.	27.3	20	6.4	.267	.733	.053	.214	.0611	.0044	.0178	27.3	66.1	55.9	612.2	91.10	150.3	.000100	.000048	.000118

$\Sigma t/a = .011871$

$A_f = 1/\Sigma t/a = 84.24$

TABLE 4A

Duluth, Minnesota
Aerial Installation

Month	Daily Mean Temp., °F	Average Possible Sunshine	Average Daylight Hours	Average, Fraction of 24 Hr. Day				Fraction of Year, t			"Adjusted" Mean Cable Temp., °F			a			t/a		
				Daylight	Night	Sunshine	Cloudy	Night	Sunshine	Cloudy	Night	Sunshine	Cloudy	Night	Sunshine	Cloudy	Night	Sunshine	Cloudy
Jan.	8.5	49	9.0	.375	.625	.184	.191	.0521	.0153	.0159	8.5	47.3	37.1	1541	229.3	378.4	.000034	.000067	.000042
Feb.	12.1	54	10.3	.429	.571	.232	.197	.0476	.0193	.0164	12.1	50.9	40.7	1291	192.2	317.1	.000037	.000100	.000052
Mar.	23.5	55	11.9	.496	.504	.273	.223	.0420	.0228	.0186	23.5	62.3	52.1	737.8	109.8	181.2	.000057	.000208	.000103
Apr.	38.6	54	13.6	.567	.433	.306	.261	.0361	.0255	.0218	38.6	77.4	67.2	351.5	52.31	86.31	.000103	.000488	.000253
May	49.4	56	15.0	.625	.375	.350	.275	.0313	.0292	.0229	49.4	88.2	78.0	206.8	30.78	50.79	.000151	.000949	.000451
June	59.0	58	15.8	.658	.342	.382	.276	.0285	.0318	.0230	59.0	97.8	87.6	129.1	19.21	31.70	.000221	.001655	.000726
July	65.6	66	15.4	.642	.358	.424	.218	.0298	.0353	.0182	65.6	104.4	94.2	93.37	13.89	22.93	.000319	.002541	.000794
Aug.	64.1	61	14.2	.592	.408	.361	.231	.0340	.0301	.0193	64.1	102.9	92.7	100.5	14.96	24.68	.000338	.002013	.000781
Sept.	54.4	52	12.5	.521	.479	.271	.250	.0399	.0226	.0208	54.4	93.2	83.0	161.8	24.08	39.73	.000247	.000939	.000523
Oct.	45.3	48	10.9	.454	.546	.218	.236	.0455	.0182	.0197	45.3	84.1	73.9	253.0	37.64	62.12	.000180	.000483	.000317
Nov.	28.4	34	9.4	.392	.608	.133	.259	.0507	.0111	.0216	28.4	67.2	57.0	580.0	86.31	142.4	.000087	.000129	.000152
Dec.	14.4	40	8.6	.358	.642	.143	.215	.0535	.0119	.0179	14.4	53.2	43.0	1153	171.6	283.2	.000046	.000069	.000063

$\Sigma t/a = .015719$

$A_f = 1/\Sigma t/a = 63.62$

TABLE 5A

Newark, New Jersey
Reel Yard Storage

a) Outer Layer of Reel (0.1 of Total Length)

Month	Daily Mean Temp., F	Average Possible Sunshine	Average Daylight Hours	Average, Fraction of 24 Hr. Day				Average, Fraction of Year, t			"Adjusted" Mean Cable Temp., °F			a			t/a		
				Daylight	Night	Sunshine	Cloudy	Night	Sunshine	Cloudy	Night	Sunshine	Cloudy	Night	Sunshine	Cloudy	Night	Sunshine	Cloudy
Jan.	32.7	51	9.6	.400	.600	.204	.196	.0500	.0170	.0163	32.7	71.5	61.3	469.6	69.88	115.3	.000106	.000243	.000141
Feb.	33.9	55	10.7	.446	.554	.245	.201	.0462	.0204	.0168	33.9	72.7	62.5	442.7	65.88	108.7	.000104	.000310	.000155
Mar.	41.1	52	12.0	.500	.500	.260	.240	.0417	.0217	.0200	41.1	79.9	69.7	310.9	46.27	76.34	.000134	.000469	.000262
Apr.	51.7	53	13.3	.554	.446	.294	.260	.0372	.0245	.0217	51.7	90.5	80.3	184.8	27.49	45.37	.000201	.000891	.000478
May	61.6	54	14.4	.600	.400	.324	.276	.0333	.0270	.0230	61.6	100.4	90.2	113.6	16.91	27.90	.000293	.001597	.000824
June	70.3	58	15.0	.625	.375	.363	.262	.0313	.0303	.0218	70.3	109.1	98.9	74.12	11.03	18.20	.000422	.002747	.001198
July	75.1	63	14.7	.613	.387	.386	.227	.0323	.0322	.0189	75.1	113.9	103.7	58.56	8.715	14.38	.000552	.003695	.001314
Aug.	73.4	60	13.7	.571	.429	.343	.228	.0358	.0286	.0190	73.4	112.2	102.0	63.66	9.473	15.63	.000562	.003019	.001216
Sept.	67.1	55	12.4	.517	.483	.284	.233	.0403	.0237	.0194	67.1	105.9	95.7	86.74	12.91	21.30	.000465	.001836	.000911
Oct.	56.7	54	11.1	.463	.537	.250	.213	.0448	.0208	.0178	56.7	95.5	85.3	144.5	21.51	35.49	.000310	.000967	.000502
Nov.	46.0	42	9.9	.413	.587	.173	.240	.0489	.0144	.0200	46.0	84.8	74.6	244.4	36.37	60.02	.000200	.000396	.000333
Dec.	35.1	47	9.3	.388	.612	.182	.206	.0510	.0152	.0172	35.1	73.9	63.7	417.4	62.12	102.5	.000122	.000245	.000168

$\Sigma t/a_{.1}$ = .027388

b) Inner Layers of Reel (0.9 of Total Length)

Jan.	DITTO	.0833	32.7	469.6	.000177
Feb.		.0833	33.9	442.7	.000188
Mar.		.0833	41.1	310.9	.000268
Apr.		.0833	51.7	184.8	.000451
May		.0833	61.6	113.6	.000733
June		.0833	70.3	74.12	.001124
July		.0833	75.1	58.56	.001422
Aug.		.0833	73.4	63.66	.001309
Sept.		.0833	67.1	86.74	.000960
Oct.		.0833	56.7	144.5	.000576
Nov.		.0833	46.0	244.4	.000341
Dec.		.0833	35.1	417.4	.000200

$\Sigma t/a_{.9}$ = .007749

$A_f = 1/(0.1\Sigma t/a_{.1} + 0.9\Sigma t/a_{.9})$

$= 1/(0.1 \times .027388 + 0.9 \times .007749) = 1/.009713 = 103.0$

Jerzy A. Olszewski joined General Cable Company in 1956 and is currently a Transmission Research Specialist, Technical Operations. He has also held positions in International Operations. He holds a B.S. in Electrical Engineering from the Loughborough University of Technology, Loughborough, England.

John J. Woods joined General Cable Company in 1964 and is currently a Manager of Application Engineering, Technical Operations. He has also held positions in Research and International Operations. He holds a B.S. in Engineering Science from the City University of New York and has persued graduate studies at the Polytechnic Institute of New York.

The Distinction Between Fire Hazard and Fire Risk: The Importance of Such Assessments to Public Safety

John R. Hall, Jr.

National Fire Protection Association

Abstract

New models and methods are rapidly becoming available to calculate not just the physical growth of fire but also the hazard and risk posed by fire. An understanding of the concepts underlying terms like "hazard" and "risk" will be essential for anyone who wishes to solve problems, or assess proposed solutions, using these new computer-based decision aids. A brief review is provided of concepts and a major research initiative now under way.

This decade has seen an explosive growth in the number and diversity of models and analysis methods, either available or under development, for the examination of fire growth, smoke spread, and fire effects on people and property. With this growth in capability has come a number of new terms like "hazard" and "risk", terms that seem deceptively familiar and simple but that are now used in a technically precise manner to distinguish one class of new models from another. In the new world of scientific fire safety decision-making, it will be important to know not only how these new models work but also what questions each is intended to address and what aspects of the fire problem each is designed to capture. This paper will review the meanings of the new terms, provide a brief conceptual overview of the new models, and describe current research now under way to develop them. Throughout this paper, it is assumed that most users wish to model the effects of changes in a product to be used in a certain class of buildings.

Many of the computer-based models in wide use today may be loosely referred to as fire growth models. Examples of these models would include (1) the various editions of the Harvard code, originally developed by Howard Emmons, (2) the highly simplified ASET, or Available Safe Egress Time Model, developed by Leonard Cooper, and (3) the FAST model, or Fire And Smoke Transport model, developed at the National Bureau of Standards. In these models, a fire is defined primarily as a rate of heat release time-curve and a particular location in a larger space. Although the models are often called fire growth models, they are really smoke and heat spread models. The specific curve defining the fire typically must be provided by the model user, who in turn may derive it based on the reference curves that have been developed for a wide range of burning items. The principal function of the model is then to use the laws of physics to simulate the build-up of heat, smoke, and toxic gases in sections of the larger space as a result of the externally defined fire.

Fire growth models vary considerably in complexity, speed, cost, and sophistication. Some are field models, providing physical characteristics as a function of specific locations in the fire-affected space. Some are zone models, providing physical characteristics only for large segments of the fire-affected space and modeling the movement of the borders or interfaces between these spaces. Some can model only one room, while others can model several rooms, including such non-room areas as concealed spaces. But none of these models address two major aspects of fire safety - the likelihood that the fire they model will occur and the practical consequences to people or property of the physical characteristics they show developing.

A model that includes both a model of fire growth and a model of the practical consequences of that growth is called a hazard model. A hazard model therefore must include a model that translates the physical phenomena of fire into damage to people or property. The leading hazard model in the U.S. is HAZARD I, developed at the National Bureau of Standards, and it

models damage to people through a modeling component called TENAB, which stands for TENABility. TENAB is a comparison program. Its point of reference may be a particular room or a moving location representing an occupant. At each point in time, TENAB calculates the instantaneous and cumulative effects fire has had on the location or occupant of interest, then compares those effects to known criteria regarding lethal or incapacitating levels or combinations of fire effects. The best current knowledge on toxic potency of gases and on heat stress enter the hazard model in this way.

To put it another way, HAZARD I uses FAST, a fire growth model, to generate a description of the hazardous conditions at each location in the building as a function of time. TENAB then calculates, based on a fixed location or a moving location representing a moving occupant, the point in time when the cumulative exposure at that location would have been lethal or incapacitating. If escape has not occurred by that time, the occupants at that location will be considered to have died.

In this way, HAZARD I directly addresses many of the concerns that have been raised about the direct use of toxic potency tests for regulation. HAZARD I uses toxic potency information, like LCt50 values, to translate the accumulating fire effects into practical consequences of incapacitation or death. But HAZARD I does not treat a single toxic potency value as safe or unsafe in itself. If a product has high toxic potency but is very difficult to ignite, then this should be captured in the initial specification of the fire curve, which will show the product entering the fire later. If a product has high toxic potency but releases mass slowly, then the time calculations of HAZARD I can reflect that fact.

What HAZARD I cannot do is compensate for limitations in the state of the art of its components, whether they be test methods for calculating input variables or physical, chemical, or biological relationships that are used to make the calculations. Like an experimental automobile, HAZARD I is an integrated system which includes some components that perform in a nearly ideal fashion and other components that are subject to considerable uncertainty and need to be carefully monitored by knowledgeable users.

HAZARD I includes another major component that it treats as part of hazard and which others have treated as part of the population-exposure element of risk. That component is EXITT, a model of human behavior in fire, which is the medium by which HAZARD I provides a dynamic picture of the exposure of occupants to a developing fire. In simple terms, HAZARD I uses FAST to determine what fire effects are in a room, uses TENAB to determine how lethal those effects are, and uses EXITT to determine whether anyone is present to be affected.

As complex and comprehensive as HAZARD I may already sound, there are many elements of hazard it does not include. One is the process of suppression, whether by automatic systems or by manual means. Others are non-lethal effects of fire on people and damage effects on property. Each of these may be thought of as a challenge for the future. HAZARD I also does not include the key defining element of a risk model, which is the relative likelihood of the conditions it models.

The simplest extension of a hazard model to a risk model would consist of adding on a single probability number. This simple extension is not satisfactory, no matter how it is considered. Suppose the probability is defined narrowly as the likelihood of the very specific situation used in HAZARD I - a specific fire in a specific location of the specific building with specific occupants in indicated locations. Then the probability will inevitably be near zero, and the significance of knowing anything about that situation will appear to be nil. At the other extreme, suppose the probability is defined broadly as the likelihood of any fire in any location of any of that class of buildings with all their variations in occupancy. Then it is unlikely that a user will know enough to be comfortable - let alone accurate - in selecting one detailed description to be representative of all that variety in a HAZARD I run.

The solution to this dilemma is the use of what is called a scenario structure. One begins with an occupancy class of interest and a product class of interest, and one wishes to model the risk of fire involving that kind of product in that kind of occupancy. The universe of fires that can occur in that occupancy class are then subdivided into what are called scenario classes. Each scenario class is defined by several characteristics, such as a room of origin, a description of the initial fire, and a description of the locations and characteristics of the building occupants when the fire began. These characteristics are referred back to the data on historical fires and other data sources to obtain a probability for that scenario class. At the same time, a representative case is identified within the scenario class. It

is designed to be representative of all the variety in the scenario class, but this will be a much more manageable and defensible task than selecting one representative of the universe of fires because each scenario class will be more homogeneous than the whole universe of fires. This representative case is called the reference scenario for that scenario class.

The identification of scenario classes and reference scenarios involves considerable judgment and a balancing of two different concerns. If the number of scenario classes is too large, then (a) the time and cost of running the model will be unacceptably large, and (b) the existing data bases may be inadequate to provide reasonably accurate probability estimates for each scenario class. But if the number of scenario classes is too small, then there will be grave, unresolveable doubts about the representativeness of many of the reference scenarios, given the tremendous variation that will exist in the scenario classes they represent.

Finding ways to deal with this dilemma, and many others, is the mission of the National Fire Protection Research Foundation's fire risk assessment research project. Begun in 1986 and due to be completed in 1990, this project is designed to construct a fire risk model around a fire hazard model and to demonstrate its general applicability to estimation of the projected impact of product design changes on the national fire death toll. Of the three developmental cases used to bring the project to its current position, one addressed wire and cable insulation in hotel and motel installations. The other two were carpets in office buildings and upholstered furniture in homes. Future work will include a developmental case on interior wall coverings in restaurants and more focused work to refine the accuracy and measure the sensitivity of the risk method's individual modeling components.

The following is a very brief listing of some major modeling challenges that have been and are being addressed in the fire risk assessment project:

o What characteristics, recorded or estimateable for most real fires, can be used to estimate when, at what size, and for what reason the fire stopped growing? Most fires are interrupted, and this affects the estimation of the hazard consequences of changing a product involved in the fire.

o What characteristics, recorded or estimateable for most real fires, can be used to estimate whether and when a product will become involved in a fire that did not begin with its ignition? The secondary ignition of a product may depend on the burning properties and location of any other item in the building.

o What data exists, recorded for either real fires or the population in general, that can be used to describe the layouts of rooms and the number, locations and conditions of occupants in enough detail to support hazard-model calculations?

o What characteristics, recorded or estimateable for most real fires, can be used to determine whether, when, and with consequences for fire spread, fires cross into or out of concealed spaces? This may be called the barrier breach model, although there is a possibility of barrier compromise prior to the fire which should be captured as well.

o How can a hazard model, designed to handle up to ten rooms, be used to estimate risk or hazard in buildings having hundreds of rooms and dozens of floors?

o How can a risk or hazard model, which calculates risk as a cumulative effect of toxic gases and heat stress, capture the many rapid fatal injuries to persons located very close to the point of ignition? This includes people smoking in bed, the torch operators who ignite the materials they are working on, and clumsy arsonists who trap themselves in fast-moving fires.

As these questions are answered, fire risk and fire hazard assessment methods will become sufficiently well developed to be used in all the major fire safety decision-making areas we now work in using less sophisticated tools. Fire hazard models may be the key to our long-stated goal of movement from specification codes to performance codes. Because they can address the net effects of many simultaneous changes in a product or a building, fire hazard models will permit greater flexibility in assessing new technology.

Fire risk assessment methods should have a similar impact but will be of particular use if ease of ignition is among the product design changes being contemplated. Fire risk assessment methods also will be the models of choice for economic decisions, such as whether to regulate, because they are the only models capable of estimating benefits in terms [illegible] lives saved that can be

validly compared to estimates of the cost of regulation. Agencies like the U.S. Consumer Product Safety Commission therefore are likely to be prime users of the new fire risk assessment tools, while building code officials are more likely to find that fire hazard models will suit most of their needs.

It is important to view all of these tools as systems in a constant state of development. As with other computerized decision aids, there will always be gaps - the gap between the version in widespread use and the version the lab boys and girls consider their best current model, the gap between the model applications that can be safely and confidently performed by the typical user in the field and the wider range of model applications that can be executed by the model developers and their peers, and lastly, the gap between the scientific state of the art embedded in the model and the state of knowledge required to answer all questions and concerns to everyone's satisfaction. Notwithstanding all these gaps between the ideal and the real, by the next decade, we can look forward to a new level of scientific power in our public and private decisions about fire safety. If I may hazard a guess, we have nothing to risk and everything to gain.

John R. Hall, Jr.
Director
Fire Analysis & Research Division
National Fire Protection Association
Batterymarch Park
Quincy, MA 02269

Dr. John Hall is Director of Fire Analysis and Research at the National Fire Protection Association, a position he has held since 1984. Prior to joining NFPA, Dr. Hall was involved with fire analysis and research at the National Bureau of Standards Center for Fire Research, the U.S. Fire Administration, and the Urban Institute. Dr. Hall has a B.A. in Mathematics from Brown University and a Ph.D. in Operations Research from the University of Pennsylvania.

FIRE MODELING: A KEY ELEMENT TO HAZARD AND RISK ASSESSMENT

William Douglas Walton

Center for Fire Research
National Institute of Standards and Technology
Gaithersburg, Maryland 20899

Abstract

The ability to predict the temperatures, species concentrations and other conditions developed in compartment fires is a key element in the analysis of fire hazard and risk. Decades of study of the phenomena associated with compartment fires have led to the development of computer-based models which can predict the fire induced environment in compartments.

This paper will review the state-of-the art of compartment fire modeling and will present examples of current models and their function.

Introduction

Although the importance of fire hazard and risk assessment will be discussed in another paper, it is evident that an estimate of the conditions developed during the course of a fire is necessary to make an assessment. The conditions most commonly of interest include the burning rate of the fire and the associated spatial distribution of gas temperatures and species concentrations. The species concentrations typically include oxygen, carbon dioxide and carbon monoxide. Other conditions such as gas flow rates, material temperatures, heat fluxes, other species concentrations and the activation time of detection and suppression devices may also be important.

The most comprehensive method for estimating the conditions resulting from a fire is the use of a computer fire model. This discussion of fire modeling will be limited to compartment fires. Compartment fires can defined as fires in enclosed spaces which are commonly thought of as rooms in buildings, but may include other spaces such as those found in transportation vehicles such as ships, planes, trains, and the like.

Fires Stages

Compartment fires are often discussed in terms of stages[1]. The stages are:

1. Ignition
2. Growth
3. Flashover
4. Fully developed fire
5. Decay

While many fires will not follow this idealization, it provides a useful framework for the discussion of compartment fires. All fires include an ignition stage but, beyond that may fail to grow or they may be affected by manual or automatic suppression activities before going through all of the stages listed above.

Fire Stage Definitions

Ignition Stage - This is the point at which the fire begins.

Growth Stage - Following ignition, the fire initially grows primarily as a function of the fuel itself, with little or no influence from the compartment. The fire can be described in terms of its rate of energy and combustion products generation. If sufficient fuel and oxygen are available, the fire will continue to grow causing the temperature in the compartment to rise. Fires with sufficient oxygen for combustion are said to be fuel controlled.

Flashover - Flashover is generally defined as the transition from a growing fire to a fully developed fire in which all combustible items in the compartment are involved in fire. During this transition there are rapid changes in the compartment environment. Flashover is not a precise term, and several variations in definition can be found in the literature. Most are based on the temperature at which the radiation from the hot gases in the compartment will ignite all of the combustion contents. Gas temperatures of 300 to 650°C have been associated with the onset of flashover, although temperatures of 500 to 600°C are most widely used[2]. Flashover has also been associated with The ignition of unburnt fuel in the hot fire gases, the appearance of flames from openings in a compartment, or the ignition of all of the combustible contents may actually be a different phenomen.

Fully developed fire - During this stage, the heat release rate of the fire is the greatest. Frequently during this stage more fuel is pyrolized than can be burned with the oxygen available in the compartment. In this case, the fire is said to be ventilation controlled. If there are openings in the compartment, the unburned fuel will leave the compartment in the gas flow and may burn outside of the compartment. During the fully developed stage, the environment within the compartment has a significant effect of the heat release rate of the burning objects.

Decay stage - The decay stage occurs as the fuel becomes consumed and the heat release rate declines. The fire may change from ventilation to fuel controlled during this period.

Compartment Fire Phenomena

In order to calculate or predict the temperatures and species concentrations generated in a compartment fire, a description or model of the fire phenomena must be created. This model will be described in terms of physical equations which can be solved to predict the temperature and species concentrations in the compartment. Such a model is, therefore, an idealization of the compartment fire phenomena. Consider a fire which starts at some point below the ceiling and releases energy and products of combustion. The rate at which energy and products of combustion are released may change with time. The hot products of combustion form a plume which, due to buoyancy, rises toward the ceiling. As the plume rises, it draws in cool air from within the compartment decreasing the plume's temperature and increasing its volume flow rate. When the plume reaches the ceiling, it spreads out and forms a hot gas layer which descends with time as the plume's gases continue to flow into it. There is a relatively sharp interface between the hot upper layer and the air in the lower part of the compartment. The only interchange between the air in the lower part of the room and the hot upper layer is through the plume. As the hot layer descends and reaches openings in the compartment walls (e.g., doors and windows), hot gas will flow out the openings and outside air will flow into the openings. This description of compartment fire phenomena is referred to as a two-layer or zone model.

The two layer model concept assumes that the composition of the layers is uniform. That is the temperature and other properties are the same throughout each layer. Although the temperature of the lower layer will rise during the course of the fire, the temperature of the upper layer will remain greater and is of the most importance in compartment fires.

Calculation of Compartment Fire Temperatures and Species Concentrations

The basic principle used to calculate the temperature in the a compartment fire is the conservation of energy. As applied to the hot upper layer, the conservation of energy can be simply stated as: the energy added to the hot upper layer by the fire equals the energy lost from the hot layer plus the time rate of change of energy within the hot upper layer. From the time rate of change of energy within the hot layer, the temperature of the layer can be computed. Conservation of energy can also be applied to the lower layer as well. Since the volume of the upper layer changes with time, and mass flows in and out of the upper layer, conservation of mass must be used along with the conservation of energy. Because the energy generated by the fire and the temperatures in compartment vary as a function of time, the application of the conservation of energy will result in a series of differential equations. The transport of energy in a compartment fire is a very complex process. In order to formulate expressions for the conservation of energy in a practical way, a number of assumptions must be made. It is possible to formulate the equations for the conservation of energy in a number of ways based on the level of detail desired. Similar techniques are used to calculate the species concentrations using the conservation of mass. Additional details may be found in the references cited.

Energy and Products Generated by the Fire

The energy generated by the fire is the primary influence on the temperature in a compartment fire and much research has been conducted in predicting the energy release rate of many fuels under a variety of conditions. As a fuel is heated and releases pyrolysis products, these products react with oxygen, generating heat and combustion products and possibly producing flames. The rate of energy release is equal to the mass loss rate of the fuel times the effective heat of combustion of the fuel. The effective heat of combustion is the heat of combustion which would be expected in a fire situation where incomplete combustion takes place. This is less than the theoretical heat of combustion as measured in the oxygen bomb calorimeter. The effective heat of combustion is often described as a fraction of the theoretical heat of combustion.

The products generated by the fire are the primary influence on the species concentrations within the compartment. Although theoretical product generation rates may be calculated for simple fuels, much less work has been done in measuring and predicting the wide range of products expected to be produced from the burning of real fuels under the wide variety of conditions found in compartment fires.

In fuel-controlled fires, there is sufficient air to react with all the fuel within the compartment. In ventilation-controlled fires, there is insufficient air within the compartment, and some of the pyrolysis products will leave the compartment, possibly to react outside the compartment. For calculating the temperatures produced in compartment fires, the primary interest is in the energy released within the compartment.

The pyrolysis rate of the fuel depends on the fuel type, its geometry and the fire-induced environment. The energy and combustion products generated in the compartment by the burning pyrolysis products then depend on the conditions (temperature, oxygen concentration, etc.) within the compartment. While the processes involved are complex, and some are not well understood there are two cases where some simplifying assumptions can lead to useful methods for approximation of the energy released by the fire. These two cases may not however provide as great a simplification in approximating the generation of combustion products.

Free-burning fires are defined as those in which the pyrolysis rate and the energy release rate are affected only by the burning of the fuel itself and not by the room environment. This is analogous to a fire burning out of doors on a calm day. This data is most useful for estimating burning rates of primarily horizontal fuels in pre-flashover fires, where the primary heating of the fuel is from the flames of the burning item itself[3]. Vertical fuels, such as wall linings and fuels located in the upper hot gas layer, will likely be influenced by the pre-flashover room environment.

Ventilation-controlled fires are defined as those in which the energy release rate in the room is limited by the amount of available oxygen. For most fuels, the heat released per mass of air consumed is a constant approximately equal to 3000 KJ/kg[4]. Therefore, the rate of energy release of the fire can be approximated from the air inflow rate.

The solution of a relatively complete set of equations for the conservation of energy, mass and species requires the solution of a large number of equations which vary with time. Although individual energy transport equations may be solved, in general there is not an explicit solution for a set of these equations. As a result, one of two approaches can be taken. The first is an approximate solution which can be accomplished by "hand" using a limiting set of assumptions. The second is a more complete solution utilizing a computer program. In either case, a number of methods have been developed. This paper will focus on the computer based methods. Each method employs assumptions and limitations which should be understood before employing the method.

Computer Methods for Predicting Compartment Fire Phenomena

Computer models are simply computer programs which model or simulate a process or phenomenon. Computer programs are used in many areas of fire protection design, including suppression system design, smoke control system design, and egress analysis. The focus here will be on computer models which predict the conditions in compartment fires.

Computer fire models can provide a faster and more accurate estimate of the impact of a fire, and the measures used to prevent or control the fire, than many of the methods previously used. While manual calculation methods provide good estimates of specific fire effects (e.g., prediction of time to flashover), they are not well suited for comprehensive analyses involving the time-dependent interactions of multiple physical and chemical processes present in developing fires.

The state of the art in computer fire modeling is changing rapidly. Understanding of the processes involved in fire growth is improving and thus the technical basis for the models is improving. The capabilities, documentation, and support for a given model can change dramatically over a short period of time. In addition, computer technology itself (both software and hardware) is advancing rapidly. A few years ago, a large mainframe computer was required to use most of the computer fire models. Today, almost all of the models can be run on microcomputers. Therefore, rather than provide an exhaustive discussion of rapidly changing state-of-the-art available computer models, the following discussion will focus on a representative selection.

There are two general classes of computer models for analyzing enclosure fire development. Probabilistic models treat fire growth as a series of sequential events or states. These models are sometimes referred to as "state transition" models. Mathematical rules are established to govern the transition from one event to another (e.g., from ignition to established burning). Probabilities are assigned to each transfer point, based on analysis of relevant experimental data and historical fire incident data. Probabilistic models do not normally make direct use of the physical and chemical equations describing the fire processes.

In contrast, deterministic models represent the processes encountered in a compartment fire by interrelated mathematical expressions based on physics and chemistry. These models may also be referred to as "room fire" models, "computer fire" models or "mathematical fire" models. Ideally, such models represent the ultimate capability: discrete changes in any physical parameter could be evaluated in terms of the effect on fire hazard. While the state of the art in understanding fire processes will not yet support the "ultimate" model, a number of computer models are available that provide reasonable estimates of selected fire effects.

The most common type of physically based fire model is the "zone" or "control volume" model, which solves the conservation equations for distinct regions (control volumes). A number of zone models exist, varying to some degree in the detailed treatment of fire phenomena. The dominant characteristic of this class of model is that it divides the room(s) into a hot upper layer and a lower cooler layer. The model calculations provide estimates of key conditions for each of the layers as a function of time. Zone modeling has proved to be a practical method for providing first-order estimates of fire processes in enclosures.

Another other general type of deterministic model is the "field" model. This type of model solves the fundamental equations of mass, momentum, and energy for each element in conservation of energy in a number of ways based on the level of detail desired. Similar techniques are used to calculate the species concentrations using the conservation of mass. Additional details may be found in the references cited.

Energy and Products Generated by the Fire

The energy generated by the fire is the primary influence on the temperature in a compartment fire and much research has been conducted in predicting the energy release rate of many fuels under a variety of conditions. As a fuel is heated and releases pyrolysis products, these products react with oxygen, generating heat and combustion products and possibly producing flames. The rate of energy release is equal to the mass loss rate of the fuel times the effective heat of combustion of the fuel. The effective heat of combustion is the heat of combustion which would be expected in a fire situation where incomplete combustion takes place. This is less than the theoretical heat of combustion as measured in the oxygen bomb calorimeter. The effective heat of combustion is often described as a fraction of the theoretical heat of combustion.

The products generated by the fire are the primary influence on the species concentrations within the compartment. Although theoretical product generation rates may be calculated for simple fuels, much less work has been done in measuring and predicting the wide range of products expected to be produced from the burning of real fuels under the wide variety of conditions found in compartment fires.

a compartment space which has been divided into a grid of small elements. Imagine an enclosure filled with a 3-dimensional grid of tiny cubes; a field model will calculate the physical conditions in each cube, as a function of time. The calculation will account for physical changes generated within the cube, and changes affected on the cube from surrounding cubes. This will permit the user to determine the conditions at any point in the compartment.

Currently, the computational demands of most field models exceed the computer resources of the typical user. One of the field models, JASMINE[5,6], "appears to offer a reliable tool for the prediction of detail thermal properties on non-spreading fire problems where radiant heat transfer is relatively less important than convection."

The above discussion provides the reader with a brief overview of computer fire modeling. For in-depth review of the topic, see references [5-31]. A brief review of selected zone fire models is provided below.

Compartment Fire Models

ASET (Available Safe Egress Time) is a program for calculating the temperature and position of the hot upper smoke layer in a single room with closed doors and windows. ASET can be used to determine the time to the onset of hazardous conditions for both people and property. The required program inputs are the heat loss fractions, the height of the fuel above the floor, criteria for hazard and detection, the room ceiling height, the room floor area, a heat release rate, and (optional) species generation rate of the fire. The program outputs are the temperature, thickness and (optional) species concentration of the hot smoke layer as a function of time, and the time to hazard and detection. ASET can examine multiple cases in a single run. ASET was written in FORTRAN by Cooper and Stroup[7].

ASET-B is a program for calculating the temperature and position of the hot upper smoke layer in a single room with closed doors and windows. ASET-B is a compact version of ASET, designed to run on personal computers. The required program inputs are a heat loss fraction, the height of the fire, the room ceiling height, the room floor area, the maximum time for the simulation, and the rate of heat release of the fire. The program outputs are the temperature and thickness of the hot upper smoke layer as a function of time. Species concentrations and time to hazard and detection, calculated by ASET, are not calculated in the compact ASET-B version. ASET-B was written in BASIC by Walton[8].

COMPF2 is a computer program for calculating the characteristics of a post-flashover fire in a single building compartment, based on fire-induced ventilation through a single door or window. It is intended both for performing design calculations and for the analysis of experimental burn data. Wood, thermoplastics and liquid fuels can be evaluated. A comprehensive output format is provided which gives gas temperatures, heat flow terms, and flow variables. The documentation includes input instructions, sample problems, and a listing of the program. The program was written in FORTRAN by Babrauskas[9].

FAST (Fire and Smoke Transport) is a multi-room fire computer program which predicts the conditions within a structure, resulting from a user-specified fire. FAST version 17 can accommodate up to five rooms with multiple openings between the rooms and to the outside. The required program inputs are the geometrical data describing the rooms and connections; the thermophysical properties of the ceiling, walls and floors, the fire as a rate of mass loss, and the generation rates of the products of combustion. The program outputs are the temperature and thickness of, and species concentrations in, the hot upper layer and the cooler lower layer in each compartment. Also given are surface temperatures and heat transfer and mass flow rates. FAST was written in FORTRAN by Jones[10]. FAST serves as the base model for the fire hazard assessment system (currently known as HAZARD I) scheduled to be released by the Center for Fire Research, NIST, in early 1989.

The HARVARD fire model predicts the development of a fire and the resulting conditions within a room (version 5) or multiple rooms (version 6), resulting from a user-specified fire or user-specified ignition. Version 5 predicts the heating and possible ignition of up to four targets, due to the original fire. The room must have at least one opening to the outside. Version 6 does the same for up to five rooms connected to each other with openings (at least one of the rooms must have an opening to the outside). The required program inputs are the geometrical data describing the rooms and openings, and the thermophysical properties of the ceiling, walls, burning fuel, and targets. The generation rate of soot must be specified, and the generation rates of other species may be specified. The fire may be entered either as a mass loss rate or in terms of fundamental properties of the fuel. Among the program outputs are the temperature and thickness of, and species concentrations in, the hot upper layer and the cooler, lower layer in each compartment. Also given are surface temperatures and heat transfer and mass flow rates. The HARVARD program was written in FORTRAN by Emmons and Mitler[11]. Further development of the HARVARD model has been discontinued and a descendant of this model known as FIRST has been introduced.

OSU (Ohio State University compartment Fire computer program) is a program for calculating heat release rate, smoke generation rate, and smoke and heat venting from single compartments. The OSU model takes into account an initiating fire and both horizontal and vertical fire spread, providing a prediction of how combustible materials in the compartment influence the course of a developing fire. The required program inputs are material thermal properties, ignition point, rate of heat and smoke release, and flame propagation parameters. In addition, certain plume properties are required, including dimensions, temperature, and emissivity. Typical model outputs include upper layer air temperature, smoke generation rate, and heat release rate. OSU was written in FORTRAN by Smith and Satija[12].

Cautions and Limitations

A discussion of computer fire models would not be complete without a word of caution concerning their use. Fire is a complex event. As the name implies these methods are models of fire development within a compartment and are based on an assumed mathematical description of the phenomena. None of the models are comprehensive in there description and the results should be viewed as estimates. In general a level of precision is implied in the model output which is in excess of the model's capabilities. Each of the models has its own individual set of limitations and the user should become familiar with them.

When using fire models the user should examine the sensitivity of the results to variations in the required inputs. If small changes in input values result in large changes in the outputs, extra caution should be exercised.

Users of computer fire models have found that using multiple models provides a useful check of the results. While all zone models are similar, there are enough differences that using two or more models to address the same problem can prove useful in screening errors. A common technique is to compare the results of a relatively simple model with those of a more comprehensive one.

Related Activities

The development of computer fire models is a very active research area. The above review is intended to offer the reader a perspective on what is currently available. One should also recognize that the information in this paper is not exhaustive. As an example, little attention has been given to fire modeling efforts and available programs outside the United States.

Most of the computer fire models discussed in this paper are available only from the authors. Some programs may also be available on fire-oriented computer bulletin boards. (ASET, ASET-B, FAST and FIRST are available in versions for MS-DOS computers on the Center for Fire Research Bulletin Board. The modem phone number is 301-921-6302.) The user should be aware that there may be significant differences among computers and versions of so-called standard computer languages. As a result, programs may not always be transferred directly from one computer to another.

There are a number of organizations in the United States which are very active in the development and coordination of computer fire models. The Ad Hoc Working Group on Mathematical Fire Modeling has been active for over ten years. This group, chaired by the National Institute of Standards and Technology plays a role in coordinating the development of the technical basis for fire models, and serves as a forum for discussion and exchange of ideas. The American Society of Testing and Materials (ASTM) has a subcommittee (ASTM E 5.39 Subcommittee on Fire Modeling) to coordinate and develop ASTM's role in the evolution of computer fire modeling. Also, the Society of Fire Protection Engineers (SFPE) has a computer committee which maintains a current list of available computer models. The serious user of computer models will need to be acquainted with the activities of these groups.

References

1. Drysdale, D., "The Pre-Flashover Compartment Fire," An Introduction to Fire Dynamics, John Wiley & Sons Ltd., Chichester, pp. 278-303 (1985).

2. Thomas, P.H., "Testing Products and Materials for their Contribution to Flashover in Rooms," Fire and Materials, Vol 5, No. 3, pp. 103-111 (1981).

3. Babrauskas, V., "Upholstered Furniture Room Fires - Measurements, Comparison With Furniture Calorimeter Data, and Flashover Predictions," Journal of Fire Sciences, Vol. 2, Jan/Feb, pp 5-19 (1984).

4. Huggett, C., "Estimation of Rate of Heat Release by Means of Oxygen Consumption Measurements," Fire and Materials, Vol. 4 No. 2., pp. 61-65 (1980).

5. Cox, G. and Kumar, S., "Field Modeling of Fire in Forced Ventilation Enclosures," Comb. Sci. and Tech., 52, 1-3, pp 7-23 (1987).

6. Cox, G., Kumar, S. and Markatos, N. C., "some Field Model Validation Studies," Proceedings, International Association for Fire Safety Science, Hemisphere Publishing (1986).

7. Cooper, L.Y. and Stroup, D.W., "ASET- A Computer Program for Calculating Available Safe Egress Time," Fire Safety Journal, Vol. 9, pp. 29-45 (1985).

8. Walton, W.D., "ASET-B A Room Fire Program for Personal Computers," Nat. Bur. of Stand. (U.S.) NBSIR 85-3144 (1985).

9. Babrauskas, V., "COMPF2- A Program for Calculating Post-Flashover Fire Temperatures," Nat. Bur. of Stand. (U.S.), NBS TN 991 (1979).

10. Jones, W.W., "A Multicompartment Model for the Spread of Fire," Smoke and Toxic Gases, Fire Safety Journal, Vol. 9, pp. 55-79 (1985).

11. Mitler, H.E., "The Harvard Fire Model," Fire Safety Journal, Vol. 9, pp. 7-16 (1985).

12. Smith, E.E. and Satija, S., "Release Rate Model for Developing Fires," 20th Joint ASME/AIChE National Heat Transfer Conference, Milwaukee, WI, August 2-5, (1981).

13. Emmons, H.D., "The Prediction of Fires in Buildings, Seventeenth Symposium on Combustion," p. 1101, The Combustion Institute, Pittsburgh, PA (1979).

14. Levine, R.S., "Mathematical Modeling of Fires," Nat. Bur. of Stand. (U.S.) NBSIR 80-2107 (1980).

15. Quintiere, J.G., "A Perspective on Compartment Fire Growth," Combustion Science and Technology, Vol. 39, pp. 11-54 (1984).

16. Rasbash, D.J. (Editor), "Computer Applications in Fire Protection: Analysis, Modeling and Design," Fire Safety Journal, Vol. 9, No. 2 (July 1985).

17. Jones, W.W., "A Review of Compartment Fire Models," Nat. Bur. of Stand. (U.S.) NBSIR 83-2684 (1983).

18. Parikh, J.S. and Beyreis, J.R., "Survey of the State of the Art of Mathematical Fire Modeling," SFPE Bulletin (March 1985).

19. Survey of the State of the Art of Mathematical Fire Modeling, Underwriters Laboratories, Inc., File NC554, Project 82NK1618 (1983).

20. Swartz, J.A. et al., Final Technical Report on Building Fire Simulation Model, Vol. I & II, National Fire Protection Association, Quincy, MA. (May 1983).

21. Curtat, M.R., and Bodart, X.E., 1st Symposium International Association for Fire Safety Science, Hemisphere Publication, p. 637, 1986.

22. Tanaka, T., "A Model of Multiroom Fire Spread," Nat. Bur. of Stand. (U.S.) NBSIR 83-2718 (1983).

23. Zukoski, E.E. and Kubota, T., "Two-layer Modeling of Smoke Movement in Building Fires," Fire and Materials, Vol. 4, No. 1, p. 17 (March 1980).

24. Siu, N.O., "COMPBRN-- A Computer Code for Modeling Compartment Fires," University of California, Los Angeles, UCLA-ENG-8257 (August 1982).

25. MacArthur, C.D. and Reeves, J.S., "Dayton Aircraft Cabin Fire Model," University of Dayton, FAA-RD-76-120, 1 (June 1976).

26. Hagglund, B., "Simulating the Smoke Filling in Single Enclosures," National Defense Research Institute, Sweden, FOA C 20513-D6 (October 1983).

27. Hagglund, B., "A Room Fire Simulation Model," National Defense Research Institute, Sweden, FOA C 20501-D6 (June 1983).

28. Mitler, H.E., "The Physical Basis for the Harvard Computer Fire Code," Home Fire Project Technical Report #34, Harvard University (October 1978).

29. Rockett, J.A. et al., "Using the Harvard Fire Simulation," Fire Science and Technology, Vol. 3, No. 1, pp. 57-62 (1983).

30. Handa, T. et al., "Some Examples of Application of Harvard V Fire Computer Code to Fire Investigation," Fire Science and Technology, Vol. 3, No. 1., pp. 63-72 (1983).

31. Pape, R. Waterman, T.E., and Eichler, T.V., "Development of a Fire in a Room From Ignition to Full Room Involvement--RFIRES," Nat. Bur. of Stand. (U.S.) NBS-GCR-81-301 (1981).

A Real Case of Fire-Hazard Assessment: The NFPA and ENMT Conduit

Irwin A. Benjamin, Frederic B. Clarke, Philip DiNenno, Sharon Steele and Henri van Kuijk

Benjamin/Clarke Associates, Inc., Kensington, Maryland

ABSTRACT

Unresolved questions concerning the toxic hazard of combustion gases from electrical non-metallic tubing (ENMT) resulted in the National Electrical Code's limiting its use to buildings of three floors or less. The role of the hazard assessment in successfully removing the NEC limitation will be described.

This paper focuses on the contribution of the ENMT to the resulting hazard. The results of the tests and the correlation with the prediction are presented and discussed.

The approach consisted of full-scale experiments to verify those parts of the method which could readily be tested, followed by its application to the likely scenarios of actual use.

I. Background and Introduction

In the early 1980's a new product, electrical non-metallic tubing, was developed and proposed for use in certain applications covered by the National Electrical Code. The product is fabricated from unplasticized poly(vinylchloride) - - PVC - - in a fashion which combines mechanical strength with considerable pliability. The novelty of the product, in combination with a heightened awareness of the role of smoke in fire hazard, led, in 1984, to a limitation on the use of ENMT to buildings of three stories or less.

In an effort to learn more about the role of this product in a building fire. The manufacturer, Carlon Corp., asked Benjamin/Clarke Associates to develop a method for toxic hazard assessment which could be used to review the safety of the use of ENMT in buildings.

This report describes a method for looking at toxic hazard and to show how it was applied in a specific case, the use of ENMT raceway, which is made of PVC. Typically, ENMT is concealed in walls, floors, ceilings or fire resistive chases. This report is specifically designed to define the behavior of ENMT in two selected fire scenarios and to determine its contribution to the fire hazard in a building.

This kind of information, difficult to obtain without the use of hazard assessment, constituted part of the evidence which persuaded the NEC to remove the 3-story limitation in 1987.

II. The Approach to Hazard Assessment

A. Logic

Ideally, the way to assess a hazard is simply to carry out a series of full-scale experiments which simulate the situations of concern. As is often the case, this proved difficult to do in practice. In addition to the usual concerns attendant to full-scale fire experiments, the difficulties of characterizing and analyzing smoke generated in concealed spaced made a straightforward full-scale test program impractical. As a result, a hybrid program, using both experimental data and engineering calculations, was undertaken.

The method consists of several steps:

1. For a given scenario, calculate the thermal environment to which the ENMT raceway will be exposed. (The environment will of course be different, depending upon whether the raceway is directly exposed to a fire or located inside walls or ceiling plenums. However, in either case the environment is predictable.)

2. For the raceway, calculate the rate of combustion or pyrolysis product released as a result of the environmental exposure. To do this, one needs laboratory-scale data on the raceway's fire performance and the results of Step 1, above.

3. Determine the concentration of product leaving the fire room and its relative toxic hazard in relation to the other combustion products expected to be present.

Since the analysis is based on computer calculations and information from small-scale tests one may well ask how well the analysis can simulate a real fire. For this reason, a series of room tests were conducted and are reported herein, which were designed to validate the method of calculation (although, for the reasons cited above, they did not deal specifically with the scenarios understudy).

B. Organization

Section III gives results of room tests conducted to validate the calculation procedures used. This part shows how the prediction of the combustion or pyrolysis product loss rate can be calculated from a series of small scale tests conducted on the cone calorimeter; and from calculations of the fire growth rate in the environment using modern modeling technique such as the Harvard Fire Code. The two in combination allow a prediction of the amount of product being generated in a given fire.

Section IV looks at two scenarios in which an ENMT raceway would typically be used and determines the concentration of pyrolysis product present in a given room as a result of a typical fire in that room. The scenarios illustrate what change in the toxic hazard could result if ENMT were used in these cases.

III. Experimental Program

A. Full-Scale Measurements

1. Test Layout and Procedure: The full-scale test program was conducted to determine whether the calculation techniques used could indeed predict a given environment. Tests were conducted at two nominal fire energy output levels, 250 and 500 kW, in an 8 x 12 foot room. The details of the room and test arrangement are shown in Figures 1 and 2 and the test description is shown in Table 1. All the tests were conducted with wood cribs which were located in the center of the burn room. Two types of non-metallic raceway were located within the room and purposely exposed to the fire environment. The fires were designed so that the 25 kg crib fire (Tests 3-5) did not directly impinge on the raceway, but the 50 kg crib fire (Tests 1 and 2) did impinge on, and did ignite, the raceway.

For this validation program a 7'10" x 12'1" room, 8'1" high, was used as an experimental chamber, with a 31.5" x 79" door, Figures 1 and 2. It was desired specifically to obtain measurements to compare with calculations made to predict the behavior of 40 lineal feet of raceway hung near the ceiling along one side and exposed to the fire plume. The raceways were suspended horizontally in a tray about 3" below the ceiling and the center of the unit was 6" from the side wall. Although using exposed non-metallic tubing raceway in a room would not be normal construction practice, it was used in this test for the purpose of demonstrating the model predictability. These demonstrations would have been far more difficult if the tubing had been used in its normal concealed location.

A series of five tests was run in accordance with Table 1. Tests were made with both ENMT (electrical non-metallic tubing) and RNMC (rigid non-metallic conduit). Both of these products are made from PVC, with negligible addition of fillers or additives. Two blank tests were run to evaluate the performance of the cribs alone in the room. The fire effluent emptied into a 43 foot long corridor that had a hairpin bend in it at midpoint. The corridor in turn emptied into a 10 by 10 foot hood which was used to collect all the combustion gases, so that a total heat release rate record could be made. The ceiling and walls of the room were of foam concrete of 44 PCF density and were covered with 2 coats of silicone paint.

2. Test Results: With the 25 kg crib the flames from the crib did not reach the ceiling, and there was no ignition of the raceway. With the 50 kg crib fire the flames hit the ceiling and travelled across the ceiling to the raceway. Ignition

occurred at about 600 seconds at the center of the raceway and from there travelled to the ends.

Figure 3 shows the measured rate of total heat release of Tests 1 and 2. The 50 kg crib alone produced about 450 kilowatts. This value increased in Test 2 to about 520 kilowatts, because of the added heat release of the of raceway, which started burning after 10 minutes. The measured upper air temperatures for Tests 1 and 2, showed similar behavior. These data were taken from Test 2 showed an average upper layer temperature about 50°C higher than Test 1 because of the additional energy created by the burning of the raceway.

Both the ENMT and RNMC are made from PVC, with no plasticizers or extenders. The former is a thin wall corrugated conduit and the latter is a heavier-walled (Schedule 40) conduit. Hydrogen chloride (HCl) is released from PVC in significant quantities starting at about 270°C. The measured raceway weight loss during the test is shown in Figure 4. Only a small portion of the HCl loss occurs prior to ignition; since the ENMT started burning between 600 and 700 seconds, data beyond this time no longer represents only the pyrolysis (non-burning decomposition) of the PVC, but also the added weight loss due to the burning of the PVC.

The measured rates of heat release for those tests which used a 25 kg crib reached a value of about 250 kw, and are shown in Figure 5. Tests 3 and 4 are of ENMT and RNMC raceways respectively and show comparable rates of heat release. Test 5, which was the crib without a raceway in the room, shows a comparable heat release rate peak and a slightly delayed response time. Heat flux measurement and weight loss for raceway in these tests were also obtained and are discussed below.

B. Comparison of Predicted and Measured Fire Environment

1. The Fire Environment: The fire conditions which most affect raceway behavior are the heat flux and temperature around the raceway. These can be calculated using a fire growth model: the one used was Harvard CFC 5 (1), which allows one to enter the actual size of the fire, which was taken from the measured weight loss rate of the cribs, and to obtain as output the temperature in the upper layer of the room, the height of the smoke layer, the radiation to an object in the room, flow out the door and various other parameters. Table 2 shows a typical input data sheet for the CFC5 code. The values of the heat of combustion of wood and the thermal conductivity of the low density concrete walls were taken from the NFPA Fire Protection Handbook and the ASHRAE Handbook respectively.

Comparison of the measured average upper layer temperatures with those predicted by the Harvard Fire Code for the burning crib are shown in Figures 6 through 8 for Tests 2, 3 and 4 respectively. In general, the predictions are quite close, with a maximum deviation of about 50°C for Test 2 where the test temperatures are higher because the tubing contributed to the fire.

The prediction of the radiative flux to the object is important since the calculation of the weight loss is based on this parameter. Figures 9 through 11 show the comparison of the predicted with the actual radiative flux to the object, measured by radiometers near the ends of the conduit and slightly below the plane of the raceway. Tests 3 and 4 show excellent agreement between the measured and predicted values. In Test 2, the agreement is good until ignition of the tubing, an event not treated by the model used.

2. Reaction of Raceway to Environment: The second step in the procedure is to calculate the rate of mass loss of the raceways as a result of the thermal exposure. To do this the response of the raceway to a given applied heat flux must be known. This response was measured by the cone calorimeter (2), a device for following weight loss of a sample under well characterized heat flux levels. Curves were developed from the test data, using a linear best-fit program, to predict the rate of weight loss of the raceway as a function of a given applied flux over a period of time. The summary of this cone calorimeter work is shown in Figure 12 in which the energy input, applied flux times time, is shown as a function of the weight loss per unit area. The values are shown for both ENMT and RNMC.

Using the calculated flux to the object shown in Figures 9 through 11,

the mass loss behavior of the raceways can be calculated from the curves in Figure 12. This procedure gives the weight loss as a function of time for the test. Figures 13 through 15 show a comparison of the measured and predicted weight loss, based on the exposure of the surface of the raceway, an area of 10.8 sq. ft., to the calculated fluxes.

Figures 13 through 15 show the ability of the procedure to predict the weight loss in the early stages of the fire, and therefore the rate of generation of HCl. The measured and predicted weight losses were in fairly good agreement for all the tests. In Tests 3 and 4, where no ignition occurred the measured weight loss reaches a plateau when all the volatiles are driven off. For the calculation curve in Test 3, this is shown as the level when all the theoretical weight of HCl has been lost. For the total amount of raceway used in Test 2, of 2.6 kg, the maximum HCl present was about 1.5 kg, based on a theoretical weight of HCl of 56 per cent. The measured weight loss shown in Figure 13 which exceeds this level represent the loss due to the burning of the raceway.

C. Significance

When PVC material is heated it will release hydrogen chloride. Since HCl is one of the first volatiles to come off from PVC as it is heated, the measured weight loss of the PVC raceway up to the time of its ignition is a measure of the release of the HCl into the atmosphere. Since it has been shown that the weight loss can be predicted from a calculation of the thermal environment flux and the response of the material to that flux, one now has a method whereby full-scale performance can be inferred by computational methods and laboratory data.

Another output from the Harvard Code is the rate of mass flow leaving the room. The mass flow contains within it the HCl which was pyrolyzed from the raceway. From the weight loss prediction curves in Figures 13 through 15 and the mass flow rate a calculation can be made of the concentration of the HCl in the air leaving the room, or the concentration of HCl into the corridor outside the room of fire origin. This is shown in Table 3. This concentration of HCl is the predicted maximum concentration, based on the assumption that all the volatiles are HCl, none of which is lost due to settlement or condensation on the walls and ceilings.

This section has shown that fire behavior and its effect on the raceway can be predicted and, as a consequence the HCl output of the fire room was predicted. The experimental program of this work was particularly designed to show the feasibility of predicting mass loss of the product if we know its environment. We now proceed to analyze specific real scenarios.

IV. Toxic Hazard Evaluation

A. Applicable Scenarios

This section discusses two situations where a raceway such as ENMT is typically used. The scenarios of interest are where the raceway is inside either a wall cavity or a ceiling plenum. The passage of heat through a wall can be accurately calculated so long as the wall's properties are known and the temperature of an object in the space behind the wall can in turn be estimated by taking into account both radiative and convective interchange with the walls.

In order for significant quantities of HCl to be released from the PVC raceway in a plenum or a cavity wall it must be subject to about 525°F (270°C) surface temperature, an equivalent flux of approximately 7 kW/sq m. To predict when this temperature might actually be reached inside a cavity, it is necessary to know the temperature-time profile on the room-side of the wall. If no experimental data are available, a fire model, such as that described in the previous section, can be used. In this case however, reliable real fire data re available: Figure 16, shows the growth of the temperature in the upper air layer of a furnished residential room. This is one example from a series of tests conducted at the National Institute of Standards and Technology, using a large fast growing fire (6). For the first two minutes the temperatures in the room do not show a significant increase, but then the room quickly becomes fully-involved, or "flashed-over", and we see the large jump in temperature.

Two scenarios involving this fire were examined. For Case 1, we assumed a raceway in a wall cavity 3 1/2" wide and faced with 5/8" gypsum board,

where the exposed wall area is 200 sq. ft. For Case 2, we assumed a raceway in a ceiling plenum above a 5/8" gypsum board. We have assumed a plenum, in accordance with Section 12-3.7 of the Life Safety Code which mandates a maximum size of 22,500 square feet, and an assumed height of 24": this represents a volume of 45,000 cubic feet. For fire protection we assumed a 5/8" Type X gypsum board ceiling. The fire area is assumed to be limited to a single room and the heated area of the ceiling was taken as 200 sq. ft.

The room temperatures from the test are reproduced in more schematic form in Figure 17, labeled "Exposure Fire". These temperatures were used to calculate the temperatures of the raceways inside the cavity and plenum, which are also shown in Figure 17. The temperatures on the raceway in the wall cavity are higher than those in the ceiling plenum because the wall cavity has far less surface area to which it can lose heat. To reach the indicated value of 500°F, just below the temperatures at which the HCl will begin to evolve, will take about 16 minutes in the wall cavity and close to 40 minutes in the plenum, after the initiation of this fire. If the plenum or cavity has no communication with the fire room, then the HCl will not enter the room; if there is air leakage through the wall or ceiling, then some HCl will enter the room volume.

B. Wall Cavity Calculation

The worst case for an analysis of the possible toxic hazard: is the raceway in a wall cavity from which the concentration of HCl is freely communicating into the room of fire origin through leakage in the wall. In this case the wall cavity has a volume of about 58 cubic feet into which the mass loss of the conduit will be initially distributed. For this particular case we can calculate the environmental exposure of the raceway from Figure 17, convert the temperature to heat flux reaching the raceway, and from the exposure calculate the associated mass loss of the raceway that will occur. Figure 18 shows the mass loss of HCl from an assumed 40 lineal feet of raceway (4 ten-foot pieces) into the adjacent cavity, as a function of time. This calculation is based on the data from Figure 12, which allows a calculation of the rate loss of the raceway from radiant flux in the cavity. There will be about 3g, or 900 parts-per-million of HCl released into the cavity 20 minutes after the fire in the room starts.

If all the HCl from the cavity goes into the fire room and is retained in the fire room (no open doors, and no loss by deposition or absorption). Then the concentration of HCl in the $26m^3$ room will be 70 ppm at 20 minutes and 500 ppm at 30 minutes. In other words, for even this very fast developing fire, over 30 minutes would be required to develop significant concentrations of HCl in the fire room assuming 100% of the HCl is leaking out of the cavity.

An immediate lethal threat is posed by the exposure fire after about 5 minutes, when it is in the post flash-over regime, and producing large quantities of carbon monoxide. The measured amount of carbon monoxide that was generated in this particular fire (7) is shown in Figure 19. After about 5.5 minutes, the concentration-time product (4) of CO reached a value of 75,000, well in excess of the 40,000 to 50,000 ppm-minutes generally considered as a value for carbon monoxide-induced incapacitation (5). Hence, carbon monoxide in this scenario is incapacitating after 6 minutes; no HCl is even generated until about 20 minutes. It is also worth noting that there were over 40,000 ppm of CO for the extended period from about 4 to 14 minutes. During this period the CO level is far in excess of a lethal amount. From this example, as shown above, a fire large enough to cause a mass loss of HCl from the raceway inside the cavity or plenum would have been burning long enough to cause a lethal atmosphere from the generation of carbon monoxide. The production of HCl from the cavity would occur considerably after the CO lethal conditions have been developed.

C. Raceway in Ceiling Cavity

From Figure 17 it is obvious that the heating of the raceway in the ceiling plenum will lag that in the wall cavity, about 40 vs 16 minutes. When HCl does come from the plenum raceway it will be distributed in 45,000 cu. ft of plenum and room space. For these reasons, the generation of HCl from the plenum into the room will be only a small fraction of that calculated for the wall cavity

and therefore not the critical scenario.

D. Significance

Two scenarios were assessed for toxic hazard: a raceway in a ceiling plenum and in a wall cavity, with a fast developing fire in a room. Data from an actual fire was used to evaluate the effect on the concealed raceways. The measured values of CO were shown to be above the lethal level long before any significant amounts of HCl would enter the room from the concealed raceway.

V. Conclusions

The major conclusions to be drawn from this work are:

1. The proposed methodology for toxic hazard analysis was shown by test to be usable for predicting the behavior of PVC raceways exposed to a fire.

2. For the typical case of the PVC raceways enclosed within a ceiling or wall plenum the size of a room fire necessary to produce HCl from this raceway would probably by itself produce carbon monoxide in excess of lethal levels before production of HCl occurred.

VI. Acknowledgments

This program was supported by Carlon, a division of The Lamson & Sessions Co. The full scale testing was done at the University of Ghent and the cone calorimeter tests at the National Institute of Standards and Technology.

VII. References

1. Documentation for CFC V, NBS-GCR-81-344, U.S. Department of Commerce

2. Development of the Cone Calorimeter - A Bench-Scale Heat Release Rate Apparatus Based on Oxygen Consumption, Babrauskas, NBSIR 82-2611, NBS 1982

3. Turbulent Ceiling - Jet Induced by Large Scale Fires, Alpert, FMRC No 22357-2, May 1971

4. Evaluation of Smoke Toxicity using Concentration - Time Products, Alexeeff and Packham, Journal of Fire Sciences, V2, No. 5, September 1984

5. Modeling of Toxicological Effects of Fire Gases: Part I; Journal of Fire Sciences V2, July/August 1984.

6. Fire Development in Residential Basement Rooms, Fang and Breese, NBSIR 80-2120, NBS 1980.

7. Fire Endurance Tests of Selected Residential Floor Construction, Fang, NBSIR 82-288, NBS 1982.

8. Sensory Irritation Evoked by the Thermal Decomposition Products of Plasticized Polyvinyl Chloride, Alarie et al, Fire and Materials, 1976, 1, 147 to 153.

VIII. Biographies

1. Irwin A. Benjamin

Deceased

2. Frederic B. Clarke, III, Ph.D.
Benjamin/Clarke Associates, Inc.
10605 Concord Street - Suite 501
Kensington, MD 20895

Frederic Clarke is President of Benjamin/Clarke Associates, Inc., a firm specializing in the characterization and analysis of fire safety problems. Until Fall, 1981 he was director of the National Institute of Standards and Technology's Center for Fire Research, the Nation's principal Federal fire laboratory. He was a member of the National Academy of Sciences Committee on Fire Toxicity, 1985-86 and is currently Technical Director of the National Fire Protection Association Risk Analysis Project.

He holds a Ph.D. in chemistry from Harvard University.

3. Philip DiNenno
Benjamin/Clarke Associates, Inc.
10605 Concord Street - Suite 501
Kensington, MD 20895

4. Sharon Steele
Benjamin/Clarke Associates, Inc.
10605 Concord Street - Suite 501
Kensington, MD 20895

Sharon Steele is an Engineering Associate at Benjamin/Clarke Associates, Inc. Her responsibilities

include the preparation of scenarios for modeling and modification of models to suit scenarios. She has applied her skills to several projects such as NFPA's Risk Analysis, Forced Ventilation in Multi-Room Facility, Residential Heat Detector Actuation, Cable Flame Spread and Tunnel Fire Hazard.

She holds a B.S. from the University of Maryland in Fire Protection Engineering.

5. Henri van Kuijk
Benjamin/Clarke Associates, Inc.
10605 Concord Street - Suite 501
Kensington, MD 20895

Henri van Kuijk is an Engineering Associate at Benjamin/Clarke Associates, Inc. with responsibilities in computer modeling of fire and smoke behavior in buildings. He has expanded the Harvard Computer Fire Code, and developed a user friendly graphic package written in Fortran to include on-line calculations.

He holds a M.S. from the University of California, Berkeley.

TABLE 1
Test Schedule

Test Number	Crib Size*	Approximate Peak Heat Release Rate (kW)	Type Raceway
1	50 kg	500	none
2	50 kg	500	ENMT
3	25 kg	250	ENMT
4	25 kg	250	RNMC
5	25 kg	250	none

* Crib located on room center line.

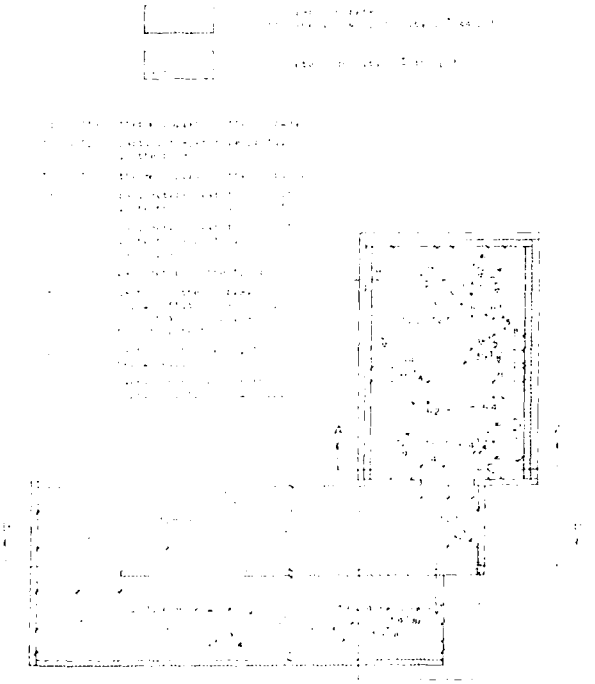

TABLE 2

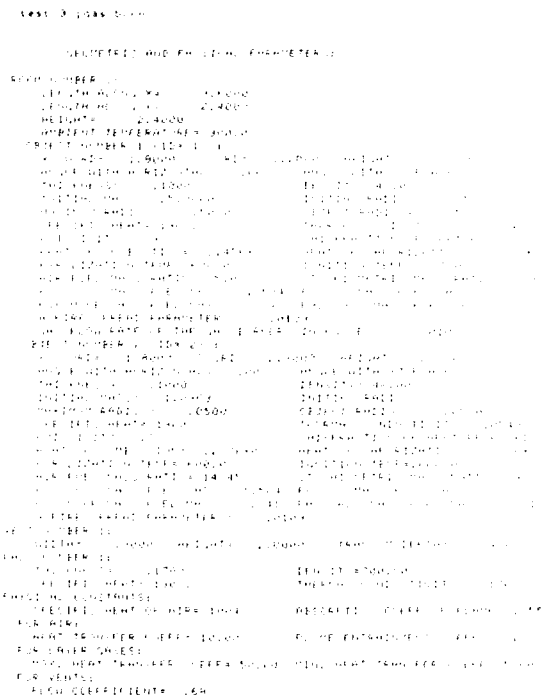

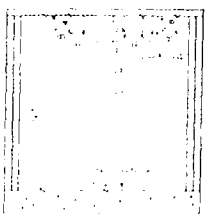

Table 3
Predicted HCl Concentrations

Test	Calculated Values		
	Maximum Rate wt. loss, g/s	Mass flow g/s	HCl ppm
2	3.7*	780	3380
3	1.25	640	1440
4	0.85	680	977

* Calculated at time of ignition.

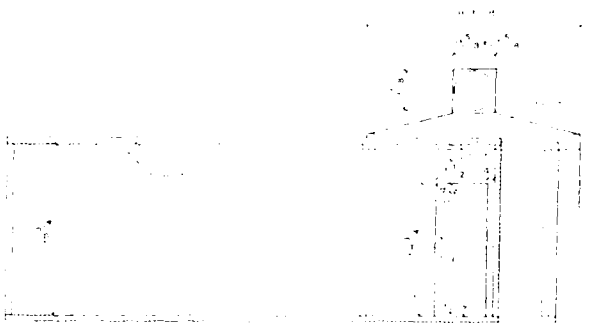

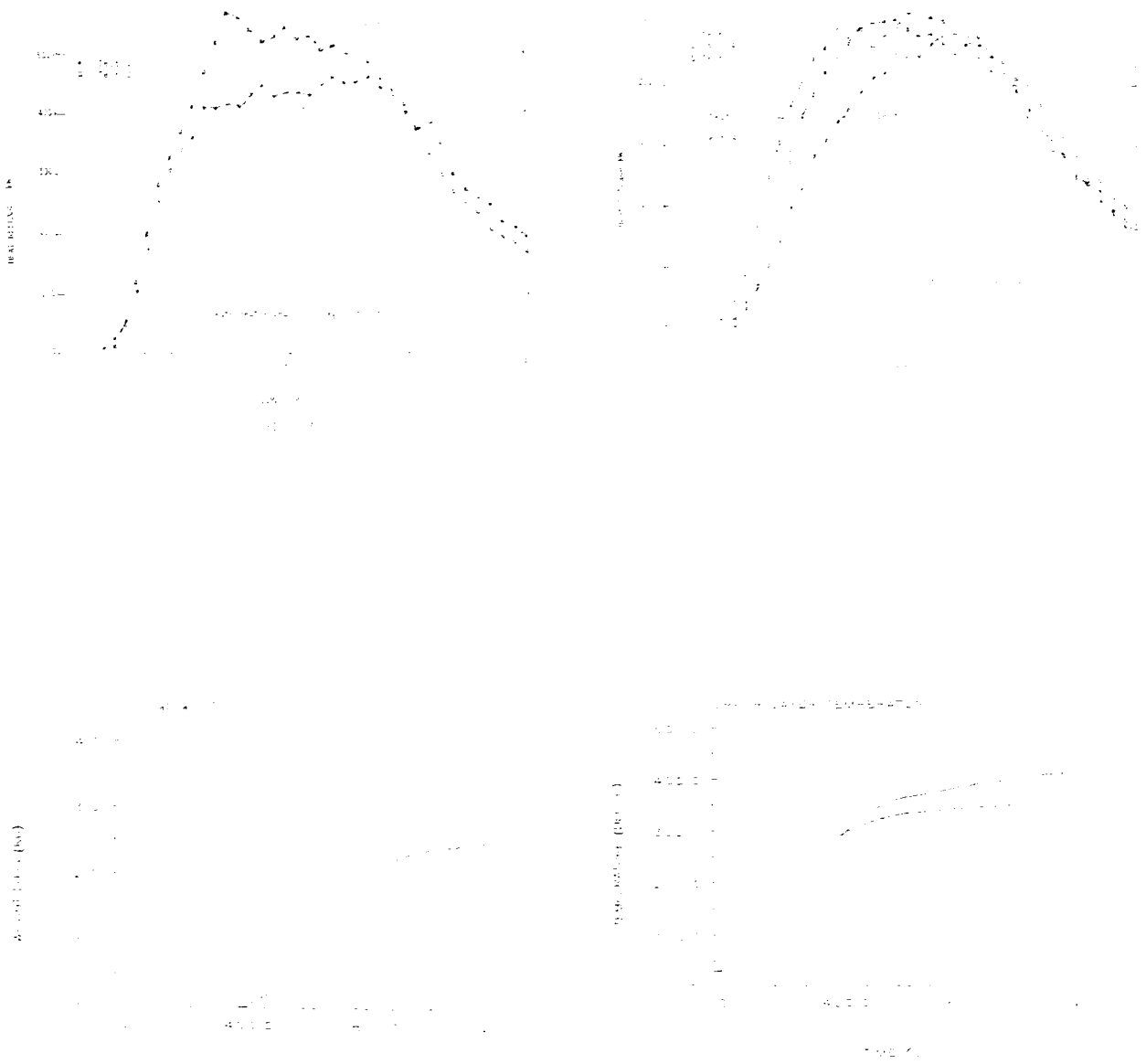

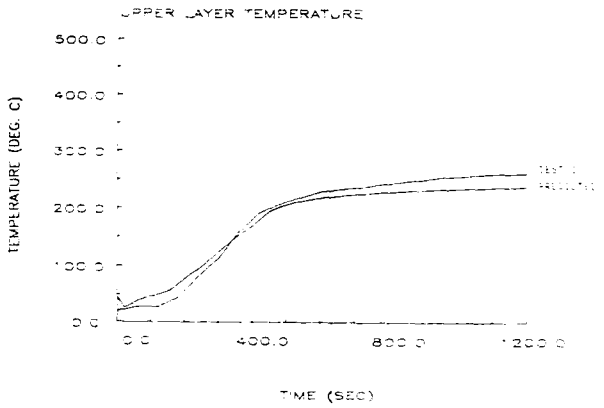

FIGURE 7

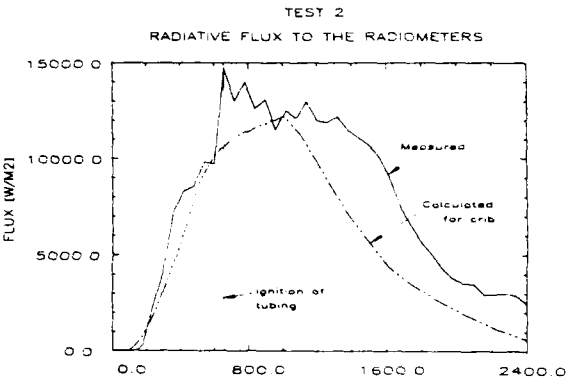

FIGURE 8

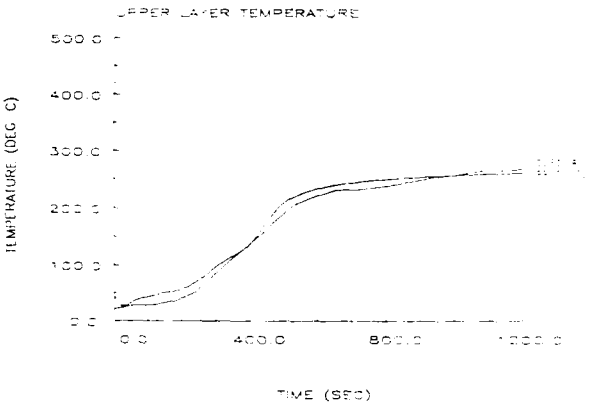

FIGURE 8

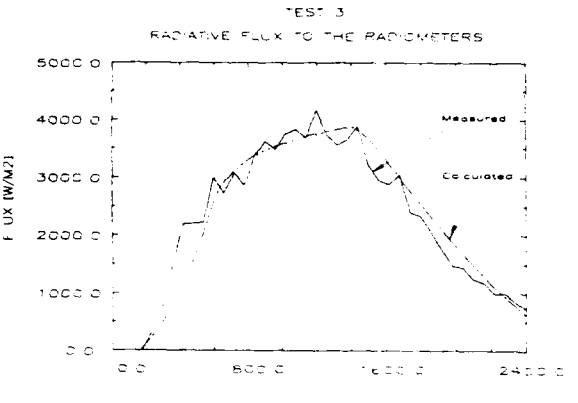

FIGURE 9

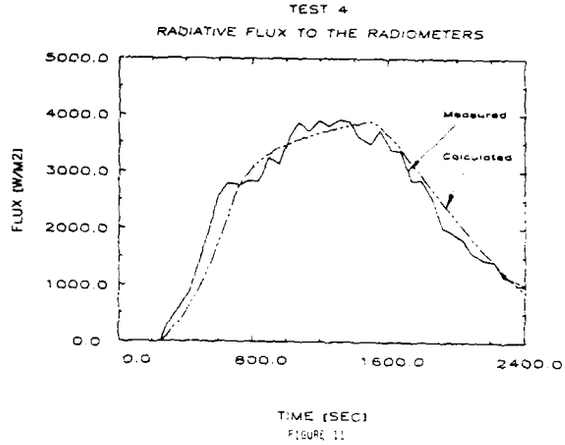

FIGURE 11

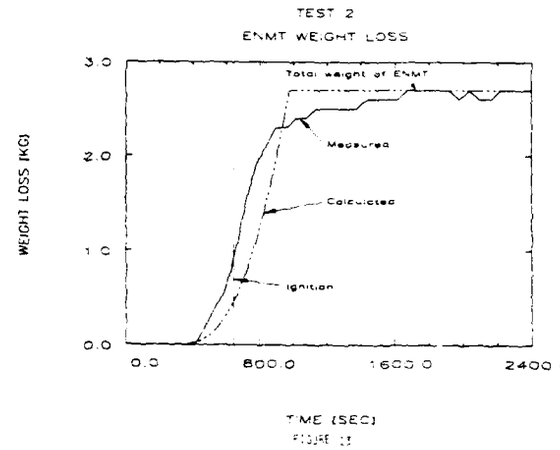

FIGURE 12

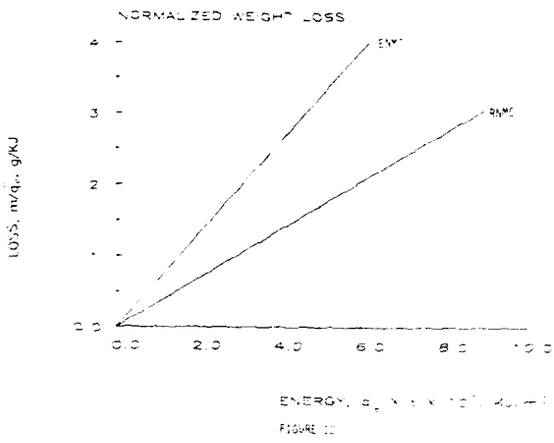

FIGURE 13

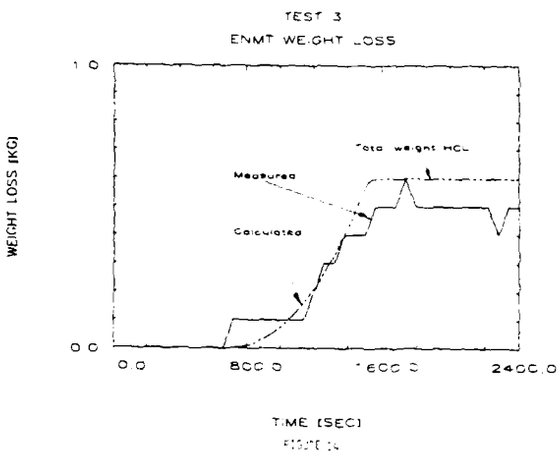

FIGURE 14

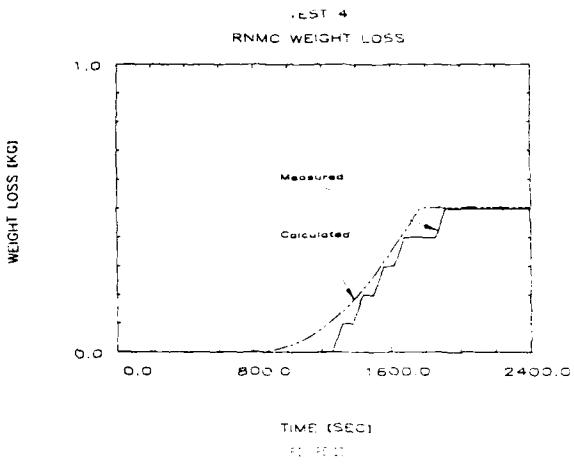
TEST 4
RNMC WEIGHT LOSS
WEIGHT LOSS (KG)
1.0
0.0
Measured
Calculated
0.0
800.0
1600.0
2400.0
TIME (SEC)

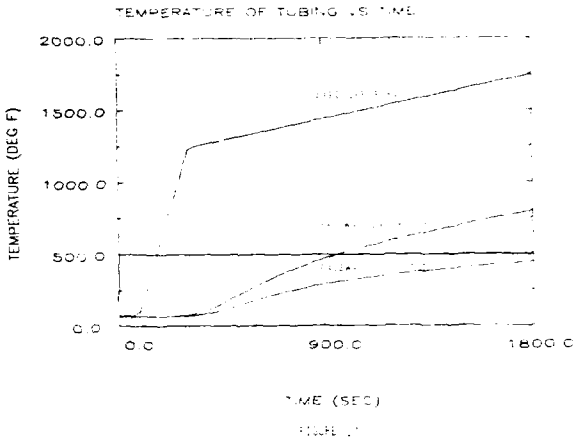
TEMPERATURE OF TUBING VS TIME
TEMPERATURE (DEG F)
2000.0
1500.0
1000.0
500.0
0.0
0.0
900.0
1800.0
TIME (SEC)

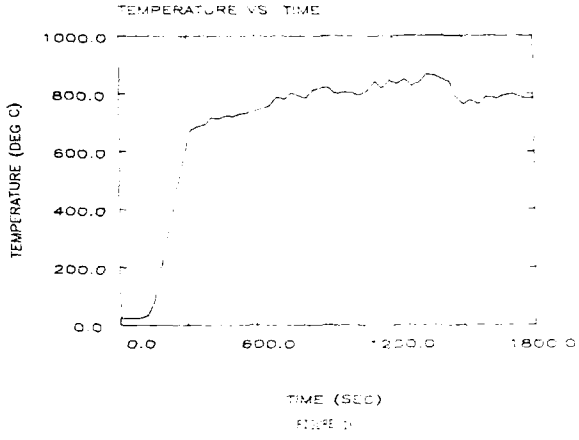
TEMPERATURE VS TIME
TEMPERATURE (DEG C)
1000.0
800.0
600.0
400.0
200.0
0.0
0.0
600.0
1200.0
1800.0
TIME (SEC)

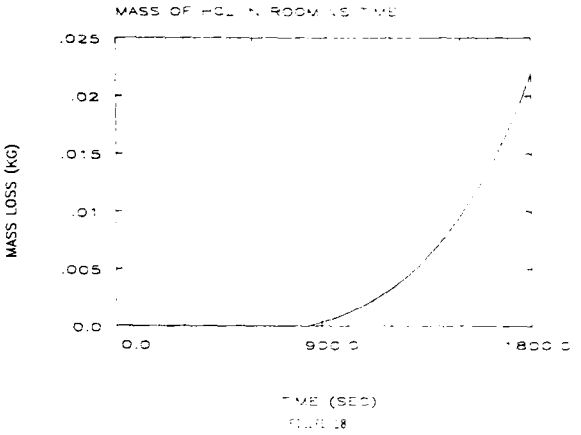
MASS LOSS (KG)
.025
.02
.015
.01
.005
0.0
0.0
900.0
1800.0
TIME (SEC)

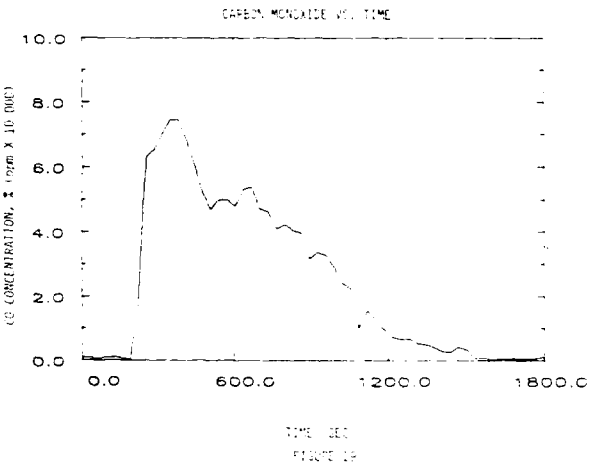
10.0
8.0
6.0
4.0
2.0
0.0
0.0
600.0
1200.0
1800.0

WIRE AND CABLE FIRE PERFORMANCE AS DETERMINED BY A CONE CALORIMETER

Almut F. Breazeale

E.I. du Pont de Nemours & Co., Inc.

ABSTRACT

The cone calorimeter, developed at the National Bureau of Standards (NBS),[1,2] is a major technological advance for use in fire hazard and risk assessment studies. This instrument, which determines fundamental fire properties of materials and products, provides critical information for assessing fire hazard and for developing new products with improved fire performance.

This paper describes the cone calorimeter, discusses the types of data that it generates and presents actual test data.

INTRODUCTION

In a closed environment fire, the heat release rate of burning combustibles provides the most significant information for predicting both the course of the fire and its effect.

To accurately measure the heat release rate of a burning sample, a calorimeter was developed at NBS. This instrument is called a cone calorimeter because the source of its constant heat flux is an electric coil shaped like a truncated hollow cone (Figure 1). The cone calorimeter also measures other performance properties of burning materials, such as heat of gasification, specific extinction area of the smoke and sample mass loss rate. For the past year, Du Pont has tested materials with a commercial version of this instrument[3] in order to develop materials with better fire performance.

CONE CALORIMETER

Principles of Operation

To measure the heat release rate of a burning sample exposed to a constant heat flux, the cone calorimeter uses the oxygen consumption principle, which states that the amount of heat released during combustion is proportional to the amount of oxygen consumed during combustion.

Figure 1.
THE CONE CALORIMETER SET UP TO TEST A SAMPLE IN A HORIZONTAL POSITION.

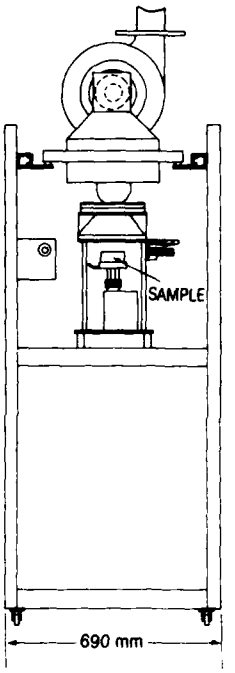

Table I[4] shows both the heat of combustion and the heat of combustion per gram of oxygen consumed for several polymers that are widely used by wire and cable manufacturers. It has been observed that the heat of combustion per unit of oxygen consumed is approximately the same for most materials (13.1 kJ/g of oxygen consumed).[4] Materials, such as polytetrafluoroethylene, that have heats of combustion per gram of oxygen consumed that are significantly different from the default value (13.1

Table I.
HEAT OF COMBUSTION
AND HEAT OF COMBUSTION
PER GRAM OF OXYGEN CONSUMED[4]

POLYMER	HEAT OF COMBUSTION, kJ/g	HEAT OF COMBUSTION/g OF O_2 CONSUMED, kJ/g O_2
Polyethylene	-43.3	-12.6
Polystyrene	-39.8	-13.0
Polyvinylchloride	-16.4	-12.8
Polyvinylidene fluoride	-13.3	-13.3
Polyacrylonitrile	-30.8	-13.6
Polyethylene terephthalate	-22.0	-13.2
Nylon 6.6	-29.6	-12.7
Polytetrafluoroethylene	-5.2	-15.6

kJ/g of oxygen consumed), can be tested accurately in the cone calorimeter by changing the default value to the appropriate value.

The data reduction software associated with the cone calorimeter, also developed at NBS,[1] calculates the heat release rate of a burning sample by automatically collecting, storing and then using the following data:

1. The amount of oxygen present in the combustion gases as a function of time;

2. The sample mass loss due to burning as a function of time; and

3. The sample area, measured in advance by the operator. It is assumed that this area does not change during testing. (The maximum sample area is 0.01 m^2.)

The amount of oxygen in the combustion gases emitted from a burning sample is measured as a function of time by a paramagnetic oxygen analyzer. This analyzer was chosen because it is well suited for measuring the range of oxygen concentrations, approximately 18 to 21 percent,[1] found in the combustion gases. Measurements are made every five seconds throughout the test.

To measure the sample mass loss due to burning as a function of time, the sample is placed on a load cell and weight measurements are recorded every five seconds. The sample holder, clamps and other non-sample items are tared prior to the test.

Basic Operation

To test a material in the cone calorimeter, an operator first sets the flux level to the desired level and then verifies the setting with a total heat flux gauge, such as a 12.5-mm-diameter Gardon gauge. Next, the sample area is measured and the sample is placed in the sample holder. The operator then places the sample holder on the load cell. The sample's surface is positioned 25 mm from the cone's open side to ensure a homogeneous flux field. The sample can be positioned either horizontally or vertically; however, the cone heater is always positioned so that the heater's open side faces the sample surface (Figures 1 and 2).

Figure 2.
THE CONE CALORIMETER SET UP TO TEST A SAMPLE IN A VERTICAL POSITION.

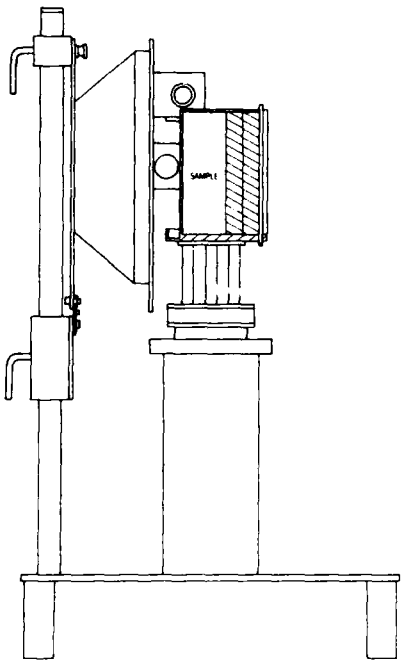

A furnace-type spark plug is immediately positioned above the sample and the time required for the gases and vapors released from the sample to ignite is measured. Beginning at the time of ignition, as a function of time, sample mass data is recorded and oxygen consumption is analyzed, as previously described. After the testing is completed, the data reduction software calculates the heat release rate and other fire properties that can be derived from the recorded data.

SAMPLES TESTED

Various samples have been tested in the cone calorimeter at Du Pont, including:

- Films of thermoplastic and thermoset materials;
- Slabs of thermoplastic and thermoset materials;
- Wires and cables; and
- Intumescent slabs and cables.

Films of Thermoplastic and Thermoset Materials

It is difficult to obtain data with thin (<0.064 cm) films or slabs of thermoplastic and thermoset materials because the combustion time is usually very short. One solution to this problem is to cut slits in the samples with an X-ACTO knife, stack the samples and tie them together with very fine wire.

The stacked arrangement increases the mass that is burned and the slits, which allow air to escape, eliminate warpage. Generally, such sample stacks burn in an orderly manner (from the top surface down), particularly if the edges of the stacks are covered with aluminum foil.

Slabs of Thermoplastic and Thermoset Materials

Slabs of thermoplastic and thermoset materials that are at least 0.32-cm thick generally have long enough combustion times to provide sufficient data for analysis. With these samples, it is also helpful to cut slits and to cover the bottom and sides with aluminum foil.

Wires and Cables

Wires and cables are generally cut into 10-cm-long pieces and placed side by side in the sample holder; remaining space in the sample holder, if any, is filled with a medium-density refractory material.

Some cables contain air voids or materials that readily liquify and flow out the ends of the cable when exposed to the high temperatures encountered during testing. This often results in the cables burning on the inside. Although this probably would not occur in a real fire situation, it can be avoided during testing by sealing the cable ends with an unfired ceramic cement in paste form.[5]

"Sauereisen" No. 1 Paste[6] is applied with a spatula and can be cured by air drying for several days at ambient temperature. The maximum service temperature of this material is 980°C, which is higher than the temperature of most burning samples in the cone calorimeter.

When using "Sauereisen" No. 1 Paste to seal cable ends, it is often helpful to cut slits into the cable jacket to allow trapped air or volatiles to escape. This prevents the cable jacket from rupturing during testing. Sealing the cable ends is not always necessary because many wires and cables burn in a controlled manner, beginning with the jacket (see Figure 7).

As previously discussed, the surface area of a burning sample is an essential factor for calculating the fire properties. Because wires and cables are generally round, the actual surface area exposed to the incident flux of several cables placed side by side in the sample holder is greater than the sum of the areas calculated from the individual lengths and diameters of the cables. However, because the same situation exists in a real fire situation, no adjustment for cable roundness is made (i.e., the surface area of a cable is the area calculated from the cable's length and diameter).

Intumescent Slabs and Cables

One common problem when testing materials, such as polyvinylchloride (PVC), that swell and char when burning is that the material rises into the cone and is exposed to much higher flux levels than those in the area 25 mm below the face of the cone. Since the fire properties of a sample are often dependent on the incident flux (as illustrated in Figure 8), exposure of part of the sample to much higher (and not well known) levels of flux makes the data difficult to interpret. One way to avoid this problem is to place a grid over the sample surface and anchor it to the sample holder with wire. However, it must be remembered that this can interfere with the natural intumescence, thereby altering the burning behavior of the sample. Increasing the distance between the sample surface and the cone is not feasible because the sample surface would no longer be exposed to a homogeneous flux.

EXPERIMENTAL DATA

Types of Data

Many types of data can be generated from the parameters measured by the cone calorimeter. We have found that the following types have the greatest general applicability:

- Critical ignition flux,
- Sample mass and mass loss rate as a function of time,
- Heat release rate during combustion,
- Total heat released,
- Heat of combustion,
- Heat of gasification and
- Specific extinction area of the smoke.

Critical ignition flux, measured in kW/m^2, is the minimum flux required for sample ignition. It can be determined by extrapolating between those values of incident flux where the sample ignites after a long period (>300 seconds) and the flux level at which the sample does not ignite (>800 seconds).

Alternatively, the critical ignition flux can be determined by measuring the time to ignition at several incident flux levels and extrapolating a plot of the "reciprocal *of time to ignition*" *versus* the "incident flux" to the flux level at which the time to ignition is infinite (1/time = 0). (See Figure 3.) Typical values for critical ignition flux for materials used for wire and cable applications range from approximately 1 to 35 kW/m^2.

Graphs of sample mass, measured in g/actual sample area, provide assurance that the sample burned in an orderly manner (i.e., pieces of the sample did not fall off the load cell during combustion). If the exposure time is long, data from these graphs can also be used to determine the amount of combustibles present in the sample.

A graph of sample mass loss rate as a function of time can be used to determine average mass loss rate and can often also provide a more detailed description of the burning behavior of the sample. (See Figure 4.) Typical values for average mass loss rate range from approximately 5 to 20 g/m^2 sec.

Figure 3.
CRITICAL IGNITION FLUX FOR A CABLE WITH FLUOROPOLYMER PRIMARIES AND AN ETHYLENE COPOLYMER JACKET. (See Table III)

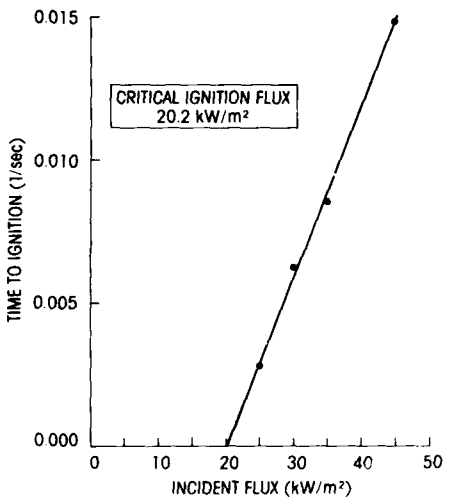

Figure 4.
SAMPLE MASS AND SAMPLE MASS LOSS RATE AT 50 kW/m^2 INCIDENT FLUX VERSUS TIME FOR A POLYVINYLCHLORIDE COMPOSITION AND A FLAME-RETARDANT POLYVINYLCHLORIDE COMPOSITION. (See Table II)

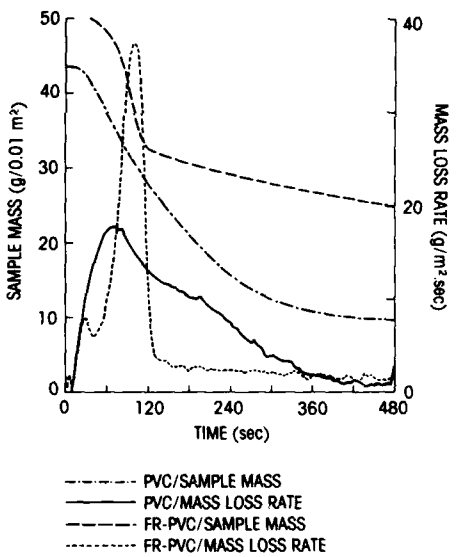

The heat release rate of a sample during combustion (measured in kW/m^2) and the total heat released during the test (measured in MJ/m^2) can be plotted by the data reduction software as a function of time. Heat release rate values can be as high as 1,000 kW/m^2 (see Figure 5), but are generally less than 500 kW/m^2. The total heat released generally ranges from 1 to 100 MJ/m^2. Average values can also be obtained.

Figure 5.
HEAT RELEASE RATE AND TOTAL HEAT RELEASED AT 25 kW/m² INCIDENT FLUX VERSUS TIME FOR A POLYETHYLENE AND A FLAME-RETARDANT, HALOGEN-FREE THERMOPLASTIC. (See Table II)

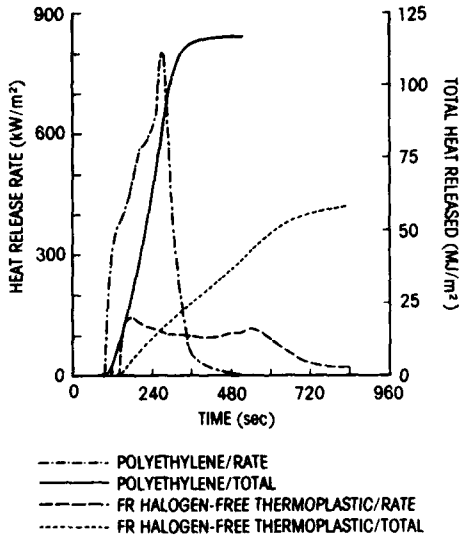

The heat of combustion, measured in MJ/kg, is the amount of heat released during sample combustion. This value may be constant during sample burning or may vary with time. In either case, the data reduction software calculates an average value for the time period. (See Figure 6.) Typical values range from 1 to 40 MJ/kg.

Figure 6.
HEAT OF COMBUSTION AT 50 kW/m² INCIDENT FLUX VERSUS TIME FOR A CABLE WITH POLYOLEFIN PRIMARIES AND A POLYOLEFIN JACKET. (See Table III)

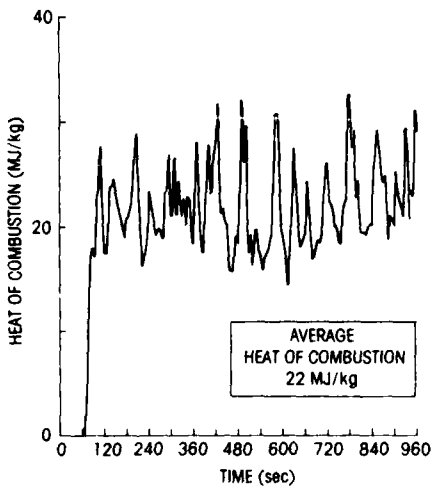

The heat of gasification, measured in MJ/kg, is the amount of heat required to form vapors that can be ignited by a flame source. The vapors result from volatile ingredients and/or the thermal decomposition of the sample. The heat of gasification can be viewed graphically or as an average value. (See Figure 7.) Typical values range from 1 to 10 MJ/kg.

Figure 7.
HEAT OF GASIFICATION AT 40 kW/m² INCIDENT FLUX VERSUS TIME FOR A CABLE WITH SILICONE PRIMARIES AND A PVC JACKET. CABLES WERE TESTED WITH AND WITHOUT THE ENDS SEALED WITH "SAUEREISEN" NO. 1 PASTE.

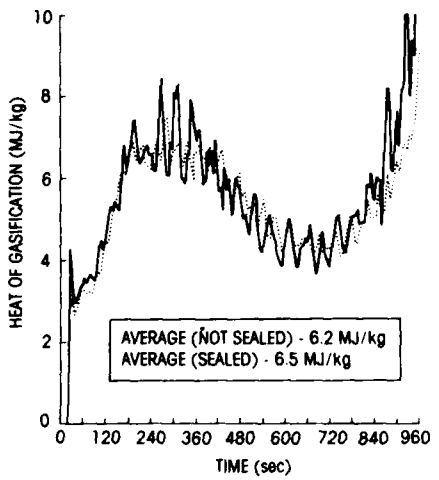

The cone calorimeter is equipped with a helium-neon laser and ancillary equipment that measure the optical properties of the combustion products. A light beam (the laser) passing through the combustion products (smoke stream) is attenuated according to Bouguer's law. The light attenuation is a function of the initial light intensity, the path length and the extinction coefficient. The extinction coefficient is measured by the cone calorimeter and then converted to the specific smoke extinction area, m^2/g. This value relates the smoke produced to the mass of the sample burned. Thus, the specific extinction area, a measure of the density of the smoke generated during sample combustion, can also be presented graphically or as an average value. (See Figure 8.) Typical values range from 0 to 1.3 m^2/g.

Figure 8.
SMOKE SPECIFIC EXTINCTION AREA AT 50 kW/m² and 25 kW/m² INCIDENT FLUX VERSUS TIME FOR SLABS OF FLAME-RETARDANT POLYOLEFIN COMPOUND 1. (See Table II)

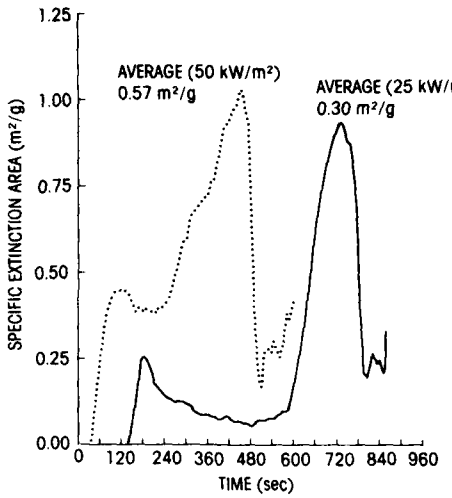

Typical Data

Cone calorimeter data for six types of cable jacketing materials are listed in Table II. This information, obtained from 0.32-cm-thick slabs at 50 kW/m^2 incident flux, makes it possible to determine and illustrate the trade-offs that occasionally must be made to produce materials with the required fire performance properties. For example:

- Compared to polyethylene, PVC is more difficult to ignite (higher critical ignition flux) and produces less heat while burning (lower heat of combustion). However, PVC produces denser smoke than polyethylene, as shown by its greater specific extinction area.

- Compared to PVC, a flame-retardant grade of PVC produces less dense smoke and requires a greater energy input to produce volatiles (higher heat of gasification). These materials are equivalent in ignitability.

- Compared to a flame-retardant grade of PVC, the flame-retardant polyolefin compounds #1 and #2 are more difficult to ignite and produce smoke of approximately the same density. However, these compounds produce more heat during combustion.

- Compared to the flame-retardant polyolefin compounds #1 and #2, the flame-retardant polyolefin compound #3 is much more difficult to ignite; produces a much less dense smoke; and generates less heat during combustion.

Table II.
FIRE PROPERTIES OF SIX JACKETING COMPOUNDS TESTED IN THE CONE CALORIMETER*

		COMPOUNDS**					
PROPERTY	UNIT	A	B	C	D	E	F
Critical Ignition Flux	kW/m²	<1.0	1.0	1.0	4.4	12.5	17.5
Ignition Time at 50 kW/m²	sec	35	23	27	46	46	59
Heat of Gasification	MJ/kg	5.8	6.9	9.1	10.0	10.0	10.0
Heat of Combustion	MJ/kg	42	12	13	28	30	20
Specific Extinction Area	m²/g	0.45	1.0	0.69	0.57	0.81	0.25
Mass Loss Rate	g/m² sec	8.3	7.2	5.5	4.8	5.1	5.1

*Data were obtained from 10-cm x 10-cm x 0.3-cm slabs at 50 kW/m² incident flux. A grid was used for the two intumescent PVC-based compounds.
**Compound A = Polyethylene. B = Polyvinylchloride. C = Flame-retardant Polyvinylchloride. D = Flame-retardant Polyolefin Compound 1. E = Flame-retardant Polyolefin Compound 2. F = Flame-retardant Polyolefin Compound 3.

Table III lists cone calorimeter data for three functionally equivalent cable samples. These cables were tested at 50 kW/m^2. The ends of the cables were not capped because preliminary experiments showed that the properties measured by the cone calorimeter were not affected by the presence of the cap for these cables (see Figure 7).

Table III.
FIRE PROPERTIES OF THREE CABLES TESTED IN THE CONE CALORIMETER*

		CABLES**		
PROPERTY	UNIT	A	B	C
Critical Ignition Flux	kW/m²	12	13	21
Time to Ignition at 50 kW/m²	sec	13	47	31
Heat of Gasification	MJ/kg	7.1	9.5	10.0
Heat of Combustion	MJ/kg	18	22	20
Specific Extinction Area	m²/g	0.73	0.23	0.34
Mass Loss Rate	g/m² sec	6.9	7.9	4.9

*Data were obtained at 50 kW/m² incident flux. Cable ends were not capped.
**Cable A = Polyvinylchloride Jacket and Silicone Primaries. B = Polyolefin Jacket and Primaries. C = Ethylene Copolymer Jacket and Fluoropolymer Primaries.

The data listed in Table III show that although cable B (polyolefin primaries and jacket) is equivalent in ignitability to cable A (silicone primaries and a PVC jacket), it produces a less dense smoke and requires somewhat more energy to form ignitable vapors.

Cable C (fluoropolymer primaries and an ethylene copolymer jacket) is considerably more difficult to ignite than cable A or cable B and produces the same lower density smoke as cable B. The heat released during combustion is judged to be equivalent for the three cables.

CONCLUSION

The cone calorimeter can provide data to aid in determining the fire hazard associated with wire and cable materials. The wide range of data that it generates, limited only by the imagination of the operator and the skill of the software writer, is also extremely useful for developing new wire and cable products to meet end-user requirements for improved fire performance.

Although this instrument is relatively new, its value to the wire and cable industry is already quite evident. The cone calorimeter truly represents a major technological advance for use in fire hazard and risk assessment studies.

References

1. U.S. Department of Commerce, National Bureau of Standards. Development of the Cone Calorimeter -- A Bench-Scale Heat Release Rate Apparatus Based on Oxygen Consumption. Babrauskas, V. NBSIR 82-2611. 1982 November. 75 p.

2. Babrauskas, V.; Mulholland, G. Smoke and Soot Data Determinations in the Cone Calorimeter. Proceedings of SPE Vinyl Division RETEC. 1987 September 16-17.

3. Custom Scientific Instruments, Inc., a Division of Atlas Electric Devices Co., 13 Wing Drive, Cedar Knolls, N.J. 07927 USA

4. Huggett, C. Fire and Materials 4(2):62;1980.

5. Turner, V.L. Du Pont Company, private communication.

6. Sauereisen Cements Company, Pittsburgh, Pa. 15238 USA

Almut Breazeale, Research Associate in Du Pont's Wire and Cable Group, Polymer Products Department, joined Du Pont in 1965 after earning a Ph.D. in organic chemistry from the University of Washington. Since that time, she has been involved in research and development work in the areas of fluoropolymers and thermoplastic and thermoset hydrocarbon polymers for various industrial applications.

THE NIBS SMOTOX WG PROGRAM

H. J. ROUX

ARMSTRONG WORLD INDUSTRIES, INC.
LANCASTER, PA 17604
NOVEMBER 17, 1988

The work of the combustion toxicity working group of the National Institute of Building Sciences, known as the NIBS SMOTOX WG, is on-going. Appropriately though, and because of recent advances in the test equipment, this work is at a critical stage, dictating the following status report.

The purpose of the NIBS SMOTOX WG is to develop a small scale performance test for potential toxic hazard. It is not the purpose of the NIBS SMOTOX WG to develop another smoke or combustion toxicity test, of which there are several, but which typically only measure toxic potency. The two best known tests of this type are the NBS Cup Furnace and the UPITT (University of Pittsburgh) combustion toxicity tests.

A toxic potency test is well suited to measure the "quality" (actually, the "lack of quality") of the smoke, once the smoke is produced by the burning product. It does not, however, measure the "quantity" of smoke produced by the burning product, the other critical ingredient in any test of potential toxic hazard.

The proposed performance test for potential toxic hazard intends to measure both the "quality" and the "quantity of smoke, simultaneously. In measuring "quantity", the test intends to consider both ease of ignition (commonly measured as time to ignition) and rate of burning, as the most important responses of a product to a fire.

A practical derivation of the above principle, in the form of a test method, is to expose the product to a given fire, allowing the product to respond to the fire in terms of ease of ignition and rate of burning, and exposing thereto, i.e., to the smoke produced, an appropriate animal specie. In this work, rats are used as a surrogate for man. The time at which the rats succumb (death, for instance) is then a measure of the potential toxic hazard of the product.

The use of time to measure potential toxic hazard is most appropriate because nearly all events relative to fire safety are time dependent. For example, there is the time of fire ignition and growth, the time to detection and subsequent alarm, the time for travel and evacuation, the time for response of the fire department, etc. There is also the time that man needs to be exposed to a given concentration of gas (or combination, or mixture of gases) to be affected in terms of incapacitation or death.

Such a scheme for a potential toxic hazard test has been developed by the WG, which takes into account time to ignition, rate of burning, and toxic potency (as represented by the concentration x time product) simultaneously.

PROPOSED TEST METHOD

Incorporated in the above derivation of the principle of potential toxic hazard is the idea that this measure of potential toxic hazard, time of death, is solely a time during the exposure of the animals to the fire. For some authorities, this is sufficient; in that it is thought that the escape of man from a toxic hazard situation is success, with any continuing or delayed health effects to man medically treatable. However, there are other authorities (which to date have prevailed in the WG) who feel that the continuing or delayed health effects to the animals must be included in the measure of potential toxic hazard. It is generally believed that these effects will be complete within 14 days after the test exposure. Consequently, a different derivation of the principle of potential toxic hazard is proposed by the NIBS SMOTOX WG.

The actual derivation of the principle of potential toxic hazard, accepted by the NIBS SMOTOX WG, is the following form of a test method. Again, the product is exposed to a given fire, but, in this derivation, for a time that is just sufficient to cause deaths of the animals during the length of the test plus 14 days post exposure. It is this fire exposure, expressed in terms of the time of fire exposure, that acts as the measure of potential toxic hazard. Obviously, there is a given for this fire exposure, which is the severity of the fire.

FIRE EXPOSURE

One of the key parameters in this test method is the fire to which the product is exposed. It is the intent of the proposed test method to place the product in a given fire, a steady fire, and to let the product respond to that fire. It is not the intent of the proposed test method to simply ignite the

product and allow it to independently burn, alone, for this is less challenging of the product and certainly not representative of a real fire exposure. The immediate question, therefore, is -- what fire?

A study of applicable fire statistics for the USA clearly indicates that the principal cause of death due to smoke inhalation alone is of a fire that has left the room of origin (equated by the WG to flashover of origin) and where the victims are located remote from the room of (fire) origin. Logic does side with these findings, in that flashover is expected to create both the volume of toxic gases and the heat pump in the room of origin to drive these gases to a remote location. A meaningful fire, therefore, that is directly applicable to the proposed test method is flashover. A consequent, apt description of flashover is a radiant flux level of 5 w/cm^2 with piloted ignition.

Herein, though, laid the cause for extensive discussion by the WG, i.e., an appropriate radiant flux level for flashover. (Piloted ignition is not a question.) Data submitted to the WG, for the definition of flashover, included radiant flux levels as low as 2 w/cm^2 and as high as 10 w/cm^2. However, practical considerations to come into play; these include a) the lack of capability of the test equipment to obtain and sustain very high radiant flux levels, b) the lack of discrimination between products that could occur at higher radiant flux levels (known to the author as the "crowd effect"), c) a suspicion that a high radiant flux level is not of importance once the product starts to burn, and most products will burn freely, with flaming, at lower radiant flux levels, and d) some evidence (from heat release research results) that the greatest effect of burning may be at moderate radiant flux levels. For the moment, the work of the WG will progress with a radiant flux level of 5 w/cm^2.

Conceivably, an equally meaningful fire is one, again with piloted ignition, that duplicates open burning (flaming). This is thought to be the fire of consequence for building contents, for it is felt (more by conception than by actual data) that it is when flaming occurs at the end of smoldering that the greatest potential toxic hazard is created by this class of products. Yet, certainly, the fire exposure in the proposed test method could be a smoldering fire, without piloted ignition, if needed for building contents.

MEASURE

In that time of fire exposure is the measure of potential toxic hazard by this proposed test method, it is suggested that this measure be reported as IT_{50}. It is "irradiation time", a sufficiently sterile term to preclude an erroneous understanding of the term for it is not equated to any given time in a real fire, but illuminating enough for it is an identification of the driving force of the fire exposure, i.e., radiant flux. The subscript 50 is derived from the legendry of toxicology, for the response of animals in a toxicity test is normally measured in terms of 50% of the animals. The IT_{50} is therefore the irradiation time (time of a given fire exposure) that is required to kill 50% of the animals during the test exposure (30 minutes) plus post exposure (14 days).

It is a principle of this proposed test method that the longer a product has to be in a fire before it creates a toxic hazard, the safer it is; because it provides more time for alarm and response, either extinguishment and/or evaluation, to the originating fire. (The originating fire is considered to be of other than the test product.) In some cases, this time may be more than sufficient to prevent a toxic hazard from originating in the first place from the product. In other cases, the product will now be part of the "crowd effort", i.e., all of the toxic hazards from all of the products in the fire. The toxic hazard in either case is still the same biological response, 50% animal deaths.

TEST EQUIPMENT

The new equipment for this proposed test method is now at Southwest Research Institute, assembled and tested. This is a most recent development. The equipment, so far, exceeds all expectations. The new equipment is actually a new combustion chamber, and the necessary chimney connection to the animal exposure chamber.

The combustion chamber is a horizontal Pyrex cylinder, of approximately 5" diameter and 13" length. There are removable Pyrex plugs at each end for ease of cleaning and of insertion of the specimen. Up to 4"x7" specimens are possible. The specimen can be continuously weighed by means of an external load cell.

There are two external radiant heaters (dual tubular lamp type), angled in order to obtain a uniform radiant flux level on the upper surface of the specimen.

The chimney connection between the combustion chamber and the animal exposure chamber is 11-3/4"x1-1/4"x12-1/2". It is divided into three channels or stacks; the two outer stacks of about 3" width through which "cool" air from the animal exposure chamber flows to the combustion chamber, and one center stack of about 6" width through which "hot" air (i.e., the products of combustion) from the combustion chamber flows to the animal exposure chamber; all in a very smooth fashion.

The animal exposure chamber is still the standard NBS chamber, of 2001 size (12,204 cu. in.). It does accommodate six animals (rats), head only exposure.

A shutter is located between the top of the chimney and the animal exposure chamber. It acts to obtain the time of fire exposure.

SUMMARY

There are many labels that can be affixed to this proposed small scale performance test for potential toxic hazard. It can be considered a comparison test of products under the same fire conditions. It does acknowledge those factors that create a toxic hazard in a real fire, i.e., thermal stability of a product and the toxic potency of the gases produced by the burning product. The proposed test method is expected to produce a scaler value (IT_{50}), which may be used in various ways. It is expected that alternative methods, e.g., predictive N-gas modeling, will be designed to determine IT_{50} without recourse to excessive trial and error testing.

In conclusion then, the essential elements of this proposed test methods are: a) a fire of consequence; a test of product(s); a scaler value for the test results; an expected comparison of test results between different products; a measure of potential toxic hazard, i.e., a measure of both the "quality" and the "quantity" of smoke, simultaneously; and a measure of the fire size, i.e., severity and time of exposure, to cause a given toxicological response (i.e., death of 50% of the animals in the 30 minute test exposure plus 14 days post exposure).

Development of a field-usable, high-strength splicing technique for 1.55 um dispersion shifted fibers.

K. OSAKA T. YANAGI Y. ASANO

Sumitomo Electric Industries, Ltd.
Taya-cho 1, Sakae-ku, Yokohama-city, Kanagawa Pref., JAPAN 244

Summary

Recently fiber optic submarine cables are ardently introduced and laid between islands and continents. For this purpose optical fibers should bear relatively high tensile stress during installation of such submarine cables. Usually one unit length of optical cable is around 50 km, therefore in order to install longer lines, cables should be spliced every 50 km. (For 1.55 um wavelength system, repeater distance is expected to become longer than 100 km.) But conventional high strength splice technique employed some chemicals or gases in order to attain high-strength splice and the splice machines tend to be toxic and difficult to operate.

We developed a new technique by fabricating a 5 um thickness thin film coatings around bare fibers to protect against any mechanical damages during splicing process. Also all processes were improved and arranged into specific machines and tools. Using these improvements, an average splice of 0.05 dB with a mean strength of 51 N have been achieved.

1. INTRODUCTION

Fusion splicing technique for optical fibers are widely accepted and are regarded as one of the most reliable connecting method in regard to lower splice loss and higher stability after reinforcement.

For longer transmission lines---long-haul lines, undersea cables---operating wavelength of 1.55um is projected to be used for the benefit of lower transmission loss. Various kinds of 1.55 um dispersion shifted single mode fibers (1.55 DSF) are proposed. The structure of such a fiber is more complicated compared with the one used at conventional 1.3 um wavelength. Because the core diameter is smaller and easier deformed. More efforts is required to achieve low splice losses.

One of the drawbacks of fusion splicing is the low strength of the spliced part. Usually the strength of an original fiber is around 70 N for primary coated 125 um fiber but decreases to 7 N after splicing. The main cause is assumed to be the contact of bare fiber with surrounding materials such as removing blade, cutting blade and v-shaped groove for alignment.

For factory splicing of single mode fibers, various splicing techniques and the coating restoration techniques have been reported. Krause employed flame fusion splicing using chrolinehydrogen gas and restored the splice point with UV curable material. Thereby he obtained fiber strengths over 4 GPa. Leach used arc fusion and obtained mean splice loss of 0.1 dB and mean splice strength around 1 % strain by minimizing the exposed fiber length and controlling fusion process. Many reseachers pointed out there are at least two essential factors to perform high strength splicing---perfect cleaving and good fiber alignment.

To lower the splice loss and to shorten the operation time, fibers should be fixed stably during fusion process. In normal splicing, bare fibers are set onto V-shaped grooves which damages the fiber surface. To overcome these difficulties we developed thin film coating techniques which have been applied to 1.3 um fibers. An average splice loss of 0.09 dB and a mean tensile strength of 20 N were obtained.

In this paper, an improvement to the above technique and its application to DSF is reported.

2. PROCEDURE

A set of high strength splice apparatuses are listed in Table 1.

2-1. Applicable optical fibers

Most of the silica based fibers in the commercial market are applicable only if their buffer coating materials can be successfully removed and fiber diameter is around 125 um. The structures and dimensions of the test fiber are shown in Table 2.

Table. 1 Apparatuses and Machines.

Process	Name of the tool, machine and equipment
1 JACKET REMOVING	Mechanical stripper with a hot iron
2 CLEANING	Ultrasonic Bath
3 CLEAVING	Cleaver
4 THIN FILM COATING	Coating Machine
5 SPLICING	Arc Fusion Splicer (Direct Core Monitoring)
6 PROOF TEST	Proof Tester
7 REINFORCE	Protection Sleeve Heater

2-2. Procedure of the splice

The procedure is divided into 7 steps. Each process is schematically illustrated in Fig. 1.

(1) Jacket removing: Certain fibers were easily removed its jacket by using heat. The optimum temperature was different and found dependent on to its jacket material. Fig. 2 shows the dependence of the stripping force on temperature. The lowest region was 80-120°C. The gap between the blade of 150-180 um was chosen to prevent damaging onto the fiber.

(2) Cleaning: Primarily stripped fibers typically have some residuals on the surface. Dipping such fibers into acetone with ultrasonic vibration was found effective for cleaning . A well-cleaned fiber is necessary to recoat in the following process.

(3) Cleaving: A new type of cutting tool was developed. A fiber end is set between two clamps, each holding a bare fiber portion and coated one, and given a certain tension. A round blade is positioned between the clamps, moving perpendicular to the fiber axis thereby making scratches onto the fiber surface. During the process the initiating flaw gets deeper and deeper and finally the fiber breaks resulting in a flat endface.

(4) Thin film coating: The bare portion of the fiber is coated one by one with UV curable resin, except for a few mm from the cut end and irradiated under a UV lamp. Thus the fiber is protected with a UV layer during the following processes.

(5) Fusion splicing: Two ends of fibers are set on the V-shaped groove and fixed with a plastic clamp. The fibers are aligned using a CCD camera and microprocessors.[6] ("Direct Core Monitoring System") Finally the fibers are fused together with a core axis offset less than 0.2 um.

(6) Proof test: To prove the strength of the spliced points, every fiber experiences a proof test by pulling for one second. The proof test conditions are listed in Table 3.

(7) Reinforcement: Spliced fibers are reinforced with heat-shrinkable tubes that are conventionally used for protection. This application is mainly intended for splices between two cables, where spliced points are accomodated in closures.

2-3. Required time

Table 4 shows the average results of time required in each process. Totally, it took about 20 minutes to finish one splice.

Table. 3 Proof Test Condition

Duration Time	1 sec
Pulling Speed	10 mm/sec
Tensile Force	2.5% (23 N for 125 um fiber)

Table. 2 Test Fiber

Diameter of the jacket	250 um
Diameter of the cladding	125 um
Diameter of the core	8 um
Cut off wavelength	1.1 um
Material of the jacket	UV Curable Resin

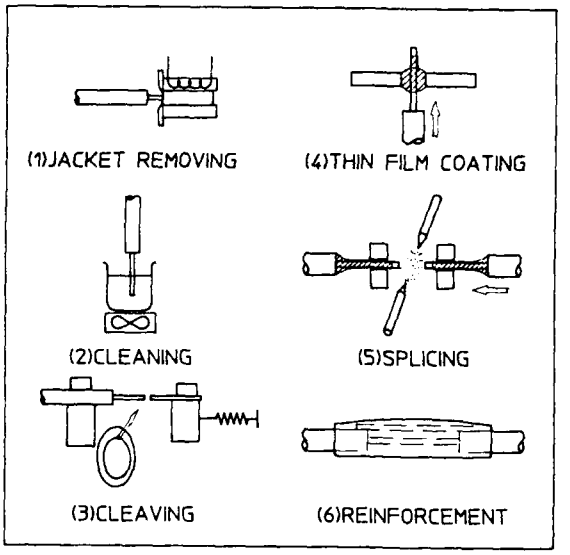

Fig. 1 Spicing Procedure

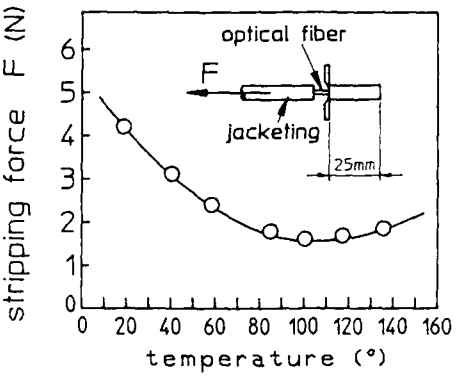

Fig. 2 Stripping force dependency on temperature

Table. 4 Process Time

JACKET REMOVING	1 min	x for both fiber ends
CLEANING	2	
CLEAVING	1	
THIN FILM COATING	3	
FUSION SPLICE	2	
PROOF TEST	3	
REINFORCEMENT	1	
TOTAL	20 min	

3. BASIC TECHNOLOGIES

3-1. Comparison with conventional methods

Fig. 3 shows a comparison between conventional methods and new method. The new method consists of seven processes, some of which are newly developed, others are modified or improved from conventional ones.

Conventional "high strength" splice method(A) started from cleaving and ended with restoration of the jacketed material. Major disadvantages are : -

(a-1) The use of chemicals is inavoidable.--- limits the applicable field.

(a-2) Cleaving characteristics are not good because difficulties arise during cleaving when jacket is not removed.

(a-3) Splice losses are not good because of the instability of fiber holding.

Conventional "normal" splice method(B) is simple and straight forward. Time required is usually less than 10 minutes per splice, but it is impossible to prevent the fibers from weakening.

The new method was developed in regard to being simple, straight forward and accurate. The machines were developed or improved to be small, lightweight so that they could be carried to the field, as well as being more accurate in order to splice 1.55 DSFs.

The asterisks in Fig. 3 indicate the newly developed processes or machices. The key technologies are cleaving and thin-film coating, that made it possible to use conventional splicer with higher strength and equivalent splice loss.[7]

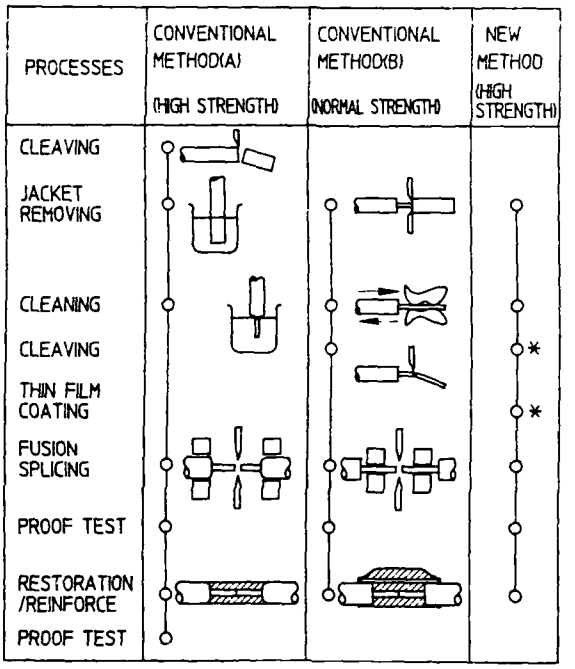

Fig. 3 Comparison of splicing methods

3-2. New cleaving technique

In order to accomplish lower splice losses, the endface of fibers should have a mirror surface and be perpendicular to the fiber axes. Conventionally fibers are scored and pulled or bent to make good results.

Gloge[8] investigated the cleaving principle using such a cleaver that gives a fiber tension, score and bending sequence. He obtained the cleaving conditions using breaking tension in the range of 125 to 175 g, scorer pressure of 1.5 to 7.5 g and 7.5 cm radius breaker. He used a straight diamond tip as a scorer and scored the fiber by touching and pulling. Haibara[9] fixed a fiber with two clamps, scored with a round blade and bent with a round breaker. In this cleaver, no tension is added to the fiber. Instead of controlling the blade pressure, a certain fiber deflection was imposed equivalent to 10 g tension. The optimum bending radius was around 6 cm.

In these two techniques, a bare fiber had to be clamped thereby the fiber was weakened.

Fig. 4 shows the schematic view and an appearance of the developed cleaver. There are two clamps, left one holds the surviving fiber coating, right one holds the bare fiber to be discarded. A round blade moves perpendicular to the fiber axis and is raised stepwise stroke by stroke, thereby the initiating score becomes

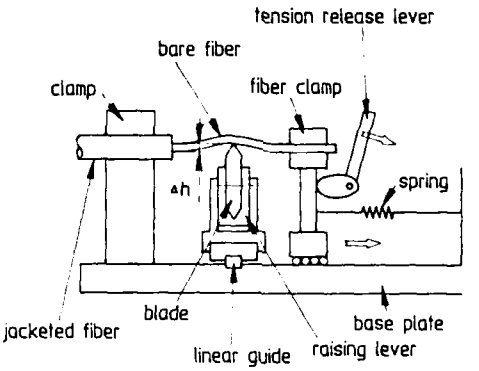

(a) schematic view of the cleaver

(b) appearance

Fig.4 Cleaving tool

larger. A tension is imposed to the fiber using a coil spring. In case of higher tension, the endface tend to become "hackle", in case of lower tension, the fibers would not be cleaved. Fig. 5 shows the relation between the tension and an average cleaved angle. 210 g tension gave the minimum angle. This value is very close to Suzuki's[10] result, where good endfaces were obtained when the fracture stress was around 20 kgf/mm^2 (=240 g). Fig. 6 shows the typical endface observed with an interferometric microscope.

The height of the blade and the fiber at the initial is experimentally changed. The height between the top of the blade and the bottom of the fiber is defined as Δh. When Δh is larger than 50 um the fibers are cut.

Fig. 6 show a histogram of the endface inclination of the fibers using the cleaver and a typical endface. All endfaces were flat, and an average inclination angle was around 0.5°. Fig. 7 shows the relation between the splice loss and the endface inclination. The solid line is the mean value of the data. This result suggests the splice loss of 1.55 DSF are much more dependent on endface angle than 1.3 um fibers.

3-3. Thin film coating technique

Cleaved fiber ends need to be protected from mechanical damages. We utilized UV curable resin chemically compatible to fiber buffer layer and fabricated a thin film around the bare fiber. Fig. 8 show the machine and the principle of coating. A fiber end is inserted into UV resin dip and fed along its axis at a constant speed, thereby a thin layer remain on the fiber surface (Fig. 8 (C)). This process is divided into 3 steps.

(1) Bridging of UV curable resin---precise control of supplied resin is necessary.

(2) Constant coating---Move the fiber into the bridging and feed in the direction of fiber axis at a constant speed.

(3) Irradiation of UV light---A fiber bundle is used to introduce UV light and to illuminate the fiber ends uniformly.

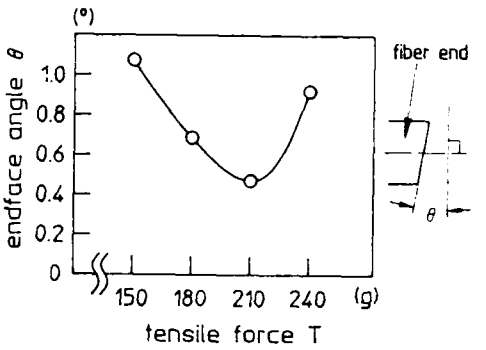

Fig. 5 Relation between tension and endface angle

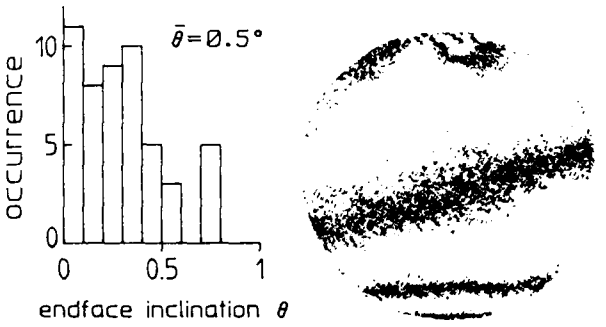

(a) Endface inclination (b) Typical endface λ=0.63μm

Fig. 6 Endface inspection

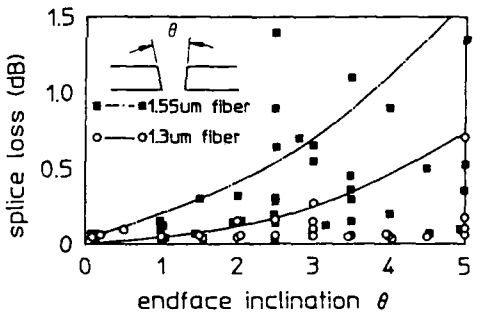

Fig. 7 Splice loss dependency

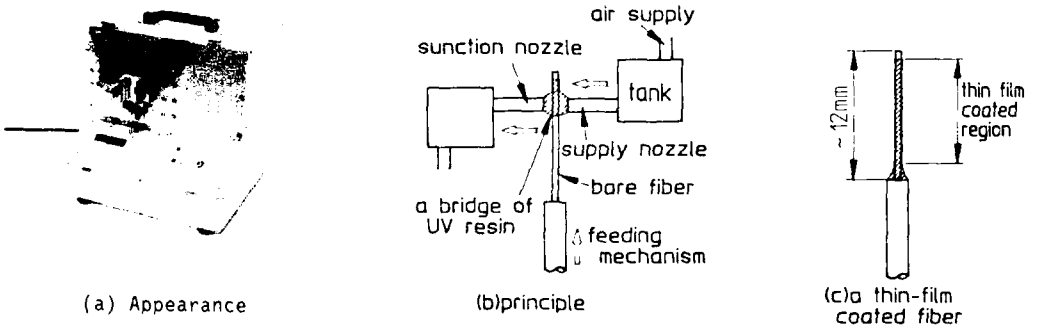

(a) Appearance (b)principle (c)a thin-film coated fiber

Fig. 8 Thin film coating machine

The coating thickness depends mainly on physical characteristics of the resin, and the coating speed. Fig. 9 shows typical relation between temperature and the viscosity. Higher viscosity cause fluctuation of the thickness and lower viscosity leave the fiber uncoated. A uniform layer was obtained by keeping the temperature constant. Fig.10 show a cross section of a coated fiber, coated region and diameter measurement along the fiber. There was a small fluctuation but it did not cause any significant loss increase when clamped.

After many fibers of various coating thickness were obtained, it was found that thicker coating cause eccentricity resulting in unstable holding and thinner coating was easily broken by usual handling. Optimum coating thickness were found around 5 um. Using such fibers, the effectiveness of thin film coating is shown in Fig. 11. The figure shows the stability of transmitted light power, when two coated fiber are butt-jointed together. Solid line indicates light power is stable when fibers are clamped on a V-groove. Dashed line shows a large decrease of light power when a original jacketed fiber is clamped. In the latter case, the light power remained unstable for more than 10 minutes because of the elasticity of the jacket material.

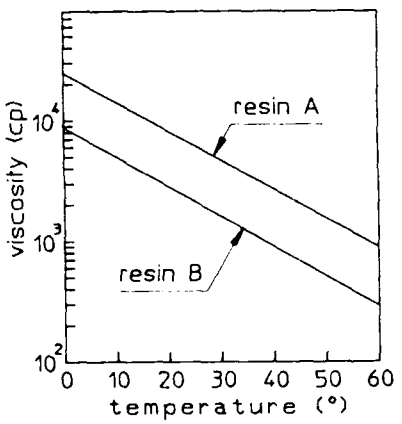

Fig. 9 Viscosity of UV curable resin

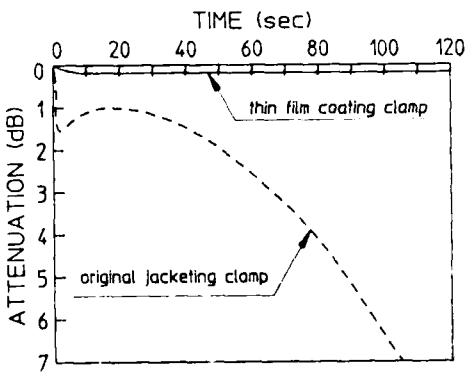

Fig. 11 Transmitted light power change

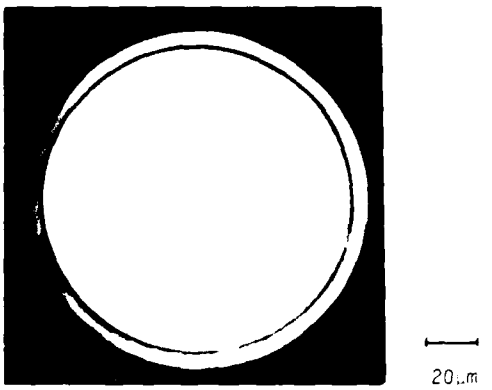

(a) a cross section

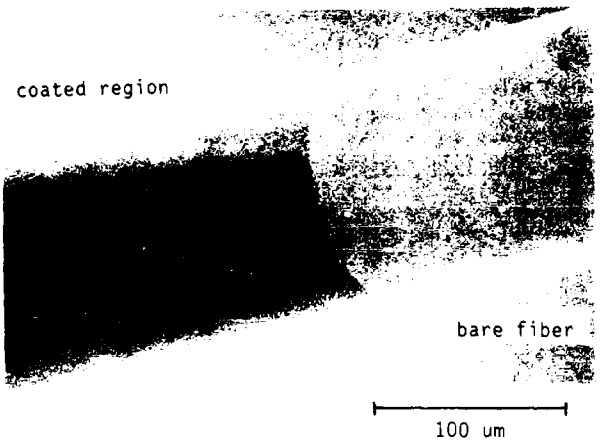

(b) SEM photograph

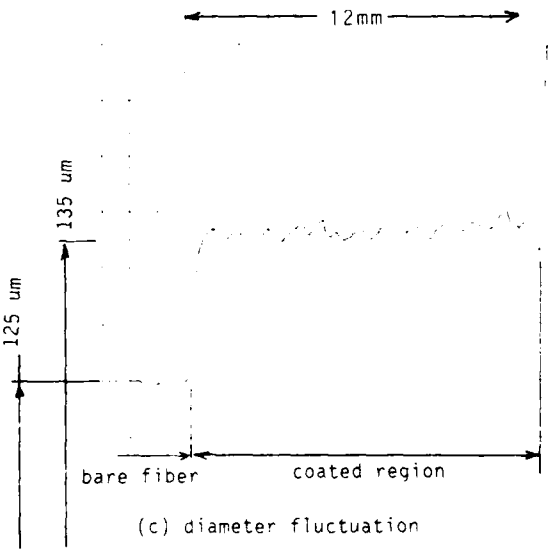

(c) diameter fluctuation

Fig. 10 Appearance of a thin film coated fiber

4. PERFORMANCE

4-1. Splice loss

Fig. 12 to 14 show the comparison of the splice loss. In Fig. 12, histogram of the splice loss of bare fibers is shown. In Fig. 13, the result for jacketed fiber clamp method is shown. In Fig. 14, the result for thin film coated fiber is shown. Thus, it is shown that the first and the last case give us very low and stable splice losses.

4-2. Strength of the splice

Figs. 15 shows the failure strength of a spliced and reinforced fiber. Thin film coated fibers show stable and consistent performance and the yield for 2% screening (18.6 N) is more than 97%.

5. RELIABILITY OF THE SPLICE

5-1. Static fatigue

Table 5 shows the test condition. A spliced fiber was reinforced with a heat-shrinkable tube. The breakability for 5000 hours was zero.

5-2. Dynamic fatigue

Fig. 17 shows the results. The mean tensile strength until failure was not dependent on strain rate.

5-3. Heat cycle

Same fibers are spliced 5 times in series with a distance of 10 meters. This sample fiber was tested under alternating temperature between -40°C to +70°C for 10 cycles. Maximum power change was 0.01 dB per splice point.

5-4. Humidity

Same sample as in 5-3 was left in 95% RH, 60°C for more than 10 hours. The loss change was less than 0.01 dB/splice.

5-5. Heat shock

Same sample was dropped into -70°C alcohol. There was no significant change.(< 0.01 dB/splice)

6. CONCLUSION

6-1. Performance of thin film coating method

The strength and splice loss were investigated by comparing with conventional methods.

The strength is 51 N on the average which is equivalent with jacketed fiber clamping method.

The splice loss is 0.05 dB which is equivalent with bare fiber splice.

The time required is 20 minutes per one splice.

6-2. Reliability of thin-film coated fiber

The long term stability (static fatigue) and dynamic fatigue, heat-cycle test were imposed. All the results showed that the reinforced portion of thin film coated fiber had good reliability.

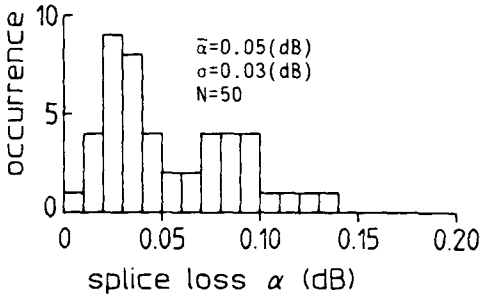

Fig. 12 Splice Loss---normal splice

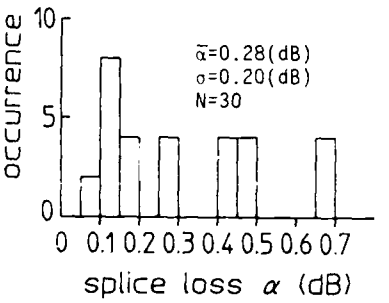

Fig. 13 Splice Loss---original jacketing clamp

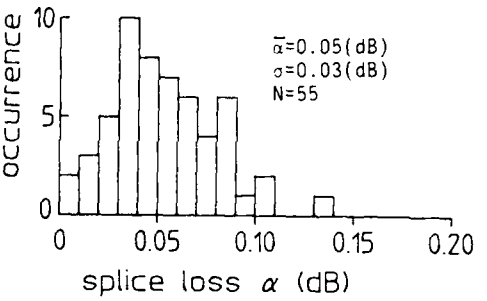

Fig. 14 Splice Loss---thin film coating

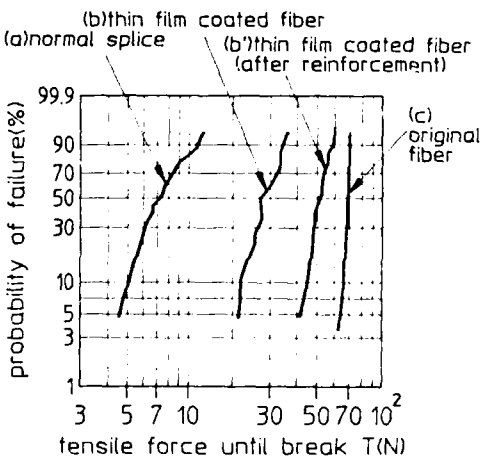

Fig. 15 Tensile strength

Table. 5 Test Conditions for reliabity of the reinforced fiber

	ITEM	CONDITION	RESULT
1	STATIC FATIGUE	0.5/1.0% strain, > 5000 Hours	good (Fig. 16)
2	DYNAMIC FATIGUE	strain rate 5 to 500 mm/min.	good (Fig. 17)
3	HEAT CYCLE	-40 to +70°C, 10 cycles	< 0.01 dB
4	HUMIDITY	95% RH, 60°C, > 10 hours	< 0.01 dB
5	HEAT SHOCK	room temperature to -70°C, 10 times	< 0.01 dB

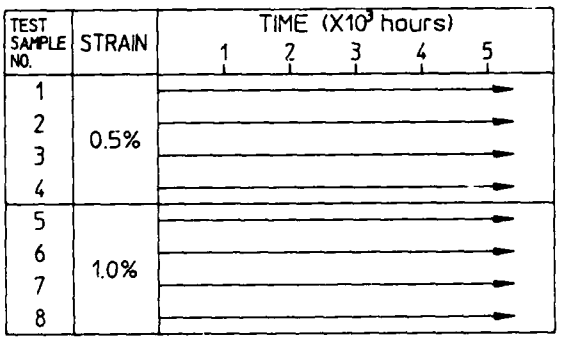

Fig. 16 Static Fatigue

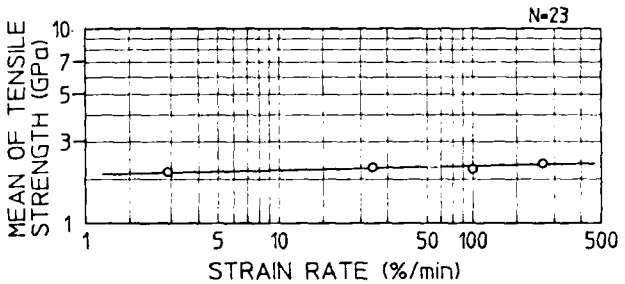

Fig. 17 Dynamic Fatigue

References

(1) Y. Negishi et al., "High-strength fiber splice applied for submarine optical fiber cable," p.263, J. Opt. Commun. 6, '85.

(2) J. T. Krause et al., "Tensile strength > 4 GPa for light guide fusion splices," Elec. Letters. p.812 Vol.17. No.21, '81.

(3) A. C. Hart et al., "Coating Technique for high strength light guide fusion splices," Applied Optics, p.1731, Vol.22, No.11, '83.

(4) T. Yanagi et al., "High Strength Splicing with Fabrication of a Thin Film," OFC '87.

(5) T. Yanagi et al., "Method for splicing optical fibers" USP 4,749,252.

(6) N. Hakamata et al., "Development of a Compact Fusion Splicer with Direct Core Monitoring System SUMIOFCAS TYPE 34," p.37, No.27, Sumitomo Electric Tech. Review, '88.

(7) K. Osaka et al., "A new and reliable cutting tool for high strength splice of optical fibers," OEC '88, to be published.

(8) D. Gloge et al., "Optical fiber and preparation for low-loss splices," B.S.T.J. Vol.52, p.1579, '73.

(9) T. Haibara et al., "Design and development of an automatic cutting tool for optical fibers," J. of LIGHTWAVE TECH. p.1434- Vol.LT4, No.9, '86.

(10) H. Suzuki et al., "A breaking dynamics study on endface forming of optical fibers," (in Japanese) p.4, No.870-13 Proceedings of the lectures, JSME, '87.

Keiji Osaka

Sumitomo Electric
Industries, Ltd.
1, Taya-cho, Sakae-ku
Yokohama, Japan

Keiji Osaka was born in 1955 and received his M.S. degree in precision mechanical engineering from Kyoto University in 1981. He joined Sumitomo Electric Industries the same year and has been engaged in research and development of high NA optical fiber fabrication and fusion splice technology. He is now a staff member of Communications R & D Dept. Yokohama Research Labs. and a member of the Institute of Electronics, Information, and Communication Engineers of Japan.

Toru Yanagi

Sumitomo Electric
Industries, Ltd.
1, Taya-cho, Sakae-ku,
Yokohama, Japan

Toru Yanagi was born in 1939. He joined Sumitomo Electric Industries in 1964 and has been engaged in research and development of fusion splice technology. He is a member of the Institute of Electronics, Information and Communication Engineers of Japan.

Yasuo Asano

Sumitomo Electric
Industries, Ltd.
1, Taya-cho, Sakae-ku,
Yokohama, Japan

Yasuo Asano received his B.S. degree in mechanical engineering from Waseda University in 1968. He joined Sumitomo Electric Industries in 1971 and has been engaged in development of jointing technologies for coaxial cables and fiber optic cables. He is now a chief research associate of Communication R & D Dept. Yokohama Research Laboratories and a member of Japan Society of Mechnical Engineers and the Institute of Electronics, Information and Communication Engineers of Japan.

MECHANICAL OPTICAL FIBER SPLICE CONTAINING AN ARTICULATED CONFORMABLE METALLIC ELEMENT

Richard A. Patterson

3M Company Austin, Texas

A new mechanical optical fiber splice has been developed which is very fast and easy to use and at the same time provides loss performance approaching "tuned" mechanical splices. The new splice derives its performance capabilities and ease of use from a unique conformable articulate metallic element which simultaneously aligns and clamps the optical fibers within the splices. This paper describes the design configuration, operating principles, and function of the new splice. Results of testing on the new splice are also provided.

Background

Optical fibers have been spliced using both fusion systems and mechanical fiber splices. Fusion splicing systems can provide low loss splices but usually require expensive fiber alignment and fusing equipment. Mechanical splices typically require less expensive assembly equipment, but without tuning, cannot provide as low initial loss as fusion splices. Tuning of mechanical splices involves adjusting the relative positions of the fibers in the splice to bring the fiber cores into better alignment. Usually, tuning of mechanical splices increases the splice assembly time, and may also require the use of loss minimization such as local light injection and detection or an additional operator.

The subject of this paper is a new single or multimode mechanical optical fiber splice which is very fast and easy to assemble, and provides insertion loss performance approaching a tuned mechanical splice. Because the new splice does not require tuning, it can be completely assembled in approximately 30 seconds following normal fiber preparation consisting of plastic coating removal and fiber end cleaving. All combinations of 250um and 900um plastic coatings can be accomodated in the new splice. The new splice is assembled using a small, inexpensive plastic holding and actuation fixture.

The new splice has shown excellent stability in long term temperature cycling, water immersion, and vibration tests. It provides low insertion loss without tuning and low back reflection. It can also withstand fiber tensile loads in excess of .75 pound without significant (.03db) change in loss.

Description of New Splice

The new mechanical splice, which is shown in exploded view Figure 1, consists of five (5) major parts. Four of these parts are molded from a highly stable glass-filled plastic material. These molded parts include the "jacket", the "cap", and two identical "end plugs". When assembled, these parts create the

case or housing for the splice. The other part of the splice is the "V" shaped metallic fiber alignment and clamping element. The element is fabricated in a series of high precision metal embossing, blanking and bend operations from a soft corrosion resistant aluminum alloy. The element contains a precision channel located at the base of the "V" section for aligning and clamping the glass optical fibers. Figure 2 is an assembly drawing showing the cap, jacket, element and end plugs in their assembled form.

The major structural member of the new splice housing is the jacket. The jacket is 1.50 inches long, .25 inches high, and .15 inches wide. The top side of the jacket is flat, and the bottom side contains a full radius along its entire length of 1.50 inches. Openings are molded in the top (flat) side, and in both ends of the jacket. The top surface of the jacket also contains fiber size designation circles.

The cavity or opening in the top side of the jacket receives both the metallic "V" shaped element and the cap. This cavity has a groove running along its full length at the bottom for locating the "closed" side of "V" shaped element. The open side of the element faces the open side of the cavity. The alignment and clamping channel in the element is positioned near the bottom of the cavity and parallel to the 1.50 inch dimension. The element cavity also has detents molded into its side walls which engage matching detent ribs in the cap. This produces a detent system that holds the cap in its initial open position and then in its final closed position.

Both ends of the jacket also contain openings which are connected to the central element cavity. These openings each have a semi-circular groove molded along the side face of the opening adjacent the radiused bottom side of the jacket. These grooves form half of the fiber entry and guiding ports in the splice. The other half of these grooves are molded into the side faces of the splice end plugs. When the end plugs are inserted into the end openings of the jacket, two precision stepped circular fiber entry ports are formed. These entry ports are in precise alignment with the fiber alignment and clamping channel within the element when the element is properly positioned in its groove inside the splice jacket.

As can be seen in Figure 2, The fiber entry ports have a small diameter section closest to the "V" shaped element cavity that opens up into a larger diameter section near the ends of the splice. The inner smaller diameter section is approximately .008 inches in diameter by .110 inches long, and accurately guides the bare glass fiber into the alignment and clamping channel within the element. The smaller diameter hole opens up into a larger diameter hole at a tapered transition section. The larger diameter portion of the port is chamferred at its outside end and provides a snug slip fit on the plastic coating of the fiber. The transition betwen the small and large entry port diameters serves as a stop for the plastic coating on the fiber when it is inserted into the splice. The snug fit between the plastic coating on the fiber and the splice housing minimizes the bending stress on the fiber as it exits the splice housing. The larger portion of the port is sized at approximately .011 inches diameter for the 250um fiber or at approximately .037 inches for the 900um fiber.

The new splice can have entry ports to accomodate 250um plastic coatings on both of the ends to be spliced, 250um coating one end and 900um coating the other end, or 900um coating both ends. These combinations have been designated by color coded splice housings. The 250um to 250um splice is all black. The 250um to 900um splice has a black jacket and white cap. The end of the splice for receiving the 250um fiber has a black plug and the end for the 900um fiber has a white plug. The 900um to 900um splice is all white. Additional fiber size identification is provided by the designation circles which are located on the top flat

portion of the jacket near the ends. The 250um port end of the splice is designated by a circle containing a triangle. The 900um port is designated by a full circle.

An additional function of the splice end plugs is to retain the element inside its cavity and prevent it from being lifted out even if the cap is removed. As can be seen in Figures 1 and 2, the element contains notches at both ends. The plugs contain projections which fit into these notches in the element when the element is properly located in its groove inside the jacket, and the plugs are fully seated in their openings. The nooks on the plugs thus hold the element in the proper position inside the jacket.

The cap for the new splice fits into the central cavity in the jacket after the element and end plugs have been installed. The cap consists of a flat top section with two parallel side skirts running under the full length of the top section. Detent ribs are molded into the outside faces of the skirts at both ends. These detents engage matching detent features inside the jacket element cavity when the cap is installed in the jacket. The first detent position holds the top of the cap approximately .050 inches above the top flat portion of the jacket. The cap can be pushed to the second detent position where the top of the cap is flush with the top of the jacket. The cap is held in this position by engagement of an additional set of detent ribs inside the jacket.

Two small notches are provided in each side of the jacket under the flat top portion of the cap. These notches allow the closed cap to be reopened with a special tool by providing access to the underside of the cap so it can be lifted.

The cap has a "U" shaped cross section. The slot which is located between the side skirts of the cap runs full length under the top of the cap. This slot contains a wider section between the side skirts at the open side of the "U" section. This wider portion transitions into a narrower section further up the inside walls of the skirts, and ends in a full radius adjacent the top of the cap. The wider section of the slot is approximately .065 inches wide and the narrower section is approximately .055 inches wide. The transition between the two slot widths are at 30° angles.

When the cap is seated in its "open" detent position inside the jacket, with its top .050 inches above the top of the jacket, the open legs of the element are located in the wider section of the slot inside the cap. When the cap is pushed into the jacket and seated fully, the legs of the element ride up into the narrower section of the cap. This forces the legs of the element together and causes the fiber alignment and clamping functions to occur inside the element on fibers which have been inserted into the splice. Figure 3 shows a cross sectional view of the new splice with the cap in its "open" position and legs of the element in contact with the wide portion of the slot in the cap. Figure 3 also shows the cap in its closed position with the legs of the element pushed together when they are forced up inside the cap as the cap is pushed flush with the top of the jacket.

The new splice is provided to the fiber installer completely assembled with the cap in its open position. The inside of the element is filled with a silicone based index matching gel at the factory. A small amount of the same gel is also injected into both the entry ports of the splice to insure that the fibers are coated with gel when they are inserted into the splice. The new splices are packaged individually in sealed compartments in a vacuum formed packaged to keep them clean and dry prior to use.

Figure 4 shows the molded plastic assembly tool that is used to hold the new splice and optical fibers during the assembly process, and to close the cap of the splice. The tool contains a pivoted handle mounted above the splice holding cradle at the center of the base. Fiber retention pads are located at

the ends of the tool to restrain the optical fibers being inserted in the splice. The tool also contains integral fiber cleave length gages at both ends to check the length of bare fiber projecting beyond the edgs of the plastic fiber coating.

Principle of Operation of the Metallic Element

The new mechanical splice obtains its fiber alignment and clamping capabilities from the "V" shaped metallic element. The metallic element is fabricated from a soft corrosion resistant aluminum alloy. The fabrication process utilizes this aluminum alloy in strip form from rolls. As the strip passes through a series at precision embossing, stamping, and blanking operations, flat element blanks like the one shown in Figure 5 are produced. The completed flat element blank contains a high precision "W" shaped cross section groove across its center portion. The chamferred sections at each end of this groove provide a funnel shaped transition to the fiber alignment channel when the element is bent into its final "V" shape.

The "W" shaped groove in the element blank contains nine individual planar surfaces, and creates two thinned sections or hinge points about which the element can be bent to create its "V" shape. The two edges of the flat element which are parallel to the main "W" shaped groove are also radiused on the opposite side so they will easily slide inside the cap after the element is bent into its "V" shape and assembled inside the splice. The notches in the corners of the element blank are engaged by the projections on the end plugs as described previously.

After the flat element blank has been cleaned, the "W" shaped groove is inspected optically for any defects. The element blank is then accurately located in a precision automatic bending fixture. This fixture clamps the element blank in the correct position, and simultaneously bends both legs of the blank about the thinned sections in the "W" shaped groove to produce a completed element as shown in Figure 6. The element is then filled with index match gel and is ready to assemble in the splice. In its final bent "V" shaped form, the distance between the radii on the back side of the legs is approximately .070 inches. This provides a snug fit of the element legs inside the wider .065 inches section of the cap groove.

When the element is bent into its final "V" shape, the original "W" shaped groove in the element is transformed into an equalateral triangular cross-section fiber alignment and clamping channel which runs full length of the element at the base of the "V". This channel is comprised of the first, fifth, and ninth flat surfaces from the original "W" shaped groove. The channel is large enough initially, so that a 125um glass fiber can be easily inserted into it from each end. The chamfers at each end of the channel make it easy to insert the fiber.

After bending, the element can be considered to contain 3 articulated parts or sections. The center section is a flat topped triangular cross section rib. This rib is attached to each of the element legs or levers through the thinned sections in the original "W" shaped groove. These thinned sections function like flexure hinge points for the element legs. When the legs are forced together as they would be wher the cap is forced down over the element, the legs pivot about the hinge points and the fiber channel surfaces on the inside of each leg are brought closer together. This reduces the cross sectional size of the fiber alignment channel. The flexure hinge and fiber channel size reduction principles are illustrated in Figure 7.

The ratio of the distance from the flexure pivot to the fiber channel surface on the inside of the element, and the flexure pivot to the end of the element leg is relatively large. This results in a high mechanical advantage in the

leg of the element with respect to the central rib and opposing element leg. The mechanical advantage is large enough to create relatively high compression loads on the fibers when they are inserted in the channel and the element legs are brought together.

The three surfaces comprising the fiber alignment channel in the "V" shaped element are relatively soft when compared to the fiber. These surfaces have a tensile yield stress of between 4,000 and 8,000 pounds per square inch. When the legs of the element are brought together on the fiber ends in the channel, the fibers embed themselves slightly into the three ductile surfaces of the channel. Since the surfaces are acting or pressing onto the fibers at equal angles of 120°, The fibers embed themselves approximately equal amounts in each surface.

The metallic element in the new splice can precisely align the geometric centerlines of fibers that have been inserted into it. If the cores in the fibers are relatively concentric to their cladding outside diameters, then the cores will also be brought into alignment within the element.Testing of the new splice on current fiber indicates that actual tolerances on core to cladding concentricity are very small. Thus, alignment of the fiber cladding centers in the new splice does align the cores sufficiently to provide insertions loss below .2db without tuning in most cases.

The new splice also has the capability to align fibers which have slightly different cladding diameters. This situation is illustrated in Figure 8. Each fiber embeds itself into the three surfaces in the alignment channel when the element is closed by the cap. If the pair of fibers in the splice are different diameters, the smaller fiber will embed itself less deeply in the channel walls and the larger fiber more deeply.
Since each fiber is embedded uniformly into the channel walls, the two differing diameter fibers will still be aligned. It is believed that the type of active fiber alignment achieved within the new splice is the most precise of any non-tuned system available today.

The new splice's high fiber retention capabilities are achieved by a combination of 1) the contact area between the fiber and the channel walls, and 2) the energy that is elastically stored in the element legs. When the legs of the splice element are forced together by the cam surface inside the cap, bending stresses are generated in the element legs These stresses are below the elastic limit of the element material in the legs. This causes the legs of the element, and to some extent the plastic case, act like springs which maintain the compressive load on the fibers in the element channel.

In order to achieve low insertion loss in the new splice, the fiber center lines must be brought into alignment. This is accomplished by the geometry and function of the metallic element. An additional requirement for low splice loss is that the cleaved fiber end faces must be brought into contact and held in contact when the element is clamped onto the fibers. Fiber end contact inside the splice occurs as a result of the normal splice installation procedure which will be described next.

Splice Installation Procedure

The following procedure is used to assemble the new splice and results in the fiber end faces being in contact when the splice cap is actuated. With practice, the splice assembly portion of this procedure can be completed in 30 seconds.

1) Place splice in holder in assembly tool shown in Figure 4.

2) Strip and cleave first fiber to desired length. (250um plastic coated fiber is stripped to 12.5 mm and 900um plastic coated fiber is stripped to 14.0 mm.)

3) Position plastic coating portion of first fiber in foam

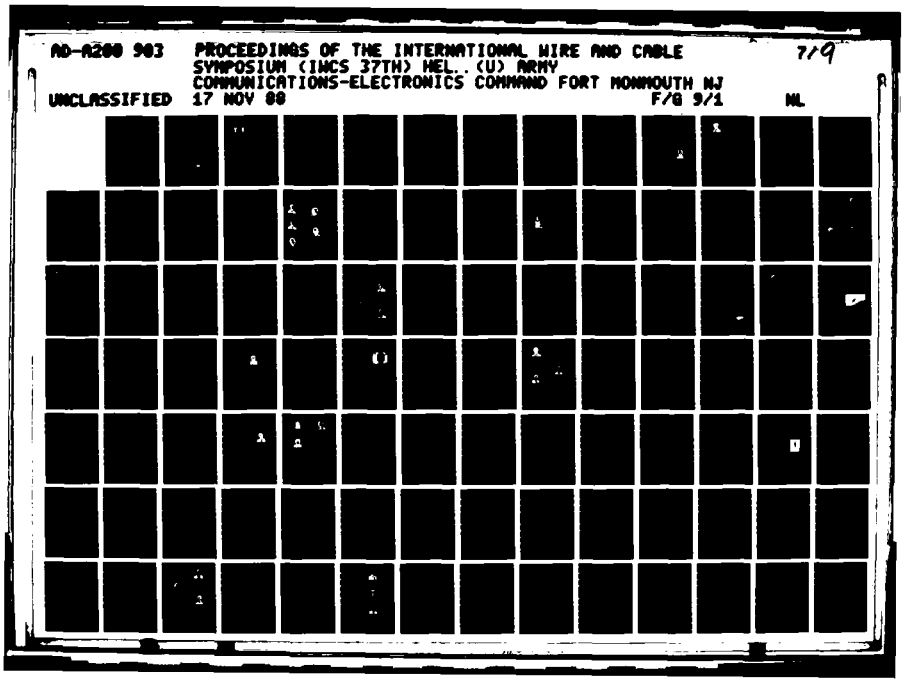
AD-A200 903 PROCEEDINGS OF THE INTERNATIONAL WIRE AND CABLE SYMPOSIUM (IWCS 37TH) HEL..(U) ARMY COMMUNICATIONS-ELECTRONICS COMMAND FORT MONMOUTH NJ
UNCLASSIFIED 17 NOV 88 F/G 9/1 NL
7/9

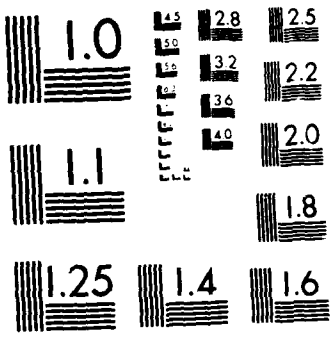

retention pad and the insert bare glass portion through the entry port and into the element until the shoulder on the fiber's plastic coating bottoms out against the chamfer inside the entry port. (The element is initially "open" and fibers can be easily inserted through the entry port into the element channel.)

4) Strip and cleave second fiber to desired length.

5) Position second fiber in foam retention pad at opposite end of assembly tool from first fiber. Insert bare glass portion of second fiber through entry port and into the element, until it comes into contact with first fiber end face. This occurs approximately at the center of the element. Fiber contact can be easily seen because a distinct buckle or bend occures in the first fiber between the splice and the foam retention pad on the tool as it is pushed slightly back out of thee splice by the second fiber.

6) Push first fiber back against second fiber until bends in both fibers between the splice and their respective retention pads are approximately equal.

7) Bring handle of assembly tool down on top of splice cap until cap is forced to its fluch closed position. The compressive force generated by the buckles in the installed fibers holds the fiber end faces in contact until the splice cap is closed and the fibers are clamped within the element.

Testing of the New Splice

A number of tests have been conducted on the new splice to verify its overall performance. These tests have included temperature cycling, tensile load retention, insertion loss, water immersion, vibration, and back reflection. The results of this testing to date is summarized in Figure 8.

FIGURE 1
METALLIC ELEMENT OPTICAL FIBER SPLICE

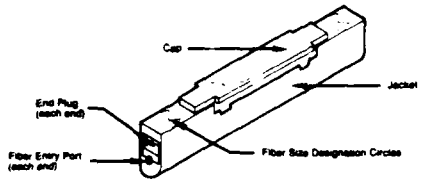

ASSEMBLED SPLICE

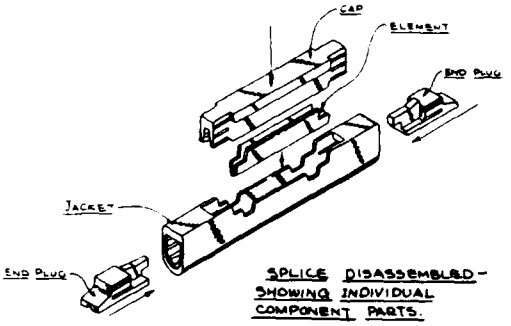

SPLICE DISASSEMBLED - SHOWING INDIVIDUAL COMPONENT PARTS.

FIGURE 2
SPLICE ASSEMBLY DRAWING

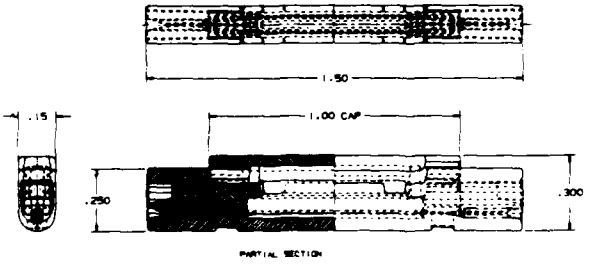

FIGURE 3
SECTION THROUGH CENTER OF SPLICE

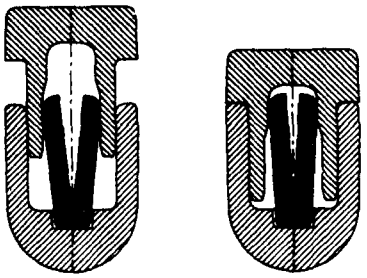

CAP OPEN
ELEMENT OPEN

CAP CLOSED
ELEMENT CLOSED

FIGURE 5
FIBER CLAMPING/CENTERING ELEMENT
(BEFORE BENDING INTO V SHAPE)

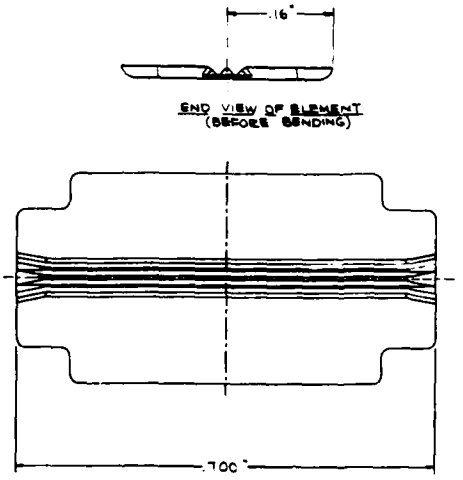

END VIEW OF ELEMENT
(BEFORE BENDING)

TOP VIEW OF ELEMENT
(BEFORE BENDING)

FIGURE 4

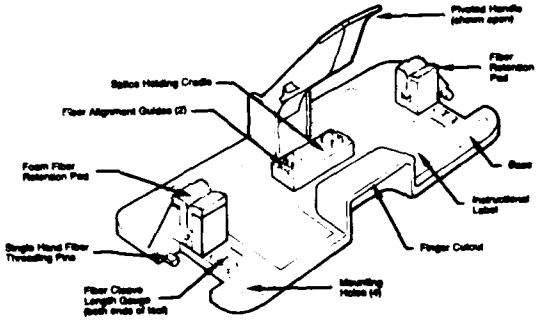

FIGURE 6
METALLIC ELEMENT AFTER BENDING

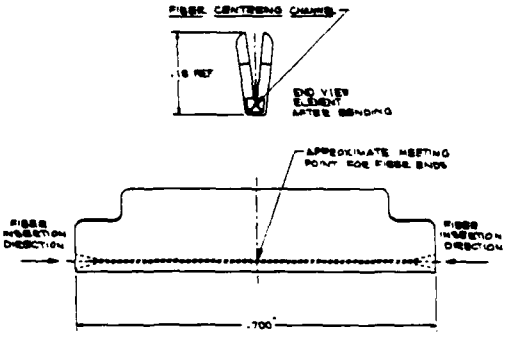

SIDE VIEW ELEMENT
(AFTER BENDING)

FIGURE 7

DEFORMABLE METALLIC SPLICE ELEMENT

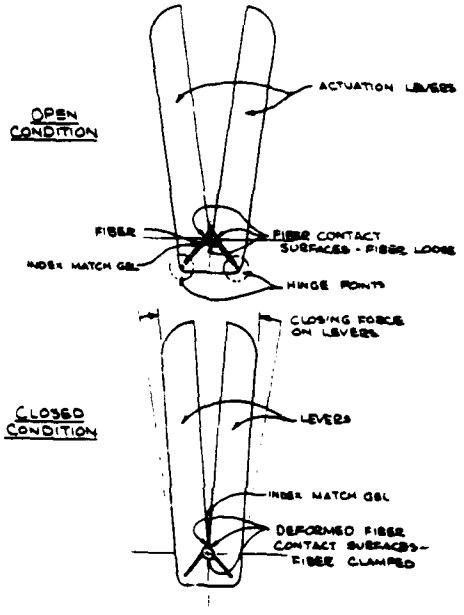

FIGURE 8

CENTERING OF DIFFERENT DIA FIBERS

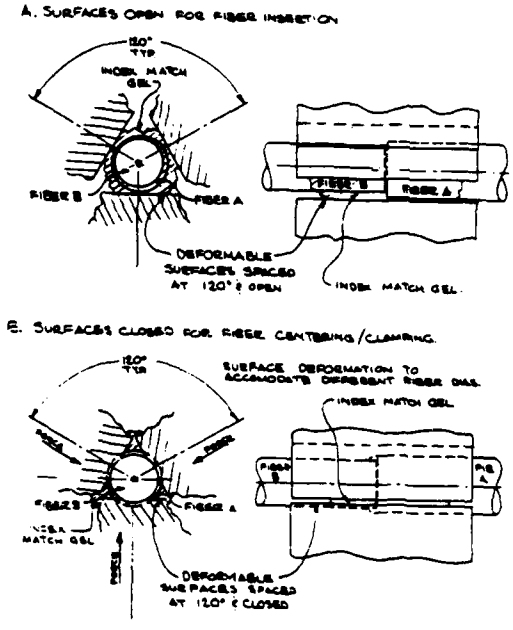

FIGURE 9

TEST RESULTS FOR NEW OPTICAL FIBER SPLICE

TYPE OF TEST	SAMPLE SIZE	TEST METHOD	RESULTS
Insertion Loss	100	Strip, cleave, insert fibers (no tuning). Measure loss with power meter.	90% of samples below .1dB with "in" tolerance fiber
Fiber Retention	100	Apply .75 lbs. for one minute. Measure change in power.	90% of samples show change less than .03 dB.
Vibration	11	Vibrate splice 1.52mm, 10 to 55 hz. variable frequency for 20 minutes in all 3 Axes. Measure change in power.	90% of samples showed a change less than or equal to .02 dB.
Temp. Cycling	16	Cycle splices from - 40° to +80°C. 2 hour holds at each extreme, one hours excursion times. Repeat 200 cycles. Measure transmission power every 5 min.	13% of splices showed loss change greater than .5dB during temperature cycling. 87% showed loss change less than .10dB.
Back Reflection	45	Blind splice, measure back reflection	All splices between-45dB and-75dB with 65% below -60dB.
Water Immersion	16	10 days immersion in distilled water at +40° c. Measure change in power.	100% of samples showed a change less than or equal to .03dB.
Index Match Gel Study		Thermogravimetric analysis. Heat gel while continuously monitoring weight.	65% of sample remained at 700 c.
		Heat age gel at+80°c for 60 days, measure index of refraction periodically.	Less than .1% change in index of refraction.
Acid - Base Solution Immersion		Immersed splices in 3% sulfuric acid solution or .2 normal sodium hydroxide solution for 10 days at+40°c. Measure power daily with OTDR.	None showed change greater than .1dB.

Undersea Single Mode Fiber Optic Rotary Mechanical Splice

R. R. Cammons, G. A. Decker, G. F. DeVeau

AT&T Bell Laboratories, 2000 Northeast Expressway, Norcross, GA 30071 Crawfords Corner Road, Holmdel, NJ 07733

ABSTRACT

A new fiber optic mechanical splice has been designed for use in the undersea cable joint environment. When used to join single mode fibers made to tight geometric requirements, it provides a low loss connection between two fibers without the aid of an optical test set to improve alignment. If used with a test set, losses are typically reduced to negligible values. The design of this splicing system is based on a widely used, highly reliable splice used in terrestrial fiber applications. The undersea splices described in this paper are designed to be incorporated inside a joint box, a device that enables one to join two multi-fiber high-strength cables. Materials were chosen to provide high reliability in the joint environment that includes surviving the high temperature of a splicebox overmolding process. In this process, molten polyethylene is injected into a mold surrounding the splicebox and cooled, isolating the high voltage current carrying joint and attached cables from the sea. Later, the splice can experience cyclic temperature swings while the cable resides in storage warehouses on land. It is exposed to shock and vibration during loading on a cable ship, transportation to the deployment site, and finally during cable laying in the ocean. After these stressful events, the splice is to remain in continuous service for 25 years. Twenty five year reliability assurance has been based on (1) extensive data gathered on its widely used terrestrial counterpart, (2) ensuring that those components in the terrestrial splice that were replaced for the undersea splice design were equal to or more rugged than those of the terrestrial version, (3) modeling and testing individual critical components and (4) assembling and successfully age testing many splices subject to extreme stress, at levels far greater than those expected for service. The device has been used during repair and integration operations in commercial deep water lightguide systems, demonstrating feasibility of reliably assembling the splices on a cable ship and durability in the ocean environment.

1. Background

Fiber splices can be subdivided into two categories:

1. splices that are incorporated into cables and other potentially high strain applications
2. those that are included in cable joints, repeaters, etc., that experience low mechanical strain during service

The first category usually implies that the splice must be similar in appearance and physical properties to unspliced fiber. The second has fewer geometric constraints, which usually implies that its cross sectional area can be far larger than that of the adjoining fibers.

Traditionally, fiber optic undersea cable systems have used arc or flame fusion splicing technology to join fibers. Fusion techniques have been applied to fibers drawn from different preforms to make system length spans before cabling as well as joining the fibers from cable spans to their counterparts emanating from repeaters. As undersea systems were put in service, fusion fiber splicing was introduced to the shipboard environment. High strength flame fusion splicing,[1] a technique that produces splices with the same mechanical characteristics, and made of the same materials as an unspliced section of fiber, did not require any lifetime prediction studies beyond the formidable problems associated with predicting the life of continuous fibers in undersea cables. However, mechanical non-fusion splices, and low strength fusion splices reinforced by mechanical splints, require another set of analyses and tests if they are to be committed to 25 year service. Typically, these types of splices represent major changes in mass and bending stiffness compared to the virgin fibers that they adjoin; moreover, they include additional materials that may experience degradation and displacement, or adversely react with each other and the materials in the splicebox, as a result of the previously mentioned polyethylene molding cycle, shock and vibration, or the splicebox environment when resting on the seabottom. Analysis of the fiber strain relief, splice mounting system, and the effect on the adjacent fiber, while experiencing mechanical shock and during long-term service, must be considered. If improperly designed, these components could induce stress in the fibers causing latent fiber failures. However, experience with the widely used AT&T connectorized splices used in land systems showed that

well designed splices were reliable and could be assembled under harsh conditions such as those in terrestrial manholes. Unlike fusion splicing, this technology relies on simple, inexpensive, rugged equipment; the resultant good performance does not require a vibration isolated, quasi-cleanroom environment on a cable ship.

It was decided, therefore, that a non-fusion splice would be suitable when jointing cables at sea, since they are easy to assemble and they would be stored in a low strain configuration inside a splicebox. The first phase of the development effort was directed at developing the splice and its assembly procedures for the undersea application; the remaining efforts were devoted to demonstrating the overall reliability of the product, and its suitability to undersea construction and repair applications.

2. Splice Design

A drawing of the undersea splice is shown in Figure 1. In deep ocean, the splicebox environmental conditions are mostly static with temperature ranging from 1C to 4C and moderate relative humidity. Assembly and storage conditions are much more variable. For instance, the undersea splicebox is overmolded with polyethylene before it is deployed in the ocean and this causes the internal temperature to be much higher than normal for about one hour. Although a typical joint requires a single molding operation, three consecutive overmolding cycles were imposed on the splices in the tests, as shown in Figure 2, to account for the unlikely possibility of having to remold a joint. All splice materials must remain adequately stable for this time period. When a cable system is in storage, temperatures can vary from -20C (-4F) to 40C (104F). These restrictions require adhesives and other mechanical parts that are dimensionally and chemically stable when repeatedly exposed to high temperature.

The general design is almost exactly the one used for a previously developed rotary mechanical splice that is used for land based systems.[2] Tests were made to see that the splice worked well at the assembly, storage, and service conditions stated above and all reliability tests were performed on samples that were exposed to multiple simulated assembly conditions as shown in Figure 2. The design changes required to transform the terrestrial rotary splice into its undersea counterpart included: replacement of the relatively low temperature material used in the terrestrial splice ferrule housing with a high temperature material, replacement of the relatively low glass transition temperature UV cured adhesive used in the terrestrial splice with a heat curable high glass transition temperature adhesive, and replacement of the buffer tubes/fiber strain reliefs with high temperature resistant substitutes. The main reason for these changes was to increase the splice's tolerance to the high temperature that it would experience during splicebox overmolding.

3. Reliability Assessment

Field service and laboratory stress tests of the terrestrial mechanical splice have shown no degradation mechanism nor failure mode. It has been in commercial service for more than three years, there are about 750,000 terrestrial splices in service, and there have been no failures after successful installation. Assuming a constant failure rate, we can statistically infer with high confidence that the terrestrial splice has a FIT rate (number of failures in 10^9 hours) of less than 1. The design philosophy behind the undersea splice was to build on this highly reliable foundation by increasing its robustness to protect it against failure modes that may be experienced in the undersea environment. Since there are only minor material differences between the terrestrial splice and the undersea version, and those differences were carefully designed to increase reliability, the undersea splice is projected to be at least as reliable as the terrestrial splice.

To check the validity of these assumptions, we have performed a battery of highly stressful tests to ensure that we did not introduce any failure modes into the product during the redesign process. The following sections describe these tests.

3.1 Aging Studies in the Laboratory

150 undersea mechanical splices were assembled and exposed three times to the thermal cycle experienced during the polyethylene overmolding of the undersea splice enclosure (Figure 2).

The assembled losses for the splices in the lifetest are displayed in Table 1. *These splices were assembled without* any optical testing or monitoring equipment since we were interested in the loss and stability of splices obtained without active alignment. Typical attenuation values when using optical monitoring equipment are less than 0.05 dB average loss and a standard deviation of 0.05 dB. All splice losses reported in this paper are for splicing singlemode fibers drawn from different preforms.

This exercise was designed to simulate the worst case splicebox assembly conditions during which multiple attempts are made to overmold the splicebox with polyethylene. Typical loss changes during the overmold process are shown in Table 2. As can be observed, there are minor changes in loss during the overmold cycle, and the result is usually a net reduction of loss.

The purpose of the lifetest was to detect thermally accelerated aging mechanisms. These 150 splices were divided up into three separate connected chains of 50 splices. All chains were immersed in distilled water (a humidity environment much more severe than expected even under worst-case service conditions), but each at a different constant temperature. One was maintained near 0C, another at room temperature, and the last at 40C. The optical loss of the chains was measured at 1.31 microns several times per month for 300 days. The tests continue.

Histories of the measurement results are shown in Figures 3, 4 and 5. The curves show the optical loss of the splices over time indicating the mechanical stability of the design. The results of the aging program suggest no thermally accelerated aging mechanism in the splices.

3.2 Shock and Vibration Testing

The undersea mechanical splice was subjected to the same shock and vibration test requirements that undersea repeater components must withstand. The specifications of this test are below:

Vibration Test Specification

Frequency (Hz)	Acceleration	Octaves/min.
5-11	0.5 in. disp.	NA
11-500	3Gs	0.1
500-1000	1G	0.25

Shock Test Specification

5 shocks, 100 Gs x 6 ms, sawtooth

All tests were performed on three axes.

Again, to ensure realism, the splices under test were subjected to the thermal effects of three simulated splicebox polyethylene overmolding cycles. None of the splices failed during these tests. Loss changes were small or non-existent. The repeater shock and vibration specification is designed to be a conservative test of discrete components in a cable system.

3.3 Index Gel Studies

A thermally cured index matching gel is applied between the abutted fiber ends to minimize optical loss and reflections. Special care was taken to ensure this material would not fail or degrade significantly over the life of the cable system.

3.3.1 Catalysis Inhibition The index gel is a two part RTV silicone material made of component parts that must be mixed together, applied between the faces of the adjoining fibers in the splice, and then cured by heating. The curing of the material can theoretically be poisoned by the presence of hydroxyls, carboxylic acid groups, sulfanates, amines, and unsaturated organic groups.

Glass slides were treated with the following:

1. 1,1,1 Trichloroethane
2. Acetone
3. 1,2 Dichloromethane (Methylene Chloride)
4. Dichlorodifluoromethane (Freon)
5. Methyl Alcohol
6. Ethyl Alcohol (denatured)
7. Sulfuric Acid (aq), dilute

The slides were allowed to air dry and then mixed gel was applied and thermally cured. The results showed that the residues of these chemicals are not harmful and there would be no inhibition to cure as long as the surfaces were dry.

3.3.2 Water absorption Another study tested the optical transmissivity of the gel on a continuous optical spectrum starting below 1.31 and extending above 1.55 microns optical wavelength. The thin layer gel samples were exposed to high heat and humidity. The results showed no increase in loss at 1.31 or 1.55 micron wavelengths. The loss did increase at 1.24, 1.39, and 1.65 micron wavelengths indicating an absorption of water. These effects disappeared when the material was placed in a dry environment showing that the water absorption is reversible. The conclusions are that heat and humidity do not detectably age or affect the chemical composition of the gel, the gel absorbs and releases water in a reversible way, and the absorbed water within the gel layer does not produce detectable optical transmission degradation at 1.31 or 1.55 micron optical wavelength regions.

3.3.3 Darkening Owing to Optical Radiation The gel has been exposed to 60,000 rads of gamma radiation at 200 rads/sec and suffered no measurable change of loss. The expected radiation dosage over the 25 year service life is typically on the order of a few rads.[3] Terrestrial rotary splices using this type of gel material have been transmitting infrared optical energy for as long as three years with no measurable increase in loss. The same is also true of multiple fiber array splices that have been in service for more than five years. We judge that it is not likely the material will significantly darken owing to photon transmission.

3.3.4 Bubble Support Deliberate attempts were made to whip up the gel with vigorous stirring during mixing of the component parts before use. The aerated gel was then applied to a splice and loss was monitored while heating the splice. Excess loss was less than 0.1 dB and this eventually disappeared. The material does not support bubbles well and introducing bubbles of optical significance owing to mispreparation of the material is not likely.

3.4 Potential Adverse Material Interactions

The properties of the materials used in the splice were investigated to see if there would be some significantly harmful chemical reaction within the splice or between the splice and the materials in the splicebox. The most likely possibility was judged to be stress corrosion cracking of the BeCu alignment sleeve in the presence of secondary and tertiary amines in the hardeners of the adhesives. This would only occur if a craftsperson did not properly mix the adhesive and the adhesive did not thoroughly cure. High temperature and high humidity tests of samples of the alignment sleeves in the presence of the pure hardener while under mechanical stress greater than service stress showed no signs of stress corrosion.

It was also noted that the alignment sleeve was resistant to stress relaxation even at temperatures higher than service conditions. Relaxation of the sleeve after 25 years under cable storage and service conditions is predicted to be well within acceptable limits.

4. Field Experience

Field experience has been favorable in terms of its compatibility with the shipboard installation environment and its optical performance. The device has been used to install a new repeatered cable span in the Optican I system during 1987 (which links two of the Canary Islands), installation of the TAT-8 shore sections and deep water sections during 1987 and 1988 respectively, and installation of a repeaterless inter-island link off the coast of Taiwan in 1988. No failures have been observed after proper installation. Yield — the number of splice attempts that do not have to be remade before closing the splicebox owing to failing the inspection criteria — is nearly 100%.

5. Conclusion

A mechanical splice was developed for use in undersea cable systems. It has been tested extensively and found to be reliable. Shipboard use has shown it to be a cost saver in terms of crew training compared to flame fusion splicing. Assembled transmission systems have been working well after almost a year of service. No special requirements were needed to modify the shipboard environment for splicing, making this splice a practical device for at-sea jointing operations.

6. Acknowledgments

We acknowledge that this has been a cooperative effort with major contributions coming from the Atlanta, Murray Hill, and Holmdel laboratories. We thank R. D. Tuminaro, J. J. Blee, E. Yanowski, J. Shea, D. W. Dahringer, S. Wong, R. Stathum, D. Menges, and E. Dalrymple for providing the bulk of the testing, contributing to the design elements of this splice, and for manuscript review. We would also like to thank the members of AT&T-TCSC for contributing to the refinement of the splicing fixtures and documentation, and providing project support. Lastly, we would like to acknowledge the strong efforts of J. C. Childs, R. Huckabee, M. J. Edwards, T. Smith, and S. Sapp for committing this device to production.

FIGURE 1

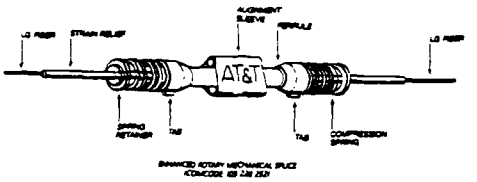

FIGURE 2
SIMULATED OVERMOLDING CYCLES

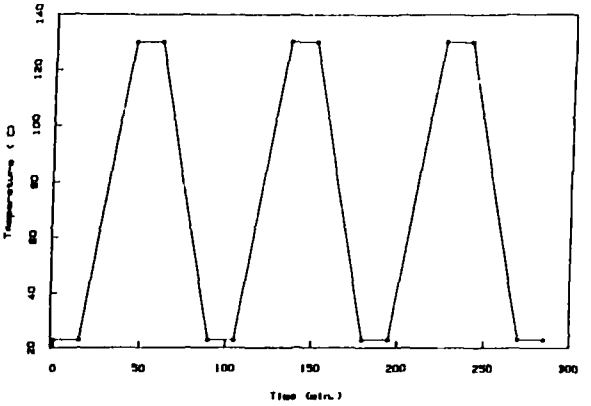

FIGURE 3

4 C AGING

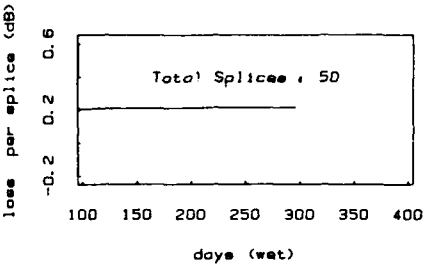

FIGURE 4

40 C AGING

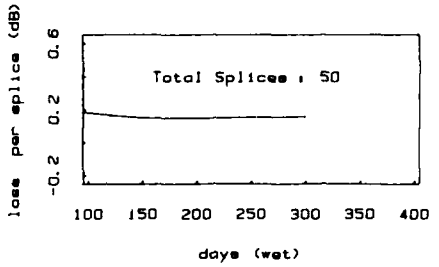

FIGURE 5

RM TEMP AGING

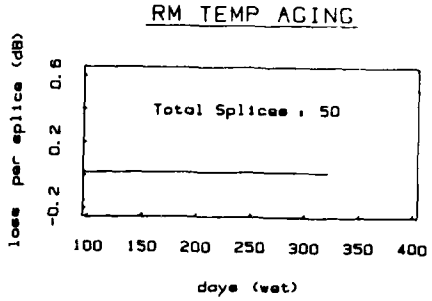

TABLE 1

TABLE OF ASSEMBLED SPLICE LOSSES

	Total Splice Loss	No. of Splices	Loss per Splice
Rotary Set 1	7.23 dB	50	0.14 dB
Rotary Set 2	8.95 dB	50	0.18 dB
Rotary Set 3	12.68 dB	50	0.25 dB

TABLE 2

LOSS CHANGES AFTER OVERMOLDING CYCLES

	Loss Change	No. of Splices
Rotary Set 1	0.13 dB	50
Rotary Set 2	1.04 dB	50
Rotary Set 3	1.40 dB	50

REFERENCES

1. G. A. Decker, R. V. Giangrossi, "High Strength Low Loss Flame Fusion Splicing Of Singlemode Fibers For Undersea Cable," SPIE, May 1-2, 1984, Arlington, VA.
2. J. A. Aberson, G. F. DeVeau, K. M. Yasinsky, "Enhanced Rotary Mechanical Splice With Fiber Positioner," 4th Annual Electrical Engineers Conference, New York, NY, April 11-14, 1988.
3. E. W. Mies, L. Soto, "Characterization Of The Radiation Sensitivity Of Single Mode Optical Fibers," ECOC (Venice, 1985).

Ray R. Commons is a Member of Technical Staff at AT&T Bell Laboratories, Norcross, Georgia. He has an Associate Degree in Mechanical Engineering from Southern Technical Institute. Since 1972, he has been working in the development and injection molding of plastic apperatus and light guide components.

George A. Decker is a Member of Technical Staff at AT&T Bell Laboratories in Holmdel, New Jersey. He joined AT&T in 1980 and has been working in the Undersea Systems Laboratory investigating high strength fusion splicing and rapidly deployable non-fusion splices with a view toward applying them to commercial undersea cable systems. George has also investigated optical measurements for analyzing the quality of fibers in optical components such as relays, cable terminations, and splices. George received his B.S.M.E. from the University of Rhode Island in 1980 and his M.S.E.S. degree from Stanford University in 1981.

George F. DeVeau is a Member of Technical Staff at AT&T Bell Laboratories, Norcross, Georgia. After joining Bell Laboratories in 1967 he was involved with multi-pair cable design and development. Since 1980, Mr. DeVeau has been engaged in the development of fiber optic splicing systems.

FUSION SPLICES WITH LOW LOSS BETWEEN SM-FIBERS OF DIFFERENT TYPES

W. Stieb and J. Schulte
Kabelmetal Electro GmbH, 3000 Hannover, West Germany

A.M. Oehler, T.M. Hauff and W.E. Heinlein
University of Kaiserslautern, 6750 Kaiserslautern, West Germany

Summary.

A new technique is reported for the minimization of splice loss between dispersion-optimized single-mode fibers and conventional single-mode fibers. These low-loss splices will be important for future dispersion-optimized optical fiber networks. For example, a loss reduction from 0.8 dB to 0.1 dB was achieved by slightly tapering the splice region. The measured splice losses are in good agreement with our calculations. The method of splice-loss minimization was applied to splices between dispersion-flattened, dispersion-shifted, matched-cladding and depressed-cladding single-mode fibers. The diameter of the slightly tapered splices is sufficiently large for the splices to be mechanically stable and independent of the environment, i.e.: the embedding medium. The simplicity of the splice-tapering technique suggests tapering the splices in a modified fusion splicer.

Introduction.

For future optical communication networks consisting of dispersion-flattened single-mode fibers (DFSM-fibers) and components with standard single-mode pigtails, such as lasers and couplers, low-loss splices between these different fibers are required. Splices between these dissimilar fibers cause high splice losses because of different mode field diameters[1] which are $2w_0$ =6.3 µm for the DFSM-fiber and $2w_0$ = 9.9 µm for the standard matched-cladding single-mode fiber (MCSM-fiber) at the 1.3 µm wavelength that we used for our study. We devised a new technique of field matching to reduce the splice loss between DFSM- and standard MCSM-fibers by slightly tapering the splice region[2] . In this contribution we expand our investigations to splices of selected fiber combinations. The field matching is based on the unlike behavior of the mode field parameters of different fibers during tapering. For example: by tapering a DFSM-fiber, the mode field expands rapidly in contrast to a standard single-mode fiber, where the mode field decreases initially and, with further tapering, increases less than the mode field of the DFSM-fiber. Thus, optimum field matching and low splice losses between different fibers can be obtained. The matched mode fields are still core-guided in contrast to the method of Mortimore et al.[3]. Therefore, the matched splices are mechanically stable and insensitive to the environment, i.e.: the embedding medium. The field matching can be performed in a modified commercial fusion splicer. The influence of dopant diffusion in the splice region[4] as a function of the tapering parameters will be discussed.

Splicing strategy: General considerations.

Two fibers with different index profiles are joined by a fusion splice. Tapering the joint reduces the diameter of the splice junction, as shown in Fig.1. The resulting tapers can be characterized by the taper ratio $TR = a_t/a_0 = \leq 1$, wherein a_t is the radius of the tapered fiber and a_0 that of the untapered fiber. These tapers act as mode transformers. The taper ratio can be chosen so that the core guidance is maintained and so that a minimum of loss results at the junction between the fibers. Thus, the surrounding medium has no influence on the mode fields. To illustrate the operation of the tapered splice one may consider the Petermann spot size parameter w_0 at the splice junction as a function of TR. The spot size w_0 of a MCSM-fiber, for example, decreases slightly with decreasing fiber diameters until TR = 0.85, while w_0 of a DFSM-fiber shows an increase[2]. Therefore, field matching is possible through a suitable choice of TR.

The splice loss is influenced by refractive-index profile diffusion: by annealing the splice, first the refractive index profiles of the fibers will be smoothed by diffusion. We calculated in our example the reduced splice loss for smoothed refractive-index profile Δ_s(MCSM) of the MCSM-fiber and Δ_s (DFSM) of the DFSM-fiber in accordance with the dopant concentrations mentioned in [4] (Fig. 2). Secondly, further annealing leads to a

diffusion process between both fibers, resulting in a common refractive-index profile Δ_c in the central region of the splice (Fig. 1). For a splice between DFSM-fiber and MCSM-fiber this leads to additional field matching. Taking into account the diffusion processes, the minimal splice loss of 0.11 dB at the 1.3 µm wavelength is obtained for TR = 0.62 (Fig. 2).

The splice-loss reduction of an untapered splice caused by profile-smoothing is approximately equal for both the 1.55 and 1.3 µm wavelengths. However, the influence of the common refractive-index profile is less effective at 1.55 µm (see Table 1). The minimal splice loss at 1.55 µm is 0.15 dB for TR = 0.75. Thus, by a suitable choice of TR the splice loss can be reduced for broad-band application.

To compare the exact values of the well-known overlap integrals of the mode fields[5] with an approximation made by assuming that the field distribution is Gaussian and neglecting the diffusion processes (Fig. 2), we calculated the splice loss for Gaussian fields with the spot size w_0. Therefore, if Gaussian field distribution is assumed, the splice loss at 1.3 µm would disappear for TR = 0.70 because the spot sizes are equal. However, the exact splice loss reveals a finite minimum.

Practical results.

All untapered splices were prepared using conventional splicing equipment. Optimum splicing parameters were the same as for splices between conventional MCSM-fibers (fusion time: 1.8 s). The measurement equipment is shown in Fig, 3. The laser beam was launched into a dispersion-optimized fiber (i.e.: DFSM-fiber or dispersion-shifted single-mode fiber (DSSM-fiber)) of 2 km length, spliced to a MCSM-fiber of minimum 5 m length. These fiber lengths are sufficiently long to suppress higher-order modes.

Following splice loss measurement of the untapered splices, the splices were clamped to a motorized, computer-controlled jig. The laser and receiver units remained fixed. The splice region was then heated with an oxybutane micro-torch and tapered symmetrically by moving the jigs. The transmitted light power was recorded vs. the taper length.

Splice between DFSM fibers.

A histogram of splice losses between identical DFSM-fibers is shown in Fig. 4. The splice losses at the 1.55 µm wavelength showed a similar behavior. These results prove that, in spite of the small spot size of DFSM-fibers, low-loss fusion splices between DFSM-fibers can be obtained.

Splice between DFSM- and MCSM-fibers.

The splice losses at 1.3 µm are shown in the histogram of Fig. 5. The mean untapered splice loss of 0.8 dB is in good agreement with the calculated value of 0.83 dB for butt-joint splices (Table 1). The transmitted light power vs. taper length is given in Fig. 5. We achieved a minimum splice loss of about 0.1 dB which is in good agreement with the calculated splice loss, assuming a common refractive index profile caused by diffusion. The mean splice loss at 1.55 µm was 0.6 dB before and 0.2 dB after tapering. Our splice losses are lower than those reported by Zell et al.[4], wherein only heating of the splice region was used to reduce the splice loss.

Splice between DSSM- and MCSM-fibers.

We calculated the splice loss between a commercially available dispersion-shifted single-mode fiber and a standard MCSM-fiber at the 1.55 µm wavelength. The results are shown in Fig. 6. For a butt-joint splice the splice loss is 0.25 dB for TR = 1.0 and for an optimum taper ratio of TR = 0.56, the splice loss (without diffusion) is 0.01 dB. Fig. 7 shows the mode field radii of the DSSM- and MCSM-fibers vs. taper ratio. The field distributions of both fibers are shown in Fig. 8. With optimum tapering the splice loss is 0.06 dB when a diffusion-smoothed refractive index profile is assumed, and 0.1 dB when a diffusion-caused common refractive index profile is assumed. This means that in the case of MCSM/DSSM splices the profile diffusion raises the splice loss.

Fig. 9 shows an example of DSSM/MCSM splice loss change during tapering together with histograms for the initial and final values of our tapering experiments at 1.55 µm. The mean splice loss before tapering is about 0.4 dB, which is higher than the expected 0.25 dB theoretical value. The splice loss increases to about 0.6 dB as the fiber is heated and before the taper process is started. It then decreases to 0.1 dB (mean value: 0.15 dB) during tapering. This last value is in good agreement with theory, although our theoretical model does not explain the initial increase. Fig. 10 shows a photograph of a tapered splice and a histogram of the taper ratios which yielded minimum splice loss values. They are between TR = 0.6 and 0.7, as theo-

retically expected for diffusion-caused common refractive index profiles.

Splice between DSSM-and depressed-cladding SM-fibers.

We calculated the splice losses between a DSSM-fiber and a depressed-cladding single-mode (DCSM) fiber for the 1.55 μm wavelength. The spot sizes w_0 are given in Fig. 11. The splice losses are shown in Fig. 12. With the exception of the lower loss of an untapered butt joint splice, the overall picture of the values listed in the table is the same as for MCSM/DSSM splices.

Splice between MCSM- and DCSM-fibers.

We calculated the loss for a splice between a MCSM-fiber and a DCSM-fiber, assuming worst-case field diameters of $2w_0$ = 11 μm ($MC_{11\mu m}$ SM-fiber) and $2w_0$ = 8 μm ($DC_{8\mu m}$ SM-fiber), respectively, for the 1.3 μm wavelength. In this case, the minimum splice loss is achieved for an untapered splice with a region of diffusion-caused common refractive index profile. The splice loss of this fiber combination can be reduced for the 1.3 μm and 1.55 μm wavelenghts from 0.5 dB to 0.3 dB simply by annealing the splice region without tapering the splice (see Table 1).

Conclusion.

We have shown that splice losses between different fibers can be reduced significantly through slight tapering of the splice region. The simple handling suggests that the tapering operation can be accomplished through modification of a conventional splicer. Our initial experience with a semi-automatic splicer, wherein we manually moved the clamps apart while maintaining the arc, showed good results. The outer diameters of the slightly tapered splices are still sufficiently large so that the matched splices can be handled like conventional splices (Fig. 10).

Our studies show that in transmission lines using dispersion-optimized fibers, i.e.: DFSM- or DSSM-fibers, conventional single-mode components can be used. The anticipated high splice losses between these fibers with large and small spot sizes can be avoided through our splice-tapering technique. Fig. 13 shows the example of a dual-wavelength DFSM-fiber transmission line using standard SM-pigtailed lasers, standard SM-fiber WDMs and standard SM-fiber repair patches. We assumed 10 repair patches along the 30-km DFSM-fiber line. Instead of an expected cumulative 17.6 dB splice loss using untapered splices, we obtained a low value of 3.5 dB (at 1.3 and 1.55 μm) by tapering. The costs of installation and maintenance of a WDM-system consisting of a dispersion-optimized SM-fiber transmission line and using only conventional SM-fiber components are much lower than those of a system requiring specially-designed components for dispersion-optimized fibers.

fiber combination	λ(μm)	taper ratio	splice loss (dB)		
			Case 1	Case 2	Case 3
Dispersion Flatt.SMF-Matched Clad.SMF	1.30	1.00	0.83	0.62	0.34
		0.68	0.24		
		0.62			0.11
		0.61		0.13	
	1.55	1.00	0.61	0.42	0.27
		0.82	0.24		
		0.75			0.15
		0.74		0.17	
Dispersion Flatt.SMF-Depressed Cladd.SMF	1.30	1.00	0.66	0.52	0.30
		0.72	0.29		
		0.70		0.21	0.14
	1.55	1.00	0.45	0.36	0.24
		0.87	0.29		
		0.85		0.25	0.18
Dispersion Shift.SMF-Matched Cladd.SMF	1.55	1.00	0.25	0.22	0.17
		0.66			0.10
		0.60		0.06	
		0.56	0.01		
Dispersion Shift.SMF-Depressed Cladd.SMF	1.55	1.00	0.17	0.18	0.15
		0.83			0.12
		0.79	0.06	0.09	
Matched Cladd.$_{11\mu m}$ Depressed Cladd.$_{8\mu m}$SMF	1.30	1.00	0.47	0.47	0.26
	1.55	1.00	0.53	0.54	0.30

Table 1.
Calculated losses between different fibers
Case 1: Ideal butt-joint splice, without profile diffusion, index-matched;
Case 2: Similar to Case 1, except that profile diffusion[3] is taken into account;
Case 3: Similar to Case 2, except for a region with common refractive-index profile Δ_c (see Fig. 1).

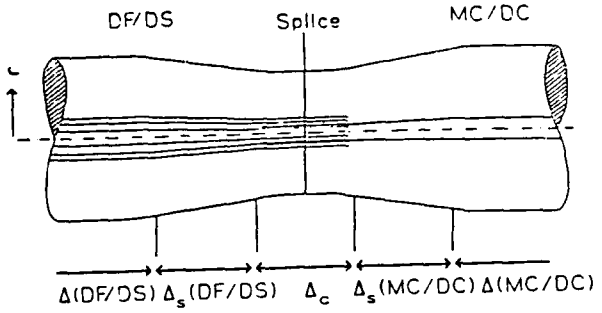

Fig. 1. Schematic of a tapered splice with assumed refractive-index profiles at different locations

MC = Matched-cladding single-mode fiber (SMF) with refractive-index profile Δ(MC);
DC = Depressed-cladding single-mode fiber with refractive-index profile Δ(DC);
DF = Dispersion-flattened SMF with refractive-index profile Δ(DF);
DS = Dispersion-shifted SMF with refractive-index profile Δ(DS);
Δ_s = Refractive-index profiles, smoothed by diffusion process in the taper regions;
Δ_c = Common refractive-index profile between the taper regions.

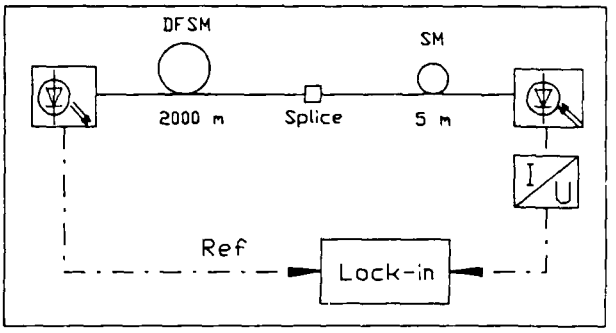

Fig. 3. Measurement set-up for DFSM-MCSM splices.

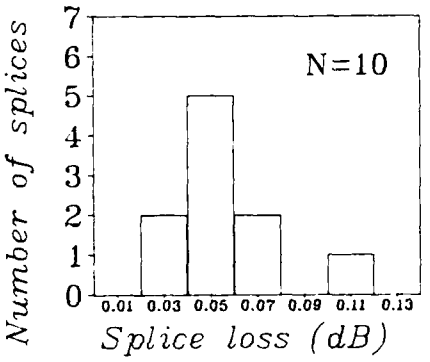

Fig. 4. Splice losses between identical DFSM-fibers

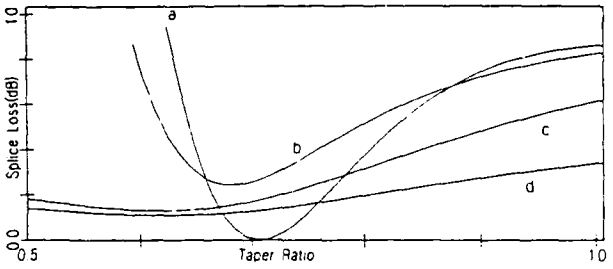

Fig. 2. Calculated losses of symmetrically-tapered splices between DFSM- and MCSM-fibers vs. taper ratio TR at the 1.3 μm wavelength

a = Gaussian field approximation (leading to spot sizes [1]);
b = Exact field distribution, neglecting diffusion;
c = Similar to b but with diffusion-smoothed Δ_s(DF), Δ_s(MC);
d = Similar to b but common Δ_c by diffusion

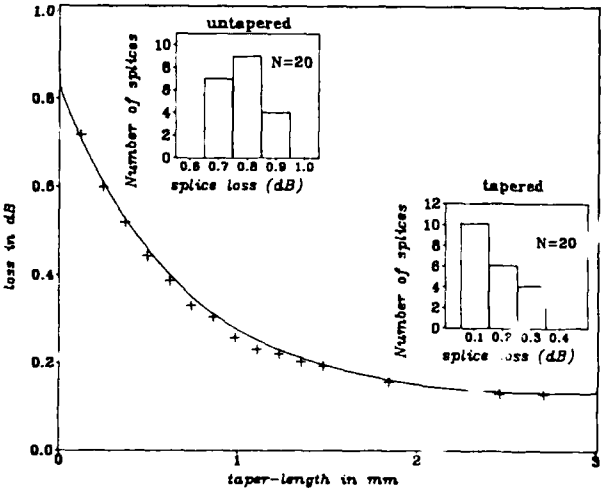

Fig. 5. DFSM/MCSM-splice loss vs. taper length and results of untapered and tapered splices.

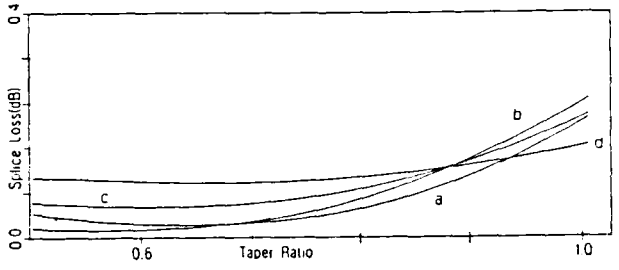

Fig. 6. Calculated losses of symmetrically-tapered splices between DSSM- and MCSM-fibers vs. taper ratio TR at the 1.55 µm wavelength
a = Gaussian field approximation (leading to spot sizes [1]);
b = Exact field distribution, neglecting diffusion;
c = Similar to b but with diffusion-smoothed Δ_s(DF), Δ_s(MC);
d = Similar to b but common Δ_c by diffusion

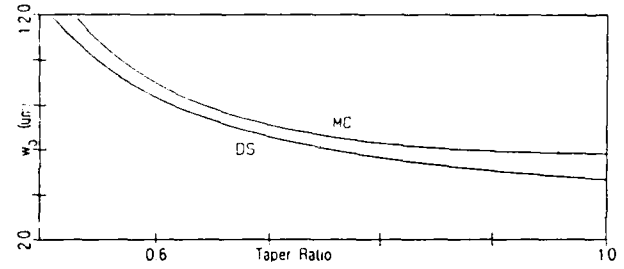

Fig. 7. Spot sizes w_0 of dispersion-shifted single-mode fiber (DS) and of matched-cladding single-mode fiber (MC), according to [1], as a function of taper ratio TR for the 1.55 µm wavelength.

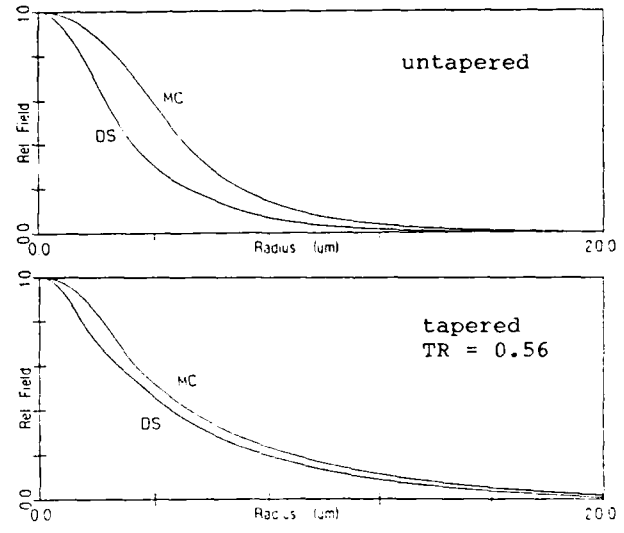

Fig. 8. Relative field of DSSM- and MCSM-fibers for the 1.55 µm wavelength.

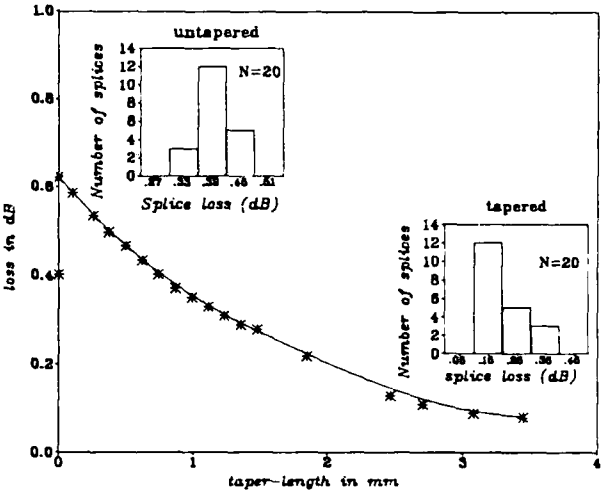

Fig. 9. DSSM/MCSM-splice loss vs. taper length and results of untapered and tapered splices.

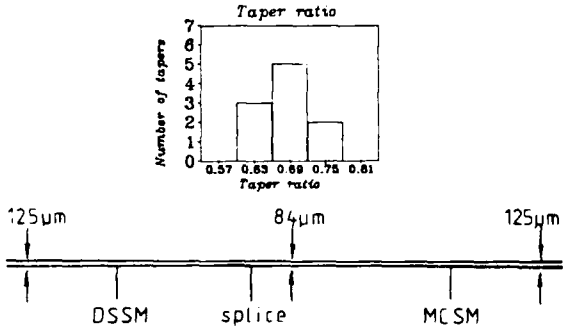

Fig. 10. Photograph of a tapered DSSM/MCSM splice and values of taper ratios for minimal splice losses.

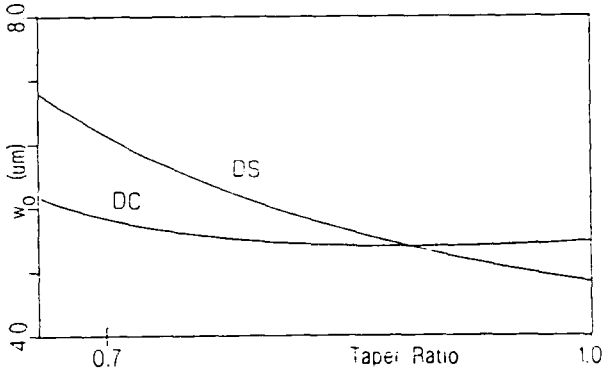

Fig. 11. Spot sizes w_0 of dispersion-shifted single-mode fiber (DS) and of depressed-cladding single-mode fiber (DC), according to [1], as a function of taper ratio TR for the the 1.55 µm wavelength.

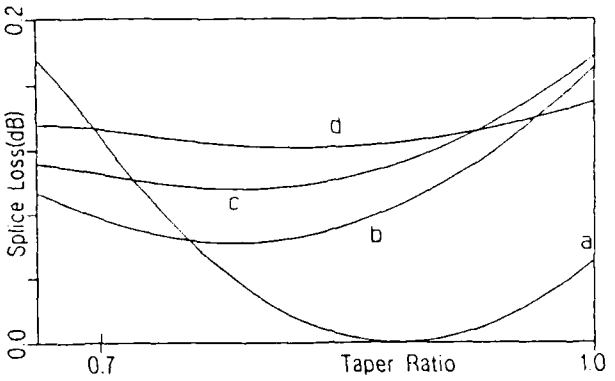

Fig. 12. Calculated losses of symmetrically-tapered splices between DSSM- and DCSM-fibers vs. taper ratio TR at the 1.55 μm wavelength

a = Gaussian field approximation (leading to spot sizes [1]);
b = Exact field distribution, neglecting diffusion;
c = Similar to b but with diffusion-smoothed Δ_s(DS), Δ_s(DC);
d = Similar to b but common Δ_c by diffusion

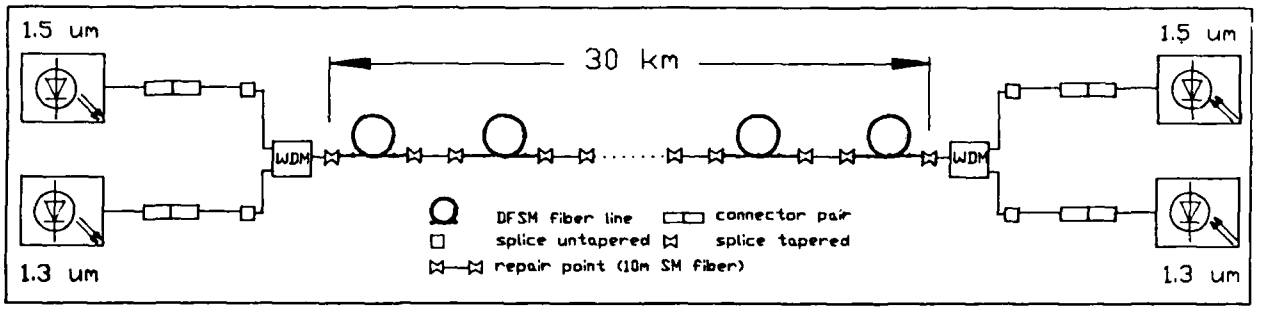

Fig. 13. Dual wavelength DFSM-transmission line, using standard SM-pigtailed lasers, SM-fiber WDMs and ten SM-fiber repair patches.

References.

1. Petermann, K. "Fundamental Mode Microbending Loss in Graded-Index and W-Fibers." Optical and Quantum Electronics, Vol. 9, 1977, p. 167-175

2. Oehler, A., Hauff, T., Heinlein, W., Stieb, W., Schulte, J. "New Field-Matching Technique for Low-Loss Splices between Conventional and Dispersion - Flattened Single-Mode Fibers." Proceeds., European Conf. on Optical Communications, 1988.

3. Mortimore, D.B., Wright, J. V. "Low-Loss Joints between Dissimilar Fibers by Tapering Fusion Splices". Electronics Letters, Vol. 22, No. 6, 1986, p. 318-319

4. Zell, W., Becker, J.A., Bachmann, P.K., Hermann, W.G. "Low-loss Fusion Splicing of PCVD-DFSM Fibers", IEEE J. of Lightwave Technology, Vol. LT-5, No.9, 1987, p. 1192-1195

5. Marcuse, D., "Loss Analysis of Single-Mode Fiber Splices", Bell System Technical J., Vol. 56, No. 5, 1977, P. 703-718

Acknowledgments.

This project was supported by the German Federal Ministry of Research and Technology, Bonn. The authors wish to thank Mr. H. Hofheimer of Cable Consultants Corp., Larchmont NY for his valuable assistance in preparing this paper.

Werner Stieb
Kabelmetal Electro
GmbH
Kabelkamp 20
3000 Hannover 1
West Germany

Werner Stieb, after receiving his electrical engineering degree from the University of Kaiserslautern in 1986, joined Kabelmetal as a development engineer in the field of telecommunication cables. As a group leader he is responsible for development of passive optical components.

Johann Schulte
Kabelmetal Electro
GmbH
Kabelkamp 20
3000 Hannover 1
West Germany

Johann Schulte received his physics degree in quantum optics in 1981 and his Ph.D. in engineering in 1986 from the Technical University/Hannover. After a research stay at IBM, Yorktown Heights NY, he joined Kabelmetal in 1987, where he is presently engaged in the development of components for optical communications.

Albrecht Oehler
Univ.of Kaiserslautern
Dept. of Theoretical
EE & Optical Communic.
P.O. Box 3049
6750 Kaiserslautern
West Germany

Albrecht Oehler was born in 1957 and received his Dipl.Ing. degree in electrical engineering from the Univ. of Kaiserslautern in 1985. Following a stay at Siemens AG in Munich, where he was engaged in exploratory development work on fiber optical transmission systems, he joined the Dept. of Theor. FE & Optical Communication at the Univ. of Kaiserslautern in 1987, where he is pursuing his Dr.-Ing. degree in fiber optics. He is engaged in theoretical studies of propagation and coupling characteristics of single-mode fiber couplers.

Thomas Hauff
Univ.of Kaiserslautern
Dept. of Theoretical
EE & Optical Communic.
P.O. Box 3049
6750 Kaiserslautern
West Germany

Thomas Hauff was born in 1960. He received his Dipl.Ing. degree in electrical engineering from the Univ. of Kaiserslautern in 1986, after which he joined the Dept. of Theoretical EE & Optical Communication to pursue the Dr.-Ing. degree in fiber optics. He has been engaged in theoretical studies of propagation characteristics of single-mode multiple-clad fibers, of stress-induced waveguides and non-linear optics.

W. E. Heinlein
Univ.of Kaiserslautern
Dept. of Theoretical
EE & Optical Communic.
P.O. Box 3049
6750 Kaiserslautern
West Germany

Walter Emil Heinlein was born in 1930. He received his Dipl.Ing. degree in electrical communications engineering in 1955 and his Dr.-Ing. degree in 1958 from the Univ. of Stuttgart. In 1957 he joined Siemens AG., Munich, where, as head of a research laboratory he performed exploratory development work on microwave applications of semiconductors, active filters and fiber optic transmission systems. Since 1975, he has been a Professor of Theoretical Electrical Engineering at the University of Kaiserslautern, where he is engaged in research on optical communications. Prof. Heinlein is co-author and author of two books. He is a member of the Optical Society of America (OSA).

Single-Mode Multifiber Technique for High-Density High-Count Subscriber Cables.

Tadashi HAIBARA, Shinji NAGASAWA, Michito MATSUMOTO and Masaaki KAWASE

NTT Network Systems Development Center
Tokai, Ibaraki, 319-11, Japan

ABSTRACT

Practical single-mode multifiber jointing techniques, an efficient fiber coat stripper, a mass-fusion splicer and a field-installable multifiber connector, have been developed.

Their performances have been evaluated for experimental subscriber lines with 10-SM-fiber ribbon cables. It has been found that average splice losses for the same ribbon and for different ribbons are 0.02dB and 0.11dB, respectively. An average connection loss of 0.42dB for field-installed connectors has been obtained.

1. Introduction

In construction of single-mode optical fiber subscriber lines, several kinds of optical cables and jointing techniques are required. Particularly, multifiber jointing techniques, including mass-fusion splicing and multifiber connectors, are indispensable for high-density, high-count optical cables such as feeder cables.

Low-loss and higher operating efficiency are required for mass-fusion splicing. A mass-fusion splicing machine for 4-SM-fiber ribbons with image processing equipment[1], a fiber cutting tool[1],[2] and a fiber holder[3] have been developed for achieving low-loss splicing. For practical use, the reduction of mis-stripping, mis-splicing and miniaturization of splicing equipment are important.

A low-loss multifiber connector for fiber ribbons, that is small, and economical, is required. A multifiber connector with a precision plastic-molded ferrule has been developed[4],[5] for this purpose. The connector is constructed in the factory for application to pre-connectorized cables. For practical use, the connector must rapidly be constructed in the field. Therefore, a multifiber connector allowing both easy construction and low-loss is desirable.

In this paper, the design and performances of the practical single-mode multifiber jointing techniques, the mass-fusion splicing equipment and the multifiber connector, are described. The results of a field trial are also presented.

2. Mass-Fusion Splice

2.1 Splice Equipments Design

Figure 1 shows the relationships between problems and solutions in achieving low-loss and highly efficient multifiber splicing. A fiber cutting tool[1],[2] and a fiber holder[3] have already been developed to solve these problems. With this equipment, some degree of low-loss splicing has been achieved[1].

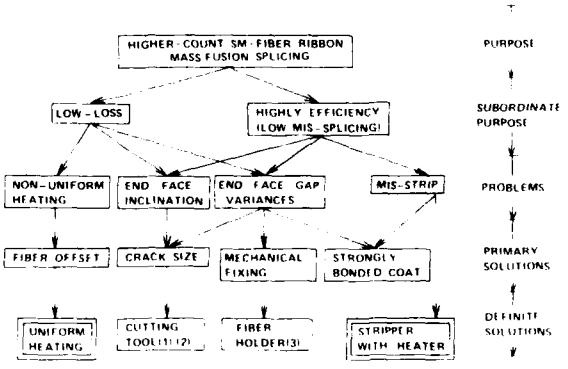

Figure 1. Relationship between purpose and solutions to achieve a low-loss and highly efficient multifiber splicing.

On the other hand, the two major problems, end face gap variances and non-uniform heating, have not been completely solved.

In this section, splicing equipment which solves these problems is described.

(1)Coat stripper with heater

Mis-splicing mainly occurs when there are large end face gap variances due to weakly bond between the fiber and its coating. Strongly bonded coat is very effective in reducing the variances directly, but the mis-stripping rate increases due to the difficulty encountered when stripping. The mis-stripping rate using a conventional stripper increases more than 50%. This is inefficient for field use. Therefore, a new coat stripper for stripping the strongly bonded coat easily needs to be developed.

The resistance required to strip the coat is determined by how much the coat shrinks and the strength of the bond between the coat and fiber. Therefore, when the coat is heated, shrinkage will be reduced due to its thermal expansion. The shrinkage **p** of unit length decreases in proportion to the temperature, described as,

$$p = C(t_0 - t) \qquad (1)$$

taking into consideration the theory of shrink fit. Where, **C** is the constant determined by thermal expansion coefficients of the coat and fiber, elastic modulus, etc., and t_0 is temperature at which shrinkage disappears.

Figure 2 shows the construction of the coat stripper. The stripper consists of a pair of blades and a ceramic heater for controlling temperature.

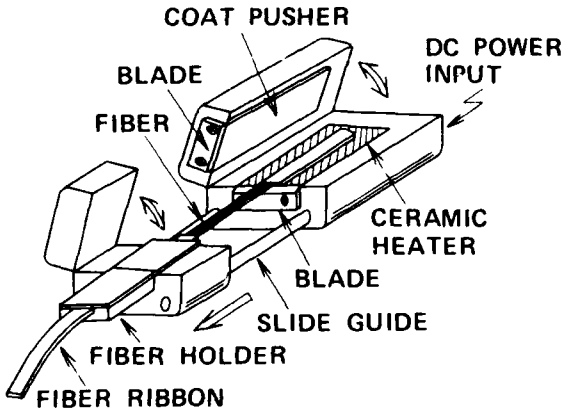

Figure 2. Construction of the coat stripper.

Figure 3 shows the effect of temperature on resistance when stripping a 10-SM-fiber ribbon. The length of coat stripped was 30mm. The filled circles are the measured values, the solid line is a calculated value based on eq.(1) and resistance at 20°C, and broken line is an average resistance in the region of 70 to 100°C. The resistance decreases as indicated by eq.(1). It was found that the effect of shrinkage disappears over 70°C.

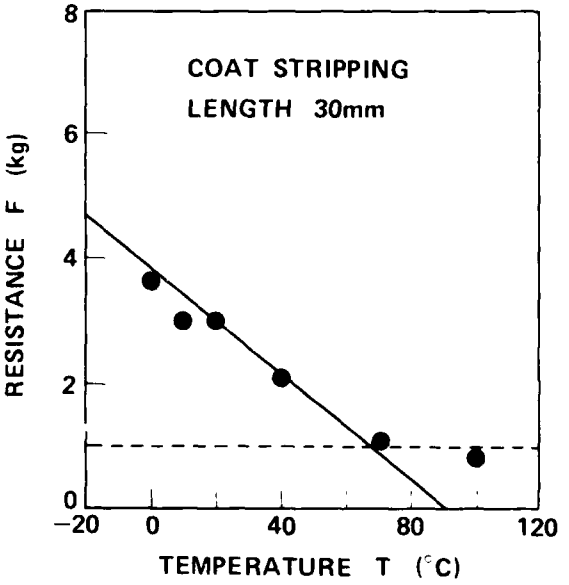

Figure 3. Effect of temperature on resistance when stripping 10-SM-fiber ribbon.

Figure 4 shows the relation between the length to be stripped vs. resistance. Open circles, triangles, and rectangles indicate resistances for three different fiber ribbons that are not heated. And the filled marks correspond to the resistances heated to 100°C. Furthermore, the cross indicates the resistance of non-bonded ribbon without using heating. When the coat is heated, the resistance decreases to about 1kg which is as same as that of the non-bonded ribbon. This result indicates that the strength of the bond force between coat and fiber disappears when heated.

During field tests it was confirmed that, when heated, the resistance of a strongly bonded coat

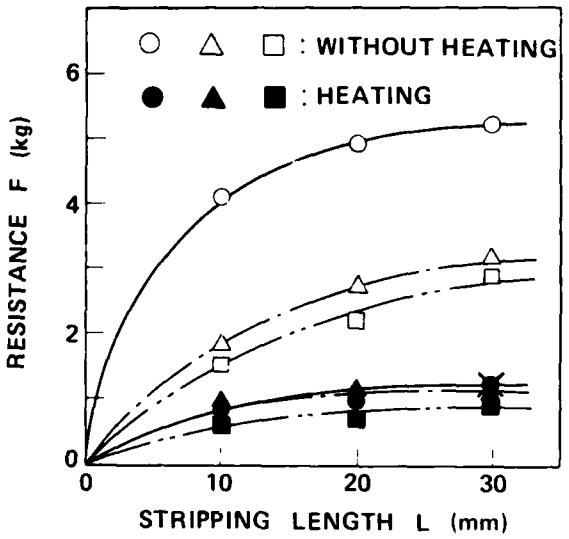

Figure 4. Relation between the length to be stripped and resistance.

is reduced and the coat can be stripped easily with blades. The stripper is $40x100x40mm^3$, small enough to make it very convenient for use in the field.

(2)Uniform heating conditions

The rate of mis-splicing and splice loss increases when the temperature varies between individual fibers. The heating technique has been studied and a low-loss splicing of less than 0.1dB has been obtained for 5-GI-fiber ribbons[6]. The offset **d** and electrodes gap **L** corresponds to the number of fibers to be spliced simultaneously, therefore the uniform conditions have been confirmed experimentally. Figure 5 shows the brightness of the 10-SM-fibers during electrical discharge, recorded by TV camera. Figure 5(a) shows a uniform heating condition and (b) shows the non-uniform case. Figure 6 shows the relation between normalized discharge current i/i_0 vs. ratio **d/L**. The discharge current **i** is normalized by the smallest value i_0 which was obtained experimentally. The open circles and triangles indicate uniform heating conditions for 10-SM-fiber ribbons and non-uniform ones, respectively. The uniform heating is obtained in the hatched region. The non-hatched regions indicate the non-uniform, low-power or excessive power regions, respectively.

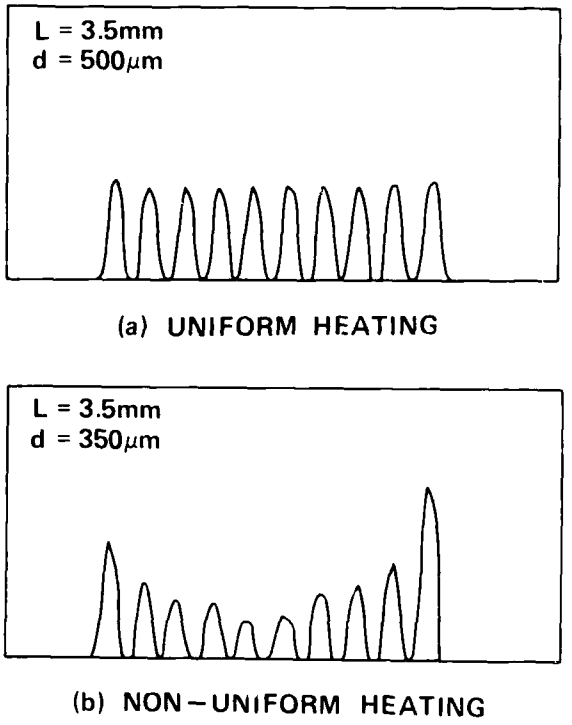

Figure 5. Brightness of 10-SM-fibers during electrical discharge.

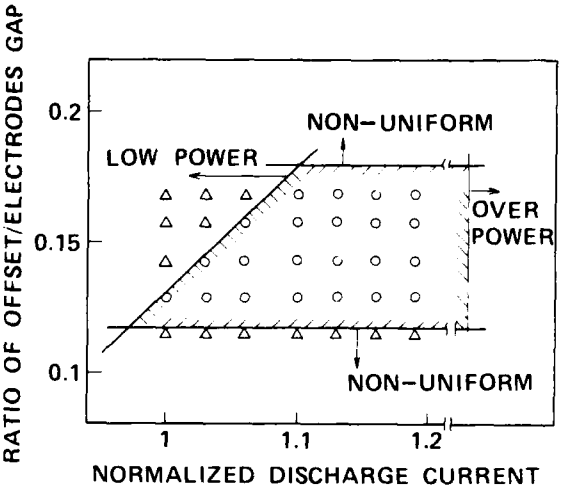

Figure 6. Relation between normalized discharge current and the ratio d/L.

Moreover, it was found that these offset and electrodes values are not only applicable to 10-SM-fiber ribbons but also easily applicable to fewer fiber ribbons, namely between 1 and 10-fiber ribbons, by controlling the discharge current.

2.2 Splicing Machine Construction and Performance

A mass-fusion splicing machine has been developed adopting a uniform heating condition. The machine is suitable for mono-coated fiber, 4-SM, 5-GI, 8-SM and 10-SM-fiber ribbon etc., by changing the pair of fiber holders and controlling the discharge current. Figure 7 shows the mass-fusion splicing machine, the coat stripper and the cutting tool. The conventional image processing procedures[1] for noting fiber end face variances are excluded from the splicing machine, because the end face variances are less than 10um which is small enough to attain low-loss splicing. Therefore, the splicing machine is simplified and miniaturized. The size of the machine is $170x110x140mm^3$.

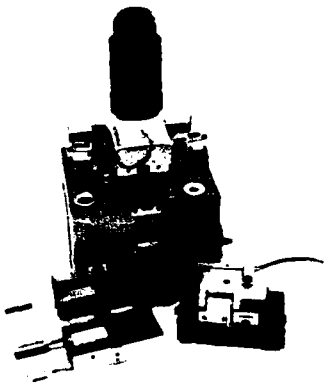

Figure 7. The mass-fusion splicing machine, the coat stripper and the cutting tool.

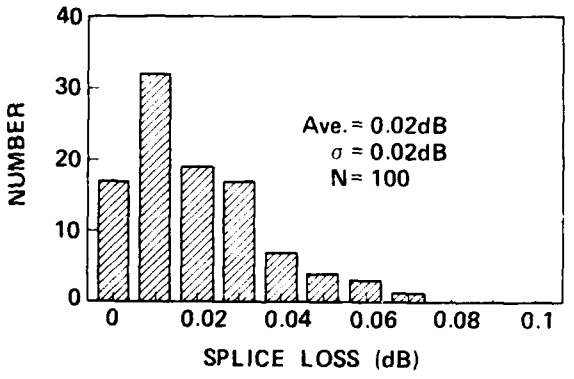

Figure 8. Splice loss distribution of one 10-SM-fiber ribbon under laboratory conditions.

Figure 8 shows the splice loss distribution of the one 10-SM-fiber ribbon under laboratory conditions. The average mode field diameter is 10um. An average splice loss of 0.02dB was achieved. In addition, average splice losses of 0.04dB and 0.02dB for 4-SM- and 8-SM-fiber ribbons respectively, were obtained. As far as we know, these are the lowest splice losses to be achieved, so far.

3. Multifiber Connector

3.1 Connector Structure

Figure 9 shows the structure of the multifiber connector for 10-SM-fiber ribbons. The connector consists of a pair of ferrules with a gum boot, two guide-pins and a clamp spring. At the ferrule end, ten fibers are positioned precisely between two guide-holes. The ferrules are aligned by the guide-pins and are held by the clamp spring. The component, made by a precision plastic molding technique suitable for mass production, has ten fiber-positioning holes with fiber-introducing guide grooves. This structure allows for easy ferrule construction. Ten bare fibers of a ribbon are inserted together into the corresponding fiber holes with the aid of the fiber-guide grooves and are fixed to the ferrule component using an adhesive. The component's dimensions are $7x3x8mm^3$. The fiber hole alignment error is less than 1um.

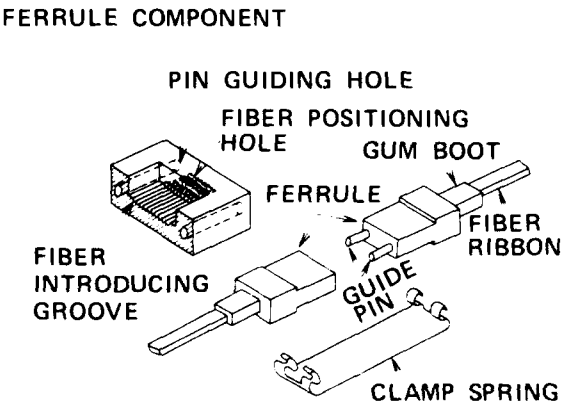

Figure 9. Structure of the multifiber connector for 10-SM-fiber ribbons.

To make ferrule construction easy in the field, a single type of ferrule with a one fiber hole diameter, which fits a specified maximum outer diameter of the fibers, should be used. Here, there is the problem of mis-alignment due to clearance between the fiber hole and the outer diameter of the fibers increasing, as illustrated in figure 10. It is important to suppress the mis-alignment due to clearance by utilizing the fiber centering effect of the adhesive[7], injected into the fiber hole for fixing the fiber. The adhesive material was investigated experimentally. Test ferrule components were formed using the same mold and were assembled with three types of fiber ribbons with difference in the fiber's outer diameter. The ribbons have 1.3um zero-dispersion 10-SM-fiber with a mode field diameter of 10um, a core-cladding eccentricity of less than 0.3um and an outer diameter variance of less than 1um per ribbon. The clearance between the fiber hole and the fiber's outer diameter was made to be 1, 2 and 4um. Two types of adhesives were used: (a) epoxy resin and (b) epoxy resin with glass fillers having an average outer diameter of 2um. Using the three types of fiber ribbons and two types of adhesives described above, the test ferrules were constructed. The test ferrules were connected to a reference ferrule, constructed with a clearance of 1um, and the connection losses were examined. Figure 11 shows the measured connection losses. The solid curves in figure 11 are the calculated probability[8], in which the fiber center is assumed to be located in a Gaussian distribution

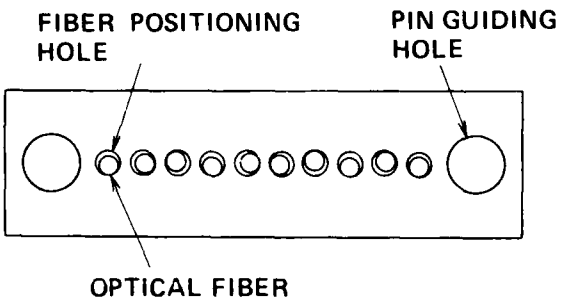

Figure 10. A cross-sectional view of a ferrule.

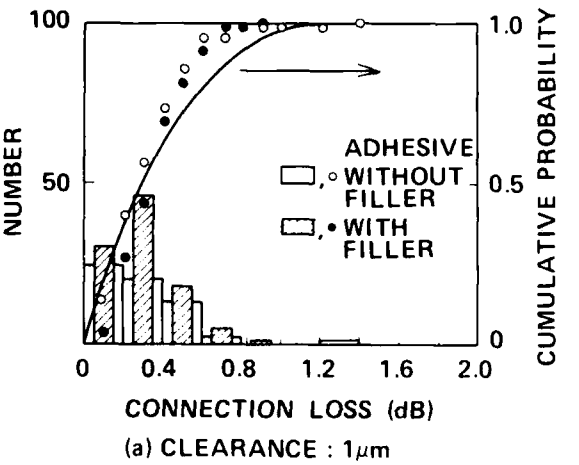

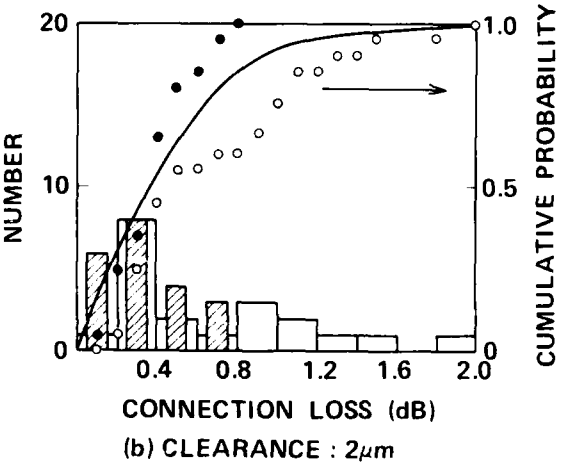

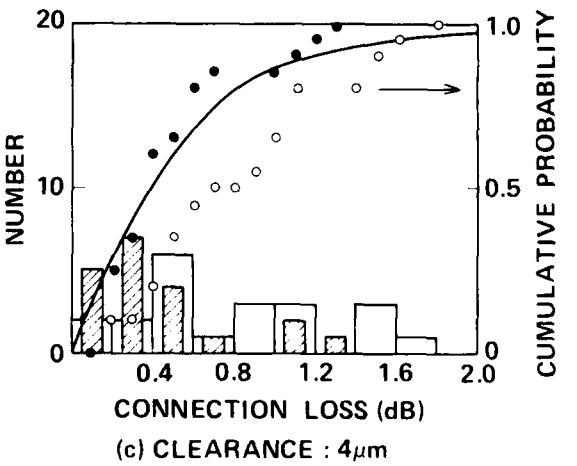

Figure 11. Connection loss distributions with clearance of 1um, 2um and 4um.

within the fiber hole with an alignment error of 1um. From figure 11, the fiber centering effect is found to be remarkable for the ferrules using glass filled epoxy resin. This is explained by the fact that glass fillers are filled round the clearance between the inner wall of the fiber hole and the fiber. Therefore, mis-alignment due to clearance was found to be suppressed using adhesive with fillers.

3.2 Connector Assembly and Performance

The assembling procedure for the multifiber connector is as follows:

(1) The coating of fiber-ribbon is removed by the stripper.

(2) The bare fiber ends are inserted into the ferrule fiber-holes filled with epoxy resin with glass fillers.

(3) The epoxy resin in the ferrule is heated for 10 minutes and is cured using a small heater capable of heating five ferrules at the same time. The heater's dimensions are $100x100x120mm^3$.

(4) The ferrule end is polished by a small polishing machine with dimensions of $120x120x150mm^3$. Three types of polishing sheets are used. It takes about 10 minutes to finish the polishing procedure.

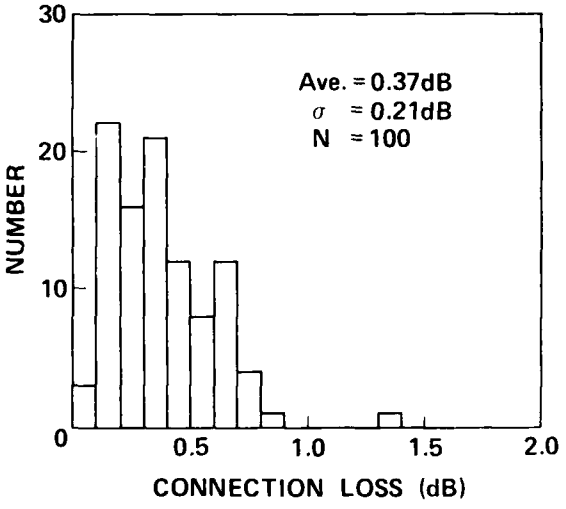

Figure 12. Connection loss distribution connected to a reference ferrule.

(5) Two ferrules are aligned by two guide pins and are held by a clamp spring. Index-matching material is used between the fiber end faces.

On the basis of the above procedure, the multifiber connectors were assembled with 10-SM-fiber ribbons in the laboratory. Assembly time was 20 minutes per ferrule. Figure 12 shows the connection loss distribution. The average connection loss was 0.37dB. Mechanical and environmental tests were also carried out. The test results are shown in Table 1. The results were found to be satisfactory.

Table 1. Results of mechanical and environmental tests for multifiber connector.

ITEMS	CONDITIONS	CHANGE OF CONNECTION LOSS
RE-CONNECTION	100 CYCLES	<0.2dB
VIBRATION	FREQUENCY : 10Hz AMPLITUDE : 10mmp.p. DIRECTION : X, Y, Z TIME : 2h FOR EACH DIRECTION	<0.1dB
HEAT-CYCLE	−30°C ~ +60°C 4h/CYCLE 10 CYCLES	<0.2dB
HUMIDITY	60°C, 90%RH Time : 100h	<0.2dB

4. Experimental Results in Field Tests

Mass-fusion splicing, using a coat stripper, a splicing machine, and a multifiber connector, have been evaluated in experimental field line tests. The experimental lines constructed of 10-SM-fiber ribbon cables, includes 100 fibers.

4.1 Mass-Fusion Splicing

As mentioned above, the splice loss of 0.02dB for same fiber ribbon has been obtained. On the other hand, splice loss may increase due to mode-

field diameter(MFD) variances, in the field. Figure 13 shows the splice loss between launched fiber whose MFD is 10.5um and tested fibers whose MFD is 8.5 to 10.5um. Splice loss increases as MFD variances grows. Therefore, the effect of this variance on the characteristic of mass-fusion splicing has been confirmed in the field.

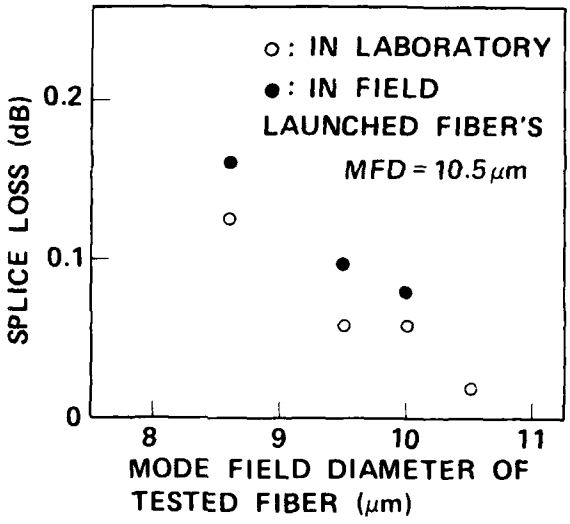

Figure 13. Splice loss between a launched fiber and tested fibers whose MFD is 8.5 to 10.5um.

Figure 14 shows the splice loss distribution. The average loss between different fibers was 0.11dB. This value is found to be highly practical in the construction of subscriber lines. But the value of 0.11dB is larger than that for the same fiber ribbon in the laboratory. It is thought that the MFD variances, human error and environmental conditions made splice loss larger.

Mis-splicing rates have also been noted; mis-strippings was 9%, mis-cuttings was 13%. The rate of mis-fusion however was 0%. The mis-stripping rate is one fifth smaller than that achieved by conventional tool, and the mis-fusion splicing rate completely vanishes, so that the total mis-splicing is significantly reduced. The splicing success rate of about 80% per one trial was achieved. Therefore, the length necessary to splice is shortened.

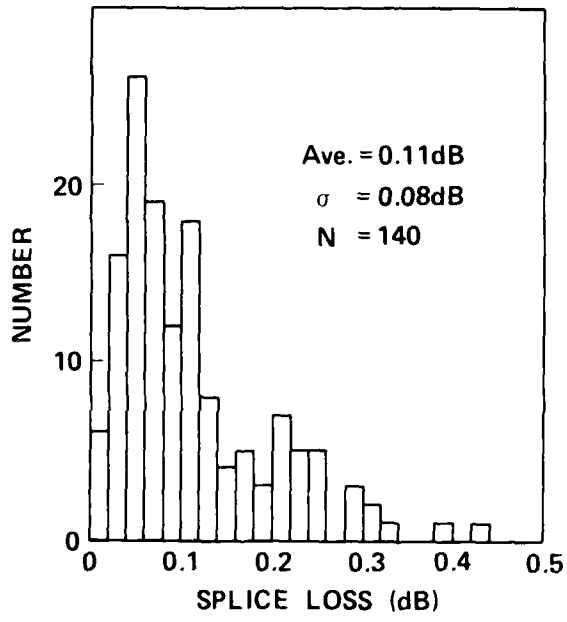

Figure 14. Splice loss distribution in field tests.

The total splicing time required for splicing a 10-SM-fiber ribbon in the field was 270sec, from start to finish. This means that the splicing time per fiber is only 27sec, which is extremely short for high-density multifiber optical cables.

Furthermore, the spliced portion of the fiber ribbon is reinforced by heat shrinkable tube.

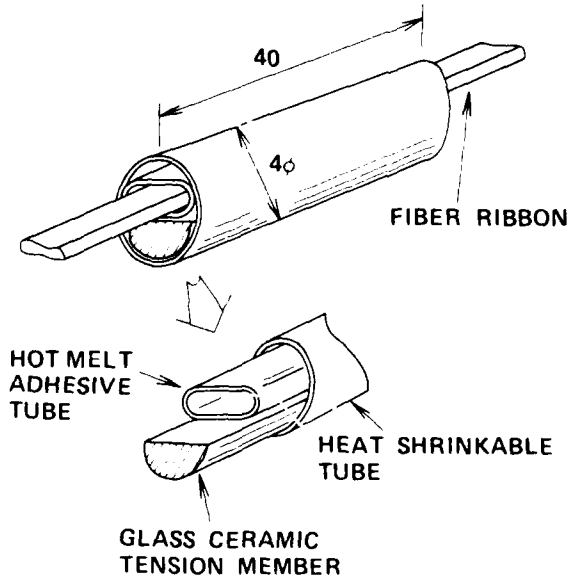

Figure 15. Construction of reinforced element.

Figure 15 shows the construction of the reinforcement element. A semi-cylindrical, glass ceramic tension member is used to depress a repeated thermal stress. No-loss-increase appears after reinforcement, and no-loss-change during the heat-cycle has been observed.

4.2 Connector

Performances of the multifiber connectors constructed in the factory and in the field have also been evaluated in the experimental lines. The factory-installed ferrules were applied to the pre-connectorized cables. The field installed ferrules were assembled by semi-skilled workers, with the cables in a manhole of the experimental lines. It took 20 minutes to assemble the ferrule, this was the same time as the indoor experiments. Figure 16 shows the 10-SM-fiber ribbon connection loss between the field- and the factory-installed ferrules. The average connection loss was 0.42dB. When the field-installed ferrules and the factory-installed ferrules were connected to a reference ferrule, the average losses were 0.38dB and 0.37dB, respectively. It was shown that the field-installed connector exhibited approximately the same loss as the factory-installed connector.

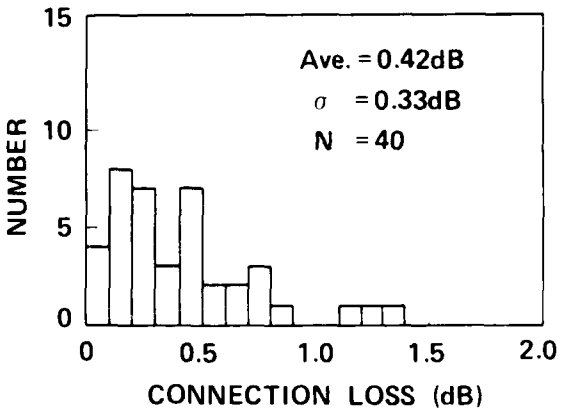

Figure 16. Connection loss between the field- and factory-installed ferrules in field tests.

5. Conclusion

Practical, low-loss and high-efficiency multifiber jointing techniques, a coat stripper, a mass-fusion splicer and a multifiber connector, have been developed.

(1)Mass-fusion splicing equipment, a stripper that can easily remove strongly bonded coat, small size mass-fusion splicing machine which can be used with 1 to 10-SM-fiber ribbon, have been developed. With this equipment, the average splice loss of 0.02dB for the same 10-SM-fiber ribbon in the laboratory and of 0.11dB for different ribbons in field trials have been achieved. Mis-splicing is significantly reduced, so that a success rate of 80% is attained after one trial. The splicing time was only 27sec per fiber.

(2)The multifiber connector, which has a self fiber centering effect due to the adhesion with glass fillers and precision plastic molding components, has been developed. So the multifiber connector is simplified and easily installed in the field. An average connection loss of 0.42dB for 10-SM-fiber ribbon has been obtained in field trials. It takes 20 minutes to assemble in the field.

As a result of the experimental line test, the mass-fusion splicing machine and the multifiber connector are found to be highly practical in field use.

ACKNOWLEDGMENT

The authors express their sincere appreciation to S. Takashima, H. Murata and I. Fuchigami for their helpful discussions and suggestions. Thanks are also due to N. Kawasaki and H. Furukawa for their valuable discussions and assistances.

REFERENCES

(1) Y.Kato, A.Ishizaki, I.Sano and S.Takashima: "Single-mode optical fiber ribbon splicer", Proceedings of 36th I.W.C.S., pp.386-391, (1987).

(2) T.Haibara, M.Matsumoto and M.Miyauchi: "Design and development of an automatic cutting tool for optical fibers", IEEE/OSA, J. Lightwave Technol., LT-4, pp.1434-1439, (1986).
(3) T.Haibara, M.Matsumoto, M.Miyauchi and M.Shirai: "Design of fiber-holder for optical fiber ribbon splice", Trans. IEICE, J70-C, pp.1164-1172, (1987).
(4) T.Satake, S.Nagasawa and R.Arioka: "A new type of demountable plastic-molded single-mode multifiber connector", IEEE/OSA, J. Lightwave Technol., LT-4, pp.1232-1236, (1986).
(5) T.Satake, N.Kashima and M.Oki: "Very small single-mode ten-fiber connector", IEEE/OSA, J. Lightwave Technol., LT-6, pp.269-272, (1988).
(6) M.Tachikura and N.Kashima: "Fusion mass splicing for optical fibers using high-frequency discharge", IEEE/OSA, J. Lightwave Technol., LT-2, pp.25-31, (1984).
(7) N.Kashima and T.Satake: "Relation between connection loss and single-mode optical fiber diameter in a multifiber connector", Trans. IEICE, E-70, pp.1120-1124 (1987).

Tadashi HAIBARA

Network Systems
Development Center,
NTT
Tokai, Ibaraki,
319-11, JAPAN

Tadashi Haibara is a Senior Engineer, belonging to the Fiber Optics Local Network Systems Project Group, in the Network Systems Development Center of NTT. He was born in 1955 and received his B.E. and M.E. degrees in precision engineering from Hokkaido University in 1979 and 1981, respectively.

He joined NTT in 1981. Since 1987 he has been in the Project Group where he has been engaged in the development of optical fiber splicing equipment. He is a member of IEICE of Japan, and received the 1987 Young Engineer Award from IEICE of Japan.

Shinji NAGASAWA

Network Systems
Development Center,
NTT
Tokai, Ibaraki,
319-11, JAPAN

Shinji Nagasawa is a Senior Engineer, belonging to the Fiber Optics Local Network Systems Project Group, in the Network Systems Development Center of NTT. He was born in 1950 and received his B.E. and M.E. degrees in electronics engineering from Chiba University in 1974 and 1976, respectively.

He joined NTT in 1976. Since 1987 he has been in the Project Group where he has been engaged in development of optical fiber connecting and splicing techniques. He is a member of IEICE of Japan.

Michito MATSUMOTO

Network Systems
Development Center,
NTT
Tokai, Ibaraki,
319-11, JAPAN

Michito Matsumoto is an Executive Engineer, belonging to the Fiber Optics Local Network Systems Project Group, in the Network Systems Development Center of NTT. He was born in 1952 and received his B.E. degree in electrical engineering from Kyusyu Institute of Technology. He received M.E. and Ph.D. degrees in electronics engineering from Kyusyu University in 1977 and 1987, respectively.

He joined NTT in 1977. Since 1987 he has been in the Project Group where he has been engaged in development of optical fiber splice technologies. Dr. Matsumoto is a member of IEICE of Japan.

Masaaki KAWASE

Network Systems
Development Center,
NTT
Tokai, Ibaraki,
319-11, JAPAN

Masaaki Kawase is an Executive Engineer, belonging to the Fiber Optics Local Network Systems Project Group, in the Network Systems Development Center of NTT. He received his B.E. and M.E. degrees in electrical engineering from Hokkaido University in 1970 and 1972, respectively.

He joined NTT in 1972. Since 1987 he has been in the Project Group where he has been engaged in development of subscriber optical transmission lines. He is a member of IEICE of Japan.

Field Measurements of Return Loss for Ferrule-Based Mechanical Splices

A. F. Judy, J. A. Aberson, G. F. DeVeau

AT&T Bell Laboratories
2000 Northeast Expressway, Norcross GA 30071

Abstract

Field OTDR measurements of installed ferrule-based splices have shown that typical return losses are below the cumulative fiber backscatter for transmission systems and hence should have no effect. Moreover they are large enough to be clearly seen on an OTDR thereby assisting in maintenance and restoration procedures through the ability to accurately locate splices. Similar measurements in the laboratory show that other splice return losses, even unmeasureably small ones, can be obtained through modifications to the present splice preparation methods.

1. Introduction

Ferrule-based mechanical splices can be designed to yield a wide range of return losses by varying the end preparation method and/or index matching gel.[1] While large reflections are not usually desirable, some customers also object to vanishingly small values because the inability to see them on an OTDR complicates fault locating procedures. Thus a logical design goal could be for the splice reflections to be large enough to see with an OTDR but small enough to negligibly impact even high-speed digital transmission systems. AT&T's Rotary Mechanical Splice is an example of this type of design, and results demonstrating its characteristics for field-installed systems will be shown and discussed. Other designs with lower (or higher) reflections could also be offered if needed. As an example, by using slightly different end-preparation methods, ferrule-based splices can be modified to achieve ultra-low reflections which may be appropriate for analog transmission systems. Some results illustrating this will be given also.

Regardless of the designed value of return loss, one must verify in the field that the desired values are attained. This is especially important when splices are installed in a high productivity mode where as many as 60 fiber splices a day are being made by a single splicing crew. This can be accomplished with commercial OTDRs using the following multi-step operation.

2. OTDR Return Loss Measurement Method

The OTDR transmits narrow pulses into a fiber and displays the reflected signal versus time or, equivalently, distance. If the distance between splices is larger than one half the OTDR's spatial pulse width, the splice reflections can be viewed separately from each other as shown in Figure 1. The return loss of the splices can in principle be determined by measuring the height of the reflections. However two complications occur. The first is that OTDRs only display a relative decibel scale so one can only measure the dB difference between two reflections. To get absolute readings one must generate a known reference reflection which the splice can be compared to. The most readily available reference is the Rayleigh backscatter from the fiber itself.

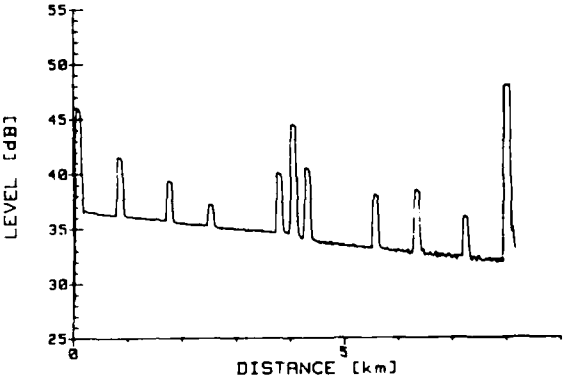

Figure 1. Typical OTDR Trace

At any point in the fiber its reflectance is:[2]

$$R_{bs} = \frac{v_g}{2} PW\, \alpha_s\, S \qquad (1)$$

where

v_g is the group velocity,

PW is the temporal pulse width of the equivalent rectangular pulse,

α_s is the fiber attenuation due to Rayleigh scattering, and

S is the proportion of backscatter that is captured by the fiber (which is a function of the fiber's spot size).

Defining the return loss as $RL = 10LOG_{10}(R)$, equation (1) shows the return loss due to backscatter (RL_{bs}) for nominal AT&T single-mode fiber to be -46.3 dB at 1.31 μm and -48.8 dB at 1.55 μm when $PW = 2\mu s$. The uncertainty in these numbers is typically a few tenths of a dB due to fiber parameter uncertainties. Note that RL_{bs} changes by -3 dB for every halving of the OTDR's pulse width. So if very narrow pulse widths are used, RL_{bs} can become too small to measure. In this case one could use as a reference the -14.7 dB Fresnel reflection from a 0° fiber end in air. This can also be used to check the RL_{bs} value.

The second complication is that even the difference between the fiber and splice reflections cannot be read directly from the OTDR. The reason is that the reflected power measured at the splice is the sum of the power backscattered from the fiber and the power reflected at the splice. (This is because the spatial width of the OTDR pulse is much wider than the splice so most of the pulse remains in the fiber while a portion is being reflected by the splice.) Thus the actual difference in decibels between the splice and fiber return loss (RL_{sp-bs}) is found from the measured difference ($RLmeas_{sp-bs}$) by:

$$RL_{sp-bs} = 10\, LOG_{10}\left(10^{(2 \cdot RLmeas_{sp-bs}/10)} - 1\right).$$

where the factor of 2 in the exponent is needed because most OTDRs display one-way loss, i.e. one-half of the measured round-trip loss. One then finds the return loss from the splice as:

$$RL_{sp} = RL_{sp-bs} + RL_{bs}.$$

For later use we also derive the equation for the backscatter that occurs when the input signal has a much wider duration than typical OTDR pulses. We begin by generalizing equation (1) to show the backscatter that occurs at the fiber's input due to a differential length, dz, of fiber that is a distance z from the input. If the input is a continuous wave signal, the reflectance will be equation (1) with an equivalent pulse width of $2dz/v_g$ and multiplied by the round-trip fiber attenuation:

$$R_{bs}(z) = dz\, \alpha_s\, S \exp^{-2\alpha z}.$$

When this is integrated over the entire length, L, one obains the cumulative reflectance:

$$R_{bs}^{cum} = \frac{\alpha_s}{2\alpha} S\left(1 - \exp^{-2\alpha L}\right).$$

For long fiber lengths the exponential term is negligible and the reflectance due to backscatter is :

$$R_{bs}^{cum} = \frac{\alpha_s}{2\alpha} S$$

which corresponds to return losses of about -31.6 dB at 1.3 μm and -31.7 dB at 1.5 μm. These are the cumulative return losses due to backscatter alone for a typical transmission system and represent a reasonable design goal for splices and connectors.

9. Field Measurement Procedure

For field tests on large numbers of splices, a computer controlled measurement is most convenient to use. This also allows disk storage of the data for later analysis or comparison. Normally we use an Anritsu OTDR (MW98A or MW910A) controlled by a HP 9826A computer using in-house software. Each splice and fiber is measured for loss and return loss using varied OTDR settings. The actual calculation of return loss usually requires combining multiple sweeps. First the entire cable will be measured with a high attenuation setting and a wide pulse width. This insures that the peak level is not clipped or distorted. Then the fiber backscatter will be measured at a lower attenuation (higher gain), with the splice reflections "masked", and at times

a narrower pulse. This ensures that the lower level backscatter signal will have minimum noise, will be free of "dead zone" distortion due to transients from preceeding reflections, and will be accurately measured between even closely spaced splices. Since these OTDRs cannot mask more than three splices on the screen, this last step alone requires numerous sweeps. The following results utilize all of the above techniques.

4. Typical Field Results

We report on two different routes that were installed by different operating companies. The first is a recently installed 48-fiber link connecting a RBOC central office to an AT&T Communications facility. It consisted of five *Lightpack®* cables and four outside plant cable splices. This installation used untuned, passively aligned (blind) Enhanced Rotary Mechanical Splices (ERMS) that were installed by the RBOC's craft.

The route's short length of 3.96 km allowed the connectors at the far end to be looped together enabling all 192 fiber splices to be measured bidirectionally from one end of the route. A comparison of the two opposite-directioned measurements on each of the 192 splices (Figure 2) shows the consistency of the measurement procedure. The root-mean-square difference is 1.6 dB for all the data and, more meaningfully, 0.8 dB for the splices greater than -45 dB.

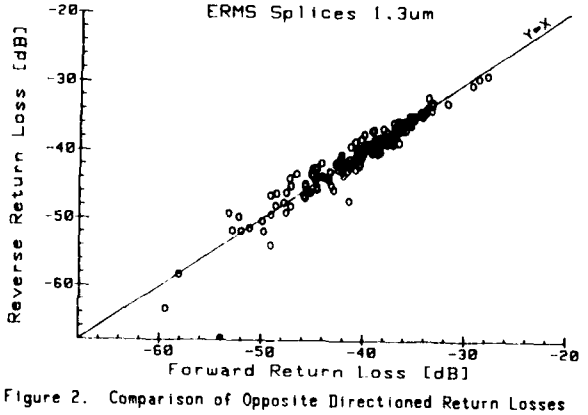

Figure 2. Comparison of Opposite Directioned Return Losses

Histograms of the splice return losses (Figures 3 and 4) show a mean value below -40 dB with a worst case value of -29 dB.

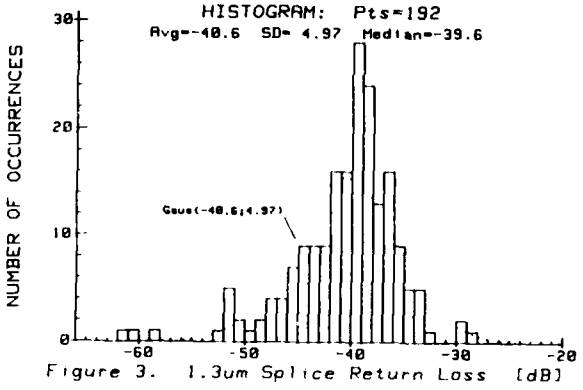

Figure 3. 1.3um Splice Return Loss [dB]

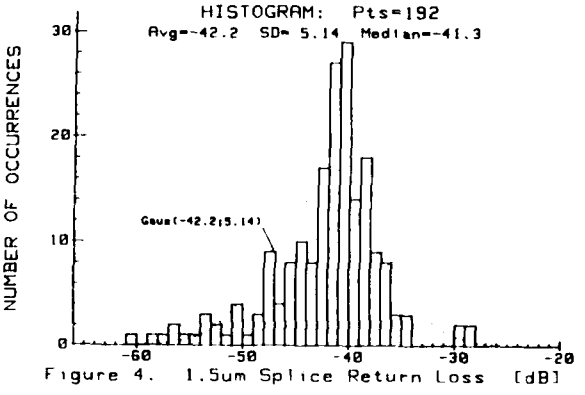

Figure 4. 1.5um Splice Return Loss [dB]

This worst case is not substantially different from the -31.6 dB cumulative fiber backscatter that a normal transmission system generates. Also it is interesting to note that while the statistics at the two wavelengths are similar, the 1.5-μm return loss is not perfectly correlated to the 1.3-μm (Figure 5). This is because the total

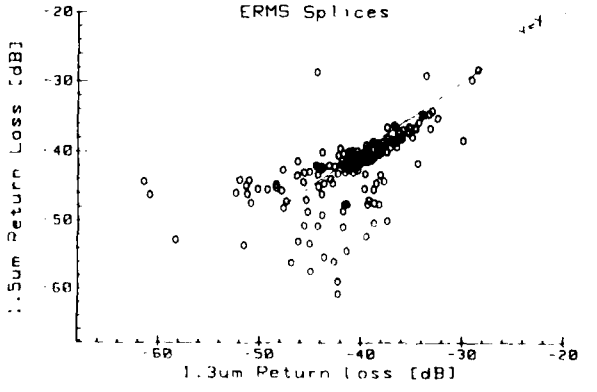

Figure 5. Comparison of Return Losses at Different Wave Lengths

reflection at a splice is the coherent sum of two reflections, one from each ferrule end. The small gap between the two ends will have slightly different phase shifts at different wavelengths resulting in differences in the coherent interference.

The second route is an 18-fiber *Lightpack* cable link installed by AT&T. It had 12 outside plant cable splices which were made with tuned, actively aligned ERMS for lowest loss. All 198 fiber splices were measured bidirectionally at 1.3 μm. Figure 6

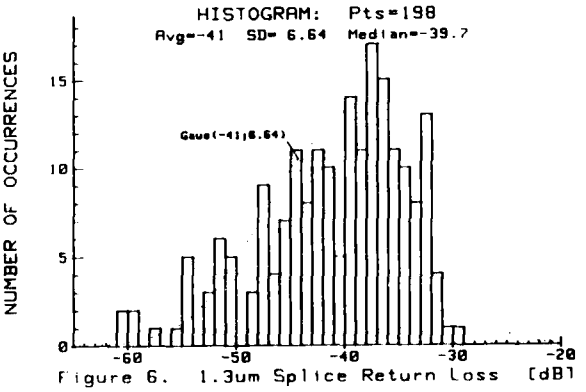

Figure 6. 1.3um Splice Return Loss [dB]

shows the return loss distribution for these tuned splices to be essentially identical to that of the untuned splices above.

5. *Experimental Results for Modified Ferrule-Based Splices*

As applications of fiber optics become more widespread and varied, special requirements on splice return losses may arise. Designers and maintainers of such new systems can still use ferrule splices; for, by simply choosing different end-face finishes, these splices can achieve virtually any return loss specified.

To illustrate, we present here laboratory results for two methods for changing the return loss characteristics of an ERMS. First, with only the substitution of a different polishing-paper material for the 0.3 μm paper now used on ERMS ferrules, the return losses shown in Figure 7 were

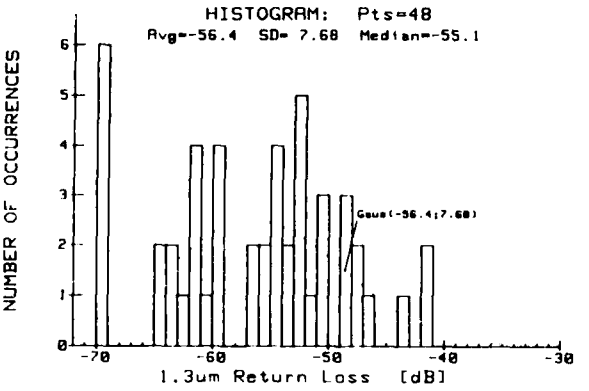

Figure 7. ERMS with Low Reflection Polish

obtained. For the 48 splices measured, the mean return loss is -56.4 dB (versus the -40 dB for the standard polish), with the worst being -41 dB (versus -29 dB previously). Of course other polishing materials could be found that will produce characteristically different results.

A second approach is to alter the standard 0° angle of the ferrule end-face. To study this, a polishing tool with a 10° wedge-angle was used with standard finishing materials to prepare ferrules. The reflections for the resulting splices were, like fusion splices, undetectable on the OTDR. Which is to say, return losses less than -70 dB can be obtained for the ERMS with 10° end-angles. And, because the pre-aligned features of the ERMS make its initial untuned configuration very close to its lowest-loss state, these angled splices are tunable and have proven to be environmentally stable for both splice loss and return loss.[3]

6. *Conclusions*

Field OTDR measurments of installed ferrule-based splices have shown that typical return losses are below the cumulative fiber backscatter and hence would not cause problems for transmission systems. Furthermore they are usually greater than the OTDR detected fiber backscatter and easily observed for accurate fault locating.

Also, two variations for end-face preparation show that ferrule splices can be tailored to

produce any level of return loss that is needed. No other splicing method has the capability to achieve such flexibility.

References

1. A. F. Judy and H. E. S. Neysmith, "Reflections from Polished Single Mode Fiber Ends", Fiber and Integrated Optics, Vol.7, No.1, pp17-26, 1988
2. E. Brinkmeyer, "Analysis of the Backscattering Method for Single-Mode Optical Fibers," J. Opt. Soc. Am., Vol.70, No.8, p.1010, August 1980
3. G. M. Alameel, J. B. Clayton, G. F. DeVeau, C. M. Miller, "Low Reflection Polish for Ferrule-based Mechanical Splices and Straight-tip Connectors", OFC '89, to be published.

Arthur F. Judy is a Distinguished Member of Technical Staff in the Lightguide Systems and Applications Engineering Group. In his 20 years at AT&T Bell Laboratories he has worked on the theory, modeling and measurement of various transmission media including coaxial, multi-pair and lightguide cable. He has BSEE and MSEE degrees from the University of Maryland.

George F. DeVeau is a Member of Technical Staff at AT&T Bell Laboratories, Norcross, Georgia. After joining Bell Laboratories in 1967 he was involved with multi-pair cable design and development. Since 1980, Mr. DeVeau has been engaged in the development of fiber optic splicing systems.

James A. Aberson has been at AT&T Bell Laboratories, Norcross, Georgia since 1980, where he has worked principally on analysis and design of fiber splicing methods and devices. Since 1986, he has been Supervisor of the Lightguide Joining Group which is responsible for all fiber splicing methods and recommendations for AT&T and its customers. He holds BS, MS and PH. D. degrees in Structures and Mechanics from North Carolina State University.

REDUCED MODE-FIELD DIAMETER SINGLE-MODE FIBER FOR SPECIALTY APPLICATIONS

Timothy C. Starkey
James W. Suggs

Corning Glass Works
Advanced Fiber Products

Fiber-optic technology has presented a unique opportunity to advance the science of tactical missiles. FOG-M and related programs have demonstrated the possibilities that exist in this area.

As payout speeds have increased, attenuation increases at the "peel point" bend have become a problem. Since bend sensitivity varies with mode-field diameter, the challenge is to reduce the mode-field diameter as much as possible, without adversely affecting other key parameters.

Corning's Advanced Fiber Products department has developed a small mode-field diameter single-mode fiber to address this concern. Bending loss tests have shown little or no increase in attenuation for bend diameters as small as 4.8 mm. This fiber offers advantages in the areas of small diameter cables and sensors as well. The high degree of bend-loss resistance could allow the use of fiber optics in more rugged environments than was previously feasible.

The design of a single-mode fiber is a tradeoff between attenuation, mode-field diameter and dispersion. All three of these parameters have an impact on a fiber's functionality and their relative impact depends on the application. For most telecommunication applications the following requirements typically apply: low attenuation to achieve the maximum distance between repeaters; mode-field diameter that offers the best tradeoff between spliceability, connectability and bend loss; and low dispersion at the operating wavelength to allow high bit-rate transmission.

These requirements have lead to a fiber with 1300 nm attenuation in the region of 0.35 dB/km to 0.40 dB/km, mode-field diameter in the range of 8.5 um to 10 um and a zero dispersion wavelength around 1310 nm. For maximum performance, dispersion-shifted fibers offer attenuation values at 1550 nm of 0.20 dB/km to 0.5 dB/km, mode-field diameters of 7.5 um to 9 um and a zero dispersion wavelength of approximately 1550 nm. This type of fiber offers the best overall performance of any commercially available fiber. As applications for optical fiber have become more demanding, the need has arisen for specialized fibers with higher performance in one or two of these areas. This can lead to performance tradeoffs in other areas, but depending on the application, this tradeoff may be appropriate.

Applications such as FOG-M, the fiber optic guided missile, rapidly deployable technical cable, fiber optic sensors and others have demonstrated the need for a fiber with enhanced resistance to bend induced attenuation increases. Bend diameters on the order of a few millimeters illustrate the potential severity of this requirement. Operation at 1550 nm creates an additional problem due to the wavelength dependence of macrobend attenuation. This is due to the increase in mode-field diameter with increasing wavelength.

Another area of recent interest is microcables. For specific applications it can be advantageous to decrease the size of the cable to a minimum. Reducing the protection afforded the fiber by the cable can increase the risk of bending loss. Smaller, more flexible cable can also be bent and kinked more easily and this can lead to a greater susceptibility to bending induced loss.

Many fiber optic sensor systems rely on coiled fiber. In particular, fiber optic hydrophones may use coils with many thousands of turns, resulting in an extremely bend intensive environment. To operate in this configuration fiber must have a high resistance to bend induced attenuation increases.

It has been demonstrated that mode-field diameter is the key to bending loss.[1] In order to significantly improve a fiber's bending performance, the mode-field diameter must be reduced. To do this while maintaining the cut-off wavelength in the region near the operating wavelength, the refractive index delta must be increased.

Corning's Advanced Fiber Products department has developed a step index single-mode fiber specifically for these specialized applications with a more highly doped core region and a smaller core diameter. The cut-off wavelength is maintained below 1300 nm, making operation at 1300 nm and 1550 nm possible. This results in a fiber with a mode-field diameter of approximately 6.5 to 7.0 um at 1550 nm and 6.0 um to 6.5 um at 1300 nm.

The attenuation values are approximately 0.6 dB/km at 1300 nm and 0.3 dB/km at 1550 nm. These attenuation rates are more than sufficient for the distances over which these fibers will be used.

As a result of the increased delta, the zero dispersion wavelength is shifted. Preliminary data indicate that it falls in the region of 1400 nm. This will still allow high data rate operation at 1300 nm and 1550 nm over length of several tens of kilometers. Narrow line width lasers can improve on this if necessary.

The attenuation and dispersion values of this fiber are such that this fiber would not be suitable for standard telecommunications applications. However, the bending performance is of primary importance. A variety of tests are possible depending on the application. Several tests have been performed on this fiber and each indicates excellent bend performance. With one turn wrapped on a 5 mm diameter mandrel, the 1300 nm and 1550 nm attenuation increases by less than 0.1 dB. 13,000 turns around a 1/2" diameter mandrel shows no increase at 1300 nm or 1550 nm. Standard fibers have attenuation increases of up to 50 dB/km in these same tests. Lateral load (sandpaper) tests show greatly improved performance over standard fibers as well.

Ordinarily, reducing the cladding and coating diameters of standard fibers causes the susceptibility to bend loss to increase. However, the excellent bend performance of this fiber can be utilized to create a reduced diameter fiber. The outside vapor deposition process used by Corning makes diameter changes very straight forward. By simply depositing less cladding material the diameter can be changed without any need to modify the core deposition process. For an experimental 80 um diameter fiber with a 135 um coating diameter, bending loss at 1550 nm is less than 0.2 dB for a 5 mm diameter bend. By comparison, fiber with an 80 um clad diameter and a typical dispersion shifted core design is dark at 1550 nm and has a 4.0 dB loss at 1300 nm under the same conditions. This indicates the magnitude of the improvement in the fiber.

While this fiber is a specialized product that is not suitable for traditional telephony applications, it does offer unique advantages in special applications. With this fiber, small diameter cables become more feasible. A variety of applications could benefit from this. Tethered vehicles need small, light weight cables, as do systems such as Ariadne. The excellent bending performance also allows the use of this fiber in tethered weapons and sensor systems where fiber has not previously been usable.

[1]Giroux et al. IWCS Proceedings 1986

OPTIMIZING POLYMER COATINGS FOR FIBER OPTIC ACOUSTIC SENSORS

N. Lagakos and J. A. Bucaro

Naval Research Laboratory
Washington, DC 20375

ABSTRACT

Polymers have been studied as coatings for single mode optical fibers used in interferometric acoustic sensors. Using the measured temperature and frequency dependence of the elastic moduli of polymers, coatings optimizing the fiber sensor response have been identified.

I. INTRODUCTION

Phase modulation of light in single mode fibers has been successfully utilized for detecting environmental changes such as pressure, magnetic and electric fields, acceleration, and temperature[1,2]. Suitable fiber coatings are used for different detections: polymeric jackets such as nylon or polyester for acoustic fields, magnetostrictive coatings such as Ni or met-glass for magnetic fields, piezoelectric materials such as PVF_2 for electric fields, and metals such as Ni or Al for temperature sensing. In each case, when a field is applied on the fiber it generates strains in the outer coating which are transferred to the fiber core causing phase modulation.

In this paper we consider the acoustic response of optical fibers in the low frequency or hydrostatic[3] regime. In this case the fiber coatings play a very important role in determining the fiber acoustic sensitivity. The necessary elastic moduli of many commercially available polymers were studied as a function of frequency ($10^2 - 10^4$ Hz) and temperature (0 - 35°C). Utilizing these results, polymers optimizing the fiber acoustic response have been identified.

II. ACOUSTIC SENSITIVITY OF FIBERS

A Mach-Zehnder interferometric sensor has been utilized to detect phase modulation in single mode fibers, and is shown schematically in Figure 1. Any phase modulation in the sensing fiber can be detected by comparing the phases in the sensing and reference fibers. Fiber couplers are used to split and recombine the light beams. The pressure sensitivity of the optical phase in a fiber is defined as $\Delta\phi/\Delta\phi P$ where $\Delta\phi$ is the shift in the phase ϕ due to a pressure change ΔP. If the given pressure change $\Delta\phi$ results in a fiber core axial strain ϵ_z and radial strain ϵ_r, then it can be shown that [4]

$$\frac{\Delta\phi}{\phi} = \epsilon_z - \frac{n^2}{2}[(P_{11} + P_{12})\epsilon_r + P_{12}\epsilon_z] \qquad (1)$$

Here P_{11} and P_{12} are the elastooptic coefficients of the core and n is its refractive index. The first term in (1) is the part of $\Delta\phi/\phi\Delta P$ which is due to the fiber length change, while the second and third terms are due to the refractive index modulation of the core, which is related to the photoelastic effect[4].

In order to calculate the sensitivity as given in Equation (1), the strains in the core ϵ_z and ϵ_r must be related to the properties of the fiber layers. The strains in a given layer are related to the stresses through the elastic moduli of that layer[5] while the displacements are expressed in terms of the strains. The constants involved in these calculations are found from the appropriate boundary conditions. The applied pressure is assumed to be hydrostatic[3]. Having calculated the various constants, the strains in the core are determined and the sensitivity is calculated using Equation (1)[6].

In general, the acoustic sensitivity is a very strong function of the elastic moduli of the outer hard polymeric coating of the fiber. High sensitivity can be achieved with coatings of low bulk modulus and high Young's modulus materials. This can be understood from the next two figures. Fig. 2 shows the acoustic sensitivity of a fiber as a function of coating thickness for different coating Young's moduli. All the other parameters of the fiber were kept constant. As can be seen from this figure, for thick coatings the sensitivity is determined by the bulk modulus which governs the fiber dimensional change. For typical fibers, however, both the bulk modulus and the Young's modulus are important. As can be seen from Fig. 3, high sensitivity requires low bulk modulus and high Young's modulus coatings. In this case, the bulk modulus determines the "maximum" fiber dimensional changes, while the Young's modulus governs the fraction of these changes, or strains, which can communicate to the fiber core.

The important role of the Young's modulus is also apparent from Fig. 4 where $\Delta\phi/(\phi\Delta P r^2)$ is shown as a function of thickness and Young's modulus of the coating. The bulk modulus was kept constant (2.5×10^{10} dyn/cm^2). As

can be seen from Fig. 4, even for small coating thickness a high Young's modulus results in high sensitivity since it can communicate high fraction of the applied stress to the fiber core, while low Young's modulus requires substantial coating thickness. Therefore, in designing a compact sensor, both bulk and Young's moduli are important.

III. POLYMERIC COATINGS

The elastic moduli of polymers required to predict the fiber acoustic sensitivity were studied as function of frequency and temperature.[7] The frequency and temperature dependence of the Young's modulus was obtained from measurements on bulk samples in the form of rods with diameter 1.5 - 3.5 cm and length 5 - 15 cm. The bulk modulus was considered to be frequency independent and was measured at only one convenient frequency (1 MHz).[7]

We have studied the elastic moduli of several commonly used thermoplastics, rubbers, and UV curable elastomers (which are listed in Table I) in the temperature range of 0 - 35° C for frequencies 10^2 to 10^4 Hz and 1 MHz which can be found in Ref. 7. The Young's and the bulk moduli measured experimentally at 1 MHz at three temperatures. The least Young's modulus variation was obtained with Rexolite (19), polystyryne (17, 18), polyvinyl chloride (21), Noryl (10), polysulfone (20), nylon (5, 6), and acrylic (9). The least bulk modulus dependence is found in polystyryne (17, 18), Rexolite (19), polysulfone (20), acrylic (9), Noryl (10), polyvinyl chloride (21), and nylon (5).

In order to obtain the frequency dependence of the elastic moduli of the polymers, the frequency dependence of the Young's modulus was studied in the range of 10^2 - 10^4 Hz at three different temperatures assuming the bulk modulus to be frequency independent. It was found that away from any transitions the Young's modulus is proportional to log of frequency, i.e. $E=A\log_{10}F+B$. The coefficients A and B of the best linear fit are listed in Ref. 7. It was found that the used equation describes well the Young's modulus in most polymers in the frequency range of 10^2 - 10^4 Hz.

In general, as it was expected, the Young's modulus decreases as temperature increases or as frequency decreases. Similarly, the bulk modulus decreases as temperature increases. The least temperature and frequency variation was obtained with Rexolite (19), polystyrene (17, 18), Noryl (10), polycarbonate (14), polysulfone (20), and nylon (6).

Using the hydrostatic analysis the acoustic sensitivity of fibers coated with various polymers was obtained from the bulk and Young's moduli listed in Ref. 7. In these calculations, the fiber o.d. was taken to be 0.35 mm, a "thin" fiber, 1 mm, as used in the tested sensors, and 4 mm, a "thick" coating case. The results of these calculations are listed in Table I. As can be seen from this Table, for fibers with thick coatings maximum sensitivity is obtained with Polyurethane Conap (29) and Uralite 3130 (30), and Teflon TFE II (1) due to their low bulk modulus. For fibers with typical thickness coatings, however, maximum sensitivity is obtained with polystyrenes (17, 18) and Rexolite (19) due primarily to their high Young's modulus, and with Teflon TFE (1,2). The smallest temperature and frequency dependence is obtained with polystyrene (18), polyvinyl chloride (21), Lucite (9), and Noryl (10). Small dependence is also obtained with Delrin (7) and Zytel (101). On the other hand, high dependence is obtained with the soft UV curable elastomers due to the large frequency and temperature dependence of their Young's modulus.

Table II, column 1, lists the most promising polymers as fiber coatings for interferometric sensors. The second column shows the calculated acoustic sensitivity of single mode fibers coated with these polymers up to 1 mm o.d. The third column shows the overall variation of the acoustic sensitivity in the temperature range of 0R - 35° C and for frequencies 10^2 - 10^4 Hz. The fourth and fifth columns show the predicted minimum detectable pressure when the reference fiber of the interferometric sensor is coated with a 0.35 mm o.d. nylon (Zytel 101) and a 110 o.d. aluminum, respectively. In these calculations it is assumed that the sensing fiber is 30m and the minimum detectable phase modulation is 10^{-6} radians.

From Table II we can see that the highest sensitivity is obtained with TFE (due primarily to its low bulk modulus) with, however, significant temperature and frequency variation. The second highest sensitivity is obtained with polystyrene (due to its high Young's modulus) with very small temperature and frequency variation. Rexolite (a cross linked styrene polymer) and TFA-340 give also high sensitivity and very small variation. Noryl gives high sensitivity and very small variation, and nylon gives small sensitivity (due to its high bulk modulus) and the smallest temperature and frequency variation. In general, good sensitivity is obtained with all Teflons as a result of their small bulk modulus.

Some of the most promising polymers have been used as fiber coatings in Fig. 5 which shows the acoustic sensitivity of four fibers coated with different coatings. For thick fiber coatings, high sensitivity is obtained with Teflon TFE and Teflon FEP 100 due to their low bulk modulus. For lower coating thickness, Noryl results in higher sensitivity due to its intermediate bulk modulus and high Young's modulus.

IV. CONCLUSION

The low frequency acoustic sensitivity of optical fibers has been reviewed and has been found to strongly depend on the elastic moduli of the fiber coatings. The elastic moduli necessary to predict the sensitivity have been studied as a function of frequency and temperature and polymers optimizing the fiber acoustic response have been identified.

REFERENCES

1. T. G. Giallorenzi, J. A. Bucaro, A. Dandridge, G. H. Sigel, J. H. Cole, S. C. Rashleigh, and R. G. Priest, IEEE J. Q. Elect., QE-18, 626 (1982).
2. J. A. Bucaro, N. Lagakos, J. H. Cole, and T. G. Giallorenzi, Physical Acoustics, 16 (Academic, New York, 1982) p. 385
3. R. Hughes and J. Jarzynski, vol XVI (Academic, New York, 1982, p. 385) Appl. Opt., 19, pp 98-197, 1980.
4. B. Budiansky, D. C. Drucker, G. S. Kino, and J. R. Rice, Appl. Opt. 18, 4085 (1979).
5. J. F. Nye, Physical Properties of Crystals. Oxford, 1976.
6. N. Lagakos and J. A. Bucaro, Appl. Opt., 20, pp 2716-2720, 1981.
7. N. Lagakos, J. Jarzynski, J. H. Cole, and J. A. Bucaro, J. Appl Phys. 59, 4017 (1986).

TABLE 1

ACOUSTIC SENSITIVITY OF FIBERS COATED WITH VARIOUS ELASTOMERS

$\Delta\phi/\phi\Delta P$ $(10^{12}(dyn/cm^2)$

POLYMER	TEMP °C	TYPICAL FIBERS (o.d.: 0.38mm) Frequency (Hz)			TOTAL YR.	FIBER (o.d.: 1mm) Frequency (Hz)			TOTAL YR.	FIBER (o.d.: 4mm) Frequency (Hz)			TOTAL YR.
		10^2	10^3	10^4	%	10^2	10^3	10^4	%	10^2	10^3	10^4	%
1) TEFLON TFE TYPE II	0	1.69	1.72	1.74	39	6.23	6.25	6.27	16	8.38	8.37	8.35	15
	23	1.36	1.48	1.60		6.10	6.33	6.56		9.31	9.34	9.36	
	35	1.06	1.17	1.27		5.88		6.09		9.81	9.84	9.86	
2) TEFLON TFE type I	0	1.99	2.18	2.37	51	5.62	5.79	5.80	10	6.79	6.81	6.83	15
	27	1.76	2.94	3.31		5.99	6.12	6.25		7.77	7.78	7.78	
	35	1.60	1.89	1.77		5.86	5.97	6.09		7.87	7.91	7.95	
3) TEFLON FEP 100	0	0.98	1.07	1.16	17	4.87	4.99	4.71	19	6.73	6.81	6.88	19
	23	1.08	1.13	1.18		4.99	5.09	5.19		8.04	8.01	7.97	
	35	1.11	1.14	1.17		5.12	5.21	5.29		8.28	8.31	8.33	
4) TEFZEL 280	0	1.43	1.50	1.57	12	4.43	4.52	4.60	15	5.59	5.63	5.67	17
	24	1.47	1.52	1.56		5.00	5.06	5.09		6.56	6.58	6.50	
	35	1.38	1.48	1.57		4.91	5.06	5.20		6.89	6.66	6.73	
5) ZYTEL 101	0	1.79	1.83	1.86	11	3.48	3.61	3.64	6	3.84	3.86	3.87	8
	22	1.77	1.80	1.83		3.65	3.66	3.66		4.07	4.06	4.04	
	35	1.66	1.69	1.71		3.64	3.68	3.72		4.17	4.18	4.19	
6) ZYTEL	0	1.66	1.69	1.71	9	3.33	3.35	3.36	10	3.70	3.70	3.70	10
	22	1.78	1.80	1.82		3.66	3.68	3.70		4.08	3.10	4.11	
	35	1.73	1.75	1.77		3.63	3.64	3.66		4.07	4.07	4.07	
7) DELRIN 150	0	1.96	1.95	1.94	9	3.88	3.87	3.86	9	3.89	3.88	3.87	10
	22	1.97	1.99	2.00		3.89	3.90	3.90		4.30	4.30	4.29	
	35	1.83	1.86	1.87		3.76	3.77	3.77		4.17	4.17	4.17	
8) DELRIN 107	0	1.83	1.89	1.95	17	3.44	3.49	3.52	12	3.78	3.80	3.82	12
	22	1.98	2.02	2.06		3.89	3.91	3.93		4.29	4.30	4.31	
	35	1.71	1.76	1.80		3.50	3.52	3.54		3.91	3.91	3.91	
9) LUCITE	0	2.45	2.50	2.56	36	3.67	3.73	3.78	14	3.97	3.97	3.96	8
	24	2.39	2.54	2.68		3.97	4.01	4.05		4.24	4.25	4.25	
	35	1.71	1.76	1.80		3.50	3.52	3.54		3.91	3.91	3.91	
10) NORYL	0	2.24	2.27	2.29	6	5.18	5.20	5.22	8	5.91	5.92	5.93	8
	22	2.36	2.39	2.41		5.59	5.60	5.61		6.42	6.41	6.40	
	35	2.31	2.34	2.37		5.55	5.59	5.62		6.39	6.42	6.45	

TABLE I (Continued)

ACOUSTIC SENSITIVITY OF FIBERS COATED WITH VARIOUS ELASTOMERS

$\Delta\phi/\phi\Delta P$ $(10^{-12}dyn/cm^2)$

POLYMER	TEMP °C	TYPICAL FIBERS (o.d.: 0.35mm) Frequency (Hz) 10^2	10^3	10^4	TOTAL VAR. %	FIBER (o.d.: 1mm) Frequency (Hz) 10^2	10^3	10^4	TOTAL VAR. %	FIBER (o.d.: 4mm) Frequency (Hz) 10^2	10^3	10^4	TOTAL VAR. %
11) POLYETHYLENE (Low Density)	0	1.87	1.87	1.87	18	5.21	5.21	5.21	4	6.29	6.29	6.29	10
	22	1.65	1.70	1.75		5.22	5.36	5.45		6.60		6.58	
	35	1.54	1.60	1.65		5.27	5.36	5.45		6.90	6.96	7.01	
12) POLYETHYLENE (Low Density)	0	1.13	1.23	1.33	43	4.32	4.48	4.66	22	6.14	6.16	6.18	26
	22	1.07	1.18	1.29		5.04	5.29	5.54		8.33	8.32	8.31	
	35	1.72	1.81	1.89		5.03	5.11	5.18		6.18	6.20	6.22	
13) POLYETHYLENE (High Density)	0	1.93	2.01	2.08	18	4.66	4.71	4.75	10	5.39	5.40	5.41	13
	22	1.71	1.78	1.85		4.75	4.81	4.86		5.74	5.75	5.76	
	35	1.72	1.81	1.89		5.03	5.11	5.18		6.18	6.20	6.22	
14) POLYCARBONATE	0	1.83	1.83	1.83	6	4.36	4.36	4.36	11	5.04	5.04	5.04	12
	22	1.86	1.85	1.84		4.38	4.49	4.59		5.04	5.21	5.37	
	35	1.88	1.92	1.96		4.59	4.75	4.90		5.33	5.53	5.73	
15) POLYPROPYLENE 6823	0	2.38	2.52	2.66	43	4.69	4.75	4.80	12	5.16	5.18	5.20	16
	22	1.59	1.55	1.52		4.59	4.77	4.94		5.63	5.64	5.64	
	35	2.13	2.05	1.97		4.80	5.00	5.20		6.08	6.12	6.17	
16) POLYPROPYLENE 7823	0	2.25	2.36	2.47	49	4.95	4.99	5.03	13	5.59	5.59	5.58	18
	27	1.36	1.48	1.59		4.76	4.98	5.20		6.35	6.37	6.38	
	35	1.25	1.52	1.78		4.80	5.14	5.48		6.73	6.79	6.84	
17) POLYSTYRENE	0	2.91	2.92	2.92	2	5.61	5.60	5.59	5	6.13	6.13	6.12	5
	25	2.91	2.94	2.97		5.73	5.75	5.76		6.30	6.30	6.30	
	35	2.93	2.95	2.97		5.85	5.87	5.88		6.44	6.45	6.46	
18) POLYSTYRENE	0	2.77	2.79	2.81	7	5.79	5.74	5.68	5	6.43	6.36	6.28	6
	22	2.87	2.90	2.92		5.94	5.96	5.98		6.59	6.61	6.62	
	35	2.84	2.98	2.91		6.00	6.02	6.04		6.70	6.70	6.70	
19) REXOLITE	0	2.77	2.79	2.81	5	5.60	5.61	5.61	5	6.19	6.19	6.18	6
	22	2.84	2.88	2.91		5.85	5.88	5.90		6.49	6.51	6.52	
	35	2.85	2.87	2.88		5.91	5.92	5.92		6.57	6.57	6.56	
20) POLYSULFONE	0	1.74		1.84	10	4.18		4.19	7	4.80		4.79	6
	22	1.84		1.89		4.32		4.33		4.98		4.94	
	35	1.88		1.91		4.41		4.46		5.07		5.11	

TABLE I (Continued)

ACOUSTIC SENSITIVITY OF FIBERS COATED WITH VARIOUS ELASTOMERS

$\Delta\phi/\phi\Delta P$ $(10^{-12}(dyn/cm^2)$

POLYMER	TEMP °C	TYPICAL FIBERS (o.d.: 0.35mm) Frequency (Hz) 10^2	10^3	10^4	TOTAL VAR. %	FIBER (o.d.: 1mm) Frequency (Hz) 10^2	10^3	10^4	TOTAL VAR. %	FIBER (o.d.: 4mm) Frequency (Hz) 10^2	10^3	10^4	TOTAL VAR. %
21) POLYVINYL CHLORIDE	0	2.07		2.16	9	3.94		3.97	7	4.31		4.32	9
	22	2.16		2.25		4.13		4.17		4.52		4.53	
	35	2.03		2.22		4.18		4.25		4.65		4.66	
22) HYTREL 7246	0	1.49		1.52	37	3.97		4.00	9	4.76		4.76	16
	22	1.12		1.14		3.93		4.22		5.33		5.39	
	35	0.96		1.17		3.82		4.16		5.66		5.65	
23) HYTREL 6346	0	1.03		1.34	43	3.49		3.82	17	4.70		4.70	9
	24	0.76		1.01		3.18		3.69		5.19		5.18	
	0												
24) HYTREL 5556	0	3.12				6.41				7.11			
	23												
	35												
29) POLYURETHANE CORIM	0	3.27		4.59	59	8.43		8.93	25	9.82		9.76	15
	22	1.48		1.83		6.72		7.38		10.28		10.33	
	35	1.43		1.77		7.05		7.82		11.45		11.52	
30) POLYURETHANE 3130	0	1.98		2.98	72	5.84		6.48	31	7.16		7.27	26
	22	1.05		1.63		5.20		6.49		8.94		9.11	
	35	0.83		1.29		4.46		6.06		9.31		9.66	
31) POLYURETHANE 1592	0	3.84		5.17	45	6.20		6.47	16	6.56		6.61	46
	22	2.92		4.09		6.58		7.01		7.44		7.50	
	35	4.46		2.84		9.82		7.43		12.08		8.17	

TABLE II

OPTIMIZED COATINGS

	$(10^{-12}/dyn/cm^2)$	Temp. and Frequency Variation %	P_{min} (Ref. Fiber: Nylon: 0.35 mm o.d. dB ref 1 Pa	P_{min} (Ref. Fiber: Al, 110 m o.d. dB ref. 1 Pa
TEFLON 1 TFE	6.13	15	37.2	34.3
POLYSTYRENE	5.96	5	37.5	34.5
REXOLITE	5.87	5	37.7	34.7
TEFLON TFA-340	5.87	6	37.7	34.7
HDRYL	5.59	4	38.3	35.1
POLYETHYLENE (Low Density)	5.26	6	39.1	35.1
TEFLON FEP 100	5.12	18	39.5	35.9
TEFZEL 280	5.05	13	39.6	36.0
POLYETHYLENE (High Density)	4.79	9	40.4	36.5
POLYPROPYLENE 6823	4.79	16	40.4	36.5
HYTREL 7246	4.09	16	42.7	37.9
NYLON 101	3.65	3	44.6	38.9

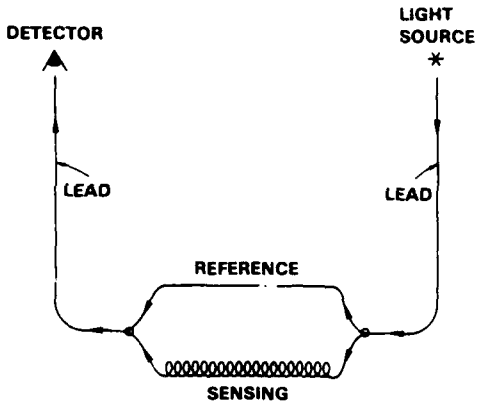

Figure 1. Fiber Optic Interferometric (Mach-Zehnder) Sensor

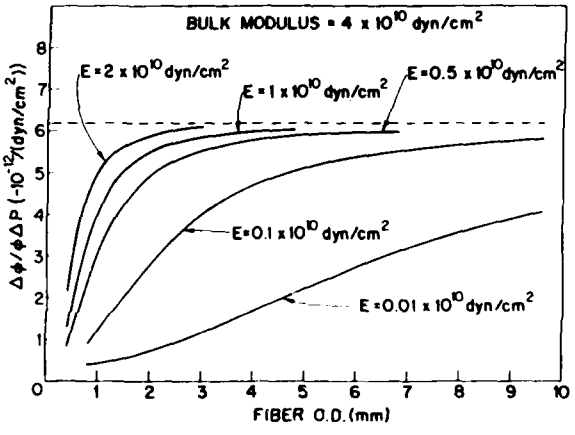

Figure 2. Calculated Acoustic Sensitivity vs Fiber Outer Diameter for Different Young's Moduli of the Outer Coating. (bulk modulus: 4 X 1010 dyn/cm2)

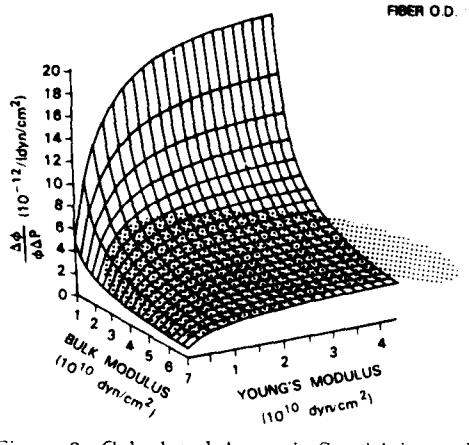

Figure 3. Calculated Acoustic Sensitivity vs Bulk and Young's Moduli of the Fiber Outer Coating

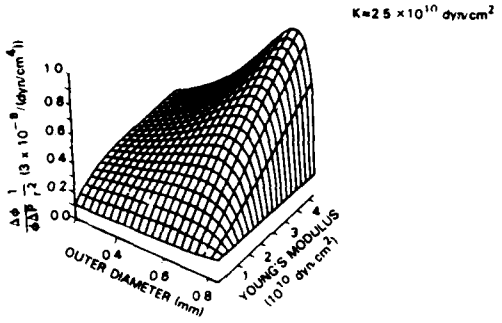

Figure 4. Acoustic sensitivity per Fiber Cross-Section vs Coating Young's Modulus and Fiber Outer Diameter.

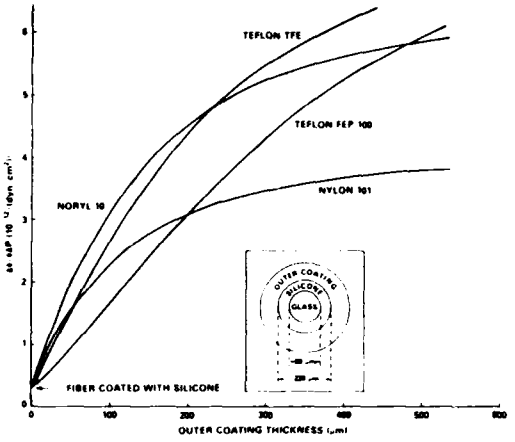

Figure 5. Calculated low Frequency Acoustic Sensitivity of Fibers with Different Outer Coatings.

A FIBER OPTIC CABLE FOR MILITARY INSTALLATIONS

J. D. Fridman, The MITRE Corporation, Bedford, MA, U.S.A.
A. Goffin, MOD Belgium, Brussels, Belgium

Abstract

An all dielectric fiber optic cable for underground installations has been developed for application in military communication networks. The cable was designed to withstand rigorous military environmental and operational specifications. The performance of the cable was tested relative to characteristics of the optical fibers to preserve stated attenuation and bandwidth margins. Cables were retested in laboratory link length simulation tests and after final installation in the network. Field tests were also performed to establish the vulnerability of the cable to explosive charges.

Introduction

Fiber optic cables used in underground installations are available world-wide from various manufacturers. They are usually designed and fabricated for commercial system applications, in which adherence to strict military standard specifications for their environmental or operational performance is not a requirement. Furthermore, most of these cable configurations use metallic shields or metallic wire rods to reinforce their structure. Therefore, they are sensitive to the coupling of high intensity electric fields or to their detection when installed within trenches.

Since available commercial cables did not fulfill a specified need, it was found necessary to develop an underground fiber optic cable subject to military environmental conditions. The cable was specified to be of all dielectric construction with dual wavelength optimized fibers, designed to withstand rigorous military standard performance tests. The performance of the cable was tested relative to characteristics of the optical fibers to preserve specific attenuation and bandwidth margins. After field installation the cable was retested to confirm and compare its actual performance against laboratory tests. This paper describes the design and tested performance of the fiber optic cable, developed for the first time to withstand the harsh environment created by military engagements.

Description of Cable

A photograph of the fiber optic cable is shown in figure 1. A cross section of the cable construction and the disposition of the fibers, fillers, reinforcing elements, Kevlar strands, and outer jacket are shown in figure 2.

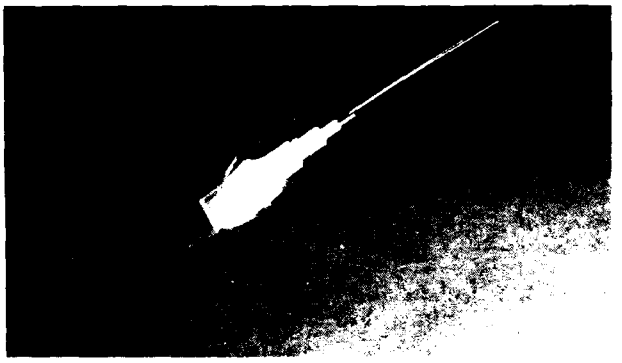

Figure 1. Cable With Four Fibers

The cable has the following characteristics:

Number of fibers	4 or 6
Outer diameter, D	12 mm
Bending radius	20 X D = 24 cm
Weight	0.140 kg/m
Pulling force	150 kg
Available lengths	1050 m and 2250 m

Fibers used in the construction of the cable are optimized for dual wavelength operation, and their characteristics are as follows:

Type	Graded Index
Core/cladding diameter	50 ± 3/125 μm multimode

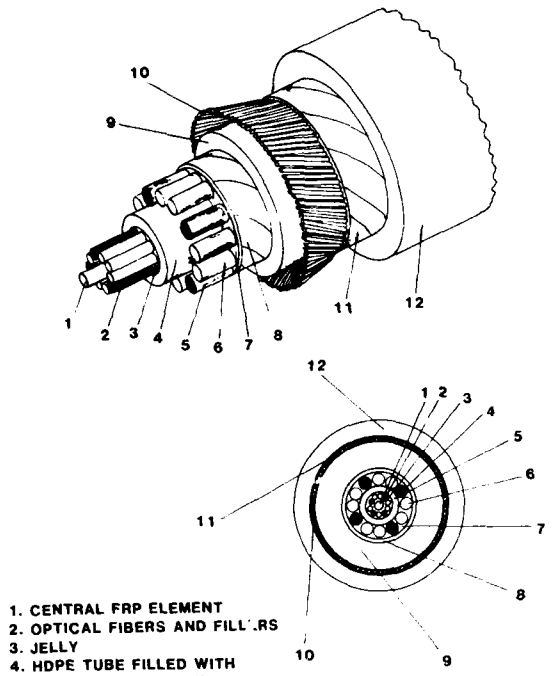

Figure 2. All Dielectric Underground Fiber Optic Cable

Buffer diameter	Double coated with acrylate at 325 or 500 μm
Attenuation	2.5 ± 0.2 dB/km at 850 nm; 1.0 ± 0.2 dB/km at 1300 nm
Bandwidth	400 MHz•km at 850 and 1300 nm
Numerical aperture	0.20 ± 0.015

Fibers are color coded in red, yellow, white, and black for the four-fiber cable, with blue and green added for the six-fiber cable. The cable has been designed and manufactured to incorporate all dielectric elements to reinforce the structure of its fiber optic core. A central dielectric element provides stiffness for optical fibers and plastic fillers in a tube filled with polybutane jelly. Four reinforcing elements and plastic fillers interspersed with jelly are then built around the tube containing the optical fibers. These structural elements are in turn wrapped with polypropylene tapes and a tight fitting plastic tube to hold the whole configuration together. The final outer structure of the cable is then made up of a layer of Kevlar strands for tensile load reinforcement and a PVC outer jacket to complement the cable construction.

The cable is specified to withstand a variety of applied mechanical loads such as flexing, compressive impact, tensile loading, and twisting with the proviso that any one of the optical fibers not increase attenuation by more than 0.5 dB/km. Cable performance has been defined over a -25°C to +50°C temperature range relative to an optical fiber attenuation change not to exceed 0.2 dB/km. In addition, the cable is specified to be made up of materials that have flame retardant characteristics. For instance, when set aflame, the cable must be self-extinguishing with a burning time not to exceed 30 seconds, over a distance less than its outer circumference. All tests and procedures to characterize the properties of the cable have been performed under the United States Department of Defense Military Standard 1678 (DOD-MIL-STD-1678), Fiber Optic Test Methods and Instrumentation.

Test Measurements

Cable Tests

The manufacturer systematically performed core and cladding geometry and attenuation and bandwidth test measurements on all optical fibers. Forty 1-km cables of four and six fibers were systematically tested for their attenuation characteristics at 850, 905, 1060, and 1300 nm. Results are illustrated in figure 3: an attenuation curve typical of

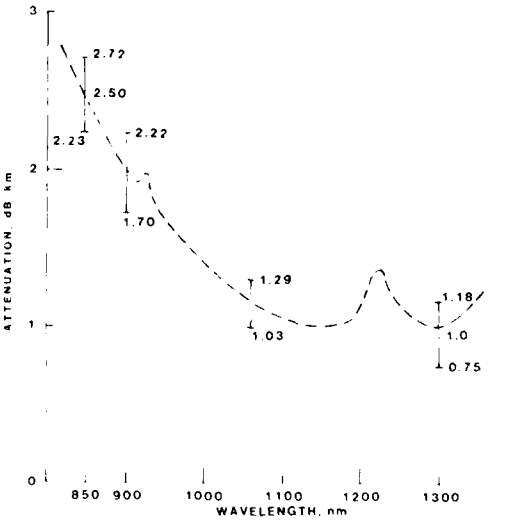

Figure 3. Cable Attenuation Measurements

such fibers is indicated (dashed line), and the spread of measured data shown. Most attenuation measurements are clustered around 1.0 ± 0.2 dB/km at 1300 nm and 2.5 ± 0.2 dB/km at 850 nm, thus meeting the specifications.

One may characterize dispersion effects in fibers by measuring the impulse response of the fiber in the time domain or the baseband frequency response in the frequency domain. Impulse response measurements were performed on all the optical fibers supplied by the manufacturer. Results obtained at 850 and 1300 nm showed a wide range of bandwidths extending from 1600 MHz·km to 400 MHz·km, with a mean of 780 MHz·km at 850 nm and 920 MHz·km at 1300 nm.

The next series of test measurements were performed on the fiber optic cables for their thermal, mechanical, and environmental characteristics. Tests were conducted over the -25°C to +50°C range at 850 nm and 1300 nm. Results obtained, shown in figure 4, indicate that the variation in the optical fiber attenuation was less than 0.2 dB/km over the full temperature range.

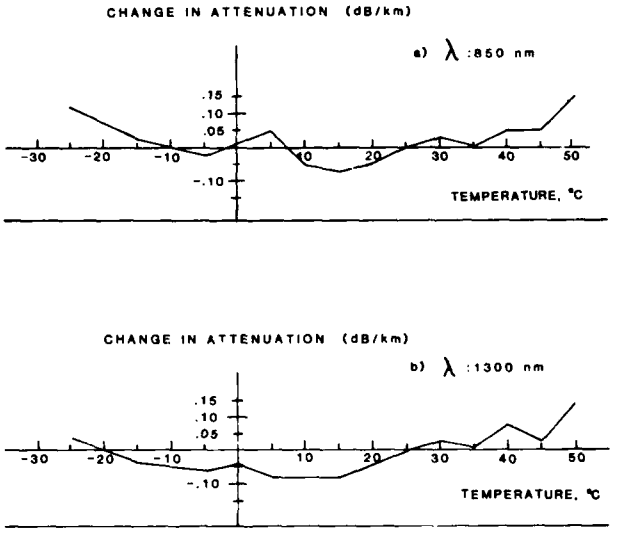

Figure 4. Thermal Characteristics of Fiber Optic Cable at a) 850 nm and b) 1300 nm

When subjected to a variety of flexing, impact, tensile loading, and twist tests per DOD-MIL-STD-1678, the mechanical behavior of the optical cables was assessed relative to an allowed increase of 0.5 dB/km at 1300 nm. The following test results were obtained on a six-fiber cable. Note that all fibers in the cable were fused together during the tests to obtain an increased measurement sensitivity.

- Cyclical Flexing: Method 2010, Procedure II. A drum 3 cm in diameter is used to cyclically flex the cable 1000 times.

  Increases in attenuation were observed to be less than 0.5 dB/km. Extending the flexing to 3200 cycles broke one fiber in the cable assembly. When measurements were repeated on a 6-cm drum, no degradation in the attenuation of the fibers was observed after 1000 cycles.

- Impact Test: Method 2030, Procedure II. From a height of 15 cm a weight of 3 kg is dropped 100 times.

  The increase in attenuation was 0.12 dB/km.

- Compressive Strength: Method 2040, Procedure II. A load of 5000 newtons is applied within 5 seconds to the cable assembly.

  At the maximal load an increase of attenuation of 2.1 dB/km was observed, but the fibers completely recovered to their initial state after a relaxation time of 2 seconds.

- Installation Tensile Loading: Method 3010, Procedure II. A 100-meter specimen cable is submitted for a duration of 5 minutes to incremental tensile loads applied over a 5-second interval.

  A residual increase in attenuation of 0.5 dB/km was observed at 3000 newtons. Other cable samples showed no residual increase for loads applied at 1000, 2000, 3000, and 4000 newtons.

- Operating Tensile Loads: Method 3010, Procedure II. A 200-newton load is applied to a 100-meter specimen cable for a period of 72 hours.

  No increase in attenuation was observed.

- Cable Twist: Method 2050, Procedure II. A 2-meter cable specimen is submitted to alternate clockwise and counterclockwise torsions of:

  180 cycles at ±180°
  20 cycles at ±360°
  10 cycles at ±720°

  No increase in attenuation was observed.

- Longitudinal Tightness: Two specimens of 1 meter length are submitted for periods of 7 and 16 days to 1 meter of water pressure.

  No water penetration was observed.

- Transversal Tightness: External sheaths of the cable are immersed in 1 meter of water.

  Dry gas was blown into one end. Less then 1 ppm of water was measured in the gas 6 weeks later.

- Flammability: Method 5010. A fiber optic cable specimen is set aflame.

  The burning time of the cable outer jacket was 10 seconds over a flame travel distance of 35 mm. Both these observables were within the specification of 30 second burn time at a flame propagation distance of 36 mm.

System Simulation Tests

Laboratory simulation tests were performed with concatenated cable assemblies. Three sets of 6-fiber cables about 1 km long were fused together with 17 splices for a total length of 19.4 km. Bandwidth and attenuation measurements were then performed at 1300 nm. A total attenuation of 20 dB was obtained. Of this attenuation 17.4 dB was directly attributed to the fibers specifically used in the cables, resulting in a 0.15 dB average loss per fusion splice. The bandwidth was measured at 64 MHz, relative to a theoretically calculated value of 65 MHz.

Installation Tests

Attenuation tests were performed throughout the final network after installation of the cables. For optimal performance of any link in the network, cables were selected and fused together to compensate for their attenuation and variations in bandwidth. Since each cable had been measured out and identified before installation, all concatenated links could be rechecked and final on-site test results confirmed. In a final field installation only one of the cables laid underground had to be replaced because of microbending losses in excess of 0.5 dB/km. This particular attenuation increase was due to a manufacturing deficiency in one fiber of the cable run that was aggravated by greater than normal earth movements during trench digging and refilling. As a further precaution the fiber optic cables were subsequently enclosed in impact resistant plastic tubing.

Explosive Tests[1]

User concern over cable plant ruggedness and survivability becomes an important issue in military applications. Hence the susceptibility to damage or failure of cables due to explosive charge detonations or other heavy shock and stress forces must be better understood. The capability of underground cables to resist dynamic forces generated by explosive blasts is a function of the cable mechanical design and rigidity, its location relative to the blast, and the magnitude of the explosion.

Tests were performed at White Sands Missile Range, New Mexico, to evaluate the response of buried fiber optic cables to accelerations and stresses developed by an explosive charge. During these tests, observations were made of cable parameters that might be affected by these forces. Transmission bit error rate measurements were made to determine cable performance changes, and cable attenuation profiles were monitored with an optical time domain reflectometer. The tests involved detonation of a 250-kg conventional charge in close proximity to copper and fiber optic cables buried both directly and in protective steel conduits to simulate a buried cable plant. The 250-kg explosive charge equivalent used in these tests was generated by 90 lb of liquid nitro-methane, detonated with a prime cord and booster charge.

Five different cables were tested, including two types of fiber optic cable. The three metallic cables were 50-mm and 16-mm coaxial (Heliax) and a composite cable produced by Cableries & Corderies du Hainaut, Dour, Belgium. This composite cable consisted of a 14-gauge twisted pair, a 22-gauge twisted pair, and two coaxial cables. These four conductors were all encased in a double sheath, one of corrugated steel and the other of lead. The cable weighed approximately 4 lb/ft, and its mechanical structure was designed to help withstand the impact of high dynamic forces. Both optical cables were of all dielectric construction. One was the six-fiber loose-tube underground cable described herein and manufactured by Opticable, S.A., Brussels, Belgium. The other, which was instrumented for this test, was a four-fiber tight-bound tactical cable. The cables were buried in trenches to depths of 1 and 3 meters at distances of 2.5, 3.5, and 5.5 m from the center of the charge casing.

The experiments demonstrated the necessity to isolate cable structures, not

designed specifically to withstand explosive blasts, in protective tubing. When laid bare, side by side in the same trenches, the coaxial cables, except the one designed to withstand the direct impact of the explosives, were crushed and damaged to a far greater extent than the fiber optic cables. Cables contained in protective steel tubing survived the tests.

Conclusions

The development of an underground, all dielectric fiber optic cable has successfully evolved from initial specifications and laboratory tests to its final production phase. Measurements made on the fibers and cable assemblies were used as a reference for the final installation and field measurements performed on the total network. Excellent correlations have been established between the cable performance in the network and its essential characteristics established during laboratory and factory measurements. Test results also indicate that fiber optic cables, unless designed specifically to withstand large dynamic forces, should be installed in steel tubing to increase their survivability if they are in the immediate vicinity of high probability impact targets. Otherwise, they may be directly buried in the ground or additionally protected in plastic tubing.

Acknowledgment

We would like to acknowledge the contributions made by Michel Andre, Opticable S.A., Mons, Belgium in the development, certification, and installation of the fiber optic cable. This work was performed in part under the sponsorship of the U.S. Air Force Electronic Systems Division, Air Force Systems Command, Contract F19628-86-C-0001.

References

1. S. F. Large and G. W. Styskal, "Fiber Optic Cable Vulnerability Test, White Sands, New Mexico," December 1982, ESD-TR-82-259.

Biographies

Jonathan D. Fridman is a Lead Engineer/Project Leader in Optical Communications at the MITRE Corporation. He is involved in the design of survivable communications systems for command centers and is responsible for the implementation of long-haul underground and tactical fiber optic systems and their associated networks. Mr. Fridman is a graduate of the Robert College Engineering School in Istanbul, Turkey. He completed master's and doctoral studies in electrical engineering and physics at Purdue, Harvard, and Brandeis Universities.

Andre Goffin is a graduate of the Royal Military Academy and the University of Louvain la Neuve in Belgium. His fields of study have been telecommunications engineering and operations research. Since 1981 he has been a Design Engineer and Project Manager at the Ministry of Defense, Belgium, where he has been involved, in particular, in the implementation of fiber optic telecommunication networks for NATO and USAFE.

SINGLE MODE BEND INSENSITIVE OPTICAL FIBER

D. BISWAS, K. KARBASSIYOON AND L. HODGES

ALCATEL CABLE SYSTEMS, INC.
ROANOKE, VA 24019

Abstract:

A single mode bend insensitive fiber (SMBI) was developed for applications where a sharp bend is of concern. This fiber outperformed standard telecommunications single mode depressed clad fiber in two types of bend tests where the fiber was wound on 75mm and 0.25 inch diameter mandrels. The bend test results, the wound fiber on canister results and its low temperature performance are discussed.

1.0 INTRODUCTION

Radiative losses occur whenever an optical fiber undergoes a bend of finite radius of curvature. Fibers can be subject to two types of bends: (a) bends having radii that are large compared to the fiber diameter, e.g., such as occur when a fiber cable turns a corner, and (b) random microscopic bends of the fiber axis that can arise when the fibers are incorporated into cables. In this paper the radiation losses due to large curvatures (macro-bending) will be addressed.

For slight bends the excess loss is extremely small and essentially unobservable. As the radius of curvature decreases, the loss increases exponentially until at a certain criticalradius the curvature loss becomes observable (1).

$$\alpha_c \text{ (dB/km)} = AcR^{1/2} e^{-\nu R} \qquad (2)$$

where: $Ac \sim 33 * \Delta^{1/4} * \frac{\lambda c^{3/2}}{\lambda^2}$

R is the curvature radius

ν is the normalized frequency

If the bend radius is made a bit smaller once this threshold point has been reached, the losses suddenly become extremely large.

A standard single mode telecommunication fiber whether depressed or matched clad, shows high bend loss when the fiber is subjected to a sharp bend.

By selecting the appropriate core profile, mode field diameter (MFD), and cutoff wavelength, the bending loss of single mode fiber can be optimized (3). Mandrel tests and pin array tests are commonly used to measure the bend loss of optical fibers. Recent experimental data (4) correlated the bend induced loss and mode field diameter of single mode matched clad and depressed clad fibers.

By adjusting the profile parameters Alcatel has developed a modified single mode fiber that has been tested to perform significantly better than a standard telecommunication fiber when subjected to a sharp bend. Procedures to evaluate bending loss performance and temperature cycling and the experimental results are discussed in this paper.

2.0 BEND LOSS PERFORMANCE

Results from mandrel testing of three (3) matched clad and three (3) depressed clad single mode fibers are shown in Figure 1.

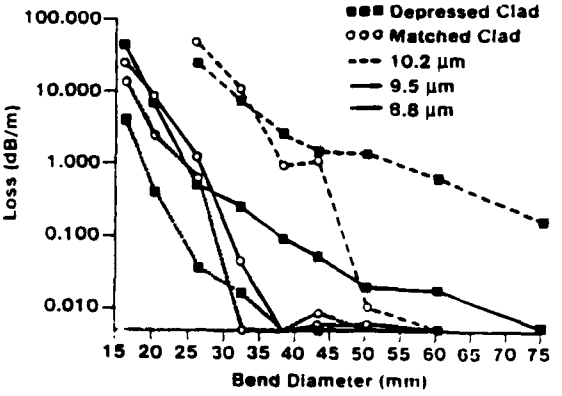

Figure 1 Mandrel Test: Loss vs Bend Diameter at 1550nm for Three Pairs of Fibers Having Similar 1300-nm MFDs (From Ref. 4)

Table 2 lists results from both bending tests comparing the attenuation performance of two groups of telco type fiber having different mode field diameters with the performance of the modified SMBI fiber.

Fiber Type	MFD	Wavelength (um)	100 Turn Bend Loss (dB)	1/4 Turn Bend loss (dB)
Standard Telco Single Mode Fiber 1	9.5	1.3	0.0	6.5
		1.55	0.10	10.5
Fiber 2	8.5	1.3	0.0	4.8
		1.55	0.12	9.5
SMBI	---	1.3	0.0	0.03
		1.55	0.0	0.30

Table 2. Attenuation Data on Bending Tests

3.0 TEMPERATURE CYCLING PERFORMANCE

The SMBI fiber is designed to provide excellent bend insensitivity at 1.3um and 1.55um wavelengths and it is particularly important when the fiber is wound on a canister and deployed at high speed. A photograph of a typical wound canister is shown in Figure 3. Typically the fiber is wound with approximately 100g tension. A small amount of adhesive is applied on each layer of fiber for better fiber pack stability. When this fiber is temperature cycled between -50°C to +60°C, the loss is negligible as seen in Figure 4.

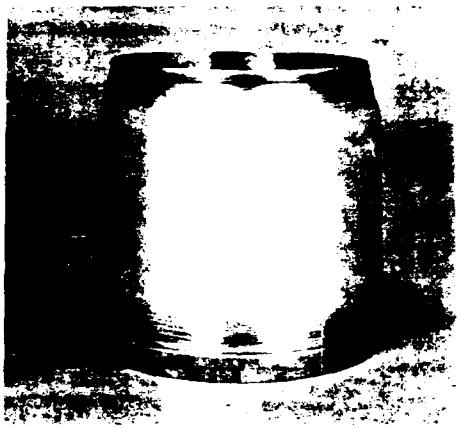

Figure 3. A Typical Wound Canister

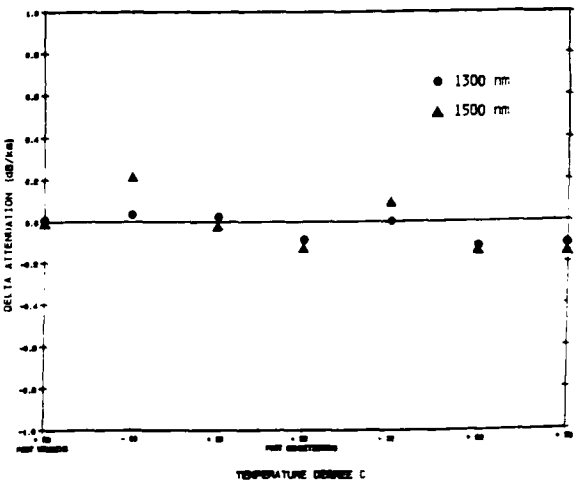

Figure 4. Temperature Cycling Data of a Wound Aluminum Canister of Single Mode Bend Insensitive Optical Fiber.

It is clearly seen that standard telecommunication fiber exhibits significantly higher bend loss when subjected to small diameter bends. In order to reduce the high loss associated with small diameter bends, Alcatel has developed a modified single mode fiber which exhibits very low bending loss. Two types of mandrel testing procedures were used to measure the attenuation due to bending:

1. 100 turn on a 75mm diameter mandrel (FOTP 62):

The test fiber is carefully wound on a 75mm diameter mandrel without overlaps or crossovers in the fiber. After winding 100 turns, an additional 1.5m of fiber is used on each side for injection and detection. The loss is measured using the standard cut back method.

2. 90 degree bend on a 0.25 inch diameter mandrel:

This test determines the loss induced in a fiber by a single 90 degree bend around a 0.25 inch diameter mandrel. This test is intended to simulate the loss which is induced when a fiber is paid out from a wound canister (or bobbin) during high speed deployment.

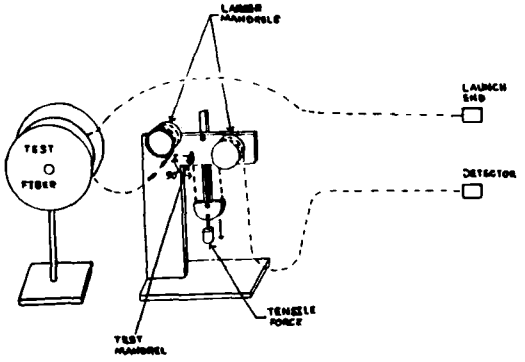

FIGURE 2. 90° Bend Test Fixture

The test fiber is wrapped around the 0.25 inch mandrel as shown in Figure 2. The fiber is positioned between two larger diameter mandrels with a support weight suspended to apply the tensile force necessary to maintain the 90° bend. The weight does not have an effect on the measurement as long as it is large enough to hold the fiber in contact with the mandrel for the 1/4 turn. The change in fiber attenuation due to the 90 degree bend can be calculated from:

$$A = -10 \log (Pr/Po) \quad [dB]$$

Where Pr and Po represent the powers through the test fiber with and without the 90° bend respectively.
Results from the 90° bend test comparing standard telco depressed clad single mode fiber with the modified single mode bend insensitive (SMBI) fiber for various mandrel diameters are shown in Table 1. The attenuation performance of the SMBI fiber is vastly superior to the telco design for bending diameter less than 1.0 inch.

Fiber Type	Wavelength um	Mandrel Diameters (inches) 1.0	0.75	0.50	0.25	0.125
Standard Telco Single-Mode	1.30	0.01	0.05	0.78	7.5	---
	1.55	0.19	1.18	4.10	11.0	---
SMBI	1.30	0.01	0.01	0.01	0.01	0.26
	1.55	0.02	0.05	0.05	0.13	2.01

Table 1. 90° Turn Bend Loss (dB) Data for Different Mandrel Diameters

4.0 SUMMARY AND CONCLUSIONS

A single mode fiber design was modified for improved bend performance. It was compared with standard telecommunication grade single mode depressed clad optical fibers. This single mode bend insensitive (SMBI) fiber showed minimal increase at 1.3 and 1.55 um wavelengths during the 100 turn and 90° bend testing. The SMBI fiber is particularly suitable where the fiber is subjected to a sharp bend. This fiber can be wound on an aluminum canister and thermally cycled between -50°C and +60°C with an insignificant loss increase at 1.3 and 1.55 um. This fiber has been deployed successfully at high speed.

Acknowledgements:

The authors would like to acknowledge Alcatel for granting permission to publish this paper.

References:

1. Gerd Keiser, Optical Fiber Communications, McGraw Hill, Inc., NY (1983), 55 pp.

2. L. B. Jeunhomme, Single-Mode Fiber Optics, Marcel Dekker, Inc., New York and Basel (1983), 270 pp.

3. T. Li, Optical Fiber Communications, Academic Press, NY, 1, 48 (1985).

4. J. Dixon, et.al., Tech. Digest, OFC'87, TUA 2 (1987).

Dipak R. Biswas received his Ph.D from the University of California, Berkeley in 1976. After working at Lawrence Berkeley Laboratory, University of Utah and Institute of Gas Technology, he joined ITT Electro-Optical Products Division. He worked on optical fiber strength and coating developments for different commercial and military applications. Currently, he is working at SpecTran Corporation (50 Hall Road, Sturbridge, MA 01566) as Director, Research and Development in fiber optics.

Kamran Karbassiyoon was awarded the B.S. degree in chemistry from Southeastern Massachusetts University in 1977. In 1979, he received a M.S. degree in chemistry from Scranton University. Kamran Karbassiyoon has been associated with ITT/Alcatel since 1981. At his present capacity he is responsible for overseeing and managing several military related programs that require special high strength fibers to satisfy the needs of bobbin winding and high speed payout of the Fiber Optic Guided Missile (FOG-M) and the Advanced Anti-Armor Weapon System - Medium (AAWS-M).

Les B. Hodges received the B.S. degree in Industrial Engineering from Virginia State University, Petersburg, VA, in 1987. He joined ITT Electro-Optical Products Division, Roanoke, VA, in 1978 as a member of the R&D optical preform development group where he was involved in the development of different types of single-mode fiber for various commercial and military applications. Since the formation of Alcatel Cable Systems Group, Roanoke, VA, in 1987, he has been working as Senior Manufacturing Engineer, responsible for the preform manufacturing processes. Mr. Hodges is a member of the Optical Society of America.

SINGLE-FIBER TACTICAL CABLES FOR SINGLE-MODE AND MULTIMODE SYSTEMS

K. Kathiresan, L. C. Hotchkiss and S. P. Gentry, AT&T Bell Laboratories, Norcross, Georgia 30071, U.S.A.

J. B. Fluevog, AT&T Network Systems, Norcross, Georgia 30071, U.S.A.

V. E. Kalomiris, U.S. Army CECOM, Ft. Monmouth, New Jersey 07703-5202, U.S.A.

ABSTRACT

The design and development of single-fiber optical cables for use in tactical applications have been completed. Development effort was guided by the detailed design criteria provided by the contracting organization, the U.S. Army CECOM. Four different cable designs were developed under this program. The cable designs include two different cable sizes, 2.5 mm and 4.0 mm, and two different fiber types, single-mode and multimode. Two different cable sizes, one lightweight and the other more rugged, were developed in this program so that different cables can be used for different applications. The cable designs are similar to the two-fiber single-mode and multimode tactical cables previously developed for the U.S. Army. The cables can be used in either one- or two-way transmission. The results of optical, environmental and mechanical performance tests for the four cable designs are presented in the paper.

INTRODUCTION

The design and development of single-fiber optical cables for use in tactical fiber-optic applications have been completed. This development program was funded by the U.S. Army Communication-Electronics Command (CECOM).[1] Four cable designs were developed under this program. The cable designs include two cable sizes and two fiber types. The two different cable sizes are 2.5-mm and 4.0 mm in diameter. The 2.5-mm design is compact and lightweight, while the 4.0-mm design is similar, except more rugged and thus can withstand more stringent mechanical environments. The 2.5-mm and 4.0-mm cables have tensile ratings of 270 Newtons and 1350 Newtons, respectively. These cables can be used in radar remoting, robotic vehicle control/communication, and other general tactical communication system applications. The cables can be deployed either from backpack, a ground vehicle or from a helicopter. The cable size should be selected based on the application and the stringency of the mechanical environment the cable will experience.

The two different fiber types are single-mode and multimode fibers. The single-mode cable uses standard 8.8-μm mode-field diameter single-mode fiber. The multimode cable uses a newly developed 50/125 mm core/cladding radiation-hardened multimode fiber. For all applications, the fibers are prooftested to 690 MPa (100 ksi). The single-mode cables can be operated at 1310 nm and 1550 nm, and the multimode cables can be operated at 850 nm and 1300 nm. The cables can be used in either one- or two-way transmission.

The operating temperature range of these cables is -55 °C to 85 °C. The design criteria for the single-fiber cables are similar to those used for the two fiber single-mode and multimode tactical cables previously developed for the U.S. Army CECOM.[2] [3] In the following, the design, development and performance test results for the four single-fiber tactical cables described above are presented.

CABLE DESIGN

The cross-sectional views of the four cable designs are given in Figure 1. All four cable designs are all-dielectric and use either the single-mode or multimode fibers described above. The fiber is coated with a dual acrylate coating which is mechanically strippable. The fiber is then tight-buffered to 1 mm (.039 inch) diameter with a blue-colored polyester elastomer. The buffering material is also mechanically strippable in

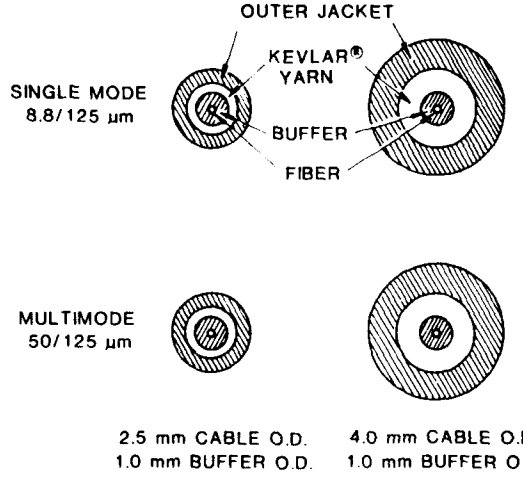

Figure 1. Single-Fiber Optical Cable Designs

order to facilitate repair and connector termination in the field. The buffering material was chosen to minimize microbending losses induced by exposure of the cable to temperature extremes of -55 ° C and 85 ° C and to meet the stringent mechanical performance requirements. Aramid yarns, which are the main tensile-load-carrying members, are stranded over the buffered fiber. Appropriate amounts of aramid yarns are used for the 2.5-mm and 4.0-mm cables to attain the 270 N and 1350 N tensile ratings, respectively. A flame-retardant polyurethane outer jacket is then extruded over the aramid yarn.

PERFORMANCE

The cables were subjected to all the required optical, environmental and mechanical performance tests. The fibers were also subjected to a battery of optical, mechanical and dimensional requirements before they are used in the cables. Typical results of these single-mode and multimode fiber performance tests can be found in the References 4 and 5. These references also include temperature cycling and accelerated aging test results for coated fibers as well as buffered fibers. Thus, performance was evaluated both for the finished cable and the individual components. In the following cable performance evaluation, two to three cable samples for each design were used for the environmental tests. For all the mechanical tests, the results correspond to triplication of tests.

First an attenuation test was conducted for the finished cables. Typically the cables were manufactured in 1-km lengths. The attenuation results for single-mode cables at 1310 nm and 1550 nm, and multimode cables at 850 nm and 1300 nm are given in Figures 2 and 3. No distinction is made for the 2.5-mm and 4.0-mm cables in these data. The requirement for single-mode cables is that the attenuation rate be less than or equal to 0.5 dB/km at 1310 nm. Corresponding requirements for multimode cables are 3.75 dB/km at 850 nm and 1.5 dB/km at 1300 nm.

The two primary environmental tests are temperature cycling and accelerated aging. The temperature cycling used for the cable evaluation is presented in Figure 4. The temperature range requirement for tactical cable is from -46 ° C to 71 ° C. However, the cables were evaluated for the extended temperature range of -55 ° C to 85 ° C. The results of temperature cycling for all four cable designs are presented in Figures 5 through 8. The requirement of maximum increase in attenuation for single-mode cables is 0.3 dB/km at 1310 nm and for multimode cables is 0.5 dB/km at 850 nm and 1300 nm. The results are given for five temperature cycles for the extended temperature of -55 ° C and 85 ° C. The -46 ° C and 71 ° C added loss data were consistently lower than the corresponding data at -55 ° C and 85 ° C. All cable designs pass the requirements showing excellent performance.

The accelerated aging test consists of subjecting the cables to a temperature of 110 ° C for 10 days. This test temperature and duration simulates the mechanical response of the cable materials to an exposure of 85 ° C for the design life of 20 years. This simulation criteria was arrived at using the viscoelastic mechanical properties equivalence principle described in Reference 6. The results of the accelerated aging tests are presented in Figures 9 through 11. The added loss requirements for accelerated aging tests are the same as

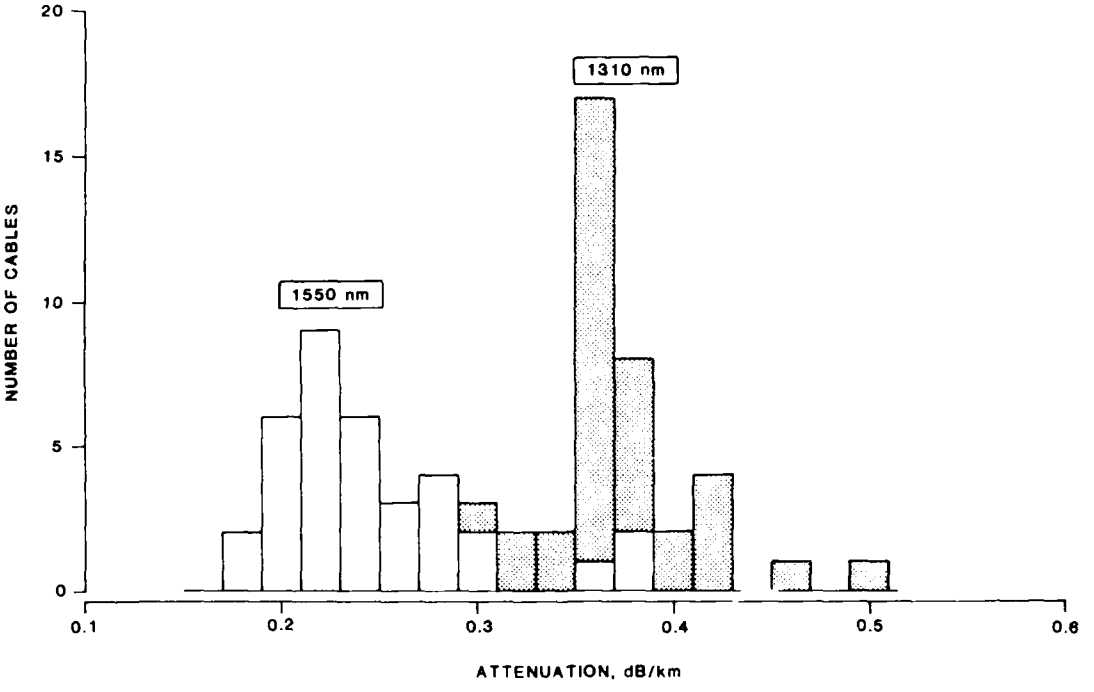

Figure 2. Single-Mode SFOCA Cable Attenuation

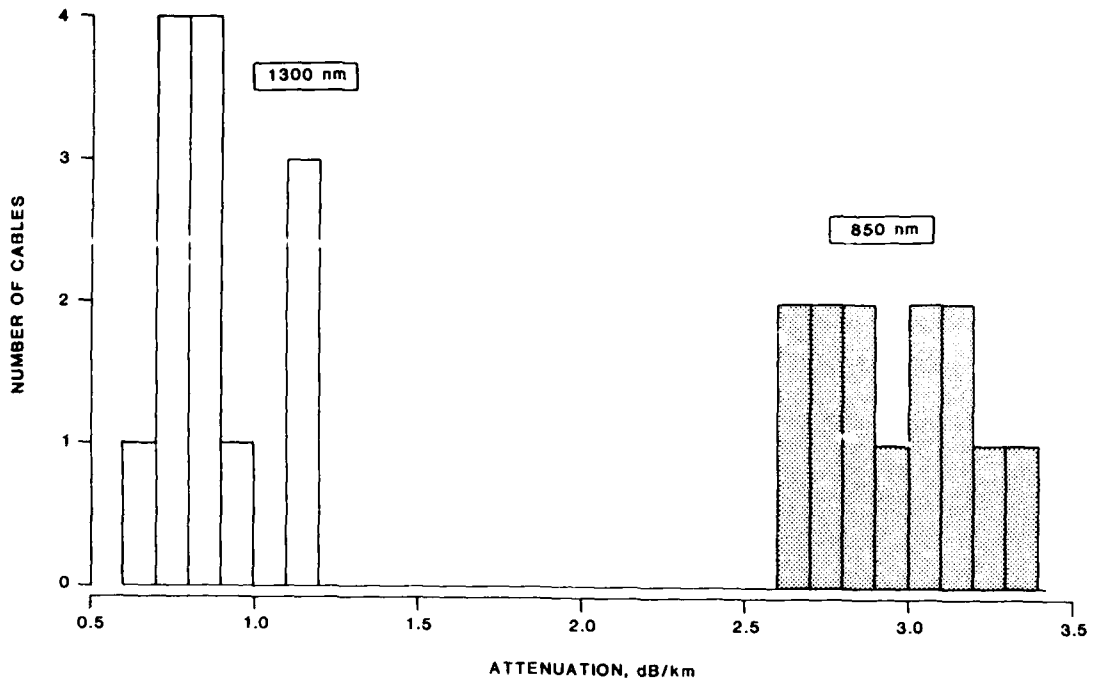

Figure 3. Multimode SFOCA Cable Attenuation

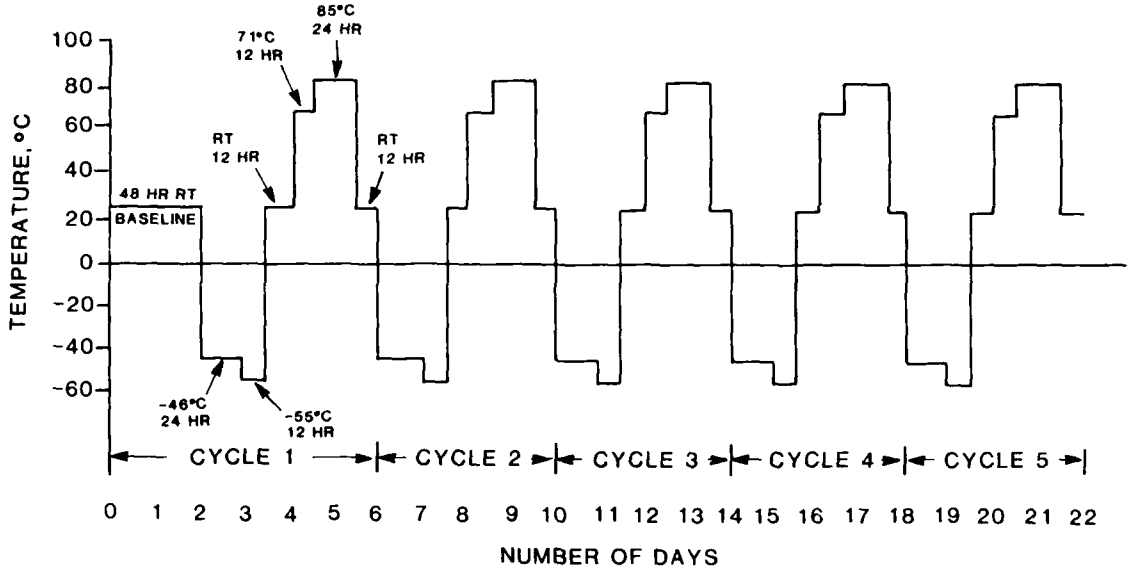

Figure 4. Temperature Cycles for SFOCA Cables

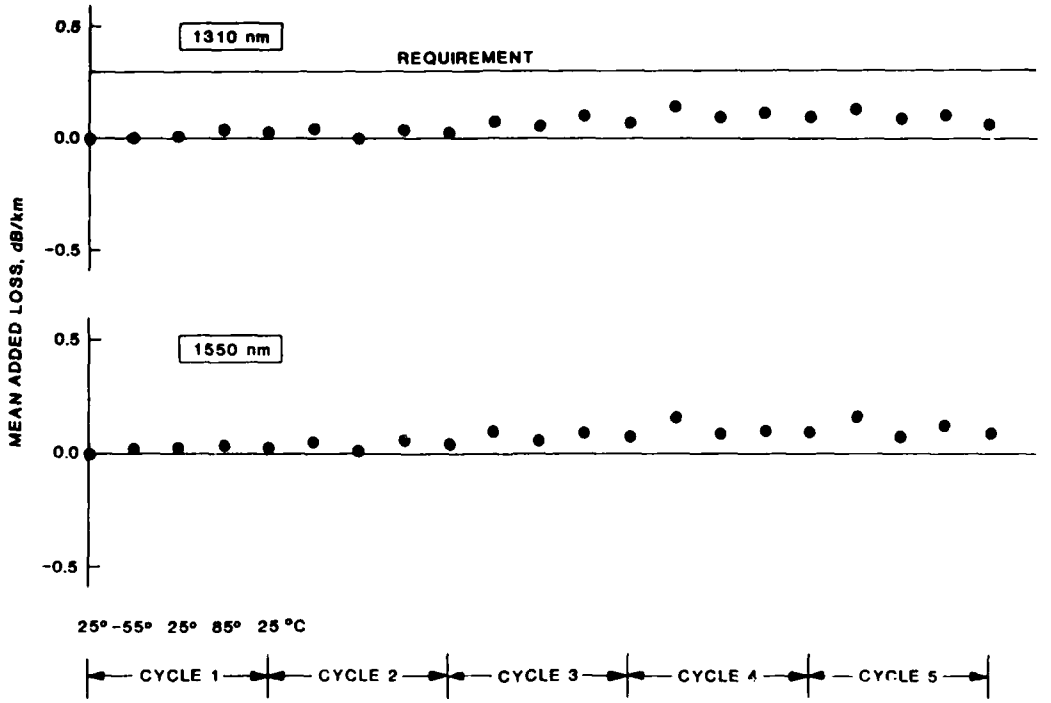

Figure 5. Temperature Cycling Test Result for 2.5 mm Single-Mode Cable

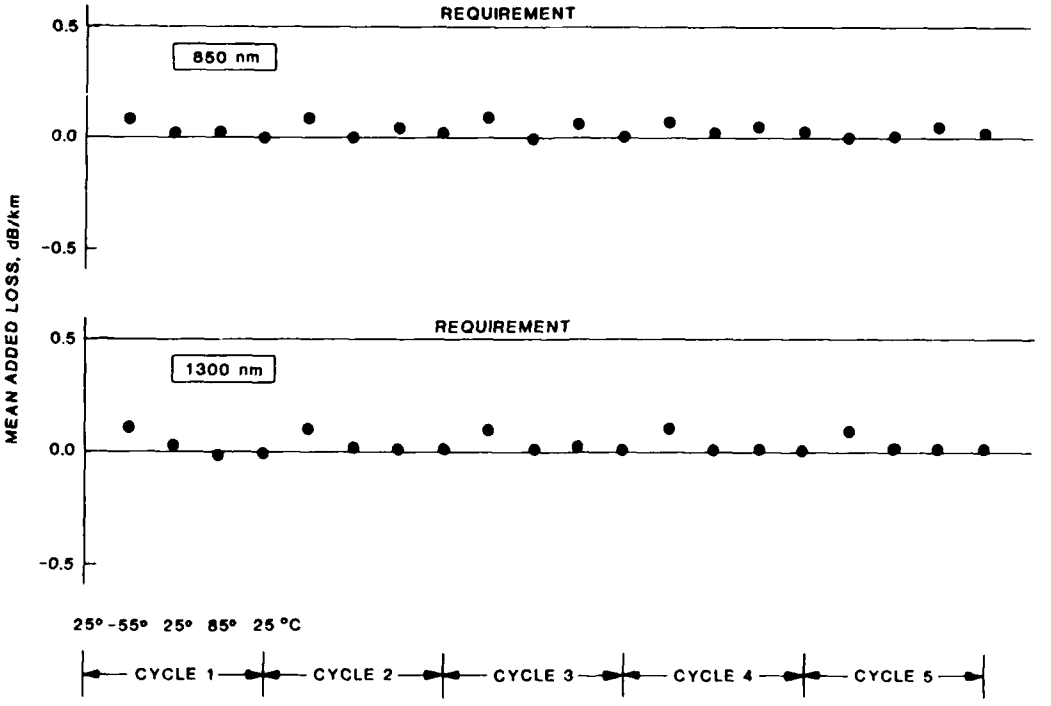

Figure 6. Temperature Cycling Test Result for 2.5 mm Multimode Cable

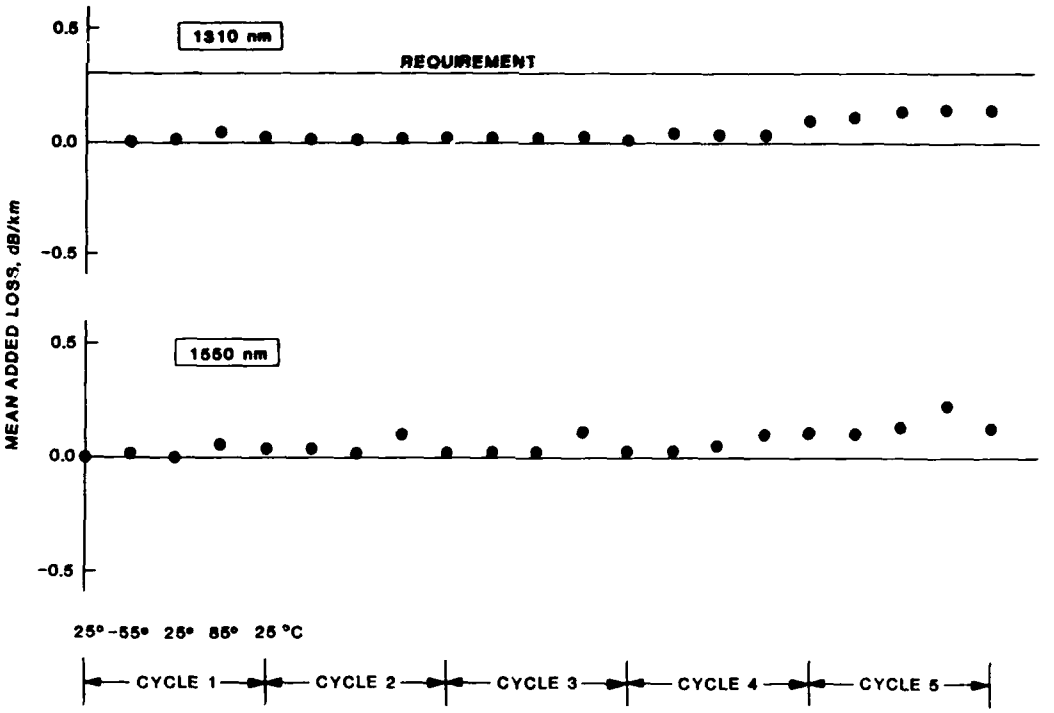

Figure 7. Temperature Cycling Test Result for 4.0 mm Single-Mode Cable

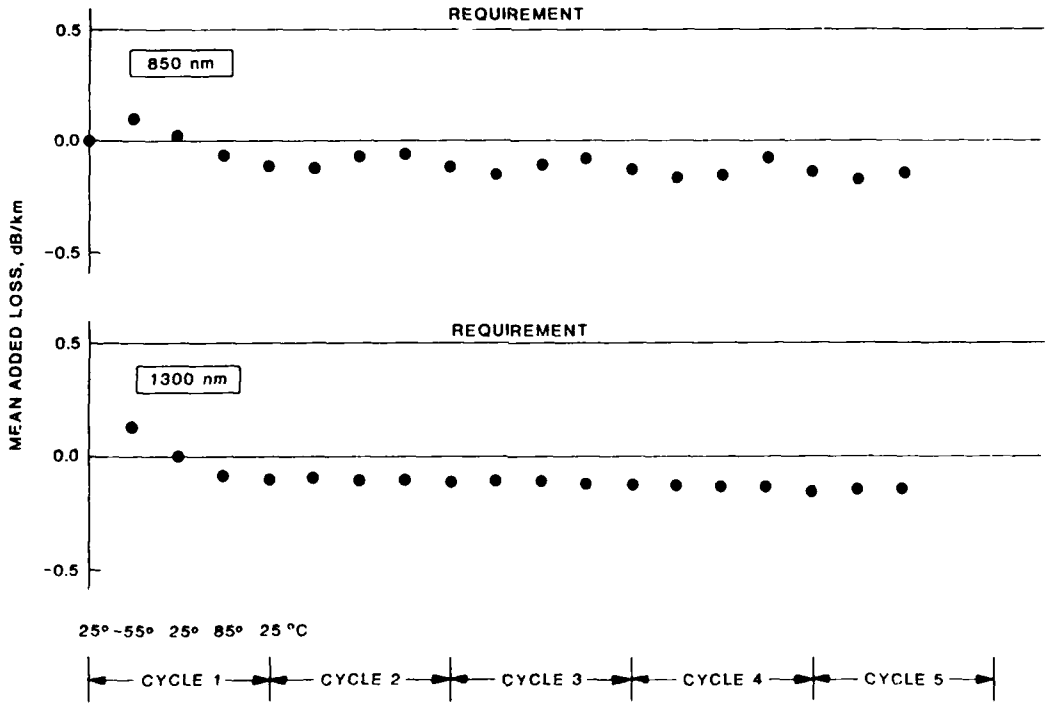

Figure 8. Temperature Cycling Test Result for 4.0 mm Multimode Cable

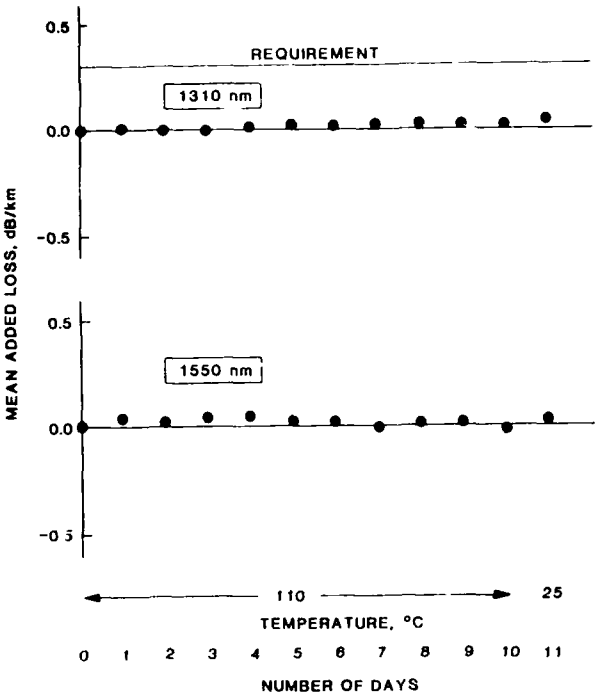

Figure 9. Accelerated Aging Test Result for 2.5 mm Single-Mode Cable

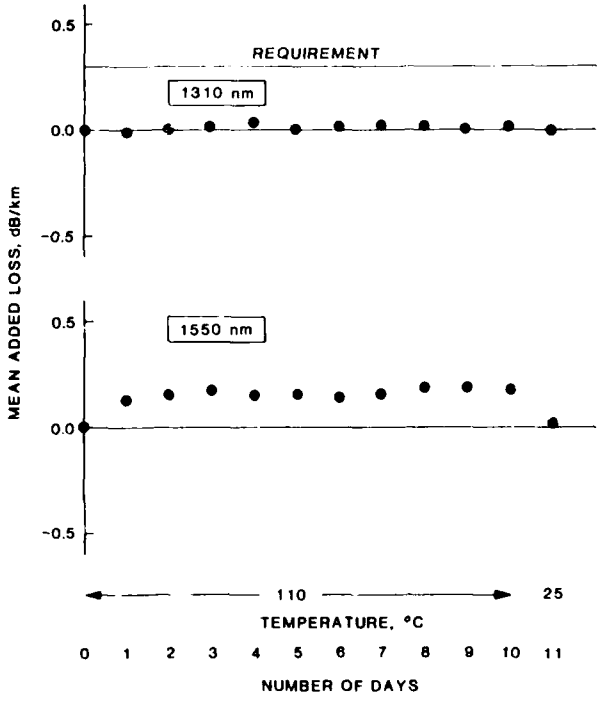

Figure 10. Accelerated Aging Test Result for 4.0 mm Single-Mode Cable

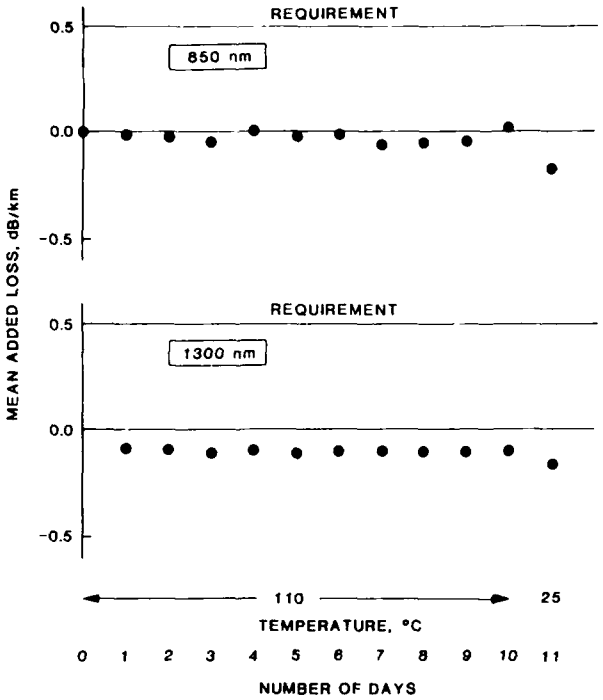

Figure 11. Accelerated Aging Test Result for 4.0 mm Multimode Cable

those for the temperature cycling tests. The 2.5-mm multimode cable design was not tested due to a shortage of cable samples. These results show excellent performance of the cable in the accelerated aging test.

The cables were also subjected to the required mechanical tests summarized in Table I. The results of the mechanical tests are also summarized in tabular form. Table II presents the results for primary wavelengths, i.e. 1310 nm for single-mode cables and 1300 nm for multimode cables. Table III presents the data for single-mode cables at 1550 nm and multimode cables at 850 nm. Though not required, a 1-mm corner bend and a radiant heat test were added to the matrix for a thorough evaluation of the cable designs. As can be seen from the tables, the 4-mm cable design either meets or surpasses all the mechanical requirements. The lightweight 2.5-mm cable meets all the test requirements, except for the knot and the 1-mm corner bend tests. However, the added attenuation at the primary wavelengths recovers after the load is removed. It should also be noted that in the 1-mm corner bend test, the cable is bent far below its minimum bend radius.

The twist bend test specified in the program uses the test procedure DOD-STD-1678, Method 2060. In this procedure a test weight of 10 kg is specified for all cables less than 6.4 mm in diameter. The 10 kg requirement of DOD-STD-1678 is very stringent for smaller diameter cables. Most industry procedures for similar tests specify weights which vary proportionally to the cable diameter. Thus, the number of cycles for the 4.0-mm cables was selected as 1000 cycles, instead of 2000 cycles which is conventionally used in tactical

TABLE I. SFOCA CABLES MECHANICAL REQUIREMENTS

NO.	TEST DESCRIPTION	REQUIREMENTS	
		2.5 mm O.D. CABLE	4.0 mm O.D. CABLE
1	OPERATING TENSILE LOAD	EIA-455-FOTP-33 180 N (40 lbf), 5 MINS ADDED LOSS, $\Delta \leq$ 0.2 dB	EIA-455-FOTP-33 300 N (65 lbf), 5 MINS ADDED LOSS, $\Delta \leq$ 0.2 dB
2	TENSILE STRENGTH	EIA-455-FOTP-33 270 N (60 lbf) ELONGATION $\leq$ 2.0% Δ - NOT SPECIFIED	EIA-455-FOTP-33 1350 N (300 lbf) ELONGATION $\leq$ 2.0% Δ - NOT SPECIFIED
3	COLD BEND	DOD-STD-1678, 2020 MANDREL DIA. = 12.5 mm -46 °C, 5 kg, 3 TURN $\Delta \leq$ 0.2 dB	DOD-STD-1678, 2020 MANDREL DIA. = 20 mm -46 °C, 10 kg, 3 TURN $\Delta \leq$ 0.2 dB
4	IMPACT	DOD-STD-1678, 2030 0.5 kg, 15 cm, 100 CYCLES $\Delta \leq$ 0.2 dB	DOD-STD-1678, 2030 1.5 kg, 15 cm, 100 CYCLES $\Delta \leq$ 0.2 dB
5	KNOT	AT&T BELL LABORATORIES DIAMETER = 12.5 mm $\Delta \leq$ 0.5 dB	AT&T BELL LABORATORIES DIAMETER = 20 mm $\Delta \leq$ 0.5 dB
6	COMPRESSION	DOD-STD-1678, 2040 10.1 cm DIA., 450 N (100 lbf) $\Delta \leq$ 0.2 dB	DOD-STD-1678, 2040 10.1 cm DIA., 1780 N (400 lbf) $\Delta \leq$ 0.2 dB
7	CYCLIC FLEXING	EIA-455-FOTP-104 MANDREL DIA. = 12.5 mm 5 kg, 2000 CYCLES $\Delta \leq$ 0.2 dB	EIA-455-FOTP-104 MANDREL DIA. = 20 mm 10 kg, 2000 CYCLES $\Delta \leq$ 0.2 dB
8	FREEZING WATER IMMERSION	DOD-STD-1678, 4050 -10 °C, 6 HOURS -2 °C, 1 HOUR $\Delta \leq$ 0.2 dB	DOD-STD-1678, 4050 -10 °C, 6 HOURS -2 °C. 1 HOUR $\Delta \leq$ 0.2 dB
9	TWIST BEND	NOT REQUIRED	DOD-STD-1678, 2060 MANDREL DIA. = 20 mm 10 kg, 1000 CYCLES $\Delta \leq$ 0.2 dB
10	CORNER BEND	NOT REQUIRED AT&T BELL LABORATORIES 1 mm RADIUS, 90 N (20 lbf) 1 minute, $\Delta \leq$ 0.5 dB	NOT REQUIRED AT&T BELL LABORATORIES 1 mm RADIUS, 300 N (65 lbf) 1 minute, $\Delta \leq$ 0.5 dB
11	RADIANT HEAT	NOT REQUIRED AT&T BELL LABORATORIES 900 °C, 10 min., $\Delta \leq$ 0.2 dB	NOT REQUIRED AT&T BELL LABORATORIES 900 °C, 10 min., $\Delta \leq$ 0.2 dB
12	FLAMMABILITY	DOD-STD-1678, 5010 60 ANGLE TEST EXTINGUISH $\leq$ 30 sec.	DOD-STD-1678, 5010 60 ANGLE TEST EXTINGUISH $\leq$ 30 sec.

TABLE II. SUMMARY OF MECHANICAL TEST RESULTS FOR CABLES AT PRIMARY WAVELENGTHS

TEST	CABLE DESIGN (FIBER TYPE/ CABLE O.D. mm/ BUFFER O.D. mm)			
	SM/2.5/1.0	MM/2.5/1.0	SM/4.0/1.0	MM/4.0/1.0
MEAN/MAX./MAX. ALLOWED INCREASE IN ATTENUATION AT 1310nm FOR SM OR 1300nm FOR MM				
OPERATING TENSILE LOAD	.00/.00/.2	.04/.08/.2	.03/.08/.2	.00/.01/.2
TENSILE STRENGTH	.00/.01/-	.01/.04/-	.00/.00/-	.00/.00/-
COLD BEND	.02/.04/.2	.00/.00/.2	.01/.01/.2	.00/.00/.2
IMPACT	.00/.01/.2	.01/.01/.2	.01/.02/.2	.01/.01/.2
KNOT	.59/.64/.5*	.40/.47/.5*	.10/.13/.5	.06/.07/.5
COMPRESSION	.00/.00/.2	.01/.01/.2	.01/.01/.2	.01/.02/.2
CYCLIC FLEXING	.00/.00/.2	.00/.00/.2	.04/.09/.2	.03/.07/.2
ICE CRUSH	.00/.00/.2	.00/.00/.2	.02/.06/.2	.07/.09/.2
TWIST BEND	-	-	.02/.04/.2	.04/.06/.2
CORNER BEND	6.10/6.36/.5***	.81/1.13/.5**	.38/.41/.5*	.33/.35/.5*
RADIANT HEAT	.02/.05/.2	.02/.06/.2	.02/.02/.2	.08/.23/.2
MAXIMUM TIME TO SELF-EXTINGUISH, sec / MAX. ALLOWED TIME TO SELF-EXTINGUISH, sec / ANY DRIP?				
FLAMMABILITY	15/30/NO	15/30/NO	25/30/NO	25/30/NO

* RECOVERED AFTER LOAD REMOVAL
** RECOVERED TO .32/.37/.5 AFTER LOAD REMOVAL
*** RECOVERED TO .27/.48/.5 AFTER LOAD REMOVAL

TABLE III. SUMMARY OF MECHANICAL TEST RESULTS FOR CABLES AT SECONDARY WAVELENGTHS

TEST	CABLE DESIGN (FIBER TYPE/ CABLE O.D. mm/ BUFFER O.D. mm)			
	SM/2.5/1.0	MM/2.5/1.0	SM/4.0/1.0	MM/4.0/1.0
MEAN/MAX./MAX. ALLOWED INCREASE IN ATTENUATION AT 1550nm FOR SM OR 850nm FOR MM				
OPERATING TENSILE LOAD	.00/.00/2.	.07/.10/.2	.04/.11/.2	.02/.03/.2
TENSILE STRENGTH	.01/.01/-	.06/.12/-	.01/.01/-	.06/.11/-
COLD BEND	.03/.09/.2	.04/.06/.2	.01/.01/.2	.00/.01/.2
IMPACT	.01/.01/.2	.01/.01/.2	.00/.01/.2	.01/.01/.2
KNOT	4.08/4.46/.5*	.40/.44/.5*	.08/.13/.5	.06/.08/.5
COMPRESSION	.00/.00/.2	.04/.05/.2	.01/.01/.2	.02/.03/.2
CYCLIC FLEXING	.00/.00/.2	.05/.09/.2	.03/.07/.2	.02/.04/.2
ICE CRUSH	.00/.00/.2	.05/.09/.2	.02/.04/.2	.02/.06/.2
TWIST BEND	-	-	.02/.05/.2	.02/.05/.2
CORNER BEND	11.81/12.22/.5***	1.30/1.39/.5**	.33/.35/.5*	.37/.41/.5*
RADIANT HEAT	.00/.00/.2	.07/.13/.2	.00/.00/.2	.09/.24/.2

* RECOVERED AFTER LOAD REMOVAL
** RECOVERED TO .73/1.13/.5 AFTER LOAD REMOVAL
*** RECOVERED TO .74/1.38/.5 AFTER LOAD REMOVAL

application. The 2.5-mm cables were not subjected to twist bend tests. EIA-RS-455 FOTP-91 does provide weights based on cable sizes, and the cables will be tested using this procedure in the future.

The weight requirements for 2.5-mm and 4.0-mm cables were 6.0 kg/km and 25 kg/km, respectively. The diameter and weight results for the cables are given in Table IV.

TABLE IV. SFOCA CABLE DIAMETER AND WEIGHT RESULTS

CABLE DESIGN FIBER TYPE/ CABLE O.D. (mm)/ BUFFER O.D. (mm)	AVERAGE DIAMETER (mm)	AVERAGE WEIGHT (kg/km)
SM/2.5/1.0	2.3	5.3
MM/2.5/1.0	2.4	5.6
SM/4.0/1.0	3.9	12.7
MM/4.0/1.0	3.8	12.8

CONCLUSIONS

The single-fiber tactical cables described herein meet and surpass all the optical, environmental and mechanical requirements imposed by the sponsoring agency, U.S. Army CECOM. Cables with different sizes and fiber types have been developed for use in varied tactical applications. The technology utilized in the design and development of these cables is similar to that of their two-fiber predecessors, enhancing field serviceability, compatibility and maintainability.

ACKNOWLEDGEMENT

A project of this nature requires support from many organizations. The authors gratefully acknowledge the extensive contributions of several members of AT&T Bell Laboratories and AT&T Network Systems.

REFERENCES

1. "Single-Fiber Optical Cable Assemblies (SFOCA)", U. S. Army CECOM Contract No. DAAB07-85-C-K556.
2. "Tactical Fiber-Optic Cable Assemblies (TFOCA)", U. S. Army CECOM Contract No. DAAB07-84-C-K551.
3. "Single-Mode Fiber Optic Communication Systems (SIMFOCS)", U. S. Army CECOM Contract No. DAAB07-85-C-K565.
4. "Final Engineering Design Model (FEDM) Test Report for Tactical Fiber Optic Cable Assemblies (TFOCA)", Report submitted to U. S. Army CECOM for Contract No. DAAB07-84-C-K551.
5. "Final Engineering Design Model (FEDM) Test Report for Single-Mode Fiber Optic Communication Systems (SIMFOCS)", Report submitted to U. S. Army CECOM for Contract No. DAAB07-85-C-K565.
6. K. Kathiresan, et al., "Selection and Test Criteria for Polymeric Materials for Tactical Fiber-Optic Cables", Proceedings of the 1988 Annual Technical Conference (ANTEC) of the Society of Plastic Engineers, Atlanta, Georgia, April, 1988.

Kris Kathiresan is a Member of Technical Staff in the Lightguide Technology Department at AT&T Bell Laboratories in Norcross, Georgia. He is responsible for the design and development of specialty cables, including military applications.

Dr. Kathiresan joined AT&T Bell Laboratories in 1985. He has a B. E. Hons in Mechanical Engineering from University of Madras, India, an M. E. in Aerospace Engineering from Indian Institute of Science, India, and a Ph. D. in Engineering Science and Mechanics from Georgia Institute of Technology, Atlanta, Georgia.

Dr. Kathiresan is a Senior Member of American Institute of Aeronautics and Astronautics and a Member of American Society of Mechanical Engineers. He is a registered Professional Engineer (Mechanical) in States of Georgia and Florida.

L. C. Hotchkiss is a Distinguished Member of Technical Staff in Lightguide Technology Department at AT&T Bell Laboratories, Norcross, Georgia. He earned a Bachelors Degree in Electrical Engineering from University of Wisconsin and a Masters Degree in Electrical Engineering from Stevens Institute of Technology. He has 30 years of experience, primarily in the design of test equipment, and is presently responsible for the design and programming of fiber optic environmental loss measuring test sets.

Sherrie P. Gentry joined AT&T Bell Laboratories, Norcross, Georgia in 1982 as a Senior Technical Associate in the Lightguide Technology Department. Her current responsibilities in the Lightguide Measurement and Computing Support Group include environmental testing of fibers and cables and fiber characterization and diagnostic measurements. She received a Bachelors in Electrical Engineering Technology from Southern Technical Institute.

Jill B. Fluevog is a Development Engineer in the Lightguide Cable Engineering Department at AT&T Network Systems, Norcross, Georgia. She joined AT&T in 1985 after receiving a Bachelors Degree in Chemical Engineering from Georgia Institute of Technology. She is responsible for the development of lightguide cable products and processes for military applications. Ms. Fluevog is a member of American Institue of Chemical Engineers, Institute of Electrical and Electronics Engineers and Society of Plastic Engineers.

Vasilios E. Kalomiris is currently a project leader responsible for fiber optic cables, connectors, and fiber optic system development at the U. S. Army CECOM, Ft. Monmouth, New Jersey. He received the 3rd Annual Engineering Excellence Award for 1986 from CECOM; served for three years as chairman of the Tri-Service Group on fibers, cables and connectors; and is a member of EIA P6.7 Working Group on Fiber Optic Cables. Most recently, he worked for ITT-EOPD as a project engineer for the air layable cable which he designed. Prior to joining ITT-EOPD, Mr. Kalomiris was associated with General Cable Corp. R&D as a research engineer for 6 years. While at General Cable he was involved with the design, development and manufacture of the prototype super-conductive power cable with flexible core. He is a member of IEEE and the Technical Chamber of Greece (Society of Professional Engineers). Education: B. A. in Mathematics, B. S. in Electrical Engineering, and M. S. in Electrical Engineering, all from the New York University, and an M. B. A. from Fairleigh Dickinson University.

OPTICAL FIBER MODULES FOR MILITARY AND SPACE APPLICATIONS

Mike Hartmann, Ron Landgraff, Bill Philipson

PCO, INC.

Optical fiber is now being widely used for commercial applications. Military applications are moving rapidly towards production. This paper summarizes the status of commercial transceiver modules, and describes some of the efforts now in progress for military applications.

Introduction

The number of applications for fiber optic communications links has grown rapidly over the past 5 years. Usage of these links has spread from Telecommunications to Computer/Datacom to Military and Government and Instrumentation.

In the Computer/Datacom and Military applications, users are demanding products with increasing levels of integration. These integrated products are described as "data links".

This paper briefly reviews the status of Data Link products in commercial and military applications. We summarize the characteristics of some of the more prominent commercial products and then highlight some of the more advanced module developments being funded by the Army to illustrate the differences in military applications. In the last section we review trends in data link products.

Data Link Modules for Commercial Applications

Fiber optic transmitter and receiver modules for data communication applications are available in a variety of performance categories. The modules are designed primarily for the transmission of serial digital data, featuring compatibility with the standard digital logic families.

Transmitter modules convert the input logic signal to infrared energy by means of a driving circuit and a light emitting diode (LED). Typically, the module includes a receptacle for mating to an optical fiber terminated with one of the standard optical connector types, SMA and ST being most popular. Modules compatible with the TTL logic families are available for use up to 50 Mb/s, while emitter coupled logic (ECL) is used for modules with ratings up to 200 Mb/s. Important transmitter specifications include wavelength of operation, maximum modulation rate, and level of optical energy coupled to the mated optical fiber.

Receiver modules convert infrared energy back to electrical signals. Again, the module housing usually accepts a standard optical connector. Two very important receiver module specifications include the minimum optical signal strength required for reliable conversion and the maximum optical signal strength that can be accepted without saturation. The difference between these two levels (sensitivity level minus saturation level) is a critical parameter in defining the operating range of an optical data link. Of equal importance are the wavelength of operation and the maximum bit rate for which the module was designed.

Receiver modules are also characterized by their compatibility with different formats of the serial digital data. Various formats for serial data transmission, such as non-return to zero (NRZ), bursty packet transmissions, continuously scrambled data, or continuous encoded data, can determine whether a given receiver module is usable in a given application. If usable, the data format can still affect the performance of the module or require the modification of the transmission protocol.

Typical of low cost, moderate performance data links are shortwavelength products utilizing 820

nanometer technology. The transmitter consists of an LED (requiring an external driving circuit) typically coupling -16 dBm of optical power into a 62.5/125 micron optical fiber at up to 50 Mb/s. A typical companion receiver is usable to 5 Mb/s, with sensitivity of -25 dBm, saturation level of -9 dBm, operation using 5 volt power supply, and an open collector output for TTL or CMOS signal levels. This type of link could operate over a 4 kilometer distance for a purchase price below $100 without restrictions on the data format. As data rate increases to 50 Mb/s, the prices rise to about $200/pair. Above 50 Mb/s, most fiber optic modules utilize differential ECL logic levels and 1300 nanometer operating wavelength. Table 1 compares the offerings of three vendors of products aimed at the 125 Mbaud data rate market. Dual-in-line metal packages with ST connector compatibility are used by all three vendors, with a selling price on the order of $600 or less in small quantities.

Table 1

	Manufacturer A	B	C
Transmitter & Receiver Packaging Size (inches) (less connector)	1.00x.48x.35	1.00x.48x.37	1.77x.94x.35
Style	16 pin DIP	16 pin DIP	24 pin DIP
Hermetic	yes	no	no
Connector	ST	ST	Mini-BNC
Data Rate (Min/Max) MBit/Sec	10/220	40/220	10/200
Electrical I/O	10 K ECL	100 K ECL	10 K ECL
Operating Temp. Range 0°C	-40 to +70	0 to 70	0 to 50
Power Supply Voltage	-5.2 ± 10%	-4.5 ± 5%	-5.2 ± 5%
Link Budget	14-17 dB	11-13 dB	13-15 dB

Data Link Modules for Military Applications

Data link products are planned for many military applications including tactical communications, underwater sensor systems, ships, aircraft and the space station. In this paper, we review some modules whose development is funded by the Army, which illustrate the major trends and requirements in the military and space areas.
The Army program calls for the development of a low data rate transmitter/receiver (DC to 1 Mb/s) and a high data rate pair (1 Mb/s to 50 Mb/s). Features of these links are summarized in Table 2.

Surface emitting LEDs were chosen for their reliability and temperature stability. Figure 1 shows a diagram of the low speed link. The low speed link uses off-the-shelf ICs, has a single 5 V power supply for the transmitter, the link will dissipate about 1.5 watts and has a ± 5 volt supply for the receiver.

Performance goals of the low speed link are summarized in Table 3.

Table 2

Features of Transmitter/Receiver Modules

- 1300 nm wavelength of operation
- Arbitrary input data format
- Miniaturized and connectorized packages: 16 pin DIP or 24 pin DIP
- Hermetically sealed
- Extended temperature range (- 46°C to +85°C)
- Single 5 volt supply or dual ± 5 volt power supply
- Back-to-back connection without overloading

Table 3

Performance of Low Speed Link

- Transmitter peak optical power coupled to 50/125 m fiber:
  - -14 dBm typical at 25°C
  - -16 dBm minimum at +85°C
  - -12 dBm maximum at -46°C
- Receiver peak optical power required for 10^{-9} BER:
  - -36 dBm typical at 25°C
  - -33 dBm minimum over -46°C to +85°C
- Receiver saturation level: -12 dBm worst case over -46°C to +85°C range.
- Link Budget:
  - 22 dB typical at 25°C
  - 17 dB worst case over -46°C to +85°C range

The high speed link is shown in Figures 2 and 3. This link uses two custom-integrated circuits and clock recovery with phase lock loops. Performance of the high speed links is summarized in Table 4.

Table 4

Performance of High Speed Link

- Transmitter peak optical power coupled to 50/125 m fiber:
  - -14 dBm typical at 25°C
  - -16 dBm minimum at +85°C
  - -12 dBm maximum at -46°C
- Receiver peak optical power required for 10^{-9} BER:
  - -36 dBm typical at 25°C
  - -33 dBm minimum over -46°C to +85°C
- Receiver saturation level: -12 dBm worst case over -46°C to +85°C range.
- Link Budget:
  - 19 dB typical at 25°C
  - 16 dB worst case over -46°C to +85°C range

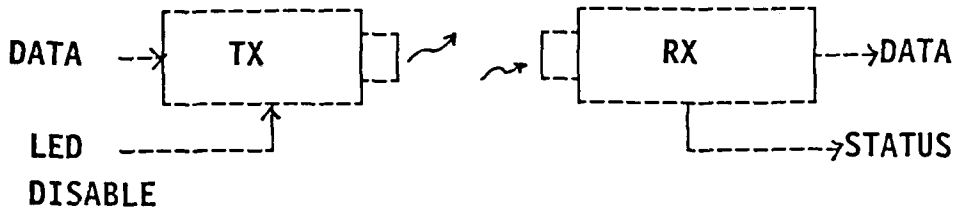

Figure 1. Low Speed Link
(DC to 1 Mbit/s)

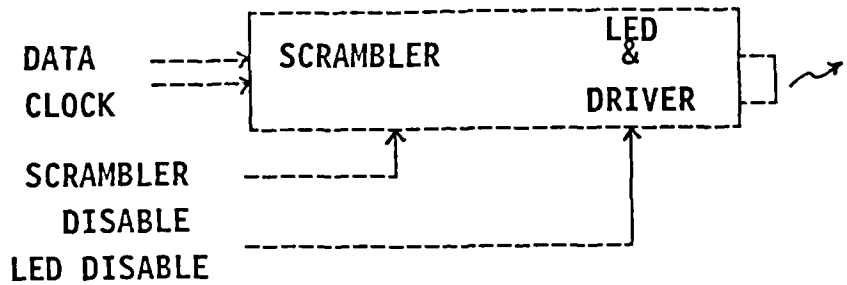

Figure 2. High Speed Link
(1 Mbit/s to 50 Mbit/s)
Transmitter Module.

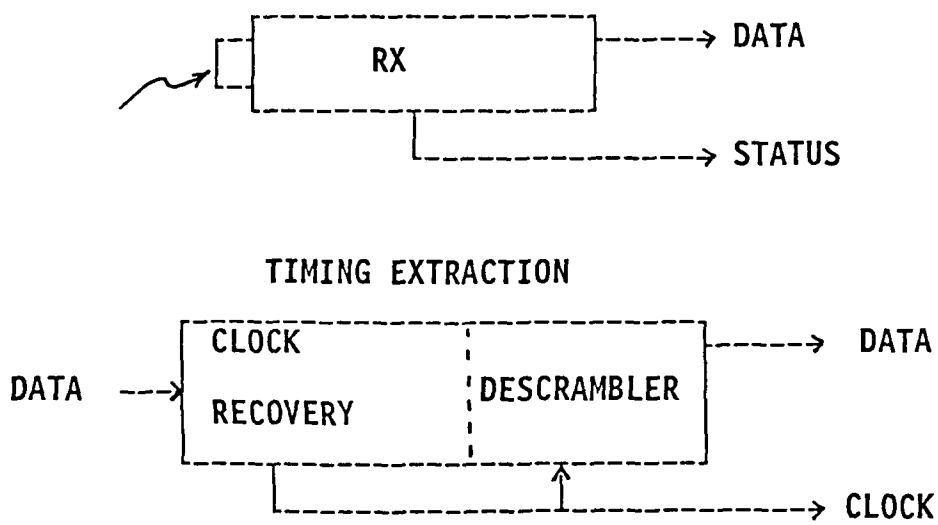

Figure 3. High Speed Link:
Receiver and Timing
Extraction Module.

Data Link Trends

In commercial applications, data rates are rising rapidly. The FDDI standard calls for 100 Mb/s of data. Several products operate to 200 Mb/s and above. The integration of more functions (coding and clock recovery) into the module is likely. The next generation of products will likely be laser based and will have data rates from 200 to 1,000 Mb/s.

For the military, data rates will rise, temperature ranges will expand to 125°C and mil-qualified parts usable in the most rugged applications (aircraft, space, etc.) will be produced. Ultimately, laser-based products will appear.

Summary

It is clear that data link products are finding application in both commercial and military applications.

On the military side, there is a strong trend towards integration of more functions in the basic data link module and a trend towards wider temperature ranges. Functions that are being absorbed into the basic module include clock recovery, multiplexing and demultiplexing, coding, alarm signals, etc. Compact packaging continues to be a major concern.

On the commercial side, data link modules are moving to lasers as sources, lower cost (as usual, prices are dropping rapidly), and lower cost packages (albeit, at a sacrifice in temperature range and link budget).

The outlook for data link products is excellent. We now have multiple, reliable vendors with the technological, financial and marketing resources to produce the products needed by our customers.

TELECOMMUNICATIONS ON TAP

Dr. Trevor R. Smith and John McDermott

STC Cable Systems Division, Newport, Gwent, NP9 OWS, U.K.

ABSTRACT

A patented technique has been developed and trialled, for installing fibre optic data link cables within live mains (ie. under pressure and flow conditions). The paper outlines some of the aspects of the design of the cable, the development of the installation and retrieval techniques, trials data and operational experience to date.

INTRODUCTION

For many years STC has manufactured power, data and telecommunication cables to be installed either underwater or in water filled conduits. The STC Dataflo technique was originally patented in 1983 and a 300 m test loop built to develop the cable design and installation system.

The objective was to develop an installed cable system using existing pipeline infrastructures. This would have the advantages of fast, easy deployment and eliminate expensive trenching. There would be limited excavation work at the entry/exit points and the cable would be installed securely in a damage-proof environment.

The pipeline is exposed only at the entry/exit points for the cable. The cable section length is variable up to 17 km, and is normally selected as the distance between valves.

An underpressure tapping is made into the pipe using specifically designed saddles. The cable is introduced to the pipe through a glanded entry system. A drag inducing device guides the cable towards the previously prepared exit point where it is accurately positioned, captured and retrieved through special seals. (See figure 1)

Cable sheath materials and pressure seals would be selected to be compatible with these pipeline liquids. In some cases there may be a requirement for the pipeline to be pigged - either to scrape deposits from the pipewall or to separate products being transported. The cable system can be designed to survive with most commonly used pigs. Foam swabs would not affect the cable system.

Once installed the cable can be simply removed or replaced if required.

CABLE DESIGN

Up to fourteen components, either fibres or fillers, are helically applied around a centre strain member. The fibres can be either single or multimode, selected for the transmission system requirements. The cable design is suitable for pipeline pressures up to 70 bar (1015 psig) and has been qualified up to 150 bar (2180 psig). The fibres are buffered and the cable is solid filled to withstand the working pressure. (Figure 2)

Cable construction materials are selected not only to be compatible with the fluids, but also to make the cable, when installed, approximately neutrally buoyant. Typical sheath materials are grades of polyetheylene, nylon or polyurethane.

The cable is designed to exist in the pipeline environment and withstand both installation and operational strains.

The central strain member will see very high tensile loads during deployment, the magnitude dependant on cable length and the fluid velocity. During and after installation the cable will be subject to dynamic stress, with fluid flow possible in either direction. If the pipeline is to be pigged this again will put additional tensile and dynamic strain on the cable.

Cable diameter is influenced by several factors. Firstly the need to keep the flow induced strain within tolerable limits (smaller diameters reduce the flow induced load). Secondly the need to be near neutral buoyancy. Thirdly pipe routing with tight bends necessitating a more flexible cable.

The cable diameter has to be accurately controlled to ensure that the dynamic and static sealing as the cable enters and exits the pipeline does not give rise to leakage.

Different forces act on the cable during installation and long term operation. It is necessary to evaluate both these conditions to ensure safe operation of the cable system. Indeed

prudent design suggests that consideration is also given to the forces that would be induced in the cable during a withdrawal operation.

The forces acting on the cable can be categorised as follows.

Primary Forces

Drag:	due to liquid flow
Friction:	due to cable weight in fluid
Pressure:	due to pressure at input and exit of cable
Buoyancy:	due to upthrust of fluid on cable
Tension:	due to final clamping forces

Secondary Forces

Gravity:	due to cable weight in inclined pipe
Capstan:	due to additional friction at bends

In addition there are the forces associated with pressure around the cable, the bending stresses on a cable due to pulling off drums and being inserted into the pipeline, and the friction forces at pipe seals.

Figure 3 gives a diagramatic representation of the forces in the pipeline.

The drag forces are a function of the flow rate. When the cable is stationary these forces are highest (note, higher forces would be induced when pulling against the flow).

Maximum cable tension increases significantly with length of installation. (Figure 4)

Friction of the cable and the capstan effects around bends only apply during installation.

A full mathematical model has been developed to determine the cable stresses and thereby confirm the cable design and installation parameters. It also is used to assist in the 'flight plan' determined for every installation.

From early trials work it was realised that there are a large number of installation parameters to be considered as the cable is launched into the pipeline network. Pressures, flow conditions, length, size of cable bends, topography etc., all have an influence on the cable. If the cable overshoots its final exit point, can it be safely withdrawn the few centimetres necessary for successful capture? As a result of this experience, it was decided that a plan of installation would be written for every scheme detailing speeds of installation against the environmental conditions. This plan became colloquially known as a 'flight plan' because it resembled an airline pilots operational procedures.

This model has been compared with experimental data and shown to give a good correlation. (Figure 5) and it has been used to show how the impact of friction and bends influences the tension along a cable length during installation. (Figure 6)

It is possible to determine windows of operation for a successful installation. (Figure 7) Should the operating conditions fall outside the acceptable window it may be necessary to redesign the cable, modify the flow rates for short term, reduce the section to give shorter length or utilise a modified installation technique.

UNDER PRESSURE TAPPING

A number of techniques are available to tap into a pipeline while it is operating under fluid flow and pressure. Most involve the placing of a saddle around the pipeline and the hole is then drilled through a valved spigot. The appropriate technique would be selected depending on pipeline material and pressure. Most underpressure tappings allow the swarf and the coupon removed from the pipeline to be withdrawn without contaminating the fluid.

The tapping would be at right angles to the pipeline unless the pipeline has to be pigged. In this case it would be at 30° to allow the cable to be introduced without obstructing the pipeline.

Experience has been obtained on ductile iron, grey iron, polyethylene and steel pipelines, with consideration now being given to asbestos cement and PVC. Current experience has covered the range 63 mm - 600 mm nominal diameter.

Tools and techniques have been developed to allow all fittings necessary for the cable to be installed under pressure during the tapping operation. These include quills, bend restrictors, seals and valves.

Access chambers for vertical entry to the pipeline are considerably smaller than for angled entry where pigging is expected.

INSTALLATION

The cable is produced in lengths to suit the pipeline section. Where necessary it can be passed through a cleaning or sterilisation process before being fed through the insertion equipment. This insertion equipment is designed to drive the cables through the seals and into the pipeline. A drag inducing device then guides the cable in the fluid flow. The cable is designed to be neutrally buoyant and minimum friction experienced between the cable and the pipe.

The cable system can be deployed in most pipeline configurations including bends and vertical sections. The deployment rate is relative to the flow in the pipe and can be up to 3.6 km/hr (ie. 1m/sec). Most pipelines operate at velocities below 3m/sec.

The insertion equipment is used to control the deployment speed and to locate the cable for capture. A 'flight plan' is developed for each installation and it is usually possible to monitor cable progress through sensors located outside the pipeline.

These sensors accurately position the cable end for capture.

A considerable amount of experimental work has been undertaken to develop drag inducing devices which ensure that the cable is held centrally and stably in the flow to enable capture to take place. These drag inducing units vary in design due to the size of pipe, pressure and flow rates.

Capture equipment enters the pipeline through the prepared underpressure tapping and the cable is withdrawn through the seals. These tappings are at 30° or 90° to the pipeline dependent on whether pigging occurs. The cable will then be tensioned to a predetermined level to ensure optimisation of cable life.

Experiment trials have involved proving these techniques for continuous cable length up to 11 km and have also involved 'pumping' a cable inside a duct up a height of 80 feet.

TERMINATION/JOINTING

Where the cable sections have to be jointed to form part of a completed cable system tails would be taken from either side of the valve and jointed using normal fibre optic techniques. Alternatively, traditional cable laying techniques may be employed to take the cables from the access pit to an adjacent building.

PIPELINE INTEGRITY/FRACTURES

The under pressure tapping techniques will not affect the integrity or certification of the pipeline. However, if the pipeline leaks or is fractured it is worth considering the position of the cable.

Being within the protected environment of the pipeline the cable is less suseptible to accidental damage than when simply trenched or buried in conduits. If the pipeline has a minor leak, clamp repairs will not affect the cable.

If there is a catastrophic failure or burst it is likely that the cable will survive the initial damage. However, the pipeline operators main priority will be the reinstatement of the piped service. If possible, the cable can be easily removed, stored and replaced when the work is complete. If it is damaged during the pipeline repair the installation of the replacement cable is simple as the end fittings are already in place.

Should any planned maintenance on the pipeline or route changes be contemplated, early consideration can be given to the cable.

CONCLUSION

The experimental stage has now been completed and the system is being introduced commercially as a proven alternative to conventional installation. The method needs trained installation crews using the specially developed cable, equipment and techniques. The advantages of installation speed and use of existing conduits/wayleaves make it an attractive proposition to both pipeline operators and telecommunication networks. It can be as easily installed both in the downtown areas, thereby reducing congestion and reinstatement costs, and in rural areas without need to disturb crops and pasture. By being installed inside a pipe, the risk of third party interference is reduced.

Water and fire mains are one of the areas now having these novel cable systems introduced.

BIOGRAPHIC NOTES

Dr. Trevor Smith holds the position of Technical Manager of STC Cable Systems Division, where he has responsibility for engineering and specialist cable manufacturing. He has been with STC since 1984. Prior to then, he has held a number of senior management positions in international manufacturing and research organisations with a particular emphasis on pipe valve and fittings development. He is a chartered Water Engineer and a chartered Gas Engineer. He holds a degree in Mechanical Engineering and a PhD for research into glass reinforced plastics, both of these awards being obtained from Nottingham University.

John McDermott joined STC in 1983 and is responsible for the marketing of specialist fibre optic cable systems.

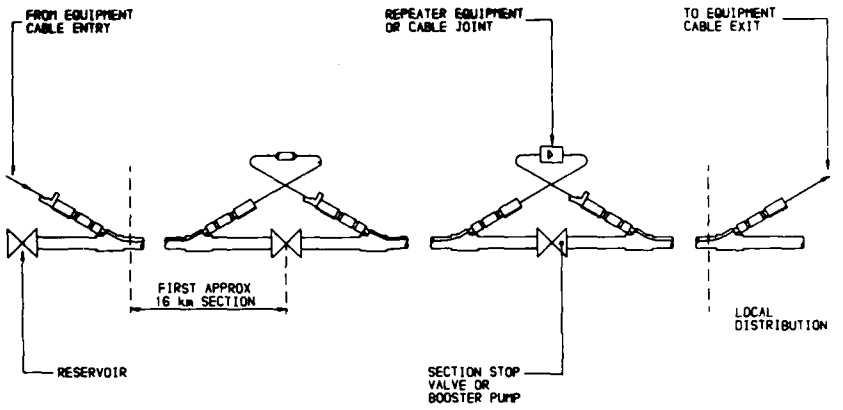
FROM EQUIPMENT
CABLE ENTRY
REPEATER EQUIPMENT
OR CABLE JOINT
TO EQUIPMENT
CABLE EXIT
FIRST APPROX
16 km SECTION
LOCAL
DISTRIBUTION
RESERVOIR
SECTION STOP
VALVE OR
BOOSTER PUMP

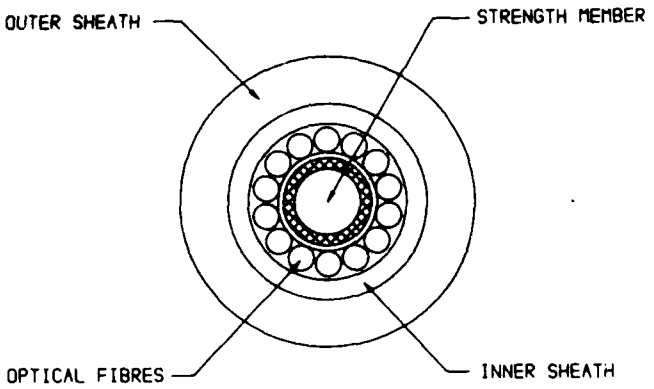
OUTER SHEATH
STRENGTH MEMBER
OPTICAL FIBRES
INNER SHEATH

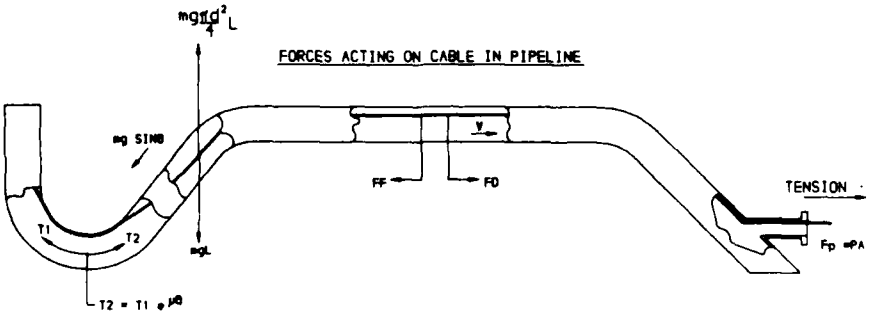
FORCES ACTING ON CABLE IN PIPELINE
mg SINθ
FF
FD
TENSION
T1
T2
mgL

FIGURE 3

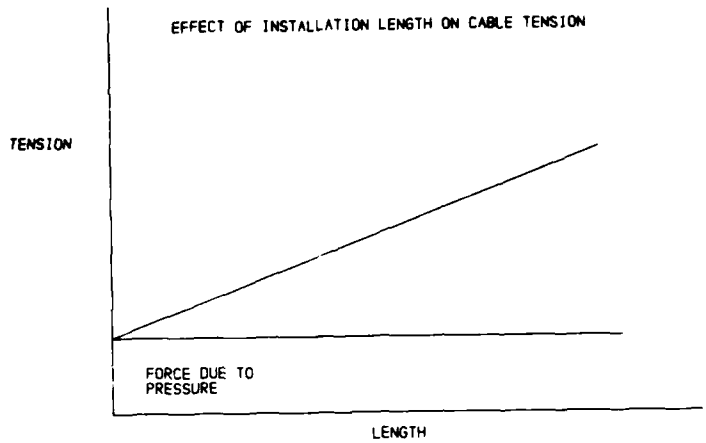
EFFECT OF INSTALLATION LENGTH ON CABLE TENSION
TENSION
FORCE DUE TO
PRESSURE
LENGTH

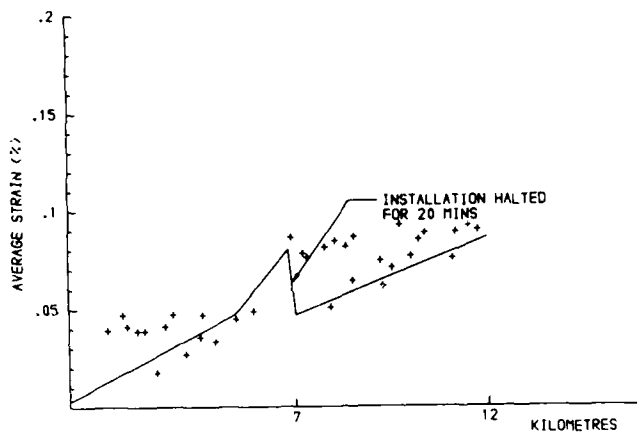
.2
.15
.1
.05
AVERAGE STRAIN (%)
INSTALLATION HALTED
FOR 20 MINS
7
12
KILOMETRES

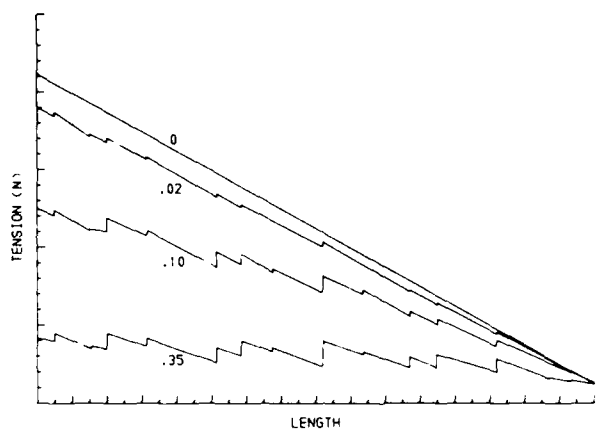
0
.02
.10
.35
TENSION (N)
LENGTH

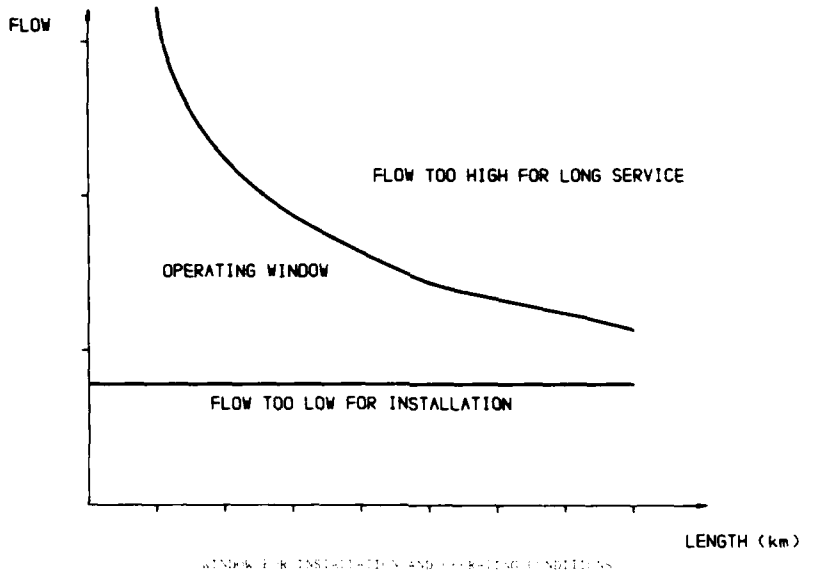
FLOW
FLOW TOO HIGH FOR LONG SERVICE
OPERATING WINDOW
FLOW TOO LOW FOR INSTALLATION
LENGTH (km)

FIGURE 7

CLASSIFICATION OF ELECTRICAL CABLES BASED ON VERTICAL FIRE PROPAGATION

M. M. Khan and A. Tewarson

Factory Mutual Research Corporation - Norwood, Massachusetts 02062

ABSTRACT

This paper presents the results of a study undertaken at Factory Mutual Research Corporation to quantify the vertical fire propagation of cables using laboratory-scale flammability apparatus, where large-scale fire radiation conditions are simulated. A new technique has been developed to quantify vertical fire propagation rate from the chemical heat energy released and burned surface area of the cable. This fire propagation rate was found to be proportional to the ratio of radiant fraction of chemical heat release rate to the thermal response of the cable; the ratio is expressed as the Fire Propagation Index (FPI). The results from the laboratory-scale (500 kW-scale) flammability apparatus were validated by conducting large-scale cable fire tests in the 5000 kW-scale flammability apparatus. A laboratory-scale test method has been proposed to classify cables based on FPI.

INTRODUCTION

Electrical wires and cables are installed in almost every occupancy and industry for the purposes of power, control, and signaling. Generally, the polymeric materials used in the wire and cable insulations and jacket materials are combustibles in varying degrees. These combustibles pose serious fire hazards in terms of fire propagation and growth, generation of heat, smoke, corrosive and toxic compounds[1].

Although there exists several national and international standard test methods for the flammability evaluation of cables, they are difficult to use to assess the fire hazard of cables in large-scale fires. In order to evaluate the realistic fire behavior of wires and cables in relation to their end use applications, it is necessary to develop a small-scale test method, where larger-scale fire conditions are properly simulated. Recently, a new small-scale test technique, where flame radiation condition of large-scale fires are simulated, has been developed for the assessment of the vertical fire propagation behavior for cables[2,3]. Data from these small-scale tests have been validated through large-scale cable fire tests[3].

In this paper, electrical wires and cables are classified based on their vertical fire propagation behavior. Using fundamental flame propagation theories, an engineering relationship has been developed for the vertical fire propagation rate for wires and cables using experimental data from small-scale (500 kW-scale) and large-scale (5000 kW-scale) cable fires. Based on this relationship, a Fire Propagation Index (FPI) has been identified to classify wires and cables into three groups. Group 1 cables are not expected to have self-sustained fire propagation (fire propagation in the presence of heat sources only). Fire propagation is expected to be self-sustained for Groups 2 and 3 cables; the fire propagation rate increases linearly with time for Group 2 cables, whereas it increases exponentially with time for Group 3 cables.

Finally, based on FPI, a small-scale test method has been proposed to classify wires and cables.

TECHNICAL BACKGROUND

Fire Propagation Velocity

In order for a flame to propagate over the surface of a combustible solid, sufficient heat must be transferred from the burning region to the unburned region to raise it to the temperature for sustained ignition. A detailed discussion pertaining to recent advances in the experimental study of the mechanisms controlling flame propagation over the surface of combustible solids has been presented in a review paper[4].

Upward flame propagation velocity for thermally thick solids, in concurrent flow (i.e., gas flow is in the same direction as that of flame propagation), is expressed as[5]:

$$V^{1/2} = \dot{q}''_f \delta_f^{1/2} / (T_{ig} - T_s)(k\rho c)^{1/2} \qquad (1)$$

where V is in m/s; $\dot{q}''_f$ is the radiant heat flux from the flame to the solid surface (kW/m^2) and δ_f is the flame length (m); T_{ig} is the ignition or pyrolysis temperature (K), T_s is the unburned solid surface temperature (K) and $(k\rho c)$ is the thermal properties of the solid: k is thermal conductivity (kW/m-K), ρ is density (kg/m^3) and c is the specific heat (kJ/kg-K).

The denominator in Eq (1) can be defined as the thermal response of the surface of the combustible solid[2,3], which is a function of time to sustained ignition:

$$t_{ig}^{1/2} \alpha (T_{ig} - T_s)(k\rho c)^{1/2}/\dot{q}'' \qquad (2)$$

where t_{ig} is the time to ignition(s), and $\dot{q}''$ is the imposed heat flux to the solid surface (kW/m^2).

$\dot{q}''_f$ in Eq (1), is taken as proportional to the radiative fraction of chemical heat release rate from the burning material surface, which essentially provides heat to the unburned surface to maintain flame spread process:

$$\dot{q}''_f \alpha (\chi_R \dot{Q}'_{ch})^n \qquad (3)$$

where χ_R is the radiant fraction, $\dot{Q}'_{ch}$ is the chemical heat release rate (kW/m), and n is less than unity.

It has been experimentally shown[6] for pool fires that flame radiative heat flux, $\dot{q}''_f$, increases and approaches an asymptote with the increase of mass fraction of oxygen, m_{O_2}, in the environment. The asymptotic value of $\dot{q}''_f$ (for m_{O_2} between 0.344 to 0.466) was found to be equivalent to the values for large-scale fires[6].

The fire propagation velocity, V, can be determined from the following expression:

$$\ell(t) = [\frac{1}{W}] [A_T/E_T] E(t) \qquad (4)$$

where $\ell(t)$ is the burn out or combustion length[3] (m) as a function of time, W is the width of the solid (m), A_T is the total burnt surface area (m^2), E_T is the total chemical heat energy released (kJ) from ignition to complete flame extinction (A_T/E_T is assumed to be constant), and E(t) is the chemical energy released (kJ) as a function of time, which is given by,

$$E(t) = \int_{t_{ig}}^{t_e} \dot{Q}_{ch}(t)\, dt \qquad (5)$$

where $\dot{Q}_{ch}$ is the chemical heat release rate (kW), integrated between ignition (t_{ig}) and extinction (t_e) times (s).

In case of a single vertical cable configuration, $\ell(t)$ in Eq (4) can be written as[2,3]:

$$\ell(t) = [\frac{1}{\pi d}] [A_T/E_T] E(t) \qquad (6)$$

where d is the outer diameter of the cable (m).

For multiple cables in vertical wall configuration (single layer)[3],

$$\ell(t) = [\frac{1}{\pi dN}][A_T/E_T] E(t) \qquad (7)$$

where N is the number of cables.

The fire propagation velocity is a function of time is thus,

$$V(t) = \frac{d\ell(t)}{dt} \qquad (8)$$

Finally, by using Eqs (1) and (3), the fire propagation velocity can be expressed as

$$V^{1/2} \alpha (\chi_R \dot{Q}'_{ch})^n/(T_{ig} - T_s)(k\rho c)^{1/2}. \qquad (9)$$

The fire propagation velocity in Eq (9) is proportional to the ratio of the radiative fraction of chemical heat release rate to the thermal response of the cable surface.

EXPERIMENTAL APPROACH

Experiments were conducted in our 10 kW-, 500 kW- and 5000 kW-scale flammability apparatuses[3], shown in Figure 1. About 35 cables of various types of insulation and jacket materials, including three solid pine cylinders, were used in the laboratory-scale apparatuses (10 kW- and 500 kW-scale). In order to validate laboratory-scale data, five cables out of 35 cables were examined in the large-scale apparatus (5000 kW-scale).

Ignition Experiments in 10 kW-Scale Apparatus

Cable samples, 0.10 m long, both ends covered with aluminum foil, were exposed to different radiant heat flux values. In the experiments, the time to piloted ignition was measured. No significant variations were found in the piloted ignition data due to vertical or horizontal configurations[2]. Figure 2 shows the relationship between time to ignition and external heat flux where a minimum value of external heat flux on the X-axis, when $(\text{time to ignition})^{-1/2}$ equals zero, is defined as critical heat flux for piloted ignition, which separates the ignition and no ignition zones. The inverse of the slope of the linear portion of the curve in Figure 2 represents the thermal response, $(T_{ig} - T_s)(k\rho c)^{1/2}$, satisfying the relationship in Eq (2), where proportionality constant is assumed to be unity.

Vertical Fire Propagation Experiments in 500 kW-Scale Apparatus

Experiments were conducted in the 500 kW-scale flammability apparatus[2,3] using 0.51 and 1.3 m single cable in vertical orientation. The cable was surrounded by a quartz tube, 0.30 m in diameter and 0.63 m in length, extended to 1.4 m by a Pyrex tube with similar diameter. Air with an oxygen concentration of 30-40% was introduced at the bottom of the quartz tube with a gas velocity[2] of 0.11 m/s, simulating flame radiation-dominated large-scale fires. The cable was surrounded at the bottom by four coaxially placed tungsten-quartz radiant heaters. The external heat flux zone (from these radiant heaters) was about 0.20 m vertical length from the bottom of the cable. In the experiments, peak external heat flux value of 50 kW/m^2 was used. Thus, both external heat flux assisted fire propagation and self-sustained fire propagation beyond external

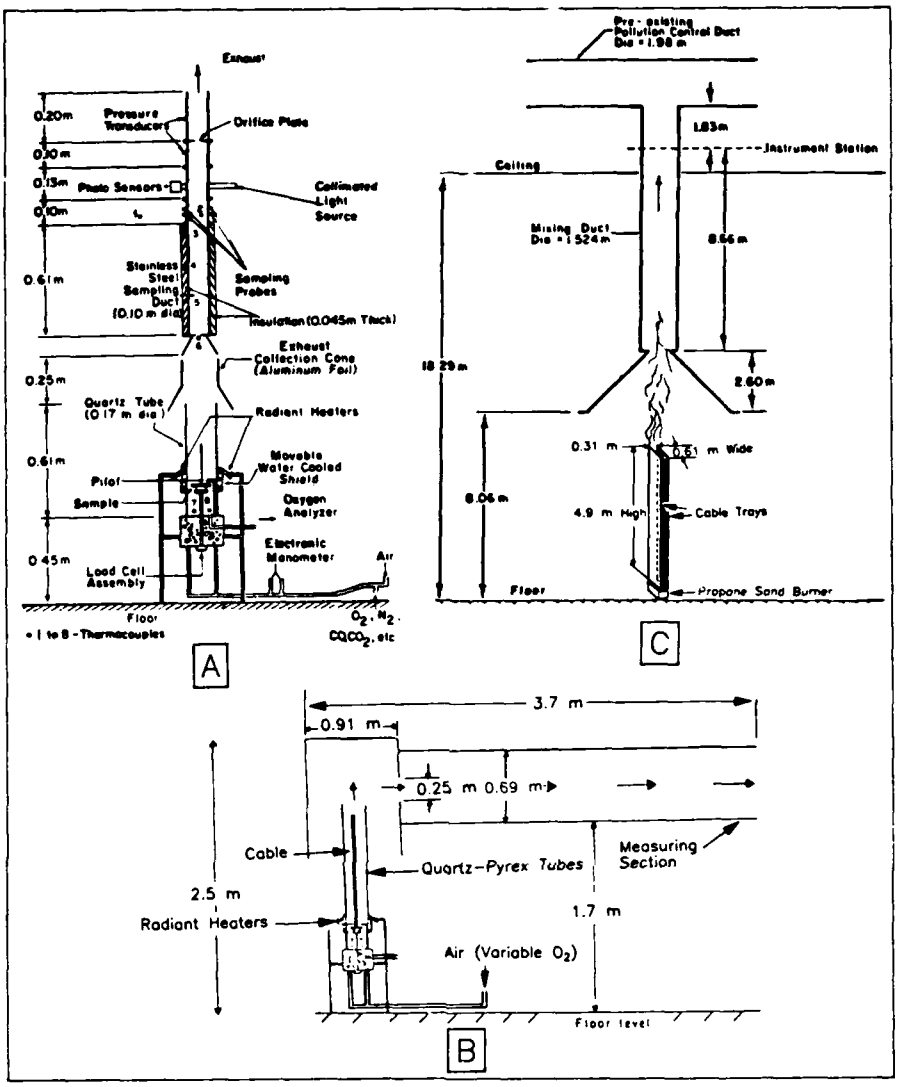

Figure 1. Flammability Apparatuses used in the Experiments: A) 10 kW-scale; B) 500 kW-scale; and C) 5000 kW-scale.

heat flux zone was quantified. All the fire products generated during fire propagation were captured in the sampling duct, where measurements were made, as functions of time, for generation rates of CO, CO_2, total gaseous hydrocarbons, optical density of smoke, and depletion rate of oxygen. In addition, visual observations were made for time to ignition and extent of fire propagation. The chemical heat release rate was calculated from the generation rates of CO and CO_2 as a function of time.

Vertical Fire Propagation Experiments in 5000 kW-Scale Apparatus

The results from the 500 kW-scale apparatus were validated by conducting large-scale cable fire tests[3] in the 5000 kW-scale flammability apparatus, which uses the same measurement principles as the 10 kW- and 500 kW-scale apparatuses. For the tests in the 5000 kW-scale apparatus, multiple cables in a vertical wall configuration were used. A single layer of cables was attached diameter-to-diameter on two vertical Marinite sheets. Each sheet was about 0.61 m wide and 4.9 m long. The two Marinite sheets were about 0.31 m apart, with cables facing each other. In such parallel configuration, flame heat flux to the cable surfaces was enhanced approximately 50%[3]. A 61 kW (210,000 BTU/hr) propane sand burner (0.305 m by 0.61 m and .305 m deep) with a flame height of about 0.5 m was used as an ignition source and was located between the sheets for uniform heating, shown in Figure 1C. Similar measurements were made in the sampling duct as in the 500 kW-scale apparatus.

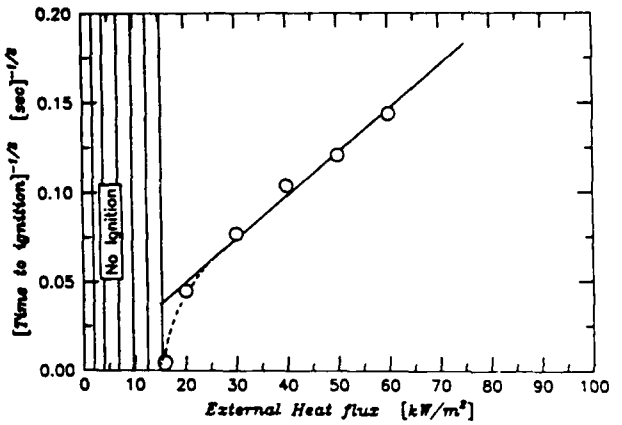

Figure 2. Relationship between time to ignition and external heat flux.

EXPERIMENTAL RESULTS

Fire Propagation Index

Figure 3 presents the fire propagation velocity versus the ratio of radiative fraction of chemical heat release rate to the thermal response of the cable surface for 0.51 and 1.3 m long single vertical cables in the 500 kW-scale apparatus. The fire propagation velocity, V (m/s), and chemical heat release rate, $Q_{ch}/\pi d$ (kW/m) (where d = outer diameter of the cable), are the peak average values[3]. χ_R, the radiative fraction, is generally equal to 0.40 for turbulent fires. V values were determined by using Eqs (6) and (8), with the experimental values of E(c) and A_T/E_T. Q_{ch} was measured in the experiments and thermal response, $\Delta T(k\rho c)^{1/2}$ (where $\Delta T = T_{ig} - T_s$), was determined from ignition experiments. In Figure 3, an excellent data correlation for cables and solid pine cylinders can be noted, which satisfies the engineering relationship in Eq (9) with n = 1/3.

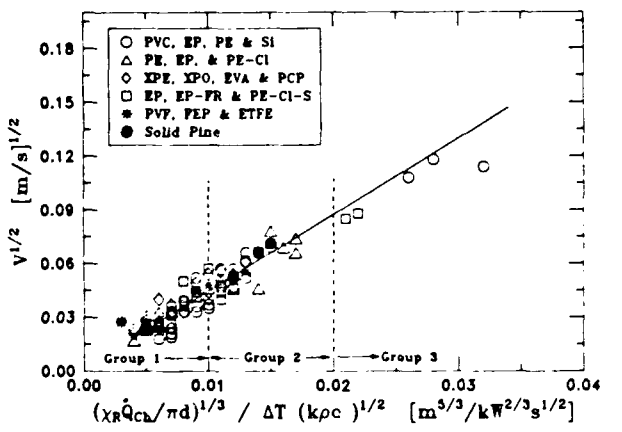

Figure 3. Fire propagation velocity versus ratio of radiative fraction of chemical heat release rate to the thermal response of the cable surface for 0.51 and 1.3 m long single vertical cables in the 500 kW-scale apparatus

It has been previously shown[3] that V values for cables, from 5000 kW-scale apparatus (calculated by using Eqs (7) and (8)) and corrected for 50% enhancement of the heat flux to the cable surface, showed an excellent correlation with the V values for the same cables (calculated by using Eqs (6) and (8)) from 500 kW-scale apparatus.

Figure 3 is divided into three regions (based on the parameter in X-axis) identified as Groups 1, 2 and 3. Cables falling in Group 1 have virtually no self-sustained fire propagation unless heat sources are provided. Cables in Group 2 have self-sustained fire propagation which increases linearly with time. Group 3 cables have very rapid self-sustained fire propagation which increases exponentially with time.

Based on the three-group regions in Figure 3, the parameter in X-axis, is thus expressed as Fire Propagation Index (FPI), which is multiplied by 10^3 for round numbers. FPI as a function of time is expressed as:

$$FPI(t) = [(\chi_R\dot{Q}_{ch}(t)/\pi d)^{1/3}/\Delta T(k\rho c)^{1/2}] \times 10^3 \quad (10)$$

For multiple cables in vertical wall configuration (single layer of cables),

$$FPI(t) = [(\chi_R\dot{Q}_{ch}(t)/\pi dN)^{1/3}/\Delta T(k\rho c)^{1/2}] \times 10^3 \quad (11)$$

where N is the number of cables.

As an example, Figures 4 through 6 show the plot of FPI as a function of time for some selected cable samples from both small-scale and large-scale experiments, where group boundaries for classification of cables are shown. For Group 1 cable, FPI is less than 10; for Group 2, FPI is equal to or greater than 10 but less than 20; and for Group 3, FPI is equal to or greater than 20.

PVF cable in Figure 4 is classified as Group 1 cable. Its fire propagation was not self-sustained. Extent of fire propagation remained within the ignition zone (heat source) both in small-scale, as well as in large-scale experiments.

Figure 5 shows fire propagation for PE/PE-Cl cable in the small-scale experiment (a large-scale experiment was not performed with this cable). Fire propagation was self-sustained for this cable and fire propagated all the way to the top of the cable at a steady rate. This cable is classified as Group 2 cable.

PE/PVC cable in Figure 6 is classified as Group 3 cable. Fire propagated very rapidly both in small-scale, as well as in large-scale experiments.

Table I presents some selected data (derived from Ref. 3) peak average values of FPI for cables with various insulation and jacket materials from small-scale (500 kW-scale) and large-scale

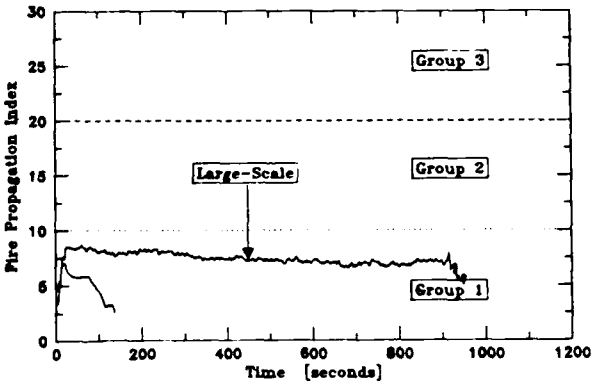

Figure 4. FPI as a function of time for PVF/none cable; diameter = 0.0050 m.

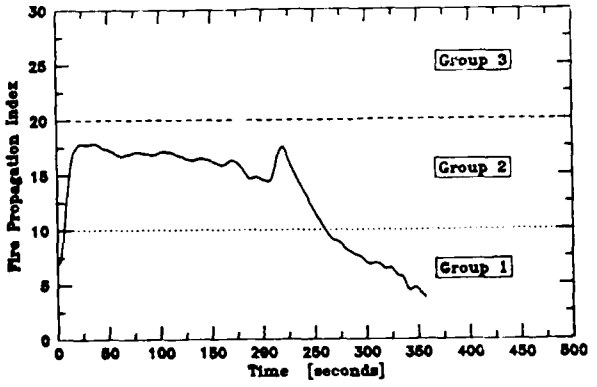

Figure 5. FPI as a function of time for PE/PE-Cl cable; diameter 0.0094 m.

(5000 kW-scale) apparatuses. Table I shows a good agreement between data from small-scale and large-scale tests in terms of FPI. This suggests that a small-scale test method for cable, where large-scale fire conditions are properly simulated, can be used for cable classification.

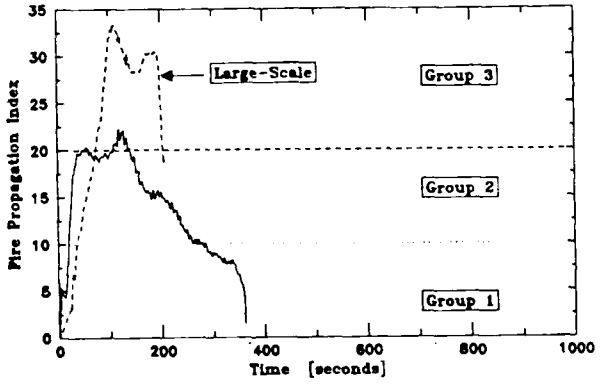

Figure 6. FPI as a function of time for PE/PVC cable; diameter = 0.011 m.

Table 1 also indicates that FPI values not only vary for cables with different insulation and jacket materials but also vary for cables with similar type of insulation and jacket materials because of differences in additives, cable construction and size of the conductor.

Standard Small-Scale Fire Test for Cables

Based on the studies we presented, it is possible to propose a standard small-scale fire test using an apparatus similar to that in Figures 1A and 1B, a single vertical cable with a length of 0.51 m (surrounded by a quartz tube of 0.61 m long and 0.30 m in diameter) and air with an oxygen concentration of 40% at a flow rate of 0.11 m/s and external heat flux of 50 kW/m^2 at the bottom as an ignition source. Fire products generated during fire propagation are captured in the sampling duct of the apparatus where measurement can be made for chemical heat release rate as a function of time. By using the radiative fraction of this chemical heat release rate per unit circumference of the cable raised to the one-third power, and thermal response data (determined from ignition experiments), a fire propagation index can be derived (Eq 10) and plotted as a function of time as shown in Figures 4 through 6. Based on the group boundaries in Figures 4 through 6, a cable can thus be classified as Group 1, 2 or 3 in terms of its fire propagation characteristics. FPI should not touch the group boundaries at any time during the test in order for a cable to qualify for a particular group classification.

CONCLUSIONS

1. Based on the application of theoretical expression for flame spread, an engineering relationship has been developed for the vertical fire propagation rate for cables using experimental data from laboratory-scale and large-scale cable fires.

2. Fire propagation rate can be calculated as a function of time using chemical energy released during fire propagation and burned surface area of the cable.

3. Oxygen concentration of 30-40% in the gas flow can be used for the laboratory-scale cable samples to simulate the fire propagation rate expected in larger-scale cable fires. Vertical fire propagation data in small-scale tests have been validated through large-scale tests.

4. Fire propagation rate is expected to depend on the type of polymeric material used in cable insulation and jacket, outer diameter, size of the conductor, cable construction and initial surface temperature of the cable.

5. A fire propagation index has been identified to classify cables. A small-scale test method thus can be used to classify cables based on this fire propagation index.

TABLE I

CLASSIFICATION OF ELECTRICAL CABLES BASED

ON FIRE PROPAGATION INDEX (PEAK AVERAGE VALUES)

Polymeric Materials		Diameter	Small-Scale (single cable) Length = 0.51 m	Small-Scale (single cable) Length = 1.3 m	Large-Scale (multiple cables) Length = 4.9 m	Cable Class.
Insulation	Jacket	(m)	FPI	FPI	FPI	(Group)
PVC	PVC	0.0036	32	N	N	3
PVC	PVC	0.0044	26	N	N	3
PVC	PVC	0.0092	15	14	N	2
PVC	PVC	0.013	11	N	N	2
PE	PVC	0.011	23	N	32	3
EP	PVC	0.011	12	11	N	2
PVC	EP	0.034	7	N	N	1
PE	PE	0.0094	17	N	N	2
PE	PE-Cℓ	0.0094	17	N	N	2
EP	EP	0.016	6	6	N	1
EP	EP	0.025	5	5	N	1
XPE	XPE	0.0095	N	13	N	2
XPE	XPE	0.011	11	N	N	2
XPE	EVA	0.012	7	N	9	1
XPE	EVA	0.022	7	6	N	1
XPE	PCP	0.015	9	N	7	1
XPO	XPO	0.016	9	9	9	1
EP	PE-Cℓ-S	0.0035	22	N	N	3
EP	PE-Cℓ-S	0.0043	21	N	N	3
EP	PE-Cℓ-S	0.016	7	7	N	1
EP-FR	None	0.028	N	7	N	1
PE-Cℓ	None	0.015	11	11	N	2
ETFE	EA	0.010	5	N	N	1
PVF	None	0.0050	6	N	7	1
FEP	FEP	0.0079	N	3	N	1
FEP	FEP	0.0092	3	N	N	1
Solid Pine[a]		0.013	N	15	N	2
Solid Pine[a]		0.019	N	14	N	2
Solid Pine[a]		0.029	N	13	N	2

a: Solid cylinder; N: Not measured; Cℓ: Chlorinated; Cℓ-S: Chloro-Sulfonated; EA: Ethylene-acrylic copolymer; EP: Ethylene-propylene copolymer; EVA: Ethylene-vinyl acetate copolymer; ETFE: Ethylene-tetra fluoroethylene copolymer; FR: Fire retarded; FEP: Fluorinated ethylene propylene; PE: Polyethylene; PCP: Polychloroprene; PVC: Poly(vinylchloride); PVF: Poly(vinylidene fluoride); XPE: Cross-linked polyethylene; XPO: Cross-linked polyolefin.

ACKNOWLEDGMENTS

Contributions towards the design and performance of the experiments in the 5000 kW-scale apparatus by Mr. J. S. Newman and experiments performed by Mr. S. D. Ogden in the 10 kW- and 500 kW-scale apparatuses are deeply appreciated.

REFERENCES

1. Khan, M.M., and Tewarson, A., "Parameters for the Assessment of Fire Hazard from Electrical Wires and Cables," Proceedings of the 33rd International Wire and Cable Symposium, November 13-15, 1984, Sponsored by the U.S. Army Communications - Electronics Command, Fort Monmouth, New Jersey.

2. Tewarson, A., and Khan, M.M., "Fire Propagation Behavior of Electrical Cables," Second International Symposium on Fire Safety Science, 1988. Hemisphere Publishing Corporation, New York, NY (in press).

3. Tewarson, A., and Khan, M.M., "Flame Propagation for Polymers in Cylindrical Configuration and Vertical Orientation," Twenty-Second Symposium (International) on Combustion, the Combustion Institute, Pittsburgh, PA, 1988 (in press).

4. Fernandez-Pello, A.C., and Hirano, T., "Controlling Mechanisms of Flame Spread," Combustion Science and Technology, 32, 1 (1983).

5. Sibulkin, M., and Kim, J., "The Dependence of Flame Propagation on Surface Heat Transfer II: Upward Burning," Combustion Science and Technology, 17, 39 (1977).

6. Tewarson, A., Lee, J.L., and Pion, R.F., "The Influence of Oxygen Concentration on Fuel Parameters for Fire Modeling," 18th Symposium (International) on Combustion, The Combustion Institute, Pittsburgh, PA, p. 563 (1981).

AUTHORS BIOGRAPHICAL SKETCHES

M. M. Khan, Factory Mutual Research Corporation, Norwood, MA 02062.

Mohammed M. Khan joined Factory Mutual Research Corporation in 1978 and is an Advanced Research Scientist. He received a Masters degree in Applied Physics from the University of Dhaka, Bangladesh and received another Masters degree from the Mechanical Engineering Department at MIT. Mr. Khan has been involved in experimental research on the flammability behavior of cables, packaging materials, and other polymeric materials. He has several publications in these fields.

A. Tewarson, Factory Mutual Research Corporation, Norwood, MA 02062.

Archibald Tewarson joined Factory Mutual Research Corporation in 1968. He is Senior Research Specialist and Manager of the Flammability Section. Dr. Tewarson received his PhD degree in Fuel Science from Pennsylvania State University. His research on the physicochemical aspects of fires includes flammability of materials, smoke, and toxic compounds generated in fires. He has over 60 publications in these fields.

USING COMBUSTION TOXICITY DATA IN CABLE SELECTION

Stanley Kaufman
James J. Refi
AT&T Bell Laboratories
Norcross, Georgia

Rosalind C. Anderson
Anderson Laboratories
Dedham, Massachusetts

ABSTRACT

As a result of New York State's combustion toxicity reporting requirements, combustion toxicity data are available on all electrical cables sold in NY. To use these data in cable selection, a method is presented for converting lethal concentration (LC_{50}) data expressed in weight of material (grams) into lengths (meters) for comparing wire and cable. Since combustion toxicity data alone should not be used for cable selection, an approach to choosing safe cables is suggested which considers flame spread, smoke emissions and LC_{50} expressed in length. A full scale validation test of this approach is proposed.

INTRODUCTION

With the adoption of New York State's combustion toxicity reporting requirements,[1] a large volume of combustion toxicity data was generated by the wire and cable industry and made available for cable purchasers and specifiers of electrical cable. The sponsors of the NY law hoped that when these data became available, it would create market demands for safer cables to which the wire and cable industry would respond.

The objective of this paper is to present an approach for using combustion toxicity data along with other fire data to help a cable specifier choose safer cables. Before being enacted, public hearings and debate surrounded the adoption of New York's toxicity reporting law. Rather than revisit those issues, we take the position that a database of combustion toxicity information exists and these data can be used wisely or unwisely. We suggest ways of viewing the data that have the greatest potential for leading to safer cables.

The data used in this paper were generated by the Arthur D. Little company under a contract with the National Electrical Manufacturers Association (NEMA). The principal investigators were Rosalind C. Anderson (toxicologist) and Peter W. Kopf (chemist).

University of Pittsburgh Test Protocol

New York state required that combustion toxicity data be generated in the University of Pittsburgh combustion toxicity test[1] illustrated in Figure 1. In this test, animals are exposed to fumes generated by materials heated in an oven. The material is heated at 20 °C/minute and animal exposure is initiated at a sample weight loss of 1%; animal exposure then continues for 30 minutes. After a 10 minute recovery period, the test animal mortality/survival ratio is noted. The test is conducted several times (4-10) with increasing sample weights, and a response curve of sample material weight versus mortality generated. A statistical method is used to calculate the mid point of the log-weight versus mortality curve and this mid point is reported as the LC_{50} value (concentration of material which causes 50% mortality of the test animals, i.e. lethal concentration) for the tested material. The unit of LC_{50} is grams.

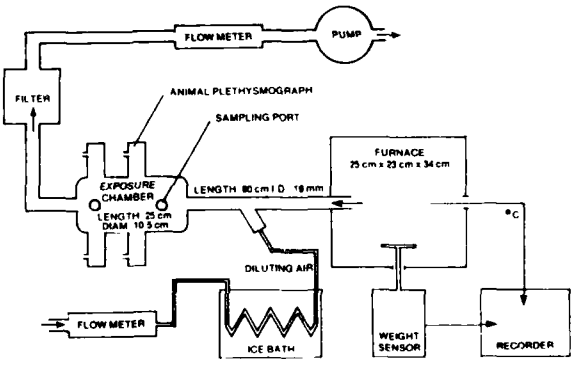

Figure 1. Test apparatus for the University of Pittsburgh combustion toxicity test.

In the NEMA study, two materials were used as intralaboratory controls, a nylon 6/6 and a commercial PVC compound. Figure 2 shows the distribution of test results for nylon; the results are tightly clustered between 5 and 10 grams.

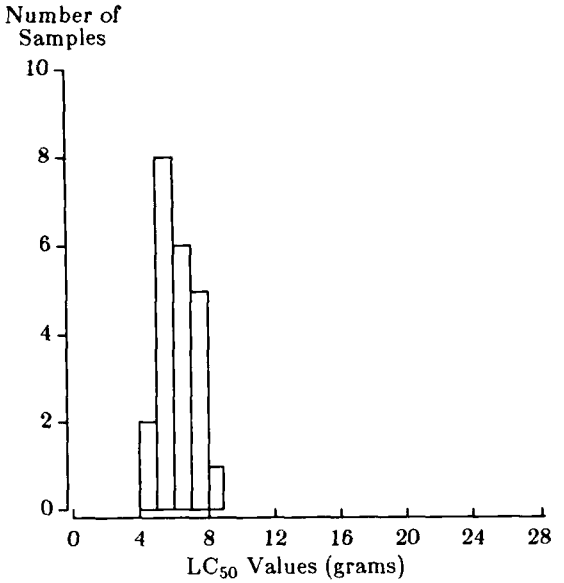

Figure 2. Histogram of the University of Pittsburgh test results on nylon 6/6 control samples.

In contrast to the results on the nylon samples, the results of the tests of the PVC control samples (Figure 3) are more widely scattered. In general, it was found that test data from halogenated materials are less reproducible in this test system than are data from materials without halogens. Replicate samples of halogenated materials vary by as much as a factor of three. The reason for this is not precisely known; however, data from the Vinyl Institute[3] suggest that smoke containing HCl is highly reactive and changes composition rapidly, and that the change in concentration is dependent on time, humidity and type of surface in contact with the smoke.

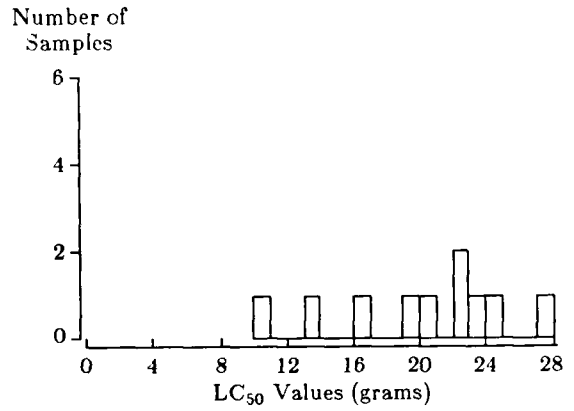

Figure 3. Histogram of the University of Pittsburgh test results on PVC control samples.

The LC_{50} and Product Comparisons

The potency of fumes is described by the LC_{50} value. This value defines, in grams, the mid point of the active portion of the concentration response curve, and provides a convenient way to compare materials. Before making conclusions based on these test values, there are two important points to note.

The first consideration is that the LC_{50} value, being expressed in units of grams, is not immediately informative about a product constructed or used on a different basis. The desirable unit for measuring safety should include both the toxicity of the material and the quantity used. For wires and cables, the critical dimension for comparison of products is the length of cable that might cause death for 50% of the test animals, rather than the weights of these cables.[4] For carpets, the dimensions for comparison would be surface area rather than weight[4].

The second important principle is that in combustion toxicology, as in most biological work, the logarithms of the test values, rather than their measured values, define the important relationships between tested products. Products for which LC_{50} values are measured as 10 and 20 grams are related similarly as products with LC_{50} values of 1 and 2 grams, or 100 and 200 grams. In each of these examples, the first product is numerically twice as toxic as the second. It can be seen from control data that except for chlorinated materials, reproducibility is within a factor of two. For this reason, it is difficult to argue that materials in which LC_{50} values differ by a factor of two have different toxicities. There is an ongoing debate among toxicologists about how different (factors of 2, 5 and 10) the LC_{50} of two materials should be before the materials are considered to have different toxicities.[5][6]

THE NEMA CLASSIFICATION SCHEME

In the NEMA classification scheme, there are 5 single material major categories and 12 multiple material major categories. In the interest of brevity, we shall consider only the single material categories.

PVC

All PVC compounds were placed in a single category regardless of plasticizer, stabilizer, filler, flame retardant or smoke suppressant. The mean LC_{50} for PVC is 17.6 grams with 98% of the population between 8.5 and 32.9 grams.

Polyolefins

Like PVC, all polyolefin plastics were placed in a single category, including unfilled polyethylenes and polypropylenes used in outside plant cable as well as

fire-resistant (filled) polymers and crosslinked polymers. Polyolefin rubbers were placed in the hydrocarbon rubber category. The mean LC_{50} is 9.9 with 98% of the population between 6.6 to 14.5.

Fluoroplastics

All fluoroplastics except polytetrafluoroethylene homopolymer (PTFE) were placed in the fluoroplastics category including three tetrafluoroethylene copolymers: (1) FEP, a fluorinated ethylene propylene copolymer, (2) PFA, perfluoroalkoxy tetrafluoroethylene copolymer, and (3) ETFE, ethylene tetrafluoroethylene copolymer. Also included were polyvinylidene fluoride (PVDF) homopolymers and copolymers, and ethylene chlorotrifluoroethylene copolymers (ECTFE). This category includes fully fluorinated polymers, FEP and PFA, partially fluorinated polymers, PVDF, ETFE and ECTFE as well as a mixed halogen polymer, ECTFE. The LC_{50} of this category is 8.9 with 98% of the population between 3.7 and 19.0 grams.

Hydrocarbon Rubbers

This category includes both thermoplastic as well as crosslinked rubbers, including polyolefin type ethylene propylene and ethylene propylene diene rubbers, natural rubber, styrene butadiene as well as polyester rubbers. As anyone familiar with rubber technology would expect, many of the rubbers contain fillers, reinforcing agents and flame retardants. The LC_{50} is 18.4 with 98% of the population between 9.7 to 32.6 grams.

Chlorinated Rubbers

This category includes chloroprene, chlorinated polyethylene and chlorosulfonated polyethylene. The LC_{50} is 22.7 with 98% of the population between 9.1 to 48.7 grams.

Summary

Figure 4 shows a histogram of the 137 LC_{50} values for all five material classes described above. Notice that rather than having a normal (Gaussian) shape, the distribution is skewed toward low values and has a long high-valued tail. A shape such as this can occur when a lower limit is imposed by the test; for example, negative LC_{50} values are impossible with this test method. Analysis of such data can be improved by taking the natural logarithm of the data as shown in Figure 5. The log-normal appearance justifies the use of log scales when portraying LC_{50} data.

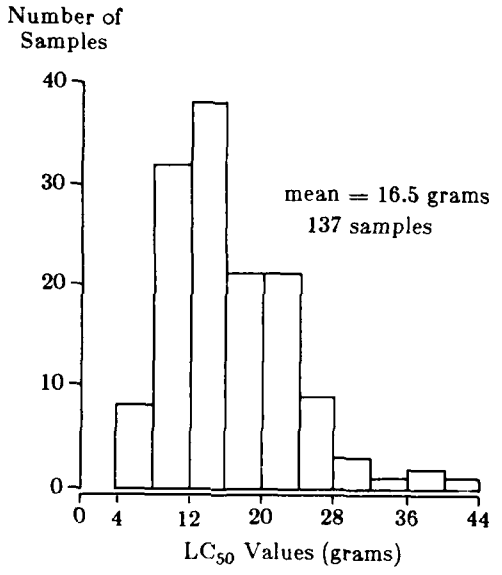

Figure 4. Histogram of the LC_{50} values for the five single material categories in the NEMA classification system.

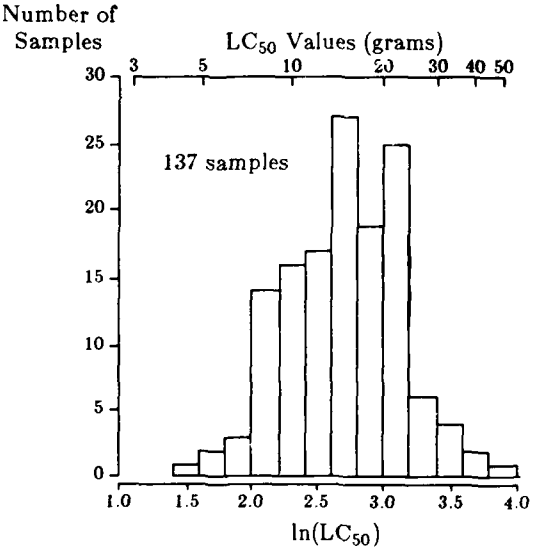

Figure 5. Histogram of the logarithm of the LC_{50} values for the five single material categories.

Figure 6 shows a logarithmic barplot of the range of LC_{50} values (98% limits) for the 5 single material categories. Because the LC_{50} values of all categories overlap, we cannot judge whether some material classes are significantly different from others.

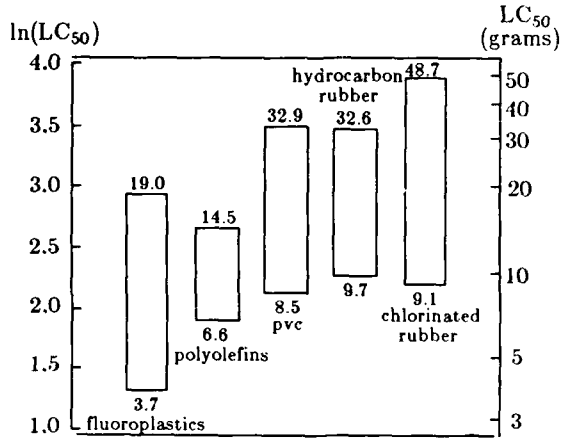

Figure 6. Logarithmic barplot of the 98% limits on the LC_{50} values for the single material categories.

A useful tool for making such judgments is to portray the LC_{50} values via the boxplots shown in Figure 7.[7] Boxplots are a convenient way to summarize and compare several sets of data. The lower edge of the box is at the first quartile of the data, the upper edge at the third quartile, and the line though the center at the median. Vertical "whiskers" extend out of the box to show the range of the data. Data values lying outside a prescribed range are considered "outliers" and plotted individually as asterisks. The notches on a box indicate a rough 95% confidence level on the median. If the notches on two boxes overlap, the medians of the two data sets do not significantly differ from each other.

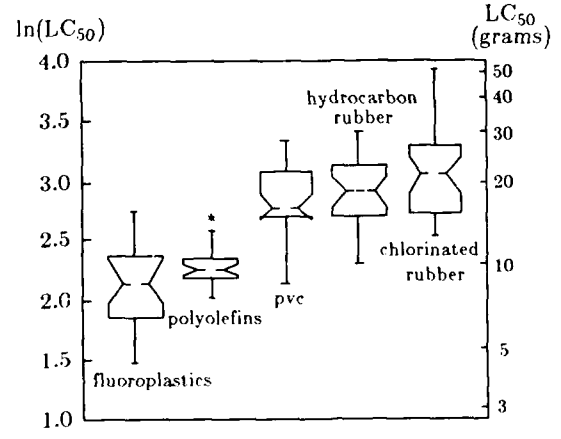

Figure 7. Logarithmic boxplots of the LC_{50} values for the single material categories.

For example, the notches for the fluoroplastics overlap those for the polyolefins and so the two classes may be considered to have similar LC_{50} values. Likewise, the PVC and hydrocarbon classes may be taken as similar to one another. Although the LC_{50} values for the chlorinated rubber materials are similar to those for the hydrocarbons, it is not clearly evident whether the chlorinated rubbers are similar to or different from the PVCs. Finally, the LC_{50} values of the fluoroplastic and polyolefin classes clearly differ from those of the PVC, hydrocarbon rubber, and chlorinated rubber classes.

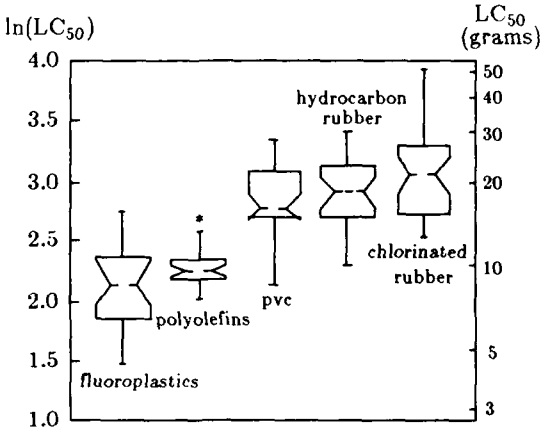

Figure 7. Logarithmic boxplots of the LC_{50} values for the single material categories.

CABLE SELECTION

The New York State Combustion Toxicity law contains a caveat on the use of combustion toxicology data. It is worthwhile to repeat that caveat here:

> This test is a measure of acute toxicity of the thermal decomposition by-products of the tested material using a specified procedure under controlled laboratory conditions. The test results alone do not constitute a characterization of the hazard, safety or risk of materials, products or assemblies under actual fire conditions. The results of this test, if used in any assessment of hazard or risk, should be considered in conjunction with all of the factors which are pertinent to an evaluation of the fire hazard of a particular end use.

The best way to compare the fire hazards of various cables is through a computer simulated hazard analysis. However, hazard analyses are too complex to be widely used. As far as we know, the only hazard analysis of cable that has been conducted and published is Bukowski's analysis[8] of fluoroplastic plenum cables. A less rigorous approach is to consider the three fire properties that are important for determining the fire hazard of a cable, viz:

1. flame spread
2. smoke emissions
3. toxic potency.

The importance of minimizing flame spread is apparent when one considers the potential for cables to spread fire through a building. Choosing a communications cable with the right flame spread properties is simply a matter of complying with the National Electrical Code which has the fire resistance hierarchy illustrated in Figure 8.[9][10] If, for example, a particular application calls for CM rated cable, then any candidate replacement cable must have a CM rating at a minimum with a CMR rating being preferable.

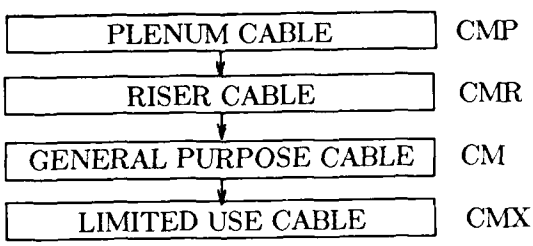

Figure 8. National Electrical Code fire resistance hierarchy for communication cables.

A candidate replacement cable should not compromise smoke emissions because smoke emissions reduce visibility and impede egress. If one is considering a cable for a plenum application, then a CMP rating is required. Since the CMP listing includes both flame spread and smoke requirements, the only additional property needing consideration is toxic potency. However if one is considering general purpose (CM) or riser (CMR) applications, smoke emissions are not specified and one has two options:

1. Measure the smoke for the candidate cables under consideration by adding smoke measurements to the prescribed flame spread tests for these cables, or
2. Upgrade to a plenum cable.

Having assured oneself that the candidate cable is no worse than present cables in flame spread and smoke properties, one is then ready to consider toxic potency. However, in no case is the use of raw LC_{50} values a suitable approach by itself for choosing the safer cable.

LC_{50} Expressed as Length

To convert LC_{50} values that are expressed in grams into a more useful form for wire and cable analysis, we need to convert to a unit of length. A few examples should help clarify and support this statement. Consider two 24 gauge insulated wires. One wire is insulated with 10 mils of solid FEP and the second with 10 mils of foamed FEP. The LC_{50} of both these wires is 8.9 grams, but the wire with foamed insulation has less material and would emit a lower level of toxic gases when burned.

Consider two hypothetical insulated 24 gauge wires with equal insulation thicknesses. The first wire is insulated with material A which has a specific gravity of 1 and a LC_{50} of 20. The second wire is insulated with an equal thickness of material B which has a specific gravity of 2 and a LC_{50} of 40. One might choose a wire insulated with material B based on its LC_{50} being twice that of material A. However, because material B has twice the specific gravity of material A, twice as much B material is used per unit length, and this exactly offsets the apparent advantage of the higher LC_{50} material.

To further consider the effect of density, let us revisit the fluoroplastic, polyolefin, and PVC boxplots of Figure 7. Because the density (ρ) for each tested material is not available, we will assign typical values for each class, namely, 0.95 g/cm^3 for polyolefin, 1.35 for PVC, and 1.76 for fluoroplastic. Figure 9 shows boxplots of the logarithm of the material volumes which produce a given LC_{50}, (LC_{50}/ρ) for the three materials. Notice that the high specific gravity of the fluoroplastics has shifted its box down and that the low specific gravity for the polyolefins has shifted it up, thereby causing these two classes to have different toxicity characteristics when viewed on a volume basis as opposed to a weight basis. Contrastingly, the polyolefin and PVC classes now approach similarity as compared to their distinctively different relationship on a weight basis.

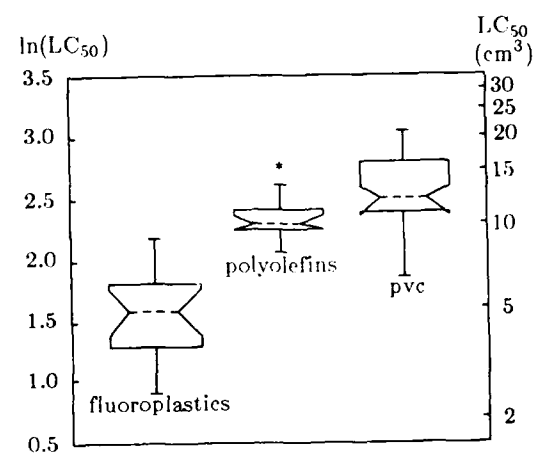

Figure 9. Logarithmic boxplots of the LC_{50} values expressed as volumes for the single material categories.

To consider the effects of density and the amount of material used, i.e., insulation and jacket thicknesses, we need to convert LC_{50} values into length. This is the length of insulated wire or cable needed to contain a weight equal to the LC_{50}. Figure 10 illustrates the method for converting from LC_{50} expressed in grams to LC_{50} values in meters.

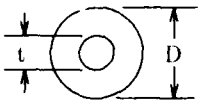

$$\text{linear density (g/m)} = 1500\pi\rho\left[(D/2+t)^2-(D/2)^2\right]$$

where:

D = conductor diameter (mils)
t = insulation thickness (mils)
ρ = density (g/cm^3)
LC_{50} (meters) = LC_{50} (grams)/linear density

Figure 10. Converting LC_5 values from grams to meters for a single insulated conductor.

Figure 11 shows the results (using 95% confidence intervals on the median) as a function of insulation thickness for 24 AWG wires insulated with PVC, polyolefin, and fluoroplastic. The polyolefin wire falls in the middle of the PVC range—indicating that the median performance for the two materials is essentially similar. As a group, the LC_{50} values in length for PVC and polyolefins are significantly higher than for fluoroplastic insulated wire.

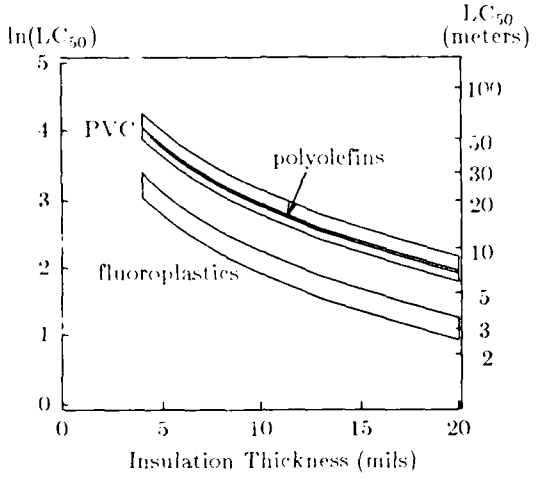

Figure 11. This figure compares the LC_{50} expressed in meters for PVC, fluoroplastics and polyolefins and shows the variation with insulation thickness.

Converting LC_{50} values from grams to meters can also be extended to cables as illustrated in Figure 12. Let's consider cables that have the same material for insulation and jacket, and compare their LC_{50} values in meters when the cables are made with four different materials. To make the comparison as realistic as possible, we will consider the physical properties of each material and adjust the insulation and jacket thicknesses accordingly. Table 1 lists the materials we are comparing: two widely used materials (PVC and fluoroplastics), and two hypothetical materials (A and B). The specific gravity and tensile strength for PVC are typical values, while the specific gravity and tensile strength for the fluoroplastics are the properties of ECTFE copolymer. The LC_{50} range (20-30 grams) of hypothetical material A was chosen to represent a material above the mean (16.5 g) of the distribution of LC_{50} values shown in Figure 5, while the LC_{50} value of 40-60 grams for hypothetical material B represents a material at the extreme high end of LC_{50} values found. The specific gravities and tensile strengths assigned to the hypothetical materials are reasonable for filled polymers.

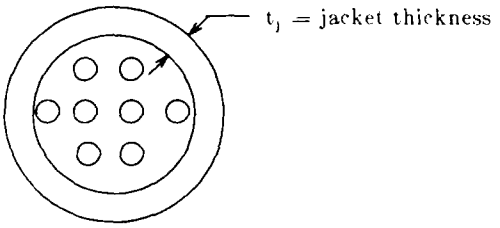

linear density of insulation (g/m) = 8× linear density of single insulated conductor

core diameter (mils) = 5(D + t)

linear density of jacket (g/m) = π(core diameter)$t_j\rho$

LC_{50} (meters) = 1500 LC_{50} (grams)/(jacket linear density + insulation linear density)

Figure 12. Converting LC_{50} values from grams to meters for an eight conductor cable.

Table 1
Cable Comparisons

Material	95% Confidence Interval on Median LC_{50}	Density (g/cm^3)	Tensile Strength (psi)
PVC	15.2-18.7	1.35	3000
Fluoroplastics	7.2-10.0	1.76	7000
Material A	20-30	1.5	2000
Material B	40-60	1.7	1500

Table 2 shows the insulation and jacket thicknesses used in the calculations from converting LC_{50} from grams to meters. The values used for PVC and fluoroplastics are typical ones used by a major manufacturer. Note that the jacket thickness for fluoroplastics is only 8 mils reflecting its superior physical properties and high cost. An insulation thickness of 8 mils (2 mils thicker than for PVC) was assigned to the hypothetical materials because they are hypothesized to have poorer physical properties than PVC. Likewise, the hypothetical materials were assigned jacket thicknesses of 30 mil 10 mils thicker than PVC.

Table 2 LC_{50} (meters) Values of 4 Pair Cables			
Material	Insulation Thickness (mils)	Jacket Thickness (mils)	LC_{50} (meters)
PVC	6	20	1.25-1.53
Fluoroplastics	5	8	0.92-1.27
Material A	8	30	0.90-1.35
Material B	8	30	1.60-2.40

Looking at the LC_{50} (meters) values we see that the PVC and fluoroplastic cables in this example have LC_{50} (meters) ranges that slightly overlap. We are therefore hard pressed to conclude that the two cables significantly differ. Hypothetical material A, which has a high LC_{50} (20-30 grams) has an LC_{50} (meters) range significantly overlapping PVC and the fluoroplastics—indicating no significant differences among these three cables. Only hypothetical material B, which has the highest LC_{50} (40-60), has a LC_{50} (meters) above the range of the other cables.

Validation Testing

If one uses LC_{50} expressed in either grams or meters in cable selection, then one has made the assumption that a correlation exists[11] between the toxic potencies (LC_{50}) determined in the Pittsburgh protocol and a real fire scenario. Certainly the test conditions of this combustion toxicology test differ from those of a developing fire.

To determine if one cable is safer than another in a real fire scenario requires full scale fire testing.[12] If, for example, the cables being considered were rated for riser use (CMR), then the UL 1666 riser cable test could be expanded to include smoke and toxic potency. Smoke measurements could be readily added, and combustion toxicity could be ascertained by directing some of the effluent to a series of animal exposure chambers. Until testing of this type is done, it will not be known whether cables with higher LC_{50} values are truly safer.

SUMMARY

The NY State database of combustion toxicity information includes LC_{50} values for cables used in buildings. These data should not be used alone for cable selection, but along with flame propagation (UL fire resistance ratings) and smoke data. To reasonably use combustion toxicity data in cable selection, the LC_{50} values should be converted to length.

ACKNOWLEDGEMENTS

We are grateful to Mr. John C. Hyder of AT&T Bell Laboratories for writing the computer program for converting LC_{50} from grams to meters.

REFERENCES

1. New York State Uniform Fire Prevention and Building Code, Article 15, Part 1120, Combustion Toxicity Testing, New York Department of State, Office of Fire Prevention and Control, Albany, NY

2. Y. C. Alarie and R. C. Anderson, "Toxicologic and acute lethal hazard evaluation of thermal decomposition products of synthetic and natural polymers," *Toxicol. Appl. Pharmacol.*, 51, 341, 1979

3. J. J. Beitel, C. A. Bertelo, W. F. Carroll, Jr., A. F. Grand, M. M. Hirschler and G. F. Smith, "Hydrogen Chloride Transport and Decay in a Large Apparatus: II. Variables Affecting Hydrogen Chloride Decay," *Journal of Fire Sciences*, Vol. 5 - March/April 1987, p 105.

4. Alarie, Yves; Matijak-Schaper, Michelle; Stock, Maryan F., "Toxicity of Thermal Decomposition Products from Commonly Used Synthetic Polymers," *Fire Sci. Technol. (NY)*, 1982 Volume:1, Number: 1.

5. H. J. Klimisch, J. E. Doe, G. E. Hartzell, S. C. Packham, J. Pauluhn, and D. A. Purser, "Bioassay Procedures for Fire Effluents: Basic Principles, Criteria and Methodology," *Journal of Fire Sciences*, Vol. 5 - March/April 1987, p 73.

6. Alarie, Y., Anderson, R. C. "Toxicologic classification of thermal decomposition products of synthetic and natural polymers," *Toxicol. Appl. Pharmacol*, 57:181-88, 1981.

7. J. M. Chambers, W. S. Cleveland, B. Kleiner and P. A. Tukey, *Graphical Methods for Data Analysis*, Wadsworth International Group, Belmont, CA, 1983

8. Bukowski, Richard W., "Toxic Hazard Evaluation of Plenum Cables," *Fire Technology*, Volume 21, Issue 4, Nov. 1986, p 252.

9. Article 800, National Electrical Code 1987, National Fire Protection Association, Quincy, Massachusetts.

10. Stanley Kaufman, "The 1987 National Electrical Code Requirements for Cable," *International Wire & Cable Symposium Proceedings 1986*, p 545.

11. Y. Alarie, R. C. Anderson, M. F. Stock R. L. Dombroske, L. W. Keller, L. W. Hayduk and R. E. Park, "Toxicity of Thermal Composition Products: An Attempt to Correlate Results Obtained in Small Scale with Large Scale Tests," *Journal of Combustion Toxicology*, Vol. 8 February 1981, p 58.

12. Frederic B. Clarke, Henri J. Van Kuijk, J. E. Bonesteel, J. G. DiPinto, R. Valentine, Marc Janssens and Paul Vandevelde, "Experimental Design for Full-Scale Evaluation of the Toxicity of the Products of Combustion from Cables," *International Wire & Cable Symposium Proceedings 1987*, p 276.

Stanley Kaufman is Supervisor of the Chemistry, Metallurgy and Product Safety Group at AT&T Bell Laboratories in Norcross, GA. He received a BS in Physics from the City College of the City University of the City of New York, and a PhD in Chemistry from Brown University.

Dr. Kaufman has spent more than a decade of his professional career at AT&T Bell Laboratories working to improve the fire safety of communication cables, and developed many of the fire-resistant plastics being used in AT&T cables. Working closely with Underwriters Laboratories, he contributed to the development of the fire tests used by UL for testing plenum and riser cables for compliance with the National Electrical Code requirements. He is a member of the National Electrical Code Committee, serving on Panel 16 which is responsible for telephone and data wiring safety. He is also a member of the NEMA Management Committee which oversaw the toxicity testing program at Arthur D. Little.

James J. Refi received the BSEE degree from Villanova University in 1966 and the MSEE degree from the Polytechnic University in 1968. He is a Distinguished Member of the Technical Staff in the Lightguide Applications and Systems Group at AT&T Bell Laboratories in Norcross, GA. Since joining Bell Laboratories in 1966, he has spent most of his career working on land coaxial and multipair cables—having authored papers on pair unbalance phenomena, lightning surges and crosstalk. He began working on lightguide in 1982 and since then has obtained a patent and authored papers on field measurements, multimode bandwidth and single-mode chromatic dispersion. Mr. Refi is currently responsible for several fiber-to-the-home applications. He is a member of the IEEE, the Optical Society of America, Tau Beta Pi and Eta Kappa Nu.

Dr. Rosalind C. Anderson is president of Anderson Laboratories, Inc. She has more than ten years of active participation in the field of combustion toxicology. With Dr. Yves Alarie at the University of Pittsburgh, she developed the Pittsburgh test. While manager of the toxicology unit at A. D. Little, Inc., Dr. Anderson was responsible for the study for New York State to investigate the potential use of a combustion toxicity test in the State Building Code. She conducted the study for the National Electrical Manufacturers Association which resulted in categories approved by New York State for the registration of millions of products in compliance with Code 15/1120. Dr. Anderson was an invited participant on the National Academy of Science Committee on Combustion Toxicology.

Dr. Anderson earned her graduate degrees at Yale University School of Medicine. She is a member of the Society of Toxicology and ASTM.

COMBUSTION TOXICITY EVALUATIONS OF POLYMERS FOR ELECTRICAL AND BUILDING APPLICATIONS

Harlan R. Bratvold, William J. Christian, Stephen P. Woynerowski

Underwriters Laboratories Inc.
Northbrook, Illinois

Since adoption of the New York State regulations on combustion toxicity, UL has installed the University of Pittsburgh test equipment and has been serving manufacturers in need of toxicity data. Combustion toxicity has been evaluated by standard protocol for individual products for direct submittal to New York State as well as to establish product classes. Two types of product classes have been established. One type involves only the products of a single manufacturer, and the class is owned and used by that manufacturer. The other type involves only the products which use materials of a specific generic makeup, and can be used by UL to classify products of any manufacturer that meet the class definition UL's experience with this test protocol and its plans regarding other protocols under development will be discussed.

Introduction

In December 1986, the New York State Fire Prevention and Building Code Council passed an amendment for combustion toxicity. New York became the first state in the nation to require testing of building materials for combustion toxicity.

The process that led to this requirement began in 1982, after the tragedy of the Stouffer's Inn fire in Westchester County, New York. There has been evidence that many of the deaths from that fire were caused by toxic combustion products. In general, it is believed that 80 percent of all lives lost due to fire are in fact smoke related.

The New York State amendment requires building products to be tested, by an approved laboratory, for combustion toxicity and data filed with the Secretary of State's office in Albany. No product can be installed or used as a part of a building or factory manufactured home within that state unless such product is tested in accordance with Article 15, Part 1120 of the New York State Fire Prevention and Building code.

Once the testing has been completed by an approved laboratory and filed with the state, the product becomes officially registered with the Secretary of State and is issued a file number which allows the product's continued use within the State of New York. This combustion toxicity test data filed with New York State will be a public record available to any interested party.

In order to fully cover all building products in question , New York State devised a three year phase-in plan. Starting December 16, 1987, electrical wire insulation and synthetic electrical conduit had to be tested for combustion toxicity and filed with them. Pipe, duct and thermal insulation must be tested and filed by December 16, 1988 and interior finish and interior floor finish by December 16, 1989. This amendment covers all products permanantly installed in a building, but does not include appliances, temporary fixtures, or electrical connecting cords.

Methods

Underwriters Laboratories Inc., in response to the needs of manufacturers, has installed the necessary University of Pittsburgh test apparatus, and has served as a recognized New York State approved test facility for combustion toxicity since May, 1987.

The combustion toxicity testing required by New York State must be conducted in accordance with the "Procedure for Evaluation of Acute Toxicity Resulting from Exposure of Mice to Thermal Decomposition Products Using a Modification of the Protocol Developed at the University of Pittsburgh."

This test procedure is a dynamic exposure method that measures toxic potency in terms of an LC50 (lethal concentration expected to kill 50 percent of the animals exposed) value. The LC50 value is a statistical number derived from a series of

test runs at various sample weight. The test apparatus is shown in (figure 1) and the procedure is performed as follows: A prescribed amount of sample is weighed and placed on a quartz pedestal in a programmable oven. The sample weight is constantly monitored by means of a weight sensing device on which the pedestal rests. Once in place, the sample is subjected to a temperature rise of twenty degrees celcius per minute. When a mass loss of 1% is detected, the combustion products from the sample are educted from the oven at a flow rate of 20 liter per minute from a quartz tube placed through the oven door. The combustion products are diluted with cool air before being inducted into a chamber where four male white mice are exposed in head only exposure mode. After passing through the exposure chamber, the combustion products are drawn through a series of filters to remove particulate matter and then through gas analyzers which continuously monitor percent oxygen, carbon monoxide, and carbon dioxide.

Calculations and Results

The test procedure requires calculation of the LC50 value by the Weil method. The formula to calculate an LC50 is:

$$\log LC50 = \log D + (f + 1) \log R$$

Where:

- D = The lowest of four dosage levels used
- R = The geometric progression factor of dosage levels
- f = Mortality factor (available in Table 1)

This method requires a minimum of four dose levels to be tested per material provided that the logarithms of successive dose levels differ by a constant (d). The geometric factor is the ratio of successive dose levels and is denoted by R, thus d = log R. For the University of Pittsburgh test, four animals are exposed per dose level. The goal is to obtain. from the animals dosed at four successive levels, a set of mortality data (r-values) that match one of those in Table 1. Each r value represents the number of mortalities achieved for one dose level.

Underwriters Laboratories has performed combustion toxicity tests on a variety of compounds commonly used in the wire and cable industry. The compounds have been actual commercially produced insulations for electrical wire and cable. Based on data acquired from these tests, approximate ranges of LC50 values on various types of wire insulation have been obtained. These ranges are summarized in Table 2.

TABLE 2

Nylon	5.757 - 6.954
Polyvinyl Chloride	8.333 - 16.262
Cross Linked Polyethylene	7.583 - 23.779
Flouroplastic	2.029 - 12.550
Nylon and PVC	10.000 - 15.072
PVC and Polyethylene	11.990 - 25.883
Rigid PVC	6.542 - 13.146
Wood	41.771 - 65.441

Note: Wood was added to the table to serve as a reference as many toxicologists have compared relative toxicity to wood.

Classification of Products

Currently, there are two ways to submit combustion toxicity data to the New York Secretary of State's office in Albany. The first involves testing of individual products by the standard protocol and direct submittal for official registration of those products tested. The second involves select testing of products of similar composition to represent a group or "classes" of products. If the class is approved by New York State, any individual product within the product class will be assigned a toxicity potency range. This range is established from the data submitted for all products tested.

Underwriters Laboratories has established two types of product classes. The first type is a proprietary product class that involves only the products of a single manufacturer or association. Establishment of an approved proprietary product class could likely result in significant savings in testing costs to an individual manufacturer who produces a product line that currently has or in the future may have, variation in material composition. UL offers its services for consulting and submittal of product classes on behalf of a manufacturer. Assuming New York State acceptance of a proposed proprietary product class, we also offer the option of acting as an organizational representative in submittal of future products for acceptance within the class(es) approved by the State of New York.

The second type of classification is a non-proprietary class. These classes are similar to proprietary classes in content and structure but are owned and managed by UL. With the assistance of knowledgeable manufacturer representatives, UL established these classes for the convenience of anyone. The class is defined by a range of various compositions and constructions tested and submitted by UL to New York State. In order to be considered for acceptance within an approved non-proprietary class a manufacturer needs to

submit its product composition for review to UL. If accepted by UL, full combustion toxicity testing of that product will not be needed resulting in a savings to the manufacturer.

Future Activities

UL is presently installing equipment for a new smoke toxicity test developed under the sponsorship of the National Institute of Building Sciences. The NIBS test attempts to address relative toxic hazards in terms of more than just toxic potency. It reflects three of the five product characteristics thought to effect toxic hazards in actual fire situations:

A) Ease of ignition.
B) Rate of smoke generation (mass loss).
C) Toxic potency.

The two characteristics it does not presently address are quantity of product in use and flame spread.

Although this test is still in the developmental stage, it holds promise of achieving ASTM and/or NFPA adoption.

Conclusion

Underwriters Laboratories is committed to providing safety testing for clients in need of demonstrating compliance with government regulations or nationally recognized standards. Combustion toxicity testing according to regulations adopted by the State of New York is one result of that commitment. UL plans to have the capability to conduct new combustion toxicity test protocols that may develop and become regulatory requirements.

H. R. Bratvold
Underwriters Laboratories Inc.
333 Pfingsten Road
Northbrook, IL 60062

Mr. Bratvold is a Senior Associate Managing Engineer in the Casualty and Chemical Hazards Department with Underwriters Laboratories. He is chairman of the subcommittee D20.30 on plastics and also serves ASTM committees on Rubber, Occupational Health and Safety, and Hazard Potential of Chemicals.

W. L. Christian
Underwriters Laboratories Inc.
333 Pfingsten Road
Northbrook, IL 60062

Dr. Christian is Manager of Research & Technology Development with Underwriters Laboratories. He is currently a member of NFPA committees on Systems Concepts for Fire Protection, Contents and Furnishings, Fire Test, and Toxicity of Combustion Products. He also serves on the ASTM Task Group on Smoke Corrosivity.

S. P. Woynerowski
Underwriters Laboratories Inc.
333 Pfingsten Road
Northbrook, IL 60062

Mr. Woynerowski is an Associate Project Engineer in the Casualty and Chemical Hazards Department with Underwriters Laboratories. He is the test cooridinator for toxicity testing and is presently assisting in the construction of the NIBS test apparatus at UL.

TABLE 1

r Values	F	t	F Values	f	q
0,0,0,4	1.00000	0.26250	0,1,3,3	0.66667	0.53116
0,0,2,4	0.75000	0.25000	0,1,4,3	0.33333	0.35136
0,0,4,4	0.50000	0.00000	0,2,2,3	0.66667	0.58794
0,1,1,4	1.00000	0.25000	0,2,3,3	0.33333	0.53116
0,1,2,4	0.75000	0.23438	0,2,4,3	0.00000	0.35136
0,1,3,4	0.50000	0.25000	0,3,4,3	0.00000	0.47140
0,1,4,4	0.25000	0.25000	1,0,3,3	1.00000	0.70711
0,2,2,4	0.50000	0.40625	1,0,4,3	0.50000	0.23255
0,2,3,4	0.25000	0.23438	1,1,2,3	1.00000	0.91287
0,2,4,4	0.00000	0.08862	1,1,3,3	0.50000	0.79057
0,3,3,4	0.00000	0.25000	1,1,4,3	0.00000	0.70711
1,0,0,4	1.00000	0.25000	1,2,3,3	0.50000	0.58976
1,0,1,4	0.83333	0.23438	1,2,4,3	0.00000	0.91287
1,0,2,4	0.66667	0.22222	1,3,4,3	0.00000	1.41421
1,0,3,4	0.50000	0.23438	2,0,4,3	0.00000	1.15470
1,1,1,4	0.66667	0.52116	2,1,2,3	1.00000	1.82574
1,1,2,4	0.33333	0.52116	2,1,3,3	0.00000	1.82574
1,1,3,4	0.00000	0.47140	2,2,2,3	0.00000	2.00000
1,2,2,4	0.33333	0.58794	0,0,4,2	1.00000	0.57735
1,2,3,4	0.00000	0.60858	0,1,3,2	1.00000	0.91287
2,0,2,4	1.00000	0.57735	0,1,4,2	0.50000	0.57735
2,0,3,4	1.00000	0.57735	0,2,3,2	1.00000	1.00000
2,0,4,4	0.00000	0.57735	0,2,4,2	0.00000	0.81650
2,1,1,4	1.00000	0.70711	0,3,4,2	0.00000	0.57735
2,1,2,4	0.50000	0.81650	0,3,4,2	0.00000	0.70711
2,1,3,4	0.00000	0.81650	1,0,4,2	1.00000	1.15470
2,2,2,4	0.00000	1.00000	1,1,3,2	1.00000	1.82574
3,0,2,4	1.00000	1.15470	1,1,4,2	0.00000	1.41421
3,0,3,4	1.00000	1.41421	1,2,3,2	1.00000	2.00000
3,1,1,4	1.00000	1.41421	1,2,3,2	0.00000	1.82574
3,1,2,4	0.00000	1.82574	0,2,3,1	1.00000	1.82574
0,0,3,3	1.00000	0.47140	0,2,4,1	0.00000	1.15470
0,0,4,3	0.66667	0.22222	0,3,3,1	0.00000	1.41421
0,1,3,3	1.00000	0.60858	0,1,4,1	1.00000	1.41421

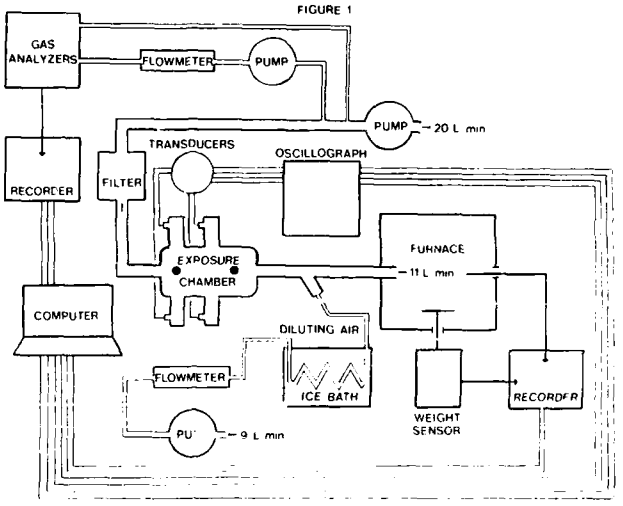

FIGURE 1

REGISTRATION CATEGORIES FOR WIRE AND CABLE PRODUCTS: TOXICITY STUDY OF THE NATIONAL ELECTRICAL MANUFACTURERS ASSOCIATION

Rosalind C. Anderson, Ph.D.

Anderson Laboratories, Inc., Dedham, Massachusetts

Abstract

Data obtained during a study of compounds and mixtures of compounds used by the wire and cable industry indicate that products can be divided into broad groupings according to their chemical and toxicological attributes. The major groupings were: compounded polyolefin, hydrocarbon rubber, PVC, chlorinated rubber and fluoroplastic. From these five groups singly and in combination, thirty-two groups were found to allow categorization and registration of most products in compliance with the New York State Building Code 15/1120. After careful review of new versus tested formulations, the categories may be used by study participants for registration of products yet to be entered into the marketplace.

Introduction

The New York State Building Code 15/11201 requires insulation and jacketing combinations used in wire and cable products to be tested for combustion product toxicity by the test method developed at the University of Pittsburgh. The test values, LC_{50} and associated physical and chemical data, are submitted to the State for inclusion in the publicly available data base. As an alternative, covered products may be registered as members of a pre-established chemical based category. The industry members, participating in the NEMA study needed to register products in as simple and inexpensive a manner as could be consistent with the requirements of the law. The approach was to establish broad categories which describe the actual compounds and mixtures of compounds in common use. The only guidance from New York State at that time was that the categories were to include chemically related products, and that the range of toxicity values was to be sufficiently narrow to substantiate the chemical similarity.

Formulations were submitted by participants of the NEMA study and were found to include fewer than 10 different generic polymers or resin systems typically used in wire and cable jacket and insulation compounds. Widely used compounds as well as certain compositionally unique compounds were selected for testing.

Most of these compounds belong to one of five families of chemicals, e.g., polyolefin compounds, hydrocarbon rubber compounds, polyvinyl chloride compounds, chlorinated rubber compounds and fluoroplastics (see Table 1). These five families used alone or as mixtures occur in a majority of the products to be registered. Pittsburgh Test data were used to affirm major category groupings of these widely used compound mixtures. Only one combination (nylon/PVC) was noted which required a major registration category outside of this matrix.

Smaller groups of compounds or mixtures, not in frequent use were designated minor registration categories. Examples are aramid compounds and EVA compounds. Low frequency mixtures included a number of the fluoroplastics combined with hydrocarbon rubber compounds or polyvinyl chloride compounds in addition to a number of very specialized products.

For single family products the categories were obvious, however, for mixtures it was necessary to establish quantitative rules to govern the categorization, depending on the proportions of components used. Because of the sensitivity of the test and the somewhat uniform toxic potencies of these chemicals, changes of less than 10% of a compound formulation or in relative proportions of compounds did not result in a large enough change of LC_{50} value to be statistically demonstrated. As a result for mixtures

of compounds as well as for ingredients of a mixture, we have elected to consider components which are present at more than 10% by weight. For example, a binary system in which one compound is present at less than 10% is considered to be a single component system.

For submission to the State, each group was described by the chemistry of the components, the statistical parameters, mean, range of LC_{50} values, boundaries, and coefficient of variation: A sample from the approximate mid point of the group was identified to represent the group. Seventeen major and fifteen minor categories were approved by New York State on December 14, 1987 and have been sufficient for the registration of all but a few single covered products.

The Pittsburgh Test

The test designated by New York State was designed at the University of Pittsburgh.[2,3] The test apparatus consists primarily of a furnace and an animal exposure chamber. After the sample is placed in the furnace on a balance the furnace is heated at a constant rate, causing the sample to decompose and/or burn. The animal chamber is connected to the furnace for a 30 minute interval after the test sample begins to loose weight. Four test animals breathe the cooled and diluted fumes. Animals are observed 10 minutes after the end of the exposure for eye damage and survival.

Data showing the weight loss, and temperatures of major events (initial weight loss, flame) are collected. The test segment is performed with at least four different starting sample weights in order to define the relationship between the logarithm of the dose and the frequency of the response (death) for the test material.

The LC_{50}

The unit of measure used for comparison of tested materials is the LC_{50}. This is a calculated value expressed in grams.[4] Other dimensions, e.g., length, volume could be used. The materials tested by this method to date have resulted in LC_{50} values of less than 0.01 grams to greater than 600 grams. Of two products, the one having the lower LC_{50} value is the more toxic.

There are no absolute rules for the interpretation of these LC_{50} values and much discussion has centered around the degree of difference between two products necessary to document that the two are not equivalent in toxicity, and the inverse, how close two numbers must be to demonstrate similar toxicity. This was addressed during the NEMA project because of the need to verify, by means of LC_{50} values, the relationship between genericly related compounds.

Definition of Identity, Replicate Testing

The repeat studies of two control products have been useful in establishing the range of LC_{50} values acceptable for use in category definitions. A series of 22 replicate tests was conducted with nylon 6/6 as the test material. The range of LC_{50} values is from 4.8 to 8.5 grams. The coefficient of variation (CV) is 18.5.

The smoke generated by halogen containing products as represented by PVC is less reproducibly tested. Ten replicate tests of a compounded PVC resulted in a range of values from 10.0 to 27.5 grams, CV 25.9.

The 22 replicate tests of nylon 6/6 represent the largest pool of repeat testing available for this test method.

The CV of 18% indicates very good agreement between test values. The chlorinated materials show greater fluctuation in repeat testing, with a coefficient of variation of 26%. The reason for the greater variability is not well defined but a number of options are readily hypothesized. The sample itself may have been less homogeneous. It has also been demonstrated that the HCl levels in smoke varies with time, humidity and surface contact.[5] In either case, exact replication of exposure conditions is difficult to assure.

In addition, in animals following exposure to HCL the effect develops slowly except in high concentration exposures. Frequently at the end of the test and 10-minute observation period, animals are alive which would not survive more than a few additional minutes. By contrast, animals exposed to smokes containing rapidly effective toxic agents seldom are in such a precarious status.

There is some question whether the test version which was selected by the New York State Building Code which is only 40 minutes in duration, is too short to give an evaluation of acid gas releasing products comparable in severity to the evaluation of products from which the

toxic agents are more rapid in action. Data available in the Arthur D. Little[6] report to New York State indicate that in a 48-hour or 14-day study the LC_{50} of some chlorine containing products would be measured as approximately twice as potent as in the 40-minute test.

Provisional Guidelines for Categories

Because a factor of two or three is encountered in the definition of identity, logically it follows that related compounds will show a broader spread in Pittsburgh Test values.

On the basis of these replicate tests, it was our aim for the NEMA registrations to structure categories such that a range of three between lowest and highest LC_{50} values would signify a family relationship, indicating similarity of toxic potency for products containing no halogen. For halogen containing compounds, a broader range of four was projected. With one exception, products which were outside the group due to unusual chemistry or LC_{50} values outside the target range were excluded from the category and were recommended for registration as single covered products.

Geometry

An important preliminary question whether the effect of geometry of the experimental sample had an effect on the LC_{50} value for these wire and cable products was resolved by a series of tests in which commercially available wires and cables were examined in several different configurations: final product with conductor in place, jacketing and insulation stripped from conductor, and the same compounds in pellet form. The results shown in Table 2 demonstrate that for these products the LC_{50} values are not dependent on the sample geometry. This was demonstrated for a variety of wire and cable products.

The Array of Test Data

The project required five to six hundred tests of products, compounds and mixtures of compounds used in the wire and cable industry as insulation and or jacketing. The test results displayed, without regard to the compound identity, indicate that a rather uniform behavior is to be observed from these products on a weight basis. The mean of the test results was 21 grams, with a heavy representation at the lower, more toxic end of the scale. The lowest value was 4 grams: highest value 73 grams, a range over two orders of magnitude. The higher values most frequent were obtained from products which were highly filled, as evidenced by residue weight data.

If a longer version of the test (24-, 48-hour observation period) had been selected by the New York State Code Council, the distribution of data points would differ as a result of changes in the values obtained from the compounds which form acid gas during thermal decomposition.

The LC_{50} range for such products might be reduced to about one-half of the value measured at the 10-minute post exposure.[6] Although the array of values would be different, the range between high and low LC_{50} values in this study would probably not have been greatly extended.

The Categories, Major and Minor

Because the LC_{50} data indicated sufficient agreement between related products, it was possible to base the category system on only five broadly defined family groups: polyolefin compounds, hydrocarbon rubber compounds, PVC compounds, chlorinated rubber compounds and fluroplastics. The compounds included in each major group are identified on Tables 3 and 4. Representatives of these families are frequently used alone as well as being used in most of the mixtures which the matrix would suggest.

For each presumptive category, examples of individual compounds which contained the major fire retardants as well as varieties of plasticiser, filler and stabilizer were tested. Individual formulations were examined to determine whether each could be included as a category member on the basis of both chemistry and measured toxicity. Compounds and mixtures which were identified as frequently used or high volume were assigned major category status. The major categories and test data summary are listed on Table 1.

Minor categories were established for products which were described infrequently in the data submitted by industry. These were found to represent 3 to at most 50 examples. In addition, these unusual products were frequently marketed by only one or possibly two manufacturers. Because of very limited use of these materials a much reduced testing program was conducted in support of these groupings. The test results fo these products, Minor Categories are described on Table 5.

The groups are not uniquely distinguished by the mean LC_{50} or the range of toxicity values. Significant overlaps are noted between groups. The lower, more toxic end of the spectrum contains compounds, fluroplastics and polyolefins which are typically used with little or no filler. The groups of PVC, hydrocarbon rubber and chlorinated rubber were higher on the continuum of LC_{50} values. Statistical measures can be used to show some differences between groups on a weight basis. The groupings do not show dissimilarities of practical importance when compared strictly on the basis of weight. These data do not demonstrate the advantage of one chemical class of compounds over another used in wire or cable products. There are, however, differences between specific compounds which are large enough to merit attention. The highest and lowest values of the study are separated by a factor of 18.

Application of Data

The groups are not dramatically different from one another in measured toxicity values although specific compounds in the study will differ significantly from others. Because the structure of the categories does not reveal individual product differences, there is no easy way to use these data for compound choices.

To use LC_{50} data in a practical way will require individual product toxicity values and specific information about how the candidate materials are to be used, e.g., the jacket and insulation thickness required to deliver the necessary physical properties. The LC_{50} values being expressed in terms of weight need to be adapted for use with compounds which are applied according to a different measurement unit.

The author wishes to acknowledge Dr. Peter W. Kopf as a major contributor to this study.

References

1. New York State Uniform Fire Prevention and Building Code, Article 15, Part 1120, Combustion Toxicity Testing, New York Department of State, Office of Fire Prevention and Control, Albany, NY.

2. Alarie, Y.C. and R.C. Anderson. "Toxicologic and acute lethal hazard evaluation of thermal decomposition products of synthetic and natural polymers," Toxicol, Appl. Pharmacol., 51, 341, 1979.

3. Alarie, Y.C. and R.C. Anderson. "Toxicologic classification of thermal decomposition products of synthetic and natural polymers," Toxicol. Appl. Pharmacol, 57:181-188, 1981.

4. Weil, C.S. Biometrics, 8:249-263, 1952.

5. Beitel, J.J., C.A. Bertelo, W.F. Carroll, Jr., A.F. Grand, M.M. Hirschler and G.F. Smith. "Hydrogen Chloride Transport and Decay in a Large Apparatus: II. Variables Affecting Hydrogen Chloride Decay," Journal of Fire Sciences, Vol. 5 March/April 1987.

6. Anderson, R.C. and P.A. Croce. Study to Assess the Feasibility of Incorporating Combustion Toxicity Requirements into Building Material and Furnishing Codes of New York State. Vol. 2: Report of Findings, May 1983.

TABLE 1

COMPOUNDS INCLUDED IN EACH CATEGORY

Class	Compounds
Polyolefin	XLPE, LDPE, PP, MDPE, PE, XHDPE, HDPE, EXPE, PPE
Hydrocarbon Rubber	TPR, SBR, EPR, Polyester, EPDM, Natural Rubber
Polyvinyl Chloride	Polyvinyl Chloride
Chlorinated Rubber	Neoprene, CSPE, CPE
Fluoroplastics	PVDF, HFP, FEP, PFA, ECTFE, ETFE

TABLE 2

LC_{50} VALUES FROM PRODUCTS AND COMPONENTS
Effect of Geometry

	LC_{50} grams		
Sample	Intact Product	Disrupted Product	Mixed Pellets
TC multi conductor PVC/Nylon	9	15	
Flat Cable multi conductor Polyester/PVC	14	17	
Armored multi conductor	16	17	
TC multi conductor Neoprene/TPR	16	19,14*	14
MV 90 single conductor CSPE/EPR	47		33
MV 90 single conductor XLPE	9		11
THHN single conductor PVC/Nylon	9** 11***	11	9

*Two separate tests

**Small diameter

***Larger diameter

NOTE: PVC = Polyvinyl chloride

TABLE 3

MAJOR CLASSES FOR SINGLE COMPOUND PRODUCTS

		LC_{50} grams*		
	# Tests	Mean	Range	CV*
Polypropylene	25	10	8-14	17
Hydrocarbon Rubber	31	18	10-31	25
Polyvinyl Chloride	31	18	9-28	28
Chlorinated Rubbers	33	23	13-51	40
Fluoroplastics	17	9	4-16	34

*Numbers rounded up at .5 or above.

TABLE 4

MAJOR CLASSES FOR PRODUCTS WITH MULTIPLE COMPOUNDS

		LC_{50} grams*		
Compounds**	# Tests	Mean	Range	CV*
PO/HR	13	13	8-18	21
PO/PVC	13	18	12-33	37
PO/CR	14	18	12-38	40
HR/PVC	16	20	13-28	22
HR/CR	19	25	16-35	26
PVC/CR	13	27	9-45	36
Nylon/PVC	9	13	9-27	23
PO/HR/PVC	9	17	13-20	13
PO/HR/CR	8	15	11-19	19
PO/PVC/CR	11	18	14-24	16
HR/PVC/CR	9	22	16-26	15
PO/HR/PVC/CR	8	20	15-25	18

*Numbers rounded up at .5 or above.

**PO - Polyolefin; HR - Hydrocarbon rubber; PVC - Polyvinyl chloride; CR - Chlorinated rubber.

TABLE 5

MINOR CLASSES, INFREQUENTLY USED COMPOUNDS OR MIXTURES

Class Name**	# Tests	LC_{50} grams* Mean	Range
Aramid	3	11	7-17
SR	5	53	41-73
EVA	6	24	16-56
PO/EVA	4	12	10-14
HR/EVA	7	23	11-40
PVC/EVA	4	29	17-47
HR/F	5	15	9-27
PVC/F	4	19	14-26
PVC/SR	3	28	26-30
CR/SR	4	37	27-47
Aramid/SR	5	50	34-70
CR/EVA	6	22	20-28
CR/F/SR	4	22	14-37
PO/CR/EVA	3	14	12-17
PC/F/SR	3	16	15-18
PO/PVC/CR/EVA	3	20	18-24

*Numbers rounded up at .5 or above.

**SR - Silicone rubber; EVA - Ethylene vinyl acetate - Ethylene Acrylate Copolymer; PO - Polyolefin; PVC - Polyvinyl chlroide; HR - Hydrocarbon rubber; F - Fluoroplastic; CR - Chlorinated rubber

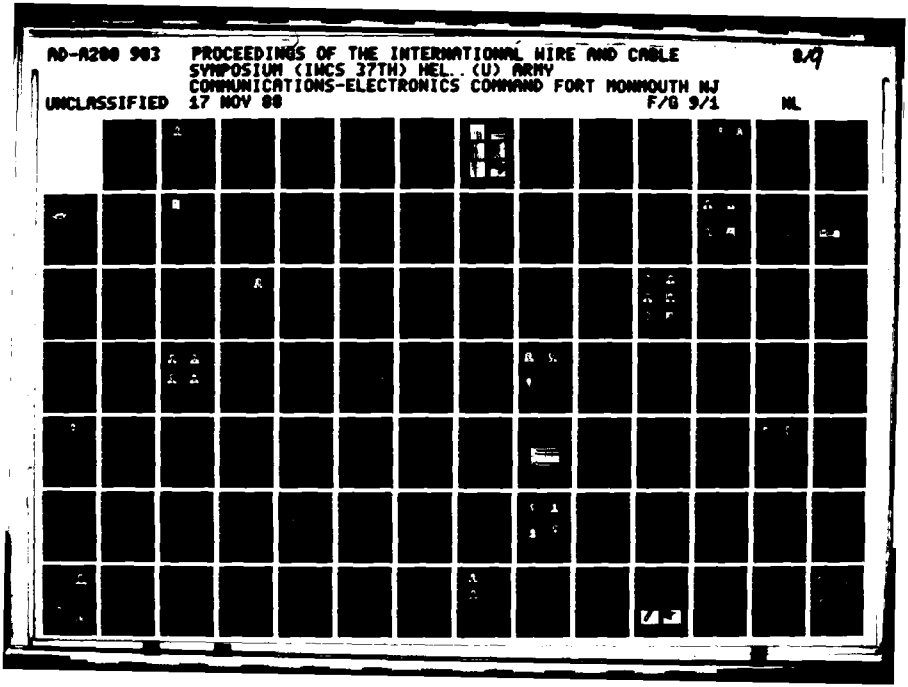
AD-A200 903
PROCEEDINGS OF THE INTERNATIONAL WIRE AND CABLE SYMPOSIUM (IWCS 37TH) HEL.. (U) ARMY COMMUNICATIONS-ELECTRONICS COMMAND FORT MONMOUTH NJ
UNCLASSIFIED
17 NOV 88
F/G 9/1
NL

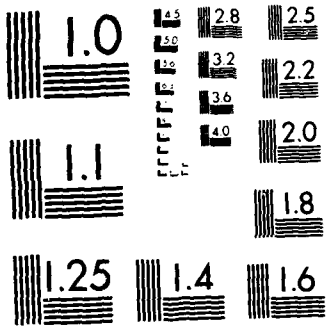

DR. ROSALIND C. ANDERSON: President Anderson Laboratories, Inc., 30 River Street Dedham, Massachusetts 02026.

Dr. Anderson has more than ten years of active participation in the field of combustion toxicology. With Dr. Yves Alarie at the University of Pittsburgh she developed the Pittsburgh Test. While manager of the toxicology unit at Arthur D. Little, Inc., Dr. Anderson was responsible for the study for New York State to investigate the potential use of a combustion toxicity test in the State Building Code. She conducted the study for the National Electrical Manufacturers Association which resulted in categories approved by New York State for the registration of millions of products in compliance with Code 15/1120. Dr. Anderson was an invited participant on the National Academy of Science Committee on Combustion Toxicology.

Dr. Anderson earned her graduate degrees at Yale University School of Medicine. She is a member of the Society of Toxicology and ASTM.

AXE EXCHANGE CABLE FIRE PERFORMANCE TESTING

Loris Colla
Telecom Australia
Metropolitan Division
Network Management
Melbourne

David J. Adams
Telecom Australia
Research Laboratories
Melbourne

Stephen Grubits
National Building
Technology Centre
Sydney, Australia

ABSTRACT

Telecom Australia is planning the introduction of halogen-free, low-smoke, fire-retardant cables for use in new Stored Programmed Control switching installations. This paper describes the work undertaken by Telecom Australia to determine the grades of commercially available materials considered suitable for use in the exchange environment.

Tests were commissioned to assess the reaction to fire for the specific application, addressing the majority of cable installation configurations.

The testing programme undertaken has determined several alternative grades of comercially available materials considered suitable for use and capable of replacing PVC as the cable sheath material.

INTRODUCTION

The all-electronic, AXE 10 Ericsson, Stored Programmed Control telephone switching system was adopted by Telecom Australia for the modernisation of the telephone switching network in 1981. AXE 10 is the basis for the evolving digital switching networks of the future and is used in more than 60 countries worldwide.

Telecom Australia AXE exchange cable design requirements were described by E. Buczma et al at the 1987 IWCS[1]. Telecom Australia adopted a halogen-free, fire-retardant conductor insulation in 1984, that evolves low levels of corrosive and toxic gases when exposed to fire. This material replaced the more expensive nylon insulation previously used in these cables and, in addition, offered superior electrical and flammability properties were required. However, until now the outer cable sheath has remained PVC.

Telecom Australia has experienced a number of exchange fires[2]. The damaged caused and the high cost of restoration resulting from the burning of relatively small amounts of PVC, strengthened our intention that its use in new installations should not be perpetuated.

The presence of irritant gases and dense smoke are features of fires involving PVC, particularly when considerable heat is generated in an enclosed space and there are high volumes of PVC cable such as in a telephone exchange.

Comprehensive examination of surfaces covered with soot is not immediately possible, and it is usually weeks after a fire that the corrosive damage caused is fully apparent. Any preventative measures are then too late, and repairs and replacements of equipment are expensive. Such damage generally exceeds many times over, that caused by the fire itself, since no equipment or apparatus installed in the vicinity of the fire escapes contamination by the corrosive vapour and the smoke. Damage caused to Printed Circuit Board Assemblies by smoke has been particularly evident.

Considerable damage can also occur to the exchange building and cases have been reported[3] where the concrete and steel reinforcement were badly damaged by hydrochloric acid attack with the result that the entire building had to be demolished. In addition, the emission of toxic fumes required the evacuation of several blocks of homes in the vicinity.

Significant damage has also been reported[4] where a fire was confined on one floor of a multi-storey telephone exchange but caused smoke and toxic related damage to equipment on the other floors of the building. In this case, smoke was given off in large volumes during the fire which was a hazard in itself by obscuring exits and totally hindering fire fighting operations.

Also smoke that deposited as fine soot on surrounding surfaces, absorbed the hydrogen chloride gas released from the PVC during the fire. With atmospheric water vapour, this gas converted to hydrochloric acid leaving a very corrosive acid soot firmly adhered to all surfaces, not only in the near vicinity of the fire, but also at locations well away from the fire source.

OBJECTIVES OF THE PROGRAMME

The overall objective of the programme was to substitute the use of PVC compounds with low-smoke, halogen-free, fire-retardant, thermoplastic materials suitable for use in Telecom exchange cables.

This entailed the following, more specific, objectives :

1. Determine the cable types that are targets for PVC replacement.

2. Determine fire scenarios and cable configurations to be used in the design of full scale fire tests.

3. Develop techniques for measurement of fire characteristics in full scale tests. The full scale test is used to predict the performance of the cable system under fire conditions that is appropriate for the intended application.

4. Establish the level of correlation of small-scale measurements of materials (ignition energy, rate of heat release, smoke produced), with the full-scale tests of relevant fire situations. Future formulation changes on new materials can therefore be readily assessed.

CABLE TYPES FOR PVC REPLACEMENT

Cables containing PVC insulation and sheath compounds have been used by Telecom Australia in all telephone exchange cabling except in the case of the AXE-10 Ericsson exchange[5]. For AXE-10, as previously discussed, the conductor insulation is a halogen-free, fire-retardant material, but the outer cable sheath has remained PVC.

As telephone switching growth is now almost exclusively provided by AXE equipment it was decided to confine the substitution of PVC to AXE cables only. It is envisaged that AXE (and its future equivalents) will replace all earlier switching equipment by about the year 2010.

SCREENING TESTS FOR CABLE SHEATHING MATERIALS

In early 1987, Telecom Australia began an evaluation programme of a number of halogen-free, non-drip, fire-retardant, low-smoke polymers capable of replacing PVC as the cable sheath material. Twenty-three commercial and experimental materials were sourced and screened according to the laboratory tests described in Table 1, for extrusion trials on cable for evaluation in the subsequent fire tests. These requirements had to be met before a material would be considered.

TABLE 1

SCREENING TESTS FOR HALOGEN-FREE, LOW SMOKE, FIRE RETARDANT SHEATHING MATERIALS

TEST	COMMENTS
1. Dimensional Stability	Cable sheath is expected to retain dimensional stability on being subject to a moderate heat flux. The test consists of a plaque 150 x 6 x 3 mm being hung longitudinally in an oven at 100°C for 5 days. The plaque must not distort in the vertical axis.
2. Minimum Oxygen Concentration (MOC)	Both this test and the Critical Temperature Index are attempts to screen out materials with inadequate combustion properties. The materials must have an MOC equal to or greater than 34%.
3. Critical Temperature Index (CTI)	The temperature at which a material will just support combustion in an oxygen concentration of 20.9% when tested in accordance to the method for MOC. The material must have a CTI of greater than 260°C
4. Smoke Evolution	This test is performed using the Arapahoe Smoke Chamber in ASTM D4100-1982. The method determines by mass the evolved smoke and particulate matter. The material must have a value less than 2%.
5. Tensile and Elongation at Break	The initial elongation values must be greater than 150% and retain at least 80% of it's initial value after ageing at 100°C for 5 days. The initial tensile break strength must be equal to or greater than 10 MPa and retain at least 80% of it's initial value after ageing at 100°C for 5 days.
6. Corrosivity	The final conductivity must be less than 100 µS/cm and the final pH greater than 3.5 when tested in accordance with the modified method of DIN 57 207 Part 23.

Six materials were found to satisfy the above conditions. These compounds are based on polyolefinic copolymers filled with hydrated alumina or a similar inorganic filler which endothermically react to liberate water at high temperatures. These types of materials also satisfied the tolerable cost penalty relative to PVC sheathed cables.

Methods of test for the combustion propagation characteristics of single specimens of these materials with a small heat source of ignition do not give a indication of actual fire behavior of multipile lengths of cable installed in the exchange.

Accordingly, the test for Early Fire Hazard Properties of Materials of Australia Standard 1530.3-1982, as described by E. Buczma et al at the 1987 IWCS[1] is applied to cables with a view to using this test as a means of grading their intrinsic ignition, flame spread, heat release and smoke evolution properties.

Australian building regulations use the AS 1530.3-1982 test methods and the requirements exclude the use of materials which have rapid flame spread and which produce considerable smoke in essential fire escape-ways.

The standard regime of increasing, impressed radiant heat applied to the test specimens in this method was originally defined following studies made at the Australian National Building Technology Centre (NBTC)[6] of the heat energy impressed on the walls of a test room when various small fires were deliberately kindled. The NBTC was commissioned by Telecom Australia to conduct both the Early Fire Hazard and full scale fire tests.

The six sheath compounds selected from the screening test programme of Table 1 were subsequently used to manufacture trial lengths of AXE exchange cables. The types and construction of the cables subjected to AS 1530.3 and the full scale fire test are listed in Table 2. The results of the tests for Early Fire Hazard properties are listed in Table 3.

TABLE 2

CONSTRUCTION OF THE AXE EXCHANGE CABLES

Cable Size No. of Wires	Cable Diameter (mm)	Sheath Thickness (mm)	Sheath Material Type
64w	9.0	1.2	SM1
64w	9.0	1.4	SM2
64w	9.3	1.3	SM3
64w	9.2	1.4	SM4
64w	8.8	0.9	PVC
8w	5.4	1.0	SM5
8w	5.2	1.0	SM4
8w	5.3	1.4	SM2
8w	5.5	1.1	SM3
8w	5.2	1.0	SM6
8w	5.0	0.7	PVC

NOTES :

1. w = wires
2. All cables consist of 0.4 mm dia copper conductors.
3. All cables consist of Noryl PX 1766 conductor insulation with a mean radial wall thickness of 0.1 mm.
4. Sheath Material (SM) codes used for the halogen-free materials under evaluation:

   SM1 = Pirelli Afumex 4710 SV

   SM2 = Pirelli SVO 100

   SM3 = ICI CFR 95

   SM4 = Megolon S 300

   SM5 = Megolon S 1

   SM6 = Mitsubishi FR 3201

TABLE 3

RESULTS OF THE EARLY FIRE HAZARD TESTS

Cable Size No of Wires	Sheath Material	Ignition Time (min)	Flame Spread (min)	Heat Evolved (kJ/m^2)	Mean Optical Smoke Density (m^{-1})
64w	SM1	11.6	2.1	101.3	0.07
64w	SM2	9.5	*	98.0	0.06
64w	SM3	9.2	*	86.8	0.18
64w	SM4	12.3	*	14.7	0.29
64w	PVC	7.1	*	49.9	1.52
8w	SM5	6.8	*	32.5	0.33
8w	SM4	7.9	1.9	78.6	0.15
8w	SM2	7.5	1.3	140.0	0.07
8w	SM3	7.8	1.6	120.0	0.10
8w	SM6	8.6	1.1	153.0	0.09
8w	PVC	6.6	*	90.5	1.55

* Flame spread time is not determined for specimens that fail to register the 1.4 kW/m^2 increase in radiant heat

CABLE CONFIGURATIONS FOR THE FULL SCALE FIRE TESTS

Inspections of several AXE exchanges were conducted to determine the most appropriate cable configuration to be used in designing the full scale fire tests.

The guiding principle used in the inspection assessment was that the cable configuration chosen for full scale fire test reflect the most common and vulnerable situation.
Examination of all exchanges revealed five possible configurations for AXE exchange cables, three vertical (Figs 1,2,3) and two horizontal (Figs 4,5).

Horizontal cable configurations were disregarded because it was considered significantly less severe than the vertical configurations.

Cables configured in the exchange as shown in Fig. 3 were chosen for incorporation in the full scale fire test. This configuration of bunched cables was considered to reflect the most common and vulnerable setting for a fire. The riser shaft cable configuration, shown in Fig. 2, although depicting a high volume of cables, was not considered as vulnerable and certainly not as common. The cable service shaft in all AXE exchange buildings is 'fire stopped' at all openings[7] and is located in isolation, away from equipment and personnel.

Therefore, the cable configuration selected for the full scale fire test was chosen to depict the cable arrangements and fire scenario shown in Fig.3 and incorporates :

- bunching of cables with three bunches of varying bunch sizes : 4,8 and 16 cables in each bunch.
- a single layer of bunches suspended vertically.
- spacing of bunches of 25 mm.
- fixing of bunches at intervals of 300 mm with a single cable tie.
- use of a ladder arrangement to support the bunches.

FULL SCALE FIRE TEST

The full scale fire test is an essential part of the PVC replacement programme. The test is used as a measure to predict the performance of the AXE cable configurations with various sheath materials under fire conditions that may be anticipated under conditions of actual use.

With the advent of many new polymeric materials whose widely differing fire performance properties are not known, there has been a proliferation of new small scale test methods, most of which originated as ad-hoc tests in laboratories. Their relevance to the performance of products in real fires was seldom a factor in their development. A few of these test methods have achieved recognition as standard methods by virture of their endorsement by standards organisations.

Intrinsic property tests, such as oxygen and temperature index are of more use in product development, quality control and in the establishment of specifications and regulations. For instance, oxygen index is not useful in establishing fire hazard standards. For materials such as those under evaluation, a small heat source for ignition can be insufficient to overcome the expected large activation energy caused by the flame retardants. Hence, higher oxygen concentrations, (higher OI levels), are required to obtain ignition. However, with a sufficiently large ignition source the resultant heat release by the fuel may be sufficient to overcome the activation energy and cause the material to continue burning.

The full scale test provides the most reliable measure of hazard potential with the intention to correlate the properties measured with the Early Fire Hazard Tests.

The full scale fire test configuration is shown in Fig. 6.

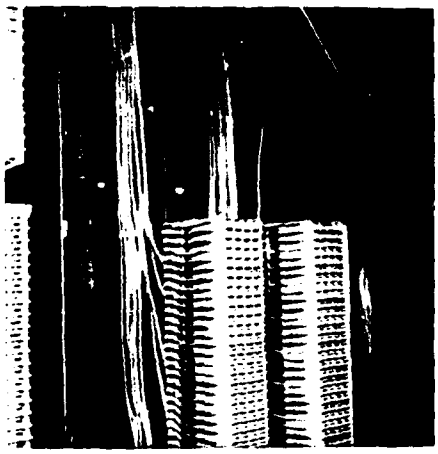

Fig. 1
Main Distribution Frame
Cable Configuration

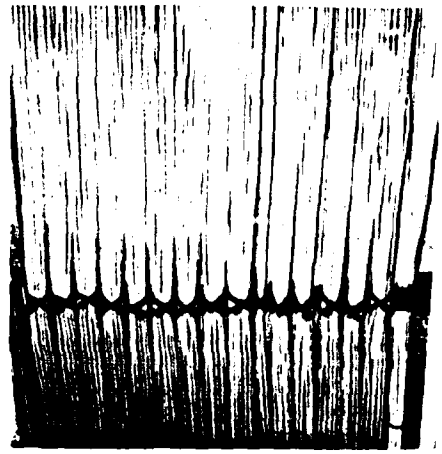

Fig. 2
Riser Shaft Cable
Configuration

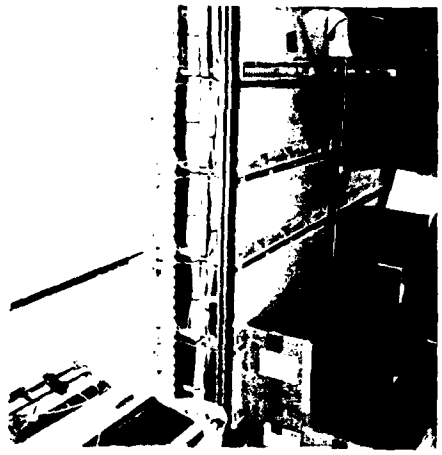

Fig. 3
Equipment Rack Cable Configuration

Fig. 4
Exchange Equipment
Shelf Cable Configuration

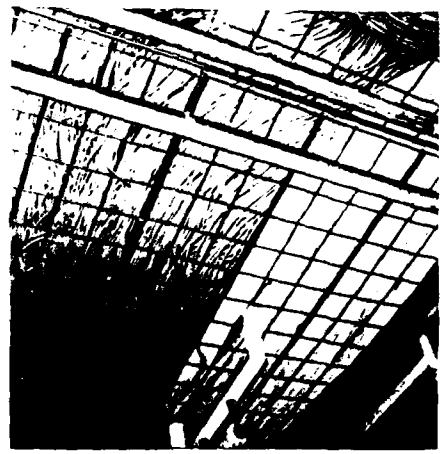

Fig. 5
Overhead Cable Configuration
from Riser Shaft to Exchange
Equipment.

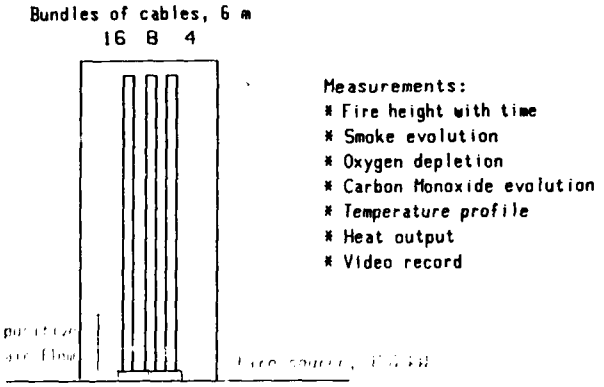

Fig. 6 Full Scale Fire Test Configuration

The emphasis of the full-scale test procedure was to reproduce the most likely fire scenario described previously. The severity of the igniting fire source was chosen to represent a likely fire severity that could be encountered. The fire source severity was chosen to be approximately a 150 kW fire of 10 minute duration which was considered to be equivalent to a waste-paper basket fire consisting of paper and cleaning rags containing flammable solvents.

A standardised and more reproducible fire source consisting of 9 sticks of 300 x 25 x 13 mm and 4 sticks of 150 x 25 x 13 mm softboard arranged to form a 5 layer high crib was used. Immediately prior to the test, the sticks were soaked in 600 mL of ethanol in a sheet metal tray measuring 305 x 457 mm. The tray was used to hold the crib during the test.

This fire source was considered to be more appropriate than the ribbon type propane gas burner heat source specified in IEC 332-3, "Tests on electric cables under fire conditions, Part 3 - Tests on bunched wires or cables". The 20 kW heat output of the IEC 332-3 burner was not considered to be sufficiently severe to represent a typical fire scenario nor does it preheat the cable significantly above the ignition source as would be the case with a real fire.

To compare the characteristics of a waste paper basket fire containing paper and cotton rags soaked with ethanol and the full scale test ignition source, heat release and radiant heat flux measurements were undertaken to achieve correlation[8]. The radiant heat flux was measured using a heat flux transducer located in the plane where the cable would be burning during the full scale fire test at approximately 300 mm above the fuel surface where the maximum radiant heat flux was expected. The heat release rate was measured by Oxygen Calorimetry.

The fire shaft test facility consisted of a 6 m high masonry shaft with a 1 m x 1 m internal cross-sectional area. The shaft was lined inside with glass-fibre reinforced plaster sheets. The shaft was provided with a 0.8 m x 2.8 m opening on the observation room side at its base and a 0.8 m square opening on the same side of the shaft near the top. Both openings in the shaft terminated within the main test building.

A centrifugal fan was used to induce a 0.2 m/s draft in the shaft and to vent the combustion products to the outside. A wire mesh cable ladder was attached to the wall of the shaft opposite the openings.

The test shaft was equipped with the following instrumentation located at the top of the shaft opening :

- Thermocouples. Three type K thermocouples to measure the temperature of the combustion products.
- Anemometer. An insulated paddle anemometer was located in the centre of the opening to monitor flow of hot gases.
- Smoke Density Meter. A photoelectric type smoke density meter was located vertically across the opening. The meter consisted of a light source that directed a near collimated beam of light to a photodetector across a 0.75 m smoke path.
- Gas Sampling Probes. A stainless steel probe was used to collect samples of the combustion products for analysis by a paramagnetic type Oxygen Analyser and an infra-red absorption type carbon monoxide gas analyser.

In addition, cotton threads were located across the face of the cables at 1.0 m vertical increments to monitor the rate and extent of flame spread. The threads were tied to microswitches which were connected to data logging equipment.

The output of the transducers and flame spread monitors were connected to a datalogger that sampled all the channels once every 10 secs.

A video camera connected to a recorder was located at the base of the shaft to view the ignition and early stages of flame propagation on the cables. A second camera was located on the floor above to view the flame spread within the shaft.

FULL SCALE FIRE TEST RESULTS

Table 4 records the results obtained for the full scale fire tests depicting the following characteristics :

- Ignition time. The time for the cables to ignite.
- Flame Spread. The time for the flames to reach the 4 m marker.
- Heat Evolved. The rate of heat evolved is calculated from the flow-rate and the temperature rise data. No attempt was made to compensate for losses in the heat release determination as the values were meant principally for comparison and ranking purposes.
- Smoke Density. The maximum smoke density (averaged over a one minute period), together with the value of the integral representing the total quantity of smoke produced.

TABLE 4

RESULTS OF THE FULL SCALE FIRE TESTS

Cable Size No of Wires	Sheath Material	Ignition Time (min)	Flame Spread (min)	Heat Evolved (kW)	Max Smoke Developed (m^{-1})	Total Smoke Developed (m^{-2})
64w	SM1	1.2	9.1	26.2	0.41	95.0
64w	SM2	0.8	6.6	44.3	0.65	95.3
64w	SM3	0.8	9.3	29.8	0.25	46.7
64w	SM4	1.5	*	13.7	0.11	22.4
64w	PVC	0.2	*	7.9	1.39	133.7
8w	SM5	0.7	*	6.9	0.06	4.9
8w	SM4	0.9	*	6.2	0.05	1.3
8w	SM2	0.8	*	7.6	0.06	7.7
8w	SM3	0.9	*	7.1	0.03	2.7
8w	SM6	0.7	7.6	15.5	0.26	20.7
8w	PVC	0.4	*	3.6	0.58	16.2

* Indicates that the flame spread did not reach the 4 m marker.

DISCUSSION OF RESULTS

Assessment of the results recorded for the Early Fire Hazard tests, (Table 3), the full scale tests, (Table 4) and the ranking of materials, (Table 5), yielded the following comparative observations concerning the flammability and smoke characteristics of the materials evaluated.

- PVC ignited the earliest.
- PVC contained the spread of flame better than most materials, (except SM5), even though its minimum oxygen concentration is the lowest of all of the materials. The rate of flame spread was similar for all materials.
- The heat released from PVC burning cable is comparatively low.
- PVC produced the highest levels of smoke and was distinctively darker in nature.
- Material SM4 comparatively displayed the best overall performance.
- The level of correlation between the Early Fire Hazard test (small scale test) and the full scale fire test results to assess comparative material ranking was satisfactory for the ignition time, spread of flame and heat evolved characteristics, (refer to Table 5).

  However, the level of correlation for the smoke density measurements was poor and requires further investigation. For the purposes of discussion here, the smoke density results obtained for the full scale tests will be used.
- All halogen-free, fire retardant materials evaluated displayed acceptable minimum fire performance requirements for use in the telephone exchange environment.

TABLE 5

RANKING OF MATERIALS

Early Fire Hazard Tests

Sheath Material	Ignition Time	Flame Spread	Heat Evolved	Smoke Density
SM1	2	7	6	2
SM2	4	5	5	1
SM3	5	4	4	4
SM4	1	3	2	5
SM5	6	1	1	6
SM6	3	6	7	3
PVC	7	2	3	7

Full Scale Fire Tests

Sheath Material	Ignition Time	Flame Spread	Heat Evolved	Smoke Density
SM1	2	5	4	4
SM2	4	6	6	5
SM3	3	4	5	2
SM4	1	3	2	1
SM5	5	1	3	3
SM6	6	7	7	7
PVC	7	2	1	6

Overall Ranking *

Sheath Material	Ranking
SM1	4
SM2	5
SM3	3
SM4	1
SM5	2
SM6	6
PVC	7

* Overall ranking was based on biasing the order of importance placed on the characteristics measured. The order of importance used was the following :

1. Smoke density
2. Flame spread
3. Ignition time
4. Heat evolved

PVC is ranked last as it contains halogen, toxic materials and produces considerable smoke during combustion.

CONCLUSIONS

The cable fire performance testing programme undertaken has determined several alternative grades of commercially available materials considered suitable for use in the AXE-10 Ericcson exchange environment and capable of replacing PVC as the cable sheath material.

The materials were comparatively assessed and rated for their fire performance behavior under fire conditions that may be anticipated under conditions of actual use.

The programme conducted here will enable a cable specification to be issued for the introduction of halogen-free, low-smoke, fire-retardant cables for use in all new AXE-10 Ericsson telephone exchanges.

REFERENCES

1. Buczma, E., Mayer, H.A., Day, A.C. "Processing of Thin Wall Flame Retardant, Non-Halogenated Insulation for Indoor Telephone Exchange Wiring, IWCS 1987.

2. Telecom Australia, Design Standards Branch, HQ Fire Loss Report, 1987.

3. Cerberus Ltd, Switzerland. Quarterly Bulletin Ceberus Alarm, December 1968.

4. Chisholm, B.A., Gwyn, P.S. "Assessment of Fire and Water Damage : Hodgson Nagi Building, Lae, Papua New Guinea." Applied Science Branch Paper No. 116, Telecom Australia Research Laboratories, Melbourne, Australia, 1988.

5. Telecom Australia Specification, Schedule OS 3122, Appendices A,B and C, June 1987.

6. National Building Technology Centre - Technical Report 481, July 1982.

7. Telecom Australia, Technical Publication HQ No. 0940, Issue 2 - Fire Stopping Systems for Cable and Busbar Openings - Manager, Design Standards Branch, H.Q. December 1983.

8. National Building Technology Centre - Technical Report 900, August 1988.

AUTHORS

Loris S. Colla
Senior Engineer
Cable Design Section
Customer Access Network Group
Network Management Unit
Metropolitan Consumer Division
28/570 Bourke Street
MELBOURNE VIC 3000
AUSTRALIA

Loris Colla graduated in 1981 from Deakin University in Victoria with a Degree in Electrical Engineering. He joined Telecom Australia in 1984 and has experience in areas of telecommunications cable design, specification and provisioning. In 1985, he joined the Cable Design Section and is currently responsible for external and internal plant aspects of copper cable design within Telecom Australia.

David J. Adams
Senior Chemist
Polymer and Chemistry Section
Research Laboratories
Telecom Australia
770 Blackburn Road
CLAYTON VIC 3168
AUSTRALIA

David Adams graduated in Chemistry from the Footscray Institute of Technology, Australia in 1975. He joined Telecom Australia in 1972 and is currently a Senior Polymer Chemist, Telecom Research Laboratories. His current area of interest covers flammability and weathering aspects of polymers.

Stephen Grubits
Section Manager
Fire Technology
National Building
Technology Centre
87 Delhi Road
NORTH RYDE, SYDNEY
NSW 2113
AUSTRALIA

Stephen Grubits is currently head of the Fire Technology Section, National Building Technology Centre. He has 20 years' experience in fire research including fire behaviour of building materials, smoke movement and control, fire test methods, fire detection and protection systems.

SPEAKER

L. Kiss
Inter-Exchange
Networks Branch
Telecom Network
Engineering
Telecom Australia
29/570 Bourke Street
MELBOURNE VIC 3000
AUSTRALIA

Les Kiss is currently Manager of the Optical Installation and Maintenance Section of the Inter-Exchange Networks Branch, Telecom Australia. He joined Telecom Australia in 1971 after graduating in Mechanical Engineering at Melbourne University in Victoria, Australia. He has had extensive experience in the external plant area, in particular in cable design and specifications and in the installation of cable plant. He currently has full responsibility for the installation and maintenance of optical fibre cables in the inter-exchange network.

NEW PLASTIC SINGLE MODE FIBER CONNECTOR FOR SUBSCRIBER NETWORKS

W. Eutin, U. Grzesik, E. Schürmann

Philips Kommunikations Industrie AG
Nachrichtenkabel und -anlagen
Schanzenstr. 30; D-5000 Köln 80
Federal Republic of Germany

Abstract

In the fiber optic telecommunications market investigations meanwhile focus on the subscriber network. In contrast to the long-haul communication routes the fiber optic connectors play an important role concerning the cost of the subscriber line. To achieve a low cost level without loosing in single mode fiber connector quality, nowadays proved to be standard, a completely new connector design was developed. The design comprises precision injection molding technique for almost all parts, including the fiber centering component which incorporates a V-groove. The mean insertion loss can be as low as 0.05 dB, the return loss was 40 dB and more.

1. Introduction

In the near future fiber optic technologies are expected to penetrate into the subscriber network. Because of the huge transmission capacity of single mode fibers which probably will satisfy all demands even on a large time scale the advisable technology will be the single mode one. This new application area requires new concepts for the connection technology: Cost is an important factor, because of the higher number of connectors per fiber kilometer; packaging and packaging density is important for the effective line-up in cross connection cabinets [1]; last but not least low insertion and high return loss characteristics either allow the implementation of low cost light emitting and receiving devices into the system or very high speed systems being vulnerable to reflections from imperfections in the transmission line. The synthesis of these two requirements, high quality and low price, which are in general judged to be diametrically opposed, does not lead to an adequate solution, if conventional techniques are used. Connector ferrules (cylindrical as well as conical) for single mode fibers always need single part machining, core alignment procedures and time-consuming grinding and polishing in order to achieve the submicron precision of the core centricity in the ferrule which is necessary if insertion losses well below 1 dB are expected. Considering this situation the question arose whether it is possible to make use of the high precision geometry of the fiber itself by coupling two fibers via their cladding in a common V-groove.

2. V-groove coupling

The influences on the insertion loss of a cladding-cladding-coupling in a V-groove can be divided into two groups: First, there are the statistically distributed spot size radii of the fibers, second, the statistical distribution of the fiber geometrical parameters. These factors had to be analyzed very carefully to give an answer to the above question.

2.1 Different spot size radii

Starting with Marcuses derivation of the loss a when coupling two fibers with spot size w_1 und w_2,

$$a = -10 \log \left(\frac{2V}{V^2 + 1} \right)^2 \quad , \quad V = \frac{w_1}{w_2} \qquad (1)$$

the distribution of the loss a was calculated when assuming spot sizes that are distributed gaussian. The theoretical calculations as well as the experimental investigations prooved that the excess loss caused by this effect is only of minor importance [2]: Coupling fibers the spot sizes of which are distributed around 9 µm with a standard deviation of 0.25 µm will result in a mean excess loss of 0.02 dB only. If 9 µm spot size fibers should be coupled to 10 µm spot size fibers both of them having 0.25 µm standard deviation the value for the mean excess loss will be slightly increased to 0.08 dB.

2.2 Fiber geometry

All fibers, regardless of the manufacturing process employed, come along with statistically distributed values for the cladding radius R, circularity and core centricity. The core position of a fiber to be coupled via its

cladding in a 90 degree V-groove is shown in figure 1: The distribution of R is described by the deviation δ from the mean $\bar{R}$, the non-circularity is characterized by the two parameters η and ψ, the core excentricity is expressed by ϵ and φ.

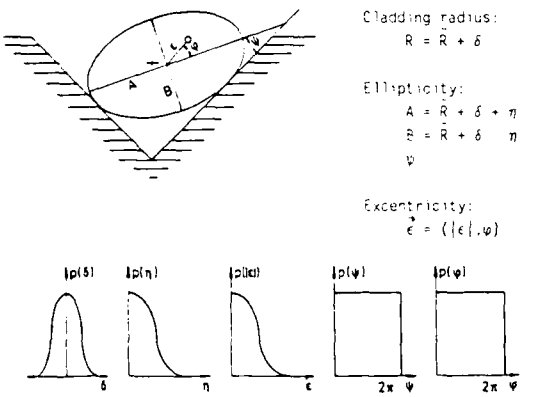

Fig.1: Fiber core position in 90° V-groove and parameter distributions

The lower part of figure 1 shows the distributions for these five parameters, they are assumed to be gaussian except for the two angles which should be uniformly distributed. So the core position is a function of these five variables. After some calculation an analytical solution is found for the mean value $\bar{a}$ of the loss:

$$\bar{a} = \frac{20 \log e}{w_0^2} \left(2 \sigma_\delta^2 + \bar{\epsilon}^2 + \sigma_\epsilon^2 + \bar{\eta}^2 + \sigma_\eta^2\right) \qquad (2)$$

The equation shows that the mean loss depends twice as strong on the width of the distribution of the cladding diameter as on the other variables.

The following example shows the influence of the various contributions of fiber geometry imperfections to the loss:

With

$\sigma_\delta = 0{,}3\ \mu m \quad \bar{\epsilon} = 0{,}5\ \mu m \quad \sigma_\epsilon = 0{,}25\ \mu m$

$\bar{\eta} = 0{,}4\ \mu m \quad \sigma_\eta = 0{,}2\ \mu m$

the partial sums $\bar{a}_\delta$, $\bar{a}_\epsilon$, and $\bar{a}_\eta$ of equation (2) resulting from radius deviations, core excentricities, and non-circularities are:

$\bar{a}_\delta = 0.08$ dB $\quad \bar{a}_\epsilon = 0.13$ dB $\quad \bar{a}_\eta = 0.09$ dB

So the overall sum $\bar{a}$ will be 0.3 dB in this example.

Statistical analysis allowed the calculation of the loss distribution as a function of given statistics of the geometry parameters. Figure 2 shows the probability density and the accumulated probability for an arbitrarily chosen set of fiber geometry parameters that results in a mean loss of 0.2 dB.

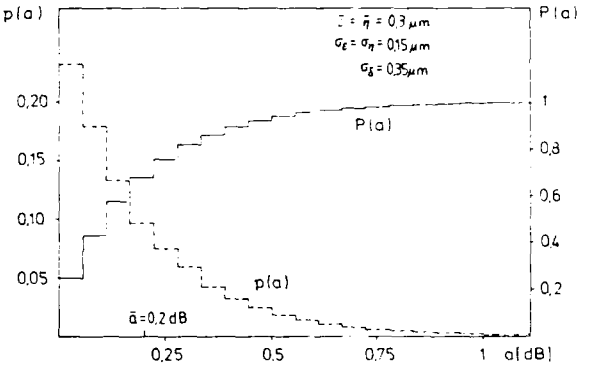

Fig. 2: Probability density p(a) and accumulated probability P(a)

The experimental investigations included fibers from different manufacturers. Very extensive coupling measurements were made [2]. For non-identical fibers from one manufacturer each a mean loss of 0.11 dB was measured. When coupling identical fibers the mean loss was as low as 0.07 dB.

These results indicate that the parameter set chosen above for the example does not meet the real quality of fiber geometry which is better than assumed in that example.

From these investigations, especially the experimental ones, it is obvious that the intended V-groove coupling is an alignment principle which is well suited for connectors. Its feasibility however depends very strong on the quality of the fiber geometry.

3. Connector Design

Figure 3 shows a photo of the connector. It basically comprises four parts, all of which are made by precision injection molded plastics: The adaptor, the two plugs and the coupling device, which is the small part between the two plugs. It contains the V-groove which couples the two fibers. Normally it is connected to one of the two plugs. The fact that the coupling device can be separated from the plugs offers the advantage to choose its materials independently. Furthermore cleaning or inspection of the V-groove or the fiber endface is readily done, if necessary. The fibers are fixed in a part of the plug that is called stamp. The floating fixture and the contour of the stamp provide the pre-alignment of the fiber in the first phase of the

connecting procedure, in the second one the fiber is precisely aligned by the V-groove. A spring exerts a gentle pressure perpendicular and horizontal to the fiber axis. Thus the fibers are in close contact to the V-groove and at the end of the connecting cycle the fiber endfaces are in physical contact.

Fig. 3: Plastic single mode fiber connector

The connection of a plug is simply done by pushing it into the adaptor, where it is locked by a slot-and-key-mechanism. Disconnection is only possible when both of the resilient arms of the plugs are pushed together at the same time, thus releasing the plug to be pulled out.
The size of the rectangular adaptor is 17 x 12 mm^2, its length is 66 mm. These are dimensions that are thought of to be not too small for easy handling and not too large for achieving high packaging densities in cross connection cabinets.

4. Connector Performance

4.1 Insertion loss

The connectors were assembled with Philips PCVD single mode fibers from the same drum. Figure 4 shows the histogramm of the insertion loss for 240 different combinations. The mean value of 0.05 dB impressingly justifies the completely new connector design. As there is still a small contribution of the fibers to the loss one can state that the connector inherent (extrinsic) mean loss will be below 0.05 dB.

Subsequent mating cycles of a connection gives no significant change in the insertion loss. The measured values, as shown in figure 5, all lie within the short-term stability of the optical attenuation measuring system.

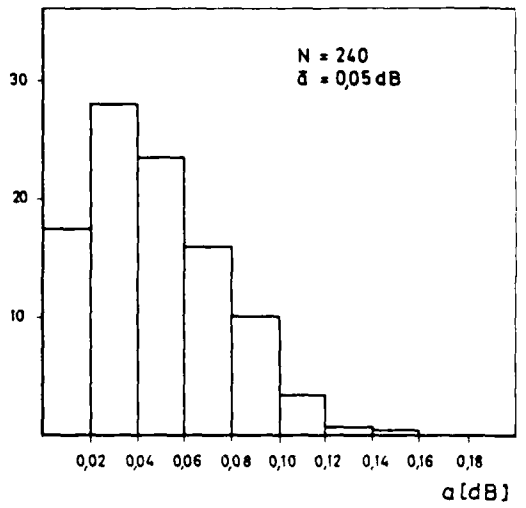

Fig. 4: Loss histogram

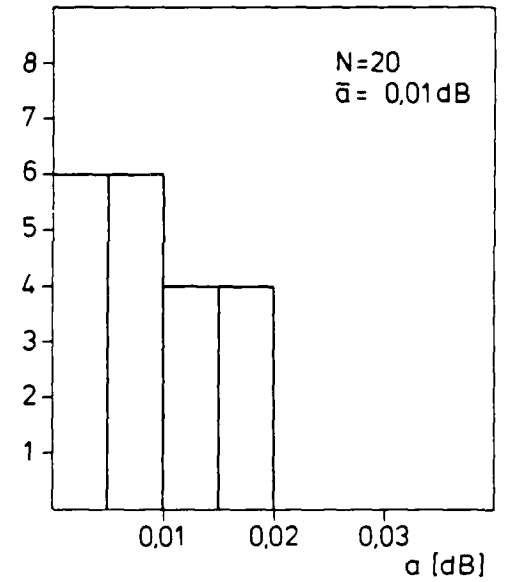

Fig. 5: Loss repeatability

Thus, as for the connector loss characteristics, an ultimate quality level is reached that can only be affected by the quality of the fiber geometry.

4.2 Temperature

Figure 6 shows the temperature dependance of the insertion loss for five different connections.

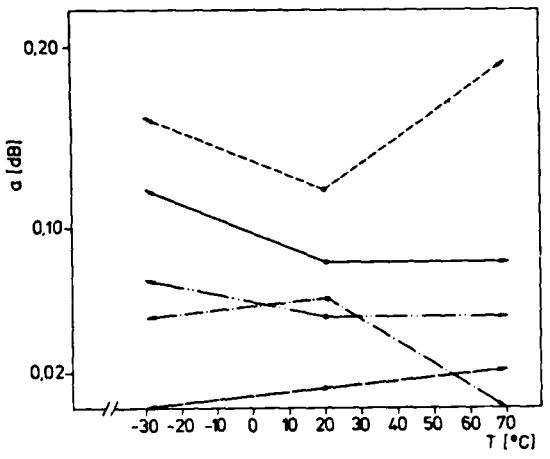

Fig. 6: Temperature dependance of loss a

The behaviour of the connectors is not identical, but it is absolutely satisfactory, because the loss variation is less than 0.1 dB over the entire temperature range of -30°C to +70°C.

4.3 Mating Durability

This test was conducted to investigate the connectors loss behaviour under progressive wear of the mechanical slides. In general this is a critical test for fiber optic connectors that make use of plastic fiber aligning parts. Figure 7 shows the loss behaviour for three situations found to be typical. The complete test was made without any cleaning of any connector part. The results again confirm the design: As no high absolute dimensional accuracy is necessary, the wear of the parts does not influence the fiber alignment.

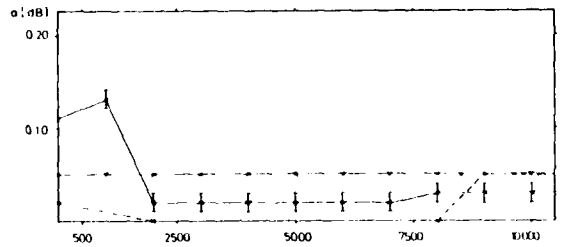

Fig. 7: Mating cycle test

The connector with the initial high loss is a quite interesting case, because it shows self-cleaning. Its higher values in the beginning of the test result from dust particles on the fiber endface (which of course have to be smoother than glass). After some cycles they are crushed and moved out of the core region.

Conclusion

This paper describes the development of a completely new single mode connector for application in subscriber networks. The essentials are:

- The connector is a very high performance component and a low cost device at the same time.
- The high performance is achieved by cladding to cladding coupling in a V-groove.
- Low cost is possible by exclusive use of plastic parts.
- The rectangular adaptor offers the advantage of easy handling and allows packaging densities which fulfill the demands of cross -connection cabinets and of main distribution frames [1].
- The design permits excellent loss characteristics over the temperature range of -30°C and +70°C and for very high mating cycles.

Acknowledgement

This work was supported by the Bundesminister für Forschung und Technologie of the Federal Republic of Germany. The authors alone are responsible for the content.

References

[1] P. Deußer, J.A. Becker: Cable Accessories For Optical Fibre Ribbon Cables In Subscriber Loop Networks. This conference

[2] J.A. Becker, U. Grzesik, W. Zell: Spleißkompatibilität von Einmodenfasern unterschiedlicher Herstellung, PKI Technische Mitteilungen, vol. 2 (1987), pp. 91-94

[3] W. Zell: to be published

Wolfgang Eutin was born in Recklinghausen, West Germany, in 1952. He received the Dipl.-Phys. degree from the Universität Düsseldorf, Düsseldorf, Germany, in 1981, where he worked on stabilized sealed CO_2 lasers. In 1981 he joined the Heinrich-Hertz-Institut, Berlin, Germany, where he was engaged in coherent fiber communication systems. Since 1985 he is with Philips Kommunikations Industrie AG, Cologne, Germany, where he is responsible for fiber optic connectors.

Ulrich Grzesik was born in Wuppertal, West Germany, in 1957. He studied Physics at the University of Cologne and the Technical University of Munich where he got his "Diplom" in 1982. The following years were spent at the Max-Planck-Institut for Quantum Optics. 1985 Mr Grzesik obtained the grade "Dr.rer.nat" for his work on frequency stabilisation of lasers. Afterwards he joined the Philips Kommunikations Industrie AG working on interconnection technology for optical fibres. From 1987 he lead a group working on optical fiber connectors for subscriber loop applications (Photograph not available at time of publication).

E. Schürmann, biography and photograph not available at time of publication

OPTICAL-FIBER FANOUT CONNECTOR USING PUSH-PULL MULTI-FIBER CONNECTOR

TAKEO KOMIYA TOSHIAKI KAKII SHUZO SUZUKI YUYA IWAMOTO

Sumitomo Electric Industries Ltd.
1, Taya-cho, Sakae-ku, Yokohama, 244, Japan

ABSTRACT

In an optical subscribers network, small and high performance fanout connectors are needed to fanout ribbon fibers to individual single fibers. Fanout connectors for use in graded index fiber subscriber lines have been developed. They are composed of a branching unit, a multi-fiber push-pull connector and five single-fiber push-pull connectors. The dimension of the branching unit have been reduced to 90(L) x 33(W) x 9(H) mm^3.

In particular, its thickness is reduced to only 9mm by using the newly developed push-pull multi-fiber connector. Considering the long-term reliability and the low bending loss of the bent fiber in the branching unit, the minimum branching length was designed. The average loss of mass produced fanout connectors was found to be 0.44dB.

1. Introduction

Optical subscriber network needs high-density high-count optical fiber cables which accommodate a number of ribbon fibers. It is very important to fanout ribbon fibers to individual single fibers in telephone offices or subscriber buildings. Usually in order to fanout a ribbon fiber, individual single fibers are divided from it and then spliced individually with particular single fibers or jumper cords. The spliced parts and the excess length of these are put in a closure or a cabinet. The problem with this method is that it requires the large space for accommmodation of the ribbon fiber fanouting portion. Therefore, demands for small and high performance fanout connectors have increased.

This paper describes the design and performance of the newly developed fanout connector with the multi-fiber push-pull type connector.

2. Design

2.1 Structure of the fanout connector

The fanout connector is composed of a branching unit, one multi-fiber connector and five single-fiber connectors, as detailed in Fig.1. The single-fiber and the multi-fiber connectors are mounted on PVC-jacketed, and Kevlar-reinforced optical fiber jumper cords. In order to realize the fanout connector which has the advantages of high fiber density and easy handling, small size single-fiber and multi-fiber push-pull connectors are necessary. The multi-fiber push-pull connector plug and adaptor and the branching unit case are plastic molded to reduce cost and weight.

2.2 Multi-fiber push-pull connector

The multi-fiber push-pull connector has a transfer-molded square ferrule [1] on which the five graded-index fibers with 50μm core and 125μm cladding diameter are positioned precisely at 0.25mm intervals between the two alignment holes for guide pins, as shown in Figs.1 and 2. Mating plugs are joined and aligned with these two guide pins of stainless steel, whose diameter is 0.7mm and tolerance is within 1μm. The deviations of the diameter and the center position of each fiber holes are designed and manufactured to be within 1μm and 3μm respectively (Fig.3).

The push-pull connecting mechanism has two features; one is easy handling. For connection only push the boot of the plug and only pull the ejector for disconnection [2][3]. The other is the mechanical characteristic; low insertion force and high mechanical coupling strength are accomplished. The mechanical coupling strength means the minimum tensile strength loaded on the fiber cord which can pull out the plug from the adaptor by force. The connecting mechanism is detailed in Fig.4. In order to reduce connector thickness to 9mm, two small springs (Spring II) for forcing the ejector are arranged on the both sides of the ferrule.

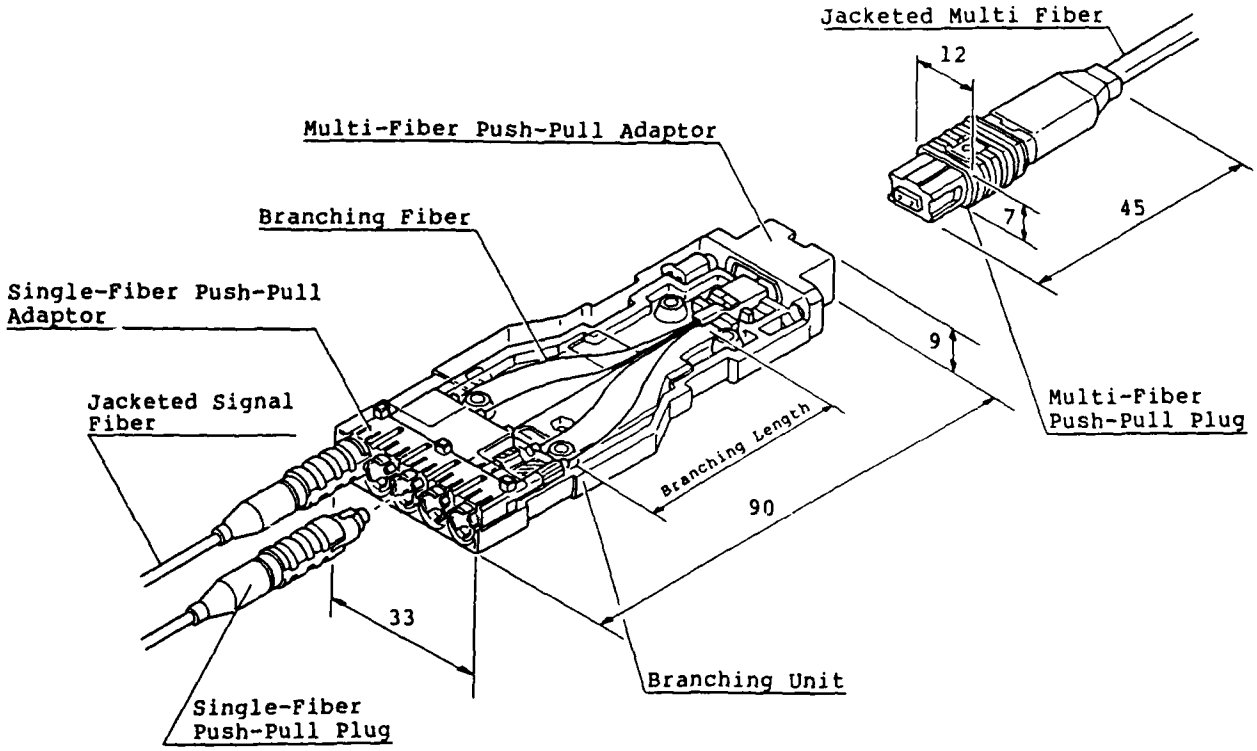

Fig.1 Perspective View of Fanout Connector

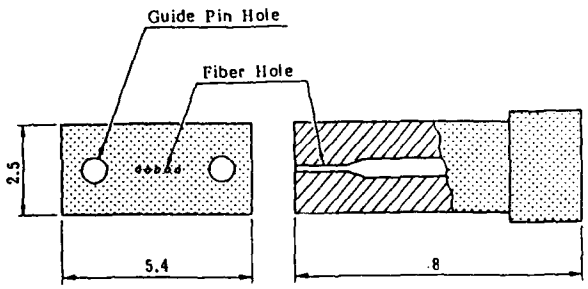

Fig.2 Structure of Plastic Square Ferrule

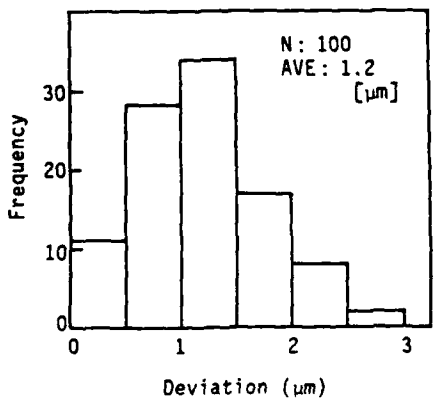

Fig.3 Fiber Holes Center Position Deviation of Plastic Square Ferrules

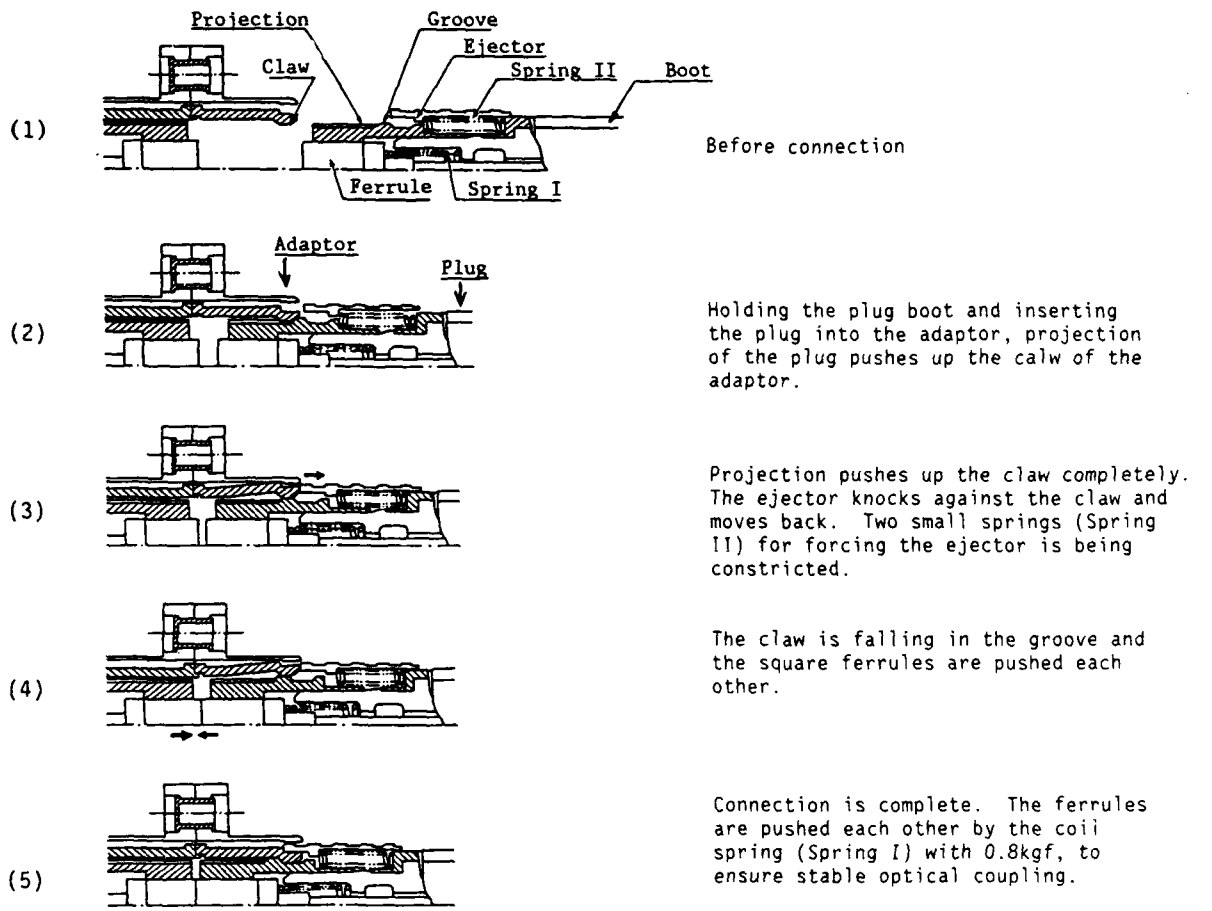

Fig.4 Mechanism of Connection

The relationship between the insertion length and insertion force was calculated and the results are shown in Fig.5-(1). The zero point of the insertion length is defined as the point where the projection first touches the claw. The calculated insertion force (F) is given by the following expression.

$$F(x) = f_1(x) + f_2(x) + f_3(x)$$

$f_1(x)$; the sum of the claw flexure force and the frictional force between the claw and the projector

$f_2(x)$; the press force of the two small springs (Spring II)

$f_3(x)$; the press force of the main spring (Spring I)

x ; insertion length

In order to realize easy handling and connection endurance, this multi-fiber push-pull connector was designed so that $f_1$max and Fmax are less than 1kgf, and 2kgf respectively. Fig.5-(2) shows the measured results. These results indicate that the measured results are generally in accordance with the calculated results, and $f_1$max and Fmax are 0.6kgf and 1.7kgf respectively and meet the requirements. The withdrawal force was also calculated and measured in the same way. These results are given in Table 1.

Considering the accident which may be caused by catching jumper codes, the minimum coupling strength was required to be greater than 10kgf. By selecting the appropriate material and designing the optimum structure as the ejector, the mechanical coupling strength of greater than 14kgf was accomplished.

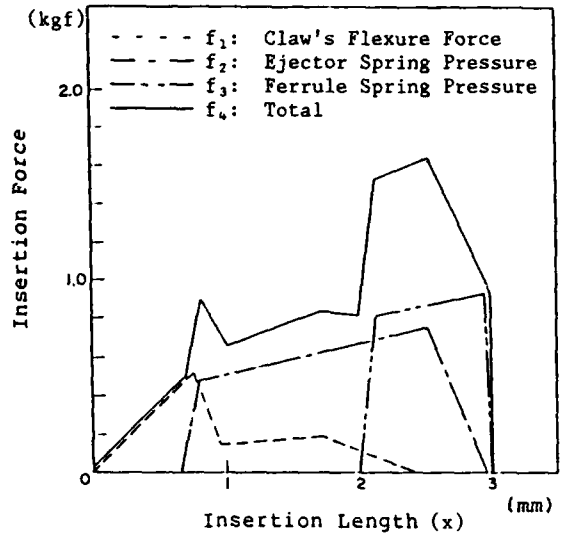

Fig.5-(1) Calculated Relationship between the Insertion Length and Insertion Force

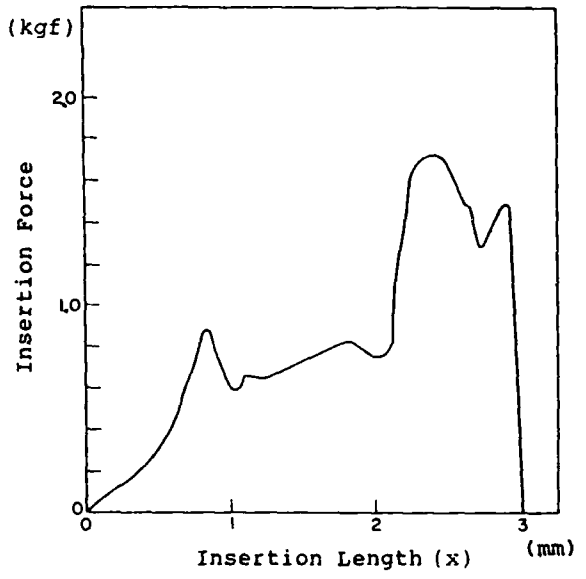

Fig.5-(2) Measured Relationship between the Insertion Length and Insertion Force

Table 1 The designed and measured results of the insertion and withdrawal forces

	Insertion force		Withdrawal force	
	Design	Measurement	Design	Measurement
F_{max}	≦ 2.0	1.7	≦ 2.0	1.1
f_1max	≦ 1.0	0.6	≦ 1.0	0.8

[kgf]

2.3 Single-fiber push-pull connector

The single-fiber push-pull connector[4] with a MP-ferrule [5] has a push-pull connecting mechanism like that of the multi-fiber push-pull connector, and can be mounted at intervals of 6mm, as shown in Fig.1.

2.4 Branching unit

As illustrated in Fig.1, the branching unit consists of a multi-fiber adaptor and five single-fiber adaptors are mounted at intervals of 6mm. The dimension of the branching unit is 90(L) x 33(W) x 9(H) mm^3.

The branching fibers which joint single-fiber adaptors and multi-fiber adaptors are bent except for the central jointing fiber. Therefore, an investigation of the time to failure caused by bending strain is very important to guarantee high reliability. The result of the calculation about the relationship between the time to failure and the bending radius is shown in Fig.6. When 0.7% proof tested fiber is used as branching fiber, the bending radius must be more than 25mm under the condition that the life time is almost equal to that of optical fiber cable used in subscriber metwork. Taking into account the minimum radius of 25mm and the 6mm intervals of single-fiber adaptors and the production precision, a minimum branching length of 40mm was designed. Bending loss of jointing fiber was negligible. Furthermore, using 2% proof-tested fiber as a branching fiber, the branching length can be shortened to 20mm.

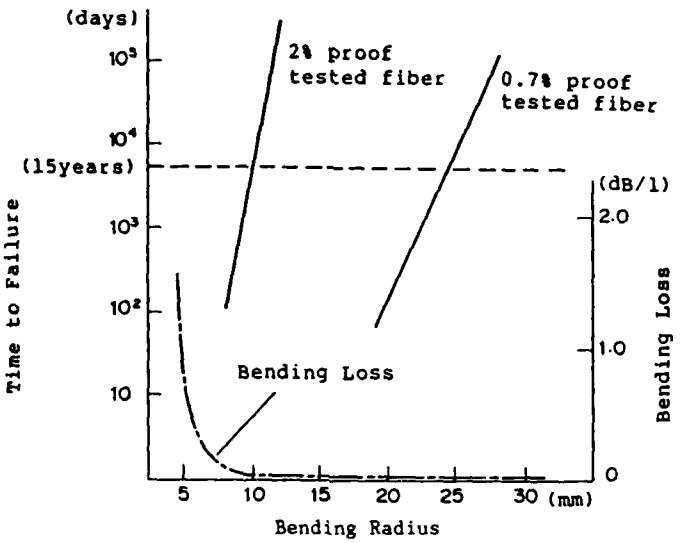

Fig.6 Relationship between Radius and Time to Failure ————

Relationship between Radius and Bending Loss — - —

fiber length: ℓ=50mm
failure probability: $1x10^{-6}$

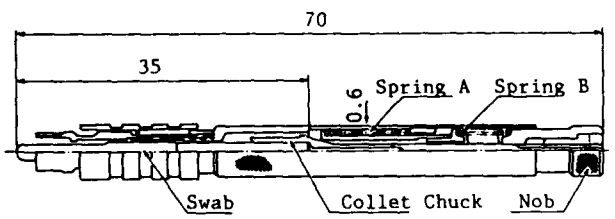

Sig.7 Cross Section of Cleaning Plug

2.5 Cleaning plug

The push-pull type connector is easily connected and disconnected. In the frequent mating of the push-pull connectors, the surface of the ferrule may be sometimes stained with dust. The cleaning plug, as shown in Fig.7 has been developed for the cleaning of the single-fiber push-pull adaptor, and has the following features.

(1) The cleaning plug can be easily connected with the single-fiber push-pull adaptor, because it has the same mechanism as that of the single-fiber push-pull connector.

(2) The cleaning effect of this plug is excellent because the swab is given sufficient pressure and rotated by the nob rotation.

(3) The swab can be easily exchanged by pushing the nob.

3. Fabrication of the branching unit

Fig.8 shows the fabrication process of the branching unit and the details of the main process are as follows.

(1) Single-fiber insertion
Bare single-fiber is inserted into the MP-ferrule filled with epoxy adhesive and cured.

(2) Polishing
The MP-ferrule's endface is polished.

(3) Single-fibers arrangement
The single-fibers with the ferrules are cut to each designed braching length. The tips of five single-fibers are arranged side by side like a five-fiber ribbon with a clamp.

(6) Unit assembly
Branching fibers with five MP-ferrules and a square ferrule, five single-fiber adaptors, a multi-fiber adaptor, and a branching unit case are assembled.

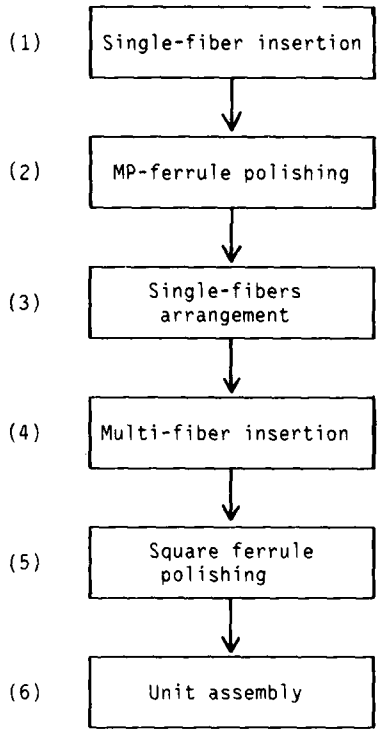

Fig.8 Fabrication process of the branching unit

4. Performance of the fanout connector

The fanout connector was mass produced, using the single-fiber and multi-fiber push-pull connectors for 50/125μm graded-index fibers. 2970 insertion losses of the 596 fanout connectors were measured at 1.3μm LED. Histogram of the insertion loss and the relationship between the fiber No. and the insertion loss are shown in Fig.9 and Table 2 respectively. The average loss was 0.44 dB. No correlation between the insertion losses and fiber No. is found. The insertion losses of the fanout connectors are summed by those of the single-fiber push-pull connectors, those of the multi-fiber push-pull connectors and the bending losses of the branching fibers. The average losses of single-fiber and the multi-fiber push-pull connectors were found to be 0.15dB and 0.26dB respectively. Therefore, the average bending loss is presumed to be about 0.03dB.

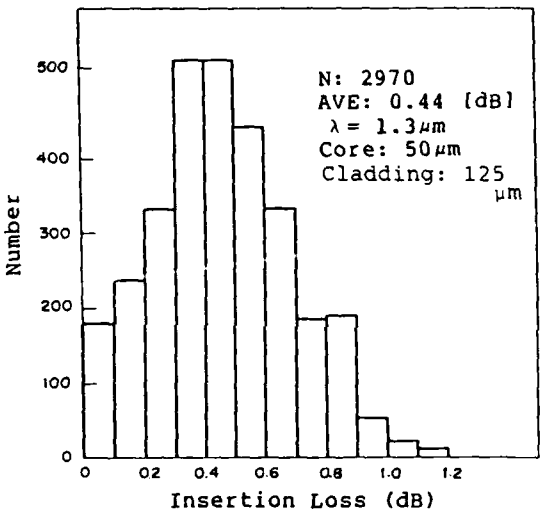

Fig.9 Historgram of Insertion Loss of Fanout Connectors

Table 2 Relationship between the fiber No. and the insertion loss of fanout connectors

Fiber No.	Average loss
1	0.43
2	0.41
3	0.44
4	0.47
5	0.44

[dB]

The return losses of the fanout connectors were measured at 1.3μm and were greater than 35dB. Fig.10 shows the results of the multi-fiber connector repeatability test. The variation in insertion loss during 1000 push-pull actions was within 0.03dB.

Various kinds of mechanical and environmental tests were carried out and the variations in insertion loss were measured. For the tensile strength test, the tensile strength was loaded on the multi-fiber cord, and the optical coupling strength of the multi-fiber push-pull connector was measured. It is defined as the maximum tensile strength at which the increment of the insertion loss reaches to 0.2dB. The optical coupling strengths (P_1, P_2, P_3) were measured by applying force an axial or radial direction of a connector as shown in Fig.11 and 8.5kg of P_1, 4.2kg of P_2 and 4.1kg of P_3 were obtained (Table 3).

The vibration test was carried out at the frequency of 10Hz and the amplitude of 10mm for 2 hours, and the fluctuation in insertion loss was within 0.05dB.

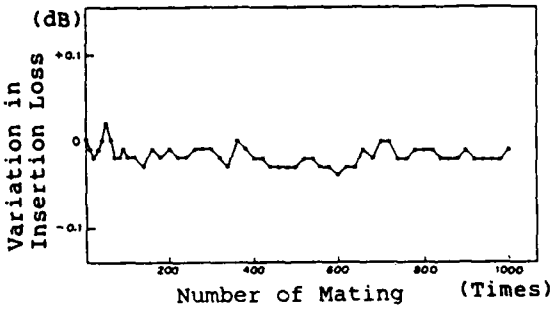

Fig.10 Repeatability of Multi Fiber Push-Pull Connector

Table 3 Optical coupling strength

Direction	Optical coupling strength
P_1	8.5
P_2	4.2
P_3	4.1

[kgf]

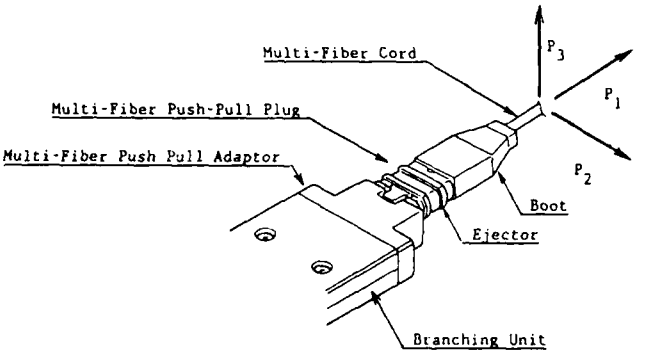

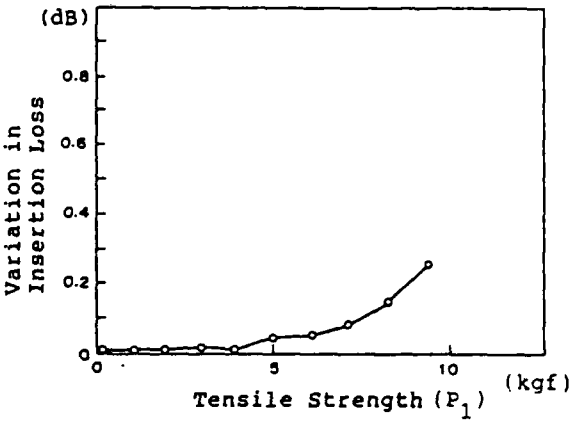

Fig.11 Tensile Strength Test on the Direction of P_1

Fig.12 shows the results of heat cycling test, from which insertion loss change was within 0.07dB over temperature range of -30°C to +60°C. The results concerning other testing items are shown in Table 4. Results of these tests demonstate that the newly developed fanout connector exhibits the stable connection performance.

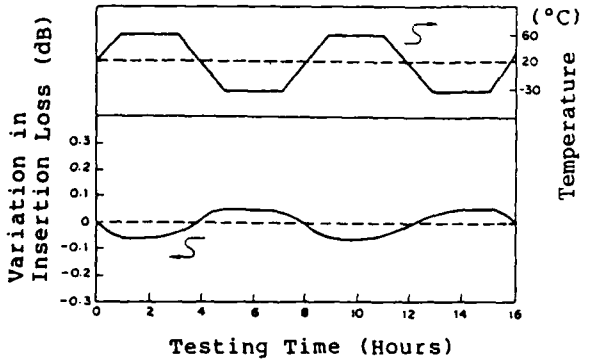

Fig.12 Temperature Cycling Test of Fanout Connector

Table 4 Performance of the fanout connector

Testing item	Condition	Result
Average loss	1.3μm LED	0.44dB
Return losss	1.3μm LD	More than 35dB
Repeatability	1000 times	Within 0.03dB
Heat cycling	From -30°C to 60°C 100H	Within 0.07dB
High temperature	80°C, 100H	ditto
Low temperature	-30°C, 100H	ditto
Humidity	60°C, 95%RH, 100H	ditto
Vibration	10Hz amplitude 10mm, 3 direction	Within 0.05dB

5. Conclusion

Fanout connectors for the use in the optical subscriber networks have been developed. They are composed of a branching unit, a multi-fiber push-pull connector and five single-fiber push-pull connectors. The branching unit size has been reduced to 90(L) x 33(W) x 9(H) mm^3. In particular its thickness is reduced to only 9mm by using the newly developed push-pull multi-fiber connector. Low insertion force has been achieved with the claw of the adaptor, and high mechanical coupling strength has been accomplished with the optimum design of the ejector of the plug. Considering the long-term reliability and low bending loss of bent fiber in the branching unit, a minimum branching length of 40mm was determined.

The average insertion loss of a number of mass produced fanout connectors was 0.44dB. Various kinds of mechanical and environmental tests were conducted to confirm the stability and reliability of the fanout connector.

The fanout connector was put to practical use in the optical subscriber network and are quite effective for raising the fiber accommodation density of the MDF (Main Distribution Frame) in telephone offices.

Reference

[1] T. Sataka, S. Nagasawa, R. Arioka, "A new Type of Demountable Plastic-Molded Single-Mode Multifiber Connector", IEEE, J. Lightwave Technol., Vol.Lt-4, 8, pp.1232∿1236, 1986.

[2] S. Nagasawa, T. Satake, I. Sankawa, R. Arioka, "Optical-fiber fanout connector for 10-fiber ribbon cable termination", IEEE, J. Lightwave Technol., Vol.Lt-4, 8, pp.1243∿1247, 1986.

[3] S. Nagasawa, I. Sankawa, T. Satake, N. Kashima, "Small-size push-on type optical fiber connector", Trans. IEICE Japan, Vol.E70, 5, pp.451∿454, 1987.

[4] K. Kashihara, M. Fukuma, T. Kakii, S. Suzuki, "Design and Performance of the New Single-Mode Fiber Connector with MP-Ferrule in Subscriber Network", IWCS 87, pp.379∿385, 1987.

[5] T. Kakii, K. Kashihara, Y. Asano, S. Suzuki, "Composite metal-plastic ferrule for single-mode fiber connector", in Tech. Dig. OFC/IOOC, TUF5, 1987.

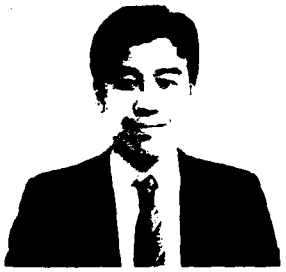

Takeo Komiya

Sumitomo Electric
Industries, Ltd.

1, Taya-cho, Sakae-ku,
Yokohama, Japan

Mr. Komiya received his B.S. degree from University of Tokyo in 1986. He then joined Sumitomo Electric Industries and has been engaged in research and development of optical fiber jointing technologies. He is a member of Communication R&D Department Yokohama Research Laboratories, and a member of the Institute of Electronics and Communication engineers of Japan.

Shuzo Suzuki

Sumitomo Electric
Industries, Ltd.

1, Taya-cho, Sakae-ku,
Yokohama, Japan

Shuzo Suzuki received a M.S. in 1972 from Tokyo University. He joined Sumitomo Electric Industries, Ltd. in 1972, and has been engaged in research and development of optical fiber, cable and jointing technologies. He is a member of the Institute of Electronics and Communication Engineers of Japan.

Toshiaki Kakii

Sumitomo Electric
Industries, Ltd.

1, Taya-cho, Sakae-ku,
Yokohama, Japan

Toshiaki Kakii was born in 1955 and received a M.E. degree from Keio University in 1980. He joined Sumitomo Electric Industries, Ltd. in 1980 and has been engaged in research and development of optical fiber jointing technologies. He is a member of the Institute of Electronics and Communication Engineers of Japan.

Yuya Iwamoto

Sumitomo Electric
Industries, Ltd.

1, Taya-cho, Sakae-ku,
Yokohama, Japan

Yuya Iwamoto received a B.S. degree in 1972 from the Tokyo Metropolitan University. He joined Sumitomo Electric Industries, Ltd. in 1972, and has been engaged in development and designing of optical fiber cable accesories.

Performance Characteristics of Plain Copper Versus Tinned Copper for Solderless Wrapped Connections

David Dunleavy

Bell Canada

ABSTRACT

This paper compares the performance characteristics of plain copper versus tinned copper for solderless wrapped connections. To satisfy real life conditions and a 40 year reliability objective, tests were conducted which subjected the connections to temperature cycling, heat aging, humidity and thermal shock. It was considered that these tests would accelerate the ageing processes that tend to cause electrical and mechanical instability. The test results indicate that plain copper meets the stability objectives for a 40 year service life in a central office environment.

INTRODUCTION

Tinned copper has long been used for indoor applications with telecommunication equipment in central offices, PBX, and PABX exchanges. Its early use was most likely due to the general belief that it improved the solderability performance, since plain copper if left exposed to the environment would readily tarnish and exhibit signs of oxide film.

With the introduction of solderless wrapping, tinned wire was kept presumably for its improved mechanical and electrical performance a result of the solid state diffusion between wire and terminal. It has been stated in a paper published in a Bell System Technical Reference (Pub 48010)[1] that the use of plain copper would reduce the life requirement by approximately one half, as well as produce noisy and unreliable connections under certain environmental conditions.

Recent research work performed by Telecom Australia[2] indicates plain copper performs equally well if not better than tinned copper conductors. In view of this and the potential cost savings of using plain copper, Bell Canada has conducted a series of tests to more closely examine the effects of diffusion and corrosion mechanisms on the long term reliability of a solderless wrapped connection.

Temperature cycling, heat ageing, high temperature humidity exposure, and thermal shock tests were conducted in order to compare the in-service and lifetime performance characteristics of both plain and tinned copper conductors for solderless wrapped connections.

SAMPLE PREPARATION AND TEST PROCEDURE

To evaluate the performance characteristics of plain copper versus tinned copper, 33 - 100 pair NE 66QC100 wire wrap connecting blocks were individually wire wrapped with equal amounts of 24 AWG (0.51 mm diameter) plain and tinned copper wire. Of the tinned wire samples, two coating specifications were used as shown in table 3. All joints were wrapped using a manually operated O.K. Wrap tool (model G100).

As shown in figure 1, the test wires ends were wrapped to tin plated terminal posts (.06" X .04") forming a connection loop.

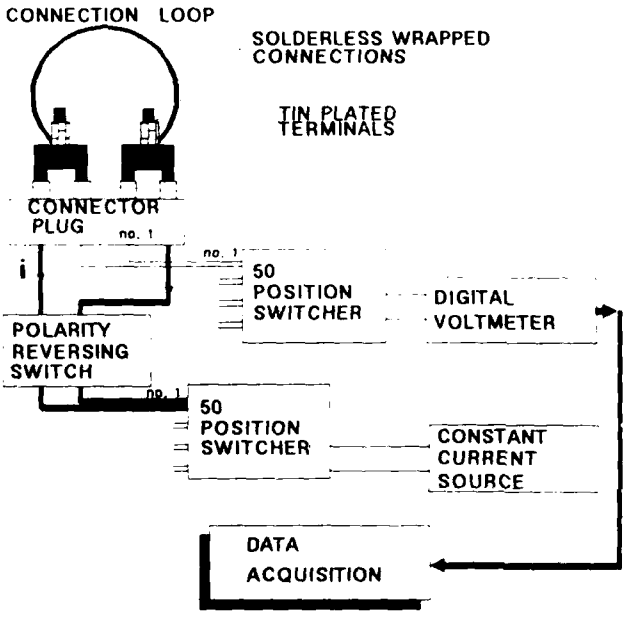

Figure 1 System Test Set up

Using a 6624A HP System DC Power Supply and a 3852A Data Acquisition control unit, 4 point resistance measurements for each of the connection loops were recorded. To eliminate thermal potentials all calculated resistances were based on forward and reverse voltage measurements by reversing the direction of the current. A second set of measurements was taken immediately after the first to assure repeatability of the test method and measuring apparatus.

Two connection loops (one copper and one tin) from each of the test blocks were fully soldered. In this way, any significant variation in connection loop resistance would provide a further measure of the system repeatability as well as the degree to which oxidation, corrosion, or tin wire intermetallic growth affects the bulk wire resistance.[3]

In order to ensure the measurement of thin film barrier resistances, the current source was initially set to zero before being increased to the 100 mA maximum as specified by ASTM for dry circuit testing[4].

Figure 2 shows a fully wired test block under measurement.

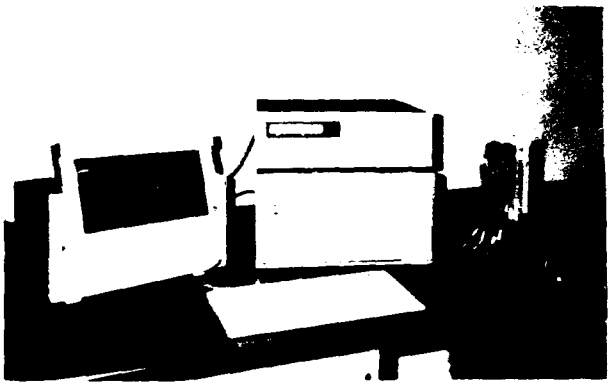

Figure 2 Test Block Resistance Measurement

TEST ENVIRONMENTS

The following tests were performed in order to compare the long term reliability behavior of both plain and tinned copper for solderless wrapped connections:

Temperature Cycling

Test blocks were placed in an environmental chamber and subjected to 100 cycles with each cycle consisting of a temperature change from -40°C to +60°C. The dwell time at each temperature extreme was 2 hours and 25 minutes. The temperature changes occurred at a rate of 150°C per hour. The chamber humidity was not controlled. Resistance measurements were performed initially and after 25, 50 and 100 cycles. All test blocks were stabilized for 3 hours at 25°C

Heat Ageing

Test blocks were exposed to a constant temperature of 118°C. Resistance measurements were recorded initially and after 10, 20, 30 and 40 days. All test blocks were stabilized for 2 hours at 25°C prior to measurement. It was expected that this test would simulate the amount of stress relaxation and metal diffusion at the contact points of the wrapped connection over its intended life.[5]

High Humidity

Test blocks were subjected to a constant relative humidity of 95% or greater for a total of 25 days. All test blocks were stabilized for 3 hours at a temperature of 25°C before being measured at 5, 10, 15, 20 and 30 day intervals.

Thermal Shock

A final group of test blocks was subjected to 10 cycles of a temperature alternating between -15°C and 118°C with a dwell time of 20 minutes at each temperature extreme. The samples were stabilized for 45 minutes at 25°C before being measured for changes in joint resistance.

RESULTS

The test results comparing plain copper to tinned copper wire are shown in tables 1, 2, and 3, as well as in figures 3 through 9. All resistance variations shown are the differences between those of their initial values and after the given testing period.

The general observations were as follows:

a) all resistance variations were well below one milliohm

b) tinned copper performed better in the temperature cycling and thermal shock tests

c) plain copper performed better in the heat ageing and high humidity tests

Repeatability of the resistance measurements was on average below 0.01 milliohms while resistance variations of the fully soldered connection loops were on average below 0.02 milliohms.

DISCUSSION OF RESULTS

The low resistance variations observed in the test results of the soldered connections clearly indicate:

a) the measurements are sufficiently accurate for use in a comparison study.

b) the effects of oxidation, corrosion, and tin intermetallic growth on bulk wire resistance are negligible.

Table 1 Results of Temperature Cycling and Thermal Shock Tests

TEST		TEMPERATURE CYCLING		THERMAL SHOCK	
		TIN	COPPER	TIN	COPPER
SAMPLE SIZE NO. OF CONNECTION LOOPS		700	700	150	150
RESISTANCE VARIATION (milliohms)	10 CYCLES			AVG .142 STD .154	AVG .204 STD .164
	25 CYCLES	AVG .071 STD .060	AVG .169 STD .128		
	50 CYCLES	AVG .134 STD .135	AVG .292 STD .188		
	100 CYCLES	AVG .152 STD .130	AVG .353 STD .238		

Table 2 Results of Heat Ageing and Humidity Tests

TEST		HEAT AGEING		HUMIDITY	
		TIN	COPPER	TIN	COPPER
SAMPLE SIZE NO. OF CONNECTION LOOPS		300	300	300	300
RESISTANCE VARIATION (milliohms)	5 DAYS			AVG .177 STD .176	AVG .034 STD .144
	10 DAYS	AVG .172 STD .128	AVG .008 STD .124	AVG .183* STD .172	AVG .031 STD .172
	15 DAYS			AVG .364 STD .185	AVG .227 STD .176
	20 DAYS	AVG .263 STD .143	AVG .047 STD .125	AVG .386 STD .204	AVG .252 STD .223
	25 DAYS			AVG .446 STD .284	AVG .298 STD .242
	30 DAYS	AVG .354 STD .173	AVG .128 STD .138		
	40 DAYS	AVG .419 STD .190	AVG .204 STD .149		

* BLOCKS NOT THOROUGHLY DRY DURING MEASUREMENT

Table 3 Properties of Wire used in Test

	ELONGATION %	TIN THICKNESS um (microinches) FREE[1]	TOTAL[2]	CONDUCTIVITY BEFORE WRAPPING % IACS[3]
COPPER WIRE	28.1	—	—	101.2
TINNED WIRE lot # 1	25.9	0.5 (20)	1.5 (50)	99.3
TINNED WIRE lot # 2	23.1	1.15 (46)	1.7 (67)	100.1

Notes:

1. measured using a Kocour thickness tester
2. measured using Atomic Absorption Spectrophotometry
3. International Annealed Copper Standard

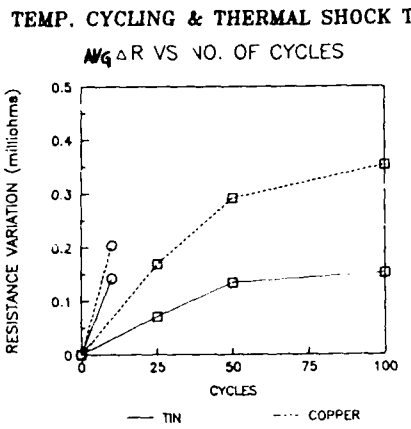

Figure 3

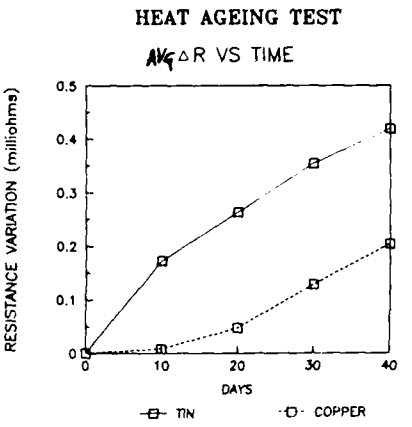

Figure 4

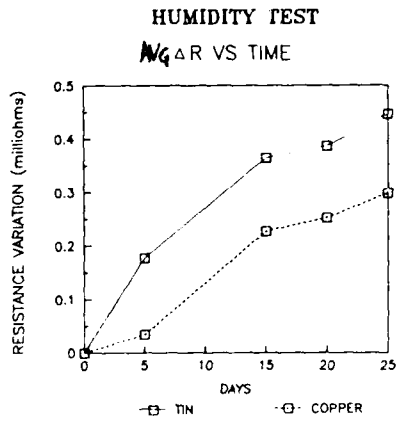

Figure 5

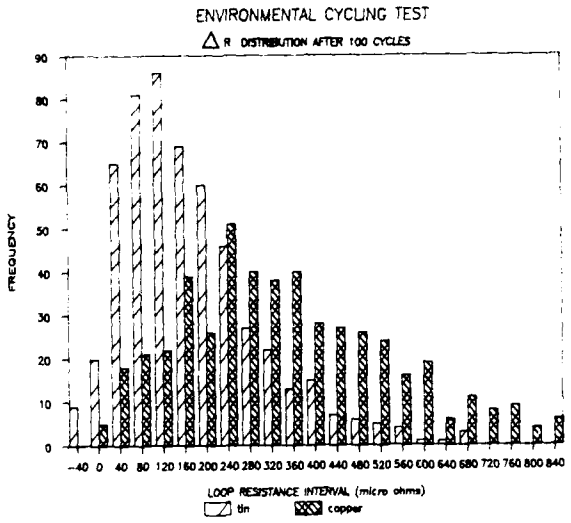

Figure 6

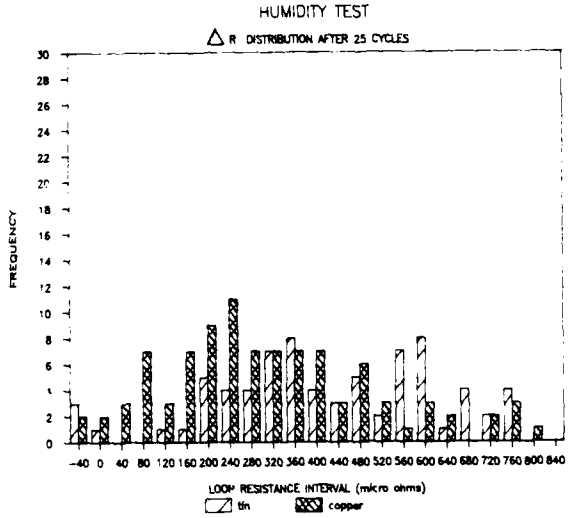

Figure 8

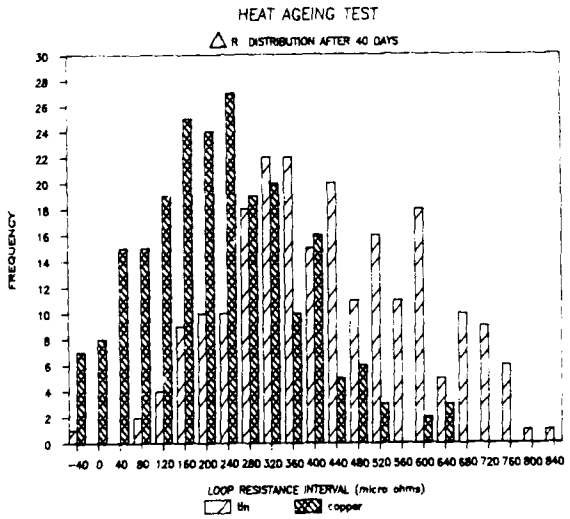

Figure 7

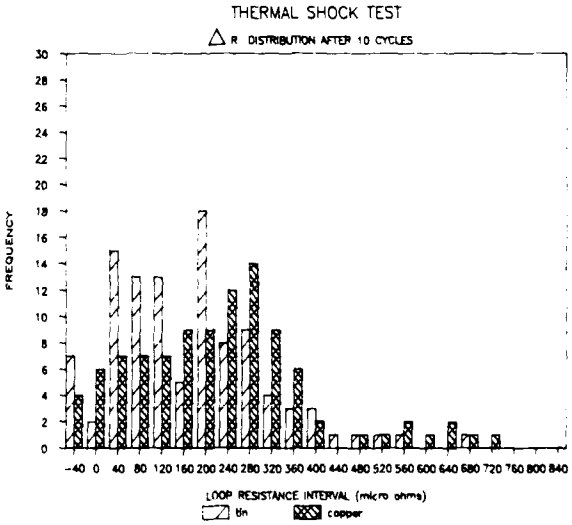

Figure 9

Since the data shows all resistances well below one milliohm, it can be safely assumed that all connections are stable and the 40-year reliability objective is satisfied. Although there were slight performance differences between plain and tinned copper in each of the tests (an estimated 0.2 milliohms per two connections), they were not considered significant in terms of affecting the lifetime reliability objective. It should be stated that these differences are very low considering the threshold of transmission impairment is quoted at 100 milliohms.[6]

However well plain copper was found to perform, there still remains unanswered questions regarding the relative performance. It was considered that these differences could be explained by the various mechanisms such as stress relaxation or diffusion. With this in mind, pull out tests were performed on freshly stripped and wrapped wire samples as well as on specimens obtained from the temperature cycling and heat ageing test. Results of this evaluation are shown in table 4.

Examination of table 4 shows that the wire-wrap pull-out forces for the tin wire groups increase slightly after the temperature cycling and ageing processes. This phenomenon is consistent with the theory of solid state diffusion.

It was also noted that wires with the thicker tin plating had a higher pull out force. This may be explained by the fact that thicker ductile coatings maximize the post-to-wire contact and ensure the greatest possible area for cold welding.[8]

Further review of the test results indicates that the pull-out forces required for the copper wire are substantially higher than those for the tin after the heat ageing process. This phenomenon may be explained as follows:

a) a higher contact surface is established between the copper wire and the post, since the copper wire can more easily deform in wrapping as seen by its elongation characteristics

b) the likelihood that the test temperature and duration was high enough to promote the slower reacting plain copper/tin post diffusion mechanism - which is hypothesized to produce a much higher limiting shear force than that for tin plated copper[9]

As for the lower pull-out forces observed for the copper samples in the temperature cycling test, this is probably due to two factors, namely:

a) the nature of the test; since heating with periodic cycling and measurement is claimed to be more severe than undisturbed heat ageing.[10]

b) the lower temperature levels and diffusion time which do not promote the same higher limiting shear forces as in the heat ageing test

CONCLUSION

Based on the test results it can be concluded that plain copper meets the stability objectives for a 40-year service life in a central office environment.

Table 4 Pull-out Force Test Results

	ELONGATION %	TIN THICKNESS um (microinches) 1 FREE	2 TOTAL	RESISTANCE VARIATION m TEMP CYCLING	HEAT AGEING	PULL OUT FORCE kg 3,4 TEMP CYCLING	HEAT AGEING	FRESHLY STRIPPED
COPPER WIRE	28.1	—	—	.353	.204	9.5	17.2	13.6
TINNED WIRE lot # 1	25.9	0.5 (20)	1.5 (50)	.161	.436	14.1	14.5	13.2
TINNED WIRE lot # 2	23.1	1.15 (46)	1.7 (67)	.145	.404	14.1	15.9	13.2

Notes:

1. measured using a Kocour thickness tester
2. measured using Atomic Absorption Spectrophotometry
3. values based on an average of 10 samples
4. representative samples were found capable of being unwrapped from the terminal without breaking [7]

REFERENCES

1. "Requirements for Solderless Wrapped Connections", Bell System Technical Reference (Publication 48010), March 1981, p. 16.

2. Boer B.T, and Mottram K.G., "Use of Plain Copper Conductors in Lieu of Tinned-Copper for Internal Cables", 22nd International Wire and Cable Symposium, 1983, pp. 1 - 7.

3. McCune T.B. and Burns J.H.,"Heat Ageing Evaluation of Common Coated Conductors", 19th International Wire and Cable Symposium, 1970 1970, pp. 122 - 130.

4. American Society for Testing and Materials B539 - 80, "Standard Methods for Measuring Contact Resistance of Electrical Connections (Static Contacts)", 1980, pp. 430.

5. "Design Evaluation of Solderless Wrapped Connections", Bell Northern Research, Standard 1021, 1973, pp. 1 - 14.

6. "Solderless Wrapped Connections - Requirements", Bell Northern Research, Standard 1972, p. 2.

7. "Solderless Wrapped Connections" Bell Telephone System Technical Publications (Monograph 2085), 1953, p. 74.

8. Davies D. G. "Micro-Mechanisms of Solderless Wrapped Joint Formation", IEEE Trans, Parts, Hybrids, Package V Php-8 No. 1, March 1972, pp. 48 to 62.

9. Mason W. P. and Anderson O.L. "Stress Systems in the Solderless Wrapped Connection and Their Permanence", The Bell System Technical Journal, September 1954, pp. 1093 - 1110.

10. Elliot S. J. "Evaluation of Solderless Wrapped Connections for Central Office Use", Bell Telephone System Technical Publications (Monograph 3339), 1958, p. 8.

David Dunleavy graduated in 1986 as a Mechanical Engineer from Concordia University. Since joining Bell Canada, he has been involved in the development of fiber optic and copper cable technology. He is presently National Study Group Secretary for CCITT Study Group VI.

PRE-CONNECTORIZED OPGW WITH MULTICONNECTOR

* ** *** **** **** ****

M. Kaiju K. Sugimoto M. Muramathu H. Hosoya S. Togo H. Yokosuka

* Chubu Telecommunications Company, Incorporated (Nagoya, Japan)
** Chubu Electric Power Company, Inc. (Nagoya, Japan)
*** Nippon Idou Tsushin Corporation (Nagoya, Japan)
**** FUJIKURA LTD. (Tokyo, Japan)

Abstract

A new and quick jointing system for OPGW has been developed. This system consists of a plant-fabricated SM multi-fiber connector, pulling hardware and a joint box. The connector permits a simultaneous eight-fiber connection, with connector loss reduced to a low level of 0.16dB. The pulling hardware protects the connector during the installation. It is a flexible stainless-steel tube. It provides resistance against various forces as well as smooth wheel passability. The organizer in the joint box is divided into two parts, respectively accommodating mated connectors and fibers, so that stability in the connecting area is maintained and the accommodation work is easy. Installed on steel towers, the prototype of this new product has been proven to exhibit such good features as easy installation characteristics and excellant optical properties. High long-term reliability of the multi-fiber connector was proven through a long-term observation of the trial products.

1. Introduction

The present trend with optical-fiber cable is that with the increased applications of optical-fiber cable, there is an increase in the number of optical fibers constituting the cable which results in tremendous time required for jointing work. Under the circumstances, there is a great demand calling for a simplification of the jointing method with improved efficiency.

The jointing work of the composite overhead ground wire with optical fibers (OPGW) is a very time-consuming task because of the necessity to construct scaffolds, wind-breaking tents and other equipment for both preparation and removal on high steel towers.

In order to solve such a problem as cited above, a system has been developed, in which OPGWs are fabricated in-plant with connectors on both ends and delivered to the site where they are installed to undergo connector-connection instead of fusion splicing. This system permits a simple connector-connection to accommodate all the cumbersome operations, eliminating the necessity for a fusion splicer and various other preparations. Therefore, it is a great on-site labor-saving contribution.

The a pulling hardware which this system consists of, protects the connector and the end of the OPGW during installation. A multi-fiber connector and the joint box which accommodates the fibers and the mated connectors make up the rest of this system.

2. Structure and Characteristics

2-1 Optical multi-fiber connector

The OPGW must be jointed with low loss since it is often used over a comparatively long distance and is provided with a number of jointing points. Consequently, connectors contained in the OPGW should demonstrate the lowest possible connector loss while providing outstanding stability. It is desirable that the OPGW permit a simultaneous multi-fiber connection which requires less time while offering more convenience than the conventional fusion splicing methods.

A remarkaly compact structure of the connector has been designed with outside dimensions measuring 26 mm in diameter and 130 mm in length (Fig. 1), accommodating eight ferrules in one single housing.

The ferrules have been made of zirconia-ceramics and have physical contact mating faces. They have also been

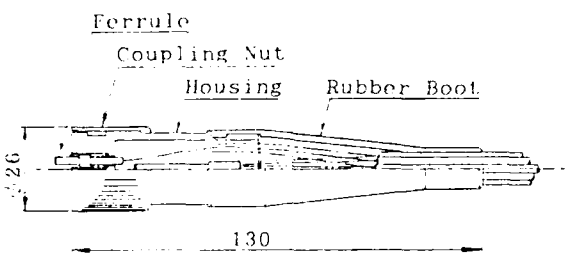

Fig.1 Structure of Multi-Fiber Connector

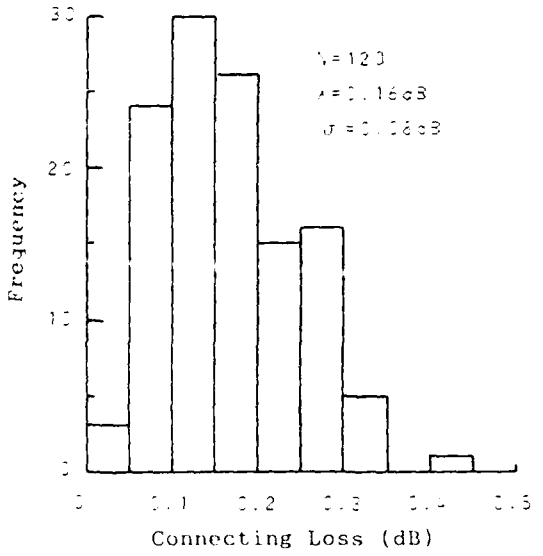

Fig.2 Connecting Loss

inspected by means of a precision measuring system. The connector exhibits stabilized characteristics with low connector loss. Taken at random, Fig. 2 shows a favorable connector loss of 0.16 dB on the average.

2-2 Pulling hardware

Since the optical multi-fiber connectors are fabricated in plant on OPGW ends , it is possible to carry out the installation with connectors on ends. It means that the installation requires rigid protectors which protect the OPGW-end connectors from various exterior forces during the operation. Meanwhile, the protectors should provide sufficient flexibility to permit the wheels to pass smoothly, and tension-resistance to permit the wire-traction.

The pulling hardware should meet the requirements which are represented in table 1.

Table 1 Requirements of Pulling Hardware

Stringing tension force	500 kgf (max.1000kgf)
Outside diameter	Max. 70 mm
Wheel passability	ϕ450 Urethane-lined wheels can be used.
Assembly properties	Attachable and detachable on site.
Water-proofability	Water-proof designed.

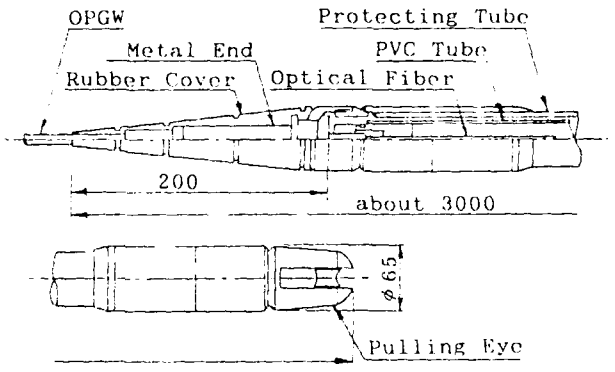

Fig.3 Structure of Pulling Hardware

In order to meet the requirements, it has been designed as shown in Fig. 3, with specifications as described below:

a. Metal end of the OPGW
1. The fiber unit is protected by a metal sleeve gripping the interior at the end of the OPGW. A sufficiently high grip force to stand the stringing tension force is achieved.
2. The end is convered by a moderately tapering rubber cover to improve wheel passability.

b. Protecting tube
1. A lace-reinforced, stainless-steel flexible tube is used to provide resistance against tension force and lateral pressure. It also improves wheel passability.
2. A PVC tube was incorporated for waterproofing, taking into consideration transit, outdoor stowage, etc.
3. The outside diameter was designed not to exceed 65 mm for the sake of wheel passability.

A wheel passability test was performed on the pulling hardware, Fig. 4, to confirm the mechanical strength and other characteristics of the trial products. Table 2 shows the test results. Fig. 5 describes the fluctuation of the tension force, which is found to increase when the pulling eye encounters the wheel (to approx. 1.7 times the designed force). This increase, however, is tolerable and poses no particular problems. Under this test it was proven that the trial products have favorabel characteristics.

Table 2. Test Results of Wheel Passability Test

Items		Results	
		Designed Tension 500kgf	Designed Tension 1000kgf
Wheel passability		No problem	No problem
Appearance	Protecting tube	No problem	No problem
	OPGW	No problem	No problem
Attenuation loss		No loss increase	No loss increase
Max. Tension		880kgf	1670kgf

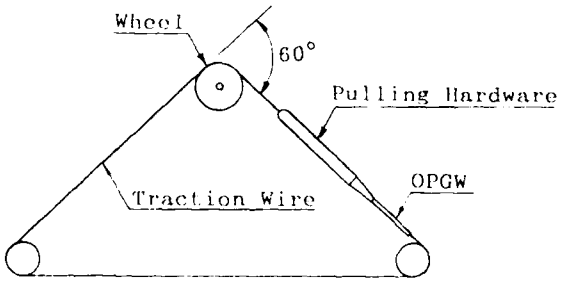

Fig.4 Wheel Passability Test

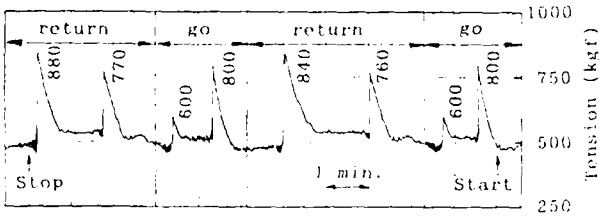

Fig.5 Example of Fluctuation of Tension Force

2-3 Joint box

A joint box which consists of an aluminum alloy box, an aluminum alloy lid, an O-ring and an organizer was developed for accommodating the mated connector as well as the optical fibers. Fig. 6 shows the structure of the joint box, with the organizer separated into two parts; one is to accommodate the mated connectors and the other is to accommodate the optical fibers. Such a design as cited above has reduced adverse factors against the inside fiber and connectors to the lowest possible level, while contributing to the ease in accommodating the optical fibers and connectors.

Taking into consideration the branch cables of the jointing; the joint box is designed to provide four cable inserting holes, an organizer part for accomodating four mated connectors and an other organizer part for accommodating four pairs of optical fiber units. The joint box is provided with an O-ring between the box and the lid and with sealing tubes in the cable insertion holes to insure waterproofing.

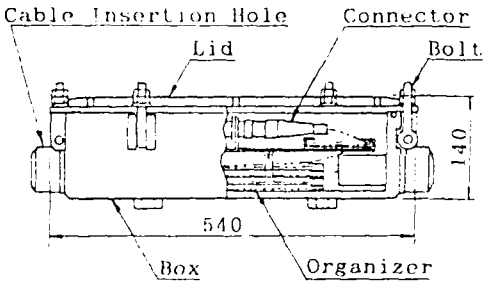

Fig.6 Structure of Joint Box

3. Field test

3-1 Installation test

Product behavior during installation, optical properties and other characteristics were tested by installing the trial products on steel towers. The test employed two OPGWs with connectors on both ends and four six-fiber connectors. The test revealed that there was a master connector loss of 0.14 dB on the average in the course of a connecting operation. Fig. 7 shows the structure of the OPGW under the test and Table 3, its specifications.

The stringing method was one in which a number of small pulleys were used on normal type OPGWs. Fig. 8 shows the stringing method, in which samples were hung on steel towers spaced 188 m and 206 m apart respectively, with three

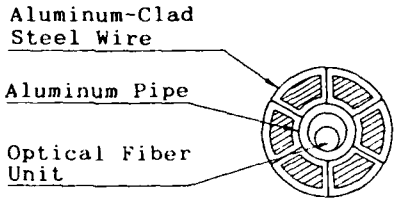

Fig.7 Cross Section of OPGW

Table 3. OPGW Construction

Nominal section area (mm²)		55
Strand construction (mm)		6/3.23 segment-shaped type
Aluminum pipe (mm)		1/5.0 (3.8)
Outer diameter (mm)		9.6
Minimum tensile load (kgf)		5,780
Estimated cross-sectional area (mm²)	Aluminum-clad steel wire	49.16
	Aluminum pipe	2.0155
Standard weight (kg/cm)		334.4
Electric resistance (20C) (Ω/km)		1.54
Equivalent elastic modulus (kg/mm²)		15,200
equivalent expansion coefficient (1/°C)		12.9×10⁻⁶

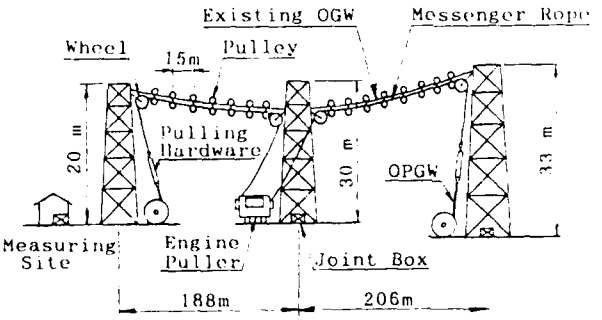

Fig.8 Field Test

connection points where fibers were hold-connected to the measuring instruments. Fig. 9 illustrates the connection diagram.

Table 4 shows the test results, in which tension force acting on the sample during the stringing operation is found to be outstandingly low (Fig. 10), permitting wheels and pulleys to smoothly pass over the sample. The test revealed no change in the pulling hardware, the ends of the OPGWs. And the connectors after stringing have shown a very favorable connector loss of 0.15 dB on the average. The pulling hardware proved to have an expectedly satisfactory effect; confirming that the conventional operating methods are applicable to the OPGW with connectors.

The connector-connection method completed the jointing work in 40 minutes. This used to require about one day in the case of the conventional fusion splicing method. Elimination of the necessity for the fusion splicer and other equipment as well as scaffolds for the splicing operation results in the economization of preparation and removal work, leading to a remarkable simplification of the OPGW jointing work.

Table 4. Test Results of stringing Test

Items		Results		
		Sample No.1	Sample No.2	
Wheel passability		No problem	No problem	
Appearance	Protecting tube	No problem	No problem	
	Connector	No problem	No problem	
	OPGW	No problem	No problem	
Jointing time		30 min.	10 min.	30 min.
Connection loss after the test		0.15dB		

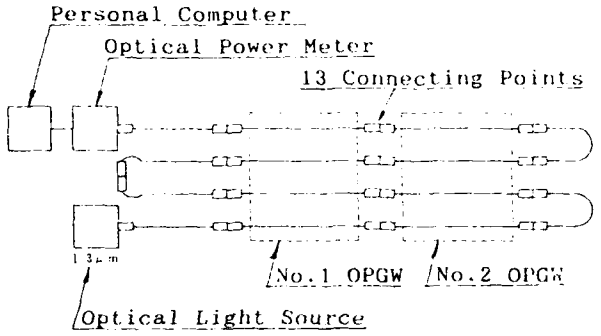

Fig.9 Connection Diagram

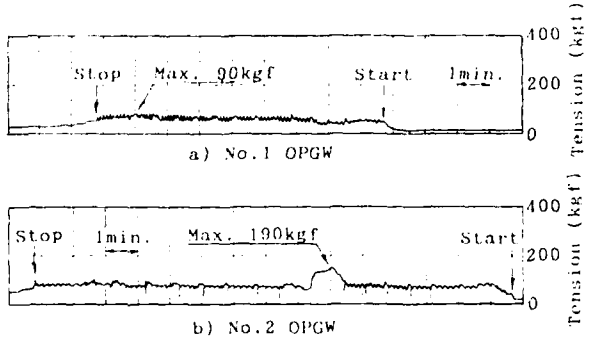

Fig.10 Fluctuation of Tension Force

3-2 Long-time reliability test

Fig. 11 shows the results of a test conducted for about nine months with respect to the fluctuation of optical power in the sample after the installation. The loss incerease during the test was as low as 0.03 dB per connecting point. Fig. 12 and 13 show that the increase in the connector loss depends on the temperature. But it is as low as 0.01 dB per connecting point during the most extreme day.

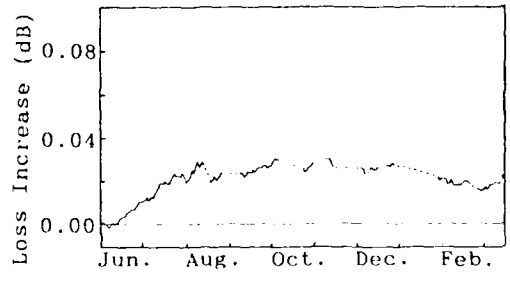

Fig.11 Loss Change after Installation

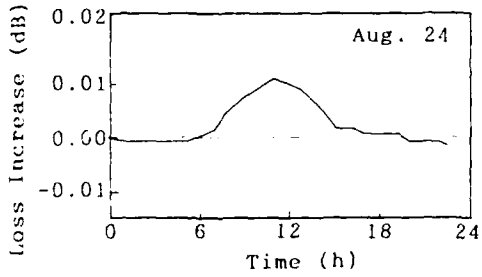

Fig.12 Example of Loss Change During The Day (Clear Day)

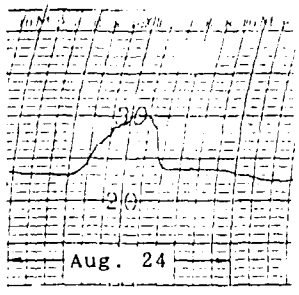

Fig.13 Temperature Change

The test revealed that the joint box consistently functioned well and retained it's original surface on both the interior and exterior, Leakage of moisture into the box was also found to be nonexistant.

Thus the OPGW with connectors has exhibited outstandingly stabilized optical characteristics and long-time reliability.

4. Conclusion

The results of the various kinds of tests on the OPGW using, multi-fiber connectors, are summarized as follows:

1. Realization of a low-loss multi-fiber connector

   A multi-fiber connector, which features stabilized and long-term characteristics with low connector loss and instantaneous connectability has been produced. It has been proven that the OPGW can be connected by means of connectors, thanks to the accomplishment of the above-cited connector.

2. Simplification of jointing operation

   Fabricating the multi-fiber connector in-plant has remarkably simplified the on-site jointing operation. Since, the scaffolds for the jointing operation are also no longer required, the preparation work has also been so simpified that it is no longer required.

3.Conventional methods are applicable

It has been confirmed that the use of the pulling hardware which protects the ends of OPGW with connectors permits conventional methods to string the OPGW without any damage to the fiber, connector, etc.

Acknowledgements

This development and testing was supported by a number of people from Chubu Electric Power Company, Inc. and Fujikura Ltd.. The authors gratefully acknowledge their contributions.

Masanori Kaiju

Technology & Operation Dept.
Chubu Telecommunications Company, Incorporated

2-2-5, Sakae, Naka-ku, Nagoya, Aichi, 460, Japan

Masanori Kaiju joined Chubu Electric Power Company, Inc. in 1981, and was engaged in research and development of computer and communication systems. He is now in Chubu Telecommunications Company, Inc. which belongs to a group of Chubu Electric Power Company, Inc.. He is in technology & operation department.

Hideyuki Hosoya

Opt-Electronics Laboratory
FUJIKURA LTD.

1440, Mutsuzaki, Sakura-shi, Chiba, 285, Japan

Hideyuki Hosoya joined Fujikura Ltd. in 1983 and has been engaged in research and development of optical fiber connectors and accessories of optical fiber cables. He is now a staff engineer of the fiber and cable accessory section in Opt-Electronics Laboratory. He is a member of the Institute of Electronics, Information and Communication Engineers of Japan.

Kathuyoshi Sugimoto

Electric Power Research & Development Center
Chubu Electric Power Company, Inc.

20-1, Kita-Sekiyama, Oodaka-cho, Midori-ku, Nagoya, Achi, 459, Japan

Kathuyoshi Sugimoto joined Chubu Electric Power Company, Inc. in 1961, and has been engaged in research and development of computer and communication systems.

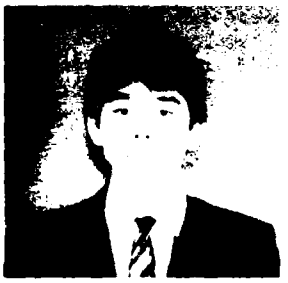

Shuichi Togo

Opt-Electronics Laboratory
FUJIKURA LTD.

1440, Mutsuzaki, Sakura-shi, Chiba, 285, Japan

Shuichi Togo joined Fujikura Ltd. in 1986 and has been engaged in research and development of optical fiber connectors and accessories of optical fiber cables. He is now a staff engineer of the fiber and cable accessory section in Opt-Electoronics Laboratory. He is a member of the Institute of Electronics, Information and Communication Engineers of Japan.

Masahiko Muramathu

Nagoya Regional Office
Nippon Idou Tsushin Corporation

2-3-1, Sakae, Naka-ku, Nagoya, Aichi, 460, Japan

Masahiko Muramathu joined Chubu Electric Power Company, Inc. in 1970, and was engaged in research and development computer and communication systems. He is now in Nippon Idou Tsushin Corporation which belongs to a group of Chubu Electric Power Company, Inc.. He is now a chief of the electrical engineering section in Nagoya Regional Office.

Hiroshi Yokosuka

Opt-Electronics Laboratory
FUJIKURA LTD.

1440, Mutsuzaki, Sakura-shi, Chiba, 285, Japan

Hiroshi Yokosuka joined Fujikura Ltd. in 1967 and has been engaged in research and development of automatic telephone cable splicing machines, joint closures and optical connectors. He is now a chief of the fiber and cable accessory section in Opt-Electronics Laboratory. He is a member of the Institute of Electronics, Information and Communication Engineers of Japan.

CABLE TRANSFER SYSTEM WITHOUT DISTURBING INTEGRITY OF INFORMATION ON PAIR

Hiroaki KUBOZONO, Yuzo TSUCHIYA *, Masato HIRATA, Tomonobu SHIMOMURA **

* NTT Tsukuba Field Engineering Development Center

** NTT Network Systems Development Center

ABSTRACT

A new technology, which makes it possible to transfer live data transmission circuits with no bit error by controlling the transitional signal level variation gradually, is presented as resistor insertion multi-connecting.

NTT has developed a cable transfer splicing system adopting this technology. The system will be introduced for actual applications in December 1988.

1. BACKGROUND

Recently, the number of non-telephon circuits, which carry data signals, facsimile signals and so on, is worldwidely increasing. These data communications require a higher quality and higher reliability network than those used only for voice communications.

To satisfy the requirement, NTT is currently replacing existing cables with improved polyethylene insulated cables, however the work sometimes causes serious problems shown as follows.

(1) Permanent signal level variation
(2) Disconnection of the circuits
(3) Transitional signal level variation

The permanent signal level variation can be reduced by designing the line loss of new cable as same as that of old cable. And disconnection of the circuits can be prevented by multi-connecting of new and old cables. However, as there was no methods to suppress the transitional signal level variation, which occurs in a short time (several milliseconds), it was impossible to transfer live data transmission circuits without disturbing the information.

Therefore, some new technology and systems, which perform transfer with no bit error by suppressing or controlling the transitional signal level variation into acceptable value, have been earnestly required.

2. PROBLEMS IN CONVENTIONAL TRANSFER METHOD

For transferring voice communications circuits, multi-connecting method has been applied. It is possible to prevent disconnection of the circuits with this method, but some bad influences, which shown in Figure 1, are caused.

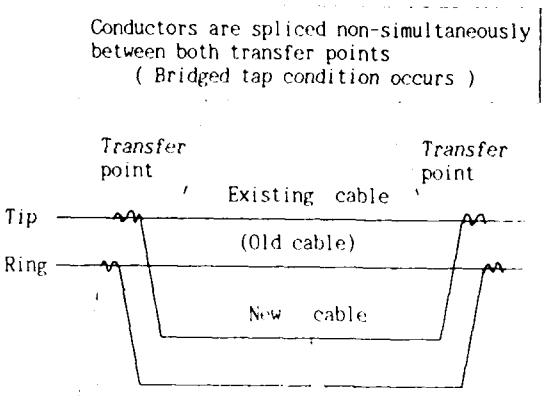

CMRR : Common mode signal rejection ratio

Figure 1 Problems in conventional transfer method

Figure 2 shows an example of the signal level variation during the existing multi-connecting transfer. The transitional signal level variations are caused in the several milliseconds.

As a result, if the data transmission circuits are transferred by this metod, the information will be influenced and caused a large amount of bit errors.

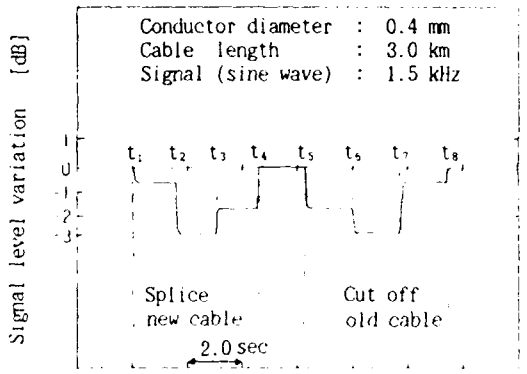

t_1: splice tip of new cable at upper side
t_2: splice ring of new cable at upper side
t_3: splice tip of new cable at lower side
t_4: splice ring of new cable at lower side
t_5~t_8: Cut off old cable conductors in the same process as above

Figure 2 Example of signal level variation

3. NEWLY DEVELOPED TRANSFER METHOD

To achieve a non-interruption and disturbance-free cable transfer, it is effective to control the transitional signal level variation, which caused during conventional transfer, gradually.

Figure 3 shows the new transfer technology using the "resistor insertion multi-connecting method" to satisfy the requirment.

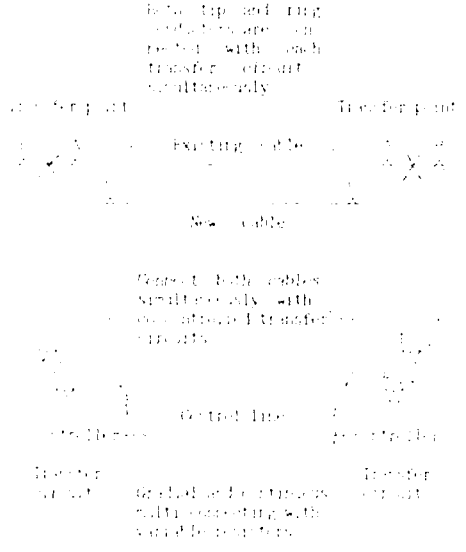

Figure 3 Resistor insertion multi-connecting transfer

3.1 Investigation of controlling the transitional signal level variation.

The instantaneous level variation is caused by the direct connection of new and existng cable conductors.

To control it gradually within the limmit allowed for data transmission systems, resistor insertion multi-connecting technology has been developed. In its process, new and existing cable conductors are first connected each other through the electrical resistors inserted in new cable, which are at a high value (Figure 4). After that, the resistances are being decreased with some stages.

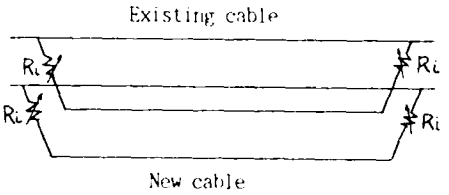

Figure 4 Resistor insetion multi connecting

(1) Experimental results

To fix the first inserted resistance valule and decreasing steps, calculations and measurements of the level variations with some resistor insertion multi-connecting models had been carried out.

Figure 5 shows the results of them.

By this experiments, the first inserted resistance value was required as over 10 k Ω, and it was necessary to decrease the resistance with small steps in the range between 5 kΩ and zero.

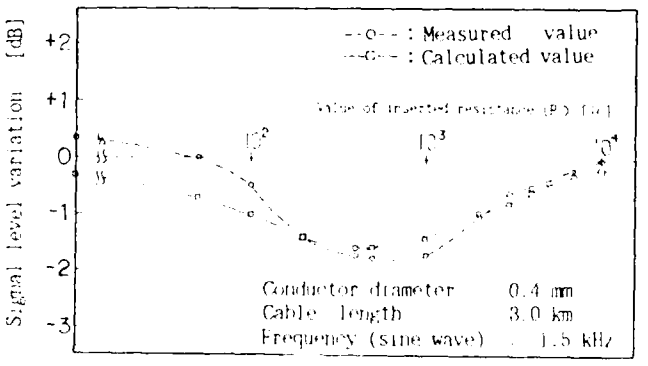

Figure 5 Signal level variation versus inserted resistance

(2) Experimental results 2

According to that result, the level variation in each steps would be suppressed at acceptable rate, however bit error will be caused because the compensation function of data transmission systems can not follow the variation if the resistance holding time is too short.

Figure 6 shows the experimental results of bit error measurement during the process under the some resistance holding time.

The data transmission systems applied to this measurement are shown in Table 1. Their receiving signal levels were set to the minimum value with signal attenuator.

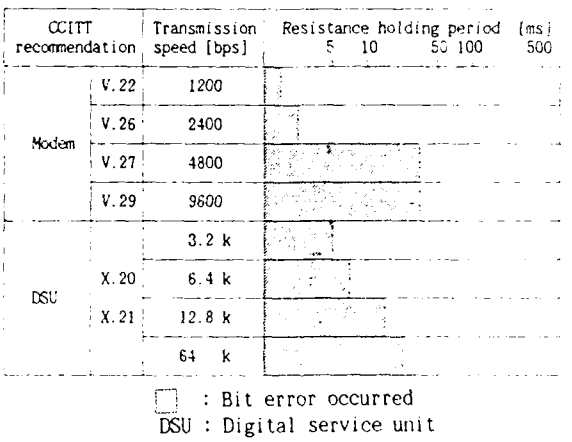

Figure 6 Results of bit error measurement

Table 1 Characteristics of data transmission systems

	Transmission speed [bps]	Transmission method	Signal sending level	Signal receiving level
Modem	1200	FSK	0 ~ -15 dBm	0 ~ -32 dBm
	2400	PSK	0 ~ -15 dBm	0 ~ -32 dBm
	4800	PSK	0 ~ -15 dBm	0 ~ -32 dBm
	9600	QAM	0 ~ -15 dBm	0 ~ -32 dBm
DSU	3.2 k ~ 64 k	Digital codec	3 V, bipolar	40 Ω

FSK : Frequency shift keying
PSK : Phase shift keying
QAM : Quadrature Amplitude Modulation
f_N : Nyquist frequency

(3) Application to transfer circuit

To apply this technology to transfer circuit, it is also necessary to cut off the old cable by the symmetrical resistance insertion in the old cable.

Furthermore, to suppress the variation of other transmission characteristics, for example, common mode signal rejection ratio of balanced pair, reflective loss, it is effective to carry out the resistor insertion process both at two conductors and at two transfer points with 2-pair transfer circuits simultaneously.

3.2 Investigation of applying to a new data transmission system

A new digitalized high speed data transmission system using 200 kbps TCM (Time compression Multiplexing) technology was developed as pre-ISDN system in the same period. A transfer curcuit having fixed resistors and relay switches as a inserted variable resistor was manufactured and its adaptability for this new system was studied.

In this transmission system, as 28 mA DC current constantly flows on the circuit, noises, which disturbing the signals, will be caused if the line resistance changes. So, the transfer circuit using stepping resistance transition could not be applied to this system with no bit error.

To clear this problem, it is necessary to realize the more continuous and gradual transition of inserted resistances.

To realize this transition, LED-CdS photocoupler was introduced as the variable resistor. Its resistance is fixed by the current flowing into the LED. So, by cotrolling the current gradually and accurately, the inserted resistances can be set to ideal value.

Figure 7 shows a block diagram of the control and calibration circuit for adapting LED-CdS photocoupler to a controllable resistor.

The control information is memorized in the memory IC as the value of the voltage. It is converted into current and supplied to the LED along the transition curve by CPU support. The resistance of the LED-CdS photocoupler is calibrated and checked with the calibration circuit.

Figure 8 shows the inserted resistance transition and Figure 9 shows examples of the signal level variation during the new multi-connecting transfer by controlled LED-CdS photocoupler.

Figure 10 shows the maximum value of level variation versus transferred cable length (the new and old cable length are the same).

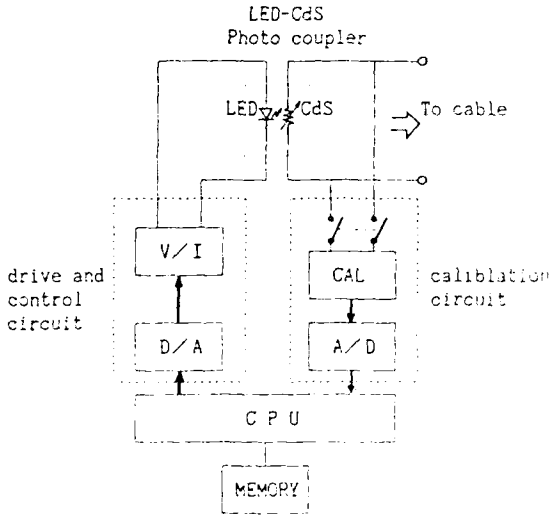

CPU : Central processing unit
D/A : Digital to analog converter
A/D : Analog to digital converter
V/I : Voltage to current converter
CAL : Measurement and caliblation circuit

Figure 7 Block diagram of resistance control circuit for LED-CdS photocoupler

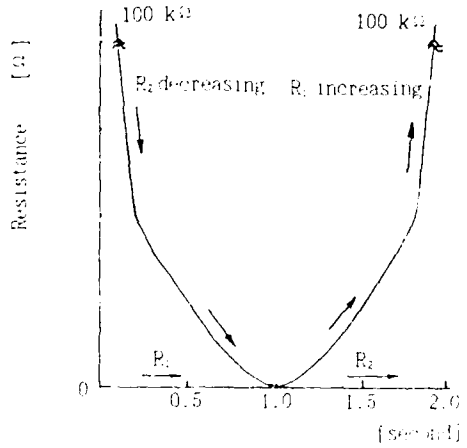

Figure 8 Transition of inserted resistance using LED-CdS photocoupler

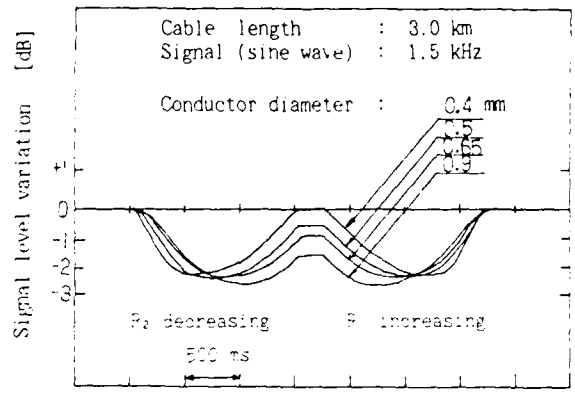

Figure 9 Signal level variation in new transfer method using LED-CdS photocoupler

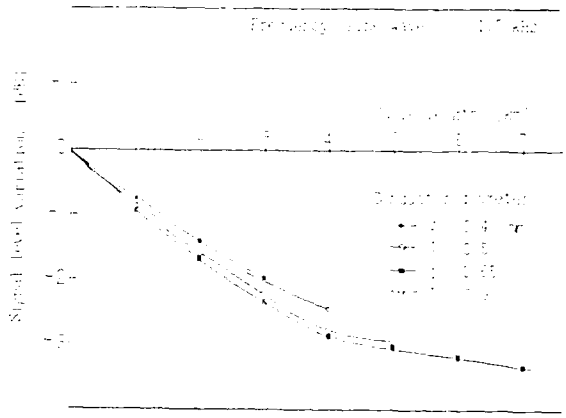

Figure 10 Maximum value of signal level variation versus tranferred cable length

4. CABLE TRANSFER SPLICING SYSTEM FOR PRACTICAL APPLICATIONS

To apply this transfer circuit to the practical applications, NTT has developed some new products and technology shown as follows.

(1) Transfer equipment using a resistor insertion multi-connecting method;

The inserted resistors are LED-CdS photocouplers. It automatically perfomes the 10-pair transfer. It also contains a new pair identification circuit adopting the lock-in amplifier principle. These functions are supported by a built-in microprocessor.

(2) A pair transferable connector;

A pair transferable connector is capable of splicing 10-pair conductors in a body with incorporated insulation displacement type contacts. Two connectors can be mated each other. It is also possible to make contact with the spliced conductors through contact holes at the bottom.

(3) Transfer splicing equipment;

It connects the connector or conductors to the transfer equipment electrically using conductive pin probes.

5. EVALUATION OF THE TRANSFER SPLICING SYSTEM

The capability of error-free transfer had been confirmed with simulating data transmission systems, which mentioned in the above, in experimental facilities since January 1986 to March 1987.

Futhermore, after some improvement, it was applied to commercial test for confirming its function and workability.

Table 2 shows the number of transferred circuits in commercial test.

Table 2 The number of transferred circuits in commercial test

Transmission method or data speed	Number of circuits	Use of circuits
Voice (telephone)	6355	Telephone, Facsimile
Voice band data (14400 bps)	4	Stock information service
Voice band data (1200 ~ 9600 bps)	493	Financial informations or trade informations, etc
Digital coded data (50 bps)	262	Remote security service
Total	7114	

In these test, it was confirmed that transfer splicing is carried out with no bit errors, and it takes about 10 minutes per 10 circuits transfer splicing.

NTT has started providing the ISDN system using 320 kbps TCM digital transmission technology in a pair metallic conductors since April 1988, which satisfy the CCITT I-series recommendations. With this circuit, it is possible to transfer with no bit error.

6. CONCLUSIONS

In transfer splicing of the metallic cable containing the data transmission circuits, it is necessary to carry out the transfer without disturbing the information on the pair.

The new transfer technology using the "resistor insertion multi-connecting method" makes it possible to control the transitional signal level variation gradually and to transfer with no bit error.

This technology has been introduced into the cable transfer splicing system for practical applications.

This actual system has been co-developed together with NTT, 3M Company and Fujikura Co.,Ltd. ever since 1985.

In addition, this system has been improved through commercial tests from April 1987 to March 1988 and will be introduced for actual application in December 1988.

ACKNOWLEDGMENTS

The authors wish to thank Takayuki Nimiya, General Manager of Line Engineering Project Group in NTT Tsukuba Field Engineering Development Center, Seiji Takashima, General Manager of Telecommunication Cable Systems & Outside Plant Project in NTT Network Systems Develpment Center and Fuminori Kozono, Assistant Manager in NTT Tokyo-Minato district headquarters.

Hiroaki Kubozono

NTT Tsukuba Field
Engineering Development
Center

1-7-1 Hanabatake
Tsukuba-shi, Ibaraki
305 Japan

Hiroaki Kubozono received his B.S degree in electrical engineering from Kagoshima University in 1983. He joined NTT in 1983 and has been engaged in development on construction and maintenance technology of metallic telecommunication cable systems. He is an engineer in the Line Engineering Project Group in NTT Tsukuba Field Engineering Development Center.

Masato Hirata

NTT Network Systems
Development Center

2-1 Uchisaiwai-cho
1-chome Chiyoda-ku,
Tokyo 100 Japan

Masato Hirata received his M.S degree in electrical engineering from Nagoya Institute of Technology in 1979. He joined NTT in 1979. He has been engaged in development of metallic conductor cable. He is a senior engineer in the Telecommunication Cable Systems & Outside Plant Project in NTT Network Systems Development Center. He is a member of the Institute of Electronics, Information and Communication engineers of Japan.

Yuzo Tsuchiya

NTT Tsukuba Field
Engineering Development
Center

1-7-1 Hanabatake
Tsukuba-shi, Ibaraki
305 Japan

Yuzo Tsuchiya received his B.S degree in materials science from University of Electro-communications in 1973. He joined NTT in 1973. After gaining experience in outside plant management in the Yokohama district headquartes, he has been engaged in development on construction and maintenance technology of metallic and optical telecommunication cable systems. He is an exective engineer in the Line Engineering Project Group in NTT Tsukuba Field Engineering Development Center. He is a member of the Institute of Electronics, Information and Communication engineers of Japan.

Tomonobu Shimomura

NTT Network Systems
Development Center

2-1 Uchisaiwai-cho
1-chome Chiyoda-ku,
Tokyo 100 Japan

Tomonobu Shimomura received his B.S in precision machinery engineering from Tokyo University in 1984. He joined NTT in 1984. He has been engaged in development of metallic conductor cable. He is an engineer in the Telecommunication Cable Systems & Outside Plant Project in NTT Network Systems Development Center. He is a member of Electronics, Information and Communication engineers of Japan.

Single-Fiber Optical Connector for Tactical Applications

B. V. Darden and B. G. LeFevre
V. E. Kalomiris

AT&T Bell Laboratories, Norcross, Georgia 30071
US Army CECOM, Ft. Monmouth, New Jersey 07703

ABSTRACT

A single-fiber, practical hermaphroditic connector has been designed for use in tactical fiber-optic communications systems and robotic vehicle applications. It is intended for use wherever two-way transmission over a single optical fiber is indicated. Development effort was guided by detailed design criteria similar to that used for the two-fiber Tactical Fiber Optic Cable Assembly (TFOCA) unit previously developed for the U.S. Army CECOM. The single-fiber (simplex) connector is available in both multimode and single-mode versions. Typically, insertion loss is less than 1 dB when installed on either 50/125-μm multimode fiber or single-mode fibers.

Many features of the successful AT&T duplex TFOCA connector have been incorporated into the simplex design. These include the same biconic components, cable retention hardware which requires neither special tools nor adhesives, waterproofing seals, and field cleanability. The connector was designed to accommodate cable diameters ranging from 2 to 5 mm. Operating temperature range is from -55° to 85°C. The new connector is 2.8 cm in diameter; a mated pair is 15.2 cm long (excluding bend limiter) and weighs 325 grams, including dust covers.

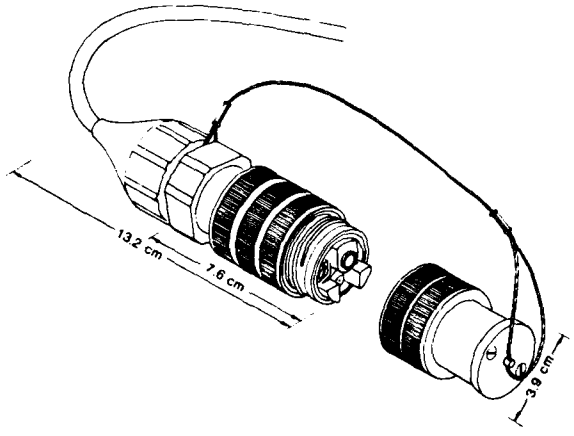

Figure 1. Duplex Connector

INTRODUCTION

In 1987 AT&T completed development of a two-fiber, hermaphroditic connector for use in tactical fiber-optic communications systems.[1] The connector, shown in Figure 1, and its companion bulkhead receptacle were designed to be rugged, waterproof, and resistant to the stringent environments experienced in tactical military applications. A duplex embodiment of AT&T's biconic connector, the tactical unit is available in multimode and single-mode versions, and insertion loss of each is typically less than 1 dB.

For many tactical fiber-optic communications systems and tethered or robotic vehicle applications, two-way transmission over a single optical fiber is indicated. AT&T has designed a single-fiber (simplex) connector for those uses. Development effort was guided by detailed design criteria similar to that used for the two-fiber Tactical Fiber-Optic Cable Assembly (TFOCA) unit previously developed for the U.S. Army CECOM. Many features of the successful duplex connector have been incorporated into the simplex design. These and other features of the new connector, along with testing results, will be described in this paper.

TACTICAL SIMPLEX CONNECTOR

Tactical systems often employ cable assemblies, typically 1-km in length, which are concatenated to complete fiber links as long as 15 kilometers without repeaters. For those uses it is desirable for the cables to be terminated with hermaphroditic connectors so that all cable ends are identical. Any cable end would mate with any other. For more traditional applications such as those where a connector mates with a bulkhead receptacle only, the hermaphroditic feature is not required. The new simplex connector is suitable for both uses described above and is available in both multimode and single-mode configurations. It meets mechanical and environmental requirements listed in Table I.

TABLE I. Connector Requirements

Insertion Loss:	1.5 dB Maximum (Multimode, Single-Mode)
Mating Durability:	1000 Complete Cycles
Coupling Torque:	0.75 inch-pound Maximum
Shock Drop:	10 ft. Drop, 6 Times
Shock:	40g Sawtooth Pulse, 11 ms Duration
Vibration:	5-500-5 Hz, 15 Minute Sweep, 4.2g
Cable Retention:	Cable Dependent - up to 300 lbs.
Tensile Strength:	≥ 300 lbs.
Flex Life:	2000 Cycles at +20°C, 1000 Cycles at -55°C
Twist Life:	1000 Cycles at +20°C
Temperature Cycling:	-55 to + 85°C
High Temperature:	MIL-STD-810D, Method 501.1 (85°C)
Low Temperature:	MIL-STD-810D, Method 502.1 (-57°C)
Temperature Shock:	-57°C to +85°C
Water Immersion:	2-Meter Depth, 24 Hours
Humidity:	MIL-STD-810D, Method 507.1 (> 90%, 30°C)
Salt Fog:	MIL-STD-810D, Method 509.1
Dust:	MIL-STD-810D, Method 510.1
Mud Immersion:	5 Minutes, 10 Times
Fungus:	MIL-STD-810C Method 508.1

Hermaphroditic connectors are readily designed and produced when an even number—2, 4, 6, etc.—of fibers are to be mated. Half of the fibers are terminated with a traditional male terminus and the others with a female. Thus, when two connectors are joined, the male termini mate with their female counterparts, and high performance connections, i.e., ≤ 1 dB, can be accomplished. However, producing a high performance hermaphroditic single-fiber connector is more difficult. Large efforts have been expended with only spare achievements to date.

The AT&T tactical simplex connector can be described as a pseudo or practical hermaphroditic unit—not hermaphroditic in the strictest sense, but hermaphroditic in its application. As shown in Figure 2, the simplex connector consists of two major components—connector plug and sleeve holder—and a dust cover.

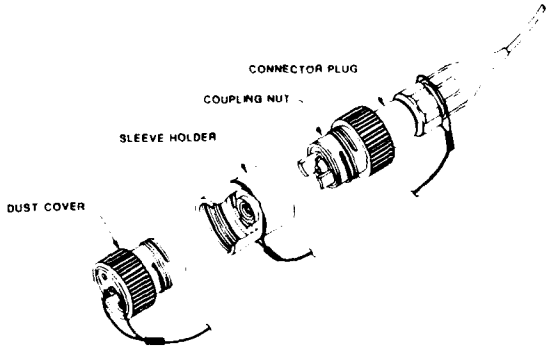

Figure 2. Simplex Tactical Connector

The connector is 2.8 cm in diameter and a mated pair weighs 325 grams, including dust covers. A companion bulkhead receptacle was developed for the system and shares a common interface. Hence, any cable end can be mated with any other or with a receptacle. The sleeve holder can be separated from the connector plug by unscrewing the connector coupling nut. When separated the sleeve holder is secured by a flexible lanyard. A captivated dust cover closes the open end of the sleeve holder.

The schematic in Figure 3 shows the connector mating sequence. Mated simplex connectors are depicted in Figure 4. For applications where the hermaphroditic feature is not required, the connector can be provided without the sleeve holder. Then the connector mates directly with a bulkhead receptacle which contains a sleeve. When the connector is unmated, a special dust cover is attached to prevent water or dust entry.

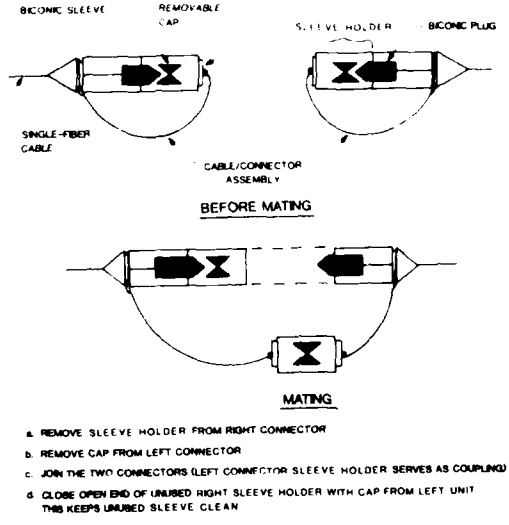

Figure 3. Mating Simplex Tactical Connectors

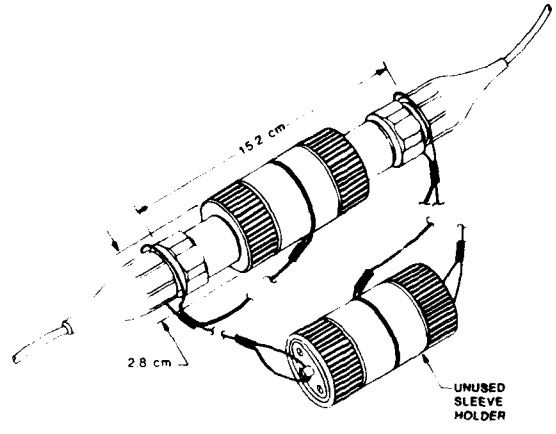

Figure 4. Mated Simplex Connectors

The sealed connector insert assembly shown in Figure 5 contains the biconic plug. A fluorosilicone bellows seal allows the plug to float axially and radially to align with its counterpart in a mated connector. It also prevents water entry around the plug during connector cleaning operations. An O-ring seals the insert-connector shell interface. The forward most part of the assembly is a threaded retaining ring. The ring secures the assembly within the connector shell; its geometric features align and orient the connector with the sleeve holder and protect the biconic plug. Arc-shaped lobes, protruding to partially encircle and shroud the plug, are of stout proportions to insure positive engagement with mating slots in the sleeve holder, and to withstand the impact if the unmated connector is dropped on its end.

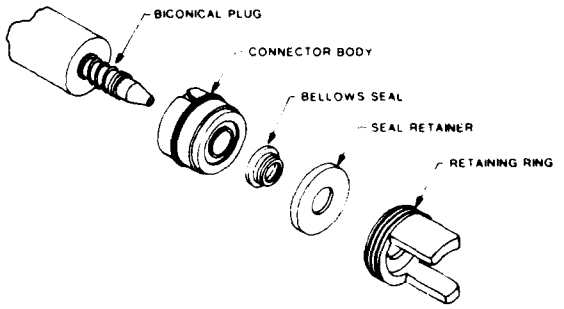

Figure 5. Connector Insert Assembly

Figure 6 shows in section the complete simplex connector assembly. A metal shell encloses the insert assembly described above and retains the cable-termination hardware. A free-turning coupling nut tightens the joint between the connector plug and sleeve holder, or between a connector plug and receptacle. Coupling threads are a modified 60° stub for strength with a double lead for quick and easy engagement. An insert-molded bend limiter at the rear of the connector compresses a seal which blocks the water-entry path along the cable, and mechanically isolates inner parts of the connector from cable twist. Other leak paths are blocked by O-rings under the end cap and at the connector shell-sleeve holder interface.

The connector is joined to the cable by capturing the aramid yarn typically used in tactical cables with a special steel retention assembly easily put together without special tools. No adhesive is used in the cable termination operation. The connector was designed to accommodate cable diameters ranging from 2 to 5 mm. Only the cable retention hardware, bend limiter, and cable seal—four pieces total—need to be replaced to change cable sizes.

Unlike duplex tactical connectors, no excess or slack fiber is stored in the simplex connector shell. If the connector should require a replacement biconic plug, the cable can be reterminated easily because of the simple retention hardware design.

A sleeve holder comprises an essentially symmetrical, cylindrical metal shell with internal coupling threads and a cavity which retains a biconic alignment sleeve. In each end of the sleeve holder is an O-ring which seals agains the connector shell to prevent water or dust entry.

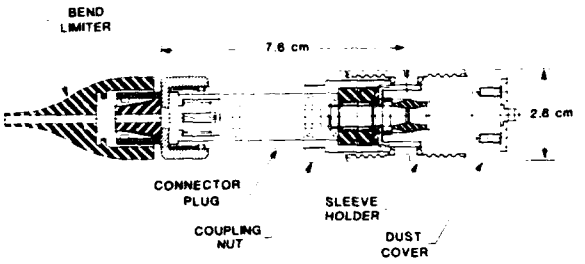

Figure 6. Simplex Connector Cross Section

BULKHEAD RECEPTACLE

The internal details of the receptacle, shown in Figure 7, are identical to corresponding parts of a connector sleeve holder. A short fiber pigtail extends from the rear of the assembly for splicing to an internal fiber or electro-optical device. The receptacle may be mounted through a D-hole in panels up to 6.4 mm thick with a standard AN-series jam nut. An O-ring under the mounting flange seals the panel-receptacle interface. The receptacle protrudes about 2.2 cm in front of the bulkhead and 3.5 cm from the rear. An unmated receptacle is protected by a lanyard-attached dust cover identical to the one provided for the connector.

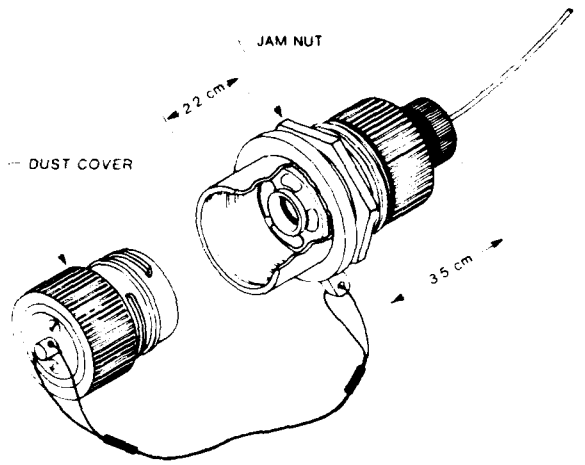

Figure 7. Bulkhead Receptacle

MATERIALS

The connector and receptacle shells and sleeve holder are aluminum die castings. The connector end cap, dust cover, and coupling nut are machined from wrought aluminum. All aluminum parts are given an anodize finish for corrosion resistance. All multimode connector parts are black and the single-mode connector is also black except for a gold-colored endcap and dust cover. These are different for identification purposes. The cable-retention hardware and other metal items are passivated stainless steel; the lanyards are plastic-coated stainless steel stranded cable. Except for the biconic plug, the connector-insert assembly is injection molded from filled resins having excellent dimensional stability, high impact strength, and good chemical and heat resistance. Seal materials are neoprene and fluorosilicone.

CONNECTOR TESTS

The connector design objectives of low loss and field ruggedness were evaluated by testing samples to the requirements listed in Table 1. The samples consisted of plug-to-plug or plug-to-bulkhead combinations terminating either 50/125 μm radiation hardened multimode or 8.8/125μm standard AT&T single-mode fiber. Except where noted, the loss (or loss change) measurements were made with 1300 nm LED sources. The results are discussed in the following section.

Insertion Loss - The primary requirement of any connector is insertion loss. For this particular study it was measured by two methods: (a) cut and insert (per EIA FOTP 34) and (b) substitution (per EIA FOTP 171). The results are summarized in Table 2. Each set of cut and insert data is the result of 20 measurements made on four samples. The substitution measurements were made with jumpers prepared by terminating 2.5 mm tactical cable. Both multimode and single-mode values averaged less than 0.6 dB. For the single-mode case a comparison between the two methods is shown graphically in Figure 8. The 0.1 dB difference may be attributed to the fact that substitution measurements involve unmatched fibers.

TABLE II. Insertion Loss (dB)

	Single-Mode			Multimode		
	N	$\bar{x}$	σ	N	$\bar{x}$	σ
FOTP 34	80	0.42	0.12	80	0.50	0.21
FOTP 171	44	0.53	0.19	-	-	-

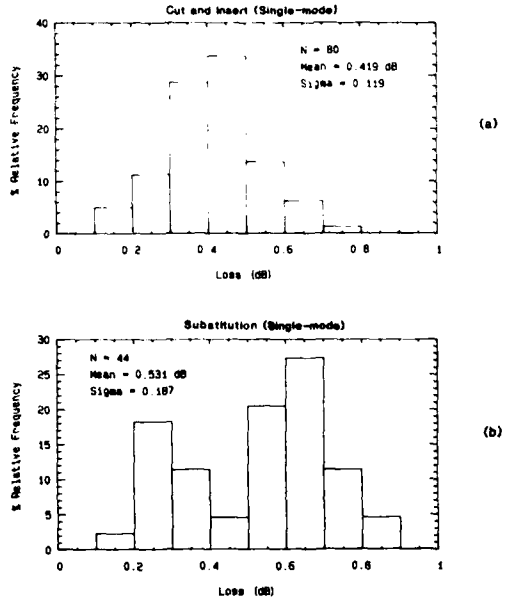

Figure 8. Insertion Loss of Simplex Connector Measured by: (a) Cut & Insert and (b) Substitution Methods

Thermal Cycling - The thermal cycling performance of the connector was measured over the range of - 55 to 85°C according to the schedule shown in Figure 9(a). Six mated pairs of connectors terminating 6-meter lengths of single-mode fiber tactical cable[2] were tested at 1300 nm using a filtered white light source. The results are shown in Figure 9(b). An average change of less than 0.1 dB occurred over the given temperature range. The same cycle for 2 mated pairs terminating multimode cable[2] showed an average change of less than 0.3 dB.

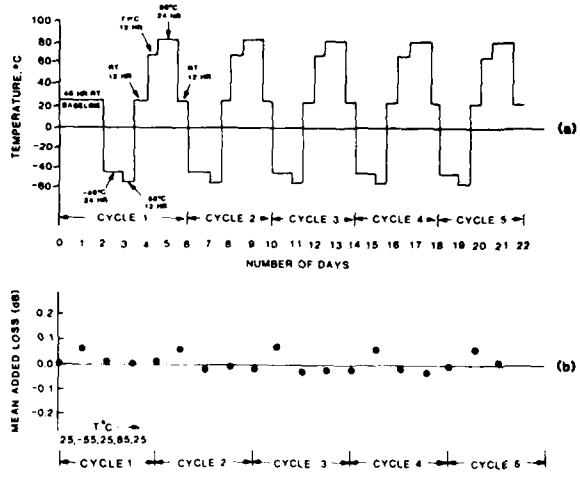

Figure 9. Thermal Cycling Performance of Single-Mode Connector: (a) Thermal Cycle, (b) Added Loss

Mating Durability - The ability of a connector to sustain a high number of successive matings without damage or excessive intermittent cleaning is an important measure of its durability. The tactical simplex connector was tested to 1000 matings without damage and with loss change less than 0.5 dB with cleaning at 375, 650 and 900 cycles. These data are shown in Figure 10.

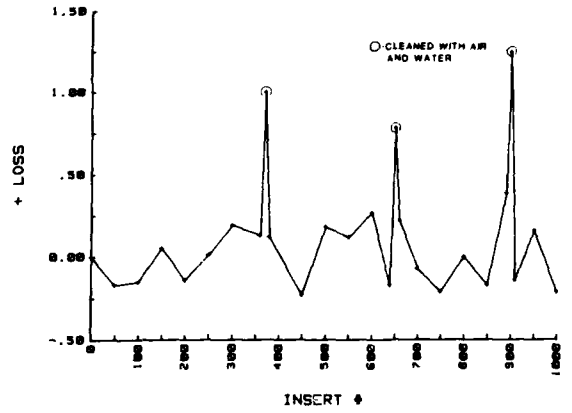

Figure 10. Mating Durability of Single-Mode Connector

Environmental Performance (General) - In addition to thermal cycling, connector samples were subjected to the environmental stresses of sustained storage temperature extremes, temperature shock simulating shipping, water immersion, humidity, dust, and mud immersion (refer to Table 1 for conditions). The connectors sustained their functionality without damage or loss change exceeding 0.3 dB. The TFOCA connector which uses the same basic materials has previously been successfully tested to salt fog & fungus exposure. On this basis the simplex connector meets all the environmental requirements of Table 1.

Mechanical Performance (General) - In addition to mating durability, connector samples were subjected to a series of mechanical tests to evaluate field-ruggedness. Three of those tests simulate transportation and field-handling conditions: shock drop, shock, and vibration. Three others: Cable retention, flex life, and twist life simulate stresses at the cable/connector interface during field-handling. These latter 3 tests were conducted on samples terminating 4.0 mm single-mode tactical cable[2]. The tensile strength requirement designates the load rating of a mated connector pair joining two cable assemblies. The connector met the mechanical requirements of Table I without damage or loss of functionality and with loss changes not exceeding 0.3 dB.

SUMMARY

A single-fiber practical hermaphroditic connector, based on biconic alignment components, has been designed and successfully tested for environmental and mechanical conditions of tactical communications and robotic field applications. Its development was facilitated by the use of proven technology and materials based on the AT&T two-fiber TFOCA connector. The simplex connector is capable of maintaining less than 1.0 dB attenuation under operating field conditions.

ACKNOWLEDGEMENTS

The authors acknowledge the assistance of the following people: J. M. Anderson for helpful discussions concerning connector design; T. E. Simmons, Jr., and G. A. Sandels for sample preparation and testing.

REFERENCES

1. J. M. Anderson, B. V. Darden, V. E. Kalomiris, "A Duplex Tactical Fiber-Optic Connector," 1987 Military Fiber Optics and Communications Exposition, Arlington, Virginia, March 16-19, 1987.

2. K. Kathiresan, L. C. Hotchkiss, S. P. Gentry, J. B. Fluevog, and V. E. Kalomiris, "Single Fiber Tactical Cables for Single Mode and Multimode Systems", *37th* International Wire and Cable Symposium, Reno, Nev., November, 1988.

B. V. Darden
AT&T Bell Laboratories
2000 Northeast Expressway
Norcross, GA 30071

Bruce V. Darden is a Member of Technical Staff at AT&T Bell Laboratories, Norcross, Georgia. He received a B.S. Degree in Engineering from North Carolina State University in 1951, and held engineering positions with Western Electric Company until 1960 when he joined AT&T Bell Laboratories. He is currently a member of the Connector Systems Development Group.

B. G. LeFevre
AT&T Bell Laboratories
2000 Northeast Expressway
Norcross, GA 30071

Bruce G. LeFevre is a Member of Technical Staff at AT&T Bell Laboratories, Norcross, Georgia. He received his B.S. (Colorado School of Mines) and PhD (University of Florida) in Physical Metallurgy. He joined AT&T Bell Laboratories in 1976 after ten years on the faculty of Georgia Institute of Technology. He has been involved in the study of metals and alloys used in the manufacture of cables and connectors, and is currently working with fiber-optic connectors.

V. E. Kalomiris
U.S. Army CECOM
Ft. Monmouth, NJ 07703

Vasilios E. Kalomiris is currently a project leader responsible for fiber optic cables, connectors, and fiber optic system development. He received the 3rd annual Engineering Excellence Award for 1986 from CECOM; served for three years as chairman of the Tri-Service Group on fibers, cables and connectors; and as a member of EIA P6.7 Working Group on Fiber Optic Cables. Most recently, he worked for ITT-EOPD as a project engineer for the air layable cable which he designed. Prior to joining ITT-EOPD, Mr. Kalomiris was associated with General Cable Corp. R&D as a research engineer for 6 years. While at General Cable he was involved with the design, development and manufacture of the prototype super-conductive power cable with flexible core. He is a member of IEEE and the Technical Chamber of Greece (Society of Professional Engineers). Education: B.A. in Mathematics, B.S. in Electrical Engineering, an M.S. in Electrical Engineering, all from the New York University, and an MBA from Fairleigh Dickinson University.

MACROBEND LOSS OF 1300nm OPTIMIZED SINGLE MODE FIBRE AT 1550nm

Su-Vun Chung

Olex Cables, a Division of Pacific Dunlop Limited,
Melbourne, Victoria, Australia.

ABSTRACT

The ratio of the mode field diameter measured at 1300nm to the effective cut-off wavelength has been identified as a useful parameter for predicting macrobend loss of 1300nm optimized single mode fibres at 1550nm. This ratio, designated the fibre's MAC number, has been shown to be directly related to the degree of mode field confinement at 1300nm. Thus it is a practical and proven indicator of bend losses. Once an empirical relation has been established, no further time-consuming bend loss measurements are required on individual fibres. For such fibres to possess enhanced bend resistance at 1550nm, we found that the ratio should be less than 8.5. However, the appearance of a secondary bend loss mechanism for some depressed cladding fibres at the 1550nm window for bending diameters greater than 50mm indicated that the scheme is strictly applicable only to fibres obeying the pure bend loss theory for the range of bending diameters recommended by CCITT G652.

1. INTRODUCTION

Most telecommunication applications employing 1300nm optimized single mode optical fibres in the network also require the cabled fibre to perform satisfactorily at 1550nm. The bending performance at this window is of concern due to the increased proportion of light in the cladding. Consequently, CCITT recommendation G652 specifies methods that can be used to qualify the bend performance of these fibres. Two methods were mentioned. For qualification purposes only, the multiple-turn (> 40 turns), large-diameter (60 or 75mm) mandrel wrap test is recommended. In cases where routine screening of every fibre is needed, a simplified single-turn, small-diameter (20-30mm) bend test was included as an alternative.

Recent tightening of the bend loss at 1550nm from 2dB to 1dB per 100 turns over a mandrel diameter of 60 or 75mm means that a significant proportion of fibres meeting the CCITT specification for mode field diameter (MFD) and cut-off wavelength will not meet the new criteria[1]. In some applications, a bend loss of 0.2dB has been specified. Thus, a method of assurance is required.
The multiple-turn wrapping test is ruled out as a routine procedure because it is economically unviable. Furthermore, spectral loss measurements employing the alternative single-turn test performed on both matched and depressed cladding fibres led us to believe that the test is unreliable for two reasons: firstly, substantial oscillations observed in the spectral bend loss curve at 1550nm for some matched cladding fibres indicate that up to 7dB difference in results can be obtained if narrow line width lasers with slightly different centre wavelengths were used. Secondly, we discovered that the mapping relation (based on pure bend loss theory) that allows an equivalent single-turn, small-diameter bend test to be constructed as a simplified alternative to the multiple-turn large diameter specification is not valid for some depressed cladding fibres due to the appearance of an unexpected spectral loss feature at the 1550nm window at large bend diameters. Its magnitude and threshold wavelength is a function of bend diameter. Thus, a practical method for ensuring satisfactory macrobend performance at 1550nm for 1300nm optimized single mode fibres is required.

We will describe a method for predicting the macrobend loss of matched cladding fibres at 1550nm based on the individually measured mode field diameter at 1300nm and the effective 2 metre cut-off wavelength. Our measurements were performed independently of a very recent CCITT contribution[2]. This paper confirms those results and provides a theoretical foundation for the measured bend losses. Further analysis led us to propose the ratio of MFD to cut-off wavelength as a new parameter for characterising the macrobend loss of single mode fibres. We designate this ratio as the fibre's MAC number. We show by simple arguments, that it is related to a newly-defined normalized spot size of the fibre, an important parameter used for the characterisation of macrobending performance of single mode optical fibres[3,4]. Spectral loss measurements on both depressed and matched cladding fibres will also be presented to highlight some unusual wavelength-dependent features at bend diameters of interest.

2. DESCRIPTION OF THE METHOD

Several recent papers on macrobend loss measurements have described the MFD as being the primary variable affecting attenuation increase[5,6]. However, extensive computations on various types of single mode fibre designs have strongly indi-

cated that the MFD normalized with respect to the core diameter of the fibre is a primary indicator of bend losses[7]. In practice, the core diameter is not measured on each fibre. Instead, it can be deduced from the 2 metre cut-off wavelength measurements if the delta of the refractive index profile is available and the relationship between the theoretical and effective cut-off wavelength is known. For matched cladding single mode fibres, the former is optimized at 0.3%. Variations can be detected from preform measurements. In the latter, the relation is linear and a ratio of 1.15 was frequently quoted[8].

We have derived a composite design chart from computations on an equivalent-step-index (ESI) fibre with a nominal refractive index delta of 0.30% and core diameter of 8.8 microns. Figure 1 shows the equi-bend loss curves with the MFD (Petermann II definition) and theoretical cut-off wavelength as the axes. For each delta, the cut-off wavelength is varied by changing the core diameter via the well-known normalized cut-off frequency parameter, Vc[9]. For an equivalent step index fibre we can write:

$$\lambda_c = 2\pi a n_{c_l} \sqrt{2\Delta}/V_c \qquad (1)$$

where λ_c - theoretical cut-off wavelength
$2a$ - core diameter
n_{c_l} - cladding refractive index = 1.447
V_c - normalized cutoff frequency = 2.405
Δ - delta = 0.3%

Thus, by keeping Δ constant, we can change the core diameter through λ_c . A family of curves is obtained if we repeat the process for each Δ. The variation of Δ about the nominal was chosen to reflect small changes due to production tolerances on the refractive index profile. The bend loss at 1550nm over 50 turns with a bending diameter of 60 mm have been calculated from the pure bend loss formula of Kuester and Chang[10] . The zero dispersion wavelengths were also calculated and included in Figure 1, using a computer program which incorporates Kobayashi's sellmeire coefficients[11] . Interpolation was employed to deduce material dispersion for arbitrarily chosen values of Δ.

Figure 1 : Equi-bend loss and equi-zero dispersion wavelength lines for an ESI fibre. Bend loss calculated at 1550 nm @ 50 Turns at 60 mm bend diameter.

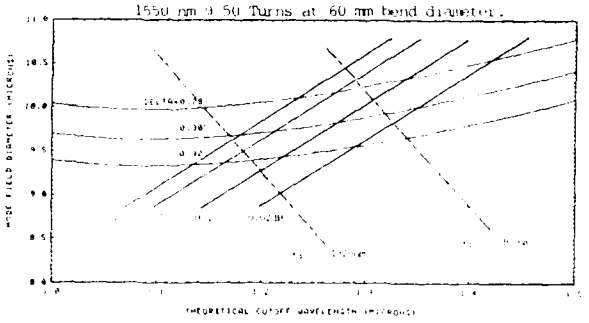

The significance displayed in Figure 1 is that due to strong influences in Δ, a fibre characterised by a large MFD and simultaneously long cut-off wavelength can show the same bend loss as another fibre with a smaller MFD and shorter cut-off. This observation led us to believe that the simple ratio of MFD over the cut-off could yield a dimensionless quantity needed for assessing the bend loss susceptibility of single mode fibres. For convenience, we designate this ratio as the fibre's MAC number. Table 1 shows the variation of this quantity at points A and B in Figure 1 for a number of equi-bend loss curves. The variation in MAC numbers is sufficiently small between A and B compared to the variation between equi-bend loss lines so that differences in the MAC number can be correlated with the bend loss measurements. By taking the ratio of MFD over cut-off, we have effectively calculated the slope of the straight line connecting the equi-bend loss curves to an imaginary origin. However, because we are only working around a very small portion of the MFD-cut-off plane, each curve effectively becomes a point so that differences in the slope between two closely spaced points along the curve tends to zero.

Table 1: Characteristics of the theoretical MAC number for the calculated bend loss at 1550nm; 50 turns; 60 mm diameter.

	MAC Number*	
BEND LOSS	POINT A	POINT B
1.0	8.21	8.18
0.5	8.04	8.04
0.1	7.75	7.74
0.02	7.42	7.45

*Points A and B lie on the equi-bend loss curves at the limits of zero dispersion wavelength identified by 1300 and 1320 nm respectively.

It can be shown simply from eq. (1) that the MAC number is related to the normalized mode field diameter in the form:

$$\text{MAC number} = 6.81K\ (\text{MFD}/2a) \qquad (2)$$

where K denotes the ratio of theoretical cut-off wavelength to the effective 2 metre cut-off and 2a is the core diameter of the ESI fibre. The ratio of the MFD over the core diameter is an indicator of mode field confinement. Various definitions of MFD appear in the macrobend and microbend loss formulae but at 1300nm, their differences are small for fibres with cut-off wavelengths close to 1300nm. Corrections can be made from measured data. A fibre in which light is tightly confined to the core, that is, one identified with a small normalized MFD or a small MAC number would be expected to be least

susceptible to bending-induced losses.

3. MULTIPLE-TURN MANDREL WRAP BEND LOSS MEASUREMENTS

As a consequence of the theoretical results in Table 1, we have carried out mandrel wrap bend tests on 75 samples of matched cladding UV-acrylate single mode fibres with an overall diameter of 250 microns. The sample length is 20 metres and the fibres were hand wound with near zero tension and twist on a smooth PVC pipe of 60.3 mm diameter. Double-sided tape is used to hold the fibre in place. The laser has a line width of 4nm and the centre wavelength is 1562nm. The excess loss due to bending is indicated by the readout from a power meter with reference and averaging facilities. The total system drift is less and 0.02dB over the period of measurement. The repeatability between measurements is better than 0.05dB. Residue twist and imperfect windings are main factors affecting measurements. The fibres were connected to the measurement system via V-grooves. No change in received power was observed when a 60mm diameter loop was inserted 2 metres from the source V-groove indicating that mode stripping is complete. All measurements were carried out at a controlled temperature of 20 ± 2°C.

The results have been presented in exactly the same format as the theoretical construction depicted in Figure 1 so that a comparison can be made. An equi-bend loss curve with a MAC number of 8.6 is fitted to the scattergram in Figure 2 to identify fibres having bend losses of 0.1dB at 1550nm over 50 turns with a mandrel diameter of 60mm. If we define the corresponding MAC number as its cut-off value, then Figure 3 confirms that it is equal to 8.5. If sufficient samples with MAC numbers greater than 9.2 are measured, curve fitting techniques can be employed to deduce an empirical formula between the bend loss and MAC number. Good agreement with the cut-off MAC number is obtained if the K factor in equation (2) is set to 1.1 and corrections are made to the measured mode field to account for the slight (≃3%) differences between the Petermann II and Gaussian mode field diameters. These adjustments to the theoretical MAC number returns a value of 8.7 and have been superimposed on the measured datain Figure 2.

Figures 2 and 3 indicate that for a fibre to meet the tighter CCITT bend loss specification of 0.5dB and bending diameter of 60mm, its MAC number must not exceed 9.2. This result will exclude fibres on the top left hand corner in Figure 2.

Figure 2: Measured bend loss for matched cladding fibres at 1550nm with excess losses over 50 turns, 60mm bending diameter.

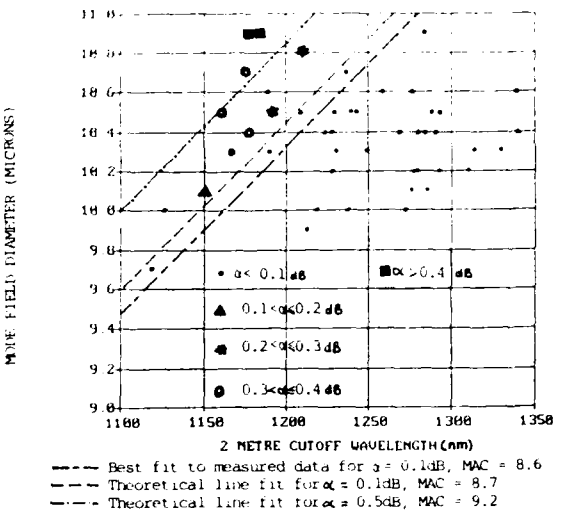

Figure 3 : Macrobend loss of matched cladding fibres plotted as a function of the MAC number of each fibre.

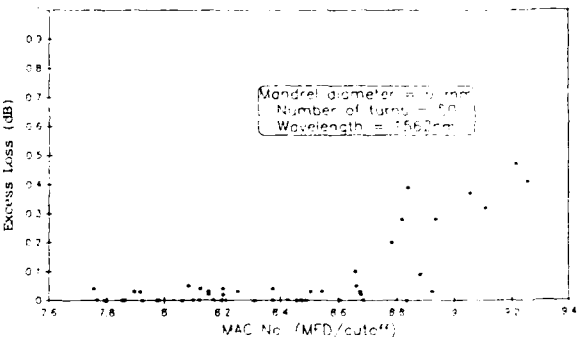

For the MAC number to be used as a reliable guide for screening fibres, an indication of its reliability is required. Measurement reproducibilities on the MFD and cut-off wavelength are typically 0.1 micron and 20nm respectively. For CCITT specified 1300nm optimized single mode fibres, the MAC numbers lie in the range 7.22 ± 0.20 to 9.73 ± 0.27. Thus, allowing for a sufficient margin to cover measurement reproducibility and various definitions of MFD, a MAC number not exceeding 8.0 is a convenient rule-of-thumb for selecting bend insensitive fibres. For fibre manufacturers, a figure of 8.5 can be used to define the allowed ranges of MFD and cut-off wavelength for enhanced bend resistant non-dispersion shifted fibres.

This scheme can be generalized to cover all single mode fibres obeying the pure bend loss theory. For example, depressed cladding fibres have an average MAC number of 7.2 compared to 8.2 for

Figure 4: Bend loss signature of depressed cladding fibre at 60mm bending diameter

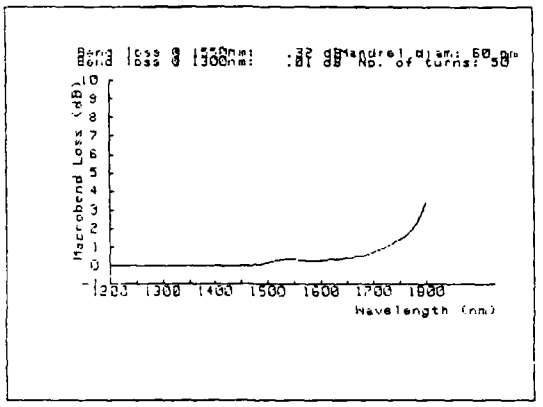

Figure 5: Depressed cladding fibre. Bend loss pedestal shifts towards longer wavelengths at 50mm

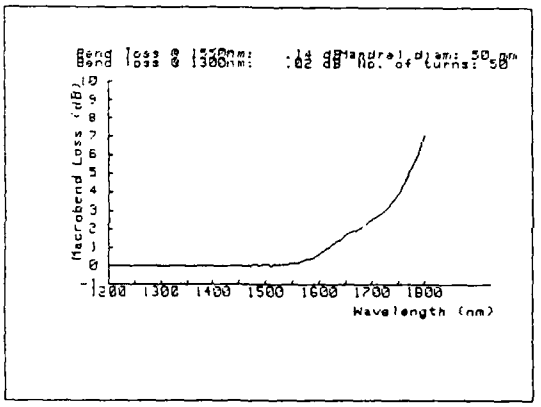

Figure 6: Depressed cladding fibre. No sign of bend loss pedestal at 40mm bend diameter.

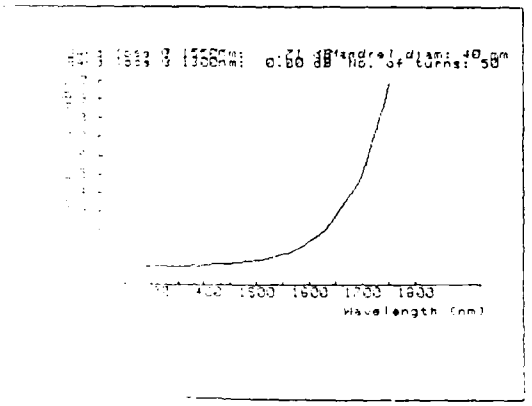

These measurements confirm recent published reports that for bend diameters greater than 50mm, depressed cladding fibres can have higher excess bend losses than matched cladding fibres[13]. Knowledge of the behaviour of the mode field is required to fully understand the phenomenon. Computer-aided modelling based on the tipped profile model has led Reed to believe that the relevant parameter is the power in a mode at some critical bend radius[14]. Extensive parametric studies have been carried out to understand the phenomenon[15].

5. SINGLE TURN BEND LOSS MEASUREMENT

The single-turn, small-diameter bend test is a CCITT G652 recommended simplified alternative to the multiple-turns mandrel wrap test for assessing bend performance at 1550nm. To obtain a spectral signature of the loss, the same spectral loss set-up was employed. Measurements were performed on short 2-metre samples of matched and depressed cladding fibres. Figure 7 shows the excess bend loss of the same depressed cladding fibre used in section 4 for a bending diameter of 20mm. No unusual feature is present that could lead one to predict the excess loss shown in Figure 4 for the multiple-turns mandrel wrap test at a bend diameter of 60mm.

Figure 7: Same depressed cladding fibre as Fig. 4 - Typical curve at small bend diameters

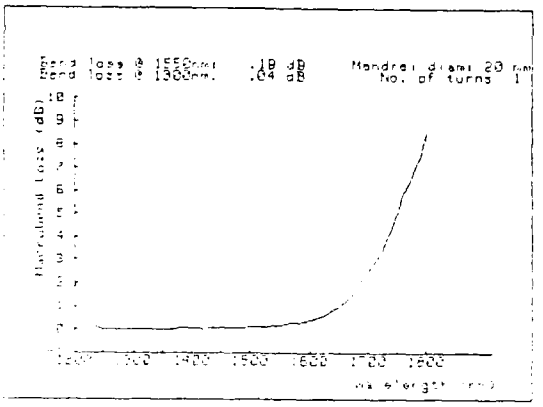

A matched cladding fibre with an MFD of 10.5 microns and cut-off wavelength of 1180nm was measured under the same conditions. Figure 8 shows the appearance of large resonant peaks and troughs at the 1550nm window. These features appearing on top of the exponentially increasing pure bend loss curve is commonly referred to as transition losses. A difference of 7dB in excess loss can be obtained if lasers with slightly different centre wavelengths in the range 1520-1570nm were used. Harris and Castle attributed the dips in the total bend loss to snychronous coupling between the fundamental mode and the leaky whispering gallery mode and that the peaks are caused by asynchronous coupling[16]. As such, the asymptotic value of the peaks should agree with the pure bend loss theory. Preliminary experiments suggest that the refractive index of the primary coated cladding mode stripper is an important parameter in limiting the magnitude of these transition losses.

Figure 8: Matched cladding fibre. Typical bend loss signature at small bend diameters.

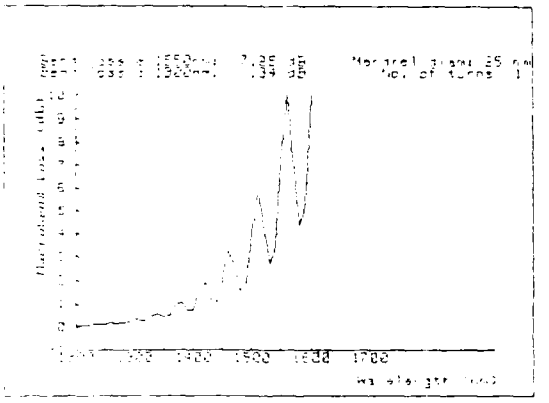

These results are timely because it is the first such reported study which suggests that the simplified single-turn single-wavelength bend test may not be a reliable method for routine testing of either matched or depressed cladding single mode fibres. An alternative is to employ a computer fit to the spectral loss data obtained from cut-off wavelength measurements with the 60mm loop replaced by a smaller diameter in the range 20 - 30mm.

6. CONCLUSION

We have established that the ratio of MFD measured at 1300nm over the 2 metre cut-off wavelength (MAC number) is a reliable indicator of the macrobend loss susceptibility of single mode fibres at 1550nm. Our measurements showed that fibres should have a MAC number less than 8.5 to ensure a bend loss of less than 0.1dB over 50 turns on a 60mm diameter mandrel. If sufficiently large samples are taken, this method can be used to screen fibres for bend loss with a high level of confidence. The MAC number scheme can also find applications in quality control. For example, poorly coated single mode fibres are known to be susceptible to microbending losses. The coating will attenuate the LP_{11} mode and thus shorten the cut-off wavelength with a corresponding increase in the MAC number. Thus, a scheme employed to screen macrobend loss susceptibility could at the same time eliminate those fibres which are prone to microbending losses. The MAC number should be of assistance to fibre users for specifying the combination of MFD and cut-off wavelength required to meet a specified bend loss. These results can be generalized to apply to all single mode fibres obeying the pure bend loss theory.

REFERENCES

1. CCITT Recommendation G652 doc. APIX-60-E p.68
2. CCITT Study Group XV-Contribution 202, Feb., 1988
3. K. Petermann and R. Kuhne, J. Lightwave Tech. Vol LT-4, 1986, p.2-7
4. M. Artiglia et al, Tech. Digest, Twelfth European Conf. Opt. Comm., Barcelona, 1986, P.341
5. A.O. Garg and C.K. Eoll, International Wire and Cable Symposium Proceedings, 1986, p.406-414
6. J.A. Dixon et al, paperTUA2, OFC/IOOC, 1987
7. S.V. Chung Ph.D. Thesis, Chap.4, Part II, 1987
8. K. Kitayama et al, J. Lightwave Tech. Vol. LT-1, No. 2, p.363-369, June 1983
9. A.W. Snyder and J.D. Love, Optical Waveguide Theory, Chapman and Hall, 1983, Chap.14
10. E.F. Kuester and D.C. Chang, IEEE J. Quantum Electron., Vol. QE-11. 1975, p.903-907
11. S.M. Kobayashi et al, Rev. Electro-Comm. Lab., Vol.26, 1978, p.453-467
12. A. Tomita and D. Marcuse, J. Lightwave Tech. Vol. LT-1, No. 3, 1983, p.449-452
13. P.F. Glodis et al, OFC/IOOC 1987, paper TUA3
14. W.A. Reed, OFC 1988, paper WE1
15. W.A. Reed, private communication
16. A.J. Harris and P.F. Castle, J. Lightwave Tech., Vol. LT-4, No. 1, 1986, p.34-40.

Su-Vun Chung
Olex Cables
A Division of Pacific Dunlop,
207 Sunshine Road,
Tottenham, Victoria,
Australia. 3012.

Su-Vun Chung was born on November 8, 1960 in Kuching, Malaysia. He received his BE in electrical and computer systems engineering and PhD in fibre optics from Monash University, Australia in 1982 and 1987 respectively. His current interests are in the areas of design and characterization of single mode fibres, systems and development of specialized optical fibre cables. He is a member of the Institution of Electrical and Electronics Engineers (IEEE).

METHOD FOR SINGLE MODE FIBRE BENDING STUDIES IN SHORT FIBRES OR CABLES

Tarja Volotinen and Leif Stensland

Ericsson Cables, P O Box 457, S-82401 Hudiksvall, Sweden

Abstract

The fundamental mode in single mode fibres is sensitive to bends especially at long wavelengths, where a large part of the power is carried in the cladding outside the core. The behaviour of the fundamental mode at these wavelengths may be difficult to study but can be simulated by the next higher order mode near its cut-off wavelength. The paper discusses shortly the theoretical justification of this idea and gives some experimental results on the correlation between the spectral behaviour of the LP11-mode near cut-off and the loss of the fundamental mode at long wavelengths. Some applications of such LP11-mode studies are proposed.

Introduction

The intrinsic attenuation of standard single mode fibres of today is very low, 0.30 - 0.40 dB/km at 1300 nm and even 0.16 - 0.25 dB/km at 1550 nm. In order to maintain this low attenuation in when the fibre is cabled, the cable must be carefully designed. Further, the cable must also maintain its low loss in different installation situations, thus the cables are often tightly specified as far as mechanical and environmental tests are concerned. Consequently, in the cabling process and in such tests, only a very low additional loss is permitted, usually of the order of 0.01 - 0.1 dB/km. It is thus very important to use extremely sensitive methods, when experimentally studying or optimizing cable constructions.

The physical process that can cause additional loss in fibres in cables is bending. There are two types of fibre bending situations, microbending and macrobending. Single mode fibres are sensitive to both types of bendings, however, the wavelength behaviour is slightly different for the two bendings. It is not always easy to identify which bending type that is present in a practical situation. On the contrary, a clear distinction between them is easy to do theoretically (see theory below).

Fibres themselves have been extensively tested for macrobend sensitivity, ref 1. The sensitivity of these measurements were, however, limited to 0.1 - 10 dB/m, which does not meet the demand from the cable mechanical and environmental tests. The situation is similar for microbend tests.

In a practical situation the two bending types may be present simultaneously. Normally, though, one of them dominates and it is important to analyse the fibre bending situation in the cable in order to choose and optimize the appropiate cable construction. In order to clearly attribute an added cabling loss in a certain situation to one of the two bending types, accurate measurements have to be performed on the cables over a wide wavelength region. If only the fundamental mode of the fibre is studied in these test, very long cable lengths are necessary. Such tests are expensive and - in temperature cycling tests - time consuming. There is thus a need for sensitive tests, which can be used on short cables. Further, there is a need for a test on the tolerance before an attenuation increase starts in a manufactured cable.

In this paper, studies of the next order higher mode, the LP11-mode, are suggested for cable and fibre bending tests. First, fibre properties are discussed end a short theoretical introduction is given. In the major part of the paper, experimental evidence is given to the correlation between the LP11-mode attenuation near the mode cut-off wavelength and the LP01-mode (the fundamental mode) at long wavelengths. Finally, the method is discussed with the reported experimental results as a background and possible further applications are indicated.

Theory

Standard single mode fibres usually have effective cut-off wavelengths around 1200 nm. The theoretical cut-off wavelengths are somewhat higher. The fibres are thus bimodal in easily accessible wavelength regions. The fundamental mode, i e the LP01-mode, is of course the interesting mode from the system point of view. However, in bent fibres, the attenuation of the fundamental mode, α_{01}, increases rather slowly versus the wavelength. It is thus necessary to use long fibres or long wavelengths for fibre bending studies. On the other hand, the attenuation of the next higher order mode, (the LP11-mode), α_{11}, increases rapidly to extremely high values as the wavelength increases towards the cut-off wavelength of the mode. The additional loss from macro- and microbends also give quite large and clear changes in the α_{11} spectral behaviour near the cut-off wavelength. In the following the LP11-mode behaviour will be discussed.

α_{11} measurements

α_{11} is measured by a special spectral measurement. In this test the fibre launch end is overfilled and a comparison is done of the transmitted power before, P_{tot}, and after, P_0, inserting a LP11-mode blocking filter, fig 1. If P_{01} and P_{11} are the power in the LP01 mode and the LP11 mode, respectively, launched in the fibre, we get

$$P_{tot}=P_{01}\cdot 10^{-\alpha_{01}\cdot L/10}+P_{11}\cdot 10^{-\alpha_{11}\cdot L/10} \quad (1)$$

$$P_0 = P_{01}\cdot 10^{-\alpha_{01}\cdot L/10} \quad (2)$$

rearranging, we get

$$\alpha_{11}-\alpha_{01}=10(\log(2\cdot P_0)-\log(P_{tot}-P_0))/L \quad (3)$$

where we have assumed that $P_{11}=2\cdot P_{01}$. (There are four LP11-modes and only two LP01-modes.)

A convenient type of diagram that will be used through out the paper is the $\log(\alpha_{01})$ and/or $\log(\alpha_{11})$ vs wavelength plot. Far from cut-off $\alpha_{01}\approx\alpha_{11}$, thus $\alpha_{11}-\alpha_{01}$ is very small, but closer to cut-off α_{11} increases by several orders of magnitude, reaching by definition 22 dB/m at the so called effective cut-off. As α_{01} is negligible in comparison to α_{11} in this region of interest, in the following α_{11} will be used instead of the correct $\alpha_{11}-\alpha_{01}$.

Macrobends

A macrobend situation occurs, when the additional loss is mostly pure bend loss. In bent fibres all modes are leaky and pure bend loss is thus really the mode attenuation due to leakage. This leakage occurs because the phase velocity of a mode wavefront in a bent fibre has to increase linearly with the distance from the bend center. Sooner or later the phase velocity will reach the speed of light in the cladding and beyond that point the mode will consist of a radiative part. Marcuse (ref 2) has given formulae for the additional macrobend loss, which can be written approximately

$$\Delta\alpha_{01}(R)=A_0\cdot(v_0\cdot R)^{-\frac{1}{2}}\cdot\exp(-B\cdot\lambda^2\cdot v_0^3\cdot R) \quad (4)$$

$$\Delta\alpha_{11}(R)=A_1\cdot(v_1^3\cdot R)^{-\frac{1}{2}}\cdot\exp(-B\cdot\lambda^2\cdot v_1^3\cdot R) \quad (5)$$

where R is the bend radius, v_0 and v_1 are the radial decay parameters for the LP01 and LP11 modes respectively, A_0 and B are constants and A_1 is a slowly varying parameter. When the wavelength increases towards infinity, v_0 decreases towards zero giving an slowly increasing LP01 attenuation mainly due to the exponential factor. The LP11-mode loss is of a similar form to that of the LP01-mode. However, v_1 decreases to zero when the wavelength approaches the theoretical cut-off wavelength of the LP11-mode. As A_1 is only slowly varying with the wavelength, it can be regarded as a constant. Thus we get an extremely rapid change of $\Delta\alpha_{11}$, which is several orders of magnitude. Also for $\Delta\alpha_{11}$ the exponential factor dominates the wavelength behaviour. Thus for different R, the $\Delta\alpha_{11}(\lambda)$-curve is shifted in wavelength, such that

$$\lambda^2\cdot v_1^3\cdot R = \text{constant} \quad (6)$$

as can also be seen in fig:s 2 and 3. However, in the region of interest, λ varies only by ± 10 % and can thus be considered almost as a constant in comparison to v_1. Thus by studying the $\Delta\alpha_{11}(\lambda)$-curve near the LP11 cut-off wavelength for a fibre in a cable, we may obtain the bending radius R, and be able to predict $\Delta\alpha_{01}$ at long wavelengths.

Microbends

Microbends occur when the bends are small but sharp, many and lying rather close. Microbends are thought to be induced by a disturbance of the fibre. Such a disturbance is often random and may be external, e.g. due to pressure against a non-smooth surface, or internal, e.g. tension in the fibre glass. Microbends are characterized as being a mode coupling situation in contrast to macrobends, where the loss is due to leaky modes. The mode coupling occurs from the guided mode, which can be the LP01- or the LP11-mode, to modes in the cladding. As these modes are highly lossy, they can be regarded as radiative modes. For mathematical simplicity they can be grouped together into a "quasimode", ref 3, with a propagation constant β_r. If the guided mode has a propagation constant β_g, the microbend loss will be determined by the disturbance spatial power spectrum at $\beta_g-\beta_r$, ref 4. If, further, the disturbance is thought to have a gaussian autocorrelation behaviour, we can write approximately

$$\Delta\alpha_{01}=C_0\cdot\sigma^2\cdot L_c\cdot\exp(-(D(v_0^2-v_r^2)L_c)^2) \quad (7)$$

$$\Delta\alpha_{11}=C_1\cdot\sigma^2\cdot L_c\cdot\exp(-(D(v_1^2-v_r^2)L_c)^2) \quad (8)$$

where C_0, C_1 and D are constants, σ is the disturbance RMS-mean deviation value and L_c its correlation length. As usual, by definition (see e.g. ref 5)

$$v^2=(\beta^2-k^2\cdot n_2^2)\cdot a^2 \quad (9)$$

where v stands for v_0, v_1 or v_r, β for β_0, β_1 (i.e. β_g) or β_r, $k=2\pi/\lambda$, n_2 the refractive index of the cladding and a the core radius. (As β_r must be smaller than $k\cdot n_2$, v_r^2 will be a negative quantity and $(v^2-v_r^2)$ will be positive for all v.)

Thus, also for microbending, the LP01 and the LP11 additional loss behaviour are similar to each other. However, in this case, L_c is small, perhaps a few tenths of a millimeter, while in the case of macro-bending R is large, several tens of millimeters. The non-zero value of v_r and the small L_c-value allow v_1 to increase to much higher values, i.e. to lower wavelengths before the exponential factor and thus $\Delta\alpha_{11}$ have decreased very much. Thus microbends give a much less rapid change in the $\Delta\alpha_{11}$ versus wavelength diagram than macrobending. Macro- and microbending can thus be easily distinguished from each other from the behaviour of α_{11}. The type of bending that is present in a cable could thus be easily inferred from α_{11}.

Practical situations

In practice both types of bends are likely to be present simultaneously. The two types of bending should not influence each other and thus the total loss should simply be the sum of the two bending losses.

Experimental results

The attenuation of the LP11 mode near cut-off has been studied and related to the LP01 loss at long wavelengths in a number of cases including

- macrobend test, different diameters
- microbend test, different sandpapers
- cabling process
- cable temperature cycling

In all these tests, 12 OVD-fibres of the matched cladding type and 12 MCVD-fibres with a slightly depressed cladding were studied. The fibres were carefully chosen to show different macro- and/or microbend sensitivities. The cable studied was a filled loose tube construction with four coloured fibres in each of six tubes. The tubes were helically placed in petroleum jelly filled slots in the central strength member. The cable was finally sheathed with polyethylene.

Measurement results of all four cases will be reported below for one fibre (fibre A) in the cable, in addition, for another fibre (fibre B), only cable measurements will be given.

Fibre attenuation measurement procedure

The attenuation of the LP01-mode was obtained by the standard cut-back method procedure with a 2 m length of the fibre as reference including one loop of 280 mm in diameter (or smaller if the fibre had a long cut-off wavelength). The attenuation of the LP11-mode of the fibres was obtained by the special spectral measurement (see theory). The spectral scans were taken between 800 nm and 1700 nm in steps of 10 nm.

Typical transmission scans of one fibre are shown in fig 1. α_{01} is evaluated from the scans 1 and 3 and α_{11} from the scans 1 and 2 by the formula (3). The results are presentated in log α versus λ diagrams. Near cut-off, for a typical fibre, log α_{11} is almost linear in λ, which was also predicted in fig 2. Thus, log α_{11} can be well represented by a straight line

$$\log \alpha_{11} = A_{11} + B_{11} (\lambda - \lambda_{ceff}) \qquad (10)$$

where if α_{11} is given in dB/m, the slope of the line i.e. B_{11} is of the order of 40 μm^{-1} for straight or macrobent fibres and about 5 μm^{-1} for microbent fibres, λ_{ceff}, finally, is the effective cut-off wavelength making A_{11}=log 22 by definition.

Macrobend tests

All fibres were subjected to macrobend tests at different bend diameters between 30 and 100 mm. In this measurement, fibre lengths of 35 or 50 m were used, depending on the bend diameter. α_{11} was obtained by the special spectral measurement procedure (the relative value was obtained by using in formula (3) as L the bent portion of the fibre, assuming that α_{11} in the straight parts is negligible). Great care was taken in assuring that no part of the fibre was unintentionally bent to smaller diameter than 280 mm. The bends were taken up on a mandrel in such a way that first half a loop of the proper bend diameter was attached to the mandrel. Later the subsequent loops were wound clockwise and counter-clockwise, respectively, on the mandrel on both sides of the first half-loop, fig 4. In order to get good reliability, rather long parts of the fibres, up to 25 or 40 m, respectively, were carefully wound on the mandrel.

Typical spectral transmission curves look like fig 5. It is obvious that the LP11-mode is much more bend sensitive than the LP01-mode. In fig 6 the log $\alpha_{11}(\lambda)$ plots are given. A number of observations can be done from these plots. The fibre in this test was a matched cladding fibre (fibre A). Short pieces of this fibre, 2 and 50 m respectively, gave very steep α_{11}-curves. These fibres were not bent to diameters smaller than 280 mm. In the macrobend test the α_{11}-curve is shifted to shorter wavelengths, when the bend diameter is decreased. This effect was predicted in fig 2 and is well known from cut-off measurements. This knowledge of the bend shift are used below, when the α_{11} spectral behaviour of cabled fibres is analysed.

Microbend test

All fibres in the cable were subjected to a standard microbend test. In this test a 50 m piece of the fibre was used. The fibre was placed on a sandpaper, usually type P 180, and pressed against it by glass plates. 4 or 6 m of the fibre were then subjected to a pressure from the glass plates of 10 N/m. α_{11} was again measured by the special spectral measurement method. When calculating the α_{11} value, only the length of fibre under the glass plates was used assuming that the loss of this part was dominant.

A fibre subjected to microbends shows a quite different α_{11} behaviour from that of a fibre under macrobending, fig 7. The wavelength dependence is less steep and the sensitivity of the LP11 mode to microbends is only one order of magnitude higher than that of the LP01-mode. As seen in fig 8 the α_{11}-curve is still approximately a straight line as in formula (10), however, the slope, i.e. B_{11}, is only about 5 μm^{-1}.

An example of microbends can also be seen in fig 8, where the α_{11}-curve for the 4 km long fibre on the measurement spool is not as steep as expected. It is believed that this effect was due to microbending on the spool, at least for the innermost fibre layers.

Cable process test

In the cable process test the fibre loss was measured at several stages for a 10 m sample and for the complete cable length, about 1.7 km. In fig 9 a large shift in the α_{11}-curve is found for the fibre after the first process step, i.e. after putting the fibre in a filled tube. This is understood as a large excess length of the fibre, buckling it to bends of diameter about 50 mm. During the stranding of the tubes, they were stretched so the excess lengths of the fibres was decreased and the fibre bend diameters increased to about 130 mm. The cable stranding should give the fibres an average bend diameter of 165 mm, when the cable is straight, thus some buckling excess fibe length remains. This kind of information cannot be obtained from the α_{01}-curve, as such a bend diameter does not change the attenuation of the LP01-mode by a noticeble amount and because of the different fibre bending sensitivities. The final sheathing of the cable changes the α_{11}-curve only very slightly and has thus not given any further stretching or compression. In fig 11 a fibre, B, from another tube is shown. In this tube the fibres were stretched in order to have little or negative excess lengths. It is clearly shown that the bending diameter in the fibre in the tube is no smaller than in the cable.

Cable temperature test

The 35 m cable sample and the complete long cable were subjected to a temperature cycling test between - 40°C and + 70°C. For the fibre A, which had rather large excess length and did show a small α_{01} increase at - 40°C, but no change at + 70°C. A significant macrobend type shift did show up in the α_{11}-curve, fig 10. For this particular fibre even the 35 m long cable sample gave the same result. This result indicates thus that temperature cycling tests may be reliably performed even on quite short cable lengths. Fig 12 shows fibre B in the other tube. Due to the fibre deficiency in the tube, the highest loss occurs at high temperatures and the α_{11}-curves have less steep slopes, indicating that some microbending is present. As in fig 10 it is quite evident that most information can be obtained from the short cable length. In this case even the high temperature, i.e. + 70°C, gave a microbend type of change of α_{11}. The cause for this is unknown.

Discussion

It has been demonstrated that in single mode fibres the LP11-mode is more sensitive to the two bending types than the fundamental LP01-mode. The LP11-mode may thus be used for probing the bending status of a fibre, even if only a short piece of it is present.

Many applications of the LP11-mode study method can be envisioned. Both fibre and cable tests are possible and advantageous. Among the fibre tests are

- macrobend sensitivity studies, especially at large bending diameters
- primary coating development
- measurement spool influence on attenuation studies
- fibre splice evaluation
- colouring of fibres

Possible cable tests are

- secondary coating development
- process parameter optimisation
- cable mechanical tests
- cable temperature test
- other environmental tests
- cable installation tests
- cable imperfection analysis

LP11-mode studies are especially efficient in identifying which of the two bending types that dominates in a particular situation. They are further easy to perform as there is no need to cut-back the fibre. The necessary reference is obtained from the fibre with the LP11-mode blocking filter.

Conclusions

Studies of the next higher order mode, the LP11-mode, in standard single mode fibres, has been proven to be a valuable tool in fibre and cable attenuation change investigations. The fibre bend diameter in cables is possible to evaluate, even on quite short samples. Further, e.g. in temperature tests, short fibres or cables can be used. On long lengths the results can be analysed to greater depths than with the usual LP01-mode studies.

Acknowledgement

The authors would like to thank Paul Morris and Optical Fibres, UK for supplying the OVD fibres used in the study and allow us to publish the result obtained on these fibres. We further like to thank the many individuals at Ericsson Cables, who have helped by doing many of the measurements, by developing the measurement evaluation programs or by preparing the manuscript. A research and educational grant from "Nordisk Industrifond" is also gratefully acknowledged.

References

1 Geittner, P et al, "Bend loss characteristics of single mode fibers", ECOC 1987, 97.

2 Marcuse, D, "Curvature loss formula for optical fibers", J Opt Soc Am 66, 216 (1976)

3 Petermann, K, "Theory of microbending loss in monomode fibers with arbitrary refractive-index profile", Arch Elektr Uebertrag 30, 337 (1976)

4 Bjarklev, A, "Microdeformation Losses of Single-Mode Fibers with Step-Index Profiles", J Lightw Techn LT-4, 341 (1986)

5 Jeunhomme, L, Single mode fibre optics, Dekker 1983

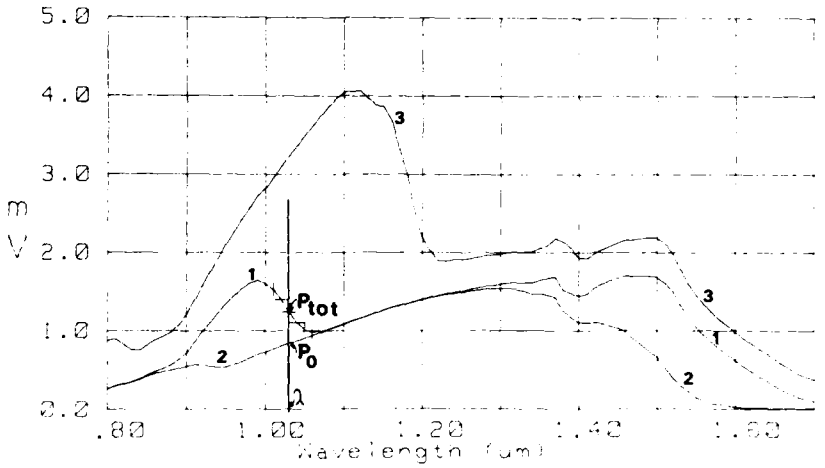

Fig 1
Transmission curves for the special spectral measurement.
Curve 1: transmission through a long fibre
Curve 2: transmission through the same fibre with an LP11 blocking filter
Curve 3: transmission through a 2 m reference fibre with one fibre loop of 280 mm in diameter
α_{11} is evaluated from P_{tot} and P_0, i.e. curves 1 and 2, α_{01} from curves 1 and 3.

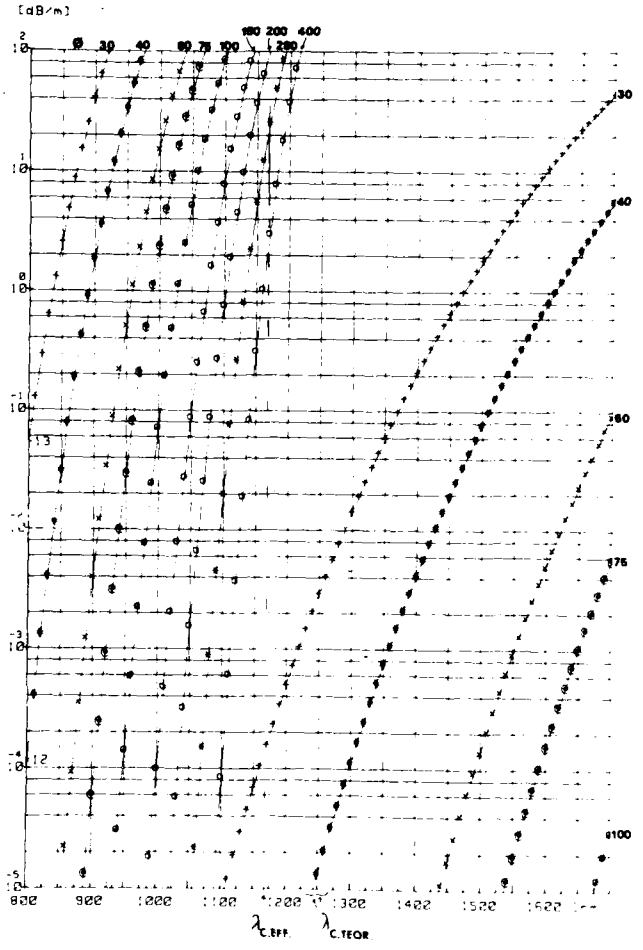

Fig 2
Theoretical plot of α_{11} (left part) and α_{01} (right part), the spectral attenuation of the next higher order mode and the fundamental mode respectively, when the fibre is macrobent to different diameters. The additional bend loss of the fundamental mode cannot be measured at bend diameters above 75 mm, while in principle the additional bend loss of the LP11-mode conveniently can be measured at large bend diameters.

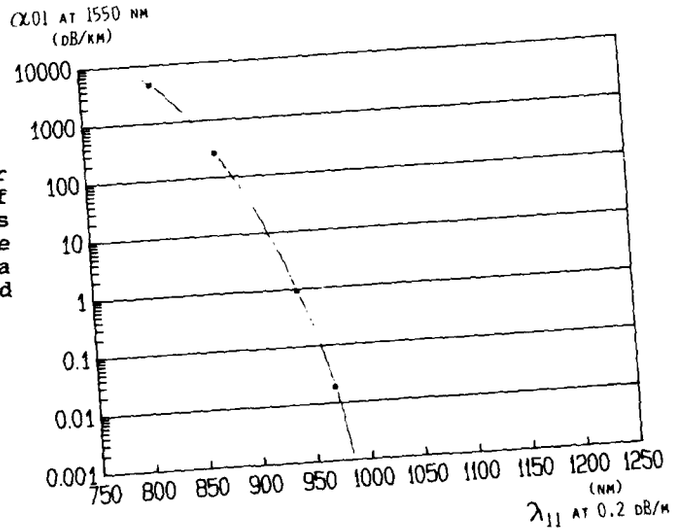

Fig 3
Relation between additional bend loss for LP01-mode at 1550 nm and the position of the LP11-mode loss curve. The latter is represented by the wavelength, where the attenuation is 0.2 dB/km, as this is a level that is conveniently evaluated from the log α_{11}-diagrams.

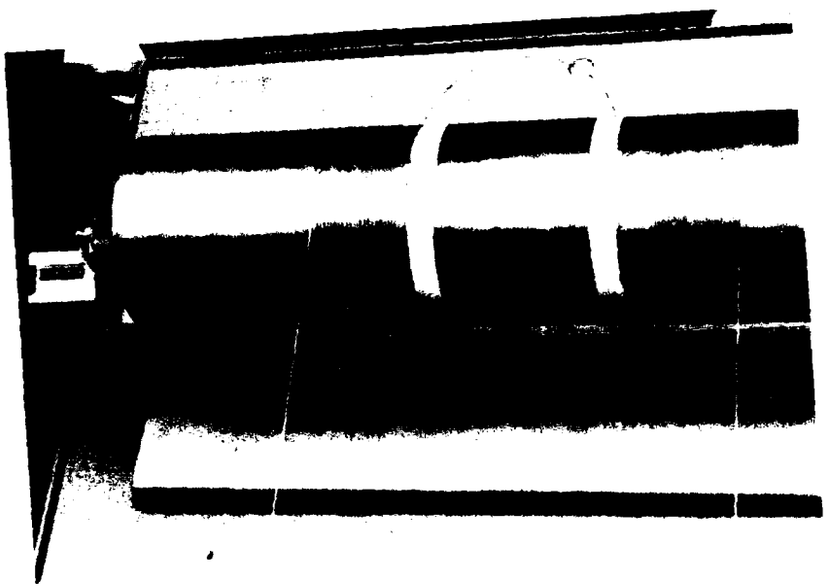

Fig 4
Photograph of a fibre in the macrobend test corresponding to curve 7 in fig 5. The bend diameter is 100 mm and 128 turns is wound on the mandrel. The first half turn can also be seen.

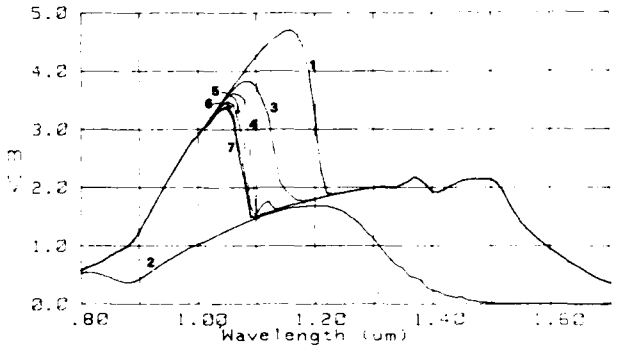

Fig 5
Transmission curves for a 50 m long fibre in a 100 mm diameter macrobend test with different lengths of the bent part of the fibre; 0 - 40 m, curves 1, 3 - 7.

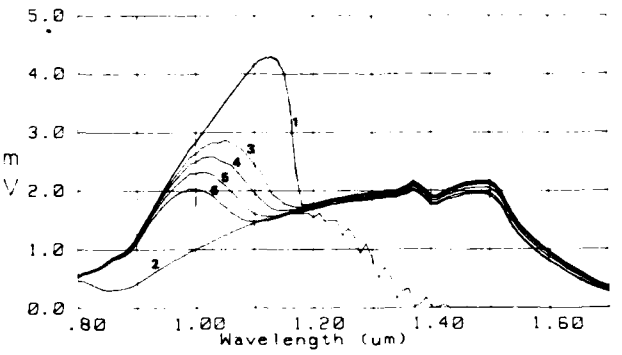

Fig 7
Transmission curves for a 50 m long fibre in a P 180 sandpaper microbend test with different lengths, 0 - 6 m, of the bent fibre.

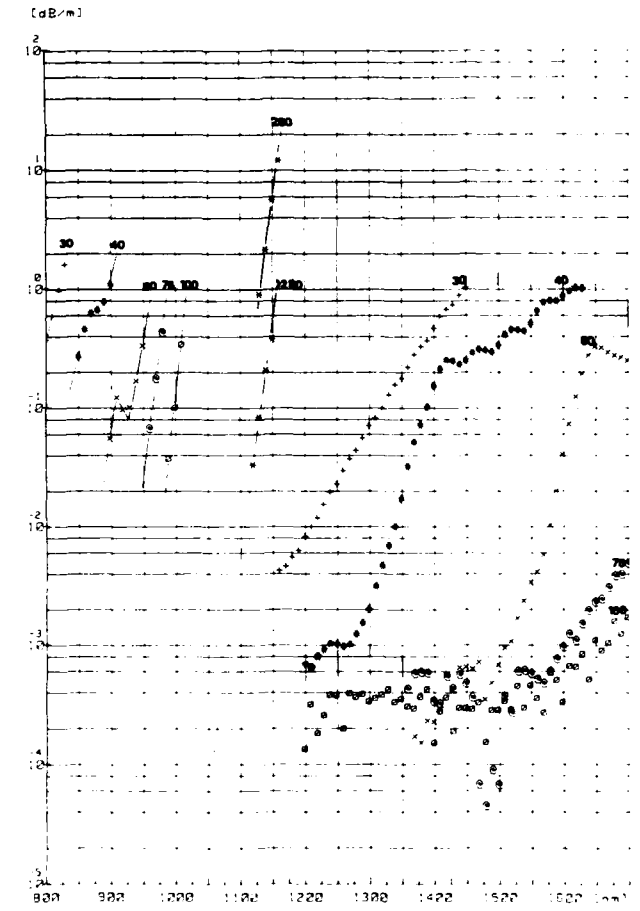

Fig 6
Log α_{11} (upper left corner) and log $\Delta\alpha_{01}$ (lower right corner) diagrams of a macrobend test with different bend diameters, fibre A.

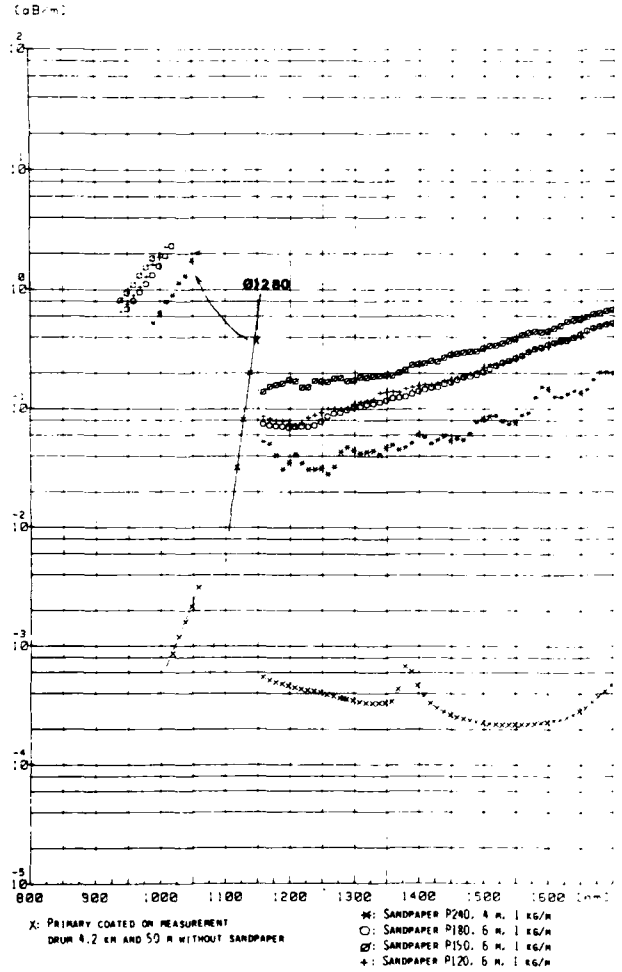

Fig 8
Log α_{11} and log $\Delta\alpha_{01}$ diagrams of a microbend test with different sandpapers, fibre A.

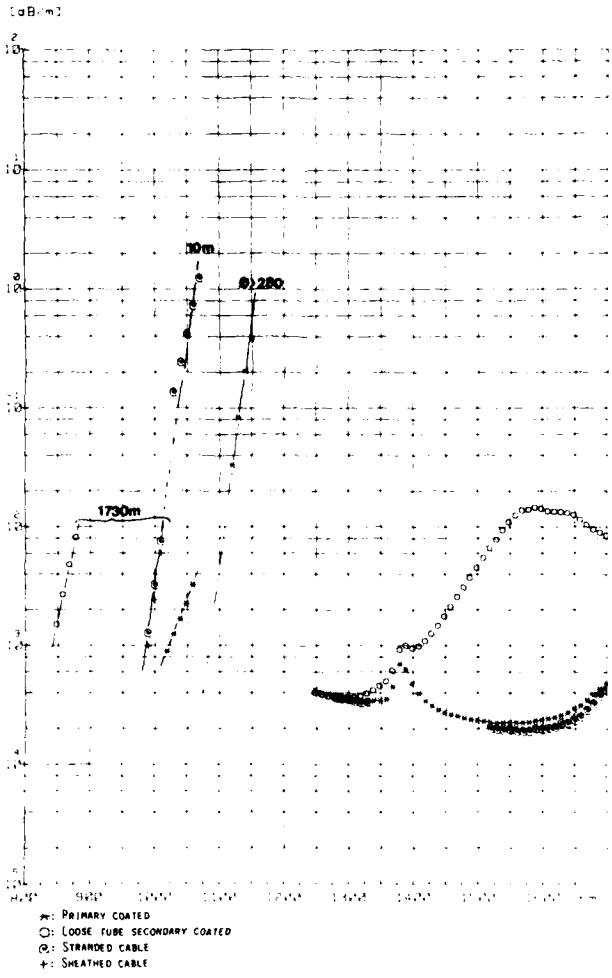

Fig 9
Log α_{11} and log α_{01} diagrams of the steps in the cable process. The manufactured cable was 1730 m long, in addition a 10 m cable sample was also tested, fibre A. For the loose tube additional loss is present both for the LP01- and the LP11-modes. For the cable, however, the LP01-mode shows no bend loss, while from the LP11-mode the fibre bend diameter can be inferred.

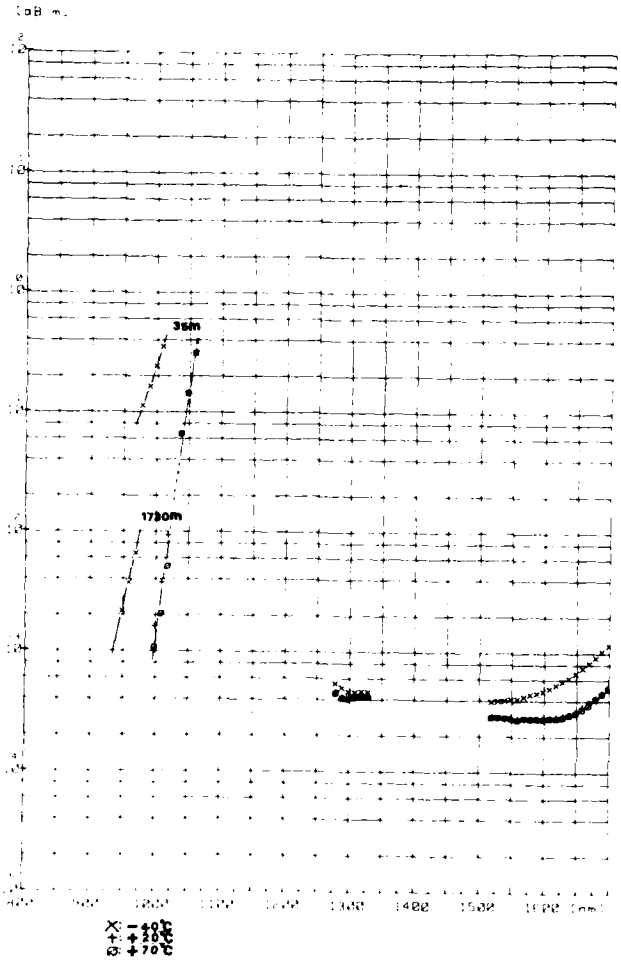

Fig 10
Log α_{11} and log α_{01}, diagrams of a temperature cycling test of a 1730 m and a 35 m cable respectively, fibre A. 35 m of the cable is a sufficiently long sample if LP11-mode is observed.

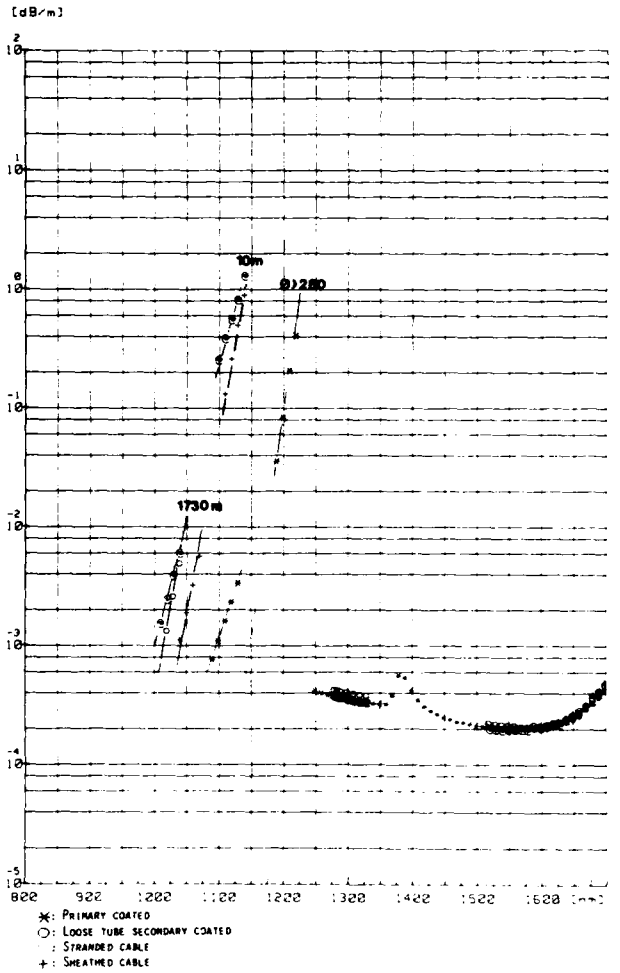

Fig 11
Log α_{11} and log α_{01}, diagrams of the steps in the cable process, 1730 m and 10 m cable respectively, fibre B. In this case the tube was made with a slight fibre length deficiency.

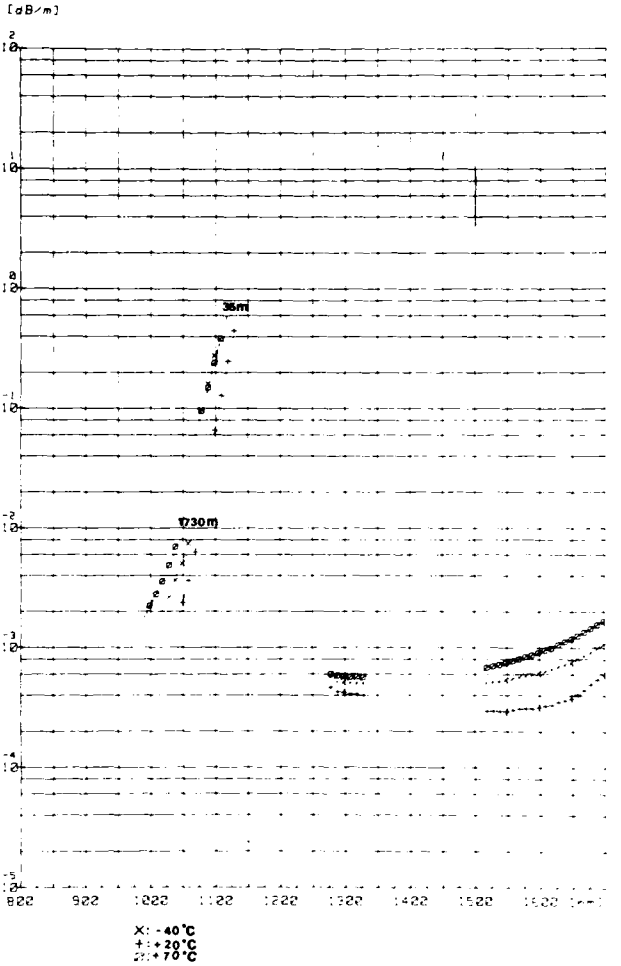

Fig 12
Log α_{11} and log α_{01}, diagrams of a temperature cycling test of a 1730 m and a 35 m cable respectively, fibre B. Due to fibre length deficiency the highest loss is obtained at high temperatures, where the fibre in under microbending.

Tarja Volotinen

Ericsson Cables AB
Telecom Cables Div.
P O Box 457
S-824 01 Hudiksvall
SWEDEN

Tarja Volotinen recieved her M Sc degree in Physics in 1978 from Helsinki University in Finland. In 1978 she joined Nokia Cables in Finland to be engaged in developing optical fibre and cable measurement techniques and quality control. In 1986 she joined Ericsson Cables in Sweden. She has responsibility for optical fibre and cable measurement techniques and is especially engaged in the fibre bending influence on cable performance.

Leif Stensland

Ericsson Cables AB
Fiber Optics
S-172 87 Sundbyberg
SWEDEN

Leif Stensland recieved the degree "Teknologie Licenciat" in optical physics from the Royal Institute of Technology in Stockholm, Sweden in 1971. Until 1982 he was with the Institute of Optical Research in Stockholm, heading a group in fibre and integrated optics. He joined Ericsson Cables in 1982 as manager of fibre and cable developments. His present responsibilities include also preform process development and measurement techniques.

MICROBENDING EFFECTS IN SINGLE MODE OPTICAL CABLES

G. GRASSO (*), F. MELI (*), E. USAI (*), F. ESPOSTO (**)

(*) SOCIETA' CAVI PIRELLI, MILANO (ITALY) - (**) SIP D.G., ROMA (ITALY)

Abstract

A new approach for calculating the loss increase in cabled fibers based only on experimentally determined fiber and cable parameters is presented.
A theoretical model for predicting the loss increase of a fiber compressed by linear pressure on a rough surface is illustrated.
A dedicated measurement apparatus for characterizing surface roughness has been developed.
The prediction of the loss increase based on the measured roughness spectrum has been confirmed by experimental tests on different types of fibers and cables.
The application of this method in cable design and technology for reducing cabled fibers sensitivity to microbending is discussed.
Further application in the field of loose type cable design and fault analysis are proposed.

Introduction

In the last years the intrinsic attenuation of silica fibers has reached its ultimate limit. Single mode fibers with attenuation lower than 0.2 dB/km at 1.55 μm are already commercially available.
In this situation even slight loss increases due to subsequent fiber handling can have a significant impact on optical system performances, especially in trunk or submarine lines where repeaterless span up to 200 km are being designed.
Therefore large efforts are being devoted to improve cable design and technology with the objective of reducing all the possible impairments of fiber attenuation due to manufacturing, installation or servicing of optical cables.
The fiber microbending phenomenon is one of the most frequent causes of loss increase in optical cables. The physics of this phenomenon is completely understood but no reliable quantitative data are available at present. Up to now the attempts to predict loss increases in single mode fiber due to microbending by applying theoretical models or experimental results obtained on short fiber lengths, have given only qualitative indications[1,2].
This paper will present a new approach to this problem which gives very reliable predictions of microbending losses of cabled optical fibers.
The results of this work, besides giving the criteria to reduce cabled fibers sensitivity to microbending, can have significant applications in the optimization of loose type cable design and in the fault analysis of manufactured cables.

Theoretical model

Fiber microbendings are generated in optical cables when the fiber is compressed by external mechanical stresses against the cable materials.
As an example in a loose tube cable with helical structure subjected to axial strain the fibers are compressed against the tube surface as soon as the cable axial strain exceeds the fiber extra length.
In case of microbendings, fiber axis curvature can be considered a random variable which can be characterized by its power spectral density, whose parameters depend on:

a) Magnitude of the compression force
b) Geometrical and physical characteristics of cable materials and fiber coatings.

Microbendings losses in single mode optical fibers are due to the coupling of the fiber fundamental mode LP01 and the higher order unguided modes. The magnitude of this coupling loss depends on the fiber characteristics and on the power spectral density of the fiber axis curvature.
Following Petermann approximation the added loss for a single mode fiber is[3].

$$\Delta\alpha(\lambda) = \frac{1}{4}\left(k n_1 \omega_0^2 \Delta\right)^2 \Phi(\Omega_c) \qquad (1)$$

n_1 : equivalent core index

k : space wave number

w_o : spot-size (Petermann definition)

$\emptyset(\Omega_f)$: power spectral density of fiber axis curvature

Ω_f : radian frequency = $1/(kn_1 \cdot w_o^2)$

This expression is valid for any type of single mode fiber as the only parameter related to the fiber characteristics is the spot-size. However for some particular classes of profile (multiple-clad), better accuracy can be obtained using in (1) for w_o the equivalent mode field parameter as proposed in.[2]

The curvature power spectral density $\emptyset(\Omega_f)$ of a fiber subjected to microbending can be calculated by modelling it as a thin elastic beam compressed against a rough surface (fig.1). Assuming elastic deformations of the materials and good uniformity of the coating, $\emptyset(\Omega_f)$ depends linearly on the surface roughness power spectral density $P(\Omega)$[4].

$$\emptyset(\Omega_f) = \frac{\Omega_f^4 \cdot P(\Omega_f) \cdot \left(1 + \frac{\pi^2 D^4}{4p^4} \sigma^4\right)^{\frac{1}{4}}}{\left(1 + \frac{H}{D} \Omega_f^4\right)^2} \qquad (2)$$

H : fiber stiffness = $E_f \cdot J_f$

E_f : fiber Young modulus

J_f : fiber moment of inertia

p : linear pressure

σ : r.m.s. of surface deformations [illegible]

D : surface effective lateral rigidity, where $\frac{1}{D} = \frac{1}{D_c} + \frac{1}{[illegible]}$

E_s : surface compression Young modulus

D_c : coating effective lateral rigidity. In case of double jacketed fiber (fig.1) if the outer shell is harder than the inner one the following approximation holds:

$$D_c \simeq [illegible]\, E_1 \cdot E_2 \cdot \left(\frac{r_2 - r_1}{r_2}\right)^{[illegible]}$$

where E_1 and E_2 are the moduli of the inner and the outer jacket and r_1 and r_2 are the radii of the respective [illegible].

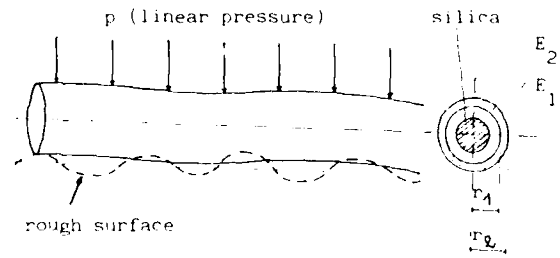

Fig.1 - Coated fiber forced against a rough surface and its section.

Inserting (2) in (1) the expression of loss increase $\Delta\alpha(\lambda)$ is obtained:

$$\Delta\alpha(\lambda) = \frac{\Omega_f^2 \cdot P(\Omega_f) \cdot \left(1 + \frac{\pi^2 D^4}{4p^4} \sigma^4\right)^{\frac{1}{4}}}{4 \cdot w_o^2(\lambda) \cdot \left(1 + \frac{H}{D} \Omega_f^4\right)^2} \qquad (3)$$

For most practical cases

$$\frac{\pi^2 D^4}{4p^4} \sigma^4 \gg 1$$

therefore

$$\Delta\alpha(\lambda) \simeq [illegible] \cdot p \qquad (4)$$

where

$$[illegible] = \frac{[illegible]}{[illegible]\sqrt{\pi}} \cdot \frac{\Omega_f^2 \cdot P(\Omega_f)}{D \cdot \sigma \cdot w_o^2(\lambda) \cdot \left(1 + \frac{H}{D} \Omega_f^4\right)^2}$$

Experimental results

[illegible]

[illegible]

As regard the roughness characteristics of the surfaces, the relevant roughness spectral components for microbending loss calculation are those within the frequency range corresponding to spatial periods of 0.5÷2 mm.
Power spectra measurements of surface irregularities were performed by using a suitable modified commercial roughness meter having vertical sensitivity of about 0.05 μm and spatial resolution of 5 μm (fig.2). With this apparatus the profile of the surface irregularities is obtained by moving, at constant speed, a sharp stylus (2.5 μm radius), kept in contact with the surface itself at very low pressure.
The vertical displacement of the stylus is trasformed by means of a photoelectric transducer in an electrical signal which is sampled and digitized by a high speed digital voltmeter. The data are then processed by a personal computer with F.F.T. algorithm.

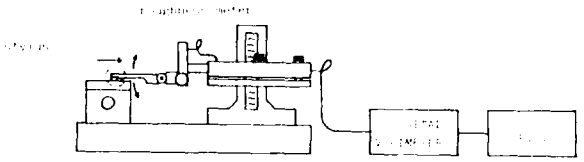

Fig.2 - Apparatus for roughness power spectrum measurement.

Suitable windowing and averaging techniques were applied in order to obtain a reliable distribution of the power density spectrum of the irregularities. Residual noise components were filtered out by fitting the data with a suitable analytical expression. In particular a Lorentzian three parameters shifted distribution was found to fit correctly the spectrum of the actual surface roughness.

$$W(\Omega) = \frac{\sigma^2}{\pi} \cdot \frac{\mu}{\mu^2 + (\Omega - \Omega_0)^2}$$

l : correlation length
Ω : central spatial frequency
μ : spectral width
σ^2 : normalization factor

The measurements were performed on surface sample lengths of 100 mm with sampling period of about 25 μm. In these conditions the noise introduced by the high and low frequency components in the spatial frequency range of interest was minimized. The results obtained show a good riproducibility of the numerical values of the characteristic parameters of the spectrum function (5).

As an example the power density spectrum obtained on a polypropylene loose tube sample is shown in fig. 3. In fig.4 an hystogram of the numerical values obtained by measuring several times the same sample is presented for the parameter μ which is the most critical from the point of view of microbending loss increase. The measurements did also show that the roughness of the filler coating is negligible compared with those of cable materials at least for the frequency range of interest.

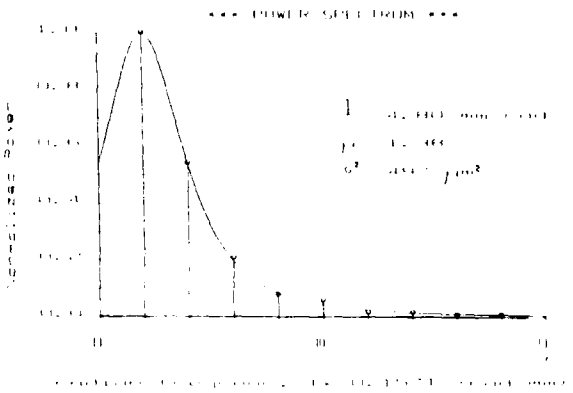

Fig.3 - Roughness power spectrum of loose tube [illegible] with center spatial frequency [illegible] ——— fitting [illegible].

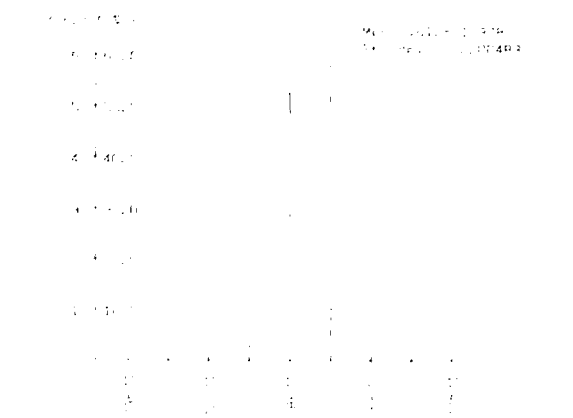

Fig.4 - [illegible]

As all the materials involved in microbendings phenomena work in compression state with small deformations, their elastic characteristics in these conditions were fully characterized using a T.M.A. apparatus. In table I the compression elastic moduli measured for some of the materials used in optical fiber and cable manufacturing are presented.

SURFACE MATERIAL		FIBER COATING	
Type	E [MPa]	Type	E [MPa]
3M Imperial®	100	Inner	3.45
P P	1000		
P B T	2000	Outer	300.00
P E E K	3500		

Tab.I - Compression elastic moduli for surface materials and coatings.

Microbending tests on fibers

Microbending sensitivity tests on optical fibers are generally carried out by submitting a short length of fiber (1÷2 m) to a compression force between two plates coated with sand paper. With this technique, in order to obtain significant loss increases, very coarse materials and high linear pressures have to be used. In these conditions the deformations induced in fiber coatings are well beyond their elastic limit. Therefore these tests are not representative of the real situation of the cabled fibers and moreover cannot been used for an experimental verification of microbending loss calculations as this model is based on the hypotesis of perfect elastic behaviour of the materials involved.

In this work microbending effects on optical fibers were characterized by using an expandable bobbin. This 300 mm diameter metallic bobbin, coated with the special rough material (3M Imperial® PSA - grade 40 μm), has been specifically developed. Its radial dimension can be varied by means of a motor driven device. This device is connected with a personal computer which controls also an optical measuring system composed of an apparatus for spectral attenuation measurement and a test set-up for fiber strain measurement by phase shift technique (fig.5).

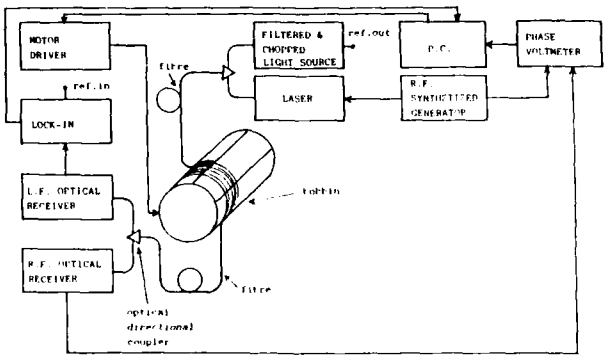

Fig.5 - Apparatus for microbending attenuation test vs linear pressure.

The test is performed by winding with zero tension a long length of fiber (500÷1000 m) on the bobbin and expanding it while monitoring fiber transmission loss versus wavelength and fiber strain. Linear pressure on the fiber is calculated from the measured fiber elongation being $p = EA\varepsilon/R$, where E is the elastic modulus, A the area of the coated fiber and R the bobbin radius. From these measurements, microbending losses as a function of wavelength and linear pressure are obtained.

Experimental tests using the expandable bobbin have been performed on a number of fibers having different refractive index profiles. The results obtained have been correlated with predicted theoretical values based on measured roughness power density spectra of the bobbin coating material (fig.6).

The loss increase vs wavelength is shown in fig.7 for a step index matched cladding 1.3 μm optimized single mode fiber (M.C./I on tab.II) with double acrylate coating. Figure 8 shows the loss increase as a function of linear pressure at a 1.3 μm for the same fiber.

In figure 9 the attenuation increases at 1.3 μm for a linear pressure of 1.9 g/mm are shown as a function of spot-size for different fibers all of step index matched cladding 1.3 μm optimized design.

In the same figures 7-8-9, the results obtained on segmented core 1.55 μm dispersion shifted fiber design are shown.

The relevant calculated results on the basis of the theoretical model are represented by the solid lines in figures 7-8-9.

The excellent agreement between the experimental and the calculated data confirms the validity of the model and of the experimental procedure adopted.

FIBER	M.F.D. [μm]		λ_c [μm]
	1.3 μm	1.55 μm	
M.C./1	10.6	12.2	1260
M.C./2	10.7	12.3	1260
D.S.	6.8	8.3	1180

Tab.II - Optical cgaracteristics of some considered fibers.

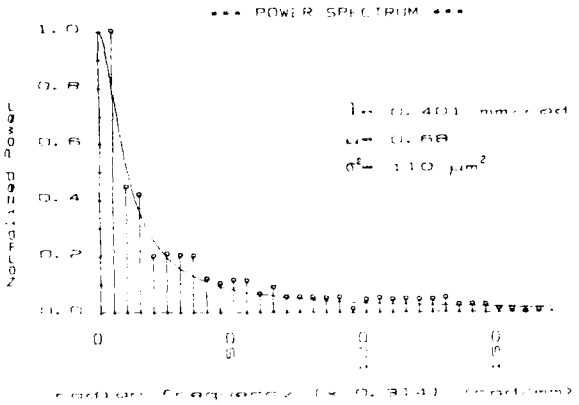

Fig.6 - Example of bobbin material roughness power spectrum (———) fitting curve.

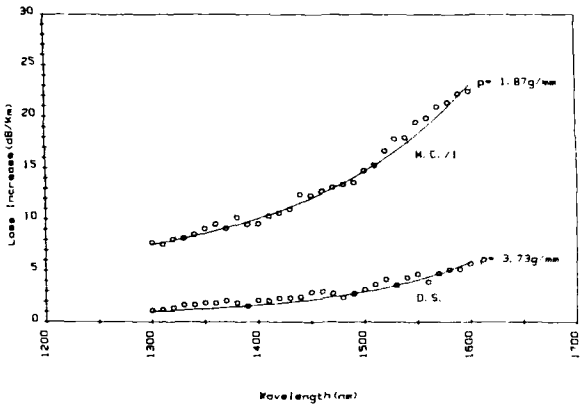

Fig.7 - Microbending loss increase vs wavelength for the M.C./1 and the D.S. fibers (o) measured, (———) calculated.

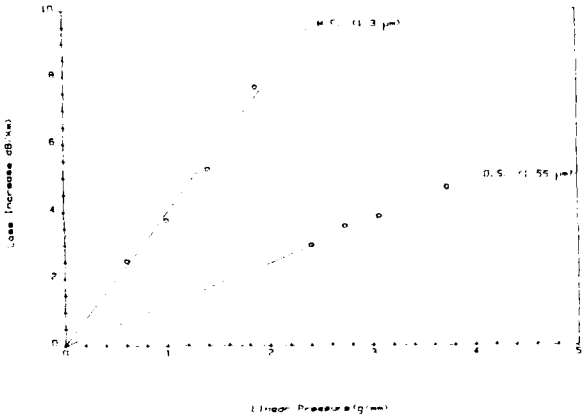

Fig.8 - Microbending loss increase vs linear pressure for the M.C./1 and D.S. fibers (o) measured, (———) calculated.

Fig.9 - Microbending loss increase vs spot-size at 1.9 g/mm (o) measured, (———) calculated.

Microbending tests in optical cables

Fiber microbendings in optical cables are generally caused both by thermal variations and mechanical stresses. The experimental tests have been performed in a condition which was the closest to the theoretical model. An unfilled loose tube cable having twelve polypropylene tubes helically stranded around a central strength member has been chosen (fig.10).

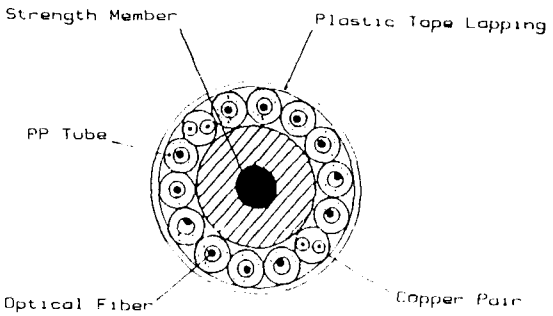

Fig.10 - Optical core structure of loose tube cable.

Each tube contained a single step index fiber matched cladding 1.3 um optimized design.
A cable sample of 200 m length was subjected to a tensile test and fiber spectral loss together with fiber strain was measured as a function of tensile load. As a result of this test, fiber loss increase vs linear pressure can be calculated taking into account the geometrical structure of the cable.
In order to compare the experimental data with the calculated values the roughness power density spectra of the polypropylene tubes were measured. Several tube samples were cut at regular distances along the cable length. The samples were longitudinally divided in two half with a specifically developed technique and the roughness profile was measured along a generatrix of the inner surface. As an example the roughness power density spectrum of tube No.10 is shown in fig.3.
The spectrum was found to have a very distinct peak at a frequency corresponding to a period of 40 mm which was associated to technological conditions during tube extrusion. This periodicity has a very limited effect on the fiber microbending loss increase as it is outside of the critical frequency range. Similar results were obtained on the other tubes.
The loss increase values measured during the cable tensile test for the fiber included into the tube No.10 are shown in figures 11-12 as a functio, of wavelength and linear pressure.

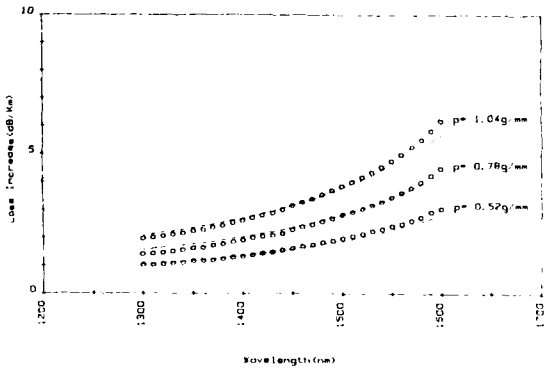

Fig.11 - Microbending loss increase vs wavelength for the M.C./2 fiber at three different linear pressures (o) measured, (———) calculated.

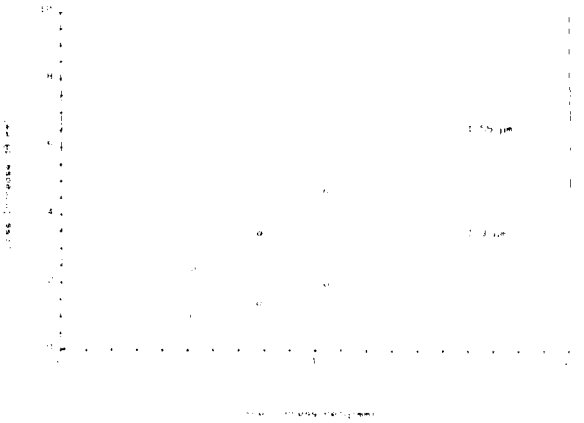

Fig.12 - Microbending loss increase vs linear pressure for the M.C./2 fiber at two wavelengths (o) measured, (———) calculated.

The solid lines correspond to the calculated data and also in this cases a very satisfactory agreement between the calculated values and the measured data was found. This agreement is substantially confirmed by Tab.III in which experimental and calculated values of loss increase at 1.3 μm, normalized for a linear pressure of 0.87 g/mm, are shown for the twelve fibers included in the cable.

TUBE	ATTENUATION [dB/km]	
	Measured	Calculated
1	1.59	1.69
2	1.26	1.12
3	1.84	1.85
4	1.84	1.79
5	1.86	1.72
6	1.52	1.61
7	1.72	1.53
8	1.56	1.42
9	1.24	1.27
10	1.55	1.82
Red	1.13	1.25
Green	1.58	1.52

Tab.III - Measured and calculated microbending loss increase at 1.3 μm and 0.87 g/mm for the fibers in a tested loose tube cable.

Further experimental tests were carried out on a helically grooved unfilled core cable (figura 13) containing one fiber per groove. The measured power density spectrum of the groove was found to have a distinct peak at a frequency corresponding to a period of 10 mm (fig.14). Measured loss increase results were also in this case in excellent agreement with the calculated values.
Tests are in progress to verify the applicability of the model to filled multifiber loose tube and grooved core cables. Preliminary results show that the effect of the filling compound is negligible if the filling compound itself is homogeneously soft along the cable. As regards multifiber cables there seems to be a significant dispersion of the measured loss increases among the fibers contained in the same hollow space (tube or groove). However the theoretical calculated values fit reasonably the average measured results.

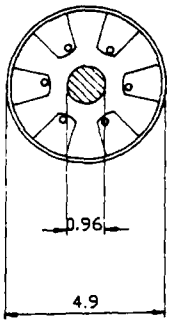

Fig.13 - Helical groove structure.

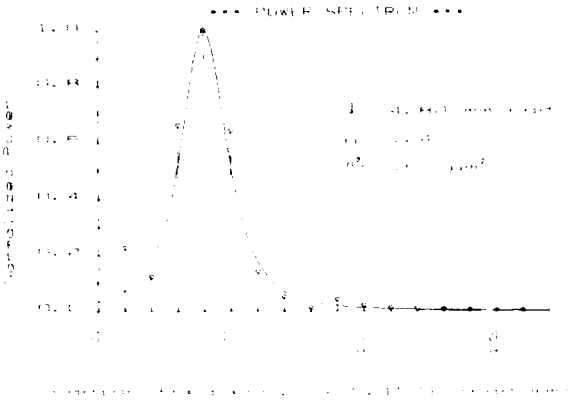

Fig.14 - Grooved cable material roughness power spectrum, with center radian frequency Ω_0 = 0.628 rad/mm (———) fitting curve.

Applications

Cable design and technology

The results of this work could have a significant impact in cable design and technology. On one hand they provide design criteria and indicate which process parameters must be controlled in order to minimize the fiber microbending sensitivity in optical cables.

On the other hand, once the cable materials and the manufacturing process are well characterized and under continuous control, they allow the optimization of cable design taking into account the predicted microbending loss increases.

From the theoretical model and the experimental results it appears that microbending loss increases in optical cables depend on material properties and its extrusion process.
A detailed analysis of the measured power density spectra shows that the surface irregularities can be considered as a combination of the ondulations, introduced by the extrusion process, and the roughness, depending on intrinsic material properties and extrusion parameters. The ondulation are characterized mainly by long period components while roughness is predominant in the short period range (fig.15 curve 1).
As regards the effect on fiber attenuation the power density spectrum of surface irregularities is filtered by a weight function which depends on materials mechanical characteristics (fig.15 curve 2). Numerical calculations performed for fibers and cable materials currently used show that the effect of the latter is negligible and that the weight function parameters are determined only by fiber coating characteristics.

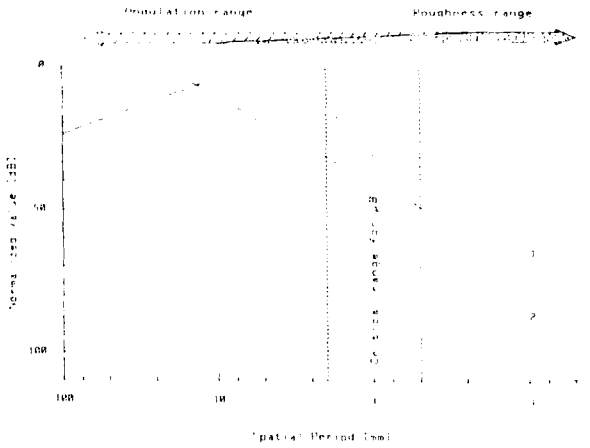

Fig.15 - Curve 1 : Roughness normalized power spectrum of tube No.10 vs spatial period.
Curve 2 : Weight function.

The microbending loss at each wavelength for a given fiber is linearly dependent on the value of the resulting spectrum at the frequency defined by the fiber spot-size.
Those frequencies, for the fiber type and wavelengths of interest, correspond to spatial periods in the range 0.5÷2.0 mm.
Moreover our experiences confirm that microbending losses are a strongly increasing function of the fiber spot-size as shown from previous literature data.[3]
From this analysis it appears that in order to reduce the fiber microbending sensitivity in optical cables the following steps should be taken:

a) optical fiber with reduced spot-size;
b) fiber coating with low intrinsic roughness and physical characteristic suitable to increase the spectral filtering effect of the weight function at the frequencies of interest (e.g. low mechanical modulus);
c) cable materials with low intrinsic roughness;
d) extrusion parameters which minimize the roughness of the extrudate;
e) manufacturing process parameters which produce low intensity ondulations at frequencies as far as possible from the critical range of interest for microbending increases.

The possibility of predicting with enough reliability the fiber microbending loss increase can be used to give a further degree of freedom in loose type cable design.
Actually with the use of this method the operating cable strain range can be extended beyond the fiber stress-free window.
As an example in case of a cable submitted to a time variant tensile load (e.g. overhead graundwire) a reduction of the empty space inside the cable, and therefore of its dimensions, is possible if a known attenuation penalty is accepted for the periods of time relative to the highest loads.
This option may lead to the design of a cable with a substantial reduction in material, manufacturing and installation costs.

Fault analysis

Four possible causes of loss increase in optical fiber cables are known at present, namely:

- a) microbending
- b) macrobending
- c) hydrogen
- d) radiation

By finding out which phenomena cause loss increase in actual cables it is possible to evaluate the significance of the impairment and to predict its future evolution.

The model illustrated in this paper can help to understand if the observed loss increase is due to microbending effect only.
For this purpose an analysis of the spectral loss increase have to be carried out.
Actually if cable materials and process are well characterized it is possible to perform an iterative procedure in order to fit the measured data with the theoretical curve.
If the fitting procedure gives positive result microbending is the only cause of the loss increase and the actual strain in the fiber, and therefore in the cable, can be evaluated. In case of negative result other causes must be considered.
In some cases loss increase at only two wavelengths (1.3 μm and 1.55 μm) are known.
From our experiences the fitting procedure developed gives useful information also in these conditions. In figure 16 an example of actual fiber loss increase found in two groove core cables, experimentally manufactured , are shown.
In cable A microbendings where intentionally introduced while in cable B some macrobending was added.
The results of the fitting procedure, performed only on fiber loss increases at 1.3 um and 1.55 um, confirm that in the case of cable A microbending is the only cause of the loss increase and that in case of cable B other causes are present.

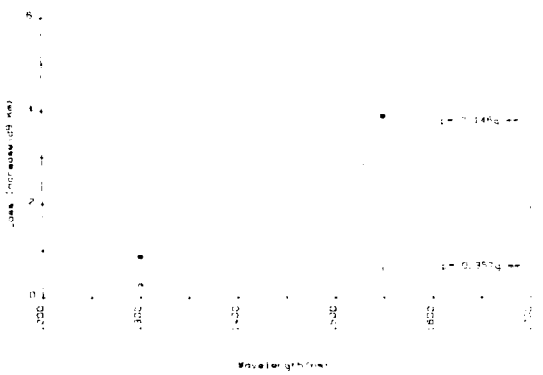

Fig.16 - Application of the fault analysis procedure in the case where only loss increases at 1.3 μm and 1.55 μm are known. (○) cable A, (●) cable B.

Conclusion

The applicability of a theoretical model for the calculation of microbending loss increases has been experimentally verified on fibers and on cables. The high degree of confidence reached between predicted and measured microbending loss data gives the possibility of using the theoretical model in different fields of application:

a) reduction of microbending sensibility of cabled fibers through the improvement of cable design and technology;

b) increase of the degree of freedom in loose type cable design by enlarging the operating strain range;

c) detection of microbending phenomena in case of loss increase found in manufactured cables.

Acknowledgments

The authors wish to thank the management of Società Cavi Pirelli and S I P for authorization to present this paper.

References

1. K. Blow, et al.
"Power spectrum of microbends in monomode optical fibres".
Electronics Letters - May 1982 - Vol.18 n.11

2. M. Artiglia, et al. - Proceedings of ECOC '87
Vol.I - pag.437.
"Bending loss characterization in single mode fibres".

3. K. Petermann
"Foundamental mode microbending loss in graded index and W fibres".
Optical and Quantum Electronics 9 (1977) 167-175.

4. D. Blodge
"Optical fiber packaging and its influence on fiber straightness and loss".
B.S.T.J. - Vol.54, n.2, February 1975.

Giorgio Grasso was born in 1949 in Rome, Italy. He received his electronic engineering degree from the University of Bologna in 1972. He joined the Central Cable Laboratory of Società' Cavi Pirelli S.p.A. in 1973 where he has been involved in the development and design of optical cables and optical fiber measurements.
At present he is responsible for the Laboratory for the development of new optical fiber characterization methods and transmission technique.
He is author of many papers and member of S.P.I.E.

Fausto Meli was born in 1956 in Piacenza, Italy. He received his nuclear engineering degree from the Polytechnic Institute of Milan in 1981. He joined the Central Cable Laboratory of Società cavi Pirelli S.p.A. in 1983 where he has been involved in the characterization of optical fiber properties. He is member of the I.E.C. Fiber Optic Test Equipment Working Group.

Elio Usai was born in 1960 in Sassari, Italy. He received his electrical engineering degree from the University of Cagliari in 1985.
He joined the Central Cable Laboratory of Società Cavi Pirelli S.p.A. in 1987. where he has been involved in the characterization of mechanical properties of optical fibers and optical cables.
He is member of the A.I.A.D.S.

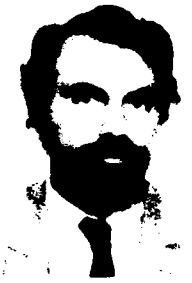

Feliciano Esposto was born in Acervia (Ancona), Italy, in 1948. He received his doctorate in physics from the University of Torino in 1976.
In 1969 he joined CSELT, where he did research on optics and optical communications, particularly holography and optical fiber characterization.
Since 1980 he is with SIP, the Italian telecommunication operating company, which like CSELT belongs to the STET group, where he has been involved in optical fiber transmission system design.
At present he is the chief of the physical carrier and apparatus design and development on the "Industrialization of New Technology" division at SIP headquarters in Rome.
Feliciano Esposto is co-author of many papers and lectures at Superior School "Guglielmo Reiss Romoli".

EFFECT OF COATING ON MECHANICAL PROPERTIES OF OPTICAL FIBERS

H. H. Yuce and A. D. Hasse

Bellcore
Morristown, NJ 07960

P. L. Key and M. J. Andrejco

Bellcore
Red Bank, NJ 07701

SUMMARY

Polymer coatings on optical fibers protect the glass surface from mechanical damage and minimize microbending losses in cables. The effectiveness of the coating for protecting the strength of the fiber can vary significantly with the specific coating. We present the strength and dynamic fatigue results for a group of eight different fibers and discuss the results in terms of the effect of the coating. We show that the coating affects both the distribution of flaw sizes in the glass as well as the rate of growth of these flaws in the presence of stress. To adequately characterize the long term mechanical reliability of polymer coated optical fibers, short term strength or proof testing must be accompanied by fatigue testing.

1. INTRODUCTION

Although low loss glass makes an excellent transmission media, coatings are necessary to make fibers practical for communications systems. Coatings can provide mechanical protection of the glass from abrasion and the environment and minimize microbending losses associated with cabling and installation. In addition, some coatings can be dyed to identify individual fibers in a multi-fiber cable[1].

There is no single coating material that can satisfy all these requirements. For example, polymer coatings, especially dual coatings consisting of an inner low modulus polymer and an outer high modulus polymer, have been shown to be especially resistant to microbending losses[2]. On the other hand, polymers are very permeable to environmental agents such as water which reduce the mechanical strength of the fiber. Coatings such as amorphous carbon[3] and titanium carbide[4] have been shown to provide an hermetic barrier to moisture but are ineffective at preventing microbending losses. The majority of fibers for telecommunications applications are coated with UV-cured epoxy acrylate[5]. The requirements for polymeric coatings have recently been summarized by Toler and Kar[6].

Polymer coatings have frequently been regarded as an inert layer which prevents mechanical contact with the fiber surface. However, a number of investigators have shown that properties of the polymer such as adhesion to the glass and water permeability can significantly affect the mechanical properties of the coated fiber[7-11]. In this paper, we present strength and dynamic fatigue results for eight fibers; four were purchased from different vendors and four were produced in our laboratory. Even though the outer surface of the glass was similar for the fibers produced in our laboratory we observed significant differences in fatigue properties among the fibers which we attribute to a coating effect.

2. EXPERIMENTAL PROCEDURE

For this study we obtained eight kilometer lengths of optical fibers. Each fiber had a nominal glass diameter of 125 μm coated with various UV-curable, epoxy acrylate polymer coatings to 250 μm diameter. Four of the fibers (designated herein as Vendor 1 - 4) were commercially available fibers. The other four fibers were produced in our laboratory by drawing from a fire polished synthetic fused silica rod (T20 Suprasil 2 Type F). Two fibers were coated in-line with two UV-curable epoxy polyurethane acrylate coatings that were purchased from two different vendors (designated as fiber A-0 and B-0). In addition, two fibers were drawn and coated with the same two UV-curable epoxy acrylates but with 1% by weight of 0.3 μm aluminum oxide powder dispersed in the coating (fibers designated A-1 and B-1). Such additions of alumina have been shown[12] to reduce the median strength of the fiber.

The mechanical properties of the eight fibers were determined by tensile testing at strain rates ranging from 0.005 %/min to 50 %/min. Generally a total of 60 samples with a gage length of 50 cm were tested at each strain rate. However, due to lack of material only 10 and 30 samples were tested at 0.005%/min for fibers A-0 and B-0. The tests were performed on a screw driven universal tensile testing machine, in a laboratory environment of 22 C ± 2 C and 45% ± 5% relative humidity with the breaking loads measured to ± 0.1N. Samples were gripped on 10 cm diameter capstans covered with a soft elastomeric sleeve. Masking tape was used to hold the fiber samples securely on the capstans.

In addition, the stripping force of the coating was measured using a commercial stripping tool mounted on a screw driven universal tensile testing machine. The gage length of the stripping test samples was 1.5 cm and the test was conducted at 50 cm/min. The stripping force was measured for fibers in the as-received condition and after exposure to 60 and 90 C water for 24 hours.

3. EXPERIMENTAL RESULTS

The dynamic tensile test results for the eight fibers are shown in Figures 1-8 plotted on Weibull axes. The tensile data can be fit to a single Weibull distribution of the form:

$$P = 1 - \exp - [\sigma\ \sigma_0]^m \qquad (1)$$

for all but the two fibers containing abrasive particles in the coating (Figures 7 and 8). In this equation P is the cumulative probability of failure at a stress less than or equal to σ and σ_0 and m are empirical distribution parameters. The values of the Weibull exponent m are listed on Figures 1-8.

In the presence of stress and certain chemical species such as water, the size of flaws existing in the glass can grow to a size that causes failure. Assuming that the growth rate of such flaws is proportional to a power function of the stress intensity, it can be shown[13] that the dynamic breaking strength σ depends upon the applied strain rate, $\dot{\varepsilon}$:

$$\sigma = B\dot{\varepsilon}^{1/(n+1)} \qquad (2)$$

where n is the crack growth exponent associated with the power law dependence of the crack growth rate and B is an experimental parameter. The median strength values of the data shown in Figures 1-8 are plotted as a function of strain rate in Figures 9 and 10. Fitting the line predicted by equation 2 to these data yields the values of n listed on Figures 9 and 10.

The results of the coating stripping test are shown in Table 1.

Table 1 - Coating Stripping Force (grams)

Fiber	As Rec'd	60°C H_2O	90°C H_2O
Vendor 1	314	319	297
Vendor 2	173	27	19
Vendor 3	282	167	195
Vendor 4	398	25	54

4. DISCUSSION

The mechanical reliability of an optical fiber depends upon the initial distribution of flaws in the fiber and upon the rate of growth of those flaws in the presence of stress and chemical species from the environment. The median initial size of the flaws in a fiber is indicated by the median short term strength with larger values of strength associated with smaller flaw sizes. The value of the Weibull exponent m indicates the breadth of the distribution of flaw sizes in the fiber with large values of m associated with a narrow distribution of flaw sizes. Thus, coatings providing good mechanical protection should result in large values of m. Similarly, the crack growth exponent n is a sensitive indicator of the effectiveness of the coating at protecting the fiber from the environment with large values of n associated with more protection and slower crack growth. Table 2 shows the eight fibers ranked in order of decreasing strength (based on median strength at a strain rate of 50% min), decreasing m values and decreasing n values.

Table 2 - Fibers Ranked In Order of Strength, m, n

Strength	m	n
A-0	3	A-1
3	1	A-0
B-0	2	1
1	A-0	B-1
4	4	B-0
2	B-0	3
B-1	A-1	2
A-1	B-1	4

Examination of this table shows that coatings vary in their ability to protect a fiber mechanically and to protect it from the environment. For example, the fiber of vendor 3 shows high strength and a large m but a low n. This is demonstrated even better by comparison of the two fibers with abrasive particles in their coating (A-1 and B-1) with the corresponding fibers without the abrasive material (A-0 and B-0). In this case the same glass was used in all four fibers. The short term strength of fiber A-0 and B-0 are almost the same since this strength is largely reflective of the initial glass condition. The difference in the coating shows up as differences in both m and n. Examination of the results of the fibers with the abrasive dispersed in the coating shows the expected low short term strength and low m values due to the abrasion of the glass by the dispersed abrasive. However, there is practically no change in the crack growth exponent n for these fibers from the abrasive-free fibers. This result indicates that the addition of abrasive does not change the effectiveness of the coating as an environmental barrier.

The results of the coating stripping test shown in Table 1 indicate that coating on vendors 1 and 3's fibers are more resistant to moisture than vendors 2 and 4. This is consistent with the ranking shown in Table 2 based on n.

In addition to a coating's barrier effect (mechanical and environmental), it should be noted that a coating can affect the local chemical environment at the crack surface in two other ways. First, polymer coatings contain mobile ionic species and contaminants which can diffuse to the coating glass interface. Second, while coatings are recognized to be fairly permeable, they do act to encapsulate the contaminants and moisture at the coating-glass interface. This encapsulation can lead to significant chemical concentrations at the glass surface which is the location of most strength reducing flaws in fibers. Numerous studies have shown a strong effect of chemical environment such as pH and ion size on the

rate of propagation of cracks in glass[14].

5. CONCLUSIONS

The long term mechanical reliability of a glass fiber depends upon applied stress, fiber strength, the rate of growth of flaws in the glass, and the fracture toughness of the glass. The polymer coating on the fiber can affect the initial distribution of flaw sizes as well as the rate of growth of those flaws in the presence of stress. Neither measurement of fiber strength nor proof testing is adequate to assure the long term mechanical reliability of optical fibers since neither provides information about the rate of crack growth. Thus, short term tests must be augmented with fatigue tests.

6. REFERENCES

1. L. L. Blyler, Jr., B. R. Eichenbaum, and H. Schonhorn; "Coatings and Jackets", in **Optical Fiber Telecommunications** (S. E. Miller and A. G. Chynoweth, ed); Academic Press; 299-341 (1979).
2. P. Bouten, D. Broer, C. Jochem, and T. Meeuwsen; "Optical Fibre Coatings: High Modulus Coatings for Fibres with a Low Microbending Sensitivity"; Proc 46th Annual Technical Conference Soc Plastics Engrs, 395-2397 (1988).
3. R. G. Huff, F. V. DiMarcello, A. C. Hart, Jr.; "Amorphous carbon hermetically coated optical fibers"; Tech Digest, OFC 1988, TUG2 (1988).
4. R. Chadhuri and P. C. Schultz; "Hermetic Coating on Optical Fibers"; Proc SPIE 717, 27-32 (1986).
5. H. Schonhorn, C. R. Kurkjian, R. E. Jaeger, H. N. Vazirani, R. V. Albarino, and F. V. DiMarcello; "Epoxy acrylate coated fused silica fibers with tensile strengths > 500 ksi (3.5 GN/m^2) in 1-km gauge lengths"; **Appl. Phys. Lett**; 29; 712 (1976).
6. J. Toler and G. Kar; "Polymeric Coatings for Optical Fibers"; Proc 46th Annual Tech Conf Soc Plastics Engrs; 372-376 (1988).
7. T. Wei; "Mechanical reliability considerations of polymer-coated optical fibers"; Proc SPIE 717; 21-26 (1986).
8. T. Wei; "Effects of Polymer Coatings on Strength and Fatigue Properties of Fused Silica Optical Fibers"; **Advanced Ceramic Materials**; 1; 237-241 (1986).
9. B. J. Skutnik, B. D. Munsey, and C. T. Brucker; "Coating Adhesion Effects on Fiber Strength and Fatigue Properties"; Proc Mat. Res Soc; 88; 27-34 (1987).
10. T. Wei and B. J. Skutnik; "Effect of Coating on Fatigue Behavior Behavior of Optical Fiber"; **J. Non. Crys. Solids**; 102; 100-105 (1988).
11. B. Skutnik; "How Coating Polymer Properties Affect Fiber Cable Performance"; Proc. 46th Annual Tech. Conf. Soc Plastics Engrs; 382-385 (1988).
12. F. A. Donaghy and D. R. Nicol, "Evaluation of the Fatigue Constant *n* in Optical Fibers with Surface Particle Damage"; **J. American Ceramic Soc**; 66; 101 (1983).
13. D. Kalish, P. L. Key, C. R. Kurkjian, B. K. Tariyal, and T. T. Wang; "Fiber Characterization - Mechanical"; in **Optical Fiber Telecommunications** (S. E. Miller and A. G. Chynoweth, ed), Academic Press; 401-433 (1979).
14. T. A. Michalske and S. W. Freiman; "A Molecular Mechanism for Stress Corrosion in Vitreous Silica"; **J. Am. Cer Soc.**; 66; 284-287 (1983).

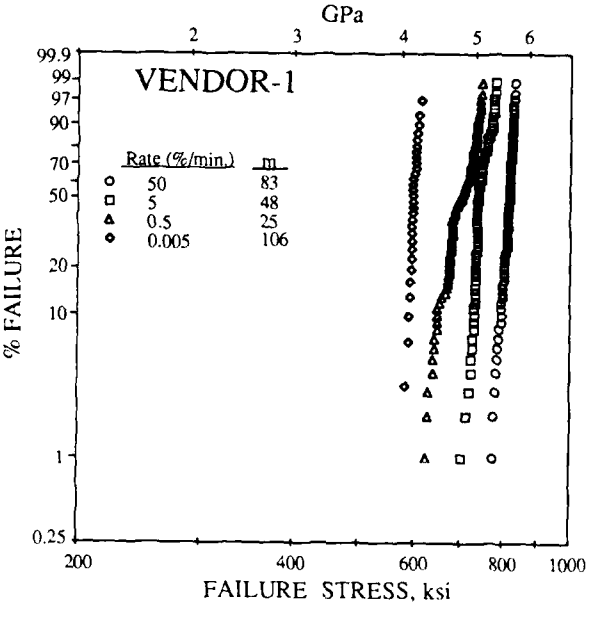

Figure 1: Weibull plot of strengths of polymer coated fiber [vendor-1].

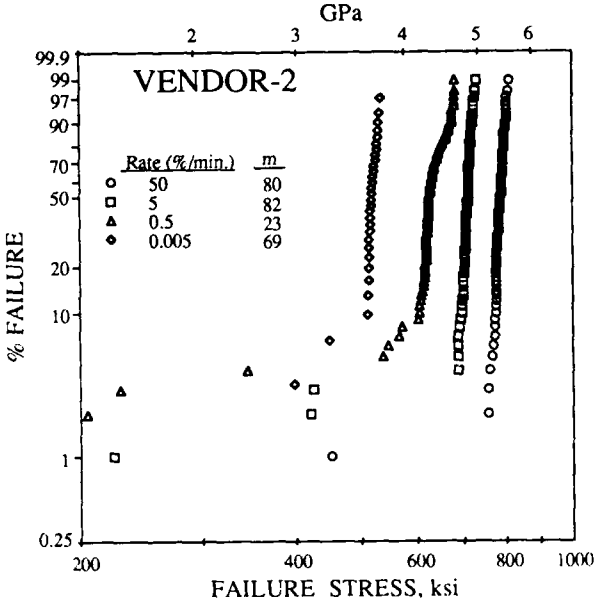

Figure 2: Weibull plot of strengths of polymer coated fiber [vendor-2].

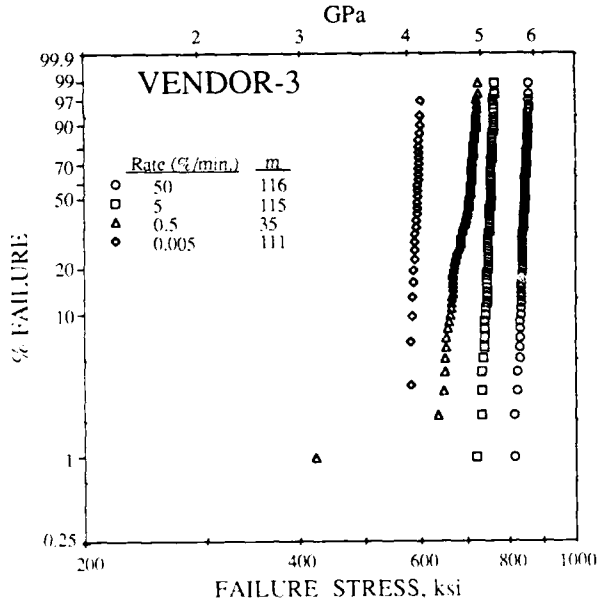

Figure 3: Weibull plot of strengths of polymer coated fiber [vendor-3].

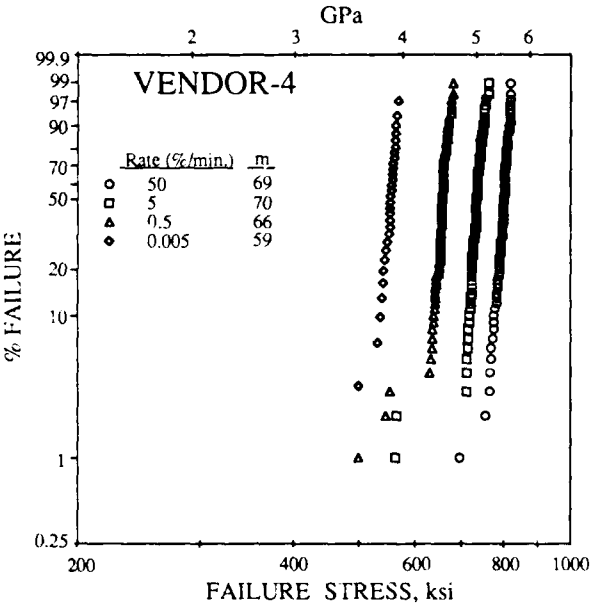

Figure 4: Weibull plot of strengths of polymer coated fiber [vendor-4].

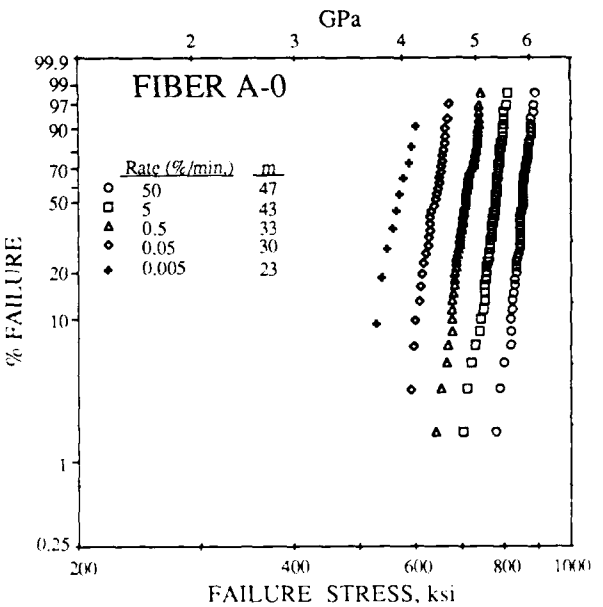

Figure 5: Weibull plot of strengths of polymer coated fiber [Fiber A-0].

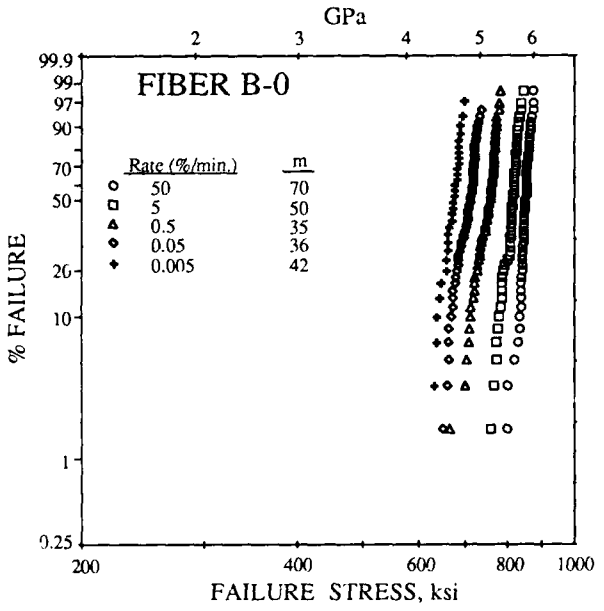

Figure 6: Weibull plot of strengths of polymer coated fiber [Fiber B-0].

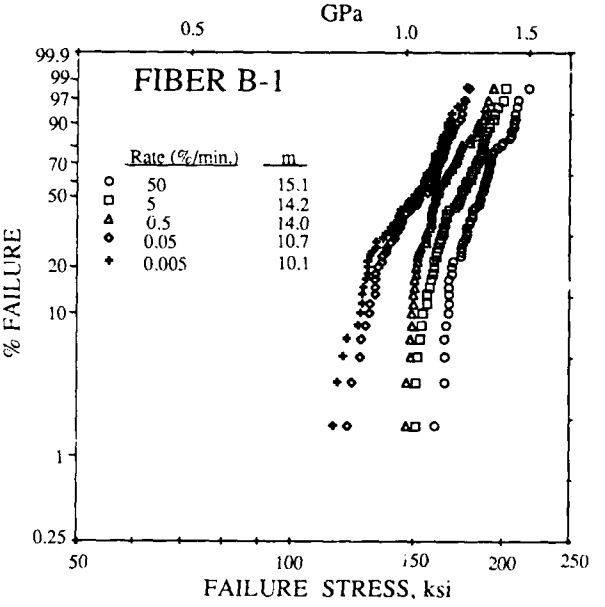

Figure 8: Strength data for Fiber B-1, with 1% by weight of alumina dispersed in the coating, at different stress rates plotted on Weibull axes.

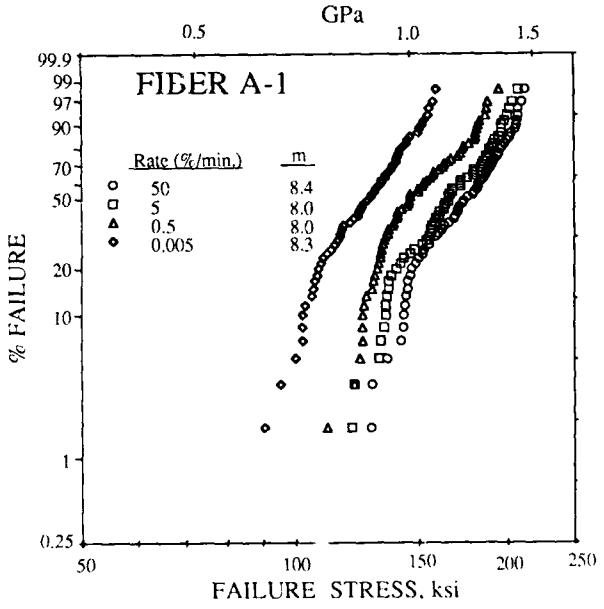

Figure 7: Strength data for Fiber A-1, with 1% by weight of alumina dispersed in the coating, at different stress rates plotted on Weibull axes.

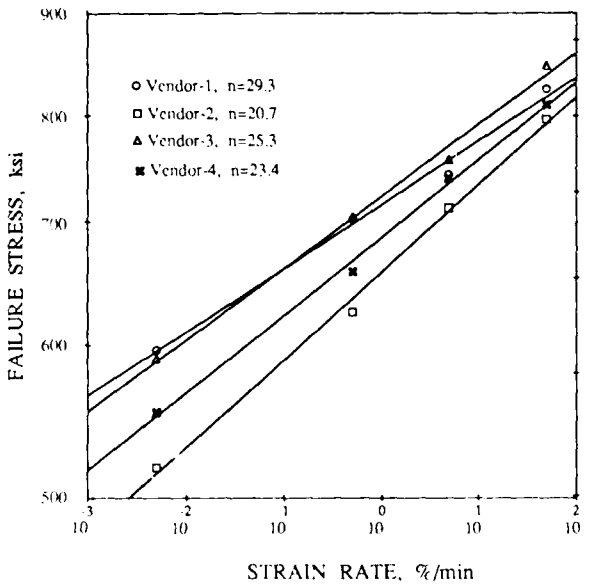

Figure 9: Mean dynamic fatigue values for polymer coated fibers.

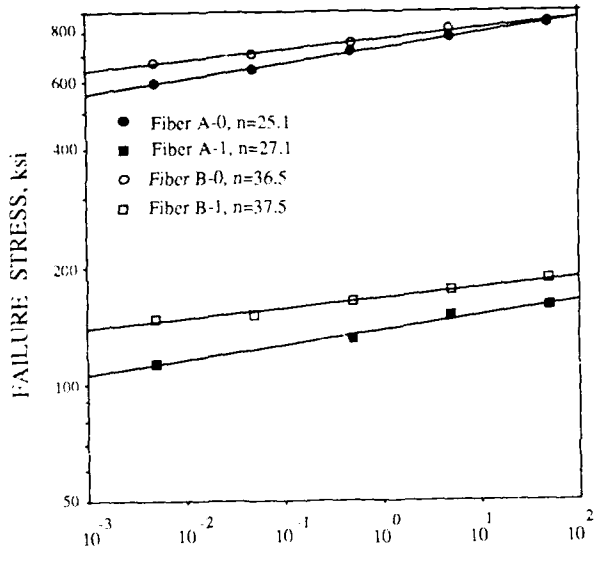

Figure 10: Mean dynamic fatigue values for polymer coated fibers.

Alan Hasse is a Staff Technologist at Bellcore in Morristown, New Jersey as part of a Cooperative Education work-study program at New Jersey Institute of Technology. At NJIT, Mr. Hasse is working toward a degree in mechanical engineering.

Leland Key is District Manager of the Metallurgical Science and Engineering Research group at Bellcore in Red Bank, New Jersey. He received a B.A. and a B.S. in mechanical engineering from Rice University, an M.S. in Engineering Science from George Washington University and a PhD in Materials Science from the University of California at Berkeley.

Hakan Yuce is a Member of the Technical Staff in the Fiber Distribution and Reliability group at Bellcore in Morristown, New Jersey. He received a B.S. in mechanical engineering from the Technical University of Istanbul, an M.S. from MIT and a PhD from Stanford.

Matt Andrejco is a Member of the Technical Staff in the Fiber and Nonlinear Optical Materials group at Bellcore in Red Bank, New Jersey. He has an A.S. degree in Math and Physical Sciences from Mercer County College.

HEAT RESISTANCE PROPERTY OF UV COAT FIBER FOR OPGW

PJ. Ohta, *N. Nirasawa, *S. Okuyama

**P.A. Hall, **I. Matsubara

*Sumitomo Electric Industries, Ltd.

**Alcan-Sumitomo Electric, Inc.

ABSTRACT

The allowable maximum temperature for UV curable acrylate coated fiber was investigated experimentally, assuming its application to an optical ground wire (OPGW). It was clarified that the practical temperature limit of UV coat fiber is about 100°C for long term (400hr) and 250°C for short term (30 minutes x 3 times). If UV coat fiber is used over these temperature limits, it may cause intolerable loss increasing at low temperature due to deterioration of coating.

1. Introduction

It is true that thermo curable silicone coated fiber has higher heat resistant property than UV curable acrylate coated fiber (UV coat fiber in short). However, UV coat fiber is the most widely used in the world. Hence UV coat fiber is sometimes required to be used in relatively high temperature environment. The application of this fiber to an OPGW is one example. But it was not so clear what the maximum temperature and duration was at which UV coat fiber was usable. This paper reports the experimental results of the heat resistant properties of UV coat fiber while assuming an accidental case of heat hysteresis which OPGW could suffer.

2. Experiments

2.1 Samples

Samples of UV coat single mode fibers and trial Six-Fiber units for OPGW were prepared. The fiber coating diameter is 0.4mm. Six-Fiber unit consists of six fiber stranded around FRP (Fiber Reinforced Plastic) rod, and a thin heat-resistant plastic wrapping tape (Fig.1).

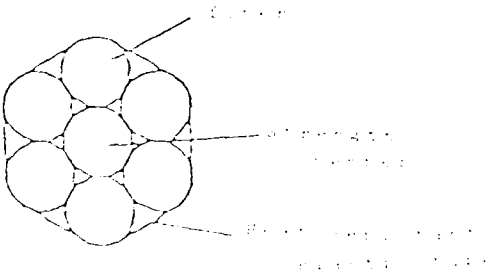

Fig.1 Six-Fiber unit

2.2 Test scheme

The heat hysteresis such as continuous heat aging and short term heat aging were imposed on the samples. The heating conditions were decided assuming those which an OPGW might suffer by accidental currents. During or after these heat experiences, the transmission loss, the young moduli and the elongations of the coating materials were measured. In addition, the temperature cycle test was conducted on the same samples to estimate whether or not they can endure normal environments after having suffered from the accidental heat hysteresises. Some tests on fiber tensile strength and fiber fatigue were also conducted before and after the heat aging. The whole evaluation scheme is shown in Fig.2.

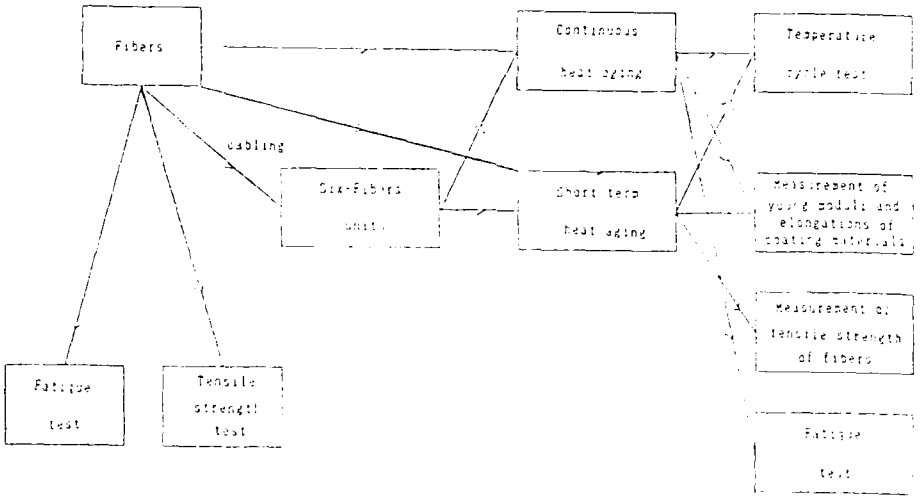

Fig.2 Evaluation scheme

2.3 Test condition and results

2.3.1 Continuous heat aging

The 1km specimens which were loosely coiled in about 300mm diameter were held at temperatures of 80°C, 100°C, 120°C and 150°C for a total of 400 hours. The transmission loss was measured at room temperature every 100 hours during and after aging which was done with cut-back method. Fig.3-a and 3-b show the transmission loss change at 1.3μm and 1.55μm wavelength under various temperatures. The changes of transmission loss and residual loss when the temperature was returned to room temperature were within the measurement accuracy. The data of the Six-Fiber units in Fig.3-b are the average loss of the six fibers.

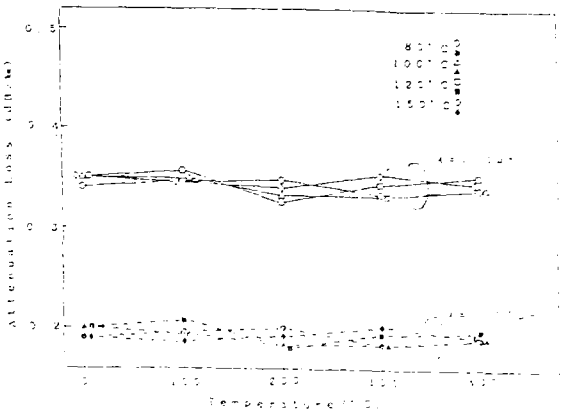

Fig.3-a Transmission loss change of fiber under various aging temperature

2.3.2 Short term heat aging

The 500m specimens which were loosely coiled in about 300mm diameter were exposed to the heat hysteresis shown in Fig.4 (peak temperatures were 180°C, 200°C and 250°C). The transmission loss was continuously monitered at 1.3μm and 1.55μm wavelengths. The maximum change of the transmission loss was recorded for every specimen at maximum temperature. Fig.5 shows the maximum value of the transmission loss after units against the maximum temperature. The transmission loss changes were less than 0.02dB/km and no residual loss changes were measured when the temperature returned to room temperature.

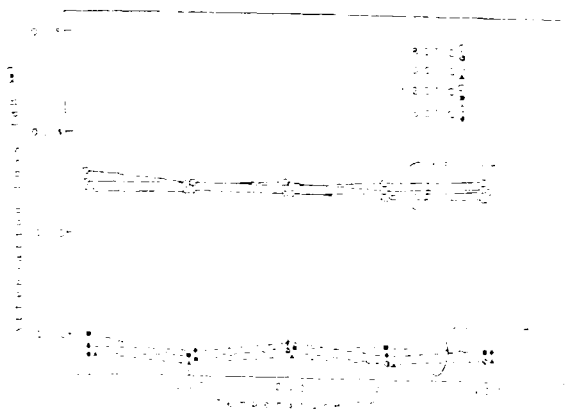

Fig.3-b Transmission loss change of Six-Fiber unit under various aging temperature

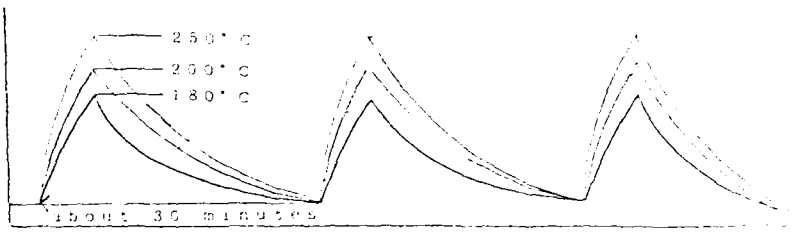

Fig.4 Heat hysteresis

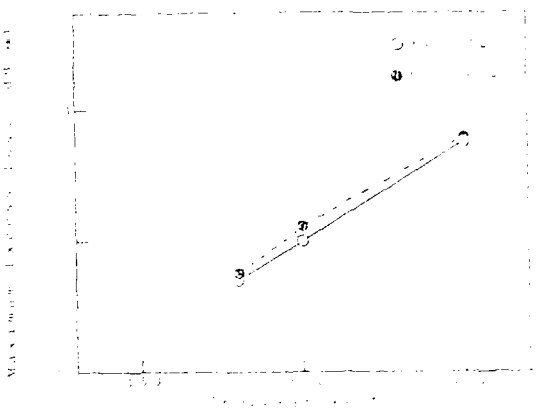

Fig.5 Maximum loss against temperature

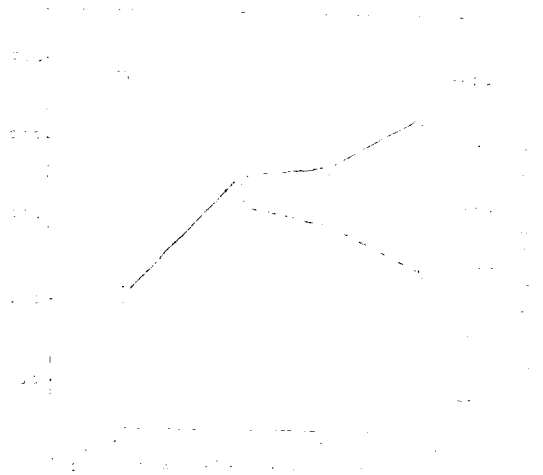

Fig.6 Residual young modulus and elongation against continuous aging temperature

2.3.3 Deterioration of coating material

The residual young moduli and elongation of UV acrylate were measured after the tests described in 2.3.1 and 2.3.2. Figs.6-a and 6-b show the results. The short term heat aging seems not to affect the young modulus and elongation up to about 250°C. But at temperatures over 250°C, heat aging should be avoided for the UV acrylate even if heating time is short, because it causes rapid material decomposition (Fig.7).

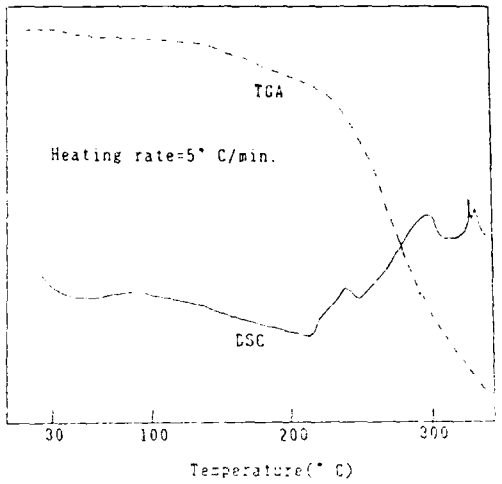

Fig.7 TGA and DSC curves of coating material

2.3.4 Temperature cycle test

The temperature cycle test (from -40°C to +100°C, 10 cycles) were done for the same samples which had experienced continuous or short term heat aging described in 2.3.1 or 2.3.2. The changes of the transmission loss were monitered continuously at 1.55μm at low temperature (-40°C) in every sample. Figs.8-a and 8-b show the peak loss value at -40°C against the heat hysteresis of the samples. The short term heat aging seems not to affect these results (Fig.8-b). However, the loss changes were observed for the fibers that experienced continuous heat aging at over 100°C (Fig.8-a). The similar tests were done also at 1.3μm wavelength, but no significant loss change was observed.

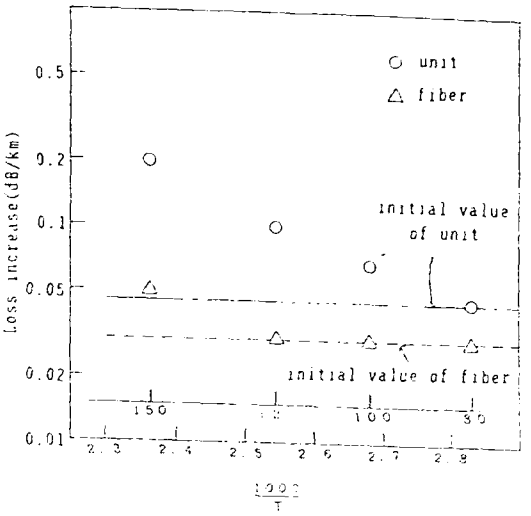

Fig.8-a Peak loss values at -40° C against continuous aging temperature

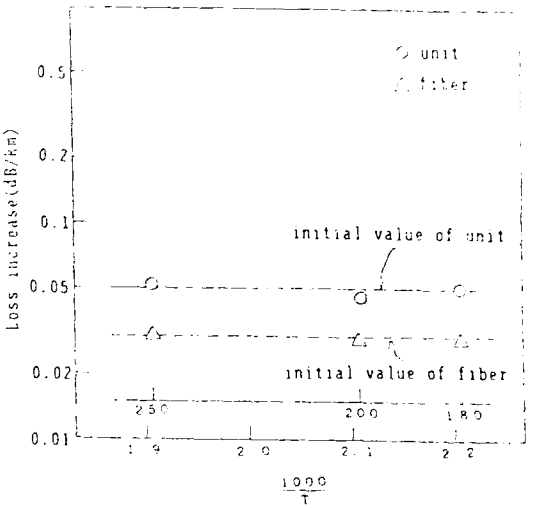

Fig.8-b Peak loss values at -40° C against short term aging temperature

2.3.5 Mechanical test

Fig.9 shows the results of the tensile strength test for the fibers of before and after the short terms aging at 180°C, 200°C and 250°C with a gauge length 30cm. The higher aging temperature, the more the tensile strength. This is thought to be caused by the effect which results and causes the moisture around the fiber to decrease when the temperature rises up.

Fib.10 shows the static fatigue property at room temperature. The data for the fibers after having experienced high temperatures have longer breakage time due to the aforemartioned reason.

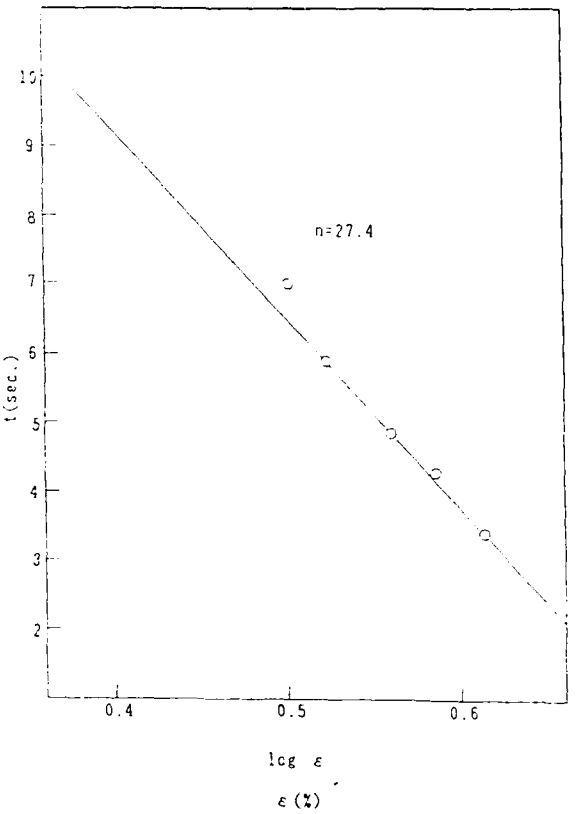

Fig.10 Static fatigue of the fiber

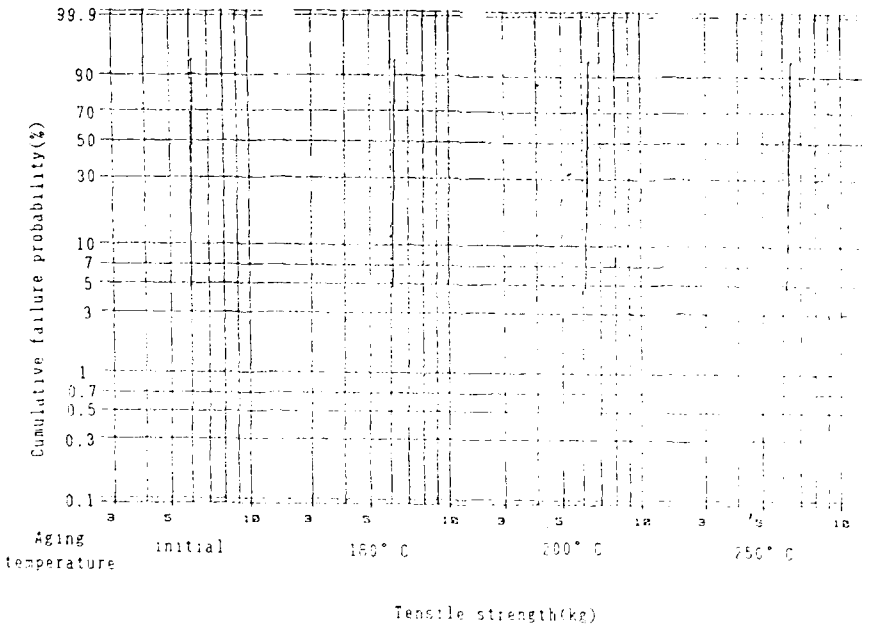

Fig.9 Tnsile strength of the fiber

4. Discussion

Both short term aging and continuous aging did not affect the transmission loss and the tensile strength of the fiber, but they surely degraded the young moduli and the elongation of coating materials. The degradation caused loss increase at low temperatures and the influence was more severe for unit fibers than fiber alone. This fact explains that the loss increase at low temperature is caused by the decrease of the buffering effect of the coating against loteral pressure due to hardening of the coating material, rather than the shrinkage of the coating material. Table 3 summarize the results described in 2.3 and we may conclude the allowable temperature for UV coat fiber is,

1) 100°C for continuous heat aging (400 hrs)

2) 250°C for short term heat aging (30 minutes x 3 times)

5. Conclusion

The practical temperature limit of UV coat fiber is about 100°C for long term (400 hrs) and 250°C for short term (30 minutes x 3 times) for OPGW application. If UV coat fiber is used over these temperatures limits, it may cause intolerable loss increasing at low temperatures due to deterioration of the coating materials or rapid decomposition of coating materials.

Table 3 Total results

Items		Continuous heat aging				Short term heat aging		
		80° C	100° C	120° C	150° C	180° C	200° C	250° C
Transmission loss	1.3 μm	good	good	good	good	good	good	good
	1.55 μm	good	good	good	good	good	good	good
deterioration of coating materials		good	good	critical	poor	good	good	good
Tensile strength		good	good	good	good	good	good	good
Temperature cycle	1.3 μm	good	good	good	good	good	good	good
	1.55 μm	good	good	critical	poor	good	good	good
Total dicision		good	good	critical	poor	good	good	good

Junichi Ohta received a M.S. degree from Tokyo Institute of Technology in 1987. He then joined Sumitomo Electric Industries and has engaged in research and development of optical fiber and cables. Mr. Ohta is a member of communication R&D Department in Yokohama Research Laboratories, and a member of the Institute of Electronics & Communication Engineers of Japan.

Nobumasa Nirasaws received his B.S. degree from University of Electrocommunication in 1983. He then joined Sumitomo Electric Industries and has been engaged in communication cable production and plant engineering section.

Shinya Okuyama received a M.S. from Tokyo Institute of Technology in 1984. He joined Sumitomo Electric Industries, Ltd. in 1984, and has been engaged in development of manufacturing optical fiber.

Phillip Hall received his B.E.E. degree in Electrical Engineering from the Georgia Institute of Technology in 1972. He joined Alcan Cable in 1981 as a Product Manager of service cable. Presently, Mr. Hall is Product Manager of the Fiber Optics Group for Alcan Cable.

Ichiro Matsubara received the B.S. degree in Electrical Engineering from Kyoto Univ. in 1966. He then joined Sumitomo Electric Industries and has been engaged in design research and development of various kinds of cables and overhead power transmission lines. Mr. Matsubara is now Executive Vice President of Alcan-Sumitomo Electric, Inc.

A New Heat Resistant Optical Fiber with Special Coating

S. Araki, T. Shimomichi, and H. Suzuki

Fujikura Ltd.
1440, Mutsuzaki, Sakura-shi, Chiba, Japan

Abstract

An optical fiber coated with a ladder siloxane polymer has been developed for use under severe conditions. This fiber is very superior in mechanical properties at elevated temperatures, and superior in static fatigue in a high humidity environment. After aging at 200 °c for a long period of time, a ladder siloxane coated fiber can maintain nearly the initial fiber strength. The n values of static fatigue in excess of 25 are found for this fiber when exposed to severe conditions, such as in atmosphere at 200 °c or water at 80 °c for prolonged periods.

1. Introduction

Ladder siloxane polymers(LSPs)[1][2] have remarkable features, such as heat resistance, high hardness, water repellency and high adhesion to a silica glass surface because of the intermediate structure between silica glass and an organic polymer. Therefore, we have considered that a thin film of an LSP existing between a silica fiber surface and a conventional coating layer may enhance the mechanical reliabilities of optical fibers under severe conditions. For example, the strength degradation of conventional coated fibers at high temperatures, above 200 °c, may be reduced by the thin coating of an LSP on a silica fiber surface. And the stress corrosion on a silica fiber surface may be reduced in an environment of high temperature and humidity.

In this work, we studied the suitability of LSPs for the thin primary coating which is advantageous in the maintenance of fiber strength, even under severe conditions. So, at first, we investigated the characteristics and the structure of LSPs to select a suitable LSP for silica fibers. Secondly, we evaluated the mechanical and the optical properties of the LSP coated fibers after long exposure above 200 °c.

2. Characteristics of ladder siloxane polymers

LSPs in their uncured state are flaky oligomers and are soluble in organic solvents. The viscosity of this resin can easily be adjusted by the use of solvents, so they are easily applied by thin film coating processes such as dipping, spinning and spray coating. LSP resin is cured by hydrolysis and condensation.

In this work, we used an LSP which has a liner organosilicon polymer between the ladder structure. The idealized structure of the LSP is shown in Fig.1. The liner organosilicon polymer plays an important role in increasing the elongation of the LSP. Table 1 shows the characteristics of the LSP in its liquid state and cured film form, respectively. A small amount of a catalyst is added to the LSP resin in order to get a high curing rate. The cured film has about 7 % elongation. The value is nearly equal to the maximum value of silica fiber elongation. Fig.2 shows the weight changes of several coating materials measured by thermogravimetry at elevated air temperatures. In the cases of thermosetting silicone and UV curable urethane acrylate, the weight decreases of these materials begin with the temperature around 150 °c, and the thermal decomposition make rapid progress at a temperature above 300 °c. On the other hand, the LSP used in this work indicates little weight change even at a temperature of 300 °c. However, oxidation of the LSP in

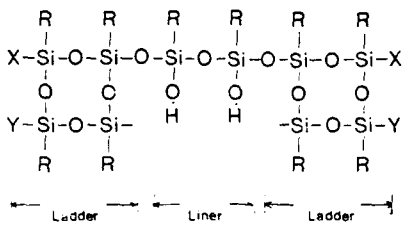

R: Pendant group (alkyl etc)

X,Y: Functional group (alkoxy,hydroxy etc)

Fig. 1 Idealized structure of the ladder siloxane polymer

air is caused by pyrolysis over the temperature range of 500 °c, and SiO2 results from the oxidation.

Table 1 Characteristics of the ladder siloxane polymer

liquid		
	viscosity 25°c	300 cps
	solvent	sec-butanol
	additive	catalyst
film	(curing condition: 200°c, 30 min)	
	elongation	7 %
	pencil hardness	4H
	refractive index n_D^{25}	1.53

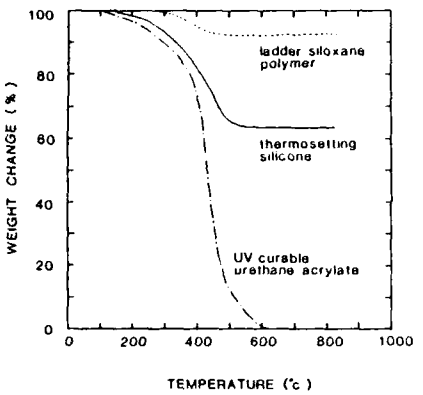

Fig. 2 Weight change of several coatings for optical fiber

3. Preparation of the ladder siloxane coated fibers

Fig.3 shows the cross section of LSP coated single mode fibers prepared in this study. The outer diameter of these fibers is 125 μm, and the thickness of the LSP layer on the fiber surface is about 7 μm. The primary and secondary coatings are 200 μm and 250 μm in diameter, respectively. In the coating process, the LSP coating is cured by heating, and subsequently, the dual coatings of UV curable resin are applied by the use of in-line applicators. The curing temperature range of the LSP is from 400 °c to 500 °c.

Prior to selection of the LSP listed in Table 1, we investigated the relationship between the elongation of an LSP and fiber strength. We prepared two kinds of LSP coated fibers (Fiber A, Fiber B). The elongation of the LSP used for Fiber A is about 7 %, while that for Fiber B is less than 1 %. A liner organosilicon polymer was not introduced into the ladder structure of the LSP used for Fiber B. Fig.4 shows the Weibull plots of the tensile strength for Fiber A and Fiber B. The tensile strength was measured at room temperature on a 3 m gage length with a 10 % strain rate. The breakage at low strength level in Fiber B mainly results from the fractures of the LSP layer during the tensile tests. These fractures seem to be due to the presence of weak points in the LSP layer. Therefore, to obtain both long and high strength fibers, the elongation of LSPs must be much the same level as that of silica fiber, and in general, LSPs must be highly adhesive to silica surfaces.

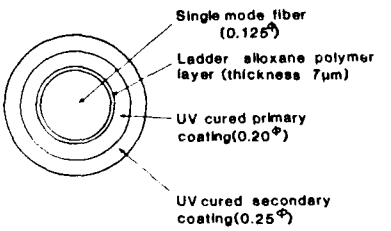

Fig. 3 Cross section of the ladder siloxane coated single mode fiber

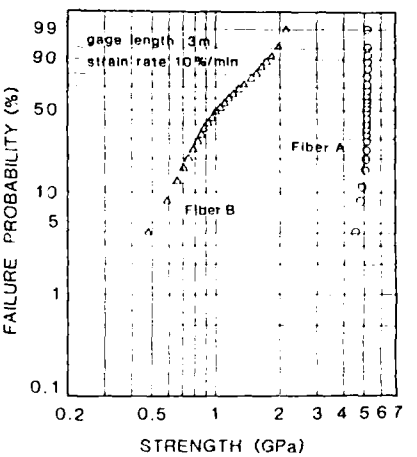

Fig. 4 Weibull plots of tensile strength for the LSP coated fiber (Fiber A,Fiber B)

4. Properties of the ladder siloxane coated fibers after aging at elevated temperatures

We investigated the tensile strength, the static fatigue, and transmission

losses of the LSP coated fibers, before and after aging in air at elevated temperatures. In addition, we compared these fibers with a conventional fiber under the same conditions. The conventional fiber has only the dual coatings(O.D.250 μm) of UV curable resin.

4.1 Tensile strength

To estimate the mechanical reliabilities of the LSP coated fibers in a high temperature environment, we measured the tensile strength after aging at 200 °c and 300 °c, respectively. Fig.5 shows the median tensile strength plots of the LSP coated fibers compared to the conventional fibers after aging at elevated temperatures. In the case of the LSP coated fibers, the tensile strength after aging at 200 °c in air for 30 days is 4.3 GPa, and this value corresponds to about 80 % of the initial strength. Although the LSP film indicates little weight change, even at the temperature of 300 °c as shown in Fig.2, the heat treatment for the fiber at 300 °c rapidly degrades the tensile strength of the fiber. After aging at 300 °c for 25 days, the median strength of the LSP coated fiber is 1.1 GPa. At the temperatures around 300 °c, it seems that the degradation of the LSP elongation is in progress, and the fracture of the LSP layer scratches the smooth surface of the silica fiber.

The strength of the conventional fiber gradually decreases with time due to the heat treatment of 200 °c, while the aging at 300 °c brings about the rapid decrease of fiber strength in only a few days. The SEM photomicrographs of the fracture surfaces for the conventional fiber and the LSP coated fiber after aging at 300 °c, are shown in Fig.6 and Fig.7, respectively. We can conclude that these fractures are caused by shrinkage of the

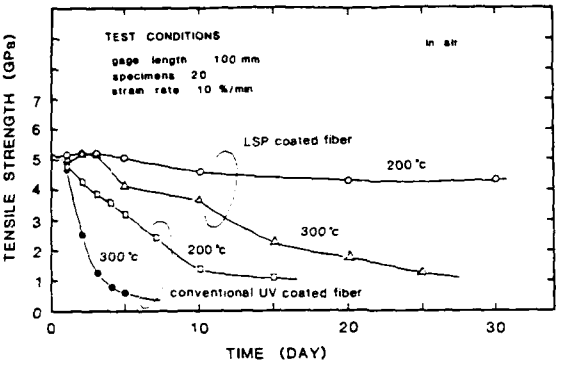

Fig. 5 Tensile strength plots of the LSP coated fiber and conventional UV coated fiber

LSP or UV cured coating layers on fiber surfaces.

Fig.8 shows the Weibull plots of the tensile strength for the LSP coated fibers after aging at 200 °c for 30 days. The tensile strength was measured at room temperature on a 100 mm gage length with a 10 %/min strain rate. The median of the tensile strength is 5.2 GPa in the initial state, while the strength after 30 day is 4.3 GPa. As shown in Fig.8, the tensile strength after 30 days decreases roughly parallel to the initial strength. The degradation of the LSP elongation seems to bring about the strength decrease, because the LSP coating layer is overcured by heat treatment of 200 °c for over a long period of time.

4.2 Static fatigue

The static fatigue of the LSP coated fiber was tested by using the mandrel bending technique under various

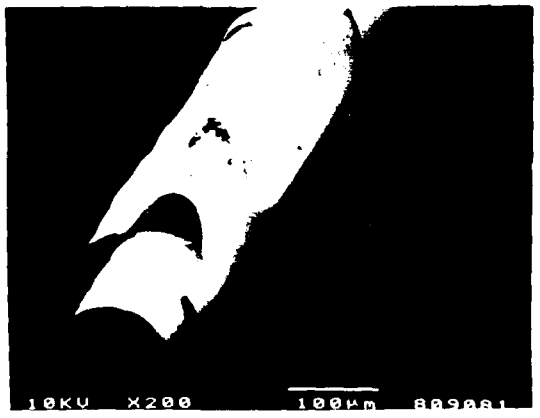

Fig. 6 SEM photomicrograph of the fracture surface for the conventional fiber coated with UV curable resin after aging at 300°C for 3days

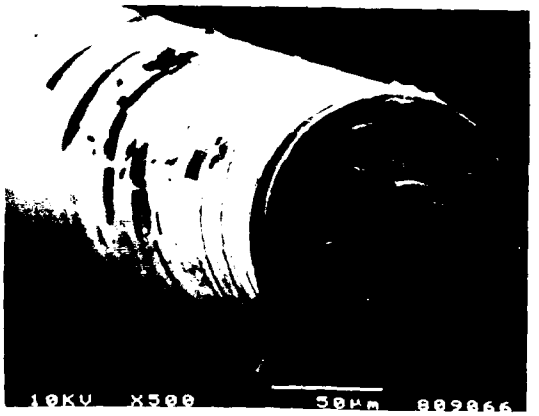

Fig. 7 SEM photomicrograph of the fracture surface for the LSP coated fiber after aging at 300°C for 25days

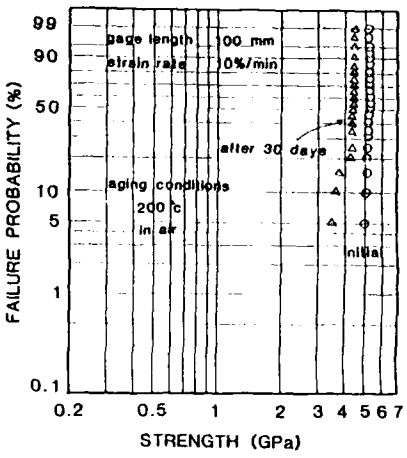

Fig. 8 Weibull plots of tensile strength for the LSP coated fiber after aging

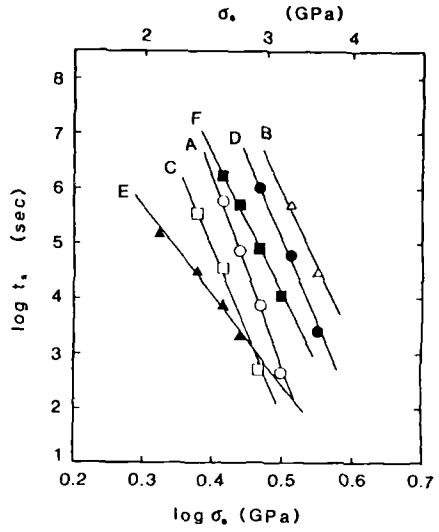

Fig. 9 Static fatigue data of the LSP coated fiber and conventional fiber under various conditions

conditions. The gage length of the static fatigue specimens was 100 cm, and 10 replicate specimens were tested at each stress level. The specimens used in our tests are divided into two parts; one is the fiber before aging, the other is the fiber after aging at 200°c for 30 days. For the fiber before aging, the static fatigue was tested in water at 80°c, in the oven maintained at 200°c, and in the atmosphere at 25°c, 50 %RH, respectively. And, the static fatigue for the fiber after aging was tested only in the atmosphere at 25°c, 50 %RH. For comparison, the static fatigue of the conventional fiber was measured in water at 80°c and in air at 25°c, 50 %RH.

In Fig.9, the static fatigue data under various conditions are plotted as median time-to-failure($\log t_s$) versus applied stress($\log \sigma_s$). On the basis of the commonly adopted empirical relation, $\log t_s = -n \log \sigma_s + \log k_s$, we calculated n and $\log k_s$ where were characteristic parameters. Table 2 shows the summary of static fatigue results. In the atmosphere at 25°c, 50 %RH, the n value and the $\log k_s$ for the LSP coated fiber after aging are 34.1 and 19.8, respectively. These values are higher than the n value(29.3) and $\log k_s$(19.7) for the LSP coated fiber before aging. And, the LSP coated fiber has 26.0 and 18.9 for the n value and $\log k_s$ in the atmosphere at 200°c, respectively. And also, the LSP coated fiber indicates a high n value and $\log k_s$ in water at 80°c, while the n value and $\log k_s$ for the conventional fiber coated with a UV curable urethane acrylate are about 16 and 10, respectively. Therefore, it becomes clear that the LSP coating acts as a water barrier.

Table 2 Summary of static fatigue results

Fiber	Type of specimen	Condition	n	$\log k_s$
A	LSP coated fiber after aging (200°c,30 days)	25°c, 50%RH	34.1	19.8
B	LSP coated fiber before aging	200°c, in air	26.0	18.9
C	↑	80°c, in water	30.1	16.9
D	↑	25°c, 50%RH	29.3	19.7
E	Conventional fiber before aging	80°c, in water	16.1	10.5
F	↑	25°c, 50%RH	25.5	16.8

4.3 Transmission loss

The purpose of this study is the realization of a heat resistant optical fiber. So, when using the LSP coated fibers in the atmosphere at temperature around 200°c, the transmission loss must be minimized and fiber strength must be stabilized for extended time periods. The loss of a UV curable resin coated fiber increases in the atmosphere around 200°c. One of the main reasons for the loss increases is thermal degradation of UV cured coatings. As it is difficult to prevent the thermal degradation, we investigated the fiber parameters(MFD, λc) of the LSP coated single mode fiber to minimize the loss increases. The spectral loss curves for two LSP coated single mode fibers are shown in Fig.10 and Fig.11, respectively. The loss curves of two fibers were measured both before and after aging at 200°c for 30 days. These fibers which were dusted with talc to prevent the adhesion of UV curable coatings, were wound under 50 g of tension onto silica glass drums(O.D. 200mm). After aging, the loss increase of the fiber(MFD

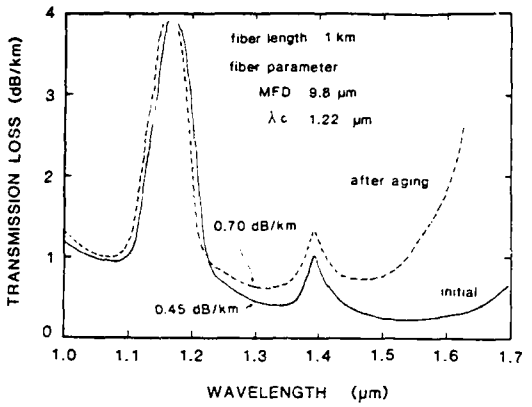

Fig. 10 Spectral transmission loss for the LSP coated single mode fiber after aging at 200°C for 30 days

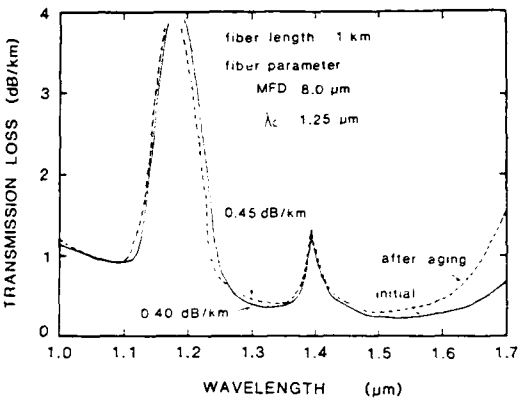

Fig. 11 Spectral transmission loss for the LSP coated single mode fiber after aging at 200°C for 30 days

9.8 μm, λ_c 1.22 μm) shown in Fig.10 is 0.25 dB/km at 1.30 um. On the other hand, the fiber(MFD 8.0μm, λ_c 1.25 μm) shown in Fig.11 indicates little loss increase at 1.30 μm. It is necessary to select the suitable fiber parameters for the LSP coated single mode fiber having UV cured coatings in order to realize a heat resistant optical fiber.

5. Conclusion

From the experimental results described above, the following conclusions were obtained.

(1) The elongation of an LSP must be much the same level as that of silica fiber to maintain the initial fiber strength. In order to increase the elongation of an LSP, it is efficient to introduce a liner organosilicon polymer to the structure of ladder polymer.

(2) The LSP coated fiber almost maintains its initial strength after aging at 200 °c in air for a long period of time. And, it is necessary to select suitable parameters for the LSP coated single mode fiber to minimize the microbending loss due to a lack of buffering efficacy of the decomposed primary layer.

(3) The static fatigue parameter's n values and log k_s for both the LSP coated fibers in an atmosphere at 200 °c, and after aging at 200 °c, are 26 ~ 34, and 16 ~ 20, respectively. The LSP coated fiber has high n values and log k_s even in a severe environment. In addition, the LSP coating acts as a water barrier.

In our study, it has become clear that the LSP coated fiber is superior in heat resistance and static fatigue. Therefore, the LSP coated fiber will prove suitable for use in a wide range of circumstances under severe conditions, such as, for ground wires, in environs of fire hazard, on ships, on oil platforms and in smelting furnace plants.

Acknowledgment

The authors would like to acknowledge the continuing guidance and encouragement of Mr. S. Tanaka and Dr. K. Inada.

References

(1) B.Bagley, C.Kurkjian and W.Quinn ; Materials Research Society Symposium Proceedings, Volume 88, 35 (1987).
(2) B.Bagley, W.Quinn and C.Kurkjian ; ANTEC 88, Atlanta, 390(1988).

Shinji Araki

Opt-Electronics
Laboratory
Fujikura Ltd.

1440, Mutsuzaki,
Sakura-shi, Chiba,
285, Japan

Mr. ARAKI received the B.E. degree in Applied Chemistry from Tokyo Metropolitan University in 1974 and joined Fujikura Ltd.. He has been engaged in research and development of optical fibers and it's coating resin. He is now assistant chief of the Telecommunication Cable Material Section in the Research and Development Division and a member of IECE of Japan.

Hideo Suzuki

Opt-Electronics
Laboratory
Fujikura Ltd.

1440, Mutsuzaki,
Sakura-shi, Chiba,
285, Japan

Mr. SUZUKI received the B.E. degree in Polymer Chemistry from Gunma University in 1971 and joined Fujikura Ltd.. He has been engaged in the study of plastic materials, polymer processing and the development of optical cables. He is now chief of the Telecommunication Cable Material Section in the Research and Development Division and a member of IEICE of Japan and the Society of Polymer Science, Japan.

Tsuyoshi Shimomichi

Opt-Electronics
Laboratory
Fujikura Ltd.

1440, Mutsuzaki,
Sakura-shi, Chiba,
285, Japan

Mr. SHIMOMICHI received the M.E. degree in Material Physics from Nagasaki University in 1985 and joined Fujikura Ltd.. He has been engaged in research and development of coating resin for optical fibers. He is now an engineer of the Telecommunication Cable Material Section in the Research and development division and a member of IECE of Japan and the Society of Ceramic, Japan.

AD-A200 903 PROCEEDINGS OF THE INTERNATIONAL WIRE AND CABLE SYMPOSIUM (IWCS 37TH) HEL..(U) ARMY COMMUNICATIONS-ELECTRONICS COMMAND FORT MONMOUTH NJ 9/9

UNCLASSIFIED 17 NOV 88 F/G 9/1 NL

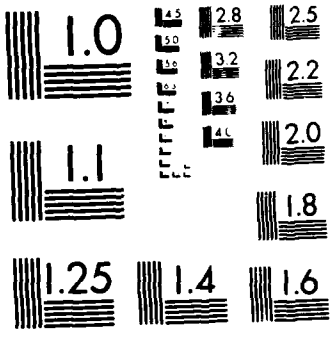

AUTHORS INDEX

International Wire & Cable Symposium

SPONSORED BY U.S. ARMY COMMUNICATIONS-ELECTRONICS COMMAND (CECOM)
FORT MONMOUTH, NEW JERSEY
14, 15 and 16 November 1989
Hyatt Regency Hotel, Atlanta, Georgia

Please provide a 300-500 word abstract (25 copies) of proposed technical paper on such subjects as design, application, materials, and manufacturing of communications and electronics wire and cable of interest to the commercial and military electronics industries. Such offers should be submitted no later than 15 March 1989 to the Headquarters, US Army Communications-Electronics Command, ATTN: AMSEL-RD-C³-PB, Fort Monmouth, New Jersey 07703-5202.

TITLE:_____

AUTHORS:_____

COMPANY:_____

ADDRESS:_____

AUTHOR(S):_____

CONTACT FOR CORRESPONDENCE:_____

ADDRESS AND TELEPHONE:_____

I. PAPER TITLE:_____

II. BACKGROUND (Why was work undertaken?):

III. PRIMARY CONCLUSION OR RESULT:

IV. DESCRIBE THE NOVELTY AND HOW THIS WORK ADVANCES THEORY OR TECHNOLOGY:

V. 300-500 WORD COMPREHENSIVE SUMMARY, INCLUDING METHODOLOGY IN REACHING CONCLUSION OR RESULT:

Fold here

Stamp

Commander
US Army Communications-Electronics Command
Attn: AMSEL-RD-C^3-PB
Fort Monmouth, NJ 07703-5202

Fold here

END

DATE

FILMED

1-89

DTIC